WORLD METEOROLOGICAL ORGANIZATION
GLOBAL OZONE RESEARCH AND MONITORING PROJECT—REPORT NO. 16

ATMOSPHERIC OZONE 1985

ASSESSMENT OF OUR UNDERSTANDING OF THE PROCESSES CONTROLLING ITS PRESENT DISTRIBUTION AND CHANGE

VOLUME III

NATIONAL AERONAUTICS AND SPACE ADMINISTRATION
FEDERAL AVIATION ADMINISTRATION • NATIONAL OCEANIC AND ATMOSPHERIC ADMINISTRATION
UNITED NATIONS ENVIRONMENT PROGRAM • WORLD METEOROLOGICAL ORGANIZATION
COMMISSION OF THE EUROPEAN COMMUNITIES • BUNDESMINISTERIUM FÜR FORSCHUNG UND TECHNOLOGIE

VOLUME III

TABLE OF CONTENTS

VOLUME III *Page*

TABLE OF CONTENTS (Continued)

TABLE OF CONTENTS (Continued)

CHAPTER 12

ASSESSMENT MODELS

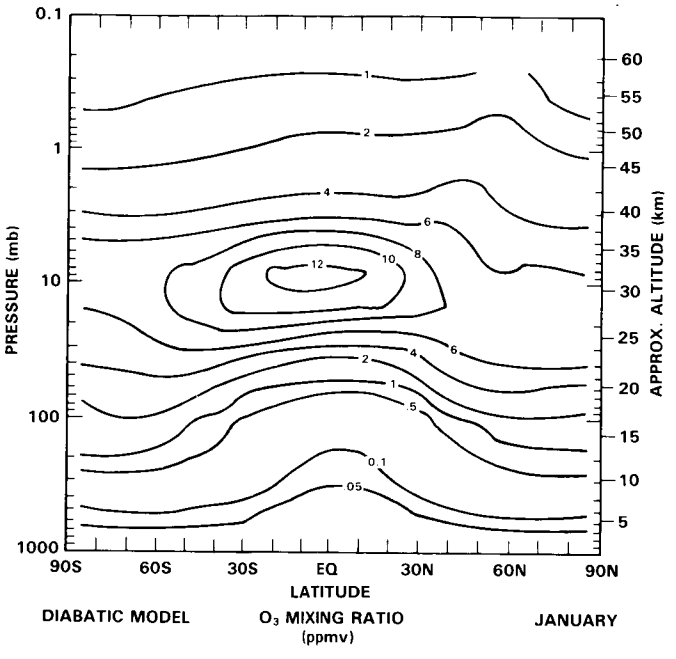

Panel Members

J.A. Pyle, Chairman

D.M. Butler
D. Cariolle
R.R. Garcia
W.L. Grose
P.D. Guthrie
M. Ko
A.J. Owens
R.A. Plumb
M.J. Prather
U. Schmailzl
M.R. Schoeberl
S. Solomon
F. Stordal
N.D. Sze
K.K. Tung
G. Visconti
D.J. Wuebbles

CHAPTER 12

ASSESSMENT MODELS

TABLE OF CONTENTS

12.0 INTRODUCTION

In this chapter the types of models used in assessment of possible chemical perturbations to the stratosphere will be reviewed. One-dimensional models have traditionally been used for this task. Their limitations are well known: the parameterisation of transport in one-dimensional models has a poor physical basis (but see Mahlman (1984), Holton (1985)); the hybrid nature of the models - part local, part global (or hemispheric) average - makes interpretation and validation non-trivial (although this problem is generally ignored). The models' great strength lies in their use as a test bed for photochemical theories; a variety of pollution studies, including multiple perturbations, can be carried out inexpensively. An additional important role in the future may lie in developing complete and efficient photochemical schemes for multi-dimensional models. One-dimensional models are discussed in Sections 12.2 and 12.3.

Two-dimensional models have been used for assessment studies in the past by relatively few groups (e.g Vupputuri, 1978/79, Pyle, 1980, Brasseur and Bertin, 1978/79, Whitten *et al.*, 1981, Gidel *et al.*, 1983). In recent years there have been considerable advances in the theoretical basis for these models and the advantages of the better dynamical treatment have lead many groups to embark on a two-dimensional modelling effort. In Sections 12.4 and 12.5 are discussed the present status of two-dimensional modelling, with a comparison of model results in Section 12.6.

Three-dimensional models have so far been little used for photochemical studies. There are beginning to be some efforts to incorporate simple chemical schemes and these are reviewed in Section 12.7.

Before a discussion of the status of photochemical modelling efforts, the problem of model validation will be mentioned. It is clear that simply to compare a model calculated profile of a particular gas with a measured profile, while being a necessary step, is unsatisfactory as a critical test for the theory behind the model. In the next Section a hierarchy of tests for photochemical models is presented.

12.1 ON THE COMPARISON OF MODELS AND DATA

To have some confidence in the models which are used to study both the current atmosphere and to make predictions about its future development, comparisons between model and data are required. In this Section, types of comparison are discussed. These vary considerably in their usefulness for testing various aspects of model behaviour. In order to reduce the subjectivity of the comparisons, strategies for field observations are suggested.

While the simplest test of the photochemical components of a model is the identification in the atmosphere of the species described in that model (a test not currently satisfied for at least HOCl and HNO_4), the next category of test is usually the comparison of modelled and observed profiles. While this is a necessary step it is certainly insufficient as a critical test. Firstly, the decision as to the goodness of fit is subjective. Differences, for example, in ozone in the upper stratosphere of about 20% are generally thought to constitute 'poor' agreement, while factors of two in comparison between modelled and measured OH are labelled as 'satisfactory'. Secondly, one and two-dimensional models are incapable of modelling the specific dynamical conditions appropriate to a given observation. Thus any discrepancy could be due to inadequately modelled transport or photochemistry. The comparison does not constitute a test because it cannot isolate the physical process being tested. The comparison is at best suggestive (consider, for example, the case of the ClO profile where systematic differences in the slope at around 30 km suggested possible inadequacies in HO_x chemistry (Whitten *et al.*, 1981)). Given these problems, single measurements of

stratospheric species for which a reasonable data base already exists do not appear to add much to the testing of models.

In order to isolate the photochemical from the dynamical contributions, a better test is to compare modelled and measured ratios of species which should be in photochemical steady state. A critical test requires the measurement of all the terms contributing to the ratio expression, which for some ratios would constitute a major logistical problem. Harries (1982) has shown that to test the ratio of NO to NO_2 measurements of O,O_3, ClO, HO_2, temperature and upward and downward solar flux are required. For the test to be critical, the measurements need to be made at exactly the same time and location. Furthermore, the requirement is for high absolute accuracies on the measurements if a useful test is to be made. Harries points to the need for measurements with absolute accuracies of $\sim \pm 2\%$ to test the NO/NO_2 ratio to $\sim \pm 10\%$.

Anderson (NASA meeting, Feldafing, 1984) has discussed the possibility of simultaneously measuring a number of important stratospheric radicals. In his resonance fluorescence technique stratospheric air flows through a chamber where the measurements are made. A rapid response will allow nearly simultaneous, highly accurate measurements of $O(^3P)$, NO, NO_2, OH, HO_2 and ClO. If O_3, CH_4, H_2O and temperature are also measured, many of the important ratios can be determined.

The rapid response is also an advantage for investigations of correlations between species within the laminar layers encountered in the stratosphere. These structures, well known for O_3 (e.g. Dobson, 1973) and recently seen in H_2O (Kley *et al.*, 1980), may be typically a few hundred metres in vertical extent. Kley *et al.* note an anticorrelation between O_3 and H_2O. Observation of similar relationships between, for example, O_3 and OH would be a powerful test of photochemical theory.

An extremely informative test, with less stringent measurement requirements, is the comparison of diurnal variations which in most situations should be independent of atmospheric dynamics. Here, the comparison of the gross behaviour of model and data is useful; failure to reproduce the observed structure points to model inadequacies. Furthermore, since it is the relative diurnal changes which are important, the observations need only have high precision with the absolute accuracy being relatively unimportant.

Two examples showing the usefulness of this approach are chosen. Figure 12-1 shows modelled and observed NO_2 in the upper stratosphere (Roscoe *et al.*, 1985b). Although the absolute magnitudes are different, the gross behaviour is modelled well, including the smaller night-time variation seen at the higher altitude, caused in the model by a less important role for $N_2O_5$with increasing height in the upper stratosphere.

Figure 12-2 shows modelled and observed measurements of the vertical column of ClO (Ko and Sze 1984). The difference in the daytime time increase has lead to important suggestions regarding the role of $ClONO_2$ (see Chapter 11).

Pallister and Tuck (1983) have suggested a particularly important role for high precision measurements of diurnal variations. Figure 12-3 shows the relative variation in ozone at altitudes between 40 and 50 km. The diurnal changes vary significantly with height as the relative roles of O_x, HO_x, NO_x and ClO_x change. For atmospheres with different levels of odd chlorine, they calculate different variations. Measurement of these variations (which would place extremely stringent requirements on the experimental technique) would be particularly useful for assessing our understanding of upper stratospheric photochemistry.

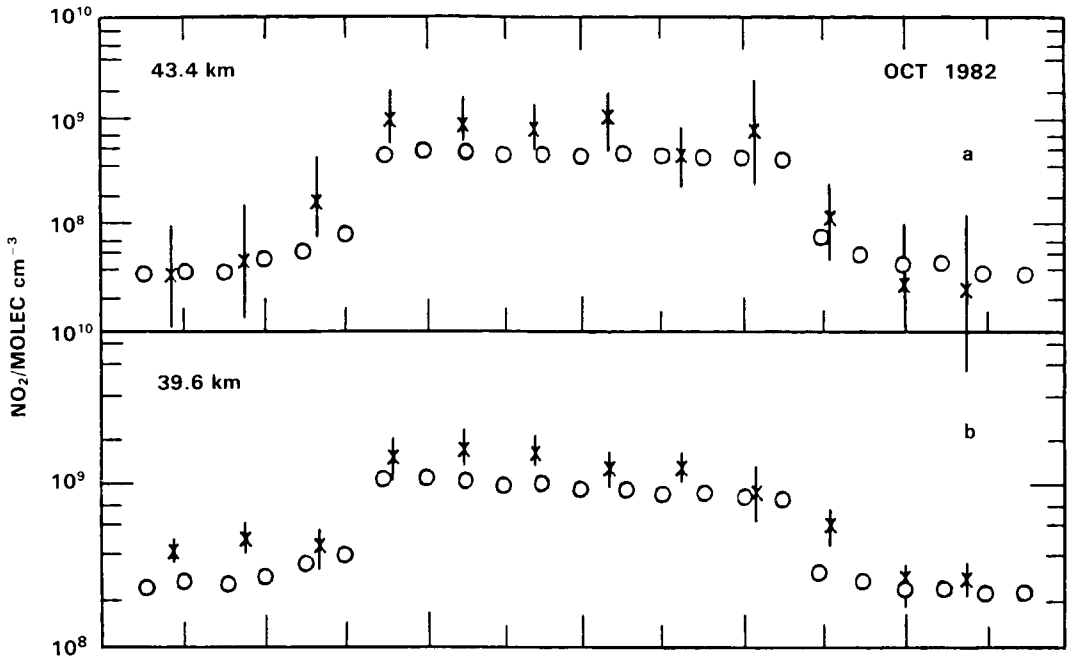

Figure 12-1. Diurnal variation of NO_2 concentration at 32°N, October at (a) ~43 Km and (b) ~40Km. *are observations by a pressure modulator radiometer; o represents model calculations. See Roscoe *et al.* (1985b).

A further category of model-data comparisons is provided by major natural perturbations to the stratosphere. These would include solar proton events, eclipses, sudden stratospheric warmings, injection of volcanic material, etc. As an example, Figure 12-4 shows the calculated decrease in ozone following the major solar proton event of August 1972. The expected decrease in ozone following the predicted increases in nitrogen oxides is modelled well.

The comparisons outlined above depend for their usefulness on the photochemical time scale being considerably less than the dynamical time scale. For many stratospheric species this is not the case and additional tests are required. To avoid the particular problems with these species and the dependence of their distributions on the synoptic situation (such that comparison of a single measured profile with a modelled profile is quite unsatisfactory) calls for more extensive data requirements. Two particular approaches can be identified. A trajectory approach can be followed in which the problem of dynamics is separated from the photochemistry by considering an isolated air parcel. Secondly, use can be made of large satellite data sets from which meaningful mean quantities can be extracted, thus avoiding the problem of day to day variability.

Austin *et al.* (1985b) have described trajectory analyses using LIMS and SAMS satellite data. Starting from a LIMS observation they calculate air parcel trajectories for periods of up to ten days (beyond which time the parcel can be expected to lose its integrity). A photochemical box model is initialised with LIMS and SAMS data and one-dimensional model results and then the photochemical calculation is carried out along the parcel trajectory, with appropriate temperatures and solar zenith angles. The parcel typically intersects one LIMS observation per day so that the model and data can be compared. Figure 12-5 shows the calculated O_3 and NO_2 at ~ 35 km compared with observations. It can be seen that the model reproduces the observed fluctuations quite well. Figure 12-6 shows scatter diagram for O_3, HNO_3 and NO_2 and the

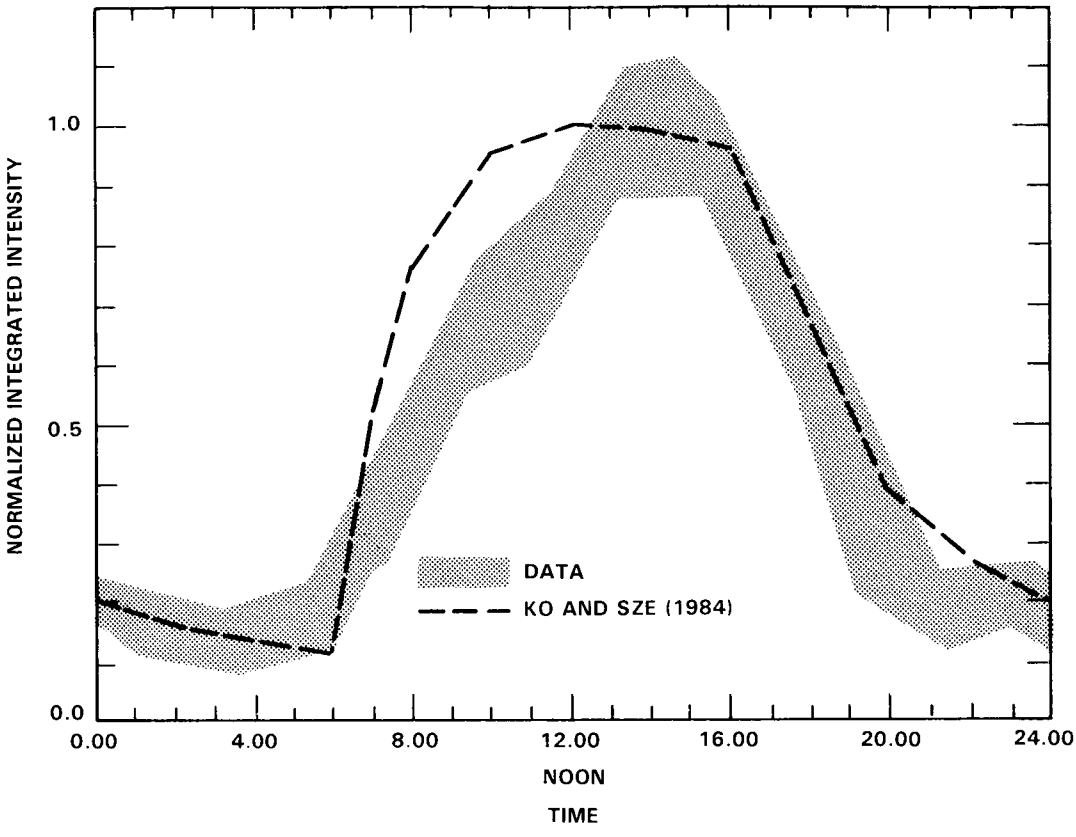

Figure 12-2. Comparison between the normalized observed integrated intensity of the ClO emission (Solomon *et al.*, 1984) and the synthetic intensity derived from calculated concentration of ClO by Ko and Sze (1984) for December, 19°N.

corresponding correlation coefficients. The good fits suggest an important future role for this kind of study, especially if more data to initialize the model becomes available. In this context, ATMOS and then the experiments on UARS provide excellent opportunities for further study.

The LIMS and SAMS experiments allow studies to be performed which rely on the extremely large amounts of data providing a good statistical base. Crutzen and Schmailzl (1983) have studied the O_x, NO_y and the HO_x budgets by using combinations of balloon and satellite data, while Jones *et al.* (1985) have investigated the role of CH_4 oxidation in the H_2O budget, using SAMS and LIMS (see Chapter 9).

Pyle and Zavody (1985a) and Jackman *et al.* (1985a) have tested some aspects of HO_x photochemistry by deriving OH fields using LIMS and SAMS data by two independent methods. One method assumes equilibrium between HNO_3 and NO_2 while the other calculates OH from its sources and sinks. The two methods agree within the errors expected of the derivations (see Chapters 9, 10.)

Finally, correlation studies using satellite data can also be used to study photochemistry. For example, the correlation between O_3 and temperature throws some light on the relative strength of the catalytic cycles affecting ozone (Barnett *et al.*, 1975a).

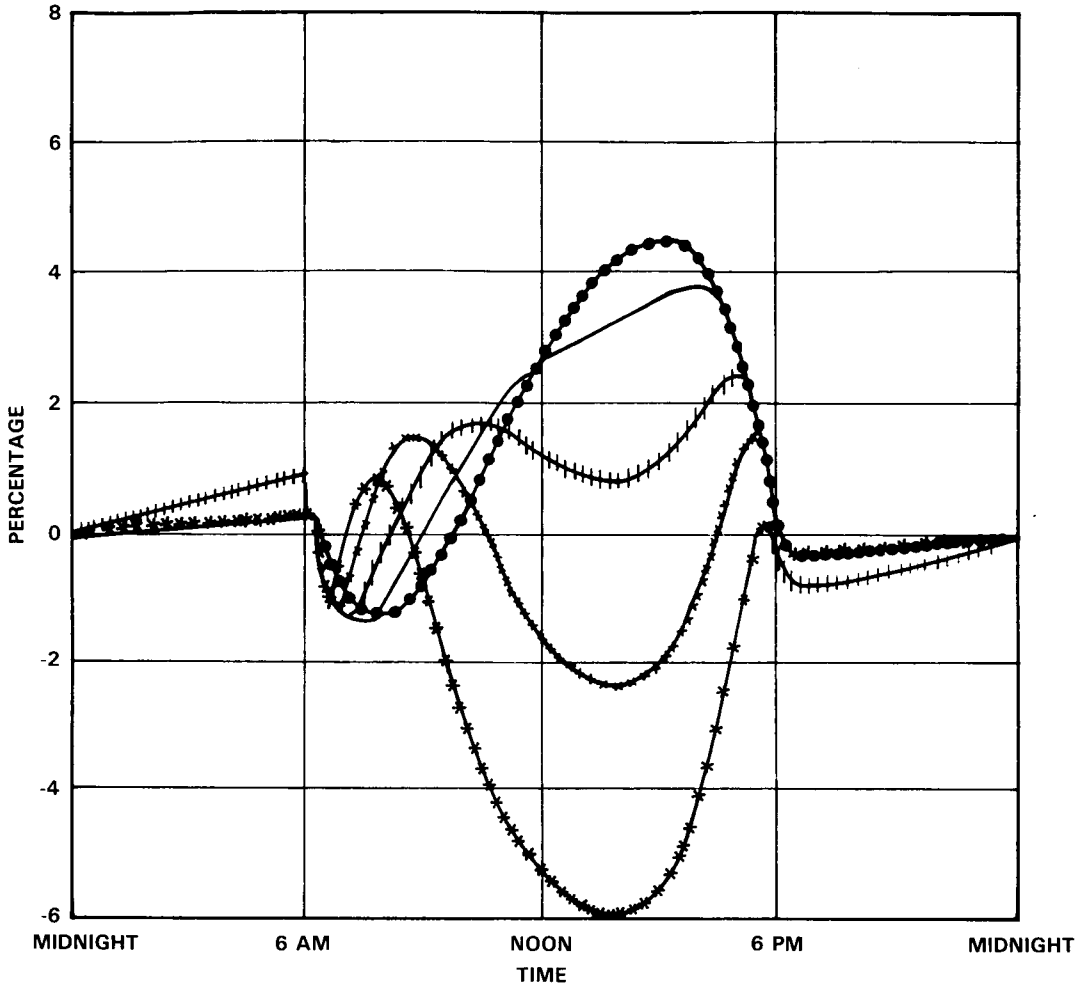

Figure 12-3. Percentage deviation from midnight values of ozone concentrations for a diurnal cycle. Key: ● ≡ 40 km; — ≡ 42 km; | ≡ 44 km; X ≡ 46 km; × ≡ 48 km. From Pallister and Tuck (1983).

In conclusion, fast photochemistry can in principle be tested using good measurements at a fixed pressure. The photochemical model then reduces to a box model and a treatment of dynamics is unnecessary. Two types of measurements appear particularly useful: measurements to test both photochemical ratios and correlations, and diurnal measurements. The former may place severe requirements on measurement accuracy while the latter requires measurements with high precision but not necessarily high absolute accuracy.

The testing of model behaviour for longer lived species is most difficult. Various methods are available. The approach needs to allow for transport so that multi-dimensional models have a particular role to play. Combinations of models and large satellite data sets are particularly useful. Trajectory analyses in which the problems of dynamics can be separated from photochemistry should be especially useful when large data sets become available.

Whichever method is used to compare model and measurements, there is a need for a careful estimate of errors in both the models and data, as pointed out by Harries (1982). While a detailed model error

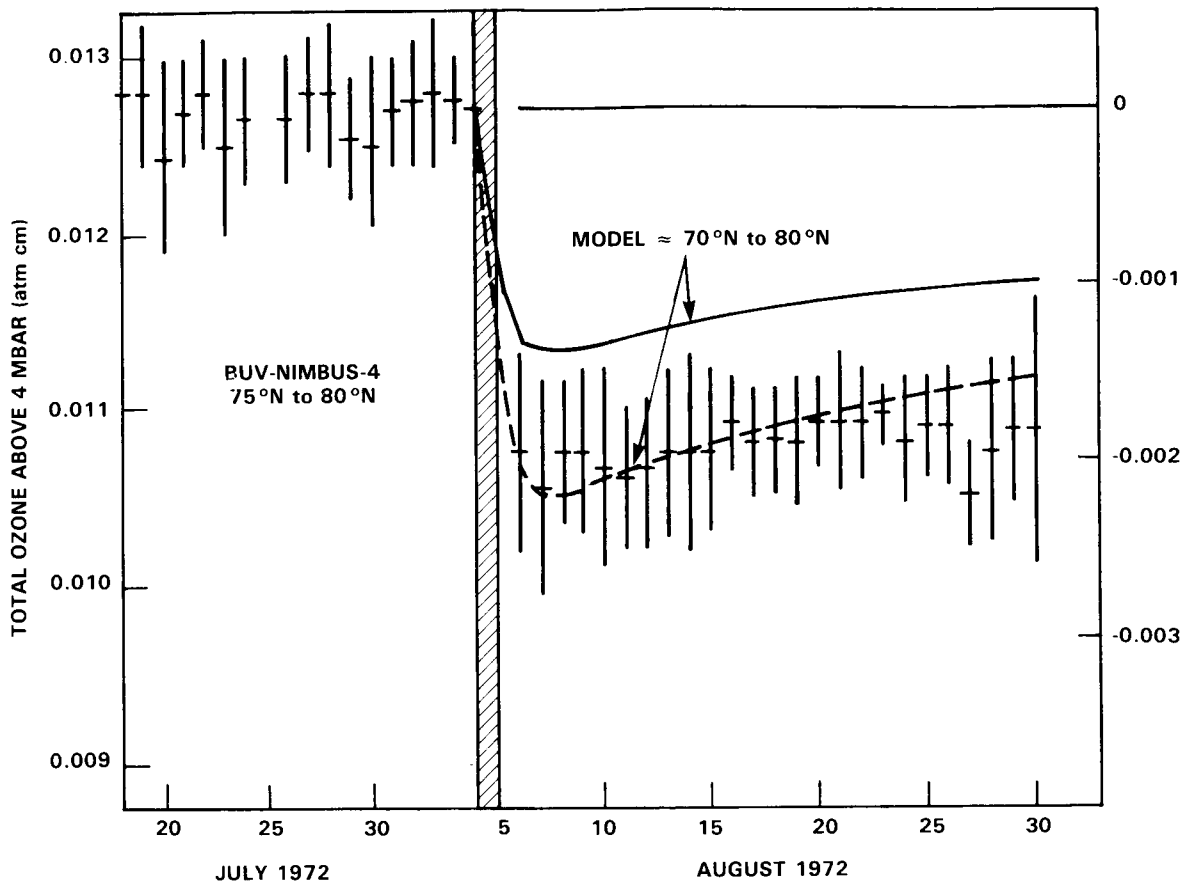

Figure 12-4. Comparison of BUV-NIMBUS-4 ozone data with model prediction for high latitudes. The model results are plotted as relative depletions with respect to the 'undisturbed' level on 4 August, before a major SPE occurred. The solid line and dashed line represent different assumed NO production rates. See Fabian *et al.* (1979).

analysis is difficult and can be an unwieldy problem, by isolating specific aspects of the model (e.g., the ratio of HNO_3 to NO_2) the comparison does become amenable to a critical examination of errors. Modellers should be encouraged to carry out such studies.

The limitations which are apparent in the present testing of models must be borne in mind when considering the discussion of the detailed comparison of models and data (Chapters 8 to 11) and, of course, in considering the assessment studies.

12.2 1-D MODELS: FORMULATION AND INTERPRETATION – RECENT DEVELOPMENTS

One-dimensional coupled transport and chemical kinetics models have been one of the basic research tools in theoretical studies of the stratosphere. In fact, much of the current theoretical understanding of the chemical structure of the stratosphere and the photochemical processes governing it has been derived with the help of one-dimensional models. Most past analyses of man's potential influence on stratospheric ozone have been done with the aid of one-dimensional models. Despite the detailed representations of

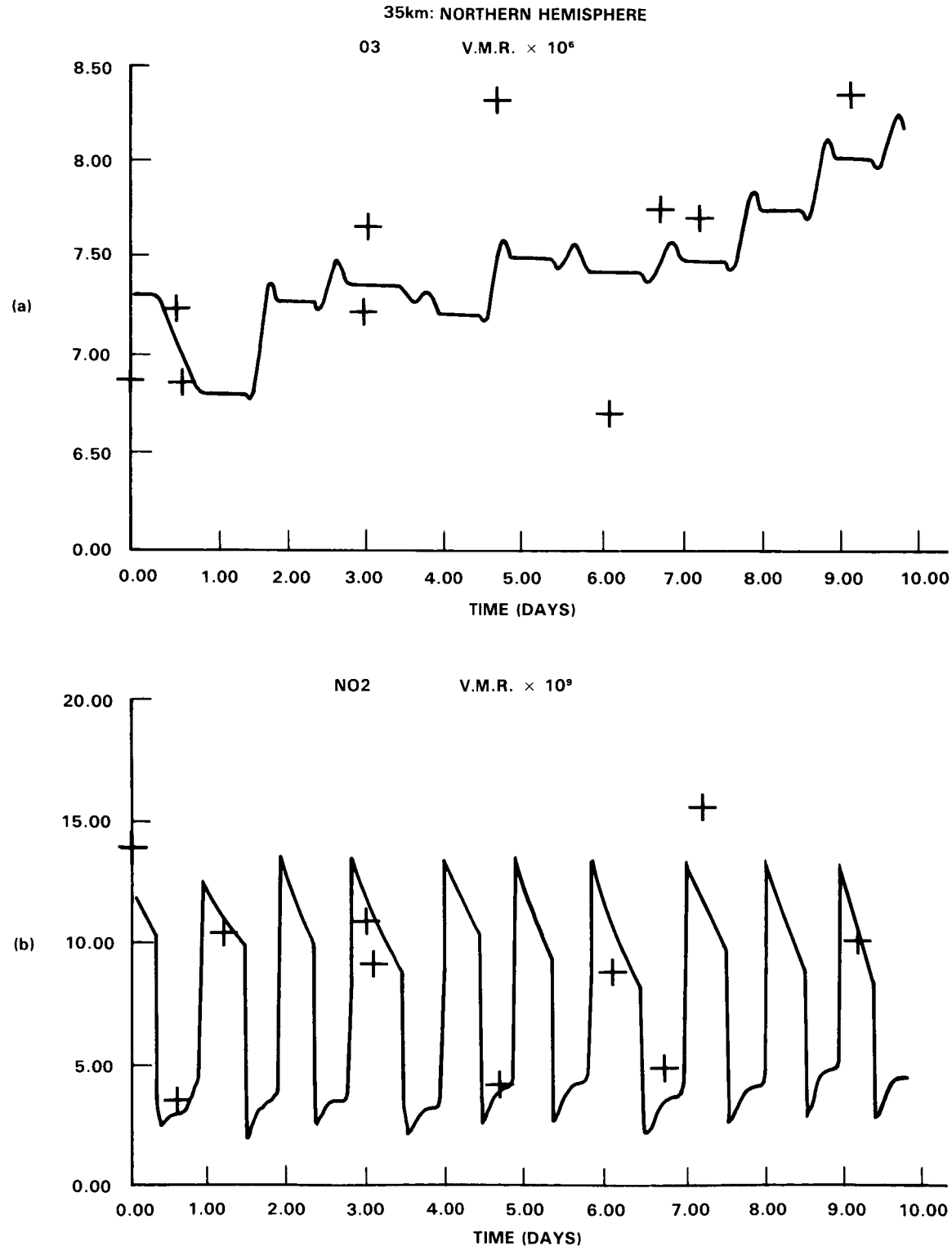

Figure 12-5. Ten-day time histories of species observed by LIMS along a trajectory at ~35 km (θ = 1100K) during February 1979. Curve is model calculation, crosses are LIMS observations within the coincidence criterion of 5 great circle degrees radius (a) O_3 (b) NO_2. After Austin *et al.* (1985b).

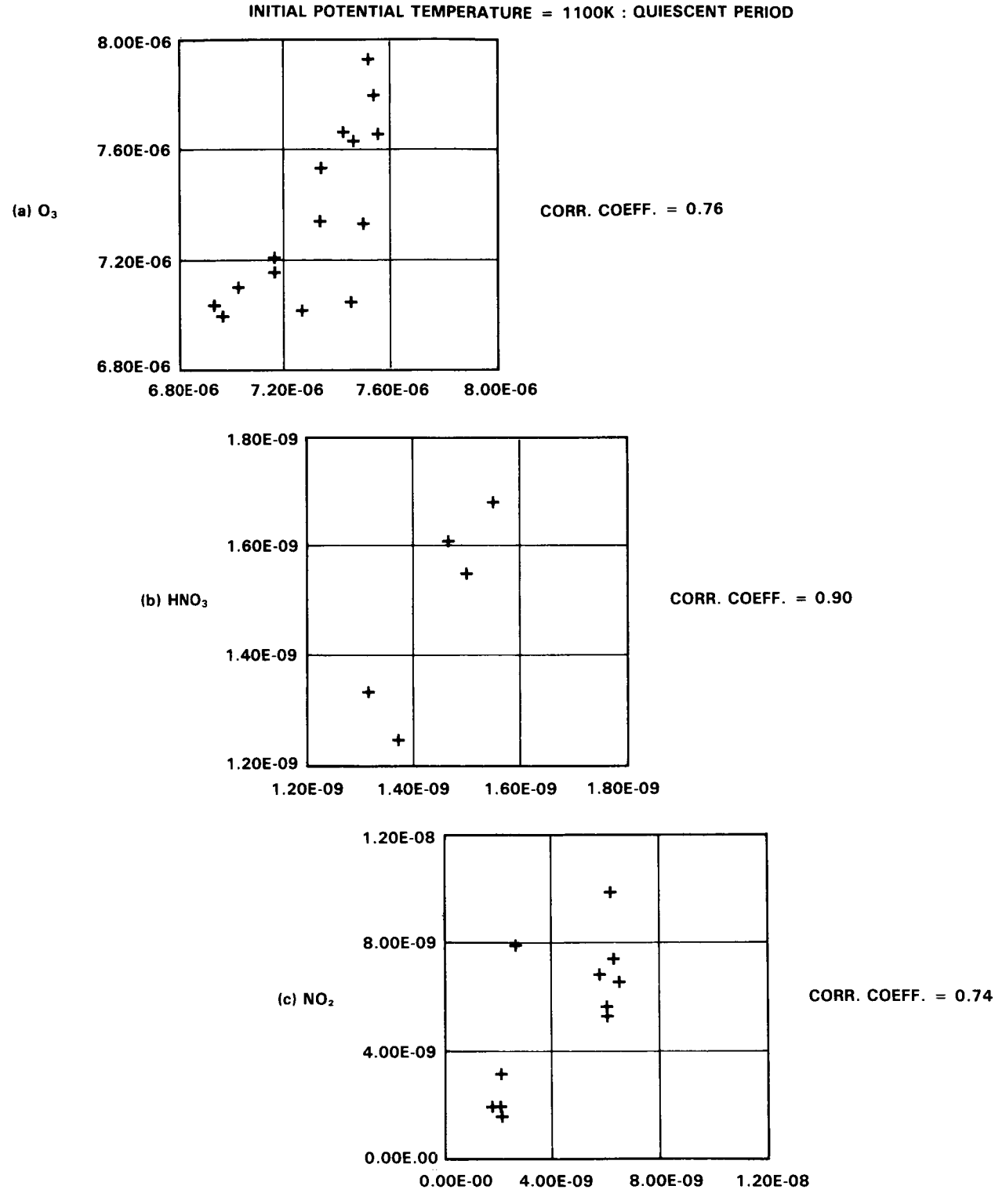

Figure 12-6. Scattergram of calculated volume mixing ratios and coincident LIMS observations. (a) O_3, (b) HNO_3, (c) NO_2. The correlation coefficient is given on each plot. ~35 km trajectory, March, from Austin *et al.* (1985b).

atmospheric chemical and radiative processes in these models, there remain recognized limitations in their formulation and interpretation.

In the 1-D model, the chemical and physical processes determining the temporal variation in the concentration of the atmospheric constituent, c, can be represented in mathematical form by the continuity equation,

$$\frac{\partial c}{\partial t} = \frac{\partial}{\partial z}\left\{K_z \varrho \frac{\partial}{\partial z}(c/\varrho)\right\} + P - Lc + S$$

where t is time, z is altitude, K_z is the one-dimensional vertical diffusion coefficient, ϱ is air density, P and Lc are, respectively, the photochemical production and loss rates, and S represents any other possible sources and sinks for c. In deriving this equation, a longitudinal and latitudinal global average of the transport flux is taken, and it is assumed that the resulting net vertical transport flux can be represented as a diffusive process.

The diffusive treatment of transport in the 1-D model is a purely empirical representation. It does not utilize observed atmospheric motions directly but rather is based on the observations of the temporal and spatial distributions of selected tracers. The K_z profiles used in different models have typically been based on chemical tracers such as CH_4 and N_2O and radionucleides from past nuclear tests. For such tracers, it is assumed that the value of K_z determined is a function of only the transporting motions, and within the scope of 1-D models is independent of both the details of the tracer field and the specific structure of the tracer source and sink distributions. While adopted profiles differ by as much as an order of magnitude at some altitudes, these K_z profiles tend to have similar characteristics: large values in the troposphere, much reduced values in the region near the tropopause, increasing with altitude in the stratosphere (see WMO 1981).

Generally, a single K_z profile is chosen to represent the transport of all species in the atmosphere. In practice, the representation of transport in the 1-D model has been limited by the lack of well-determined globally averaged data for the tracers and by uncertainties in understanding of the balances among sources, sinks and transport processes affecting the trace species distributions. Recent analyses suggest that it may not be possible to find a K_z at least with current chemistry that adequately fits atmospheric data for all long-lived tracers, such as N_2O and CH_4, at the same time (e.g. Wuebbles 1983b). Using a separate K_z for each species would provide additional variables in the model that would enable any observational data to be fit, but without necessarily representing any physical aspect of the atmosphere. Unless there is established a physically well-defined basis for each species to have its own K_z it would not be reasonable to consider this.

Dynamically based transport parameterizations have been proposed in which K_z depends on species and chemical gradients (Holton 1985, Mahlman *et al.*, 1985). Although not fully developed and exploited, these techniques may provide a better physical basis for representation of globally averaged transport in 1-D models.

A further limitation of 1-D models is that it is difficult to average accurately the global rates for photochemical production and loss. Only local variables, such as solar flux intensity, ozone concentrations, and temperature, can be used. This complicates interpretation of 1-D results, and has led to much discussion on the meaning of calculated distributions of various species. Despite these difficulties, the

1-D model has nonetheless been found to capture many of the important features of trace gas behaviour in the stratosphere, and remains a useful theoretical tool.

For multi-year time-dependent calculations, such as those for assessment analyses, it is extremely expensive to calculate the full diurnal variations throughout the calculation. To get around this, several different techniques for simplified diurnal treatments or diurnal averaging have been developed. Some models treat diurnal averaging by occasionally updating multiplicative factors on each photodissociation rate and chemical rate constant based on detailed diurnal models. Others simplify this approach in various ways. Still others simplify diurnal changes by calculating day-time and night-time averages separately throughout their calculations. For those models that do not continually update the effects of diurnal variations, several studies (e.g. Herman and McQuillan 1985; Wuebbles and Connell 1985) indicate that the influence of diurnal averaging must be carefully considered for the perturbed atmosphere. Herman (1985) indicates that significant errors in the calculated ozone change can result unless diurnal averaging factors calculated for the ambient atmosphere are updated for the perturbed atmosphere. Wuebbles and Connell (1985) show that much of this error appears to result from "false" increases in NO_3 and N_2O_5, that can be corrected for simply by recognizing that almost all NO_3 produced during the day would be photolyzed. The remaining error appears to be related to significant difference in NO_2/NO, HO_2/OH and ClO/Cl ratios between the current atmosphere and a highly perturbed atmosphere.

12.3 1-D MODELS: INTERCOMPARISON OF NO_y DIFFERENCES

The current interest in assessment studies, particularly cases with very high chlorine amounts, has lead to a recent intercomparison of 1-D models. The initial intercomparison revealed major differences in the calculated stratospheric total odd nitrogen. Possible reasons for these differences, which have an important impact on the calculated ozone perturbation, are discussed in this section.

Organizations participating in the initial stages of the 1-D model intercomparison are shown in Table 12-1. For the present atmosphere, each using the "best case" versions of the models, with 1985 NASA recommended chemical rate constants, as given in Appendix A, resulted in maximum total odd-nitrogen in the upper stratosphere ranging from 13 ppbv (in the Harvard model) to 23 ppbv (in the NASA GSFC model of Stolarski).

A special series of calculations was done with each model to analyze the causes of the large differences in calculated NO_y. In these calculations, along with using the same chemical rate constants, each

Table 12-1. Initial participants in 1-D model intercomparison. Numbers are used to identify models corresponding to plotted results in Figures 12-7—12-11.

Model	Organization
1	Du Pont (A Owens)
2	NASA GSFC (J Herman)
3	AER, Inc. (N D Sze)
4	Harvard Univ. (M Prather)
5	NASA GSFC (R Stolarski)
6	NASA Langley (L Callis)
7	LLNL (D Wuebbles)

model assumed the same K_z profile (based on the DuPont model), the same atmosphere (U.S. Standard Atmosphere, 1976), the same boundary conditions, the same tropospheric water vapor, same albedo (25%), and generally the same solar zenith angle (30° equinox). For these calculations, model calculated NO_y ranged from 12 to 22 ppbv. A detailed comparison of results indicated strong differences between models in the photodissociation rates of O_2, N_2O, and NO. Since photolysis is the major sink for N_2O, the production of odd-nitrogen, through $O(^1D)+N_2O \rightarrow 2NO$, is dependent on differences in calculated N_2O amounts and, therefore, in photolysis rates of N_2O in the upper stratosphere. In turn, N_2O photolysis is dependent on O_2 absorption in the Schumann-Runge bands. Likewise, the major sink for odd-nitrogen in the upper stratosphere is through the reaction $N+NO \rightarrow N_2+O$, where the atomic nitrogen, N, is produced through the photolysis of NO.

In order to narrow further the differences between models, another special calculation was suggested (the NASA test case shown in Figures 12-7–12-11) in which the prior conditions were combined with a fixed ozone distribution based on the U.S. Standard Atmosphere (1976). The results to be discussed include an updated photodissociation treatment of O_2 in model 5 (a change from the approach of Hudson and Mahle (1972) to Frederick and Hudson (1979a)), and changes in the treatment of both O_2 and NO photolysis for model 4 (for O_2, Logan *et al.* (1978) with reduced continuum is used and, for NO, 67% predissociation with N_2 quenching as in Nicolet and Cieslik (1980) is employed). The results for this test case gave a range in NO_y, shown in Figure 12-7, of 13 to 19 ppbv, with most of the decrease in the spread of NO_y coming primarily from the changes in photodissociation treatments described above.

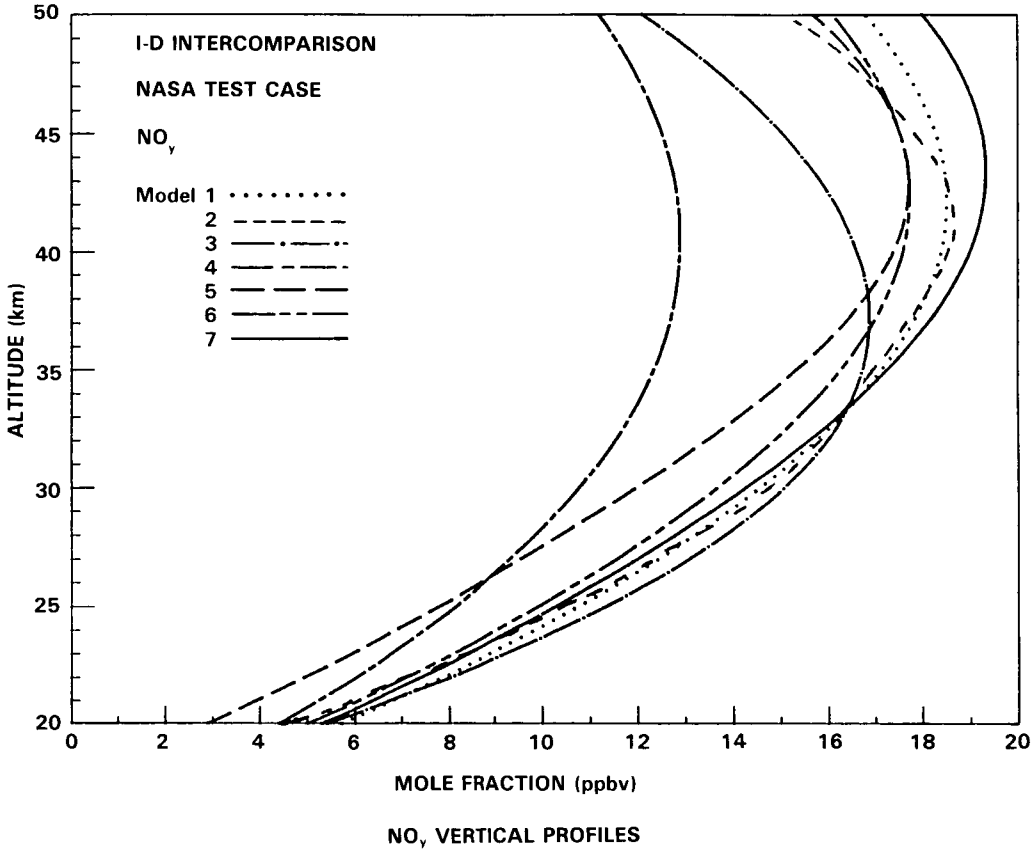

Figure 12-7. NO_y as calculated by the 1-D models of Table 12-1.

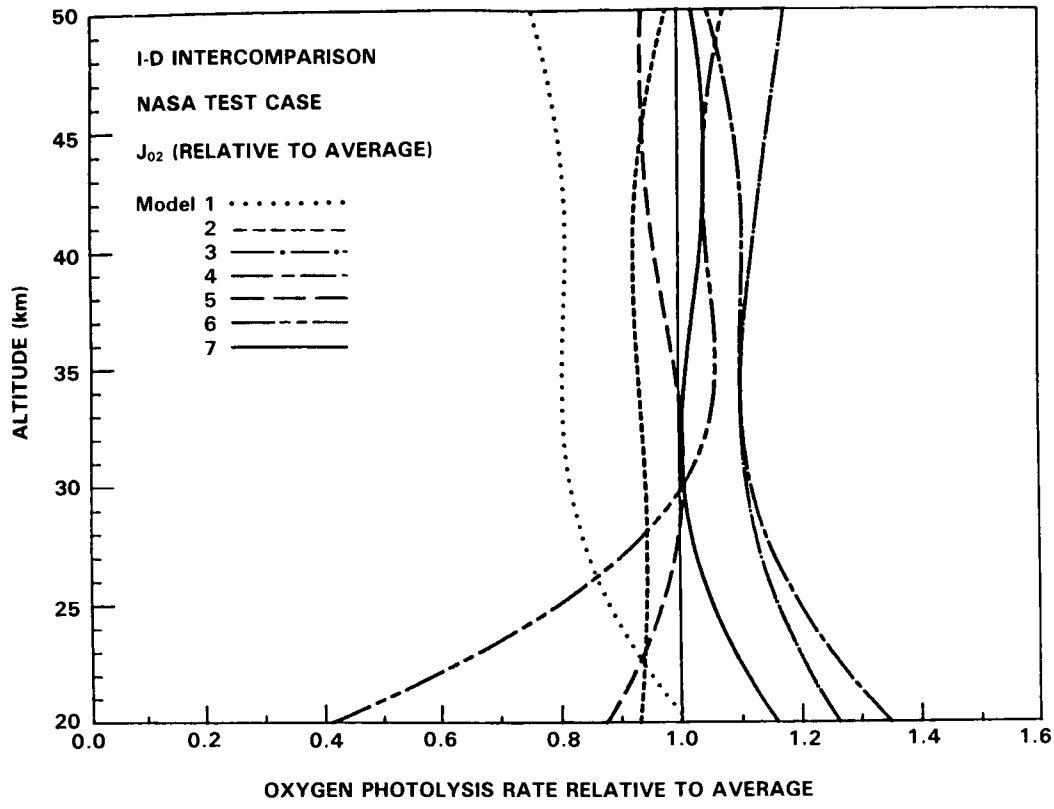

Figure 12-8. JO_2 for the 1-D models of Table 12-1 relative to the average of all model results.

Calculated photodissociation rates for O_2, N_2O, NO and O_3 are shown in Figure 12-8 through 12-11 respectively, relative to the average of all model results. Note that the relative scale for each figure is different. The photodissociation rate of O_2 differs by about twenty percent in the upper stratosphere, if the DuPont results are not included (the DuPont model calculates photodissociation rates based on a global integration of zenith angle rather than the 30° equinox used in all other models for the NASA test case). The much larger apparent differences in the photodissociation rates for N_2O, shown in Figure 12-9, suggest that discrepancies in O_2 Schumann-Runge band absorption is primarily responsible for the model differences. The calculated photodissociation rates for N_2O differ by about 20% in the upper stratosphere increasing with decreasing altitude to 60% by 30 km. As shown in Figure 12-10, much larger differences are found for nitric oxide photodissociation rates, with a factor of about 2 difference at 50 km, increasing to almost a factor of 3 at 40 km. Much smaller differences of approximately 10-15% were found in the photodissociation rates for ozone in Figure 12-11.

The underlying causes of the variations in the NO_y are possibly indicated by examining the differences in photodissociation rates. For example, the low NO_y levels calculated in the Harvard model correspond to larger N_2O and NO photodissociation rates in the upper stratosphere than found in other models, and therefore less production and more destruction of total odd-nitrogen than calculated in other models.

The results described above suggest that the major differences between models for calculated NO_y are possibly related to the formulations used for the Schumann-Runge bands. All models basically use the formulation recommended in chapter 7, with the exception of the Harvard model, which employs opacity

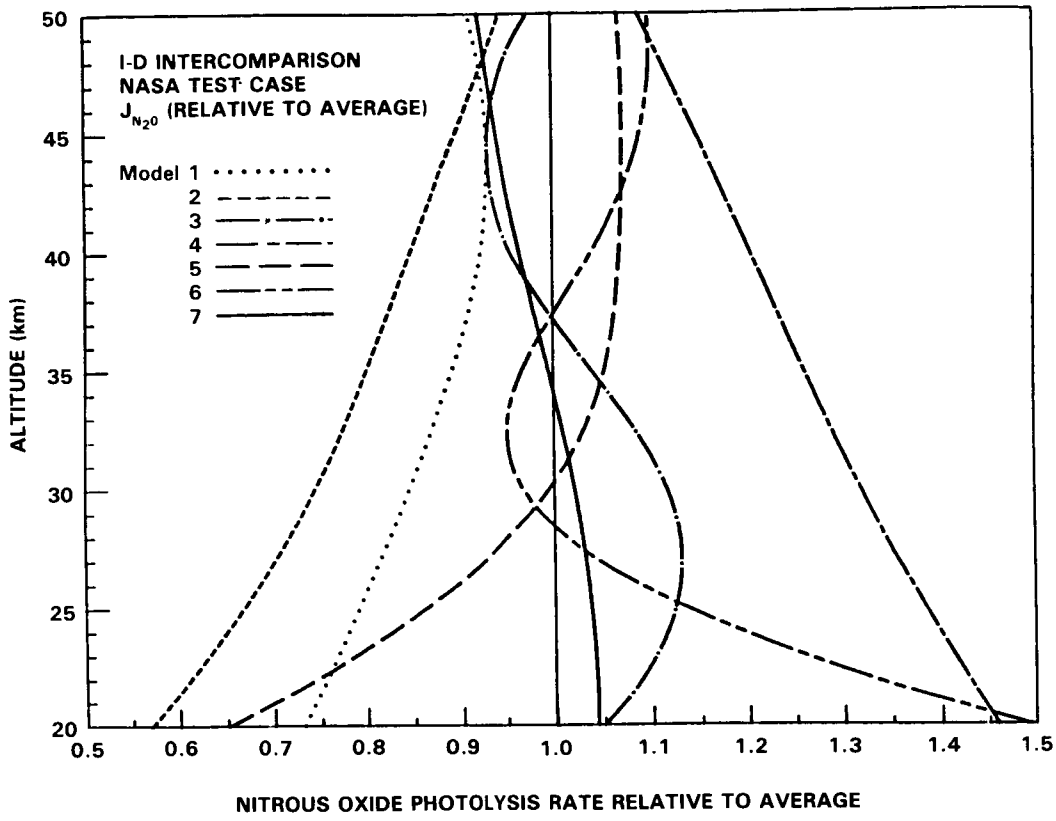

Figure 12-9. As Figure 12-8 for JN_2O.

distributions as described in Logan *et al.* (1978), and the DuPont model, which used the formulation of Nicolet and Peetermans (1980).

Production of stratospheric ozone is dominated by photolysis of O_2 in the Herzberg continuum (205-240nm). All models used similar cross-sections for the Herzberg continuum, resulting in similar photolysis rates for O_2 in the stratosphere. Penetration of sunlight in the region of the S-R bands (180-205nm) is responsible for the primary losses of N_2O and NO. The N_2O cross-section increases more than a factor of 10 from 205nm to 185nm, emphasizing differences in the treatment of radiative transfer for S-R bands (1,0) through (10,0). Similarly, photolysis of NO occurs in the δ(0,0) and δ(1,0) bands which overly the S-R(5,0) and (10,0) bands of O_2, respectively. Stratospheric photolysis is dominated by the δ(0,0) band, which when excited may either predissociate, radiate or be kinetically quenched (see Nicolet and Cieslik 1980). The Harvard formulation (Logan *et al.*, 1978, updated with new continuum values from 192nm to 240nm from Cheung *et al.*, 1984b) allows for deeper penetration of ultraviolet in the S-R bands than that of Frederick *et al.* (1981).

These results point to two fundamental uncertainties in the treatment of ultraviolet radiation in stratospheric models. First, there is considerable diversity in calculated photolysis rates even among models which are purportedly using the same treatment of radiative transfer. Second, there are different formulations currently in the literature for ultraviolet transmission in the Schumann-Runge bands. Both of these differences have significant effects on model calculations for odd-nitrogen. The first discrepancy may be resolved simply by comparing results for a few restricted cases with more accurate solutions of radiative

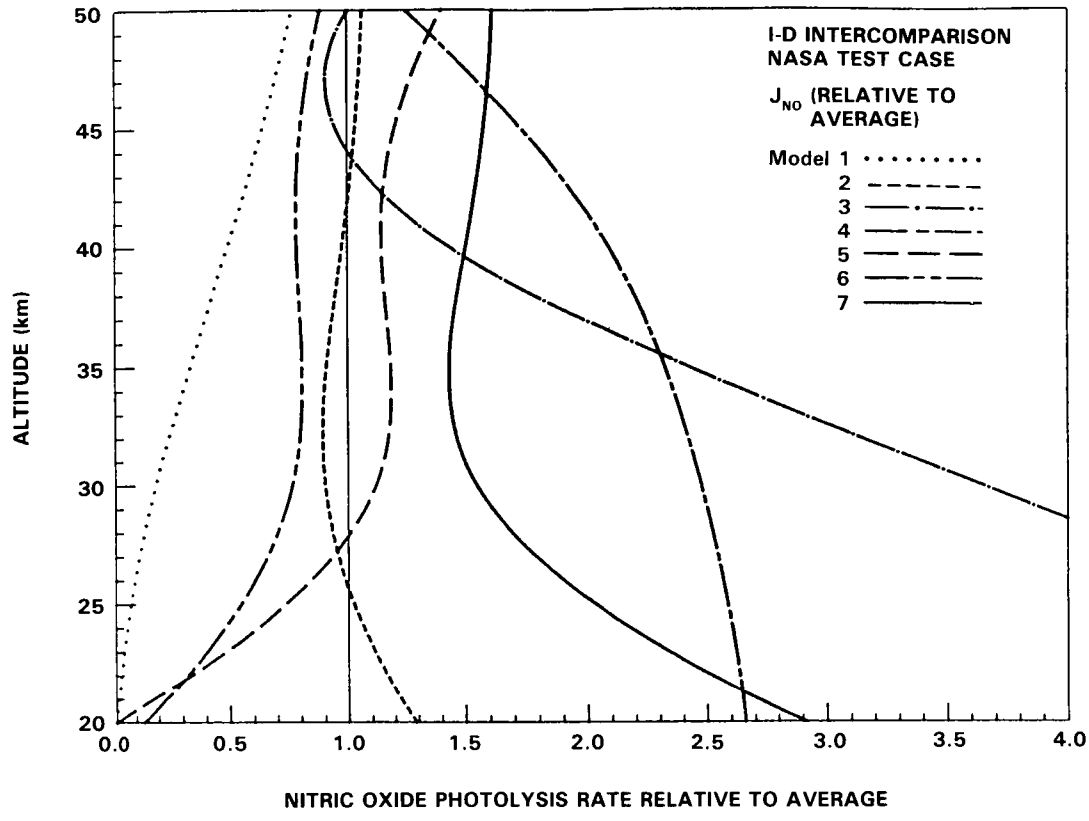

Figure 12-10. As Figure 12-8 for JNO.

transfer. The second problem requires validation of the S-R band models with both laboratory (Yoshino *et al.* 1983) and *in situ* stratospheric data (Herman and Mentall, 1982a, Frederick and Mentall, 1982, Anderson and Hall 1983). Improved models will need both further laboratory data for O_2 at lower temperatures and observations of stratospheric transmission of sunlight with a resolution of approximately 0.1nm in the S-R bands.

Assessing perturbations to the stratosphere requires an ability to simulate the response of ozone to changes in odd-nitrogen or nitrous oxide. Discrepancies among theoretical treatments of the Schumann-Runge bands of O_2 have lead to differing amounts of NO_y and thence to varying changes in total ozone for a given increase in chlorine. Validation of radiative schemes - in the ultraviolet where the greatest differences occur - is essential for both 1-D and 2-D photochemical models.

12.4 TWO-DIMENSIONAL MODELS — SOME THEORETICAL IDEAS

While 1-D models have been the principal tool for assessment studies of the effects of stratospheric pollutants, in recent years a number of two-dimensional models with detailed descriptions of radiation, dynamics and photochemistry has been developed. Some of these models have been used for assessment purposes (e.g. Vupputuri 1978/79; Pyle 1980; Haigh and Pyle 1982; Steed *et al.*, 1982, Brasseur and Bertin 1978/79) and they are expected to play an increasingly important role in the next few years.

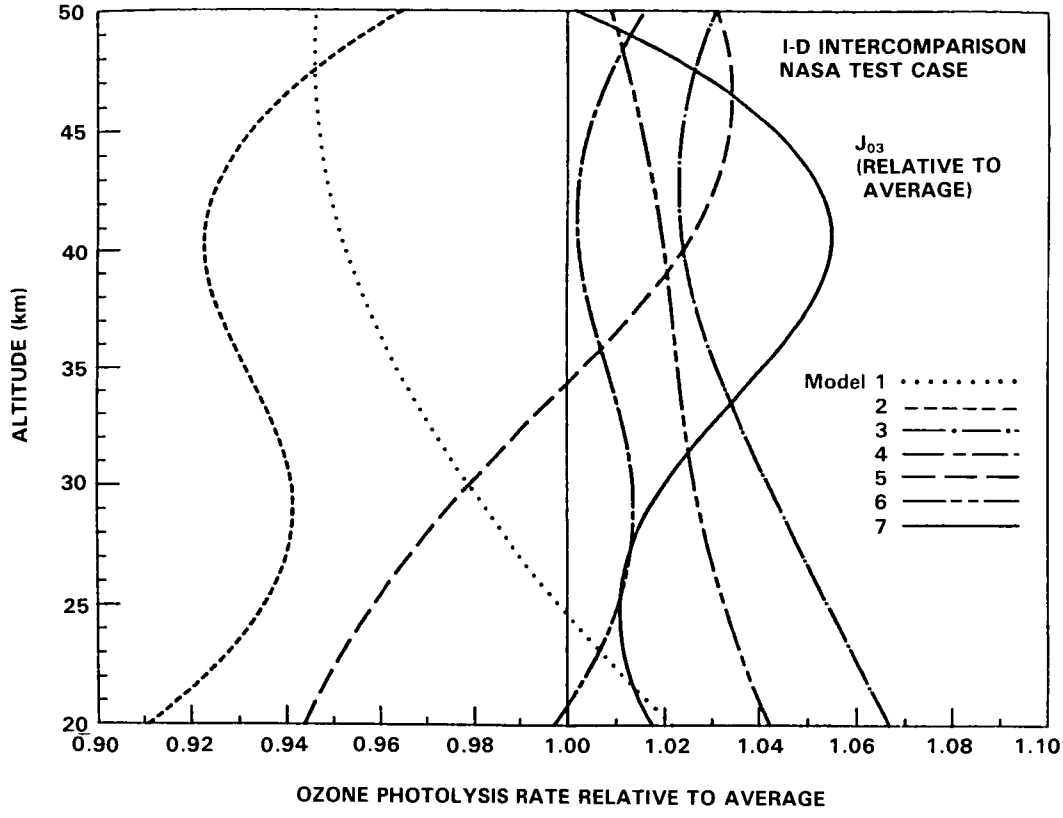

Figure 12-11. As Figure 12-8. for JO_3.

The two-dimensional approach has a number of advantages compared with that using one-dimensional models. The total ozone record is a convincing demonstration of the vital role of meridional motions in the stratosphere. Two-dimensional models can include this transport; one-dimensional models cannot. Recent developments using satellites, balloons, aircraft and ground based measurements have significantly increased the geographical coverage of data; a two-dimensional approach (at least) is an advantage in interpreting this data. Two-dimensional models also have the considerable benefit for assessment purposes that they can include a number of the important feedbacks between dynamics, radiation and photochemistry.

While the advantages of the two-dimensional approach are clear, how best to construct a two-dimensional model of the three dimensional atmosphere has been a vexed question for some time. Taking y and z as meridional and vertical coordinates, the zonal mean continuity equation for tracer of mixing ratio χ can be written

$$\frac{\partial}{\partial t}\,\overline{\chi} + \overline{v}\,\frac{\partial}{\partial y}\,\overline{\chi} + \overline{w}\,\frac{\partial}{\partial z}\,\overline{\chi} = -\frac{1}{\cos\phi}\,\frac{\partial}{\partial y}\,\overline{(v'\chi'\cos\phi)} - \frac{1}{\varrho}\,\frac{\partial}{\partial z}\,(\varrho\,\overline{w'\chi'}) + \overline{S} \qquad (12.1)$$

where v, w are meridional and vertical velocity components, $\partial y = a\partial\phi$, a is the Earth's radius, ϕ is latitude, ϱ is density and S is the net source of χ.$\overline{(\ )}$ represents a zonal average, $\overline{(\ )} = 1/2\pi \int_0^{2\pi} (\ )d\lambda$, and $(\ )'$ a departure therefrom, $(\ ) = \overline{(\ )} + (\ )'$. The transport terms on the left hand side of 12.1 represent advection by a zonal mean circulation. The transport terms on the right hand side contain departures from

the zonal mean (eddies) for which in a two-dimensional framework there is no *a priori* description. A central problem in two-dimensional modelling is the treatment and the proper interpretation of the eddy terms.

Much debate has centred on the relative roles of mean meridional motions and eddy motions in transporting heat, momentum and tracer mixing ratios. In his classic paper, Brewer (1949) explained the dryness of the stratosphere in terms of a mean meridional circulation with rising motion at the equator, poleward flow in the stratosphere with sinking motion at higher latitudes. As discussed by Dobson (1956), such a circulation, hereafter referred to as the Brewer-Dobson circulation, also appeared to be required to explain the observations of ozone.

Murgatroyd and Singleton (1961) calculated the meridional circulation of the middle atmosphere driven by radiative sources and sinks. The circulation is similar to the Brewer-Dobson circulation in the lower stratosphere and has a single cell from summer pole to winter pole in the upper stratosphere and mesosphere. Murgatroyd and Singleton concluded that their circulation was supported by the observed zonal mean tracer distributions, although they stressed the limitations of their calculations which followed the neglect of eddy processes. Thus these authors concluded that tracer transport is controlled mainly by a mean meridional circulation.

The alternative view was taken by Godson (1960). He studied the distribution of ozone in polar latitudes, noting that ozone is carried polewards in episodes which he associated with baroclinic eddies. Newell (1963a) also argued that eddy motions produced dominant transport in the lower stratosphere. Similarly, the observations of the spread of Tungsten-185 from nuclear bomb tests could best be explained in terms of diffusive mixing rather than a mean meridional transport (Feely and Spar 1960).

Subsequent theoretical studies, both analytical and modelling, have shown that the debate about the principal transport process, whether it be a mean circulation or the eddies, was based on false premises. In the conventional Eulerian formalism, the mean meridional circulation and eddy transports are not in fact independent but are intimately related to one another. For example, the close cancellation of mean and eddy transport has been demonstrated in many three-dimensional modelling studies (see e.g. Hunt and Manabe 1968). Theoretically, this result is expected and is summarized in various "non-acceleration" or "non-transport" theorems (see e.g. Andrews and McIntyre 1976) which state that in the absence of transience or damping of a small amplitude wave, the wave exerts no effects on the zonal mean state. A circulation is driven by the wave which exactly cancels the effect of the wave on the zonal mean.

There have been a number of excellent reviews of these ideas (see e.g. Murgatroyd 1982, Mahlman *et al.*, 1984) which it is not necessary to repeat. Instead, we will sketch here the impact of theoretical and observational studies on attempts to build two-dimensional tracer transport models, starting with the early work of Prabhakara (1963) and tracing developments to the present day. It is clear from Equation (12.1) that the definition of advective and eddy transport is not unique. Given the same three-dimensional circulations, different sets of mean circulation and eddy fluxes can be obtained depending on the averaging processes and coordinates adopted. It will be seen that different approaches to describing both the mean motions and the eddies are possible and that the state of the art is dynamic and not static. The different approaches currently in use will be discussed in Section 12.6. No one approach will be pronounced correct (indeed the diversity of approaches is important). Some approaches have particular advantages and these will be stressed. The chosen approach needs a firm physical base and analysis of model results must be carried out with due consideration of the limitations of the model.

The first two-dimensional numerical model for tracer transport was developed by Prabhakara (1963), who attempted to combine mean meridional motions with the diffusion model suggested by the observa-

tions of radioactive fallout (Feely and Spar 1960). Prabhakara used the Murgatroyd and Singleton mean circulation, which was scaled to be only 20 per cent of the original value in a pragmatic attempt to model the ozone distribution. Eddy transport was modelled by Fickian diffusion with the zonal mean horizontal and vertical fluxes of the mixing ratio of χ given by

$$\overline{v'\chi'} = -K_y \frac{\partial \bar{\chi}}{\partial y} \quad ; \quad \overline{w'\chi'} = -K_z \frac{\partial \bar{\chi}}{\partial z} \tag{12.2}$$

where K_y, K_z are horizontal and vertical diffusion coefficients. With some adjustments to the estimated K_y and K_z (the estimates based on the distribution of radioactive tracers) Prabhakara was able to obtain realistic latitudinal and temporal variations in total ozone. As will become evident, Prabhakara's work is of particular interest in view of the recent developments in two-dimensional modelling.

Subsequent work lead to criticism of Prabhakara's model on two counts. Firstly, the circulation obtained by Murgatroyd and Singleton did not correspond to the circulation deduced from Eulerian eddy statistics, particularly in the winter lower stratosphere where such statistics imply an indirect cell with rising motion at the pole and sinking in middle latitudes (see, e.g. Vincent 1968). Of course, as we see below, there is no *a priori* reason to expect the transport circulation to be identical to the mean meridional circulation in pressure coordinates. Secondly, observed horizontal eddy fluxes in the lower stratosphere were found to be counter-gradient (Newell 1964). Simple Fickian diffusion will only model downgradient fluxes.

The next advance was a treatment of eddy transport by Reed and German (1965) in which countergradient fluxes were permitted. They described the fluxes of a quasi-conservation tracer χ using a tensor of diffusion coefficients such that

$$\begin{pmatrix} \overline{v'\chi'} \\ \overline{w'\chi'} \end{pmatrix} = - \begin{pmatrix} Kyy & Kyz \\ Kzy & Kzz \end{pmatrix} \begin{pmatrix} \frac{d\bar{\chi}}{dy} \\ \frac{d\bar{\chi}}{dz} \end{pmatrix} \tag{12.3}$$

Expressions for the Ks were based on a mixing length hypothesis, with parcel trajectories assumed to be straight lines at some known angle to the mean isentropes. These assumptions lead to the result Kyz = Kzy, which produces a symmetric tensor and a diffusive flux. If the slope of the mixing surface (the parcel trajectory) is greater than the slope of the isentropes (and Kyz, Kzy depend on these mean quantities) then the horizontal component of the flux calculated from Equation 12.3 will be countergradient.

Reed and German's work paved the way for a number of numerical models which included both the mean circulation and eddy transports (Rao 1973, Harwood and Pyle 1975). The mean circulation can be calculated using the momentum and thermodynamic equations:

$$\frac{\partial \bar{u}}{\partial t} + \bar{v}\frac{\partial \bar{u}}{\partial y} + \bar{w}\frac{\partial \bar{u}}{\partial z} - f\bar{v} = -\frac{1}{\cos^2\phi}\frac{\partial}{\partial y}(\overline{u'v'}\cos^2\phi) - \frac{1}{\varrho}\frac{\partial}{\partial z}(\varrho\overline{u'w'}) \tag{12.4}$$

$$\frac{\partial \bar{\theta}}{\partial t} + \bar{v}\frac{\partial \bar{\theta}}{\partial y} + \bar{w}\frac{\partial \bar{\theta}}{\partial z} = -\frac{1}{\cos\phi}\frac{\partial}{\partial y}(\overline{v'\theta'}\cos\phi) - \frac{1}{\varrho}\frac{\partial}{\partial z}(\varrho\overline{w'\theta'}) + \bar{Q} \tag{12.5}$$

where $\bar{u}$ is the mean zonal wind, $\bar{\theta}$ is potential temperature, f is the Coriolis parameter, and $\overline{Q}$ is the net diabatic heating rate.

Both equations contain eddy flux terms. The eddy heat fluxes can be written in terms of the K-tensor. If the eddy momentum flux is known, then solution for the mean circulation is straightforward. However, angular momentum is not a rationally conserved quantity and Reed and German's approach cannot be used. Rao (1973) described the momentum fluxes in terms of the vertical wind shear. Harwood and Pyle (1975) chose instead to specify the horizontal eddy momentum fluxes using values derived from satellite data. These models, which will here be called classical Eulerian models, succeeded in producing realistic fields of stratospheric winds, temperatures and constituent mixing ratios. They still play a role in assessment studies.

Although some features of these models are satisfactory, the treatment of the eddies is open to criticism. Mahlman (1975) used results from a GCM to study the flux gradient relationship and found that the flux was not always diffusive in character. Other studies criticised the approximations made by Reed and German (1965): their assumptions regarding the conservative nature of the tracer, the particle trajectory (a straight line) and the mean mixing surface slope and its variance were all considered dubious (e.g. Matsuno 1980, Danielsen 1981). It is these approximations which determine the nature of the K tensor and the ensuing transport.

More generally, specification of a fixed K-tensor, particularly for assessment purposes, is unsatisfactory for several reasons. If the mean meridional circulation and the K tensor are specified independently, there is no guarantee that the sum of mean advection and eddy fluxes will give the correct net transport. Further, the specification of fixed Ks inhibits dynamical feedback whereby the eddies depend on the background zonal wind field which is related, via solar heating, to the temperature and ozone fields. Finally, the treatment of the eddy momentum fluxes can also be criticised. The physical basis for a K-theory approach for momentum is especially poor. On the other hand, if the fluxes are specified from observations, these values may not be consistent with the eddy fluxes of heat and tracers which are determined using the K-tensors.

The interest during the 1970s in possible perturbations to the ozone layer prompted analytical studies of transport in the middle atmosphere and, in particular, a reappraisal of simple models of the atmosphere and their treatments of eddy processes. These studies produced two significant advances. Firstly, the relationship between the mean meridional circulation and the eddies was clarified. The two are mutually dependent. As we have seen, under certain restricted circumstances (steady waves with no damping — and see the remarks at the end of Section 6.3.3), the wave produces no net effect on the zonal mean atmosphere.

Secondly, explicit solutions of the eddy perturbation equations using linear wave theory led to a complete reassessment of Reed and German's work. To summarise, (and see Plumb 1979, Matsuno 1980, Holton 1980, Danielson 1981, Pyle and Rogers 1980b, etc.) although a tensor approach is possible, it was found that because many of Reed and German's approximations were invalid, the form of the tensor became quite different from that originally proposed.

These results led to various new approaches in two-dimensional modelling. Ideally, Andrews and McIntyre's work pointed to the desirability of using a Lagrangian procedure for defining eddy and mean transport. In such a system, averages are taken following the trajectories of air parcels, rather than around some fixed latitude circle. Thus the mean circulation in this system is the mass transport circulation. However, experience tracing air parcels in a GCM indicates that in practice such an approach is impractical. Hsu (1980), for example, showed how material tubes can become hopelessly entangled, since on the time scale

of a few tens of days dispersion and diffusion cannot be ignored. Some of the practical problems of the Lagrangian system have been discussed by McIntyre (1980a) who suggested that the phenomena demonstrated by Hsu, which violate the premises of the non-acceleration, non-transport theorems, should be thought of as planetary wave 'braking.' (See Section 6.3.4)

Nevertheless, in the spirit of the work of Andrews and McIntyre, Dunkerton (1978) proposed a mass transport circulation based on a reformulated thermodynamic equation. Adopting the definition of Andrews and McIntyre (1976), a residual circulation is defined as

$$\bar{v}^R = \bar{v} - \frac{1}{\varrho}\frac{\partial}{\partial z}\left(\varrho\frac{\overline{v'\theta'}}{\bar{\theta}_z}\right) \tag{12.6}$$

$$\bar{w}^R = \bar{w} + \frac{1}{\cos\phi}\frac{\partial}{\partial y}\left(\frac{\overline{v'\theta'}\cos\phi}{\bar{\theta}_z}\right) \tag{12.7}$$

then the thermodynamic and continuity equations become, after some approximation,

$$\bar{w}^R\frac{\partial\bar{\theta}}{\partial z} = \bar{Q} \tag{12.8}$$

$$\frac{1}{\cos\phi}\frac{\partial}{\partial y}(\bar{v}^R\cos\phi) + \frac{1}{\varrho}\frac{\partial}{\partial z}(\varrho\bar{w}^R) = 0 \tag{12.9}$$

Equation 12.8 contains no eddy terms following the transformation in Equations 12.6-12.7. Thus the residual circulation depends just on the diabatic heating and the lapse rate and is similar to the diabatic circulation. Dunkerton then identified this circulation with a Lagrangian mean circulation of air parcels in the stratosphere provided that the waves are approximately steady and conservative. This would be the net circulation for tracer transport and is similar to the circulation proposed by Brewer (1949) and Dobson (1956). Although Dunkerton ignored diffusion, his work represented a significant conceptual improvement in the understanding of the net transport stream function.

Next, the tracer equation, in the absence of diffusion or transience and ignoring the effect of the photochemical lifetime on eddy transport, becomes

$$\frac{\partial\bar{\chi}}{\partial t} + \bar{v}^R\frac{\partial\bar{\chi}}{\partial y} + \bar{w}^R\frac{\partial\bar{\chi}}{\partial z} = \bar{S} \tag{12.10}$$

The approximations of no chemistry (except in the zonal mean source, $\bar{S}$), transience, dissipation or dispersion lead to a particularly simple tracer continuity equation.

Following Dunkerton's work there have been a number of 2-D model studies which have used the diabatic circulation, or alternatively the residual circulation, as the transport circulation. (In this chapter the term 'transport circulation' is used somewhat loosely. For definitions of different circulations and their relationships see Table 6.1). The studies include Pyle and Rogers (1980a), Holton (1981), Garcia and Solomon

(1983), Guthrie *et al.*, (1984) Ko *et al.*, (1985). For example, Holton (1981), including some of the terms dropped by Dunkerton (1978), obtained the following thermodynamic equation.

$$\frac{\partial\bar{\theta}}{\partial t} + \bar{v}^R\frac{\partial\bar{\theta}}{\partial y} + \bar{w}^R\frac{\partial\bar{\theta}}{\partial z} = \bar{Q} - \frac{1}{\varrho}\frac{\partial}{\partial z}\left\{\varrho\,\frac{\overline{v'\theta'}\cdot\nabla\bar{\theta}}{\bar{\theta}_z}\right\} \tag{12.11}$$

For steady and conservative waves the flux $\overline{v'\theta'}$ is parallel to the θ surface and the eddy forcing vanishes (Andrews and McIntyre 1976, Clark and Rogers 1978, Plumb 1979). Thus in this case, too, the transport circulation is driven by the diabatic heating. A more complete residual circulation (e.g. Garcia and Solomon 1983) would include the eddy term in both the thermodynamic and momentum equations.

Finally, the work of Tung (1982) should be mentioned, as it offers some conceptual advantages for tracer modelling. The isentropic coordinate system used by Tung adopts the potential temperature as the vertical coordinate. The vertical velocity is proportional to the diabatic heating. The zonal mean circulation in isentropic coordinates is a close approximation to the diabatic circulation and the definition of a residual circulation is not required. (Notice that the zonal mean circulations in isobaric and isentropic coordinates are not identical).

It is clear that to neglect of eddies from Equation 12.11 is an oversimplification. In the absence of any friction, the circulation would be strongly zonal with extremely weak meridional flows (see, e.g. Mahlman *et al.*, 1984). It is precisely the irreversible effects of chemistry, transience, dissipation and dispersion which give rise to a transport circulation and thus these processes must somehow be included. It cannot be argued that these are small terms which can be ignored since those same arguments would imply that the transport circulation itself is negligible. After the cancellation of the large standing wave components and the induced mean circulation it is these very terms which become important in driving the mean circulation and possibly in leading to enhanced mixing. A fully self-consistent interactive two-dimensional model is not possible without an adequate description of these processes, at present not available. This relationship between the eddies and the induced circulation and the subsequent formulation of the eddy treatment has been discussed by a number of authors (Plumb 1979, Matsuno 1980, Pyle and Rogers 1980b, Danielsen 1981, Tung 1982). An important result, where relevance to Equation 12.11 was pointed out by Andrews and McIntyre (1976), is that

$$\overline{v'\chi'}\cdot\nabla\bar{\chi} = \overline{\chi'S'} - \frac{1}{2}\frac{\partial}{\partial t}\overline{\chi'^2} \tag{12.12}$$

Thus the eddy flux of χ is directed along the surfaces of constant mixing ratios (and not across them) if χ is exactly conserved or the waves are steady and frictionless. In this case it is clear that the fluxes are not diffusive in character. On the other hand, photochemistry or a growing or decaying wave can produce cross-gradient flux components.

Solving the eddy perturbation equation with the linear wave approximation and expressing the fluxes in K-tensor form it is found that the Ks can be seprated into symmetric and antisymmetric components (Plumb 1979, Matsuno 1980).

$$\underset{\approx}{K} = \underset{\approx}{K_s} + \underset{\approx}{K_a}$$

(Notice that this shows the approximation Kyz = Kzy, used by Reed and German (1965), is not generally valid (i.e. when $\underset{\approx}{K_a}$ is significant compared with $\underset{\approx}{K_s}$)).

These K tensors depend on Lagrangian eddy statistics and the dissipation or photochemical relaxation rates. The eddy flux arising from the antisymmetric component is advective in character and can thus be conveniently combined with the mean circulation to give an effective transport circulation. This eddy-induced advection opposes the mean circulation (Dunkerton 1978, Plumb 1979). Plumb and Mahlman (1985) point out that the transport circulation is related to the Lagrangian circulation, the diabatic circulation and the residual circulation but is not identical to any (see Table 6.1). The difference between the circulations is related to the breakdown of non-acceleration conditions. Nevertheless, GCM results (Plumb and Mahlman, 1985) show that in the stratosphere the transport, diabatic and residual circulations are very similar and, in practice, many modellers have implicitly assumed them to be equal.

The symmetric, diffusive components can be further separated. A part simply depends on the time dependence of Lagrangian eddy statistics (the parcel displacements) which are difficult to determine in practice. (Note, however, that Lagrangian eddy statistics can easily be determined within linear wave theory - see Chapter 6 for a more complete discussion). This part represents dispersion. Secondly, an additional part depends also on the photochemical relaxation rates. Matsuno (1980) argued that this part would be small but Pyle and Rogers (1980b, 1984) have shown that it can play an non-negligible role.

A number of methods of deriving the Ks arising from the transient eddies have been discussed. Luther (1973) used Reed and German's approach to derive Ks from heat flux data. His values have been much used in classical Eulerian models. Typical values for Kyy are found to be a few $x10^6 m^2 s^{-1}$ and for Kzz, 0.1-1 $m^2 s^{-1}$.

Kida (1983a, b) has derived a global average Kyy from the tracer dispersion in a simple GCM and obtains a Kyy $\sim 3\times10^5 m^2 s^{-1}$ and Kzz $\sim 10^{-1} m^2 s^{-1}$, considerably smaller than Luther's values. Tung (1982) argued that the eddy motions are predominantly directed along the isentropes in the atmosphere. This implies that the effects from Kyz and Kzz are considerably smaller than that from Kyy in isentropic coordinates. Tung (1984) has studied observed atmospheric Eulerian statistics and argues for a Kyy value $\sim 4\times10^5 m^2 s^{-1}$ in the stratosphere, although this number could be an order of magnitude greater in disturbed conditions. In subsequent model studies, Ko *et al.*, (1985) found that the calculated distributions of HNO_3 are quite sensitive to the Kyy and that the observed HNO_3 distribution can best be simulated using Kyy $\sim 3\times10^5 m^2 s^{-1}$.

Newman, Schoeberl and Plumb (1985b) have investigated the possibility of deriving Kyy from the observed fluxes of potential vorticity. Since q is conserved on pressure surfaces they argue that Kzz is unimportant for potential vorticity and derive Kyy from $\overline{v'q'} = -K_{yy}\,\partial\bar{q}/\partial y$. Using stratospheric data they find a maximum Kyy $\sim 4\times10^6 m^2 s^{-1}$ at $\sim$ 1 mb with a value of $\sim 5\times10^5 m^2 s^{-1}$ typical of the middle stratosphere. They also find some regions of negative Kyy in high latitudes when the vortex is displaced from the pole. Clearly, simple two-dimensional ideas of transport must be used with caution in high latitudes.

Yet another approach has been taken by Plumb and Mahlman (1985). They have used the flux of pairs of tracers from a GCM to derive latitudinally dependent Ks (and the transport circulation). They find Kyy in the stratosphere to be generally $\sim$ a few $\times10^5 m^2 s^{-1}$ but with significant regions (the 'surf zones' of McIntyre and Palmer (1983)) where Kyy $\sim 4\times10^6 m^2 s^{-1}$. Kzz is important in the troposphere but much smaller in the stratosphere when it arises from small scale, but resolved motions. A pragmatic conclusion of their work is that although the wave amplitudes can become very large, theories based on small amplitude disturbances seem to work reasonably well, if used as above to motivate the formulabic of the K tensor.

The part of the K tensor that depends on photochemical relaxation (leading to the so-called chemical eddies) has been determined by Pyle and Rogers (1980b), among others. They showed how this component

of the tensor could be related to chemical lifetimes and eddy statistics. Expanding small amplitude waves into Fourier components and assuming linearity they calculated Eulerian statistics by solution of the quasi-geostrophic potential vorticity equation (not a particularly convenient method for purely chemically-orientated problems). Pyle and Rogers calculate photochemical Kyy values in excess of $10^6 m^2 s^{-1}$ for ozone in the mid stratosphere.

The limitations of the various derivations of the Ks must be remembered. Calculations based on satellite data use Eulerian statistics and necessarily only allow for the planetary scale since the smaller scales are not resolved. Calculations based on GCM results will be limited by the accuracy of the GCM itself. Most GCMs appear to have relatively weak eddies compared with the atmosphere (see Chapter 6).

In summary, the results discussed above on the residual circulation and the treatment of eddy transport have an important bearing on approaches to two-dimensional modelling. Firstly, various of Reed and German's approximations lead to an incorrect treatment of eddy fluxes. The parcel trajectories are, in fact, ellipses and not straight lines (Matsuno 1980) and the fluxes due to steady and conservative planetary waves are advective and not diffusive in character. A K-tensor treatment should therefore include an anti-symmetric component. That the Reed and German approach has in practice worked reasonably satisfactorily perhaps suggests that the fluxes modelled by the symmetric component, due to dispersion, photochemistry, etc., play a major role. Nevertheless the Reed and German derivation of the Ks cannot be justified in principle.

Secondly, the residual and diabatic circulations are only approximations to the transport circulation, but good approximations in the stratosphere. They are not as good an approximation in the troposphere and during disturbed situations such as stratospheric sudden warmings. These are situations where, in any case, any two-dimensional model treatment should not be expected to be satisfactory.

Thirdly, if the residual circulation approach is used, there must nevertheless still be some eddy transport to be treated, otherwise an inconsistency arises: without eddy forcing in the zonal momentum equation, we expect only a weak circulation.

Fourthly, the relative importance of advective and eddy processes in the transport of tracers can only be determined on a species by species basis. It is clear that the role of chemical eddies depends on the chemical reactivity of the individual species. The contribution from transient motions depends on both the K and local gradient of species concentrations. (See Chapter 6 for a detailed discussion of transience). Eddy transport could be particularly important for species that exhibit large gradients created by advection and/or chemical interactions.

Finally, the eddy transport is related to global Lagrangian statistics which to date have not been derived from observations. Approximate relationships to Eulerian statistics derived from linear wave theory have been used, but nevertheless a totally satisfactory determination of the Ks is difficult. In lieu of theoretical methods for determining the Ks, one could derive or validate the values of Ks by comparing the calculated tracer distributions with observed distributions. This will be discussed in the next section.

12.5 CURRENT MODELS

In parallel with the development in the formulation of transport processes in 2-D models, the chemical contents of 2-D models have also matured over the past decade. Most 2-D models now contain realis-

tic chemistry packages, comparable or identical to those in current 1-D models both in the number of species, reactions and diurnal treatment.

Current two-dimensional models can usefully be categorised in at least two ways. Firstly, they can be separated, according to their dynamical treatment of the mean circulation and the eddies, into so-called classical Eulerian models or models which employ a residual (or similar) circulation. The traditional models thus have a mean circulation with, for example, an indirect circulation in middle and high latitudes of the winter hemisphere. They use a similar approach to Reed and German for the description of the eddy transport. On the other hand the diabatic/residual circulation models explicitly recognize the cancellation between eddies and the mean motions and generally use somewhat smaller K values.

Secondly, the models can be classified by the degree to which the model is interactive. The role played by non-conservative eddy processes in driving the atmosphere away from equilibrium must not be forgotten (see Sections 12.4, 12.8 and Chapter 6); until these processes can be modelled adequately two-dimensional models cannot be fully interactive and will be driven by the *specified* eddy forcing. Nevertheless, even a limited degree of feedback within the models can be extremely useful in assisting understanding. For example, the ultraviolet heating in the upper stratosphere is dependent on the ozone concentration, which is temperature dependent. A change in ozone will change the heating rate and probably the temperature, thus altering the ozone concentration. These are potentially important feedbacks for inclusion in any assessment of ozone perturbation. For example, experiments with and without this feedback using a 2-D model showed significantly different results for the calculated ozone depletion by fluorocarbons (STRAC, 1979, pp 167-175).

The importance of an interactive model is also seen in results discussed by Harwood and Pyle (1980). They showed that the ozone column amounts in their model were extremely sensitive to the radiative heating rate in the lower stratosphere, a difficult region in which to make accurate radiation calculations. Moving from a model which assumed radiative equilibrium in the lower stratosphere to one which employed fixed, calculated heating rates there (both reasonable approximations) changed the ozone column by up to 70 D.U. The reason for such large sensitivity lies in the heating rates in both experiments being fixed. In this region of the stratosphere the model meridional circulation, and hence the temperature and tracer distributions, will be largely dominated by the diabatic forcing (which should depend on the nonconservative eddy processes). Radiative feedback in which changed temperatures alter the heating rates could also be expected to change the ozone distributions and reduce the sensitivity. Ignoring the radiative feedback (albeit for the understandable reason that the radiative calculation is very difficult) probably leads to an erroneous conclusion (and this cautions against overinterpretation of a 2-D feedback). In this case it seems likely that a Newtonian cooling scheme, necessarily of low accuracy but including the feedback capability, would be advantageous.

Other dynamical feedbacks are also important. For example the propagation of waves depends on the background zonal wind field. Thus planetary wave transport in the stratosphere and gravity wave mixing in the mesosphere should depend on the background fields, which themselves will be related to the momentum transport by the waves.

While the feedback processes are not always necessarily important for assessment studies, inclusion in simple two-dimensional models is nevertheless an extremely useful method of examining the important processes which govern the fields of temperature and trace gases in the middle atmosphere. The problems of interactive modelling are discussed in detail in Chapter 6 (see also Section 12.8).

ASSESSMENT MODELS

Table 12.2 summarizes some current two-dimensional models, categorising the approaches from the most simple, with specified circulations, to more complex models including many of the important feedback processes. In the remaining part of this section some of these models will be discussed in more detail with an emphasis on the more important results.

Table 12-2

Classical Eulerian Models

Specified mean circulation, fixed Ks	Hidalgo & Crutzen	(1977)
	Brasseur	(1978/79)
	Ko *et al.*	(1984)
	Pyle	(1980)
	Whitten *et al.*	(1981)
Calculated mean circulation, fixed Ks	Rao Vupputuri	(1973)
	Harwood & Pyle	(1975)
	Haigh & Pyle	(1982)
	Haigh	(1984)

Transformed and other alternative formulations

Diabatic Circulation	**Examples**	
Fixed heating rates, fixed Ks (often small)	Prabhakara	(1963)
	Pyle & Rogers	(1980)
	Guthrie *et al.*	(1984)
	Stordal *et al.*	(1985)
Fixed heating rates, Luther's Ks	Miller *et al.*	(1981)
	Cariolle & Brard	(1984)
Isentropic coordinate system, fixed heating rates	Ko *et al.*	(1985)
Computed heating rates + chemical eddies	Rogers & Pyle	(1984)
Residual Circulation		
Fields derived from a circulation model.	Holton	(1981)
Calculated fields.	Garcia & Solomon	(1983)
Transport Circulation		
Derived from GCMs	Plumb & Mahlman	(1985)
	Pitari and Visconti	(1985)

There have been a number of modelling studies employing the classical Eulerian approach with a specified mean circulation and a fixed K tensor. The circulation and temperature may be taken from various compilations (e.g. Newell *et al.* 1974, Louis 1974) or be precomputed. Luther's (1973) K tensor has been extensively used, although some workers have chosen to modify the Ks to produce a satisfactory fit to certain observations. This latter approach presupposes that any discrepancy between observation and theory is due to inadequately modelled eddy transport rather than, for example, a deficiency in the model photochemical scheme. While the Ks should by no means be regarded as fixed, unique quantities, treating them as adjustable parameters is equally unsatisfactory. This applies whether the approach is the classical Eulerian or uses a transformed mean circulation. These specified circulation models have been used to study stratospheric perturbations by high flying aircraft (Cunnold *et al.* 1977, Hidalgo and Crutzen 1977) and by fluorocarbons (Pyle 1980, Gidel *et al.* 1983).

Recently, using a specified circulation model with complete chemistry, Ko *et al.* (1984) have presented a very detailed analysis of the latitudinal and seasonal distribution of stratospheric trace gases and addressed the question of the role of transport and chemistry in determining trace gas distributions. Their model consistently underestimated the concentration of the upward diffusing species (e.g. N_2O) in the tropical stratosphere while at the same time overestimating the abundance of the downward diffusing species in the lower stratosphere. This suggests that the transport parameterization in this classical Eulerian model may have underestimated the upwelling at the equatorial tropopause either because of too weak a circulation or too strong horizontal mixing. The authors identified N_2O_5 as a major reservoir for NOy in the winter hemisphere at high latitudes and identified this sequestration by N_2O_5 as responsible for the winter minimum in NO_2 column produced in the model. However, the observed NO_2 column abundances show much larger seasonal contrast.

The study described by Pyle (1980) produced the interesting result that the predicted depletion of ozone due to fluorocarbons showed significant latitudinal and seasonal variations with the largest depletions occuring in the winter polar latitudes. This argues for the need for multi-dimensional models in any assessment studies and, furthermore, suggests the importance of a monitoring programme with sufficient high latitude stations.

Two-dimensional classical Eulerian models in which the mean circulation is calculated have been described by Rao Vupputuri (1973) and Harwood and Pyle (1975). As discussed in the previous section, Harwood and Pyle circumvented the problem of modelling the horizontal eddy flux of momentum by using values derived from satellite data. This removes some degree of dynamic feedback with, in some regions, the mean circulation depending strongly on the prescribed momentum fluxes. The other terms which drive the circulation, the net diabatic heating and the eddy fluxes of heat, are however model dependent. This model does produce a hemispherically asymmetric total ozone distribution in good qualitative agreement with observations (see Figure 12-12, from Haigh (1984)), due to the circulation driven by the specified, asymmetric momentum fluxes.

In common with more sophisticated models, the temperature structure in the above model, while qualitatively satisfactory, has somewhat too cold a winter polar lower stratosphere and correspondingly too strong a polar night jet. For these calculations a detailed radiation code is used with the 15μ CO_2 band modelled using a Curtis matrix approach (Williams 1971). When the ozone, temperature and net heating rates are all calculated self consistently, the summer stratopause is found to be very close to radiative equilibrium, in agreement with the arguments of Dickinson (1975). Somewhat different results were obtained by Kuhn and London (1969) and Murgatroyd and Goody (1958) who presumably used ozone and temperature data which were not necessarily mutually compatible.

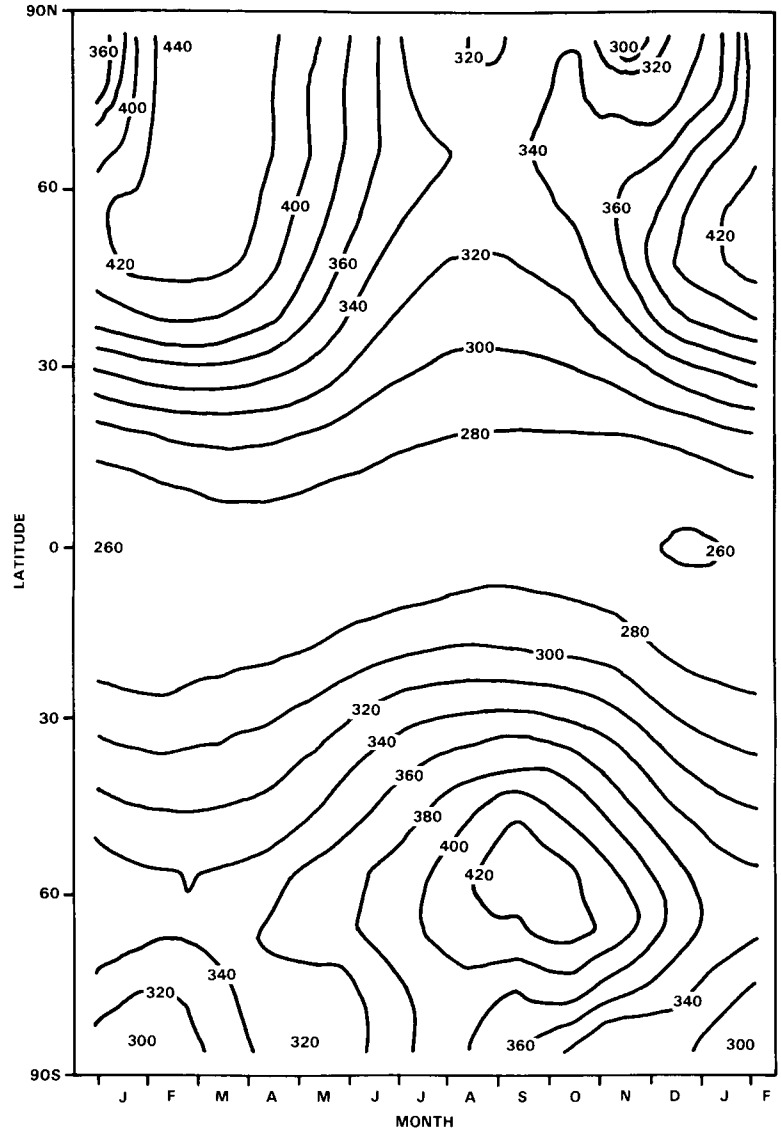

Figure 12-12. Latitude-time section of total ozone (matm-cm) from Haigh (1984).

These classical Eulerian circulation models also show a strong cancellation between eddy and mean motion transport. Some of this may be for the reasons discussed (nonacceleration, etc.), but given the diffusive nature of the model eddy transport, the cancellation perhaps is not unexpected. What is perhaps most surprising is that the modelling of satisfactory tracer distributions seems to suggest that the small residual between eddy and mean transport has also been modelled well (see, e.g. Harwood and Pyle 1977, Ko *et al.*, 1984). It could simply reflect a suitable choice of Kyz/Kyy to simulate successfully the observed slope of the mixing surfaces in the model.

Haigh and Pyle (1982) have used their model with calculated circulations to investigate stratospheric perturbations. Experiments were carried out to study the effect of emitted fluorocarbons and increasing levels of CO_2, singly and together, on stratospheric ozone. Without radiation feedback the CO_2 experiment could not, of course, have been performed. Indeed, the result of the coupled perturbation empha-

sized the importance of radiation feedback since the two perturbations were found not to be linearly additive. This was because of the different temperatures in the three runs acting differently on the temperature-dependent catalytic cycles. Figure 12-13 shows the ozone concentration change at the equator for these three calculations.

Figure 12-14 shows distributions of N_2O calculated with the above model (Gray and Pyle, 1985). Figure 12-14a shows a standard model calculation (similar to that described in Jones and Pyle 1984) in which the N_2O maximum is at the equator and little of the structure revealed by the SAMS experiment on Nimbus 7 (see Chapter 10) is seen. Figure 12-14b shows a model calculation in which the model is subjected to a prescribed equatorial momentum forcing, chosen so as to reproduce the equatorial semiannual oscillation of the zonal wind. The momentum forcing drives a circulation which modulates the net circulation and gives rise to features akin to the "double-peaks" described by Jones and Pyle (1984). Such a simple experiment, which suggests the importance of equatorial dynamics on some aspects of the tracer distributions, is only possible in a model in which the circulation can be calculated. Moreover, the validity of the experiment is not particularly compromised either by the crudeness of the momentum forcing or indeed by any other

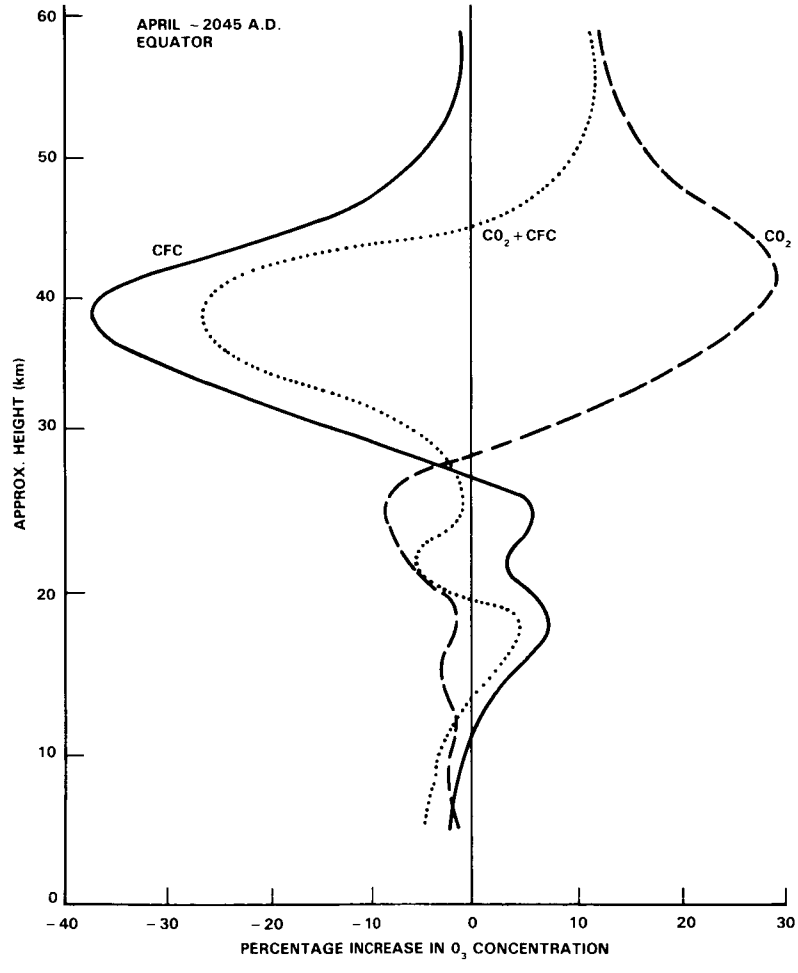

Figure 12-13. Percentage change in ozone concentration calculated for the year 2045 due to (a) increased CO_2 (b) increased fluorocarbons (c) the coupled perturbation, from Haigh and Pyle 1982.

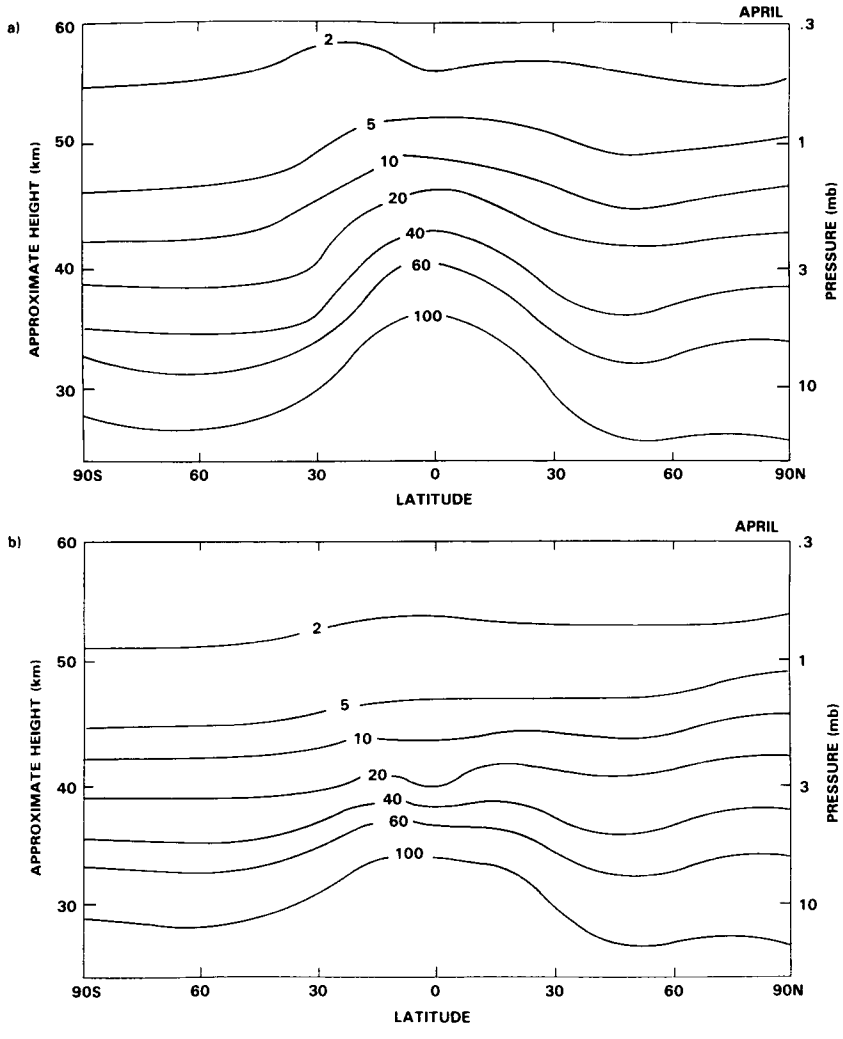

Figure 12-14. Modelled N_2O for April from the 2-D model study of Gray and Pyle (1985); (a) is the basic model run (b) includes the semi-annual oscillation.

deficiencies in the model. Simple, physically-limited models can play an important role in increasing our understanding of stratospheric processes.

Turning to the transformed circulation models, the simplest of these use a fixed diabatic circulation. Prabhakara (1963) developed the first such model (although he, apparently, did not treat the circulation as being a 'residual' in any sense). He experimented with various Ky and Kz coefficients - the eddy transport was purely Fickian diffusion - and succeeded in obtaining a reasonable latitudinal distribution of total ozone.

A more detailed model using the residual mean circulation deduced from a spectral 3-D model (see Holton, 1981) was used to simulate the distribution of N_2O. Other models have used fixed diabatic heating rates to compute the diabatic/residual circulation. Miller *et al.* (1981), Guthrie *et al.* (1984) and Stordal *et al.* (1985), for instance, use Murgatroyd and Singleton's calculated heating rates above 25 km multiplied by 0.4. Although the use of the scaling factor could partially be justified by the argument that the summer stratosphere is probably much closer to equilibrium than suggested by Murgatroyd and Singleton, such

an arbitrary adjustment is somewhat unsatisfactory. These models, however, use different methods to obtain the heating rate below 25 kms. Miller *et al.* (1981) used simple extrapolation of the Murgatroyd and Singleton values. Their model was probably not very sensitive to the choice of circulation in the lower stratosphere because of the large eddy diffusion coefficient adopted. Guthrie *et al.* (1984) and Stordal *et al.* (1985) adopted the heating rate from Dopplick (1979). Another approach to specifying heating rates is that of Ko *et al.* (1985) who obtained a global fit of the data of Murgatroyd and Singleton and Dopplick by using a sum of hyperbolic functions and thus avoided any problem of mismatch at the boundary.

Although the use of residual/diabatic circulations has been adopted in model studies since about 1981, the choice of values for the eddy coefficients to be used in conjunction with the diabatic/residual circulation remains open. Miller *et al.* (1981) and Cariolle and Brard (1984) chose to use the coefficients from Luther (1973). In contrast, Holton (1981) and Tung (1982) argued that the eddy mixing may play a secondary role relative to advective transport and large values of Ks in residual circulation models appear to be in conflict with the theoretical estimates of Kida (1983) and Tung (1984) if the eddy term is to represent mixing from transient motions. However, the work of Pyle and Rogers (1980 a,b) indicated that the chemical eddy term could have Ks whose values may be comparable to those of Luther's.

The work of Guthrie *et al.* (1984) and Ko *et al.* (1985) helps clarify the role of eddy mixing in transport of trace gases. Guthrie *et al.* used values of Kyy $\sim 2\times10^5 m^2s^{-1}$ and Kzz $\sim 0.2\ m^2s^{-1}$ to simulate the distribution of upward 'diffusing' trace gases such as N_2O, F-11, and F-12. By comparing their model results with models using large values of Kzz, they concluded that altitude profiles of upward 'diffusing' trace gases can be simulated better with smaller values of Kzz when used with the residual circulation. However, as noted by Ko *et al.* (1985), the distributions of upward 'diffusing' species, while sensitive to Kzz, are not very sensitive to the values of Kyy. Ko *et al.* argued that it is more advantageous to deduce Kyy from the observed distributions of downward 'diffusing' species which show large latitudinal gradients. One such candidate species for which extensive global data are available is HNO_3. By systematically varying the values of Kyy and comparing the model simulated column abundance of HNO_3 with observation from LIMS, they concluded that values of Kyy $\sim 3\times10^5\ m^2s^{-1}$ would be appropriate for use with the diabatic circulation. Figure 12-15 shows the observed latitudinal variation of nitric acid column compared with model calculations using various values of Kyy. The low latitude values are best fit with values close to $3\times10^5 m^2s^{-1}$. Notice, though, the weaker (or smaller) diffusion leads to considerable underestimation of the column abundance.

Values of Kyy and Kzz of $\sim 10^5$ and $10^{-1}\ m^2s^{-1}$, respectively, are closest to the numbers suggested by Kida (1983), Tung (1984), and Plumb and Mahlman (1985) (away from the zero wind line 'surfzone', actually $\sim 30° - 40°$ in latitudinal extent). There is some consensus among modellers that values of this order are suitable for the residual circulation approach. However, Miller *et al.* (1981) and Cariolle and Brard (1984) produce satisfactory tracer distributions with larger Ks. The uncertainty in the derived Ks due to limitations in GCMs and inadequate resolution in atmospheric data should not be forgotten.

Rogers and Pyle (1984) allowed some degree of radiation/dynamics feedback in their diabatic model by calculating the heating rates, although they used precomputed, time-varying temperatures from a classical Eulerian model. Secondly, they included the chemical eddy transport which arises when a tracer is not inert. The eddy correlations $\overline{v'^2}$, $\overline{v'w'}$ and $\overline{w'^2}$, which along with the photochemical lifetimes define the Ks, were calculated using a planetary wave model forced by climatological 100 mb heights. (Notice that Rogers and Pyle assumed linear, small amplitude waves and thus arrived at expressions involving Eulerian statistics).

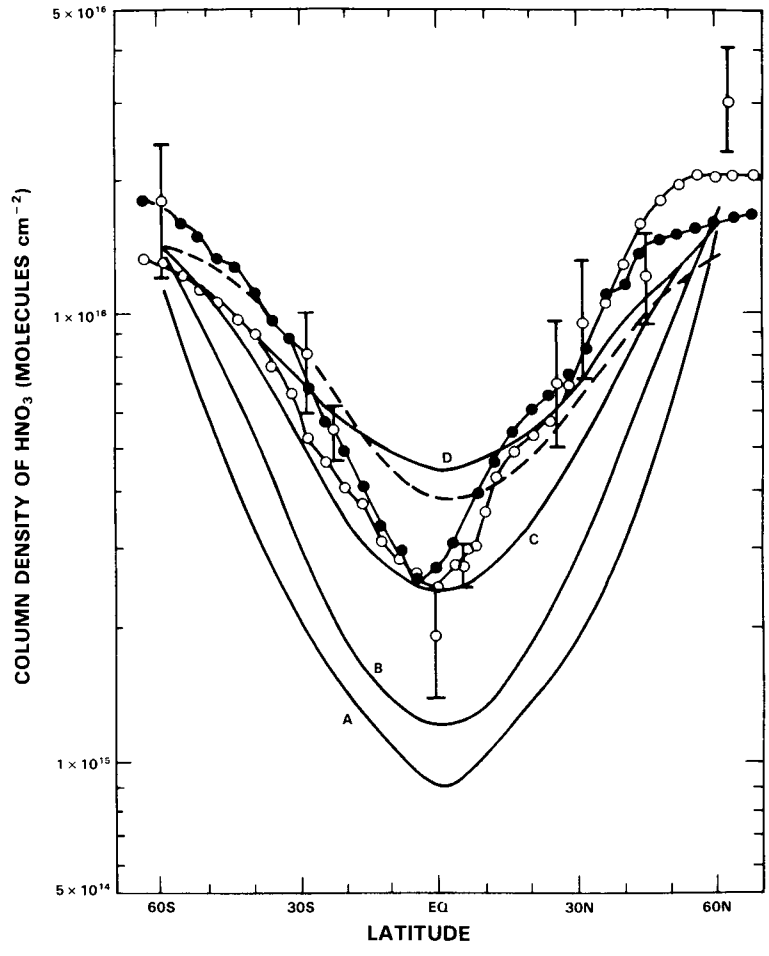

Figure 12-15. Calculated latitudinal distribution of the stratospheric column density of HNO_3. The calculated results are for (curve A) $K_{yy} = 0$, (curve B) $K_{yy} = 1 \times 10^9$ cm^2 s^{-1}, (curve C) $K_{yy} = 3 \times 10^9$ cm^2 s^{-1} and (curve D) $K_{yy} = 1 \times 10^{10}$ cm^2 s^{-1}. The data are April/May 1980 (bars) from Girard *et al.* [1982], May (dash-solid circle curve) and December (dash-open circle curve) from Gille *et al.* [1984b]. The calculated column density from the classical Eulerian model of Ko *et al.* [1984] (dashed curve) is included for comparison. From Ko *et al.* (1985).

Two conclusions may be drawn from their work. Firstly, in agreement with Guthrie *et al.* (1984) they conclude that the absence of a large cancellation between mean and eddy motions in the diabatic model helps physical interpretation. For example, Figure 12-16 shows the ozone budget at 64 mb from two model runs, a) the classical Eulerian model and b) the diabatic model. In Figure 12-16a the evident feature is the close cancellation between eddies and mean motion terms. The photochemistry appears negligible. Figure 12-16b shows, on the contrary, that the net transport is in fact comparable with the photochemistry. For time scales appropriate to two-dimensional models ozone in the lower stratosphere cannot be regarded as inert.

Secondly, the chemical eddies can play a role in determining the distribution of tracers. In their experiments Pyle and Rogers (1984) showed that using the correct chemical eddy K coefficient (dependent on the appropriate lifetime) can make significant differences to the calculated column abundances. For

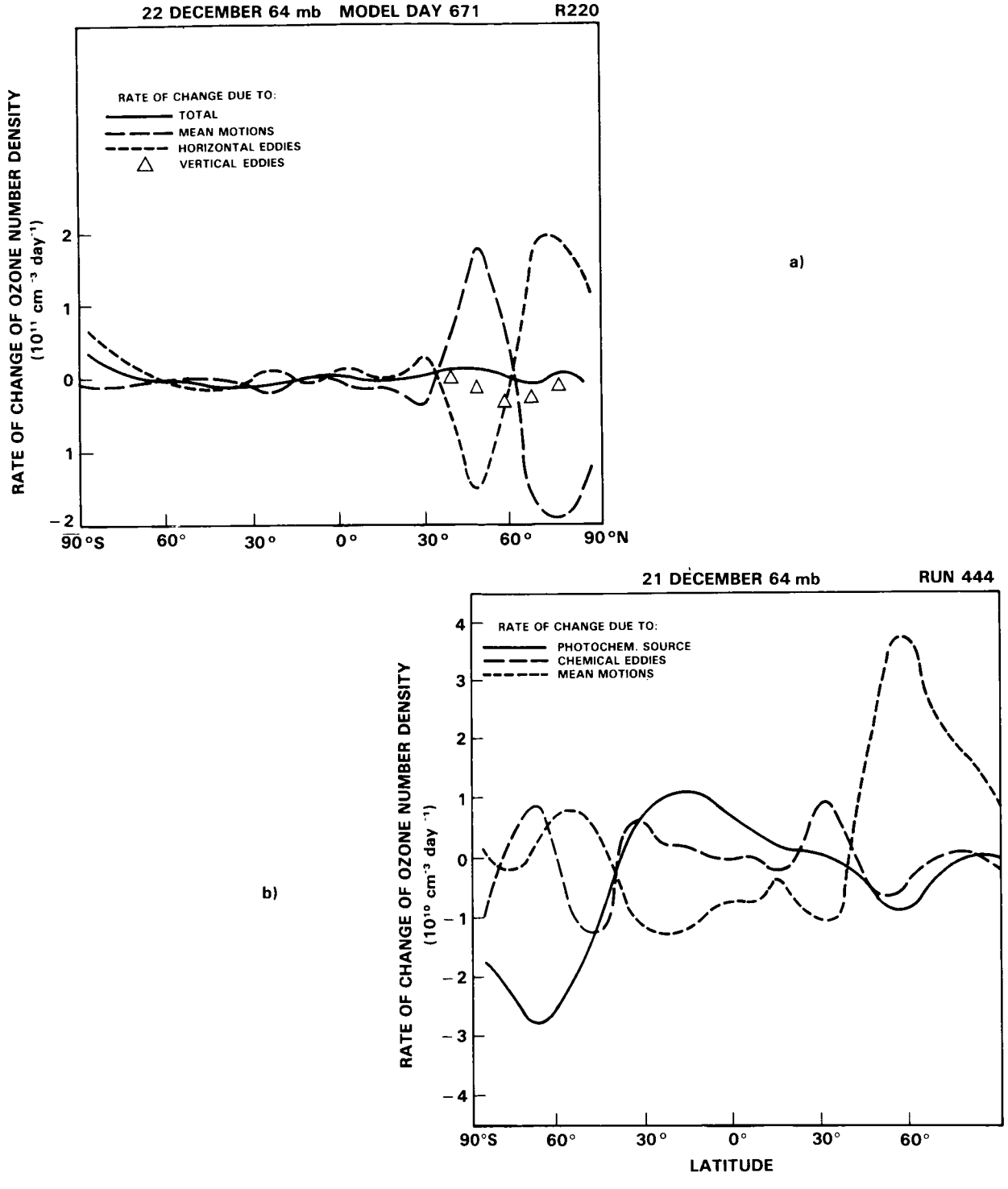

Figure 12-16. a) Zonal mean meridional section of the ozone tendency at 64 mb for December from a typical Eulerian circulation simulation (after Harwood and Pyle 1975). b) Zonal mean meridional section of the ozone tendency at 64 mb for December from a modified diabatic circulation simulation. Pyle and Rogers (1984).

example, using a K appropriate to NO_x leads to changes in the O_3 and HNO_3 high latitude columns of approaching 10% and 50% respectively.

Another residual circulation model which includes some dynamical feedback is that developed by Garcia and Solomon (1983). They solved the coupled thermodynamic and momentum equations above 100 mb and include some eddy forcing by diffusive heat and momentum fluxes, treated as a Rayleigh friction. Radiation is modelled using Newtonian cooling. The calculated circulation, temperature structure and distribution of chemical species generally agree satisfactorily with observations. In their first experiments, they used a Kyy of $10^5 m^2 s^{-1}$, but their Kzz increased from a small value ($10^{-1} m^2 s^{-1}$) in the lower stratosphere to rather large values ($\sim 10^1 m^2 s^{-1}$) in the middle and upper stratosphere. As a consequence, their vertical distribution of N_2O did not fall off with altitude as sharply as the data or as in Guthrie's *et al.* model. Their more recent calculations with smaller Kzz produce much closer agreement with observations. The model also includes chemical eddy transport parameterized in terms of the photochemical relaxation time constant which, as expected, is found to be important in the transition region where the photochemical and zonal transport time scales are comparable. The model has been used in a detailed investigation of the nitrogen budget of the stratosphere. The polar distributions of the nitrogen compounds are sensitive to the use of the residual circulation. The model supports the idea that NO_2 is carried down from the lower thermosphere to the stratosphere in the polar night. An important model conclusion (Solomon and Garcia 1984 a,b) is that N_2O_5 is the major NO_y reservoir in high latitudes (see Ko *et al.* 1984) and the model calculations appear to be consistent with the observations of the Noxon cliff (1979).

An important addition to the above model is the representation of breaking gravity waves. The seasonal behaviour of the model meridional temperature and circulation in the mesosphere is then in good agreement with observations and the computed eddy diffusion coefficients are consistent with the behaviour of mesospheric turbulence inferred from MST radar echoes. (Garcia and Solomon 1985) Figure 12-17

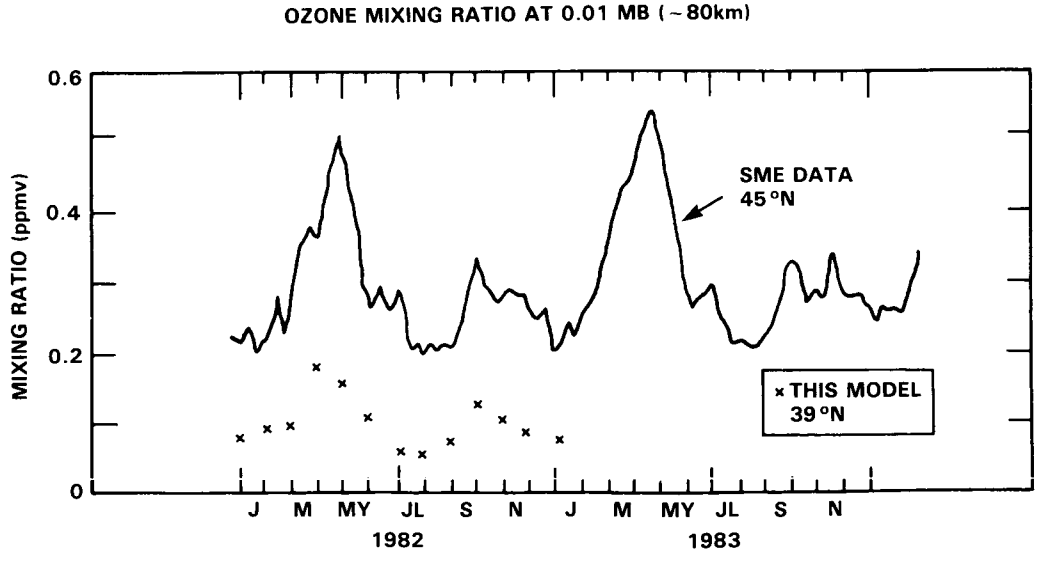

Figure 12-17. Observed [Thomas *et al.*, 1984a] and calculated O_3 mixing ratios near 85 km as a function of season at mid-latitude. From Garcia and Solomon (1985).

shows SME ozone data at ~ 80 km compared with model calculations. The qualitative agreement is excellent with maxima in March and September, corresponding to times of weak winds in the middle atmosphere and hence enhanced absorption of propagating gravity waves. This absorption leads to reduced gravity wave breaking, and hence mixing, in the upper mesosphere. Water vapour, and hence hydrogen radicals, are then reduced in the spring and autumn, leading to enhanced O_3.

Finally, the work of Plumb and Mahlman (1985) should be stressed. They are developing a model whose transport is derived from general circulation model statistics. This has the advantage that the transport circulation can be derived self-consistently with the K tensor (see Section 6.6.2). It is expected that this approach will continue to yield much useful information about stratospheric transport processes and their inclusion in two-dimensional models. A disadvantage of the model is that the validity of the transport depends on the GCM, with its own strengths and weaknesses.

This review of current two-dimensional modelling efforts suggests two conclusions, one general and one specific. Firstly, it is clear that the variety of models, using sometimes quite different approaches, has contributed to the understanding of stratospheric processes. The richness of approach is an advantage and no one approach can necessarily be regarded as always superior. This is particularly exemplified by simple model experiments where the nature of the feedback processes is the important consideration.

Secondly, major problems are still associated with the treatment of eddy processes. This applies to whichever two-dimensional approach in followed. The residual circulation approach has the advantage that the steady, conservative waves need not be considered. However, it is precisely the situations when the non-acceleration conditions break down that the eddies are important and need to be treated. A consensus appears to be developing, based on observations, general circulation model results and experience with 2-D models, that smaller K values should be used in residual circulation models with perhaps Kyy being a few $\times 10^5 m^2 s^{-1}$ (but see the comments above). It must be stressed that this smaller Kyy does not mean that the modelled eddy transports are any less important. This is shown by reference to Figure 12-15. The model is still sensitive to the choice of Kyy for species with large mean latitudinal gradients.

Some current residual circulation models employ constant K coefficients. Plumb and Mahlman's results argue against this, and this too is perhaps supported by Figure 12-15 where a Kyy increasing in the winter subtropics might produce a better fit to the data.

The progress in recent years is encouraging. For example, the consensus regarding the size of Ks is based not just on experience with models but also on theoretical arguments or models in which the large scale waves are treated explicitly. Despite some difficulties, it can be said that two-dimensional modelling is on a firmer footing than hitherto. While much work remains to be done, the physical basis of the models and, perhaps as important, the model limitations (most important being the treatment of non-conservative eddy processes) are generally well understood.

12.6 A COMPARISON OF TWO-DIMENSIONAL MODELS

The models discussed in this section are shown in Table 12-3.

(i) *Source gases*

The simulation of long-lived trace gases gives a good indication of the diversity of two-dimensional models. It also indicates a chief advantage of two- over one-dimensional models: the ability to simulate latitudinal

Table 12-3. 2-D Models Used In This Report

	TYPE	INVESTIGATORS
MPI	Eulerian	Schmailzl, Crutzen
RAL	Eulerian	Gray, Pyle
AER	Eulerian	Ko, Sze
L'Aquila	Diabatic	Visconti
EERM	Diabatic	Cariolle
GSFC	Diabatic	Guthrie
Du Pont	Diabatic	Owens
NOCAR	Residual Circulation	Garcia, Solomon
AER	Diabatic, Isentropic	Ko, Sze, Tung
Oslo	Diabatic	Stordal, Isaksen
RAL	Diabatic	Rogers, Pyle

and seasonal variations. In this section we will concentrate on model results for the long-lived tracers N_2O, CH_4, CFC-11 and CFC-12. The calculations that will be discussed were nominally performed with the same set of chemical reaction rate constants, solar fluxes, and photolytic absorption cross sections (see Appendix A and Chapter 7), so model differences due to chemistry have been minimized. There are still some differences, including the radiative treatment, diurnal model formulation, and treatments of the Schumann-Runge bands, as discussed in greater detail below.

For the simulation of source gases, two-dimensional models fall roughly into two general classes - those in which advection and diffusion play approximately equal roles, and those in which advective transport dominates. The former include classical Eulerian models (eg. MPI, RAL) and those with a diabatic circulation but with eddy diffusion coefficients of the same order as those of Eulerian models (eg. Du Pont, EERM) while the latter (eg. L'Aquila, LLNL, NASA GSFC, the NOAA/NCAR model (NOCAR), Oslo) use diabatic or residual circulations and small eddy diffusion coefficients ($Kzz \sim 10^{-1} m^2 s^{-1}$ $Kyy \sim 10^5 m^2 s^{-1}$. $Kyz \sim 0$). These coefficients are about a factor of ten smaller than in the former models. The advective models have a Brewer-Dobson type atmospheric circulation, with rising air motions in the tropics and descending motions towards the poles.

Long-lived trace gases with sources in the troposphere (eg. N_2O, CH_4, CFC-11, CFC-12) are injected into the stratosphere primarily in the tropics (20 °S to 20 °N). As the tropical air parcel is transported upward by the mean circulation, destruction of source species occurs by photolysis or reactions with $O(^1D)$ and OH. Destruction continues as the parcels are advected poleward in the stratosphere, and the parcels then descend at high latitudes with lower concentrations of the source gases. The source gas mixing ratios are thus greater at the equator than at the poles, and the isolines descend to lower altitudes near the poles.

In models with larger eddy coefficients, horizontal mixing reduces the equator-to-pole gradients, giving flatter isolines. For all the source gases, as will be discussed below, this same general picture emerges.

Figure 12-18 shows the calculated N_2O mixing ratio as a function of altitude and latitude for July in three models, two (GSFC, NOCAR) advective and one with large eddy diffusion (Du Pont). The advective

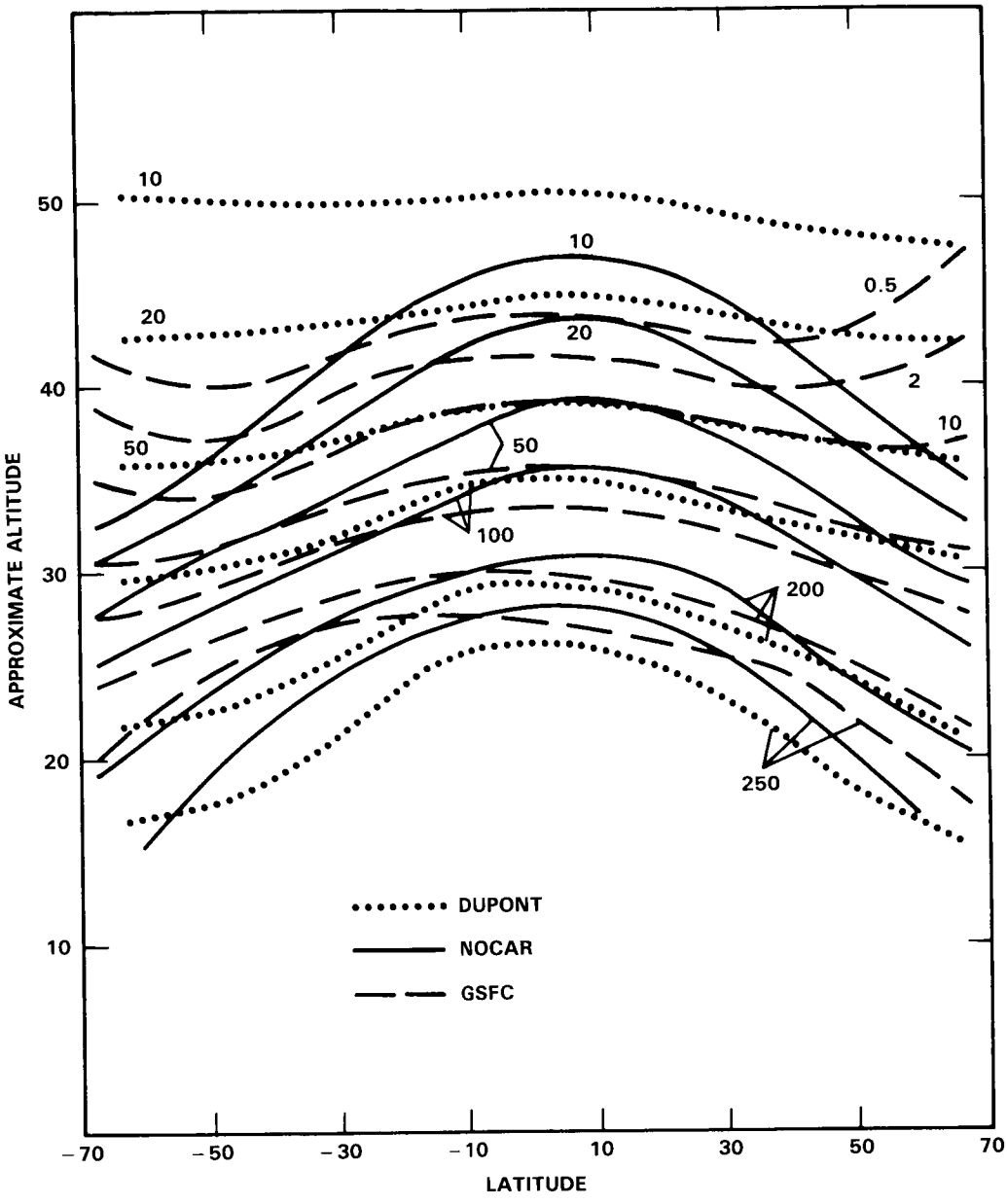

Figure 12-18. Latitude-height cross-section of the N_2O distribution (ppbv) from three different 2-D models.

models gives more rapidly downward-sloping contour lines at low and mid latitudes. The NOCAR model in particular strongly mirrors the underlying equator-to-pole circulation. Toward the poles, the upturn in the GSFC model is due to the structure of the Murgatroyd and Singleton (1961) wind field.

Figures 12-19a and 12-19b show the vertical profiles of N_2O calculated by several of the models at the equator and midlatitudes, respectively. Because of the differing latitudinal gradients illustrated in Figure 12-18, there is a large spread in the predicted profiles, especially in the mid to upper stratosphere. The

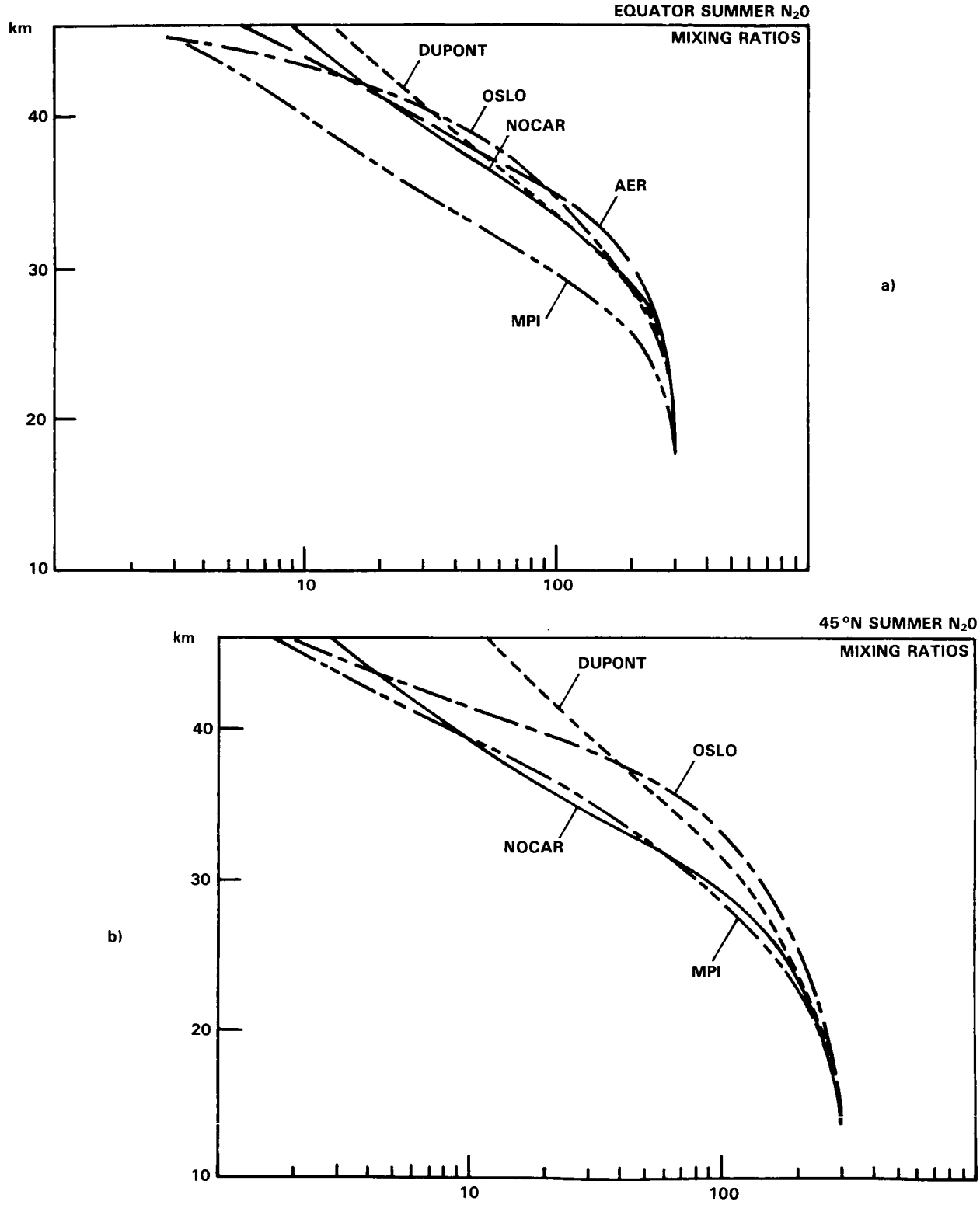

Figure 12-19. Vertical profiles of N_2O (ppbv) calculated by various models. a) Summer, 0°; b) Summer, 45°N.

model range approaches a factor of two for both low and mid latitudes at 30-35 km altitude and a factor of four at 40 km.

A latitude section of the modelled N_2O mixing ratio at the 35 km level is shown in Figure 12-20. The latitudinal distribution is quite flat in the MPI (Eulerian) model, although considerably more structure is evident between 30S and 30N in RAL's classical Eulerian model. Interestingly, the RAL model has similar structure in this low-latitude region to the residual circulation NOCAR model. In high latitudes the models are quite different, with the NOCAR model showing a continued decrease. The RAL model, with a strong high latitude indirect cell, predicts increasing N_2O with latitude.

An interesting feature of the satellite observations of N_2O is the presence of a 'double peak' structure in March, April and May when, on a given pressure surface, there is a local minimum in mixing ratio at the equator with maxima in the sub-tropics. This is in contrast to the usual situation with a single low latitude maximum. Jones and Pyle (1984) discussed this feature in detail. Using a classical Eulerian two-dimensional model they were unable to reproduce the double peak. Using the same model, Gray and Pyle (1985) have now satisfactorily modelled the feature (Figure 12-14). They hypothesise that it is related to the low latitude semiannual oscillation. The circulation induced by a low latitude westerly forcing (chosen to reproduce the observed semiannual oscillation of the zonal wind) has descending motion at the equator, sufficient to produce the local minimum there. The model also reproduces somewhat similar features in CH_4 and O_3 and leads to a significantly improved low latitude seasonal variation.

Some representative mixing ratio cross sections for CH_4 are shown in Figure 12-21. As is the case for N_2O, the residual circulation model (NOCAR) shows a much larger latitudinal gradient than the classical Eulerian model (MPI). The large difference in latitudinal gradient between a model with large eddy diffusion values (Du Pont) and one with small coefficients, both using essentially the same wind field, is shown

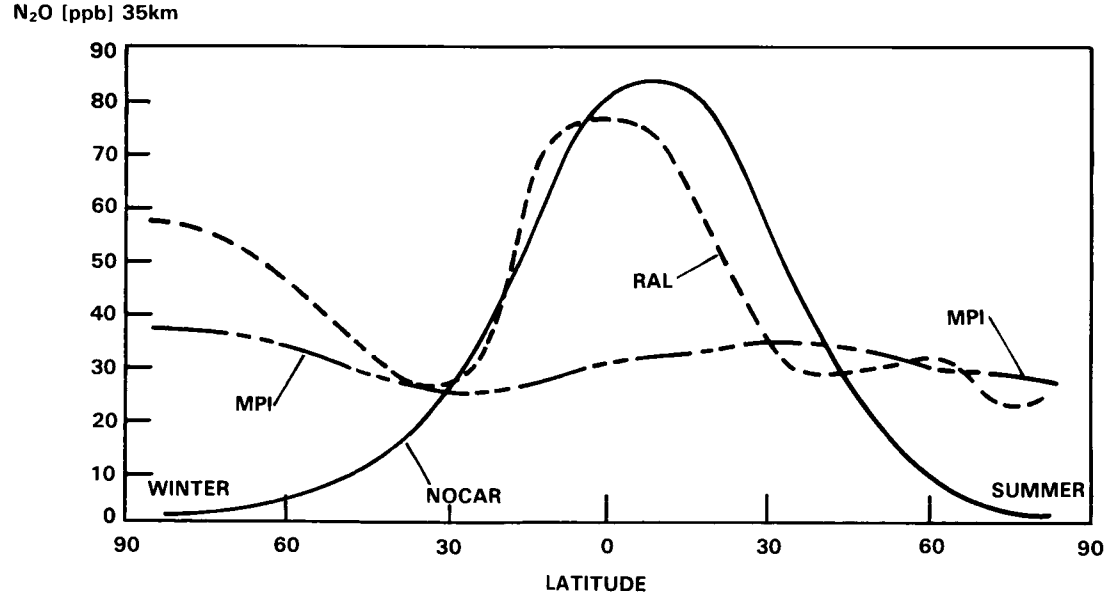

Figure 12-20. Latitude section of N_2O volume mixing ratio at 35 km for three different 2-D models.

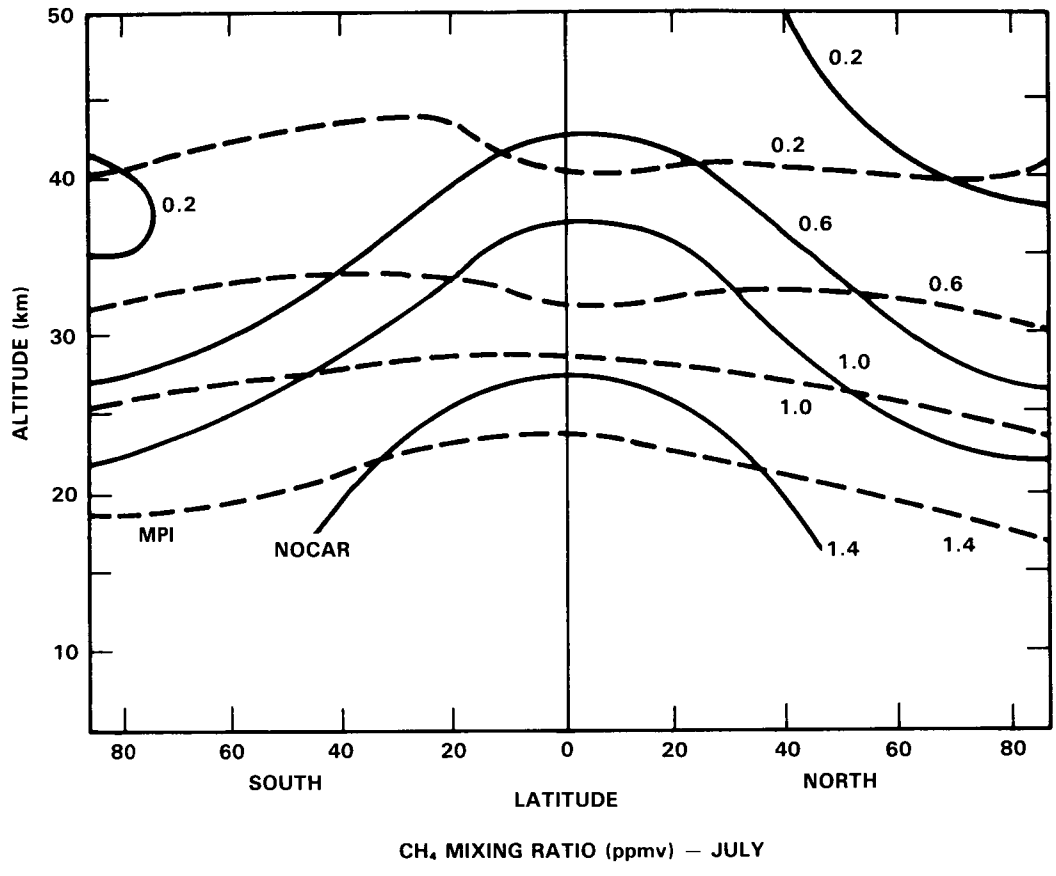

Figure 12-21. Cross-sections of CH_4 from the MPI and NOCAR 2-D models.

in Figure 12-22. While the latitudinal change from equator to 60 degrees at 40 km altitude in the summer hemisphere is less than a factor of 2 in the Du Pont model, it is an order of magnitude in the GSFC model. This large difference in model predictions for CH_4 in the upper stratosphere is one point on which satellite data may provide a significant test.

Vertical profiles for methane computed in several models are shown in Figure 12-23 for the equator and midlatitude (summer). The models with classical diffusion coefficients (Du Pont, RAL) fall off far less rapidly above 40 km than the residual circulation model (AER). The range of model predictions approaches a factor of 2 at midlatitudes near 30 km, while at the equator all the models agree within about 50% for all altitudes below 40 km. At higher latitudes, the upper-stratospheric differences between the various model predictions are considerably larger.

The modelled vertical profiles for CFC-11 at the equator and 45 °N are shown in Figure 12-24. There is good agreement between the models (after scaling to the same tropospheric mixing ratio) at midlatitudes, with agreement at all altitudes better than a factor of two. Model agreement is not so good at the equator or at high latitudes. The reason for the good gross agreement between models for CFC-11 may be its relatively rapid destruction rate in the lower stratosphere, so that its vertical profile is dominated by the photochemical sink. Nevertheless, important differences in transport are evident in discrepancies between the models.

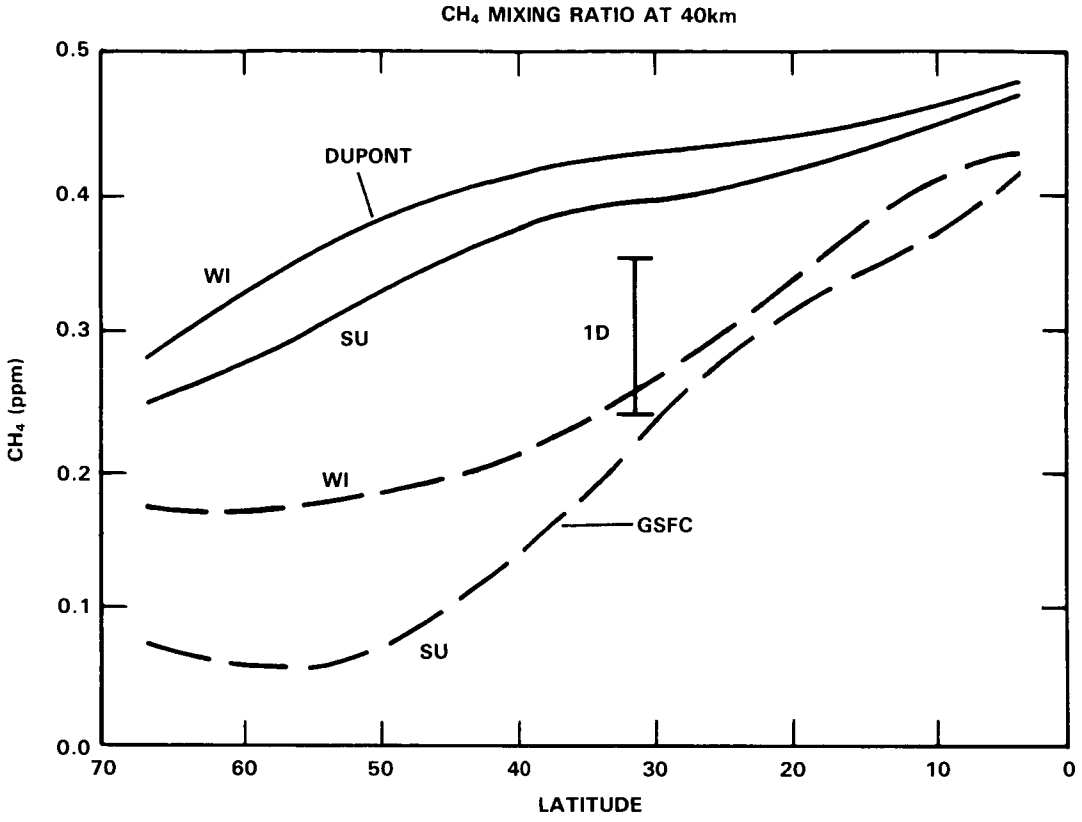

Figure 12-22. CH_4 mixing ratios versus latitude at 40 km for two different models for winter and summer. The range of 1-D model values is also shown.

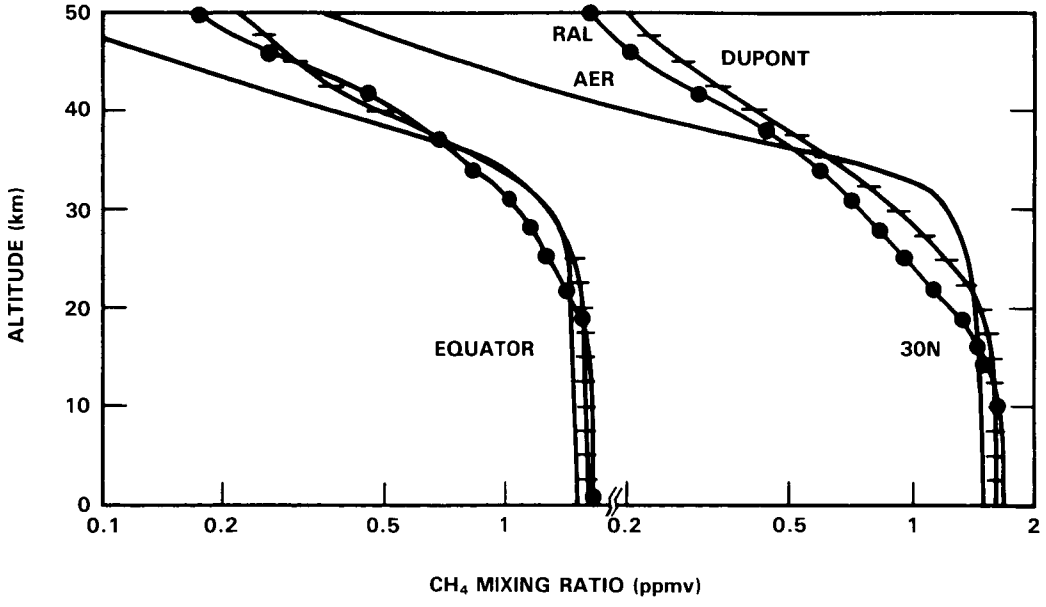

Figure 12-23. Vertical profiles of CH_4 calculated by various models at the equator and 30°N.

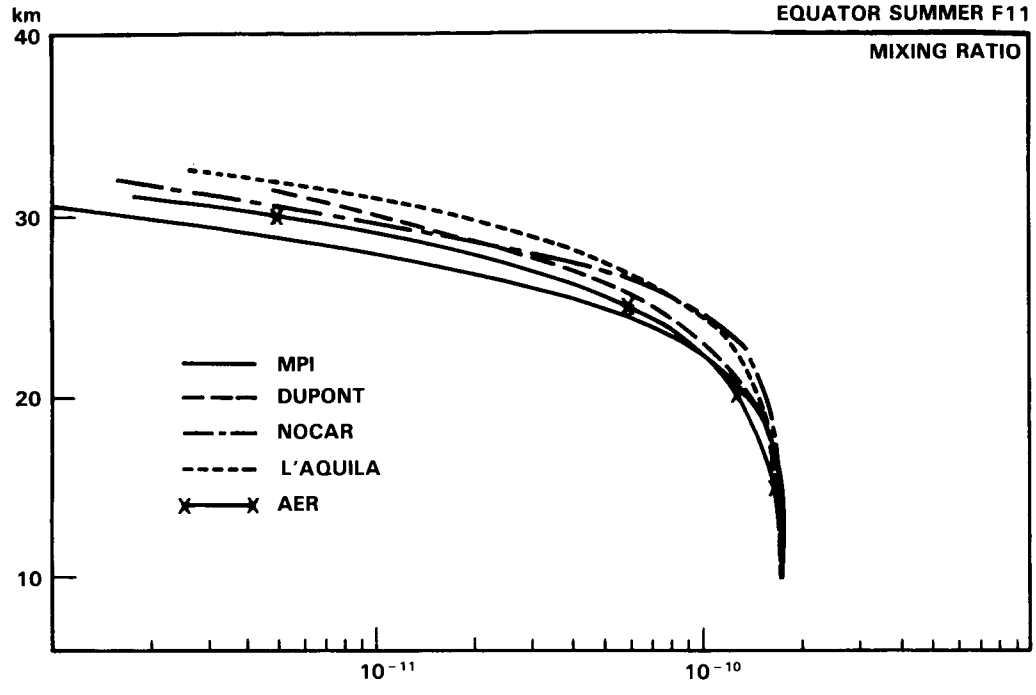

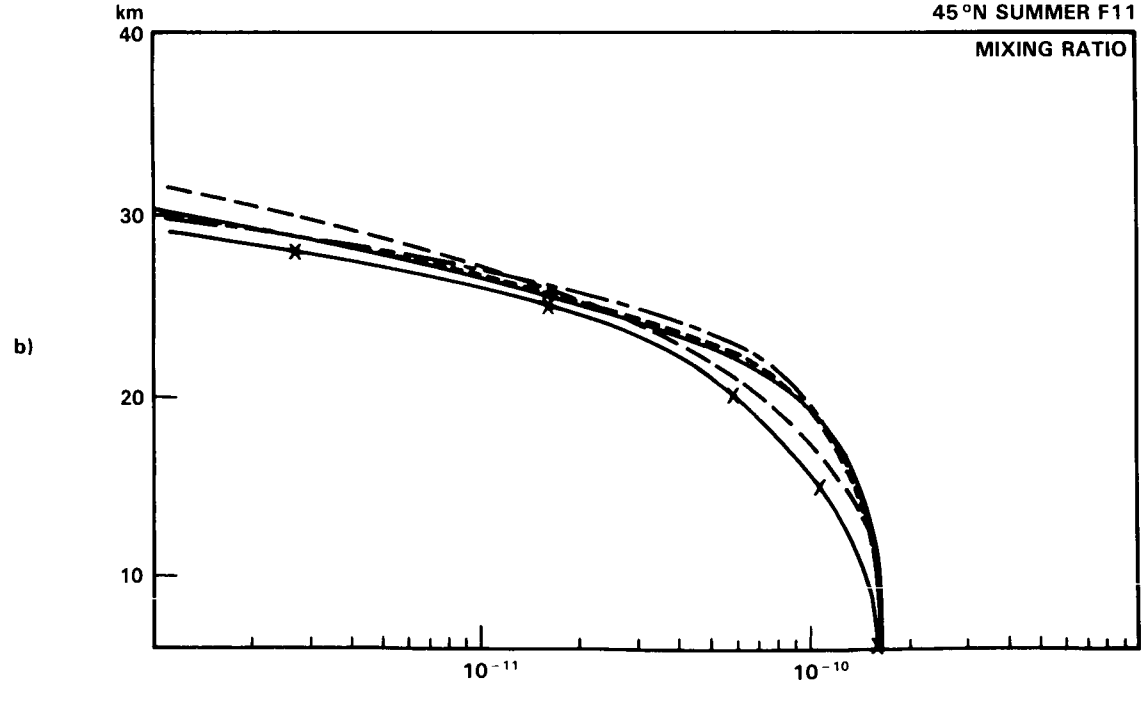

Figure 12-24. Vertical profiles of $CFCl_3$ volume mixing ratio calculated by various models. a) Summer, 0°; b) Summer, 45°N.

For the longer-lived CFC-12, the model agreement is poorer at both equatorial and midlatitudes, as shown in Figure 12-25. As is the case for N_2O, a greater latitudinal gradient is shown by the residual circulation models. The model range is a factor of two at 25-30 km and continues to be large at higher altitudes. The difference in latitudinal gradient between Eulerian (MPI) and residual (NOCAR) transport schemes are shown in Figure 12-26. At 25km altitude, the modelled equatorial values of 200ppt decrease to 40 ppt at 50 degrees latitude for the NOCAR model but only to 140 ppt for MPI.

In summary, there is a distinct difference in the results between models with large eddy diffusion compared with those with small eddy diffusion. The latter consistently show larger latitudinal and seasonal variations in the middle and upper stratosphere, as expected. Differences are still found between models of the same basic type. For example, for long-lived tracers with sources in the troposphere, the diabatic circulation in some models produces an upward bend in the isolines, while the residual circulation in other models gives isolines that continue to slope downward toward the pole. Furthermore, general conclusions regarding the relative performance of classical Eulerian compared with the transformed models are difficult to make. For example, there is some suggestion that the satellite CH_4 and N_2O data show latitudinal gradients more characteristic of the advection-dominated models, although there are still important differences from model to model. Moreover, the classical Eulerian RAL model reproduces the CH_4 and N_2O data well. In fact, in low latitudes, the satellite data shows flatter fields than are found in the model (Jones & Pyle 1984). Of course, the argument is not really about the size of the eddy diffusion but about the balance between mean and eddy transport.

One of the major problems in developing a diabatic circulation model is the lack of a definitive set of self-consistent atmospheric heating and temperature fields. The Murgatroyd and Singleton wind field, used in many models (Du Pont, EERM, LLNL, NASA, Oslo), is based on very old data and does not give a summer stratosphere near radiative equilibrium, as recent studies have implied. For diagnostic studies in the near term, more realistic ozone fields and more sophisticated radiation schemes for infrared cooling should provide an improved estimation of stratospheric winds.

Because of the large differences in source gas latitudinal gradients predicted by the models with either large or small horizontal and vertical mixing, satellite data with good coverage of the globe (from, e.g. SAMS and LIMS) should prove useful in validating transport schemes. The satellite data have already become a useful tool for testing 2-D models and their transport schemes.

In this discussion, we have not mentioned one-dimensional models. Three one-dimensional models (Du Pont, Harvard, LLNL) were compared with the mid-latitude vertical profiles shown in Figures 12-19, 23, 24 and 25 (for N_2O, CH_4, CFC-11 and CFC-12). In general, the 1-D models fall within the range of values spanned by the 2-D models and have a similar degree of consistency within themselves. The long standing problem of simultaneously fitting the observed midlatitude vertical profiles of these four tracers using the same eddy diffusion profile is shared to some extent by two-dimensional models. In two dimensions, it is, for example, possible for a model to fit the midlatitude profiles of these species satisfactorily (eg. Guthrie *et al.*, 1984), but then to have difficulty in reproducing the profiles at lower and higher latitudes.

(ii) HO_x

The models show striking similarity in the morphology of the HO_x distributions. Figure 12-27 shows a height-latitude cross-section for daytime average OH. The salient features are the broad peak between 40 and 45 km, the steep gradient toward the winter pole, and the saddle-shaped minimum near the tropopause.

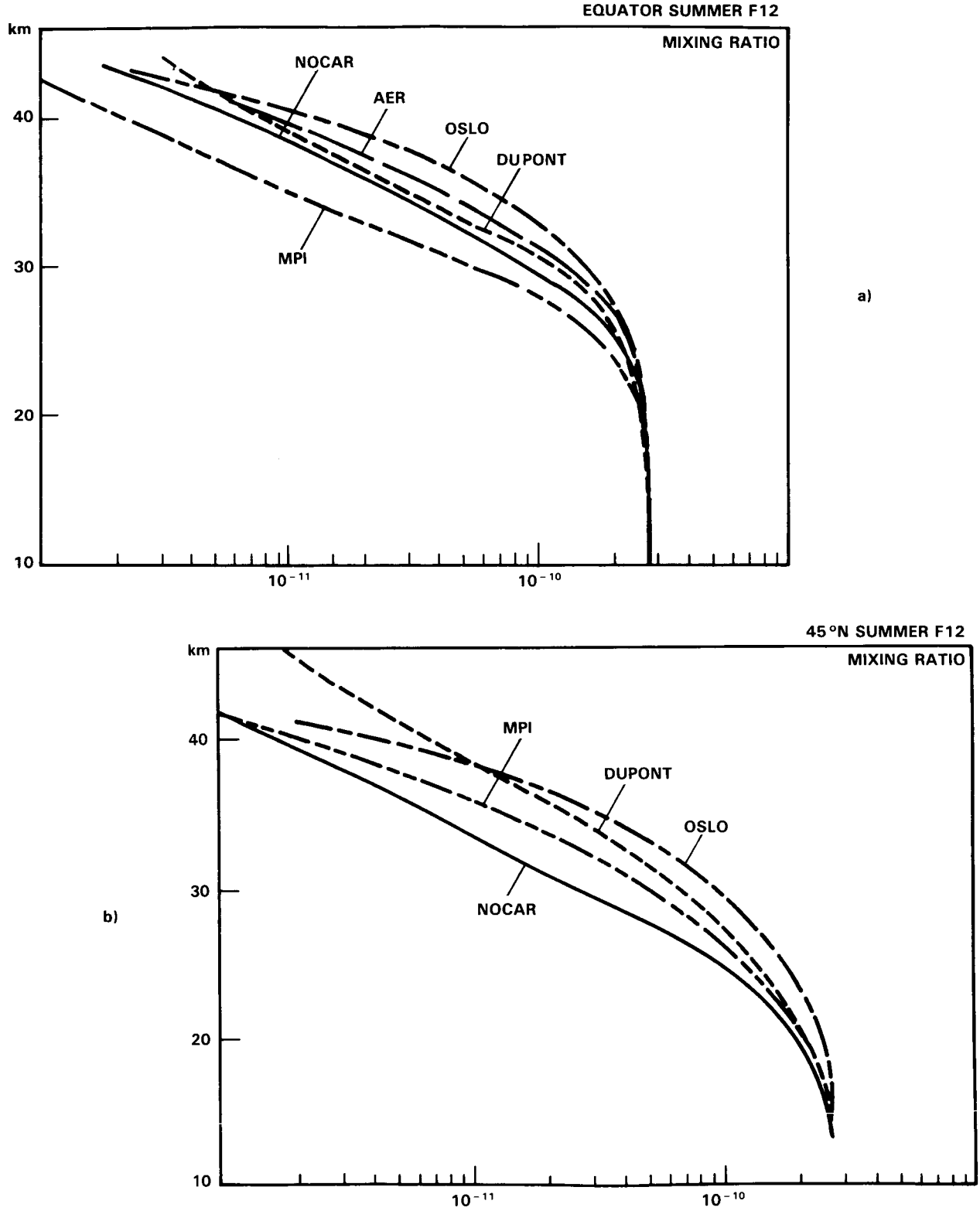

Figure 12-25. Vertical profiles of CF_2Cl_2 volume mixing ratio calculated by various models. a) Summer, 0°; b) Summer, 45°N.

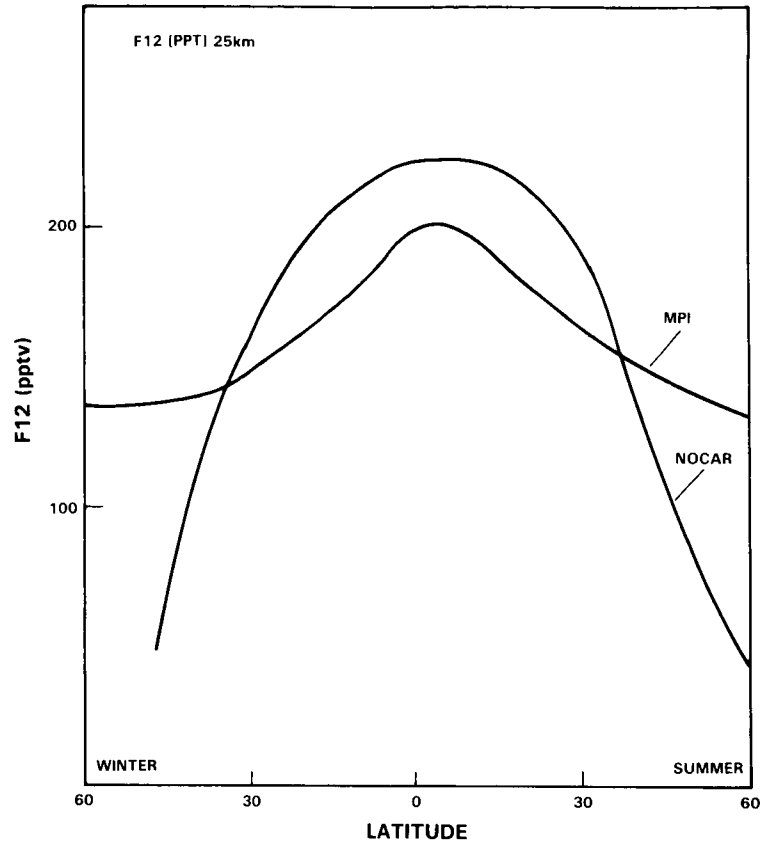

Figure 12-26. Latitude section of CF_2Cl_2 volume mixing ratio at 25 km for the MPI and NOCAR models.

All of the models considered here show peak values of 2 to 2.5 $\times$ 10^7 molecules/cm^3. The exact height of the saddle minimum and the slope of the poleward decrease at the saddle vary slightly between models, (presumably due to small differences in ozone, water vapour, and temperature distributions).

Similar structures appear in the HO_2 and H_2O_2 cross sections, although the peaks are substantially broader and flatter than in the case of OH (Figures 12-28 and 12-29). As might be expected, the centroids of the distributions follow the sun northward and southward through the course of a year with little or no phase lag.

In comparing the model distributions with available data, some discrepancies appear. The range of model profiles for daytime average OH is shown in Figure 12-30, along with measurements. The agreement seems quite good, with the intermodel range and the range of the measurements being quite comparable (see Chapter 9 for a more complete discussion).

The situation seems quite different for HO_2 (Figure 12-31). The models again agree well with each other but there is barely overlap between the range of model profiles and the range of measurements, although the available measurements are extremely limited. The difference between range centers is at least a factor of three and approaches an order of magnitude. Both ranges (model and measurement) include seasonal differences.

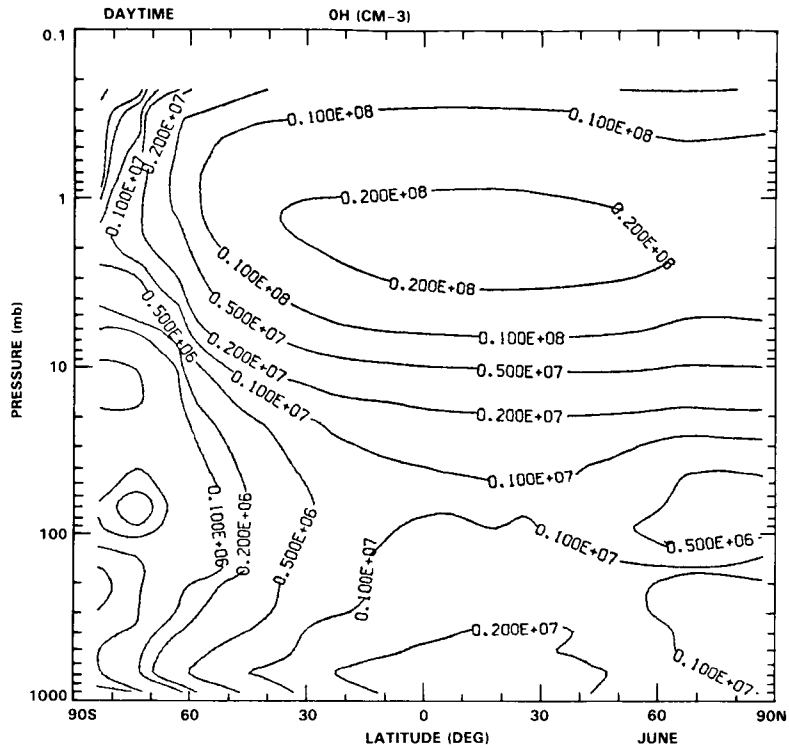

Figure 12-27. Latitude-height cross section of daytime average OH (molecules cm^{-3}) from the GSFC 2-D model.

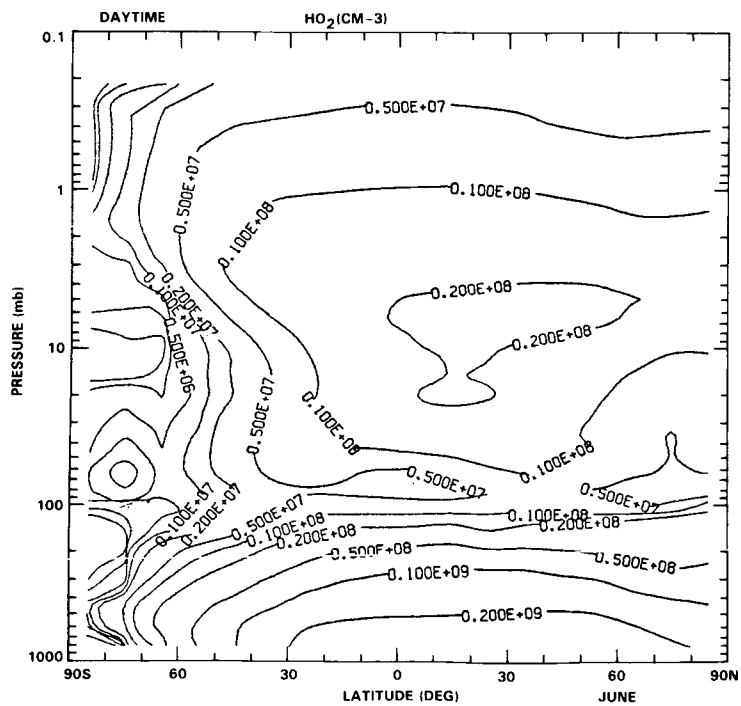

Figure 12-28. As Figure 12-27 for HO_2.

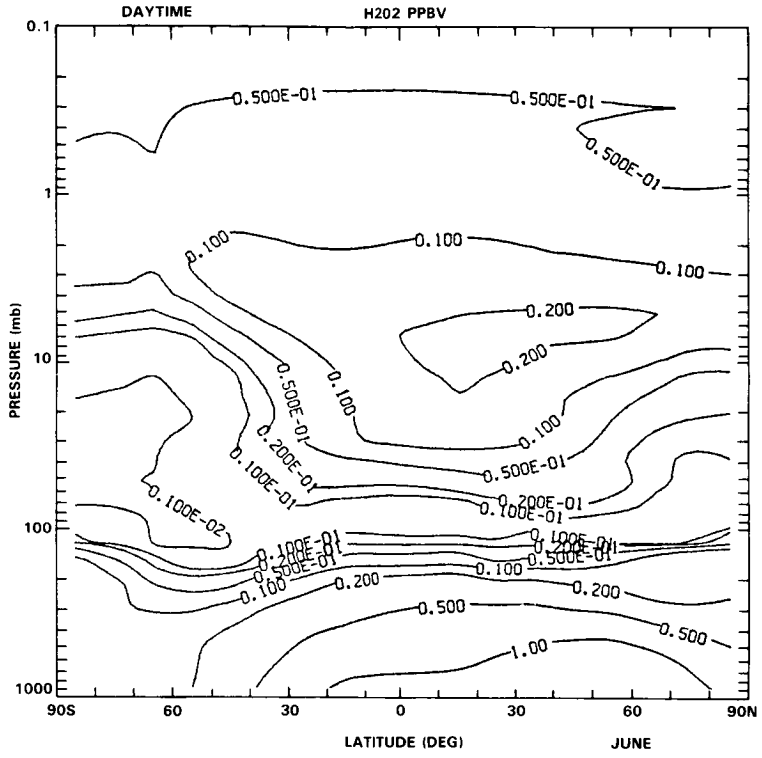

Figure 12-29. As Figure 12-28 for H_2O_2 volume mixing ratio (ppbv).

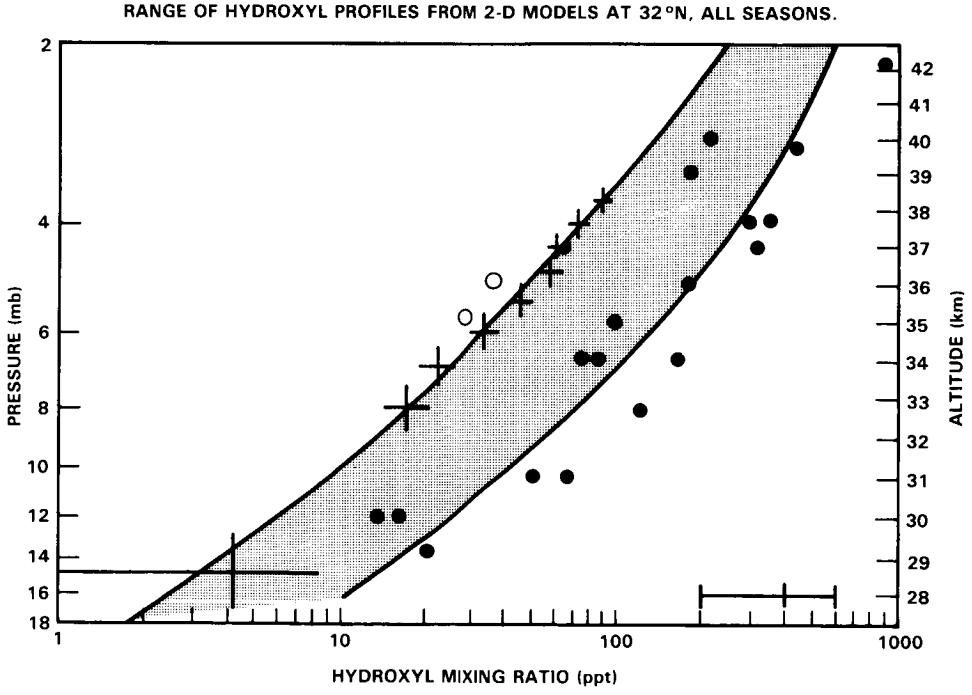

Figure 12-30. Shaded region shows the model range of 2-D model calculated OH at 32°N compared with available observations (see Chapter 9).

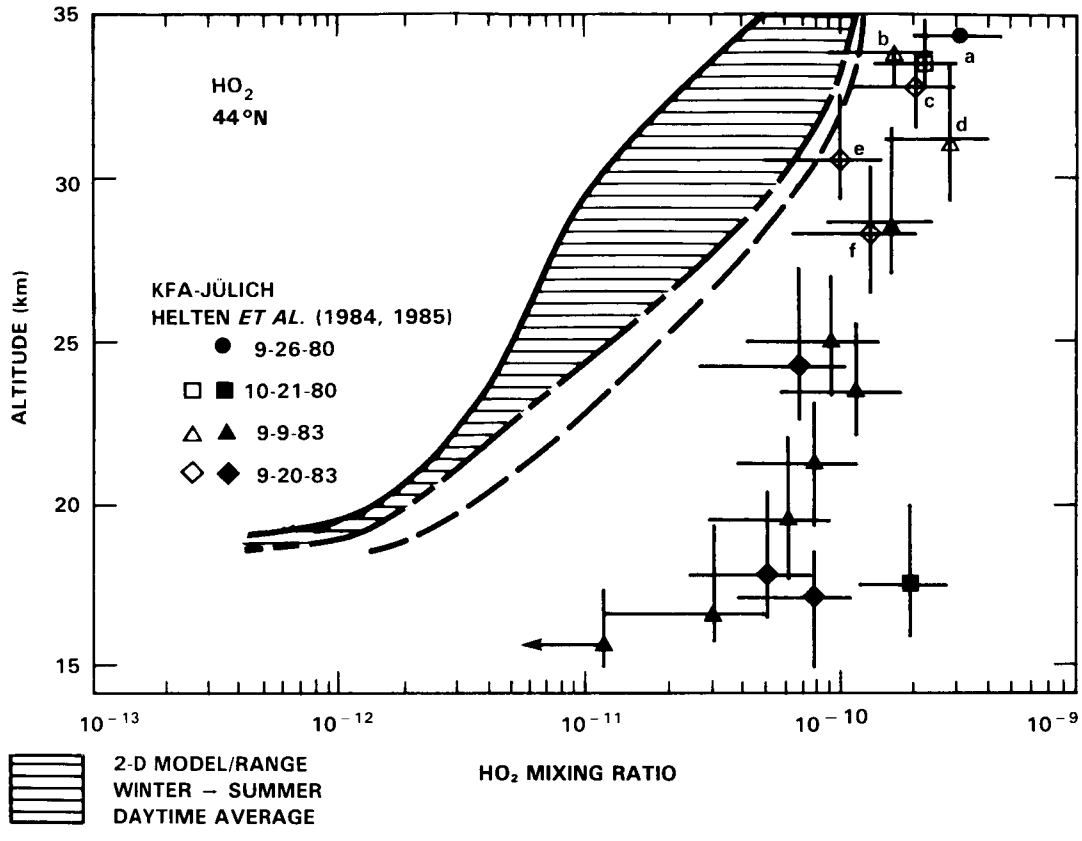

Figure 12-31. As Figure 12-30 for HO_2.

In the case of hydrogen peroxide (H_2O_2) the range, defined by reported detections and the upper limits from both Chance and Traub (1984) and de Zafra *et al.* (1984) is very broad and the detailed profile is essentially undefined. The range of model profiles for 30°N, winter is shown in Figure 12-32. Although the model range is fairly broad, it clearly falls above the upper limit of Chance and Traub between 24 and 32 km.

The increased model spread for H_2O_2 can be understood by the quadratic dependence of H_2O_2 on HO_2, and then on total HO_x. Any model differences in the production of HO_x (due, for example, to the different ozone distributions) or in the HO_2/HO_x ratio (due, for example, to differences in temperature distributions) will be magnified in the H_2O_2 comparison. It is this particular sensitivity which prompted the suggestion by Connell *et al.* (1985) that measurements of H_2O_2 along with other members of the HO_x family would make a very useful test of atmospheric chemistry.

If the difference between models and measurements persists with additional HO_2 and H_2O_2 measurements it will indicate a possible problem with our understanding of the partitioning of the HO_x family,

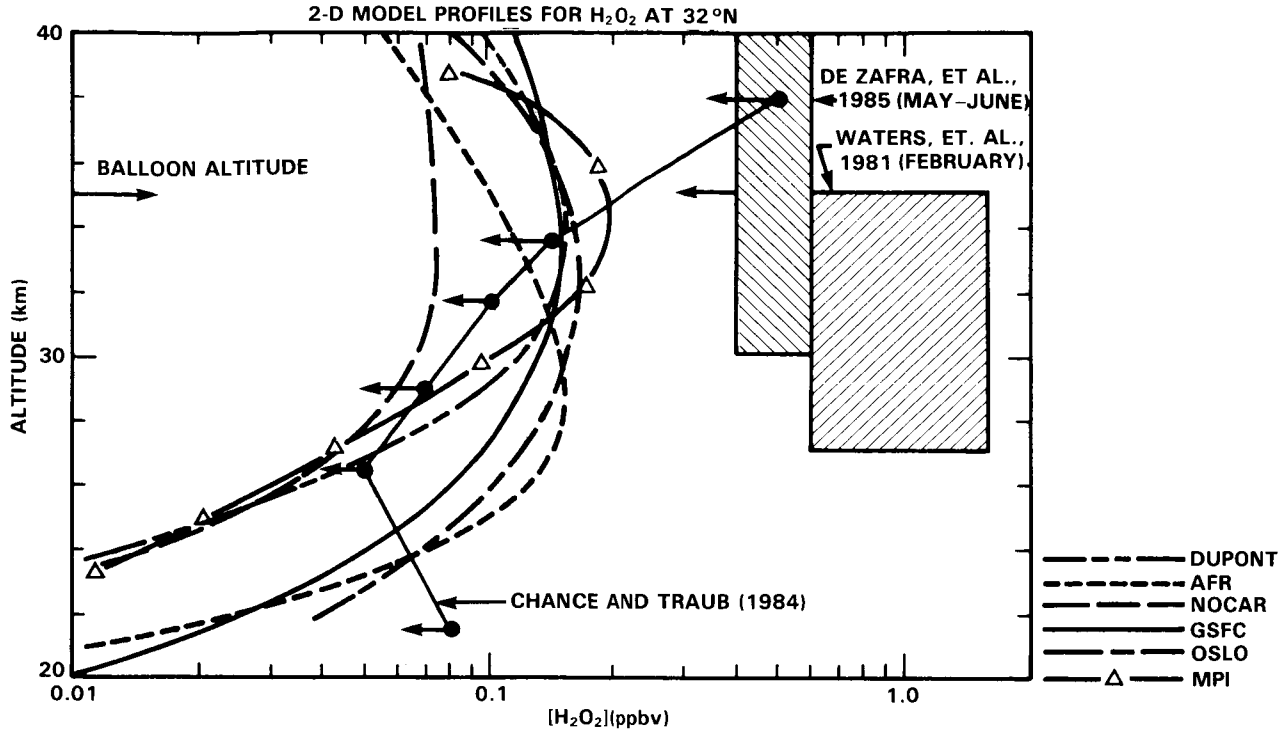

Figure 12-32. Range of 2-D model calculated H_2O_2 at 30°N, winter compared with measured upper limits.

although that partitioning would appear to be controlled by well-understood photochemical processes. This is discussed further in Chapter 9. Any such problem must be common to all the models given the agreement between them.

(iii) *Odd nitrogen*

In this subsection, distributions of odd nitrogen species calculated by a number of two-dimensional models will be compared. Differences in their behaviour will be discussed, with particular emphasis on the origin of variations in model calculated abundances of total odd nitrogen ($N+NO+NO_2+NO_3+2\times N_2O_5+HNO_3+HNO_4+ClONO_2$). This parameter is of critical importance to the ozone balance in the contemporary atmosphere, as well as to the evaluation of possible future perturbations in ozone.

Figure 12-33 presents contour plots of the NO_y distributions calculated in the models by Ko *et al.* (1985) and Gray and Pyle (1985), which are respectively formulated in the residual and classical Eulerian frameworks. Like CH_4 and N_2O, NO_y is very long-lived in the lower stratosphere, and its horizontal gradients depend sensitively on the competition between horizontal mixing and advection by the mean meridional circulation. Therefore the meridional cross section of NO_y calculated in the advection-dominated model of Ko *et al.* (1985) exhibits a steeper slope with latitude than does the classical Eulerian model.

Figure 12-34 presents vertical profiles of the calculated NO_y abundances from several two-dimensional models. The model by Pyle *et al.* makes use of the NO photolysis parameterisation of Cieslik and Nicolet (1973), while the others employ the parameterisation by Allen and Frederick (updated to account for re-

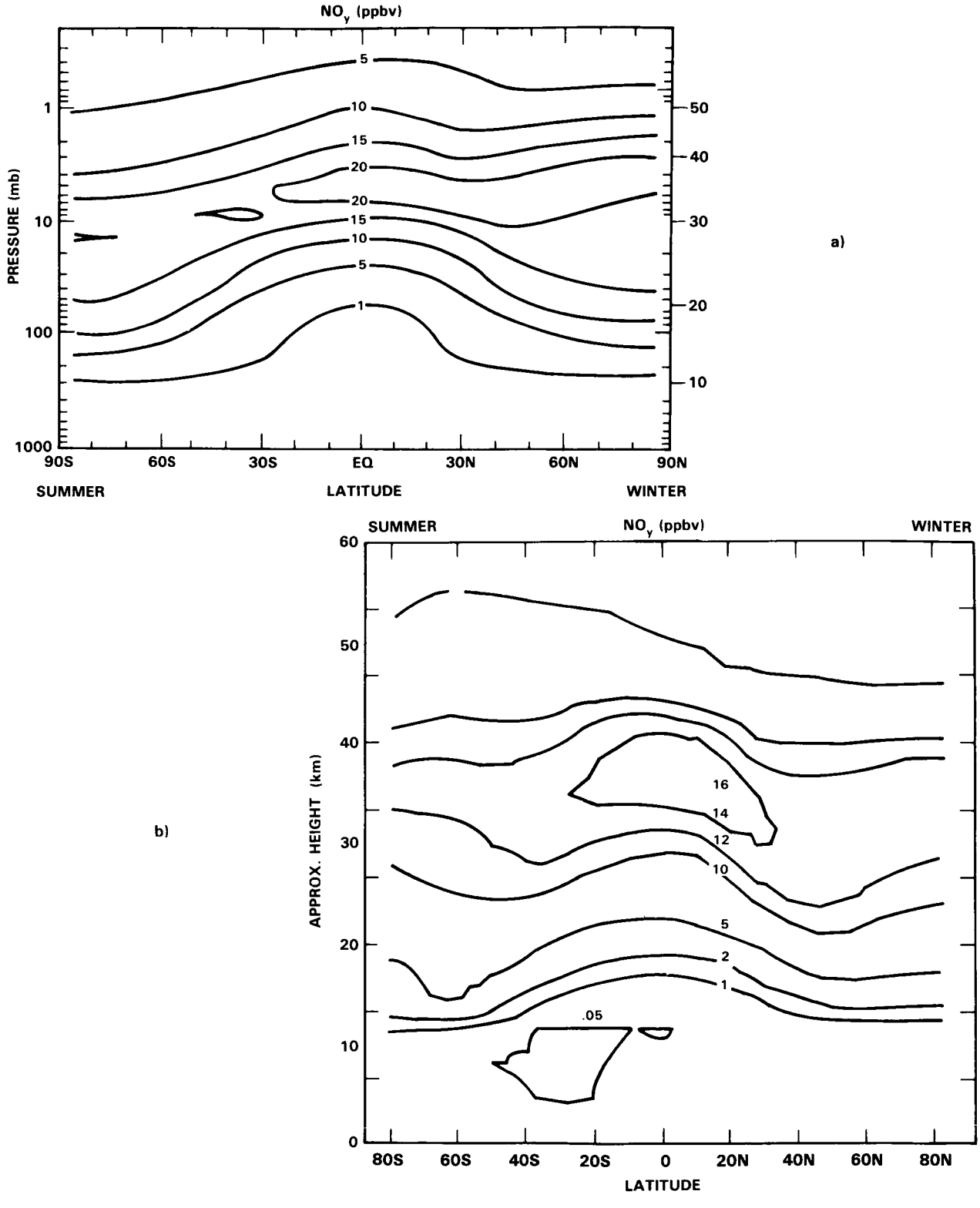

Figure 12-33. Latitude-height cross sections of NOy (ppbv) from a) The AER diabatic model (Ko *et al.,* 1985); b) The RAL Eulerian model.

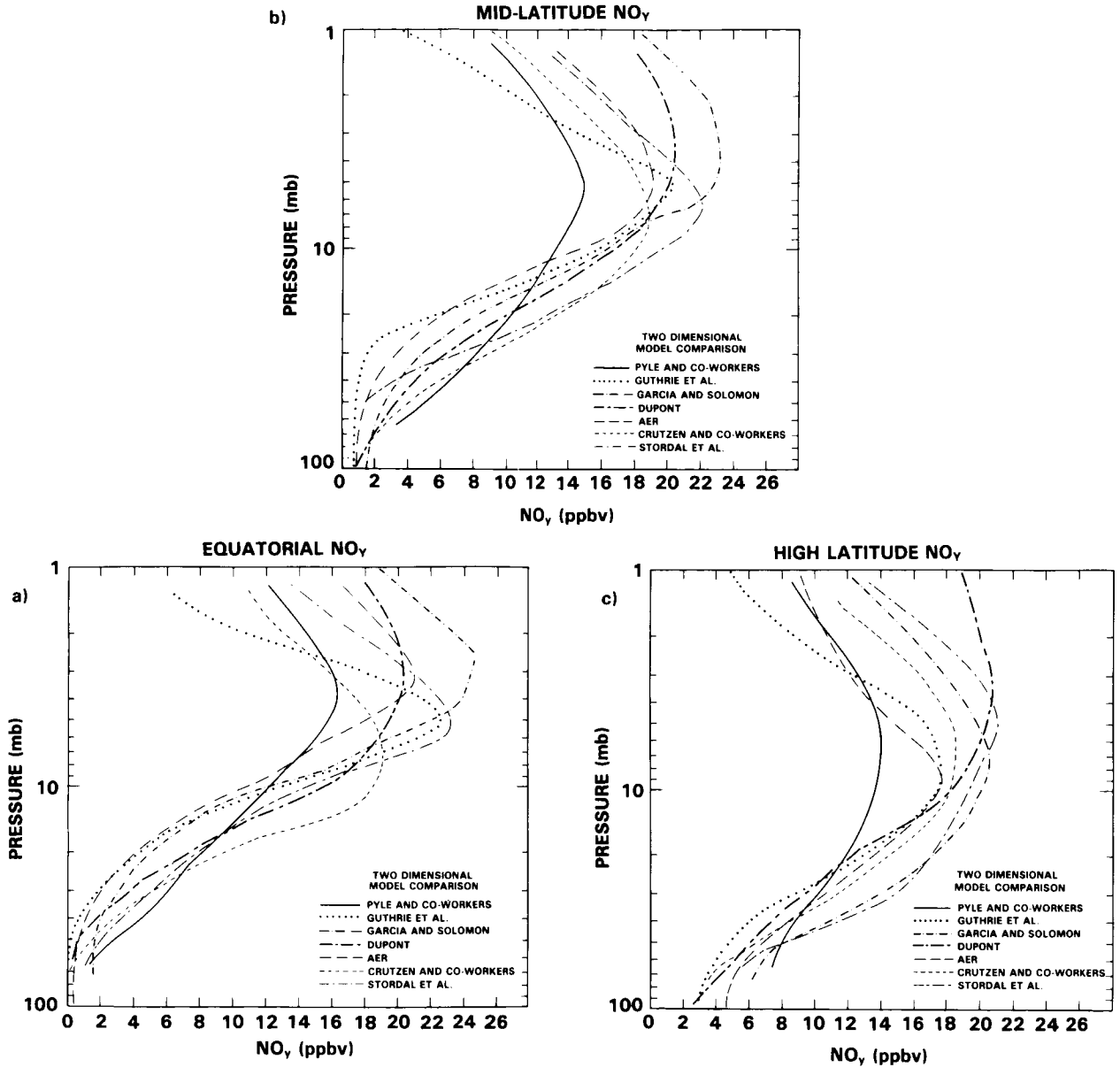

Figure 12-34. 2-D model profiles of NO_y at various latitudes. a) 0°; b) Mid-latitude, 26-35°N. c) High latitude

cent changes in our knowledge of the O_2 Herzberg continuum and Schumann-Runge band cross sections), or the similar parameterisation presented by Frederick *et al.* (1983a), which is used in the model of Garcia and Solomon (1983). The latter parameterisation includes the effect of self-absorption by the NO molecule, and the corresponding NO photolysis rates are therefore smaller (order of 40% for a 60° solar zenith angle without this effect near 40 km.). On the other hand, the NO photolysis rates obtained by Cieslik and Nicolet are larger than those presented by Frederick and co-workers in this region. As discussed in more detail in the subsection comparing one-dimensional models, the calculated abundance of NO_y near and above the peak at about 40 km is very sensitive to the NO photolysis rate, which controls the density

of atomic nitrogen and the loss of NO_y through the reaction N+NO. The model variations in NO_y abundance near the peak are consistent with these differences in the adopted photolysis rates.

Another factor that plays a critical role in the differences between modelled NO_y abundances, particularly in the lower stratosphere, is the approach taken for the transport of NO_y and for the HNO_3 rainout around the tropical tropopause region. This is perhaps easiest to examine conceptually by assuming transport in the residual Eulerian framework. The air parcels entering the stratosphere probably do so principally in the tropics, as discussed above. In residual Eulerian models, then, the NO_y mixing ratio of air ascending into the lower stratosphere is highly dependent on the treatment of transport (i.e. the vertical velocity near the tropopause and the vertical eddy diffusivity between the tropopause and the NO_y peak near 40 km), and, on the treatment of HNO_3 rainout in the tropical upper troposphere. The meridional transport in the lower stratosphere has equator to poleward flow in both hemispheres in such models (and the rate of vertical eddy mixing is very slow by comparison), so that the NO_y content of the extra-tropical lower stratosphere will also be strongly influenced by variations in the NO_y that is input in the tropics. These effects should be expected to be less pronounced in classical Eulerian models due to more mixing, both in the vertical and horizontal directions. These differences are clearly manifested by the comparison of the calculated NO_y abundances of the models of Guthrie *et al.* (residual Eulerian with rapid HNO_3 rainout in the tropics) and Pyle *et al.* (classic Eulerian with slower HNO_3 rainout). The Garcia-Solomon model has no troposphere, and prescribes an inflow of NO_y at the tropical tropopause as a boundary condition, based on the measurements reported by Loewenstein *et al.* (1978a).

In the low stratosphere, the NO_y budget is a balance between slow photochemistry and slow vertical transport. Given the great difficulty in modelling the net radiation sources and sinks in the equatorial lower stratosphere (Houghton 1978) which determines the vertical velocity in these models, the large differences in NO_y shown in Figure 12-34 are not surprising.

More recently, the LIMS data on NO_2 and HNO_3 have become available, providing a database against which our knowledge of NO_y may be tested. These data will be discussed in Chapter 10 and compared to the models. It should be noted that a more complete database of NO_y, particularly around the tropical tropopause and lower stratosphere, could be of great value in improving our knowledge of this very important aspect of stratospheric modelling. That these fluxes are important in determining NO_y can be seen by results from the RAL model. Using the Allen & Frederick parameterisation instead of the Ciezlik and Nicolet values for NO photolysis, leads to an increase in NO_y at the peak of only $\sim$ 3ppbv and makes little difference to the slope of the profile.

The partitioning of odd nitrogen among NO, NO_2, NO_3, N_2O_5, HNO_4 and HNO_3 is determined largely by fast photochemistry (outside of the polar night region). The ratio of HNO_3 to NO_2 depends upon the model OH abundances and HNO_3 photolysis rates. Figure 12-35 presents a comparison of model calculated HNO_3/NO_2 ratios at about 30° in summer, showing that these models are in rather good agreement on this photochemical parameter. The differences are probably largely due to differences in calculated O_3 and associated optical depth effects. Figure 12-36 shows the HNO_3 profiles calculated by these models. Comparison of Figures 12-36 and 12-35 reveals that the differences in model HNO_3 profiles are driven principally by the calculated differences in NO_y, and thus similar ranges should be expected to apply to the calculated abundances of NO, NO_2, etc. Because of the large amount of data available for many of the NO_y species, presentation of the data and remarks regarding the comparison to models will be deferred to the chapter devoted to NO_x.

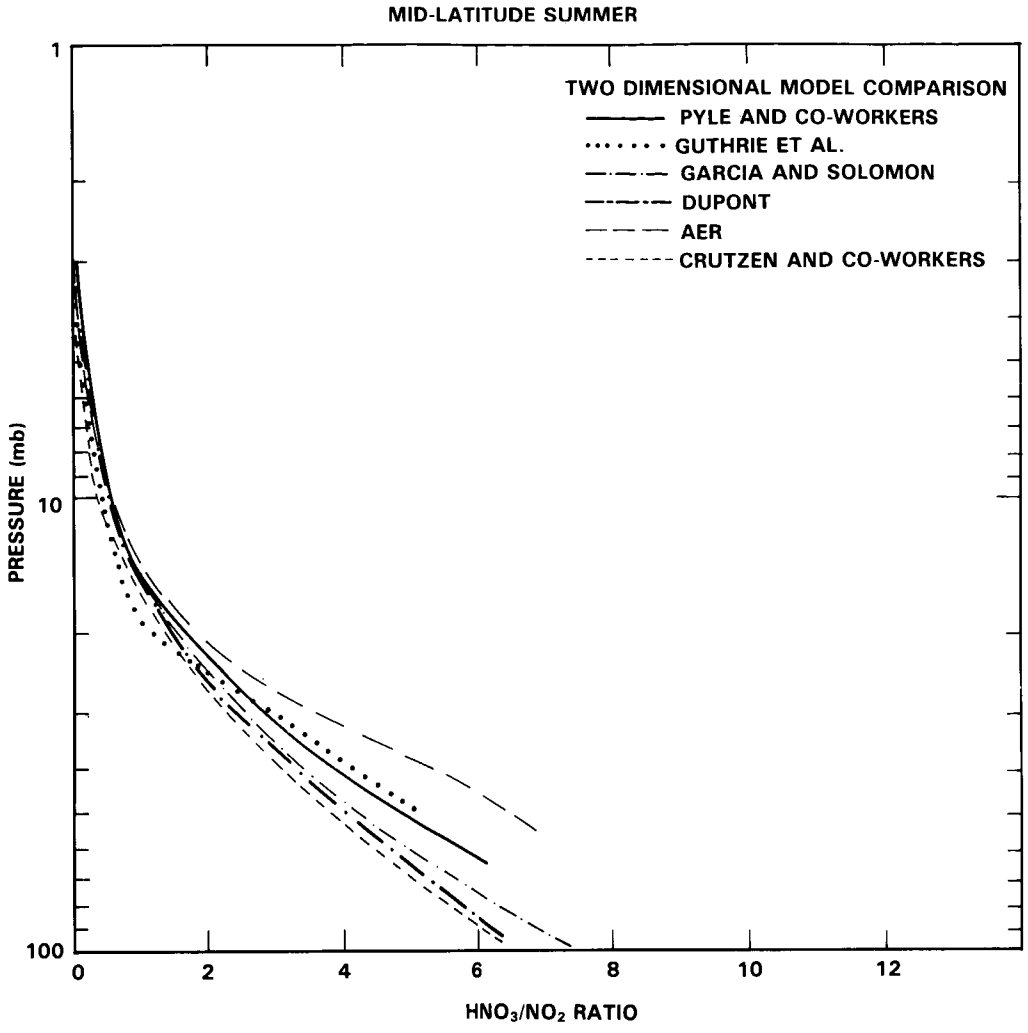

Figure 12-35. 2-D model profiles of HNO_3/NO_2 at ~30°, Summer.

Finally, we will briefly mention the morphology of a few constituents that have not yet been measured, at least not as a function of latitude. Figure 12-37 presents contour plots of the computed N_2O_5 distributions from the residual Eulerian model of Stordal *et al.* In addition to the variations in these constituents driven by the calculated gradients in NO_y (eg. Figure 12-34 above) and the sharply descending contours at high latitude characteristic of the residual circulation models, there are also strong variations with latitude which are due to calculated gradients in photochemical production and loss terms. This is particularly pronounced in the calculated N_2O_5 distribution in high latitude winter, where almost all the available NO_x ($N+NO+NO_2+NO_3+2 \times N_2O_5$) is chemically converted into N_2O_5 in present models.

The sequestering of NO_x in the N_2O_5 reservoir species has potentially important consequences on O_3 in high latitudes, as discussed by Ko *et al.* (1984) and suggests the need for global measurements of this species.

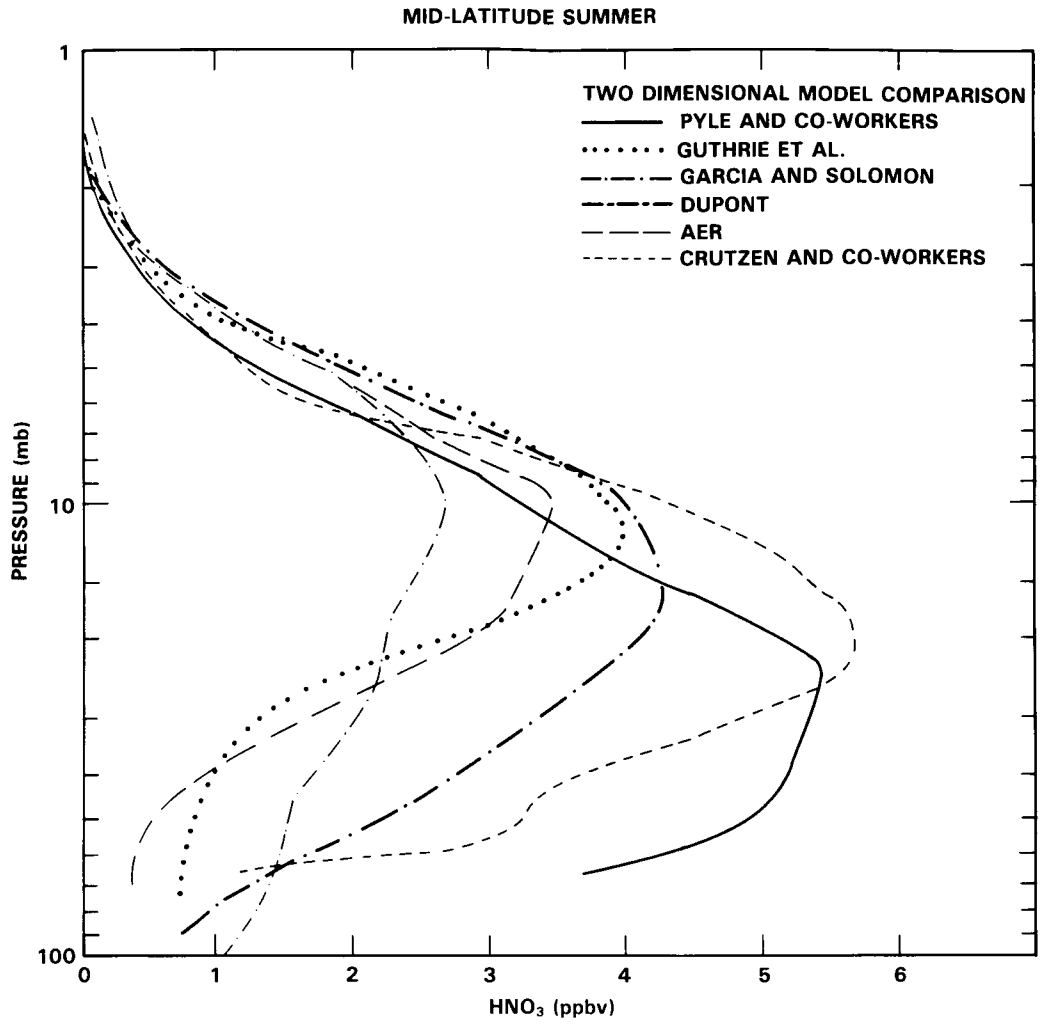

Figure 12-36. 2-D model profiles of HNO_3, ~30°N.

(iv) *ClO_x*

This subsection will provide an overview of model results for odd chlorine species, beginning with a discussion of the latitude-altitude distributions of the species from 2-D model calculations. The overall morphology of the species' behaviour as functions of altitude and latitude is sufficiently similar that only the results from one model (the AER model) will be given. In anticipation of the comparison of model results with observations to be presented in the ClO_x chapter (Chapter 11), a comparison of the calculated profiles for ClO, HCl, and $ClNO_3$ from different models will be presented. Detailed description of the diurnal behaviour of the chlorine species will be discussed in Chapter 11.

In the models, production of total chlorine (Cl_y) is from the photodecomposition of the halocarbons (CH_3Cl, CCl_4, CH_3CCl_3, F-11 and F-12) and removal is via transport into the troposphere followed by rainout and other deposition. Figure 12-38 shows the latitude-altitude cross-section of model calculated Cl_y. Cl_y is well mixed in the upper stratosphere because of the lack of photochemical removal processes.

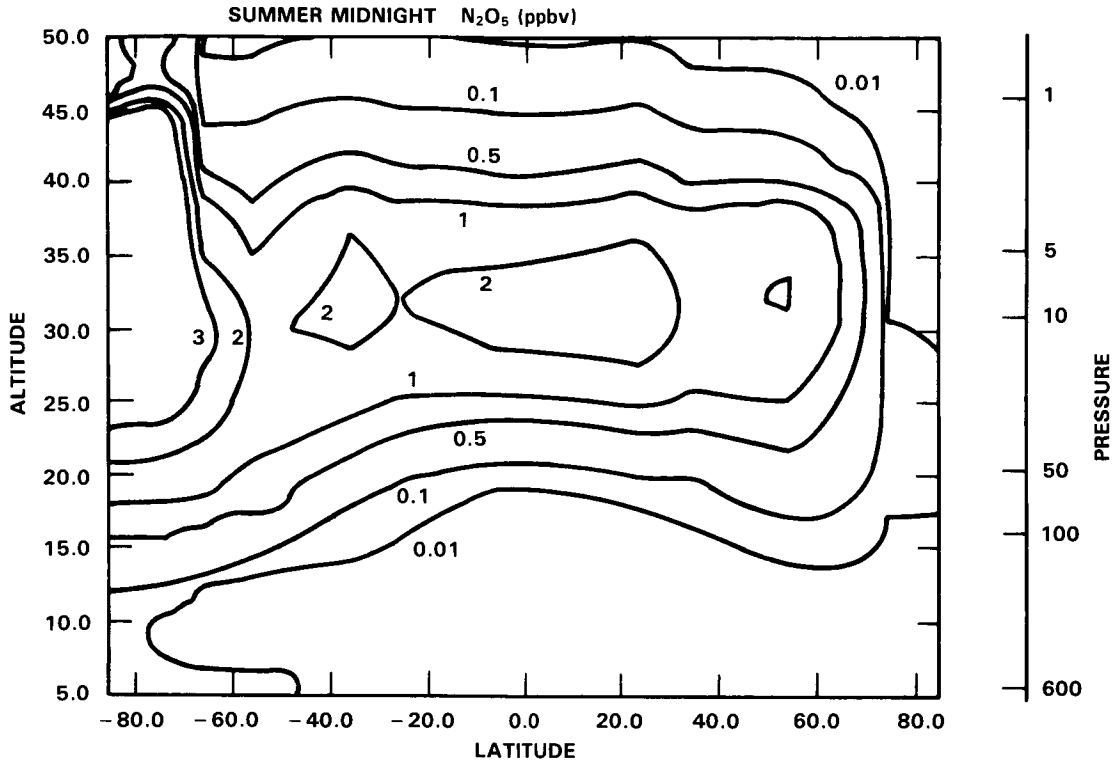

Figure 12-37. Latitude-height cross-section of N_2O_5 from the model of Stordal *et al.* (1985).

The calculated distributions in the lower stratosphere differ in various models and are dependent on the transport scheme used and the heterogeneous removal process assumed in the troposphere.

In the stratosphere, the chlorine species can be conveniently separated into HCl and Cl_x which comprises Cl, ClO, and $ClNO_3$ and HOCl. The species in the Cl_x group have interconversion lifetimes of a few hours or shorter, while transformation between HCl and ClO_x has a typical time constant of approximately one day or longer (Ko and Sze, 1984). Species in the ClO_x group exhibit large diurnal variation, but the concentrations of HCl and the ClO_x group show little variation throughout the day.

Figure 12-39 shows the calculated altitude-latitude cross-section of HCl. In the upper stratosphere, the bulk of the Cl_y is in the form of HCl as evident from the similarity between the distributions of HCl and Cl_y. The distribution in the lower stratosphere is influenced by the formation of $ClNO_3$ where its concentration reaches comparable magnitude to that of HCl.

Figure 12-40 shows the calculated altitude-latitude cross-section of the noontime concentration of ClO_x. Note the factor of 2 increase in concentration of ClO_x from the equator to 60° around 40 km in the northern hemisphere. This feature in the model results is consistent with the model results on CH_4 which show a factor of 2 decrease from the equator to the high latitudes around 40 km. Since CH_4 mediates the conversion of ClO_x to HCl via the reaction $Cl + CH_4 \rightarrow HCl + CH_3$, lower concentrations of CH_4 in the high latitudes should favour formation of ClO_x at high latitudes (cf. Solomon and Garcia, 1984b). Superimposed on the latitudinal behaviour is the seasonal variation reflecting the change in OH concentration where

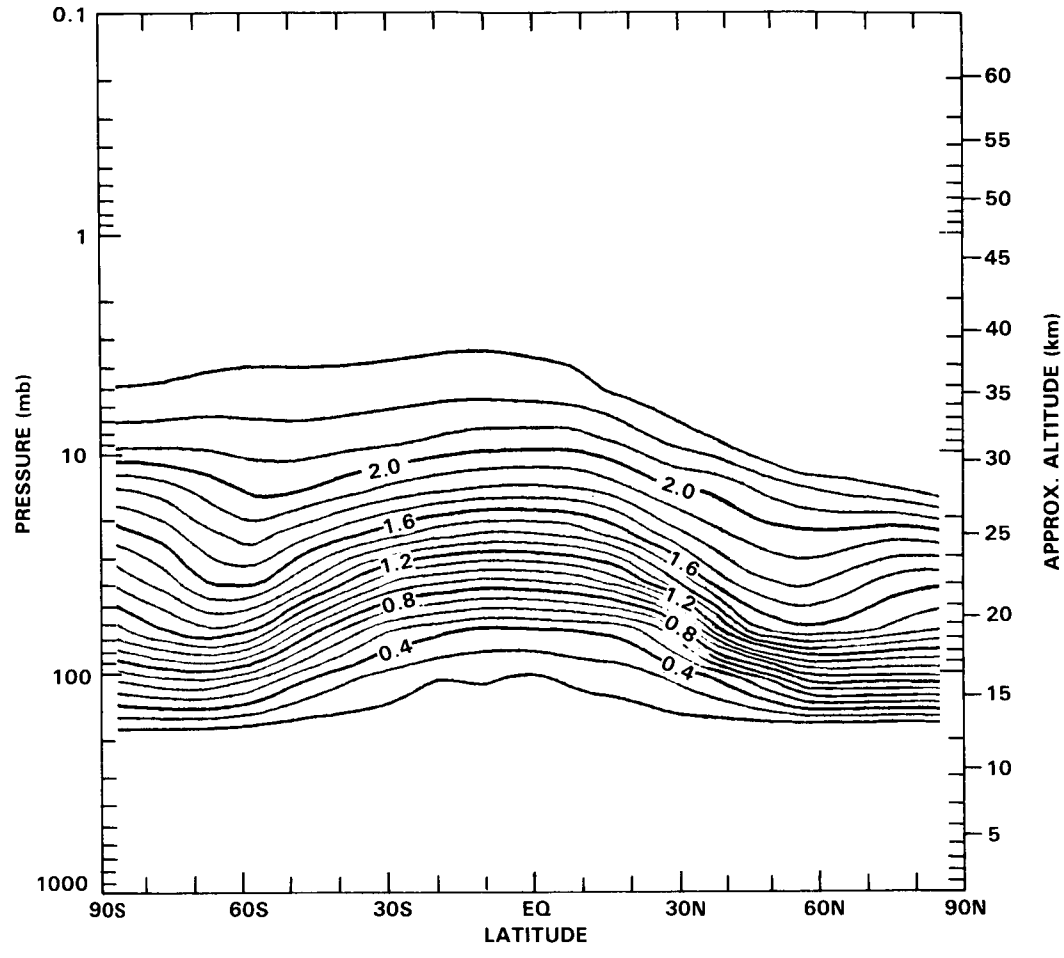

Figure 12-38. Calculated volume mixing ratio of Cl_y as a function of latitude and altitude for April. The contour levels are labelled in units of ppbv. The result is from the AER model. The photochemical scheme is identical to that in Ko *et al.* (1984) except for updating of reaction rates. The dynamical scheme is a refinement of the scheme described in Ko *et al.* (1985). The source of Cl_y is from photodecomposition of CH_3Cl, CH_3CCl3, CCl_4, CFC-11, and CFC-12 and removal is by washout and rainout in the troposphere with lifetime of about ten days.

higher OH concentration in the sunlit hemisphere will also help to convert HCl to ClO_x via the reaction $OH + HCl \rightarrow H_2O + Cl$.

The calculated cross-sections for the noontime concentrations of Cl, ClO, $ClNO_3$, and HOCl are shown in Figure 12-41. The figures show that $ClNO_3$ has the highest concentration in the lower stratosphere whereas ClO and HOCl become more important in the upper stratosphere. The species ClO and $ClNO_3$ exhibit latitudinal features similar to that of ClO_x.

The above features are common to all model results although the latitudinal gradient in upper stratospheric ClO_x in the classical Eulerian models are less pronounced because of the smaller latitudinal contrast in CH_4 (see above).

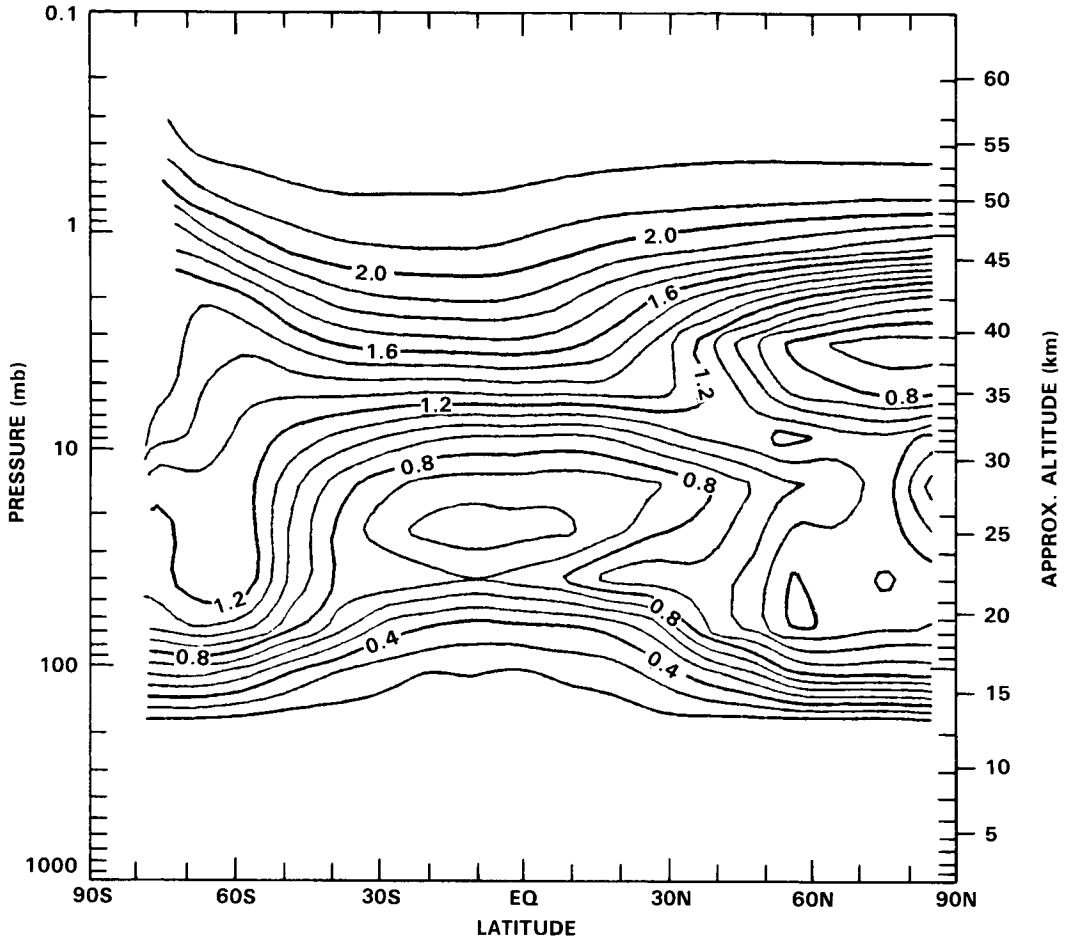

Figure 12-39. Same as Figure 12-38, for HCl (ppbv).

Figure 12-42 gives the altitude profiles of Cl_y from different models. The relatively small spread (2.1-2.5 ppbv) in the calculated values in the upper stratosphere results from the slightly different scenarios for the halocarbon emissions and transport parameters assumed in the models. The spread of values among the models in the lower stratosphere is, however, larger. In general, compared to models using the classical Eulerian circulation, those models using a diabatic or residual circulation and small eddy diffusion coefficients have lower concentrations at the tropical regions and higher concentrations at the high latitudes in the lower stratosphere. This is best illustrated by the calculated column abundances of HCl, which will be discussed in more detail in Chapter 11. In a classical Eulerian model (e.g. MPI), the ratio of the abundance at 60 °N to that at the equator is about a factor of 2. In models using diabatic/residual circulations (NOCAR, AER), the ratio is about 3:1 which is in better agreement with the observations.

Figure 12-43 shows calculated profiles of ClO, HCl, and $ClNO_3$ from different models corresponding to mid-latitudes (~ 30 °N) and summer condition. Given the diversities in the treatment of dynamic transport and diurnal variation in the various models, it remains difficult to isolate a single cause for the discrepancies. However, much of the difference could be explained in terms of the differences in the calculated Cl_y (Figure 12-42) and then differences in the partitioning of Cl_y species related to the coupling to the NO_x chemistry. To isolate the effect of partitioning, the ratios $ClNO_3$/ClO and ClO/HCl are plotted

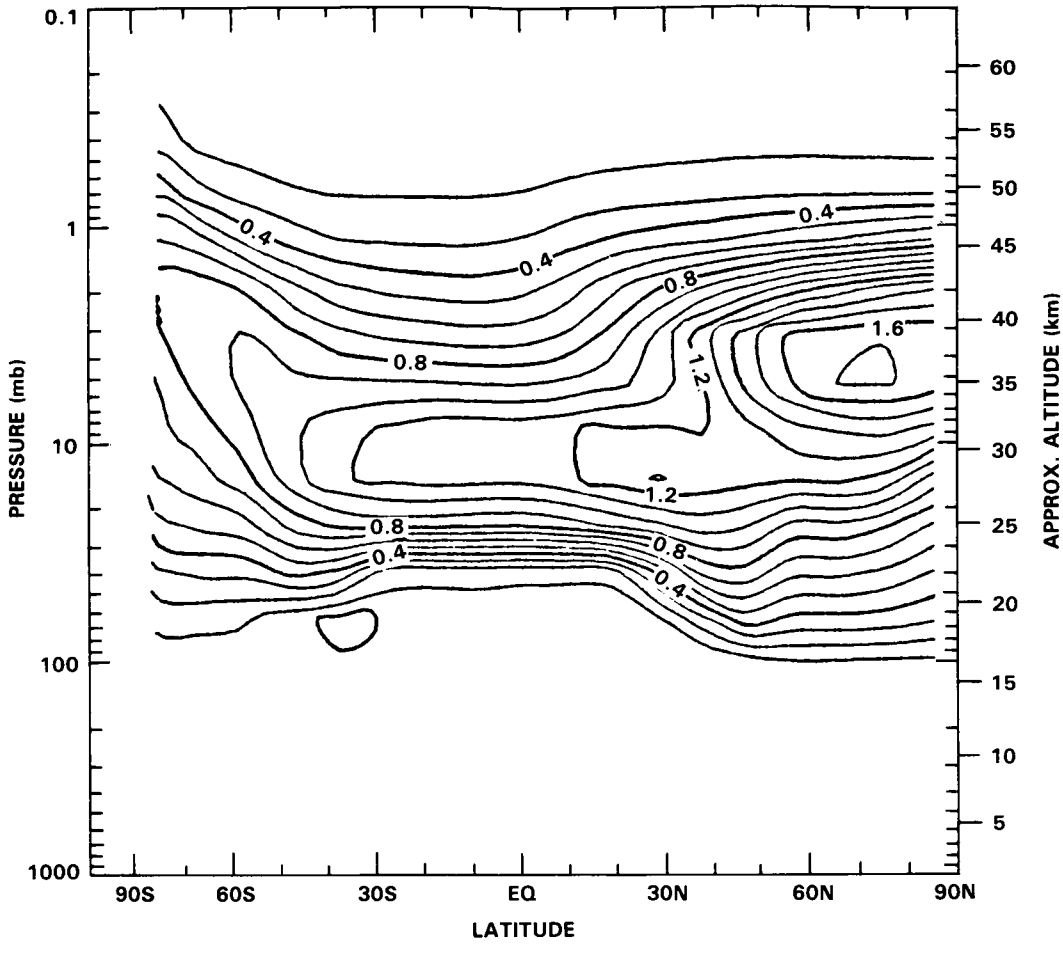

Figure 12-40. Same as Figure 12-38, for ClO_x, which is the sum of Cl, HOCl, $ClNO_3$ and ClO.

in Figure 12-44. The factor of 2 discrepancy in the ratios among the models below 30 km can be attributed in part to the differences in the calculated NO_y, where higher NO_y tends to favour the production of $ClNO_3$ at the expense of ClO, resulting in a larger $ClNO_3$/ClO ratio and smaller ClO/HCl ratio.

(v) O_x

The observed seasonal and latitudinal distribution of the total ozone column is shown in Figure 12-45a. Important features that models should simulate are: low equatorial abundances; an increase towards high latitudes; the seasonal variations at mid and particularly high latitudes; the spring maximum in both hemispheres, at the polar region in the Northern Hemisphere but at 50° - 60° latitude in the Southern Hemisphere; a fall minimum in both hemispheres around 60° latitude.

In general, models with high diffusion (mostly classical Eulerian models) underestimate the latitudinal contrasts (Figure 12-45b-e). The equatorial abundances are generally overestimated due to too strong an eddy transport. The seasonal variation at high latitudes is usually less than observed.

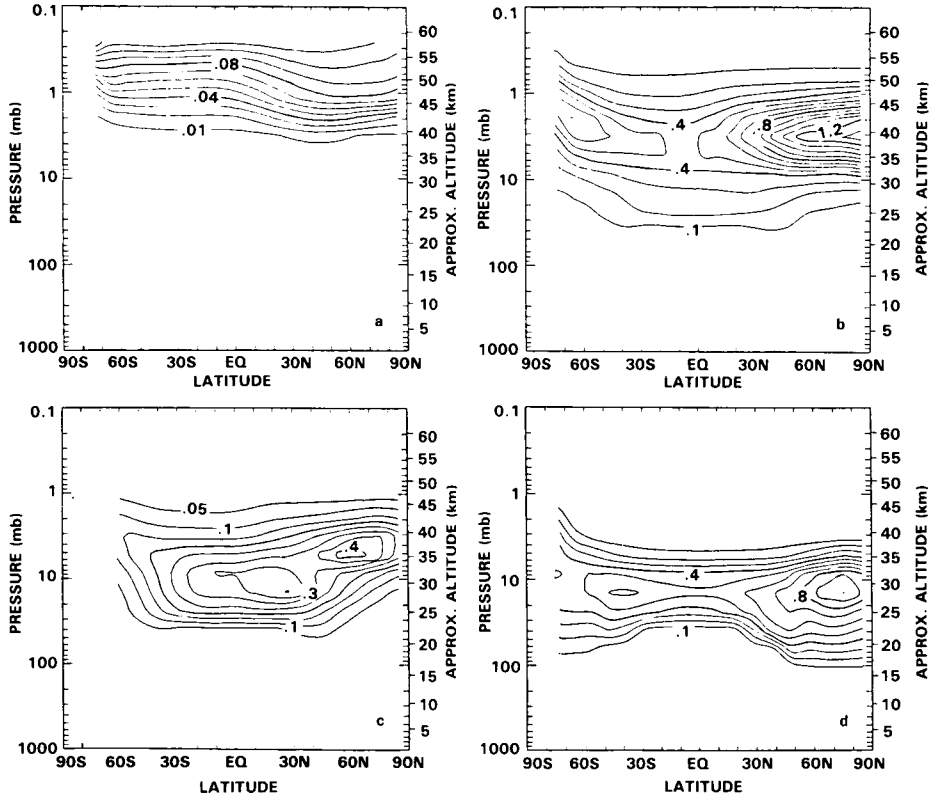

Figure 12-41. Same as Figure 12-38, for Cl in (a), ClO in (b), HOCl in (c), and $ClNO_3$ in (d).

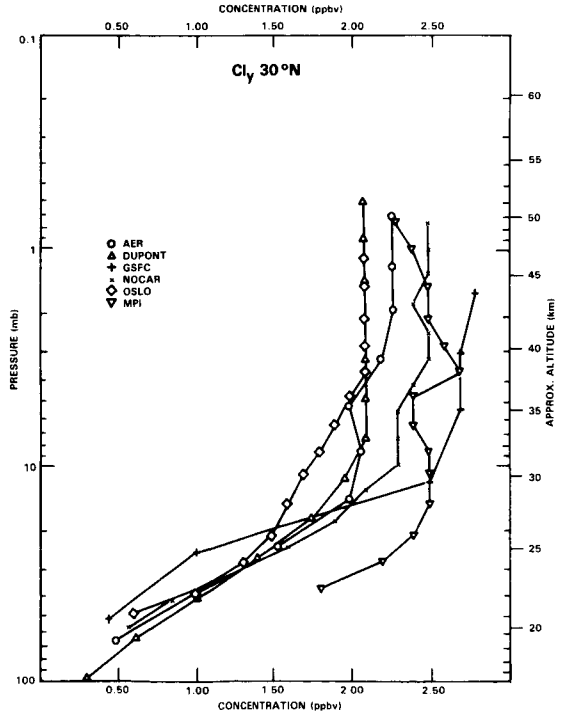

Figure 12-42. Calculated profiles of Cl_y from different models for ~30°N for summer conditions.

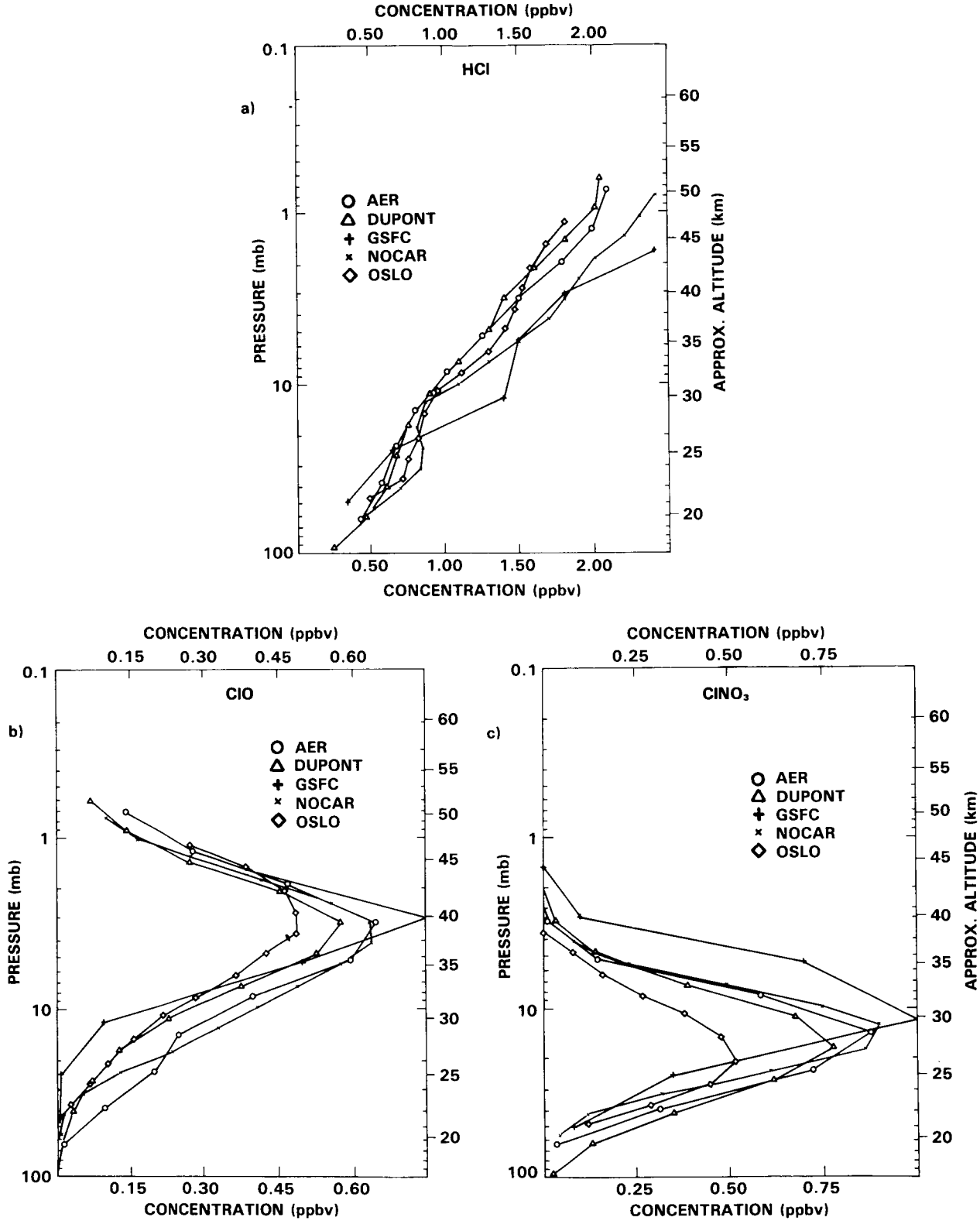

Figure 12-43. Calculated profiles of (a) HCl, (b) ClO, and (c) $ClNO_3$ for different models for mid latitudes (~30°N) for summer conditions.

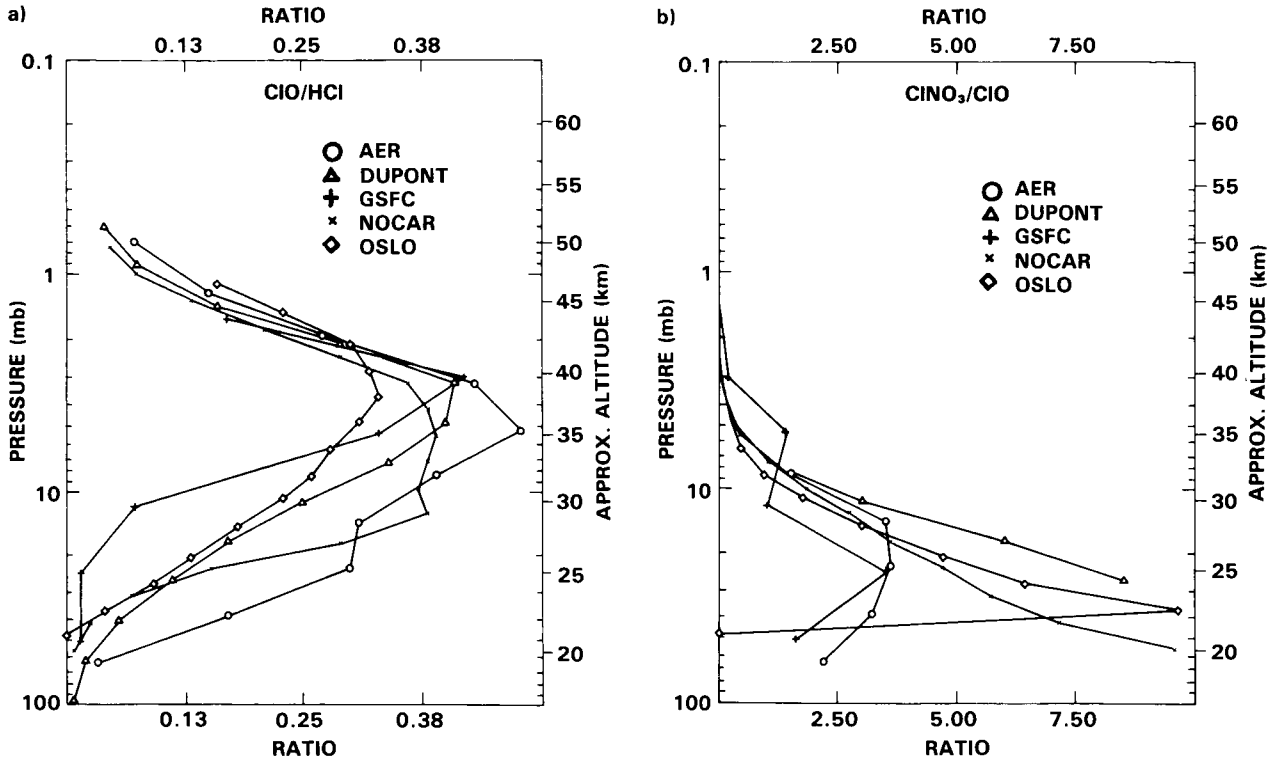

Figure 12-44. Calculated ratio of (a) ClO/HCl and (b) $ClNO_3$/ClO from different models as deduced from results indicated in Figure 12-43.

The agreement with the observations varies from model to model and essentially reflects how well the cancellation between the mean Eulerian circulation and the eddy fluxes is achieved. The Eulerian model of Crutzen and Schmailzl (1983) simulates the ozone columns in reasonable agreement with the observations, not surprising since the diffusion coefficients in this model are chosen to give the best fit to observed ozone abundances (Hidalgo and Crutzen, 1977).

The diabatic circulation models all get equatorial abundances in good agreement with the observations (see Figure 12-45). Since only low horizontal diffusion is used, larger latitudinal gradients in the observed range can be obtained. Indeed, the abundances at high latitudes are sometimes too high (Ko *et al.*, 1985 Figure 12-45h). Figure 12-45f-h show that there is a substantial individual variation between the diabatic and residual circulation models, reflecting mostly differences in adopted values of diabatic heating rates and diffusion coefficients. For instance, the model of Ko *et al.* (1985) uses hemispherically symmetric heating rates giving only small differences in the ozone columns of the two hemispheres. In the model of Stordal *et al.* (1985) (Figure 12-45g) the adopted asymmetric heating rates give rise to an interhemispheric asymmetry in ozone which is even larger than observed, with the spring abundances in their model considerably lower than observed in the Southern Hemisphere.

Figure 12-46a presents mid-latitude O_3 height profiles for summer and winter conditions from a 2D model (Solomon and Garcia, 1984b), chosen to illustrate the seasonal variations at mid-latitude. This model represents values in the middle of the model range and has a seasonal variation which is typical of all the models. The seasonal variation in the upper stratosphere is small. It increases at lower altitudes and

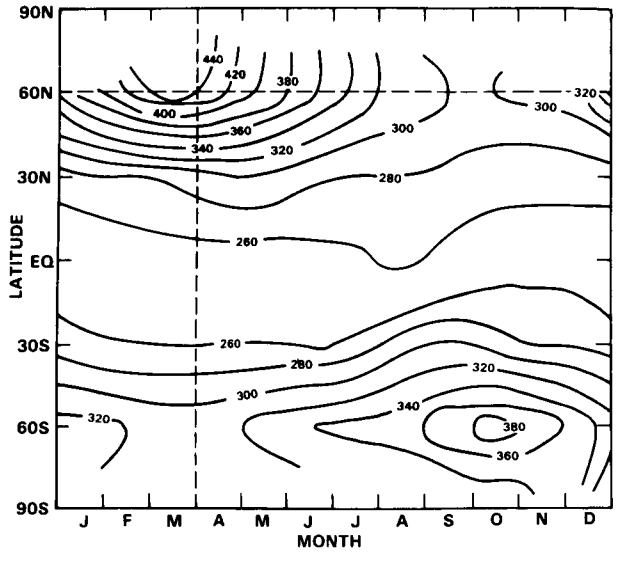

a) Observations

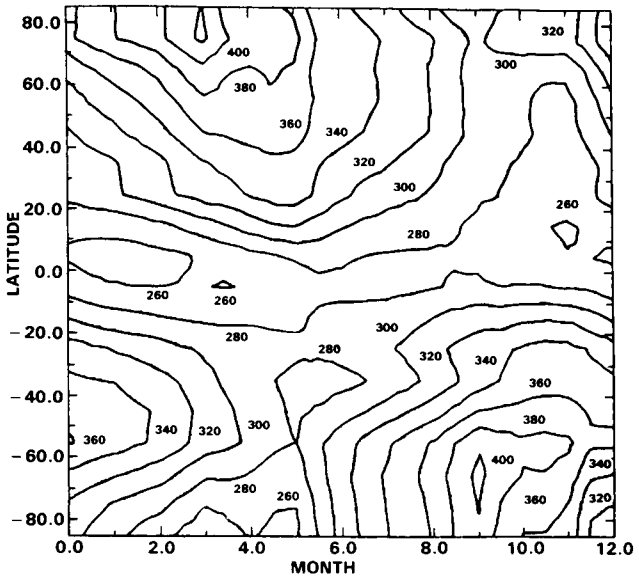

b) MPI

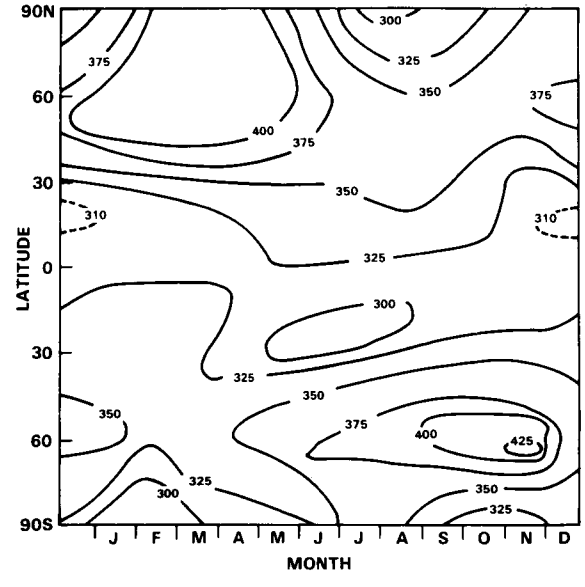

c) RAL (Eulerian)

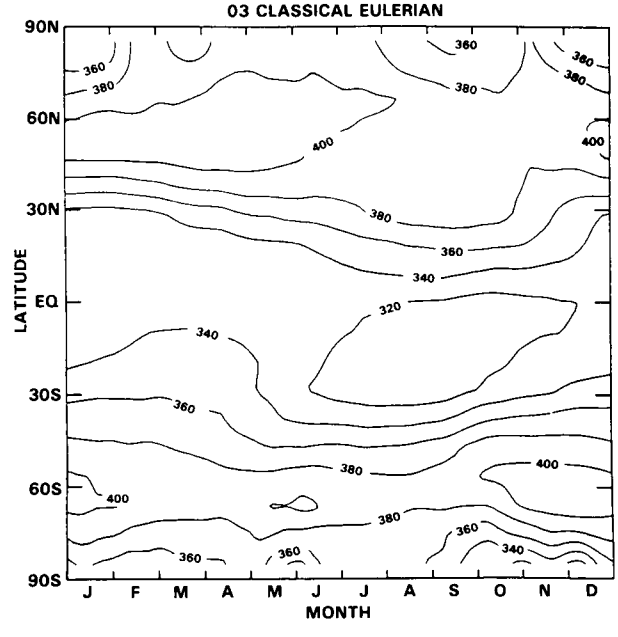

d) AER (Eulerian)

Figure 12-45. Total ozone columns as function of latitude and time of the year (m. atm cm).

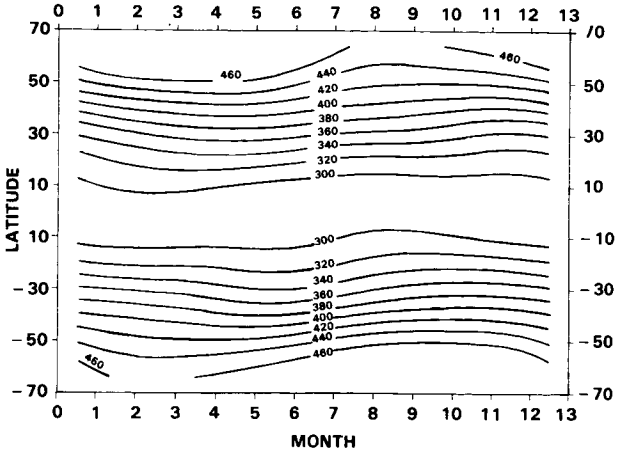

e) DuPont

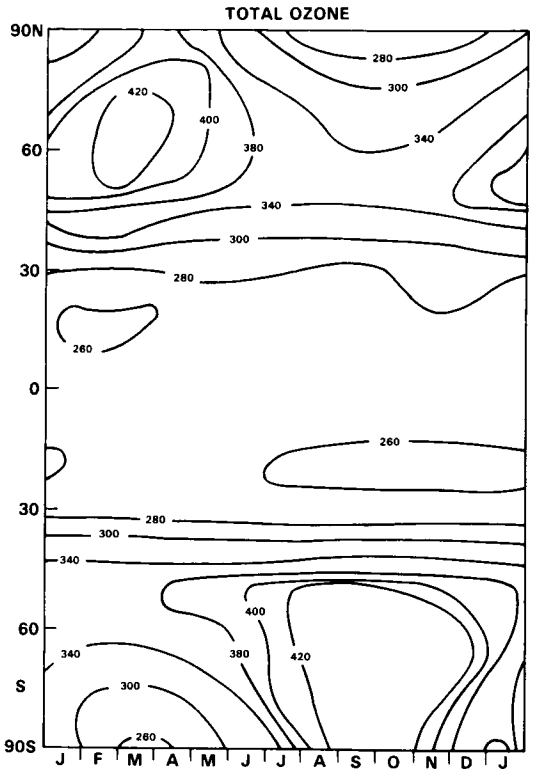

f) RAL (Diabatic)

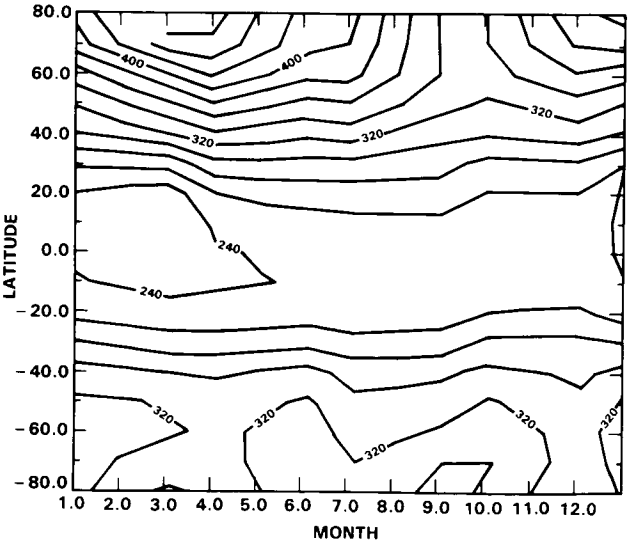

g) UOslo

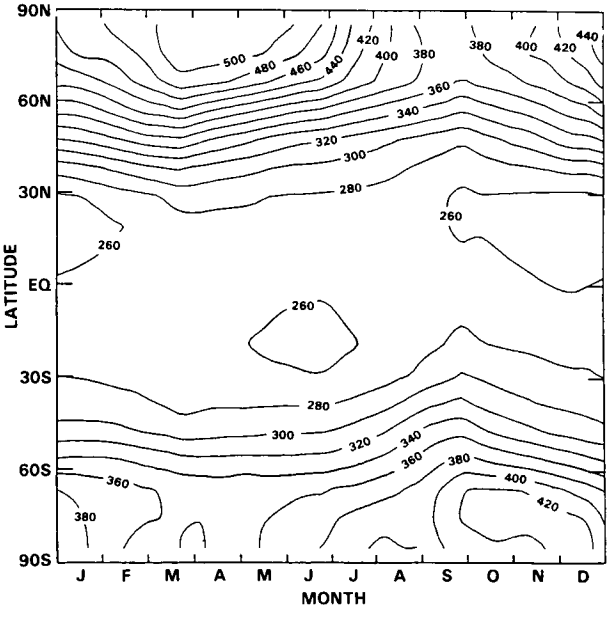

h) AER (Diabatic)

Figure 12-45. Continued

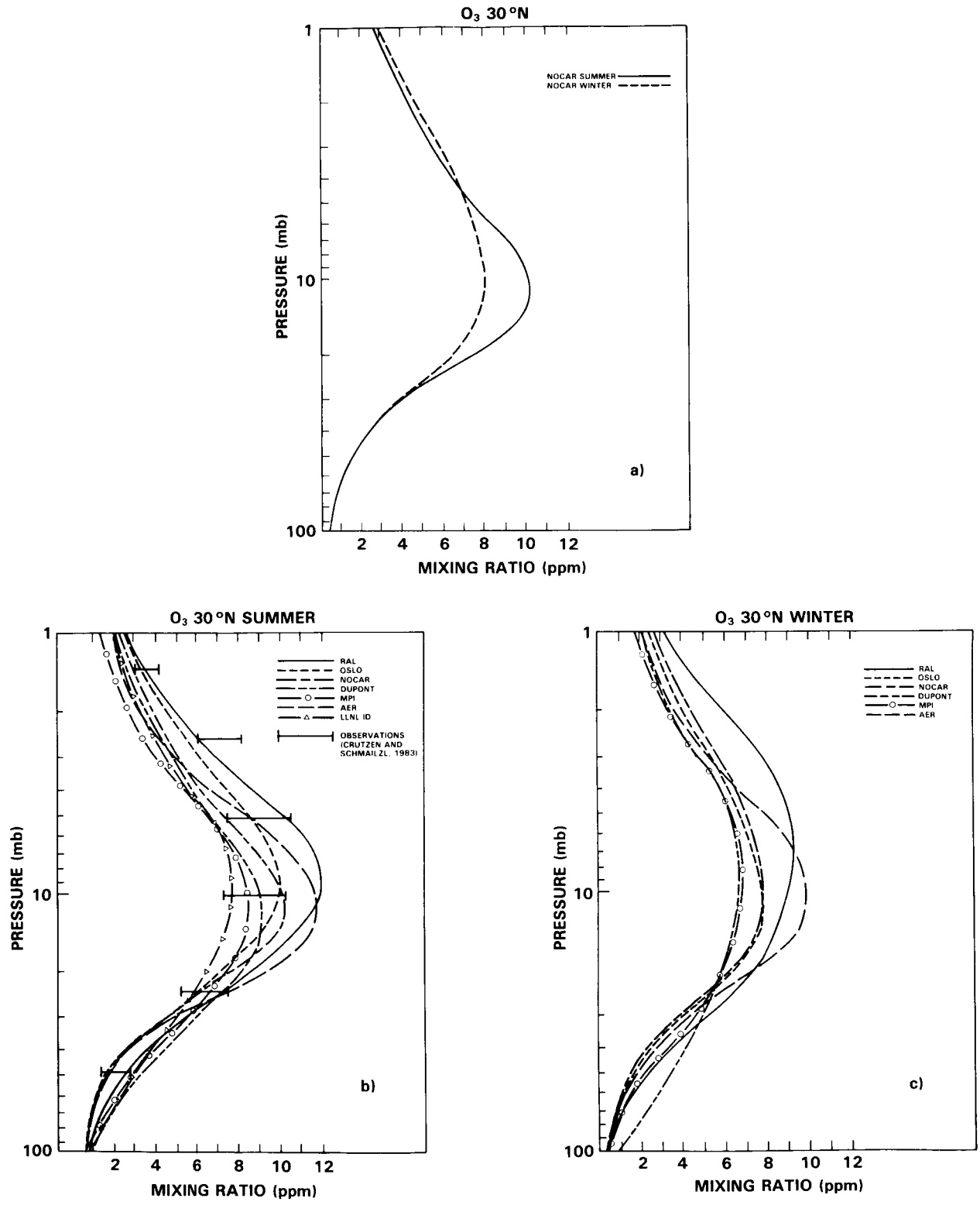

Figure 12-46. Altitude profiles of O_3 volume mixing ratio, 30°N. a) Summer and Winter, NOCAR model; b) Summer profiles, various models; c) Winter profiles, various models;.

amounts to about 2 ppm in the peak region. There is no substantial seasonal variation in the altitude of the peak.

The summer profiles for 30° latitude for several models are shown in Figure 12-46b. In the 40 km region the models consistently underestimate O_3 compared to the observations except for the RAL model which has low concentrations of ClO_x and NO_x (see Figure 12-34). In this region, ozone is photochemically controlled, and the direct effect of transport is of minor importance. However, transport processes influence the ozone abundances indirectly through transport of NO_y and Cl_y. The discrepancy between models and observations could be due to lack in the present understanding of the ozone loss chemistry, possibly in all of the HO_x, NO_x and ClO_x cycles, since they all contribute similarly to the ozone loss in the altitude region in question. The other possibility is that the production of ozone through the oxygen photolysis is not presently represented adequately in the models. The inability of models to simulate ozone in the photochemically controlled upper stratosphere represents a major limitation of current photochemical theory. This must be kept in mind when estimated effects of photochemical perturbations are evaluated. For illustrative purposes the profile from a 1-D model (LLNL) is included in Figure 12-46b. The 1-D profile falls within the range of 2-D model profiles. The problem of modelling ozone in the 40 km region appears to be independent of the dimensionality of the models.

From Figure 12-46c where winter profiles are shown, it is seen that the models underestimate ozone around 40 km regardless of the time of year. Note that the spread between the models is about the same in the winter as in the summer season.

Figure 12-47a-b shows latitude-altitude cross sections of ozone mixing ratios under solstice conditions. Results from the two AER models (one diabatic and one Eulerian) have been chosen since the two models have identical photochemistry and only differ in the transport representation. However, all the 2-D models from which data is used in this chapter show common features in the photochemically controlled domain. The region of maximum mixing ratios is located in the tropics at about 30 km in all models. The peak values range from about 9 to 12 ppm, which is also the range of the values observed from satellites. The modelled latitudinal extent of the peak is also similar in the models.

The most significant differences between the models occur in the lower stratosphere in the dynamically controlled region. In general, the mixing ratio surfaces slope more steeply downward and poleward at mid and high latitudes in the diabatic type of models (Figure 12-47a) than in the classical Eulerian models (Figure 12-47b). This behaviour can be attributed mainly to the difference in horizontal mixing in the two kinds of models and has important consequences for the latitudinal distribution of the total ozone columns. The highest ozone concentrations occur in the lower stratosphere. The slope of the mixing ratio surfaces in this region will therefore determine the latitudinal variation of the maximum ozone concentrations and thereby the total columns as well. The large latitudinal gradient in the distribution of total ozone columns in the AER diabatic model (Figure 12-45h) is therefore a reflection of the steep downward and poleward slopes of the mixing ratio surfaces in the lower stratosphere in this model (Figure 12-47a).

12.7 CHEMISTRY IN THREE-DIMENSIONAL MODELS

During the past decade a number of three-dimensional atmospheric models incorporating a formulation of chemically active trace species has been developed. The complexity of both the physics and chemistry in these models varied widely. Earlier studies of ozone transport with three-dimensional models had been conducted by Hunt (1969) and by London and Park (1973, 1974), but the study of Cunnold *et al.* (1975,

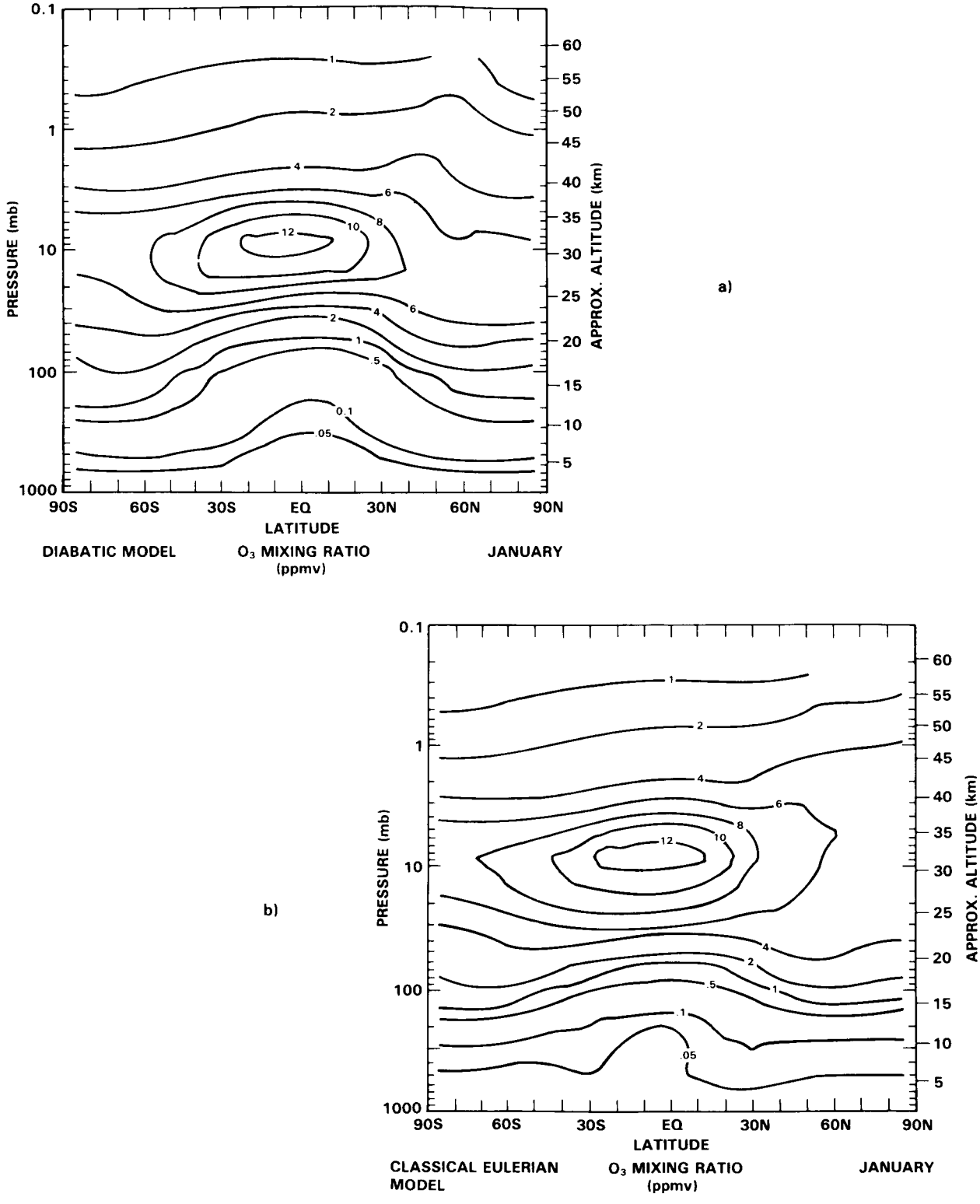

Figure 12-47. Ozone mixing ratio cross-sections, solstice conditions (ppmv). a) AER Diabatic model; b) AER Eulerian model.

1980) was notable in that for the first time multi-year simulations were conducted to study the relative importance of chemistry and dynamics in maintaining the distribution of ozone. A low resolution (six zonal wave-numbers) quasi-geostrophic model was used to simulate the gross features of the wind and temperature fields of the atmosphere. The model included simplified ozone chemistry and a specified (altitude dependent only) NO_x distribution. Despite the extremely simplified treatment of both the chemistry and the dynamics, the model was successful in simulating a number of features of the observed ozone fields, in particular the seasonal evolution of total column ozone. Schlesinger and Mintz (1979) employed the same simplified treatment of the chemistry in a primitive equation GCM which included comprehensive physics. Unfortunately, the model was integrated for such a short time (six weeks from winter solstice), that the ozone had insufficient time to evolve to a satisfactory wintertime distribution. In addition, the model winter hemisphere had an extra meridional cell in both the troposphere and stratosphere not present in the observations.

Mahlman *et al.* (1980) conducted two ozone tracer experiments using the general circulation model described by Manabe and Mahlman (1976). They employed the 'off-line' approach adopted by Mahlman and Moxim (1978) in which wind and temperature fields from the GCM simulations are stored and later used as input to a separate tracer model. In this approach the constituents (ozone in this instance) are free to react chemically as they are transported, but the chemistry cannot affect the dynamics. In the first experiment, the ozone mixing ratio at the top model level (10 mb) was specified constant everywhere. At other model levels the ozone was treated as an inert tracer with parameterized removal in the troposphere. In the second experiment, a simplified ozone chemistry was incorporated at the 10 mb level with NO_y ($NO + NO_2 + HNO_3$) specified. At all other levels the treatment of ozone was identical with that for the first experiment. These experiments were integrated for four model years. The intent of these studies was to examine the roles of chemical and dynamical processes in maintaining the ozone distribution, and determine the role of those processes in producing the observed poleward and downward slope of isolines of quasi-conserved species in the lower stratosphere. These studies indicated an important role for transient waves in irreversibly mixing constituents into the winter polar vortex. Mahlman *et al.* (1980) concluded that inclusion of ozone photochemistry in the lower stratosphere was necessary to obtain a good ozone simulation.

Grose *et al.* (1984, 1985) have recently conducted simulations of the transport of stratospheric constituents using a spectral, primitive equation model (Blackshear *et al.* 1986) with a detailed formulation of the chemistry, including those species and reactions currently thought to be important for determining the ozone distribution in the stratosphere. The transport simulation is done 'off-line'. Chemistry is incorporated by grouping certain species together into families. This family concept partitions the species into groups so that, although there may be rapid chemical conversions between individual members of the family, the characteristic lifetime of the family is long in comparison to that of individual species. A 5-month simulation was conducted transporting O_x, NO_y, Cl_y, and HNO_3. The results of the simulations were quite encouraging, when compared with LIMS and other satellite observation. These simulations share deficiencies common to most model studies of the stratospheric ozone distribution. In particular, the ozone mixing ratio is lower than observed in the upper stratosphere, and the nitric acid maximum in winter high latitudes is underpredicted. These deficiences appear to be associated with our understanding of the chemical mechanisms involved, rate coefficients, spectroscopic data, or some combination thereof. Cariolle and Deque (1984) have also utilized a spectral, primitive equation model to study ozone transport. Although the ozone chemistry in the model has been coupled with the dynamics, the chemistry has been linearized using relaxation times inferred from a 2-D photochemical model. The results from a first integration of 45 days show a successful simulation of the zonally averaged total O_3 column in the Southern Hemisphere that deviates from the observation by less than 10%. In this hemisphere the ozone variability is found

to be the result of the action of transient medium-scale waves with zonal wavenumbers 4, 5 and 6, in fairly good agreement with observation. Due to the short integration time compared to the photochemical relaxation time, the O_3 content simulated in the winter northern hemisphere was underpredicted. These results have now been improved by increasing the integration period to 6 months and by replacing the simple Newtonian cooling approximation by a more comprehensive radiative code.

Rose and Brasseur (1985) have utilized a hemispheric, primitive equation model with coupled ozone chemistry and lower boundary at 10 km to study ozone transport during a stratospheric warming. A simplified ozone chemistry was included with a zonally average chemical source term and specified NO_x (altitude dependent). The integration period was 21 days and the preliminary results presented make it difficult to judge the degree of success of this study.

As yet there are no reported results of simulations conducted using a GCM with a complete formulation of the chemistry but progress has been demonstrated with a variety of approaches as described in the foregoing discussion. Due to the severe computational burden imposed by this problem, the most fruitful approach in the near term will probably result from use of a comprehensive GCM with coupled chemistry, but using the 'family' concept. However, it should be noted that even with the development of such a model, a number of problems exist in our current understanding of both dynamics and chemistry which will inhibit our ability to achieve an accurate ozone simulation. These problems are addressed in other sections of this document.

12.8 ON THE USE OF MODELS FOR ASSESSMENT STUDIES

1- and 2-D models are now commonly used in studies of the middle atmosphere. Given the approximations in these models and their inability to explain adequately some of the limited number of measurements available, how do these limitations affect our confidence in assessment studies? How do we relate the 1- and 2-D model assessment calculations; has the use of 2-D models improved our assessment capability? In this section we consider these questions. Two problems are considered. First, how might certain model deficiencies in treatments of photochemistry affect assessment studies? Secondly, in what way do the 2-D models improve assessment studies? One of the advantages of 2-D models is the increased potential for radiative-dynamical-photochemical coupling. This is considered in some detail at the end of the section.

Turning first to limitations in photochemistry, we ask how discrepancies in models for the current atmosphere affect our ability to make such assessments. Consider the inability of most models to match the observations of stratospheric ozone. Calculated ozone abundances are generally 20 to 50% below observed values at $\sim$ 40 km and above but are as much as 20% greater than the observed concentration near the ozone peak between 20 and 30 km. The magnitude of this discrepancy varies from model to model (and also depends on which observations are selected for comparison). The pattern is common to both 1-D and 2-D models, and points possibly to a fundamental problem with photochemical theory. Various hypotheses have been put forward, ranging from revisions in the molecular oxygen cross-sections, readjustments of kinetic rates within possible uncertainties or proposals of heretofore unknown chemical reactions. No simple solution is currently acceptable and resolution of these differences may have to result from a gradual evolution of the models combined with continued observations with greater absolute accuracy.

If we accept that the models are deficient somehow in their photochemistry then we should determine how these errors would affect our predictions for the perturbed stratosphere. For example, it is hard to imagine that small changes ($\pm$50%) in the kinetic rate constants or a revision in O_2 photolysis rate would

grossly alter the calculated ozone depletions at high levels of chlorine. However, a new, hidden chemical cycle might have significant impact on our ability to make assessments. Any of these revisions are likely to alter the calculations of small perturbations to ozone, and research is needed to test how the proposed solutions to the high-altitude ozone problem would affect models of a hypothetical high-chlorine, high-methane atmosphere of the future.

The key element in determining the onset of major ozone reductions predicted by 1-D models at high levels of chlorine is the abundance of odd-nitrogen (NO_y) in the middle stratosphere. The 1-D model intercomparison described above found differences as large as 50% in peak NO_y around 36 km, but generally less than 20% in modelled values for NO_y between 20 and 30 km. This range in NO_y translates into a 20% uncertainty in the amount of chlorine (i.e. from 16 to 19 ppbv) needed to achieve major ozone reductions in current 1-D models.

Observations of stratospheric odd-nitrogen species show large latitudinal and seasonal gradients which are reasonably reproduced in the upper stratosphere by 2-D models (see Chapter 10). The 1-D model results are generally representative of the mid-latitude profiles from the 2-D models. However, there are large differences between the 2-D models in NO_y, especially in the equatorial lower stratosphere where the agreement with data is generally poor. For example, the diabatic models predict low NO_y, especially below 25 km in the tropics. These results (see Section 12-7) point to the importance of a satisfactory treatment for tropospheric NO_y (its rainout, possible lightning source, etc.) and of the vertical transport in the equatorial lower stratosphere if the NO_y budget is to be modelled adequately.

How would these large differences in NO_y in 2-D models affect the calculated ozone depletions at high chlorine? At first, one might believe that the chlorine levels, at which large ozone depletions are predicted, should scale with the NO_y as is found in 1-D models. However, this scaling may not be applied directly to 2-D models because the source of the NO_y differences is related to transport phenomena. For example, in the residual circulation models, the subtropical lower stratosphere has low NO_y values. Similarly this region would have low levels of active chlorine (Cl_x) relative to organic chlorine (e.g. CFCs). In this case, the importance of high-chlorine scenarios may only be judged on the basis of latitudinally and seasonally averaged destruction of ozone. The 1-D models attempt to simulate this averaging through their sluggish vertical transport of ozone, NO_y and Cl_x. The 2-D models include realistic seasonal variations. We may regard the diversity in NO_y concentrations of the lower stratosphere in current 2-D models as a range in the ages of air injected into the stratosphere, and hence as a range in the time over which the photochemistry has had a chance to perturb stratospheric ozone. Thus the range in stratospheric NO_y may imply a proportional range in the amount of Cl_x from tropospheric sources, with corresponding differences in the impact of photochemical perturbations to ozone. In any case it is clear that the 2-D model response is more complex than the 1-D case.

When one represents a three-dimensional system such as the atmosphere in a model of lower dimensionality (1-D or 2-D) one must in some sense average out some of the physical behaviour which occurs in the real system. When such models are used to predict the results of perturbations to the system, there is always the possibility that the averaging process has constrained the model so as to miss important interactions in the real atmosphere. One way of testing models in this context is to ask whether models of the same system at high dimensionality reveal phenomena which would affect the perturbation assessment. In particular one can look at two-dimensional models of the atmosphere to understand the effects that a more complete treatment of transport and seasonal variation would have on the global or mid-latitude 'average' profiles which are calculated by one-dimensional models. Based on such comparison it appears

that there are systematic differences between profiles generated by the two types of models, but that the differences can be understood in terms of the different transport representations.

A conclusion of a comparison of 1- and 2-D models, for both present day and perturbed atmospheres, is that there is at present no indication that the addition of meridional transport in 2-D models invalidates in a gross sense the results of 1-D perturbation assessments. Thus both types of model predict ozone depletions in a stratosphere with increased chlorine content. Because of the non-linear nature of the problem, this does not preclude the possibility of such a discrepancy for a different perturbation problem. Furthermore, it is clear that there are some questions (for example, possible latitude-dependent ozone changes) which 1-D models are incapable of answering. Moreover, there are systematic differences between 1- and 2-D model assessment studies (see Chapter 13) which remain to be explained.

Agreement in a gross sense between 1- and 2-D models is perhaps not surprising. For example, the transport parameterisation in 1-D models must describe broadly the flux of source gases from troposphere to stratosphere and agreement for these gases in low latitudes is inevitable. Since the latitude band from 30°S to 30°N encompasses half the volume of the atmosphere, gross agreement between a 1-D model and the globally averaged results of a 2-D model can be expected. However, detailed agreement at a particular latitude must be regarded as fortuitous. Furthermore, the hybrid nature of the 1-D model - part low latitude model, part global model and part local model - makes difficult the interpretation of assessment studies.

The difference between the diffusive transport in a 1-D model and predominantly advective transport in a 2-D model (especially in the residual mean or diabatic formulation) shows up quite strongly in the case of total NO_y. Figure 12-48a shows the budget of NO_y taken from the AER model for the mid-latitude

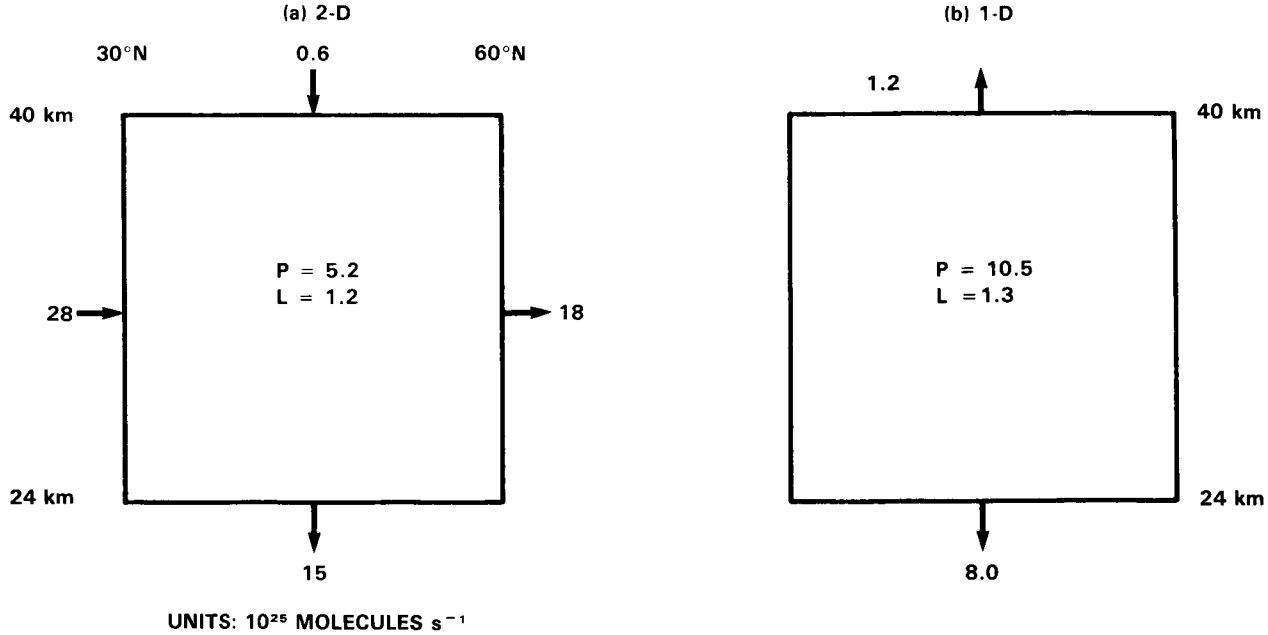

Figure 12-48. The budget of NO_y as calculated by 2-D (a) and 1-D (b) models. The integrated photochemical production rate (P) and removal rate (L) in the region are given in units of 10^{25} molecules/sec.) The calculated fluxes across the boundary (in units of 10^{25} molecules/sec) are also given for the region indicated. For comparison purpose, the values for the 1-D model are scaled to correspond to the same volume and surface areas given in Figure (a).

region (30° to 60°) between 24 to 40 km. The local concentration of NO_y is determined by the balance of the horizontal and vertical transport fluxes with the photochemical term playing a relatively minor role. In contrast, the calculated concentration in a 1-D model is maintained by the net photochemical production with diffusive transport out of the region. However, these differing effects are not surprising given that NO_y is effectively a long lived tracer and that, in its conceptual formulation, the 1-D model should approximate global averaged (not 30° to 60°) fluxes.

In summary, while the 1-D models remain useful tools for assessment it is becoming clear that 2-D models provide a much more detailed picture of the atmospheric response to perturbations. For example, 2-D model studies indicate that ozone changes will be largest in high latitudes and that there will be some local ozone production due to the self healing effect in low latitudes. The high latitude changes suggest that some monitoring efforts should be centered on this region.

Turning to the question of the degree of feedback in 2-D models, we note that the continuity equation for ozone contains transport and photochemical terms. In one- and two-dimensional models, the transport terms can be formulated in a number of different ways and they can either be specified or calculated. If calculated, they are dependent on the radiative heating and on the eddy fluxes of heat and momentum. The photochemical term depends on the ultraviolet flux and on the distribution of the other interacting species. To make predictions of changes to the ozone layer, the interactions among all these terms must be considered.

If the coupling between chemistry, radiation and dynamics is ignored (if, for example, K_z is specified in a 1-D model, or if the meridional velocities are specified in two-dimensional models) then it is possible to make a rough estimate of the error in an assessment, since this just depends on the errors in individual species concentrations.

However, the stratosphere is highly coupled with, for example, the wind fields dependent on the radiative heating which depends on the ozone field which itself is transport dependent. At first sight this appears to suggest a major limitation of 1-D and 2-D models as assessment tools. Indeed, experiments with a 2-D model (Harwood and Pyle, 1980) show that changes in the mean meridional circulation, changes in the eddy coefficients and changes in the specified eddy momentum fluxes all have a major impact ($> 10\%$) on the calculated ozone column amounts. Assessment of a perturbed stratosphere seems to require that changes in radiative and dynamical processes be modelled to high accuracy.

It is possible that the above limitations of simplified models may not be quite so serious as they seem. Perturbation experiments with a 2-D model (Haigh and Pyle, 1982) and with a GCM (Fels *et al.*, 1980) suggest that the primary adjustment of the stratosphere to changes in solar heating rates is radiative rather than dynamical. Solar heating changes due to ozone perturbations can lead to adjustments of the dynamical fields, of the longwave cooling, or both. In the two papers cited the main change is to the longwave cooling, giving rise to an altered temperature structure but with only small changes to the meridional circulation. An important exception in the calculations by Fels *et al.*, was in the region around the tropical tropopause where the dynamical adjustment was significant.

Some insight into the radiative/dynamical adjustment problem can be gained from consideration of the equations governing the global mean meridional circulation. If the quasi-geostropic approximation is

made, the steady-state zonal mean fields must obey the following momentum and thermodynamic equations in the residual Eulerian formulation:

$$-f\bar{v}^* = -K_R\bar{u} + F \tag{12.13}$$

$$\bar{w}^*\frac{HN^2}{R} = Q - C - \alpha\bar{T} \tag{12.14}$$

where for simplicity, nonlinear terms have been omitted and where infrared cooling has been written in terms of a global cooling rate, C, plus Newtonian relaxation with coefficient α. In the momentum equation a Rayleigh friction term, K_R, has been included. The terms Q and F represent externally imposed radiative and momentum forcing, respectively.

In the stratosphere, Q is due principally to absorption of UV radiation by ozone and F to the convergence of the Eliassen-Palm flux of planetary waves.

In addition to 12.13 and 12.14, the zonal mean fields also obey the continuity equation

$$\bar{v}^*_y + \bar{w}^*_z = 0 \tag{12.15}$$

(where compressibility and spherical geometry have been neglected), and the geostrophic balance equation

$$-f\bar{u}_z = \frac{R}{H}\bar{T}_y \tag{12.16}$$

Straightforward manipulation of the set 12.13 - 12.16 leads to a second order partial differential equation for the mean meridional streamfunction, χ^*:

$$\bar{\chi}^*_{zz} + \frac{N^2}{f^2}\frac{K_R}{\alpha}\bar{\chi}^*_{yy} = \frac{F_z}{f} + \frac{N^2}{f^2}\frac{K_R}{\alpha}\frac{Q_y}{\Gamma} \tag{12.17}$$

where $\Gamma = HN^2/R$. The mean meridional circulation can be obtained from χ^* through the relationships

$$\begin{aligned}\bar{v}^* &= -\bar{\chi}^*_z \\ \bar{w}^* &= \bar{\chi}^*_y\end{aligned} \tag{12.18}$$

It is instructive to consider how Equation 12.17 depends on the magnitude of the ratio K_R/α. In particular, if $(K_R/\alpha) << 1$, which appears to be the case throughout most of the stratosphere, Equation 12.17 reduces to

$$\bar{\chi}^*_{zz} \cong \frac{F_z}{f} \tag{12.19}$$

which implies that the mean meridional circulation is forced mainly by the EP flux convergence. If F is zero, then there is no mean meridional circulation and the stratosphere is in radiative equilibrium, i.e.

$$Q = C + \alpha\bar{T} \tag{12.20}$$

The work of Dickinson (1975) and Harwood and Pyle (1980) suggests that this is indeed the case in the summer stratosphere, where planetary wave activity is essentially absent.

It follows from these considerations that a change in the short wave heating rate Q due to ozone perturbations will be compensated for through adjustment of the temperature field (cf, Equation 12.20). The Fels *et al.* (1980) finding that significant dynamical adjustment occurred in the tropics is also consistent with the foregoing arguments since $f \rightarrow 0$ at the equator and the factor $N^2 K_R/f^2 \alpha$ in Equation 12.17 may not be small even if $(K_R/\alpha) << 1$.

Although the smallness of the ratio (K_R/α) in the stratosphere implies that its mean meridional circulation is rather insensitive to changes in the solar heating rate, it must be borne in mind that circulation changes could still be produced indirectly if the wave forcing, F, is altered. For example, the temperature changes produced by perturbed solar heating will affect the zonal mean wind through geostrophic adjustment (Equation 12.16). One can then envisage a change in the propagation characteristics of planetary waves in the stratosphere which, in turn, could lead to a different EP flux divergence. Investigation of this possibility would of course require the simultaneous computation of the zonal mean state and at least one planetary wave harmonic.

If the main effect of coupling during a stratospheric perturbation is to change the temperature structure then a requirement is for the models to contain an interactive radiation scheme. Since the photochemistry is temperature dependent, the adjustment needs to be calculated accurately. (The requirement for the determination of temperature dependent rate constants is also emphasized.) In the upper stratosphere, 1- and 2-D models should be able to treat the radiation transfer to high accuracy. If simple treatments are still to be used, they should be based on the Planck function perturbation, rather than the temperature perturbation (as in Newtonian cooling approaches). The radiation transfer becomes more complex in the lower stratosphere (Houghton, 1978) and more difficult to model (Haigh, 1984). Nevertheless, when considering perturbations to the ozone layer this is a crucial area which must be modelled well before assessments can be treated with confidence.

12.9 CONCLUSIONS

Middle atmosphere models which include a detailed description of photochemistry have been discussed, with an emphasis on two-dimensional models whose use has increased considerably since the publication of WMO 1981. During this time, theoretical advances have lead to major improvements in the formulation (and the understanding of the formulation) of 2-D models. The theoretical basis of 2-D models, and the associated limitations, are now generally well understood. The existing 2-D models provide a generally good description of the spatial and temporal variations of most stratospheric trace gases (or, at least, of those gases for which a reasonable observational data base exists). Practically, however, there are still some problems in overcoming the model limitations.

Improvements in 2-D models have stemmed from two areas of work. Firstly, important understanding of the relationship between eddies and the mean circulation has followed from the work of Andrews and McIntyre (1976) and many others. Secondly, the treatment of eddies in two-dimensional models has also received considerable attention.

Two-dimensional models can now be classified in at least two ways. Firstly, there are the classical Eulerian models. Secondly, there is a new generation of modified Eulerian models which use the residual

or diabatic circulation as the mean circulation and typically employ smaller eddy transport coefficients than the classical models. Eddy transport is important in both classes of models - finding the correct balance between the mean circulation and the eddies is necessary for a good model description. Secondly, some models use fixed temperature and circulation fields while others attempt to include a degree of feedback. Inclusion of feedback can help to elucidate the importance of particular radiative, dynamical or photochemical processes. Notice, though, that a completely interactive 2-D model would require an interactive description of eddy forcing, which we do not have.

While the theoretical basis of 2-D models is now well established, a comparison of the performances of various models reveals a number of practical problems. For example, comparison of classical Eulerian models with modified Eulerian models shows as large differences between models of a given type as between the two types of model.

The above differences make difficult general recommendations for the improvement of models. Nevertheless there are some clear problems. A comparison of the low-latitude profiles of odd nitrogen revealed large differences between the models. While the treatment of NO photolysis is important in defining the stratospheric sink of NO_y, it is clear that the different model treatments are not the sole reason for the differences (and this was true for a similar comparison of 1-D models). In particular, there appear to be problems in the treatment of transport in the equatorial lower stratosphere/upper troposphere. In this region the radative heating is the small, poorly defined difference of small heating and cooling terms. However, an accurate nett heating rate is required for an adequate description of the flux of source gases into the mid-stratosphere. The equatorial lower stratosphere needs further study.

While recent studies have tended to point towards the need for smaller eddy transport coefficients in transformed models compared with classical Eulerian models, there remain important uncertainties. Some diabatic models, for instance, produce a good description of the stratosphere using larger Ks; the evidence for smaller Ks is partly based on the results of general circulation models, which have their own particular problems. More studies using satellite data, and any available data with finer spatial resolution, are required to address the question of the spatial and temporal structure of eddy transport coefficients for 2-D models.

Another problem requiring attention, particularly in view of the need to carry out assessment studies, is a more detailed analysis of the difference between 1- and 2-D model results. While the advantages of the 2-D models are obvious, the relationship between results of the 1- and 2-D model, and the systematic differences between them, are less clearly understood.

Finally, as models of the stratosphere have become increasingly complex, the testing of models has become no easier. Simple subjective comparison of a model and an observed profile does not constitute a particularly satisfactory test. While large data sets, for example, from satellites, improve the capability of making meaningful comparisons, it is clear that much depends on the ingenuity of the experimentalists and theoreticians to construct experiments, either in the field or on the computer, which can test isolated aspects of theory.

CHAPTER 13

MODEL PREDICTIONS OF OZONE CHANGES

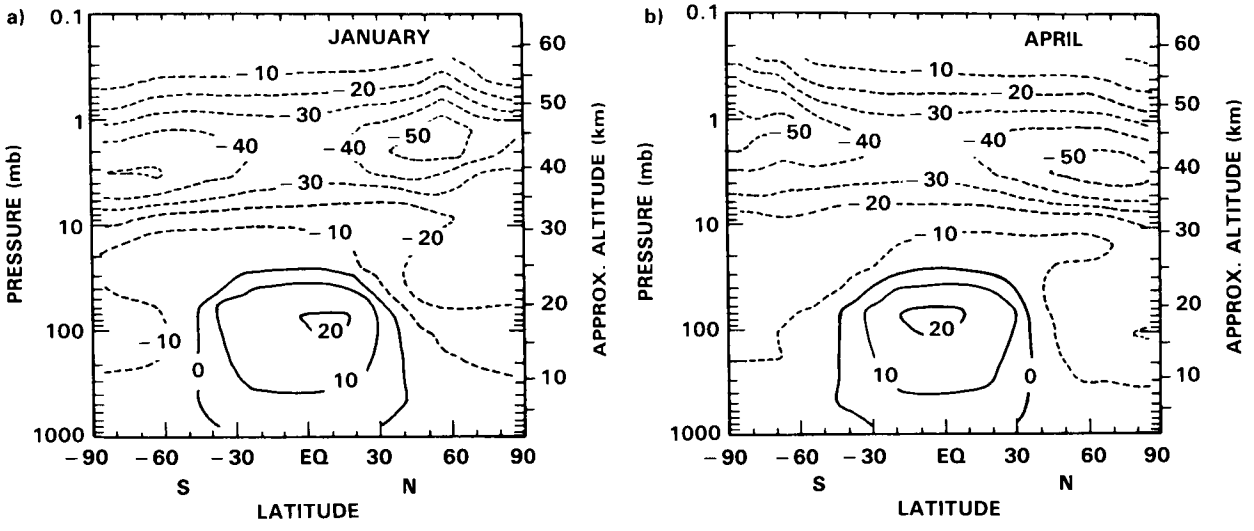

Panel Members

H.S. Johnston and F. Kaufman, Co-Chairmen

R.J. Cicerone
C.E. Kolb
M. Prather
U. Schmailzl
S. Solomon
N.D. Sze
D.J. Wuebbles

CHAPTER 13

MODEL PREDICTIONS OF OZONE CHANGES

TABLE OF CONTENTS

13.0 INTRODUCTION

For more than a dozen years, the present and future stratosphere has been modeled in increasing detail in order to estimate the effects of human activity on the composition of the atmosphere and particularly of the ozone layer. In chronological order, potential perturbations have included stratospheric flight, that is, injection of nitrogen oxides (CIAP, 1974; NRC, 1975), chlorofluoromethane release (NRC, 1976), halocarbon release in general (NRC, 1979; NASA, 1979), and the increased use of fertilizers which may increase the release of nitrous oxide from the soil and thereby increase NO_x in the stratosphere. This report is regarded as the update of the WMO Report No. 11 (1981). Among the threats to stratospheric ozone, the halocarbons, particularly CFC-11 ($CFCl_3$) and CFC-12 (CF_2Cl_2), have remained the principal ones, both because of their inertness in the troposphere and lower stratosphere and their continued usage as shown by their measured build-up over the past 15 years. Their ultimate photolysis in the mid-to-upper stratosphere (Rowland and Molina, 1975), where their chlorine atoms are released and take part in the catalytic cycle $Cl + O_3 = ClO + O_2$ and $ClO + O = Cl + O_2$ that removes odd oxygen, $O + O_3$, has been established.

Considering this simple outline of the Cl_x problem, it is perhaps surprising that model predictions of ozone-column changes have varied so widely since 1974 (NRC, 1984, p. 101) from high values of 15% to 20% depletion to low values of 3% to 5%. These model calculations all used one-dimensional eddy-diffusion to represent transport. Their variations were largely due to chemical and photochemical rate parameters, both from improved laboratory measurements and from inclusion of reactions in the mechanism that had earlier been overlooked. One might reasonably hope that the uncertainty of laboratory measurements has been reduced and that omission of critical steps is now less likely. Section 13.1 discusses these questions.

Since the 1981 WMO report, increased emphasis has been given to two important ideas, which are points of focus in this chapter: (a) The one-dimensional model predictions of ozone-column changes as a result of CFC increases are strongly dependent on concurrent increases of other trace gases, methane, nitrous oxide, and carbon dioxide (Wuebbles *et al.*, 1983; Callis *et al.*, 1983a; Sze *et al.*, 1983; DeRudder and Brasseur, 1984; Owens *et al.*, 1985a,b). Methane and nitrous oxide interact chemically with various processes that affect ozone. Carbon dioxide and also the CFCs, nitrous oxide, and methane are active in the "greenhouse effect", which (in addition to increasing surface temperature) reduces stratospheric temperatures (Chapter 15), slowing down chemical reactions that destroy ozone, and thus increasing ozone. Some combinations of increasing trace gases (Chapter 3) along with continued use of CFCs lead to ozone-column increases, instead of decreases, in the one-dimensional models. (b) Some two-dimensional models predict strong latitude gradients for ozone-column reductions as a result of increasing CFCs (Pyle, 1980; Haigh and Pyle, 1982; Haigh, 1984; Ko *et al.*, 1985; Solomon *et al*, 1985b), in the sense of larger ozone reductions in temperate and polar regions than the global average of the two-dimensional result or of the one-dimensional result. The formulation used for atmospheric dynamics (Chapter 12) affects the strength of this latitude gradient.

This chapter could have been written as a review of all articles published on this subject during the past four years, but a different approach was taken to avoid the wide variety of specific scenarios and input parameters used by the different authors. On the basis of model studies in the recent literature, a series of standard scenarios was set up for both one-dimensional and two-dimensional models. A group of modelers was invited to calculate ozone changes (and temperature changes in some cases) using these scenarios, using NASA 1985 recommendations for chemical and photochemical rate coefficients (Appendix 1) and solar spectral irradiances (Chapter 7) but otherwise using their own treatment of atmospheric motions, boundary values, and numerical methods. It is the purpose of this chapter: (a) to examine the predictions of several one-dimensional models for a number of prescribed scenarios (Section 13.1.1) in steady-state

or time-dependent approximations; (b) to examine a small number of two-dimensional steady-state calculations for a limited number of scenarios, to compare the results of the various two-dimensional models with one another, and to compare these results with those of one-dimensional models; and (c) to examine in various ways the sensitivity of the calculated predictions to the values of input parameters in order to assess recognized uncertainties in these predictions.

Most of the model calculations presented in this chapter are new and represent the generous input of modelers, listed below, both within and outside of the Chapter panel membership. We are most grateful for their help.

Panel members: R.J. Cicerone, H.S. Johnston (co-chair), F. Kaufman (co-chair), C.E. Kolb, M. Prather, U. Schmailzl, S. Solomon, N.D. Sze, D.J. Wuebbles.

Other contributors: G. Brasseur, C. Bruehl, P. Connell, P.J. Crutzen, A. Owens, R. Stolarski.

13.1 RESULTS OF MODEL CALCULATIONS

13.1.1 Scenarios For a Perturbed Atmosphere

A set of scenarios for the future evolution of the atmosphere has been selected for the 1-D and 2-D model simulations of stratospheric ozone. They are restricted in number by necessity and have been chosen to represent typical, but not necessarily most likely, scenarios. For those gases with dominant industrial sources such as the halocarbons, a range in the growth of emissions is considered. For those species with natural or uncertain sources, there is the choice of assuming that concentrations remain fixed or of extrapolating the currently observed rates of increase into the next century. Both steady-state and time-dependent scenarios have been selected and are listed in Table 13-1.

The chlorofluorocarbons are the centerpiece of chemical modeling studies for the perturbed atmosphere because (1) increases in chlorine (from halocarbons) are expected to deplete stratospheric ozone, and (2) the CFC's are known industrial pollutants with the most rapidly increasing concentrations observed among atmospheric trace gases. Chapter 3 discusses the manufacture, use, and release of halocarbons to the atmosphere. Calculated increases in the atmospheric burden of CFC's during the next 80 years range over a factor of three, depending on estimates for growth in industrial production of these compounds. The scenarios selected have a 0%, 1.5%, and 3% annual compounded growth in emissions of CFC-11 and CFC-12 as reasonable cases. It is important to note that in the modeled atmosphere, CFC-11 and -12 act as surrogates for all chlorocarbon growth in the atmosphere; growth in other industrial sources of stratospheric chlorine—such as CFC-113, CFC-22, CCl_4, and CH_3CCl_3—has not been explicitly included. Estimates of long-term growth for CFC-11 and -12 rarely exceed 3%, but inclusion of the diversity of halocarbons might lead to "effective" rates greater than this (see Quinn *et al.*, 1985). For specific effects of related CFC's see Wuebbles (1983a). Some model calculations of ozone perturbations will be presented as a function of total chlorine content of the stratosphere; results are then relatively insensitive to the specific source of stratospheric chlorine.

Bromine is also recognized as a catalytic agent leading to depletion of stratospheric ozone (Wofsy *et al.*, 1975). The halons 1211 and 1301 are expected to lead to increases in stratospheric bromine (see Chapter 3). No time-dependent scenario specific to these bromocarbons has been considered here: only the steady-state impact of a general increase in stratospheric bromine is examined (Prather *et al.*, 1984).

Table 13-1. Scenarios

STEADY-STATE SCENARIOS

*S0: Definition of 1980 reference, ambient atmosphere:

CO_2	= 340 ppmv,	N_2O	= 300 ppbv,	CH_4	= 1.6 ppmv,
CO	= 100 ppbv,	CH_3Cl	= 0.7 ppbv,	CCl_4	= 100 pptv,
CFC-11	= 170 pptv,	CFC-12	= 285 pptv,	CH_3CCl_3	= 100 pptv,

CH_3Br = 20 pptv (assumed only stratospheric source of bromine),
CFC-11 flux = 309 Gg/yr = 8.4E6 /cm²/sec,
CFC-12 flux = 433 Gg/yr = 1.34E7/cm²/sec.

S0A: Definition of background chlorine, circa 1960 atmosphere:
Same as above without CFC-11, CFC-12, CH_3CCl_3.

S1A: CFC-11 and -12 in steady state at 1980 fluxes.
*S2A: Cl_x = 8 ppbv (approx: from CFC-11 = 0.8 ppbv, CFC-12 = 2.2 ppbv).
*S2B: Cl_x = 8 ppbv plus 2 × CH_4 (concentration), 1.2 × N_2O.
S2C: Cl_x = 8 ppbv plus 2 × CH_4, 1.2 N_2O and 2 × CO_2.
*S3A: Cl_x = 15 ppbv (approx: from CFC-11 = 1.6 ppbv, CFC-12 = 4.4 ppbv).
*S3B: Cl_x = 15 ppbv plus 2 × CH_4 (concentration), 1.2 × N_2O.
S3C: Cl_x = 15 ppbv plus 2 × CH_4, 1.2 × N_2O, and 2 × CO_2.
S4: 1980 with 2 × CH_4 concentration.
S5: 1.2 × N_2O.
S6: 2 × CO.
S7: 2 × CO_2.
S8: NO_x injection from stratospheric aircraft 1000 molec $cm^{-3}s^{-1}$ or 2000 molec $cm^{-3}s^{-1}$ at 17 km and 20 km.
S9: Bromine increase from 20 pptv to 100 pptv.

TIME-DEPENDENT SCENARIOS (Based on 1980 Start-up Atmosphere Above)

T1A: CFC emissions at 1980 production rates, others (N_2O, CH_4, CO, CO_2) at fixed concentrations.
T1B: Time-dependent CFC's (fixed flux) plus increasing concentrations of CH_4 (1% per yr), N_2O, (0.25% per yr), and CO_2 (DOE scenario).
T1C: Same as T1B, but without increase in CH_4 and N_2O.
T2A: CFC emissions begin at 1980 rates and grow 1.5% per yr. (compounded), others fixed.
T2B: Same as T2A but with increasing CH_4 (1% per yr), N_2O (0.25% per yr), and CO_2 (DOE scenario).
T3A: CFC emissions grow at 3% per yr (compounded), others fixed.
T3B: Time-dependent CFC's (3% per yr) plus increasing concentrations of CH_4 (1% per yr), N_2O (0.25% per yr), and CO_2 (DOE scenario).

*Also used as 2-D model scenario

Other trace gases are strongly coupled with stratospheric photochemistry involving ozone. A prerequisite to predicting ozone in the future is an understanding of how the concentrations of stratospheric H_2O, CH_4, N_2O, and NO_x will evolve. Radiatively active trace gases, dominated by CO_2, further impact ozone directly by reducing stratospheric temperatures and indirectly through changes in global climate (see Chapter 15). There is insufficient information on stratospheric water vapor to characterize trends on a global basis (Mastenbrook and Oltmans, 1983). Possibly, water vapor may be altered with changing climate as CO_2 increases, but no global models are currently able to predict the distribution and physical processes controlling water vapor in today's stratosphere (see Chapter 5). The concentrations of methane and nitrous oxide are currently observed to be increasing at annual rates of approximately 1% and 0.25%, respectively. Sources of these gases and the cause of their increases are not well defined. Theories differ as to the causes of the current change (see Chapter 3). Without a model of the evolution of the fluxes of these gases, the scenarios here consider the two possibilities of continued growth at these rates or of constant abundance. Two anthropogenic sources of odd-nitrogen that may lead to ozone perturbations are considered: (1) fleet of stratospheric aircraft that is mainly of interest for historical comparison with previous calculations; (2) the NO_x emitted in the upper troposphere by commercial aviation in the 1990's that may lead to significant increase in tropospheric ozone (Wuebbles *et al.*, 1983).

The scenarios for time-dependent change in atmospheric composition are summarized in Table 13-1 and focus on those gases which directly affect the stratosphere: CFC's, N_2O, CH_4, and CO_2. For CFC's, growth is in terms of emissions; these gases do not approach steady-state in the next 100 years. For the others, concentrations are specified as discussed above. Increases in CO_2 (DOE scenario, Wuebbles *et al.*, 1984) are assumed to affect only stratospheric temperatures.

The use of steady-state scenarios allows for a simple examination of the effects of a perturbing influence on the atmosphere. In this case, only the initial and final states need be specified, not the complete history of the system. A steady-state scenario can therefore never refer to a specific time in the future, but it may be chosen to have conditions typical of a future time. The baseline case (0) for the steady-state scenarios listed in Table 13-1 is selected from observed atmospheric concentrations circa 1980, and a background chlorine atmosphere is defined simply as the 1980 atmosphere without CFC's and CH_3CCl_3. Three types of chlorine perturbations are considered for the steady-state scenarios: (1) CFC-11 and -12 emissions at 1980 (estimated) rates; (2) CFC-11 and -12 concentrations fixed at levels resulting in approximately 8 ppbv total chlorine (Cl_x); and (3) CFC-11 and -12 concentrations fixed to yield 15 ppbv of Cl_x. Other scenarios examine the specific effects of increased levels of $CH_4(\times 2)$, $N_2O(\times 1.2)$, and $CO_2(\times 2)$ which might be expected if current growth were extrapolated approximately 75 years. These increased concentrations are also coupled with the chlorine perturbations (2) and (3) above, in an attempt to consider a likely condition for the atmosphere in the middle of the next century. As such, these coupled, steady-state scenarios are the focus of the 2-D model calculations. Steady-state scenarios include additional perturbations due to CO, tropospheric NO_x, NO_x from stratospheric aircraft, and bromine which are analyzed by 1-D models. These cases are regarded as sensitivity studies for hypothetically isolated parameters, even though interactions in the real atmosphere make it impossible to change these quantities one at a time.

13.1.2 Assessment Calculations with 1-D Models

For the scenarios given in Table 13-1, the calculated ozone changes according to one-dimensional models are given in Tables 13-2, 3, and 4. Steady-state calculations for hypothetical single species scenarios are discussed first. There is a long record of diagnostic calculations for such scenarios with which to compare model results. In addition to historical purposes, steady-state analyses of individual perturbations are useful for interpreting the mechanisms that influence a given species effects on atmospheric ozone. For analysis

of their nonlinear interactions and for comparison with 2-D model results, steady-state calculations with coupling of several assumed species perturbations are discussed. Steady-state multiple species perturbations provide a means for interpreting the effects on ozone from complex time-dependent scenarios to be discussed later.

13.1.2.1 Steady-State Perturbations

For the purpose of this report, six groups using one-dimensional models of the troposphere and stratosphere calculated the steady-state perturbations to be discussed here. Included are results from models

Table 13-2. Change in Total Ozone from Representative One-Dimensional Models for Steady State Scenarios Containing Cl_x Perturbations. Numbers in Parentheses Refer to Calculated Changes when Including Temperature Feedback.

		Change in Total Ozone (%)					
	Scenario	LLNL (Wuebbles)	Harvard (Prather)	AER (Sze)	DuPont (Owens)	IAS (Brasseur)	MPIC (Bruehl)
S1A	CFC 1980 Flux only	−7.0 (−7.2)	−5.3	−5.3	−4.9 (−6.1)	(−7.9)	(−9.4)
S2A	8 ppbv Cl_x only	−5.1 (−5.7)	−2.9	−4.6		(−4.1)	(−9.1)
S2B	8 ppbv Cl_x + 2 × CH_4 + 1.2 × N_2O	−3.4 (−2.8)	−3.0	−3.3	−3.1	(−2.3)	(−6.0)
S2C	8 ppbv Cl_x + 2 × CH_4 + 1.2 × N_2O + 2 × CO_2	(+0.2)			(−1.4)	(0.0)	(−5.2)
S3A	15 ppbv Cl_x only	−12.2 (−12.4)	−17.8	−15.		(−8.8)	(−22.0)
S3B	15 ppbv Cl_x + 2 × CH_4 + 1.2 × N_2O	−7.8 (−7.2)	−8.2	−8.8	−7.2	(−5.6)	(−13.7)
S3C	15 ppbv Cl_x + 2 × CH_4 + 1.2 × N_2O + 2 × CO_2	(−4.6)				(−3.5)	(−13.6)

Relative to atmosphere with about 1.3 ppbv background Cl_x and with no CFC (S0A).

Table 13-3. Change in Ozone at 40 km for Steady State Scenarios Containing Cl_x Perturbations. Numbers in Parentheses Refer to Calculated Changes Including Temperature Feedback.

	Scenario	Change in 40 km Ozone (%) LLNL (Wuebbles)	Harvard (Prather)	AER (Sze)	DuPont (Owens)	IAS (Brasseur)	MPIC (Bruehl)
S1A	CFC 1980 Flux only	−63 (−56)	−64	−62	−62 (−57)	(−81)	(−59)
S2A	8 ppbv Cl_x only	−55 (−50)	−57	−56		(−67)	(−57)
S2B	8 ppbv Cl_x + 2 × CH_4 + 1.2 × N_2O	−50 (−45)	−50	−49	−58	(−62)	(−50)
S2C	8 ppbv Cl_x + 2 × CH_4 + 1.2 × N_2O + 2 × CO_2	(−35)			(−49)	(−55)	(−45)
S3A	15 ppbv Cl_x only	−74 (−68)	−78	−77		(−83)	(−76)
S3B	15 ppbv Cl_x + 2 × CH_4 + 1.2 × N_2O	−69 (−64)	−73	−64	−74	(−81)	(−71)
S3C	15 ppbv Cl_x + 2 × CH_4 + 1.2 × N_2O + 2 × CO_2	(−58)				(−78)	(−67)

Relative to atmosphere with about 1.3 ppbv background Cl_x and with no CFC (S0A).

at Lawrence Livermore National Laboratory (D. Wuebbles), Harvard University (M. Prather), Atmospheric and Environmental Research, Inc. (D. Sze), E.I. DuPont de Nemours & Company (A. Owens), the Belgium Institute for Aeronomy (G. Brasseur), and the Max Planck Institute (MPIC) in Mainz, West Germany (Bruehl and Crutzen). Each of these models has updated model chemistry to correspond to the rates prescribed in this report (Appendix A). However, treatments of other physical and chemical processes are done differently in each of these models. In particular, as discussed in Chapter 12 many of the models make different assumptions about transport parameters, diurnal averaging procedures, and photodissociation cross sections.

Table 13-4. Changes in Ozone for Steady State Scenarios. Results Are Relative to Present Atmosphere (S0), Except for AER and DuPont Calculations, Which Are Relative to Background Atmosphere Without CFCs (S0A). Numbers in Parentheses Refer to Calculated Changes When Including Temperature Feedback.

		Change in Total Ozone (%)					
	Scenario	LLNL (Wuebbles)	Harvard (Prather)	AER (Sze)	DuPont (Owens)	IAS (Brasseur)	MPIC (Bruehl)
S4	2 × CH_4	+2.0 (+2.9)	+0.3	+0.9	+1.7	(+1.6)	(+1.4)
S5	1.2 × N_2O	−2.1 (−1.7)	−2.6	−1.8	−2.3	(−1.1)	(−1.2)
S6	2 × CO	+1.1 (+1.1)	+0.3	+0.6	+0.8		(+0.8)
S7	2 × CO_2	(+3.5)		(+2.6)	(+2.8)	(+3.1)	(+1.2)
S8a	NO_x, injection 17 km, 1000 molec. $cm^{-3}s^{-1}$	−1.8 (−1.3)				(−1.4)	
S8b	NO_x, 17 km, 2000 molec. $cm^{-3}s^{-1}$	−5.7				(−3.4)	
S8c	NO_x 20 km, 1000 molec. $cm^{-3}s^{-1}$	−5.7 (−4.6)				(−3.9)	
S8d	NO_x, 20 km, 2000 molec. $cm^{-3}s^{-1}$	−12.2				(−8.8)	
S9	Br_x 20 to 100 pptv	−3.0					

Tables 13-2 and 13-4 give the calculated changes in total ozone from each of the 1-D models relative to a calculated reference atmosphere (scenarios SO or SOA in Table 13-1) for the steady-state scenarios. Table 13-3 gives the change in ozone at 40 km from each model for those scenarios involving chlorine (Cl_x) perturbations. In contrast to prior reports, most of the models now include radiative submodels that calculate atmospheric temperatures, and thereby include temperature feedback effects on atmospheric

chemistry and photochemistry. Results in Tables 13-2 through 13-4 including temperature feedback are represented in parentheses. Since the primary purpose of this section is to describe the mechanisms important to ozone change from the steady-state perturbations, and because of the complexity of discussing in depth the results from many different models, many of the figures in this section will be based on the results of a single model, primarily that at LLNL. Relevant differences in calculated results between models will be described in the text.

Chlorocarbons only

A standard scenario for comparing model results for chlorine perturbations has historically been the calculation of CFC-11 and CFC-12 constant emissions to steady state. Results in Table 13-2 indicate a range in model-calculated change in total ozone of -5 to -7% for models without temperature feedback and -6 to -9% with temperature feedback; these results are for scenario S1A, which assumes a constant flux of CFC-11 and CFC-12 at 1980 levels to steady state. These values may be compared to the -5 to -9% ozone change in WMO (1981), and -2 to -4% determined in NRC (1984). Small changes in a number of chemical rate constants in the latest evaluation (see Appendix A) have tended to increase the calculated impact on ozone for this scenario since the 1984 NRC assessment. With and without temperature feedback,the calculated changes in total ozone range from -3 to -9% for 8 ppbv Cl_x (S2A relative to atmosphere without CFC's), and from -9 to -22% for 15 ppbv Cl_x (S3A). As will be discussed later, some of the differences between models, particularly for large Cl_x perturbations, is related to the ambient amounts of total odd-nitrogen calculated.

Percentage changes in ozone as a function of altitude for three scenarios are shown in Figures 13-1, 13-2 and 13-3 for the LLNL model. All of the models produce large percentage decreases in ozone in the upper stratosphere, near 40 km. As seen in Table 13-3, most models calculate similar ozone changes in this region. Figure 13-4 gives the change in calculated (AER) ozone concentration as a function of altitude for the same cases as Figures 13-2 and 13-3; the small percentage changes around 25 kilometers represent large changes in ozone concentration. Figure 13-5 shows the vertical distributions in the rates of reaction for the primary odd-oxygen loss mechanisms as calculated for the current atmosphere by LLNL. As indicated in this figure, the chlorine catalytic cycle peaks in the region near 40 km, where a large percentage decrease in ozone is calculated. Small increases in ozone are calculated for ozone in the lower stratosphere, primarily due to the ozone recovery mechanism (increased O_2 photolysis and resultant ozone production at lower altitudes as ozone is destroyed above) and due to Cl_x interference with the dominating NO_x catalytic cycle (see Figure 13-5) from $ClONO_2$ production.

Table 13-5 shows model calculated atmospheric lifetimes for CFC-11, CFC-12, and N_2O. Differences for the calculated lifetimes occur between models due to several factors: (1) use of different transport parameterizations, and (2) use of different assumptions for photolysis calculations.

Until recently, it was generally thought that the change in total ozone calculated in 1-D stratospheric models for chlorocarbon perturbations was approximately linear, that is, the percentage change in total ozone relative to the amount of stratospheric chlorine (Cl_x) was nearly constant. In contrast to previous model results in WMO (1981), a study by Cicerone *et al.* (1983a) indicated that for small Cl perturbations (<4 ppbv), the response of total ozone in their updated model is highly nonlinear. They reported very little calculated change in total ozone for these amounts of Cl_x and found the extent of the nonlinearity to be sensitive to the detailed treatment of physical and chemical processes in the model. Herman and McQuillan (1985) did not find this nonlinear relation and suggest that the presence of a nonlinear response

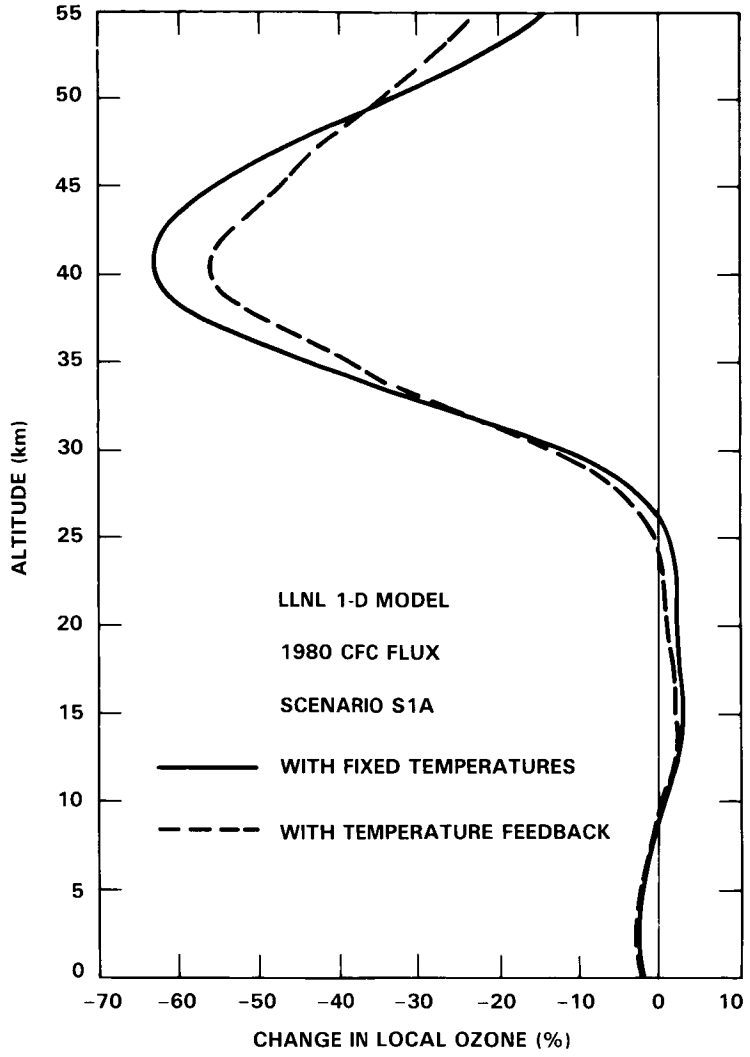

Figure 13-1. Calculated percentage change in local ozone at steady state for constant CFC-11 and CFC-12 fluxes at 1980 rates relative to the atmosphere with no CFC.

is dependent on model assumptions about diurnal averaging. All models used in this study appear to have an approximately linear response in total ozone response to small Cl_x changes.

For large Cl_x perturbations (>12 ppbv), Prather et al. (1984) found a significant nonlinearity in the ozone-Cl_x relationship, with a rapid decrease in the total ozone column occurring for incremental additional Cl_x when the Cl_x level approximately exceeds that of stratospheric odd-nitrogen. The nonlinearity for large Cl_x perturbations may have significant implications for the interpretation of effects if chlorocarbon emissions increase substantially. Other models (e.g. Wuebbles and Connell, 1984; Stolarski, 1984) have found a similar behavior.

Figure 13-6 shows recent model results from Owens and Fisher of DuPont, which illustrates a number of interesting points. The independent variable is total Cl_x in the upper stratosphere, regardless of the scenario by which it was achieved. The calculated ozone change is presented as a function of stratospheric

Table 13-5. Calculated Lifetimes of CFC-11, CFC-12, and N_2O in Representative 1-D Models.

	t (years)		
	CFC-11	**CFC-12**	**N_2O**
LLNL	75	137	118
Harvard (Prather)	84	144	166
AER (Sze)	64	126	152
DuPont (Owens)	68	140	165
IAS (Brasseur)	87	154	166

Cl_x for several different values of stratospheric NO_y. For large NO_y (about 30 ppbv) the decrease of ozone is small and very nearly linear with increasing Cl_x, but for small background NO_y (13 ppbv) ozone is strongly and nonlinearly reduced by Cl_x . This effect of NO_y is large: with 31 ppbv NO_y, 18 ppbv Cl_x is calculated to reduce ozone by 4.5%; but with 13 ppbv NO_y, 18 ppbv Cl_x is calculated to reduce the ozone column by 45%. There are several interactions between the NO_x and Cl_x systems, and a major one is indicated by Figure 13-5. In the 20 to 40 km range of the "1985" stratosphere, the NO_x catalytic cycle is the most important mechanism of ozone destruction. An increase in Cl_x causes an ozone reduction by way of the Cl_x catalytic cycle, but ClO binds catalytically active NO_2 into the inactive form of chlorine nitrate, which reduces the dominant mid-stratospheric ozone-reducer (NO_x) to give an ozone increase by virtue of a double negative. When Cl_x approximately exceeds NO_y, then chlorine becomes the dominant source of ozone reduction in the middle stratosphere, and further increases of Cl_x have their full effect on ozone with relatively minor counter effect from reducing the NO_x ozone-reducer.

Methane

Model results for a doubling of methane, from approximately 1.6 to 3.2 ppmv, give an increase of ozone ranging from 0.3% to 2.9%, as shown in Table 13-4. Results from most of the models are relative to the 1980 reference atmosphere (SO, 2.5 ppbv Cl_x) but results from AER and DuPont are relative to non-CFC reference case (SOA, 1.3 ppbv Cl_x). Each of the models gives similar qualitative changes in ozone with altitude to that in the LLNL model, shown in Figure 13-7. Absolute differences between models appear to be explainable in terms of the sensitivity of changes in ozone from CH_4 increase due to differences in local amounts of Cl_x, NO_x, and HO_x as a function of altitude. This sensitivity will be discussed in the following paragraphs.

In the LLNL model, a doubling of methane increases ozone from the surface to 45 km. In terms of total ozone change, the largest absolute increases in ozone occur around 15 km and around 35 km. In the troposphere and lower stratosphere methane oxidation produces ozone through the CH_4-NO_x-smog-reactions (Crutzen, 1973a; Johnston, 1984; Chapter 4). A doubling of surface CH_4 concentrations increases net photochemical production of ozone between the surface and 18 km by about 50%. This result will depend critically on the tropospheric and lower stratospheric abundance of NO. If NO concentrations are

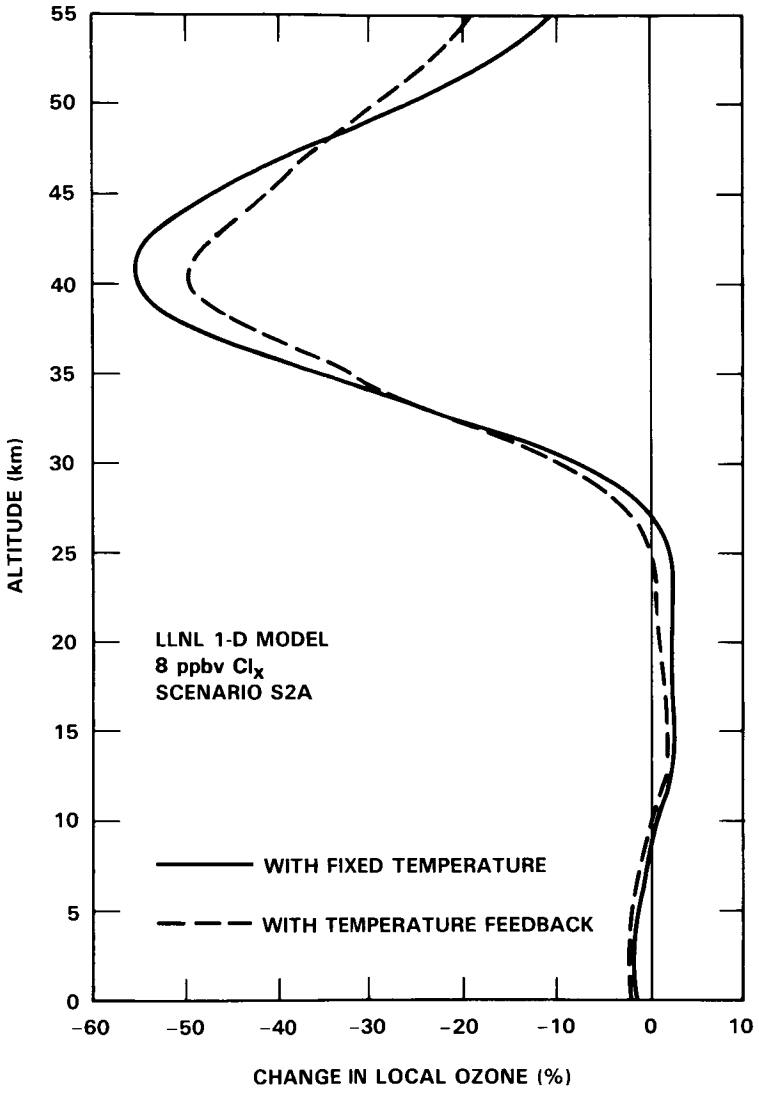

Figure 13-2. Calculated percentage change in local ozone at steady state for 8 ppbv stratospheric Cl_x relative to background with 1.3 ppbv Cl_x.

small enough, the added HO_x from methane oxidation would decrease ozone. For the present simulation, the CO surface mole fraction was held fixed. Since CH_4 is a source of CO in the atmosphere, the impacts on tropospheric OH and O_3 would be somewhat larger if a constant surface flux boundary condition were assumed for CO.

The changes in ozone above the tropopause result from direct effects of the increased CH_4 and indirect effects due to the HO_x produced by methane oxidation. For a doubling of methane, stratospheric OH concentrations are increased between 20 and 50% and stratospheric HO_2 is increased up to 100% in the LLNL model. The resulting increase in HNO_3 and HNO_4 production reduces NO_2 concentrations. There is a subsequent reduction of 5 to 15% in the NO_x catalytic loss rate from $NO_2 + O$ and an increase in O_3 due to this mechanism throughout much of the stratosphere.

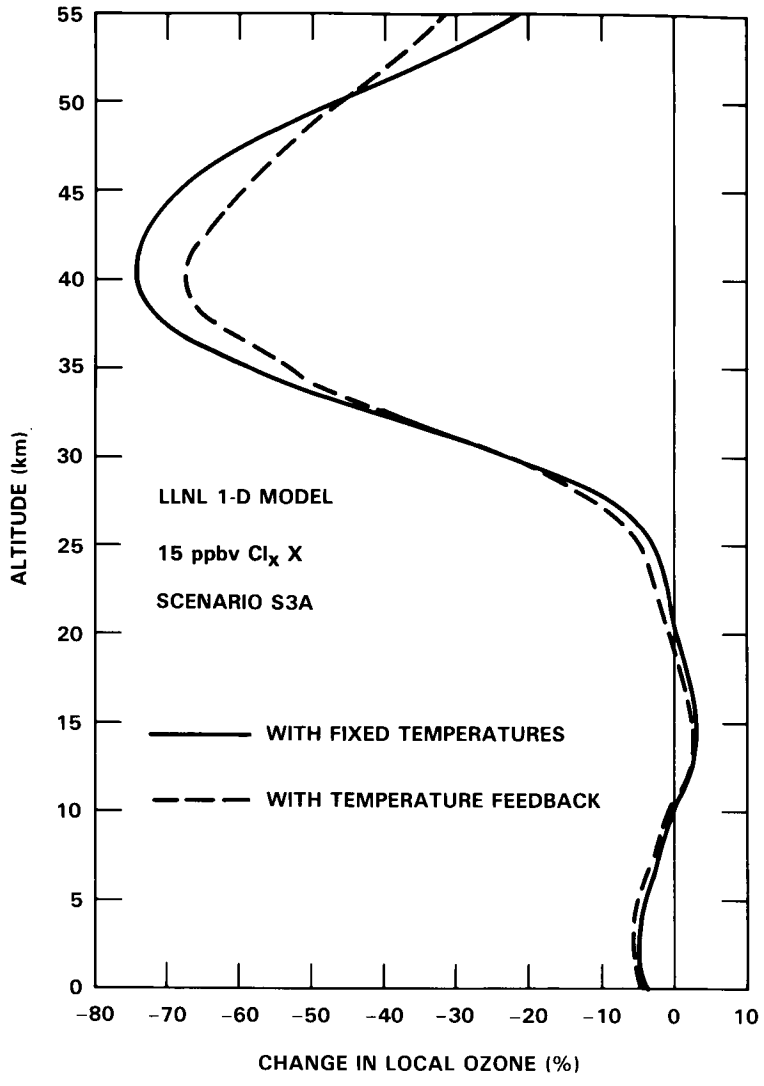

Figure 13-3. Calculated percentage change in local ozone at steady state for 15 ppbv stratospheric Cl_X relative to background with 1.3 ppbv Cl_X.

Methane is both a source and sink for Cl_X in the stratosphere [$CH_4 + Cl = HCl + CH_3$, OH (from methane) + $HCl = Cl + H_2O$]. The pronounced ozone increase near 35-40 km in the LLNL model primarily results from an approximately 25% decrease in ClO, where the Cl_X loss to methane exceeds the Cl_X recovery from the methane produced OH. Production of HCl by the reaction of Cl with CH_4 is the primary loss process for active chlorine radicals,and this loss of Cl_X is greater than the increase of Cl_X from the methane-produced hydroxyl radicals. Above 45 km, the increased HO_X from methane oxidation leads to direct ozone catalytic destruction and a resultant net decrease in ozone at these altitudes (compare Owens *et al.*, 1982a).

Nitrous Oxide

The reaction $O(1D) + N_2O = 2\ NO$ provides the major source of odd nitrogen (NO_X) in the stratosphere. Stratospheric formation of NO_X from N_2O occurs primarily in the middle stratosphere, from

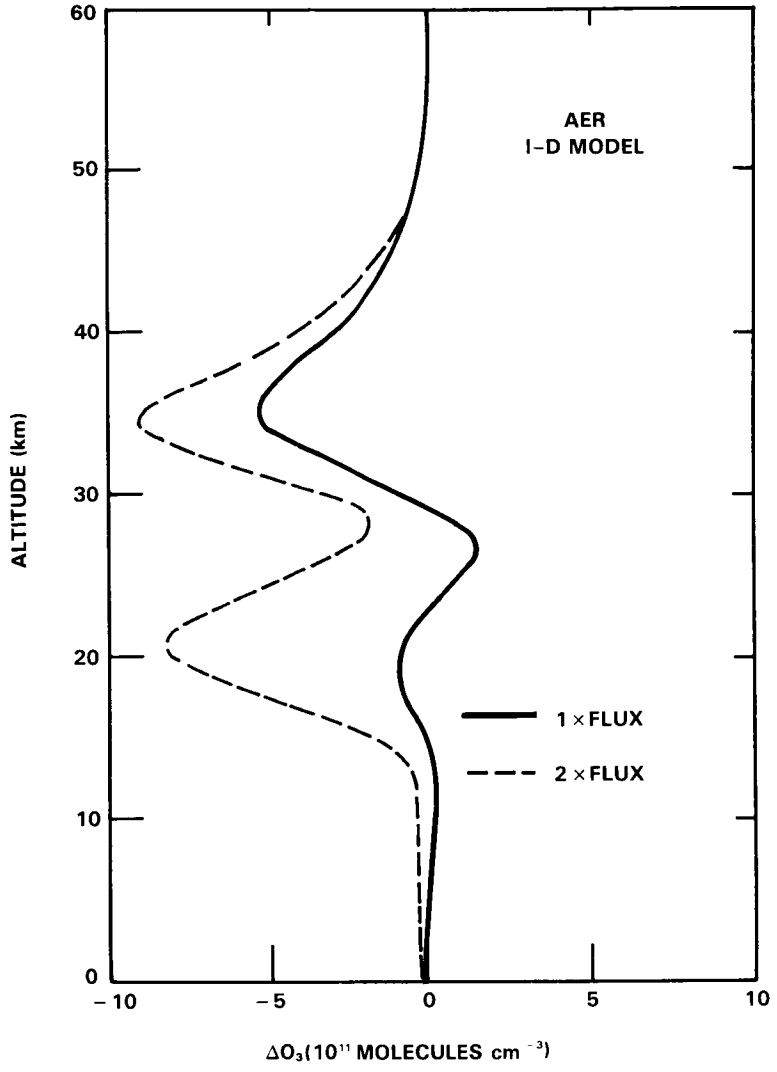

Figure 13-4. Calculated change in ozone concentration (molecules cm^{-3}) by AER 1-D model as a function of altitude relative to a baseline with no CFC. A flux at the lower boundary equal to the 1980 CFC production rate is adopted for the 1x case (about 8 ppbv stratospheric Cl_x) and the 2x case corresponds to twice the above flux (about 15 ppbv stratospheric Cl_x).

about 20 to 40 km. As shown in Figure 13-5, catalytic destruction of ozone by NO_x is most efficient in this region, and increases in N_2O should lead to decreases in stratospheric ozone. From Table 13-4 model results indicate that an increase in the background concentrations of N_2O by 20% from about 300 to 360 ppbv, gives a decrease in total ozone ranging from 1.1 to 2.6%. As seen in Figure 13-8, peak ozone destruction occurs near 35-40 km in the LLNL model. Similar behavior is found in the results from other models. The small calculated increase in upper tropospheric and lower stratospheric ozone is due to increased efficiency of the CH_4-NO_x-smog reactions from the added NO_x. The small decrease in ozone in the lower troposphere results from a combination of increased HO_x, due to larger UV penetration (since O_3 is decreased at higher altitudes) and consequent reaction of local $O(^1D)$ with H_2O, plus decreased NO_x due to increased conversion of HNO_3 and HNO_4 in the calculated downward flux of odd nitrogen from the stratosphere.

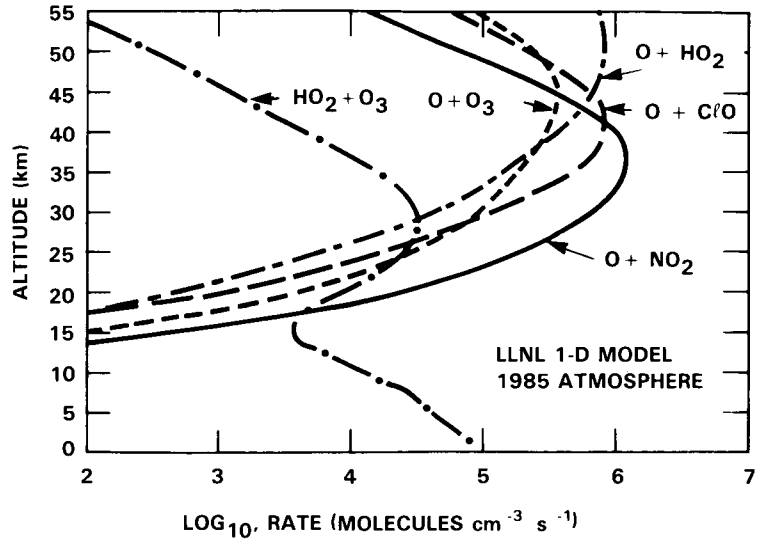

Figure 13-5. Calculated rates of key odd oxygen loss processes for 1985 atmosphere.

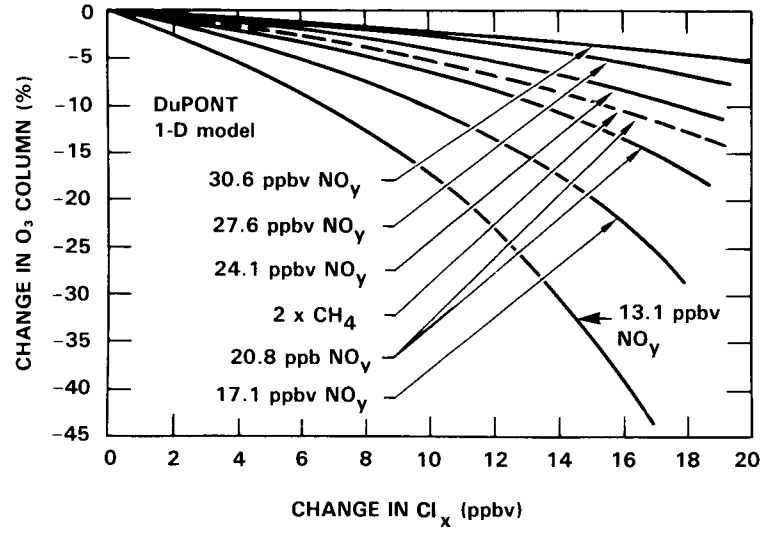

Figure 13-6. Calculated percentage change in ozone column as a function of stratospheric Cl_x for various levels of stratospheric NO_y and CH_4.

Carbon Monoxide

The perturbation scenario considered for CO is the doubling of present surface concentrations (from approximately 100 to 200 ppbv). For five 1-D models, the resultant changes in calculated total ozone vary from an increase of 0.3% to 1.1% (see Table 13-4). As seen in Figure 13-9 most of the change in ozone occurs in the troposphere. As discussed in Chapter 4, carbon monoxide participates in the chemistry of the free troposphere as a sink for OH by its oxidation to CO_2, and as a source (or sink) for ozone by the "smog" reactions. For the LLNL model, doubling CO increases tropospheric ozone source terms by about 14% and the total atmospheric column by 1.1%.

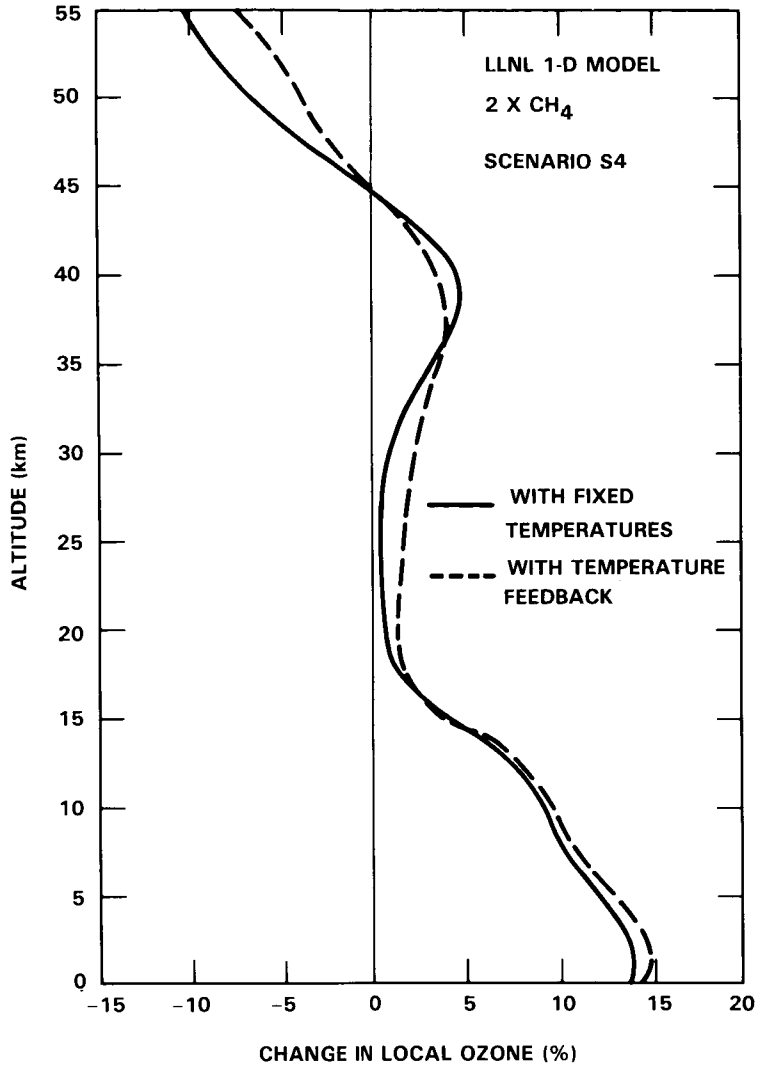

Figure 13-7. Calculated percentage change in local ozone as a result of doubled atmospheric methane.

There is a close relationship among OH, CH_4, and CO concentrations; therefore, an increase of any one of these species has significant effects on the others and on other important trace gases (Levy, 1971, 1972; Wofsy *et al.*, 1972; Wofsy, 1976; Sze, 1977; Chameides *et al.*, 1977b). This calculation of doubled carbon monoxide with other surface concentrations held constant seems especially artificial, and it is to be emphasized that these single specie scenarios are artificial sensitivity studies (analogous to partial derivatives in the calculus of multiple variables).

Carbon Dioxide

The calculated changes in ozone as a function of altitude as a result of doubling CO_2 are shown in Figure 13-10. The maximum percentage effect is near 40 km. Unlike the other trace gases that can perturb stratospheric ozone, carbon dioxide (CO_2) does not affect ozone through direct chemical interactions. Absorption of solar radiation by stratospheric ozone and infrared emission to space by carbon dioxide are primarily responsible for balancing radiative energy in the stratosphere. Thus, an increase in CO_2 concentration

C-2

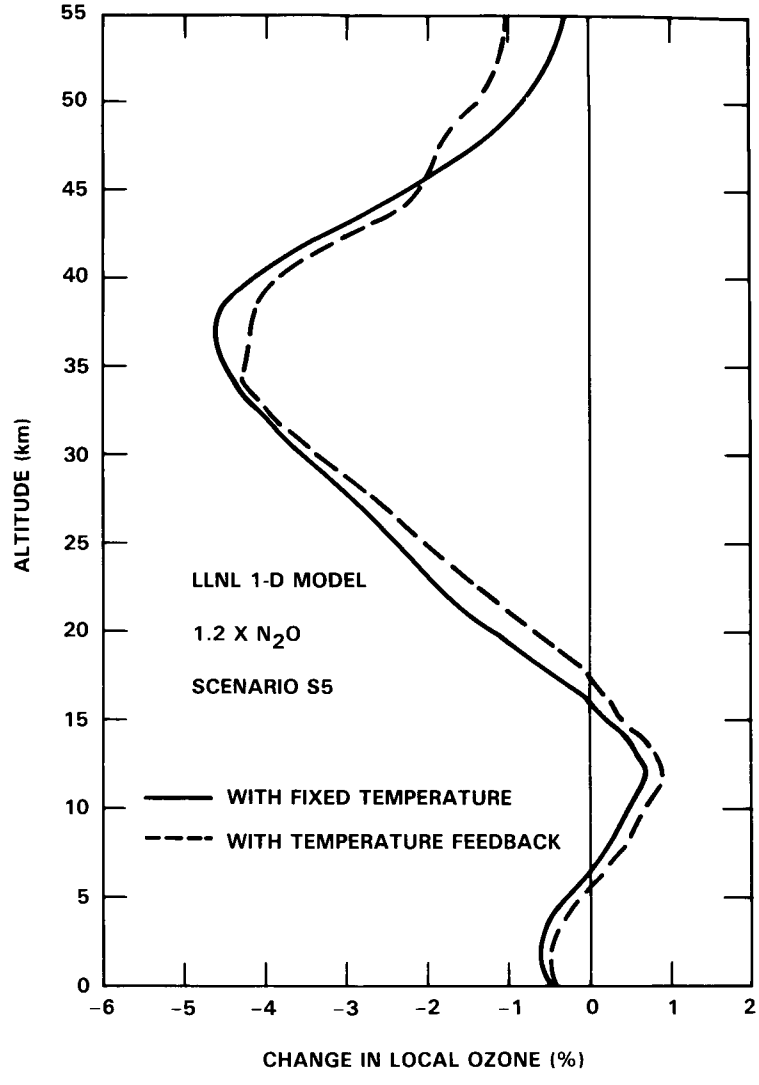

Figure 13-8. Calculated percentage change in local ozone for 20% increase in nitrous oxide.

alters the heat balance, reducing stratospheric temperatures, and leading to a slowing down of temperature-dependent ($O + O_3$, $NO + O_3$) ozone-destruction reactions. This results in a net increase in stratospheric ozone concentrations. (For very high chlorine perturbations, the opposite effect of CO_2 may occur: lower temperature reduces the rate of $Cl + CH_4$, increasing the concentration of ozone destroying Cl and ClO relative to inert HCl).

For a doubling of CO_2 the various models calculate changes in temperature at 40 km between -7 and -9 K, calculate changes in local ozone at 40 km between +9 and +19%, and calculate changes in the ozone column between 1.2 and 3.5% (Table 13-6). All of the 1-D radiative convection models, except that of LLNL, calculate increases in surface temperature also; whereas the LLNL model has a fixed surface temperature. A sensitivity study by Wuebbles (1983a) indicates that this feature causes the LLNL model to overestimate the total ozone increases by about 0.4%.

Table 13-6. Percentage Changes in Ozone Column, Ozone at 40 km, and Temperature at 40 km for Scenario S7, a Doubling of CO_2 Relative To Present Atmosphere as Calculated by 1-D Models.

Model	Ozone Column %	Ozone at 40 km %	Temp. at 40 km K
LLNL (Wuebbles)	+3.5	+19.3	−8.0
AER (Sze)	+2.6	+9.4	−8.4
DuPont (Owens)	+2.8	+11.5	−7.4
IAS (Brasseur)	+3.1	+18.8	−9.0
MPIC (Bruehl)	+1.2	+13.0	−7.1

Nitrogen Oxides

Historically, concern about the possible impact of anthropogenic trace gas emissions on ozone began in the early 1970's with studies of the effects from potential emissions of nitrogen oxides (NO_x) from high-flying supersonic aircraft (e.g., see Johnston, 1971; CIAP, 1974; NRC, 1975). Although no such fleets are currently proposed, the scenarios assumed at that time for hypothetical fleets of stratospheric aircraft flying at altitudes of 17 and 20 km remain useful as an indication of the effects of nitrogen oxide emissions on atmospheric ozone. Results from the LLNL model for NO_x emissions of 1000 molecules $cm^{-3}s^{-1}$ and 2000 molecules $cm^{-3}s^{-1}$ injected at altitudes of 17 and 20 km are given in Table 13-4 and Figure 13-11. Also shown in Table 13-4 are results from the model by Brasseur. Calculated changes in total ozone are comparable to model results in the mid-1970's (compare section 13.2.2.2). As seen in Figure 13-11, the primary effects of the emitted NO_x occur near the altitude of injection, in the region where the NO_x catalytic cycle is the dominant cause of ozone loss (Figure 13-5).

Of more immediate concern are impacts on ozone from surface emissions of odd nitrogen and from the emissions of NO_x from subsonic aircraft in the troposphere and lower stratosphere. Several studies suggest that these emissions may be influencing tropospheric ozone concentrations, with a net increase in ozone generally expected from the methane-NO_x-smog reactions (e.g. Logan *et al.*, 1981; Liu *et al.*, 1983; Callis *et al.*, 1983; Wuebbles *et al.*, 1983; Wuebbles, 1983a).

Bromine

Sources of stratospheric bromine are discussed in Chapter 3. Although bromine chemistry is in many respects similar to that for chlorine, there are also significant differences. Dissociation and reactions of CH_3Br and other important bromine sources occur at lower altitudes than for the major chlorine sources. While the reaction of Cl with CH_4 to produce HCl limits the abundance of active chlorine radical species in the stratosphere, the reaction of Br with CH_4 is endothermic and therefore negligibly slow. Also, the

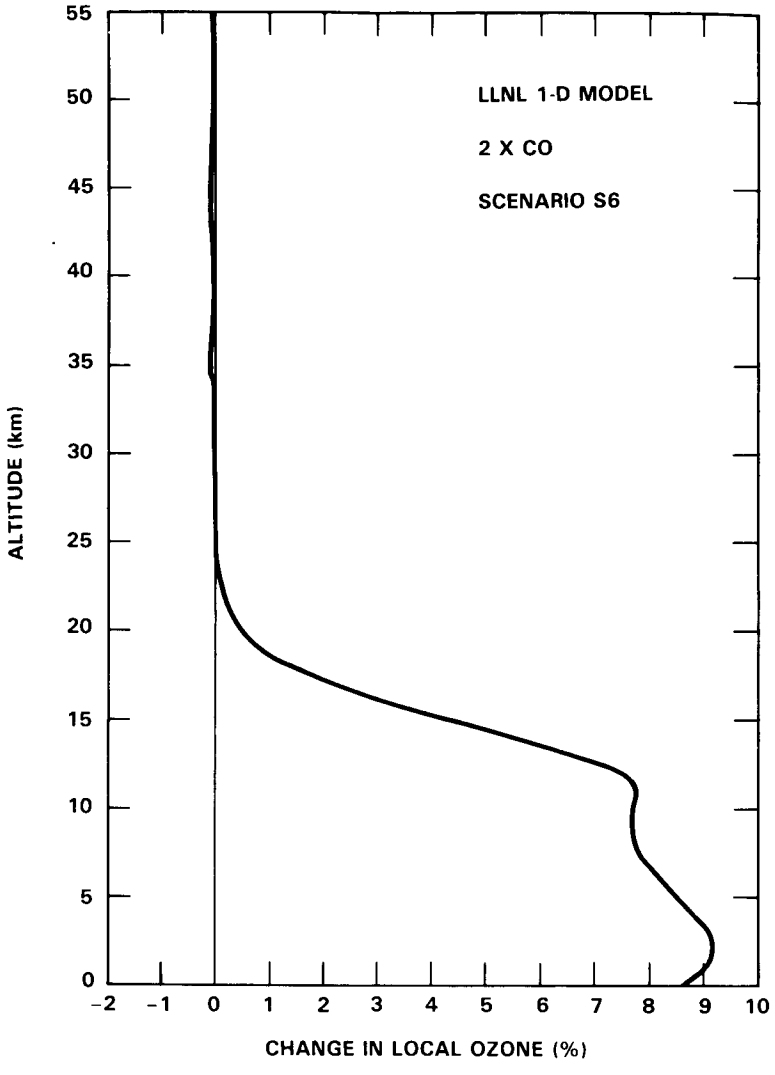

Figure 13-9. Calculated percentage change in local ozone for doubling of carbon monoxide.

photolysis of HBr is more rapid than that of HCl, and the reaction of OH with HBr is more rapid than its rate with HCl. Consequently, the majority of Br_x is present as the active species BrO. On a molecule for molecule basis, bromine is a much more efficient sink for stratospheric odd oxygen than chlorine. The details of Br_x chemistry are given in Chapter 2, Section 4.

The bromine perturbation scenario, posed as a sensitivity test only, considered is an increase in surface mole fraction of CH_3Br from 20 to 100 pptv. As seen in Table 13-4, the LLNL model was the only model used to calculate the perturbation. It gave a total ozone change of -3% (without temperature feedback), in good agreement with the -4% calculated change in total ozone for the same scenario by Prather *et al.* (1984). The relative change in ozone abundance as a function of altitude is shown in Figure 13-12. The major contribution to the change in the ozone column occurs around 20 km. The largest relative change in ozone (7% decrease) is at 15 km with a secondary peak at about 40 km.

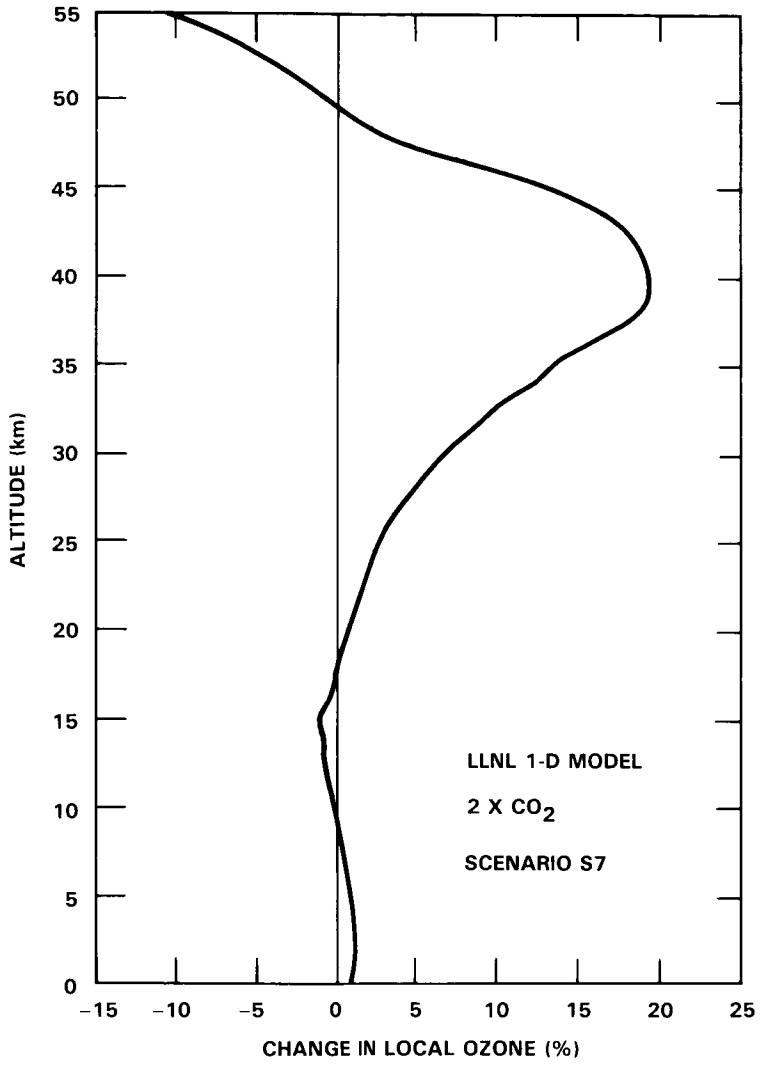

Figure 13-10. Calculated percentage change in local ozone for doubling of carbon dioxide.

Because the ozone depletion occurs mostly below the ozone concentration maximum, little increase in the penetration of UV, active in dissociating oxygen, is calculated. For this scenario the lower stratospheric ozone decrease results mostly from an increase of the rate of BrO + BrO. The reaction BrO + ClO contributes throughout the middle stratosphere. The small secondary peak at 40 km is caused largely by BrO + O.

Combined Scenarios

The calculated steady-state changes in total ozone and ozone at 40 km are shown in Tables 13-2 and 13-3 respectively, for several combined scenarios (S2, b, c, and S3 b and c) involving chlorocarbon emissions to give about 8ppbv or 15 ppbv of upper stratospheric Cl_x, doubled methane, nitrous oxide increased by 20%, and, in some cases, doubled carbon dioxide. Calculated changes in ozone versus altitude are shown in Figure 13-13. Each of the models used tend to show similar behavior, with large ozone decreases calculated in the upper stratosphere, and ozone increases in the troposphere and lower stratosphere. The addition of the CO_2 perturbation reduces the ozone decrease in the upper stratosphere.

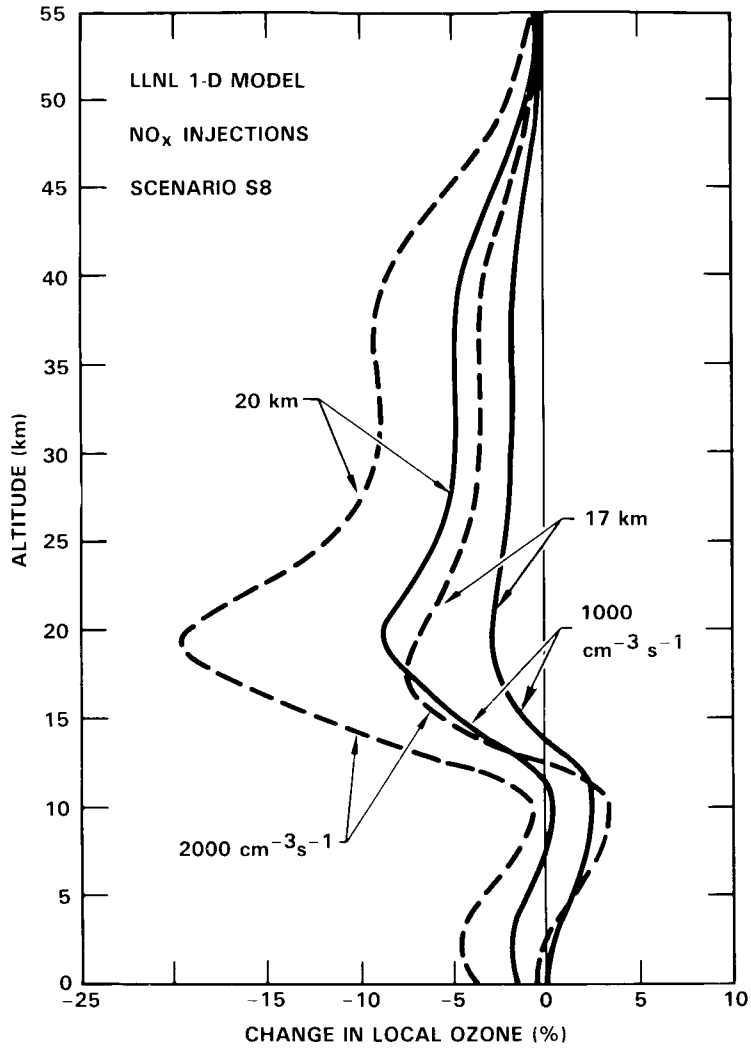

Figure 13-11. Calculated percentage changes in local ozone for 17 and 20 km NO_x injections of 1000 and 2000 molecules cm^{-3} s^{-1}.

The single-specie scenarios discussed above give the qualitative explanations for the multi-specie scenario, but the calculated changes in total ozone are much less than the sum of the individual perturbations involved. The upper stratospheric ozone decrease primarily results from increased chlorine in the assumed scenarios, while the methane change dominates the effects on ozone in the troposphere and lower stratosphere. The ozone recovery mechanism and interaction between NO_x and Cl_x chemistry also plays a role in the lower to middle stratosphere.

13.1.2.2 Time-Dependent Perturbations

Time-dependent calculations including multiple-specie perturbations are regarded as the most nearly realistic of the one-dimensional model assessments. Several studies have considered such time-dependent multiple-species scenarios (e.g. Wuebbles *et al.*, 1983; Callis *et al.*, 1983a; Sze *et al.*, 1983; DeRudder and Brasseur, 1984; Owens *et al.*, 1985a,b; Brasseur *et al.*, preprint 1985).

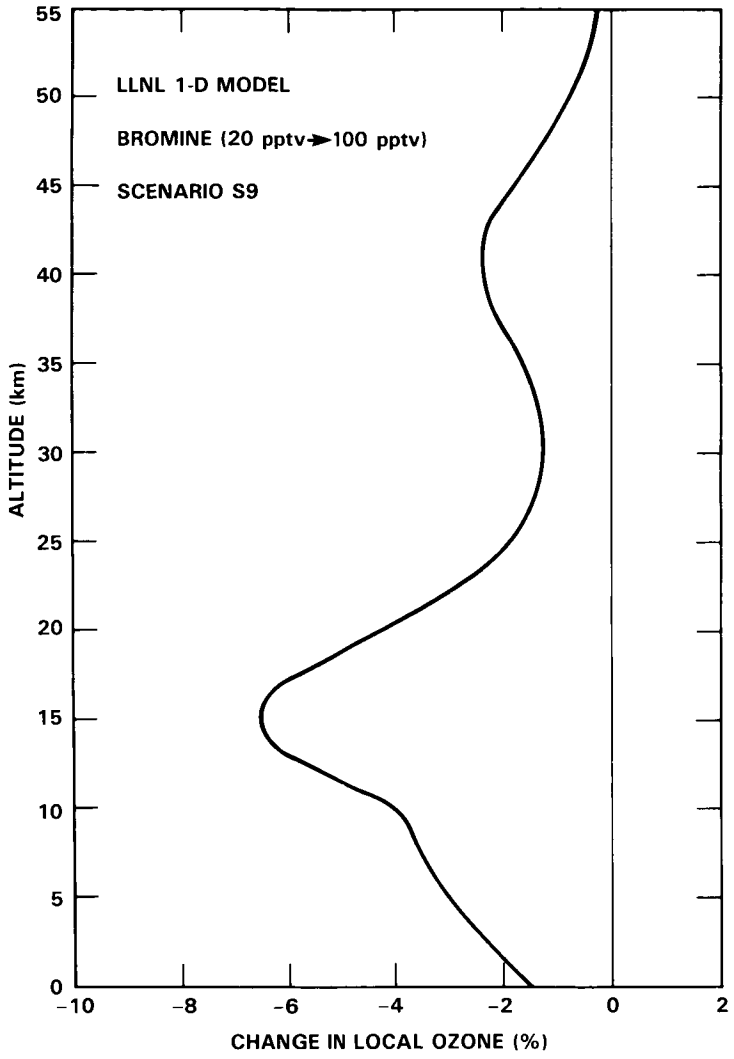

Figure 13-12. Calculated percentage change in local ozone when surface CH_3Br concentration is increased from 20 to 100 pptv.

Shown in Figure 13-14 are the calculated changes in total ozone from several models for scenario T2B, where CFC-11 and CFC-12 emissions are assumed to increase 1.5% per year, CH_4 concentrations to increase 1% per year, N_2O concentrations to increase 0.25% per year, and CO_2 to increase about 0.5% per year, corresponding to the analyses of Edmonds *et al.* (1984) as discussed in Wuebbles *et al.* (1984). Calculations with temperature feedback tend to give a smaller decrease in total ozone for this scenario than calculations with fixed temperatures, primarily due to the impact of temperature-ozone interaction from increasing CO_2 concentrations.

Figure 13-15 shows the change in ozone at 40 km for this same scenario. With the exception of the Brasseur model, similar changes in ozone at this altitude are found in those models with similar temperature treatments. Figure 13-16 shows the change in ozone with altitude for this scenario at selected times and calculated with the LLNL model.

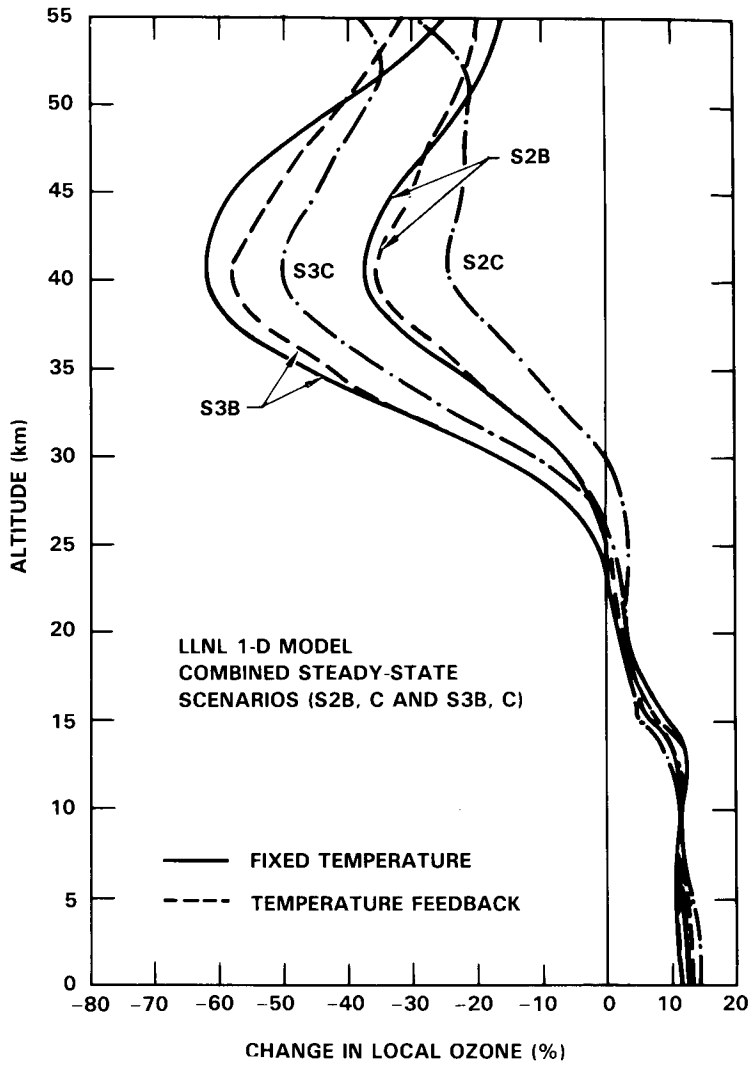

Figure 13-13. Calculated percentage change in local ozone for steady-state combined scenarios: S2B (8 ppbv Cl_x, 2 × CH_4, 1.2 × N_2O); S2C (S2B and 2 × CO_2); S3B (15 ppbv Cl_x, 2 × CH_4, 1.2 × N_2O); S3C (S3B and 2 × CO_2), all referred to background with 1.3 ppbv Cl_x.

Figure 13-17 shows the changes calculated with the LLNL model in total ozone for other scenarios (Table 13-1) as a function of time. Several conclusions can be reached from these results. Future ozone changes can be drastically affected by the choice of specific trace gas scenarios. With these 1-D models, even the sign of the change in total ozone depends on the specific changes in CFC's, CH_4, CO_2, and N_2O. Also, little change in global-average ozone may be expected in the next few decades from the combined scenarios unless significant sustained growth in CFC emissions or drastic differences in present growth rates of other source gases were to occur (see Section 13.1.3 for another, latitude-dependent interpretation of this statement in terms of two-dimensional models). Over this time period, effects of projected CO_2 and CH_4 concentrations are expected at least partially to counterbalance the calculated decrease in ozone due to CFC's alone. As suggested by Figure 13-16, significant differences are calculated in the altitude distribution of ozone in even those model calculations showing little change in total ozone calculated for combined source gas scenarios. Large decreases occur in ozone above about 30 km and increases or small

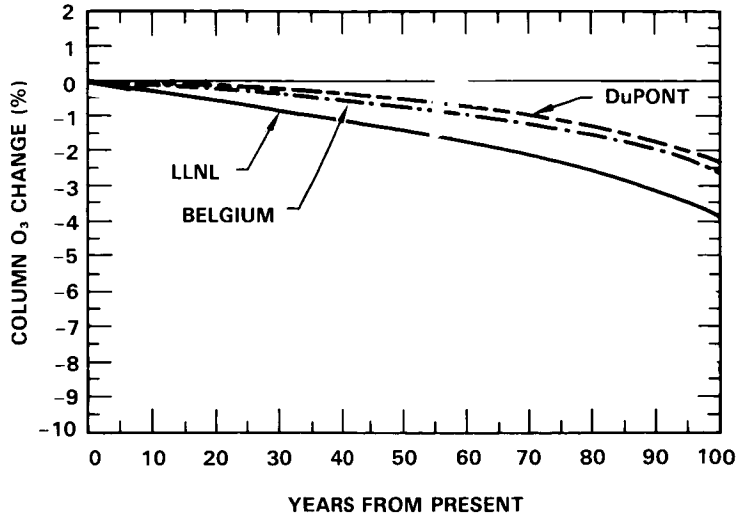

Figure 13-14. Calculated (by four different 1-D models) change in ozone column as a function of time for scenario T2B (CFC emissions begin at 1980 rates and grow 1.5% per yr compounded, CH_4 increases at 1% per yr, N_2O increases at 0.25% per yr, and CO_2 increases according to the DOE scenario).

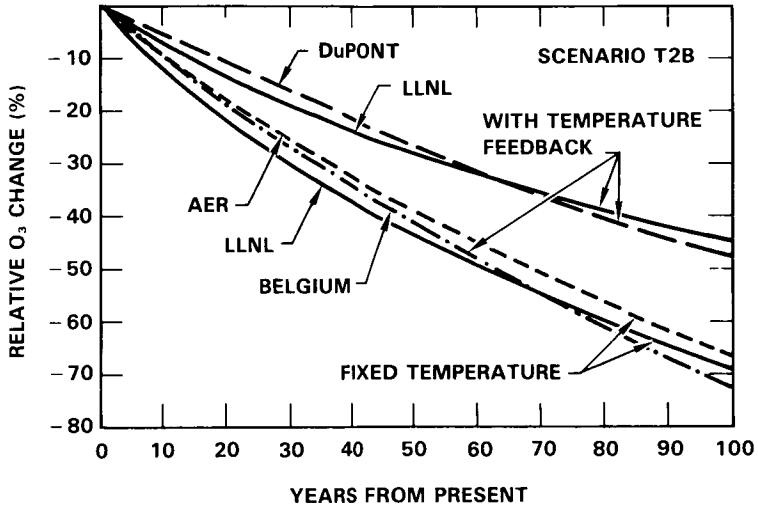

Figure 13-15. Calculated percentage change in local ozone at 40 km altitude with time for scenario T2B (compare Figure 13-14).

decreases below. Calculated increases in tropospheric ozone are extremely sensitive to the assumed CH_4, CO, and hydrocarbon perturbations but not to the Cl_x scenarios.

Results for scenario T3B (Figure 13-17), which assumes a 3% per year growth in CFC emissions along with the previously defined scenarios for CH_4, N_2O, and CO_2, show large ozone decreases even with the concurrent increase of the trace gases. After 70 years the ozone decrease is 10% and still strongly increasing.

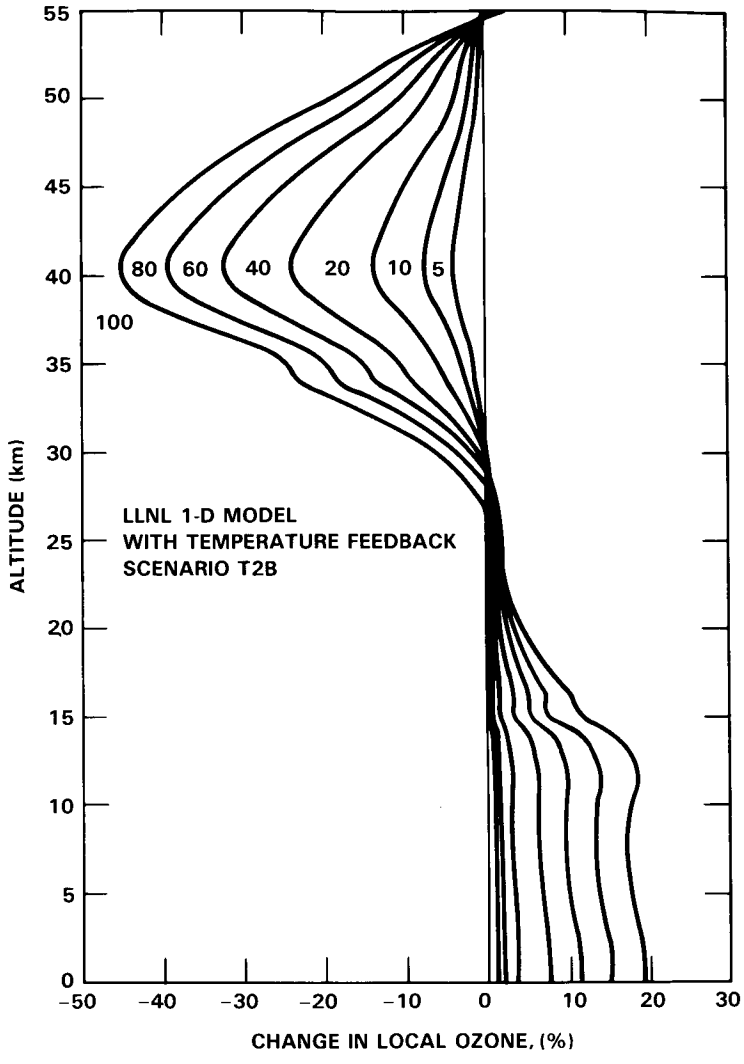

Figure 13-16. Calculated percentage change in local ozone at selected times (5 to 100 years) for scenario T2B (compare Figure 13-14).

13.1.3 Assessment Calculations with 2-D Models

In recent years, many detailed photochemical and dynamical two-dimensional models of the stratosphere have been developed (Chapter 12). These have achieved a measure of success in simulating the zonally and seasonally averaged distributions of constituents influenced both by photochemistry and transport in the stratosphere, such as methane and nitrous oxide (see Miller *et al.*, 1981; Gidel *et al.*, 1983; Garcia and Solomon, 1983; Jones and Pyle, 1984; Guthrie *et al.*, 1984; Ko *et al.*, 1984, 1985). Ozone densities below about 20-25 km are predominantly controlled by transport of ozone from the middle and upper stratosphere. Since most of the ozone column abundance at extra-tropical latitudes is located in this dynamically dominated region, it is important to examine ozone perturbations using multi-dimensional models that include at least a first order representation of transport in the meridional (height-latitude) plane. Such studies reveal latitudinal variations in ozone depletions, which are of importance for ozone monitoring programs, and they provide insight beyond that obtained with comparable one-dimensional model studies.

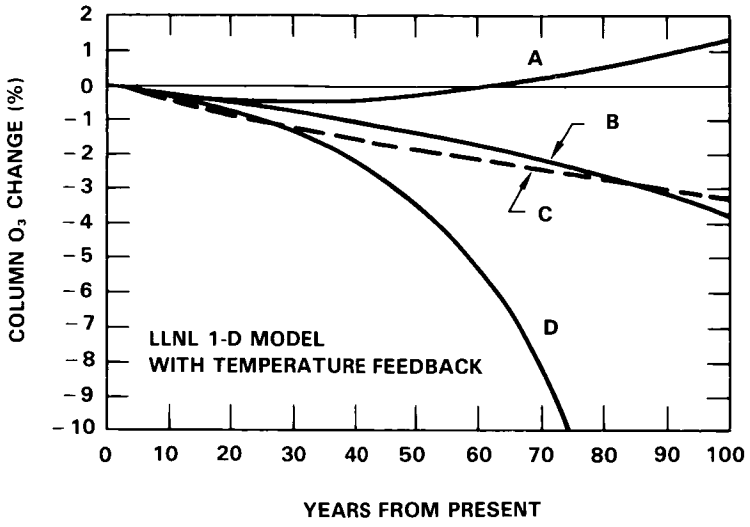

Figure 13-17. Calculated changes in ozone column with time for time-dependent scenarios: T1B (CFC flux continues at 1980 level, CH_4 increases 1% per yr, N_2O increases 0.25% per yr, and CO_2 increases according to the DOE scenario); T1C (same as T1B, but without increases in CH_4 and N_2O); T2B (CFC emissions begin at 1980 rates and increase at 1.5% per yr, other trace gases change as with T1B); T3B (same as T2B except CFC emissions increase at 3% per yr).

The work by Pyle (1980), Haigh and Pyle (1982), and Haigh (1984) using a two-dimensional chemical model suggests, for example, that substantial latitude gradients in ozone depletions should be expected, with much larger depletions occurring in the lower stratosphere at high latitude than at lower latitudes. Indeed, the total column changes predicted in high latitudes by Haigh (1984) using a two-dimensional model with detailed radiation and photochemistry were about two or even three times larger than those calculated with comparable one-dimensional models. (Of course, 1-D models do not calculate latitudinal features, but the point of this comparison is that the nominally global average result given by 1-D models systematically underestimates the ozone reductions that are predicted by 2-D models to occur in high temperate and polar regions. This two-dimensional consideration needs to be added to all one-dimensional results in order not to overlook the worst-case ozone reduction). Haigh (1984) also predicted a similarly large ozone column depletion at high latitudes even when simultaneous carbon dioxide increases were considered in the calculations. This result is also quite different from that obtained in one-dimensional models, wherein the effect of simultaneous carbon dioxide and chlorocarbon perturbations leads to a decrease in the anticipated total column change (see for example, Wuebbles *et al.*, 1983).

Some two-dimensional model perturbation studies (for example, Brasseur and Bertin, 1978/79; Gidel *et al.*, 1983; Steed *et al.*, 1982) suggest less latitude gradient in ozone depletion than that found in the studies by Pyle (1980) and Haigh (1984). It is of interest to understand the origin of these differences between these two-dimensional models.

In this subsection, perturbation studies with three two-dimensional models will be presented. The model referred to here as MPIC is that of Gidel *et al.* (1983); the calculations were done by Schmailzl and Crutzen. The model (GS) is that of Garcia and Solomon (1983) and Solomon and Garcia (1984b). The model (AER) is that described by Ko *et al.* (1985). The photochemical reaction rates used were those of NASA-JPL (1985) or Appendix 1, and the solar flux, oxygen and ozone cross sections were taken from Chapter 7,

but the authors used different methods in the treatment of the Schumann-Runge bands and used different boundary conditions. Table 13-7 shows the scenarios used in each model.

For each of these scenarios, the global, seasonal average reduction of ozone is given in Table 13-8. These results are analyzed and discussed in a later section, but first the two-dimensional structure of the ozone reductions is presented by various graphical means.

Perturbation by Cl_x Only

Figure 13-18 presents latitude-altitude cross sections of the percentage ozone depletion obtained for winter and spring from the MPIC model for scenario SMA (Cl_x increase, 6.8 ppbv; reference Cl_x, 2.7 ppbv). Similar plots are shown for all four seasons according to the AER model for scenario S2A (Cl_x increase, 6.8 ppbv: reference Cl_x, 1.3 ppbv) in Figure 13-19 and for scenario S3A (Cl_x increase, 14.2 ppbv; reference Cl_x, 1.3 ppbv) in Figure 13-20. Results of the GS model for winter and spring are given as a latitude-altitude plot of percentage ozone reduction in Figure 13-21 for scenario S2A.

For these three models, essentially the same Cl_x perturbation is represented by Figure 13-18a (winter, MPIC), Figure 13-19a (January, AER), and Figure 13-20a (December, GS). Certain similarities and differences can be noted. In all three models, the maximum percentage ozone reduction at 40 km is 50 to 60%, which is in agreement with 1-D results (Table 13-3 and Figures 13-1 to 13-3). At this altitude, the AER and GS models show similar latitude profiles with ozone-reduction maxima near the poles. Both show a saddlepoint minimum of ozone reduction of about 35% near the equator. The MPIC maximum percentage

Table 13-7. Two-dimensional Model Scenarios.

Code	Cl_x/ppbv			$2\times CH_4$ $1.2\times N_2O$	Model	Symbol
	Total	Ref.	Incr.			
S2A	8.	1.3	6.7	no	Garcia and Solomon (1983)	GS
S2A	8.2	1.3	6.9	no	Ko *et al.* (1985)	AER
S3A	15.5	1.3	14.2	no		AER
S2C	8.	1.3	6.7	yes	Garcia and Solomon (1983)	GS
SMA	9.5	2.7	6.8	no	Gidel *et al.* (1983)	MPIC
—	2.7	1.3	1.4	no		MPIC
—	9.5	1.3	8.2	no		MPIC
SMB	9.5	2.7	6.8	yes		MPIC
SMC	18.	2.7	15.3	yes		MPIC

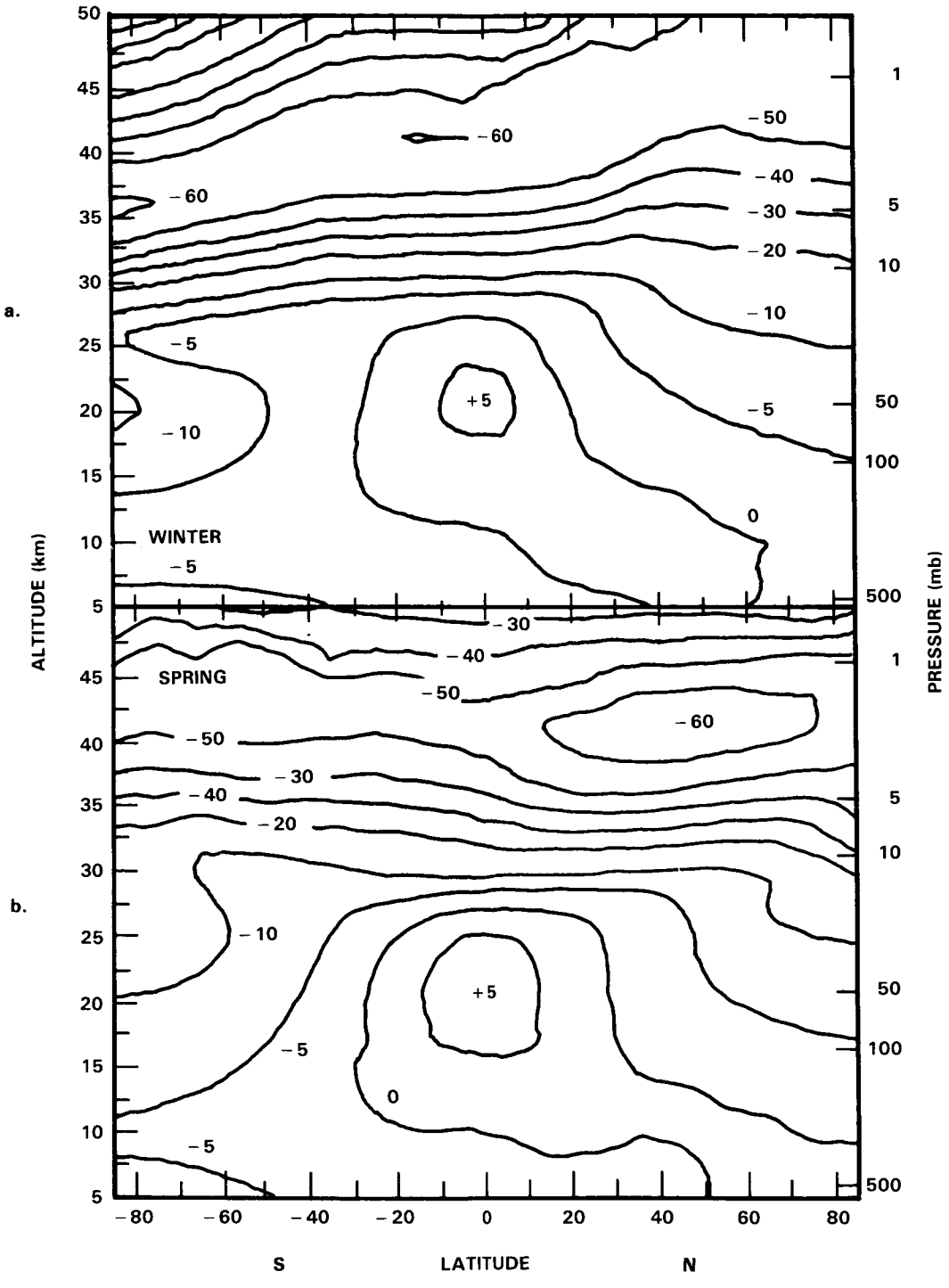

Figure 13-18. Calculated steady-state local percentage ozone change as a function of latitude and altitude—for 1980 fluorocarbon emission given 9.5 ppbv Cl_x relative to reference atmosphere w3ith 2.7 ppbv Cl_x, or an increase of 6.8 ppbv (Table 13-7, Scenario SMA, MPIC 2-D Model). a. Southern Hemisphere winter, b. Southern Hemisphere spring.

Table 13-8. Percentage Change in Global, Seasonal Average Ozone According to Two-dimensional Models for Steady-state Scenarios Containing Cl_x Perturbations, and Model "Sensitivity" of Ozone to Cl_x. Sensitivity, S, Is Percent Ozone Decrease Divided by ppbv Cl_x Increase.

Cl_x/ppbv			$2\times CH_4$	% Ozone	S	
Initial	Final	Increase	$1.2\times N_2O$	Decrease	−%/ppbv	Model
1.3	2.7	1.4	no	1.9	1.36	MPIC
2.7	9.5	6.8	no	7.2	1.06	
1.3	9.5	8.2	no	9.1	1.11	
2.7	9.5	6.8	yes	4.5	0.66	MPIC
2.7	18.	15.3	yes	11.1	0.73	
1.3	8.2	6.9	no	8.5	1.23	AER
1.3	15.5	14.2	no	18.	1.27	

ozone reduction is an almost uniform ridge from 85° N at 45 km to 85° S at 35 km. In all three models the −20% contour is flat almost from pole to pole at an altitude of about 30 km. At 20 km altitude the three models show qualitatively similar features, an ozone increase in the tropics and ozone reduction at extra-tropical latitudes; but the quantitative values differ: GS varies as −5% at 90° S, +15% at the equator, −5% at 90° N; AER values are −10% at the South Pole, +20% at the equator, −30% at the North Pole; and MPIC varies as −10% at 80° S, + 5% at the equator, −5% at 80° N.

The model results for this scenario during the spring season can be compared among Figure 13-18b (MPIC) and Figures 13-19b and 13-20 (AER). For the AER and MPIC models, the results for the Northern Hemisphere are qualitatively similar with a maximum ozone-reduction closed counter near 40 km, but this feature is absent for the MPIC model in the Southern Hemisphere. Along the high altitude maximum ozone-reduction ridge, the AER model shows somewhat greater latitude variation than the MPIC model. In the middle stratosphere the two models show similar flat contours of ozone reduction. In the lower stratosphere the AER model shows larger ozone increases in the tropical region and larger ozone reductions in temperate and polar regions than the MPIC model.

The percentage changes in the ozone vertical column are shown as a function of latitude and season in Dobson contour maps. The result of the MPIC model for Cl_x perturbation SMA is given in Figure 13-22a; and the results of the AER model are shown for scenarios S2A and S3A in Figure 13-23. The scenario for Figure 13-22a (MPIC) is essentially the same as that for Figure 13-23a (AER), which provides a direct comparison between the models. For the MPIC model, larger ozone reductions are obtained at high latitudes than at low latitudes by almost a factor of two in the winter (Figure 13-22a). However, for the AER model there are much greater differences with latitude, more than a factor of four in February, for example (Figure 13-23a). The contour intervals of ozone change are the same (every 2%) for Figures 13.22a and 13.23a, and it is obvious by inspection that the AER model shows more variation with latitude and season than the MPIC model. A direct comparison is given by Figure 13-24, which gives the latitude dependence of ozone column reduction for these two models (spring).

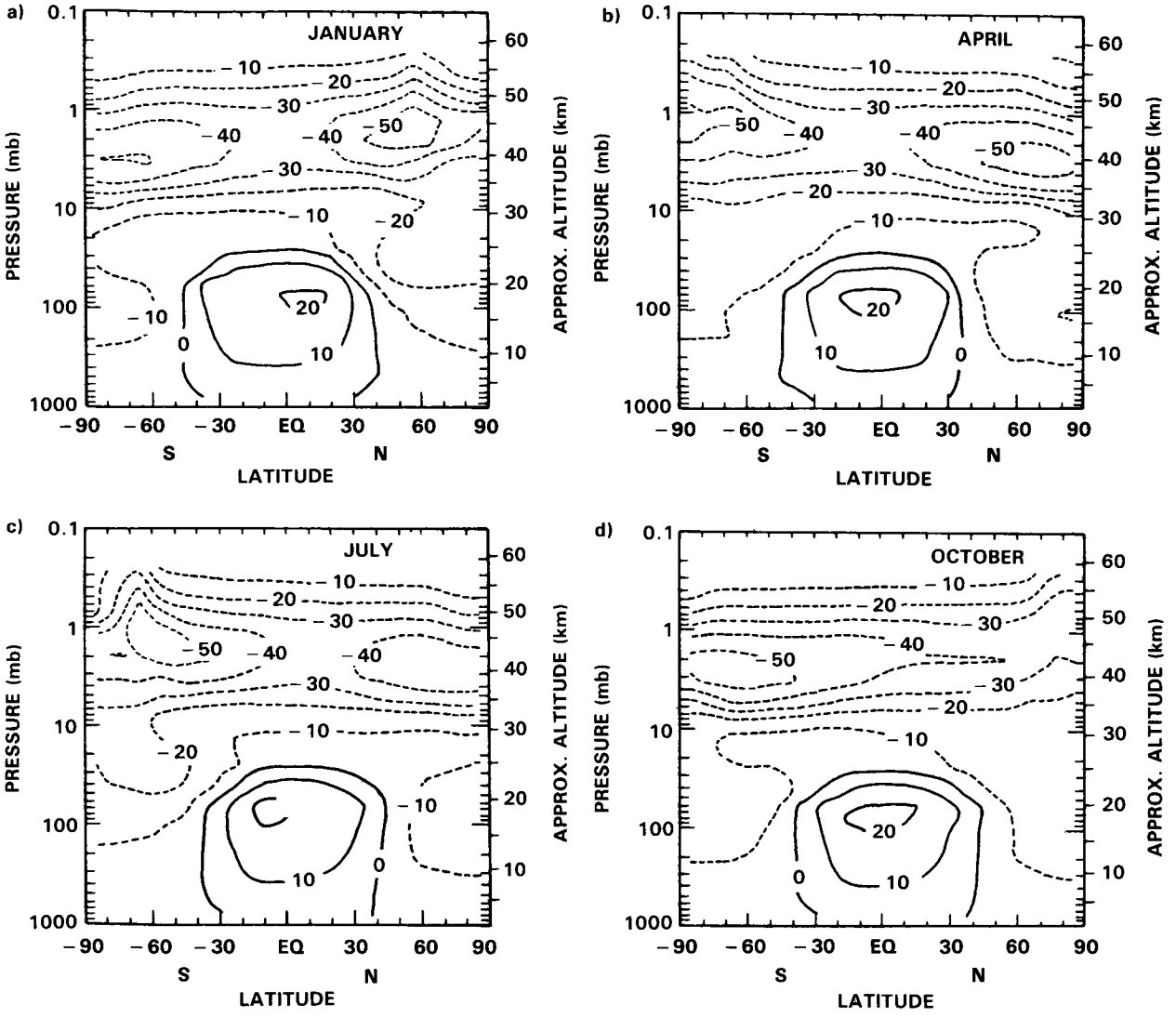

Figure 13-19. Calculated steady-state local percentage ozone change as a function of latitude, season, and altitude—for fluorocarbon emission giving 8.2 ppbv Cl_x relative to reference atmosphere with 1.3 ppbv Cl_x, or an increase of 6.9 ppbv (Table 13-7, Scenario S2A, AER 2-D Model). a. January, b. April, c. July, d. October.

Some of the reasons for these latitudinal gradients in ozone depletion were examined using the model by Garcia and Solomon. Figure 13-25 presents the calculated distribution of ozone mixing ratio obtained in that model (see Solomon *et al.*, 1985b) along with the calculated odd oxygen replacement time (the local concentration of ozone divided by twice the molecular oxygen photolysis rate by solar radiation at wavelengths below 242 nm) for the present day atmosphere. Assuming a typical time scale for meridional transport of ozone of the order of 100 days in the stratosphere, the shaded area shows the region that is substantially controlled by dynamics (i.e. below about 25-30 km, poleward of about 40-50° in both summer and winter). Near 40 km ozone is photochemically controlled, and its lifetime reveals little gradient with latitude except in the polar night region. The latitude gradients in ozone depletion obtained near 40 km in the AER and GS models are the direct result of calculated gradients in methane. Large gradients in methane have indeed been observed near 40 km by the SAMS satellite and are reasonably well reproduced

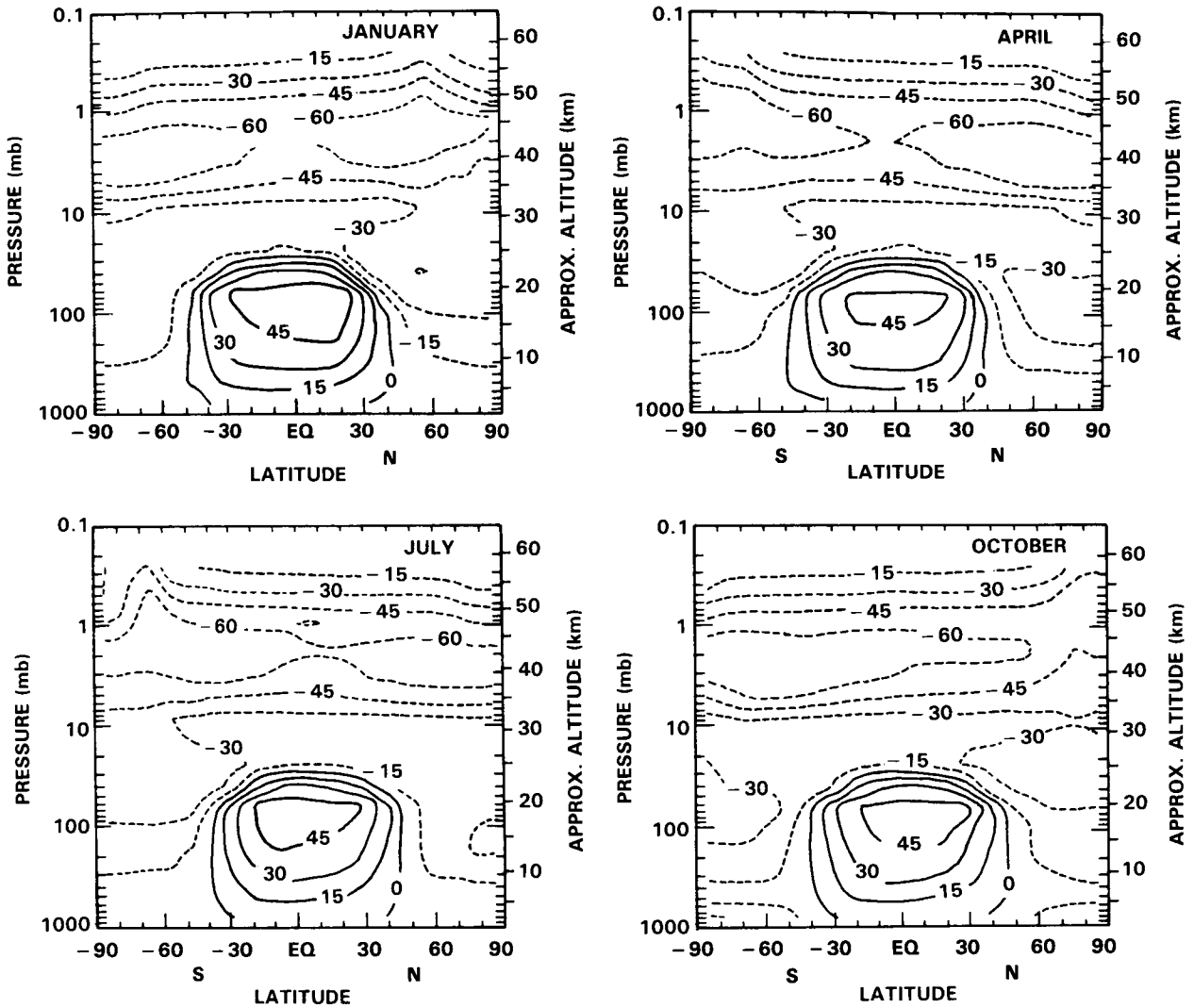

Figure 13-20. Same as Figure 13-19, but with 15.5 ppbv Cl_x or a change of 14.2 ppbv (Scenario S3A).

in some two-dimensional models (see Jones and Pyle, 1984; Solomon and Garcia, 1984b; Ko *et al.*, 1984). The satellite data suggest a gradient in methane at 40 km of about a factor of three from the tropics to about 70° latitude. Methane, in turn, controls the partitioning of active chlorine between the inert reservoir, HCl, and the ozone-destroying species, Cl and ClO, near 40 km. The methane gradient therefore results in a greater abundance of catalytic chlorine free radicals at high latitudes, where methane abundances are substantially lower than they are in the tropics at 40 km (Solomon and Garcia, 1984b). As the chlorine content in the atmosphere increases, its perturbing influence is therefore predicted to be much greater at high latitude. This effect is not observed in the winter MPIC model because the calculated methane gradient is much smaller (see Chapter 12). The reason for this difference between models is discussed further below.

The ozone changes obtained at lower altitudes largely control the behavior of the total column. As already mentioned, below about 25 km at middle and high latitudes, ozone is principally controlled by dynamics because the ozone photochemical replacement times are long. Photochemical self-healing therefore

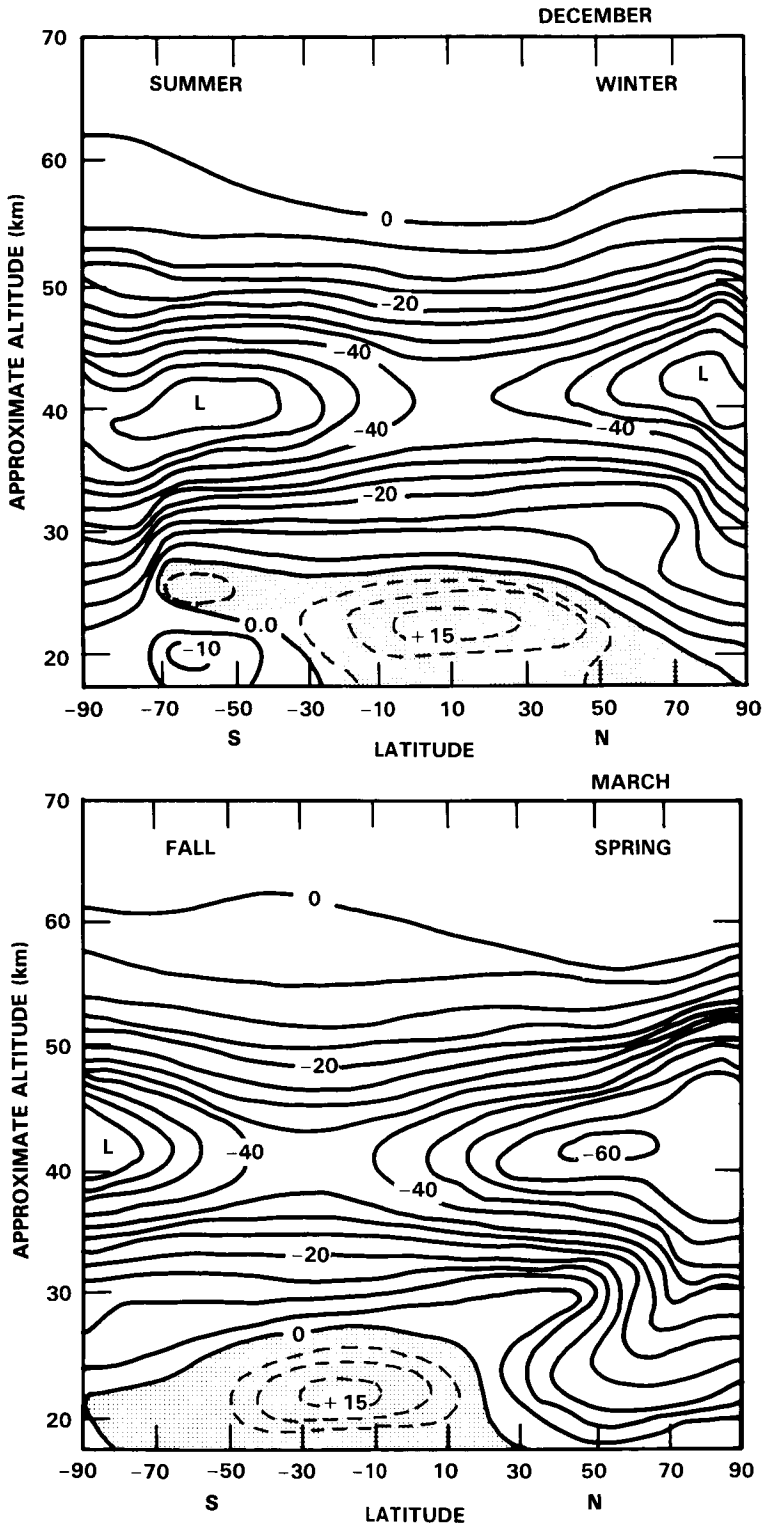

Figure 13-21. Calculated steady-state local percentage ozone change as a function of latitude and altitude—for 1980 fluorocarbon emission giving 8.0 ppbv Cl_x relative to reference atmosphere with 1.3 ppbv Cl_x, or an increase of 6.7 ppbv (Table 13-7, Scenario S2A, GS 2-D model).

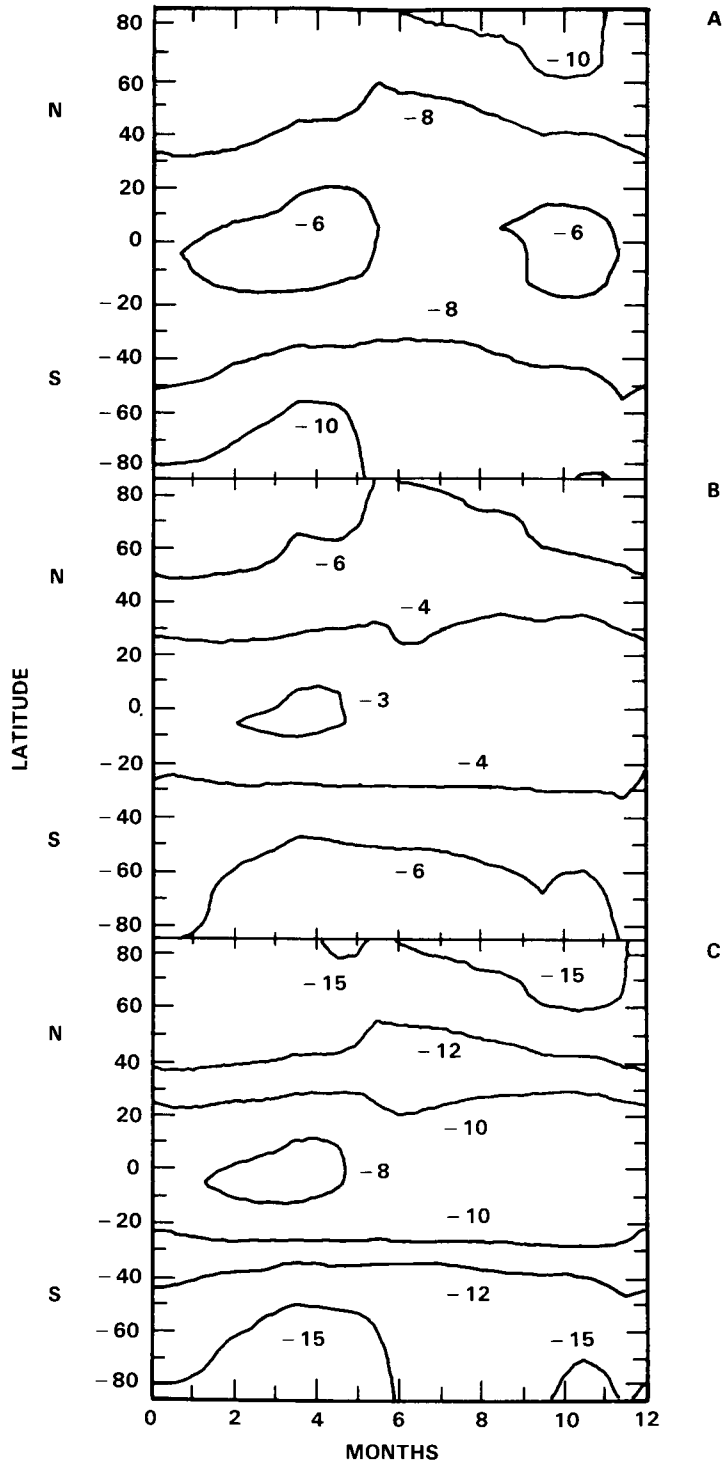

Figure 13-22. Calculated steady-state percentage change of the ozone column relative to a reference atmosphere with 2.7 ppbv Cl_x as a function of latitude and season for three scenarios in Table 13-7: (A) SMA, 1980 fluorocarbon emission giving 9.5 ppbv Cl_x or an increase of 6.8 ppbv Cl_x; (B) SMB, which is same as SMA, but also $2 \times CH_4$ and $1.2 \times N_2O$; (C) SMC, twice the 1980 fluorocarbon flux giving 18 ppbv Cl_x or 15.3 ppbv change and increase of methane and nitrous oxide (MPIC 2-D model).

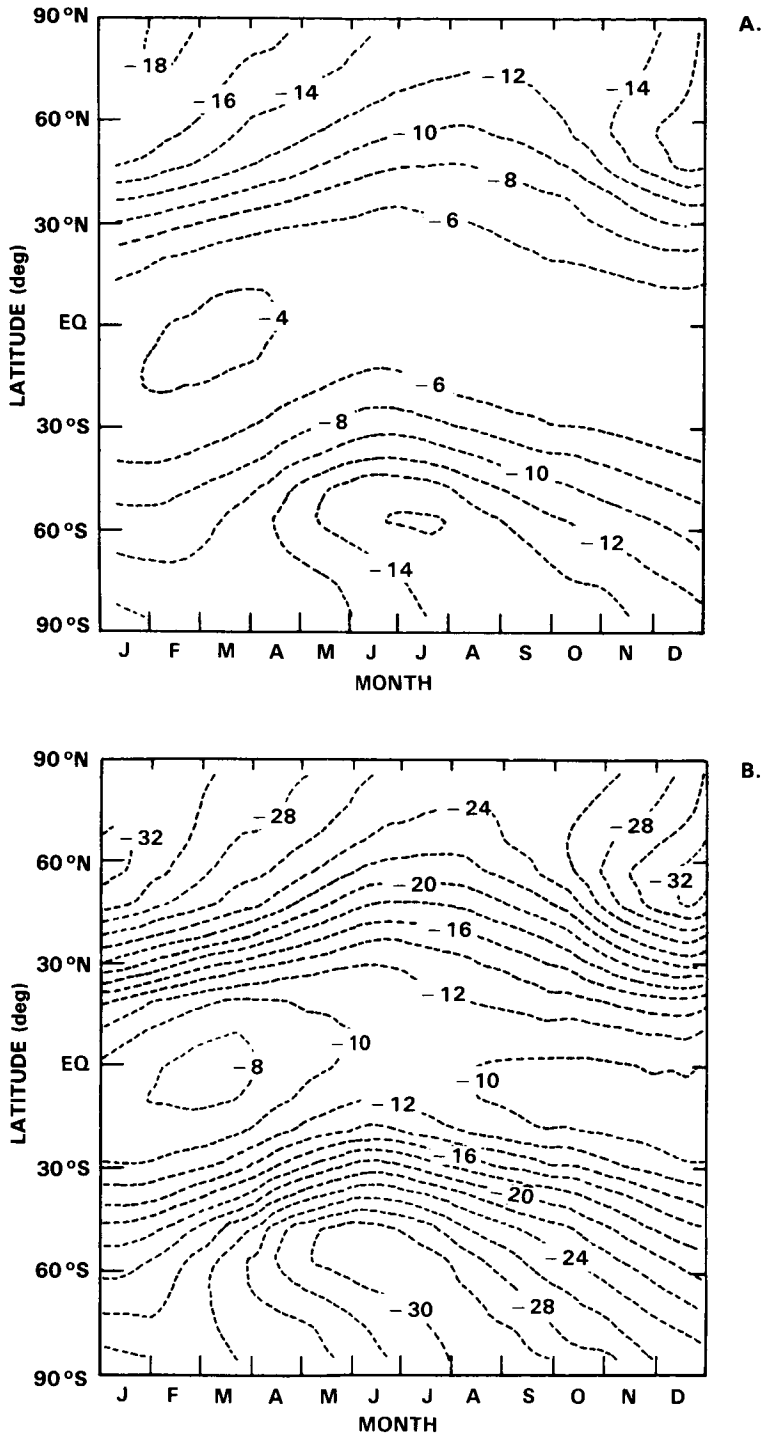

Figure 13-23. Calculated steady-state percentage change of the ozone column relative to a reference atmosphere with 1.3 ppbv Cl_x as a function of latitude and season for two scenarios in Table 13-7: (a) S2A, 1980 fluorocarbon emission giving 8.2 ppbv Cl_x or an increase of 6.9 ppbv Cl_x; (b) S3A, twice the 1980 flux of CFC giving 15.5 ppbv Cl_x or an increase of 14.2 ppbv Cl_x. The global average ozone changes are −8.5% and −18%, respectively. (AER 2-D model).

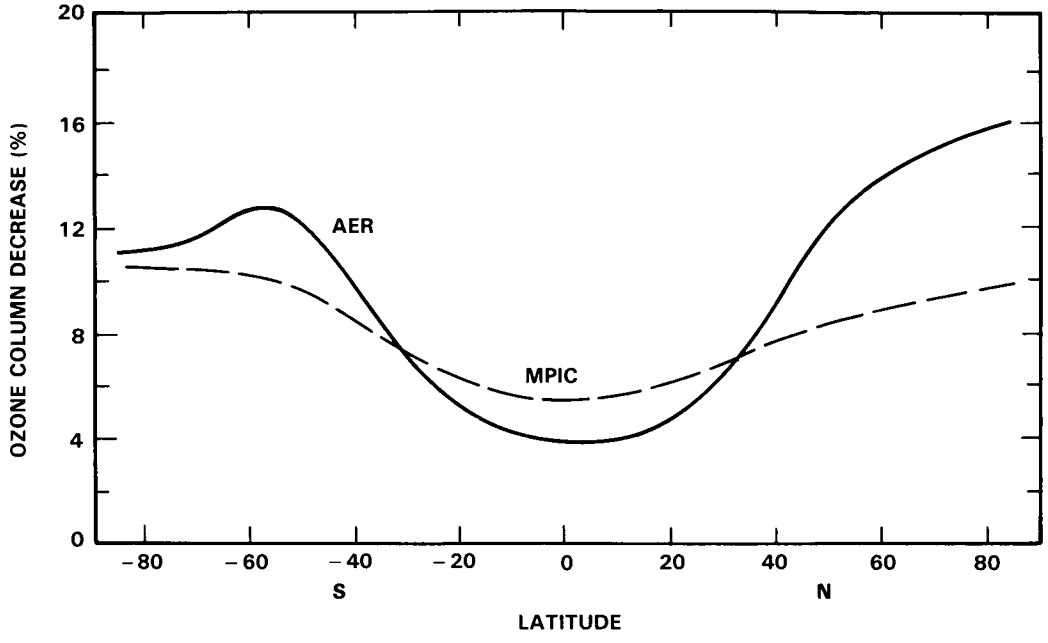

Figure 13-24. The effect of type of atmospheric dynamics used in two-dimensional models on the latitudinal variation of calculated ozone-column reduction (April). The increase of Cl_x is about 7 ppbv in each case: AER model, scenario S2A; MPIC model, scenario SMA.

occurs too slowly compared to dynamics to significantly increase the ozone densities at the lower altitudes. Particularly in the winter, it is likely that transport will be largely downward and poleward, at least in the zonal and seasonal average. This brings down air parcels that are severely depleted in ozone, having come from the photochemically controlled region above 35 km where ozone changes are expected to be large in all the models. The ozone change characteristic of the upper stratosphere may be thought of as "frozen" as air descends into the winter lower stratosphere, where photochemistry is too slow to change it locally. On the other hand, oxygen photolysis occurs on a time scale that is substantially shorter than the dynamical time scale at altitudes as low as about 20 km in the tropics. Therefore, photochemical self-healing can be very effective at tropical latitudes, yielding important increases in local ozone density that offset the depletions occurring at higher altitudes, similar to but larger than that seen in the one-dimensional models.

An important element in the evaluation of latitudinal gradients in the ozone changes to be expected, however, is the strength of horizontal mixing. If horizontal mixing rather than vertical motion dominates the transport of ozone into high latitudes in the lower stratosphere, the large changes in ozone due to descending motion will be reduced by mixing with air in which self-healing may occur. It therefore is important to understand the temporal and spatial structure of downward flow (particularly in the winter and spring) and the competition between mixing and advection. As discussed in more detail in Chapter 12, the primary differences between the models presented here are due to their differences in the formulation of dynamics. The MPIC model is a classical Eulerian model in which large eddy diffusion coefficients are employed. The AER and GS models are isentropic and residual Eulerian models, respectively, and employ much smaller horizontal mixing coefficients relative to the MPIC model. This implies that the latitudinal gradients in methane and in ozone depletion should be expected to be greater in the AER and GS models than in the MPIC model. More detailed comparisons and discussions of these two types of models are presented in Chapter 12.

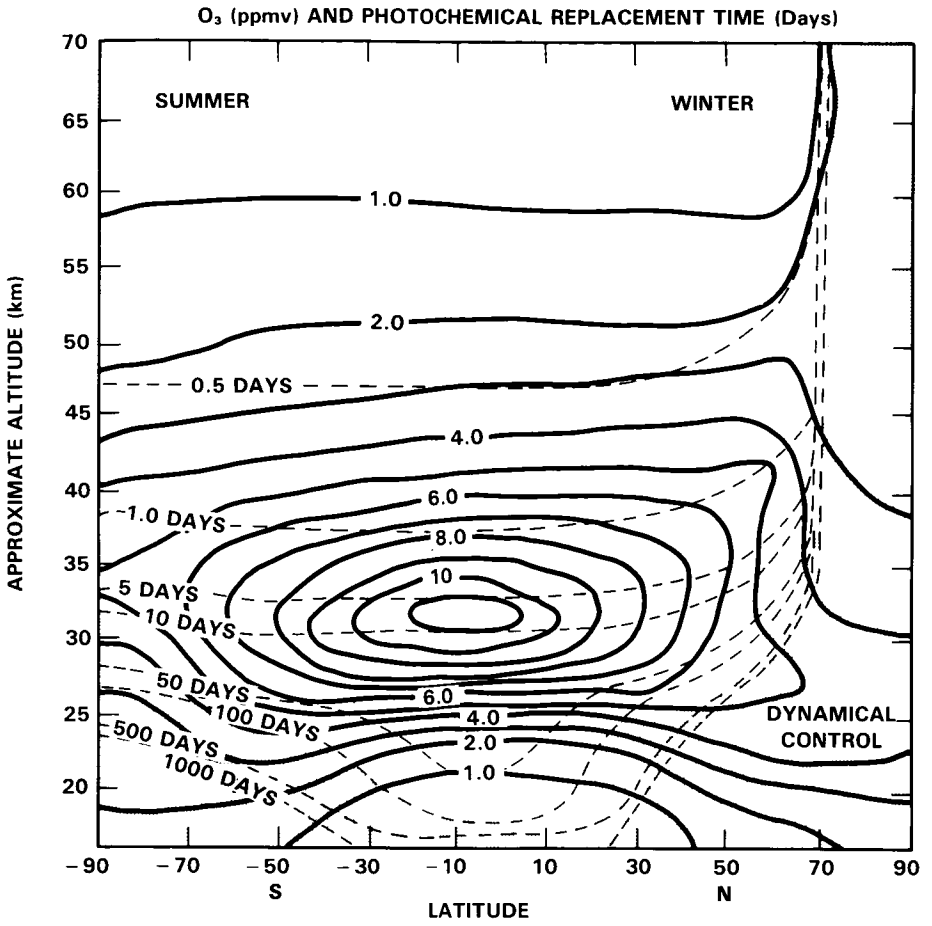

Figure 13-25. Computed local photochemical ozone replacement time (t = local ozone concentration divided by twice the rate of molecular oxygen photolysis) in days (dashed lines) and ozone mixing ratio in ppmv (solid lines) for the end of December from the GS model. Note the long ozone photochemical replacement times (> 100 days) in the lower stratosphere, particularly at high latitudes in the winter hemisphere. The shaded area indicates the region where ozone is likely to be dynamically controlled.

Mixed Scenarios

Two-dimensional steady-state model studies were carried out in which it was assumed that methane increased by a factor of two and nitrous oxide increased by a factor of 1.2 while Cl_x increased by 6.7 ppbv (GS), 6.8 ppbv (MPIC), and 15.3 ppbv (MPIC), compare Table 13-7. Latitude-altitude contour maps of percentage ozone change are presented for the GS calculation for (NH) winter and spring (Figure 13-26a,b), for the MPIC model with 6.8 ppbv increase of Cl_x for (NH) winter (Figure 13-27a) and for spring (Figure 13-27b), and for 15.3 ppbv Cl_x for winter (Figure 13-28). Several interesting comparisons can be made among these figures.

The general effect of increasing the methane abundance is to reduce the magnitude of the calculated ozone changes. For the GS model, the qualitative features of the altitude-latitude contours are unchanged, Figure 13-21 vs Figure 13-26, but there are interesting quantitative differences. The high altitude polar maxima of ozone reduction are 55% without increasing CH_4 and N_2O and 45% with the combined scenario.

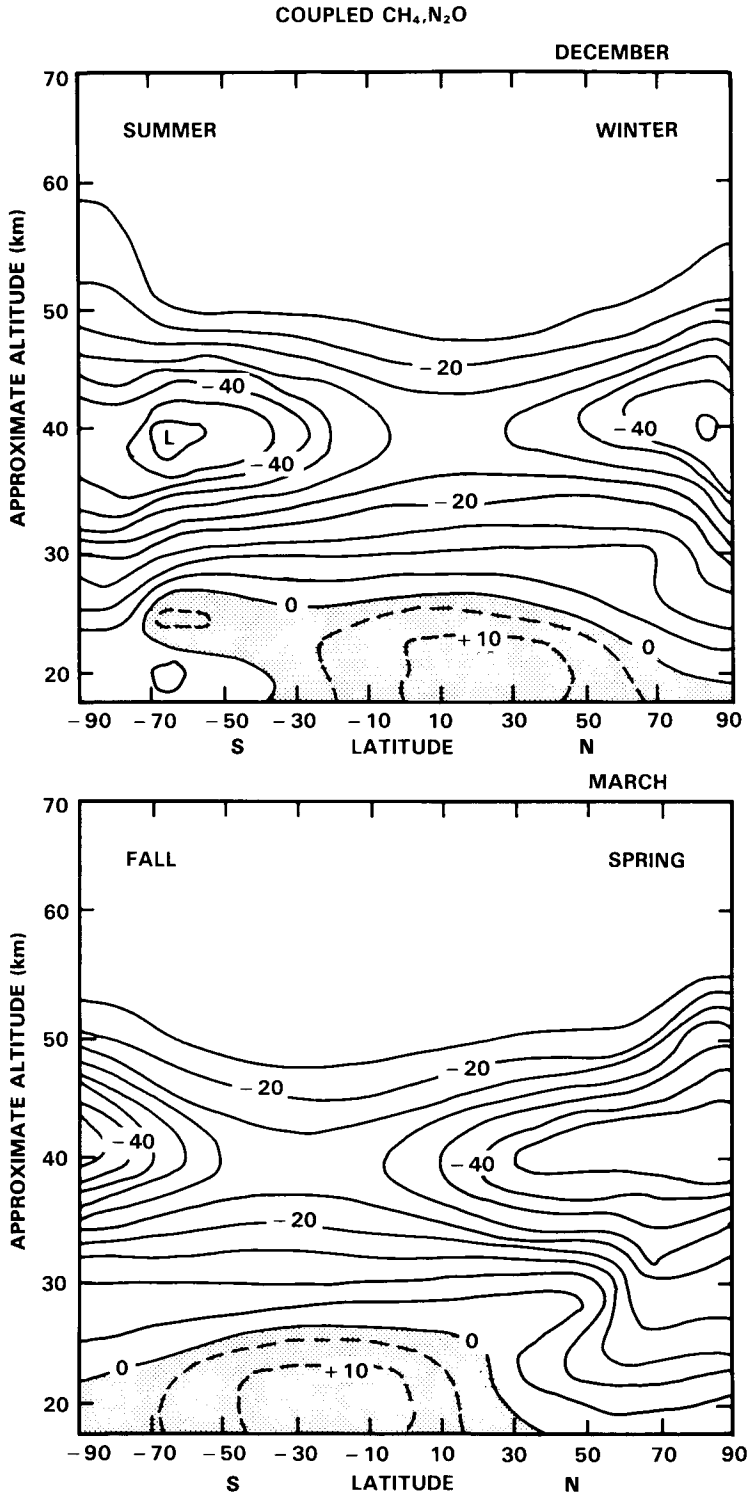

Figure 13-26. Effect of coupled perturbations—compare with Figure 13-21 Calculated steady-state local percentage ozone change as a function of latitude and altitude—for 1980 fluorocarbon emission giving 8.0 ppbv Cl_x relative to reference atmosphere with 1.3 ppbv Cl_x, or an increase of 6.7 ppbv and $2 \times CH_4$, $1.2 \times N_2O$ (Table 13-7, Scenario S2C, GS 2-D model).

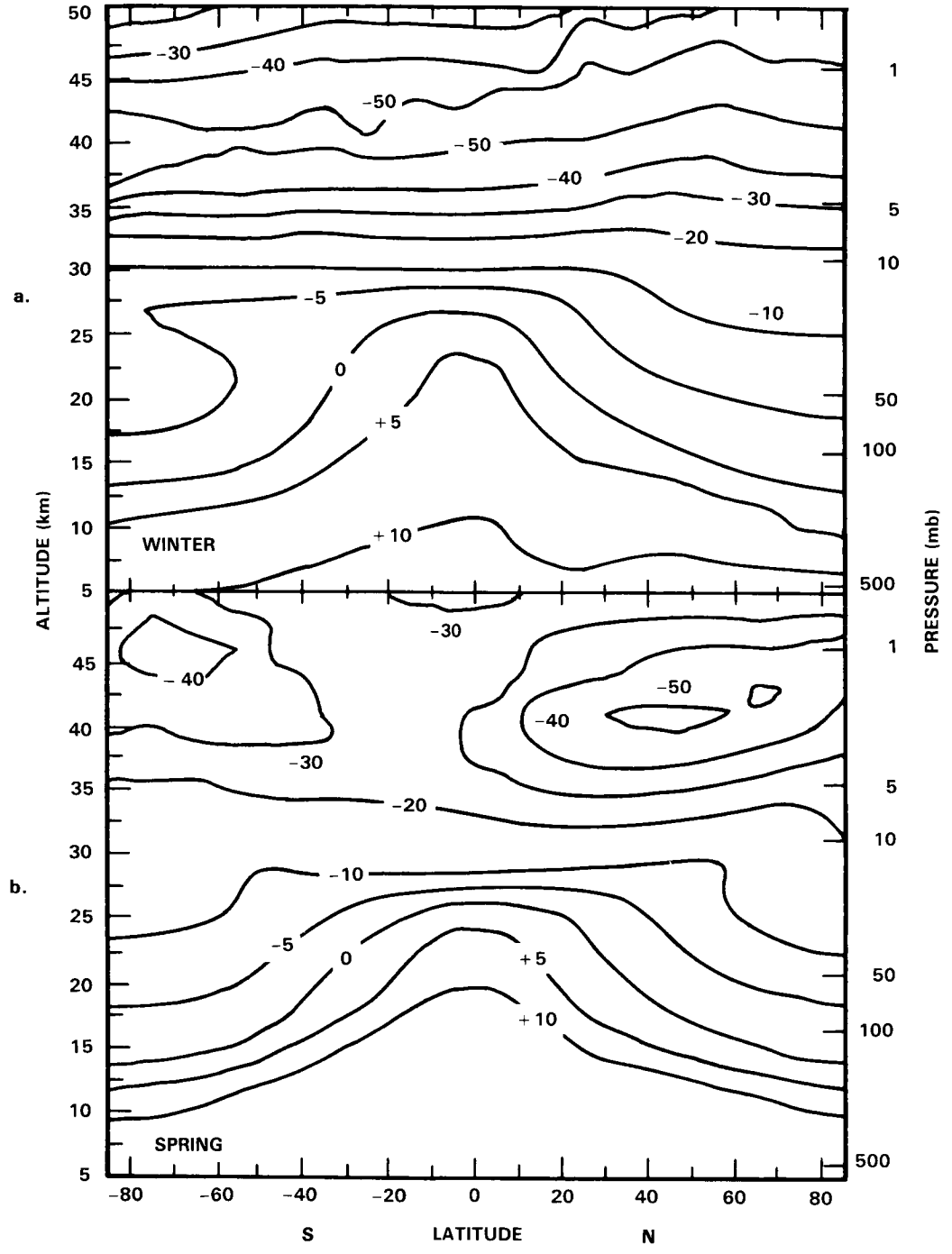

Figure 13-27. Effect of coupled perturbations—compare Figure 13-18. Calculated steady-state local percentage ozone change as a function of latitude and altitude—for 1980 fluorocarbon emission given 9.5 ppbv Cl_x relative to reference atmosphere with 2.7 ppbv Cl_x, or an increase of 6.8 ppbv and doubled methane, 1.2 × N_2O (Table 13-7, Scenario SMB, MPIC 2-3 Model).

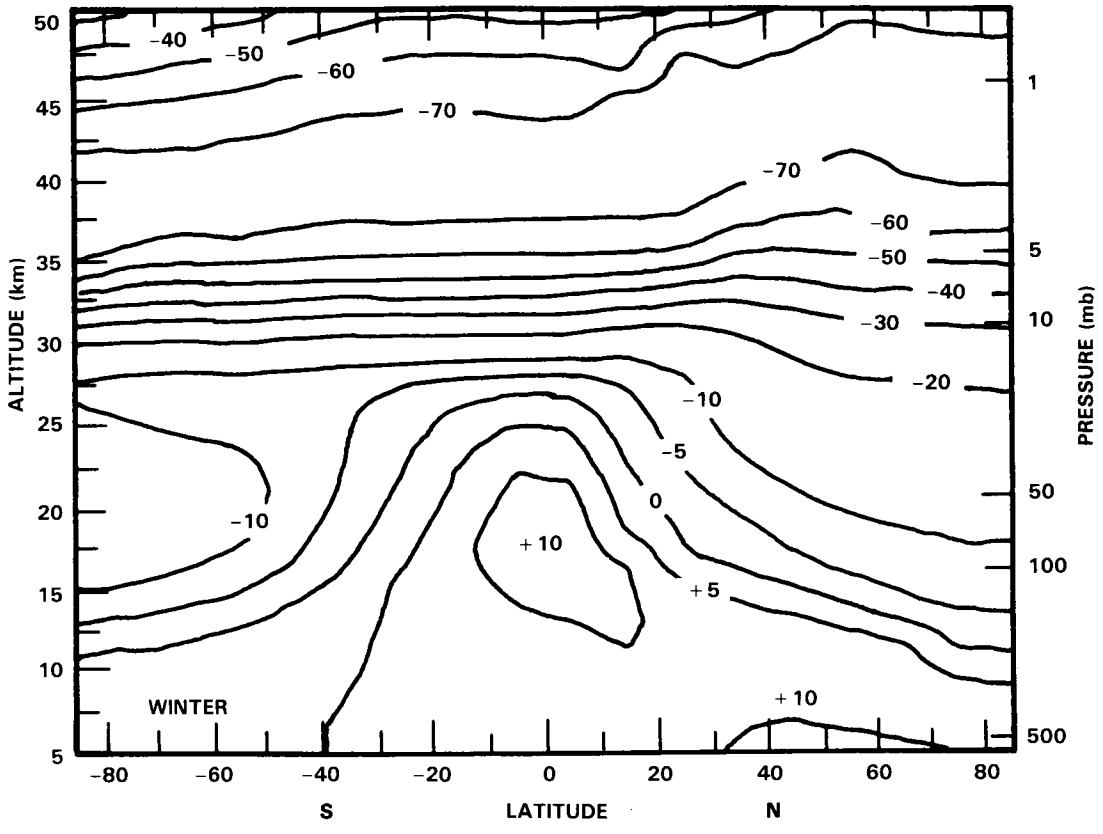

Figure 13-28. Same as Figure 13-27a but for twice the 1980 fluorocarbon flux, giving an increase of 15.3 ppbv Cl_x (Scenario SMC, MPIC model).

The saddlepoint near the equator is reduced from 35-40% (S2A) to 25-30% (S2C, combined scenario). The calculated latitudinal gradient in ozone depletion at 40 km is slightly greater than in the chlorine only case. In both cases the ozone depletion near 30 km is almost independent of latitude. The region of increased ozone in the lower stratosphere (at 18 km) is very nearly the same in both cases, but it covers a slightly greater range of latitude at low altitude for the case of the combined perturbation. In the region of ozone increase, the maximum value of the increase is 15% for S2A and 10% for S2C. These maximum values near the equator are consistent with the interpretation as ozone self healing (greater penetration of oxygen-dissociating radiation to lower altitudes as ozone is reduced), since larger ozone reduction in the upper stratosphere shows larger ozone increase at 20 km at the equator. The GS model results in Figures 13-21 and 13-26 extend down only to 18 km, and thus do not show effects in the lowest stratosphere.

The MPIC cases in winter of 6.8 ppbv added Cl_x (Figure 13-18a) and Cl_x plus change of methane and nitrous oxide (Figure 13-27a) are given down to 5 km altitude, and these figures allow for comparisons throughout the stratosphere. Ozone reductions are somewhat smaller in the combined scenario in the upper and middle stratosphere, but the structure of the contours is similar. In the lower stratosphere and upper troposphere, there is a larger region of ozone formation in the case of added methane and nitrous oxide than for the case of Ci_x only. Ozone decreases in Figure 13-18a are turned into ozone increases in Figure 13-27a in the lower Southern Hemisphere (summer) stratosphere above about 40°, and in this region there is insufficient solar radiation at wavelengths below 242 nm for this ozone increase to be "ozone self healing" in the same sense that it was discussed in connection with the GS model (additional ozone

formation from oxygen photolysis). The explanation might be called "ozone self-healing of the second kind". As ozone is reduced by Cl_x in the upper stratosphere, there is increased penetration of solar radiation at wave lengths below the ozone cross-section maximum (250 nm) which produces significant oxygen dissociation at wavelengths around 210 nm down to about 20 km in the tropics. Also, there is increased penetration of solar radiation above 250 nm, which produces significant singlet atomic oxygen (from ozone photolysis) at wavelengths below 310 nm, down to the surface of the earth. This singlet atomic oxygen, in part, reacts with water vapor or with methane to produce hydroxyl radicals. The hydroxyl radicals undergo a series of reactions that both destroy and produce ozone (Chapter 4). In particular, there are the methane-NO_x-smog reactions, which give a net formation of ozone in the lower stratosphere and upper troposphere (Chapter 4). In the lower stratosphere the NO_x species slowly but non-negligibly destroy ozone, and hydroxyl radicals convert the catalytically active NO_2 into the inert reservoir species HNO_3. In this way hydroxyl radicals destroy an ozone destroyer, and this increases ozone by way of a double negative. Even though the time scale for meridional transport of ozone is about 100 days, the residence time of carbon-14 and presumably ozone at about 20 km is the order of one year (Telegadas, 1971; Johnston *et al.*, 1976), and the relatively slow HO_x and NO_x photochemistry, which is largely driven by the penetrating solar radiation near 300 nm, significantly modifies ozone even at high latitudes at this longer time scale. Nitrous oxide is photochemically inactive at these low altitudes, and the increase of ozone as methane is increased (Figure 13-18 vs 26) identifies the methane-NO_x-smog reactions as an important component in the model at these low altitudes. The "ozone self-healing of the second kind" and related photochemical reactions that slowly destroy ozone make important contributions to the model-calculated ozone column. This discussion is supplementary to that for "ozone self-healing" in connection with solar radiation near 200 nm, which dissociates molecular oxygen.

The MPIC model for spring with 6.8 ppbv added Cl_x and with increased methane and nitrous oxide (Figure 13-27b) shows in the upper stratosphere the two polar maxima and the equatorial saddlepoint minimum that are characteristic of the GS and AER models at almost all seasons, with or without the combined scenario (Figures 13-19, 20, 21, 26). The MPIC model without added methane for spring (Figure 13-18b) also shows this structure to some extent.

An interesting feedback between chlorine and nitrogen oxides in the stratosphere is illustrated by the two-dimensional MPIC model. Table 13-9 shows that as Cl_x increases the maximum mixing ratio of NO_y ($NO + NO_2 + NO_3 + 2N_2O_5 + HNO_3 + HNO_4 + ClNO_3$) increases. Upon photolysis, nitrous oxide (N_2O) is converted to nitrogen and oxygen; and when nitrous oxide reacts with singlet atomic oxygen, the principal product is nitric oxide (NO), which is the dominant source of stratospheric nitrogen oxides (NO_y). Nitrous oxide is photolyzed by solar radiation with wavelengths below about 210 nm, but singlet atomic oxygen is mostly formed from ozone photolysis at wavelengths near 300 nm. The absolute amount of solar radiation around 300 nm is greater than that around 200 nm, so that reduction of ozone by Cl_x in the upper stratosphere more strongly increases nitric oxide formation (radiation near 300 nm) than it increases nitrous oxide photolysis (radiation near 200nm) in the middle stratosphere. The net effect is to increase the column of nitrogen oxides as stratospheric chlorine increases, which is demonstrated in Table 13-9.

Model calculations indicate that ozone changes may have already occurred in the present day atmosphere (2.7 ppbv total chlorine) compared to the atmosphere of 1965 (about 1.3 ppbv total chlorine), and these calculations have implications for ozone monitoring. Figure 13-29 presents a contour plot of the calculated percentage ozone changes for this period from the GS model for a Cl_x only scenario and neglecting temperature feedback, and Figure 13-30 shows the same calculation from the MPIC model. These changes should be considered upper limits because the mitigating effects of simultaneous methane and carbon dioxide

Table 13-9. Effect of Increasing Cl_x on Maximum Value of Stratospheric NO_y Mixing Ratio and on Nitrous Oxide and Chlorofluorocarbon Lifetimes. MPIC 2-D Model.

Scenario	ppbv Cl_x at 40 km	ppbv NO_y Maximum	Lifetime/Centuries		
			N_2O	CFC-11	CFC-12
1964	1.3	18	1.85	—	—
1985	2.7	18	1.8	0.5	1.5
1980 CFC Emission	9.5	22	1.65	0.5	1.4
1980 CFC Emission, $2\times CH_4$, $1.2\times N_2O$	9.5	24	1.65	0.5	1.4
Twice 1980 CFC Flux, $2\times CH_4$, $1.2\times N_2O$	18.	28	1.5	0.5	1.3

increases have not been considered (see one-dimensional model calculations). At 40 km, both models indicate large local ozone reductions in the north polar region (GS,30%; MPIC, 20%) and in the south polar region (GS, 30%; MPIC, 10%), and both models give at least a 10% ozone reduction from pole to pole. The GS model shows significant local ozone reductions even at 25 km in the summer and winter polar regions, due to downward transport. This suggests that a monitoring strategy aimed at detecting an ozone response at the earliest possible time should provide measurements at high latitudes, both in the lower and upper stratosphere. Further, detailed measurements of the latitudinal distributions of methane and HCl would be of value in evaluating how realistic these predicted gradients in ozone depletion at high latitude might be. Most of the ozone at high latitudes is located at low altitudes (below 25 km) where it is not readily accessible to satellite observations. This poses a severe challenge to attempts to detect changes in the ozone column and vertical profiles at high latitudes, where large changes in total ozone may occur at the earliest times as the atmospheric chlorine content increases. However, a carefully designed program would be needed to detect a clear trend against the extreme zonal and temporal variability at high latitudes in late winter and spring, particularly in the Northern Hemisphere.

Comparisons

The AER and GS models represent one method of treating atmospheric motions in two dimensional models, and the MPIC model represents a different method (Chapter 12). In comparison with atmospheric observations, one method is more successful than the other in some cases, and the reverse applies in other cases. As pointed out in Chapter 12, for example, the AER and GS models severely underestimate nitrogen oxides in the lower stratosphere, at 30 degrees north for example, as compared with the observations by the LIMS satellite. For 30° north during March, NO_y vertical profiles are given in Figure 13-31 as calculated by AER and by MPIC, and these are compared with the observed LIMS profile of NO_2 and HNO_3 at night, which is a lower limit to NO_y. For this example, the AER model underestimates nitrogen oxides by a factor between 3 and 8 over the range of 25 to 20 km, whereas the MPIC model is more

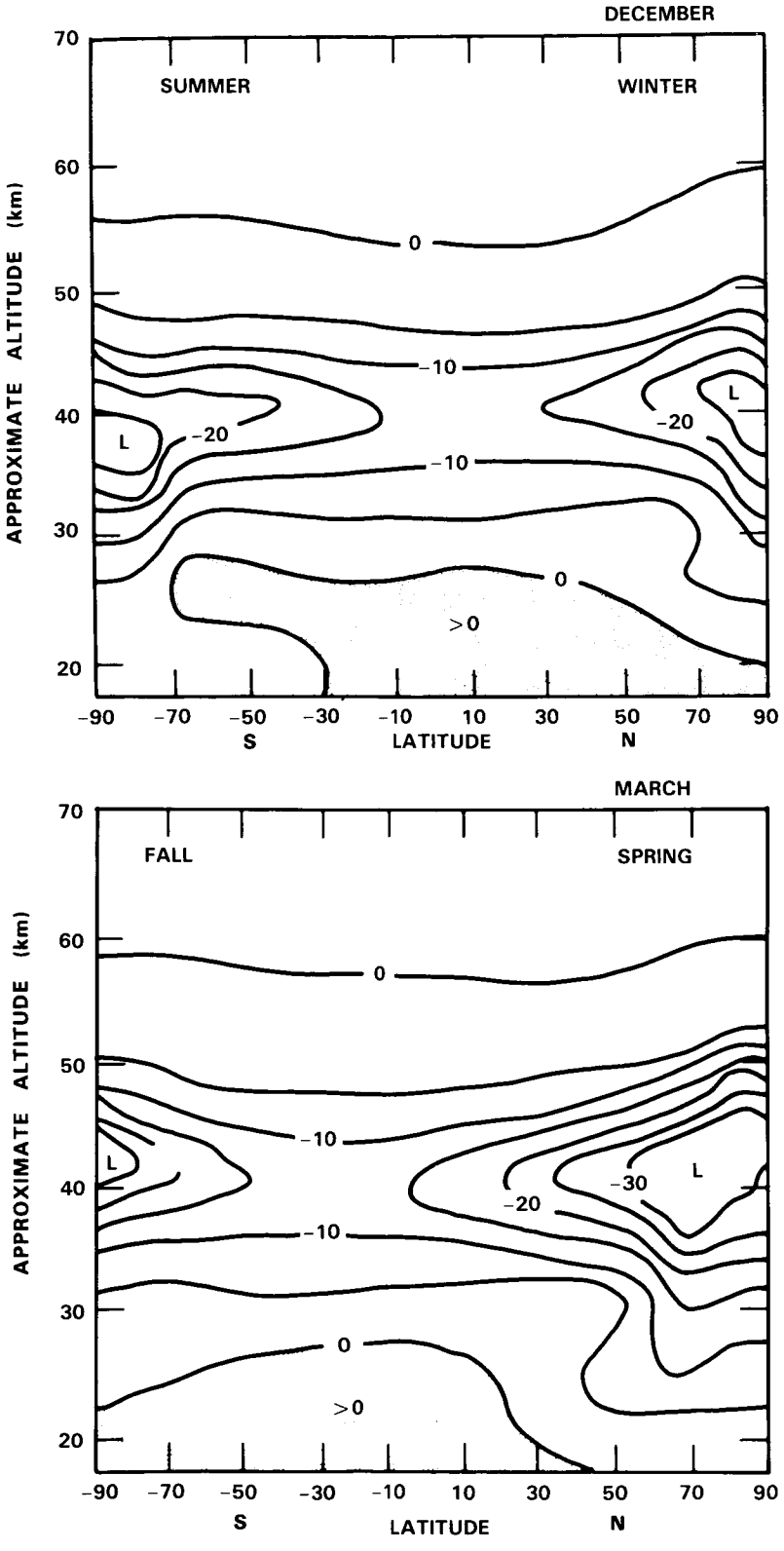

Figure 13-29. Calculated local percentage ozone changes from 1965 (1.3 ppbv Cl_x) to 1985 (2.7 ppbv Cl_x) using GS model and Cl_x only perturbation.

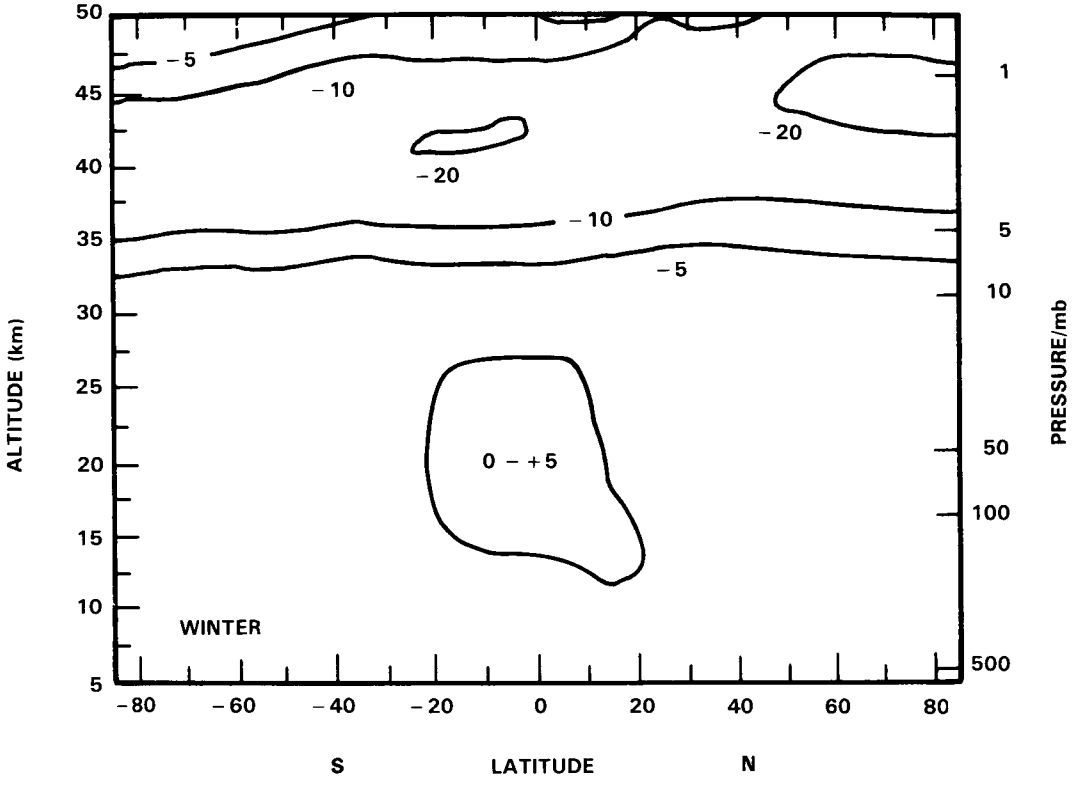

Figure 13-30. Similar to Figure 13-29 (MPIC 2-D model).

successful in this range. In the middle and upper stratosphere, both models give satisfactory agreement with observations. In the upper stratosphere the AER and GS models more nearly reproduce the methane latitudinal variations. In spite of the differences in treatment of atmospheric motions and in spite of the various agreements and disagreements between model calculations and observations, these two types of model give the same general practical results so far as ozone changes by chlorine is concerned, for example, Figure 13-24. Both types of model show ozone depletion by added chlorofluorocarbons at all latitudes, both show a strong latitudinal gradient with minimum ozone reduction in the equatorial region.

It is interesting to compare two-dimensional global average calculations against local properties in the same model. The global average vertical profile of ozone reduction for scenario S2A (6.7 ppbv increase of Cl_x) according to the Garcia-Solomon model is shown by Figure 13-32, and the local profiles are shown for 4° N and 61° N. The ozone decrease at high latitude is substantially larger than the global average at all altitudes. For the AER model with S2A perturbation, the ozone-column decrease is plotted as a function of latitude for all four seasons with the global average value indicated by a dashed line (Figure 13-33), and a similar graph is given as a function of months of the year for 0, 28, 47, and 66 degrees north latitude (Figure 13-34).

13.1.4 Comparison of 1-D and 2-D Results

Percentage changes of total ozone as calculated by one-dimensional models for various scenarios including chlorofluorocarbons are summarized in Tables 13-2 and 13-3. Many of these cases are illustrated by figures in Section 13.1.2, giving the vertical profile of calculated ozone change as a function of altitude.

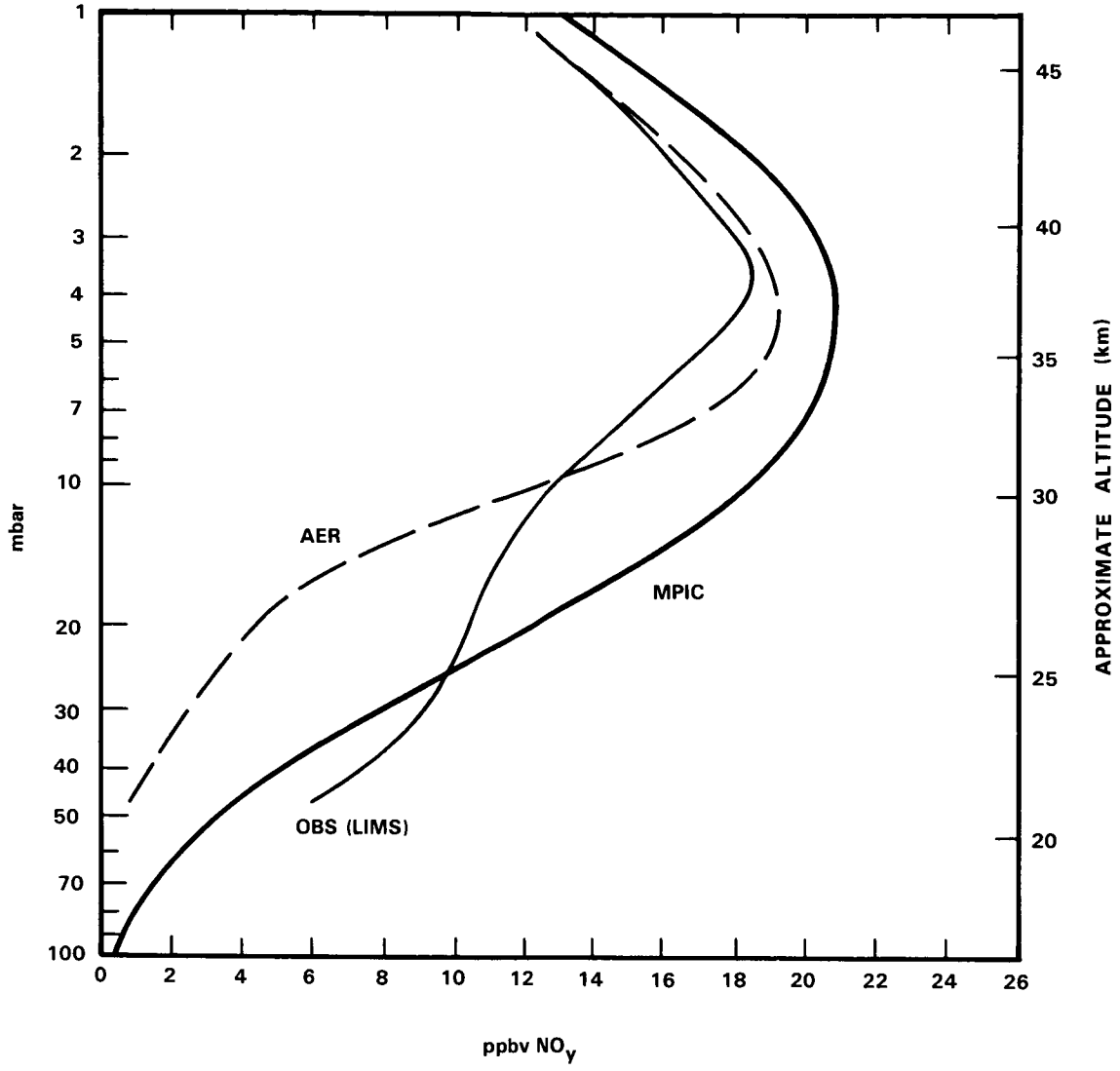

Figure 13-31. Comparison of calculated NO_y according to AER and MPIC 2-D models with LIMS satellite observed NO_2 + HNO_3 at night at 30° N during March.

Global-average percentage ozone changes according to two-dimensional models are given by Table 13-8. The seasonal and latitudinal dependence of the change of the ozone vertical column as calculated by 2-D models are shown by figures in Section 13.1.3. This section compares the results of these 1-D and 2-D models with respect to calculated ozone changes.

Three profiles of percentage change in local ozone from the AER 2-D model at 0°, 30°N, and 60°N in April are compared with the AER 1-D model profile in Figure 13-35 for 8 ppbv Cl_x relative to 1.2 ppbv Cl_x as reference. The 1-D profile does not correspond closely to any local 2-D profile. For instance, the calculated self-healing effect occurs at a higher altitude (23 to 30 km) in the 1-D model than those of the 0° and 30°N profiles calculated by the 2-D model, which calculates no significant self-healing for the 60°N profile. The 1-D model calculates larger ozone reductions above 40 km than the 2-D model, due in part to differences between the 1-D and 2-D model atmospheres (that is, temperature and air density)

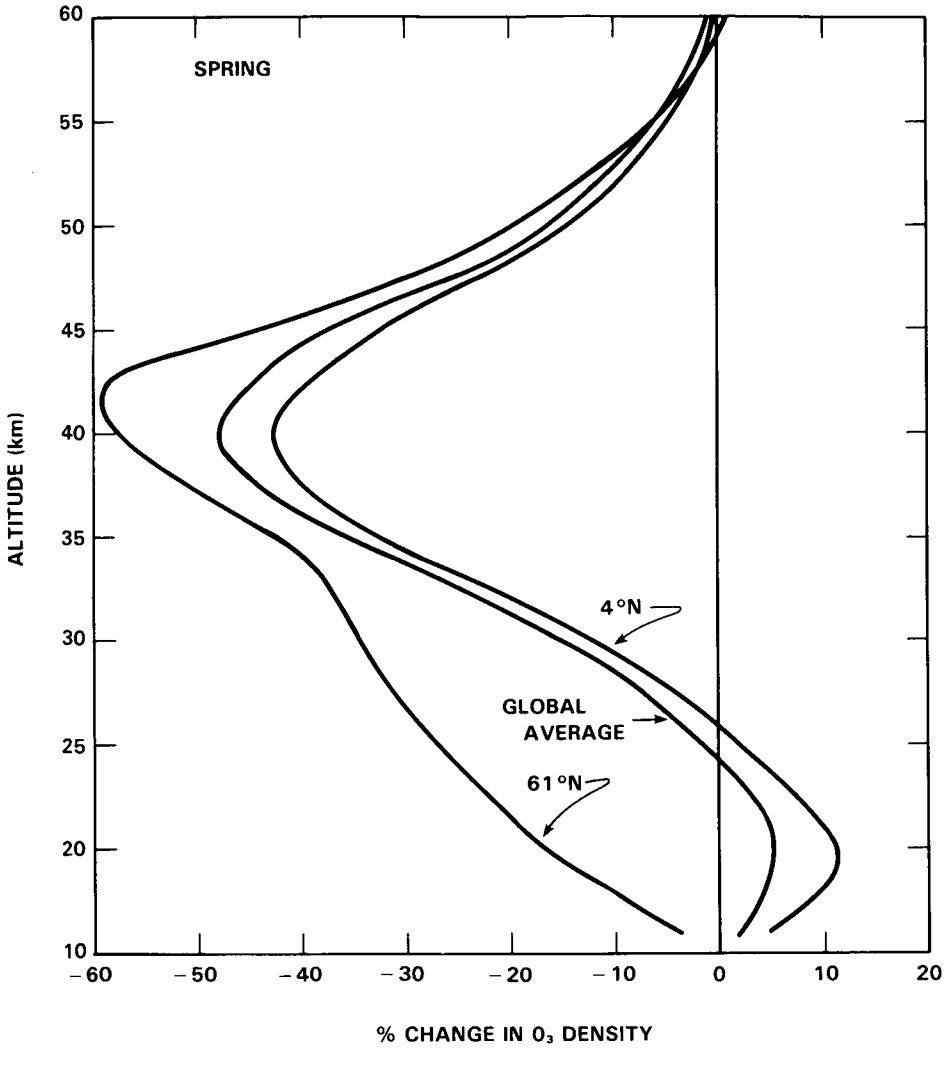

Figure 13-32. Vertical profiles of the calculated ozone changes shown in Figure 13-21 for 4° N, 61° N, and for the global average. (GS 2-D model, 6.7 ppbv increase of Cl_x).

and in part to the differences in the concentrations of transport dominated species such as water and methane between the two models.

For the AER models, the calculated ozone reduction at the spring equinox is plotted against latitude in Figure 13-36, together with the 1-D model result for the same perturbation. An important feature of this comparison is that the 2-D model gives much larger ozone reductions over the temperate and polar zones than that given by the 1-D model.

The global average 2-D results from Table 13-8 are compared with the 1-D results from Tables 13-2 and 13-3, and these comparisons are given in Tables 13-10 and 13-11. These tables are organized in terms of a quantity called "sensitivity", S, which is defined as the percentage ozone reduction divided by the ppbv of increased Cl_x. For about a 7 ppbv increase of Cl_x, the sensitivity of the 2-D models is 1.06 and 1.32 % per ppbv, and the 1-D models give values between 0.41 and 1.06. In general the global average

Table 13-10. Comparison of 1-D and 2-D Model (Global Average) Results with Respect to Sensitivity S and Linearity L, Where Cl_x Is the Only Perturbation. Sensitivity Is Percentage Ozone Reduction Divided by ppbv Cl_x Increase. Linearity Is S(2)/S(1), Which Is 1.00 if the Ozone Reduction Is Directly Proportional to Cl_x Increase.

Cl_x/ppbv			% Ozone	S	L	
Initial	Final	Increase	Decrease	−%/ppbv		Model
1.3	8.2	6.9	8.5	1.23		2-D
1.3	15.5	14.2	18.	1.27	1.03	AER
1.	8.	7.	4.6	0.66		1-D
1.	15.	14.	15.	1.07	1.63	AER
		7.	5.1	0.73		1-D
		14.	12.2	0.87	1.20	LLNL
		7.	2.9	0.41		1-D
		14.	17.8	1.27	3.10	Harvard
1.1	8.1	7.	9.1	1.30		1-D
2.5	8.1	5.6	7.4	1.32		
2.5	14.8	12.3	20.6	1.67	1.27	MPIC
1.0	7.5	6.5	4.1	0.63		1-D
1.0	14.0	13.0	8.8	0.68	1.08	IAS
2.7	9.5	6.8	7.2	1.06		2-D MPIC

2-D ozone reduction is greater than that of the 1-D models. For about a 14 ppbv increase of Cl_x, the sensitivity of the AER 2-D model is 1.27 % per ppbv, and the range of 1-D results is 0.87 to 1.67, which averages to a value almost as large as that of the AER 2-D model (compare Figure 13-36).

For ozone reductions with doubled methane and with a 20% increase in nitrous oxide in addition to increases in Cl_x, 1-D and 2-D model results (MPIC) are compared in terms of "sensitivity" in Table 13-11. Added methane reduces the sensitivity of both 2-D and 1-D models. For about 7 ppbv Cl_x increase, the global average MPIC model gives 35% greater ozone reduction than the average of the five 1-D models in Table 13-11. For about 14 ppbv Cl_x increase, the 2-D model is 16% more "sensitive" than the average of these 1-D models. The number of 2-D model calculations in this study is small, but within this small sample it is found that the global average ozone reduction calculated by the 2-D models is greater than that calculated by 1-D models for the same scenario.

For 1-D models, the reduction of ozone by increased Cl_x is not a linear function, as illustrated by Figure 13-6. A plot of "change of ozone column" against "change of Cl_x" shows downward curvature. The term "sensitivity" defined above increases with "change of Cl_x". An interesting question is whether 2-D models are linear or nonlinear in this sense of the word. In this study there are not enough 2-D model

Table 13-11. Comparison of 1-D and 2-D (Global Average) Model Results with Respect to Sensitivity S and Linearity L (for Definitions See Table 13-10). Increasing Cl_x and $2\times CH_4$ and $1.2\times N_2O$.

Cl_x/ppbv			% Ozone	S	L	
Initial	Final	Increase	Decrease	−%/ppbv		Model
2.7	9.5	6.8	4.5	0.66		2-D
2.7	18.	15.3	11.1	0.73	1.10	MPIC
1.1	8.1	7.0	6.0	0.86		1-D
2.5	8.1	5.6	4.3	0.77		
2.5	14.8	12.3	12.0	0.98	1.27	MPIC
		7.	3.4	0.49		1-D
		14.	7.8	0.56	1.15	LLNL
		7.	3.0	0.43		1-D
		14.	8.2	0.59	1.37	Harvard
		7.	3.3	0.47		1-D
		14.	8.8	0.63	1.47	AER
		7.	3.1	0.44		1-D
		14.	7.2	0.51	1.16	DuPont
1.0	7.5	6.5	2.3	0.35		1-D
1.0	14.0	13.0	5.6	0.43	1.23	IAS

results to test for linearity by means of a plot such as that of Figure 13-6. For any 2-D model used here, there are only three values of Cl_x: a reference value, a value near 8 ppbv, and a value near 15 ppbv. These three points can be used to estimate linearity in terms of change of sensitivity with increase of Cl_x. In Tables 13-10 and 13-11, a quantity "linearity" L is defined as the ratio of two sensitivities. If this ratio is 1.00 the change of ozone is linear over the range of Cl_x included in the test. For nonlinearity in the sense of that shown by 1-D models (Figure 13-6), the value of L is greater than 1.00. With opposite curvature L is less than one.

For added Cl_x as the only perturbation, the AER 2-D model is compared with the 1-D models of this study for linearity in Table 13-10 as ratio of sensitivities, S. The values of L are given as the sixth column of the table. For the AER 2-D model the global average value of L is 1.03, whereas the value for the AER 1-D model for the same range of Cl_x is 1.63. The AER 1-D model result is strikingly more nonlinear than global average results from the AER 2-D model. The other 1-D models give values of L between 1.20 and 3.1. As discussed in Chapter 12, these differences in linearity among the models is related to the amount of NO_y predicted by the models. Over the range of 1 to 15 ppbv Cl_x, the global average results of the AER 2-D model are much more nearly linear than the results of the 1-D models.

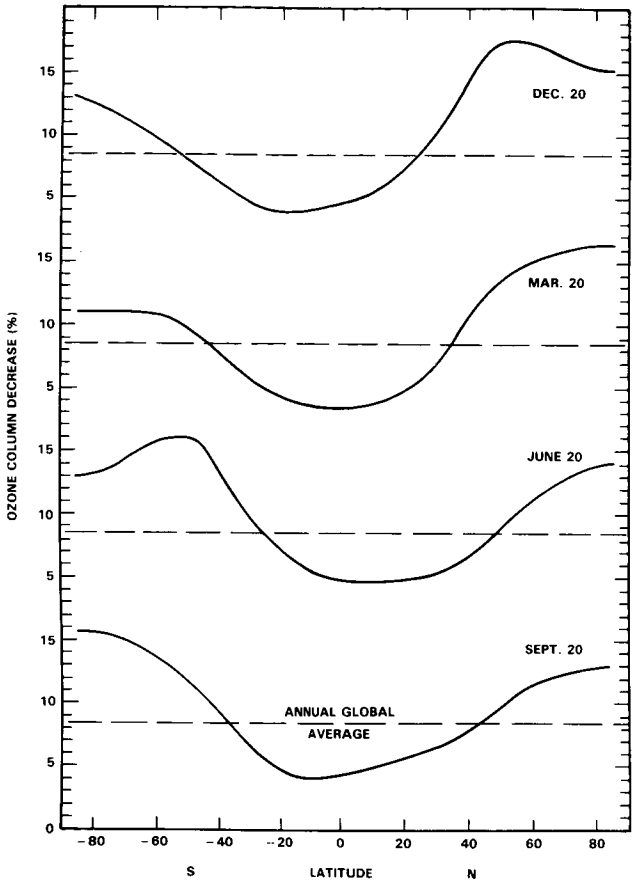

Figure 13-33. Calculated ozone-column decrease as a function of latitude for each of four seasons for conditions of Figure 13-23a with the annual, global-average value included as horizontal line (AER 2-D model).

A similar result is obtained in Table 13-11, where increases of methane and nitrous oxide are included. The MPIC 2-D model gives 1.10 as its value of L, where 1.00 represents linearity, and the MPIC 1-D model has the value 1.27. The ozone-reduction results of the MPIC 2-D model are much more nearly linear than those of the MPIC 1-D model. The 1-D models of Table 13-11 cover the range 1.15 to 1.41 in the ratio L. With added methane and nitrous oxide, the 1-D models are less nonlinear than they are in the cases of added Cl_x only.

By use of the sensitivity function S for specific values of latitude and season for two different increases in Cl_x, one can calculate a two dimensional map of the function L, which gives the local and seasonal degree of nonlinearity of the 2-D models. For the AER 2-D model, values of S for both 6.9 and 14.2 ppbv are listed for seven latitudes and for four seasons in Table 13-12. Also included in the table are the values of L for the same range of seasons and latitudes. At all seasons and latitudes, local changes of ozone according to the 2-D model are much more nearly linear than any of the 1-D models (compare Table 13-10). The range of values of L is 0.82 to 1.08, while the global average value is 1.03. The values of L between 28 °S and 28 °N are all greater than that for the global average, that is more nonlinear; and values in the polar region are somewhat less than 1.00, which corresponds to slight nonlinearity in the opposite sense.

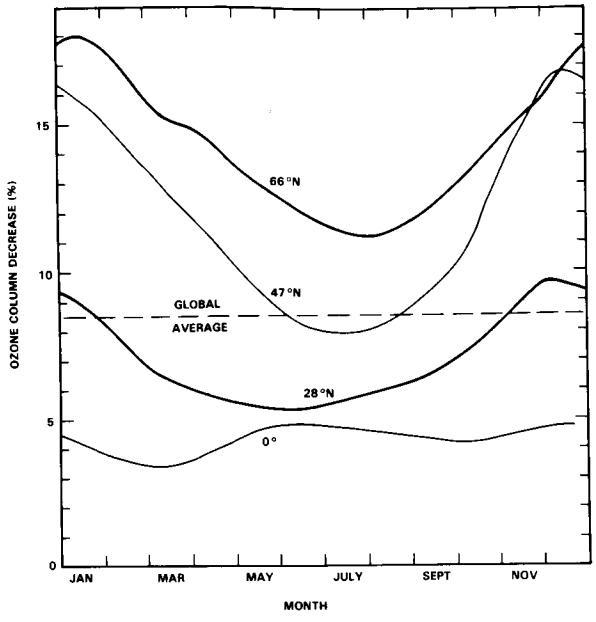

Figure 13-34. Same as Figure 13-33, except displayed as a function of the months of the year at 4 selected latitudes.

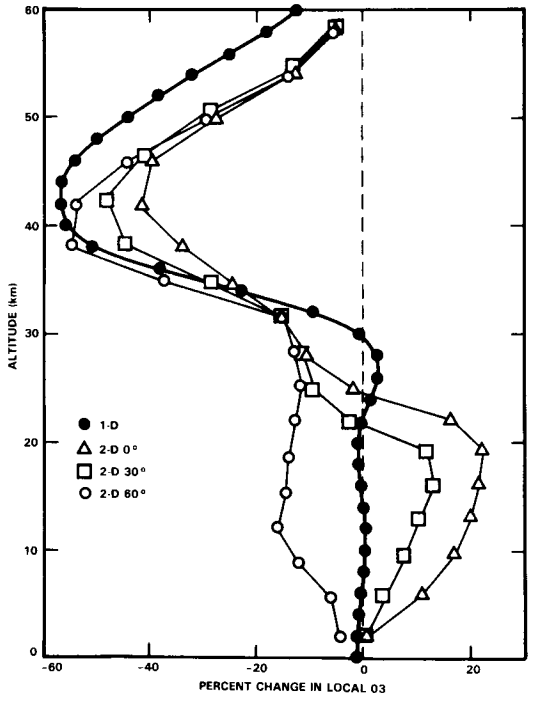

Figure 13-35. Comparison of percentage change of local ozone as a function of altitude as calculated by the AER 1-D model with three such profiles at 0, 30 and 60 degrees N calculated by the AER 2-D model for April.

Table 13-12. Local and Seasonal Ozone Sensitivity S (Percent Ozone Decrease Divided by ppbv Cl_x Increase) and Test for Local and Seasonal Linearity L (S for 14.2 ppbv Cl_x/S for 6.9 ppbv Cl_x) in Terms of AER Two-dimensional Model.

		Latitude						
Case	**Season**	**85°S**	**56°S**	**28°S**	**0**	**28°N**	**56°N**	**85°N**
S(14.2)	W	1.70	1.37	0.71	0.63	1.37	2.23	2.15
	Sp	1.71	1.93	1.05	0.59	0.93	1.78	1.91
	Su	2.05	2.13	1.37	0.71	0.87	1.48	1.78
	F	2.02	1.65	0.90	0.68	1.19	1.89	1.80
S(6.9)	W	1.79	1.30	0.64	0.61	1.29	2.47	2.48
	Sp	1.64	1.84	0.97	0.56	0.86	1.80	2.33
	Su	2.07	2.28	1.20	0.67	0.81	1.47	2.00
	F	2.18	1.71	0.81	0.63	1.08	1.91	1.92
L	W	0.95	1.06	1.11	1.04	1.06	0.90	0.87
	Sp	1.04	1.05	1.08	1.05	1.08	0.99	0.82
	Su	0.99	0.93	1.06	1.07	1.07	1.01	0.89
	F	0.93	0.96	1.11	1.08	1.10	0.99	0.94

Global Average: S(14.2) = 1.27; S(6.9) = 1.23; L = 1.03.

AER 1-D: S(14.) = 1.07; S(7.) = 0.66; L = 1.63

For Cl_x perturbations including increase of methane and nitrous oxide, values of the sensitivity function S and the linearity test function L are given for the MPIC 2-D model as a function of latitude and season in Table 13-13. The global average value of L is 1.10, and the range of values in Table 13-13 is 0.96 to 1.22. The difference between the maximum value and minimum value of L is 0.26, which happens to be exactly the same as that for the AER model (Table 13-12). This result indicates that the latitudinal and seasonal variation of linearity of the MPIC model and the AER model are about the same. On the average, however, the MPIC model with L of 1.10 is more nonlinear than the AER model with average L equal to 1.03.

In 1-D models the nonlinear phenomenon is thought to be driven by the strong chemical interactions between the chlorine (Cl_x) and nitrogen (NO_y) species. Prather *et al.* (1984) argued that as stratospheric concentration of Cl_x approaches that of NO_y a significant portion of NO_y in the *lower* stratosphere will be tied up in the form of $ClNO_3$, a chlorine reservoir species formed by recombination of NO_2 and ClO. Formation of $ClNO_3$ reduces the concentrations of other forms of NO_y species, including NO, NO_2, HNO_3, and HNO_4, resulting in higher OH in the lower stratosphere (since OH is removed mainly by reaction

Table 13-13. Local and Seasonal Ozone Sensitivity S (Percent Ozone Decrease Divided by ppbv Cl_x Increase) and Test for Local and Seasonal Linearity L (S for 15.3 ppbv Cl_x/S for 6.8 ppbv Cl_x in Terms of MPIC Two-Dimensional Model, Including Double Methane and 20% Increase of Nitrous Oxide.

		Latitude						
Case	Season	85°S	55°S	25°S	0	25°N	55°N	85°N
S(15.3)	W	1.02	0.86	0.67	0.59	0.66	0.93	0.96
	Sp	1.05	0.98	0.64	0.50	0.64	0.90	0.98
	Su	0.97	0.95	0.64	0.62	0.68	0.80	1.00
	F	0.97	0.89	0.63	0.60	0.64	0.85	0.98
S(6.8)	W	0.91	0.80	0.59	0.55	0.57	0.94	0.98
	Sp	0.92	0.90	0.55	0.45	0.58	0.92	1.02
	Su	0.93	0.91	0.53	0.56	0.60	0.72	0.91
	F	0.97	0.87	0.54	0.55	0.55	0.72	0.96
L	W	1.12	1.08	1.12	1.08	1.15	0.99	0.98
	Sp	1.14	1.10	1.16	1.12	1.11	0.98	0.96
	Su	1.05	1.04	1.22	1.10	1.13	1.11	1.11
	F	1.00	1.02	1.19	1.10	1.16	1.18	1.14

Global Average: S(15.3) = 0.73; S(6.8) = 0.66; L = 1.10.

MPIC 1-D: S(12.3) = 0.98; S(5.6) = 0.77; L = 1.27

with HNO_3 and HNO_4 in the lower stratosphere). These factors, higher OH and lower NO, contribute to the greater efficiency of the chlorine catalyzed ozone removal cycles at the high chlorine concentrations. However, the region of the chemically induced nonlinearity occurs in the lower stratosphere of the model (below 30 km), where $ClNO_3$ formation is appreciable. This is also the region where transport is known to play an important role in regulating the distribution of O_3. Since the description of transport is quite different in 1-D and 2-D models, the effect of nonlinear chemistry on lower stratospheric ozone is different in these models.

The linear response of column ozone to stratospheric chlorine perturbations (Table 13-12, Figure 13-23) calculated by the AER 2-D model at high latitudes during winter and spring may be explained in a qualitative manner by the poleward-downward ozone transport argument put forward by Solomon *et al.* (1985b). The effect of nonlinear local chemistry on lower stratospheric ozone at high latitudes is small relative to the meridional ozone transport effect.

Isaksen and Stordal (1985) tested their two-dimensional model for linearity out to Cl_x increases of 21 ppbv and for three levels of NO_y. For the standard NO_y level, they found the global average ozone reduction to be nearly linear with increasing Cl_x out to 12 ppbv and then to become significantly nonlinear

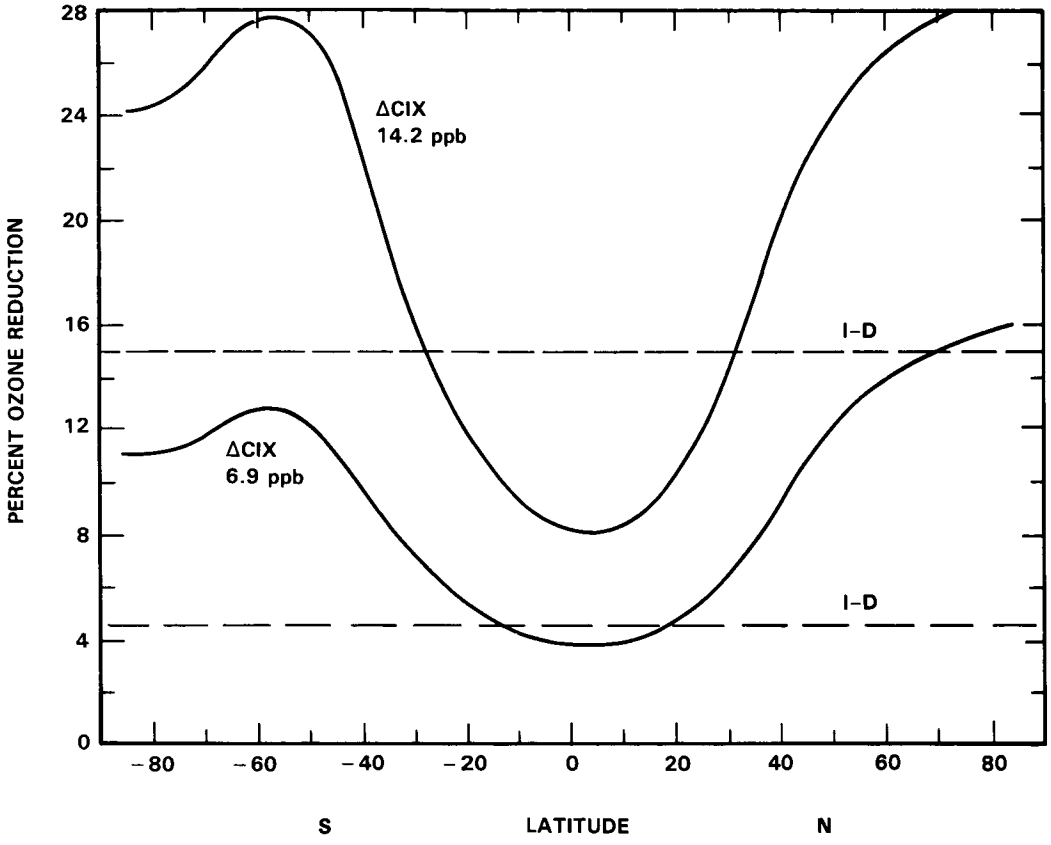

Figure 13-36. Comparison of percentage ozone-column reduction as a function of latitude as calculated by AER 2-D model with the values calculated by AER 1-D model for the same perturbation. For one case total Cl_x is 8.2 ppbv and the other it is 15.5 ppbv, and the reference case is 1.3 ppbv Cl_x.

by 20 ppbv. Their case of low NO_y was distinctly more nonlinear than the standard case, and the case of high NO_y was more nearly linear than the standard case.

In summary, for a given Cl_x perturbation the global average ozone reduction calculated by these 2-D models is greater than the value calculated by 1-D models, the 2-D models show strong latitude gradients of ozone reduction so that temperate and polar zones show larger ozone reductions than that found by 1-D models, and between 0 and 12 ppbv Cl_x the calculated ozone reductions as a function of increasing Cl_x is nearly linear for 2-D models and highly nonlinear for the 1-D models.

13.2 DISCUSSION OF CURRENT MODEL PREDICTIONS AND ASSESSMENT OF RECOGNIZED UNCERTAINTIES

13.2.1 Uncertainties in Model Predictions

The predictive value of the model results presented above cannot be judged without consideration of their sensitivity to uncertainties in model input data and assumptions. Recognized uncertainties include several factors: a) halocarbon release rate scenarios; b) long term trends in other photochemically active trace gases; c) long term trends in species that affect the climate ; d) the rate coefficients of photochemical

processes; e) atmospheric dynamics; and f) trends in solar radiation. It is possible to assess separately and quantitatively some of these uncertainties, while others can only be qualitatively noted and flagged for future concern.

13.2.2 History of Model Predictions for Assumed Perturbations

The history of model calculations gives a graphic hindsight picture of uncertainty in photochemical modeling. The calculated effects on ozone by two standard assumed perturbations have been evaluated approximately every year since 1974 by the group at Lawrence Livermore National Laboratory using the then current photochemistry (WMO, 1981, pages 3-26). The one-dimensional model, including vertical eddy diffusion, is calculated to steady-state for these perturbations. The assumed perturbations are: (1) A large fleet of stratospheric aircraft emitting 2000 molecules of nitric oxide per second per cubic centimeter over a one kilometer band centered at 20 kilometers; (2) chlorofluorocarbons 11 and 12 emitted steadily at the 1974 production rates. These perturbations were considered separately; and the photochemical rate coefficients, boundary values, and eddy diffusion function were those recognized at the time of the calculation. Between 1974 and 1981, the steady-state change of the ozone vertical column calculated for each perturbation underwent large excursions as new atmospheric species were found to be important and as values of rate coefficients were remeasured, or in some cases measured for the first time. For example, the calculated effect on the ozone column by the stratospheric aircraft went from -10% in 1974 to $+4\%$ in 1978 to -7% in 1981; and the calculated steady-state effect on the ozone column by the CFCs went from -14% in 1975 to -7% in 1977 to -19% in 1979 and to -5% in 1981. These excursions were recognized as growing pains in the science of stratospheric modeling.

This study is brought up to date by Figure 13-37. There have been no large changes in these calculations during the last four years. The calculated change in the ozone vertical column by the standard CFC perturbation has changed from -5% in 1981 to -4% in 1984 to -7% in 1985, and that for the standard NO_x perturbation has changed from -7% in 1981 to -12% in 1984 to -11 % in 1985. However, as can be seen from Section 13.2.3.1 (below), there is still room for future large changes in these perturbation calculations on the basis of recognized uncertainties in photochemical rate coefficients.

Since 1977, the changes in the NO_x effect have been strongly negatively correlated with changes in the CFC effect. The varying predictions of Figure 13-37 are not due to changes in rate coefficients in the Cl_x or NO_x systems, but instead are largely caused by revisions in the rate coefficients in the HO_x system (WMO, 1981; Johnston, 1984). Increases in the calculated hydroxyl radical concentration at 25 km are strongly correlated with greater ozone reductions by CFCs and with lesser ozone reductions by NO_x. The cause of this effect is that hydroxyl radicals bind catalytically active NO_2 into the inactive form of nitric acid, but they also release catalytically active chlorine atoms from inactive hydrochloric acid. The sensitivity of these calculations to the calculated concentration of hydroxyl radicals at altitudes between 20 and 30 km emphasizes the need for these radicals to be measured in this range of the atmosphere.

13.2.3 Sensitivity to Chemistry and Photochemistry

Two types of uncertainty can arise in connection with photochemical processes. The first type is due to experimental uncertainties in measured photochemical rate coefficients included in the model. The second type concerns chemical species or photochemical reactions that are omitted from the model, either from lack of quantitative data or because no one has thought of them yet. The first class of sensitivity of model calculations to photochemical uncertainties is subject to quantitative analysis using evaluated rate data with assessed uncertainties (DeMore *et al.*, 1983, 1985; Appendix A) and previously developed methods.

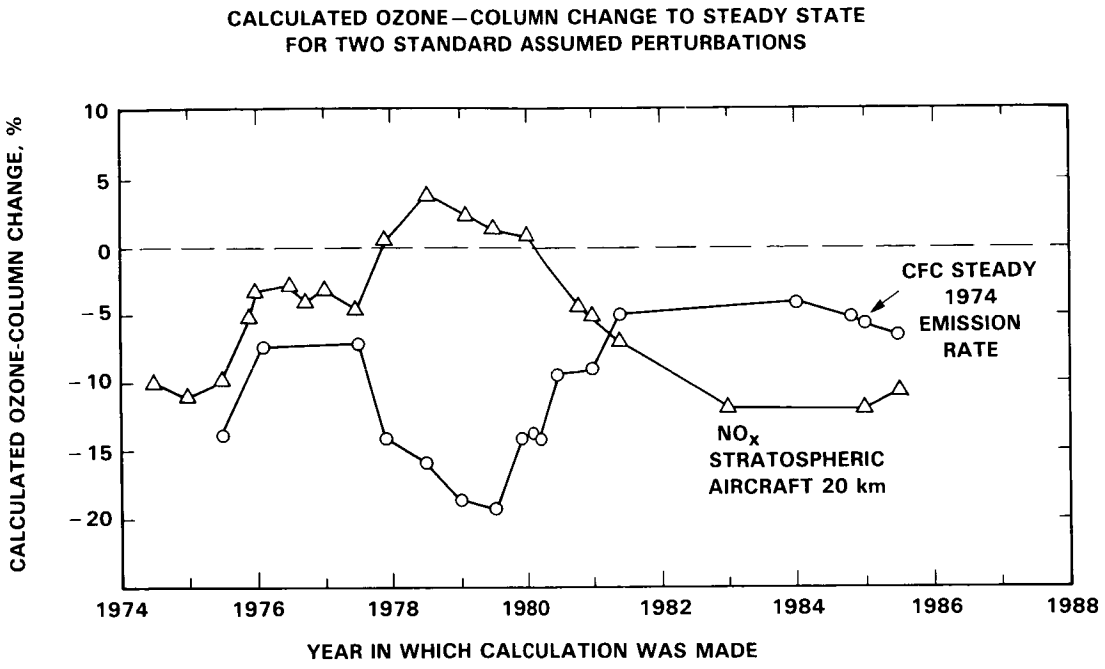

Figure 13-37. Calculated ozone-column change to steady state for two standard assumed perturbations: (a) 2000 molecules cm^{-3} s^{-1} of nitric oxide emitted over one kilometer interval centered at 20 km (originally based on a hypothetical, large fleet of stratospheric aircraft); (b) CFC-11 and CFC-12 emitted continuously at 1974 rate. These calculations were made at LLNL over this 11 year period using then current photochemical parameters, eddy diffusion functions, and boundary conditions.

13.2.3.1 Ensemble Sensitivity to Uncertainty in Rate Parameters

A method of evaluating the effects of uncertainties in rate parameters was introduced by Stolarski *et al.* (1978) and was used in the NRC 1979 evaluation (NRC, 1979, Appendices A and D). It uses a Monte Carlo simulation where individual rate parameter values for each reaction are chosen at random within an assumed probability distribution, which is based on the assessed uncertainties of the rate coefficients (DeMore *et al.*, 1983, 1985). With enough calculations of this type (typically several hundred to several thousand), the ozone-change probability distribution implied by the joint uncertainty in all the modeled reaction rates can be obtained.

Two separate Monte Carlo uncertainty analyses were performed for this assessment with currently recommended values and evaluated uncertainties for chemical and photochemical rate coefficients (Appendix A).

The first of these studies (Grant *et al.*, 1985) utilized the LLNL 1-D model with fixed concentration boundary conditions and without temperature feedback for the steady-state scenario S3B (15 ppbv Cl_x vs a background of 1.3 ppbv Cl_x, $2xCH_4$, $1.2xN_2O$) as presented in Table 13-2. In performing this study, the maximization of information gained per model run was a major concern. Since the standard error is proportional to the square root of the sample size, it was impractical to reduce the error sufficiently simply by increasing the number of model runs. In order to significantly decrease the number of samples required to achieve the needed level of estimation accuracy, a variance reducing technique known as Latin Hypercube

Sampling (LHS), (McKay *et al.*, 1979; Iman *et al.*, 1981; Iman and Shortencarier, 1984) was chosen. A detailed account of the sampling procedure used will be published (Grant *et al.*, 1985).

In the LLNL study, two sets of 50 Monte Carlo runs plus a base line calculation were performed for each of the ambient (no CFC) and perturbed (S3B, Cl_x = 15 ppbv, $2xCH_4$, $1.2xN_2O$) scenarios. Two pair of runs, each predicting extremely large ozone perturbations (beyond 3.5 standard deviations) were eliminated to avoid unduly influencing the analysis. These two sets of runs also gave NO_y levels much smaller than indicated by available measurements. The calculated ozone change, its single standard deviation, and the moments of skewness and kurtosis are shown in Table 13-14 for the remaining 98 paired runs. Distribution histograms for the total ozone column perturbations and for ozone perturbations at 20, 30, and 40 km are displayed in Figure 13-38.

As indicated by Figure 13-38 and Table 13-14 the uncertainty for the column total is less than that for individual altitudes, indicative of a tendency for the variations applied to alter the O_3 profile in addition to changing total ozone. The column total and the perturbations for the altitudes of 20 and 30 km display the negative skewness previously observed by Stolarski *et al.* (1978). These estimates also show a more peaked distribution than a normal distribution with the same standard deviation.

For the total ozone column, the calculated single standard deviation range was -1.9% to -13.5% for the full Monte Carlo calculation with the S3B scenario, and this result compares fairly well with range of -4.2% to -14.4% calculated for the nine single reaction variation treatment presented in the next section for the same perturbation scenario.

The second Monte Carlo treatment using current reaction rate evaluation inputs was performed by Stolarski and Douglass using the Goddard Space Flight Center one-dimensional model (Rundel *et al.*, 1978) as an update of their previous Monte Carlo studies (NRC, 1979; Stolarski, *et al.*, 1978). These studies have been performed as a function of CFC flux into the model atmosphere and carried to steady-state; the CFC flux is imposed on a 1 ppbv background of Cl_x from CH_3Cl and CCl_4 but no Cl_x from CFC's. The calculation is parameterized in terms of 1985 CFC input flux which was taken to be 9.2×10^6 cm^{-2} for CFC-11 and 1.28×10^7 cm^{-2} s^{-1} for CFC-12. Boundary conditions for species like N_2O and CH_4 were set at today's measured values with small uncertainties due to measurement uncertainties.

Table 13-14. Statistical Moments for Percent Change in Ozone (Perturbed Chemistry Relative to Ambient) Relative to That for the Unvaried Baseline Case Obtained for 98 Paired Runs (Grant, *et al.*, 1985).

Altitude km	Baseline % Change	Standard Deviation	Moment of Skewness	Moment of Kurtosis
Total Column	−7.7	5.80	−1.58	1.76
20	+3.9	6.28	−1.88	3.24
30	−11.2	9.96	−1.18	0.22
40	−69.1	8.96	0.90	−0.34

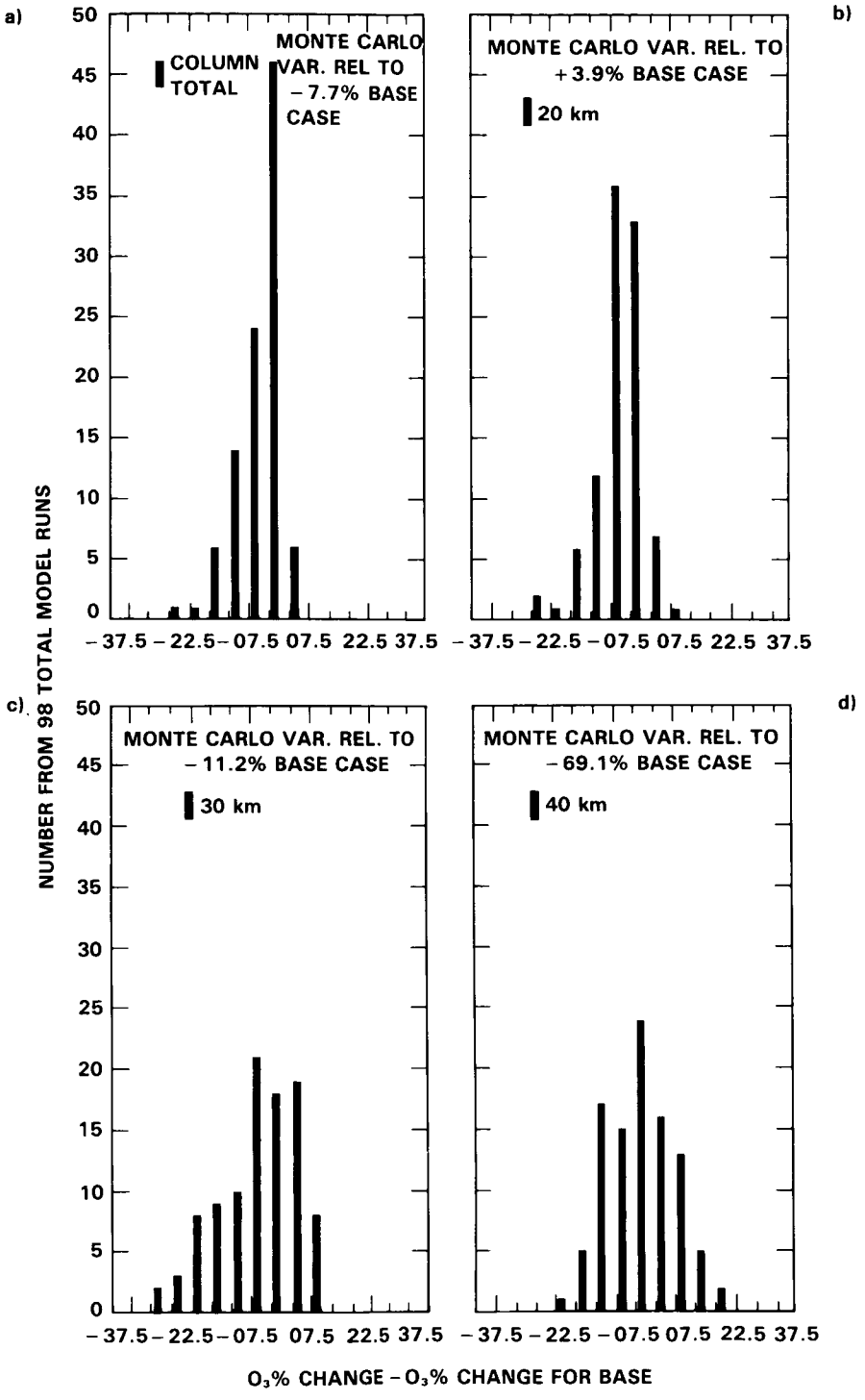

Figure 13-38. Monte Carlo calculated ozone changes in LLNL 1-D model. Distribution obtained for percentage change in ozone column (perturbed chemistry relative to ambient) relative to percentage change obtained for unvaried baseline case. (a) Ozone column with baseline case change of −7.7%. (b) Ozone at 20 km with baseline case change of +3.9%. (c) Ozone at 30 km relative to baseline case change of −11.2%. (d) Ozone at 40 km relative to baseline case change of −69%. (LLNL model).

species necessary to maintain these mixing ratios were then determined, and these fluxes are held constant when a CFC perturbation is imposed on the model. This means that when significant ozone depletions occur in the model, the concentrations of these species will decrease, contrary to the present observed trend.

The results of the Goddard Monte Carlo calculations are displayed in Figure 13-39, the solid line shows the calculated depletion in the ozone column as a function of CFC flux when the recommended values for all input parameters are used in the model. The dashed curve is the mean depletion in the ozone column for 329 cases in which probability distributions were included for all input parameters. These two curves do not coincide, and the differences are statistically significant. Use of recommended values for the cases of steady-state CFC release at the present-day fluxes gives a column ozone change of -5.0%, while including the uncertainties, shifts this mean to -6.2% with a standard error of the mean of less than 0.3%. The curves cross for larger CFC fluxes and diverge until at 3.5 times the present CFC flux, the recommended values give -40%, and the mean is -31% with a standard error of the mean of approximately 1%. Also shown in Figure 13-39 are the one standard deviation uncertainties about the mean derived from the data for the 329 cases. They are seen to increase as the size of the perturbation increases. For the present-day CFC fluxes, the standard deviation is 5.5% thus nearly encompassing zero on one side and reaching almost -12% on the other. As larger perturbations are considered, the 1 sigma limits do move clearly away from zero but increase significantly in magnitude until at 3.5 times the present-day fluxes $-31\% \pm 17\%$ is obtained.

All of these statistical parameters must be considered an approximate guide inasmuch as the output probability distributions are asymmetrical. Figure 13-40 shows a series of calculated probability histograms of the depletion of the ozone column for perturbations of 1,1.5, 2, and 3 times the present-day CFC fluxes as compared to an atmosphere with no CFC's. The distribution for the current CFC fluxes is clearly asymmetrical with a mean of -6.2% and a most probable value of between -2 and -3%. The median for this distribution increases as the fluorocarbon flux increases, and the distribution spreads toward higher values and becomes more symmetrical.

In a study initiated too late for complete inclusion in this report, Stolarski and Douglass (1985) have found that the uncertainty range of the Monte Carlo calculations can be narrowed from considerations of atmospheric observations. The Monte Carlo calculation seeks out all possible combinations of cases within the range of the assessed uncertainties of the photochemical coefficients, but certain combinations yield calculated species concentrations or distributions that are outside the range of extensive atmospheric measurements. These cases are then excluded from the study. This screening procedure was applied to the concentrations of NO, NO_2, and ClO at 25 km. Keeping only those cases that fell within the range of measurements of these three species at 25 km resulted in 125 cases, which had a mean ozone depletion calculated for steady-state fluorocarbon emissions at the 1980 rate of -3.0% and a standard deviation of 2.2%. This type of treatment of the ozone-CFC problem has the potential of bringing together and using simultaneously the full body of critically evaluated photochemical data and a large body of atmospheric observations, including satellite data. The method will, however, require careful development, including how to handle observational errors. A serious limitation is that of one-dimensional modeling and the uncertainty concerning what latitude and season of the real world observations are to be compared with the calculations of the model.

13.2.3.2 Sensitivity to Uncertainty in Individual Rate Parameters

The Monte Carlo calculations show large changes in model predictions arising from the joint uncertainties of all the rate coefficients. A special study was carried out to try to identify some individual reactions that are especially important sources of these large changes in model predictions. The effect on calculated

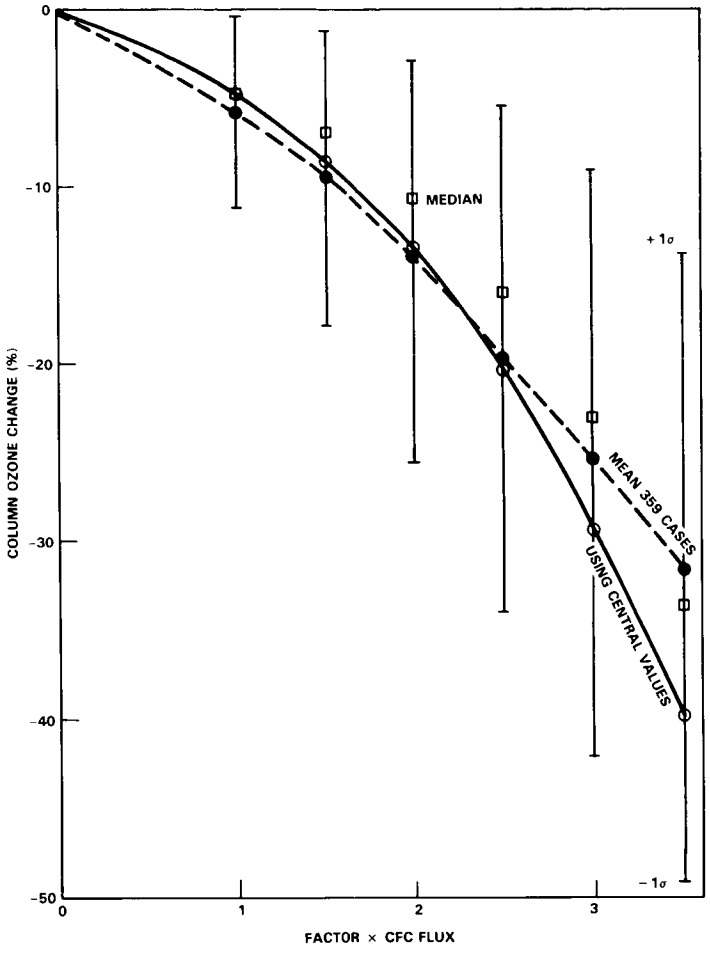

Figure 13-39. Monte Carlo calculated ozone-column changes (mean values, dashed line; medians, squares; standard deviation, range bar) for CFC flux factors normalized to 1985 values. The calculated changes based on the recommended rate parameters are shown as the solid line (Stolarski and Douglass model).

ozone depletion induced by varying nine selected photochemical rate coefficients within their ranges of evaluated uncertainties has been assessed.

This assessment of the impact of uncertainty in selected individual rate parameters has been performed for steady-state scenario S3B using the LLNL one-dimensional model without temperature feedback. This baseline scenario, as shown in Table 13-2 predicts a -7.8% change in column O_3 relative to a CFC-free atmosphere upon addition of 15 ppbv Cl_x, a doubling of current CH_4 and a 1.2 factor rise in current N_2O.

The effect of uncertainties in selected individual rate constants was evaluated by changing individual rate parameter expressions by their one-sigma evaluated levels (DeMore *et al.*, 1985) and recalculating the steady-state ozone change for the transition from a CFC-free atmosphere with current CH_4 and N_2O levels to a S3B scenario atmosphere.

In analogy with previous studies of this type, sensitivity parameters, $r_i(max)$, $r_i(min)$, and $r_i(ave)$ can be defined such that:

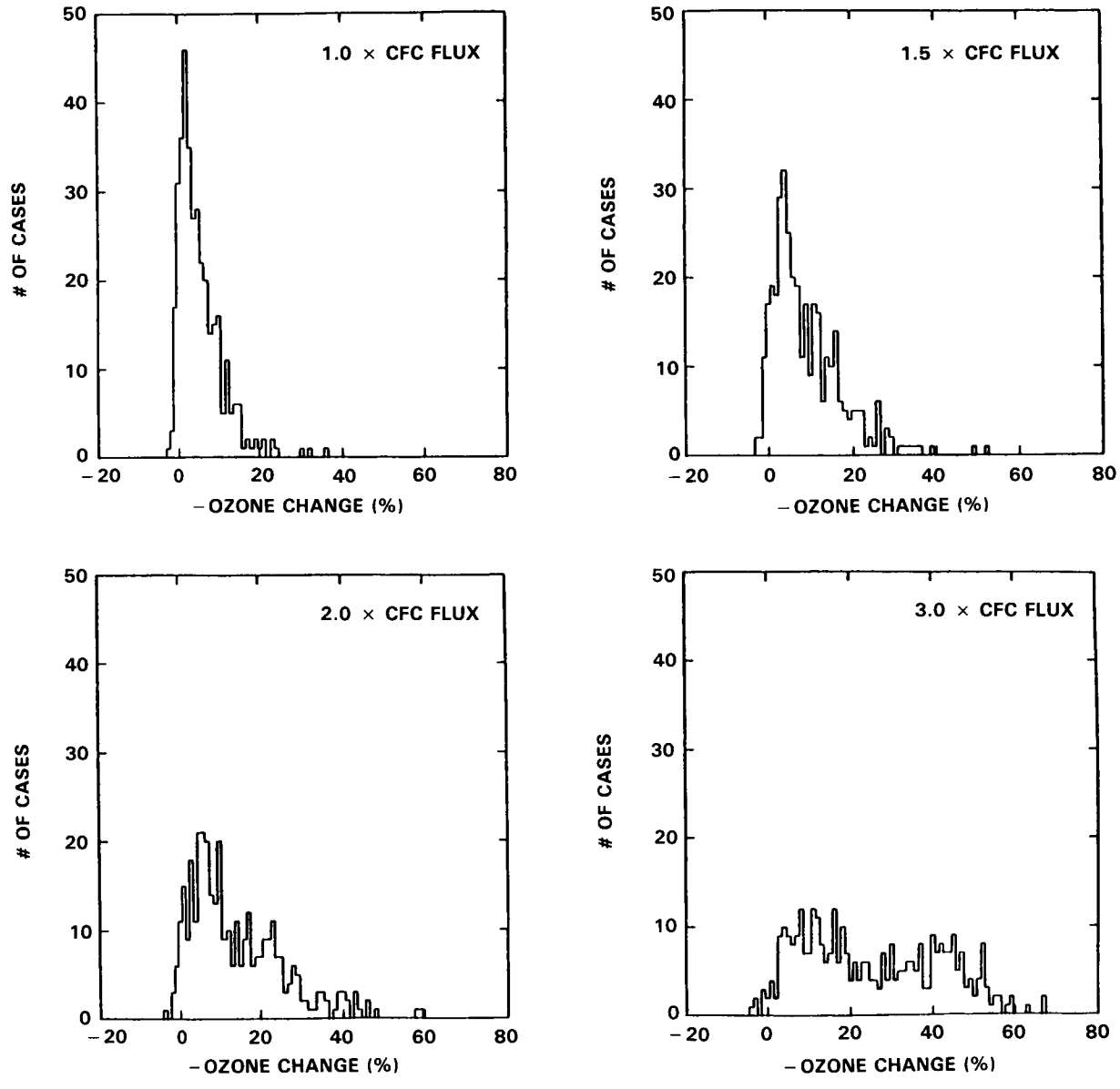

Figure 13-40. Monte Carlo calculated ozone-column-change distribution functions for four different CFC fluxes, at 1.0, 1.5, 2.0, and 3.0 times the 1985 CFC flux (Stolarski and Douglass model).

$$r_i(\text{max}) = \frac{R(\text{max}) - R(\text{rec})}{R(\text{rec})} \Big/ \frac{k(\text{max}) - k(\text{rec})}{k(\text{rec})}$$

$$r_i(\text{min}) = \frac{R(\text{min}) - R(\text{rec})}{R(\text{rec})} \Big/ \frac{k(\text{min}) - k(\text{rec})}{k(\text{rec})}$$

$$r_i(\text{ave}) = [r_i(\text{max}) + r_i(\text{min})]/2$$

where k(rec) is the evaluation panel's recommended rate parameter, k(max) is [k(rec) + one sigma] and k(min) is [k(rec) − one sigma], R(rec) is the calculated ozone change using the recommended rate constant

(−7.8%), R(max) is the ozone change using k(max), and R(min) is the ozone change using k(min). For many reactions, the NASA Evaluation Panel defines a one sigma uncertainty parameter, f, such that k(max) = f k(rec) and k(min) = k(rec)/f. For these cases:

$$\frac{k(max) - k(rec)}{k(rec)} = (f - 1)$$

$$\frac{k(min) - k(rec)}{k(rec)} = (1 - f)/f$$

DeMore *et al.* (1983) define:

$$f(T) = f(298) \exp \{(\Delta E/R)[1/T - 1/298]\}$$

where f(298) is the one-sigma correction for the room temperature rate constant and $\Delta E/R$ is the uncertainty in the temperature dependent part of a bimolecular rate parameter as supplied by the evaluators. The values of f are, therefore, often temperature dependent but were evaluated only at 230 K for this assessment.

A single standard deviation error contribution factor, u_i, was calculated from

$$u_i = r_i(ave) \ln(f_i)$$

for each reaction. Nine reactions identified as important in Cl_x perturbation studies were selected for assessment. The reactions along with their calculated r_i, f_i, and u_i factors are displayed in Table 13-15. The sign of the sensitivity factor and the error contribution factor indicates whether increasing the reaction rate parameter causes a larger (+) or smaller (−) decrease in column ozone for the S3B scenario.

The square root of the sum of the squares of the error contribution factors, u_i, for the nine reactions is written as $<u>$; and the one standard deviation cumulative uncertainty is calculated as:

$$U = \exp <u>$$

and it has the value of 1.84. Thus, at the one sigma (68%) confidence level, the variation in the calculated −7.8% ozone change for the S3B scenario due to evaluated uncertainties in these nine reactions are within the range −7.8%/1.84 to −7.8%×1.84, which is −4.2% to −14.4%.

The NRC 1979 study presented a similar analysis based on a 1978 constant CFC emission scenario for 20 reactions, including several shown in Table 13-15. In general, the r_i values reported there are similar to or smaller in magnitude than the cases in this table, while the evaluated f_i factors for overlapping reactions are nearly the same. However, all the f_i values in the 1979 analysis ignored the uncertainty in the temperature dependence of the assessed rate coefficients, so that the stated f_i values and the resulting calculated uncertainties were underestimated. As a result, the overall two-sigma uncertainty factor for the NRC (1979) twenty-reaction case was 1.72, slightly smaller than the one-sigma uncertainty value found for the nine-reaction case presented here.

This result should be discussed in context with the Monte Carlo calculation that uses atmospheric observations to screen the distribution of cases. It appears that within the range of uncertainty of the photochemical parameters, the models would predict unrealistic values for the concentrations or profiles of some measured species in the contemporary atmosphere. At present there is no systematic way to use

atmospheric observations to screen this method of sensitivity to uncertainty in individual rate parameters, unlike the situation with the Monte Carlo method. Unless an appropriate screening method can be developed for this method, future research on uncertainty analysis should probably be concentrated on the Monte Carlo method.

13.2.3.3 Uncertainties Due to Chemistry Omitted From the Models

As discussed in Chapter 2, several classes of reactions have been proposed which have the potential to significantly affect the impact of Cl_x and NO_x on stratospheric chemistry. However, current deficiencies

Table 13-15. Single Rate Constant Variation Studies.

No.	Reaction	Sensitivity Factors r_i(max)	r_i(min)	r_i(ave)	Experimental Uncertainty Factor f_i	Error Contribution Factor u_i
1.	$ClO + O = Cl + O_2$	+0.60	+0.68	+0.64	1.43	+0.23
2.	$Cl + CH_4 = HCl + CH_3$	−0.48	−0.46	−0.47	1.16	−0.07
3.	$OH + HCl = Cl + H_2O$	+0.56	+0.79	+0.68	1.32	+0.19
4.	$OH + HNO_3 = H_2O + NO_3$	−0.51	−0.56	−0.53	1.30	−0.14
5.	$OH + HNO_4 = H_2O + O_2 + NO_2$	−0.16	−0.33	−0.25	2.20(a)	−0.20
6.	$O(^1D) + M = O(^3P) + M$	+0.60	+0.63	+0.62	1.32	+0.17
7.	$O(^1D) + N_2O = 2\ NO$ $= N_2 + O_2$	−0.51	−2.00	−1.26	1.30(b)	−0.33
8.	$ClO + NO_2 + M = ClONO_2 + M$	−0.31	−0.37	−0.34	1.56(c)	−0.15
9.	$O_2 + h\upsilon$ (S-R) = 2.0	−0.58	−0.85	−0.72	1.40(d)	−0.24

(a) Since the quoted uncertainty in the activation energy for this reaction is unsymmetrical ($\Delta E/R$ = +270 and −500) the r_i was calculated for a k(max) of 1.96k(rec) and a k(min) of k(rec)/2.46; the f_i value used in the calculation of u_i is the square root of 1.96×2.46.

(b) The stated uncertainty of 1.30 is taken to be uncertainty in the branching ratio to 2 NO, not in the overall rate, which was held unchanged.

(c) The one-sigma variation on the rate was calculated for $M = 3.69 \times 10^{17}$ cm^{-3} and T = 230K, taken to be characteristic of 30 km altitude conditions. The uncertainty in both k_0 and k_∞ was accounted for according to the intermediate regime equation recommended by DeMore et al., 1983. This analysis yielded a k(max) = 1.54k(rec) and a k(min) = k(rec)/1.59, and the f_i value of 1.56 is the square root of 1.54×1.59.

(d) The factor of 1.40 was applied to the effective photoabsorption cross section and thus affects both the atmospheric transmissivity as well as the oxygen photodissociation rate.

in either detailed laboratory verification of the proposed kinetic mechanisms and rate parameters or *in situ* measurements to establish sufficient levels of proposed stratospheric species prevent a solid case for their inclusion at this time. Of course, these same deficiencies also currently prevent a quantitative assessment of the uncertainty these unrepresented reaction classes pose.

Two reaction classes of potential, but as yet unproven, importance bear special notice. These are upper stratospheric reactions of meteor deposited sodium compounds and lower stratospheric heterogeneous reactions of reservoir species.

Sodium Chemistry

Stratospheric sodium chemistry poses a striking picture with basic sodium compounds formed in the mesosphere from meteor ablated atomic sodium meeting acid compounds formed from Cl_x, NO_x, and CO_2 in the lower stratosphere to form salt and water in the upper stratosphere (Murad *et al.*, 1981). Model results predict that downward diffusing molecular sodium will be found in the form of NaOH, NaO_2, and/or NaO (Liu and Reid, 1979; Sze *et al.*, 1982). Each of these gas phase compounds react at a gas kinetic rate with HCl and probably quite rapidly with other acid gases such as HNO_3 (Silver *et al.*, 1984a; Silver and Kolb, 1985). If NaCl is formed by reaction with HCl during the day, it is quickly destroyed by photodissociation releasing atomic Cl (Rowland and Rogers, 1982).

The rate of condensation of the mesospheric and upper stratospheric gaseous sodium compounds is unknown, and therefore their concentration is difficult to model; furthermore, no attempt has yet been made to measure them. However, if as little as one percent of the downward diffusing sodium reaches the 40 km level in molecular form, a significant amount of atomic chlorine could be liberated from HCl through catalytic reactions such as (Silver and Kolb, 1985):

$$NaO_2 + HCl = NaCl + HO_2$$

$$NaCl + h\nu = Na + Cl$$

$$Na + O_2 + M = NaO_2 + M$$

$$\text{Net:} \quad HCl + O_2 + h\nu = HO_2 + Cl$$

Heterogeneous Reactions of Reservoir Species

The mid and lower stratosphere contain a persistent but highly variable layer of sulfuric acid aerosols. These aerosols are generally assumed to be composed primarily of supercooled liquid sulfuric acid and water in an approximately 75% H_2SO_4/25% H_2O weight ratio but they also contain significant impurities such as Cl-, Br-, and NH_4+ (Cadle and Grams, 1975).

Model calculations have indicated that reactions which form or liberate NO_x and Cl_x from their reservoir species: HNO_3, HO_2NO_2, $ClONO_2$, HCl, and HOCl can play a key role in Cl_x and NO_x stratospheric processes. A number of such reactions including:

$$ClONO_2 + HCl = HNO_3 + Cl_2$$

$$N_2O_5 + H_2O = 2\ HNO_3$$

$$HO_2NO_2 + H_2O = HNO_3 + H_2O_2$$

$$ClO + H_2O = HCl + HO_2$$

have been demonstrated to be very slow in the gas phase but quite rapid on the surfaces of laboratory apparatuses. As discussed in Chapter 2, it is quite conceivable that such reactions may proceed at a significant rate as heterogeneous processes on stratospheric sulfuric acid aerosols. Definitive heterogeneous kinetic experiments are clearly needed to allow further assessment of their heterogeneous reservoir reactions.

13.2.4 Uncertainty of Model Predictions to Choice of Boundary Conditions

For some species, especially nitrous oxide and methane, there is uncertainty as to whether to use constant concentration or constant flux boundary conditions in model calculations. To illustrate this point, the AER one-dimensional model was used to calculate the steady-state ozone reduction as a function of stratospheric Cl_x as the only perturbation; but one calculation was made assuming constant surface concentration of nitrous oxide as boundary condition and the other assuming constant surface flux (Figure 13-42). For small amounts of added Cl_x, the two different boundary conditions give essentially the same calculated ozone reductions, but for large Cl_x perturbations there is a substantial difference in the two calculated ozone reductions.

The reason for this difference can be illustrated by a simple mechanism, using A to represent nitrous oxide as the example:

Gross release from the surface, rate = P
Gross removal by the surface, rate = k[A]
Stratospheric destruction = flux rate F = f[A]

where f is a complicated function depending on the structure of the atmosphere between the surface and the upper stratosphere and the chemical and radiation field in the stratosphere. At steady state

$P = k[A] + f[A]$, $[A] = P/(k + f)$, and $F = P - k[A]$.

There are two limiting cases

(i) $f << k$, then $[A] = P/k$, an equilibrium constant, and the constant-concentration boundary condition is appropriate. If the stratospheric destruction coefficient f changes, the flux F changes , but the surface concentration remains constant.

(ii) $f >> k$, then $[A] = P/f$ is inversely proportional to f, $F = P$ = constant gross surface production rate, so that the constant flux boundary condition is appropriate. If the stratospheric destruction coefficient changes, the surface concentration changes but the flux remains constant.

For both nitrous oxide and methane, the production and destruction at the earth's surface (soils and waters) are complex, incompletely solved biological, geological, chemical problems. In the absence of good knowledge of the rates of surface sources and sinks, it is not obvious which type boundary conditions is better, some modelers use one and some use the other, and for large chlorine perturbations it makes a difference (for example, Figure 13-41).

13.2.5 Sensitivity to Trends of Trace Gas Species

Model calculations of the ozone distributions in future perturbed atmospheres are strongly dependent on the assumed rate of growth of trace gas species (for example, Figure 13-17; all cases in Sections 13.1 and 13.2 with mixed scenarios). Source strengths for several species (e.g. CFCs) are determined by technology and world-wide industrial growth. Emissions for others (e.g. N_2O, CH_4, CO_2, CO, NO_x) are a mixture of industrial, agricultural, and natural processes (see Chapter 3). The resulting atmospheric concentrations depend on the rate of photochemical destruction within the atmosphere, on dynamical redistribution of the tracer (stratospheric-tropospheric exchange), and on surface losses. Major perturbations to stratospheric ozone are calculated to have a direct impact on the lifetimes of N_2O, CFC-11, CFC-12, and CCl_4 (see, for example Table 13-9). These effects are based on the redistribution of stratospheric ozone and the ultraviolet radiation field, and they can be predicted with some confidence by 2-D, and probably even, 1-D models. The sources of some of these trace species involve the biosphere, soils, and the oceans; and thus the uncertainties of the biosphere, soils, and the oceans are part of the uncertainty of atmospheric models.

13.2.6 Ozone Changes Calculated to Occur in the Troposphere

Some models show calculated ozone changes in the troposphere, for example, Figures 13-1, 2, 3, 18, 19, 20. These portions of the calculated ozone-column change must be regarded as being especially uncertain. Present models are primarily designed for stratospheric simulations. Large uncertainties exist in connection with lack of knowledge of tropospheric NO_x distributions, heterogeneous processes, and non-methane hydrocarbons. Chapter 4 discusses tropospheric processes.

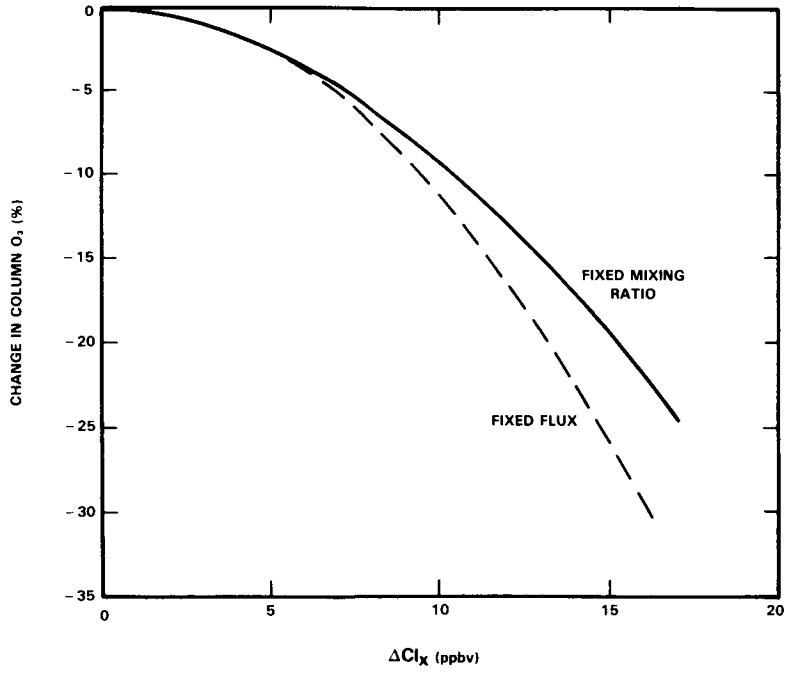

Figure 13-41. Comparison of use of fixed flux boundary condition and fixed surface concentration boundary condition for nitrous oxide in CFC perturbation calculations. Calculated ozone-column changes as a function of stratospheric Cl_x level with AER 1-D model.

13.2.7 Some Dynamical Uncertainties in Assessment Calculations

Ozone is jointly controlled by dynamics and photochemistry throughout the stratosphere. At high altitudes during daylight hours, photochemistry is fast, but the distribution of photochemically active trace species depend on longer-lived source molecules which are strongly influenced by atmospheric dynamics. At low altitudes in the stratosphere, dynamics moves and mixes ozone faster than it is formed from oxygen photolysis (Figure 13-25), but slow photochemical reactions operating over long ozone residence times significantly increase or decrease local ozone concentrations. This subsection discusses some recognized uncertainties and some recent insights in model treatment of atmospheric motions. (Fuller, more general discussions of these problems are given in Chapter 12).

In one-dimensional models, all transport is represented as vertical in direction and diffusive in nature, since transport is accomplished by an eddy diffusion coefficient function. In typical one-dimensional model studies, Northern Hemisphere mid-latitude tracer data have been used to parametrize empirically the eddy diffusion function to obtain agreement with observations of these species. Recently, a new suggestion has been put forward concerning eddy diffusion functions (Holton, 1985; Mahlman, 1985): a different eddy diffusion coefficient should be used for each species, depending on transport time scales (obtained from considerations of higher dimensional models) and the variation of its lifetime with height and latitude. This procedure is likely to affect perturbation calculations, since increasing chlorofluorocarbon abundances yield changes in photochemical lifetimes, and therefore associated changes in the lifetime-dependent eddy diffusion coefficients used in one-dimensional models. A detailed study of the possible importance of this procedure in one-dimensional perturbation calculations has not yet been performed.

To evaluate seasonal and latitudinal variations in the local ozone response, at least a two-dimensional (height-latitude) representation is required. In recent years a new insight has developed concerning the importance of using two-dimensional models for CFC perturbation calculations: if advection is sufficiently rapid, much larger ozone reductions are calculated at certain seasons for polar and temperate zones than the global average or for corresponding one-dimensional models (Pyle, 1980; Haigh and Pyle, 1982; Haigh, 1984; Garcia and Solomon, 1983; Solomon *et al.* 1985b). The discussion of this effect in terms of Garcia and Solomon's model is as follows. All current one- and two dimensional models calculate large ozone reductions by GFCs in the upper stratosphere near 40 km (Sections 13.1.2 and 13.1.3). The tropical lower stratosphere is characterized primarily by upward motion in the seasonal mean sense, so that the large ozone depletions occurring at 40 km are not transported downward to lower altitudes at those latitudes. At high latitudes, particularly in winter, the direction of net transport is downward in the zonal, seasonal average. The chemical lifetime of ozone in the middle and lower stratosphere at high latitudes is long in the winter because of the solar zenith angle and small fraction of sunlit hours in a day. Transport into the middle and high latitude lower stratosphere is dominated by vertical advection, bringing down strongly depleted ozone from the 35 to 40 km heights into lower altitudes. Large ozone depletions occur at high latitudes throughout the stratosphere relative to that found in the tropics. However, the ozone abundance at high latitudes in winter is influenced not only by vertical advection but also by horizontal mixing associated with breaking planetary waves (McIntyre and Palamer, 1983; Leovy *et al.*, 1985). An important topic for future research is to study the competition between these two diffferent transport processes.

Different two-dimensional models, as discussed extensively in Chapter 12, use different treatments for advective transport and horizontal mixing. In this study there are representatives for each of two different approaches, one represented by the diabatic and residual Eulerian models of AER and GS, and the other by the classical Eulerian model of MPIC. The two types of model differ substantially in their prediction of NO_y in the lower stratosphere. Figure 13-31, but even so they give comparable predictions of global

ozone reduction. Tables 13-10 and 13-11. Both types of model show greater ozone-column reductions in polar regions than in tropical regions; but in general, the AER and GS models give a greater range to seasonal and latitudinal ozone changes than the MPIC model, as illustrated by Figure 13-24. These differences are important in terms of considerations of ozone depletions by CFCs, and the nature of two-dimensional atmosphere dynamics should be vigorously pursued.

Most of the ozone at middle and high latitudes lies below 20 km where it is likely to be subject to mixing and dispersion associated with stratosphere-troposphere exchange processes (Allam and Tuck, 1984b; Chapter 5). These processes are crudely parametrized in two-dimensional models. A great deal of further research into the transport processes occurring in the lowest part of the stratosphere and upper troposphere is needed to improve estimates of ozone column changes.

Comparison between the ozone changes calculated by the two-dimensional classical and residual Eulerian models and consideration of the important effects of changes occurring in the region below 20 km is determining the behavior of the ozone column at extra-tropical latitudes suggest that dynamical uncertainties associated with current two-dimensional models correspond to a factor of at least two in the uncertainty in the evaluation of the ozone column change.

13.2.8 A Recently Published Article

Farman *et al.* (1985) published an article entitled "Large losses of total ozone in Antarctica reveal seasonal ClO_x/NO_x interactions" in which they report seasonally variable 5 to 30% reduction of the south polar ozone column during 1980-84 relative to 1957-73. Current two-dimensional models (Figures 13-29 and 13-30) give 15 to 25% reduction of local ozone at 40 km at the poles, and the MPIC model shows between 2 and 3% reduction of the ozone column there. The results reported in the article give much larger ozone reductions in Antarctica than those given by the models. The article has not yet been assimilated by the modeling community, and it is premature for this report to do more than to note it with great interest and to recommend that it be given close attention in the near future.

13.2.9 Discussion of Total Uncertainty

When one looks at (i) the wide spread of model calculations of the ozone column change for the same assumed perturbations over the last ten years (Figure 13-37), (ii) the range of ozone column changes calculated by different one-dimensional models in 1985 for the same scenario (Table 13-2), and (iii) the large uncertainty implied by a study of the variation of individual rate coefficients over their assessed uncertainty range (Section 13.2.3.2; NRC, 1979), one gets the impression that the total uncertainty is very large and that the solution to this problem is still far away. This impression is probably correct, but a recent development indicates that the effect of the assessed uncertainty on photochemical coefficients is not as large as (iii) indicates. The Monte Carlo treatment of one-dimensional models, when it covers the range of assessed uncertainty in photochemical parameters and is screened by atmospheric observations of many species and at several altitudes (Stolarski and Douglass, 1985; Section 13.2.3.1), promises to be a powerful method of calculating the effect of chlorofluorocarbons on the ozone column for any given scenario for future changes of chlorofluorocarbons and other gases. After this method is carefully developed, it may be hoped that the uncertainty in calculating ozone changes due to the assessed uncertainty of rate coefficients will be no more than a factor of two.

Two-dimensional models supply information about seasonal and latitudinal ozone changes. This study used two-dimensional models representative of two substantially different treatments of atmospheric dy-

namics. For a given perturbation scenario, these two models gave satisfactory agreement concerning global-average ozone reduction (Table 13-8), but they give different latitude trends (Figure 13-24). Both models indicate that there is greater ozone reduction at temperate and polar latitudes than at tropical latitudes, but one model gives almost a factor of two greater ozone reduction at temperate zones during certain seasons than the other. It is estimated here (Section 13.2.7) that uncertainty in how to formulate atmospheric dynamics in the models contributes about a factor of two to the uncertainty of model predictions. This uncertainty factor is based on the judgment of experts in the field, and it is not a statistically derived number.

In terms of (i) the assessed uncertainties in photochemical parameters as reduced by constraints introduced by atmospheric observations and (ii) the recognized uncertainties in atmospheric dynamics, there may be as little as a factor of four uncertainty in model predictions of ozone changes, given a prescribed scenario for future changes of CFCs and other trace gases (CH_4, N_2O, CO_2, stratospheric NO_x, tropospheric NO_x). In view of this range of recognized uncertainty, one should not be unduly surprized if a -7% ozone change calculated in 1985 should be found to be -4% or -12% when calculated in 1988, for example.

The uncertainties due to unknown factors, such as unrecognized chemical species or unknown photochemical reaction rates, cannot be quantified.

Even if numerically accurate models were complete in photochemistry and satisfactorily approximated those aspects of atmospheric motions and other physical processes that strongly affect ozone, the models still could not predict future ozone changes due to increasing chlorofluorocarbons unless they were supplied with the future trends of other trace species. As the models continue to improve and as the body of field measurements continue to expand, the inability to predict future trends of the trace species may become the major source of uncertainty.

13.3 SUMMARY AND CONCLUSIONS

The calculations presented in this chapter were carried out by means of three two-dimensional and six one-dimensional models using prescribed scenarios for natural and anthropogenic perturbations (Tables 13-1, 7), prescribed values of insolation (Chapter 6), and a prescribed up-to-date set of chemical and photochemical parameters (Appendix A). Differences among results therefore reflect differences in the assumptions and methods of the models themselves (boundary values, eddy diffusion functions, diurnal averaging, numerical methods). The results are presented in terms of scenarios, which were selected to demonstrate the role of certain individual species and to illustrate possible future situations. The principal results of these model calculations of ozone changes are:

(i). The long-term release of chlorofluorocarbons at the 1980 rate would reduce the ozone vertical column by about 5% to 8% according to one-dimensional models (Scenario S1A of Table 13-2, relative to 1.3 ppbv Cl_x as background) and by a global average of about 9% according to two-dimensional models (Table 13-8), which involves a reduction of about 4% in the tropics, about 9% in temperate zones, and about 14% in polar regions (Figures 13-24, 33, 34). A major finding of recent years, which is emphasized in this report, is that two-dimensional models predict large seasonal and latitudinal variations in chlorine-induced ozone-column reductions, so that there are larger ozone reductions at some seasons in temperate and polar zones than that for the global average or that for one-dimensional models.

(ii). All models with all scenarios predict that this level of stratospheric chlorine (steady state produced by 1980 CFC flux) will reduce local ozone at 40 kilometers by a large amount, 60 to 80 % (Table 13-3; Figures 13-18 - 21).

(iii). At about 80% of the present level of CFC release, coupled with doubling methane and increasing nitrous oxide by the factor of 1.2, one-dimensional models give ozone decreases of about 3% (Table 13-2, Scenario S2B), and a two-dimensional model gives an ozone decrease of about 4% (Table 13-8). If doubled carbon dioxide is added to the list of changes by other trace species, one-dimensional models predict ozone-column changes between +0.1 and −3.5% (Scenario S2C of Table 13-2). One-dimensional models predict that the magnitude and even the sign of the ozone-column changes due to increasing CFCs depend on the future trends of carbon dioxide, methane, and nitrous oxide.

(iv). If the release rate of CFCs should become twice the present level or if stratospheric Cl_x reaches 15 ppbv, the one-dimensional models predict that there will be 3% to 12% reduction of the ozone column, regardless of realistically expected increases in carbon dioxide, nitrous oxide, and methane (Table 13-2, Scenario S3C).

(v). The two-dimensional models calculate that between 1960 and 1985 there were large (about 20%) local percentage ozone reductions at 40 km in the polar stratosphere (Figures 13-29, 30). These calculations did not include the effects of increasing methane and carbon dioxide, which would tend to decrease the calculated ozone reduction.

(vi). For atmospheric perturbations considered one at a time, the one-dimensional models calculate the ozone steady-state vertical column to be increased by carbon monoxide, carbon dioxide, and methane; and they calculate it to be decreased by chlorofluorocarbons, nitrous oxide, and stratospheric aircraft (Table 13-4, Figures 13-7 to 12). These individual perturbations do not have an additive effect on ozone.

(vii). For *some* scenarios one-dimensional models predict an ozone reduction in the upper stratosphere and an ozone increase in the lower stratosphere or troposphere, to give an ozone column increase. Two-dimensional model results (Figures 13-18, 19, 20, 21) suggest that these particular one-dimensional results be interpreted as an ozone-column increase in tropical regions and an ozone-column decrease at temperate and polar regions; and even if there is a global average ozone increase, there might be significant ozone column decreases in the temperate zone.

(viii). Time-dependent scenarios were considered using one-dimensional models with CFC growth rates assumed to be 0%, 1.5%, and 3% per year. For a coupled scenario with increasing methane, carbon dioxide and nitrous oxide, the ozone column effects are relatively small for CFC increases at 0% and 1.5% (Figure 13-17, Scenarios T1B and T2B). At 3% CFC growth and the coupled scenario (Figure 13-17, Scenario T3B) the calculated ozone column decrease is 10% after 70 years and still rapidly decreasing.

(ix). Over the range 1 to 15 ppbv of stratospheric chlorine, one-dimensional models are strongly non-linear in terms of ozone-column change as a function of added Cl_x (Figures 13-6, 41; Tables 13-10, 11), but the two-dimensional models are nearly linear (Tables 13-10, 11) over this range of added Cl_x. If Cl_x increases up to 21 ppbv are considered (see note at end of Section 13.1.4), a two-dimensional model shows the same pattern of nonlinearity as the one-dimensional models. The onset of the nonlinearity occurs close to the region where the Cl_x mixing ratio exceeds the background NO_y mixing ratio.

(x). The changes in model predictions during the last four years have been less than the record of the previous six years (Figure 13-37). Even so, there remain substantial recognized uncertainties in the field of stratospheric photochemical model predictions. Two investigators carried out Monte Carlo calculations over the full range of the assessed uncertainties (Appendix A) of photochemical parameters. In

one calculation, the ozone-column changes were calculated for an increase of 14 ppbv Cl_x, a doubling of methane, and a 20% increase of nitrous oxide. Within plus or minus one standard deviation of the unsymmetrical distribution of calculated ozone-column changes, the range was -1.9% to -13.5%, where the standard result was -7.7% (Table 13-14). The second Monte Carlo calculation considered only CFC perturbations, and varied the 1980 CFC flux by factors between 1 and 3.5 (Figure 13-40). Use of the recommended photochemical parameters with the current (1985) CFC release rate gave the calculated steady-state ozone-column change of -4.8%, and the Monte Carlo calculation over the full range of the assessed uncertainties of the photochemical parameters gave the average ozone-column changes of -5.7% and the (one standard deviation) range of -0.3% to -11.1%. A recent development by Stolarski and Douglass (1985) is that considering the atmospheric observations of many species and at several altitudes excludes many of the Monte Carlo cases. When this screening is carried out, the central value of calculated ozone change is the value most nearly consistent with atmospheric observations and the standard deviation of the calculated ozone changes is substantially reduced.

(xi). The past and future changes of the trace species, methane, nitrous oxide, and carbon dioxide, involve the biosphere and its great complexity. As stratospheric modeling matures during the next few years, the biggest uncertainty in making future predictions will probably be the uncertainty in formulating the scenarios for future changes in methane, nitrous oxide, and carbon dioxide.

13.3.1 Future Research

Regarding future research in model predictions, it is particularly important to encourage the development of two-dimensional models. Two-dimensional models have progressed to the point where they include sophisticated photochemistry, and further development requires continued deep study of atmospheric transport and dynamics. Two-dimensional models importantly give large latitudinal gradients in calculated ozone-column reductions, such that much larger ozone-column reductions are indicated in temperate and polar regions than the global average or the result of one-dimensional models.

One-dimensional models still play a vital role in rapidly surveying a wide range of scenarios, and in providing first approximations to many problems and to new ideas. The new Monte Carlo method that screens the results against atmospheric observations should be given top priority; it probably should become the standard tool for one-dimensional ozone-change assessment studies. As this method is developed and refined, it should be extended to two-dimensional models.

The value of both one-dimensional and two-dimensional models depends on the quality of the input photochemical and atmospheric data. Sensitivity studies carried out here show that model predictions are still strongly changed within the recognized uncertainty limits of the photochemical data and field measurements. To reduce this element of uncertainty, there should be continued support for research in photochemistry and in atmospheric measurement of trace species.

CHAPTER 14

OZONE AND TEMPERATURE TRENDS

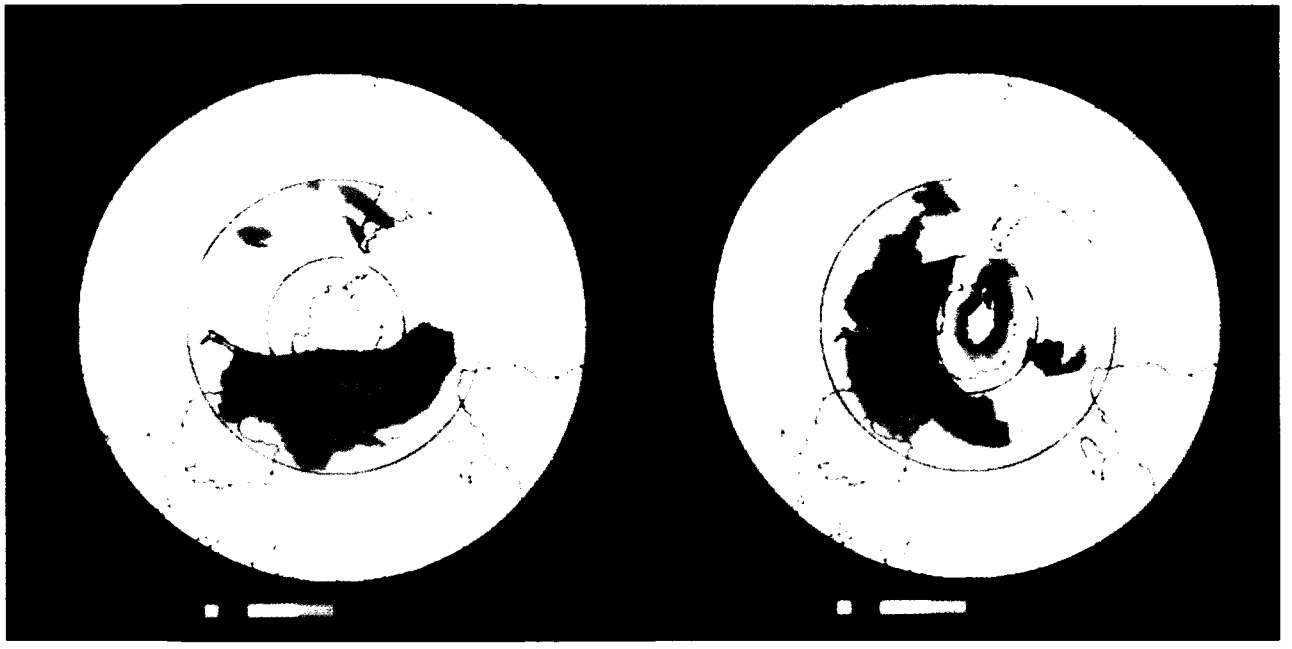

Panel Members

K. Labitzke and A.J. Miller, Co-Chairs

J. Angell
J. DeLuisi
J. Frederick
J. Logan
C. Mateer
B. Naujokat
G. Reinsel
G. Tiao

CHAPTER 14

OZONE AND TEMPERATURE TRENDS

TABLE OF CONTENTS

14.0 INTRODUCTION

Within this chapter we discuss the measurements of temporal changes in ozone and temperature. Our responsibility is to examine the data within the context of natural atmospheric variability and data problems and compare the results to numerical model calculations. In addition, we define the major issues of what is required to achieve the goals.

We note that ozone and temperature are considered within the one chapter in that they are very closely coupled via radiative, dynamic and photochemical processes, e.g. Chapter 8. Changes in one result in changes in the other such that a complete examination of trends must verify both parameters in a consistent system against a unified fully coupled predictive model. As we will see, below, the history of this subject is such that sophisticated statistical trend analyses have been accomplished first on the ozone data such that we can present quantitative results. Similar analyses for temperature, however, are only just beginning so that the results are more qualitative although prevocative.

For each parameter the initial consideration is by instrument type as each system has its unique elements that must be considered in long-term trend evaluation. Within each instrument discussion further breakdown is accomplished by altitude.

14.1 OZONE TRENDS

14.1.1 Total Ozone

Over the past several years there have been several studies conducted in an attempt to detect any evidence of a total ozone trend (e.g. Hill *et al.*, 1977; Reinsel, *et al.*, 1981; St. John *et al.*, 1982, Angell and Korshover, 1983b; Bloomfield *et al.*, 1983). Most recent statistical analyses have adopted a time domain approach to estimating a global trend. The ozone value $X_{t,j}$ at time t and observing station j is represented by $X_{t,j} = \omega_j h_t + \&_{t,j}$ where h_t represents a predicted global trend, e.g. one caused by CFC's; ω_j is a multiplier that indicates the magnitude of the observed trend at station j; and $\&_{t,j}$ represents an error process to account for other influences on ozone. The $\&_{t,j}$ series is typically assumed to be an autoregressive process (e.g., Hill *et al.*, 1977; Reinsel *et al.*, 1981; St. John *et al.*, 1982). This model is fit separately to the ozone record from each station, and a global trend estimate is obtained by combining the station values ω_j. Bloomfield *et al.*, (1983), on the other hand, introduce a frequency domain statistical model. This model extends variance-components analysis to the time series case and incorporates both temporal and spatial association found in the ozone data. A key feature of this model is the inclusion of a common global term representing natural global variations in ozone.

Reinsel *et al.* (1981) found an increase of 0.28% in global total ozone over the period 1970-1978 with a standard error of 0.67%, while St. John *et al.* (1982) found an increase of 1.5% with a standard error of 0.5% from '70 - '79 and Bloomfield *et al.* (1983) found an increase of 0.1% for the same period with a standard error of 0.55%. Thus, there is little overall support for the suggestion of a statistically significant trend in total ozone.

Reinsel *et al.* (1985 - personal communication) have recently extended the analysis using data through 1983. Time series models were used to obtain a trend estimate for each station, where level shifts to account for instrument recalibration were also included in the model for five stations (Mt. Louis, Mt. Abu, Lisbon, Buenos Aires, and Hradec Kralove). The overall trend estimate for total ozone change over the entire period 1970-1983, with associated 95% confidence limits, is (-0.003 ± 1.12) % per decade.

Trend analyses were also performed using the f10.7 solar flux series and the sunspot number series separately as explanatory variables for the total ozone series at each station. Results were quite similar in both cases, and the overall total ozone trend estimates for the period 1970-1983 are summarized as follows:

(-0.00 ± 1.12) % per decade with no solar effect in model
(-0.17 ± 1.10) % per decade with f10.7 solar flux in model
(-0.14 ± 1.08) % per decade with sunspot series in model

The f10.7 solar flux series (as well as the sunspot series) was found to be mildly related to total ozone overall, with the estimated effect of f10.7 solar flux on total ozone (averaged over 36 stations) equal to (0.63 ± 0.53)% ozone change per 100 units of f10.7 solar flux. This estimate corresponds to about a one percent change in total ozone from solar cycle minimum to maximum.

These analyses all indicate no significant overall trend in total ozone during the fourteen year period 1970-1983, and suggest a mild relation between total ozone and f10.7 solar flux. The trend estimates are about 0.2% per decade more negative with the inclusion of data for 1983 than comparable estimates based on data through 1982.

A major question of the statistical analyses has been the general lack of global coverage of the ground-based observations suggesting possible spatial biases. For the most recent trend estimates given above by Reinsel *et al.* (1985, personal communication), Figure 14-1 shows a plot of the trend estimates as a function of latitude. Altogether, there does not seem to be any latitudinal effect, but if we examine this diagram by region we see an interesting pattern. For example, all of the North American stations are below the Indian network as are 6 of 7 European stations. While the analysis of Reinsel *et al.* (1981) takes this type of regional networking into consideration, it suggests that more consideration should be given to the representativeness of the data set. This will be discussed further below.

One element that deserves further discussion is the above observation that the total ozone trend through 1983 is more negative than the earlier results. This is related, at least, in part, to the strong ozone minimum seen in the winter period 1982-1983. This effect is shown in Figure 14-2 for the global scale where we present the monthly average total ozone integrated over the domain 60N to 60S for the period May '79 through November '83 as measured from the operational TOVS system (Planet, *et al.*, 1984). We see that in the early part of the record the ozone values were higher than the general average level then seemed to level off until the winter of '82-'83 when the values dropped to their lowest level. This period of "ozone hole" is currently being examined in great detail and appears to be related possibly to two events. The first is the volcanic eruption of El Chichon (Mexico) in April '82 which spewed large amounts of material into the stratosphere (McCormick and Swissler, 1983); the second is the El Nino event of '82-'83 which was accompanied by large-scale circulation changes in the atmosphere. Quiroz, (1983a) through examination of stratospheric temperatures, has shown the difficulty of separating the signals from these events. As the record continues, the ozone values appear to be returning slowly to their previous levels. We might expect, then, that the ozone trend extended through 1984 will be slightly more positive than that for 1983. One additional point is that the above decrease does not appear to be caused by the volcanic cloud in an instrument sense (i.e. Mateer and Asbridge, 1980, Angell *et al.*, 1985).

We might also ask the question as to how often major perturbations such as the 82-83 phenomena occur and what will be their impact on a near real-time trend assessment. In Figure 14-3 we show the average monthly deseasonalized total ozone values for North America and Europe for the periods from the late 50's through 1983 (Reinsel *et al.*, personal communication). Taken in this context the '82-'83

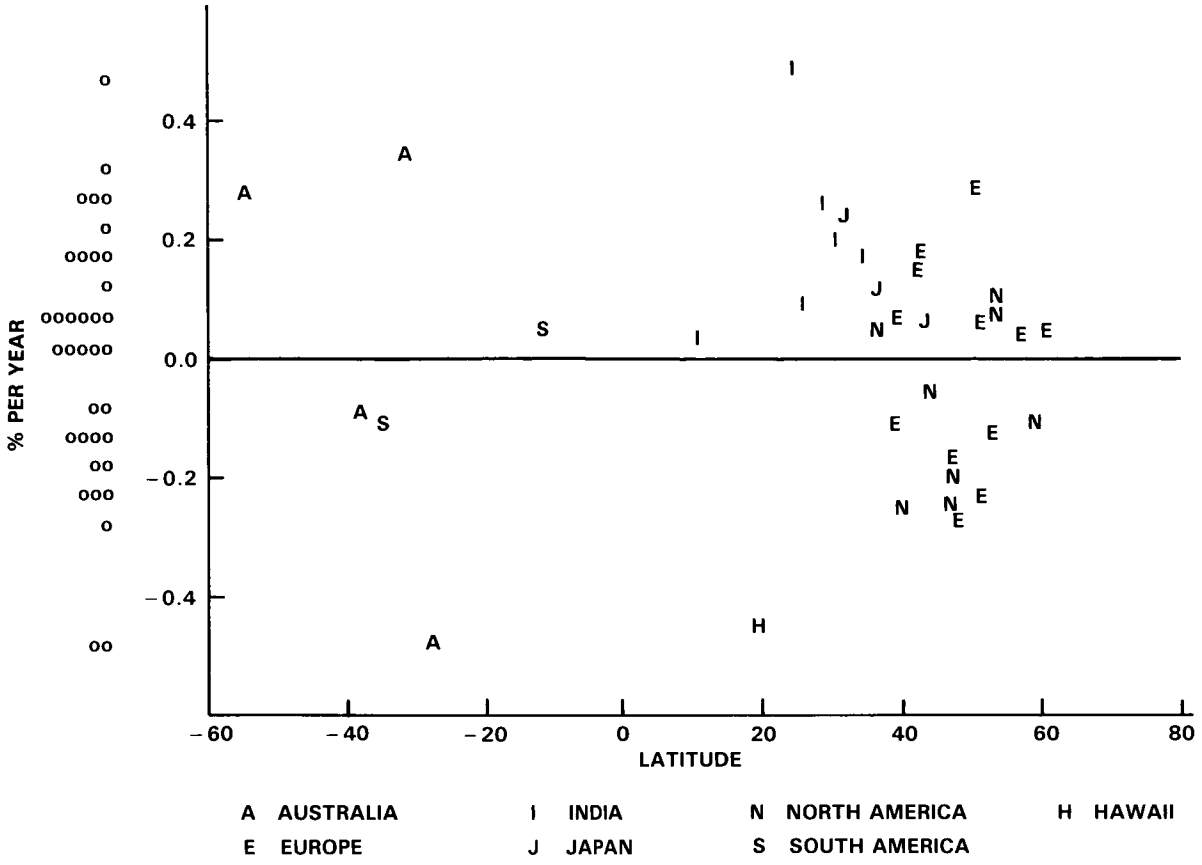

Figure 14-1. Histogram and scatter plot of total ozone trend estimates using data through 1983. (Reinsel *et al.*, personal communication).

winter results do not look all that remarkable and we can see major perturbations at not infrequent intervals. Taking the results of Figures 14-2 and 14-3 together, it appears that real-time assessment of the total ozone variation may be easily influenced by current conditions and that this will require further analysis of the data.

Recently Farman *et al.* (1985) have published the data in Figure 14-4 showing a large secular decrease in total ozone for the month of October over their station at Halley Bay, Antarctica. Since 1957 the total ozone over Halley Bay has decreased during the month of October by about 40%. Other months show significantly less trend. Satellite data from the Nimbus 7 TOMS instrument and the SBUV instrument confirm these findings and show a minimum which is spatially confined to the high south polar latitudes. As is shown in Figure 14-5 (taken from Bhartia *et al.*, 1985) the minimum is surrounded by a large maximum which displays some wave structure. The minimum is distorted into an oblong shape and rotates along with the maximum. Figure 14-5 shows a 5-day sequence in October of 1983 in which the rotation is about 50°. There is a marked tendency for the minimum to be displaced off the pole towards the direction of Halley Bay. For comparison, Figure 14-6 (Bhartia *et al.*, 1985) compares October 3, 1979 to October 3, 1983 showing that 1979 had a similar structure to 1983 except that the deep minimum was missing. These data indicate that some mechanism is at work in the cold southern polar night or polar twilight that is not generally included in models. This clearly warrants further investigation.

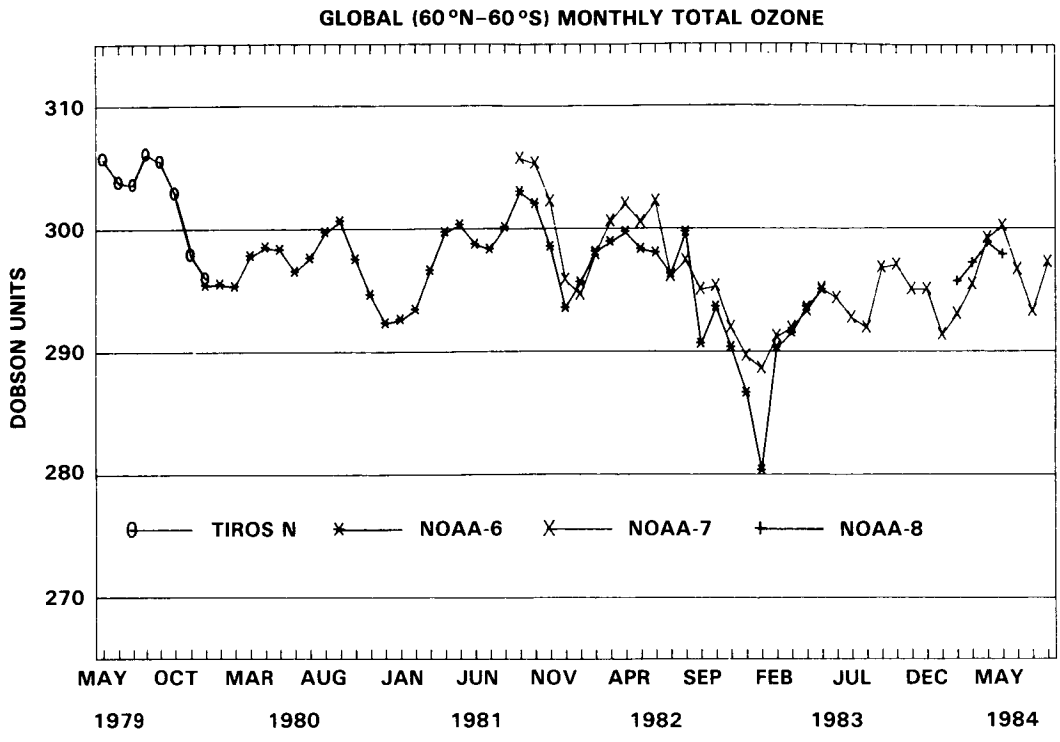

Figure 14-2. Global (60°N-60°S) monthly total ozone determined from NOAA TOVS system. (Planet *et al.*, 1984.)

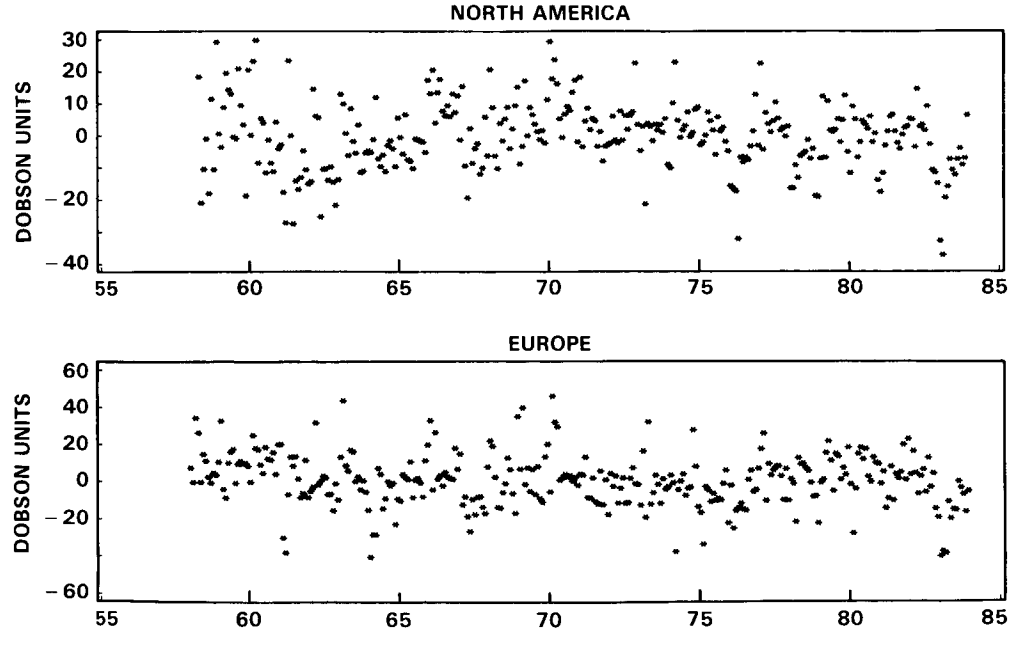

Figure 14-3. Monthly average deseasonalized total ozone; North America (top), Europe (bottom). Units: Dobson units. (Reinsel *et al.*, personal communication).

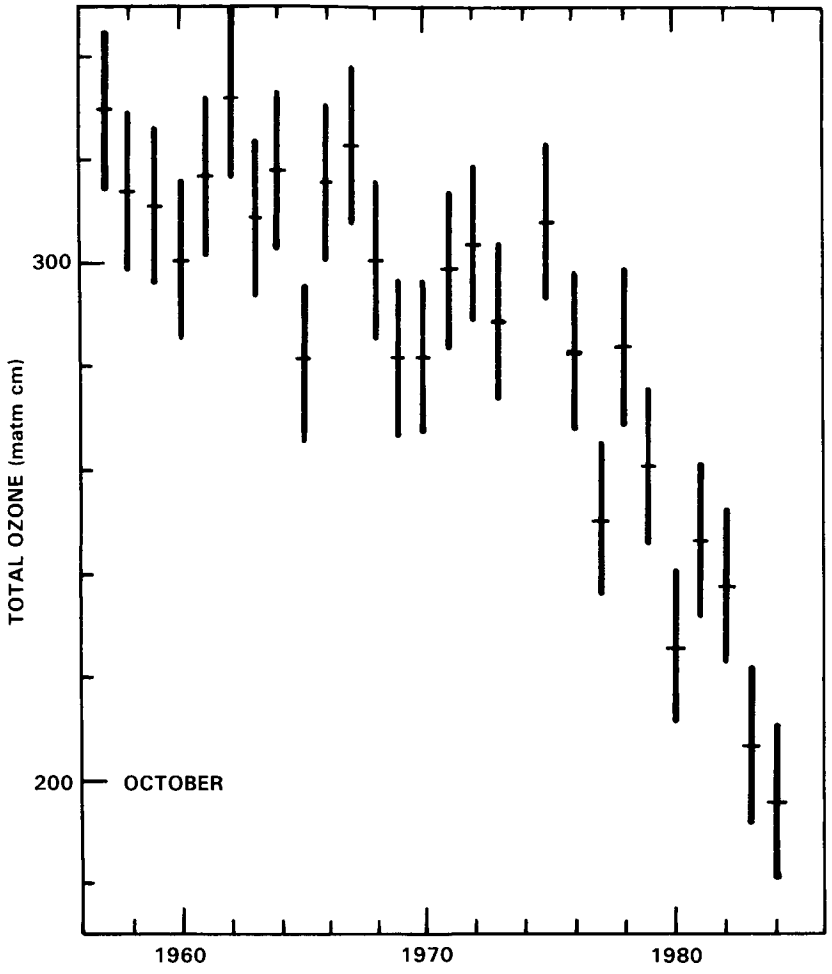

Figure 14-4. Monthly means of total ozone at Halley Bay for October of the years 1957 through 1984. (Farman *et al.*, 1985.)

14.1.2 OZONE PROFILES

14.1.2.1 Ozone Balloonsonde

In a recent update of ozone variations determined from balloonsondes, Angell and Korshover (1983b) determined that in the tropospheric layer of north temperature latitudes, 2-8 km, the data suggest a 12% increase in ozone between 1970 and 1981. This is accompanied by a 1-3% decrease in the region 16-32 km. Since then, several on-going studies have focused on the quality of the ozonesonde data for trend detection (Tiao *et al.*, personal communication; Logan, 1985) and the discussion is presented here with the authors' kind permission. Formal publication is planned for the near future. From Tiao *et al.*, Ozonesonde data from 13 stations have been processed to obtain monthly averages of ozone in 14 fractional Umkehr layers, (1A, 1B, 1C, 1D, 2A, 2B, 3A, 3B, 4A, 4B, 5A, 5B, 6A, 6B), (e.g. Table 14-3) and an additional layer above 6B. For each station, the daily sonde data (in partial pressure) were first integrated into ozone readings (in Dobson units) within each layer, and monthly averages for each layer were then computed from the integrated readings. The data were screened to meet the following criteria:

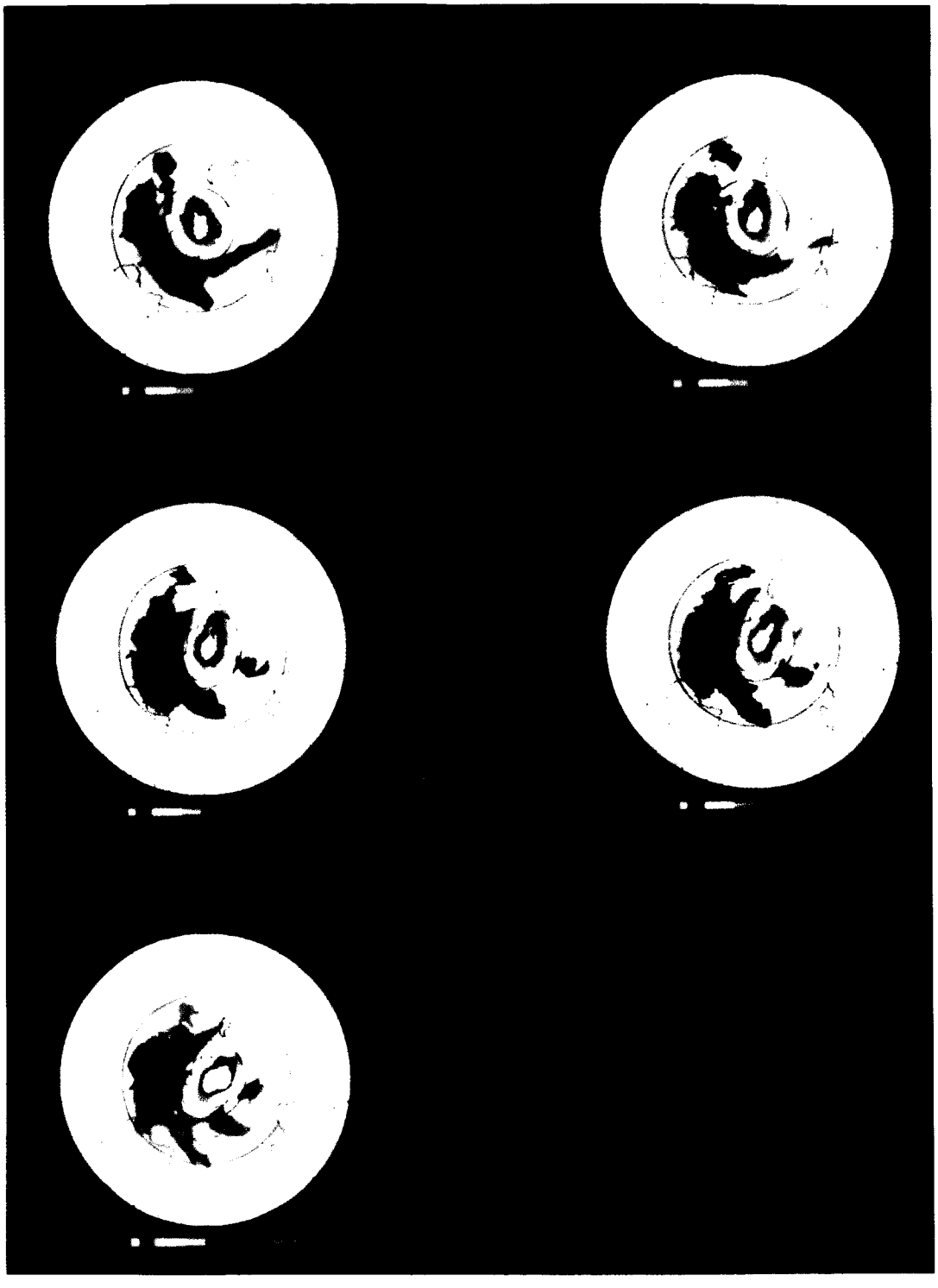

Figure 14-5. Sequence of 5 days (October 1, 1983-October 5, 1983) of total ozone measurements from the Nimbus 7 TOMS instrument. (Bhartia *et al.,* 1985.)

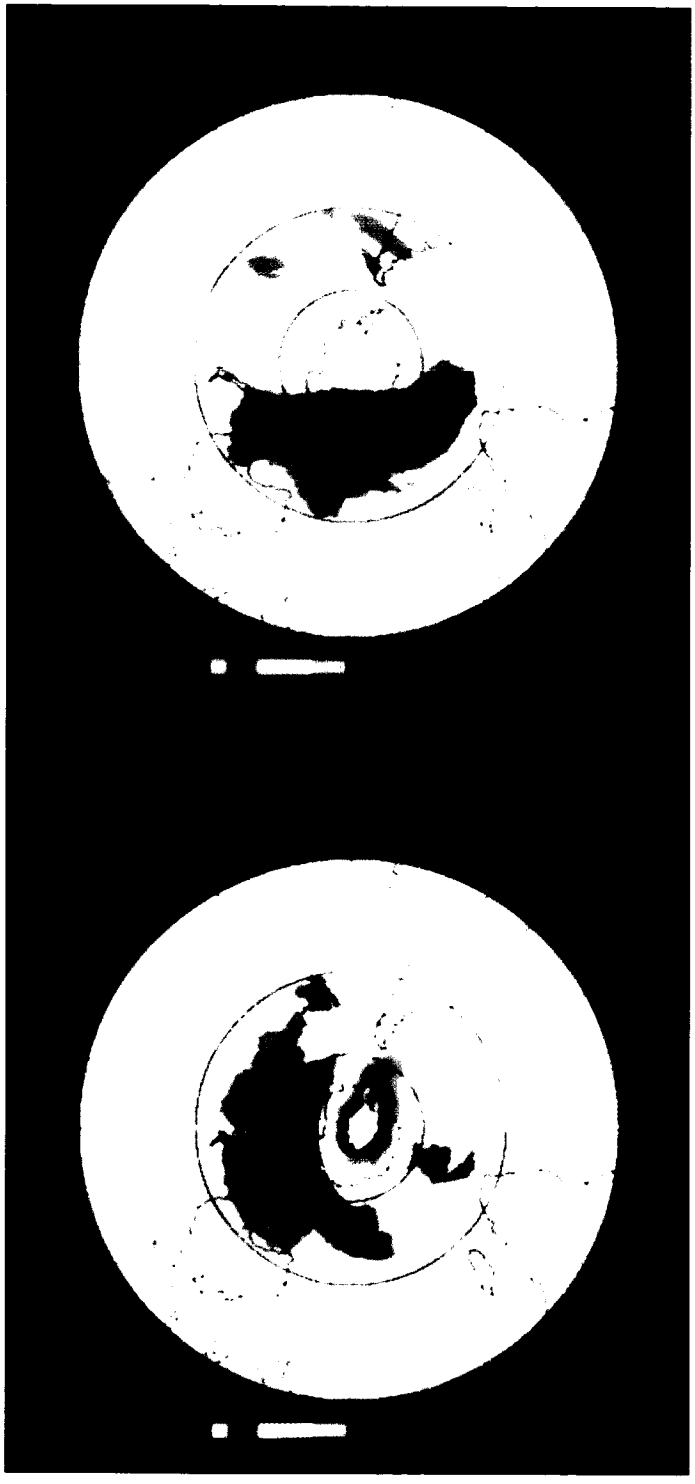

Figure 14-6. Comparison of October 3, 1979 with October 3, 1983 total ozone measurements from the Nimbus 7 TOMS instrument. (Bhartia *et al.*, 1985.)

- The correction factor (Chapter 8) was between .8 to 1.3 for ECC and .8 to 1.4 for Brewer.
- The balloon reached a burst level of 15.8 mbar (top of layer 5B).
- There were no zero partial pressure readings recorded in each daily sondes.
- The total ozone reading for the daily sonde data had a nonzero value.

The station locations, data span and methods of measurement are given in Table 14-1 (Tiao *et al.*, personal communication), where the Canadian stations changed from the Brewer system to the ECC at the designated times.

One of the first elements examined were the correction factors for the various instruments and, as examples of this parameter, we present in Figure 14-7 (Reinsel *et al.*, personal communication), the results at Goose Bay, and Hohenpeissenberg. At Goose Bay we see that the individual months show large variations with a small tendency for decrease till 1980 where the change to ECC was effected. The impact of this change will be discussed further below. For Hohenpeissenberg the diagram also shows some interesting month-to-month variations and we note, in particular, the tendency for the corrections to increase during the first few years followed by the strong minimum in the late '70's.

The cause of these tendencies in the correction factors is unclear and may be related to instrument manufacture, personnel changes or changes in the Dobson system. The major point is that we can not expect the correction factors to be random about some average value and that we will have to consider, in detail, the possible impacts of these variations. As Hilsenrath *et al.* (1985) have indicated, this brings into question whether or not the factors should be applied as they are, as a percentage change to the profile, or in some height dependent manner.

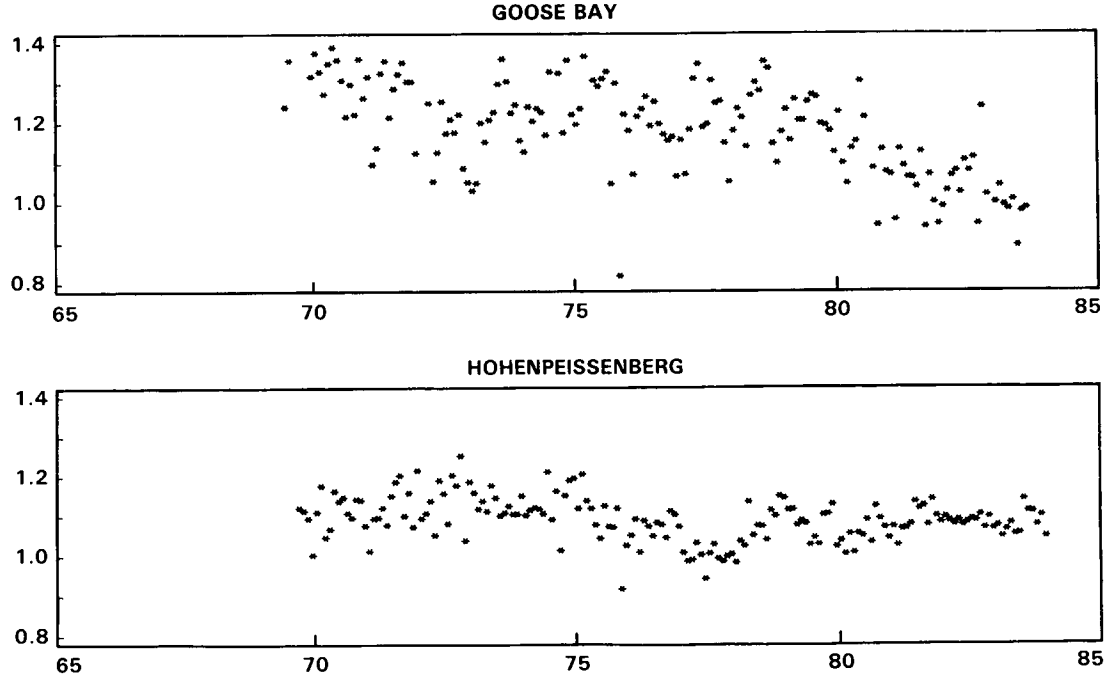

Figure 14-7. Monthly average ozone balloonsonde correction factors at Goose Bay (top), Hohenpeissenberg (bottom). (Reinsel *et al.*, personal communication)

Table 14-1. Ozone Balloonsonde Stations

Station	Data Span	Methods
Hohenpeissenberg	1/70 - 2/83	Brewer
Biscarrosse	3/76 - 1/83	Brewer
Lindenberg	1/75 - 2/83	Brewer
Payerne	9/68 - 12/81	Brewer
Aspendale	6/65 - 5/81	Brewer
Churchill	10/73 - 1/83	Brewer/ECC 9/79
Edmonton	10/70 - 12/82	Brewer/ECC 9/79
Goose Bay	6/69 - 12/82	Brewer/ECC 12/80
Resolute	1/66 - 1/83	Brewer/ECC 12/79
Wallops Island	5/70 - 4/82	ECC
Kagoshima	1/70 - 12/82	ECC
Sapporo	12/68 - 12/82	ECC
Tateno	3/68 - 12/82	ECC

The above notwithstanding, trend estimates (1970) have been obtained from the monthly averages using standard models reported previously with and without an intervention at the 4 Canadian sites for the changes of measurement method. As a cross-validation an overall trend estimate for each station was obtained by calculating a weighted average of the individual estimates of the 15 layers. These estimates may then be compared with the corresponding trend estimates obtained from the Dobson total ozone reading on the ozonesonde file. The results are shown in Table 14-2 (Tiao *et al.*, personal communication). For the nine non-Canadian stations, the trends from weighted averages are in close agreement with those from Dobson total ozone readings on the sonde file. For Churchill, Edmonton and Resolute, the agreement seems much better without the intervention level adjustments. This is in direct contrast to what we would expect and reflects, again, the question as to whether the correction factors between the Brewer Mast and ECC sondes are applied in a consistent manner.

Finally, in Table 14-3 (Tiao *et al.*, personal communication) we present the combined ozone trend estimates (Table 14-2) in the various layers along with their 95% confidence limits. We see that with and without the data intervention at the 4 Canadian sites the negative trends in the lower stratosphere appear statistically significant and of the same magnitude, about -5% per decade. In the lower troposophere, however, the values are very different although they remain positive. Thus, there is evidence to suggest the existence of overall negative trends at layers 3A and 3B, and perhaps also at 2B and 4A.

The results for the troposphere have recently been examined by Logan (1985) and her analysis indicates that the surface ozone at mid-latitudes displays two modes of seasonal behavior: a broad summer maximum within a few hundred kilometers of populated and industrialized regions in Europe and the United States; and a summer minimum in sparsely populated regions remote from industrial activity, in Canada and Tasmania, for example. She argues, in addition, that the current data base for different regions, in combination with limited historical data indicates that summertime concentrations of ozone near the surface in rural areas of Europe and the central and eastern U.S. may have increased by approximately 10-20 ppb (30-100%) since the 1940's. The seasonal cycle of ozone in the middle troposphere over Europe, the United States, and northern Japan is very similar to that at the surface, with a summer maximum,

Table 14-2. Ozone Trend Estimates (% Per Year) As Determined from Balloon Ozonesondes versus Those Determined from Dobson Measurements. (Tiao *et al.*, personal communication.)

Station	Ozonesonde		Total Ozone Readings on Sonde File
Aspendale (6/65-5/82, Brewer)	−.115 (.055)		−.162 (.075)
Biscarrosse (3/76-1/83, Brewer)	−.416 (.114)		−.587 (.185)
Hohenpeissenberg (1/70-2/83, Brewer)	−.174 (.052)		−.220 (.088)
Lindenberg (1/75-2/83, Brewer)	−.287 (.128)		−.269 (.266)
Payerne (9/68-12/81, Brewer)	−.149 (.045)		−.181 (.074)
Kagoshima (1/70-12/82, ECC)	.136 (.090)		.215 (.155)
Tateno (3/68-12/82, ECC)	.085 (.082)		−.055 (.094)
Sapporo (12/68-12/82, ECC)	.148 (.103)		.203 (.138)
Wallops Isl. (5/70-4/82, ECC)	.034 (.075)		.037 (.122)
Churchill (10/73-1/83, Brewer/ECC 9/79)	.473* (.118)	−.310** (.197)	.282 (.234)
Edmonton (10/70-12/82, Brewer/ECC 9/79)	.405* (.095)	.027** (.152)	.360 (.149)
Goose Bay (6/69-12/82, Brewer/ECC 12/80)	.029* (.060)	−.095** (.077)	−.123 (.099)
Resolute (1/66-1/83, Brewer/ECC 12/79)	−.194* (.045)	−.240** (.070)	−.164 (.074)

* without intervention adjustment.
** with intervention adjustment.

Table 14-3. Ozone Trend Estimates and 95% Confidence Intervals

Layer	KM	95% Interval (%/yr.) (w/o Intervention)	95% Interval (%/yr.) (with Intervention)
Above 6B	35+	−.05 ± .38	.22 ± .56
6B	30-35	.04 ± .33	.27 ± .54
6A		.22 ± .31	.46 ± .51
5B	25-30	.15 ± .17	.18 ± .21
5A		.05 ± .18	−.02 ± .27
4B	20-25	−.07 ± .15	−.16 ± .22
4A		−.21 ± .22	−.30 ± .21
3B	15-20	−.33 ± .25	−.48 ± .26
3A		−.56 ± .31	−.71 ± .27
2B	10-15	−.30 ± .53	−.48 ± .49
2A		−.17 ± .67	−.64 ± .75
1D	5-10	.93 ± 1.04	.08 ± .88
1C		1.44 ± 1.23	.57 ± .74
1B	0-5	1.43 ± .87	.66 ± .53
1A		1.72 ± 1.17	.75 ± .83

but it is quite different from that at 300 mb, which is characterized by a maximum in spring. There is good evidence for an increase in ozone in the middle troposphere over Europe during the past 15 years, and weaker evidence for a similar increase over Northern America and Japan. From this she argues that the summer maximum in ozone and the observed trends are due to photochemical production associated with anthropogenic emissions of NO_x, hydrocarbons and CO from combustion of fossil fuels. A strong seasonal variation in ozone observed at Natal, Brazil (6°S) may also result from emissions of NO_x and hydrocarbons, in this case from agricultural burning. Maximum concentrations at Natal are similar to values found at mid-latitudes in summer.

With the limited network of ozonesonde stations, however, the question remains as to whether the tropospheric ozone increase is due to local pollution effects or is symptomatic of a more general atmospheric behavior.

14.1.2.2 Umkehr Measurements.

Although there have been several recent analyses of Umkehr data (eg Angell and Korshover, 1983b; Reinsel *et al.*, 1983; Bloomfield *et al.*, 1982), these have been limited in that they did not consider the impact of stratospheric aerosols on the observations. This has been discussed by DeLuisi (1979) and Dave *et al.* (1979) and it has been concluded that aerosols tend to induce significant negative errors in the Umkehr measurements in the uppermost layers 7-9, with the largest percentage error occurring in layer 9.

Based on this, Reinsel *et al.* (1984) have completed a statistical analysis of the Umkehr data where atmospheric aerosols are taken into account. In the statistical trend analysis, time series models have been estimated using monthly averages of Umkehr data over the past 15 to 20 years through 1980 at each of 13 Umkehr stations and at each of the five highest Umkehr layers, 5-9, which cover an altitude range of approximately 24-48 km. The time series regression models incorporate seasonal, trend, and noise factors and an additional factor to explicitly account for the effects of atmospheric aerosols on the Umkehr measurements. At each Umkehr station, the explanatory series used in the statistical model to account for the aerosol effect is a 5 month running average of the monthly atmospheric transmission data at Mauna Loa, Hawaii, the only long running aerosol data available. A random effects model is used to combine the 13 individual station trends for each Umkehr layer. The analysis indicates statistically significant trends in the upper Umkehr layers 7 and 8 of the order of -0.2 to -0.3% per year over the period 1970-1980, with little trend in the lower layers 5 and 6.

The results are shown graphically in Figure 14-8 (Reinsel *et al.*, 1984) where we have added, for comparison numerical model calculations from Wuebbles *et al.* (1983). We see that there is substantive agreement between the observations and the model calculations.

There are several points to be raised on these results of the Umkehr analysis. The first is that the results, including the sign, are very sensitive to the inclusion of a stratospheric aerosol impact (i.e. Reinsel *et al.*, 1983, 1984). For this data record, the major impact is due to the volcanic eruption at Mt. Agung in 1963 and to lesser extent that of Tiera Del Fuego in 1974 and possibly Mt. St. Helens in 1980. The

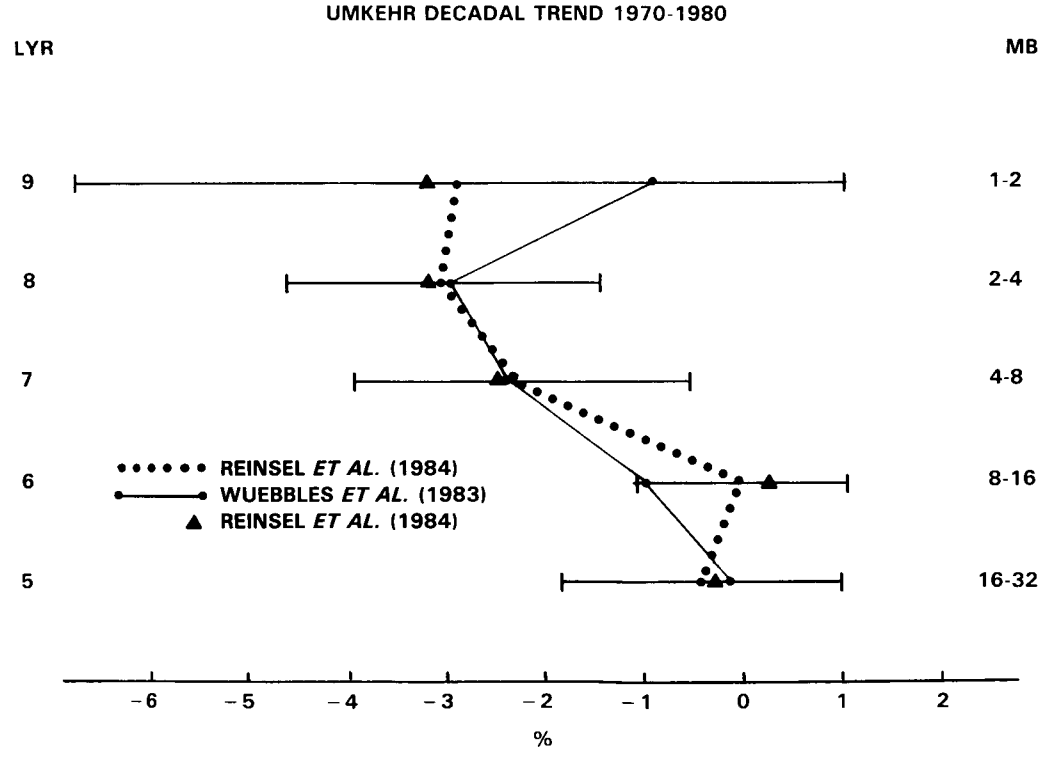

Figure 14.8. Umkehr decadal trend 1970-1980. Units: percent per decade. (Reinsel *et al.*, 1984.)

use of a single station such as Mauna Loa to account for the aerosol on a global basis is fraught with difficulty and great care must be taken on the interpretation of the results. This was evidenced most recently by the events of the volcanic eruption of El Chichon. Attempts (DeLuisi, personal communication) to consider this event within the framwork of the previous analysis have not been free of difficulty. One suggestion by DeLuisi is that there existed an actual decrease of ozone associated with the volcanic debris, possibly due to heterogeneous chemistry or injected chlorine, but this is still quite uncertain. Considerably more work will be required before we will be able to utilize the Umkehr data through the El Chichon event with some confidence.

Another point for consideration is the global representativeness of the 13 station network, an element touched on in the total ozone trend section. For the Umkehr data, Reinsel *et al.* (personal communication) have examined the spatial sampling by examining the approximate 4 year period of the global SBUV data. Their results are presented in Figure 14-9 where the trends over the period November '78 - April '82 have been determined from SBUV zonal averages. Superposed on these curves are the values determined in $10° \times 10°$ longitude/latitude boxes from the SBUV data that includes the Umkehr site. In layer 8, for example, we see that the North American and European stations are biased on the high side of the curve and that Japanese stations tend to bring the overall average into line. Thus, the overall results can be very sensitive to the availability of the stations. This is taken to extreme in the Southern Hemisphere where we see that the Australian station happens to coincide with the relative peak in the zonal average. Because of this fortuitous sampling the overall station average is rather close to the total SBUV area weighted trend. That the ground-based results are so sensitive to the spatial sample is, of course, precisely why the NOAA operational satellite ozone measurement program was initiated. This will be discussed further below.

As the final element in this section we discuss the inclusion of a solar flux variation within the trend analysis. For the Umkehr data, Reinsel *et al.* (personal communication) have included the f10.7 cm solar radio flux as an additional independent variable.

For each Umkehr layer, 5 to 9, and for a given Umkehr station, the model was used:

$$Y_t = \mu + S_t + \omega X_t + \gamma_1 V_{1t} + \gamma_2 V_{2t} + N_t$$

where

Y_t =monthly average for month t of a station's observations at a given layer
S_t =seasonal component (annual and semi-annual)
x_t =0 for $t < T$ (T denotes 12/1969)
=$(t - T)/12$ for $t > T$
ω =annual rate of change parameter (trend)
V_{1t} =a smoothed version of the transmission data at Mauna Loa
γ_1 =a parameter providing an empirical measure of the aerosol effect on Umkehr data
V_{2t} =monthly mean of 10.7 cm solar radio flux (2800 MHz)
γ_2 =a parameter for an empirical measure of the solar effect on Umkehr data
N_t =an autocorrelated noise term, modelled as an autoregressive process to account for non-independence of data
μ =intercept which is very close to the average value

A term to account for a shift in mean level due to instrument recalibration was also included in the model for some stations, as described above.

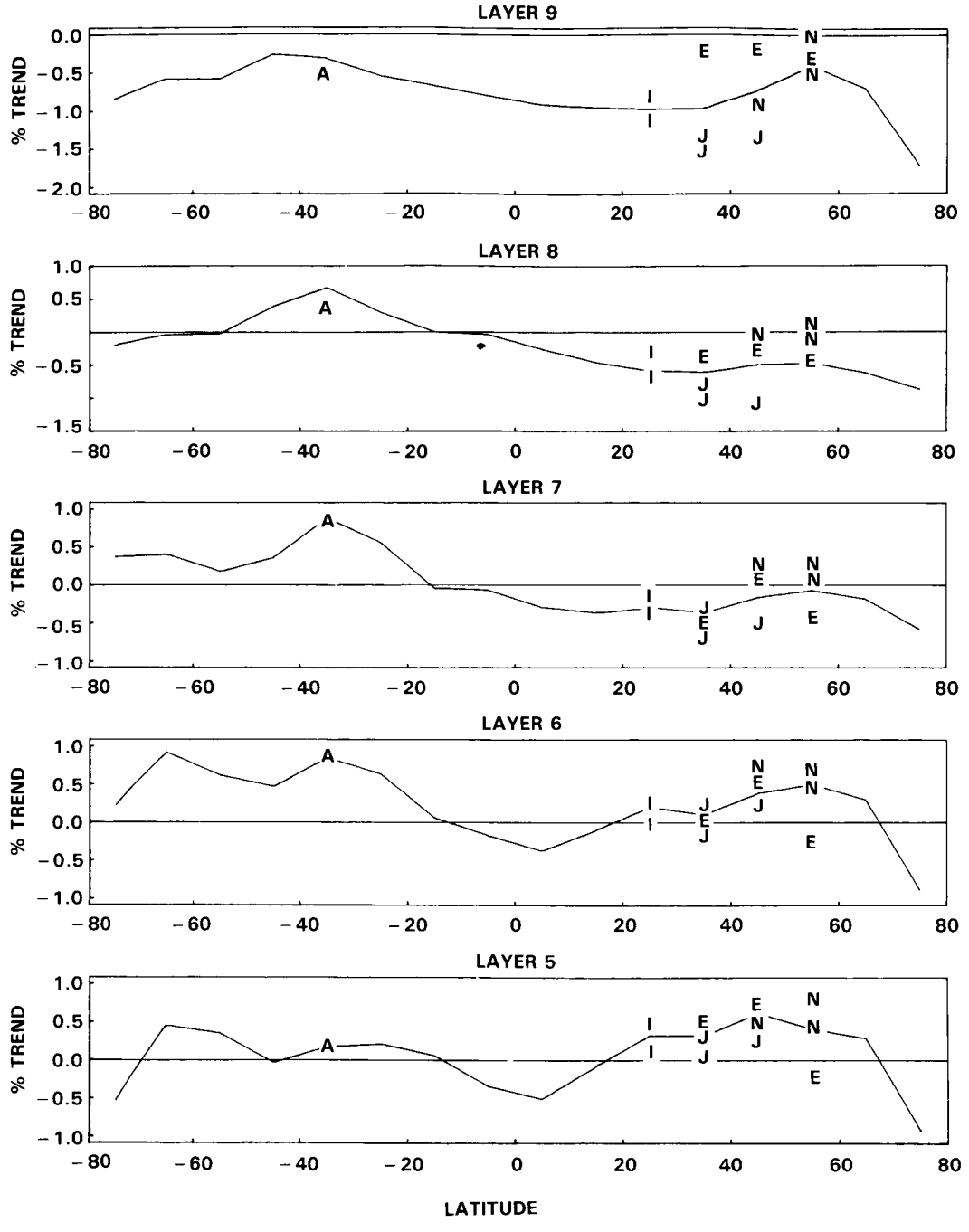

Figure 14-9. SBUV zonal trend estimates in Umkehr layers compared to "Umkehr station blocks" for period November 1978-April 1982. (Reinsel *et al.*, personal communication)

The trend estimates including the solar flux series are shown in Figure 14-8 as the solid triangles (Reinsel *et al.*, personal communication). We see that there is very little impact on the decadal trend with this term added. The overall estimates for the regression coefficients of the solar flux series with accompanying 95 percent confidence intervals are 0.81 $\pm$ 2.56, 0.46 $\pm$ 1.80, 2.04 $\pm$ 1.32, 1.53 $\pm$ 0.78 and 1.18 $\pm$ 0.86 percent, respectively, for layers 9 through 5. These coefficient estimates represent percentage change in ozone per 100 units change in solar flux. The solar effect is largest in layer 7, and statistically significant in layers 7 to 5. The estimates correspond to a solar effect on ozone from solar cycle minimum to maximum of about 1.3, 0.8, 3.4, 2.5, and 2.0 percent, respectively, for layers 9 through 5.

It is not at all clear as to why the solar flux term should have a significant regression coefficient in layers 7 and 6 and not in layers 9 and 8, and raises serious questions on the effect of the solar flux variations.

14.1.2.3 Satellite Measurements

Although the ozone satellite data are not yet of sufficient length to be able to examine decadal trends, the Solar Backscatter Ultraviolet system (SBUV-2) is now operational on the NOAA satellite series. We may expect, then, that these data will take their place among the long-term data sets such as Umkehr, ozonesondes etc., and in this section we will outline the basic operational program including validation. This will be compared to current estimates of anthropogenic impact such that the capabilities of early ozone trend detection will be delineated. We note that the SBUV-2 satellite measurements are restricted to daytime only total ozone and vertical profiles in the stratosphere above the ozone concentration maximum. There is no satellite profile capability for the troposphere anticipated for the near future.

14.1.3 OPERATIONAL SBUV-2 OZONE MONITORING SYSTEM

A critical issue in the search for long term ozone trends using satellite-based sensors concerns the separation of instrument sensitivity changes from true atmospheric variability. A thorough examination of this requires careful characterization of the instrument over its entire lifetime. A significant improvement in the new SBUV-2 as compared to previous system is the inclusion of an onboard calibration lamp to assist in tracking any instrument-related changes in the ratio of backscattered ultraviolet radiance to incident solar irradiance. This ratio is the fundamental measurable upon which the derived ozone abundance depends. However, the new calibration check is only one of several evaluations that must be conducted on a regular basis toward reaching the goal of obtaining a long term data base with negligible instrumental drift. Additional support in this regard will be provided by NASA's Shuttle-borne SBUV (SSBUV). Regular flights of this freshly calibrated instrument in coincidence with measurements from a free-flying SBUV-2 have the objective of detecting and correcting for possible sensitivity drifts in the long term measurements.

When we incorporate the above internal calibrations at a rate of twice per week, and include effects for daily sampling fluctuations, instrument noise and absolute calibration differences between operational instruments launched over two years, the operational system is determined to be able to detect a global ozone change of about 1.5% per decade at the 95% confidence level. This is considerably less than the 2.8% per decade estimate as predicted by Wuebbles *et al.* (1983) for Umkehr level 8.

A requirement to detect long term ozone trends of the magnitude predicted by theoretical scenarios for chlorofluoracarbon chemistry places strict performance requirements on the operational SBUV-2 sensors. To ensure a data base of the highest possible quality from the long term measurements program

it is necessary to examine continuously the performance of the SBUV-2 instruments and to compare the output products with independent measurements of high accuracy and precision. These procedures should, in principle, allow detection and removal of any instrument anomalies, provide support for the validity of the SBUV-2 inversion procedure, and will allow estimates of the ozone trend from independent data sets.

14.1.4 GROUND-BASED VALIDATION SYSTEM

14.1.4.1 Dobson/Umkehr Data

The basic NOAA satellite ozone validation program contains the following elements:

- 16 Primary Dobson stations - triennial calibration against Boulder standard instrument
- Other Dobson and M-83 sites with oversight via satellite consistency, WMO, U.S. and AES calibration programs
- 16 primary Umkehr sites - includes 7 automated instruments
- Other Umkehr sites as available
- Aerosol impact evaluation by GMCC
- Balloonsonde measurements monitored by GMCC at 3 sites on a once-per-week schedule
- Other balloonsonde as available
- SSBUV
- Other sources as available:
  Ozone rocketsondes
  Solar observations

Within previous studies of ground-based data and comparisons with satellite data, several elements that have been clearly exhibited are the variability between stations and that instruments change in time. Based on this experience, it is clear that we must utilize a small subset of data sites that are well coordinated and able to be recalibrated at regular intervals such as three years. Within the limitations of personnel and resources NOAA has selected 16 Dobson/Umkehr sites as this primary data base.The stations are:

1) Fairbanks, Alaska
2) Mauna Loa, Hawaii
3) Boulder, Colorado
4) Huancayo, Peru
5) Haute Province, France
6) New Zealand (tentative)
7) Perth, Australia
8) Edmonton, Canada
9) Goose Bay, Canada
10) Arosa, Switzerland
11) New Delhi, India
12) Varanasi, India
13) Sapporo, Japan
14) Tateno, Japan
15) Aspendale, Australia
16) Invercargill, New Zealand

Of these, sites 1-7 are the recently automated Dobson stations and stations 8-15 have long-term records extending at least to the mid 60's.

When a matchup of satellite and ground-based data at individual points is considered, two major sources of error are included. The first involves the noise characteristics of the individual instruments plus any space-time window involved in the matchups; the second is the difference in calibration between instruments at individual stations. We define the first to have a variance of σ_1^2 where σ_1 is a representative value at a station for η_1 matchups. For the second source, we define σ_2^2 as the variance of the average difference (satellite minus station) at η_2 stations.

The combined variance for the two errors is then:

$$\text{var} = \frac{\frac{\sigma_1^2}{\eta_1} + \sigma_2^2}{\eta_2}$$

The standard deviation, SD, is $(\text{Var})^{1/2}$ and the 95 percent confidence level is given by twice the standard deviation.

Total Ozone

Based on the results of comparisons of Bhartia *et al.* (1984) for comparisons of Dobson with SBUV for '79-'80, we find the following representative values:

$\sigma_1 \sim 5\%$ $\quad$ $\sigma_2 \sim 2.5\%$
$\eta_1 \sim 100$ $\quad$ $\eta_2 \sim 58$

with the result that

var = 0.11
SD = 0.33% $\quad$ 2×SD = 0.67%

Thus, for a yearly average, SBUV can be compared to the Dobson network to an overall 95 percent confidence precision within one percent.

One caveat with the above is that there is an implicit assumption that each station is independent of the others and that no latitudinal biases exist. Both assumptions appear reasonable based on the results presented by Bhartia *et al.* (1984).

Vertical Profiles

Umkehr - SBUV

Based on the results of Bhartia *et al.* (1984) for '79-'80 the following values are representative:

$\sigma_1 \sim 8\%$ $\quad$ $\sigma_2 \sim 7\%$
$\eta_1 \sim 36$ $\quad$ $\eta_2 \sim 11$

Consequently:

var = 4.62
SD = 2.15% 2×SD = 4.3%

Therefore, as shown in the two year SBUV data comparisons, on a yearly basis the SBUV can be compared to the Umkehr observations to within five percent.

The above, however, is somewhat misleading in that it does not address two concerns for long-term measurements. The first is that with a small number of co-location stations, particular emphasis must be placed on station history and performance; the second is the impact of stratospheric aerosols on the data. The approach to the former is that the ARL-GMCC group in Boulder, who maintain the Dobson international standard instrument, has been tasked to develop a cross-calibration program for a set of Umkehr stations on a three-year rotating basis. This, in conjunction with the added automated Dobson instruments funded by EPA would increase the number of available sites to about 16 and decrease the σ_2 standard deviation to about four percent. This changes the previous statistics to:

var = 1.11
SD = 1.05% 2×SD = 2.11%

an improvement of about a factor of two.

On the question of the aerosol impact, there has been considerable recent effort by John DeLuisi (ARL/GMCC) and Carl Mateer (AES, Canada) on determining correction factors for the Umkehr measurements. This is an on-going project and the principal thrusts have been along two lines. The first is the accumulation of precise lidar measurements; the second has been simple statistical regression of the Umkehr data against the long-term atmospheric transmission data (solar radiation) at Mauna Loa as presented by Reinsel *et al.* (1984). This latter approach is expected to be less precise than the former in that we would expect some natural region-to-region variation of aerosols and the record includes stations with modifications in time. The above not withstanding, if we examine the transmission record, (which does not include the recent El Chichon event) we can ask how great an error would result with a 16 station network if the Mt. Agung eruption was not recognized and no adjustments were made for stratospheric aerosols. Utilizing these measurements and the results from Reinsel *et al.* (1984), we would expect a bias in layer 9 of about 11.2 percent with a 95 percent confidence limit of ~ 4.8 percent and a bias in layer 8 of about 7.3 percent with a 95 percent confidence limit of ~ 3.1 percent.

The implication of the above is that if we do not recognize an aerosol impact at all, then a significant error results in the Umkehr estimates. On the other hand, if we do recognize the event even in as course a manner as making lidar measurements at one site such as Mauna Loa, then the combined 95 percent confidence limits of the SBUV and Umkehr comparisons (assuming no aerosol impact on the high level SBUV data, which is rather reasonable) for a calibrated 16 station network are:

Layer 8	Layer 9
±3.79%	±5.24%

Within the above scenario the results can be translated to our ability to detect a trend utilizing the 16 station network as a calibration mechanism for the SBUV-2 system assuming that the latter had no internal calibration mechanism. The 95% confidence limits for a decadal trend over various periods are:

10 years	4.2%
15 years	2.3%
20 years	1.5%

Thus, while this system is not expected to provide trend estimates over 10 years to within the model calculations of 2.8%, it does become sufficient at 15 years and beyond. We note that to be able to discuss a 2.4% decadal trend within 10 years would require about 45 observing stations.

14.1.4.2 Balloon Ozonesonde Data

For the low altitude, routine ozonesonde balloon program, again based on the results of Bhartia *et al.* (1984) for '79-'80, the following values are representative, noting that in their comparisons they reference all data to the Umkehr layers (i.e., they integrate the balloon ozone profile within the Umkehr layers):

$\sigma_1 \sim 11\%$ $\sigma_2 \sim 5\%$
$\eta_1 \sim 20$ $\eta_2 \sim 10$

var = 3.1
SD = 1.76%
2×SD = 3.52%

For Umkehr layer 6, this translates to a 95% trend detection capability of about 3.9% per decade.

In the case of upper altitudes, ARL-GMCC has developed a high altitude system capable of utilization to about 40 km and these are being launched in support of SBUV-2 about once-per-week. Sites selected are:

Hilo, Hawaii
Boulder, Colorado
Poker Flat, Alaska or Edmonton, Canada

Note that these data are coincident with Umkehr observations and will serve as an additional check on these systems and the impact of aerosols.

Assuming a 15% noise value for the ozonesonde at 40 km and a 10% value for SBUV-2 with a 1.2% standard deviation between stations, the 95% confidence limits for a *decadal* trend over various periods are:

10 years	3.5%
15 years	1.9%
20 years	1.2%

Thus, as for the Umkehr observations, the data base is within the model trend estimates at 15 years and beyond.

14.2 TEMPERATURE TRENDS

14.2.1 Troposphere

In the troposphere the trend evaluation is based on 63 selected radiosonde stations. The impact of including satellite data to supplement the rawinsondes is currently being evaluated.

Figure 14-10 (which is an update of earlier work, Angell and Korshover, 1983a; personal communication by authors) shows the time variation of the mean temperature in the tropospheric 850-300 mbar layer for climatic zones, hemispheres and world (climatic zone boundaries at 10°, 30° and 60°) as estimated from radiosonde data. A 1-2-1 weighting has been applied twice to successive seasonal deviations from long-term seasonal means. The variation in sea-surface temperature (SST in the eastern equatorial Pacific) is shown at the bottom, and the arrows show the dates of Mt. Agung and El Chichon volcanic eruptions. Tick marks are in June-July-August of indicated years. In the Northern Hemisphere the temperature is indicated to have decreased from 1958 to about 1965, remained approximately constant from 1965 to 1975, and increased thereafter, so that the temperature in 1983 is comparable to the temperature in 1958. In the Southern Hemisphere, however, this temperature is indicated to have decreased from 1958 to about 1965, and increased thereafter, so that the temperature in 1983 is higher than in 1958. Because of the close relation between sea-surface temperature in the eastern equatorial Pacific (bottom trace of Figure 14-10) and tropospheric temperature in the tropics a few seasons later, there is also a good relation between this SST and global tropospheric temperatures a few seasons later. The pronounced increase in this SST (El Nino) two seasons after the El Chichon volcanic eruption makes it difficult to detect any cooling effect of the eruption.

14.2.2 Lower Stratosphere

Based on the same rawinsonde stations which have been used for the troposphere, the time variation in the mean temperature in the 100-30 mbar layer has been prepared, Figure 14-11, (update of Angell and Korshover, 1983a; personal communication by authors). The evidence for a long-term cooling of this layer is better in the Southern Hemisphere than in the Northern Hemisphere. A temperature increase is apparent following the eruptions of Agung and El Chichon, but there is no obvious association with SST in eastern equatorial Pacific. We note also the pronounced cooling in polar latitudes in 1982 and 1983 following the El Chichon volcanic eruption. However, no generally accepted hypothesis is yet available to explain it.

We should stress that the 63 station data base was selected on the basis of global coverage, albeit with some gaps over the ocean areas and the southern Hemisphere. In addition, Angell and Korshover (1983a) have compared their statistical methodology for surface temperature against independent gridded analyses with quite favorable results.

For the investigation of long-term temperature changes in the lower stratosphere another series of temperature data for the Northern hemisphere is available from the Stratospheric Research Group, Free University Berlin. This data set which starts in July 1964 for most pressure levels, consists of daily hemispheric analyses of temperatures (and geopotential heights), based largely on radiosonde observations. The daily hemispheric analyses have been analyzed by hand and have been digitized into a latitude-longitude grid. Monthly mean statistics have been derived afterwards.

Figure 14-12 shows filtered zonal mean 30-mbar temperatures (°C). A 39 point filter has removed the annual and the quasi-biennial cycles (Labitzke *et al.*, 1985). Looking at these curves, several features can be noticed:

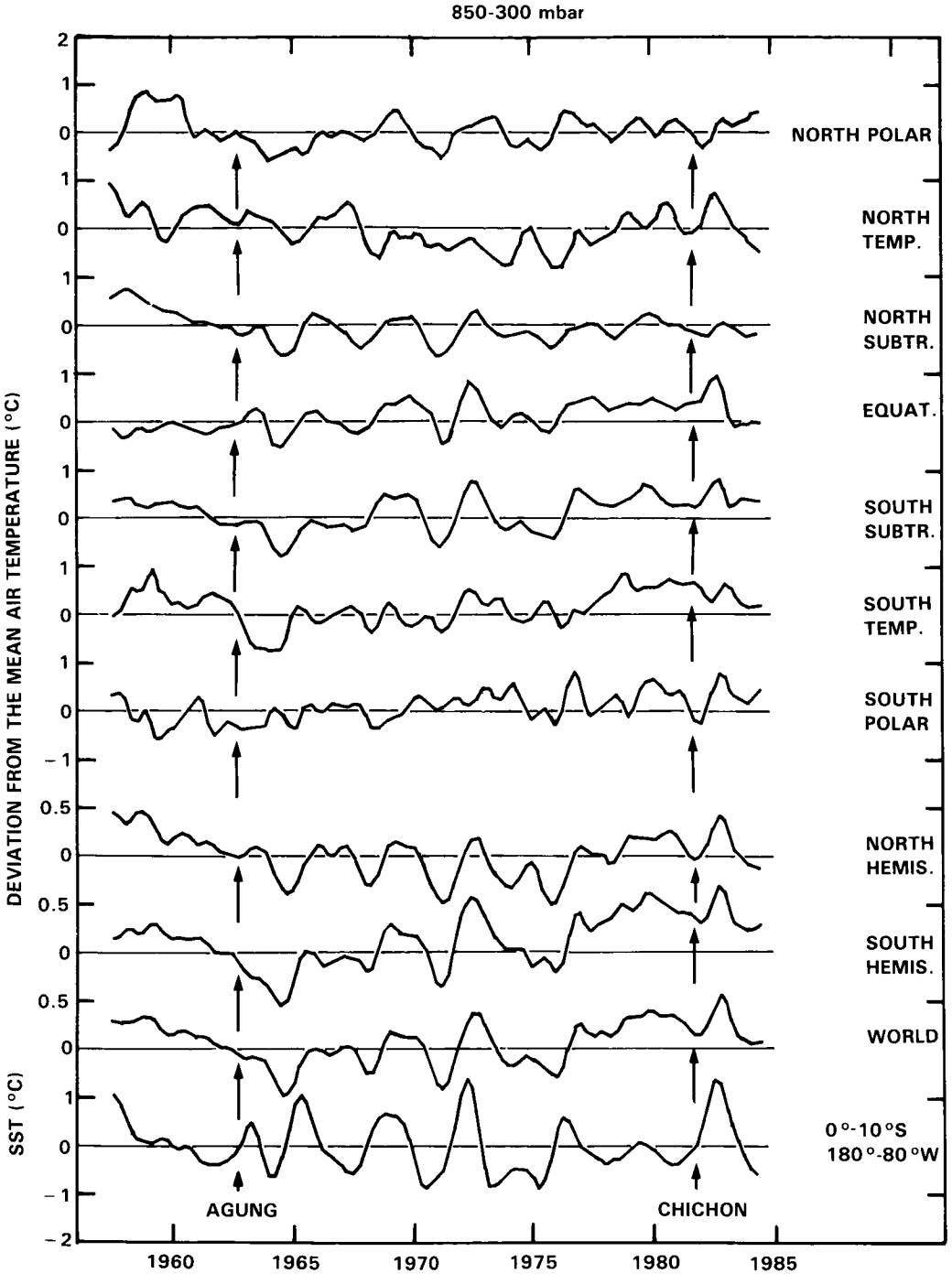

Figure 14-10. Time variation of the mean temperature in the tropospheric 850-300 mbar layer for climatic zones, hemispheres and world (climatic zone boundaries at 10°, 30° and 60°) as estimated from radiosonde data. A 1-2-1 weighting has been applied twice to successive seasonal deviations from long-term seasonal means. The variation in sea-surface temperature (SST in the eastern equatorial Pacific) is shown at the bottom, and the arrows show the dates of Agung and El Chichon volcanic eruptions. Tick marks are in July-June-August of indicated years. (Update Angell and Korshover, 1983a; personal communication).

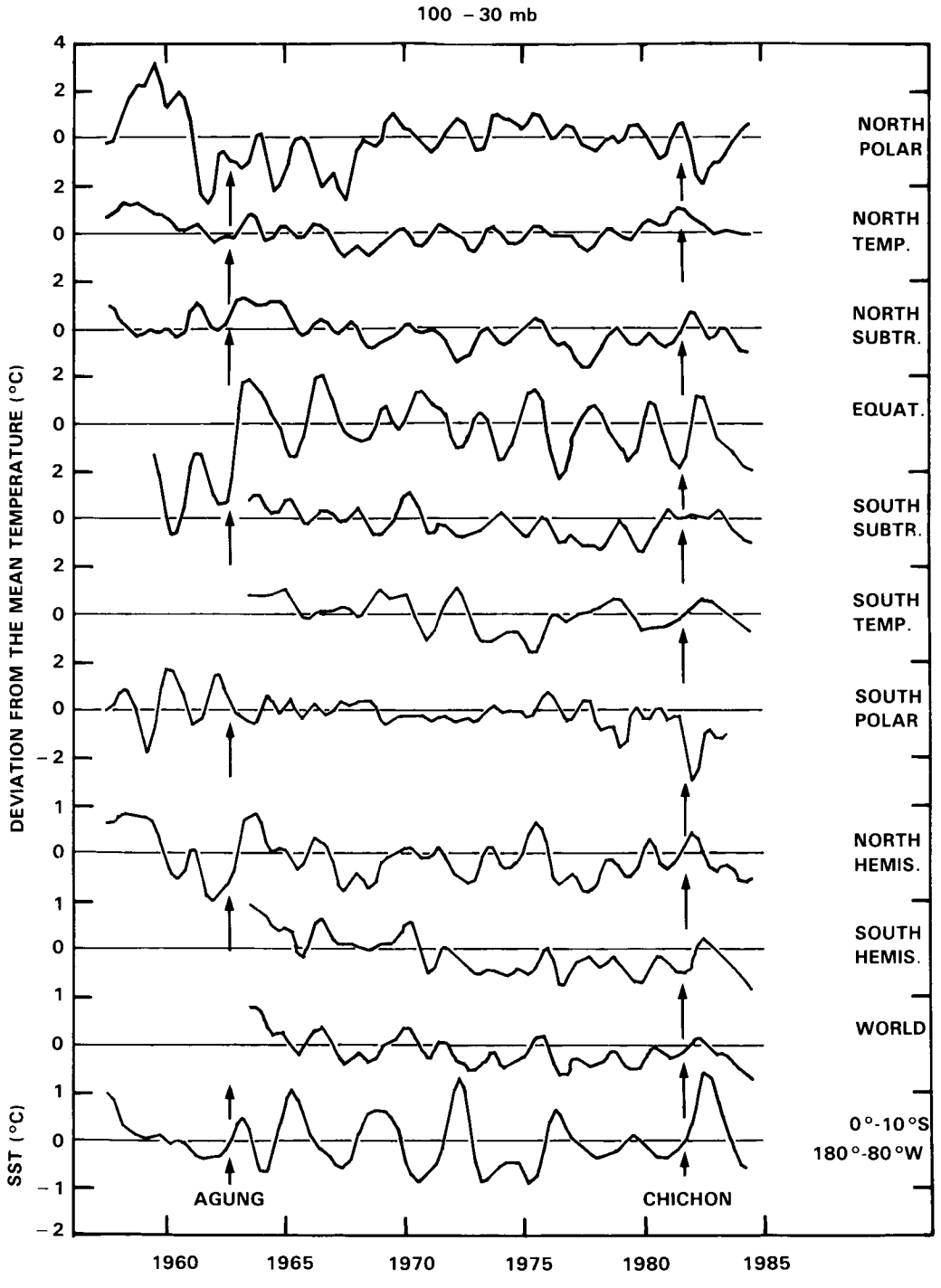

Figure 14-11. Time variation of the mean temperature in stratospheric 100-30 mbar layer for climatic zones, hemispheres and world as estimated from radiosonde data. Otherwise, see legend of Figure 14-10.

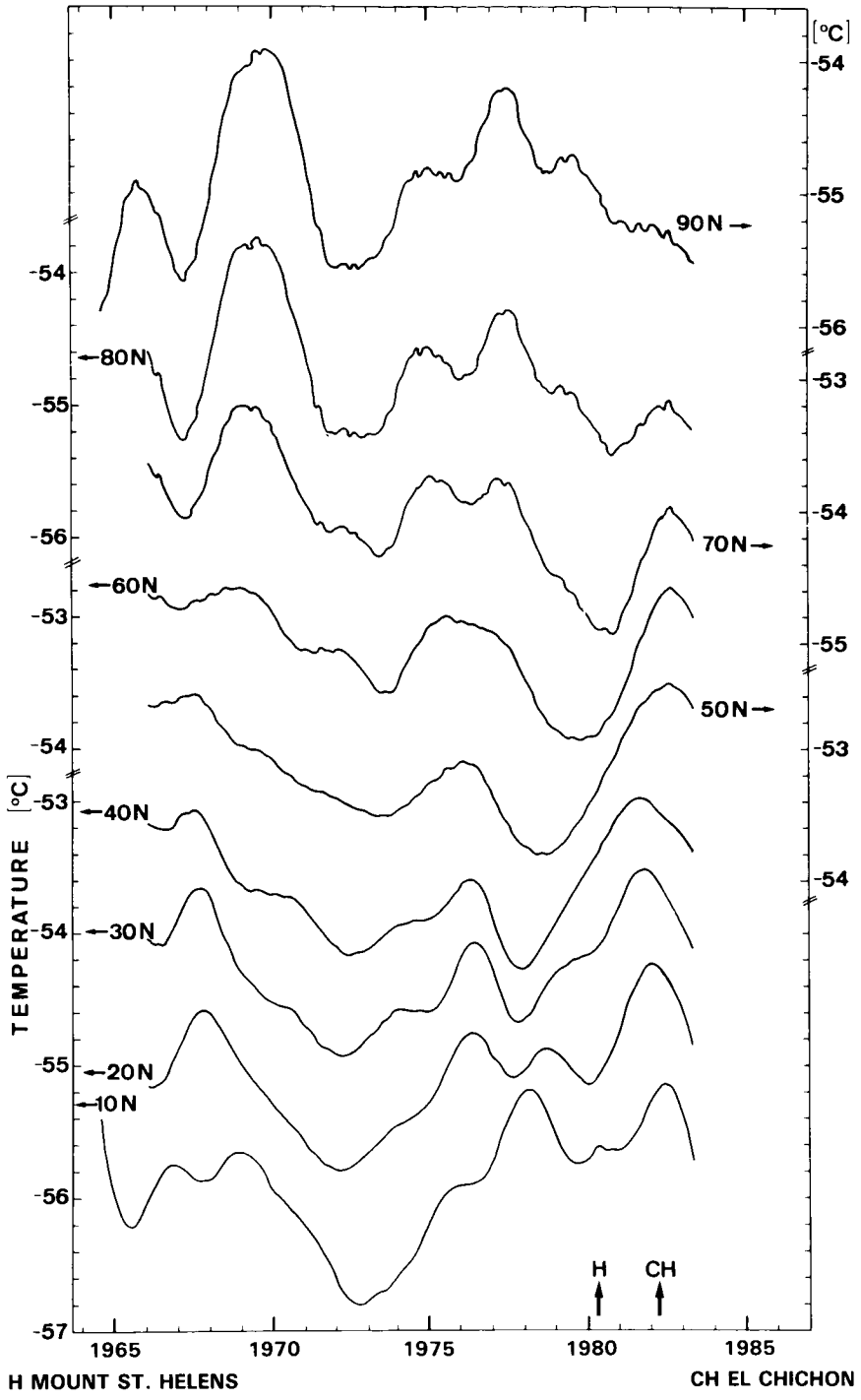

Figure 14-12. Zonal means of filtered monthly mean 30-mbar temperatures (°C). (Update of Figure 7, Naujokat, 1981).

Large variations with a time-scale of several years exist. The causes of these variations are not clear. At higher latitudes the variations appear to be connected with the appearance of intense midwinter warmings or undisturbed cold winters (Labitzke and Naujokat, 1983). Between 70 and 40 °N a "trend" of about −0.6 °/10 years can be seen from 1965 to 1979 in the data, if maxima or minima are considered. This

"trend" is interrupted after 1979 at 40°N, after 1980 at 50°N, and after 1981 at 60°N. The interruption was earlier over low latitudes where the "cooling" stopped in 1972.

The cause of the warming over the tropics from about 1972 to 1979 is not clear at this time. However, a warming attributed to the increased aerosol load after volcanic eruptions was demonstrated for the summer and fall of 1963 and 1982, when the stratosphere warmed markedly over the tropics from the eruptions of Agung and El Chichon, Figure 14-13. (Labitzke *et al.*, 1983; Quiroz, 1983a; Parker and Brownscombe, 1983).

The departures of the annual mean temperatures, averaged over 2 years, are summarized in a time-latitude cross-section, Figure 14-14. The warming episode in 1982 appears to be related to the increased volcanic aerosol load. Labitzke (1985) has associated the continued cooling over high latitudes, Figure 14-14, to be a result of extremely low winter values which may be connected with a cooling due to the increased aerosols in the polar night region and the formation of polar stratospheric clouds.

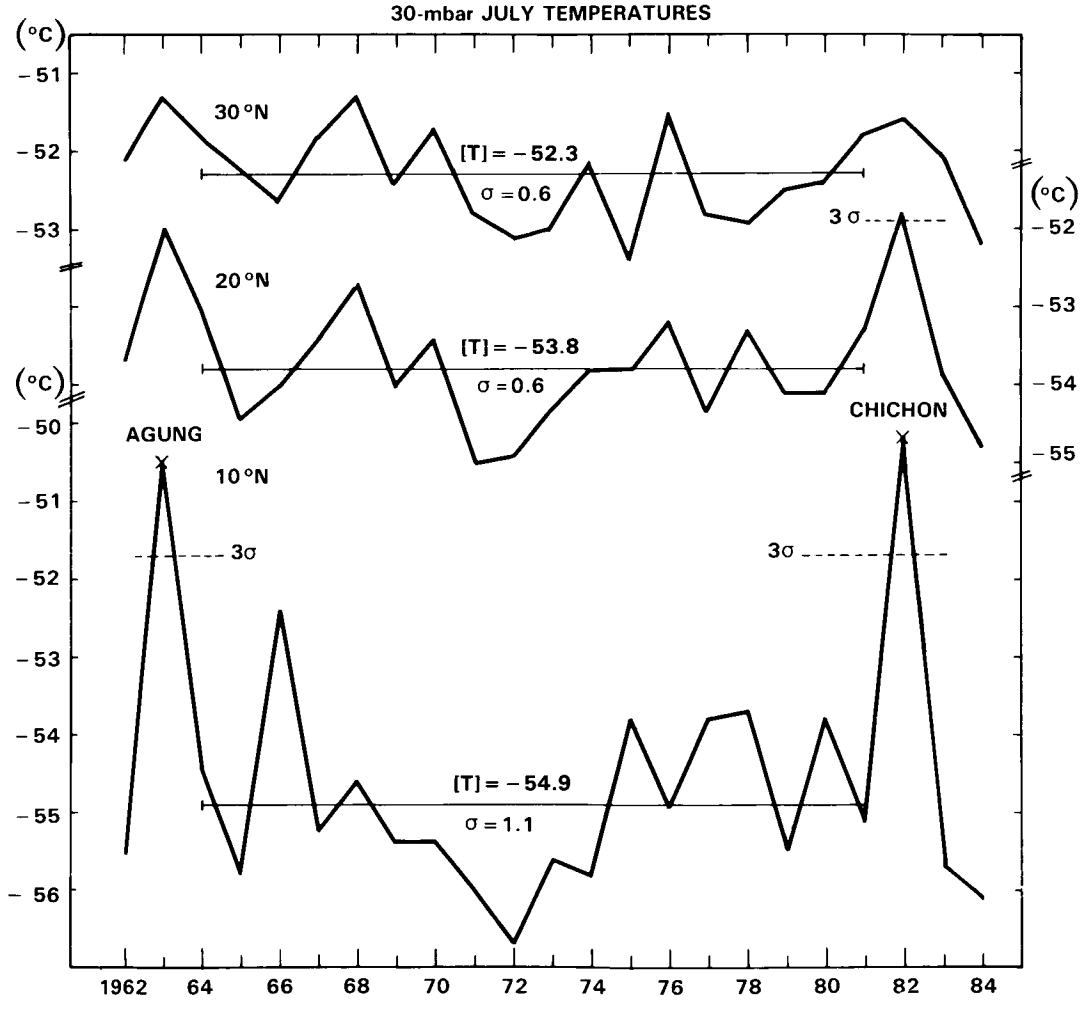

Figure 14-13. Zonal mean 30-mbar temperatures (°C) during July at 10, 20, and 30°N, for the period 1962 through 1984. The 18-year average [T] is for the period 1964-1981. (Update of Figure 11, Labitzke and Naujokat, 1983).

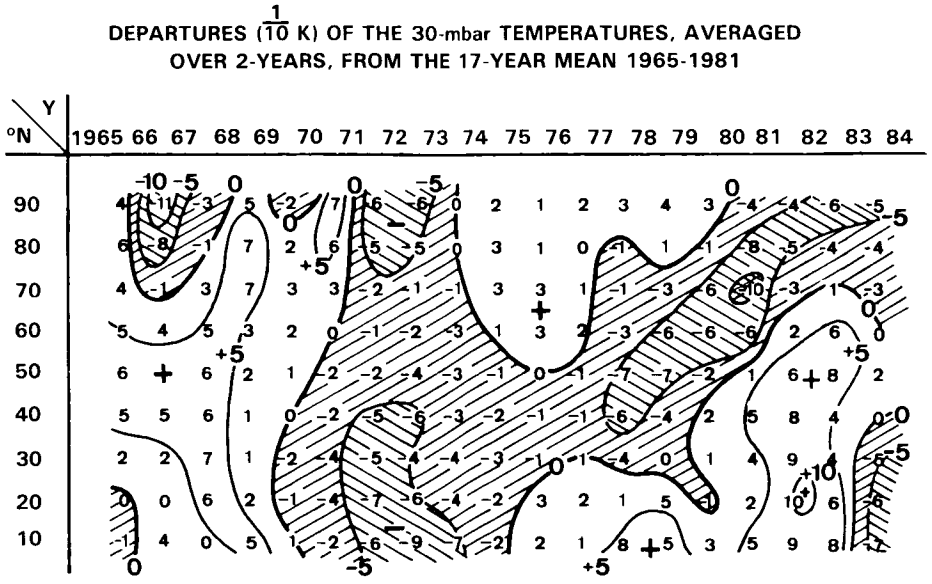

Figure 14-14. Time-latitude distribution of the deviations (1/10 K) of the annual averages, smoothed over 2 years, from the 17-year mean 1965-1981. (Update of Figure 9, Labitzke and Naujokat, 1983).

An even clearer picture emerges, if only July, i.e., a relatively quiet summer month, is considered, Figure 14-15. The data series for July starts in 1962 and the time-latitude section shows clearly the warming after Agung (March 1963) and after El Chichon (March 1982).

A serious difficulty that must be addressed is that the results from Figure 14-11 and 14-12 are inconsistent. For example, in the North Temperate regions of the former there is virtually no trend indicated

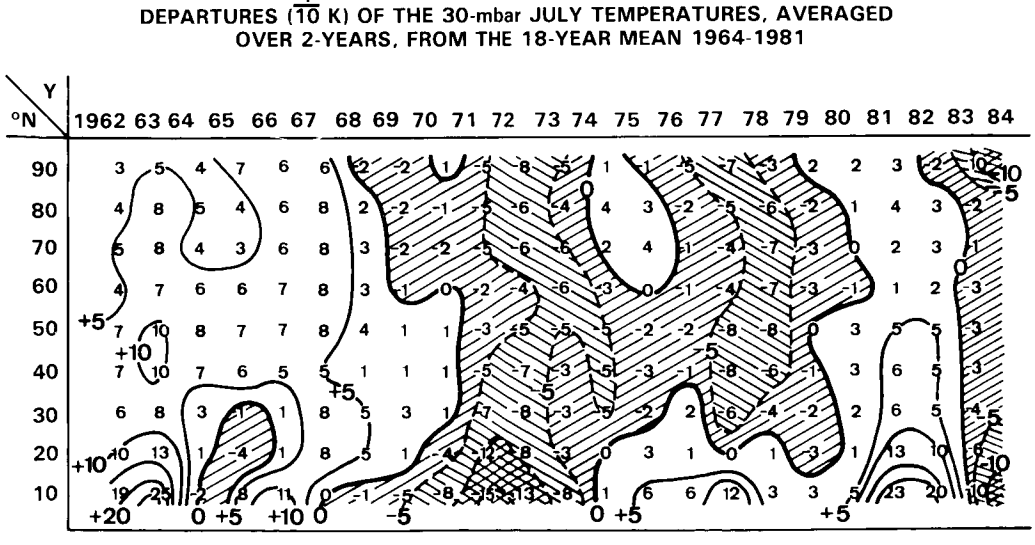

Figure 14-15. Time latitude distribution of the deviations (1/10 K) of the July averages, smoothed over 2 years, from the 18-year mean 1964-1981. (Update of Figure 9, Labitzke and Naujokat, 1983).

for the period 1965-1979, while a pronounced negative trend exists in the latter. Examination of similar diagrams for the 100-and 50-mbar levels (not shown) shows that the cause is not simply the difference between thickness and on-level temperature and this question must be resolved by further analysis.

14.2.3 Upper Stratosphere

Recent calculations, (e.g., Wuebbles, 1983b; de Rudder and Brasseur, 1985) with fully coupled one-dimensional models suggest that a 1.5 °C decrease should have been observed from 1970-1980 in upper stratospheric temperature. There have been several studies seeking this effect in available observational data. Angell and Korshover (1978) found a 3 to 5 °C decrease in mean annual temperatures in the middle and upper stratosphere (26-55 km) between 1970 to 1976. This cooling was found at Western Hemisphere rocketsonde stations at all latitudes. Quiroz (1979a) restricted his study to summer (June, July, and August), seasonal mean temperatures at 35 and 50 km from 1965 to 1977 at seven Western Hemisphere rocketsonde stations. This study used summer data because of the well-known reduced daily temperature variability during that season. In addition to many careful quality control procedures, Quiroz applied adjustments for solar radiation of as much as 3.0 °C where necessary. This study also showed a decline in temperature of 3 to 6 °C between 1970 to 1976.

In a more recent study by Johnson and Gelman (1985) the Western Hemisphere rocketsonde network reports were again the primary data base, but the period of record was extended to include 1965 to 1983 and additional quality control procedures to the data were used.

Quiroz (1979a) has discussed some of the problems involved in using rocketsonde data as published by World Data Center A for Meteorology, Ashville, N.C., (in print through 1976 and extended on microfilm through 1983). Quiroz points out that the published monthly averages may include data from falling sphere sondes, and may also need to have appropriate adjustments ("correction") applied, based on the work of Ballard (1967), Krumins (1972), or Staffensen *et al.* (1972). In addition, some observations are reported to have abnormally high or abnormally low fall velocities, which render the observational data from these soundings suspect.

Within Johnson and Gelman (1985) June monthly mean values for the 40-45 km layer were calculated for all Western Hemisphere rocketsonde stations for which data were available. The quality control scheme was as follows: (1) All falling sphere or experimental sensor soundings were rejected. (Quiroz and Gelman (1976) discuss the problems in using the data from sphere soundings.) (2) Any soundings flagged in the data books as having doubtful or missing temperatures in the 40 to 45 km region were rejected. (3) All soundings with a 43-km fall velocity more than two standard deviations from the mean June 43-km fall velocity for the station were rejected. (4) Adjustments for radiation were applied in a similar manner to that used by Quiroz (1979a). (5) If fewer than three soundings were available for a station for the month, or if the soundings were all at the beginning or end of the month, the mean was not included.

Mean temperatures for each June were then used to calculate linear least-squares regression coefficients with latitude of the stations as the independent variable. The resulting coefficients were used to calculate area-weighted mean temperatures for 25 °N to 55 °N. Results are displayed in Figure 14-16. A 2 to 3 °C temperature drop in the early 1970s is indicated in this diagram similar to the findings by Quiroz (1979a) and Angell and Korshover (1978a). We note, however, that this temperature decline coincides with a change in the principal observing system for the Arcasonde system to the Datasonde system.

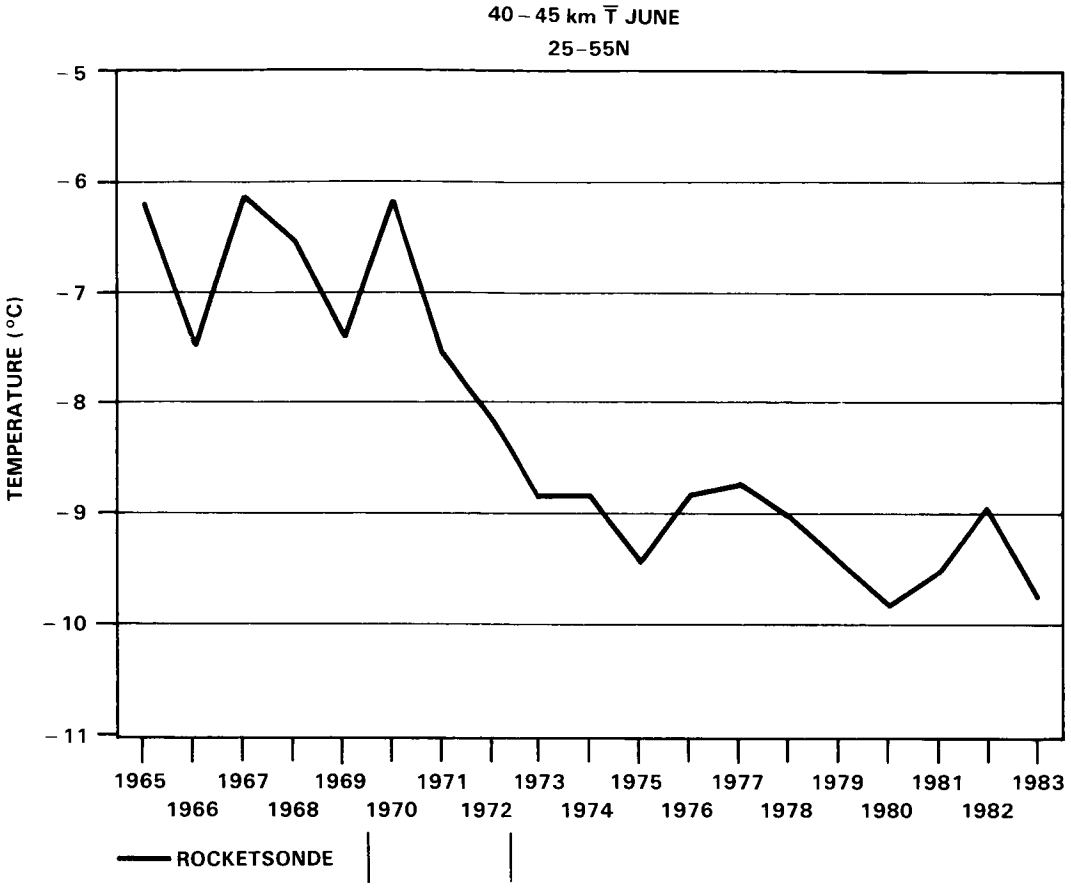

Figure 14-16. 40-45 km layer mean rocketsonde temperatures averaged over the north America (25-55 north latitude) for June in years 1965 to 1983. Heavy ticks indicate beginning and end of transition from Arcasonde to Datasonde observing systems.

In order to study this temperature decrease more closely, similar mean temperatures were calculated for the 25-30 km layer using both rocketsondes and support radiosondes. Results are displayed in Figure 14-17. There is no discernable long-term trend in radiosonde temperatures for this limited data sample and period; however, in the 1965-1971 time period the rocketsonde temperatures averaged 1.11 °C higher than the radiosonde means while in the 1972-1978 time period the rocketsondes averaged 1.06 °C lower than the radiosonde temperatures. This approximately 2 °C decrease in rocketsonde mean temperatures again corresponds to the change in observing systems.

From this, Johnson and Gelman (1985) conclude that the change in rocketsonde temperatures in the early 1970s simply reflects a previously uncompensated change in the rocketsonde temperature measurement system. It remains, then, to determine the true temperature variation taking the above into consideration. As a simple exercise to determine a possible order of magnitude effect, we have fitted a linear regression model to the 40-45 km temperature data for the limited period 1973-1983. This is after the major instrument transition and the data should be uniform in quality. The results indicate a negative trend of −0.75 °C/decade with a standard error of ± 0.34 °C/decade. Wuebbles (1983b), although not for this specific time period, suggests that a temperature decrease should exist on the order of −0.9 °C/decade at about 45 km. Thus, substantive agreement at this altitude is suggested.

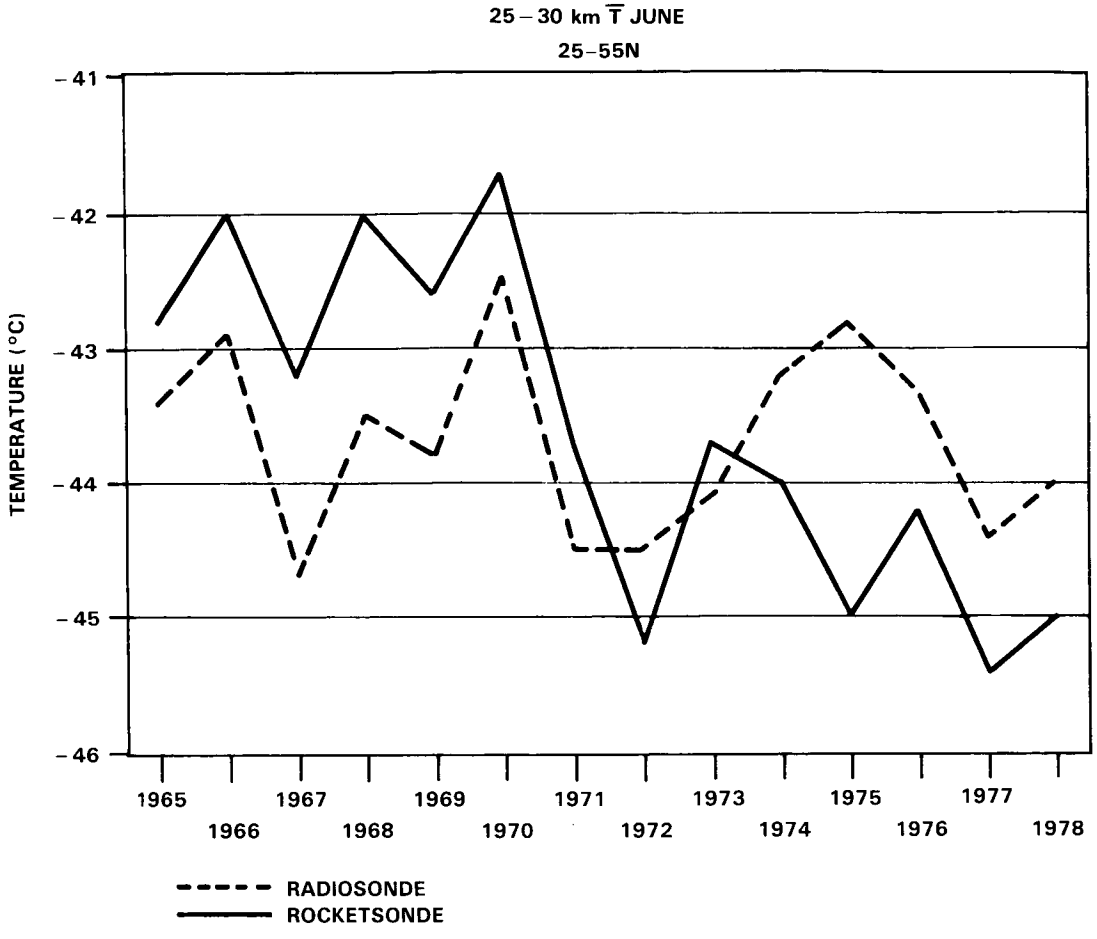

Figure 14-17. As in Figure 14-16, except for 25-30 km. Solid line indicates mean temperatures derived from support radiosondes; dashed line for corresponding rocketsondes.

Clearly, the above will have to be examined further with the more complete data sets in order to verify these preliminary findings. We note especially that the results presented above for the lower stratosphere summertime only can be quite different from yearly averages, Figures. 14-12–13.

14.2.4 Capability of Satellites to Measure Trends

As for the ozone trend section described above, the data of the long-term measurement program of statospheric temperature within the NOAA operational satellite program are not yet of sufficient length to determine decadal trends. We will discuss here, then the potential of this system and its capability to meet the monitoring requirements. Following Wuebbels *et al.* (1983b), a 3% decrease in ozone at about 2 mbar should be associated with about a 1.5 °C decrease in temperature. Following the notation in the Ozone Section, 14-1, the combined variance for a satellite-rocketsonde comparison is

$$\text{variance} = \frac{\frac{\sigma_1^2}{\eta_1} + \sigma_2^2}{\eta_2}$$

In contrast to the ozone comparisons when the different instruments are independently operated, the U.S. meteorological rocketsonde program utilizes a single instrument type with consistent manufacture. In theory, then, if the errors are purely random, σ_2 is zero and the relationship changes to

$$\text{variance} = \frac{\sigma_1^2}{\eta_1 \eta_2}$$

In practice, σ_2 is not zero. This may be due to essentially non-random errors in the satellite data or to possibly some particular equipment feature at a specific site. Gelman (private communication) has indicated that a representative value of σ_1, is about 4 °C and η_1 about 50. Depending on the particular period of study, however, σ_2 can range from 1.6 to 2.5 °C with a value for η_2 of 10. Note that the goal is to be able to discern a trend of 1.5 °C/10 years or 0.15 °C/year - at the 95% confidence limit. In Table 14-4 we see the results of the computation with varying values of σ_2. The worse case scenario suggests that we will be able to detect the temperature impact within 15 years. In the theoretical extreme, if we can achieve a lower value of σ_2, to the value of 1.6, then we will be able to detect a change of 1.2 °C over ten years and if we can ultimately bring it to zero, the value is 0.4 °C over a decade.

The nature of the problem is depicted in Figure 14-18, where we show the period Sept. 1981-Oct. 1983. We note that at the time of this document the data from the Eastern Test Range (Cape Kennedy, Antigua, Ascension Island) were being reprocessed and were not available for this analysis. The data from these sites should be forthcoming in the near future. We also note that the data from Shemya indicated an inconsistency with time that precluded their usage. The σ_2 value at 1 mbar is 1.9 °C while that at 2 mbar is 1.0 °C. In both cases, however, it is clear that it is the value at Primrose Lake that is the major departure from the average and, hence, to the standard deviation. The question is whether the values at Primrose Lake are part of a pattern of satellite bias with latitude or are merely a reflection of some difficulty at site. That there are no other U.S. run sites at these latitudes makes the interpretation extremely difficult. Data from the USSR network are currently under examination.

Finally, we point out that at 2 and 1 mbar, the average value of the TOVS-rocketsonde difference at low to mid-latitudes is about −1 °C and −9 °C, respectively. For the NOAA-6 period Oct. 1980-Sept-1981, not shown, a similar pattern of difference with latitude is indicated, but the average in low latitudes is about −5 °C and −8 °C. Thus a substantive change of about 4 °C is indicated at 2 mbar and about 1 °C at 1 mbar between the operational instruments. This is thought to be caused by the use of filters in the TOVS system that are not exactly reproducable one-to-the-other and stresses the need for a long-term validation/calibration program.

Table 14-4. 95% Confidence Estimates of 10 Year Trends (K/10 Years), as Determined from TOVS Satellite Data with Rocketsonde Verification: σ_2 is the Between Station Standard Deviation (See Text) and t is the Length of the Data Series (Years).

σ_2 (K)			
t(Years)	2.50	1.60	0
10	1.78	1.19	0.4
15	0.97	0.64	0.2

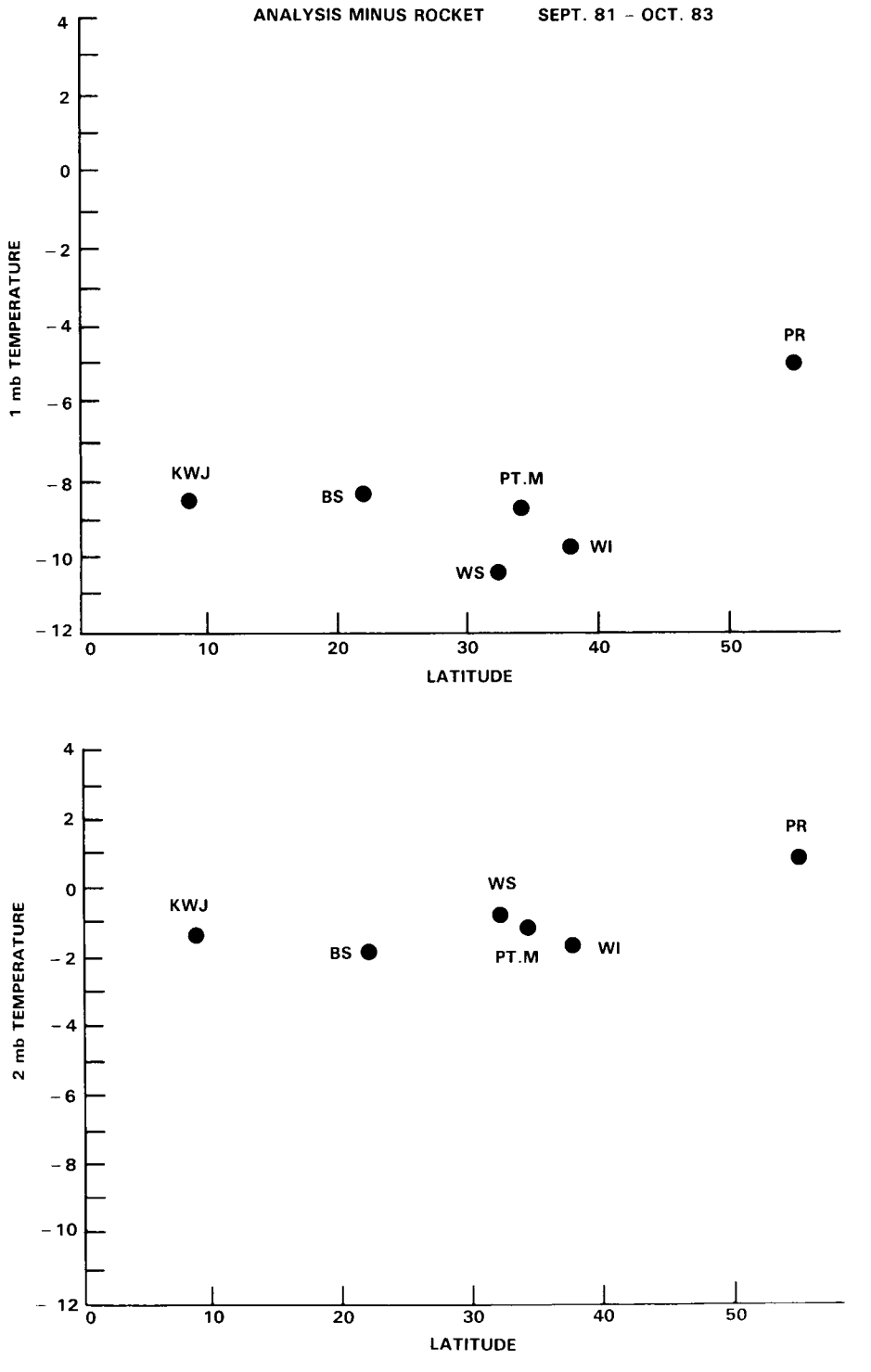

Figure 14-18. NOAA-7 TOVS analysis minus rocketsonde at 2- and 1-mbar for the period Sept. 1981-Oct. 1983.

As stated at the outset, the ozone and temperature are so intimately coupled through radiation, photochemistry and dynamics that any monitoring program must include both parameters as essential components. Toward this, we have indicated above that the requirement exists for a high quality, independent stratospheric temperature measurement system with which to verify the satellite instrument-to-instrument consistency. Such a system does not exist and is a major weakness of the monitoring program.

14.3 SUMMARY

14.3.1 Ozone

- Global trend estimates of total ozone determined from the Dobson spectrophotometer network indicate little overall support for the suggestion of a statistically significant trend during the fourteen year period 1970-1983.

- Trend estimates from 13 ozone balloonsondes indicate statistically significant positive trends in the lower troposphere and negative trends in the lower stratosphere. The interpretation of these results, however, is clouded by uncertainties in instrument behavior and the lack of a global station network.

- Ozone trend estimates from 14 Umkehr stations indicate significant negative trends from 1970 to 1980 in the middle stratosphere that are in substantive agreement with results from one-dimensional numerical models. The observational results are sensitive to the inclusion of a term to account for stratospheric aerosol impact on the measurements and the spatial distribution of the sites, but do not appear sensitive to the inclusion of a 10.7 cm flux variation (an indicator for solar flux variation).

- Examination of the NOAA SBUV-2 satellite measurement program indicates that if the system operates as designed, it is capable of global ozone trend detection in the middle to upper stratosphere as well as total ozone to within about 1.5% over a period of one decade at the 95% confidence level. This is an estimate for the measuring system only, and does not include consideration of natural atmospheric variation which can be quite complex.

- As with other long-term measurement programs, however, it is necessary to examine continually the SBUV-2 instrument performance and satellite products and compare them with independant data. We note, moreover, that the SBUV-2 are inherently limited to total ozone and ozone profiles between 25 and 55 km. If we are to be able to determine ozone trends, unambiguously, from the surface to the overlap region with the SBUV-2 profiles, a high-quality measurement program must exist.

14.3.2 Temperature

- The large cooling in rocketsonde temperatures reported for the early 1970's appears now to be due to a change in the rocketsonde temperature measurement system. Taking this into account, statistically significant negative trends are observed in June rocketsonde data at 40-45 km from 1973-1983 that are in substantive agreement with results from one-dimensional numerical models. These preliminary results will have to be examined further with a more complete data set.

- Examination of the NOAA TOVS stratospheric satellite temperature measurement program indicates that it is essential that the instrument-to-instrument consistency be verified by a high quality, independent data system. Such a system does not exist.

OZONE AND TEMPERATURE TRENDS

- Two independent analyses of lower stratospheric temperatures during the period 1965-1979 are suggestive of a downward temperature trend. Inconsistencies between the two analysis, however, preclude firm conclusions.

CHAPTER 15

TRACE GAS EFFECTS ON CLIMATE

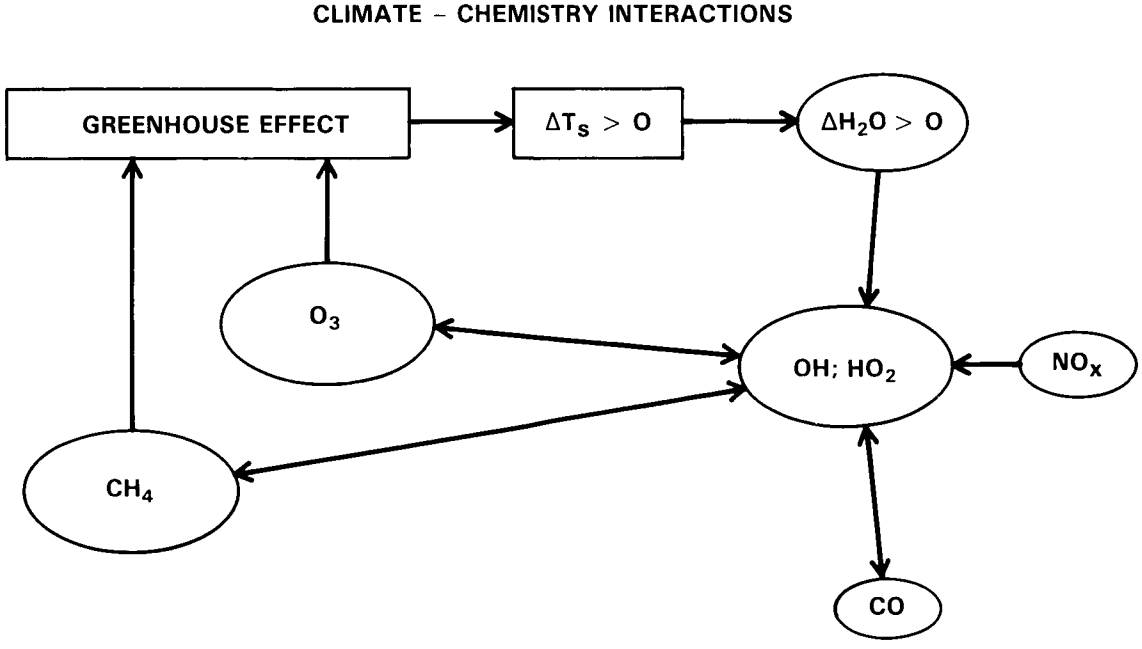

Panel Members

V. Ramanathan, Chairman

L.B. Callis, Jr.
R.D. Cess
J.E. Hansen
I.S.A. Isaksen
W.R. Kuhn
A. Lacis
F.M. Luther
J.D. Mahlman
R.A. Reck
M.E. Schlesinger

CHAPTER 15

TRACE GAS EFFECTS ON CLIMATE

TABLE OF CONTENTS

TABLE OF CONTENTS (Continued)

15.0 INTRODUCTION

15.0.1 Background and Objectives

It is now generally recognized that anomalies in radiative forcings induced by trace gases of anthropogenic origin can become the dominant factor governing climate change on decadal to longer time scales. One particular example is the greenhouse effect of CO_2 increase which has been the subject of scientific curiosity since the latter half of the nineteenth century (Tyndall, 1863; Arrhenius, 1896 and Chamberlin, 1899). Interest in the CO_2 problem gained tremendous momentum during the last two decades; this time period witnessed the development of a hierarchy of climate models with interactive clouds, oceans and cryosphere to examine the climate change that might result from CO_2 increase in the atmosphere. The last two decades also witnessed an unprecedented surge of interest in understanding the sensitivity of the ozone layer to chemical perturbations. The combination of these two developments gave rise to a series of scientific discoveries (see WMO, 1982).

First was the finding that the greenhouse effects of many polyatomic trace gases (e.g., CFCs,) were greater than that of CO_2 increase on a molecule per molecule basis. To cite one example, addition of one molecule of $CFCl_3$ (CFC11) or CF_2Cl_2 (CFC12) to the atmosphere was calculated to have the same surface warming effect as that due to an addition of 10^4 molecules of CO_2. Subsequently, it was uncovered that perturbations in stratospheric ozone can have perceptible effects on tropospheric climate through radiative-dynamical interactions between the stratosphere and troposphere. Furthermore, tropospheric ozone, which until recently was assumed to have negligible climate impact, was shown to be very effective in enhancing the greenhouse effect. Over the years, other gases (CH_4, N_2O, to cite a few) were added to the list of important greenhouse gases, and the list is still growing. Finally, it has been estimated that if the present rates of growth in the concentration of numerous trace gases continue unabated for the next several decades, the surface warming due to trace gases could surpass the observed temperature changes of the past century. In such estimates, the combined effect of increases in trace gas amounts (other than CO_2) was comparable to the greenhouse effect of CO_2 increase. The estimated effects on stratospheric climate were also substantial and far exceed the decadal scale natural variations. General circulation model studies suggested that the tropical tropopause temperatures are sensitive to perturbations in ozone and CFCs.

In effect, these unexpected developments forced the scope of the problem dealing with the greenhouse theories of climate change to be broadened from the CO_2-climate problem to the trace gas-climate problem. This broadening of the scope of the problem posed a number of new theoretical, modeling and observational challenges that could be largely ignored when dealing with the CO_2-climate effects alone. For example, we can no longer ignore the interactions between radiation, chemistry and dynamics, since these determine the stability of the O_3 layer to chemical perturbations. Radiative/dynamical interactions in the troposphere and stratosphere, as well as exchange of trace gases between these two regions, have emerged as key issues because of the potential importance of stratospheric H_2O and O_3 to climate. On the observational front, it became clear that long-term trends in CH_4, N_2O, CFCs, stratospheric and tropospheric O_3, and H_2O are just as important as the trend in CO_2 for understanding long-term climate trends. These requirements have placed extremely stringent demands on the observational platforms both with respect to instrument precision and sampling accuracies.

The two primary objectives of this report are (1) to describe the new scientific challenges posed by the trace gas-climate problem and to summarize current strategies for meeting these challenges, and (2) to make an assessment of the trace gas effects on troposphere-stratosphere temperature trends for the period covering the pre-industrial era to present and for the next several decades. We will rely heavily on the

numerous reports published on the CO_2-climate problem with respect to climate modeling issues, such as: model sensitivity; uncertainty in model results; role of feedback processes such as cloud and ice-albedo feedback. We will discuss in some detail the role of the oceans in governing the transient climate response to time varying CO_2 concentrations. Although the issue of transient climate response is discussed extensively in published reports dealing with the CO_2-climate problem, recent work has shed some new light onto this issue. Furthermore, the transient climate response is a crucial issue for assessing the trace gas effects on past and future temperature trends.

15.0.2 Observed Temperature Trends and Theories of Climate Change

The most frequently used index of climate change is the observed trends in surface-air temperature over the land areas of the globe. The instrumental record of surface-air temperature has recently been extended backwards in time to the year 1860 by Kelly *et al.* (1984). Kelly *et al.'s* time series of annual land averaged (Northern Hemisphere only) surface-air temperature is shown in Figure 15-1. The coldest decades in the record occur prior to the 1900's and the warmest decades are centered around the 1940's. The cooling trend that began around the 1940's ended in the 1970's, and temperatures during the early 1980's are comparable to the peak temperatures registered during the 1940's. Overall, the post-1940 period has been consistently warmer than the pre-1900 period. This tantalizing feature has given rise to numerous theories and plausibility arguments of climate change, most of which involve the observed increase in CO_2 and its greenhouse effect.

Various factors that govern climate change on decadal to longer time scales have been uncovered. Many of the factors fall under the category of externally (external to the climate system) induced variations in the climate forcing terms. The first set of factors involves global scale changes in the radiative heating such as due to: trace gases including CO_2, frequency of volcanic events and variations in solar insolation. Factors involving regional scale changes include changes in radiative forcing (turbidity, deforestation and desertification), thermal forcing (urban heat island) and thermodynamic forcing (alteration of evaporation and precipitation by deforestation is one example). Decadal scale climate change may also result from internal fluctuations in the interactions within the land-ocean-cryosphere-atmosphere system. Such internal fluctuations include variations in ocean heat storage, sea-ice and glaciers.

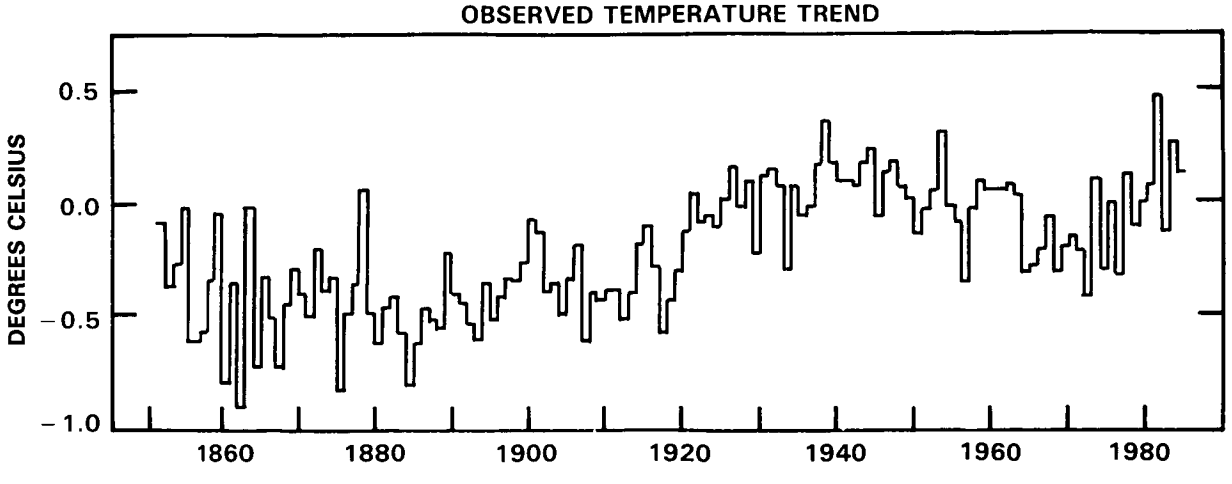

Figure 15-1. Observed surface-air temperature trends for land masses of the Northern Hemisphere (Kelly *et al.*, 1984).

Of the various factors mentioned above, accurate determination of trends has been possible only for CO_2 concentrations (at least since the 1950's). The greenhouse effect of CO_2 has received the most attention (in the literature) as a mechanism for climate change. For all other climate forcing terms, the measurements are either non-existent or, when they exist, the accuracies are insufficient to determine decadal trends. The lack of measurements has prevented identification of the causal factors for the temperature trends of the last 125 years. Nevertheless, the magnitude of the temperature variations revealed in Figure 15-1 provides a valuable measure for assessing the importance of trace gas effects.

Stratospheric temperature trends are discussed in Chapter 14 of this report. The stratospheric temperature records that are representative of hemispheric averages are available only for the past two to three decades. This limited temperature record indicates significant decadal variations of the order of 2-5 K in the mid- to upper-stratospheric temperatures.

15.0.3 Greenhouse Theory

The greenhouse effect is best illustrated by considering the annual and global average radiative energy budget of the earth-atmosphere system. The incoming solar radiation, the reflected solar radiation and the outgoing longwave radiation at the top of the atmosphere have been determined by satellite radiation budget measurements and the values inferred from these measurements are shown in Figure 15-2. The surface-atmosphere system emits to space roughly 236 W m^{-2}, which balances the absorbed solar radiation. The emitted radiation is mostly contained in wavelengths longer than 4 μm and hence, it is referred to as longwave, infrared (IR) or terrestrial radiation.

At a surface temperature of 288 K, the longwave emission by the surface is about 390 W m^{-2}, whereas the outgoing longwave radiation at the top of the atmosphere is only 236 W m^{-2} (see Figure 15-2). Thus, the intervening atmosphere causes a significant reduction in the longwave emission to space. This reduction in the longwave emission to space is referred to as the greenhouse effect. The most important radiatively active atmospheric constituents that contribute to this greenhouse effect are H_2O, CO_2 and clouds. Together these three constituents contribute roughly 90% of the total effect and the H_2O contribution is the largest. The remaining 10% is due to O_3, CH_4 and N_2O. Climate model estimates, as well as simple back-of-the-envelope type calculations, suggest that without the greenhouse effect but with the solar absorption held fixed (at the present-day value) the global average surface temperature would be about 254 K (WMO, 1982).

The radiatively active constituents absorb as well as emit longwave radiation, but the net effect is to reduce the longwave radiation to space. The fundamental cause for the reduction is the decrease in tropospheric temperature with altitude. The radiatively active gases absorb radiation emitted by the warmer surface but emit to space at the colder atmospheric temperature; hence, the net effect is to reduce the radiation to space.

The stratospheric emission and absorption of longwave radiation make an appreciable contribution to the total greenhouse effect and, furthermore, add a considerable degree of complication to the simplified picture presented above. These complications arise because of the increase in temperature with altitude in the stratosphere and because of the non-uniform ozone mixing ratio.

When the concentration of a radiatively active gas is increased, the longwave radiation to space is diminished, which upsets the global energy balance shown in Figure 15-2. If the increase in the gas concentration does not alter the solar absorption, then the greenhouse effect will lead to an increase of radia-

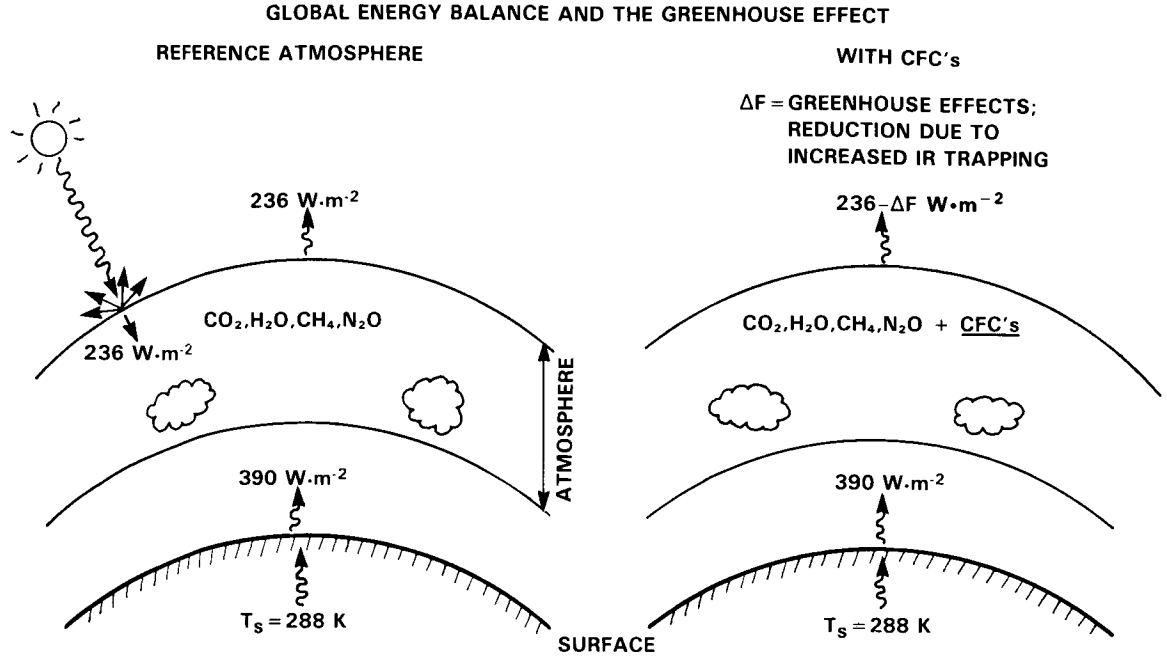

Figure 15-2. Global energy balance and the greenhouse effect.

tive energy available to the surface-atmosphere system. To maintain a balance with the net incoming solar radiation, the surface-troposphere system should warm (in response to the excess radiative energy, i.e., radiative heating) and radiate more longwave radiation to space until the longwave emission to space balances the absorbed solar radiation (i.e., until the energy balance at the top-of-the atmosphere is restored). Hence, the greenhouse theory is based on this fundamental concept of global energy balance for the surface-atmosphere system as a whole. Almost all of the modern day climate models (since the pioneering study of Manabe and Wetherald, 1967) are built around this concept of global-annual energy balance for the surface-atmosphere system. Numerous studies undertaken prior to the Manabe and Wetherald study, and a few recent studies, have misunderstood the implication of this concept of surface-atmosphere energy balance and have made erroneous interpretations of the surface temperature change due to CO_2. These studies infer surface temperature change from surface energy balance alone and ignore the energy balance of the surface-atmosphere system.

15.0.3.1 Effect of Solar Absorption

There is a frequently held misconception about the greenhouse effect. In order to draw an analogy between the CO_2-warming effect and the actual greenhouse, it is frequently mentioned that CO_2 increase enhances the greenhouse effect because it allows solar radiation to penetrate to the surface while absorbing longwave radiation. While it is true that CO_2 is nearly transparent to solar radiation, the transparency to solar radiation is not a necessary condition for enhancing the atmospheric greenhouse effect. For example, H_2O absorbs solar radiation very strongly longwave of 0.9 μm yet it is the strongest greenhouse gas. This is because almost all of H_2O solar absorption occurs within the troposphere (almost entirely within the first 5 km from the surface). Since the troposphere and surface are efficiently coupled by convection, large-scale motions and radiation, energy deposited within the lower half of the troposphere warms the troposphere as well as the surface. Hence, gaseous absorption of solar radiation in the lower troposphere

will have a surface warming effect. However, solar absorption that occurs within the stratosphere (as in the case of O_3) would have a surface cooling effect by reducing the energy available to the surface troposphere system. In summary, solar absorption by a radiatively active gas will add to or ameliorate the greenhouse effect depending on the altitude of solar absorption.

The role of climate models in the greenhouse theory is to estimate the climate response to the excess radiative heating induced by the greenhouse effect. The response, of course, depends on feedback processes involving the land, ocean, and atmosphere (including clouds). In addition to models, empirical studies based on observed satellite data (Cess, 1976) have played an important role in estimating the climate response.

15.0.4 The Trace Gas-Climate Problem

Chemical pollutants in the atmosphere can modify the climate through one or more of the following processes:

(i) Radiatively active gases: If the pollutants are radiatively active in the longwave region, they will enhance the atmospheric greenhouse effect. In particular, several polyatomic trace gases (of anthropogenic origin) have strong absorption features in the 7-13 μm (Figure 15-3). This spectral region is referred to as the atmospheric "window" since in this region the atmosphere is relatively transparent. In the 7-13 μm

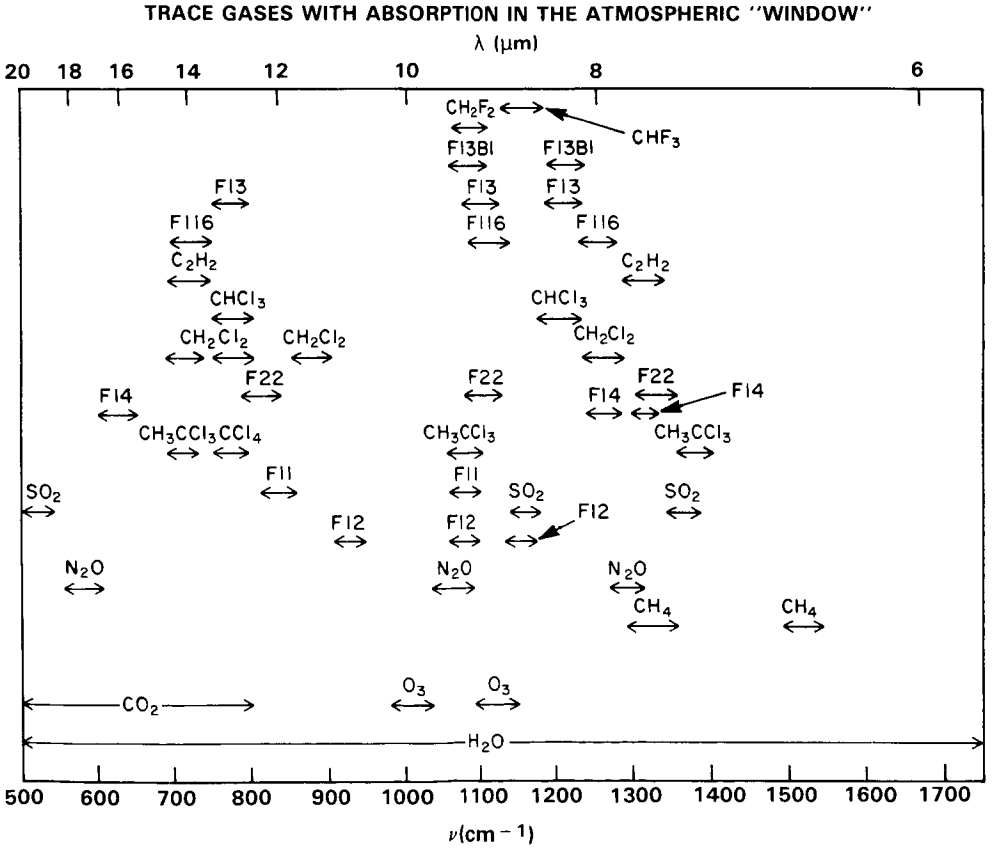

Figure 15-3. Spectral locations of the absorption features of various trace gases. (Kiehl, private communication). The spectral region between 7 to 13 μm is referred to as the atmospheric "window".

C.3

region, roughly 70-90% of the surface and cloud emission escapes to space. Consequently, pollutants with strong absorption features in the 7-13 μm region are quite effective in enhancing the greenhouse effect. In addition, perturbing gases such as CO_2 and O_3, which govern the magnitude of stratospheric longwave emission and absorption, have significant impacts on stratospheric climate.

(ii) Chemically active gases: Gases such as CO and NO, which by themselves have negligible radiative effects, can alter the concentrations of radiatively active gases such as CH_4 and O_3 by chemical interactions.

(iii) Radiatively and chemically active gases: Gases such as CH_4, are chemically active as well as radiatively active. Methane oxidation in the troposphere can lead to increased tropospheric O_3, and the greenhouse effect of the increased tropospheric O_3 can be comparable to that of CH_4 increase. Likewise, breakdown of CFCs in the stratosphere produce reactive chlorine which destroys O_3, and the effect of the O_3 decrease can either amplify or ameliorate the CFC greenhouse surface warming depending on the vertical distribution of the O_3 decrease.

(iv) Ozone change and stratosphere-troposphere radiative interactions: O_3 absorbs solar radiation in addition to absorbing and emitting longwave radiation; hence, stratospheric O_3 modulates the solar and longwave radiation reaching the troposphere. Stratospheric O_3 influences tropospheric climate through a complicated set of stratospheric-tropospheric radiative interactions in both the solar and longwave radiation regimes. The greenhouse effect of tropospheric O_3 also plays a significant role in determining the sensitivity of climate to O_3 change. Consequently, it is very difficult to generalize the nature, the sign, or the magnitude of the potential climate change due to O_3 perturbations.

(v) Radiative-chemical interactions: These effects arise because of the strong temperature dependence of the reaction rates of the various chain reactions in the stratosphere that ultimately govern the stratospheric O_3 concentration. The net effect of this dependence is such that a temperature increase (decrease) in the upper stratosphere leads to O_3 decrease (increase). Hence, stratospheric cooling due to increased CO_2 leads to an increase in O_3 which tends to compensate some of the CO_2 induced cooling. This O_3-temperature feedback results in a negative feedback on temperature perturbations in the stratosphere. Furthermore, a local O_3 decrease allows deeper penetration of sunlight and permits enhanced O_3 production at lower levels. This interaction between O_3 change and penetration of sunlight has a significant impact on the profile of O_3 change.

(vi) Interactions involving stratospheric dynamics: Large-scale motions in the stratosphere have a strong impact on some of the climate change processes described earlier. First, the climate effect of O_3 change depends crucially on the vertical and latitudinal distribution of O_3 change in the lower stratosphere which is determined by the interactions between transport and chemistry. The second interaction concerns the effect of altered dynamics due to changes in stratospheric diabatic heating (from O_3 change) on the transport of constituents. Perhaps the most important dynamics-transport effect concerns the interaction between trace gas perturbation, tropopause temperature, and stratospheric H_2O.

(vii) Climate-chemistry interactions: The greenhouse warming of the surface causes an enhancement in the evaporation of moisture from the land and oceans resulting in an increase in the tropospheric H_2O. This, in turn, through photolysis and H_2O chemistry can perturb OH in the troposphere. Since OH plays a dominant role as a cleansing and oxidizing agent for tropospheric gases (including pollutants), the altered OH can potentially perturb the concentration of radiatively active species such as CH_4 and O_3 (and possibly others).

The above description basically gives the scope of the problem that we will be dealing with in this report. The nature of the various interactive processes and the potential surface temperature effect of various radiative perturbations are described schematically in Figure 15-4. The surface temperature change shown in Figure 15-4 for O_3 is for a uniform change in O_3 within the troposphere and stratosphere. Since the surface temperature effects of O_3 depend very strongly on vertical distribution of the O_3 change, the results shown in Figure 15-4 can not be scaled for non-uniform O_3 change. Finally, the climate sensitivity to radiative perturbation depends on feedbacks involving temperature, H_2O, clouds, ice and snow cover, and on feedbacks between the ocean and the atmosphere (and possibly the biosphere). A comprehensive discussion of these topics is beyond the scope of this report and, furthermore, is unnecessary since several detailed reports (Charney, 1979; Smagorinsky, 1982) are available on this topic.

15.0.5 The Need for Model Studies

The nature of the radiative forcing arising from the myriad of interactive processes mentioned earlier is so complex that numerical models with varying degrees of complexity are needed to identify the magnitude of the various processes. The array of models needed for the trace gas-climate problem include:

(i) 1-D radiative-convective models to identify the important greenhouse effects and tropospheric-stratospheric radiative interactions.

(ii) 1-D radiative-convective chemistry models to examine the role of radiative-chemistry interaction in the stratosphere.

(iii) 2-D transport-chemistry models to estimate the magnitude of seasonal and latitude variations of O_3 change.

(iv) 2-D "fixed dynamical heating rate" models to examine the possible magnitude of temperature changes in response to trace gas perturbations.

(v) 3-D stratospheric models: These models with comprehensive treatment of radiation and dynamics can play a central role in elucidating the role of dynamics in governing the interaction between radiative perturbations and temperature perturbations. Furthermore, these models are necessary to examine the potentially important problem of how alterations in stratospheric meridional and vertical thermal gradients impact tropospheric dynamics through stratosphere/troposphere dynamical interactions. There is also another important class of 3-D models concerned primarily with atmospheric transport and chemistry. Such models are essential for evaluating the robustness of the conclusions of the 1-D and 2-D models concerning O_3 perturbations as well as for understanding the nature of interactive chemistry and transport. These 3-D models should ultimately lead to the development of self-consistent 3-D models that account for the interactions between radiation, chemistry and dynamics.

(vi) 3-D climate models with and without interactive oceans: In these models, the perturbations in trace gases are prescribed. The model determines the climate change (troposphere and stratosphere) due to the imposed perturbations. These models, in conjunction with the 1-D radiative-convective models, play a central role in the assessment of trace gas effects on climate.

More detailed discussions of these models are given in Section 15.2.

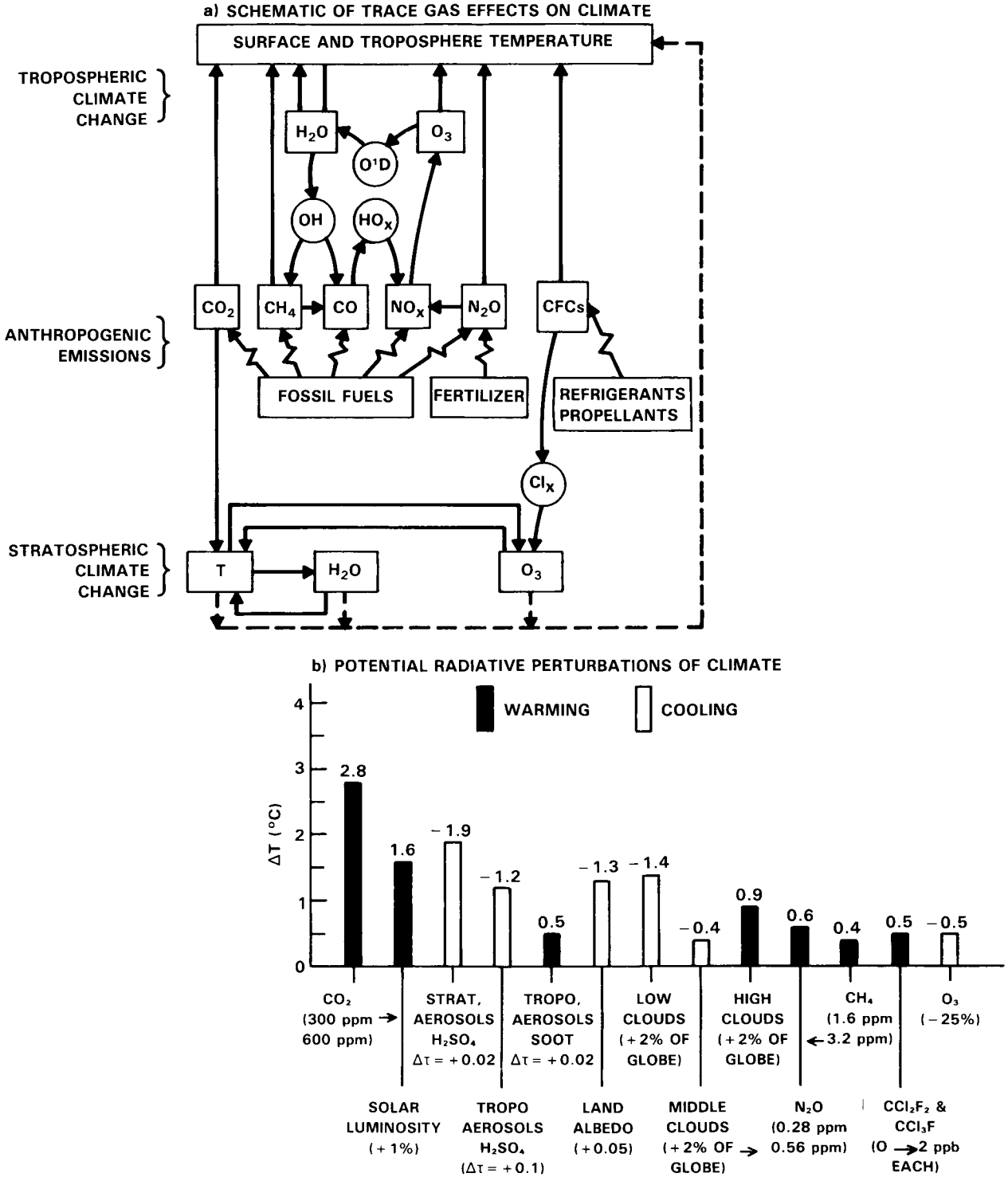

Figure 15-4. (a) Examples of climate effects due to chemically and radiatively active gases (Ramanathan, 1980). (b) One dimensional radiative-convective model estimates of surface temperature effects of various global radiative perturbations. All of the results, except for CH_4, and the figure are adapted from Hansen *et al.*, 1981. The CH_4 result was obtained as follows: The radiative forcing of doubled CH_4 as given in WMO (1982) is multiplied by the climate sensitivity of Hansen *et al.* (1981) model to obtain ΔT_S.

15.1 NATURE OF RADIATIVE FORCING

Radiative forcing due to trace gases can be considered either in terms of the changes in the fluxes of radiative energy into and out of the entire system (i.e., surface-troposphere system) or in terms of the change in the vertical distribution of the radiative heating rates. The choice between the two quantities depends on the region of interest. Within the troposphere, the vertical mixing of sensible and latent heat by convection and large scale motions is considered to be quite rapid compared to the time scales associated with radiative adjustments. As a result, the vertical distribution of the tropospheric temperature change is largely governed by dynamical processes while the mass weighted tropospheric temperature change is governed by the radiative forcing of the column. Hence, as a first approximation, we can ignore the details of the vertical distribution of the tropospheric radiative forcing and focus, instead, on the radiative forcing of the entire surface-troposphere system. Since the surface-troposphere radiative forcing is simply the change in the net radiative flux at the tropopause, it is rather straightforward to assess the importance of trace gas radiative forcing. The only minor complication is that we have to account for changes in stratospheric temperature and longwave emission in order to compute the flux changes at the tropopause. Within the stratosphere, however, time scales associated with radiative adjustments are comparable to, or faster than, those associated with dynamical processes. As a result, the magnitude of the stratospheric climate change is influenced strongly by the vertical distribution of the radiative heating rate perturbation within the stratosphere.

The trace gas radiative forcing is estimated from radiation model calculations by fixing all other parameters (e.g., temperature, humidity) in the model and then computing the changes in the radiative flux due solely to the change in the constituent of interest. Such estimates are fundamental to a proper understanding of the temperature response yielded by climate models. The longwave absorption features of the trace gases that are considered in this report are shown in Tables 15-1a and 15-1b.

15.1.1 Greenhouse Gases With Weak Solar Absorption

With the exception of H_2O, O_3 and NO_2, all other gases shown in Tables 15-1a and 15-1b have either weak or no absorption bands in the solar spectrum. Increasing the concentration of the gases with weak solar absorption subjects the troposphere to a net radiative heating accompanied by either a strong (e.g., CO_2) or weak (e.g., CH_4) longwave cooling of the mid to upper stratosphere.

15.1.1.1 CO_2 - Current Understanding and Recent Findings

The best known example of tropospheric heating/stratospheric cooling is the radiative forcing due to doubling of CO_2 (Figure 15-5). The significant enhancement of the cooling rate from the middle stratosphere to lower mesosphere shown in Figure 15-5 is due to the increase in emission to space from the wings of the non-overlapping Lorentzian lines within the CO_2 15 μm band system. The vertical distribution of the cooling rate perturbation (Figure 15-5a) is largely governed by the vertical temperature gradient (the temperature increases with altitude from 15 to about 50 km and decreases above 50 km). Since the 15 μm Planck function (i.e., CO_2 emission) increases exponentially with temperature, the cooling rate perturbation follows the temperature profile.

As opposed to the stratospheric effects, the CO_2 increase enhances the tropospheric radiative heating (Figure 15-6). The surface-troposphere radiative heating (flux change at the tropopause) has strong latitudinal gradient varying from about 4.5 to 5 W m^{-2} in the tropics to about 2 W m^{-2} in the polar region. The

Table 15-1a. Summary of Spectroscopic Data As Given in WMO (1982). More Recent Compilation Can Be Found in Smith *et al.* (1985).

Molecule	Band[1]	Rough spectral range (cm^{-1})	Band Strength[2] at 296 K (cm^{-2} atm^{-1})	Comments[3]
H_2O	rotation	0 - 1650	1306	Current improvements underway —
	υ_2	640 - 2800	257	problem of the continuum absorption
CO_2	15 μm system?	550 - 800	$\simeq$ 220	Current improvements underway
	10 μm system?	850 - 1100	0.04	
	4-3 μm system?	2100 - 2400	$\simeq$2440	
O_3	υ_3		312	V_3 band intensity to be multiplied by
	υ_1?	950 - 1200	13	1.11?. Problem of the half-widths
	$\upsilon_2+\upsilon_3-\upsilon_2$?		10	(constant with quantum?)
	υ_2	600 - 800	16	
N_2O	υ_2	520 - 660	24	Current improvements underway
	υ_1	1200 - 1350	218	Line intensities re-examined
	υ_3?	2120 - 2270	1247	
CH_4	υ_4	950 - 1650	134	Current improvements underway
CH_3D	υ_3 and υ_6	1000 - 1425	105	
SO_2	υ_3	1300 - 1400	763	Current improvements underway for
	υ_1?	1000 - 1200	87	these three bands
	υ_2?	400 - 600	97	
NO_2	υ_3	1550 - 1650	1515	Current improvements underway for
	υ_2?	600 - 900	92	these three bands
NH_3	υ_2	500 - 1350	534	Data recently revised
	rotation?	20 - 400	440	
HNO_3	υ_4	1330	680	A difficult molecule. Requires additional
	υ_2	1670 - 1750	500	work
OCS	υ_3?	1950 - 2100	1954	The fundamental υ_2 band is not compiled
	υ_1	810 - 890	27	and should be
H_2CO		compilation starting at 270 cm^{-1} plus far infrared		Bands active in the thermal IR should be compiled
HOCl	υ_1	compilation starting at 3400 cm^{-1}		Bands active in the thermal IR should be compiled
CH_3Cl	υ_1, υ_4, $3\upsilon_6$	compilation starting at 2900 cm^{-1}		Bands active in the thermal IR should be compiled. The data does exist
H_2O_2		1200-1350	318	Preliminary
C_2H_2	υ_5	640 - 810	951	Should be developed
	$2\upsilon_5 - \upsilon_5$?	640 - 820	112	
HCN	υ_2	580 - 850	822	Other bands available
C_2H_6	υ_9	700 - 950	36	Other bands available
C_2H_4	υ_7	900 - 1100	455	Preliminary
C_3H_8		735 - 760	2	Preliminary
CFCs		800 - 1200		Not yet compiled in data catalogs —
F11		850 - 1250		Laboratory spectra available
F12		1070 - 1250		
F13				

[1] A question mark indicates bands less important than the main bands but which could eventually play a role in radiation modeling (to be checked).
[2] Actually, the sum of the strengths of the lines present in the compilation (296 K). Isotopic band intensities are not added except for the estimate of a band system intensity (e.g., the 15 μm CO_2 system).
[3] Most comments were taken from L.S. Rothman (private communication).

Table 15-1b. Absorption Features of Atmospheric Trace Gases — More Recent Compilations.

Molecule	Rough Spectral Range (cm^{-1})	Band Intensity (cm^{-1} (atm cm)$^{-1}$ 296K) Measurement Range	Recent Value	Reference*
1. CFCs				
$CFCl_3$ (F11)	800–900	1540–1828	1828	K,P,S
	1050–1100	531–721	679	
CF_2Cl_2 (F12)	875–950	1265–1490	1446	K,P,S
	1060–1125	1141–1226	1141	
	1125–1175	728–821	767	
CF_3Cl (F13)	750–825	116–145	116	P
	1075–1125	1758–2311	1758	
	1175–1240	2116–2767	2116	
CF_4 (F14)	600–650	39–57	39	P,S
	1250–1300	3850–5472	5472	S
$CHClF_2$ (F22)	780–840		219	N;R
	1080–1140		637	
	1280–1340		101	
C_2F_6 (F116)	880–740		135	P
	1080–1150		975	
	1220–1280		3374	
2. Others				
CCl_4	730–810	1214–1869	1325	P
$CHCl_3$	740–820	797–1107	930	P
	1190–1250	129–190	129	
CH_3CCl_3	700–750		277	N;R
	1050–1110		154	
	1360–1410		13	
CHF_3	1110–1160	2224–3540	2693	P,S
CH_2F_2	1060–1120	1230–1485	1230	P,S
$CBrF_3$	1060–1110		1908	P
	1180–1240		1914	
PAN	570–620		72	N;R
	760–820		296	
	1130–1190		301	
	1270–1330		251	
	1700–1760		531	

*K: Kagan *et al.* (1983); P: Pugh, L.A., and K. Narahari Rao (1976); N;R: Measured values by Niki (Ford Motors, Dearborn, MI) and cited in Ramanathan *et al.* (1985); S: Smith *et al.* (1985).

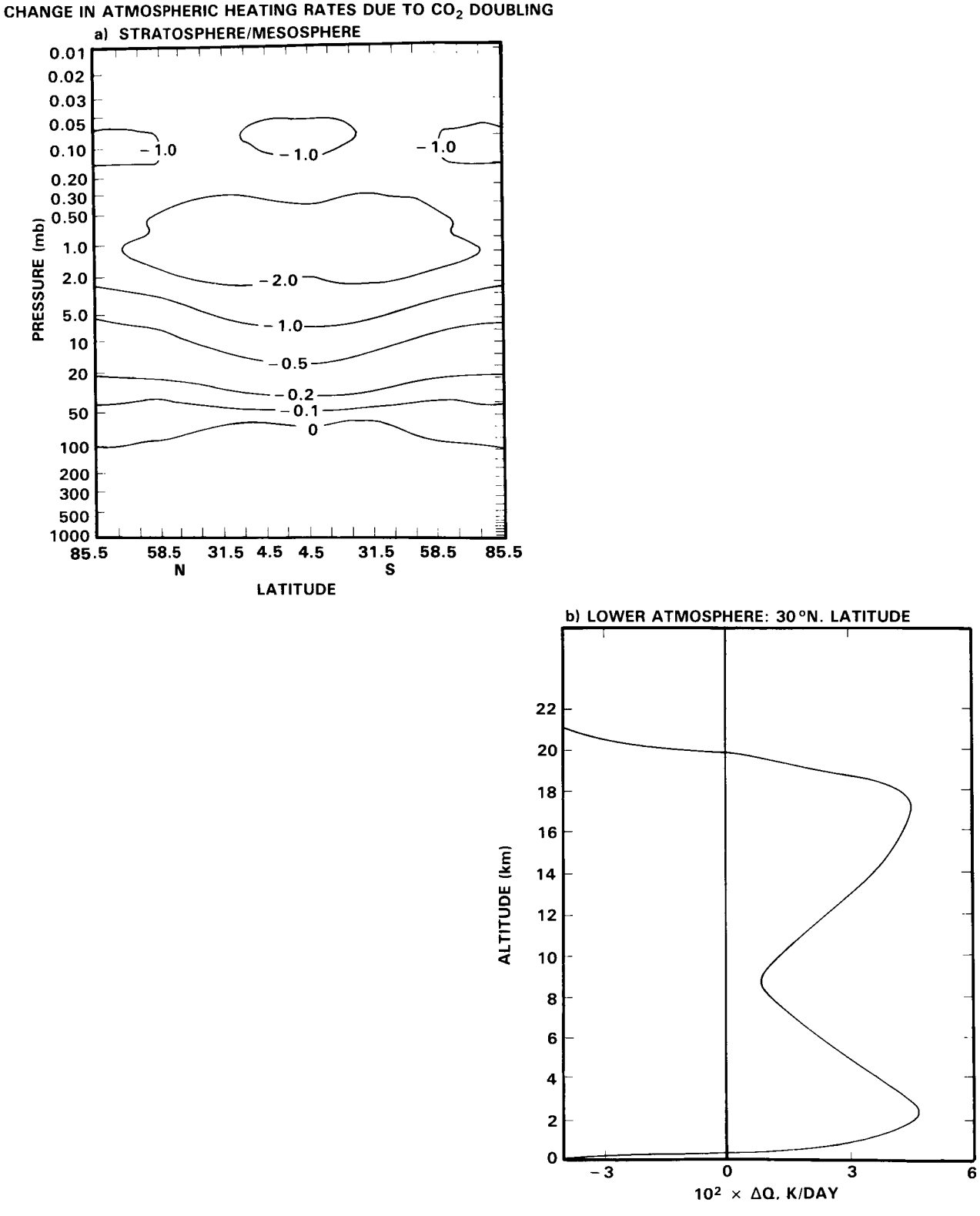

Figure 15-5. Computed change in radiative heating rates for a doubling of CO_2: (a) Stratosphere-mesosphere; Fels *et al.,* 1980; (b) troposphere & lower stratosphere; Ramanathan, 1981

global average value of the surface-troposphere heating (ΔQ) is about 4.2 W m^{-2} (for a CO_2 doubling) and ΔQ scales roughly as:

$$\Delta Q = c \ln F$$

where c is a constant and F is the ratio of CO_2 concentration to a reference value. For a doubling of CO_2, the global average ΔQ consists of roughly 1.6 W m^{-2} due to enhancement in downward emission from the stratosphere (mostly due to CO_2) and about 2.6 W m^{-2} due to decrease in the upward flux at the tropopause, and both these quantities vary significantly with latitude (Figure 15-6).

In addition to the 15 μm bands, CO_2 has absorption features in the 7.6 μm and 10 μm (2 bands) region and also has several bands in the solar spectrum (Table 15-2). The 7.6 μm and 10 μm bands have frequently been ignored by climate models. For CO_2 doubling, the 7.6 μm bands have a negligible effect

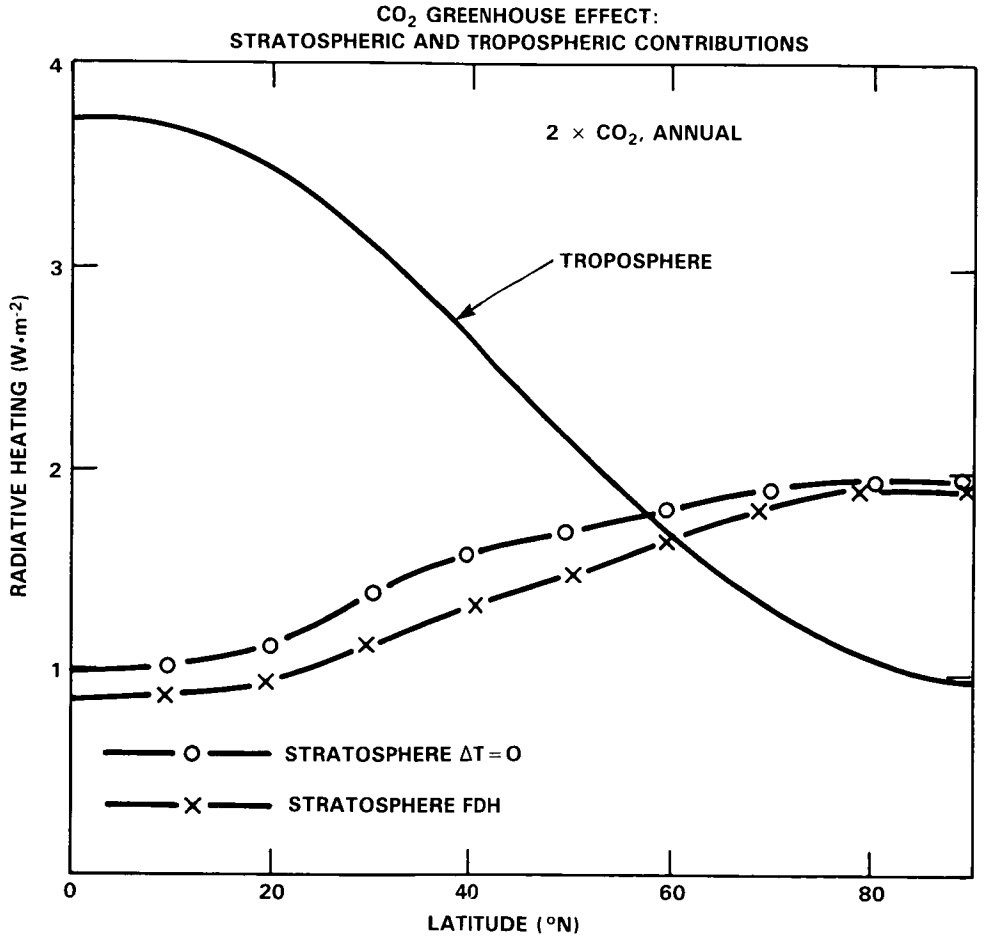

Figure 15-6. Separate contributions from the troposphere and the stratosphere to the total heating of the surface-troposphere system, due to doubled CO_2, for annual mean conditions. The stratosphere contribution is given by the increase in the downward radiative flux from the stratosphere. Stratospheric temperatures are held fixed as CO_2 is increased for the $\Delta T = 0$ curve, whereas they are allowed to change according to the fixed dynamical heating assumption (See Section 15.2.1) for the FDH curve. (Ramanathan *et al.*, 1979).

and the two bands in the 10 μm region contribute roughly 5 to 10% (of the 15 μm greenhouse effect). The solar bands have negligible impact on the stratospheric heating rates and on the surface-troposphere radiative forcing. However, they have a non-negligible impact on the partitioning of the forcing between the surface and the troposphere. For example, for a doubling of CO_2, the increased CO_2 solar absorption within the troposphere reduces the surface absorption of solar radiation by about 0.3 W m^{-2} and enhances the tropospheric solar absorption by about 0.4 W m^{-2} (Hansen *et al.*, 1981). In the 15 μm region, H_2O also has strong absorption features, and the overlapping of H_2O absorption with CO_2 bands ameliorates the greenhouse effect. Most climate models include the overlapping effect of H_2O lines but ignore the strong H_2O continuum absorption (in the 15 μm region) which was only discovered in the early 1970's. Table 15-3 illustrates the influence of H_2O-CO_2 overlap on the CO_2 radiative forcing for midlatitude summer conditions when the ameliorating effect of H_2O-overlap is expected to be large. The H_2O absorption reduces the surface heating (i.e., enhanced CO_2 downward emission) by an order of magnitude but ameliorates the surface-troposphere heating by only 15%, half of which is due to the continuum absorption. The model results in Table 15-3 are for clear-sky conditions, and the inclusion of clouds (accounted for in most climate models) ameliorates the surface-troposphere heating by another 10 to 20%.

In summary, the radiative forcing due to CO_2 arises from a complex chain of processes, and it is reasonably straightforward to account for most of these processes. However, attempts (in the published literature) to oversimplify the radiative calculations have led to significant errors and misinterpretations of the greenhouse effects (e.g., Newell and Dopplick, 1979; Idso, 1980).

Table 15-2. Long-Wave and Solar Bands of CO_2

Spectral Region, μm	Band Type
	Long-Wave Bands
12–18	Fundamental, isotopic, and hot bands (Total of 76 bands)
10	Two hot bands (9.4 and 10.4 μm region)
7.6	Isotopic bands
	Solar Bands
4.3	Fundamental, isotopic, and hot bands (see Dickinson [1972] for a listing of the number of bands in each spectral region)
Others	There are numerous combination and overtone bands between 1 and 3 μm. See Dickinson (1972) for more details.

Table 15-3. Effects of 12-18 μm H_2O Absorption on the Radiative Forcing Due To CO_2 Doubling. Clear-sky Tropical Atmosphere Conditions. (Kiehl and Ramanathan, 1983)

	Radiative Forcing (W m^{-2})	Comments
(i) Surface-troposphere heating		
CO_2 only	6.4	Change in the net
CO_2 + H_2O lines	5.9	longwave flux at
CO_2 + H_2O lines + continuum	5.4	the tropopause
(ii) Surface heating		
CO_2 only	6.9	Increase in the
CO_2 + H_2O lines	3.6	downward emission
CO_2 + H_2O lines + continuum	0.4	

15.1.1.2 Gases with Absorption Bands in the 7-13 μm Region

The atmosphere is relatively transparent in this spectral region as revealed dramatically in the spectral distribution of the longwave emission to space measured by the NIMBUS 3 IRIS instrument (Figure 15-7). The maximum emission by the planet occurs in the 7-13 μm region where roughly 70-90% of the radiation emitted by the surface and clouds escapes to space. CH_4, N_2O and most other anthropogenic trace gases (in particular, the polyatomic trace gases) have strong absorption features in this spectral region and, hence, are effective in enhancing the greenhouse effect. CH_4 and N_2O, in their present-day concentrations of 1.65 and 0.30 ppmv, respectively, contribute about 3.5 W m^{-2} to the radiative forcing of the surface-troposphere system, which is comparable to the greenhouse effect due to a doubling of CO_2.

The vertical distributions of the forcing due to increases in CH_4, N_2O and CFCs are shown in Figure 15-8. The corresponding radiative forcing of the surface-troposphere system and that of the surface alone are shown in Table 15-4 for comparison purposes. The model results shown in Figure 15-8 and Table 15-4 are clear-sky estimates computed with tropical atmospheric profile. The tropical profile is chosen since CFC effects on atmospheric radiative heating rates are a maximum in the vicinity of the tropical tropopause (e.g., see Dickinson *et al.*, 1978). The surface-troposphere radiative forcing for globally averaged conditions is also significantly smaller than the tropical clear-sky values shown in Table 15-4; for example, for CO_2 doubling, the clear-sky tropical profile yields a value of 5.4 W m^{-2} (see Table 15.3 and also Table 3 of Kiehl and Ramanathan, 1983) as opposed to about 4.2 W m^{-2} for globally averaged conditions.

The CH_4 and N_2O effects shown in Figure 15-8 are similar to those of CO_2 in many respects. They all show tropospheric heating and stratospheric cooling. Furthermore, the surface radiative heating (i.e., downward emission at the surface) is only a small fraction of the total greenhouse effect, as in the case

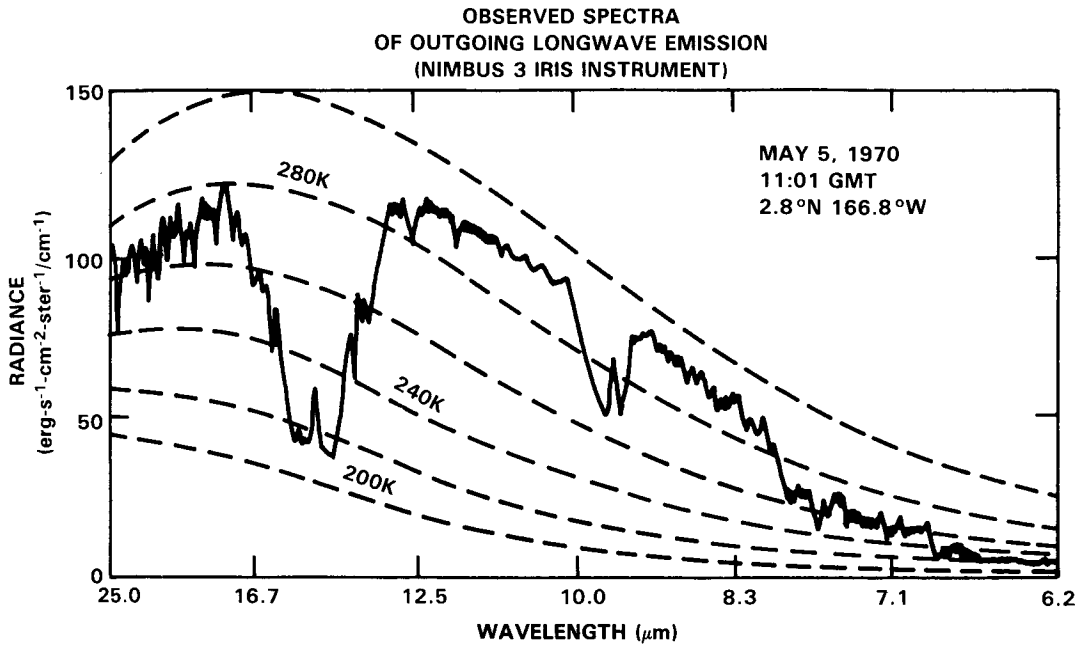

Figure 15-7. Sample spectra from the IRIS instrument on board NIMBUS-3 satellite. The dashed lines indicate the effective radiation temperature for different wavelengths. Source: Hanel *et al.,* 1972.

Table 15-4. Surface-Troposphere Radiative Forcing Due To Increase in CH_4, N_2O and CFCs for Clear-sky Tropical Profile (Source: Kiehl, 1985).

Units: W m^{-2}

	$2 \times N_2O$	$2 \times CH_4$	CFC 11 & 12 (0 → 2 ppb)	$2 \times CO_2$**
Surface-troposphere forcing*	0.7	0.9	1.2	5.38
Surface forcing	0.12	0.15	1	0.4

* Downward stratospheric emission contributes about 10% for N_2O; and about 2% for CH_4 and CFCs.

** The CO_2 results are taken from Kiehl and Ramanathan (1983). The values given here are taken from their narrow band Malkmus model results (see Table 3 of Kiehl and Ramanathan, 1983).

of CO_2. However, the enhancements in stratospheric cooling rates for CH_4 and N_2O doubling are an order of magnitude smaller than that of a doubling of CO_2.

The CFC effects differ significantly from CH_4, N_2O and CO_2 in the following aspects: (a) the maximum in the local heating rate occurs at the tropopause and (b) the CFC surface heating (i.e., downward

TRACE GAS INCREASE AND ATMOSPHERIC RADIATIVE HEATING RATES
(TROPICAL ATMOSPHERE); SOURCE: KIEHL (1985)

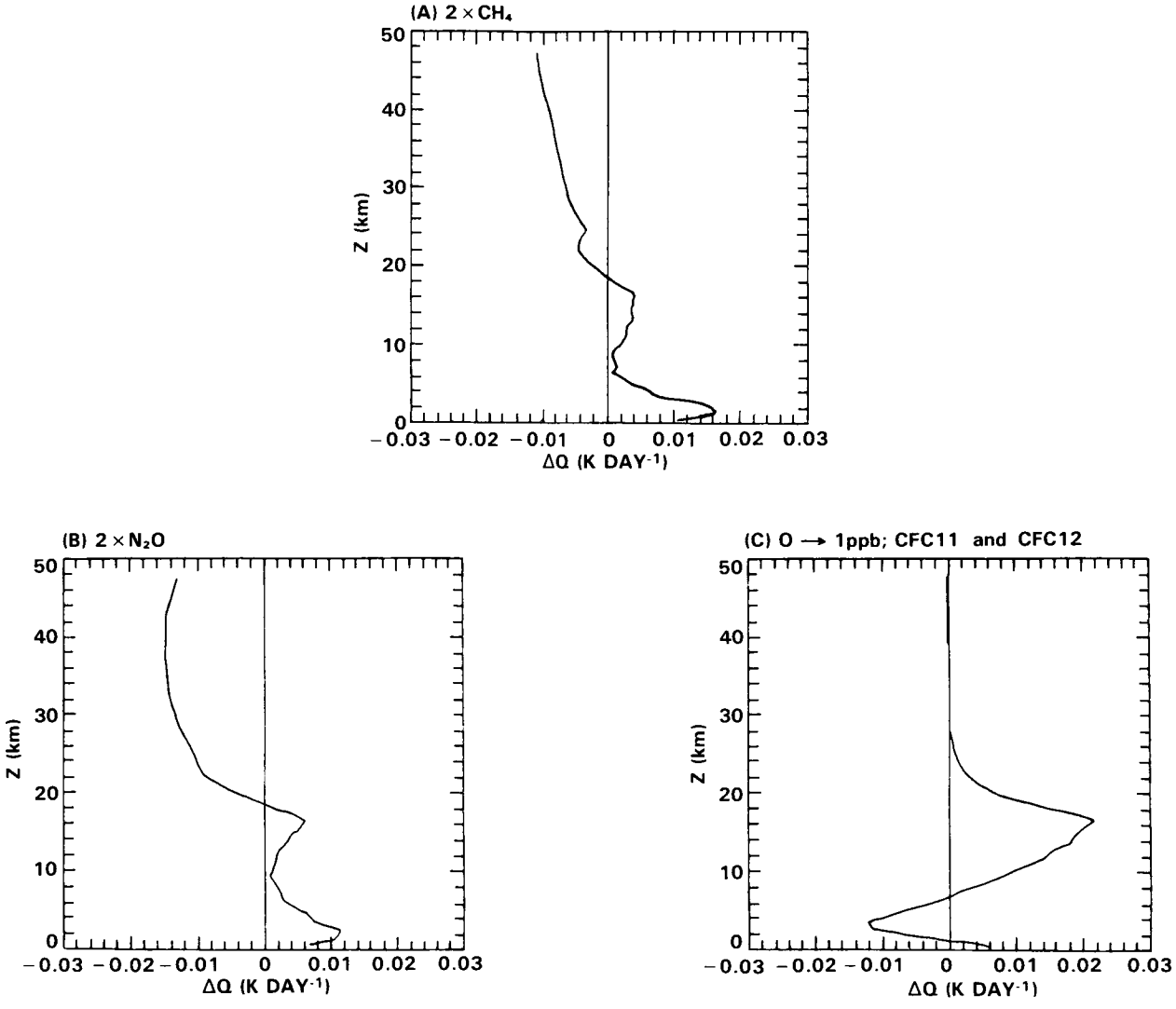

Figure 15-8. Computed change in radiative heating rates (ΔQ) due to trace gas increase. The calculations are for clear-sky conditions and employ tropical profile.

emission at the surface in Table 15-4) is almost equal to the surface-troposphere forcing, whereas, for the other gases the surface heating is only a small fraction of the total effect. By scaling the CFC greenhouse effect of about 1.2 W m^{-2} at the tropopause for a 0 to 1 ppbv (each of CFC11 and 12) increase with that (5.4 W m^{-2}; see Table 15-3) for a CO_2 doubling, we see that the radiative forcing resulting from the addition of 1 molecule each of CFC11 and 12 is more than that due to the addition of 10^4 molecules of CO_2. The principal reasons for the extreme efficiency of CFCs are: CFC band strengths are several times stronger than those of CO_2 (see Tables 15-1a and 1b); CFC absorption increases linearly with its concentration, whereas the CO_2 greenhouse effect scales logarithmically with the CO_2 amount; and CFC absorption occurs in the atmospheric window (see WMO, 1982, for further discussions).

15.1.2 Greenhouse Gases with Strong Solar Asorption: O_3

On a global-annual average, stratospheric O_3 absorbs about 12 W m^{-2} of solar radiation and about 8 W m^{-2} of 9-10 μm radiation emitted by the surface-troposphere system. It also emits about 4 W m^{-2} (2.5 W m^{-2} up to space and 1.5 W m^{-2} down to the troposphere). Thus, stratospheric O_3 contributes to a net heating of the stratosphere which is balanced by longwave cooling due to CO_2 and H_2O. In effect, stratospheric O_3 helps modulate the solar and longwave fluxes to the troposphere.

The largest impact of stratospheric O_3 change is felt in the stratosphere itself (Figure 15-9). The solar heating rate perturbation peaks in the vicinity of the stratopause. With respect to the longwave heating rate perturbation (Figure 15-9b), O_3 reduction causes a decrease in the lower stratospheric heating rates (due to decreased absorption of surface emission) and an increase in the mid to upper stratosphere heating rates (due to decreased emission).

Reduction in stratospheric O_3 can modify the surface temperature via two competing processes: more solar radiation is transmitted to the surface-troposphere system, thereby contributing to a surface warming; on the other hand, the cooler stratosphere (due to decreased solar and longwave absorption) emits less to the troposphere which would tend to cool the surface. The solar warming and the longwave cooling effects are comparable in magnitude, and the magnitude as well as the sign of the net effect depends very critically on the magnitude of the stratospheric temperature change which in turn depends strongly on latitude and season.

The magnitude of the longwave cooling effect depends on the altitude of O_3 reduction, whereas the magnitude of the solar warming effect depends solely on the reduction in total column amount. Consequently, changes in stratospheric O_3 can have different effects on the surface temperature depending on the vertical distribution of the O_3 change. This dependence is revealed in Figure 15-10 which shows the computed change in surface-troposphere radiative heating for two different profiles of O_3 change. While the uniform O_3 reduction leads to a net radiative cooling, the non-uniform O_3 change profile (denoted by CFM; Figure 15-10b) leads to a net increase in the heating. For the CFM perturbation, most of the decrease in O_3 occurs in the upper stratosphere and, hence, the reduction in longwave emission (due to stratospheric cooling) is not "felt" by the troposphere with the result that the solar warming dominates over the longwave cooling effect. The profile shown in Figure 15-10a is the ozone change vs. altitude calculated by models using the photochemistry which was current in 1979. Today's (1985) one-dimensional models show significantly less ozone change in the lower stratosphere (see Chapter 13). Two-dimensional models show a highly latitude-dependent ozone change in the lower stratosphere with increases predicted at low latitudes and decreases at high latitudes. (see Chapter 13).

Since the net effect on tropospheric radiative forcing is obtained as a difference between solar and longwave effects, it depends strongly on latitude and season. In middle to higher latitudes, even the sign of the effect depends on season (e.g., see the CFM curve in Figure 15-10).

Although the troposphere contains only about 10% of the total O_3, the longwave opacity of present tropospheric O_3 amounts is nearly the same as that of present stratospheric O_3 amounts (due to the pressure broadening effects on the O_3 9.6 μm band line shape). Furthermore, both solar and longwave effects of tropospheric O_3 change influence the surface temperature in the same direction in contrast to the opposing solar and longwave radiative effects induced by stratospheric O_3 change. As a result, surface temperature is significantly more sensitive to changes in tropospheric O_3 than to stratospheric O_3 changes. In fact,

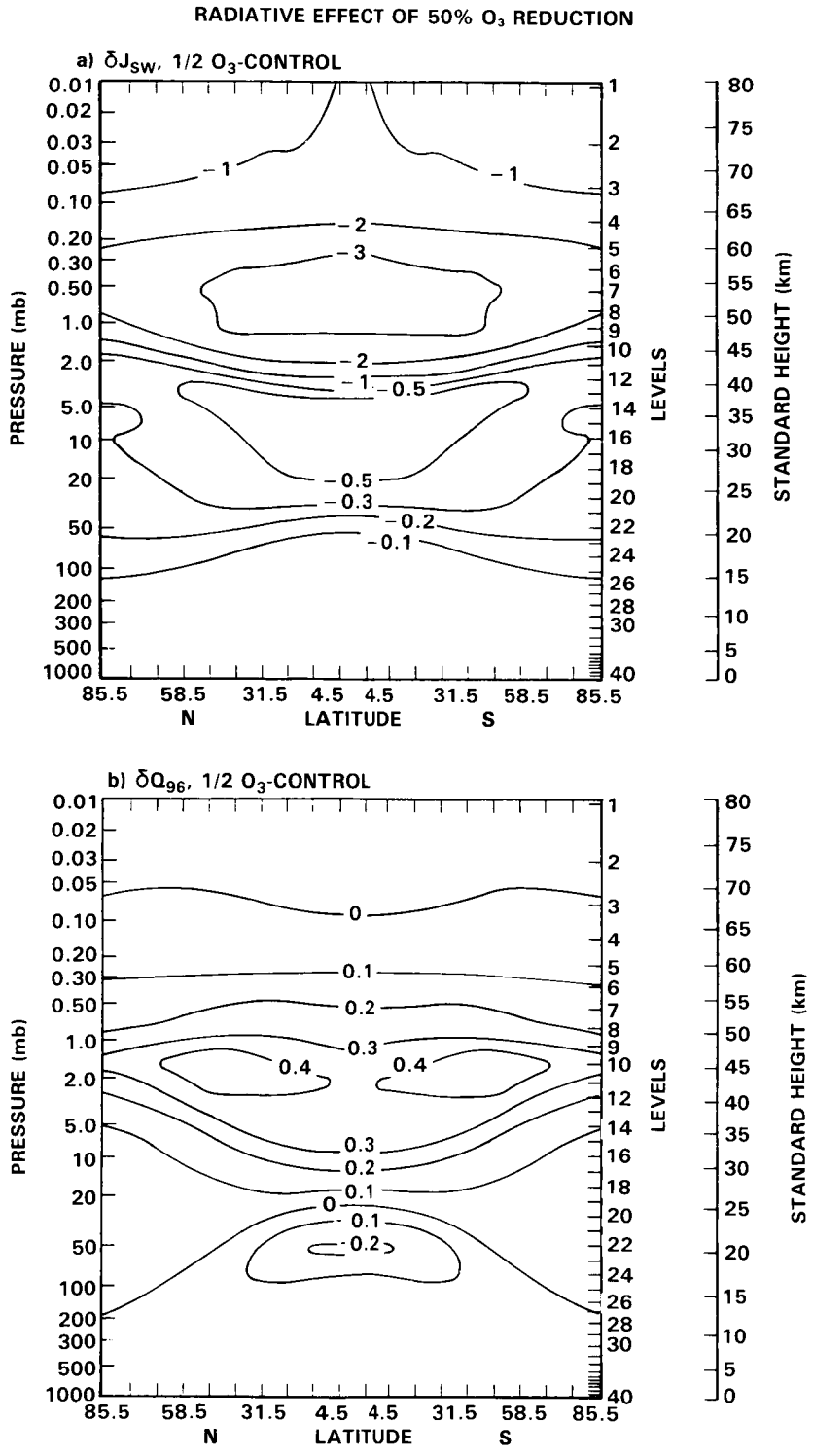

Figure 15-9. Radiative drives (K day^{-1}) for the ozone reduction experiments: (a) δJ_{SW}, the change in shortwave heating due to a 50% ozone reduction; and (b) $\delta Q_{9.6}$, the change in 9.6 μm O_3 band heating rate due to a 50% ozone reduction, with the temperatures in all cases held fixed at the control values. Source: Fels *et al.*, 1980.

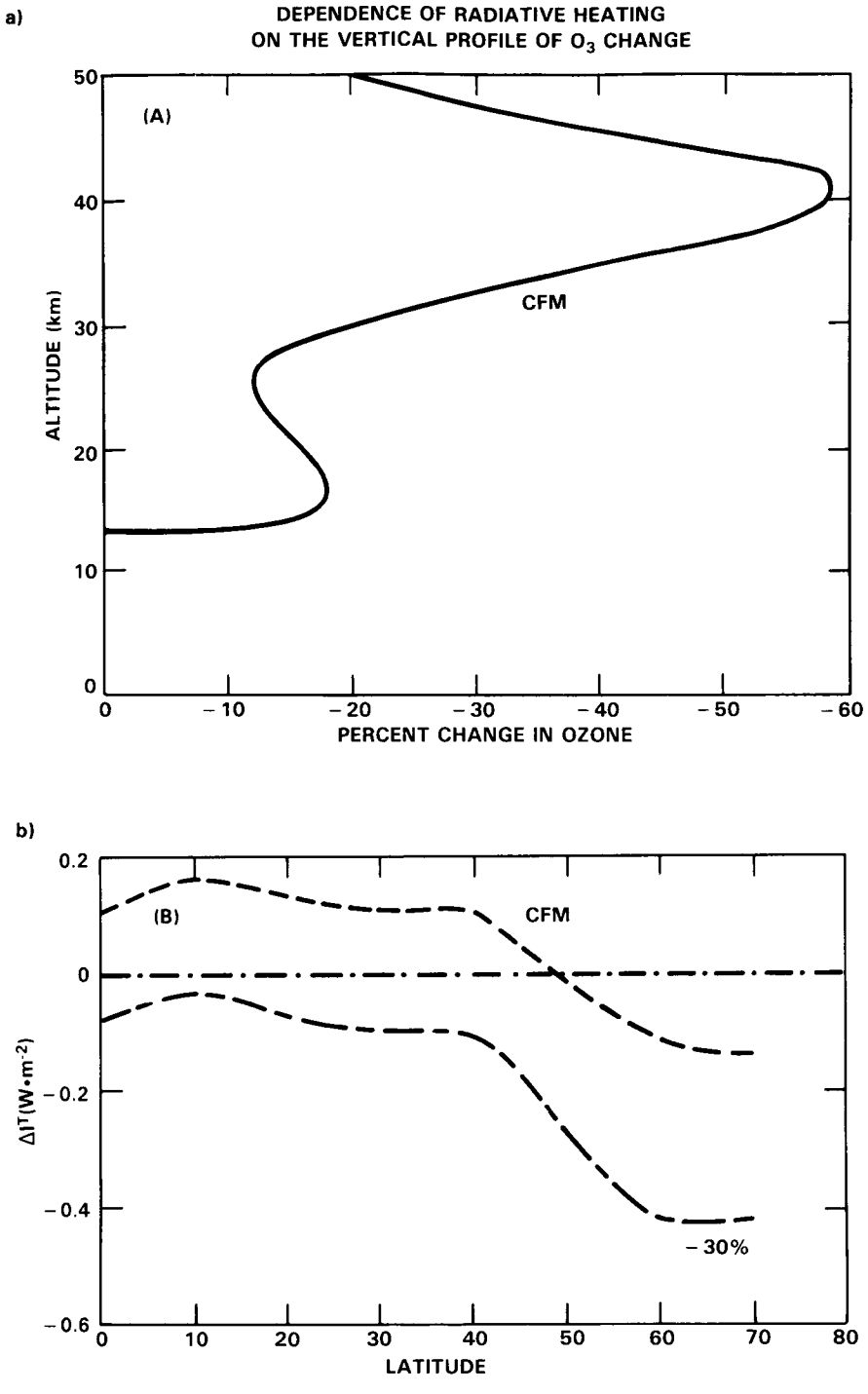

Figure 15-10. The dependence of computed change in the net radiative flux at the tropopause to assumed vertical profile of O_3 change. (a) The CFM profile is similar to the profile yielded by photo-chemical models which were current in 1979 for the effect of adding CFC's while holding other gases constant. Present models show less effect in the lower stratosphere and even give increases especially at low latitudes; (b) the computed change in the net flux at the tropopause for the CFM profile and for a 30% uniform O_3 reduction. Source: Ramanathan and Dickinson, 1979.

for a uniform O_3 change, tropospheric O_3 change is about two to three times as effective as stratospheric O_3 change in altering the radiative forcing (e.g., see Table 15-5).

The strong dependence of the computed surface temperature change to the altitude and latitude of of O_3 perturbation is summarized in Figure 15-11 (adapted from Wang *et al.*, 1980). This figure shows the computed surface temperature change (per cm-atm of O_3 change) as a function of the altitude at which O_3 is perturbed. For both the tropical and mid-latitude profile, the computed surface temperature change is most sensitive to ozone change (on a per molecule basis) within the upper troposphere and lower stratosphere. The larger sensitivity of the tropical profile is mainly due to the warmer tropical surface temperature and the colder tropical tropopause temperature both of which tend to maximize the greenhouse effect of O_3.

15.1.3 Additiveness of the Greenhouse Effects

The question to be addressed here is: would the computed change in tropospheric radiative forcing due to the simultaneous addition of two or more gases to the atmosphere be the same as that of summing up the effects of adding each gas separately? This question arises because the absorption features of several gases appear in the same spectral region. For example, the CF_4, CH_4 and N_2O bands occur in the 6-8 μm region; N_2O bands in the 15 μm region overlap with CO_2 bands; CFC bands overlap with O_3 bands; etc. To a large extent, model calculations show that the error involved in the additive assumption is less than 5% or so.

The above conclusion becomes invalid once one or more of the added gases alters a radiatively active constituent through chemical interactions. For example, both CFCs and CH_4 influence O_3 through chemistry. CH_4 is estimated to lead to an increase in O_3 in the upper troposphere and lower stratosphere, whereas

Table 15-5. Computed Surface-Troposphere Radiative Forcing Due To Uniform Reduction in O_3; Globally Averaged Conditions with Average Clouds.

O_3 Perturbation	Radiative Forcing[1] ($W\ m^{-2}$)	Source
−25% in the total column	−0.6 to −0.7 $W\ m^{-2}$	Inferred from Hansen *et al.* (1981)[2]
−25% in the stratosphere	−0.1 to −0.2 $W\ m^{-2}$	Ramanathan and Dickinson (1979)
−25% in the troposphere	−0.4 to −0.5 $W\ m^{-2}$	Fishman *et al.* (1979a)

[1] The values cited here account for stratospheric temperature changes to the imposed perturbations.

[2] These authors give results for surface temperature change and the radiative forcing was inferred by multiplying the temperature change with their model sensitivity (i.e., λ as given by Eq. 1 defined in Section 15.2.2) which is about 1.4 $W\ m^{-2}\ K^{-1}$.

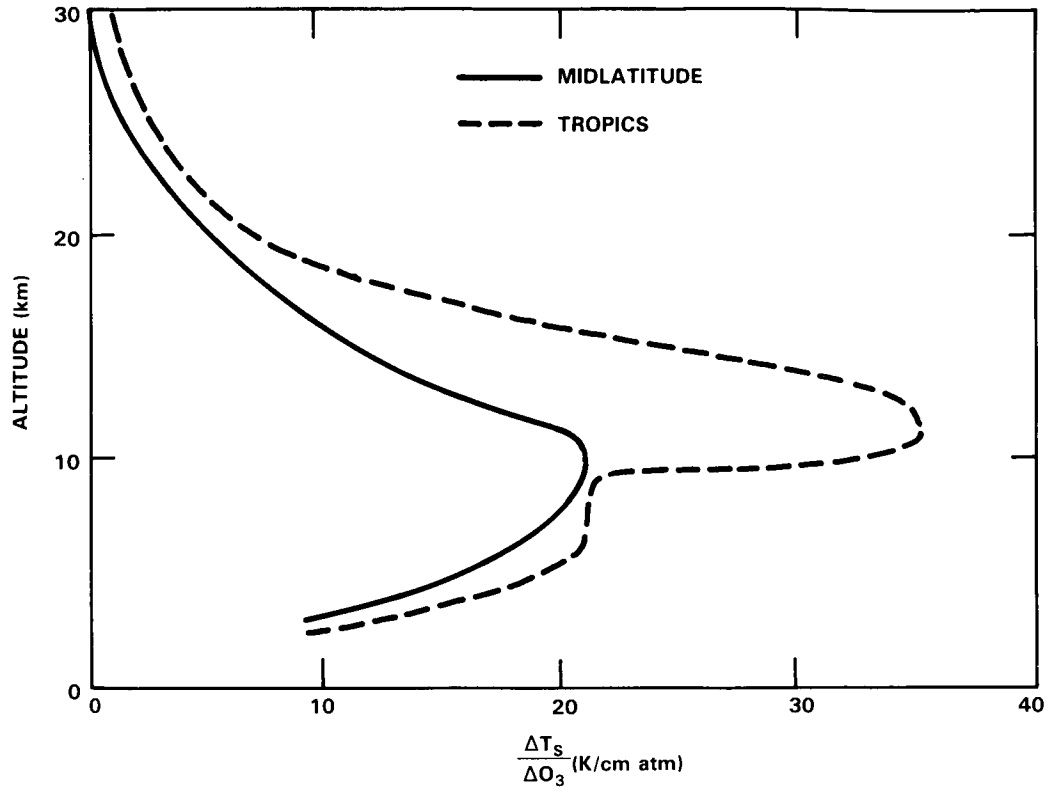

Figure 15-11. Computed change in surface temperature (per unit local O_3 change) as a function of altitude at which O_3 is perturbed. The surface temperature sensitivity curve is shown for midlatitude (solid) and tropical (dashed) atmosphere conditions. Source: Wang *et al.*, 1980.

an increase in CFCs would lead to a decrease in O_3 in the stratosphere. Simultaneous addition of CH_4 and CFCs may not produce the same change in the vertical profile of O_3 as that obtained by superposition of the individual O_3 changes produced by CH_4 and CFCs. Since the tropospheric effects depend on the vertical distribution of the O_3 perturbation, the validity of the additiveness assumption needs to be examined in the case of trace gases that chemically impact other radiatively active gases.

15.1.4 Effects of Aerosols

Stratospheric aerosols of volcanic origin undergo episodic variations while tropospheric aerosols can undergo episodic or secular variations. It is necessary to understand the nature and magnitude of the "signature" of aerosols on the observed trends of surface-troposphere-stratosphere temperatures before we can identify the role of trace gases on long term (decadal) climate trends. The above necessity is the primary motivation for including a brief discussion on aerosols in the present chapter.

A detailed description of our current understanding of aerosol effects on climate can be found in WCP (1983). Aerosols can impact climate either directly by absorption and scattering of solar and longwave radiation or indirectly by altering optical properties of clouds (Lenoble, 1984). Aerosols can influence cloud optical properties in one of the following two ways (Lenoble, 1984): (1) Aerosols lodged within a water droplet or ice crystal can alter the radiative properties of the cloud; (2) aerosols can also serve

as condensation or freezing nuclei and influence the size and concentrations of droplets or ice crystals which in turn govern the radiative properties of clouds (Twomey *et al.*, 1984). The aerosol-climate problem is so complicated that after decades of research, it is still difficult to make any general statements about whether aerosols cool or warm the climate. However the direct radiative effects are relatively better understood than the indirect effects and hence we will focus on the direct radiative effects of aerosols.

The visible optical depth of the background stratospheric aerosols is of the order of 0.01 or less, and hence, has a negligible impact on climate (WCP, 1983). The background tropospheric aerosol is estimated (by climate models) to cause a global surface cooling of about 1 to 3 K (see Table 2.2 of WCP, 1983). However, small changes in the assumed optical properties of aerosols (e.g., single scattering albedo and/or backscattered fraction; also see Lenoble, 1984) can change the computed effect from cooling to warming.

With respect to climate change, aerosols of volcanic origin in the stratosphere and of anthropogenic origin in the troposphere have the potential for influencing temperature trends within the stratosphere and troposphere on time scales ranging from a few years to several decades.

The stratospheric volcanic aerosols have been shown to affect the tropospheric climate in the following way. Aerosols produce two competing effects: (1) the scattering and absorption of solar radiation by the aerosols reduce the solar radiation reaching the troposphere and (2) they increase the atmosphere's longwave opacity. By decreasing the direct solar radiation and increasing the scattered radiation, the aerosol contributions can cool the troposphere. The increased longwave opacity and solar absorption can also heat the stratosphere. As the volcanic cloud ages, some SO_2 is oxidized to sulfuric acid to produce more aerosols (Hofman and Rosen, 1983); existing aerosols increase in mean radius (Hofman and Rosen, 1982), which in turn increases the Mie scattering in the visible spectral region. To account fully for aerosol effects upon climate, it is necessary to follow the cloud dispersion, the oxidation of SO_2, the change in the size distribution, the geographical location, the height and vertical structure of the aerosol cloud. To use this information effectively in a model, it is also necessary to know the aerosol refractive index (Reck and Hummel., 1981), from which the aerosol extinction, single scattering albedo and the asymmetry factor may be calculated.

One of the best documented and better understood effects of volcanic aerosols is their effect on stratospheric temperatures. Stratospheric temperature statistics recorded over the last two decades clearly reveal the low latitude warming in the lower stratosphere following the eruption of Agung in 1963 and El Chichon in 1982 (WCP; 1983). In the special case of the effects of the El Chichon eruption of 4 April 1982 (McCormick *et al.*, 1984; Michalsky *et al.*, 1984), isolation of its stratospheric signal from the thermal effects of the El Niño event and the quasibiennial oscillation indicates that a temperature increase of 1-3 °C at 30 mb occurred between the equator and 35 ° latitude (Labitzke *et al.*, 1983; Quiroz, 1983a). Harshvardhan *et al.* (1983) used a nine-layer zonally averaged energy balance model with ice-albedo feedback to estimate that the maximum surface cooling should have been 0.3-0.4 °C, 2.5 years following the eruption. They expected the largest zonal temperature change to occur around 70 °N with a value 0.5-0.6 °C. Their model also predicted an increase in the reflected solar radiation at the top of the atmosphere of about 3-4 W m^{-2}.

Episodic aerosol disturbances in the troposphere have also been shown to lead to regional climatic effects. The most important of these disturbances are arctic haze (Leighton, 1983), Saharan dust (Fouquart *et al.*, 1984) and urban aerosols (Galindo, 1984). Amongst these disturbances, arctic haze may turn out to be an important issue for the trace gas-climate problem for several reasons. First, observations indicate that arctic haze contains large amounts of anthropogenic compounds like soot and sulfuric acid (Blanchet and List, 1984). Secondly, it has been shown recently (Wilkness and Larson, 1984) that con-

tinental air masses (containing soot and other anthropogenic gases) can be transported over very long distances (e.g., from Asia to Arctic). Hence, the arctic haze can exhibit a secular trend in the future. Thirdly, the arctic haze has a substantial impact on the springtime solar heating rates (Porch and MacCracken, 1983). Under clear-sky conditions, the haze layer can enhance the heating rate by as much as 50%. The climatic effects of the haze are expected to be concentrated in the arctic region and might change with time (since the haze is of anthropogenic origin). Since the trace gas effects on tropospheric climate are also expected to be large in the arctic region (see Sections 15.4 and 15.5), the potential effects of the haze on arctic climate can make it difficult to infer the trace gas effects.

In summary, aerosols can produce a sizeable "noise" in meteorological data which makes it very difficult to establish a direct relationship between trace gas increases and climate change. While some models exist (Lenoble, 1984) to predict the climatic consequences of stratospheric aerosols, more research needs to be done in measurements and in modeling to establish the role of tropospheric aerosols in climate. In particular, we need to establish trends (if any) in the tropospheric aerosols and their radiative properties. Perhaps, the best hope for assessing aerosol effects is to monitor the albedo of the planet from satellites with a high degree of precision (within 0.1%).

15.1.5 Current Status in Trace Gas Radiative Treatment

Numerous approximations are invoked within climate models to simplify the treatment of the radiative effects of trace gases (e.g., the use of band models). For example, an international study entitled "the intercomparison of radiation codes used in climate models (ICRCCM)" undertook the task of comparing clear-sky longwave fluxes and cooling rates computed by about 40 radiation models including line-by-line, narrow-band and broad-band models (see the appendix for further discussion of the band models). The results of this study have been published as a World Climate Research Programme report by Luther and Fouquart and this report will be referred to as ICRCCM (1984). The principal findings of the ICRCCM (1984) study, which focused on clear-sky longwave calculations for H_2O, CO_2 and O_3 are given below:

(1) The line-by-line models are in very good agreement with each other (within 1% in the computed fluxes). (2) The radiation codes used in climate models differ significantly from each other. For example, the net radiative flux change (for clear-sky mid-latitude summer condition) at the tropopause due to CO_2 doubling (i.e., the radiative forcing of CO_2 doubling) yielded by the models ranged from 4.5 to 7.5 W m^{-2}. To give another example, the range in the computed downward flux at the surface for a mid-latitude summer atmosphere (with only water vapor) is about 60 W m^{-2}. (3) Because of large uncertainties in H_2O line shapes and in the physics of the H_2O continuum, there is an urgent need to validate line-by-line calculations with accurate laboratory data and with flux measurements in the atmosphere.

Since H_2O, CO_2 and O_3 are discussed in great detail in the ICRCCM study, the present discussion will focus on the other trace gases listed in Table 15-1. Climate models generally employ narrow-band or broad-band models for CH_4 and N_2O and employ various versions of the optically thin approximation for all other gases in Table 15-1.

The validity of the optically thin approximation is discussed in detail in WMO (1982; see the appendix by Cess in that report). For concentrations of CFC's (and others in Table 15-1) of several ppbv or less, the optically thin approximation when employed in conjunction with the exponential sum-fitting method has been shown (Ramanathan *et al.*, 1985) to yield the same accuracy as the more detailed narrow-band model. The next step is to assess the accuracy of the approaches used in narrow- and broad-band models.

The effect of simplified model approaches can be evaluated by intercomparing models of varying complexity. This technique for evaluating models is illustrated in Annex 1 for the ν_4 band of CH_4 (located at 1300 cm^{-1}). The following is a summary of the analyses given in the Appendix:

(a) It is possible to define and derive a self-consistent narrow-band or broad-band model that agrees excellently with line-by-line calculations both for homogeneous and for inhomogeneous optical paths (i.e., atmospheric path);

(b) The choice of spectral interval for the narrow-band model is quite arbitrary. The spectral interval has to be chosen by comparing with line-by-line calculations.

(c) Line half-width and its temperature dependence are available for only a minor fraction of the several thousand lines within each band. The lack of this data is a major source of uncertainty in line-by-line calculations.

For CFC's and all other gases except CH_4 and N_2O, the relevant narrow-band model parameters are unavailable. Even the integrated band strengths are unavailable for many potentially important gases such as CFC113 and 114. Furthermore, for many of the gases the hot bands (i.e., bands for which the lower vibrational state is an excited state) overlap strongly with the fundamental bands (e.g., see Varanasi and Ko, 1978 for CFC11 and 12). In such instances, it is important to determine the strengths of the hot bands for accurate modeling of the opacities in band models.

15.2. THEORY AND MODELS

15.2.1 Stratospheric Response to Perturbations

The study of climatic impacts *within* the stratosphere due to added trace constituents is of special interest for several reasons. First, for reasonable projections of future trace constituent distributions, the expected temperature changes in the upper stratosphere are nearly an order of magnitude greater than the expected surface changes. Second, these expected temperature changes are essentially independent of ocean temperature changes and cloud feedback effects. Both processes are a source of considerable uncertainty in assessing tropospheric climate change.

Climate change in the stratosphere is also different because temperature change there is coupled directly with photochemical processes. The strongest link is with the temperature dependence of the equilibrium ozone. For example, the cooling effect of increasing CO_2 in the upper stratosphere superficially involves virtually no chemistry. However, as temperatures drop, ozone amounts increase, leading to a local *heating* effect. This is an important *negative* feedback. In addition, increases of the trace gases, particularly CH_4, H_2O, N_2O and chlorofluorocarbons, tend to lead to O_3 decreases (and cooling effects) in the upper stratosphere. However, such local decreases of O_3 affect the incoming solar ultraviolet radiation such that greater penetration into the lower stratosphere would be allowed. This acts to increase local *heating* there, but more importantly, increases production of O_3 below. This process produces a very significant "self-healing" effect on the total O_3 column, while leading to significant changes in the *shape* of the ozone profile. This, in turn, affects the local temperature.

The almost bewildering array of interactive feedback processes in the stratosphere implies that they can be understood only through careful, self-consistent modeling of the radiative-photochemical-dynamical

system. Ultimately, this modeling must be done with fully interactive, time-dependent, three-dimensional models.

For a number of reasons, such complete models remain impractical today. The most well known reason is the tremendous computational requirements for a fully comprehensive model. However, even if such resources were now available, the current strategy of using a hierarchy of models ranging from the very simple to the very complex would still be the appropriate one. This is because there remain significant uncertainties in our understanding of many aspects of the radiative-photochemical-dynamical system. Useful reductions of such uncertainties require a wide range of considerably more focused research activities. Without improved understanding and modeling capability in all components of the problem, the power of more comprehensive modeling treatments tends to be diminished.

These difficulties are amplified by the very serious uncertainties in the projected changes in atmospheric trace constituent amounts. To explore such problems, typically a generous range of possibilities (scenarios) is considered.

This situation has led to a wide variety of modeling approaches, all of which work to reduce the complexity of the problem and emphasize various sets of scientific questions. Some of these modeling approaches are surveyed below.

15.2.1.1 Role of Radiative-Photochemical-Diffusive Models

The simplest approach that comes close to allowing an understanding of the complex interactions among radiation, photochemical and transport processes is the so-called one-dimensional (1-D) model. These models allow no horizontal variations and thus may logically be considered to represent globally averaged (in the horizontal) conditions. Historically, however, they often have been used to represent local conditions, usually at some appropriate "midpoint" latitude such as 30°. Historically, the 1-D models have usually considered only photochemical problems, with the required transport being parameterized by carefully chosen but empirical "eddy" diffusion coefficients (e.g., McElroy *et al.*, 1974, Hunten, 1975).

Such 1-D models have been shown to be very powerful tools for understanding complex chemical feedbacks in spite of their simplicity. Moreover, they have served as the basic tool for most of the previous assessments of the expected impacts on stratospheric ozone changes due to various anthropogenic activities (e.g., National Research Council, 1979). Typically, these models have prescribed temperatures and thus have only indirect implications for stratospheric climate changes.

More recently, some investigators have begun efforts to couple these chemically oriented 1-D models with the Manabe and Wetherald (1967) type radiative-convective 1-D climate models. These include Luther *et al.* (1977) and Boughner (1978).

To date, the main concern has been with including the effects of climatic feedback on calculated ozone changes. As the effects of radiatively important trace species other than CO_2 become the object of more serious climatic attention, the inclusion of photochemical feedbacks in the climate system will gain more research attention. However, in such cases the limitations of the 1-D model framework will become more severe. This is particularly so for the calculation of chemical/climatic feedbacks through stratospheric water, a trace substance whose spatial distribution seems to be fundamentally dependent upon 3- D processes.

15.2.1.2 Two-Dimensional Effects

In both climatic and chemical problems, there are many physical processes that at best are poorly represented in 1-D models. The next logical step is to construct a 2-D model in the meridional-vertical plane. This allows inclusion of many important sun-angle dependent processes. Most models in this category have prescribed transport processes in various combinations of zonally symmetric and "eddy" mechanisms.

In the past, the main concern has been with the problem of self-consistent prescription of mean and eddy transport processes. Recently, conceptual progress (Plumb and Mahlman, 1985) and semi-empirical successes (e.g., Garcia and Soloman, 1983; Ko *et al.*, 1985; Guthrie *et al.*, 1984) have been achieved. This progress has been mainly in the "transport/chemistry only" models in which the transport doesn't really change as the constituents or the climate of the stratosphere change.

Early attempts to produce self-consistent dynamical response in 2-D models were given in Vupputuri (1978) and Pyle and Rogers (1980a). In these models the eddy fluxes are essentially specified (usually through local eddy diffusion coefficients), but the meridional circulation is calculated self-consistently in response to these fluxes. In a more fundamental sense, these models are not really climate models either since the fundamental eddy forcing remains prescribed through large changes in constituents. They might, however, capture an important part of the 2-D "non-dynamical" part of the climatic response to trace constituent changes. Such models can yield temperature changes that are very close to the "fixed dynamical heating" (FDH) limit described in the next section.

15.2.1.3 Three-Dimensional and Dynamical Effects

Since it is clear that both chemical and dynamical processes are inherently three-dimensional, it is inevitable that 3-D climate/chemical models will play an increasing role in analysis of such trace gas/climate problems. However, even as such models are employed, they can provide information which at times may show ways in which full 3-D processes may not have to be modeled explicitly once they are well understood. For example, the work of Mahlman *et al.* (1985) indicates that all long-lived stratospheric gases exhibit predictable structure provided that the complete 3-D structure is solved for one of them and the chemistry of each of the gases of interest is known. In this context, it is likely that full 3-D solutions will not be required for each of the ever growing list of radiatively active gases that may influence climate.

In the context of predicting stratospheric climate change, it is of interest to inquire whether 3-D models are really required. The answer to this probably can be supplied only with a properly posed 3-D model. An early attempt in this regard was offered by Fels *et al.* (1980). They pointed out that there are two possible extremes of stratospheric climatic responses to changes in trace constituents. These are (1) "dynamical adjustment" and (2) "radiative adjustment." For dynamical adjustment, the net dynamical heating (sum of adiabatic heating mechanisms in the thermodynamic equation) adjusts so that the temperature doesn't change. For radiative adjustment (see also Fels and Kaplan (1975), and Ramanathan and Dickinson (1979)) the temperature changes so that the *net dynamical heating* doesn't change.

Since the net dynamical heating is a function of the degree to which the stratosphere is dynamically forced, "radiative adjustment" means in this context that *no further changes* in dynamical forcing occur as a result of changing trace constituents. This is why Fels *et al.* (1980) refer to this as the "fixed dynamical heating" (FDH) limit. The attractive feature of the FDH limit (if valid) is that, in principle, climatic calculations can be performed with purely radiative models. However, this requires that such radiative models perturb about *realistic* atmospheric structure (either real or modeled). The experiments of Fels

et al. (1980) suggest strongly that mid and high latitudes of the stratosphere are rather well described by the FDH limit. For *tropical* wind systems, however, considerable dynamical adjustment is expected. They offer a mechanistic model that explains why significant dynamical adjustment is expected mainly in the tropics.

The calculations of Fels *et al.* (1980) pertain to annual mean conditions and may not necessarily reflect the validity of the FDH model for other seasons (in particular, the winter polar regions where dynamical processes play a crucial role in maintaining the thermal structure). Nevertheless, it seems safe to conclude that, on an annual mean basis, the stratospheric temperature response to radiative heating perturbations is governed to a large extent by longwave radiative adjustment processes.

15.2.2 Troposphere Response and the Role of Feedbacks

One of the fundamentally important concepts which has emerged out of the numerous 1-D, 2-D and 3-D climate model studies is that the surface temperature change is largely determined by the radiative forcing of the surface-troposphere system (i.e., net flux change at the tropopause). The computed surface temperature change is neither strongly dependent on the vertical distribution of the radiative heating within the troposphere nor does it depend strongly on the manner in which the radiative heating is partitioned between the surface and the troposphere. The reason for the insensitivity of the computed surface temperature change to the vertical heating distribution has been explained in the introduction to Section 15.1.

The model results that helped forge this concept are numerous and only a few examples will be given below: (a) The radiative forcing of the surface-troposphere system due to a 2% increase in solar insolation and due to a CO_2 doubling agree within about 10%. But, the partioning of this forcing in terms of surface forcing and tropospheric forcing is vastly different. Yet, almost all climate model studies, including the general circulation model studies (e.g., Wetherald and Manabe, 1975; Hansen *et al.*, 1984) show that the computed surface temperature change for the 2% solar radiation increase is within 10% of that due to CO_2 doubling; (b) Likewise, as shown in Section 15.1, the vertical distribution of the radiative heating due to CFCs and CH_4 or CO_2 are drastically different. Yet, the computed surface temperature change due to the individual gases scales almost linearly with respect to their radiative forcing of the surface-troposphere system. The conclusions derived from these studies apply only to small deviations from the observed climate and should not not be generalized to large perturbations.

Three different types of climate models have been used to compute the climate change due to trace gas perturbations: energy balance models (EBMs), radiative-convective models (RCMs) and general circulation models (GCMs).

15.2.2.1 Energy Balance Models: the Zero Climate Feedback Limit

The concept of surface-troposphere radiative forcing is particularly useful for inferring the role of feedback processes since it enables the problem to be formulated in terms of a zero-dimensional climate model. Denoting the perturbation in surface/troposphere radiative heating (i.e., the radiative forcing) as ΔQ, the surface temperature change ΔT_s can be related to ΔQ by the relation (Dickinson, 1985):

$$\Delta T_s = \frac{\Delta Q}{\lambda} \tag{1}$$

where λ is referred to as the climate feedback parameter. The net (solar + longwave) radiative forcing, ΔQ, is the net (down minus up) radiative flux change at the tropopause due to the trace gas change. The change in the net flux is computed by holding the surface and tropospheric temperatures fixed at the reference value but allowing the stratospheric temperatures to come to equilibrium with the radiative heating perturbation. These subtle requirements of computing ΔQ have been ignored at times (in the literature) with catastrophic errors. For example, Equation (1) has been applied by estimating ΔQ at the surface which tends to underestimate ΔT_s by a factor of two to four (see Ramanathan, 1981) or by estimating ΔQ at the top of the atmosphere without allowing the stratosphere to come to equilibrium which tends to underestimate ΔT_s by a factor of two (see the discussions in Schneider, 1975)

In general, λ estimated by the hierarchy of simple and sophisticated climate models lies in the range of:

$$1 < \lambda < 4 \text{ Wm}^{-2}\text{K}^{-1}.$$

For the simplest case in which the earth-atmosphere system radiates as a black body with an effective radiating temperature of 254 K, $\lambda = 4\sigma T^3$ ($=3.7$ W m^{-2} K^{-1}). For this case, a doubling of CO_2 (note $\Delta Q \approx 4.2$ W m^{-2}) would yield a surface warming of about 1.1 K. This simple model implicitly assumes that the troposphere and surface are coupled so that the same temperature change occurs in the troposphere or at the surface, i.e., the lapse rate is assumed to be an invariant of climate. More importantly, this model ignores all climate feedback processes involving temperature, humidity, clouds and others. The only feedback this model includes is the negative feedback between temperature and longwave emission (Dickinson, 1982). Hence, the climate response obtained from a model with fixed lapse rate, fixed atmospheric composition and fixed planetary albedo is referred to as zero climate feedback case and the change in surface temperature for this case is denoted by $(\Delta T_s)_0$.

The EBM given by (1) imposes the energy balance at the top-of-the tropopause. There are also surface energy balance models (SEBMs) which solve for ΔT_s by imposing surface energy balance. A recent review by Schlesinger and Mitchell (1985) shows that a wide range of values for λ may be obtained (0.3 to 10 W m^{-2}K^{-1}) for SEBMs depending upon modeling assumptions. In several cases where the λ is outside the range of 1 to 4 W m^{-2}K^{-1}, the cause has been traced to the assumptions that violated the first law of thermodynamics (Cess and Potter, 1984).

There are also 1-D (latitude) and 2-D (latitude and altitude) EBMs which have played an important role in illustrating the magnitude of several climate feedbacks. These EBMs are reviewed in North *et al.* (1981).

15.2.2.2 Radiative-Convective Models

Radiative-convective models determine the equilibrium vertical temperature distribution for an atmospheric column and its underlying surface for given insolation and prescribed atmospheric composition and surface albedo. An RCM includes submodels for the transfer of solar and longwave radiation, the turbulent heat transfer between the earth's surface and the atmosphere, the vertical redistribution of heat within the atmosphere by dry or moist convection, the atmospheric water vapor content and cloud amount. The radiative transfer models used in RCMs are frequently identical to those used in GCMs. The vertical heat redistribution by convective atmospheric motions is modeled as an adjustment whereby the temperature lapse rate of the atmosphere is prevented from exceeding some given value. The amount of water vapor is detemined in RCMs either by prescribing the absolute humidity or the relative humidity; in the

latter case the amount of water vapor increases (decreases) with increasing (decreasing) temperature. Finally, the fractional cloudiness and the temperature or altitude of the cloud tops are either prescribed or predicted.

The zero-climate feedback limit in the RCM is obtained by prescribing the lapse-rate, absolute humidity and planetary albedo and by holding them fixed as surface and atmospheric temperatures vary. The computed surface temperature change for the zero climate feedback case, $(\Delta T_s)_0$, generally ranges from 1.3 K (Manabe and Wetherald, 1967; Ramanathan, 1981) to 1.2 K (Hansen *et al.*, 1984). Both of these values are reasonably close to the value of 1.1 K obtained from the zero-dimensional EBM (Section 15.2.2.1). Hence, $(\Delta T_s)_0$ is a nearly model-independent parameter and is a useful measure of the radiative forcing due to a given change in atmospheric composition.

To indicate the importance of the climate feedback processes listed in Table 15-6, we introduce a climate feedback factor, F, which is defined as:

$$F = \frac{\Delta T_s}{(\Delta T_s)_0} \tag{2}$$

where ΔT_s is the change in surface-air temperature with the feedback. The $(\Delta T_s)_0$, ΔT_s and F obtained for CO_2 doubling with various hypothesized feedbacks are shown in Table 15-6.

The water vapor feedback (second row in Table 15-6) is one of the better understood feedback processes and was introduced in the RCM by Manabe and Wetherald (1967) based on the fact that the observed zonally averaged relative humidity is quite insensitive to seasonal changes in temperatures. With fixed relative humidity, the water vapor amount increases with an increase in surface temperature according to the Clausius-Clapeyron relation. Since H_2O is the most important greenhouse constituent, the H_2O-T_s feedback increases computed ΔT_s by roughly 50 to 80% depending on the model (see Manabe and Wetherald, 1967; the review paper by Ramanathan and Coakley, 1978; F in Table 15-6). The increased solar absorption by H_2O contributes roughly 10% to the H_2O-T_s feedback.

Other parameters such as lapse rate, cloud top temperature, cloud cover will have a significant impact on λ. The numbers in Table 15-6 indicate the potential importance of these feedbacks. However, the magnitude and even the sign in some instances (e.g., clouds) of these feedbacks are not well known.

Another important feedback concerns the snow and ice albedo feedback. With an increase in surface temperature, snow and ice cover will melt which may lead to a decrease in the areal extent of snow and ice cover; this will lead to a decrease in surface albedo and a corresponding increase in the absorbed solar radiation. This positive feedback has been the subject of scores of EBM, RCM and GCM studies. Generally, according to Dickinson (1985), several models have converged to the conclusion that the ice-albedo feedback amplifies global average ΔT_s by about 15% (also see last column of Table 15-6); note, however, that the magnitude of amplification by any one feedback depends on the other feedbacks included. It should also be noted that the ice-albedo feedback has a significant impact on polar surface temperature change.

15.2.2.3 General Circulation Models

The principal prognostic variables of an atmospheric GCM are the temperature, horizontal velocity, and surface pressure, which are governed, respectively, by the thermodynamic energy equation, the horizontal momentum equation, and the surface pressure tendency equation. With the mass continuity equation and

Table 15-6. Feedback Analysis Using the Oregon State University 2-Layer RCM. (Source: Schlesinger, Private Communication)

Feedback Mechanism	T_S ($1\times CO_2$) (°C)	ΔT_S (°C)	F[2]
None $[\Delta T_S)_0]$[1]	15.28	1.35	
Water Vapor[3]	14.53	1.94	1.4
Lapse Rate[4]	9.53	0.88	0.7
Cloud Temperature[5]	15.28	1.73	1.3
Cloud Cover	15.28	1.38	1.0
Cloud Optical Depth[7]	15.28	1.39	1.0
Surface Abedo[8]	15.43	1.56	1.2
Water Vapor[3] and Lapse Rate[4]	9.38	1.19	.9
Cloud Temperature[5]	14.20	2.79	2.1
Cloud Cover[6]	15.12	1.81	1.3
Cloud Optical Depth[7]	15.39	1.70	1.3
Surface Albedo[8]	14.58	2.39	1.8
Water Vapor[3], Cloud Temperature[5], and Surface Albedo[8]	14.14	3.85	

[1] $(\Delta T_S)_0$ is calculated by the RCM without feedbacks.
[2] $F = \Delta T_S/(\Delta T_S)_0$.
[3] With the fixed relative humidity profile of Manabe and Wetherald (1967).
[4] With the moist adiabatic lapse rate.
[5] With fixed cloud temperature prescribed equal to that of the $1\times CO_2$ simulation with no feedback.
[6] With variable cloud cover prescribed similarly to that of Wang *et al.* (1981) and cloud albedo, absorptivity and transmissivity.
[7] With variable optical depth τ prescribed similarly to that of Wang *et al.* (1981) and cloud albedo, absorptivity and transmissivity parameterized in terms of τ following Stephens *et al.* (1984).
[8] With variable surface albedo prescribed as in Wang and Stone (1980).

the hydrostatic approximation and appropriate boundary conditions, these equations form a closed system for an adiabatic and frictionless atmosphere. But the general circulation of the atmosphere is the large-scale, thermally driven field of motion in which there are interactions between the heating and motion fields. Therefore, several additional prognostic variables, with corresponding governing equations and appropriate boundary conditions, must be added to simulate the heating. Of these, the most important is the water vapor, which is governed by the water vapor continuity equation. Because the atmosphere is largely heated by the underlying surface through the exchange of sensible and latent heat, and because snow lying on the ground can have a large influence on the surface albedo, the ground temperature, soil moisture, and mass of snow on the ground are prognostic variables, governed by energy, water, and snow

budget equations for the ground. In addition to the prognostic variables, GCMs have many diagnostic variables, among which clouds may be one of the most important.

The equilibrium changes in surface air temperature ΔT_s simulated by 7 selected GCMs for a doubled CO_2 concentration are presented in Table 15-7. The first four studies were performed with atmospheric GCMs coupled to a swamp ocean model which has zero heat capacity and no horizontal or vertical heat transports. These coupled atmospheric GCM/swamp ocean models are run without a seasonal insolation cycle to prevent the freezing of the ocean in the latitudes of the polar night. The last three studies were performed with atmospheric GCMs coupled to a fixed-depth mixed layer ocean model which has heat capacity, prescribed horizontal heat transports (zero except in Hansen *et al.*, 1984), and no vertical heat transports. These coupled atmospheric GCM/fixed-depth mixed layer ocean models are run with the seasonal insolation cycle.

Table 15-7 shows that the models without the seasonal insolation cycle give surface air temperature warmings of 1.3 to 3.0 K for a doubling of CO_2, while the models with the seasonal insolation cycle give annual average warmings of 3.5 to 4.2 K (also see footnote 2 in Table 15-7). It is difficult to identify the specific causes for the wide range of surface air temperature warming simulated by the models with a swamp ocean because these models differ in geographical domain, land/ocean distribution and orography as well as in their treatment of clouds, snow and sea ice (Schlesinger, 1984). It is therefore gratifying that the three simulations with the atmospheric GCM/fixed-depth mixed layer ocean model having a global

Table 15-7. Surface Air Temperature Change Induced by a Doubled CO_2 Concentration As Simulated by Selected General Circulation Models.

Study	ΔT_s (K)
Manabe & Wetherald (1975)	2.9
Manabe & Wetherald (1980)	3.0
Schlesinger (1983)	2.0
Washington & Meehl (1983)	1.3
Washington & Meehl (1984)	3.5
Hansen *et al.* (1984)	4.2[2]
Manabe & Wetherald[1]	4.0

[1] Unpublished study. See Schlesinger and Mitchell (1985).

[2] This version of the Hansen *et al.* GCM has less sea-ice than observed. They also report results with an alternate version of the GCM which has roughly 15% more sea-ice than observed and this "alternate" version yielded a ΔT_s of 4.8 K.

domain, realistic land/ocean distributions and orography, and interactive clouds produce comparable global mean surface air temperature warmings.

15.2.2.4 The Importance of Cloud Feedback

One of the least understood and potentially important feedbacks is the feedback involving clouds. The issues to be addressed are threefold. The first concerns the response of cloud cover, cloud base and cloud tops to temperature changes; the second concerns the change in cloud radiative properties (i.e., albedo and emissivity); and the last is the relationship between the above changes and the radiative forcing due to the clouds. The limited number of studies on this tough problem have led to the following conflicting inferences. Empirical studies using satellite radiation budget data in conjunction with cloud cover data have indicated that even if cloud cover changes substantially, the radiative changes would be negligible (Cess, 1976). Similar empirical studies, but using different satellite data sets (see Cess *et al.*, 1982), have suggested that an increase (decrease) in clouds would lead to a large radiative cooling (heating). The implication of these studies is that an increase (decrease) of global average clouds by about 4% i.e., from 50 to 54% (or decrease to 46%) would be sufficient to ameliorate (amplify) the CO_2 effect by a factor of 2 or more. Recent GCM studies, on the other hand, indicate that cloud feedback could amplify the CO_2 warming by about 25 to 50%.

The GCM studies have largely ignored the so-called cloud-optics feedback (Charlock, 1982; Somerville and Remer, 1984). In this feedback, the cloud liquid water increases with an increase in T_s such that the cloud albedo increases with an increase in T_s. The increase in cloud albedo provides a negative feedback. RCM calculations (Charlock, 1982, and Somerville and Remer, 1984) suggest that the cloud optics feedback may reduce ΔT_s by a factor of 1.5 to 2.

The fundamental difficulty in the way of realistic attack on the cloud problem is the fact that the processes that govern cloud formations and their radiative effects occur on scales ranging from several meters to several tens of kilometers. Theoretical, modeling and observational breakthroughs are needed to bridge the gap between the spatial scales of climate models and the scales of cloud formation. In the interim, we have to acknowledge the potentially large source of uncertainty in model estimates of climate sensitivity and explore imaginative ways of verifying model sensitivity with observations.

15.2.3 The Implications of H_2O-Climate Feedback

Most climate models and, in particular, all of the GCMs indicate that an increase in tropospheric water vapor content will accompany the greenhouse warming of trace gases. The increase in H_2O is a strong function of latitude and altitude ranging from 5 to 15% in the low latitudes to as much as 50% in the polar regions (e.g., see Washington and Meehl, 1984). As described earlier (Section 15.2.2) this H_2O feedback amplifies the surface warming by about 50 to 80%. In addition to providing the positive climate feedback, the increase in tropospheric H_2O has important implications to tropospheric chemistry (Hameed *et al.*, 1980; Callis *et al.*, 1983a; WMO, 1982).

The increase in H_2O can lead to increased production of tropospheric OH which, in turn, may lead to enhanced oxidation of CH_4, CO and O_3 (see Figure 15-4), and possibly other chemicals. Since OH plays a dominant role as a cleansing agent of tropospheric pollutants, surface-troposphere temperature changes (through the H_2O feedback) can have substantial influence on the concentrations of other greenhouse gases (e.g., O_3 and CH_4) in the troposphere. The nature and magnitude of this climate-chemistry feedback is discussed in Section 15.3.

The second important role of H_2O feedback concerns the interactions between low-latitude tropopause temperatures and stratospheric H_2O. The direct radiative forcing of trace gases such as CFCs and O_3 are particularly large in the vicinity of the tropical tropopause (Figures 15-8 and 15.9). Furthermore, GCM results reveal a large change in tropical tropopause temperatures in response to O_3 change (Figure 15-12) or to CFCs (Dickinson *et al.*, 1978). Since the stratospheric H_2O concentration is believed to depend critically on this temperature, substantial cooling (or warming) of the tropopause may lead to a substantially drier (or wetter) stratosphere.

Large changes in stratospheric water vapor have important radiative and chemical consequences. For example, a doubling of stratospheric H_2O from 3 to 6 ppm can lead to a 0.6 K surface warming (Wang *et al.*, 1976). Since H_2O is a controlling factor in stratospheric HO_x chemistry (Liu *et al.*, 1976), altered stratospheric H_2O can also influence stratospheric concentrations of O_3 and CH_4.

15.3 EFFECTS ON ATMOSPHERIC AND SURFACE TEMPERATURES

Most of the trace gases that have been detected in the atmosphere are listed in Table 15-8 together with information pertinent to their presently known sources, sinks, lifetimes, and present concentrations. The direct greenhouse effects of these gases will be discussed first, to be followed by discussions of the effects arising from chemical perturbations.

15.3.1 Direct Effects

Most of the gases shown in Table 15-8 have absorption features in the longwave spectrum (see Tables 15-1a and 15-1b). Many of the gases shown in Table 15-8 have a substantial surface warming effect at 1 ppbv level (see Figure 15-13). For reference purposes, Figure 15-13 also shows the surface warming due to uniform increases in tropospheric O_3 between 0 to 12.5 km, CH_4 and N_2O. All of the gases shown in Figure 15-13 have strong absorption features in the "window" region of 7-13 μm. Bands of gases such as CF_4 occur in the same wavelength as CH_4 and N_2O bands. Because of this band overlap, CF_4, in spite of having the strongest band (band strength of about 5000 cm^{-2} atm^{-1}, see Table 15-1b) of the gases shown in Figure 15-13, does not have as large a surface warming as some of the other CFCs. The direct greenhouse effects have also been estimated by numerous recent studies (e.g., Brühl and Crutzen, 1984; Wang *et al.*, 1985; Ramanathan *et al.*, 1985; Owens *et al.*, 1985b).

The radiative-convective model (RCM) results for ΔT_S due to increases in CFCs, CH_4 and N_2O have differed significantly among models. Recent studies (Ramanathan *et al.*, 1985 and Owens *et al.*, 1985b) have attempted to clarify the sources for the discrepancy. For CFCs, most of the differences were traced to the use of different spectroscopic data and to differences in model sensitivity. When these results were scaled to the same model sensitivity of $\Delta T_S = 2$ K for a doubling of CO_2 and to the most recent CFC band strengths of Kagann *et al.* (1983), all of the models (Ramanathan, 1975; Reck and Fry, 1978; Lacis *et al.*, 1981; Ramanathan *et al.*, 1985) except the Owens *et al.*, (1985) model, yield a surface warming of 0.52 to 0.56 K for a 0 to 2 ppbv increase in each of CFC11 and CFC12. The Owens *et al.*, model yields a ΔT_S of 0.45 K (see Owens *et al.*, 1985b for a more complete discussion of this intercomparison). A similar scaling procedure of model sensitivity (i.e., $\Delta T_S = 2$ K for CO_2 doubling) for doubling of CH_4 and N_2O shows a spread of about 0.2 to 0.3 K for doubling of CH_4 and about 0.35 to 0.45 K for doubling of N_2O (see Table 9 of Owens *et al.*, 1985b). These differences strongly suggest the need for an ICRCCM (1984) type intercomparison study for the trace gases shown in Figure 15-13.

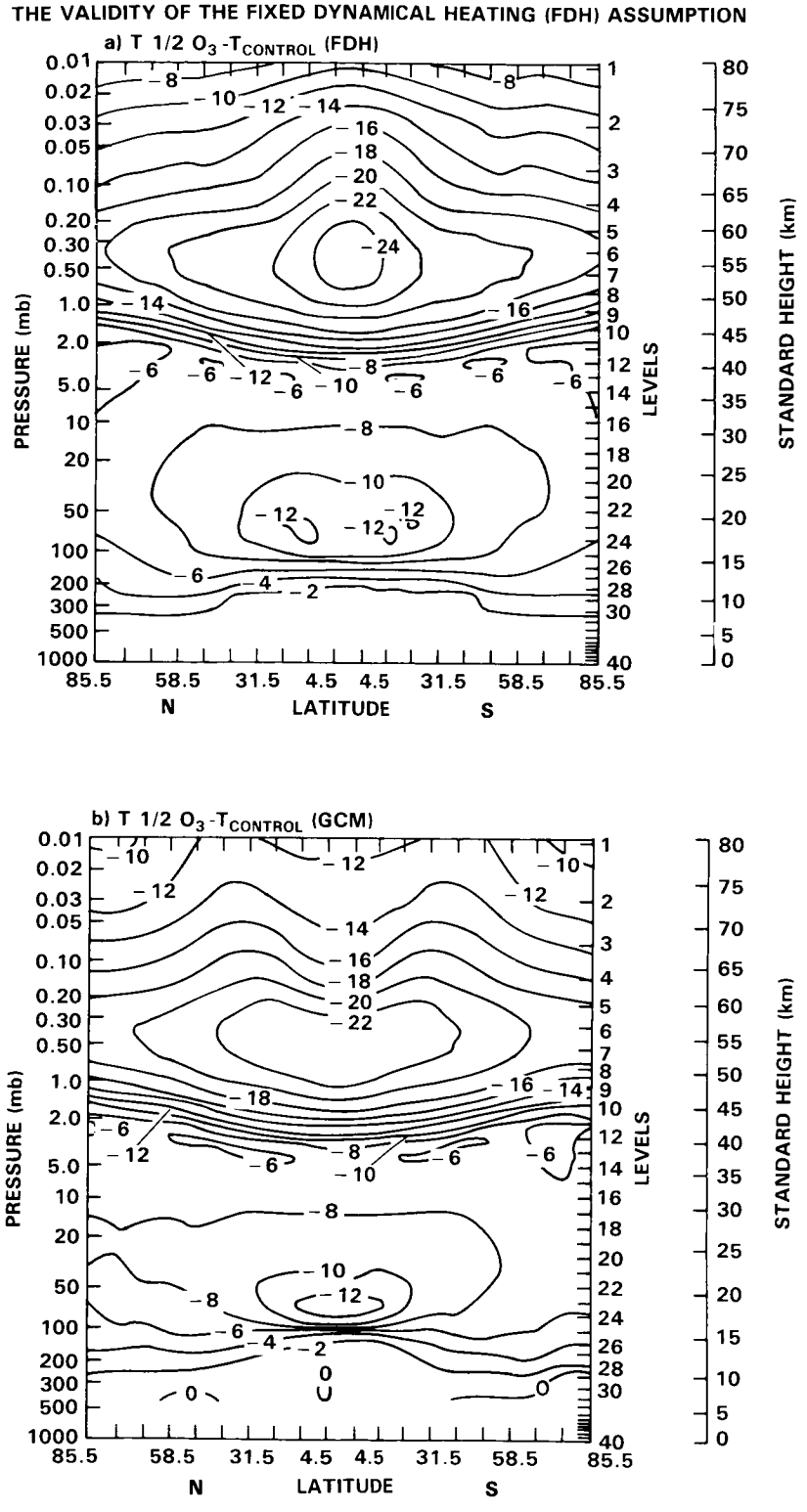

Figure 15-12. Temperature change due to 50% ozone reduction as simulated by (a) the FDH model and (b) the GCM. (Fels *et al.,* 1980).

Table 15-8. Estimates of the Abundance of Trace Chemicals in the Global Atmosphere of Years 1980 and 2030. Source: Ramanathan, Cicerone, Singh and Kiehl (1985)

Chemical Group	Chemical Formula	Dominant Source*	Dominant Sink*	Estimated Average Residence Time (τ_j) (years)	Year 1980 Global Average Mixing Ratio (ppb)†	Year 2030 probable global average concentration (ppb)*** Probable Value	Possible Range	REMARKS (also see text for details)
Carbon Dioxide	CO_2	N,A	O	2	339×10^3	450×10^3	—	Based on a 2.4% per year increase in anthropogenic CO_2 release rates over the next 50 years
Nitrogen Compounds	N_2O	N,A	S(UV)	120	300	375	350 - 450	Combustion and fertilizer sources
	NH_3	N,A	T	0.01	<1	<1	—	Concentration variable and poorly characterized
	$(NO+NO_2)$	N,A	T(OH)	0.001	0.05	0.05	0.05 - 0.1	Concentration variable and poorly characterized
Sulfur Compounds	CSO	N,A	T(O,OH)?	1(?)	0.52	0.52	—	Sources and sinks largely unknown
	CS_2	N,A	T	1(?)	<0.005	<0.005	—	Sources uncharacterized
	SO_2	A(?)	T(OH)	0.001	0.1	0.1	0.1 - 0.2	Given the short lifetime the global presence of SO_2 is unexplained
	H_2S	N	T(OH)	0.001	<0.05	<0.5	—	
Fully Fluorinated Species	CF_4(F14)	A	I	>500	0.07	0.24	0.2 - 0.31	Aluminum industry a major source
	C_2F_6(F116)	A	I	>500	0.004	0.02	0.01 - 0.04	Aluminum industry a major source
	SF_6	A	I	>500	0.001	0.003	0.002 - 0.05	
Chlorofluoro-carbons	$CClF_3$(F13)	A	S(UV),I	400	0.007	0.06	0.04 - 0.1	All chlorofluorocarbons are of exclusive man-made origin. A number of regulatory actions are pending. The nature of regulations and their effectiveness would greatly affect the growth of these chemicals over the next 50 years.
	CCl_2F_2(F12)	A	S(UV)	110	0.28	1.8	0.9 - 3.5	
	$CHClF_2$(F22)	A	T(OH)	20	0.06	0.9	0.4 - 1.9	
	CCl_3F(F11)	A	S(UV)	65	0.18	1.1	0.5 - 2.0	
	CF_3CF_2Cl(F115)	A	S(UV)	380	0.005	0.04	0.02 - 0.1	
	$CClF_2CClF_2$(F114)	A	S(UV)	180	0.015	0.14	0.06 - 0.3	
	CCl_2FCClF_2(F113)	A	S(UV)	90	0.025	0.17	0.08 - 0.3	
Chlorocarbons	CH_3Cl	N(O)	T(OH)	1.5	0.6	0.6	0.6 - 0.7	Dominant natural chlorine carrier of oceanic origin
	CH_2Cl_2	A	T(OH)	0.6	0.03	0.2	0.1 - 0.3	A popular reactive but non-toxic solvent
	$CHCl_3$	A	T(OH)	0.6	0.01	0.03	0.02 - 0.1	Used for manufacture of F22; many secondary sources also exist
	CCl_4	A	S(UV)	25 - 50	0.13	0.3	0.2 - 0.4	Used in manufacture of fluorocarbons; many other applications as well
	CH_2ClCH_2Cl	A	T(OH)	0.4	0.03	0.1	0.06 - 0.3	A major chemical intermediate (global production=10 tg/yr); possibly toxic
	CH_3CCl_3	A	T(OH)	8.0	0.14	1,5	0.7 - 3.7	Non-toxic, largely uncontrolled degreasing solvent
	C_2HCl_3	A	T(OH)	0.02	0.005	0.01	0.005 - 0.02	Possibly toxic, declining markets because of substitution to CH_3CCl_3
	C_2Cl_4	A	T(OH)	0.5	0.3	0.07	0.03 - 0.2	Possibly toxic, moderate growth due to substitution to CH_3CCl_3
Brominated and iodated species	CH_3Br	N	T(OH)	1.7	0.01	0.01	0.01 - 0.02	Major natural bromine carrier
	$CBrF_3$(F13B1)	A	S(UV)	110	0.001	0.005	0.003 - 0.01	Fire extinguisher
	CH_2BrCH_2Br	A	T(OH)	0.4	0.002	0.002	0.001 - 0.01	Major gasoline additive for lead scavenging; also a fumigant
	CH_2I	N	T(UV)	0.02	0.002	0.002	—	Exclusively of oceanic origin
Hydrocarbons, CO, H_2	CH_4	N	T(OH)	5 - 10	1650	2340	1850 - 3300	A trend showing increase over the last 2 years has been identified
	C_2H_6	N	T(OH)	0.3	0.8	0.8	0.8 - 1.2	Predominantly of auto exhaust origin
	C_2H_2	A	T(OH)	0.3	0.06	0.1	0.06 - 0.16	No trend has been identified to date
	C_3H_8	N,	T(OH)	0.03	0.05	0.05	0.05 - 0.1	No trend has been identified to date
	CO	N,A	T(OH)	0.3	90	115	90 - 160	No trend has been identified to date
	H_2	N,A	T(SL,OH)	2	560	760	560 - 1140	
Ozone	O_3 (Tropospheric)	N	T(UV, SL,O)	0.1 - 0.3	F(Z)**	12.5%		A small trend appears to exist but data are insufficient
Aldehydes	HCHO	N	T(OH,UV)	0.001	0.2	0.2	—	Secondary products of hydrocarbon oxidation
	CH_3CHO	N	T(OH,UV)	0.001	0.02	0.02	—	1980 concentration estimated from theory

*N - Natural; A - Anthropogenic; O - Oceanic; S - Stratosphere; UV - Ultraviolet Photolysis; T - Troposphere; OH - Hydroxyl radical removal; I - Ionospheric and extreme UV and electron capture removal; SL - Soil sink.

†These concentrations are integrated averages; for chemicals with lifetimes of 10 years or less, significant latitudinal gradients can be expected in the troposphere; for chemicals with extremely short lifetimes (0.001-0.3 years) vertical gradients may also be encountered.

**Varies from 25 ppbv at the surface to about 70 ppbv at 9 km. The concentration was increased uniformly by the same percentage from the surface to 9 km.

***These values are not used in the present assessment.

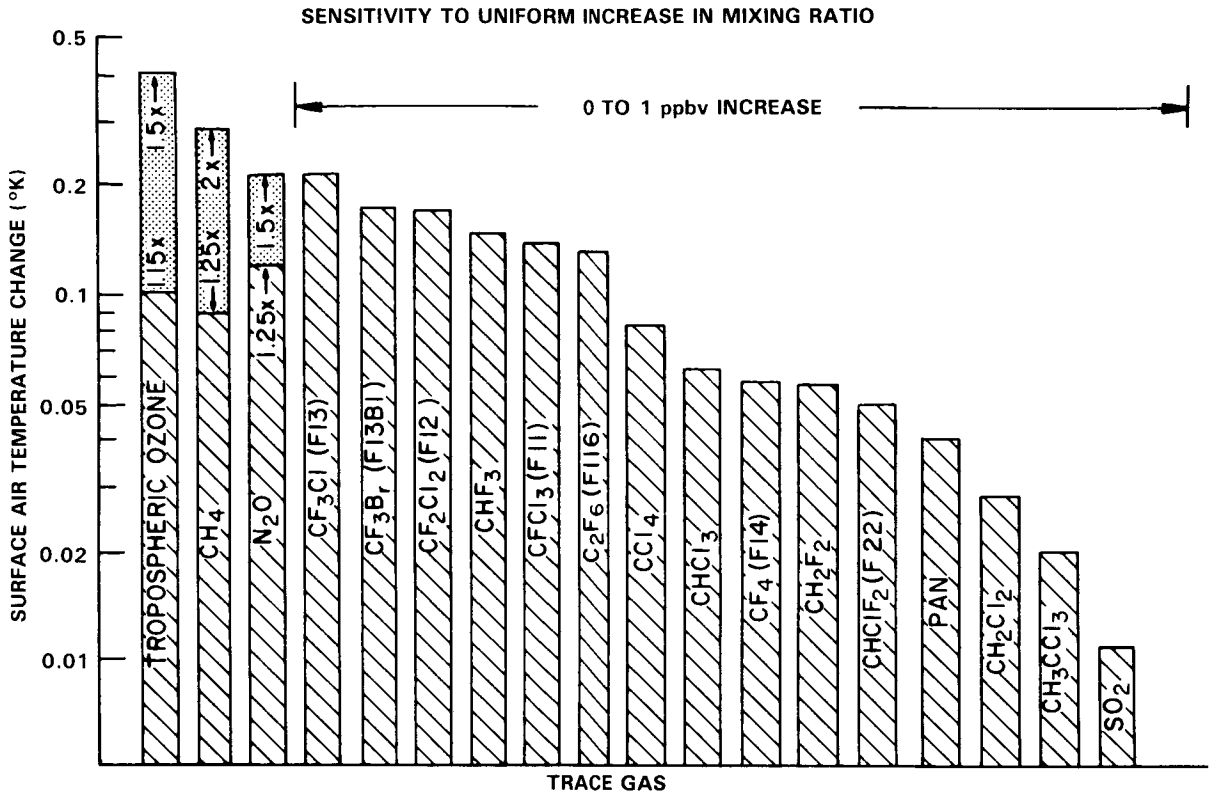

Figure 15-13. Computed surface air temperature change due to a 0 to 1 ppbv increase in trace gas concentrations. Tropospheric O_3, CH_4 and N_2O increases are also shown for comparison. For these three gases, the factor of increase is indicated in the figure. For example, for tropospheric O_3, the bottom part of the shaded region is the temperature change due to a uniform increase in O_3 from 0 to 12 km by a factor of 1.15. Source: 1-D radiative-convective model results of Ramanathan *et al.* (1985).

It is important to note that increasing levels of these gases are essentially additive and have the potential to add directly and significantly to the greenhouse effect of the present day atmosphere. Furthermore, several of the important gases shown in Table 15-8 (e.g., F13; F116; F13B1; CF_4) have lifetimes in excess of 100 years, and hence, if their use increases in the future, these gases have the potential for a substantial impact on climate on time scales of several hundred years.

15.3.2 Indirect Effects

In addition to the direct effects, many of the trace gases perturb temperatures indirectly through physical or chemical mechanisms that cause the distributions, or concentrations of other optically active constituents to be changed. The nature of some of the interactions leading to these indirect effects were shown in Figure 15-4. Most well known of these is perhaps the stratospheric destruction of O_3 due to reaction with chlorine and chlorine oxides formed as a result of stratospheric photolysis of chlorine bearing compounds (e.g., CF_2Cl_2, $CFCl_3$, CCl_4, and CH_3Cl). The altered atmospheric levels O_3 will affect both the tropospheric and stratospheric radiative budgets at both solar and infrared wavelengths. Furthermore, temperature changes can perturb chemistry through the H_2O feedback (Section 15.2). These and other examples are discussed in the following paragraphs.

15.3.2.1 H_2O-Temperature Feedback Effects on Tropospheric Chemistry

As discussed in Section 15.2.3, climate models including GCMs indicate that an increase in tropospheric humidity accompanies the computed surface/troposphere warming (due to the greenhouse effect of trace gases). For example, a 2 K tropospheric warming in the RCM (due to CO_2 doubling) leads to an increase of H_2O that ranges from about 10 to 30% (Figure 15-14). The increase in H_2O can lead to enhanced OH production through the reaction (Hameed *et al.*, 1980):

$$O(^1D) + H_2O \rightarrow 2OH \quad (1)$$

which also acts as a direct loss reaction for ozone as O(1D) is in instantaneous equilibrium with O_3. Further loss of ozone may take place through the reactions:

$$OH + O_3 \rightarrow HO_2 + O_2 \quad (2)$$

$$HO_2 + O_3 \rightarrow OH + 2O_2 \quad (3)$$

However, at high NO_x levels, ozone is efficiently produced through the catalytical cycle:

$$HO_2 + NO \rightarrow NO_2 + OH \quad (4)$$

$$NO_2 + h\nu \rightarrow NO + O \quad (5)$$

$$O + O_2 + M \rightarrow O_3 + M \quad (6)$$

The main source for HO_2 is OH reacting with CO (see discussions later under the CO section) rather than reaction (2). Hence, reactions (4) to (6) lead to a net O_3 production. However, due to the large observed variations in tropospheric NO levels, with extremely low values in some remote regions, one could expect either ozone production or ozone destruction as a result of the reactions (1) to (6).

Tropospheric CH_4 levels may also be reduced by the reaction

$$CH_4 + OH \rightarrow CH_3 + H_2O \quad (7)$$

For a doubling of CO_2, the 1-D latitudinal energy balance model (Hameed and Cess, 1983), with a ΔT_S of 3.1 K, shows a decrease in tropospheric O_3 and CH_4 of 11% and 17% respectively; the radiative-convective model, with a ΔT_S of 2 K, computes a decrease of 5-7% for tropospheric O_3 and 9-14% for CH_4. Because of the nonlinearities in the H_2O-T coupling and other nonlinearities in the chemistry, simultaneous perturbations may exacerbate the effect (e.g., see Figures 15-15 and 15-16). For example, a doubling of CO_2 with a CFC increase (due to steady state injection of CFC11 and CFC12 at the 1977 emission rate) results in a computed decrease of about 16% for O_3 (see Figure 15-15) and about 26% for CH_4 (Callis *et al.*, 1983a).

The O_3 and CH_4 changes resulting from the H_2O-T coupling have a negative feedback effect on the computed ΔT_S. For a CO_2 doubling, the computed surface warming decreases by about 10% with the inclusion of the decreases in O_3 and CH_4 (Hameed and Cess, 1983). All of the results described above

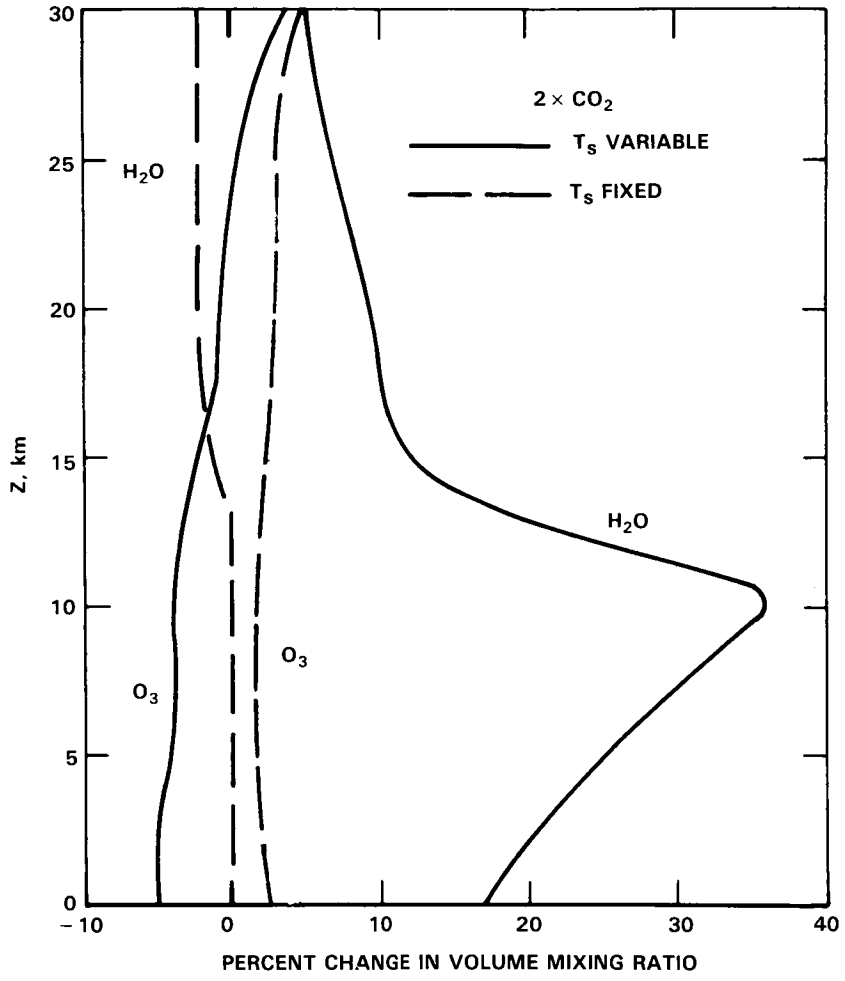

Figure 15-14. Indirect effects of CO_2 doubling on H_2O and O_3. Solid: both stratospheric and tropospheric temperatures are allowed to vary; dash: only stratospheric temperatures are allowed to vary in response to CO_2 increase. Source: 1-D model results of Callis *et al.* (1983a).

depend very strongly on the assumed background levels of NO_x (Hameed *et al.*, 1979; also see Figure 15-15), since the ozone formation as described above as well as the products in the methane oxidation scheme depend on NO concentrations.

15.3.2.2 Effects of CO_2

Carbon dioxide does not react chemically to any significant degree in the troposphere or stratosphere. However, the stratospheric temperature decrease that is computed to result from CO_2 increase (Manabe and Wetherald, 1967) will alter the reaction rates and can lead to stratospheric O_3 increases (Boughner and Ramanathan, 1975). The O_3 increase can, in turn, have a negative feedback on the CO_2-induced stratospheric cooling. Numerous coupled 1-D model studies (Boughner, 1978; Owens *et al.*, 1985) have estimated this feedback. For a doubling of CO_2, the model calculations generally indicate a column O_3 increase of 2 to 6% (see Table 6 of Owens *et al.*, 1985). This O_3 increase is mainly concentrated above 20 km where the enhanced solar heating (due to O_3 increase) reduces the stratospheric cooling due to

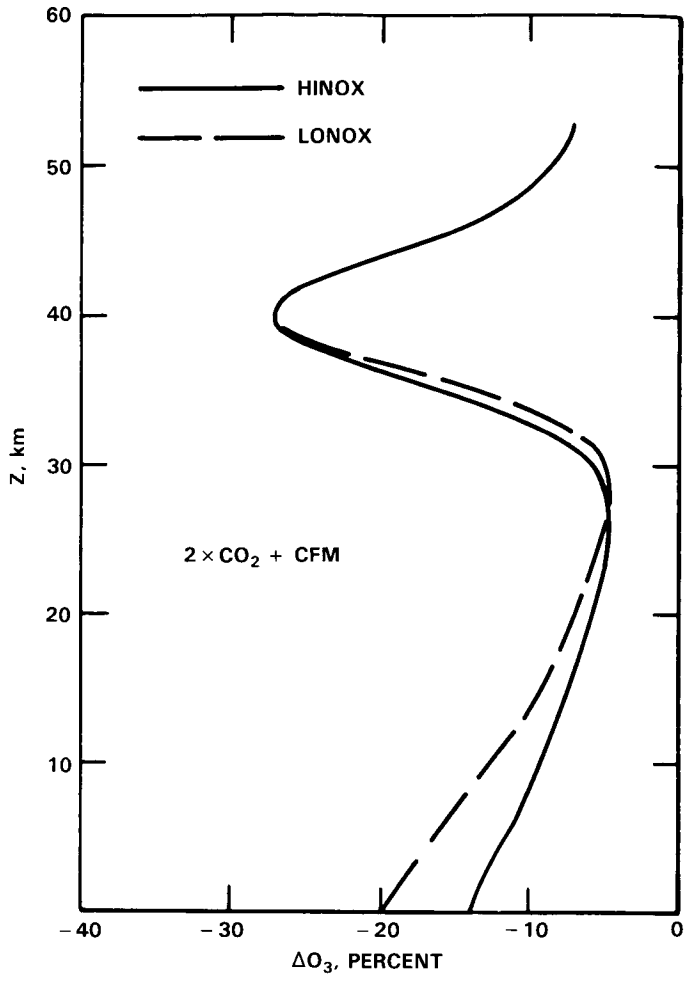

Figure 15-15. Computed changes in O_3 due to the combined effects of CO_2 doubling and CFM increase. Source: 1-D model results of Callis *et al.* (1983a). HINOX and LONOX refer to high and low concentrations of assumed background values for NO_x.

CO_2 increase by about 20% (Figure 7 of Owens *et al.*, 1985). The effect of the O_3-T feedback on surface temperature is negligible.

15.3.2.3 Effects of CH_4

Recent studies (Blake and Rowland, 1985 and Blake *et al.*, 1982) show that tropospheric concentrations of CH_4 have been increasing at a rate of about 1 percent per year over the last 4-6 years. The causes of this increase are not known at present. Both changes in the release rate of methane and in the loss rate due to changes in OH concentrations, reaction (7), affect atmospheric CH_4 levels. In addition, as the methane oxidation by reaction (7) is a main loss path of OH in the free troposphere, increases in the release rate of methane lead to a decrease in OH, and thereby to a further increase in methane levels. With continued increases in methane in the future, this positive feedback mechanism could become increasingly important. Recent 2-D model studies (Isaksen and Hov, 1985) suggest that this feedback may account for 30% of the methane increase at present. However, since the magnitude of this feedback depends on the assumed emission of NO_x, the contribution of this feedback to the observed CH_4 increase is highly model dependent

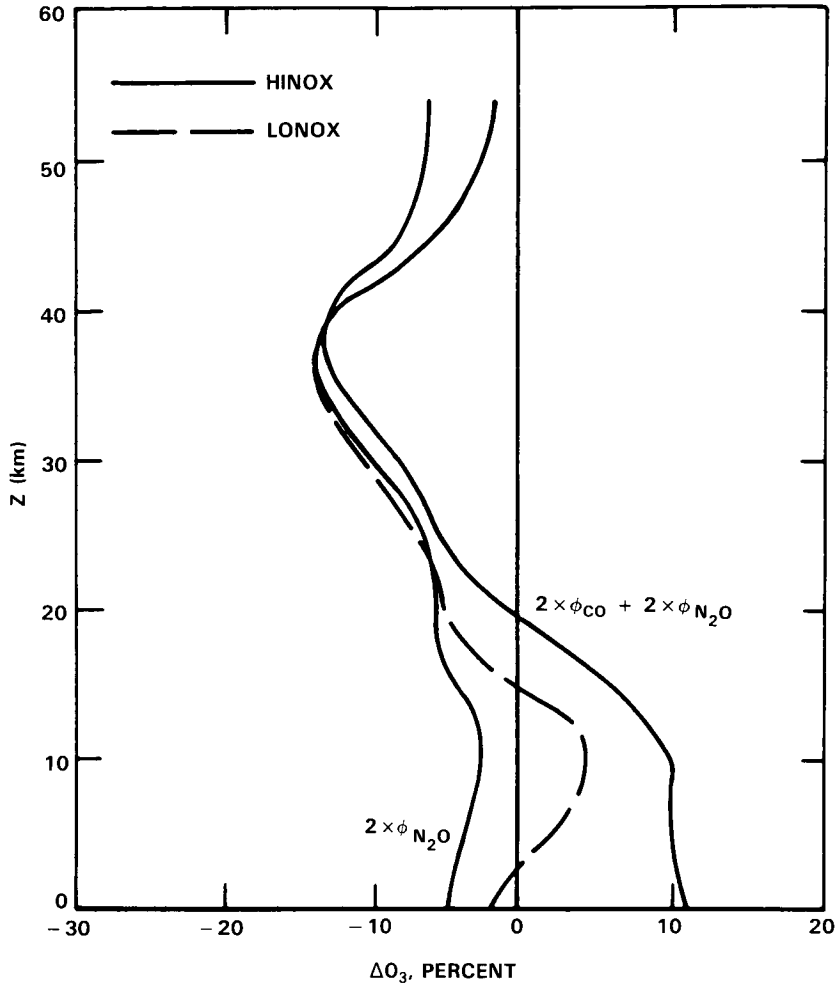

Figure 15-16. The indirect effects of increases in fluxes (ϕ) of CO and N_2O on O_3. Source: 1-D model results of Callis *et al.* (1980).

(Crutzen, private communication). A reduction of tropospheric OH levels due to CH_4 increase will also lead to reduction of the rate of scavenging (by OH) of CH_2F_2, $CHClF_2$, CH_2Cl_2, CH_3CCl_3, and SO_2 leading to increased lifetimes (and hence, concentrations) of these species with attendant perturbations to the infrared radiative balance. Increases in tropospheric methane will, provided sufficient amounts of NO_x are present, lead to enhanced ozone production through reaction (4) and the reaction:

$$CH_3O_2 + NO \rightarrow CH_3O + NO_2 \qquad (8)$$

followed by reactions (5) and (6), where productions of CH_3O_2 and HO_2 are enhanced. 2-D model estimates show that tropospheric ozone increases due to increased methane levels vary strongly with latitude, height and season (Crutzen and Gidel, 1983; Isaksen and Stordal, 1985). In 2-D models, the most pronounced ozone increase is obtained at equatorial latitudes, with ozone increases of approximately 20% in the middle and upper troposphere for a doubling of present methane levels (see Figure 15-17). In the 1-D model, the greenhouse effect of enhanced tropospheric O_3 amplifies the CH_4 greenhouse effect by as much as 75% (Table 8 of Owens *et al.*, 1985b).

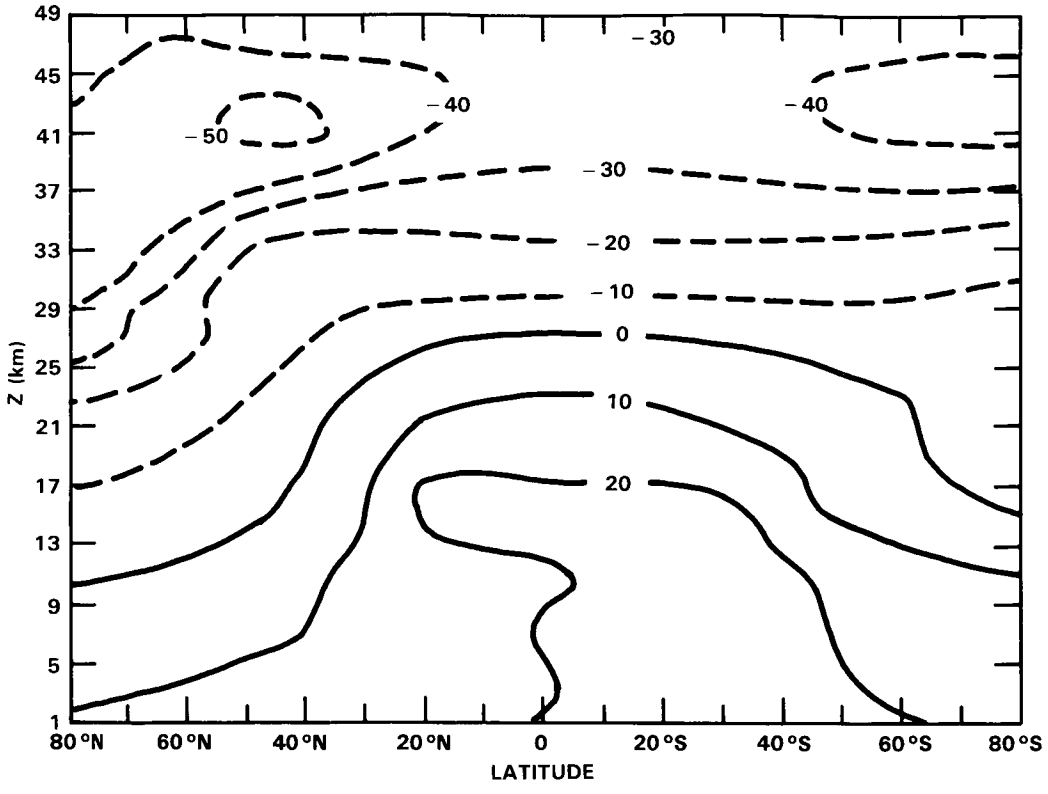

Figure 15-17. Latitudinal-height cross-section of future ozone changes (in %) due to releases of CFCs (CFC11 and CFC12), N_2O and CH_4, estimated in a 2-D diabatic circulation model (Isaksen and Stordal, 1985). The following assumptions are made with regard to future release rates and concentration rates: CFCs are in steady state with 1980 release rates, N_2O increases with a factor 1.4 from its 1980 value (300 ppb at the surface), CH_4 increases with a factor 2 from its 1980 value (1.65 ppm at the surface). The numbers given are for February.

Furthermore, increases in CH_4 are calculated to lead to similar, but less pronounced increases in lower and mid-latitudinal stratospheric ozone through their effect on HO_x, Cl_x and NO_x species (WMO, 1981). For example, CH_4 can mitigate the ozone destruction by the chlorine catalytic cycle in the middle stratosphere (around 40 km) because it can transform the Cl atoms to HCl (Brühl and Crutzen, 1984). An additional effect is that oxidation of methane may lead to substantial increases in H_2O levels in the middle and upper stratosphere (see Callis *et al.*, 1983a; Owens *et al.*, 1985b).

15.3.2.4 Effects of N_2O

Weiss (1981) has reported data that suggest that atmospheric N_2O, currently at levels of 300 ppbv, was increasing at the rate of 0.2 percent per year between the years of 1976-1980. Khalil and Rasmussen (1983) suggest an increase of 0.3 percent per year between the years of 1978-1981.

The indirect effects of increases of atmospheric N_2O arise from the reaction:

$$N_2O + O(^1D) \rightarrow 2NO \qquad (9)$$

Reaction (9) is the principal source of stratospheric NO_y (= NO + NO_2 + HNO_3 + NO_3 + HNO_4 + HNO_2 + 2 × N_2O_5 + ...). Consequently, increases in atmospheric N_2O levels will lead to increases in stratospheric NO_y and the subsequent reduction of stratospheric O_3 by catalytic destruction through the reactions

$$NO + O_3 \rightarrow NO_2 + O_2 \quad (10)$$

$$NO_2 + O \rightarrow NO + O_2 \quad (11)$$

If increases in N_2O occur at the same time as increases in the chlorine bearing compounds (e.g., CF_2Cl_2, $CFCl_3$, and CCl_4), the net effect will depend upon the details of the projected increases and their vertical distributions. Increasing stratospheric NO_y levels will provide a buffer for the stratospheric O_3 against catalytic destruction by Cl_x (= Cl + ClO + HOCl + $ClNO_3$ + ClO_2 + ...) through the reaction

$$NO_2 + ClO + M \rightarrow ClNO_3 + M \quad (12)$$

where $ClNO_3$ represents a temporary reservoir of relatively inactive chlorine. It will also affect the partitioning of chlorine species through the reaction

$$ClO + NO \rightarrow Cl + NO_2 \quad (13)$$

The chemical perturbations induced by N_2O increase are so complicated that even the sign of the tropospheric O_3 change is uncertain. For example, for a doubling of N_2O surface flux (leading to a 93% increase in surface concentration of N_2O) the computed 0-10 km column change in O_3 ranges from −2% to +4% depending upon the background levels of tropospheric NO + NO_2 (see Figure 15-16); the stratospheric O_3 column decreases by about 7%.

15.3.2.5 Effects of CO

Carbon monoxide is itself not radiatively active and therefore does not manifest any direct effects on the earth-atmosphere radiative balance. However CO does scavenge atmospheric OH through the reaction

$$CO + OH \rightarrow CO_2 + H \quad (14)$$

The reduction of tropospheric OH, as noted earlier, can, in turn, affect the abundance of numerous other species including O_3, CH_4, and hydrocarbons which are not fully halogenated (Sze, 1977; Logan *et al.*, 1978 to name a few). This has been discussed earlier in reference to CH_4 increase.

Large interhemispheric differences in the present day atmosphere are exhibited by CO due primarily to anthropogenic emissions (Logan *et al.*, 1981). In addition, increases in tropospheric CO have been suggested by recent studies (Rasmussen and Khalil, 1981; Fraser *et al.*, 1981; Graedel and McRae, 1980; and Khalil and Rasmussen, 1984). Clearly, consideration should be given to the indirect climatic effects of CO, particularly since model calculations (e.g., Hameed and Cess, 1983) have suggested the effects to be significant.

For a doubling of the surface flux of CO (leading to a factor of 2.5 increase in CO), the OH decrease through reaction (14) can lead to increases in CH_4 of about 40 to 50% and to increases in column O_3

of about 12% (Callis *et al.*, 1983a; Hameed *et al.*, 1979 and Hameed and Cess, 1983). In the model calculations (Callis *et al.*, 1983a), the increase in CH_4 also leads to stratospheric H_2O increase of about 7 to 12%.

15.3.2.6 Effects of NO_x (NO + NO_2)

As pointed out repeatedly in the earlier discussions, the indirect effects of trace gases depend critically on the tropospheric concentration of NO_x. Photochemical model calculations have also revealed the significant sensitivity of the computed tropospheric O_3 to the concentration as well as the vertical distribution of NO_x (Fishman and Crutzen, 1978; Liu *et al.*, 1980). Tropospheric NO_x has a variety of natural and anthropogenic sources (e.g., Logan, 1983): combustion and biogenic emissions are major surface sources; high flying aircraft, downward transport from stratosphere are important upper tropospheric sources. In addition, lightning may also contribute significantly in the upper troposphere. The removal of NO_x is through wet and dry deposition, mostly after its conversion to soluble species such as HNO_3 and N_2O_5. The exact removal process is not well understood and difficult to model without a realistic 3-dimensional model.

The indirect climate effect of NO_x arises because of its effect on O_3. Within the troposphere, the chemistry and photochemistry of NO_x is an important source of O_3 through reactions (4) to (6). Within the upper troposphere of the Northern Hemisphere (NH) the NO_x emission from high flying aircraft is considered to be as important a source as natural sources of NO_x (Liu *et al.*, 1980).

Although all models agree that anthropogenic NO_x emissions at the surface and by aircraft will result in the increase of tropospheric O_3, problems in modeling NO_x distribution make it difficult to obtain a reliable quantitative evaluation of the O_3 increase, particularly in the boundary layer where non-methane hydrocarbons play an important yet complex role in the photochemical production of O_3. In the upper troposphere, model calculated O_3 increase in the Northern Hemisphere ranges from a few percent (Isaksen, 1980, Derwent, 1982; Crutzen and Gidel, 1983) to as high as 30 percent (Liu *et al.*, 1980). The major difference is due to assumed natural background NO_x sources in the upper troposphere. In the lower troposphere, estimated O_3 increase in the Northern Hemisphere is about 20 percent (Isaksen, 1980).

From the above discussion, it is probably reasonable to assume a 5% increase in the Northern Hemisphere tropospheric O_3 for the decade of 1970 (e.g., Liu *et al.*, 1980; Isaksen, 1980) due to anthropogenic NO_x emissions. The Northern Hemisphere surface-troposphere radiative heating due to this O_3 increase is roughly a third of that due to the observed CO_2 increase for the decade of 1970.

15.3.2.7 Effects of Halogenated Hydrocarbons

A large number of halogenated hydrocarbons (Table 15-8) have direct effects (Figure 15-13) as well as indirect effects in both the troposphere and the stratosphere. Species not fully halogenated may be expected, at elevated concentrations, to contribute to the reduction of tropospheric OH with subsequent effects on tropospheric O_3 and CH_4 and taking place. However, this effect is expected to be small provided the concentrations of the species remain of the order of a few ppbv or less.

Some of these species released in the troposphere will be photodissociated in the stratosphere with the release of halogens which may catalytically destroy O_3. Of most concern at present and for the immediate future is the catalytic destruction of ozone by chlorine released from the photodissociation of CF_2Cl_2 and $CFCl_3$. This destruction occurs due to the reactions

$$Cl + O_3 \rightarrow ClO + O_2 \quad (15)$$

$$ClO + O \rightarrow Cl + O_2 \quad (16)$$

Recent estimates suggest that steady state emissions of CF_2Cl_2 and $CFCl_3$ may reduce the column sum of O_3 by 3-5% with local reductions of 30 to 50% between 35 to 45 km (Cicerone *et al.*, 1983a, Wuebbles *et al.*, 1983; Owens *et al.*, 1985a; to name a few). Reductions in stratospheric O_3 of such magnitudes will have a significant impact on stratospheric thermal structure (Figure 15-18). Furthermore, within the upper stratosphere, the computed cooling due to CFC-induced O_3 reduction is as large as that due to CO_2 doubling (compare the "CFCs" curve with the "2 CO_2" curve in Figure 15-18).

Since the effect of stratospheric O_3 change on surface temperature depends very critically on the vertical distribution of O_3 change, the computed surface temperature effects have fluctuated in magnitude as well as in *sign* over the years. For example, the computed O_3 perturbation profiles that were reported prior

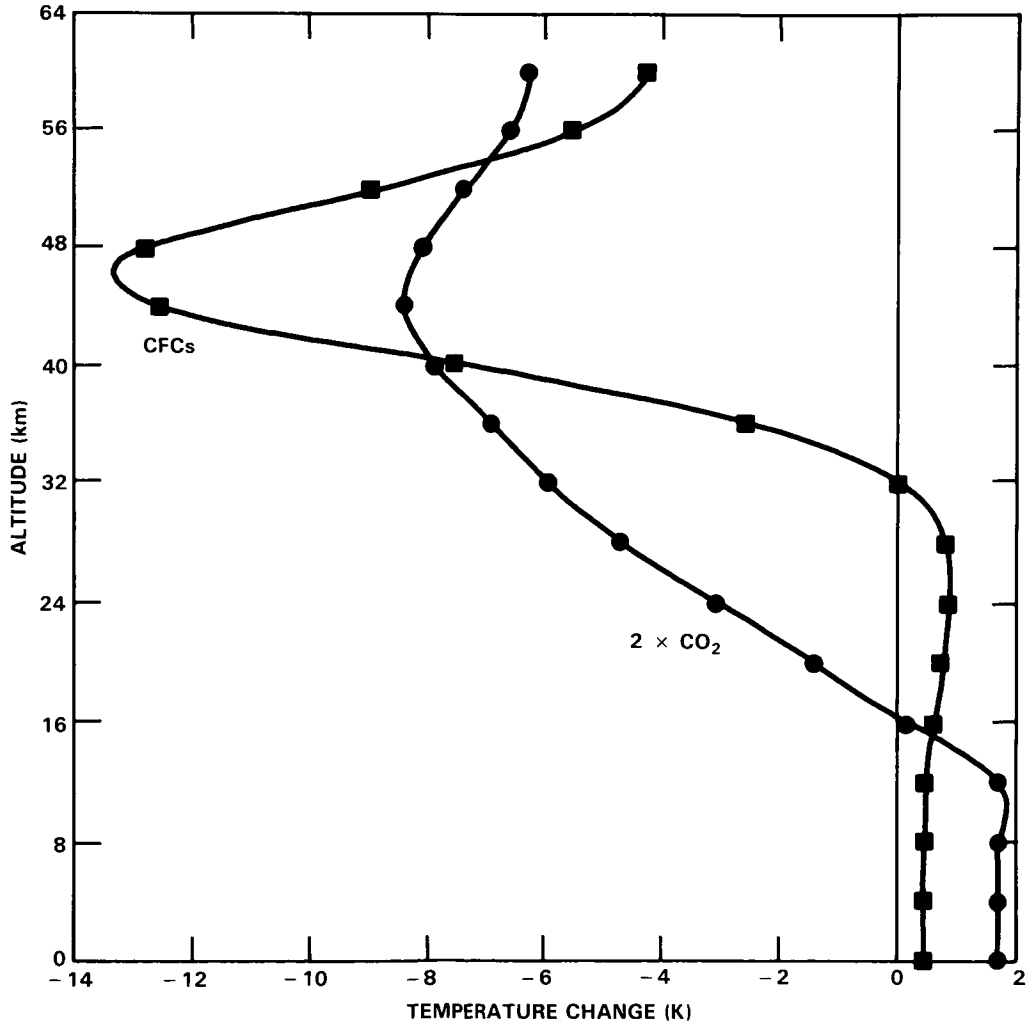

Figure 15-18. Calculated temperature changes due to releases of CFC11 and CFC12 in the steady state (open squares); solid circles: computed effect for 2 × CO_2. (Ref: Owens *et al.*, 1985a).

to the early 1980's yielded a slight surface cooling (Wang *et al.*, 1980). The more recent profiles of O_3 change yield both a surface cooling (Callis *et al.*, 1983a) and a surface warming (Owens *et al.*, 1985a; Ramanathan *et al.*, 1985). The primary source of the difference is the magnitude of O_3 changes in the upper troposphere and lower stratosphere, an issue which is somewhat unresolved at this time.

Irrespective of the sign of the computed surface temperature effect, the magnitude is non-negligible. For example, the recent studies of Owens *et al.* (1985) and Ramanathan *et al.* (1985) estimate a surface warming of 0.1 K due to O_3 change resulting from steady state injection of CFCs at constant mid-1970's emission rates which is about 25-30% of the computed warming due to the direct greenhouse effect of the CFCs. Furthermore, O_3 effects on climate depend on season and latitude (see Section 15.1.2) and both of these effects have been ignored in current climate model studies. Clearly, the O_3-climate effects resulting from the addition of chlorines to the stratosphere deserves continued study.

15.4 TRANSIENT CLIMATIC EFFECTS OF INCREASING ATMOSPHERIC CO_2

15.4.1 Observed Increases In CO_2

Measurements taken at Mauna Loa, Hawaii show that the CO_2 concentration has increased from 315 ppmv in 1958 to 342 ppmv in 1983 (Elliott *et al.*, 1985, see Figure 15-19), an 8% increase in 25 years. A variety of direct CO_2 measurements and indirect reconstructions indicate that the pre-industrial CO_2 concentration during the period 1800 to 1850 was 270 $\pm$10 ppmv (WMO, 1983b). Analyses of the future usage of fossil fuels suggest that the CO_2 concentration will reach twice the pre-industrial value by 2100 (Nordhaus and Yohe, 1983). The change in surface air temperature induced by a doubling of CO_2 as simulated by climate models was discussed in Section 15.2.2. The computed changes in global mean surface air temperature ranged from 1.3 to 4.2 K with the three most recent GCM results falling near the upper end of this range (see Table 15-7). Since such a global warming represents about 25 to 100% of that which is estimated to have occurred during the 10,000-year transition from the last ice age to the present interglacial (Gates, 1976; Imbrie and Imbrie, 1979), there is considerable interest in the identification of a CO_2-induced climatic change, and in the potential impacts of such a change on the spectrum of human endeavors.

The majority of the simulations of CO_2-induced climate change have been performed to determine the change in the equilibrium climate of the earth resulting from an abrupt increase in CO_2 such as doubling from 300 to 600 ppmv. These equilibrium climate change simulations have not been concerned with the time required for the climate change to reach its equilibrium. More recent studies have focused on the transient response of climate to both abrupt and realistic increases in the CO_2 concentration.

15.4.2 Transient Effects

The equilibrium temperature increase corresponding to the CO_2 increase from the year 1850 to 1980 can be determined using Equation 1 of Section 15.2.2 with the direct radiative forcing ΔQ scaled to that for a CO_2 doubling, ΔQ_{2X}. This scaling yields (Augustsson and Ramanathan, 1977):

$$\Delta Q = \Delta Q_{2x} \left\{ \frac{\ln[C(1980)/C(1850)]}{\ln 2} \right\} \quad (1)$$

where C is the CO_2 concentration. Combining these equations and noting that $(\Delta T_s)_{2X} = \Delta Q_{2X}/\lambda$ (see Equation 1 of 15.2), yields

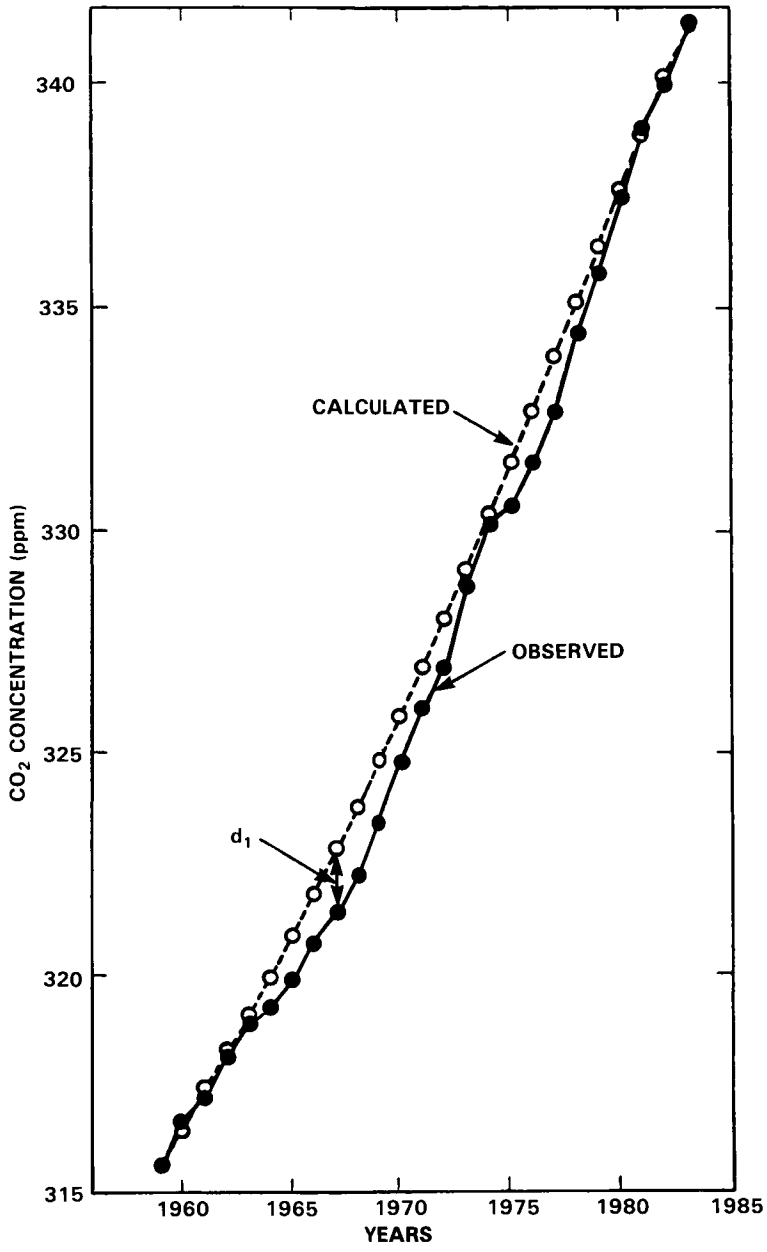

Figure 15-19. Concentration of atmospheric CO_2 at Mauna Loa Observatory, Hawaii from 1958 to 1983. The "calculated" curve is the curve used in the climate model calculations shown in Figure 15-21.

$$\Delta T_s = (\Delta T_S)_{2x} \left\{ \frac{\ln[C(1980)/C(1850)]}{\ln 2} \right\} \tag{2}$$

If we assume that $(\Delta T_s)_{2x} \approx 4$ K based on the results from the GFDL, GISS and NCAR models, then for the CO_2 concentration increase from 270 (year 1850) to 338 ppmv (year 1980), $\Delta T_s = 1.3$ K. However, the reconstructed Northern Hemisphere surface air temperature record (see Figure 15-1) indicates a warming from 1880 to 1980 of about 0.6 K. Does this difference mean that the sensitivity of the GCMs is too large by a factor of two? The likely answer is: not necessarily, since the actual reponse of the climate system

lags the equilibrium response because of the thermal inertia of the ocean. This can be illustrated by the energy balance model

$$C_s \frac{d\Delta T_s}{dt} = \Delta Q - \lambda \Delta T_s$$

where C_s is the heat capacity of the upper ocean. When equilibrium is achieved, $d\Delta T_s/dt = 0$ and $(\Delta T_s)_{eq} = \Delta Q/\lambda$. However, the transient solution

$$\Delta T_s(t) = (\Delta T_s)_{eq}(1 - e^{-t/\tau_\epsilon})$$

shows that equilibrium is approached exponentially with a characteristic "e-folding" time $\tau_\epsilon = C_s/\lambda$. In the following two sections the studies of this lag of the climate system are reviewed.

15.4.3 Results From Simplified Models

The transient response of the climate system to an abrupt CO_2 increase has been investigated with planetary energy balance, radiative-convective and simplified atmospheric general circulation models in conjunction with box-diffusion, box-advection-diffusion and two-box ocean models as well as with simplified oceanic general circulation models. The box-diffusion ocean model consists of a fixed-depth mixed layer (the box) surmounting the thermocline and deep ocean in which vertical heat transport is treated as a diffusive process with prescribed thermal diffusivity $\varkappa$. The box-advection-diffusion ocean model is a box-diffusion model with a prescribed value for oceanic upwelling. The two-box ocean model is comprised of a fixed-depth mixed-layer box and an intermediate water box which exchange heat vertically with a prescribed ventilation time.

The results from 6 studies of the transient response to abrupt heating are presented in Table 15-9. Hoffert *et al.* (1980), using a box-advection-diffusion model, and Schneider and Thompson (1981), using a two-box ocean model, obtained e-folding times of 10 to 20 years. A slightly larger e-folding time of 25 years was obtained by Bryan *et al.* (1982) and Spelman and Manabe (1984) with a simplified coupled atmosphere-ocean general circulation model in which the geographical domain was restricted to a 120°-longitude sector extending from equator to pole, with the western half of the sector occupied by land at zero elevation and the eastern half by ocean with a uniform depth of 5000 m. On the other hand, Hansen *et al.*, (1984) used a box-diffusion ocean model and obtained 27, 55 and 102 year e-folding times corresponding to assumed λ values of 2.15, 1.4 and 1 $Wm^{-2}\,K^{-1}$, respectively. Bryan *et al.* (1984) used an uncoupled global oceanic general circulation model and found an e-folding time of about 100 years in response to an imposed 0.5 K upper ocean surface warming. Lastly, Siegenthaler and Oeschger (1984) obtained a 60 year e-folding time in their study using a box-diffusion model.

The studies presented in Table 15-9 indicate that the e-folding time τ_e lies between 10 and 100 years. If $\tau_e \sim 10$ years then the actual response of the climate system would be quite close to the equilibrium response and the disparity between the latter for the 1850 to 1980 warming and that observed would mean that the climate sensitivity of recent GCMs is larger than that of nature. On the other hand, if $\tau_e \sim 100$ years, then the actual response of the climate system would be quite far from the equilibrium response, thus indicating that the sensitivity of GCMs may not be inconsistent with the observed temperature records.

Table 15-9. e-Folding Time τ_e for Abrupt Heating from Selected Climate Model Studies.

Study	Model	τ_e (Years)
Hoffert *et al.* (1980)	Planetary energy balance climate model and a box-advection-diffusion ocean model	8-20
Schneider & Thompson (1981)	Planetary energy balance model and a two-box diffusion ocean model	13
Bryan *et al.* (1982) Spelman & Manabe (1984)	Coupled atmosphere-ocean general circulation model with simplified geography and topography	25
Hansen *et al.* (1984)	Radiative-convective climate model and a box-diffusion ocean model	27 55 102
Bryan *et al.* (1984)	Global oceanic general circulation model	100
Siegenthaler & Oeschger (1984)	Planetary energy balance climate model and a box-diffusion ocean model	60

The factors that contribute to the wide range in τ_e have been investigated by Wigley and Schlesinger (1985) using their analytical solution for the energy balance climate/box-diffusion ocean model and by Hansen *et al.* (1984) using numerical solutions of the box-diffusion model and a 3-D GCM. Both studies found that τ_e depends (approximately) quadratically on λ^{-1} and linearly on the thermal diffusivity $\varkappa$. As shown in Figure 15-20, the analytic result of Wigley and Schlesinger (1985) is in close agreement with the numerical results obtained by Hansen *et al.* (1984) for $\varkappa = 1$ cm^{2}s^{-1}. However, in view of this dependence of τ_e on λ and $\varkappa$ the determination of whether τ_ϵ 10 or 100 years requires a coupled global atmosphere-ocean general circulation model (AOGCM) in which both the climatic gain (λ^{-1}) and the oceanic heat transport are self-determined. Long term integrations from a simulation with such AOGCMs are currently not available. However, preliminary results from an AOGCM indicate that an energy balance/multi-box ocean model with a self-consistent $\varkappa$ adequately describes the time evolution of the $2 \times CO_2 - 1 \times CO_2$ differences in the surface-air temperature (Schlesinger *et al.*, 1985). The required thermal diffusivity $\varkappa$ for the energy-balance climate/box-diffusion ocean model to represent the transient response of the AOGCM was determined to be 2.25 cm^{2}s^{-1} (Schlesinger *et al.*, 1985).

15.4.4 Results for a Realistic CO_2 Increase

The discussions thus far have been for the transient response of the climate system to an instantaneous doubling of the CO_2 concentration. However, the CO_2 concentration has not abruptly changed in the past, nor is it likely to in the future, at least not by an instantaneous doubling. Instead, the CO_2 concentration has increased more or less continuously over the observational period since 1958 (Figure 15-19).

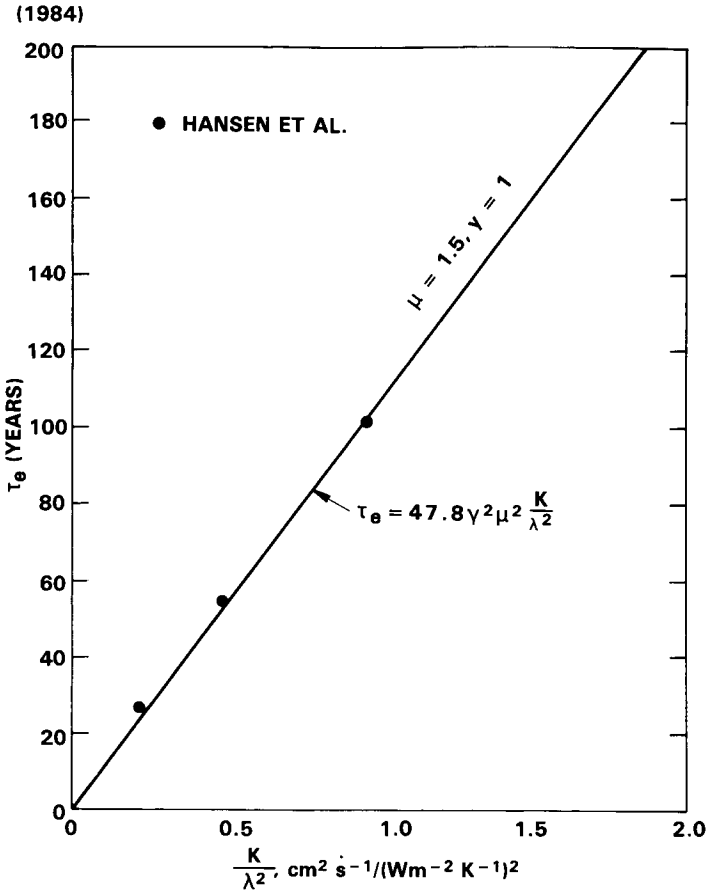

Figure 15-20. The e-folding time τ_e versus $\varkappa/\lambda^2$ for abrupt heating perturbations. The linear relation (line) is predicted by the analytical solution of Wigley and Schlesinger (1985). The data points are from the numerical computations of Hansen *et al.* (1984) for $\varkappa = 1$ cm^{2}s^{-1}.

Recently, Hansen *et al.* (1984) and Wigley and Schlesinger (1985) have estimated the temperature change from 1850 to 1980 induced by the increasing CO_2 concentration during this 130-year period. Figure 15-21, based on the study of Wigley and Schlesinger (1985), shows the 1850-1980 surface temperature change as a function of the equilibrium surface for a doubled CO_2 concentration. Let us assume that the latter is 4 K based on the recent equilibrium warmings simulated by the GFDL, GISS and NCAR atmospheric GCM/fixed-depth mixed layer ocean models. If the climate system had no thermal inertia, the 1850-1980 surface temperature change would be in equilibrium with the instantaneous 1980 CO_2 concentration, and the warming would be given by Equation (2). As shown in this figure, this instantaneous equilibrium warming would be 1.3 K. However, when the heat capacity and vertical heat transport of the ocean are considered, as shown by the curves for the oceanic thermal diffusivities $\varkappa = 1$ and $\varkappa = 3$ cm^{2}s^{-1}, the 1850-1980 warming is reduced to about 0.5 to 0.7 K. This level of CO_2-induced warming does not conflict with the temperature changes revealed in the observational record (see Figure 15-1).

Figure 15-21 also shows that even if the CO_2 concentration were to increase no further in the future, the earth's surface temperature would continue to increase by about 0.7 K (= the balance of the 1.3 K equilibrium warming for our example) in its approach to its new equilibrium value. This delayed approach to the new equilibrium surface temperature brings out the following important issue concerning the transient

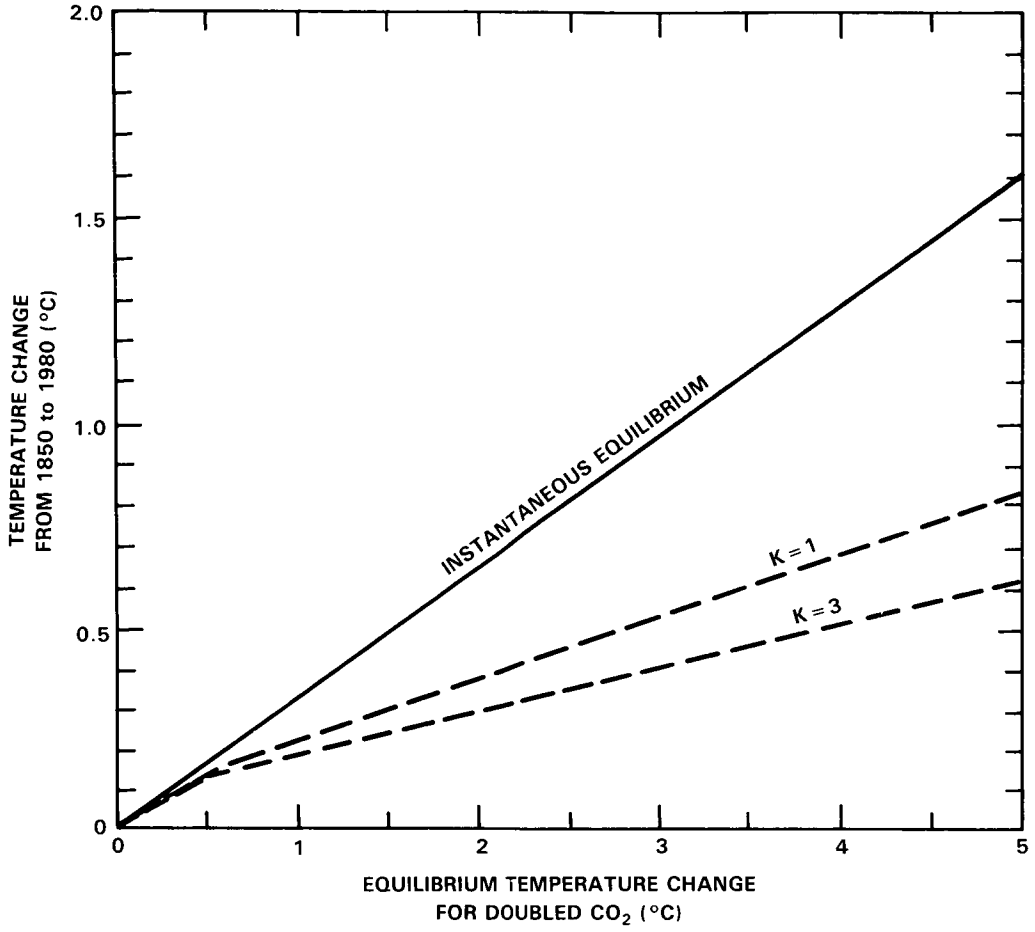

Figure 15-21. The temperature change from 1850 to 1980 versus the equilibrium temperature change for doubled CO_2. The instantaneous equilibrium curve is given by equation (2). The curves $\varkappa = 1$ and $\varkappa = 3$ are from the results of Wigley and Schlesinger (1985).

effects: the present warming is "small" and perhaps within the natural variation of climate because the ocean sequesters heat within its interior but, because of this, when the warming becomes demonstrably evident, continued future warming is inevitable, even if the CO_2 concentration were prevented from increasing further. As shown in Section 15.5, this hidden but inevitable future warming can itself increase in the future as other greenhouse gases such as N_2O, CH_4 and CFCs are added to the earth's atmosphere.

15.5 TRACE GAS EFFECTS ON OBSERVED AND FUTURE CLIMATE TRENDS

Greenhouse forcing of the climate system has accelerated in recent years due to the growth of a number of trace gases. We illustrate this quantitatively by estimating the decadal increment in greenhouse forcing for several trace gases and compare this with the forcing due to increasing CO_2 in the same decades.

15.5.1 Conceptual Framework for the Assessment

The potential effects of trace gases on past and future temperature trends have been estimated by numerous studies (Hansen *et al.*, 1984; Brühl and Crutzen, 1984; Wang *et al.*, 1985; Ramanathan *et al.*,

1985; to cite just the recent analyses). The present assessment, while it combines the salient features of the earlier work, is an independent analysis of the trace gas effects on past and future climate trends.

We do not explicitly employ a climate model but, instead, compute the zero-climate-feedback surface temperature change, $(\Delta T_S)_0$, from the radiative-convective model of Lacis (1985). The computed $(\Delta T_S)_0$ is then multiplied by the feedback factor, F (see Equation 2, Section 15.2.2.2), to obtain the expected climate forcing, ΔT_S.

The $(\Delta T_S)_0$ is the equilibrium change in surface air temperature which would occur as a result of a change in atmospheric composition in the absence of any climate feedbacks. As described in Section 15.2.2, $(\Delta T_S)_0$ is a nearly model independent measure of the radiative forcing. For example, for a doubling of CO_2, $(\Delta T_S)_0$ for RCMs is in the range of 1.2 to 1.3 K; the RCM used in this study yields a value of:

$$[\Delta T_S(2 \times CO_2)]_0 = 1.26 \text{ K} \quad (1)$$

The $(\Delta T_S)_0$ also avoids current uncertainties in *climate sensitivity*; also, since it refers to *equilibrium* response, it is independent of uncertainties in climate response time.

The next issue concerns the choice of the feedback factor, F. Climate feedbacks and climate sensitivity are discussed in Section 15.2.2. It is sufficient for our purposes to note that the estimate of equilibrium global mean climate sensitivity reported by the National Academy of Sciences (Charney, 1979; Smagorinsky, 1982) is

$$\Delta T_S\ (2 \times CO_2) = 3 \pm 1.5 \text{ K} \quad (2)$$

The above climate sensitivity range covers a factor of three, with ΔT_S ranging from 1.5 to 4.5 K. It is easier to justify the lower and the upper limits than the mean value of 3 K. For example, RCMs generally yield a value of 2 K while GCMs with seasonal cycle and realistic geography yield values ranging from 3.5 to 4.2 K (see Table 15-7). Hence, in this report, we avoid the use of a mean value for ΔT_S, but instead adopt the range recommended by the National Academy reports:

$$1.5 \leq \Delta T_S\ (2 \times CO_2) \leq 4.5 \text{ K} \quad (3)$$

Since the zero-climate-feedback forcing for doubled CO_2 is 1.26 K for the present RCM, the climate sensitivity range given by (3) corresponds to the feedback factor F[$= \Delta T_S/(\Delta T_S)_0$; Equation (2) of 15.2.2.2] of:

$$1.2 \leq F \leq 3.6 \quad (4)$$

It is because of this large range for F that we have avoided the use of a specific climate model in the present analyses. In order to account for the climate sensitivity yielded by RCMs and GCMs, we adopt the following two values:

$$\Delta T_S\ (2 \times CO_2) = 2 \text{ K; i.e., } F \approx 1.6$$

$$\Delta T_S\ (2 \times CO_2) = 4 \text{ K; i.e., } F \approx 3.2 \quad (5)$$

15.5.2 Greenhouse Forcing from 1850 to the 1980's

The sources and observed trends for the trace gases are discussed extensively in Chapters 3 and 12 of this report. Hence, only a brief summary is given in the ensuing discussions.

CO_2. The abundance of atmospheric CO_2 was 315 ppmv in 1958 when Keeling initiated accurate monitoring. Thus, since a variety of techniques indicate that the CO_2 abundance was 270 ± 10 ppmv in 1850 (WMO, 1983b), the mean decadal growth of CO_2 for the period 1850-1958 was about 4 ppmv/decade. By contrast, the current rate of growth of CO_2 is about 15 ppmv/decade. The decadal greenhouse forcing due to CO_2 growth is illustrated in Figure 15-22 for the period 1850-1960 and for recent decades.

Chlorofluorocarbons. The release rates of CF_2Cl_2 (F12) and $CFCl_3$ (F11) into the atmosphere can be estimated from production data available from the manufacturers (CMA, 1982). Under the assumption of 150 and 75 year lifetimes for F12 and F11, respectively, decadal growth rates are obtained (Rind and Lebedeff, 1984) which are in good agreement with recent atmospheric measurements (GMCC, 1983). The resulting decadal climate forcings are shown in Figure 15-22. It is apparent that these chlorofluorocarbons now add substantial climate forcing, though their contribution was negligible in the period 1850-1960.

Less abundant chlorine and fluorine compounds, such as $CHClF_2$ (F22), CCl_4, CF_4 and CH_3CCl_3 also have significant growth rates and infrared absorption strengths (see Tables 15-1, 15-1b and 15-8). However, the growth histories and absorption strengths are on the whole less well known than for F11 and F12. CCl_4 apparently had a higher growth rate in the 1960's and 1970's than it does now, while F22 and CH_3CCl have grown rapidly in recent years, with a higher growth rate than that of F11 and F12. In Figure 15-22 we include a greenhouse contribution for these other CFCs with a net radiative forcing that is 20 percent of that for F11 and F12. However, this is meant more as a reminder that these other CFCs need to be considered, rather than as an accurate estimate of their greenhouse contribution.

CH_4. Methane has been measured to be increasing for the last several years at a rate of the order of 1 percent/year (Blake *et al.*, 1982; Blake and Rowland, 1985; Rasmusson and Khalil, 1984b; Ehhalt *et al.*, 1983b). Also, measurements of air bubbles trapped in polar ice cores (Craig and Chou, 1982; Rasmusson and Khalil, 1984b) indicate that the methane abundance was about 0.7 ppmv from 25,000 years ago to 500 years ago, with an increase beginning sometime between 200 and 500 years ago. We estimate the CH_4 greenhouse forcing for Figure 15-22 by taking the abundance at 1 ppmv in 1850, 1.4 ppmv in 1958, 1.5 ppmv in 1970 and 1.65 ppmv in 1980; the growth rate is taken as 1.5 percent/year in the 1980's.

N_2O. Nitrous oxide was measured to be increasing at a rate of about 0.2 percent/year in the 1970's (Weiss, 1981). Recent measurements (NRC, 1983) suggest that the current growth rate may be closer to 0.3 percent/year. These values are used to estimate the N_2O greenhouse forcing for Figure 15-22. Although it seems likely that N_2O may have had a small rate of increase in the period 1850-1958, there are no observations providing a quantitative measure. However, in the near future, ice core data should yield a reliable pre-industrial value (Gammon, private communication).

Stratospheric H_2O. Since the abundance of water vapor in the troposphere is controlled basically by atmospheric temperature and other meteorological variables, changes in tropospheric H_2O are considered as a climate feedback mechanism rather than as a forcing mechanism. However, in the upper stratosphere H_2O is produced by methane oxidation, and therefore increase of methane may increase stratospheric H_2O. The change of stratospheric H_2O would be delayed after any increase in tropospheric

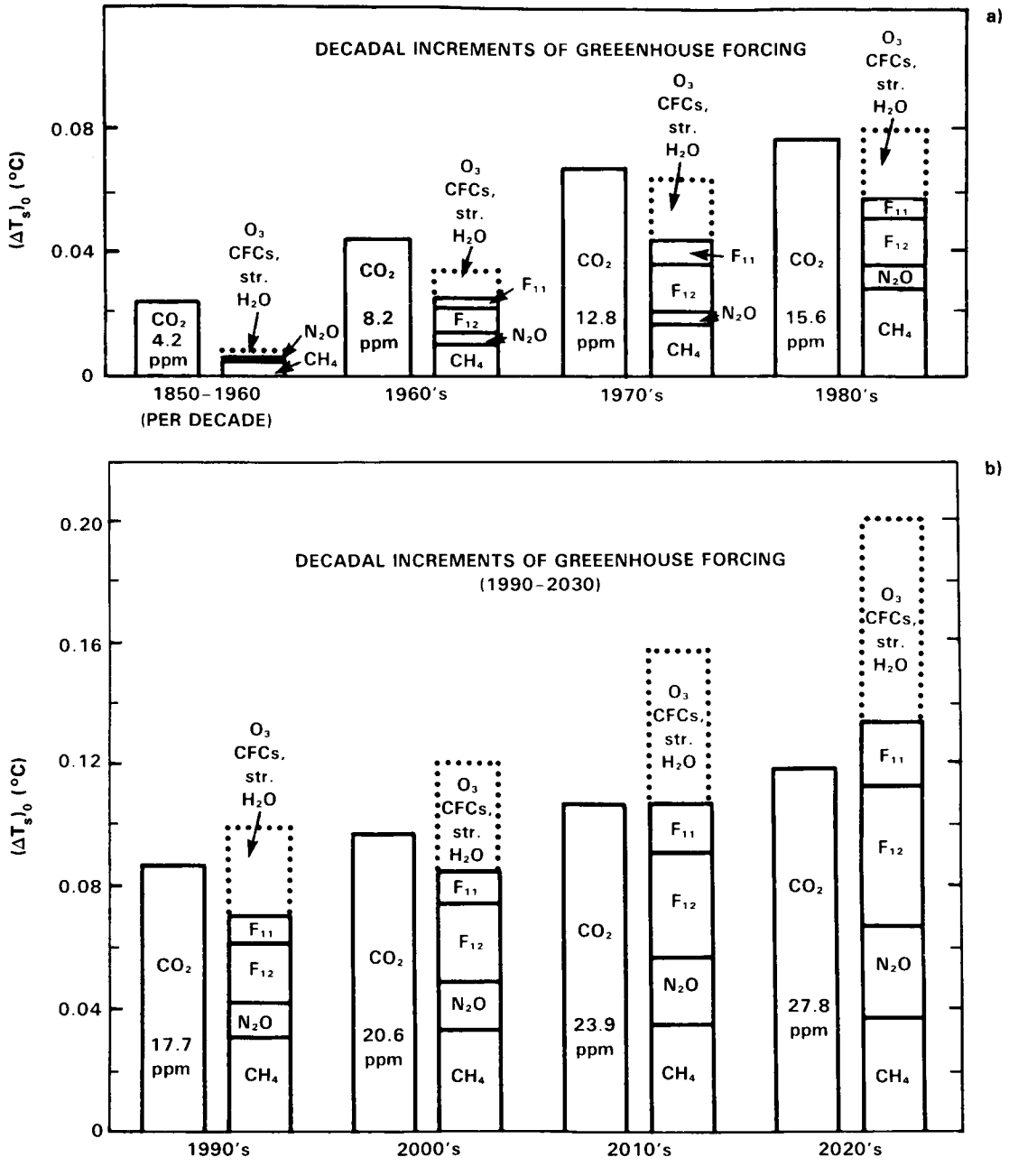

Figure 15-22. Decadal additions to global mean greenhouse forcing of the climate system. $(\Delta T_s)_0$ is the computed temperature change at equilibrium ($t \rightarrow \infty$) for the estimated decadal increases in trace gas abundances, with no climate feedbacks included. Formulas for $(\Delta T_s)_0$ as a function of the trace gas abundances are given by Lacis *et al.* (1981). (a) Past additions. Except for O_3 and stratospheric H_2O trends, the estimated trace gas increases are based on measurements as discussed in section 15.5.2; (b) Future additions. Adopts Case A scenario discussed in Section 15.5.3 and given in Table 15-10, which assumes that the sum of all trace gases other than those expressly indicated provides a forcing similar in magnitude to that of CFC11 and CFC12.

CH_4 by the time required for transport from the troposphere to the upper stratosphere. The greenhouse forcing of H_2O in Figure 15-22 is based on the added stratospheric H_2O which Wuebbles (private communication, 1985) estimates to be associated with increase of CH_4. It is apparent that the greenhouse warming from added stratospheric H_2O is about 50% as great as the direct CH_4 greenhouse warming. These estimates do not include the CH_4-O_3 feedback (see Section 15.3).

O_3. Ozone is an effective greenhouse gas because of its strong absorption band at 9.6 μm. Present understanding of atmospheric chemistry, as described elsewhere in this volume, suggests that growth of atmospheric CFCs will eventually deplete stratospheric O_3 substantially and increase tropospheric O_3, with a net column-integrated reduction of O_3. The net greenhouse effect of this would be a slight warming, because of the greater greenhouse efficiency of tropospheric ozone molecules (Ramanathan and Dickinson, 1979; Lacis, 1985; Owens *et al.*, 1985a). In addition, as discussed in Section 15.3, increases of atmospheric methane, carbon monoxide and nitric oxides tend to increase tropospheric O_3 (also see Cicerone, 1985). However, a recent 3-D transport model study (Levy *et al.*, 1985) indicates the potential importance of transport in governing the O_3 distribution. The relative importance of transport and hydrocarbon/nitrogen oxide chemistry in governing tropospheric ozone production is as yet an unresolved issue (Levy *et al.*, 1985).

Recent measurements of O_3 are not inconsistent with a long-term trend of increasing tropospheric ozone (Angell and Korshover, 1983b; Bojkov and Reinsel, 1985; Logan, 1985). For example, analyses of Northern Hemisphere ozonesonde data from 11 stations reveal a statistically significant 1.1% per year increase in the free troposphere ozone over a 15 year period; Southern Hemisphere ozone seems to have undergone very little change in the same period (Bojkov and Reinsel, 1985). These and other findings (Logan, 1985; Angell and Korshover, 1983b) based on observed ozone data are also consistent with estimates of ozone production from anthropogenically released hydrocarbons and nitrogen oxides (Isaksen, 1980; Vukovic *et al.*, 1985; Isaksen and Hov, 1985); NO_x emissions from aircraft (Liu *et al.*, 1980) and CO from incomplete combustion (Logan *et al.*, 1978). In spite of this apparent consistency between theory and observations, the large natural variability of tropospheric ozone when considered in conjunction with the poor spatial coverage of the ozone measurement stations prevents firm conclusions regarding trends.

We estimate the potential O_3 greenhouse effect by using trends for O_3 which were computed by Wuebbles *et al.* (1983) on the basis of scenarios for atmospheric methane, nitrous oxides and carbon dioxide; however, we decreased this computed $(\Delta T_s)_0$ by the factor 0.5, because much of the O_3 change would be confined to the hemispheric or smaller scale. The resulting tropospheric O_3 climate forcing, indicated by a dotted bar in 15-22, is very uncertain, but is obviously a potentially important contributor to the greenhouse effect.

The following major conclusions follow directly from Figure 15-22:

(1) Non-CO_2 greenhouse gases are now adding to the greenhouse effect by an amount at least comparable to the effect of CO_2; this is a fundamental change from the situation during the period 1850-1960.;

(2) The rate of increase of the total greenhouse forcing is now 3-10 times greater than the mean rate for the period 1850-1960, due to both increase in the growth rate of CO_2 and recent growth of other trace gases.

(3) The cumulative value of $(\Delta T_s)_0$ for the period 1850-1980 is 0.56 K; CO_2 increase contributes 0.4 K and the other trace gases contribute the balance of 0.16 K. The radiative forcing of 0.56 K would yield an equilibrium surface-air temperature change of about 0.9 K [= 0.56 × 1.6] and

about 0.6 K for CO_2 increase alone for a climate model whose equilibrium sensitivity is $\Delta T_s(2 \times CO_2) = 2$ K. These results are consistent with the earlier RCM estimates of Brühl and Crutzen (1984; 0.6 K for CO_2 alone and 1 K for all gases) and that of Ramanathan *et al.* (1985; 0.6 K for CO_2 alone and about 0.9 K for all gases) for surface-air temperature. The range in the equilibrium surface-air temperature change is 0.7 to 2 K, where we have adopted Equation (4) to multiply the $(\Delta T_s)_0$ of 0.56 K with the range in F.

(4) The computed stratospheric cooling for the period 1850-1980 is slightly under 1 K between 25-30 km and about 3 K between 35-45 K. These calculations do not include the effects of CFC-induced O_3 change which can amplify the cooling due to CO_2 increase by about 20%.

15.5.3 Greenhouse Forcing Projected Into the Next Century

We consider three scenarios (Case A, Case B and Case C) projecting trace gas greenhouse forcing into the future. The three scenarios are summarized in Table 15-10. The use of more than one scenario seems essential because of major uncertainties in our understanding of the causes of the trace gas changes and the great difficulties in projecting economic, population and other key factors. We compare these scenarios with the range of trace gas forcings estimated by Ramanathan *et al.* (1985) for 2030. The scenarios adopted by Ramanathan *et al.* (1985) are shown in Table 15-8 (see the column under the heading probable range).

The Case A scenario is an extrapolation of current growth rates for measured gases, and it includes an allowance to approximate the effect of several gases that are poorly measured and/or have uncertain absorption strengths. The resulting radiative forcing for this scenario is shown in Figure 15-22b and is near the middle of the range estimated by Ramanathan *et al.* (1985). The Case B scenario includes only five greenhouse gases that are measured reasonably well and it assumes rapidly decreasing growth rates. The resulting radiative forcing is near the lower limit of the range estimated by Ramanathan *et al.* (1985).

In Case A (current growth rates), CO_2 increases at a constant growth rate from 270 ppmv in 1850 to 315 ppmv in 1958, as observed by Keeling for the interval 1958-1984 and subsequently with a 1.5 percent growth of the annual increment. $CFCl_3$ and CF_2Cl_2 emissions are from reported rates to date and assume 3%/yr increased emission in the future, with atmospheric lifetimes for the gases of 75 and 150 years, respectively. CH_4 increases at a constant growth rate from 1 ppmv in 1850 to 1.4 ppmv in 1958, 0.6%/yr in the 1960's, 1%/yr in the 1970's and 1.5%/yr thereafter. N_2O increases according to the semi-empirical formula of Weiss (1981), the rate being 0.1%/yr in 1958, 0.2%/yr in 1980, 0.4%/yr in 2000 and 0.9%/yr in 2030. Potential effects of several other trace gases (such as O_3, stratospheric H_2O, and chlorine and fluorine compounds other than F11 and F12) are approximated by multiplying the CFC effect by a factor of 2.

In Case B (reduced growth rates) the annual increment in CO_2 is reduced from 1.5% today to 1% in 1990, 0.5% in 2000 and 0 in 2010, which compares to $\approx$4% during the period 1900-1970 and is below projected rates for population growth; the resulting ΔCO_2 is constant at 1.9 ppmv yr^{-1} after 2010. The annual growth in CF_2Cl_2 and $CFCl_3$ emissions are reduced from 3% today to 2% in 1990, 1% in 2000 and 0 in 2010; because of their finite lifetimes, the annual increments in atmospheric abundance decrease with time after 2010. The methane annual growth rate decreases from 1.5% today to 1% in 1990 to 0.5% in 2000. N_2O increases are based on Weiss' (1981) formula, but the parameter specifying annual growth in anthropogenic emissions decreases from 3.5% today to 2.5% in 1990, 1.5% in 2000 and 0.5% in 2010. No increases are included for other chlorofluorocarbons, O_3, stratospheric H_2O or any other gases.

Table 15-10. Trace Gas Scenarios.

Trace gas	Case A Current growth rate	Case B Reduced growth rate	Case C*
CO_2	1.5%/yr growth in annual CO_2 increment**	1.5%/yr growth to 1990 1.0% yr from 1990-2000 0.5%/yr from 2000-2010 0%/yr after 2010 in annual CO_2 increment	Time-dependent; averages about 2%/yr growth in annual CO_2 increment
$CFCl_3$; CF_2Cl_2	3%/yr growth in emissions	3%/yr growth to 1990 2%/yr from 1990-2000 1%/yr from 2000-2010 0%/yr after 2010	1.5%/yr growth in emissions
CH_4	1.5%/yr growth in CH_4 abundance	1.5%/yr growth to 1990 1.0%/yr from 1990-2000 0.5%/yr after 2000	1%/yr growth in CH_4 abundance
N_2O	Weiss (1981) formula 3.5%/yr growth to 1990; yields 0.2%/yr growth in abundance in 1980, 0.4%/yr in 2000, 0.9%/yr in 2030	Weiss formula with 3.5%/yr growth in emissions 2.5%/yr from 1990-2000 1.5%/yr from 2000-2010 0.5%/yr after 2010; yields 0.2%/yr growth in abundance in 1980, 0.33%/yr in 2000, 0.34%/yr in 2030	0.25%/yr growth in N_2O abundance
O_3 and other trace gases	Assumed greenhouse forcing by these gases is the same as that of CF_2Cl_2 and $CFCl_3$	None	Includes only O_3 effects. O_3 change is explicitly computed from a chemistry model

* This the same scenario used in the Model Predictions Chapter (See their Case 4; Chapter 12.)

** The CO_2 increment in 1985 was taken as 1.5 ppmv, and this increment increased by 1.5%/yr in Case A. This case is appropriate if fossil fuel use increases by 1.5%/yr and the "airborne fraction" of CO_2 remains constant, for example. Note that this growth rate is much less than the 4%/yr growth rate that existed in the 100 years before 1973.

The Case C scenario is adopted from the "model predictions" chapter (Case 4 of Chapter 13). The Case C scenarios fall in between Case A and Case B. Case C, like Case A, adopts current growth rates but chooses the lower limit of the observed growth rates. For example, it adopts 1.5%/yr growth in $CFCl_3$ and CF_2Cl_2 emissions as opposed to the 3%/yr growth assumed in Case A; the growth in CH_4 abundance is reduced to 1%/yr instead of 1.5%/yr in Case A. Furthermore, trace gases other than CO_2, $CFCl_3$ and CF_2Cl_2, CH_4, N_2O and O_3 are not included in Case C.

The Case A, Case B and Case C scenarios are summarized in Table 15-10; the time dependent concentrations for Case A and Case B are shown in Table 15-11. The computed greenhouse forcings are

Table 15-11. Trend in concentrations. From 1985 to 2100, the concentrations are derived from the scenarios A and B shown in Table 15-10.

Date	CO_2 (ppm)		CH_4 (ppm)		N_2O (ppb)		CCl_3F (ppb)		CCl_2F_2 (ppb)	
1850	270		1.00		282		0		0	
1900	290		1.17		284		0		0	
1958	315		1.40		293		.01		.03	
1970	325		1.51		297		.07		.13	
1985	346		1.79		305		.24		.40	
	A	B	A	B	A	B	A	B	A	B
2000	372	371	2.24	2.12	319	318	.42	.41	.72	.71
2015	404	400	2.80	2.28	343	335	.71	.61	1.22	1.07
2030	445	428	3.50	2.46	383	353	1.15	.78	1.99	1.41
2050	515	466	4.71	2.72	483	377	2.13	.96	3.72	1.80
2100	818	562	9.91	3.49	1432	439	9.68	1.24	17.00	2.60

illustrated in Figure 15-23 for the period 1960-2030. Case A yields a forcing that has a slightly larger forcing than the nominal scenario of Ramanathan *et al.* (see Figure 15-24). Case A yields a forcing equivalent to doubled CO_2 (with $1 \times CO_2$ defined as 315 ppmv) before 2030; Case C yields this level slightly after 2030; while Case B yields this level of forcing before 2060. The time to reach effective doubled CO_2 forcing is greatly accelerated by the non-CO_2 trace gases, which provide roughly half of the greenhouse forcing. A comparison of the forcing by CO_2 and other trace gases is illustrated clearly in Figure 15-24, taken from Ramanathan *et al.* (1985); although the relative contributions of the various trace gases in their scenario are somewhat different from either Case A or B, the results are qualitatively very similar. The following points should be noted first before comparing the Ramanathan *et al.* (1985), hereafter referred as R, results with those shown in Figure 15-23. The 1-D RCM model of R computes both surface temperature (T_g) surface-air temperature (T_s). In the R model, the computed DT_s is larger than DT_g by 10% - 13%. For CO_2 doubling, the R model yields a $\Delta T_g \sim 1.9$ K and a $\Delta T_s \sim 2.1$ K. The R model results in Figure 15-24 shows that, for the period 1980–2030, the equilibrium surface warming, i.e., ΔT_g, is 1.54 K ($\Delta T_s \sim 1.7$ K) due to all gases including CO_2 and that due to CO_2 increase alone is 0.71 K ($\Delta T_s \sim 0.8$ K). For the same period of 1980–2030, the Case A scenario in Figure 15-23 yields [for the ΔT_s ($2 \times CO_2$) = 2 K model] a ΔT_s of 1.8 K for all gases including CO_2 and a ΔT_s of 0.8 K for the CO_2 increase by itself. The cumulative ΔT_s for the Case B and Case C scenarios are respectively 1.1 and 1.25 (see Figure 15-23). The stratospheric O_3 decrease due to CFCs also causes a surface warming, and the magnitude of about 0.1 K (see Figure 15-24) is roughly 30% of the direct greenhouse effect of CFCs. Other studies (e.g., Owens *et al.*, 1985) also yield a warming of about 0.1 K due to CFC-induced stratospheric O_3 decrease.

The computed stratospheric temperature changes due to CO_2 and other trace gases are substantial (see Figure 15-25). Above 30 km, the cooling due to CO_2 increase (alone) is more than doubled by the other trace gases. The primary contribution to the enhancement in stratospheric cooling is the (computed) O_3 decrease due to CFC increase. To the extent that trace gases (other than CO_2) cause a large

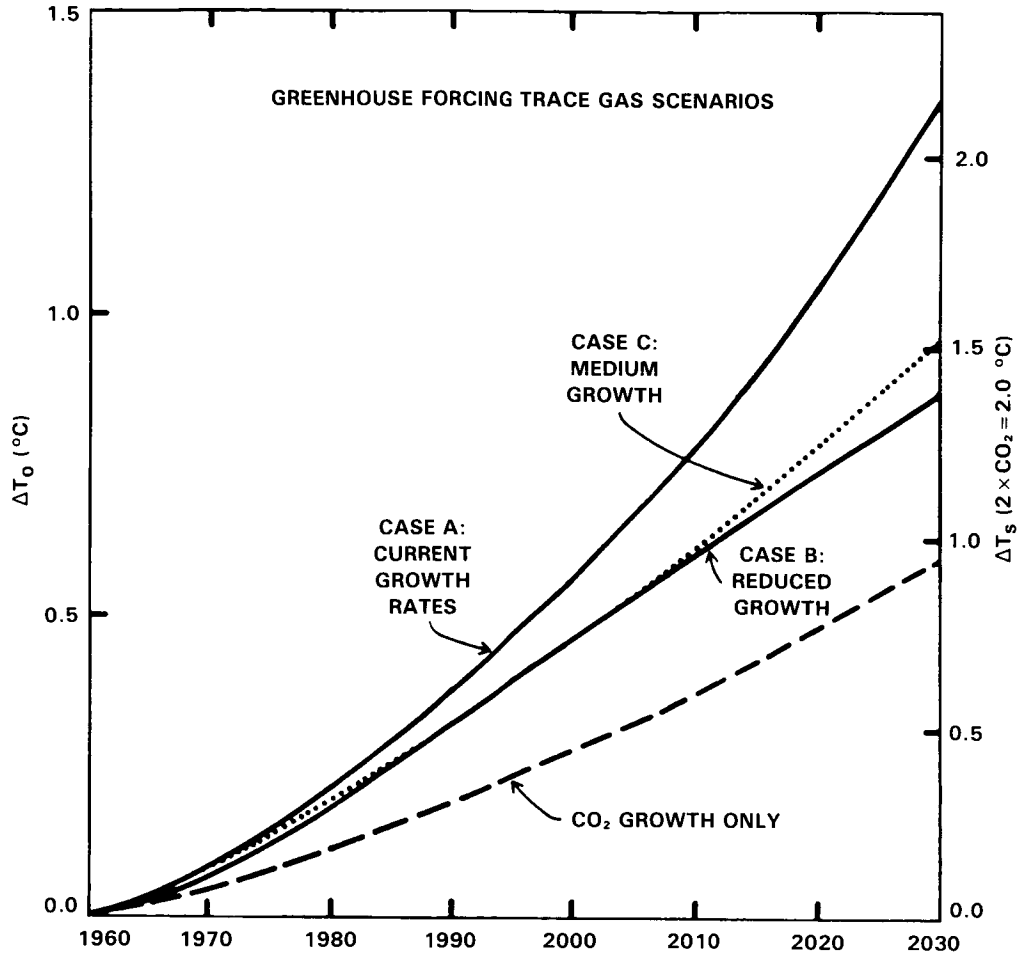

Figure 15-23. Greenhouse forcing for three trace gas scenarios: Case A, which uses current growth rates, and Case B, which assumes substantial reductions in growth, as described in the text. Case C is similar to Case A but with medium growth rate. The "CO_2 growth only" curve applies to Case A scenario. See Table 15-10 for further details. ΔT_0 is the equilibrium greenhouse warming for no climate feedbacks. The "doubled CO_2" level of forcing occurs when the CO_2 and trace gases added subsequent to 1958 provide a radiative forcing equivalent to doubling of CO_2 from 315 ppm to 630 ppm.

surface/troposphere warming and a much larger stratospheric cooling, their direct climatic effects are virtually indistinguishable from those of CO_2.

15.5.4 Regional Effects

There is general agreement that climate sensitivity is not globally uniform. Both empirical evidence from past climate changes and global climate models indicate that the surface air temperature response is magnified at high latitudes and thus somewhat muted at low latitudes, in comparison to the global mean response. This high latitude enhancement is expected on theoretical grounds, because the ice-snow albedo feedback only operates at high latitudes and because the relative stability of the atmosphere there tends to confine surface warming or cooling to low altitudes. The high latitude enhancement of the warming is illustrated in Figure 15-26, which shows model results for the annual mean surface air temperature increase from the 4 × CO_2 experiment of Manabe and Stouffer (1980). Qualitatively similar results are obtained with other general circulation models (Hansen *et al.*, 1984; Washington and Meehl, 1984).

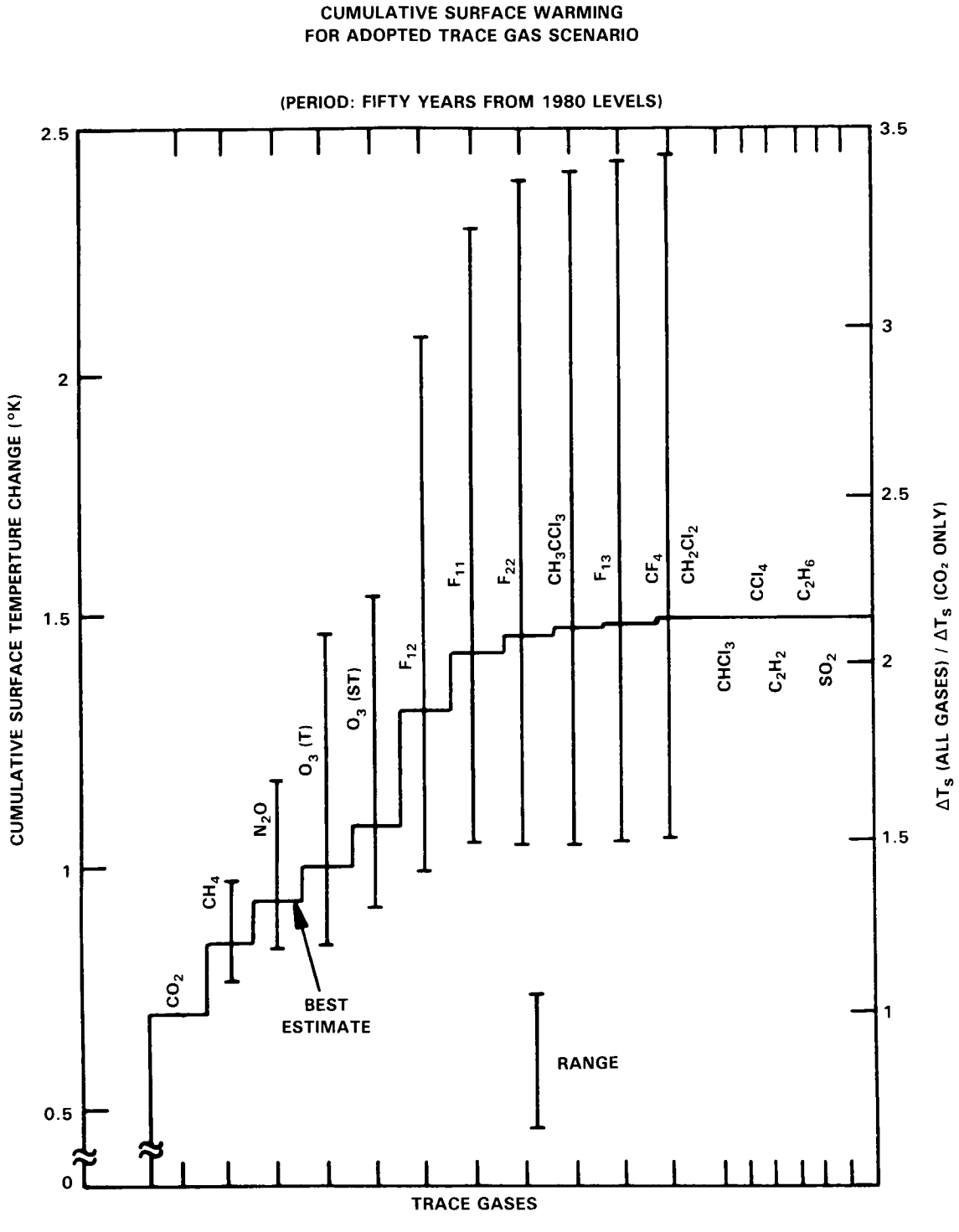

Figure 15-24. Cumulative equilibrium surface warming resulting from the trace gas scenario of Table 15-8 (source: Ramanathan *et al.,* 1985). In this 1-D model, the surface-air temperature change is larger than the surface temperature change by about 10%. The $(\Delta T_s)_0$ can be obtained by dividing the indicated surface temperature change by a feedback factor (F) of about 1.5.

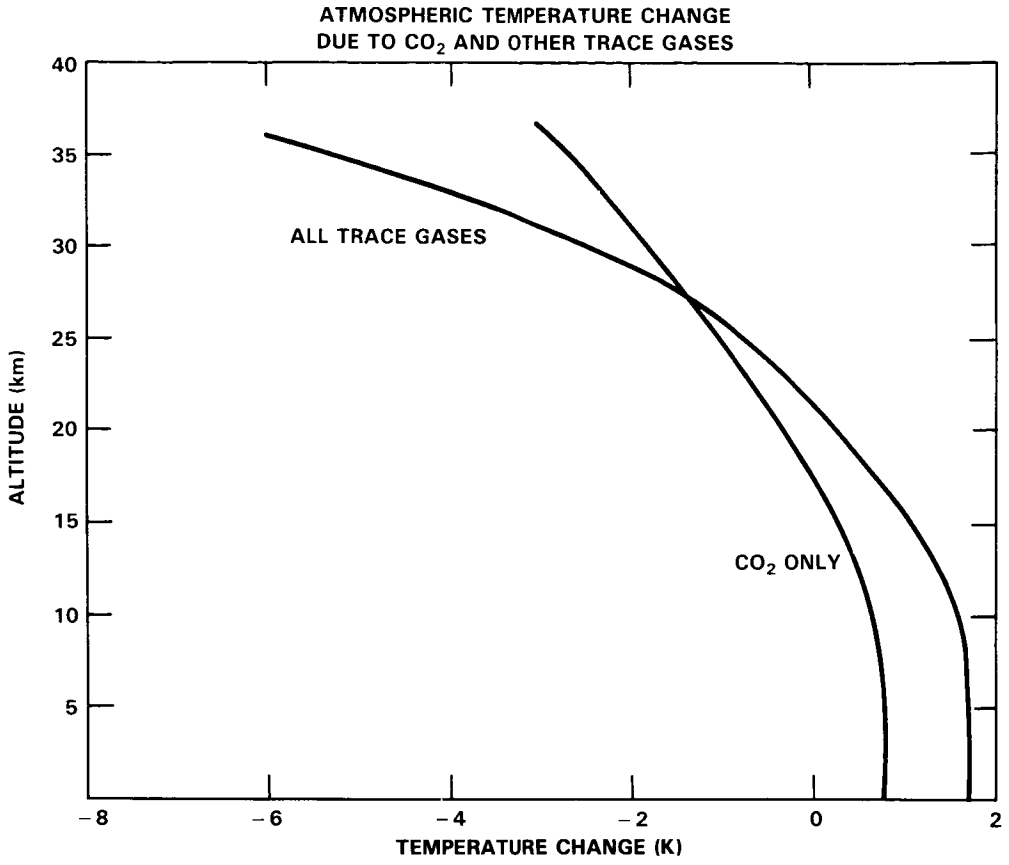

Figure 15-25. Atmospheric temperature change due to CO_2 and other trace gases. Radiative-convective model results employing the scenario in Table 15-8. (Source: Ramanathan *et al.*, 1985).

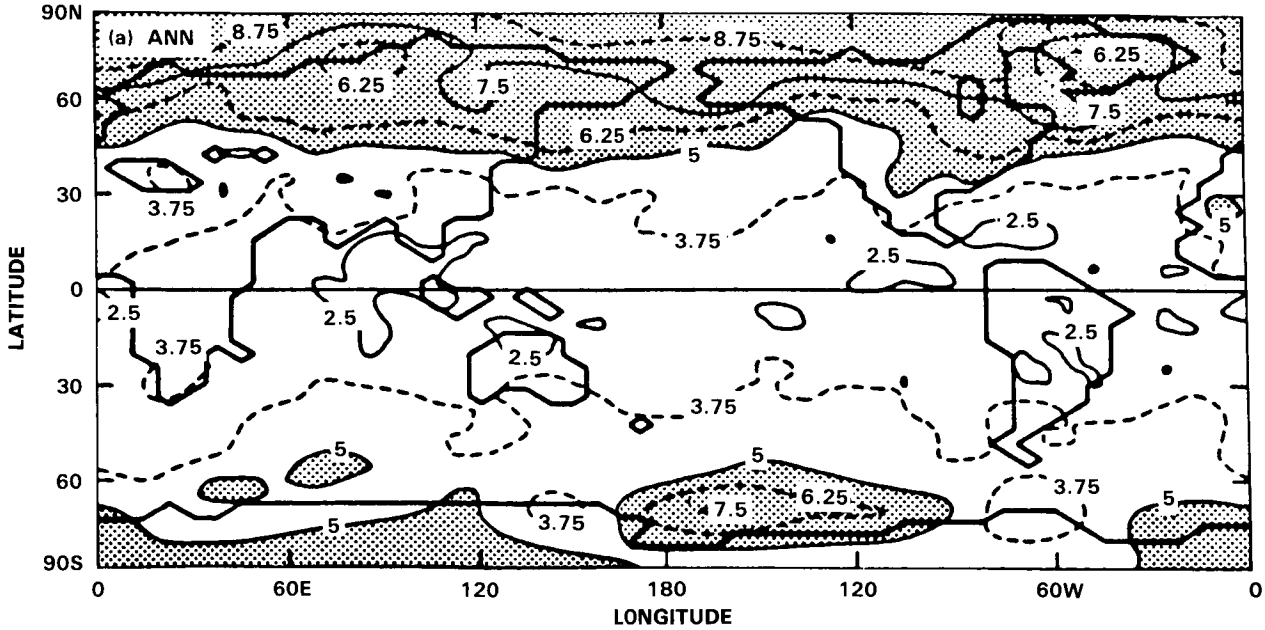

Figure 15-26. Geographical distribution of the annual mean surface air warming (°C) in the 4 × CO_2 experiment of Manabe and Stouffer (1980).

15.5.5 Equilibrium and Transient Temperature Response

The climate forcings discussed above are given in terms of the equilibrium ($t \rightarrow \infty$) response with no climate feedbacks. In order to convert these forcings to an expected temperature response, it is necessary to account for (1) climate feedback mechanisms, and (2) the finite response time of the climate system. As explained in Section 15.4, these two effects are not independent; a greater positive climate feedback leads to a longer climate response time. Also note that, although climate forcings usually can be computed with an accuracy of the order of 20 percent for a given change in atmospheric composition, the uncertainties in the strength of climate feedbacks and in the climate response time are much greater.

The transient temperature response involves additional complications because of the difficulty in properly accounting for the climate system's thermal inertia, which is due mainly to the large effective heat capacity of the oceans. Ocean circulation and mixing are not yet adequately observed, and ocean general circulation models are just reaching the point at which they can be applied to the transient climate problem. However, the essence of the ocean's effect in delaying the greenhouse warming can be demonstrated with a simple "box diffusion" model for the ocean (Oeschger *et al.*, 1975; Cess and Goldenberg, 1981; Hansen *et al.*, 1981). In this model, it is assumed that heat perturbations are rapidly mixed as a passive tracer into the deeper ocean in a way that can be approximated as one-dimensional diffusion. Although this model does not account for the buoyancy effects of sea-surface temperature changes in modifying the penetration depth of the radiative forcing, it provides a reasonable fit to the globally averaged results of a coupled ocean-atmosphere GCM (see Bryan *et al.*, 1984 for further elaboration of this issue). The effective diffusion coefficient is estimated from measurements of transient tracers to be κ = 1-2 $cm^2\ s^{-1}$ (Oeschger *et al.*, 1975; Ostlund *et al.*, 1976; Broecker *et al.*, 1980). The resulting relationships between equilibrium climate sensitivity, vertical diffusion coefficient and ocean response time have been illustrated in Section 15.4 above.

The expected warming of the ocean mixed layer is shown in Figure 15-27a for the trace gas scenario Case A (current growth rates for CO_2, CH_4, N_2O, CF_2Cl_2 and $CFCl_3$ plus an allowance for other trace gases) and in Figure 15-27b for the trace gas scenario Case B (reduced growth rates, only CO_2, CH_4, N_2O, CF_2Cl_2 and $CFCl_3$ included). In both cases, results are shown for two values of equilibrium climate sensitivity [$\Delta T_s(2 \times CO_2)$ = 2 K and 4 K] and for two values of the vertical diffusion coefficient (κ = 1 $cm^2\ s^{-1}$ and 2 $cm^2\ s^{-1}$).

In order to facilitate interpretation of the transient results, the equilibrium ΔT_s results are summarised below for the model with ΔT_s ($2 \times CO_2$) = 2 K. For the 1850–1980 period, both Case A (Figure 15-27a) and Case B (Figure 15-27b) have an equilibrium ΔT_s of 0.9 K (see major conclusion no. 3 in Section 15.5.2). For the 1980-2030 period, the equilibrium ΔT_s for Case A and Case B are about 1.8 and 1.1 K respectively (as inferred from Figure 15-23). Hence the range in equilibrium ΔT_s, in view of the range in climate sensitivity given by Equation (3), is 0.7 to 2 K for the 1850 - 1980 period while for the 1980 - 2030 period the range is 0.8 to 2.4 K for Case B and is 1.4 to 4.1 K for Case A.

These models show a warming of the mixed layer between 0.4 and 0.8 K for the period 1850-1980. This range is not inconsistent with the estimated increase of 0.54-0.6 K in Northern Hemisphere surface air temperature in that period (Kelly *et al.*, 1984; also see Figure 15-1). While the agreement with observed temperature trends is encouraging, it is difficult to conclude much from this comparison because (1) other climate forcings are likely to have operated over this time scale; for example, variations in stratospheric and tropospheric aerosols, changes in ground albedo due to desertification and changes in forest cover, and possible variations of solar irradiance are some of the other important radiative forcings; (2) the observations of surface air temperature are uncertain because of poor spatial coverage, especially in the nineteenth

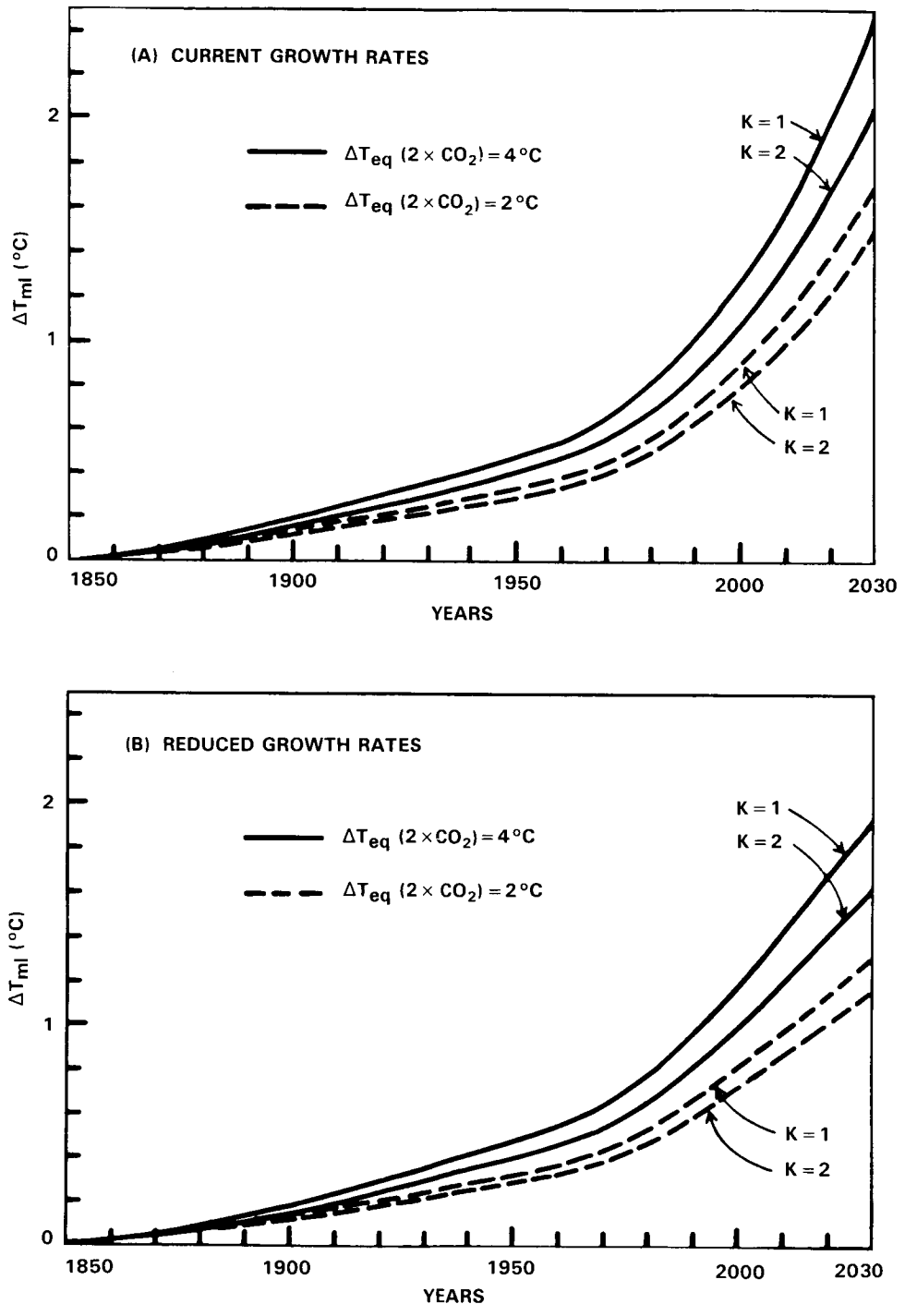

Figure 15-27. Ocean mixed layer temperature response to the two trace gas scenarios in Table 15-10 in a 1-D radiative/convective model with a box-diffusion ocean: (a) Case A (current growth rates for CO_2, CH_4, N_2O, CF_2Cl_2, and $CFCl_3$ plus an allowance for other trace gases), and (b) Case B (reduced growth rates with only CO_2, CH_4, N_2O, CF_2Cl_2, and $CFCl_3$ included). Results are shown for two values of the equilibrium climate sensitivity and two values of the vertical diffusion coefficient (in cm^2s^{-1}).

century; (3) these model calculations refer to the ocean mixed layer, while observations are of surface air over land and ocean; this surface air temperature may be more sensitive than the mixed layer temperature; for example, in three-dimensional doubled CO_2 experiments with fixed ocean temperature the global surface air temperature increased by about 0.3 K.

The computed surface-air temperature change for the period from 1850 to 2030 is in the range of 1.2 to 2.4 K (see the lowest estimate in Figure 15-27b and the largest estimate in Figure 15-27a). The equilibrium change for the cases shown in Figure 15-27 is in the range of 2 to 5.4 K and the difference between the two ranges reflect the potential influence of the oceans in delaying the "signal." If the oceans indeed have a significant delaying effect on the equilibrium warming, and if the decadal rates of increase in trace gas concentrations continue unabated (at the present rates) for the next several decades, then the climate system would be increasingly in a state of disequilibrium with the radiative forcing by the trace gases (Hansen *et al.*, 1984).

15.5.6 Conclusions

The assessment presented here reveals the following features:

(a) From the pre-industrial era to the 1950's, the greenhouse effect of CO_2 was the major source of anthropogenic impact on climate; this picture changed drastically since the early 1960's. During the last two decades or so, trace gases other than CO_2 have begun to contribute as much as the CO_2 increase to the upward trend in anthropogenically induced radiative forcing.

(b) The cumulative effect of the increase in CO_2 and other trace gases for the period from 1850-1980 is an equilibrium surface warming of 0.7 to 2 K, where the threefold uncertainty is due to current uncertainties in climate sensitivity. The contribution of the non-CO_2 trace gases to the cumulative equilibrium surface warming is about 30% (see the results cited under major conclusion no. 3 in Section 15.5.2). Time dependent calculations with a box-diffusion ocean model suggest that about 0.4-0.8 K of the (0.7 to 2 K equilibrium value) surface warming should have occurred during 1850 to 1980.

(c) A variety of scenarios that employ the upper and lower range of the observed growth rates of trace gas concentrations or their emission rates, show that if the current growth rates of trace gases continue unabated for the next several decades, trace gases other than CO_2 can have as much impact as CO_2 on future trends of surface-troposphere-stratosphere temperatures. For the various trace gas scenarios considered in this study, the equilibrium surface warming for the period 1980 to 2030 range from 0.8 to 4.1 K. This wide range is due to the range in the assumed scenario as well as that due to the uncertainty in climate model sensitivity.

(d) Thus for the 180 year period from 1850 to 2030, our assessment suggests a trace gas induced cumulative equilibrium surface warming in the range of 1.5 to 6.1 K. Because of the huge thermal inertia of the world oceans, only about 40 to 50% of the above equilibrium warming will be realized by the year 2030. Consequently, if the current rate of increase in trace gas concentrations continue unabated for the next several decades the climate system would be increasingly in a state of disequilibrium with the radiative forcing by the trace gases.

(e) In addition to CFC11, CFC12, CH_4, N_2O and O_3, radiatively active gases with long lifetimes of the order of 100-500 years (F13, F114, F115, F14, F13B1; see Table 15-8) may also become important

if their growth rates increase for the next several hundred years. The current concentrations of these gases are so small that they are projected to have a negligible impact on a 50-100 year time scale.

15.6 SCIENTIFIC CHALLENGES FOR THE FUTURE

The basic theme that emerges out of the discussions thus far is that the climatic effects of trace gases other than CO_2 are largely determined by the interactions between radiation, air-chemistry, transport of gases and large scale dynamics. The primary challenge then is to improve our understanding of the role of the above interactions in governing the observed distributions of temperatures and trace gases; and more importantly, improve our insights into their role in governing the sensitivity of the climate system to anthropogenic perturbations. Our current understanding of the above interactions is largely derived from globally averaged 1-D models or from highly parameterized zonally averaged 2-D models.

In what follows, the discussions will focus more on the challenges that are unique to trace gases other than CO_2. Hence, we do not cover some fundamentally important modeling issues such as cloud-feedback and the role of oceans; these issues are covered in ample detail in documents related to the CO_2-climate problem.

15.6.1 Theoretical and Modeling Issues

15.6.1.1 Interactions in the Troposphere

Additions of both chemically active gases (e.g., CO, NO_x) and radiatively active gases (e.g., CH_4) were shown to lead to substantial increases in tropospheric O_3 and CH_4 which in turn enhance the greenhouse effect. This indirect climate effect was shown to be as large as the direct radiative effect (Section 15.3). Furthermore, CH_4 and O_3 concentrations were also modulated by the feedback between temperature and H_2O. The principal constituents that are responsible for these chemistry-climate interactions in the troposphere are the radicals OH and HO_2. These interactions, which are illustrated schematically in Figure 15-28, are not only important for understanding climate sensitivity to trace gases but are also important for understanding the causal mechanisms for the observed trends in CH_4 and O_3. Many of the gases shown in Figure 15-28 have strong spatial and temporal variations. Hence, current analyses of these interactions, which are largely based on 1-D models, should be viewed merely as illustrative of the potential importance of the interactions (shown in Figure 15-28).

As a first step towards a more quantitative understanding of the interactions, the following key issues should be addressed:

(i) The relative role of transport and chemistry in governing the behavior of O_3, NO_x, CO (and others in Figure 15-22) should be determined. The transport processes include: downward transport of O_3 and NO_x from the stratosphere, upward transport of pollutants (e.g., CO) from the boundary layer, and lateral transport. A quantitative study of this issue requires not only interactive transport-chemistry models, but also simultaneous measurements of O_3, NO_x, CO and H_2O (as a minimum set) at a few selected locations to verify the model assumptions and simulations (Levy *et al.*, 1985).

(ii) Since the T-H_2O feedback is an important issue for the chemistry involving OH and since the temperature change (due to the trace gas greenhouse effect) is expected to be a strong function of latitude, attention should be given to the latitudinal and seasonal dependence of the interactions in Figure 15-22.

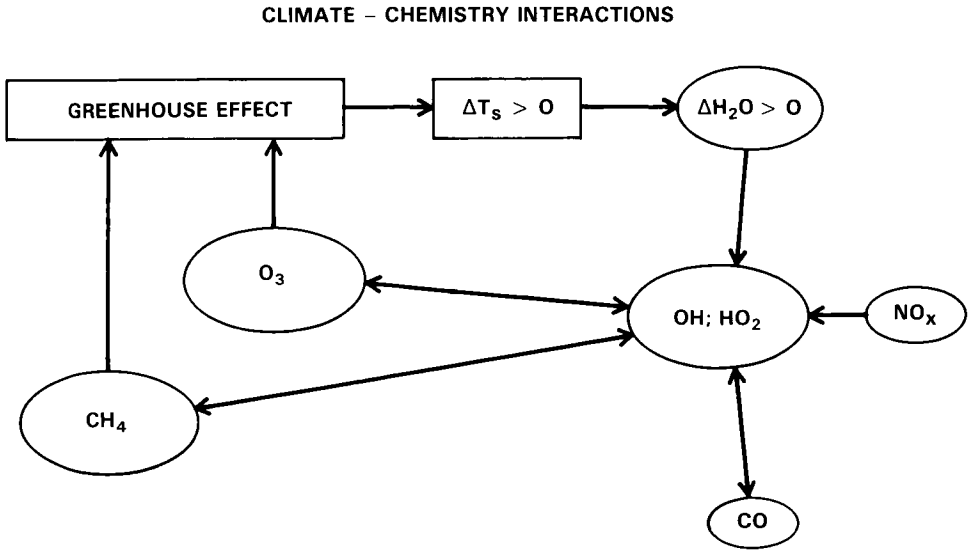

Figure 15-28. Schematic of the climate-chemistry interactions involving OH and HO_2 chemistry in the troposphere. Surface temperature increase ($\Delta T_S > 0$) due to the greenhouse effect of trace gases (including CO_2) leads to an increase in H_2O which contributes to an increase in OH. The addition of NO_X, CO and CH_4 reacts with OH and HO_2 to alter CH_4 and tropospheric O_3 which in turn modulates the greenhouse effect.

(iii) The response of biogenic source molecules such as CH_4 and N_2O to surface temperature changes are not well known and should be examined for their potential role as a feedback mechanism.

15.6.1.2 Sensitivity of Stratospheric H_2O

An important issue that has repeatedly come up during the last five years but still has not received a careful scrutiny concerns the sensitivity of stratospheric H_2O to perturbations in tropical tropopause temperatures. As discussed in earlier sections, GCMs and other models reveal the tropical tropopause temperatures to be quite sensitive to perturbations in CO_2, CFCs and O_3. However, current studies have focused largely on zonal average temperatures, whereas the entry of low levels of H_2O into the stratosphere may depend on the extreme (cold) tropical tropopause temperatures rather than the zonally averaged value. Model studies with a special emphasis on the geographical regions where H_2O enters the stratosphere in conjunction with special observational programs (for determining H_2O, temperature and cloud distribution) are needed to shed new insights on this problem.

15.6.1.3 Interactions in the Stratosphere

The continued growth of halogenated hydrocarbons in the troposphere presages reduced O_3 in the stratosphere. The subsequent effects of such changes on atmospheric opacity, thermal and dynamical structure in the stratosphere, and stratosphere-troposphere exchange bear directly on concerns about climate-chemistry issues. For example, the radiative effect of stratospheric O_3 perturbation due to CFCs can add as much as 30% to the surface warming due to the direct greenhouse effect of CFCs. Furthermore, latitudinal effects of the O_3 change on thermal structure are important. To date, most of the coupled radiative-chemical calculations of O_3 change have been performed with 1-D models. There is a strong need to develop coupled radiative-chemical-dynamical models (both 2-D and GCMs) and to examine the full scope of the climate-chemistry impact on tropospheric climate.

15.6.2 Observational Challenges

One of the most challenging issues on the observational front is the accurate determination of the long term (decadal) trends in CH_4, N_2O, CO, HO_x, NO_x, tropospheric and stratospheric O_3 and finally, tropospheric and stratospheric H_2O. As mentioned repeatedly in this report, there are significant uncertainties in our current estimates of the rate of growth of CO, O_3 and NO_x. The main source of the problem is the significant spatial and temporal variation of CO, O_3 and NO_x. The primary challenge is to design a strategy that will minimize the sampling errors, and such strategies can only evolve from active interactions between modeling and observational groups. The measurements of the above gases are also crucial for validating coupled transport-chemistry models.

Another equally challenging issue is the determination of trends in the radiative forcing (of the climate system) and the constituents that contribute to the radiative forcing. Included in this category are: solar radiation and its spectral variation at the top-of-the atmosphere, planetary albedo and its spectral distribution in 2 or 3 wavelength regions (e.g., UV, visible and IR), stratospheric aerosols, tropospheric aerosols including arctic haze, and important radiatively-active trace gases including CO_2, CH_4, N_2O, O_3 vertical distribution, F11, F12, F22, CH_3CCl_3, and stratospheric H_2O. Since the effects of aerosols, cloud-feedback and ice-albedo feedback are manifested in the planetary albedo, accurate determination of the planetary albedo should be one of the fundamental goals of future observational programs. The measurements described above are crucial for inferring the causal mechanisms for climate change. Of equal importance is continued monitoring of stratospheric, tropospheric and surface temperatures. These measurements, if they are made with high quality, excellent calibration and redundancy checks, can provide perhaps the only attractive approach for verifying the climate sensitivity of the models.

Finally, we have to develop and maintain an adequate spectroscopic data base for trace gases. For all of the CFCs and for a number of other compounds (e.g., CH_3CCl_3; PAN; CF_3Br) which have strong greenhouse effects, spectroscopic line parameters are either unavailable or unpublished. Furthermore, for the available data, there are significant discrepancies in the measured band strengths (e.g., F11 and F12 band strengths differ by 20 to 30% between different measurements). Moreover, current measurements do not separate out the contribution of the hot bands in the spectra; such identifications are crucial for incorporating the temperature dependence of the opacity in climate models. The availability of such measurements will promote line-by-line calculations which can then serve as a basis for treatment of the radiative effects of trace gases in climate models.

In preparing the ensuing assessment, the panel benefitted significantly from consultations with the following scientists: Dr. J.T. Kiehl for computing radiative heating due to trace gases; Dr. S. Liu for contributing to the subsection on NO_x and Drs. M. Geller, S. Manabe, F.S. Rowland, P.J. Crutzen, R.E. Dickinson, R. Gammon, A. Ghazi, N. Husson, M.A.H. Smith, N. Sundararaman, D. Wuebbles and R.T. Watson for their comments on the text. The panel thanks G. Escobar for preparing and proofreading the chapter.

ANNEX 1: ACCURACY OF BAND MODEL APPROACHES FOR CH_4

Band models may be divided into two categories: narrow-band models in which the longwave spectrum is divided into spectral intervals ranging from 1 cm^{-1} in width, and broad band models which employ analytical expressions either derived from theory or laboratory data to treat the absorption within the entire band. In the evaluation of a band model, two issues are involved: (1) the ability of the band model to accurately characterize the total band absorptance for a homogeneous optical path through the

gas (i.e., constant temperature and pressure), and (2) the ability of the band model to characterize absorption and emission along inhomogeneous paths (i.e., atmospheric applications). In order to treat inhomogeneous paths, a scaling approximation must be invoked in the band model.

The second item above is of particular importance with respect to broad-band models. Although several broad-band scaling approximations have been suggested (Chan and Tien, 1969; Cess and Wang, 1970; Edwards and Morizumi, 1970), there has not been a definitive examination of their accuracies.

The strategy of the present section is as follows. A reference line-by-line calculation will first be described, followed by the presentation of narrow-band and broad-band models that are tuned, for a homogeneous gas, to the line-by-line calculation. Thus, a hierarchy of band models is obtained, with these band models yielding virtually identical homogeneous band absorptances for the homogeneous case. The scaling approximations for the narrow-band and broad-band models are evaluated by applying the models to atmospheric profiles (the inhomogeneous case). Accompanying this will be a brief discussion concerning pitfalls associated with the use of narrow-band models.

The line-by-line calculations used the line locations and intensities from a JPL data tape (Orton and Robiette, 1980), with the line intensities being renormalized to a total band intensity of 129 $cm^{-2}atm^{-1}$ at 296 K (e.g., Varanasi *et al.*, 1983). The Lorentz half-width per unit pressure, γ^0, was taken to be

$$\gamma^0(cm^{-1}\ atm^{-1}) = 0.06\ (296/T) \tag{1}$$

for all lines, based upon Varanasi *et al.* (1983) who obtained a nitrogen-broadened value of 0.063 (with a standard deviation of 0.003) for 77 lines within the wavenumber interval 1300-1353 cm^{-1}. In that there are roughly 12,500 lines on the JPL tape, this comprises a rather extensive extrapolation. Although the line-by-line calculations serve as a reference, there are still some uncertainties associated with line-by-line model results because our knowledge of line half-widths is meager at best.

The narrow-band model is a modification of the Goody random band model (Goody, 1952), for which the transmittance of a spectral interval $\Delta\omega$ is given by

$$T_{\Delta\omega} = \exp\{-(S_{\Delta\omega}/\Delta\omega)[1 + (S_{\Delta\omega}\ w/\pi\gamma)]^{-1/2}\} \tag{2}$$

where $S_{\Delta\omega}$ is the sum of the line strengths within the interval, w is the absorber amount, and γ is defined by

$$S_{\Delta\omega}\gamma = C[\Sigma(\gamma S_{JK})^{1/2}]^2 \tag{3}$$

where S_{JK} denotes the individual line strengths and the summation is over all lines within $\Delta\omega$. Conventionally, $C = 4/\pi$ to be consistent with the limit of strong nonoverlapping lines (e.g., Goody, 1964). But if there is a significant number of coincident or near-coincident lines, $C < 4/\pi$ since coincident lines would be linearly summed. For present purposes, $\Delta\omega = 5\ cm^{-1}$, with elaboration on this choice to be given later.

Turning next to the broad-band model, that due to Ramanathan (1976) is adopted, for which the total band absorptance is expressed by

$$A = 2A_0 \ln\left[1 + \Sigma \frac{u}{\sqrt{4 + u(1 + 1/\beta}}\right] \tag{4}$$

where $u = Sw/A_0$ with S the total band intensity, A_0 is the bandwidth parameter, β is proportional to the ratio of a mean line half-width to a mean line spacing, and here the summation refers to the two overlapping $^{12}CH_4$ and $^{13}CH_4$ isotope bands.

The relevant coefficients appearing within both the narrow-band and broad-band models have been evaluated through regression fits to homogeneous-gas line-by-line calculations, with the result that

$$C = 0.762 \tag{5}$$

$$A_0(cm^{-1}) = 102.8(T/300) \tag{6}$$

$$\beta = 0.0838(300/T) \tag{7}$$

As discussed above, one would anticipate that $C < 4/\pi = 1.273$ if coincident lines are a factor, which may indeed be the case for the ν_4 band due both to line splitting and the presence of a Q branch. But the considerable difference between Equation (5) and $C = 4/\pi$ might include other factors as will shortly be discussed.

A comparison of both the narrow-band and broad-band models with the line-by-line results is illustrated in Figure 15-29. A single curve is used for both band models since there is no distinguishable difference between them. Similar agreement with the line-by-line results exists for temperatures spanning the range from 220 K to 300 K.

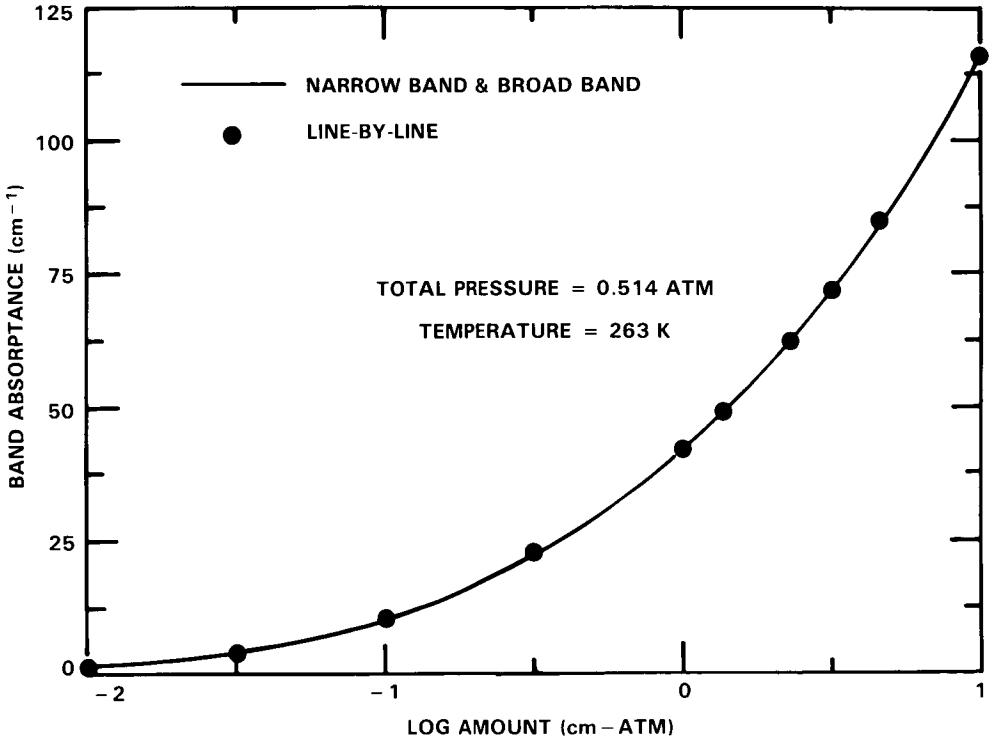

Figure 15-29. Comparison of narrow-band, broad-band and line-by-line determinations of the CH_4 total band absorptance. The CH_4 amount in cm-atm refers to STP.

As discussed in more detail by Cess *et al.* (1985), the virtual equivalence of the band models with the line-by-line calculations allows an evaluation of band-model scaling approximations. For this purpose the McClatchey *et al.* (1971) midlatitude summer atmosphere has been employed, neglecting overlap with water vapor and clouds. Table 15-12 summarizes calculations for the reduction in infrared flux at the top of the model atmosphere (25 km), at the tropopause (13 km), and at the surface, for an increase in methane volumetric mixing ratio from 1.75×10^6 to 3.5×10^6.

The use of Curtis-Godson scaling within the narrow-band model is as described by Rodgers and Walshaw (1967). Although this two-parameter scaling is exact in the weak-line and strong-line limits, the present atmospheric methane abundance lies between these two asymptotic limits. Thus, methane serves as a good test of Curtis-Godson scaling, and Table 15-12 confirms the validity of this often-used scaling approximation.

For the broad-band model, three different three-parameter scaling approximations are compared in Table 15.12 (Chan and Tien, 1969; Edwards and Morizumi, 1970; Cess and Wang; 1970). All three scaling approximations overestimate the flux reduction at the surface, with Chan-Tien scaling producing the smallest errors for the three flux reduction calculations.

On a similar point, several band models which have been employed in atmospheric radiation calculations are compared in Table 15.13 with the line-by-line results. These include the conventional random band models of Goody (1952) and Malkmus (1967), the broad-band model of Donner and Ramanathan (1980), and a broad-band model due to Cess and Chen (1975) which they developed for Jovian applications, but which was utilized for terrestrial applications by Hameed *et al.* (1980). The primary failing of the latter band model can be traced to the assumption by Cess and Chen (1975) that individual multiplets could be treated as a single Lorentz line; i.e., they neglected line splitting.

Returning to the narrow-band model, the present CH_4 example serves to illustrate certain pitfalls associated with random band models. Consider first the present choice of 5 cm^{-1} intervals. As pointed out by Kiehl and Ramanathan (1983) for CO_2, significant errors occur if one employs spectral intervals greater than 10 cm^{-1}. This is due to the statistics of the band, as manifested by the averaging procedure of Equation (3), being variable throughout the band. One way of minimizing this effect is to choose small

Table 15-12. Comparison of model calculations for the change in infrared flux due to an increase in CH_4 mixing ratio from 1.75×10^6 to 3.5×10^6. The respective scaling approximations are listed in brackets, while the numbers in parentheses denote the percentage differences from the line-by-line values.

Model	Flux Reduction (W/m^2) Top	Tropopause	Surface
Line-by-Line	1.78	1.78	2.40
Narrow Band [Curtis-Godson]	1.79 (0.6)	1.78 (0.0)	2.41 (0.4)
Broad Band [Chan-Tien]	1.77 (−0.6)	1.78 (0.0)	2.61 (8.8)
Broad Band [Edwards-Morizumi]	1.79 (0.6)	1.79 (0.6)	2.63 (9.6)
Broad Band [Cess-Wang]	1.85 (3.9)	1.83 (2.8)	2.67 (11.3)

Table 15-13. Comparison of model calculations for the change in infrared flux due to an increase in CH_4 mixing ratio from 1.75×10^6 to 3.5×10^6. Curtis-Godson scaling is used for the Malkmus and Goody models, while Chan-Tien scaling is employed for the Donner-Ramanathan and Cess-Chen models. The numbers in parentheses denote the percentage differences from the line-by-line values.

Model	Flux Reduction (W/m^2) Top	Tropopause	Surface
Line-by-Line	1.78	1.78	2.40
Malkmus	1.99 (11.8)	1.97 (10.7)	2.61 (8.8)
Goody	2.05 (15.2)	2.04 (14.6)	2.72 (13.3)
Donner-Ramanathan	1.55 (−12.9)	1.57 (−11.8)	2.17 (−9.6)
Cess-Chen	1.00 (−43.8)	1.00 (−43.8)	1.44 (−40.0)

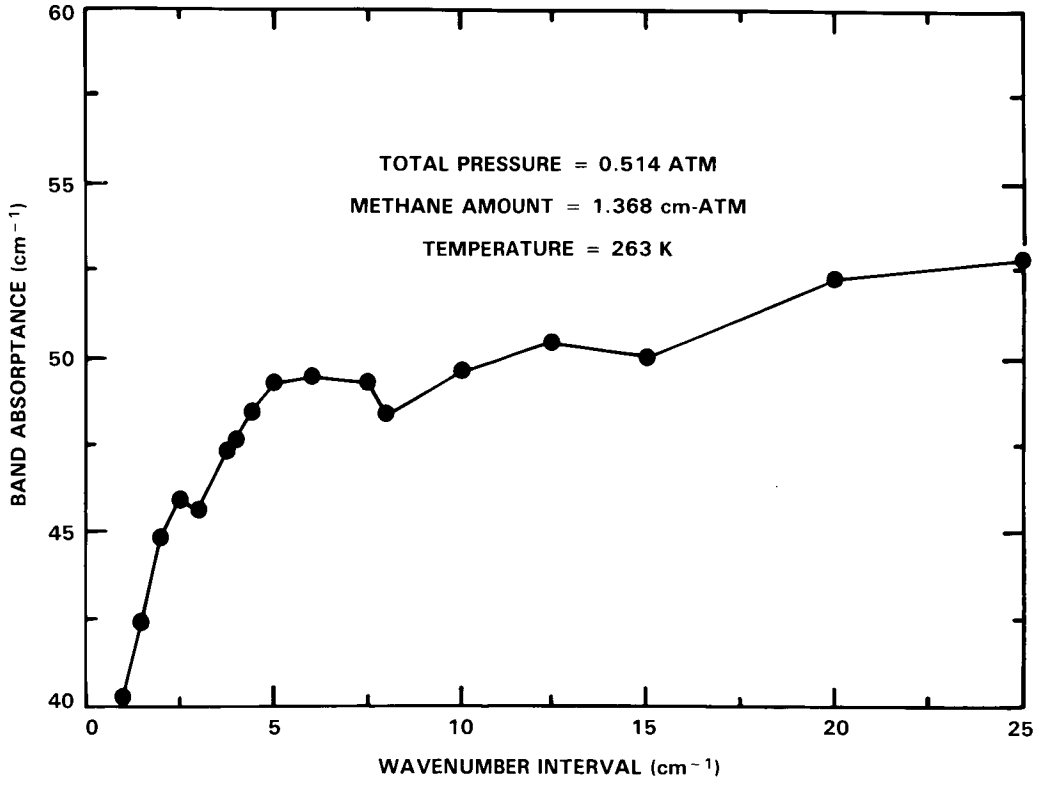

Figure 15-30. Narrow-band CH_4 total band absorptance as a function of wavenumber interval ($\Delta\omega$) as employed within the narrow band model. The methane abundance of 1.368 cm-atm (at STP) coincides with the atmospheric column abundance for a CH_4 mixing ratio of 1.75×10^{-6}.

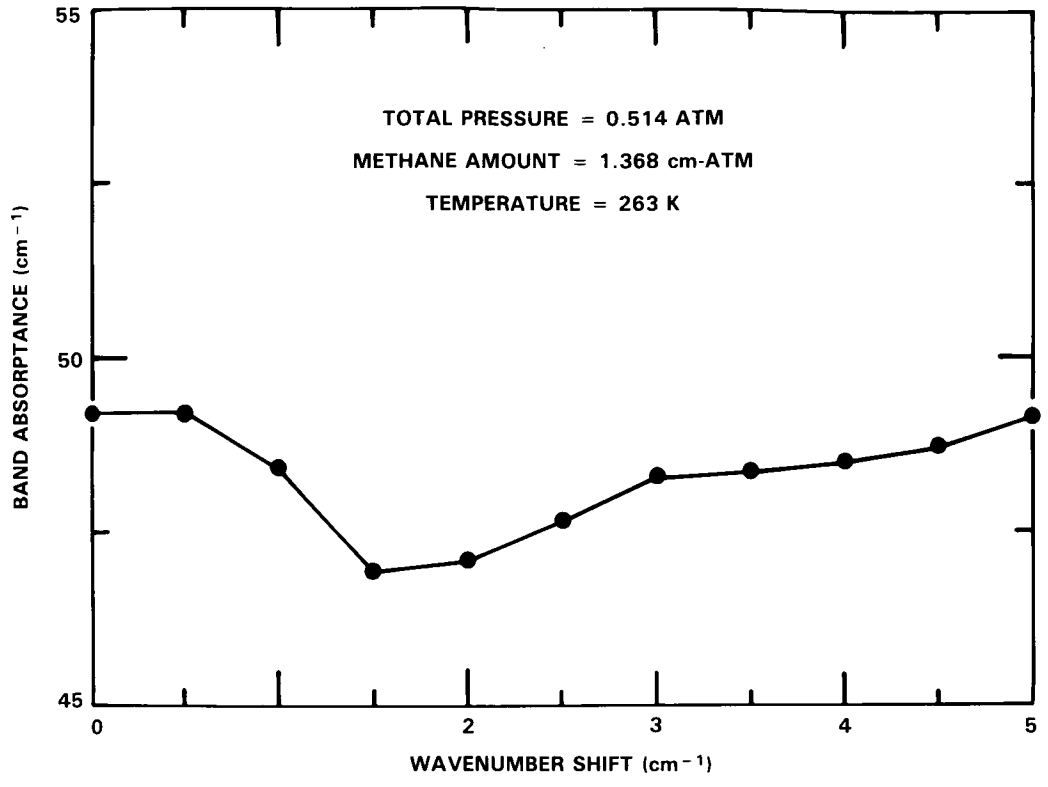

Figure 15-31. Narrow-band CH_4 total band absorptance for $\Delta\omega = 5 cm^{-1}$ and as a function of wavenumber shift of the interval spacing. The methane abundance of 1.368 cm-atm (at STP) coincides with the atmospheric column abundance for a CH_4 mixing ratio of 1.75×10^{-6}.

intervals with the hope that this will produce near-uniform statistics within each interval. But if the intervals are too small, there will not be a sufficient number of lines within each interval to yield meaningful statistics.

Ideally, one would anticipate that there should be an interval range over which the computed band absorptance is invariant to the choice of interval size, with the intervals being sufficiently large so as to contain a statistically meaningful number of lines, but at the same time sufficiently small so that Equation (3) produces meaningful statistical averages. However, as illustrated in Figure 15-30, CH_4 does not produce such a clearly defined range of intervals. The small plateau from roughly 5 to 8 cm^{-1} was the sole motivation for our choice of a 5 cm^{-1} interval size.

A second issue concerns the location of the intervals. Figure 15-31 illustrates a band absorptance calculation in which the locations of the interval spacings ($\Delta\omega$ = 5 cm^{-1}) are progressively shifted, with a shift of 5 cm^{-1} denoting a return to the original interval locations. For example, wavenumber shift = 0 corresponds to interval locations of 1200-1205 cm^{-1}, etc., while for wavenumber shift = 1 cm^{-1} these are 1201-1206 cm^{-1}, etc. As may be seen in Figure 15-31, this can result in a 5 percent variation in band absorptance, an effect that is again related to a variation in band statistics within the 5 cm^{-1} intervals as the interval positions are shifted.

In addition to the problem of coincident or near-coincident lines, as previously discussed with respect to Equation (3), the effects portrayed within Figures 15-30 and 15-31 additionally influence the evaluation

of C as given by Equation (5). For this reason, the present narrow-band models should not be applied to conditions well removed from those for which Equation (5) was evaluated.

As a final point, it must be emphasized that CH_4 represents an extreme case concerning the points raised with respect to Figures 15-30 and 15-31, since the ν_4 band possesses both line splitting and a Q branch. Experience with vibration-rotation bands of other gases (D.P. Kratz and R.D. Cess, private communication) indicates that these problems are somewhat less severe in the absence of line splitting, and are considerably less severe in the absence of both line splitting and a Q branch.

APPENDIX A

KINETICS AND PHOTOCHEMISTRY

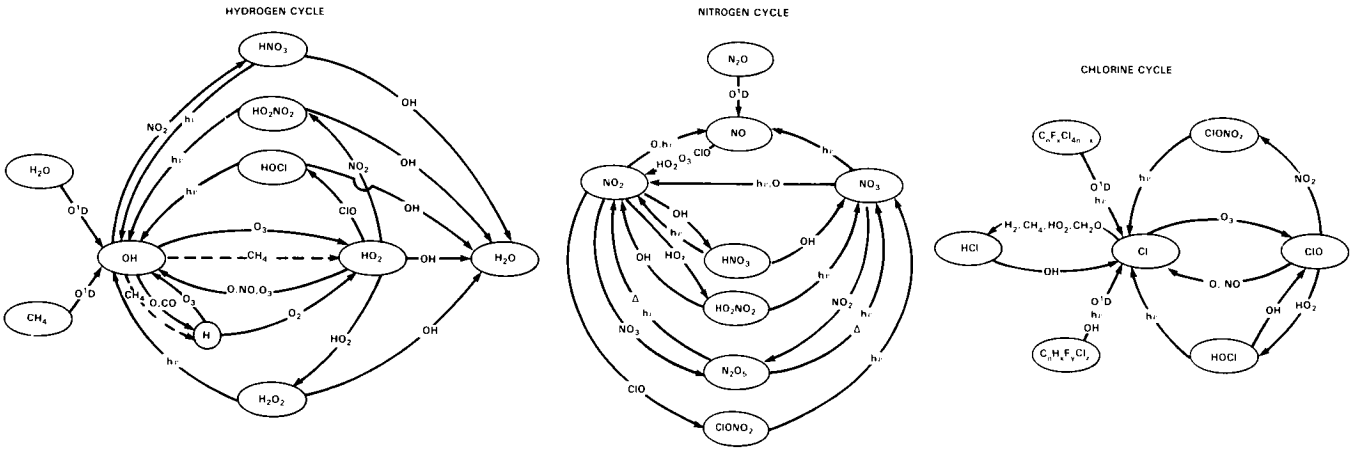

Panel Members

W.B. DeMore, Chairman

D.M. Golden
R.F. Hampson
C.J. Howard
M.J. Kurylo
J.J. Margitan
M.J. Molina
A.R. Ravishankara
R.T. Watson

APPENDIX A

KINETICS AND PHOTOCHEMICAL DATA BASE

The data for chemical kinetics rate constants and photochemical cross sections used in the present assessment were taken from a compilation prepared in early 1985 by the NASA Panel for Data Evaluation. That compilation is entitled "Chemical Kinetics and Photochemical Data for Use in Stratospheric Modeling", and is published by the Jet Propulsion Laboratory as JPL Publication 85-37.*

The NASA Data Evaluation Panel was established in 1977 by the NASA Upper Atmosphere Research Program for the purpose of providing a standardized, critical tabulation of the latest kinetics and photochemical data for use by modelers in computer simulations of stratospheric chemistry. The 1985 edition represents the seventh evaluation prepared by the panel. In earlier years the evaluations were updated annually; however, with the steadily increasing completeness and reliability of the data, future reevaluations are expected to be held approximately biennially.

Chapter 2 of the present assessment is an independent appraisal of the overall quality of the chemistry data base, along with discussions of other topics such as the best methods for testing the completeness of the chemical model and the question of error appraisal in data evaluation. Chapter 13 presents the results of model calculations using the data base, and also provides calculations which show the sensitivities of model predictions to uncertainties in the chemical data.

The following tables of data for chemical rate constants and equilibrium constants are excerpted from JPL 85-37, and are included for convenience to the reader who may not have immediate access to the complete publication.

*A copy of JPL Publication 85-37 may be obtained from the Documentation Section, Bldg. 111-116B, Jet Propulsion Laboratory, Pasadena CA 91109.

Table 1. Rate Constants for Second Order Reactions

Reaction	A-Factor	E/R±Δ(E/R)	k(298K)	Uncertainty Factor/298K
	O_x Reactions			
$O + O_2 \xrightarrow{M} O_3$	(See Table 2)			
$O + O_3 \rightarrow O_2 + O_2$	8.0×10^{-12}	2060±250	8.0×10^{-15}	1.15
	$O(^1D)$ Reactions			
$O(^1D) + N_2O \rightarrow N_2 + O_2$	4.9×10^{-11}	0±100	4.9×10^{-11}	1.3
$\rightarrow NO + NO$	6.7×10^{-11}	0±100	6.7×10^{-11}	1.3
$O(^1D) + H_2O \rightarrow OH + OH$	2.2×10^{-10}	0±100	2.2×10^{-10}	1.2
$O(^1D) + CH_4 \rightarrow OH + CH_3$	1.4×10^{-10}	0±100	1.4×10^{-10}	1.2
$\rightarrow H_2 + CH_2O$	1.4×10^{-11}	0±100	1.4×10^{-11}	1.2
$O(^1D) + H_2 \rightarrow OH + H$	1.0×10^{-10}	0±100	1.0×10^{-10}	1.2
$O(^1D) + N_2 \rightarrow O + N_2$	1.8×10^{-11}	-(107±100)	2.6×10^{-11}	1.2
$O(^1D) + N_2 \xrightarrow{M} N_2O$	(See Table 2)			
$O(^1D) + O_2 \rightarrow O + O_2$	3.2×10^{-11}	-(67±100)	4.0×10^{-11}	1.2
$O(^1D) + O_3 \rightarrow O_2 + O_2$	1.2×10^{-10}	0±100	1.2×10^{-10}	1.3
$\rightarrow O_2 + O + O$	1.2×10^{-10}	0±100	1.2×10^{-10}	1.3
*$O(^1D) + HCl \rightarrow$ products	1.5×10^{-10}	0±100	1.5×10^{-10}	1.2
$O(^1D) + CCl_4 \rightarrow$ products	3.3×10^{-10}	0±100	3.3×10^{-10}	1.2
$O(^1D) + CFCl_3 \rightarrow$ products	2.3×10^{-10}	0±100	2.3×10^{-10}	1.2
$O(^1D) + CF_2Cl_2 \rightarrow$ products	1.4×10^{-10}	0±100	1.4×10^{-10}	1.3
$O(^1D) + CF_4 \rightarrow CF_4 + O$	1.8×10^{-13}	0±100	1.8×10^{-13}	2.0
$O(^1D) + CCl_2O \rightarrow$ products	3.6×10^{-10}	0±100	3.6×10^{-10}	2.0
$O(^1D) + CFClO \rightarrow$ products	1.9×10^{-10}	0±100	1.9×10^{-10}	2.0
$O(^1D) + CF_2O \rightarrow$ products	7.4×10^{-11}	0±100	7.4×10^{-11}	2.0
$O(^1D) + NH_3 \rightarrow OH + NH_2$	2.5×10^{-10}	0±100	2.5×10^{-10}	1.3

*Indicates a change from the previous Panel evaluation (JPL 83-62).
#Indicates a new entry that was not in the previous evaluation.

Table 1. (Continued)

Reaction	A-Factor	E/R±Δ(E/R)	k(298K)	Uncertainty Factor/298K
$O(^1D) + CO_2 \rightarrow O + CO_2$	7.4×10^{-11}	-(117±100)	1.1×10^{-10}	1.2
$*O(^1D) + HF \rightarrow OH + F$	1.4×10^{-10}	0±100	1.4×10^{-10}	2.0
		HO_x Reactions		
$H + O_2 \xrightarrow{M} HO_2$	(See Table 2)			
$H + O_3 \rightarrow OH + O_2$	1.4×10^{-10}	470±200	2.9×10^{-11}	1.25
$H + HO_2 \rightarrow$ products	7.4×10^{-11}	0±400	7.4×10^{-11}	1.6
$O + OH \rightarrow O_2 + H$	2.2×10^{-11}	-(117±100)	3.3×10^{-11}	1.2
$O + HO_2 \rightarrow OH + O_2$	3.0×10^{-11}	-(200±200)	5.9×10^{-11}	1.2
$O + H_2O_2 \rightarrow OH + HO_2$	1.4×10^{-12}	2000±1000	1.7×10^{-15}	2.0
$*OH + HO_2 \rightarrow H_2O + O_2$	1.7×10^{-11}	-(416±200)	7.0×10^{-11}	1.3
$\xrightarrow{M} H_2O + O_2$	$3.0\times10^{-31}[M]$	-(500±500)	$1.6\times10^{-30}[M]$	2.0
$OH + O_3 \rightarrow HO_2 + O_2$	1.6×10^{-12}	940±300	6.8×10^{-14}	1.3
$OH + OH \rightarrow H_2O + O$	4.2×10^{-12}	242±242	1.9×10^{-12}	1.4
$\xrightarrow{M} H_2O_2$	(See Table 2)			
$*OH + H_2O_2 \rightarrow H_2O + HO_2$	3.1×10^{-12}	187^{+100}_{-300}	1.7×10^{-12}	1.3
$OH + H_2 \rightarrow H_2O + H$	6.1×10^{-12}	2030±400	6.7×10^{-15}	1.2
$HO_2 + HO_2 \rightarrow H_2O_2 + O_2$	2.3×10^{-13}	-(590±200)	1.7×10^{-12}	1.3
$\xrightarrow{M} H_2O_2 + O_2$	$1.7\times10^{-33}[M]$	-(1000±400)	$4.9\times10^{-32}[M]$	1.3
$HO_2 + O_3 \rightarrow OH + 2O_2$	1.4×10^{-14}	580^{+500}_{-100}	2.0×10^{-15}	1.5
		NO_x Reactions		
$N + O_2 \rightarrow NO + O$	4.4×10^{-12}	3220±340	8.9×10^{-17}	1.25
$N + O_3 \rightarrow NO + O_2$	-	-	$<1.0\times10^{-15}$	-
$N + NO \rightarrow N_2 + O$	3.4×10^{-11}	0±100	3.4×10^{-11}	1.3
$N + NO_2 \rightarrow N_2O + O$	-	-	3.0×10^{-12}	3

*Indicates a change from the previous Panel evaluation (JPL 83-62).
#Indicates a new entry that was not in the previous evaluation.

Table 1. (Continued)

Reaction	A-Factor	E/R±Δ(E/R)	k(298K)	Uncertainty Factor/298K
$O + NO \xrightarrow{M} NO_2$	(See Table 2)			
$O + NO_2 \rightarrow NO + O_2$	9.3×10^{-12}	0^{+0}_{-150}	9.3×10^{-12}	1.1
$O + NO_2 \xrightarrow{M} NO_3$	(See Table 2)			
$O + NO_3 \rightarrow O_2 + NO_2$	1.0×10^{-11}	0±150	1.0×10^{-11}	1.5
$O + N_2O_5 \rightarrow$ products	-	-	$<3.0\times10^{-16}$	-
$O + HNO_3 \rightarrow OH + NO_3$	-	-	$<3.0\times10^{-17}$	-
$O + HO_2NO_2 \rightarrow$ products	7.0×10^{-11}	3370±750	8.6×10^{-16}	3.0
$O_3 + NO \rightarrow NO_2 + O_2$	1.8×10^{-12}	1370±200	1.8×10^{-14}	1.2
$NO + HO_2 \rightarrow NO_2 + OH$	3.7×10^{-12}	-(240±80)	8.3×10^{-12}	1.2
$*NO + NO_3 \rightarrow 2NO_2$	1.3×10^{-11}	-(250±250)	3.0×10^{-11}	1.3
$OH + NO \xrightarrow{M} HONO$	(See Table 2)			
$OH + NO_2 \xrightarrow{M} HNO_3$	(See Table 2)			
$*OH + HNO_3 \rightarrow H_2O + NO_3$	(See ≠ below)			1.3
$OH + HO_2NO_2 \rightarrow$ products	1.3×10^{-12}	$-(380^{+270}_{-500})$	4.6×10^{-12}	1.5
$HO_2 + NO_2 \xrightarrow{M} HO_2NO_2$	(See Table 2)			
$O_3 + NO_2 \rightarrow NO_3 + O_2$	1.2×10^{-13}	2450±140	3.2×10^{-17}	1.15
$O_3 + HNO_2 \rightarrow O_2 + HNO_3$	-	-	$<5.0\times10^{-19}$	-
$NO_2 + NO_3 \xrightarrow{M} N_2O_5$	(See Table 2)			
$\#N_2O_5 + H_2O \rightarrow 2HNO_3$	-	-	$<2\times10^{-21}$	-
$*OH + NH_3 \rightarrow H_2O + NH_2$	3.5×10^{-12}	925±200	1.6×10^{-13}	1.4

* Indicates a change from the previous Panel evaluation (JPL 83-62).
\# Indicates a new entry that was not in the previous evaluation.
≠ $OH + HNO_3$ pressure and temperature dependence fit by

$$k(M,T) = k_0 + \frac{k_3[M]}{1 + \frac{k_3[M]}{k_2}}$$

with $k_0 = 7.2 \times 10^{-15} \exp(785/T)$, $k_2 = 4.1 \times 10^{-16} \exp(1440/T)$, $k_3 = 1.9 \times 10^{-33} \exp(725/T)$

Table 1. (Continued)

Reaction	A-Factor	E/R±Δ(E/R)	k(298K)	Uncertainty Factor/298K
$NH_2 + HO_2 \rightarrow$ products	-	-	$3.4x10^{-11}$	2
*$NH_2 + NO \rightarrow$ products	$3.8x10^{-12}$	-(450±150)	$1.7x10^{-11}$	2
*$NH_2 + NO_2 \rightarrow$ products	$2.1x10^{-12}$	-(650±250)	$1.9x10^{-11}$	3
$NH_2 + O_2 \rightarrow$ products	-	-	$<3x10^{-18}$	-
*$NH_2 + O_3 \rightarrow$ products	$4.8x10^{-12}$	930±500	$2.1x10^{-13}$	3
	Hydrocarbon Reactions			
*$OH + CO \rightarrow CO_2 + H$	-		$1.5x10^{-13}(1+0.6P_{atm})$	1.3
$OH + CH_4 \rightarrow CH_3 + H_2O$	$2.4x10^{-12}$	1710±200	$7.7x10^{-15}$	1.2
*$OH + C_2H_6 \rightarrow H_2O + C_2H_5$	$1.1x10^{-11}$	1090±250	$2.8x10^{-13}$	1.25
$OH + C_3H_8 \rightarrow H_2O + C_3H_7$	$1.6x10^{-11}$	800±250	$1.1x10^{-12}$	1.5
$OH + C_2H_4 \rightarrow$ products	(See Table 2)			
$OH + C_2H_2 \rightarrow$ products	(See Table 2)			
$OH + H_2CO \rightarrow H_2O + HCO$	$1.0x10^{-11}$	0±200	$1.0x10^{-11}$	1.25
$OH + CH_3OOH \rightarrow$ products	$1.0x10^{-11}$	0±200	$1.0x10^{-11}$	2.0
$OH + HCN \rightarrow$ products	$1.2x10^{-13}$	400±150	$3.1x10^{-14}$	3.0
*$OH + CH_3CN \rightarrow$ products	$4.5x10^{-13}$	900±400	$2.2x10^{-14}$	2.0
$HO_2 + CH_2O \rightarrow$ adduct	-	-	$4.5x10^{-14}$	10.0
$O + C_2H_2 \rightarrow$ products	$2.9x10^{-11}$	1600±300	$1.4x10^{-13}$	1.3
$O + H_2CO \rightarrow$ products	$3.0x10^{-11}$	1550±250	$1.6x10^{-13}$	1.25
$O + CH_3 \rightarrow$ products	$1.1x10^{-10}$	0±250	$1.1x10^{-10}$	1.3
$CH_3 + O_2 \rightarrow$ products	-	-	$<3x10^{-16}$	-
$CH_3 + O_2 \xrightarrow{M} CH_3O_2$	(See Table 2)			
$CH_2OH + O_2 \rightarrow CH_2O + HO_2$	-	-	$2x10^{-12}$	10
*$CH_3O + O_2 \rightarrow CH_2O + HO_2$	$8.4x10^{-14}$	1200±300	$1.5x10^{-15}$	2

*Indicates a change from the previous Panel evaluation (JPL 83-62).
#Indicates a new entry that was not in the previous evaluation.

Table 1. (Continued)

Reaction	A-Factor	E/R±Δ(E/R)	k(298K)	Uncertainty Factor/298K
$HCO + O_2 \rightarrow CO + HO_2$	3.5×10^{-12}	-(140±140)	5.5×10^{-12}	1.3
$CH_3 + O_3 \rightarrow$ products	5.4×10^{-12}	220±150	2.6×10^{-12}	2
$CH_3O_2 + O_3 \rightarrow$ products	-	-	$<1\times10^{-17}$	-
$CH_3O_2 + CH_3O_2 \rightarrow$ products	1.6×10^{-13}	-(220±220)	3.4×10^{-13}	1.25
*$CH_3O_2 + NO \rightarrow CH_3O + NO_2$	4.2×10^{-12}	-(180±180)	7.6×10^{-12}	1.2
$CH_3O_2 + NO_2 \xrightarrow{M} CH_3O_2NO_2$	(See Table 2)			
$CH_3O_2 + HO_2 \rightarrow CH_3OOH + O_2$	7.7×10^{-14}	$-(1300^{+500}_{-1300})$	6.0×10^{-12}	3.0
#$NO_3 + CO \rightarrow$ products	-	-	$<1\times10^{-15}$	-
#$NO_3 + CH_2O \rightarrow$ products	-	-	6×10^{-16}	1.5
	ClO_x Reactions			
$Cl + O_3 \rightarrow ClO + O_2$	2.8×10^{-11}	257±100	1.2×10^{-11}	1.15
$Cl + H_2 \rightarrow HCl + H$	3.7×10^{-11}	2300±200	1.6×10^{-14}	1.25
$Cl + CH_4 \rightarrow HCl + CH_3$	9.6×10^{-12}	1350±150	1.0×10^{-13}	1.1
$Cl + C_2H_6 \rightarrow HCl + C_2H_5$	7.7×10^{-11}	90±90	5.7×10^{-11}	1.1
$Cl + C_3H_8 \rightarrow HCl + C_3H_7$	1.4×10^{-10}	-(40±250)	1.6×10^{-10}	1.5
$Cl + C_2H_2 \rightarrow$ products	-	-	1×10^{-12}	10
$Cl + CH_3OH \rightarrow CH_2OH + HCl$	6.3×10^{-11}	0±250	6.3×10^{-11}	2.0
$Cl + CH_3Cl \rightarrow CH_2Cl + HCl$	3.4×10^{-11}	1260±200	4.9×10^{-13}	1.2
$Cl + CH_3CCl_3 \rightarrow CH_2CCl_3 + HCl$	-	-	$<4\times10^{-14}$	-
$Cl + H_2CO \rightarrow HCl + HCO$	8.2×10^{-11}	34±100	7.3×10^{-11}	1.15
$Cl + H_2O_2 \rightarrow HCl + HO_2$	1.1×10^{-11}	980±500	4.1×10^{-13}	1.5
$Cl + HOCl \rightarrow$ products	3.0×10^{-12}	130±250	1.9×10^{-12}	2.0
$Cl + HNO_3 \rightarrow$ products	-	-	$<1.7\times10^{-14}$	-
$Cl + HO_2 \rightarrow HCl + O_2$	1.8×10^{-11}	-(170±200)	3.2×10^{-11}	1.5

*Indicates a change from the previous Panel evaluation (JPL 83-62).
#Indicates a new entry that was not in the previous evaluation.

Table 1. (Continued)

Reaction	A-Factor	E/R±Δ(E/R)	k(298K)	Uncertainty Factor/298K
→ OH + ClO	4.1×10^{-11}	450±200	9.1×10^{-12}	2.0
$Cl + Cl_2O \rightarrow Cl_2 + ClO$	9.8×10^{-11}	0±250	9.8×10^{-11}	1.2
$Cl + OClO \rightarrow ClO + ClO$	5.9×10^{-11}	0±250	5.9×10^{-11}	1.25
$Cl + ClONO_2 \rightarrow$ products	6.8×10^{-12}	-(160±200)	1.2×10^{-11}	1.3
$Cl + NO \xrightarrow{M} NOCl$	(See Table 2)			
$Cl + NO_2 \xrightarrow{M} ClONO\ (ClNO_2)$	(See Table 2)			
$Cl + ClNO \rightarrow NO + Cl_2$	2.3×10^{-11}	0^{+500}_{-250}	2.3×10^{-11}	3.0
$Cl + O_2 \xrightarrow{M} ClOO$	(See Table 2)			
$Cl + ClOO \rightarrow Cl_2 + O_2$	1.4×10^{-10}	0±250	1.4×10^{-10}	3.0
→ ClO + ClO	8.0×10^{-12}	0±250	8.0×10^{-12}	3.0
*$ClO + O \rightarrow Cl + O_2$	4.7×10^{-11}	50±100	4.0×10^{-11}	1.3
$ClO + NO \rightarrow NO_2 + Cl$	6.2×10^{-12}	-(294±100)	1.7×10^{-11}	1.15
$ClO + NO_2 \xrightarrow{M} ClONO_2$	(See Table 2)			
$ClO + HO_2 \rightarrow HOCl + O_2$	4.6×10^{-13}	$-(710^{+250}_{-700})$	5.0×10^{-12}	1.4
$ClO + H_2CO \rightarrow$ products	$\sim1.0\times10^{-12}$	>2060	$<1.0\times10^{-15}$	-
*ClO + OH → products	1.0×10^{-11}	-(120±150)	1.5×10^{-11}	1.6
$ClO + CH_4 \rightarrow$ products	$\sim1.0\times10^{-12}$	>3700	$<4.0\times10^{-18}$	-
$ClO + H_2 \rightarrow$ products	$\sim1.0\times10^{-12}$	>4800	$<1.0\times10^{-19}$	-
ClO + CO → products	$\sim1.0\times10^{-12}$	>3700	$<4.0\times10^{-18}$	-
$ClO + N_2O \rightarrow$ products	$\sim1.0\times10^{-12}$	>4260	$<6.0\times10^{-19}$	-
ClO + ClO → products	-	-	-	-
$ClO + O_3 \rightarrow ClOO + O_2$	1.0×10^{-12}	>4000	$<1.0\times10^{-18}$	-
→ $OClO + O_2$	1.0×10^{-12}	>4000	$<1.0\times10^{-18}$	-
*$OH + HCl \rightarrow H_2O + Cl$	2.6×10^{-12}	350±100	8.0×10^{-13}	1.2

*Indicates a change from the previous Panel evaluation (JPL 83-62).
#Indicates a new entry that was not in the previous evaluation.

Table 1. (Continued)

Reaction	A-Factor	E/R±Δ(E/R)	k(298K)	Uncertainty Factor/298K
$OH + HOCl \rightarrow H_2O + ClO$	3.0×10^{-12}	150^{+850}_{-150}	1.8×10^{-12}	10
$OH + CH_3Cl \rightarrow CH_2Cl + H_2O$	1.8×10^{-12}	1112±200	4.3×10^{-14}	1.2
$OH + CH_2Cl_2 \rightarrow CHCl_2 + H_2O$	4.5×10^{-12}	1032±200	1.4×10^{-13}	1.2
$OH + CHCl_3 \rightarrow CCl_3 + H_2O$	3.3×10^{-12}	1034±200	1.0×10^{-13}	1.2
$OH + CHFCl_2 \rightarrow CFCl_2 + H_2O$	8.9×10^{-13}	1013±200	3.0×10^{-14}	1.3
$OH + CHF_2Cl \rightarrow CF_2Cl + H_2O$	7.8×10^{-13}	1530±200	4.6×10^{-15}	1.2
$OH + CH_2ClF \rightarrow CHClF + H_2O$	2.0×10^{-12}	1134±150	4.4×10^{-14}	1.2
$OH + CH_3CCl_3 \rightarrow CH_2CCl_3 + H_2O$	5.4×10^{-12}	1820±200	1.2×10^{-14}	1.3
$OH + C_2Cl_4 \rightarrow$ products	9.4×10^{-12}	1200±200	1.7×10^{-13}	1.25
$OH + C_2HCl_3 \rightarrow$ products	5.0×10^{-13}	-(445±200)	2.2×10^{-12}	1.25
$OH + CFCl_3 \rightarrow$ products	$\sim1.0\times10^{-12}$	>3650	$<5.0\times10^{-18}$	-
$OH + CF_2Cl_2 \rightarrow$ products	$\sim1.0\times10^{-12}$	>3560	$<6.5\times10^{-18}$	-
$OH + ClONO_2 \rightarrow$ products	1.2×10^{-12}	333±200	3.9×10^{-13}	1.5
$O + HCl \rightarrow OH + Cl$	1.0×10^{-11}	3340±350	1.4×10^{-16}	2.0
$O + HOCl \rightarrow OH + ClO$	1.0×10^{-11}	2200±1000	6.0×10^{-15}	10
$O + ClONO_2 \rightarrow$ products	3.0×10^{-12}	808±200	2.0×10^{-13}	1.5
$O + Cl_2O \rightarrow ClO + ClO$	2.9×10^{-11}	630±200	3.5×10^{-12}	1.4
$O + OClO \rightarrow ClO + O_2$	2.5×10^{-11}	1160±300	5.0×10^{-13}	1.5
$NO + OClO \rightarrow NO_2 + ClO$	2.5×10^{-12}	600±300	3.4×10^{-13}	1.5
$\#Cl + CH_3CN \rightarrow$ products	-	-	$<2.0\times10^{-15}$	-
$\#Cl + NO_3 \rightarrow ClO + NO_2$	-	-	7.6×10^{-11}	2.0
$\#ClO + NO_3 \rightarrow$ products	-	-	4.0×10^{-13}	2.0
$\#OH + Cl_2 \rightarrow HOCl + Cl$	-	-	6.5×10^{-14}	1.2

*Indicates a change from the previous Panel evaluation (JPL 83-62).
#Indicates a new entry that was not in the previous evaluation.

Table 1. (Continued)

Reaction	A-Factor	E/R±Δ(E/R)	k(298K)	Uncertainty Factor/298K
#$HCl + ClONO_2 \rightarrow$ products	-	-	$<1.0\times10^{-18}$	-
#$HCl + HO_2NO_2 \rightarrow$ products	-	-	$<1\times10^{-20}$	-
		BrO_x Reactions		
$Br + O_3 \rightarrow BrO + O_2$	1.4×10^{-11}	755±200	1.1×10^{-12}	1.2
$Br + H_2O_2 \rightarrow HBr + HO_2$	1.0×10^{-11}	>2500	$<2.0\times10^{-15}$	-
$Br + H_2CO \rightarrow HBr + HCO$	1.7×10^{-11}	800±200	1.1×10^{-12}	1.3
*$Br + HO_2 \rightarrow HBr + O_2$	-	-	8.0×10^{-13}	3.0
$BrO + O \rightarrow Br + O_2$	3.0×10^{-11}	0±250	3.0×10^{-11}	3.0
$BrO + ClO \rightarrow Br + OClO$	6.7×10^{-12}	0±250	6.7×10^{-12}	2.0
$\rightarrow Br + Cl + O_2$	6.7×10^{-12}	0±250	6.7×10^{-12}	2.0
$BrO + NO \rightarrow NO_2 + Br$	8.7×10^{-12}	-(265±130)	2.1×10^{-11}	1.15
$BrO + NO_2 \xrightarrow{M} BrONO_2$	(See Table 2)			
$BrO + BrO \rightarrow 2\ Br + O_2$	1.4×10^{-12}	-(150±150)	2.3×10^{-12}	1.25
$\rightarrow Br_2 + O_2$	6.0×10^{-14}	-(600±600)	4.4×10^{-13}	1.25
$BrO + O_3 \rightarrow Br + 2\ O_2$	$\sim1\times10^{-12}$	>1600	$<5.0\times10^{-15}$	-
$BrO + HO_2 \rightarrow$ products	-	-	5.0×10^{-12}	3.0
$BrO + OH \rightarrow$ products	-	-	1.0×10^{-11}	5.0
*$OH + HBr \rightarrow H_2O + Br$	1.1×10^{-11}	0±250	1.1×10^{-11}	1.3
$OH + CH_3Br \rightarrow CH_2Br + H_2O$	6.1×10^{-13}	825±200	3.8×10^{-14}	1.25
$O + HBr \rightarrow OH + Br$	6.6×10^{-12}	1540±200	3.7×10^{-14}	1.3
#$OH + Br_2 \rightarrow HOBr + Br$	-	-	4.8×10^{-11}	1.3
		FO_x Reactions		
$F + O_3 \rightarrow FO + O_2$	2.8×10^{-11}	226±200	1.3×10^{-11}	2.0
$F + H_2 \rightarrow HF + H$	1.6×10^{-10}	525±250	2.7×10^{-11}	1.3

*Indicates a change from the previous Panel evaluation (JPL 83-62).
#Indicates a new entry that was not in the previous evaluation.

Table 1. (Continued)

Reaction	A-Factor	E/R ± Δ(E/R)	k(298K)	Uncertainty Factor/298K
$F + CH_4 \rightarrow HF + CH_3$	3.0×10^{-10}	400±300	8.0×10^{-11}	1.5
*$F + H_2O \rightarrow HF + OH$	4.2×10^{-11}	400±200	1.1×10^{-11}	3.0
$F + O_2 \xrightarrow{M} FO_2$	(See Table 2)			
$F + NO \xrightarrow{M} FNO$	(See Table 2)			
$F + NO_2 \xrightarrow{M} FNO_2(FONO)$	(See Table 2)			
$NO + FO \rightarrow NO_2 + F$	2.6×10^{-11}	0±250	2.6×10^{-11}	2.0
$FO + FO \rightarrow 2\ F + O_2$	1.5×10^{-11}	0±250	1.5×10^{-11}	3.0
$FO + O_3 \rightarrow F + 2\ O_2$	-	-	-	-
$\rightarrow FO_2 + O_2$	-	-	-	-
$FO + NO_2 \xrightarrow{M} FONO_2$	(See Table 2)			
$O + FO \rightarrow F + O_2$	5.0×10^{-11}	0±250	5.0×10^{-11}	3.0
$O + FO_2 \rightarrow FO + O_2$	5.0×10^{-11}	0±250	5.0×10^{-11}	5.0
#$CF_3O_2 + NO \rightarrow CF_3O + NO_2$	3.9×10^{-12}	-(400±200)	1.5×10^{-11}	1.3
#$CF_2Cl_2O_2 + NO \rightarrow CF_2Cl_2O + NO_2$	3.1×10^{-12}	-(500±200)	1.6×10^{-11}	1.3
#$CFCl_2O_2 + NO \rightarrow CFCl_2O + NO_2$	3.5×10^{-12}	-(430±200)	1.5×10^{-11}	1.3
#$CCl_3O_2 + NO \rightarrow CCl_3O + NO_2$	5.7×10^{-12}	-(330±200)	1.7×10^{-11}	1.3
	SO_x Reactions			
$OH + H_2S \rightarrow SH + H_2O$	5.9×10^{-12}	65±65	4.7×10^{-12}	1.2
*$OH + OCS \rightarrow$ products	3.9×10^{-13}	1780±500	1.0×10^{-15}	10
$OH + CS_2 \rightarrow$ products		-	-	-
$OH + SO_2 \xrightarrow{M} HOSO_2$	(See Table 2)			
$O + H_2S \rightarrow OH + SH$	1.0×10^{-11}	1810±550	2.2×10^{-14}	1.7
$O + OCS \rightarrow CO + SO$	2.1×10^{-11}	2200±150	1.3×10^{-14}	1.2
$O + CS_2 \rightarrow CS + SO$	3.2×10^{-11}	650±150	3.6×10^{-12}	1.2

*Indicates a change from the previous Panel evaluation (JPL 83-62).
#Indicates a new entry that was not in the previous evaluation.

Table 1. (Continued)

Reaction	A-Factor	E/R±Δ(E/R)	k(298K)	Uncertainty Factor/298K
$O + SH \rightarrow H + SO$	-	-	1.6×10^{-10}	5.0
$S + O_2 \rightarrow SO + O$	2.3×10^{-12}	0±200	2.3×10^{-12}	1.2
$S + O_3 \rightarrow SO + O_2$	-	-	1.2×10^{-11}	2.0
$S + OH \rightarrow SO + H$	-	-	6.6×10^{-11}	3.0
$SO + O_2 \rightarrow SO_2 + O$	2.4×10^{-13}	2370±500	8.4×10^{-17}	2
$SO + O_3 \rightarrow SO_2 + O_2$	3.6×10^{-12}	1100±200	9.0×10^{-14}	1.2
$SO + OH \rightarrow SO_2 + H$	-	-	8.6×10^{-11}	2.0
$SO + NO_2 \rightarrow SO_2 + NO$	-	-	1.4×10^{-11}	1.3
$SO + ClO \rightarrow SO_2 + Cl$	-	-	2.3×10^{-11}	3.0
$SO + OClO \rightarrow SO_2 + ClO$	-	-	1.9×10^{-12}	3.0
$SO + BrO \rightarrow SO_2 + Br$	-	-	$>4.0 \times 10^{-11}$	-
$SO_2 + HO_2 \rightarrow$ products	-	-	$<1.0 \times 10^{-18}$	-
$CH_3O_2 + SO_2 \rightarrow$ products	-	-	$<5.0 \times 10^{-17}$	-
*$SH + O_2 \rightarrow OH + SO$	-	-	$<1.0 \times 10^{-17}$	-
$Cl + H_2S \rightarrow HCl + SH$	-	-	7.3×10^{-11}	1.4
$Cl + OCS \rightarrow SCl + CO$	-	-	$<1.1 \times 10^{-16}$	-
$ClO + OCS \rightarrow$ products	-	-	$<2.4 \times 10^{-16}$	-
$ClO + SO_2 \rightarrow Cl + SO_3$	-	-	$<4.0 \times 10^{-18}$	-
#$SH + H_2O_2 \rightarrow$ products	-	-	$<5 \times 10^{-15}$	-
#$SH + O_3 \rightarrow HSO + O_2$	-	-	3.2×10^{-12}	3.0
#$HSO + O_3 \rightarrow$ products	-	-	1×10^{-13}	5.0
#$SH + NO_2 \rightarrow HSO + NO$	-	-	3.2×10^{-11}	1.5
#$SH + NO \xrightarrow{M} HSNO$	(See Table 2)			
#$HOSO_2 + O_2 \rightarrow HO_2 + SO_3$	-	-	4.0×10^{-13}	3.0

*Indicates a change from the previous Panel evaluation (JPL 83-62).
#Indicates a new entry that was not in the previous evaluation.

Table 1. (Continued)

Reaction	A-Factor	E/R ± Δ(E/R)	k(298K)	Uncertainty Factor/298K
#$SO_2 + NO_2 \rightarrow$ products	-	-	$<2\times10^{-26}$	-
#$SO_3 + NO_2 \rightarrow$ products	-	-	1.0×10^{-19}	10
#$SO_2 + O_3 \rightarrow SO_3 + O_2$	3.0×10^{-12}	>7000	$<2\times10^{-22}$	-
#$CS + O_2 \rightarrow OCS + O$	-	-	2.9×10^{-19}	2.0
#$CS + O_3 \rightarrow OCS + O_2$	-	-	3.0×10^{-16}	3.0
#$CS + NO_2 \rightarrow OCS + NO$	-	-	7.6×10^{-17}	3.0
	Metal Reactions			
#$Na + O_3 \rightarrow NaO + O_2$	5×10^{-10}	0±400	5×10^{-10}	1.5
$\rightarrow NaO_2 + O$	$<3\times10^{-11}$	0±400	$<3\times10^{-11}$	-
#$Na + O_2 \xrightarrow{M} NaO_2$	(See Table 2)			
#$NaO + HCl \rightarrow$ products	2.8×10^{-10}	0±400	2.8×10^{-10}	3.0
#$NaOH + HCl \rightarrow NaCl + H_2O$	2.8×10^{-10}	0±400	2.8×10^{-10}	3.0

*Indicates a change from the previous Panel evaluation (JPL 83-62).
#Indicates a new entry that was not in the previous evaluation.

Table 2. Rate Constants for Three-Body Reactions

Reaction	Low Pressure Limit $k_0(T) = k_0^{300}(T/300)^{-n}$		High Pressure Limit $k_\infty(T) = k_\infty^{300}(T/300)^{-m}$	
	k_0^{300}	n	k_∞^{300}	m
$O + O_2 \xrightarrow{M} O_3$	(6.0±0.5)(-34)	2.3±0.5	-	-
$O(^1D) + N_2 \xrightarrow{M} N_2O$	(3.5±3.0)(-37)	$0.6^{+2}_{-.6}$	-	-
*$H + O_2 \xrightarrow{M} HO_2$	(5.5±0.5)(-32)	1.6±0.5	(7.5±4.0)(-11)	0±1
$OH + OH \xrightarrow{M} H_2O_2$	(6.9±3.0)(-31)	$0.8^{+2.0}_{-0.8}$	(1.0±0.5)(-11)	1.0±1.0
*$O + NO \xrightarrow{M} NO_2$	(9.0±2.0)(-32)	1.5±0.3	(3.0±1.0)(-11)	0±1
$O + NO_2 \xrightarrow{M} NO_3$	(9.0±1.0)(-32)	2.0±1.0	(2.2±0.3)(-11)	0±1
$OH + NO \xrightarrow{M} HONO$	(7.0±2.0)(-31)	2.6±1.0	(1.5±1.0)(-11)	0.5±0.5
$OH + NO_2 \xrightarrow{M} HNO_3$	(2.6±0.3)(-30)	3.2±0.7	(2.4±1.2)(-11)	1.3±1.3
*$HO_2 + NO_2 \xrightarrow{M} HO_2NO_2$	(2.0±0.5)(-31)	2.7±1.5	(4.2±1.0)(-12)	2.0±2.0
*$NO_2 + NO_3 \xrightarrow{M} N_2O_5$	(2.2±0.5)(-30)	4.3±1.3	(1.5±0.8)(-12)	0.5±0.5
$Cl + NO \xrightarrow{M} ClNO$	(9.0±2.0)(-32)	1.6±0.5	-	-
*$Cl + NO_2 \xrightarrow{M} ClONO$	(1.3±0.2)(-30)	2.0±1.0	(1.0±0.5)(-10)	1.0±1.0
$\xrightarrow{M} ClNO_2$	(1.8±0.3)(-31)	2.0±1.0	(1.0±0.5)(-10)	1.0±1.0
$Cl + O_2 \xrightarrow{M} ClOO$	(2.0±1.0)(-33)	1.4±1.4	-	-
$ClO + NO_2 \xrightarrow{M} ClONO_2$	(1.8±0.3)(-31)	3.4±1.0	(1.5±0.7)(-11)	1.9±1.9
$BrO + NO_2 \xrightarrow{M} BrONO_2$	(5.0±2.0)(-31)	2.0±2.0	(1.0±0.5)(-11)	1.0±1.0
$F + O_2 \xrightarrow{M} FO_2$	(1.6±0.8)(-32)	1.4±1.0	-	-
$F + NO \xrightarrow{M} FNO$	(5.9±3.0)(-32)	1.7±1.7	-	-
*$F + NO_2 \xrightarrow{M}$ Products	(1.1±0.6)(-30)	2.0±2.0	(3.0±2.0)(-11)	1.0±1.0
$FO + NO_2 \xrightarrow{M} FONO_2$	(2.6±2.0)(-31)	1.3±1.3	(2.0±1.0)(-11)	1.5±1.5
*$CH_3 + O_2 \xrightarrow{M} CH_3O_2$	(4.5±1.5)(-31)	2.0±1.0	(1.8±0.2)(-12)	1.7±1.7

Note: $k(Z) = k(M,T) = \left(\frac{k_0(T)[M]}{1 + k_0(T)[M] / k_\infty(T)}\right) 0.6^{\{1 + [\log_{10}(k_0(T)[M]/k_\infty(T))]^2\}^{-1}}$

The values quoted are suitable for air as the third body, M.

*Indicates a change from the previous Panel evaluation (JPL 83-62).

Table 2. (Continued)

Reaction	Low Pressure Limit $k_0(T) = k_0^{300}(T/300)^{-n}$		High Pressure Limit $k_\infty(T) = k_\infty^{300}(T/300)^{-m}$	
	k_0^{300}	n	k_∞^{300}	m
$CH_3O_2 + NO_2 \xrightarrow{M} CH_3O_2NO_2$	(1.5±0.8)(-30)	4.0±2.0	(6.5±3.2)(-12)	2.0±2.0
*OH + $SO_2 \xrightarrow{M} HOSO_2$	(3.0±1.0)(-31)	3.3±1.5	(1.5±0.5)(-12)	0^{+2}_{-2}
*OH + $C_2H_4 \xrightarrow{M} HOCH_2CH_2$	(1.5±0.6)(-28)	0.8±2.0	(8.8±0.9)(-12)	0^{+2}_{-2}
*OH + $C_2H_2 \xrightarrow{M} HOCHCH$	(5.5±2.0)(-30)	0.0±0.2	(8.3±1.0)(-13)	$-2.0^{+2.8}_{-1.8}$
#$CF_3 + O_2 \xrightarrow{M} CF_3O_2$	(4.5±1.0)(-29)	2±2	(8±6)(-12)	1±1
#$CFCl_2 + O_2 \xrightarrow{M} CFCl_2O_2$	(5.0±0.8)(-30)	2±2	(6.0±1.0)(-12)	1±1
#$CCl_3 + O_2 \xrightarrow{M} CCl_3O_2$	(1.0±0.7)(-30)	2±2	(2.5±2)(-12)	1±1
#$CFCl_2O_2 + NO_2 \xrightarrow{M} CFCl_2O_2NO_2$	(3.5±0.5)(-29)	4±2	(6.0±1.0)(-12)	2±2
#HS + NO $\xrightarrow{M}$ HSNO	(2.4±0.4)(-31)	3±1	(2.7±0.5)(-11)	0^{+2}_{-2}
#Na + $O_2 \xrightarrow{M} NaO_2$	(1.9±1)(-30)	1.1±0.5	(2.0±1.8)(-10)	0±1

Note: $k(Z) = k(M,T) = \left(\frac{k_0(T)[M]}{1 + k_0(T)[M] / k_\infty(T)}\right) 0.6^{\{1 + [\log_{10}(k_0(T)[M]/k_\infty(T))]^2\}^{-1}}$

The values quoted are suitable for air as the third body, M.
*Indicates a change from the previous Panel evaluation (JPL 83-62).
#Indicates a new entry that was not in the previous evaluation.

Table 3. Equilibrium Constants

Reaction	A/cm³ molecule^{-1}	B/°K	Log K_{eq}(300)
$HO_2 + NO_2 \rightarrow HO_2NO_2$	2.33×10^{-27}	10,870	-10.90
$*NO_2 + NO_3 \rightarrow N_2O_5$	1.52×10^{-27}	11,153	-10.68
$Cl + O_2 \rightarrow ClOO$	2.43×10^{-25}	2,979	-20.30
$ClO + O_2 \rightarrow ClO \cdot O_2$	$<1.3 \times 10^{-26}$	<5,230	<-18.30
$F + O_2 \rightarrow FOO$	5.32×10^{-25}	7,600	-13.27
	1.15×10^{-25}	3,582	-19.75
$CH_3O_2 + NO_2 \rightarrow CH_3O_2NO_2$	1.30×10^{-28}	11,192	-11.68

K/cm³ molecule^{-1} = A exp (B/T) [200 < T/K < 300]
*Indicates a change from the previous Panel evaluation (JPL 83-62).

APPENDIX B

SPECTROSCOPIC DATABASE

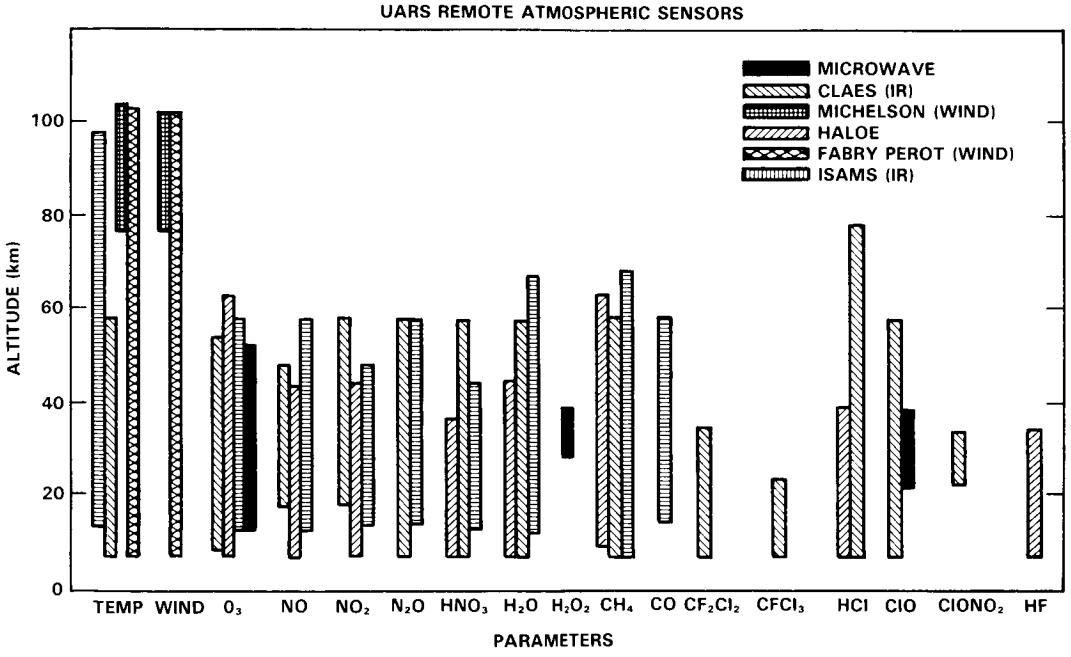

Panel Members

N. Husson, Chairperson

A. Barbe
L. R. Brown
B. Carli
A. Goldman
H. M. Pickett
A. E. Roche
L. S. Rothman
M. A. H. Smith

APPENDIX B

SPECTROSCOPIC DATABASE: INFRARED TO MICROWAVE

TABLE OF CONTENTS

B-0 INTRODUCTION

It is now well recognized that accurate modeling of radiative transfer phenomena in a planetary atmosphere requires very good knowledge of the parameters describing the radiation absorption or emission properties of the optically active gases involved in the medium considered. The increasing impact of physical techniques for the remote sensing of the thermal structure and composition of the earth's atmosphere requires continuous research to achieve a better understanding of molecular spectra of radiatively active gases and necessitates the compilation of accurate relevant spectroscopic data.

The purpose of the appendix is to review the status of spectroscopic database and current laboratory spectroscopy in the infrared to the microwave for atmospheric remote sensing. Reviews of this type have been given by the WMO as part of a meeting on potential climatic effects of ozone and other minor trace gases (WMO, 1983) and by NASA (Smith, 1985), and in the proceedings of a CMA-NBS workshop on atmospheric spectra held in 1983 (CMA-NBS, 1985).

This appendix is divided into eight sections beginning with the introduction in Section B-0. In Sections B-1 and B-2, several aspects of quantitative atmospheric spectroscopy are considered, using a classification of the molecules according to the gas amounts in the stratosphere and upper troposphere, and reviews of quantitative atmospheric high-resolution spectroscopic measurements and field measurements systems are given. Laboratory spectroscopy and spectral analysis and prediction are presented in Section B-3 with a summary of current laboratory spectroscopy capabilities. Spectroscopic data requirements for accurate derivation of atmospheric composition are discussed in Sections B-4 and B-5, where examples are given for space-based remote sensing experiments of the atmosphere: the ATMOS (Atmospheric Trace Molecule Spectroscopy) and UARS (Upper Atmosphere Research Satellite) experiments. Section B-6 is devoted to a database assessment including:

- a review of the basic parameters involved in the data compilations;
- a summary of information on line parameter compilations already in existence: the AFGL (Air Force Geophysics Laboratory) catalog (McClatchey *et al.*, 1973; Rothman *et al.*, 1983 a,b; 1985), the GEISA (Gestion et Etude des Informations Spectroscopiques Atmospheriques; word translation: Management and Study of Atmospheric Spectroscopic Information) catalog (Chedin *et al.*, 1980; 1985, Husson *et al.*, 1982; 1985), the JPL catalog (Poynter *et al.*, 1981, 1984);
- a summary of current laboratory spectroscopy studies.

Finally, the major recommendations for further work in laboratory spectroscopy to support atmospheric measurements are presented in Section B-7.

B-1 OVERVIEW OF ATMOSPHERIC SPECTROSCOPY

During the last twenty years, atmospheric spectroscopy has proven to be a powerful tool for the identification and quantification of previously unknown stratospheric gases as well as for more accurate quantification and monitoring of known species. The initial detection of stratospheric HNO_3 (Murcray *et al.*, 1968) and NO_2 (Goldman *et al.*, 1970) and the increased interest in stratospheric chemistry in relation to the effects of supersonic transports (SST) and chlorofluorocarbons (CFC) on the ozone layer have served to intensify the atmospheric spectroscopy studies. Indeed, most of the atmospheric species involved in the various photochemical cycles of the stratosphere, and particularly in the ozone photochemistry, are currently being measured, or scheduled to be measured, with high sensitivity spectrometers from the ground, aircraft, balloon and spacecraft.

SPECTROSCOPIC DATABASE

Simultaneous measurements of O_3 and related species are required for a more complete evaluation of the ozone problem. Therefore, the discussion of atmospheric spectroscopy and ozone has to include all of the possibly related species.

Traditionally, classical spectroscopy has focused mostly on spectral line positions and energy levels. Modern theoretical and experimental developments made spectroscopy a very effective quantitative tool, and the identification and quantification of atmospheric species from their spectra has become a major part of today's atmospheric science. This requires the study of absolute line intensities and line shapes in addition to line positions.

The atmospheric long geometric path obtainable at large zenith angles is a major factor in increasing the sensitivity of spectroscopic measurements to trace constituents. Some species are not observable from the ground and require high altitude platforms such as balloons or aircraft to minimize the interference by other species (especially H_2O). Most of the measurements are made in either solar absorption or atmospheric emission modes. In general, the absorption measurements yield higher spectral resolution, but the emission measurements yield larger dynamic range. In ground-based measurements, signal-to-noise ratios over 1,000 have been achieved. In aircraft and balloon borne measurements, a signal-to-noise ratio of ~ 100 is typical.

In this text, several aspects of quantitative atmospheric spectroscopy, its current status and accuracies, and its anticipated developments as a part of modern atmospheric measurements are presented. The discussion will concentrate on the infrared to microwave spectral region, but many of the concepts addressed apply to the entire electromagnetic spectrum. The evaluation will be made mostly in relation to the assessment of current knowledge and the requirements for future measurements and interpretation of ozone and related species.

B-2 QUANTITATIVE HIGH-RESOLUTION ATMOSPHERIC SPECTROSCOPY

The major quantitative spectral parameters include:

- individual line parameters;
- total and spectral band model parameters;
- approximate line or band absorption coefficients;
- continuum coefficients;

The line parameters include:

- line positions, energy levels, absolute transition probabilities, and energy level populations;
- quantum number dependence and temperature dependence of Lorentz halfwidths;
- non-Lorentzian line shapes (cores and wings).

The two series of above parameters are classified in order of decreasing accuracy.

A complete knowledge of the line parameters allows line-by-line simulations of atmospheric spectra which can lead to very accurate quantification of atmospheric gases. Indeed, this has become a standard tool of modern atmospheric spectroscopy, and extensive improvements in line parameter data banks are currently being made. The existing line parameters compilations and their accuracies are discussed separately

in this Appendix. Considerable research is also being devoted to semi-empirical quantification methods for line wings and the various coefficients which are needed to supplement the line-by-line simulations.

In general, the molecules of interest can be classified according to their optical depths in the stratosphere and upper troposphere as in Table B-1.

Table B-1. Classification of Atmospheric Molecules[1]

Category	Constituent Type	Optical Path	Molecules
[1]	"major"	long	H_2O, CO_2, O_3, N_2O, CO, CH_4, O_2, N_2, atomic O
[2]	"minor"	medium	NO, NO_2, NH_3, HNO_3, HF, HCl, OCS, H_2CO, HCOOH, HCN, C_2H_2, C_2H_6, CF_2Cl_2, $CFCl_3$, CF_4, CCl_4, CHF_2Cl
[3]	observed "trace"	small	ClO, $ClONO_2$, HO_2, OH
[4]	predicted "trace"	small	N_2O_5, CH_3Cl, HOCl, HNO_4, HNO_2, H_2O_2, HBr, SO_2, H_2S, H_2SO_4, C_3H_8, C_2H_4.

[1]According to the optical depths of the molecules in the stratosphere and upper troposphere.

In category [1] of Table B-1, the long geometric path, relative to the optical depth, of field measurements gives rise to spectral features of many weak transitions (isotopes, hot bands, etc.) not usually encountered in ordinary laboratory spectroscopy. For the infrared active molecules such as H_2O, CO_2, O_3, N_2O, CO and CH_4, this means that high rotational and vibrational quantum numbers for the participating energy levels, high order terms in the Hamiltonian expansions, and various resonance interactions between specific levels must be known. Indeed, for the polyatomic molecules in this list, it has proven necessary to do simultaneous analysis of several bands, taking into account high-order rotational terms and extensive vibration-rotation interactions. In addition, hyperfine line parameters are now needed not only for the microwave lines, but also for light diatomic molecules (e.g., NO and OH) observed in the infrared. For the infrared inactive molecules, such as N_2 and O_2, electric quadrupole line transitions and pressure-induced transitions are significant (pressure-induced transitions of CO_2, N_2O and CH_4 should have only a small effect on atmospheric spectra).

In category [2], the medium geometric path involves relatively simpler spectra for the small molecules (NH_3, HCN). However, the spectra of the larger molecules (CCl_4, $ClONO_2$) can be quite complex. The spectroscopic analysis of some of the larger molecules where the full line structure cannot be resolved requires the application of semi-empirical methods, such as band models, for quantification of these molecules from atmospheric spectra.

In categories [3] and [4], the small geometric path implies much simpler spectroscopic analysis. However, some of these molecules are unstable, and others are large molecules, so that the quantitative analysis can be quite complicated. Nevertheless, the "linear region of the curve of growth" approximation is applicable to most of these species so that the halfwidth and line shape dependence are not very significant for their quantification in the atmosphere.

The above list includes all of the species that have been measured to date in the stratosphere and upper troposphere by infrared and/or microwave spectroscopy. Other stratospheric infrared active species not listed here, such as NO_3, have been identified and quantified by their visible and ultraviolet (UV) spectra. It is important to realize, however, that with the current improvement in instrumental and theoretical techniques, it is anticipated that new species will be identified which may have strong catalytic effects. Thus, category [4] includes several potential species predicted by current photochemical/dynamic models but not yet confirmed. While the line parameters for some of these species are accurately known, only a first order quantification is needed for the initial identification.

The spectral resolution of the measurements is an important parameter in atmospheric spectroscopy. While many quantitative measurements can be made successfully from medium resolution spectra, the true stratospheric halfwidth of spectral lines is of the order of 0.001 to 0.02 cm^{-1}. Only 10 years ago, none of the field spectrometers were capable of measuring infrared atmospheric spectra at this resolution. Currently, a number of such high resolution field instruments are available and used for more sensitive quantitative atmospheric spectroscopy, for both absorption and emission spectra. These include grating, Fourier, laser and microwave spectrometers as well as others.

An extensive summary of the last 10 years [1975-1985] of atmospheric spectroscopic measurements of the species in Table B-1 is given in Table B-2; it is limited to spectral measurements of medium to high resolution only (better than 0.5 cm^{-1}), thus excluding lower resolution spectrometers and wide band filter instruments used extensively in many atmospheric measurements. Only results published in refereed journals and papers in preparation have been included. Table B-3 includes spectroscopic systems now under development for stratospheric and upper tropospheric species measurements, with classifications similar to those in Table B-2. The explanations of the instrumental abbreviations used in Tables B-2 and B-3, as well as the institution abbreviations of Table B-3, are given in Annex B-1 and Annex B-2, respectively, at the end of this appendix.

Despite the large number of spectral lines involved in the atmospheric spectrum (more than 500,000 lines), it is usually effective to perform detailed laboratory measurements only on a relatively small number of lines in preselected regions. Such measurements can yield relative or absolute intensity and line shape quantification with accuracy on the order of 1% to 5%. Combining such results with modern spectroscopic theories allows, in many cases, determination of line parameters in much wider spectral regions with accuracies of 10% or better. The selection of intervals for quantitative analysis will be specific to the planned experiment. Several laboratories are now equipped with high resolution quantitative spectroscopy systems, and are suited for such measurements. These include grating, Fourier, laser and microwave spectrometers with specialized absorption cells for various temperatures, pressures and optical paths for stable as well as unstable and corrosive gases. These are described separately in the following section.

Table B-2. Review of High-Resolution Microwave to Infrared Spectroscopic Field Measurements of Atmospheric Gases (1975-1985).

Spectral Region (cm^{-1})	Measurement Accuracy	Reference	Vehicle†	Instrument‡	Resolution* (cm^{-1})	Method**
H_2O						
20-130	50%	Clark & Kendall (1976)	Balloon	FTS	0.2	Emiss.
20-120		Kendall & Clark (1978)	Balloon	FTS	0.06	Emiss.
36-85		Carli *et al* (1980)	Balloon	FTS	0.003	Emiss.
1600-1610		Niple *et al* (1980)	Balloon	FTS	0.02	Absorp.
1599-1608	30%	Louisnard *et al* (1980)	Balloon	Grille	0.1	Absorp.
3229-3238	20%	Farmer *et al* (1980)	Balloon	FTS	0.15	Absorp.
30-110		Kendall & Clark (1981)	Balloon	FTS	0.06	Emiss.
30-80	10%	Naylor *et al* (1981)	Balloon	FTS	0.15	Absorp.
1323-1327,1602-1608	15%	Girard *et al* (1983)	Aircraft	Grille	0.1	Absorp.
794-798, 945-950	15%	Goldman *et al* (1983a)	Ground	FTS	0.02	Absorp.
1288-1326, 1595-1600, 1840-1846, 2860-2870, 2940-2950	10-20%	Louisnard *et al* (1983)	Balloon	Grille	0.1	Absorp.
1600-1608		Girard and Louisnard (1984)	Balloon	Grille	0.1	Absorp.
3815-3825		Lippens *et al* (1984)	Spacelab	Grille	0.1	Absorp.
3949-3951	15%	Park *et al* (1984)	Balloon/	FTS/	0.04/	Absorp./
			Balloon	FTS	0.15	Absorp.
1350-1570	15-20%	Rinsland *et al* (1984b)	Balloon/	FTS/	0.02/	Absorp./
			Aircraft	FTS	0.06	Absorp.
1335-1350,		Murcray *et al* (1985a)	Balloon/	Grating/	0.5/	Emiss./
278-400,			Balloon/	Grating/	0.25/	Emiss./
1600-1608,			Balloon/	Grille/	0.1/	Absorp./
80-220,	15%		Balloon/	FTS/	0.03/	Emiss./
2900-3000			Balloon	Grating	0.04	Absorp.
1450-1650		Kunde *et al* (1985)	Balloon	FTS	0.05	Emiss.
1450-1650		Murcray *et al* (1985b)	Balloon	FTS	0.08	Emiss.
HDO						
7-85		Carli *et al* (1980)	Balloon	FTS	0.003	Emiss.
1469-1513	15-20%	Rinsland *et al* (1984b)	Balloon/	FTS/	0.02/	Absorp./
1450-1486			Aircraft	FTS	0.06	Absorp.
CO_2						
2382-2392	10%	Farmer *et al* (1980)	Balloon	FTS	0.15	Absorp.
794-798, 945-950	5%	Goldman et al (1983a)	Ground	FTS	0.02	Absorp.
2046-2056		Louisnard *et al* (1983)	Balloon	Grille	0.1	Absorp.
3505-3509	15%	Park *et al* (1984)	Balloon/	FTS/	0.15/	Absorp./
			Balloon	FTS	0.04	Absorp.
700-800		Kunde *et al* (1985)	Balloon	FTS	0.05	Emiss.
700-800		Murcray *et al* (1985b)	Balloon	FTS	0.08	Emiss.
O_3						
20-90	40%	Clark & Kendall (1976)	Balloon	FTS	0.2	Emiss.
1011-1012		Frerking *et al* (1977)	Ground	LHS	0.007	Absorp.
20-120		Kendall & Clark (1978)	Balloon	FTS	0.06	Emiss.

Table B-2. Review of High-Resolution Microwave to Infrared Spectroscopic Field Measurements of Atmospheric Gases (1975-1985). — Continued

Spectral Region (cm^{-1})	Measurement Accuracy	Reference	Vehicle†	Instrument‡	Resolution* (cm^{-1})	Method**
O_3 — Continued						
1043.14-1043.18		Abbas *et al* (1978)	Ground	LHS	0.0002	Absorp.
7-85		Carli *et al* (1980)	Balloon	FTS	0.003	Emiss.
1720-1725		Goldman *et al* (1980)	Balloon	FTS	0.02	Absorp.
2778-2804, 3044-3056	25%	Farmer *et al* (1980)	Balloon	FTS	0.15	Absorp.
30-80	10%	Kendall & Clark (1981)	Balloon	FTS	0.06	Emiss.
30-80		Naylor *et al* (1981)	Balloon	FTS	0.15	Emiss.
6.876, 7.032	15%	Waters *et al* (1981)	Balloon	MWS		Absorp.
1001-1004	10%	Goldman *et al* (1983a)	Ground	FTS	0.02	Absorp.
1045-1085, 2046-2056, 2130-2138	10%	Louisnard *et al* (1983)	Balloon	Grille	0.1	Absorp.
2084-2085		Marche *et al* (1983)	Ground	SISAM	0.02	Absorp.
1080-1085	10%	Girard *et al* (1983)	Aircraft	Grille	0.1	Absorp.
2130-2135		Girard and Louisnard (1984)	Balloon	Grille	0.1	Absorp.
700-800, 1100-1200		Kunde *et al* (1985)	Balloon	FTS	0.05	Emiss.
900-1060,		Robbins *et al* (1985)	Balloon/	Grating/	0.25/	Emiss./
80-220			Balloon	FTS	0.03	Emiss.
975-994, 1044-1090, 1109-1172		Rinsland *et al* (1985c)	Ground	FTS	0.005	Absorp.
700,800, 1100-1200		Murcray *et al* (1985b)	Balloon	FTS	0.08	Emiss.
N_2O						
2200-3500	10-30%	Farmer *et al* (1980)	Balloon	FTS	0.15	Absorp.
10-40		Carli *et al* (1980)	Balloon	FTS	0.003	Emiss.
1177-1187	20%	Coffey *et al* (1981a)	Aircraft	FTS	0.06	Absorp.
1878-1881	15-20%	Rinsland *et al* (1982c)	Balloon	FTS	0.02	Absorp.
1247-1249	5%	Goldman *et al* (1983a)	Ground	FTS	0.02	Absorp.
1323-1327, 2134-2143	15%	Girard *et al* (1983)	Aircraft	Grille	0.1	Absorp.
1288-1295	10-30%	Louisnard *et al* (1983)	Balloon	Grille	0.1	Absorp.
2205-2212		Muller *et al* (1985)	Spacelab	Grille	0.1	Absorp.
1150-1300		Kunde *et al* (1985)	Balloon	FTS	0.05	Emiss.
1150-1300		Murcray *et al* (1985b)	Balloon	FTS	0.08	Emiss.
CO						
40-65		Carli *et al* (1980)	Balloon	FTS	0.003	Emiss.
2145-2167	20-50%	Farmer *et al* (1980)	Balloon	FTS	0.15	Absorp.
2040-2050, 2134-2143	10%	Girard *et al* (1983)	Aircraft	Grille	0.1	Absorp.
2046-2056, 2130-2138	10-25%	Louisnard *et al* (1983)	Balloon	Grille	0.1	Absorp.
Solar CO						
2046-2056, 2134-2143		Girard *et al* (1983)	Aircraft	Grille	0.1	Absorp.
2130-2138		Louisnard *et al* (1983)	Balloon	Grille	0.1	Absorp.
CH_4						
2900-3030	10-30%	Ackerman *et al* (1978/79)	Balloon	Grille	0.1	Absorp.
3000	15-25%	Farmer *et al* (1980)	Balloon	FTS	0.15	Absorp.
1228-1249	10%	Goldman *et al* (1983a)	Ground	FTS	0.02	Absorp.

Table B-2. Review of High-Resolution Microwave to Infrared Spectroscopic Field Measurements of Atmospheric Gases (1975-1985). – Continued

Spectral Region (cm^{-1})	Measurement Accuracy	Reference	Vehicle†	Instrument‡	Resolution* (cm^{-1})	Method**
CH_4 — Continued						
1323-1327, 2863-2871, 2929-2947	15%	Girard *et al* (1983)	Aircraft	Grille	0.1	Absorp.
1288-1326, 2860-2870, 2940-2950		Louisnard *et al* (1983)	Balloon	Grille	0.1	Absorp.
3010-3020		Lemaitre *et al* (1984)	Spacelab	Grille	0.2	Absorp.
1350-1570	15-20%	Rinsland *et al* (1984b)	Balloon/ Aircraft	FTS/ FTS	0.2/ 0.6	Absorp./ Absorp.
2974-3020		Muller *et al* (1985)	Spacelab	Grille	0.2	Absorp.
1335-1350, 2821-3385		Zander *et al* (1985)	Balloon/ Balloon	Grating/ FTS	0.5/ 0.1	Emiss./ Absorp.
1200-1400		Kunde *et al* (1985)	Balloon	FTS	0.05	Emiss.
1200-1400		Murcray *et al* (1985b)	Balloon	FTS	0.08	Emiss.
O_2						
20-100		Clark & Kendall (1976)	Balloon	FTS	0.2	Emiss.
6-85		Carli *et al* (1980)	Balloon	FTS	0.003	Emiss.
30-110		Clark & Kendall (1980)	Balloon	FTS	0.05	Emiss.
30-110		Kendall & Clark (1981)	Balloon	FTS	0.06	Emiss.
1603-1604		Goldman *et al* (1981b)	Balloon	FTS	0.02	Absorp.
1440-1680		Rinsland *et al* (1982b)	Balloon	FTS	0.02	Absorp.
80-220		Traub & Chance (1985)	Balloon	FTS	0.03	Emiss.
Atomic O						
68.6-68.9, 158.2-158.4		Carli *et al* (1985a)	Balloon	FTS	0.003	Emiss.
157-159		Clark *et al* (1985)	Balloon	FTS	0.01	Emiss.
NO						
1902-1917	25-50%	Ackerman *et al* (1975)	Balloon	Grille	0.1	Absorp.
1890-1892, 1908-1910, 1914-1916	40%	Fontanella *et al* (1975)	Aircraft	Grille	0.1	Absorp.
1898-1903		Bradford *et al* (1976)	Ground	FTS	0.06	Absorp.
1846, 1857, 1915	20-50%	Blatherwick *et al* (1980)	Balloon	FTS	0.02	Absorp.
1845-1860, 1910-1925	20-30%	Murcray *et al* (1980)	Balloon	FTS	0.02	Absorp.
1845-1848, 1859-1863, 1913-1917	20%	Coffey *et al* (1981a)	Aircraft	FTS	0.06	Absorp.
1913-1917		Girard *et al* (1983)	Aircraft	Grille	0.01	Absorp.
1840-1846	15-25%	Louisnard *et al* (1983)	Balloon	Grille	0.1	Absorp.
36-64		Carli *et al* (1983)	Balloon	FTS	0.003	Absorp.
1897-1903	20%	Rinsland *et al* (1984a)	Ground	FTS	0.01	Absorp.
1987		Webster & Menzies (1984)	Balloon	TDL	0.0002	Absorp.
1914-1919		Laurent *et al* (1985)	Spacelab	Grille	0.1	Absorp.
NO_2						
1595-1601	20-30%	Ackerman *et al* (1975)	Balloon	Grille	0.1	Absorp.
1603-1608	20%	Fontanella *et al* (1975)	Aircraft	Grille	0.1	Absorp.
1604-1607	20-50%	Blatherwick *et al* (1980)	Balloon	FTS	0.02	Absorp.

Table B-2. Review of High-Resolution Microwave to Infrared Spectroscopic Field Measurements of Atmospheric Gases (1975-1985). — Continued

Spectral Region (cm^{-1})	Measurement Accuracy	Reference	Vehicle†	Instrument‡	Resolution* (cm^{-1})	Method**
NO_2 — Continued						
1600-1610		Niple *et al* (1980)	Balloon	FTS	0.02	Absorp.
1600-1610	20%	Coffey *et al* (1981a)	Aircraft	FTS	0.06	Absorp.
36.5-39.0		Kendall & Clark (1981)	Balloon	FTS	0.06	Emiss.
1602-1608	15%	Girard *et al* (1983)	Aircraft	Grille	0.1	Absorp.
1595-1600	6-50%	Louisnard *et al* (1983)	Balloon	Grille	0.1	Absorp.
2880-2930	15-25%	Camy-Peyret *et al* (1983)	Ground	FTS	0.01	Absorp.
67-68		Carli *et al* (1983)	Balloon	FTS	0.003	Emiss.
2880-2930		Flaud *et al* (1983)	Ground	FTS	0.01	Absorp.
2890-2930	25-50%	Kendall & Buijs (1983)	Balloon	FTS	0.04	Absorp.
1595-1600		Girard & Louisnard (1984)	Balloon	Grille	0.1	Absorp.
1575-1610		Kunde *et al* (1985)	Balloon	FTS	0.05	Emiss.
1595-1599		Laurent *et al* (1985)	Spacelab	Grille	0.1	Absorp.
1600-1615		Roscoe *et al* (1985a)	Balloon	Grating	0.5	Emiss.
OH						
60-90		Kendall & Clark (1979)	Balloon	FTS	0.06	Emiss.
61.0-61.4, 83.6-84.0		Carli *et al* (1983)	Balloon	FTS	0.003	Emiss.
80-220		Chance & Traub (1985)	Balloon	FTS	0.03	Emiss.
61-62, 83-84		Carli *et al* (1985a)	Balloon	FTS	0.003	Emiss.
118-189						
Solar OH						
825-960	50%	Goldman *et al* (1981c)	Balloon	FTS	0.02	Absorp.
810-960		Goldman *et al* (1983b)	Balloon/	FTS/	0.02/	Absorp./
			Ground	FTS	0.01	Absorp.
2400-3300		Grevesse *et al* (1984)	Ground	FTS	0.01	Absorp.
HF						
4038-4040	20%	Zander (1975)	Balloon	Grating	0.08	Absorp.
4038-4040		Farmer & Raper (1977)	Balloon	FTS	0.15	Absorp.
41.0-41.2		Carli *et al* (1980)	Balloon	FTS	0.003	Emiss.
3833-4040	25%	Buijs *et al* (1980)	Balloon	FTS	0.05	Absorp.
4038-4040	20%	Farmer *et al* (1980)	Balloon	FTS	0.15	Absorp.
160-250	20%	Traub & Chance (1981)	Balloon	FTS	0.03	Emiss.
4038-4041	6-20%	Zander (1981a,b)	Balloon	Grating	0.04	Absorp.
4038-4041	50%	Girard *et al* (1982)	Aircraft	Grille	0.2	Absorp.
3944-4009	40%	Girard *et al* (1983)	Aircraft	Grille	0.2	Absorp.
4039-4041,	20%/	Park *et al* (1984)	Balloon/	FTS/	0.02/	Absorp./
3877-3878	30%		Balloon	FTS	0.04	Absorp.
160-250	20%	Farmer *et al* (1985)	Balloon	FTS	0.03	Emiss.
163.9-164.1		Carli *et al* (1985a)	Balloon	FTS	0.003	Emiss.
HCl						
2923-2947	40%	Ackerman *et al* (1976)	Balloon	Grating	0.22	Absorp.
2923-2928		Bradford *et al* (1976)	Ground	FTS	0.06	Absorp.
2929-2947	25%/	Farmer *et al* (1976)	Ground/	FTS/	0.15/	Absorp./

Table B-2. Review of High-Resolution Microwave to Infrared Spectroscopic Field Measurements of Atmospheric Gases (1975-1985). — Continued

Spectral Region (cm^{-1})	Measurement Accuracy	Reference	Vehicle†	Instrument‡	Resolution* (cm^{-1})	Method**
HCl — Continued						
	10%		Aircraft	FTS	0.15	Absorp.
2926-2927	25-50%	Farmer and Raper (1977)	Balloon	FTS	0.15	Absorp.
2841-2844, 2924-2946	30%	Raper *et al* (1977)	Balloon	FTS	0.15	Absorp.
2925-2946	15%	Buijs *et al* (1980)	Balloon	FTS	0.05	Absorp.
40-83		Carli *et al* (1980)	Balloon	FTS	0.003	Emiss.
2841-2844, 2924-2946	20-50%	Farmer *et al* (1980)	Balloon	FTS	0.15	Absorp.
124-126, 144-146	27%	Chance *et al* (1980)	Balloon	FTS	0.03	Emiss.
140-250	20%	Traub & Chance (1981)	Balloon	FTS	0.03	Emiss.
2775-2776, 2942-2943	20-25%	Marche *et al* (1980a,b)	Ground	SISAM	0.03	Absorp.
103.0-105.5		Kendall & Clark (1981)	Balloon	FTS	0.06	Absorp.
2942-2946	17-24%	Zander (1981a,b)	Balloon	Grating	0.04	Absorp.
2942-2946	25-30%	Girard *et al* (1982)	Aircraft	Grille	0.1	Absorp.
2942-2946	25%	Girard *et al* (1983)	Aircraft	Grille	0.1	Absorp.
40-83,110-187		Carli *et al* (1985a)	Balloon	FTS	0.003	Emiss.
140-250,	15%/	Farmer *et al* (1985)	Balloon/	FTS/	0.03/	Emiss./
2821-3385	22-27%		Balloon	FTS	0.1	Absorp.
2803-3057		Fast *et al* (1985)	Balloon	FTS	0.1	Absorp.
HBr						
49.9-50.1, 83.3		Carli *et al* (1985a)	Balloon	FTS	0.003	Emiss.
ClO						
853.122	30%	Menzies (1979)	Balloon	LHS	0.001	Absorp.
6.816	25%	Parrish *et al* (1981)	Ground	MWS	<0.001	Emiss.
6.816	40%	Waters *et al* (1981)	Balloon	MWS	<0.001	Emiss.
853.125	30-40%	Menzies (1983)	Balloon	LHS	0.001	Absorp.
856.5, 859.8		Mumma *et al* (1983)	Ground	LHS	0.001	Absorp.
6.8163-9.2941	5-25%	Solomon *et al* (1984)	Ground	MWS	<0.001	Emiss.
22.8-23.0		Carli *et al* (1985b)	Balloon	FTS	0.003	Emiss.
OCS						
2050-2060	10-30%	Mankin *et al* (1979)	Aircraft	FTS	0.06	Absorp.
2046-2056	30-50%	Louisnard *et al* (1983)	Balloon	Grille	0.1	Absorp.
2040-2050	15%	Girard *et al* (1983)	Aircraft	Grille	0.1	Absorp.
H_2CO						
2806-2808, 2868-2871	75%	Barbe *et al* (1979)	Ground	SISAM	0.03	Absorp.
HCOOH						
1100-1108	75%	Goldman *et al* (1984a)	Balloon	FTS	0.02	Absorp.
NH_3						
825-935		Murcray *et al* (1978)	Ground	FTS	0.06	Absorp.
927.22-927.30	20-25%	Hoell *et al* (1980)	Ground	LHS	−0.001	Absorp.

C-4

Table B-2. Review of High-Resolution Microwave to Infrared Spectroscopic Field Measurements of Atmospheric Gases (1975-1985). — Continued

Spectral Region (cm^{-1})	Measurement Accuracy	Reference	Vehicle†	Instrument‡	Resolution* (cm^{-1})	Method**
HNO_3						
1324-1336	30%	Fontanella *et al* (1975)	Aircraft	Grille	0.1	Absorp.
860-890		Bradford *et al* (1976)	Ground	FTS	0.006	Absorp.
9-25		Carli *et al* (1980)	Balloon	FTS	0.003	Emiss.
1720-1725		Goldman *et al* (1980)	Balloon	FTS	0.02	Absorp.
1720-1725	20%	Coffey *et al* (1981a)	Aircraft	FTS	0.06	Absorp.
875-900	22%	Lippens & Muller (1981)	Ground	FTS	0.13	Absorp.
1323-1327	20-30%	Girard *et al* (1982)	Aircraft	Grille	0.1	Absorp.
1323-1327	20-30%	Girard *et al* (1983)	Aircraft	Grille	0.1	Absorp.
1320-1326	10-20%	Louisnard *et al* (1983)	Balloon	Grille	0.1	Absorp.
867-873	50%	Goldman *et al* (1984c)	Balloon	FTS	0.02	Absorp.
1320-1326		Girard & Louisnard (1984)	Balloon	Grille	0.1	Absorp.
884		Murcray *et al* (1985b)	Balloon	Grating	0.25	Emiss.
850-925		Kunde *et al* (1985)	Balloon	FTS	0.05	Emiss.
870-900		Pollitt *et al* (1985)	Balloon	Grating	0.25	Emiss.
860-900		Murcray *et al* (1985b)	Balloon	FTS	0.08	Emiss.
N_2						
2395-2420		Camy-Peyret *et al* (1981)	Ground	FTS	0.01	Absorp.
2395-2420		Goldman *et al* (1981b)	Ground	FTS	0.06	Absorp.
2395-2420		Rinsland *et al* (1981)	Balloon	FTS	0.15	Absorp.
HCN						
3270-3290	10%	Coffey *et al* (1981b)	Aircraft	FTS	0.06	Absorp.
25-60		Carli *et al* (1982)	Balloon	FTS	0.003	Emiss.
3287-3287.5, 3299-3300	25%	Rinsland *et al* (1982a)	Ground	FTS	0.01	Absorp.
3270-3300	50-75%	Smith & Rinsland (1985)	Balloon	FTS	0.15	Absorp.
CH_3Cl						
2870-3010		Kendall & Buijs (1983)	Balloon	FTS	0.04	Absorp.
H_2O_2						
6.83	50%	Waters *et al* (1981)	Balloon	MWS	<0.001	Emiss.
51-54, 93-96, 111-113		Kendall & Clark (1981)	Balloon	FTS	0.06	Emiss.
90-150		Chance & Traub (1984)	Balloon	FTS	0.06	Emiss.
$CFCl_3$ (F-11)						
830-860	20%	Wllliams *et al* (1976)	Balloon	Grating	0.3	Absorp.
830-860		Bradford *et al* (1976)	Ground	FTS	0.06	Absorp.
830-860	8%	Lippens & Muller (1981)	Ground/ Ground	FTS/ FTS	0.13/ 0.13	Absorp./ Emiss.
824-864	16-24%	Zander *et al* (1983)	Ground	FTS	0.01	Absorp.
840-860		Kunde *et al* (1985)	Balloon	FTS	0.05	Emiss.
840-860		Murcray *et al* (1985b)	Balloon	FTS	0.08	Emiss.

Table B-2. Review of High-Resolution Microwave to Infrared Spectroscopic Field Measurements of Atmospheric Gases (1975-1985). — Continued

Spectral Region (cm^{-1})	Measurement Accuracy	Reference	Vehicle†	Instrument‡	Resolution* (cm^{-1})	Method**
CF_2Cl_2 (F-12)						
918-925		Bradford *et al* (1976)	Ground	FTS	0.06	Absorp.
900-940	20%	Williams *et al* (1976)	Balloon	Grating	0.3	Absorp.
920-940, 1160-1162	24%	Zander *et al* (1983)	Ground	FTS	0.01	Absorp.
920-925		Kunde *et al* (1985)	Balloon	FTS	0.05	Emiss.
910-930		Murcray *et al* (1985b)	Balloon	FTS	0.08	Emiss.
$ClONO_2$						
1291-1293	25%	Murcray *et al* (1979)	Balloon	FTS	0.02	Absorp.
779-781	60-80%	Rinsland *et al* (1985b)	Balloon	FTS	0.02	Absorp.
CHF_2Cl (F-22)						
828-830	75%	Goldman *et al* (1981d)	Balloon	FTS	0.02	Absorp.
828-830	20-24%	Zander *et al* (1983)	Ground	FTS	0.01	Absorp.
C_2H_2						
776-778	40%	Goldman *et al* (1981a)	Balloon	FTS	0.02	Absorp.
776-777	22%	Zander *et al* (1982)	Ground	FT5	0.01	Absorp.
3250.5-3251, 3304.8-3305.3	15%	Rinsland *et al* (1985a)	Ground	FTS	0.01	Absorp.
C_2H_6						
822-823	17%	Zander *et al* (1982)	Ground	FTS	0.01	Absorp.
821-823	40%	Goldman *et al* (1984b)	Balloon/ Aircraft	FTS/ FTS	0.02/ 0.06	Absorp./ Absorp.
2975-2990, 2976-2977		Coffey *et al* (1985)	Aircraft/ Ground	FTS/ FTS	0.06/ 0.01	Absorp./ Absorp.
CCl_4						
785-810	30%	Williams *et al* (1976)	Balloon	Grating	0.3	Absorp.
CF_4						
1275-1290		Goldman *et al* (1979)	Balloon	FTS	0.02	Absorp.
HO_2						
8.859-8.866	15%	De Zafra *et al* (1984)	Ground	MWS	<0.001	Emiss.

† Type of instrument platform.

‡ See Annex B-1 for explanation of the instrument abbreviations.

* For interferometric spectra, this is either the apodized or the unapodized resolution, depending on how the data were analyzed.

** Emission or absorption measurements.

A slash (/) indicates that two experiments were treated in the article. A comma (,) indicates multiple spectral regions.

Note: It is inevitable, in any extensive compilation such as this, that a few works will inadvertently be overlooked. Our apologies to any authors whose publications have thus been accidentally omitted.

Table B-3. Some Examples of High Resolution Infrared to Microwave Atmospheric Spectrometer Systems in Progress

Institution¶	Instrument*	Resolution†	Spectral Interval[s]	Vehicle‡	Method**
JPL	FTS	10	500 - 5000	Shuttle	Absorp.
	FTS	10	500 - 5000	Balloon	Absorp.
	TDL	0.2	330 - 3300	Balloon	Absorp.
MET.FRANCE	Grille	100	1000 - 4000	Aircraft	Absorp.
NASA Goddard	Cold FTS	20	650 - 2000	Balloon	Emiss.
NCAR	TDL	1	800 - 1300	Aircraft	Absorp.
LPMOA Orsay	FTS	10	650 - 4000	Balloon	Absorp.
LPM Reims	FTS	3	1000 - 1600	Ground	Absorp.
	LHS	0.3	1000	Ground	Absorp.
SAO Harvard	FTS	4	80 - 250	Balloon	Emiss.
U. Calgary	FTS	15	20 - 90	Balloon	Absorp.
U. Denver/AFGL	Cold FTS	60	650 - 2500	Balloon	Emiss.
U. Denver	FTS	3	650 - 2500	Balloon	Absorp.
	LHS	0.3	1000	Ground	Absorp.
U. München	Cold FTS	100	650 - 2000	Balloon	Emiss.

¶ see Annex B-2 for explanation of the institution abbreviation
* see Annex B-1 for explanation of the instrument abbreviation
† Resolution in units of 10^{-3} cm^{-1}. For interferometric spectra, it is either the apodized or the unapodized resolution, depending on how the data were analyzed.
s spectral interval in units of cm^{-1}
‡ type of instrument platform.
** emission or absorption measurements

B-3 LABORATORY SPECTROSCOPY BY SPECTRAL ANALYSIS AND PREDICTIONS

Laboratory measurement capabilities in the infrared and microwave regions have undergone significant evolution in the past ten years. Examples of current laboratory spectroscopy capabilities are listed in Table B-4. Where the exact frequency range was not known we have used near infrared (IR) to mean the region near 2μm, mid-IR to mean the region near 10 μm, and far-IR to mean the region near 100 μm. There are approximately 60 microwave groups of similar capability. Rather than list them all, we have summarized them in the last entry in the table. Instrument and institutional abbreviations are expanded in Annex B-1 and B-2, respectively.

With the advent of computer assisted data analysis, it is now possible to reproduce the experimental absorption profile with model lineshapes to within experimental errors. However, due to our lack of understanding of the systematic errors in instrument performance, the significance of the derived lineshape parameters is less certain. With care, line positions can be retrieved to 1/20 to 1/100 of the instrumental width, and intensities and collisional widths can be retrieved to 5%. Systematic effects which degrade these accuracies include multiple lines, channeling, source power variations with frequency, and continuum contributions. Development of believable capabilities for measurement of intensities and widths which are more accurate than 5% will require much more work and a coordinated program of intercomparisons between different laboratories. Moreover, it should be emphasized that accurate laboratory data are more readily obtained for the more stable trace species such as CH_4, etc., compared to the reactive compounds such as $ClONO_2$ and HNO_3, due to the difficulty in manipulating these compounds in the laboratory.

Use of predictive models has always been an essential part of interpreting the spectrum. A model Hamiltonian is used to assign the spectrum and predict the relative intensities and energies of the levels involved in the transition. The complexity of the model varies with the complexity of the molecule, but challenges the state of the art only when there are multiple interacting vibrational states. Typically, line positions can be fit to better than one part in 10^7 in frequency. Prediction of line centers can be made with known errors deduced from the fit, although care must be taken in extrapolating out of the range of measured quantum numbers.

Relative intensities within a band can also be predicted from the molecular Hamiltonian. Absolute intensities require measurements of gas concentration in the infrared or permanent dipole moments in the rotational region. In the case of resonances or severe centrifugal interaction, corrections to the predicted intensities may be required. Halfwidth predictions require collision theory which is not as well developed as the theory used for frequency and intensity predictions. Current approximate theories, such as the Anderson-Tsao-Curnutte (ATC) method (Anderson, 1949; Tsao and Curnutte, 1962) or the Quantum Fourier transform (QFT) method (Davies, 1975), reproduce widths to 10% if adjustable parameters are used (Robert and Bonamy, 1979; Lacome *et al.*, 1983; Gamache and Davies, 1985). More exact available theories require several orders of magnitude more computing resources.

Table B-4. Examples of Some Current Infrared to Microwave Laboratory Spectroscopy Capabilities.

Institution†	Instrument*	Resolution‡	Spectral Interval¶	Sample Cells
AFGL	FTS	3	400–4000	
Duke U.	Submillimeter	0.003	3–35	2 m
IROE	FTS	1.3	10–200	1.4 m
ISM-CNR	FTS	20	IR	20 m
JPL	Laser Sideband	0.01	10–100	2 m cooled, DC discharge
	Submillimeter	0.003	3–35	
	TDL	1	mid-IR	
	FTS (Bomem)	4	400–4000	0.8 m
	FTS (Nicolet)	60	8–4000	
JRC Ispra	TDL	1	mid-IR	cooled cells
	FTS (Bruker)	30	mid-IR	60 m, 256 m
Kitt Peak NSO	FTS	5	500–4000	384 m White cell
LIR Orsay	FTS	3	600–4000	cooled cells
	TDL	1	mid-IR	
LPM Reims	SISAM	20	IR	
	FTS	2	800–4000	4 m cooled, 30 m,
	LHS heterodyne	0.1	mid-IR	3 km
LPMOA Orsay	FTS (Bomem)	20	400–9000	
LSM-ENEA	TDL	3	620–760	1 m
LSM Paris	FTS (Bomem)	1	600–10000	40 m cooled
	TDL	1	mid-IR	
NASA Ames	FTS (Bomem)	4,60	400–4000	30 cm cryogenic, 35 m, 3000 m
	FTS (Nicolet)	60		35 m, 3000 m White cells
	TDL	1	mid-IR	
NASA Goddard	TDL	1	mid-IR	
	FTS	60	4–4000	
	CO_2 laser heterodyne	0.1	900–1100	
NASA Langley	TDL	1	mid-IR	5, 10, 25,
	FTS (Nicolet)	60	400–4000	50 cm cooled
NBS Boulder	CO_2 difference laser	0.01	10–200	

Table B-4. Examples of Some Current Infrared to Microwave Laboratory Spectroscopy Capabilities. — Continued

Institution†	Instrument*	Resolution‡	Spectral Interval¶	Sample Cells
NBS Washington	FTS (Bomem)	4	8–4000	cooled cells
	FTS (Nicolet)	60		35 m, 3000 m White cells
	TDL	0.1, 1	mid-IR	
	difference frequency	1	near-IR	
NCAR	FTS	20	IR	atmospheric spectra
NOAA/NESDIS	TDL	1	mid-IR	8 m cooled
	grating spectrometer			
NPL	FTS	15	10–200	13 m
NRC Canada	FTS (Bomem)	4	400–4000	
OSU	FTS (Nicolet)	60	400–4000	2 km cooled
RAL	FTS (Bomem)	4	400–4000	cooled 5 m, 20 m, 1000 m
U. Bologna	FTS	12	IR-Visible	20 m
U. Denver	grating spectrometers			
	FTS (Eocom)	60	500–400	atmospheric spectra
	FTS (Bomem)	20		
	FTS (Bomem)	4		
U. Louvain	Intracavity (CO_2,CO)	0.01		
	Laser Stark spectrometer			
U. Oulu	FTS	3	far-IR up to 1000	
U. Stony Brook	grating spectrometer	100	IR	5 cm to 100 m
	TDL	1		cooled
(+60 institutions) see text	microwave	0.001	0.3–3	2 m some cooled

† See Annex B-2 for explanation of the institution abbreviation.
* See Annex B-1 for explanation of the instrument abbreviation.
‡ unapodized in units of $10^{-3}cm^{-1}$
¶ in units of cm^{-1}

B-4 USE OF SPECTROSCOPIC DATA TO DERIVE ATMOSPHERIC COMPOSITION

Analysis of atmospheric data consists of identifying the species that give rise to individual features in the atmospheric spectra and retrieving important atmospheric parameters as a function of altitude (vertical profiles). The general tasks involved are:

- line-by-line identification of observed features (including detection of new species);
- upper limits of species not directly observed;
- retrieval of volume mixing ratios of observed species;
- retrieval of pressure and temperature profiles.

To accomplish these tasks, the observed spectra are often compared to synthetic spectra, the computation of which requires good knowledge of:

- the spectroscopic parameters and line shapes;
- the instrumental effects of the spectrometer;
- the pressure and temperature profiles of the atmosphere;
- the estimates of the concentrations or volume mixing ratios of species as a function of altitude;
- the geometric path.

In an analysis of atmospheric data, identifications of spectral features are often made by computer matching of the observed line centers of the spectral lines to values given in the spectroscopic database and by visual inspection of plots computed with approximate atmospheric parameters. Once the features in a spectrum are generally identified, then one can say with confidence that the absorptions of a particular species are not observed and obtain upper limits of concentration.

The retrievals of vertical concentration profiles and pressure or temperature profiles from the spectra are done using various methods (such as least squares techniques, equivalent-width method, etc.). The measurements are made for altitudes from sea level to 120 km where atmospheric pressures range from 1 to 10^{-6} atm and temperatures from 300 K to 180 K. In practice, the vertical profiles can be obtained through the "onion-peel" approach; in this, parameters for the uppermost altitudes (pressure, temperature, number density, etc.) are retrieved first and then held fixed in the computed spectra when determining the parameters at lower altitudes. A complimentary method of retrieving vertical profiles involves the fitting of an observed radiance profile to a simulated profile, with the fitting done simultaneously at every altitude point over the range of intensity. The simultaneous spectral radiance profiles are generated using available spectroscopic data and assuming an atmospheric model for the gas (or gases) of interest. As a practical matter, researchers may select small spectral intervals that contain absorptions of just a few (or one) species whose vertical profiles are to be obtained by the retrieval technique. The interval may be as small as 1 cm^{-1} or as large as a few hundred cm^{-1}, depending on the application.

As indicated in Section B-3, the essential molecular parameters required for the interpretation of atmospheric data are positions, strengths, widths and lower state energies of those species which contribute to the atmospheric spectrum. The required accuracies of these molecular parameters will vary according to how they are to be used. The identification of the spectral features and determination of upper limits can be readily accomplished with only moderately accurate parameters. In a spectrum recorded at 0.01 cm^{-1} resolution, with a signal-to-noise ratio of 100:1, features can be readily matched by computer if the line positions in the database are given to only 0.003 cm^{-1} and strengths to only $\pm$ 20% with ground

state energies known to 5%. In fact, many of the features in the ongoing atmospheric atlases, such as those from the University of Denver (Blatherwick, *et al.*, 1982; Goldman *et al.*, 1982), the Kitt Peak Solar Atlas (Delbouille *et al.*, 1981) and the IROE-CNR Atlas (Baldecchi *et al.*, 1984) have been assigned and quantified using current database compilations. These databases must be as complete as possible and contain the parameters of all lines that might be observed. For the trace species, this can generally be achieved by study of the fundamentals and a few of the weaker overtones and hot bands. For the major gases, parameters of many bands and several isotopes with strengths ranging over four to six orders of magnitude are needed. In all, the database appropriate for today's technologies probably consists of over 500,000 entries.

Molecular parameters of features in the selected intervals will be utilized in the computer retrieval of atmospheric parameters and therefore must be known with better accuracies. For example, Figure B-1 shows a comparison between observed and computed spectra overlaid with the differences between the two (the residuals labelled O-C) plotted below. The observed spectrum is a laboratory spectrum of CH_4 recorded at 0.01 cm^{-1} resolution with a signal-to-noise ratio of 500:1 using the FTS (Fourier transform spectrometer) at Kitt Peak NSO. As an illustration, different types of errors have been introduced in the parameters of the computed spectrum. In the left panel, the positions of the three strong lines (a, b, c) are in error by 0.0001, 0.0005 and 0.0030 cm^{-1}, respectively, while at the right, the strengths of the same three lines (d, e, f) are in error by 1%, −5% and 15%, respectively. Visually, the two spectra appear to be in good agreement in both panels, but the residuals in the difference plots are considerably different around each line. Whether or not these errors will adversely affect the retrieval of atmospheric parameters depends on the signal-to-noise ratio of the observed spectrum. If the signal-to-noise ratio of the observed spectrum of Figure B-1 were 100:1, the errors in lines b and e would be substantially masked. However, the errors in lines c and f would still interfere with the functioning of an algorithm which uses the residuals to direct its action. The retrieval mechanism would try to adjust atmospheric parameters to compensate for errors in the molecular parameters, thus resulting in an incorrect retrieval of atmospheric physical and chemical properties.

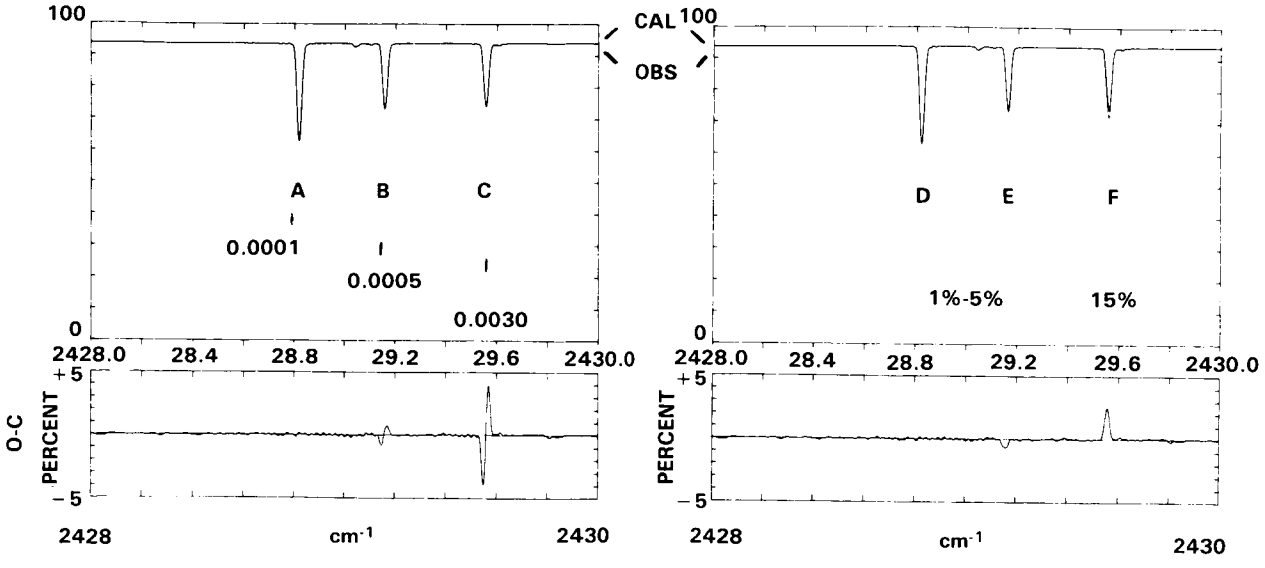

Figure B-1. A Comparison of Observed and Synthetic Spectra of CH_4.

SPECTROSCOPIC DATABASE

An example of how uncertainties in a particular spectroscopic parameter (line strengths) impact the accuracy of a retrieved vertical profile is shown by Figure B-2. For this, a profile of ozone was generated using a specific value of strengths for a series of lines and a particular profile. The profile was then recalculated, but included a 3% change in the strengths of all O_3 lines, and the ozone profile was adjusted to force a fit between the two calculations. In Figure B-2, the standard deviation in percent between the adjusted ozone profile and the assumed profile is shown (on the vertical axis) versus altitude. The uncertainty in the line strengths is seen to give rise to errors of 2.5% to 3% over the altitude range of 20 to 50 km, and there is, to first order, a one-to-one correspondence between the uncertainty in the spectroscopic parameter and the induced error in the retrieved ozone. For reference, the impact of adding an 0.5 K bias and an 0.25 K random error to the temperature knowledge is also shown (lower trace), along with the errors associated with the combination of the two (upper trace).

As discussed in the main body of this document, understanding of the atmospheric chemistry and circulation requires detailed knowledge of vertical profiles of many diverse molecular species. The detection of some of the important trace species, which contribute only a small percentage of intensity to an atmospheric spectrum, can be achieved only with complete spectroscopic knowledge of all species whose transitions overlap the region of the target species. A good example is provided by the recent detection of ClO at 22.9 cm^{-1} (Carli *et al.*, 1985b). This feature has been observed in emission spectra recorded with the same instrument during two balloon flights, one in 1979 and another, with a better signal-to-noise ratio, in 1983. This identification was made possible only after new laboratory data of ozone isotopes and vibrationally-excited ozone became available. These species contribute to the submillimeter stratospheric spectrum with features that have an intensity comparable to that of ClO and cause a background structure which, if not identified, must be considered as measurement noise. Without these new laboratory data, even the 1983 field measurements, with better signal-to-noise ratio, could not be interpreted.

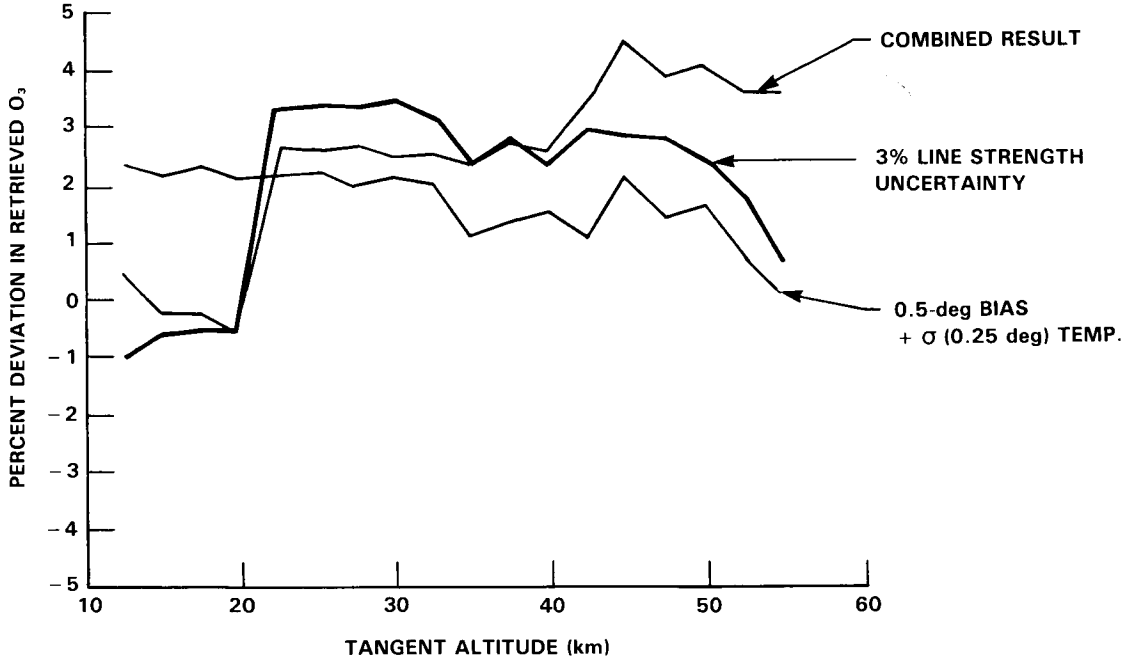

Figure B-2. Effect of Line Strength and Temperature Uncertainties on the Retrieval of Atmospheric Ozone Density.

Another example is provided by the recent study of $ClONO_2$ in the 780 cm^{-1} region (Rinsland *et al.*, 1985b). After balloon-borne spectra (recorded at 0.02 cm^{-1} resolution and long geometric path) revealed several inadequacies in the database for this region, new laboratory research was done to improve the positions and strengths of O_3 and to provide a semi-empirical spectral model for $ClONO_2$ parameters. Once completed, it also became clear that the atmospheric spectrum also contained features arising from the solar atmosphere. In particular, solar OH, $\Delta v = 1$, lines were found to be important in the $ClONO_2$ region, and new work on this species was done. Finally, the improved database was used to do a least squares fitting of the balloon spectra involving O_3 and CO_2 with residuals to 1% and $ClONO_2$ with residuals to 4%.

Thus it should be emphasized that the complete spectroscopic needs of remote sensing are difficult to specify completely until the data from a specific application are examined in detail. One may predict the needs according to species known to be found in the atmosphere or from chemical models that predict the probability of their existence, but quite often a new and interesting analysis of atmospheric data also results in a redefinition of the spectroscopic parameters required.

B-5 EXAMPLES OF SPECTROSCOPIC DATA REQUIREMENTS FOR SPACE-BASED REMOTE SENSING OF THE ATMOSPHERE

B-5.1 The Spectroscopic Requirements of ATMOS

The objective of the ATMOS (Atmospheric Trace Molecule Spectroscopy) investigation is to measure the concentrations and distribution of gases in the upper atmosphere. In May 1985, the ATMOS instrument, a modified Michelson interferometer, orbited the earth aboard the space shuttle at an altitude of 350 km to record the infrared absorption spectrum in the 2 to 16 um region at a resolution of 0.01 cm^{-1} (unapodized). This spectrometer obtained an interferogram every 1.1 seconds with signal-to-noise ratios in the transformed spectrum of 100:1 or better, using the sun as the optical source and optical filters with widths of 600 to 1500 cm^{-1}. The mission provided data from 19 occultations (sunrise and sunset) for a total of 2000 individual spectra. In a typical orbit, the atmospheric data covered altitudes ranging from 16 to 350 km with a vertical resolution of better than 2 km. Yearly reflights are planned.

The species to be investigated during 1985 are shown in Table B-5. They include the major gases (which account for 85% of the observed absorption features), several chemical families of species (nitrogen, hydrogen, halogen) and also hydrocarbons and sulfur compounds.

Analysis will include retrieval by least squares techniques of the pressure-temperature vertical profiles and volume mixing ratios of detected species, as well as upper limits of species not observed, and identification of spectral features. For the first two tasks, small portions of spectra containing unblended, single transitions of one of the targeted species, will be carefully selected from the large volume of available ATMOS spectra and used in the least squares retrieval of parameters. These regions are generally one to two cm^{-1} wide. Efforts will be made to choose windows in which only absorptions of an individual target molecule appear, if possible. Table B-6 lists the general spectral regions where tentative windows are found along with the molecule targeted for detection in each interval.

The interpretation of ATMOS data requires accurate line positions, strengths, widths, and lower state energies of the species listed in Table B-5. Additional parameters may be required for radicals of major gases, species that arise from the outgassing of the shuttle and species previously undetected in the upper atmosphere as well as features from the solar spectrum. As summarized in Table B-7, the required ac-

Table B-5. Species to be Investigated by ATMOS

Major gases	
	H_2O, CO_2, O_3, N_2O, CO, CH_4, N_2, O_2
Minor and Trace gases	
Nitrogen family:	NH_3, NO, NO_2, N_2O_5, HNO_2, HNO_3, HNO_4, HCN
Hydrogen family:	H_2O_2, HO_2, H_2CO, HCOOH, HDO
Halogen family:	Chlorofluorocarbons [$CFCl_3$ (F-11), CF_2Cl_2 (F-12), CF_2HCl (F-22)], CH_3CCl_3, CH_3Cl, CCl_4, HCl, HF, ClO, HOCl, $ClONO_2$, COF_2, COClF, CH_3F, CF_4
Hydrocarbons, Sulfur compounds and others:	
	C_2H_2, C_2H_4, C_2H_6, C_3H_8, OCS, SO_2

curacies of individual parameters vary greatly according to the use made of them. Positions must be known at least to a third of a line width so that the spectral features can be identified and detection windows selected. For the retrieval of vertical profiles, it is desirable that positions be good to 0.0005 cm^{-1} (or better), although in practice, one can often recognize and compensate for small errors in positions through computer software.

Knowledge of line shapes and Doppler and Lorentz widths are needed for data covering the lower part of the stratosphere. Below 35 km, where the pressure is greater than 0.01 atm, the Lorentz contribution to the line profile becomes increasingly important, particularly at longer wavelengths. The accuracies needed for general feature identification are crude (50%), but better accuracies (2% to 5%) are needed for the retrieval of vertical profiles.

The line strengths are needed with accuracies of 20% to 2%, depending on usage. To identify the spectral features, select detection windows for targeted species, and determine upper limits, strengths to 20% are sufficient. However, for transitions used in the vertical profile retrievals, requirements are much more stringent. With the ATMOS data, the volume mixing ratios are obtained using 5 to 25 transitions per molecule for which strengths (and widths) are known to 5% (a total of 1000 lines). For the retrieval of pressure-temperature profiles, some one hundred CO_2 lines are to be used for which line strength accuracies of 1% to 2% are needed.

Over the next decade, the ATMOS project will generate a wealth of atmospheric data which can be analyzed in a reasonable time period only if computerized methods of data reduction and analysis are employed. The task requires (among other things) that a comprehensive computer-accessed database be available. The majority of the parameters can be of modest accuracies (0.003 cm^{-1} for positions and 20% for strengths in the worst case), but for some 1000 selected transitions, accuracies of 0.0005 cm^{-1} for positions and 1 to 5% for strengths are needed.

Table B-6. General Spectral Regions of the ATMOS Analysis

Region†	Targeted Species
650- 750	CO_2
750- 880	CO_2, HNO_2, HNO_3, HNO_4, ClO, $ClONO_2$, $CFCl_3$ (F-11), CF_3Cl (F-13), C_2H_2, C_2H_6, COClF, $COCl_2$, COF_2, CCl_4, OCS
920- 960	NH_3, C_2H_4
1040-1080	O_3
1100-1120	HCOOH
1150-1180	CF_2Cl_2 (F-12)
1200-1400	H_2O, H_2O_2, HOCl, CH_4, CF_4, N_2O_5, N_2O, SO_2, HNO_3
1460-1540	H_2O, O_2
1600-1700	H_2O, NO_2, O_2
1890-1930	CO_2, N_2O, NO
2000-2100	CO_2, OCS
2140-2200	N_2O, CO, O_3
2230-2240	N_2O
2300-2450	CO_2, N_2O, N_2
2580-2590	N_2O
2670-2690	CH_4
2720-2740	HCl
2800-2870	O_3, H_2CO
2900-3080	CH_4, CH_3Cl, HCl, H_2CO, O_3, C_2H_6
3200-3310	H_2O, HCN
3380-3445	N_2O
3800-3870	H_2O
4030-4150	HF
4495-4510	CH_4
4600-4630	CH_4, CO_2

† cm^{-1}

Table B-7. ATMOS Spectroscopic Parameter Accuracy Requirements

Uses	Positions†	Strengths	Widths‡	Lower States	# of Lines
a. Identify species	0.003	20%	50%	20%	4×10^5
b. Upper limits	0.003	20%	50%	20%	10^3
c. VMR profiles*	0.0005	5%	5%	5%	10^3
d. P-T profiles**	0.0005	2%	2%	1%	10^2

† cm^{-1}
‡ air-broadened
* volume mixing ratios
** pressure-temperature profiles

B-5.2 UARS Program Spectroscopic Requirements

The Upper Atmosphere Research Satellite (UARS), which is scheduled for launch in the fall of 1989, will provide global synoptic monitoring of the earth's upper atmosphere from a 600 km orbit for a period of two years.

The goals of the UARS program have been defined (Banks, 1978) as:

- to understand the mechanisms that control upper atmosphere structure and variability;
- to understand the response of the upper atmosphere to natural and anthropogenic perturbations;
- to define the role of the upper atmosphere in climate and climate variability.

To accomplish these goals, three categories of measurements will be performed (Reber, 1985):

- *atmospheric composition and structure:* This involves the measurement of upper atmospheric species distribution and temperature and is directed towards the study of global photochemistry with emphasis on ozone layer chemical cycles;
- *dynamics:* Involving the measurement of upper atmospheric wind and temperature fields;
- *energy input:* Involved primarily with the measurement of solar irradiance and particle energy deposition.

To illustrate the spectroscopic requirements of the UARS project and to keep within the infrared to microwave guidelines of this report, only the four experiments dealing with chemical species are discussed here; comprehensive details of all of the experiments, and their requirements are available as part of the UARS Project Spectroscopy Requirements Document (Roche, 1985), being generated by the UARS spectroscopy working group.

A list of all species to be measured by the four composition/structure experiments, CLAES (Cryogenic Limb Array Etalon Spectrometer), ISAMS (Improved Stratospheric and Mesospheric Sounder), MLS (Microwave Limb Sounder), and HALOE (Halogen Occultation Experiment), is given in Table B-8 with associated spectral intervals. Figure B-3 displays this information on an altitude grid along with details of two other UARS experiments. As seen from this table and figure, UARS will provide (in certain cases, for the first time) global measurements of stratospheric and lower mesospheric chlorine species including ClO, $ClONO_2$, HCl, CF_2Cl_2(F-12), and $CFCl_3$(F-11). It will also provide more complete measurements of the global distribution of ozone and important species in the stratospheric O_x, NO_x and HO_x chemistry and should provide improved measurements of global temperature and pressure.

All four experiments view the earth limb between approximately 10 and 100 km altitude and depend on the inversion of either emitted or absorbed radiances to infer the altitude distribution of species concentrations and temperature. As discussed previously, the inversion process requires data on spectroscopic line parameters including line position, intensity, halfwidth, and line shape for all species of interest over a temperature range of at least 180 to 300 K and an atmospheric pressure range from a few to several hundred millibars. Furthermore, since two of the experiments (HALOE and ISAMS) employ gas cells with relatively high concentrations of the target gases, self-broadened halfwidths and line shapes will be required for these species in addition to air-broadened data.

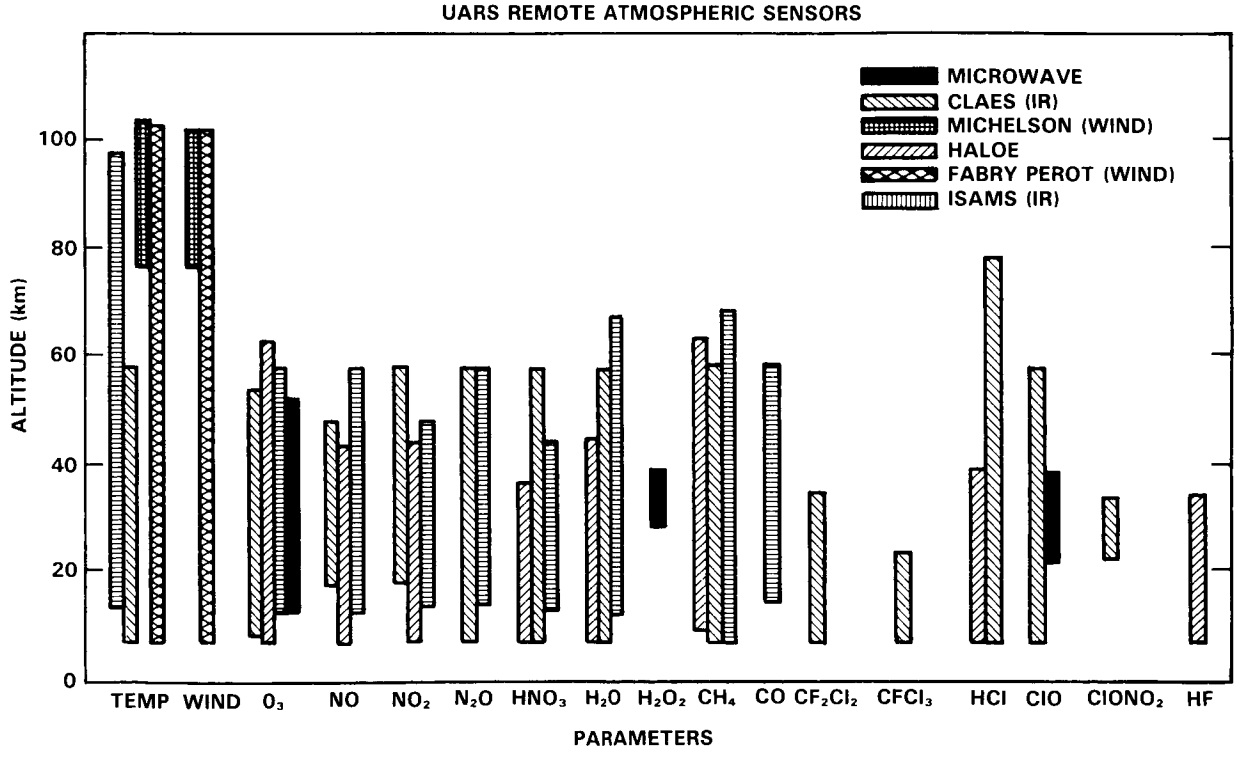

Figure B-3. UARS Remote Atmospheric Sensors.

Table B-8. UARS Atmospheric Spectroscopy Measurements

Atmospheric Composition and Structure				
Instrument	**Description**	**Species/Parameter**		**Spectral Interval/ Line Frequency [cm^{-1}]**
CLAES Cryogenic Limb Array Etalon Spectrometer	Solid-hydrogen cooled spectrometer sensing atmospheric infrared emissions	HCl		2838-2848
		NO		1892-1902
		NO_2, H_2O		1600-1610
		N_2O, CH_4, $ClONO_2$		1288-1298
		CF_2Cl_2 (Fl2), CO_2		920-930
		HNO_3		874-884
		$CFCl_3$ (F11), O_3, Aerosol		835-845
		O_3, Pressure, Temperature		787-797
ISAMS Improved Stratospheric and Mesospheric Sounder	Mechanically cooled spectrometer sensing atmospheric infrared emissions	CO_2	Pressure Modulated Radiometer	2325, 666
		H_2O, NO_2		1590
		CO		2174
		NO		1887
		N_2O		1266
		CH_4		1298
		O_3	Radiometric	1030
		HNO_3		884
MLS Microwave Limb Sounder	Microwave radiometer sensing atmospheric emissions	ClO		6.866
		H_2O_2		6.874
		O_3		6.926
		H_2O		6.159
		O_2 - Pressure		2.117
HALOE Halogen Occultation Experiment	Gas filter/radiometer sensing sunlight occulted by the atmosphere	HF	Gas Correlation	4047-4109
		HCl		2910-2970
		CH_4		2870-2912
		NO		1883-1917
		CO_2/Pressure	Radiometric	3537-3608
		NO_2		1591-1607
		H_2O		1506-1522
		O_3		976-1017

To assess the accuracy requirements for these spectroscopic parameters, each experiment has to exercise specific inversion algorithms against simulated data, in a similar manner to that described above in Section B-4, and establish the impact of uncertainties in spectroscopic input data on the accuracy of retrieved geophysical parameters. As Table B-8 indicates, this is a nontrivial task in view of the number of species and spectral intervals being studied. Further, each spectral interval containing one or more target species will have a set of interfering species whose line parameters need to be known, and selected spectral intervals may also require accurate knowledge of continua such as collision-induced O_2 and N_2 absorption bands, continuum absorption in H_2O, and aerosol effects.

In general, the more complete and accurate the spectroscopic parameters are, the more accurate the geophysical parameters will be (at least to the inherent sensitivity and calibration limits of the individual experiment). It is also important to note that, in many instances, the availability of improved spectroscopic data even after launch and orbital data acquisition can be used to advantage to upgrade geophysical data.

The specialized and detailed accuracy requirements of these four diverse experiments will constitute the major portion of the UARS requirements document mentioned above. General accuracy requirements over stratospheric temperature (T_{strat}) and pressure (P_{strat}) ranges are summarized in Table B-9. However, many common requirements exist for all the experiments, and most of these are included in Section B-7.

B-6 DATABASE ASSESSMENT

There are several spectroscopic databases for high resolution atmospheric transmission and emission simulations. The AFGL compilation became available in 1973 (McClatchey *et al.*, 1973) and has since been updated on the average of every two years (Rothman *et al.*, 1983a,b). The GEISA compilation began in 1976 for internal use and was published for the first time in 1980 (Chedin *et al.*, 1980); most of its data (Chedin *et al.*, 1985: Husson *et al.*, 1985) are in common with the AFGL compilation. In addition, an atlas of microwave and submillimeter transitions is available from JPL (Poynter and Pickett, 1984). The initial emphasis of each of the three compilations varied. The AFGL compilation was intended for terrestrial atmospheric problems, the GEISA compilation for terrestrial and giant planetary atmospheres, and the JPL catalog for astrophysical studies. The GEISA compilation also provided software for efficient use of its database. These databases now overlap in that they include many of the same molecular transitions relevant to remote sensing. Table B-10 summarizes the parameters that are currently incorporated into the compilations. The parameters are given in order of frequency for all significant transitions of molecular and atomic species of interest (provided that they are available in a suitably quantitative form).

Until 1984, the AFGL and GEISA compilations included for each absorption line of a given molecule, the following parameters:

- the resonant frequency in vacuum cm^{-1};
- the intensity in $cm^{-1}/(molecule\ cm^{-2})$ at 296 K;
- the collision halfwidth HWHM (halfwidth at half-maximum), in $cm^{-1}\ atm^{-1}$ at 296 K;
- the lower state energy of the associated transition in cm^{-1};
- the quantum identifications (vibrational, rotational, electronic level, hyperfine, and splitting designation if necessary);
- the entry date, isotope and molecule codes.

Table B-9. Typical Spectroscopic Parameter Accuracy Requirements for UARS Composition Measurement Experiments

Parameter	CLAES	HALOE	ISAMS	MLS
Line Position	± 0.001 cm^{-1}	± 0.001 cm^{-1}	± 0.001 cm^{-1}	± 30 kHz
Line Intensity	$<5\%$ over T_{strat}	$<5\%$ over T_{strat}	$<6\%$ over T_{strat}	$<2\%$ over T_{strat}
Collision-Broadened Halfwidths	$<5\%$ over T_{strat} and P_{strat} *Air-Broadening* for all species	$<5\%$ over T_{strat} and P_{strat} *Air-Broadening* for all species *Self-Broadening* for HF, HCl, NO, CH_4	$<5\%$ over T_{strat} and P_{strat} *Air-Broadening* for all species *Self-Broadening* for PMR species	$<2\%$ over T_{strat} and P_{strat} *Air-Broadening* for all species
Absorption Continua	Collision-induced O_2 band, H_2O continua, $<5\%$	Collision-induced O_2 band, H_2O continua, $\simeq <3\%$	Collision-induced O_2 band, H_2O continua, $<5\%$	

However, some basic modifications have been made recently in the compilations (in addition to inclusion of new species). For example, the impact of the temperature variation of the halfwidth $\gamma(T)$ of a line on the accuracy of radiative transfer computation is now accepted to be very important (as explained by Chedin *et al.*, 1985). As a result, in 1984, the temperature-dependence of halfwidth has been introduced as a new parameter in the GEISA catalog by giving the value of the exponent "n" in the expression $\gamma(T) = \gamma(T_O)(T_0/T)^n$, where $\gamma(T)$ is the collision halfwidth at T, and T_O is a reference temperature (e.g., 296K).

In addition, five new parameters will be included (or at least are to be considered when reliable information becomes available) in the 1985 new AFGL format:

- the transition moment in debyes;
- the self-broadened halfwidth in cm^{-1} atm^{-1} at 296 K;
- the pressure shift of the line in cm^{-1} atm^{-1} at 296 K;
- approximate error estimates for frequency, intensity and halfwidth;
- references for frequency, intensity and halfwidth.

The major part of all the above-mentioned line parameters is also included in the JPL catalog (see Table B-10).

As can be seen, the compilations attempt to present for each transition, molecule-dependent unique parameters from which synthetic spectra can be calculated. Issues such as line shape or coupling between the radiation field and matter have been left to individual computer algorithms used in calculating synthetic spectra. Likewise, phenomena such as continua which are not amenable to discrete quantization

Table B-10. Spectroscopic Database Parameters

Parameter†			Database			
	Type	**Unit**	**AFGL GEISA**	**JPL**	**GEISA84**	**AFGL85**
MOL	molecular specie index		x	x	x	x
ISO	isotopic variant index		x	x	x	x
ν	resonant frequency	cm^{-1}	x	x	x	x
S	intensity of transition	$cm^{-1}/(molecule\ cm^{-2})$	x	x	x	x
R	transition moment	Debye				○
g	upper state degeneracy			x		
γ	air-broadened halfwidth	$cm^{-1}\ atm^{-1}$	x		x	x
γ_s	self-broadened halfwidth	$cm^{-1}\ atm^{-1}$				○
E″	lower state energy	cm^{-1}	x	x	x	x
n	temperature-dependence of halfwidth				○	○
δ	pressure shift of transition	$cm^{-1}\ atm^{-1}$				○
v′	upper vibrational quanta		x	x	x	x
v″	lower vibrational quanta		x	x	x	x
Q′	upper rotational quanta		x	x	x	x
Q″	lower rotational quanta		x	x	x	x
e	error estimates for major parameters			x		○
ref	citations for major parameters					○

† Reference temperature 296 K
○ New parameter for GEISA (1984 Edition) or AFGL (1985 Edition)

are not included on the databases. In some cases, bands of heavier molecules whose transitions are separated by a fraction of a Doppler width and are hence unresolvable by most laboratory and field instruments have been relegated to a separate file on the most recent AFGL compilation where pseudo-band models have been supplied.

Table B-11 summarizes the present situation with respect to the molecules classified in Table B-1. These species are a subset of those available on the compilations. In the second column, arbitrary spectral intervals have been given (in reciprocal centimeters) which roughly correspond to the submillimeter region (if present) and various regions of the infrared spectrum, further subdivided for important species where different qualities of the data prevailed. The third column presents the log of the minimum and maximum line intensities in units cm^{-1}/(molecule cm^{-2}) at 296 K. This information is given as a very good guide in evaluating the effect of a species on long path attenuation problems and includes the extremes of the three databases. In some cases, very weak transitions have been retained due to either consideration of hot bands necessary for nonlocal thermodynamic equilibrium problems, or flame spectra, or transitions in the millimeter region. The number of transitions, again, represent the union of the databases. The fifth column (under quality) gives an evaluation of the three most significant parameters in terms of calculating atmospheric spectra and retrieval of atmospheric profiles, namely the frequencies (ν), strengths (S), and halfwidths (γ) of the transitions. The designation "A" is a judgement that the data are good for many applications; "B" signifies that the data are good for some applications considered here but need improvement; and "C" indicates that the data require major improvement. It must be realized that for major constituents, the classification of A, B, or C in a particular spectral region is, for the most part, very difficult since regions containing strong transitions, with very accurate parameters, usually also contain less accurate parameters for hot bands, isotopic lines, or weak bands in resonance. The sixth column lists the current availability of data in each interval on the AFGL, GEISA, and JPL databases, respectively. Under the comments heading, remarks on present deficiencies, problems, and other highlights of a species have been given. The need for self-broadened widths, which are required by some of the experiments discussed in Section B-5-2, has been abbreviated as "SB."

In addition to current work involved with adding completed work to the databases, there are many laboratory measurements which are in progress. A sampling of this work is listed in Table B-12. (Instrument and institutional abbreviations are expanded in Annex B-1 and B-2.) Because it was necessary to suppress many of the details of these investigations, it may appear that there is considerable overlap in the studies in progress. In the case of linewidth and intensity measurements, this duplication is desirable as a check for systematic errors, as discussed above. In addition, measurements using different techniques often provide complimentary data sets. For example, diode laser systems are typically used to measure a few lines to high resolution, while Fourier instruments typically are used to measure many more lines at necessarily lower resolution.

B-7 CONCLUSIONS AND RECOMMENDATIONS

The status of the spectroscopic database and current laboratory research given in this appendix is related to the accuracies with which atmospheric composition can be determined from spectral measurements. Further limitations are imposed by the inherent uncertainties of different atmospheric experiments and by the optical paths involved. With the present capabilities available for laboratory spectroscopic measurements and calculation of those spectroscopic parameters which cannot be measured, it is now routine to obtain line positions with high absolute accuracy (± 30 kHz in the microwave, 0.001 cm^{-1} or better in the infrared). Intensity and halfwidth measurements are more difficult. While relative intensities can

Table B-11. Summary of Spectroscopic Databases

Specie	Spectral Interval†	Intensity Range‡	Number of Transitions	Quality* ν	S	γ	Database** A	G	J	Comments***
H_2O	0-500	-32,-18	49000	A	A	B	x	x	x	Better precision needed due to
	500-5000	-27,-19		B	B	B	x	x		interference with other species
	5000-17900	-27,-20		C	C	C	x	x		$\lvert \Delta K \rvert > 2$ lines need improvement; SB
CO_2	400-1400	-27,-19	60000	A	B	B	x	x		Strengths to 1% needed for P,T
	1800-2400	-37,-18		A	B	B	x	x		retrievals for ATMOS and UARS; SB
	2400-9700	-27,-20		A	B	B	x	x		
O_3	0-300	-26,-21	49000	A	B	B	x	x	x	Better precision needed due to
	500-1200	-25,-20		A	B	B	x	x		interference with other species;
	1600-2900	-26,-21		B	B	B	x	x		Missing transitions needed between
	2900-3100			C	C	B	x	x		8.3-6.3 μm and $<$ 3.2 μm
N_2O	0-50	-25,-22	16000	A	A	A	x	x	x	Not all available measurements
	500-1400	-24,-19		A	A	A	x	x		have been incorporated; SB
	1600-5200	-24,-19		B	B	A	x	x		
CO	0-150	-24,-21	600	A	A	B	x	x	x	SB
	1900-6400	-24,-19		A	A	B	x	x		
CH_4 and CH_3D	0-100	-29,-27	27000	A	A	B	x	x	x	Some hot bands missing
	900-2000	-29,-19		A	B	B	x	x		
	2200-3200	40,-19		A	B	B	x	x		Some transitions missing between
	4100-6100	-23,-20		C	C	B	x	x		2-1.6 μm; SB
O_2	0-300	-35,-25	2200	A	A	B	x	x	x	Pressure induced bands needed;
	1400-16000	-30,-23		A	B	B	x	x		coefficients available
N_2	2000-2600	-34,-28	100	A	B	C	x	x		Pressure induced bands needed
O	68-158	-22,-21	2	A	A	C			x	
NO	0-100	-35,-22	7400	A	A	B	x	x	x	SB
	1500-4000	-44,-19		A	B	B	x	x		
NO_2	0-100	-25,	26000	A	A	C			x	SB
	600-3000	-24,-19		A	B	B	x	x	x	
NH_3	0-400	-29,-21	7000	A	A	B	x	x	x	6 μm region to be revised; 3 μm
	400-2200	-28,-19		B	B	B	x	x		region needed
HNO_3	0-100	-26,-21	57000	A	A	C	x	x	x	Several strong fundamentals missing;
	840-1750	-23,-17		C	C	C	x	x		7.7 μm bands needed
HF	0-8000	-24,-17	60	A	A	B	x	x		SB

Table B-11. Summary of Spectroscopic Databases (continued)

Specie	Spectral Interval†	Intensity Range‡	Number of Transitions	Quality* ν	S	γ	Database** A	G	J	Comments***
HCl	0-400	-24,-18	200	A	A	B	x	x	x	SB
	2400-8500	-24,-19		A	A	B	x	x		
OCS	0-40	-28,-21	700	A	A	B	x	x	x	
	800-2100	-23,-18		A	B	B	x	x		3.4 and 2.4 μm bands needed
H_2CO	0-100	-38,-19	2700	A	A	C	x	x	x	
	2700-3000	-20,-19		A	A	C	x	x		5.7 μm band needed
HCOOH	0-100	-28,-21	1888	B	A	C			x	Available data not yet incorporated
	1060-1160	-22,-20	3388	B	B	C		x		
HCN	0-150	-24,-18	800	A	A	B	x	x	x	
	550-3450	-25,-19		A	A	B	x	x		
C_2H_2	600-3400	-25,-18	1200	A	A	B	x	x		
C_2H_6	700-1000	-25,-21	5400	C	C	C	x	x		Major improvement required; 3.3 μm Q-branch strengths needed
CF_2Cl_2, $CFCl_3$, CF_4, CCl_4, CHF_2Cl										Band models and cross sections are available
ClO	0-100	-29,-21	6000	A	A	B	x	x	x	
	760-900	-24,-20		A	C	B	x	x		
$ClONO_2$	0-100	-24,-22	8500	A	A	C			x	
HO_2	0-100	-25,-20	6200	A	A	C			x	high resolution IR data needed
OH	0-100	-31,-18	8500	A	A	C	x	x	x	New extended rotational
	1250-10000	-81,-19		A	B	C	x	x		prediction forthcoming
N_2O_5	—	—	—		—			—		Cross sections available
CH_3Cl	2900-3200	-25,-21	6700	A	B	C	x	x		Incomplete vibrational spectrum
HOCl	0-300	-26,-19	15600	A	A	C			x	Missing fundamental
	1150-3800	-23,-20		A	B	C	x	x		
HNO_4 — HNO_2 —		—	—		—			—		Incomplete data
H_2O_2	0-300	-26,-20	3300	A	A	C			x	Missing data for high quantum numbers
	1150-1350	-23,-20		A	B	C	x	x		Only one IR band at present, 3 μm region needed

Table B-11. Summary of Spectroscopic Databases (continued)

Specie	Spectral Interval†	Intensity Range‡	Number of Transitions	Quality* ν	S	γ	Database** A	G	J	Comments***
HBr	0-350	-24,-18	300	A	A	B	x	x	x	
	2200-9800	-24,-19		A	A	B	x	x		
SO_2	0-200	-24,-20	18200	A	A	C	x	x	x	
	400-2550	-23,-19		A	B	C	x	x		
H_2S	0-600	-27,-19	4100	A	A	C	x	x	x	Missing fundamentals
	990-1600	-23,-21		A	A	C	x	x		Available data not yet incorporated
H_2SO_4	—	—	—		—			—		No data
C_2H_4	900-1100	-21,-18	200	B	B	C		x		Only a single band at present
C_3H_8	—	—	—		—			—		No data

† Spectral intervals are given in units of cm^{-1}.
NB: 1 μm corresponds to 10,000 cm^{-1}.

‡ Spectral intensities range is the log of the minimum and maximum line intensities in units of cm^{-1}/(molecule cm^{-2}).

* The quality codes indicate: A, good for many applications; B, good for some applications but needs improvements; C, needs major improvements. The three columns refer to line position (ν), line strength (S), and halfwidth (γ).

** Database codes are: A, AFGL (1985); G, GEISA (1984); J, JPL (1984) catalog.

*** The need for self-broadened widths has been abbreviated as "SB".

Table B-12. Some Examples of Infrared to Microwave Current Laboratory Spectroscopy Efforts

Molecule	Spectral Coverage (cm^{-1})	Instrument[1]	Data Type[2]	Accuracy[3]	Institution[4]
H_2O	2-4	MW	line shapes	2%	JPL
	20-350	FTS	F	0.0001 cm^{-1}	NRC Canada
	0-300(H_2O,HDO)	MW,FTS	F	0.00001 cm^{-1}	JPL
	500-2000(HDO)	FTS	F	0.004 cm^{-1}	AFGL
	700-1200(continuum)	grating,TDL	I,W	10%, 5%	U. Stony Brook
	900-5000($\Delta K > 1$)	FTS	I	5%	JPL
	1000-2000	FTS	F(calib.)	0.0001 cm^{-1}	JPL
	1250-1380(H_2O,HDO)	TDL	I,air-W,N_2-W	3%	NASA Langley, CWM
	1400-1800	grating,TDL	I,W	10%, 5%	U. Stony Brook
	1500-1523	TDL	I,N_2-W,self-W	3%	NOAA/NESDIS,CWM
	1523-1600	TDL	I,N_2-W,self-W	3%	NOAA/NESDIS
	1600(HDO)	FTS	F	0.001 cm^{-1}	JPL
	2100-2900(HDO)	FTS	F,I	0.001 cm^{-1}, 5%	LPMOA Orsay
	5000-5500(^{18}O)	FTS	F,I	0.001 cm^{-1}, 5%	LPMOA Orsay
	7550-7660	FTS	air-W,self-W	10%	Douglas RL, Kitt Peak NSO
	16000-25000	FTS	F,I	0.001 cm^{-1}	LPMOA Orsay
	10000-25000	FTS	F,I	0.001 cm^{-1}	JPL

Table B-12. Some Examples of Infrared to Microwave Current Laboratory Spectroscopy Efforts (continued)

Molecule	Spectral Coverage (cm^{-1})	Instrument[1]	Data Type[2]	Accuracy[3]	Institution[4]
CO_2	500-4000(high temp)	FTS	F	0.0005 cm^{-1}	AFGL
	600-750	grating,TDL	I,W	10%, 5%	U. Stony Brook
	670-720	TDL	self-,N_2-W		NOAA/NESDIS
	700-800(hot band)	FTS	F	0.005 cm^{-1}	LSM Paris
	700-800(hot band)	TDL	I,self-W,N_2-W	5%	LIR Orsay
	700-1100	FTS	F,I	0.001 cm^{-1}, 5%	JPL
	800-1100	FTS	F,I,W,	0.002 cm^{-1}, 5%	OSU
	900-1000	CO_2 laser	self-W,N_2-W,O_2-W	3%-5%	LIR Orsay
	1800-4200(isotopes)	FTS	F,I	0.0004 cm^{-1}, 2%	NASA Langley, CWM
	1900-4000(isotopes)	FTS	F	0.0004 cm^{-1}	AFGL
	2086-2307	FTS	F	0.0005 cm^{-1}	LIR Orsay
	2270-2600	FTS	F,I, self-W,N_2-W	0.005 cm^{-1}, 3%	LSM Paris
	2200-2400	grating,TDL	I,W	10%, 5%	U. Stony Brook
	2300-2400	FTS	I	2%	NRC Canada
	2400-2600(continuum)	FTS	self-W,N_2-W		U. Rennes, LSM Paris
	7550-7660	FTS	F	0.005 cm^{-1}	Douglas RL, Kitt Peak NSO
O_3	FIR-500	MW,FTS	F,I	0.0001 cm^{-1}	JPL,IROE, U. Bologna
	500-900	FTS	F,I	0.001 cm^{-1}, 10%	JPL, U. Denver LPM Reims, NASA Langley, CWM
	600-5000	FTS	F,I,W	0.001 cm^{-1}, 5%, 3%	RAL
	950-1200	FTS,LHS	I,N_2-W,O_2-W	2%, 2%	LPM Reims
	950-1400(isotopes)	FTS,TDL	F,I,W	0.004 cm^{-1}, 10%, 2%	LPMOA Orsay NASA Langley, CWM
	2050-2150	FTS	N_2-W,O_2-W	5%	LPM Reims
	3000-3200	FTS	F,I	0.001 cm^{-1}, 10%	LPM Reims
N_2O	900-5000	FTS	F,I	0.0001 cm^{-1}, 2%-5%	JPL
	1000-1350 (hot band)	FTS	F	0.001 cm^{-1}	LSM Paris
	1100-1110	FTS,TDL	F,I	0.002 cm^{-1}, 10%	NBS Washington
	1100-1300	grating,TDL	I,W	10%, 5%	U. Stony Brook
	1830-1950	FTS,TDL	F,I	0.002 cm^{-1}, 10%	NBS Washington, U. Oulu
	2160-2270	FTS	F,I,self-W,N_2-W,O_2-W	0.001 cm^{-1}, 3%	LSM Paris
	2200-2400	FTS	F,I	0.001 cm^{-1}, 2%	JPL
	2200-2400	grating,TDL	I,W	10%, 5%	U. Stony Brook
	2400-2900	TDL	F,I,W	0.001 cm^{-1}, 2%	JPL
	3000-5000	TDL	F,I,W	0.001 cm^{-1}, 2%	JPL
CO	30-100	SMM	F	10^{-4} cm^{-1}	NBS Boulder
	2000-2200	grating,TDL	I,W	10%, 5%	U. Stony Brook
CH_4	1000-2000	FTS	F,I	$10^{-4}cm^{-1}-10^{-3}cm^{-1}$, 2%-10%	JPL, U. Dijon
	1000-1500	FTS	F,I,self-W,air-W	0.0005 cm^{-1}, 5%, 3%	RAL
	1000-1300(CH_3D)	TDL,FTS	F,I	0.005 cm^{-1}	LIR Orsay, JRC Ispra
	1100-1500(isotopes)	FTS,TDL	I,air-W,N_2-W	3%	NASA Langley, CWM
	1200-1400	grating,TDL	I,W	10%, 5%	U. Stony Brook
	2800-3200	grating,TDL	I,W	10%, 5%	U. Stony Brook
	3750-4750	FTS	F,I	2×10^{-4}-$2\times10^{-3}cm^{-1}$, 2%-10%	JPL, U. Dijon
	5800-6150	FTS	F,I	4×10^{-4}cm, 2%-15%	JPL
	7601-7606	Photoacoustic	air-W		Douglas RL, Kitt Peak NSO
O_2	6-30 (singlet delta)	SMM	F	0.1 MHz	JPL

Table B-12. Some Examples of Infrared to Microwave Current Laboratory Spectroscopy Efforts (continued)

Molecule	Spectral Coverage (cm^{-1})	Instrument[1]	Data Type[2]	Accuracy[3]	Institution[4]
N_2	---				
O atom	---				
NO	1800-1950	FTS	N_2-W,Ar-W	3%	LSM Paris
	1800-2000	FTS	F,I,self-W,air-W	0.0005 cm^{-1}, 5%-3%	RAL
	1800-1950	grating,TDL	I,W	10%, 5%	U. Stony Brook
	3700-3880	DFL	I,self-W	2%	NBS Washington
NO_2	10-200	FTS	F	0.0001 cm^{-1}	IROE, LPMOA Orsay, U. Bologna
	1570-1620	FTS	F,I	0.001 cm^{-1}, 2%-15%	JPL
NH_3	900	FTS	F	0.001 cm^{-1}	JPL
	1400-1490	FTS	F,I	0.0002 cm^{-1}, 2%-10%	JPL
	1500	FTS	F,I	0.001 cm^{-1}, 10%	JPL
HNO_3	850-1740	TDL,FTS	F,I	0.001 cm $^{-1}$, 20%	NBS Washington, U. Denver
	850-1350	FTS	F	0.001 cm $^{-1}$	LSM Paris, LPMOA Orsay
	1240-1370	FTS	F	0.002 cm $^{-1}$	RAL
	1310-1340	TDL	I	10%	JPL
HF	40-160	FTS	N_2-W,O_2-W	5%	IROE, SAO Harvard, U. Bologna
	3500-4300	DFL	I,self-W,N_2-W	1%	NBS Washington
HCl	20-160	FTS	N_2-W,O_2-W	5%	IROE, U. Bologna, SAO Harvard
	2600-3100	FTS	HF-W	10%	NASA Langley
	2600-3000	FTS	N_2-W	3%	RAL
	2650-3080	FTS	I,self-W,N_2-W	2%	NASA Ames
	2700-3050	DFL	I,self-W,N_2-W	1%	NBS Washington
	2900-3100	grating,TDL	I,W	10%, 5%	U. Stony Brook
OCS	490-1920	FTS,TDL	F,I	0.0002 cm^{-1}, 10%	NBS Washington, U. Oulu
	839-887	TDL	self-W,N_2-W	5%	LIR Orsay
	1050	Stark	I		U. Louvain
	2000-2200	grating,TDL	I,W	10%, 5%	U. Stony Brook
H_2CO	1800	FTS	F,I	0.001 cm^{-1}	JPL
HCOOH	---				
HCN	3200-3400	FTS	F,W	0.02 cm^{-1}, 10%	NASA Langley
C_2H_2	650-800	grating,TDL	I,W	10%, 5%	U. Stony Brook
	1250-1350	TDL	air-W,N_2-W	3%	NASA Langley, CWM
C_2H_6	---				
CF_2Cl_2	860-950	grating,TDL	I,W	10%, 5%	U. Stony Brook
	700-1200	FTS	band	5%	NBS Washington
	1050-1200	grating,TDL	I,W	10%, 5%	U. Stony Brook
$CFCl_3$	150-1100	grating,TDL	I,W	10%, 5%	U. Stony Brook
	700-1200	FTS	band	5%	NBS Washington
	810-850	grating,TDL	I,W	10%, 5%	U. Stony Brook

Table B-12. Some Examples of Infrared to Microwave Current Laboratory Spectroscopy Efforts (continued)

Molecule	Spectral Coverage (cm $^{-1}$)	Instrument[1]	Data Type[2]	Accuracy[3]	Institution[4]
CF_4	---				
CCl_4	---				
CHF_2Cl	---				
ClO	---				
$ClONO_2$	10-200	FTS	F	0.0001 cm^{-1}	IROE, U. Bologna
HO_2	1040-1140	TDL	F,I,W	0.001 cm^{-1}, 20%	Aerodyne Research
	1340-1440	TDL	F,I,W	0.001 cm^{-1}, 20%	Aerodyne Research
	3370-3500	TDL	F,I,W	0.001 cm^{-1}, 20%	Aerodyne Research
OH	30-105(OH,OD)	SMM	F	0.5 MHz	JPL
	60-200	DFL	air-W	5%	SAO Harvard, NBS Boulder
N_2O_5	3-30	MW,SMM	F,I	0.05 MHz	JPL
	800-2800	FTS	I		LPMOA Orsay
CH_3Cl	---				
HOCl	10-200	FTS	F	0.0001 cm^{-1}	IROE, U. Bologna
HNO_4	1-10	MW	F,I	0.05 MHz	NBS Washington, JPL
HNO_2	1240-1280	TDL	F,I	0.001 cm^{-1}, 10%	NBS Washington
H_2O_2	10-200	FTS	F	0.0001 cm^{-1}	IROE, U. Bologna
	1250-1380	TDL	air-W	5%	NASA Langley, CWM
SO_2	3-100	SMM	F	0.1-0.5 MHz	Duke U., JPL
H_2S	10-100	FTS	F	0.0001 cm^{-1}	IROE, U. Bologna
	2000-2800	FTS	F,I	0.001 cm^{-1}, 10%	LPMOA Orsay
	6100-6500	FTS	F,I	0.001 cm^{-1}, 10%	LPMOA Orsay
H_2SO_4	---				
C_3H_8	500-4000	FTS	band		NBS Washington
C_2H_4	800-1100($^{13}C,^{12}C$)	FTS	F	0.001 cm^{-1}	U. Louvain, LSM Paris
	1780-2380($^{13}C,^{12}C$)	FTS	F	0.001 cm^{-1}	U. Louvain, LIR Orsay
CH_3CCl_3	1000-1200	grating,TDL	I,W	10%, 5%	U. Stony Brook

Notes: 1. See Annex B-1.
2. Data Type: F = frequency, I = intensity, W = linewidths, Band = random band model.
3. The accuracy, when available, refers to F in cm^{-1} or MHz and to I or W in %.
4. See Annex B-2.
5. 0.0001 cm^{-1} $\cong$ 1 MHz

It is inevitable, in any extensive compilation such as this, that works will inadvertently be overlooked. Our apologies to any authors whose works have thus been accidentally omitted.

often be determined with a precision of 2 to 5%, absolute intensities are usually known with confidence to only 10 to 15% for stable molecules. With particularly careful measurements, accuracies of 5% can be achieved, but greater absolute accuracy (1 to 3%) requires intensive collaborative effort by several laboratories to reduce systematic errors. The situation is similar for halfwidths, where the present measurements result in absolute accuracies usually no better than 5%. Many of the spectroscopic parameters needed for the future UARS program require greater accuracy than can be achieved at the present time.

The major requirements for further work in laboratory spectroscopy for atmospheric measurements and climate modeling are summarized below, in order of importance. Specific details for many of these requirements will be found in Tables B-7, B-9, and B-11 of this appendix, in Chapter 15 of this report, in the report of Smith (1985), and in the UARS Spectroscopic Requirements document (Roche, 1985). The first two of the requirements given here have much greater importance than those in the remainder of the list.

1. *Line Positions and Intensities.* Accurate line positions and intensities are important for many of the atmospheric remote sensing techniques and for climate studies. However, the spectral parameters for several infrared bands of major and trace constituents are either totally missing or of poor accuracies. This problem, in general, is more severe between 3000 to 10,000 cm^{-1} where significant contributions from molecules such as O_3, CH_4, and HNO_3 are not available. Even where intensities are available, for example, in the 15 μm band system of CO_2, improvements are needed in both the experimental accuracies and the theoretical modeling of these data.

2. *Line Widths.* Knowledge of spectral line halfwidths and their dependence on temperature is deficient for nearly all the atmospheric gases. Accurate measurements of air-broadened halfwidths (and self-broadened and N_2-broadened halfwidths in special cases [see Table B-9] are needed). Efforts to improve theoretical calculations of line widths for atmospheric molecules should also be encouraged.

3. *Line Shapes.* Deviations from the Lorentz lineshape can be critical for analysis of atmospheric spectral data (see Chedin and Scott, 1984) and for calculation of atmospheric heating and cooling rates in almost all wavelength regions, such as in the 15 μm region and the 4.3 μm band head of CO_2, the 6.3 μm H_2O band and in many regions in the microwave. Continued laboratory and theoretical studies of these deviations are needed.

4. *Unresolved Bands.* The use of band models to represent unresolved rotational structure is required for heavy molecules such as chlorofluorocarbons. More accurate measurements of band intensities or absorption coefficients and integrated intensities of strong isolated features such as Q-branches are desired. Accurate band model representations for radiatively important trace gases are also needed in climate studies where line-by-line calculations over very large spectral regions are impractical or impossible.

5. *Pressure Induced Bands.* The currently available absorption coefficients for the important pressure induced bands of O_2 and N_2 (in the 6 μm and 4 μm regions, respectively) are quite approximate, especially at typical stratospheric temperatures. Additional laboratory measurements and modeling efforts are needed.

6. *Water Vapor Continuum.* H_2O continuum absorption is important in the interpretation of tropospheric absorption spectra and in climate studies, but presently available representations do not adequately model the temperature-pressure dependence of the continuum. More work in this area is needed.

7. *Non-LTE Radiative Transfer.* Emission or absorption by molecules such as O_2, O_3, HCl, OH, NO, H_2O and CO_2, which are not in local thermodynamic equilibrium (LTE) at certain altitudes in the upper atmosphere, can significantly affect atmospheric measurements in many cases. Improvements are needed in parameters for transitions between the high vibrational levels involved in non-LTE radiative transfer.

8. *Other Effects.* Several other effects such as pressure induced line shifts, collisional narrowing, and line mixing, which are normally neglected in most atmospheric spectroscopic studies, can be significant in some cases. Measurements and theoretical modeling of these effects should be encouraged. In particular, accurate measurements of pressure induced line shifts would be useful for validation of theoretical line width calculations.

There are also several comments and recommendations which may be made in regard to the maintenance and improvement of the spectroscopic database.

- Since the analysis of atmospheric spectral measurements increasingly involves the use of computers, the entire database should be computer accessible.
- Laboratory investigators should consistently report absolute accuracies along with measured values for line positions, intensities, and halfwidths.
- Where multiple measurements exist for a given set of parameters (e.g., CO_2 line positions and intensities), a critical evaluation of the measurements should be made, and the best possible set of parameters (with error bars) should be determined and incorporated in the database.
- As can be seen from section B-5-2, several UARS investigations desire line intensity and halfwidth accuracies better than those reported in this document or routinely measured in the community. Since improved line parameter accuracies directly benefit the accuracy of retrieved geophysical parameters, there should be an organized effort, involving many laboratories, to establish absolute line intensity standards in the infrared. A related effort should be made for line widths in the infrared and microwave.

In this appendix the status of spectroscopic data in the visible and ultraviolet regions has not been addressed, except to the extent that some visible-region line parameters are included in the AFGL and GEISA compilations. However, a number of ground-based, balloon-borne, rocket-borne or space-based atmospheric ultraviolet and visible remote sensing experiments are presently in operation or are planned for the future. As in the infrared to microwave region, the accuracy of the results derived from these short-wavelength atmospheric observations is also affected by the uncertainties in the available spectroscopic data. Therefore it is recommended that the database in the visible to ultraviolet region be reviewed and evaluated in the near future.

Increasingly more sophisticated atmospheric remote sensing experiments are being discussed for possible implementation in the later part of this century and beyond. Examples of the types of instruments under discussion may be found in the Earth Observing System (EOS) science and missions requirements working group report (Butler, 1984). The increasing number of observations from space will require better knowledge of spectroscopic parameters at conditions prevalent in the upper stratosphere, mesosphere, and possibly at even higher altitudes. Efforts toward remote sensing of the troposphere from space will also require improved knowledge of halfwidths, line shapes, continua, and aerosol extinction, as well as line parameters for additional molecules which are not important in the stratosphere. Improved knowledge of these same spectroscopic parameters, along with accurate representations of absorption and emission in broad spectral regions covering many molecular bands, will also be required for climate studies.

Acknowledgements

Thanks are expressed to Drs. A. Chedin, K. Chance, and V. Ramanathan for valuable comments to preliminary versions of this appendix.

Annex B-1
Explanation of Instrument Abbreviations

FTS:	Fourier Transform Spectrometer (Michelson Interferometer)
TDL:	Tunable Diode Laser Spectrometer
MW:	Microwave Spectrometer
SMM:	Submillimeter (Far-Infrared) Spectrometer
DFL:	Difference Frequency Laser
LHS:	Laser Heterodyne Spectroscopy
SISAM:	French interferometer (spectromètre interférentiel à selection par l'amplitude de modulation)

Annex B-2
Explanation of the Institution Abbreviations

Aerodyne Research:	Aerodyne Research, Inc., Billerica, MA, USA
AFGL:	Air Force Geophysics Laboratory, Hanscom Field, MA, USA
Douglas RL:	MacDonnell Douglas Research Laboratories, St. Louis, MO, USA
CWM:	College of William and Mary, Williamsburg, VA, USA
Duke U:	Duke University, Durham, NC, USA
IROE	Istituto di Ricerca sulle onde Elettromagnetiche del CNR, Firenze, ITALY
ISM CNR:	Istituto di Spettroscopia Molecolare del CNR, Bologna, ITALY
JPL:	Jet Propulsion Laboratory, California Institute of Technology, Pasadena, CA, USA
JRC Ispra:	Joint Research Center, EEC, Ispra, ITALY
Kitt Peak NSO:	National Solar Observatory, Kitt Peak, Tucson, AZ, USA

LIR Orsay:	Laboratoire d'Infrarouge, Université d'Orsay, FRANCE
LPM Reims:	Laboratoire de Physique Moléculaire, Faculté de Sciences des Reims, FRANCE
LPMOA Orsay:	Laboratoire de Physique Moléculaire et d'Optique Atmosphérique, Campus d'Orsay, FRANCE
LSM-ENEA:	Laboratoria di Spettroscopia Molecolare del ENEA, Frascati, ITALY
LSM Paris:	Laboratoire de Spectronomie Moléculaire, Université de Paris 6, FRANCE
MET. FRANCE:	Météorologie Nationale, FRANCE
NASA Ames:	NASA Ames Research Center, Moffett Field, CA, USA
NASA Langley:	NASA Langley Research Center, Hampton, VA, USA
NASA Goddard:	NASA Goddard Space Flight Center, Greenbelt, MD, USA
NBS Boulder:	National Bureau of Standards, Boulder, CO, USA
NBS Wash.:	National Bureau of Standards, Washington, DC, USA
NCAR:	National Center for Atmospheric Research, Boulder, CO, USA
NOAA/NESDIS:	National Oceanic and Atmospheric Administration, National Environmental Satellite Data and Information Service, Washington, DC, USA
NPL:	National Physical Laboratory, Teddington, UNITED KINGDOM
NRC Canada:	National Research Council of Canada, Herzberg Institute of Astrophysics, Ottawa, Ontario, CANADA
OSU:	Ohio State University, Columbus, OH, USA
RAL:	Rutherford Appleton Laboratory, Chilton, Didcot, Oxon, UNITED KINGDOM
SAO Harvard:	Smithsonian Astrophysical Observatory, Harvard, Cambridge, MA, USA

U. Bologna:	Instituto Chimica Fisica e Spectroscopia, Università, Bologna, ITALY
U. Calgary:	University of Calgary, Calgary, Alberta, CANADA
U. Denver:	University of Denver, Department of Physics, Denver, CO, USA
U. Dijon:	Laboratoire de Spectronomie Moléculaire de l'Université de Dijon, Dijon, FRANCE
U. München:	München Universität, München, FRG
U. Louvain:	Université Catholique de Louvain, Département de Physique, Louvain la Neuve, BELGIUM
U. Oulu:	University of Oulu, Physics Department, Oulu, FINLAND
U. Rennes	Département de Physique Atomique et Moléculaire, Université de Rennes, Rennes, FRANCE
U. Stony Brook:	Laboratory for Planetary Atmospheres Research, State University of New York at Stony Brook, Stony Brook, NY, USA

APPENDIX C

INSTRUMENT INTERCOMPARISONS AND ASSESSMENTS

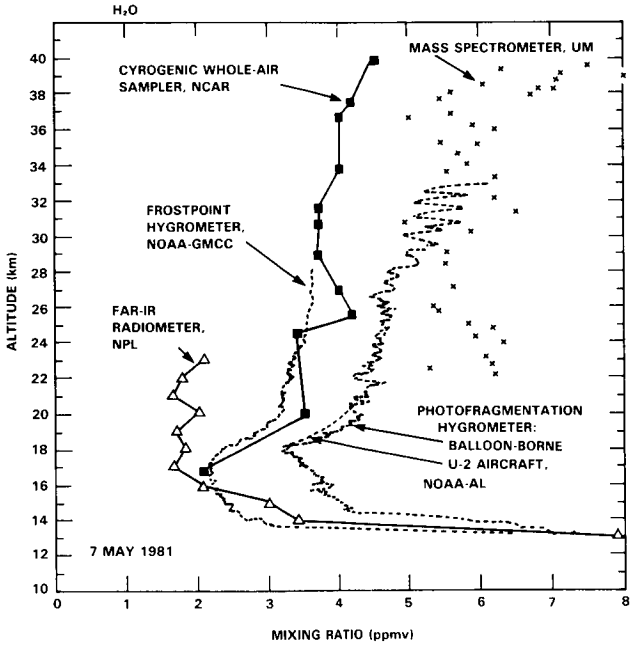

Panel Members

D.L. Albritton and R.J. Zander, Co-Chairmen

C.B. Farmer
E. Hilsenrath
W.G. Mankin
D.G. Murcray
S. Pollitt
D.E. Robbins
H. Roscoe

APPENDIX C

INSTRUMENT INTERCOMPARISONS AND ASSESSMENTS

TABLE OF CONTENTS

C-0 INTRODUCTION

The word "stratospheric" means different things to different people. For the layperson, *Webster's Thesaurus* has expanded on the meaning of this adjective by listing several synonyms:

> "*stratospheric* adj syn EXCESSIVE, dizzy, exorbitant, extravagant, immoderate, sky-high, steep, stiff, unconscionable, unmeasurable."

While it would be interesting to see how well each of these translates over to the field of stratospheric research, the synonym that does indeed strike at the heart of an important scientific issue is the last one: "unmeasurable".

To be sure, not all of the stratospheric trace constituents are unmeasurable, as experimentalists would quickly and correctly point out. But the lexicographers have indeed caught a germ of truth; such measurements are generally extremely challenging to carry out and often end up being somewhat equivocal. Yet, it is vital to have reliable estimates of the uncertainty in the observations, since they are the touchstone against which the theoretical understanding is tested.

In the series of assessments that have addressed the status of this understanding of the physics and chemistry of the atmosphere (e.g., WMO, 1982), several questions have generally arisen regarding the quality of the measurements of stratospheric trace constituents:

- Are the current data of adequate quality to constrain the models in useful ways?
- Are the rather large differences between measurements that have been made at different times, at different places, and with different methods due to atmospheric variability or instrumental uncertainty (or both)?
- Have the estimates of experimental uncertainty been tested quantitatively?
- Recognizing the growing need for simultaneous and comprehensive data on a photochemically coupled suite of trace gases, is measurement reliability currently at a state such that only one instrument or method need be included for each key species in a campaign?

In recent years, the community has devised a way to address these questions in an arduous, but effective way: a formal and rigorous intercomparison of instruments and techniques.

The features of the most successful (i.e., the most instructive) of these instrument intercomparisons have been the following:

- involve several different techniques for measuring the same species,
- measure at the same place and time and under typical operating conditions, insofar as possible,
- state the accuracy and precision estimates in advance of the intercomparison,
- each investigator prepare his/her results independently and separately (i.e., "blind") from the others and in a publication-ready status,
- jointly (or via an independent party) compile the separate results and assess the state of agreement,
- publish all results and conclusions in a refereed journal, and
- repeat the whole process occasionally.

Over the past few years, there have been several field campaigns devoted specifically to this goal, namely, the assessment of instrument reliability, as opposed to solely obtaining data to answer a geophysical question. Some of these intercomparison campaigns have been carried out in a fashion close to the above "ideal".

INTERCOMPARISONS

Table C-1 lists chronologically some examples of the formal instrument intercomparisons that have occurred in the past decade and those that are planned for the very near future. Moreover, numerous research institutions have participated, as the list in the table demonstrates. In this Appendix, the focus is on the middle group of campaigns, for which published or publication-ready results are available. These are the ones that have been carried out in recent years, but yet sufficiently long ago to permit a definitive assessment of some of the results. Furthermore, most of these campaigns have incorporated many of the features of the "ideal" noted above.

Table C-1. Examples of past and planned instrument intercomparisons and the participating research institutions

Intercomparison Campaigns:

• Ozonesondes: Hohenpeissenberg	1970, 1978
• Balloon-borne Ozone Instruments: UV absorption photometer and mass spectrometer	1978
• International Ozone Campaign: variety of ozone instruments	1981*
• Water Vapor Instrumentation: primarily balloon-borne *in situ* methods	1981, 1983*
• Balloon Ozone Intercomparison Campaign: primarily balloon-borne *in-situ* and remote methods	1983*, 1984*
• Balloon Intercomparison Campaign: remote methods addressing several species	1982*, 1983*
• Global Tropospheric Experiment - Chemical Instrumentation Tests and Evaluation:	
— aircraft-borne OH, NO, and CO methods	1983, 1984
— aircraft-borne NO_2, HNO_3, and PAN methods	1986
• The Middle Atmosphere Program: Global Budget of Stratospheric Trace Constituents (MAP-GLOBUS): variety of methods and species	1983, 1985

Participating Research Institutions*

AES	Atmospheric Environment Service (Canada)
CNRS-FSR	Centre Nationale de la Recherche Scientifiques, Faculte des Sciences de Reims (France)
CNRS-SA	Centre Nationale de la Recherche Scientifique, Service d'Aeronomie (France)
DU	Denver University (U.S.A.)
HU	Harvard University (U.S.A.)
IASB	Institut d'Aeronomie Spatiale de Belgique (Belgium)
IROE	Instituto de Ricerca sulle Onde Electromatnetiche (Italy)
JPL	Jet Propulsion Laboratory (U.S.A.)
MN	Meteorologie Nationale (France)
MOH	Meteorologisches Observatorium Hohenpeissenberg (Federal Republic of Germany)
NASA-GSFC	National Aeronautics and Space Administration, Goddard Space Flight Center (U.S.A.)
NASA-JSC	National Aeronautics and Space Administration, Johnson Space Center (U.S.A.)

Table C-1 (Continued)

NASA-WFC	National Aeronautics and Space Administration, Goddard Space Flight Center, Wallops Flight Facility (U.S.A.)
NBS	National Bureau of Standards (U.S.A.)
NCAR	National Center for Atmospheric Research (U.S.A.)
NOAA-AL	National Oceanic and Atmospheric Administration, Aeronomy Laboratory (U.S.A.)
NOAA-GMCC	National Oceanic and Atmospheric Administration, Geophysical Monitoring for Climate Change (U.S.A.)
NPL	National Physical Laboratories (U.K.)
ONERA	Office Nationale d'Etudes et de Recherches Aerospatiales (France)
SAO	Smithsonian Astrophysical Observatory (U.S.A.)
UL	Universite de Liege (Belgium)
UM	University of Minnesota (U.S.A.)
UO	University of Oxford (U.K.)
UT	University of Tokyo (Japan)

*Emphasized in this Appendix

This Appendix emphasizes balloon-borne techniques and instruments that address the height profiles of the trace species in the lower stratosphere. Although ground-based total-column methods offer an independent and valuable constraint, most of the recent campaigns have not completed a full intercomparison of the integrated vertical profiles and the groundbased results. Lastly, the comparison of vertical-profile data with satellite measurements is a challenging study in itself and is outside the scope of this summary.

Some of the chemical species have been addressed rather thoroughly in more than one campaign. Beginning with the most extensively studied trace constituent, this Appendix describes the approach taken and the results that have been obtained. Lastly, the conclusions reached regarding the current status of the measurement capabilities are summarized, and the needs for future intercomparisons and assessments are listed.

C-1 OZONE (O_3)

For obvious reasons that are developed in this and previous reports, there has been substantial effort directed toward an assessment of the reliability with which stratospheric ozone can be measured. Indeed, more intercomparisons have addressed this species than any other. There have been three major research efforts in this regard in the last few years, each having a rather different focus:

- INTERCOMPARISON OZONE CAMPAIGN - the first integrated intercomparison of a *wide variety of techniques*,

- BALLOON OZONE INTERCOMPARISON CAMPAIGN - primarily *in situ balloon-borne instruments*, and

- BALLOON INTERCOMPARISON CAMPAIGN - primarily *remote balloon-borne instruments.*

The goals, approach, and results of each are summarized here.

C-1.1 Intercomparison Ozone Campaign

The multi-faceted, three-week, Intercomparison Ozone Campaign has been the most extensive investigation of the experimental aspects of atmospheric ozone (Chanin, 1983a and 1983b and accompanying papers).

Characteristics

(a) *Organization and location:* Figure C-1 gives a graphical summary of the campaign. The study, which was conducted at several sites located across southern France, combined ground-based observing stations with several ozonesonde launches and two large-gondola balloon launches. This approach was to include as many different methods as possible, with the goal of obtaining the first overall "status report" on how well ozone can be measured.

(b) *Variety of ozone instruments:* The observational techniques included not only those that had been used routinely as part of network operations, but also those newly developed ones still undergoing field

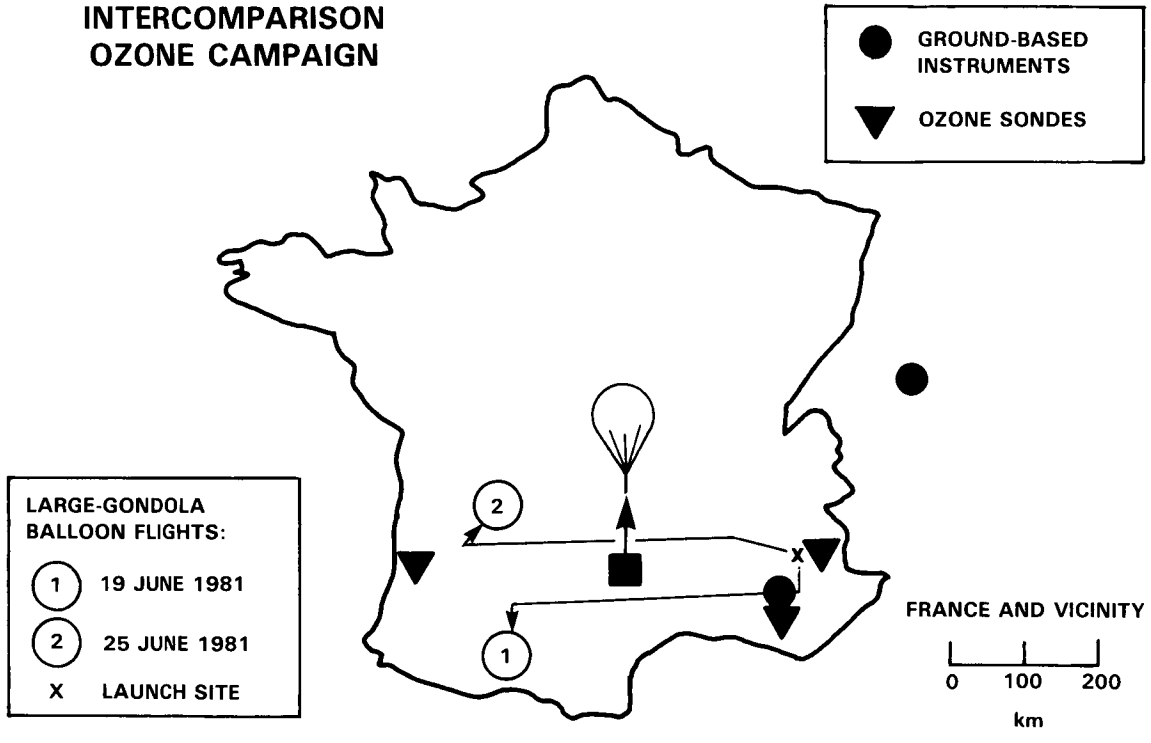

Figure C-1. Geographical locations of the components of the Intercomparison Ozone Campaign. (Adapted from Chanin [1983a]).

trials. Several research institutions were represented and both vertical-profile and total-column instruments were employed:

- ground-based:
  - CNRS-FSR: Dobson spectrometer (column)
  - CNRS-FSR: high-resolution IR absorption interferometer (column)
  - CNRS-FSR: Umkehr method (profile)
  - CNRS-SA: differential absorption lidar (profile)

- balloon-borne:
  - NASA-WFC: electrochemical concentration cell (ECC) sonde (*in situ,* profile)
  - MN: Brewer-Mast sonde (*in situ,* profile)
  - NASA-JSC: UV absorption photometer (*in situ,* profile)
  - CNRS-SA: chemiluminescence ozonometer (*in situ,* profile)
  - IASB and NASA-GSFC: solar UV absorption photometers (*in situ,* remote)

The large gondola carried the last four types of balloon-borne methods.

There were a total of fourteen ozonesondes launched on small balloons during the three weeks (four Brewer-Mast and ten ECC) from western and eastern France, respectively. Each set of soundings had sequential launches, with time separations of hours or greater, since the goal was to compare the ozonesondes to other types of instruments, rather than to compare sonde versus sonde. The other techniques were represented by a single instrument each, except for the solar UV absorption photometers, of which there were two from different institutions on the gondola.

Results

The price paid for variety was, of course, a resulting set of observations that were somewhat separated in space and time and a modest number of samples, both of which hindered some of the intercomparisons. Nevertheless, there had never been such an extensive look at how well ozone can be measured. The results stand as a benchmark in experimental science.

(a) *Total column:* The four ground-based instruments - Dobson, IR and UV spectrometers, and lidar - gave total-column ozone values that agreed within $\pm 5\%$ during the three-week period, *provided* the data were taken at the same place and time. On one day during one of the large-balloon flights, twelve different methods (ground-based and balloon-borne) were used to deduce the total column of ozone, and the values obtained were with $\pm 10\%$. If the results from the ECC sondes were excluded, the dispersion was reduced to $\pm 5\%$.

(b) *Vertical profile:* Because of larger variability of ozone in the region below about 20 km and because so few of the observations were coincident in space and time, the assessment of the performance of the instruments in this lower part of the atmosphere was limited to noting general agreement. However, above 25 km, which was the emphasis of the campaign, several results stand out:

(i) The electrochemical sondes exhibit substantial discrepancies among themselves. The dispersion between the results increased with increasing altitude, reaching a factor of two at 33 km for one day's series. While the soundings were at different times during that day, it is unlikely that all of these discrepancies could be rationalized by atmospheric variability alone.

(ii) The *in situ* UV absorption and chemiluminescence instruments differed by as much as ±15% at the ozone maximum, the major uncertainty being attributed to the lack of inflight calibration in the latter.

(iii) The data from both of the remote solar UV absorption photometers were consistently about 20% larger than those from the *in situ* UV absorption instrument. Figure C-2 shows this reproducible difference, which had been seen on earlier balloon flights also.

(iv) The profiles obtained from the Umkehr method scattered ±20% from the others in the height range 15-30 km, but the correction for aerosols had not been made completely.

C-1.2 Balloon Ozone Intercomparison Campaign (BOIC)

This series of three balloon campaigns were conducted at Palestine, Texas, in three parts:

BOIC 1 - June, July 1983
2 - October 1983
3 - March 1984.

The primary goal was to assess the ability to perform stratospheric ozone measurements by balloon-borne instruments (Hilsenrath *et al.*, 1985).

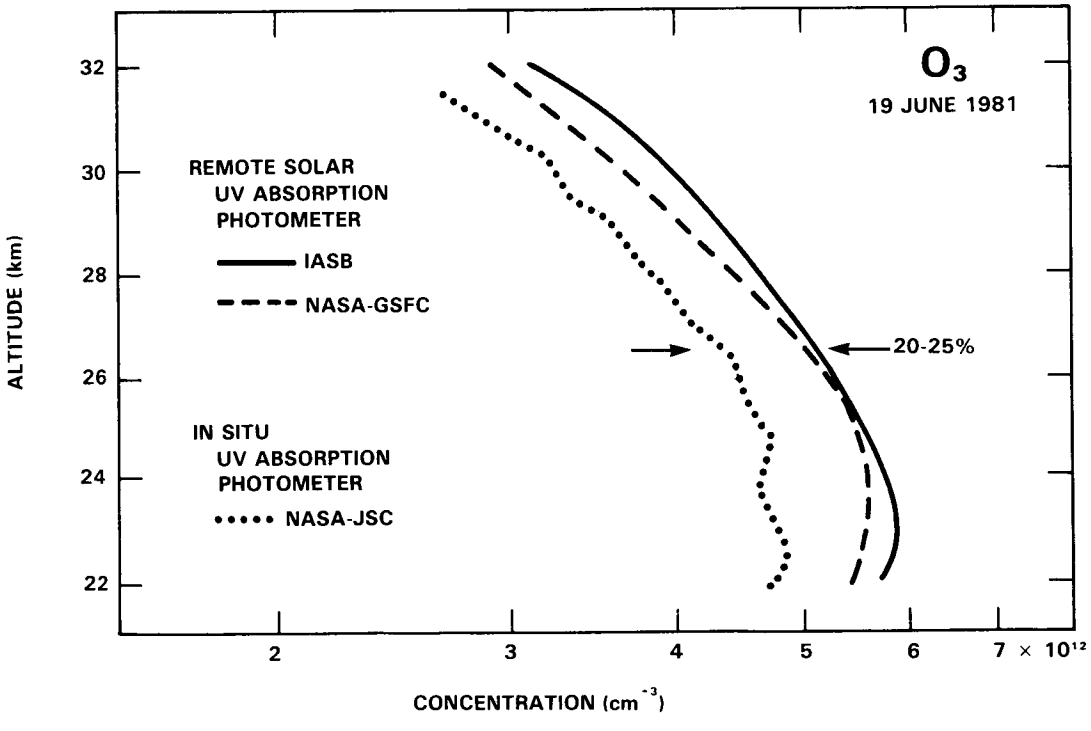

Figure C-2. Comparison of results of two remote solar UV absorption photometers with those taken simultaneously by an *in situ* UV absorption photometer. The data are from the Intercomparison Ozone Campaign. The result of the *in situ* UV absorption photometer are from one profile. The results of the NASA-GSFC and IASB remote UV absorption photometers are averages of data from three and two profiles (ascents and descents), respectively. (Adapted from Aimedieu *et al.*, [1983]).

Characteristics

(a) *Organization:* The campaign employed three instrument ensembles: a large multi-instrument gondola, a smaller gondola with fewer instruments, and a series of small ballons, each carrying a set of three electrochemical ozonesondes. Specifically, the institutions and techniques were:

- multi-instrument gondola:
  - — HU, NASA-GSFC (2), NASA-JSC, and NOAA-AL (2): *in situ* UV absorption photometer, six instruments,
  - — NASA-GSFC and NASA-WFC: remote solar UV absorption photometer, two instruments, and
  - — NASA-WFC and NOAA-GMCC: ECC sondes, several instruments.

- secondary gondola, one of each of the following:
  - — UM: mass spectrometer,
  - — NASA-JSC: *in situ* UV absorption photometer,
  - — NASA-WFC: remote solar UV absorption photometer, and
  - — NASA-WFC and NOAA-GMCC: ECC sonde, one from each institution.

- triplets; a set of three sondes flown together and representing four institutions and different methods:
  - — AES, NASA-WFC, and NOAA-GMCC: ECC, and
  - — MOH: Brewer-Mast.

The optimum plan was to have simultaneous flights of both gondolas to 40 km, accompanied by a series of triplet flights, thereby intercomparing measurements of all of the methods and research groups. However, two successive balloon failures for the multi-instrument gondola forced BOIC into three parts:

• BOIC 1:	multi-instrument gondola	10 July, 1983	(only to 26 km)
	secondary gondola	18 July	
	triplets	19 June - 7 July	
• BOIC 2:	multi-instrument gondola	24 October, 1983	(only to 22 km)
	triplets	1 week	
• BOIC 3:	multi-instrument gondola	21 March, 1984	(to 42 km)
	secondary gondola	24 March	

Only on the third attempt did the main gondola reach 42 km. Because of this lengthening of the time required to complete the campaign, not all of the institutions could participate in all aspects, as indicated. The primary data for the high altitudes are from BOIC 3 and the best statistics for the ozonesondes are from BOIC 1.

(b) *Ground-based observations:* Total ozone and Umkehr profiles were taken by Dobson and Brewer spectrophotometers, which were located at Palestine to limit the effect of spatial variations on the intercomparisons.

(c) *Ground-based comparison with an ozone reference:* Most of the *in situ* instruments were compared with the ozone reference photometer of NBS, both in advance of BOIC at the Gaithersburg, Maryland laboratory and at the launch site on BOIC 1 and 2. The ozone concentrations employed were those that would be encountered in the stratosphere, but the pressure remained at one atmosphere.

(d) "*Blindness*": In almost all cases, the flight data were reduced separately, each group being unaware of the other's data, and the results were submitted to an independent party and then intercompared jointly. Some data were corrected for errors that this initial intercomparison revealed. The comparisons at the launch site with the NBS reference were also done "blind".

Results

By focusing only on balloon-borne instruments, BOIC could enhance the statistics of the observations by having multiple instruments of a given type and by having numerous launches of the triplets of electrochemical sondes. Therefore, even though only one of the three attempts with the main gondola reached optimum altitude, BOIC has revealed several key features of the current ability to measure ozone from balloon platforms:

(a) *Comparison with NBS reference:* The largest differences between the *in situ* instruments and the NBS reference occurred for the electrochemical sondes. The departures were often systematic for each method/institution and ranged from 20% low to 10% high. The sondes exhibited response times on the order of a minute.

Four of the *in situ* UV absorption photometers (NOAA-AL #1 and #2 and NASA-JSC #1 and #2) agreed with the reference within $\pm 2\%$. The two photometers of NASA-GSFC consistently were about 8 to 12% lower than the NBS reference for both BOIC 1 and 2. The flow requirements of the HU photometer precluded a comparison with the reference

(b) *In situ* UV absorption photometers: The six *in situ* photometers of HU, NASA-GSFC (2), NASA-JSC, and NOAA-AL (2) were on the main gondola on BOIC 3 and hence could be intercompared at altitudes to 42 km. The left-hand side of Figure C-3 shows the percentage differences of the results of five of the photometers (NASA-GSFC #2 reported no data) from the average of the measured profiles on ascent. The salient feature is that four of the five photometers agreed within about $\pm 3\%$ over much of the middle stratosphere. The NASA-GSFC #1 instrument, which was low compared to the NBS reference, was also low in the stratosphere by about the same amount; hence, it is not unreasonable to assume that a yet-unknown, persistent error of 5-10% exists in that particular instrument. The NOAA-AL #1 photometer was designed to operate only up to 30 km, and the increasing discrepancy between it and its partner (NOAA-AL #2) at altitudes above 35 km is attributed to inlet wall losses, as described below. Therefore, if the data from the NASA-GSFC #1 and NOAA-AL #1 photometers are excluded from the set for these reasons, the right-hand side of Figure C-3 likely reflects the state of the art with which ozone can be measured in the stratosphere by *in situ* UV absorption photometry.

(c) *Electrochemical sondes:* The ECC sondes (NASA-WFC and NOAA-GMCC) that accompanied the main gondola gave results that agreed to $\pm 10\%$ with the average of the *in situ* UV absorption photometer data in the region of the ozone maximum. Above about 30 km, the sonde data drop to values much lower than the photometer results, exceeding 20% at 38 km and higher.

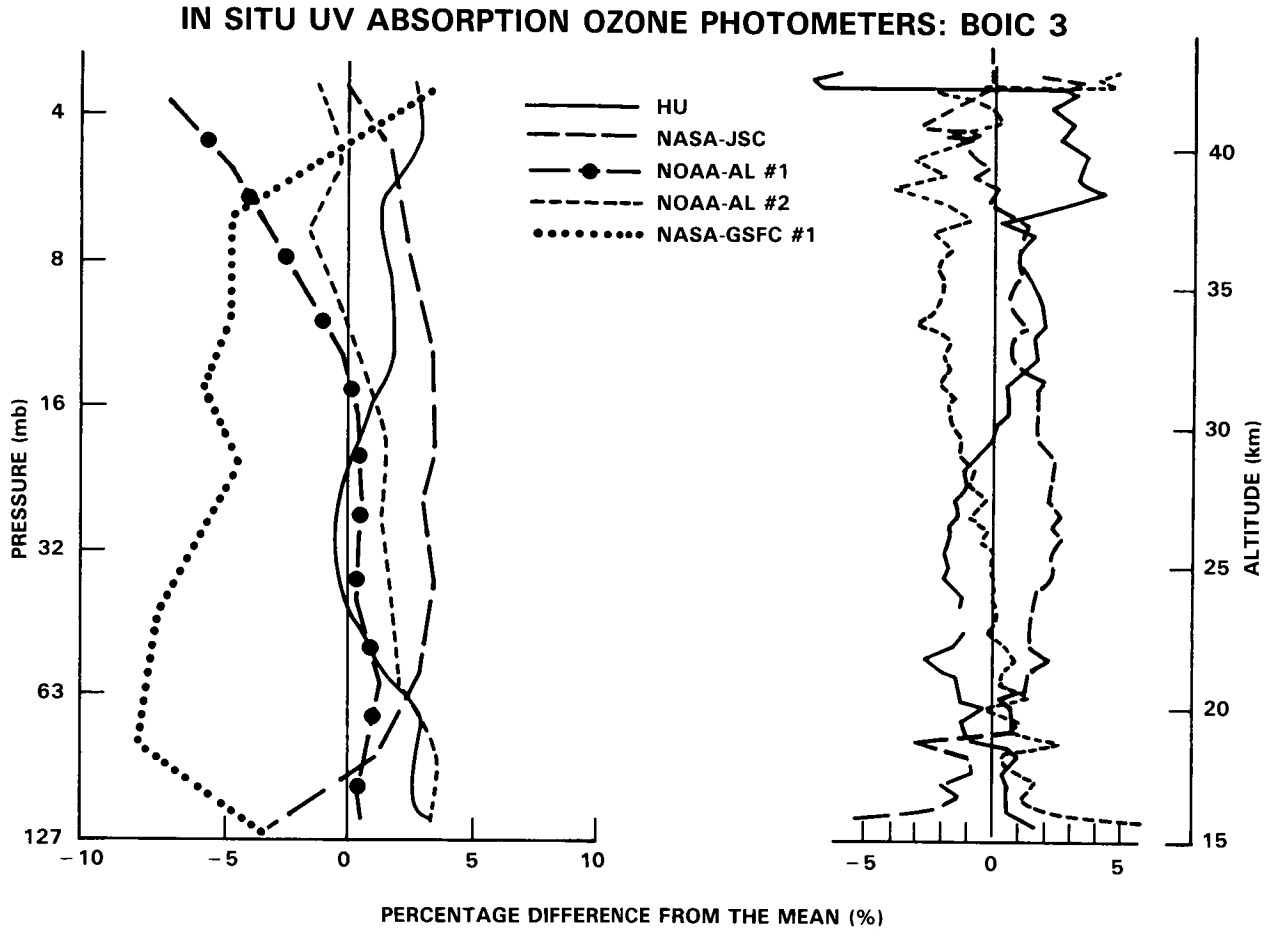

Figure C-3. Percentage difference of the results of *in situ* UV absorption photometers from the mean. The right-hand diagram contains the same data as the left-hand diagram, except that the results from the NASA-GSFC #1 and NOAA-AL #1 instrument have been deleted from the former (see text for reasons). Note the different ordinates: left-hand, pressure, and righthand, altitude. The data are from the Balloon Ozone Intercomparison Campaign 3 and are averages over height intervals. (Adapted from Hilsenrath *et al.*, [1985]).

Since numerous sondes flew in the triplet series of BOIC 1, reliable precision estimates are now possible. For the sondes of a given research group, the sonde-to-sonde difference for simultaneous measurements was typically 5% in the stratosphere, but with occasional outliers. This figure is almost doubled when those of different groups were flown together. The agreement between the sondes of different groups is reflected in Figure C-4, which shows the average departure, by Umkehr layer, of the sondes from each institution from a mean profile from all soundings (a) before, and (b) after normalization to the ground-based measurements of the total ozone column.

(d) *Remote UV absorption photometers:* Balloon and instrument failures almost thwarted a BOIC testing of the remote UV absorption method, a technique that the earlier intercomparisons had found wanting. However, on the BOIC 3 flight of the small gondola, one of these instruments was intercompared with an *in situ* UV absorption photometer. The result was consistent with the earlier observations; namely, the remote method gave results that were 5-10% higher over much of the altitude range covered.

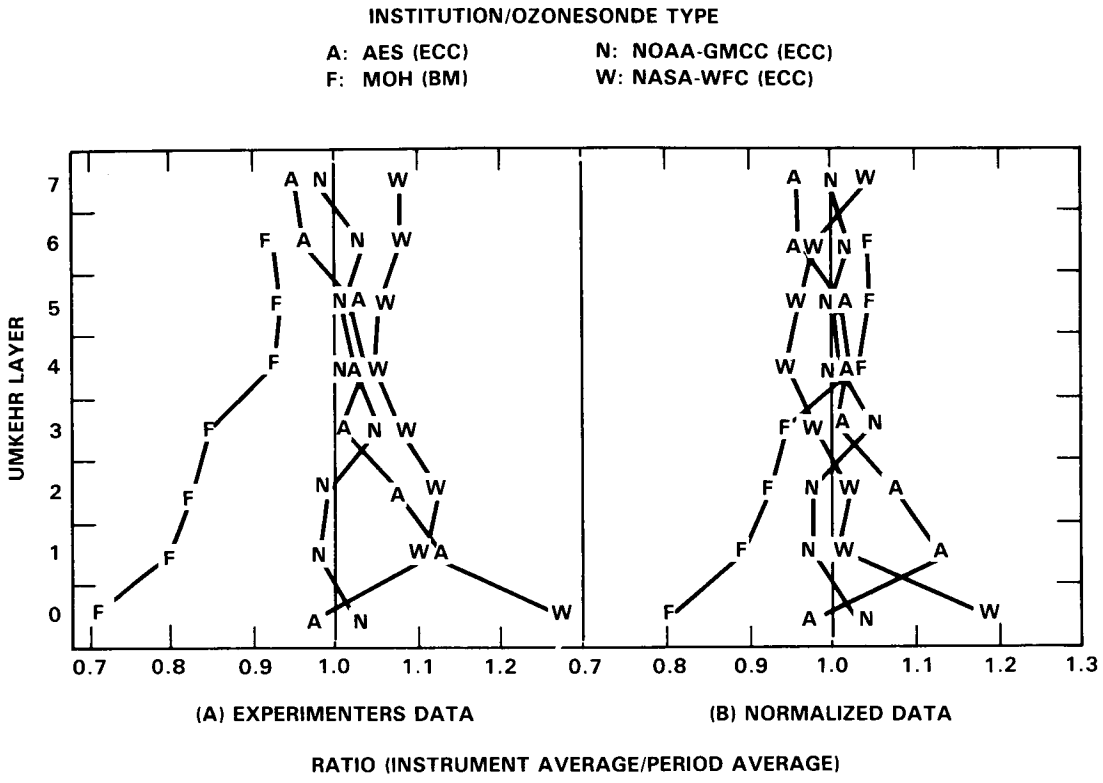

Figure C-4. Average percentage departure of each electrochemical sonde type from the mean of all soundings. Left-hand diagram: before normalizing to separately measured total ozone column. Right-hand diagram: after normalization. The sonde types are Brewer-Mast (BM) and electrochemical concentration cell (ECC). The data are from the Balloon Ozone Intercomparison Campaign 1. (Adapted from Hilsenrath *et al.,* [1985]).

(e) *Gondola and inlet-tube losses:* BOIC made a special effort to explore the oft-discussed, but rarely quantified *in situ* measurement uncertainties of losses of ozone to surfaces. At float, the differences between the *in situ* UV photometers nearly doubled and preliminary analyses suggest correlations with gondola orientation. Three of the UV instruments (HU, NASA-JSC, and NOAA-AL #2) could change their flow rates while inflight by ground command and thereby could assess whether ozone loses were occurring internally in the instrument. None showed any discernable effects even at 42 km. The NOAA-AL #1 UV photometer was not designed for measurements above 30 km and, when carried above this altitude on BOIC 3, showed distinctly lower values than its partner above 35 km (dot-dash line in Figure C-3) strongly suggesting losses on its smaller-diameter inlet lines.

C-1.3 Balloon Intercomparison Campaign

The Balloon Intercomparison Campaign (BIC) a Palestine, Texas was an ambitious and complex program whose primary goal was to assess the accuracy with which balloon-borne remote-sensing instruments can determine the composition of the stratosphere (Watson, 1986). The full implementation required a set of near-simultaneous launches of heavy gondolas on separate large balloons. Each gondola carried several instruments, many of which could measure the stratospheric abundance of numerous species.

However, balloons are not trains, and a gap of 13 days occurred between the launches of some of the main gondolas in the first BIC program in 1982. However, the launches in the second BIC program in 1983 were much closer together:

- BIC 1: 3 gondolas 22 September 1982
  1 gondola 5 October 1982
  aircraft
  ground sites

- BIC 2: 2 gondolas 17 June 1983
  2 gondolas 20 June 1983
  aircraft
  ground sites

Understandably, the time span that occurred in BIC 1 complicated some of the assessments of the intercomparisons, as did the fact that the aerosols from the El Chichon volcano were present in the lower part of the stratosphere at the balloon-site latitude during that time period. Consequently, this Appendix relies heavily on the BIC 2 data, since the more detailed analyses required for some of the BIC 1 data are still underway. Nevertheless, the whole BIC series was a logistical tour de force and has provided an unprecedented examination of the performances of balloon-borne remote-sensing techniques.

Simultaneous aircraft flights and sequences of ground-based observations provided vertical column abundances of many species, and these data could be compared to an integration of the height-profile data from the balloons. This Appendix includes only the results from the aircraft flights in BIC 2 and the Palestine ground site, for which the comparisons are the most straightforward.

Characteristics

(a) *Organization:* A number of laboratories used a total of seven different techniques to measure ozone, and their distributions among the primary BIC launch dates are the following (Robbins *et al.*, 1986):

	BIC 1	BIC 2
• balloon-borne *in situ*:		
— AE: ECC sondes	8 launches	8 launches
— NASA-JSC: UV absorption photometer	22 Sept.	14 June
• balloon-borne remote:		
— NPL: mid-IR emission grating spectrometer	5 Oct.	20 June
— JPL: microwave emission spectrometer	22 Sept.	17 June
— AES: solar UV absorption spectrophotometer	22 Sept.	
— ONERA: IR grille absorption spectrometer		20 June
— SAO: far-IR emission spectrometer		20 June

A study of the ozone data from ground-based, ECC, and satellite measurements indicated that little change occurred in the ozone structure above about 22 km between 22 September and 5 October on BIC 1; hence, the NPL data are considered comparable to the others that were obtained earlier on 22 September, but the intercomparisons were limited to higher altitudes. A Brewer spectrophotometer was operated by AES at Palestine for measurements of the total vertical column of ozone for both BIC 1 and 2.

(b) *Uncertainty analysis:* A unique feature of BIC was the detailed uncertainty analyses that each of the investigators applied to their technique. Altitude-dependent uncertainties for each known random and systematic component were combined to construct a 95% confidence interval expected for the flight data. Figure C-5 shows these confidence levels, expressed as a percentage, for the seven techniques that addressed ozone in BIC. The IR techniques exhibit substantial possible uncertainty, greater than 25%. The others anticipated lower uncertainties, 10% or less at the ozone maximum. The key utility of these careful estimates is that the instrumental differences observed inflight can be assessed in terms of whether they are larger than the combined uncertainties, i.e., whether they are significant. Disagreement beyond such conservative confidence limits for a pair of data sets would clearly indicate a highly significant discrepancy.

Results

(a) *Overall agreement:* If one disregards the ECC measurements above 29 km on BIC 1, the results of all techniques, with one exception, agree to within ±15% for 22-38 km for BIC 1 and 2. This agreement is within the 95% confidence limits; in fact, it is well within, which suggest that these limits are conservative.

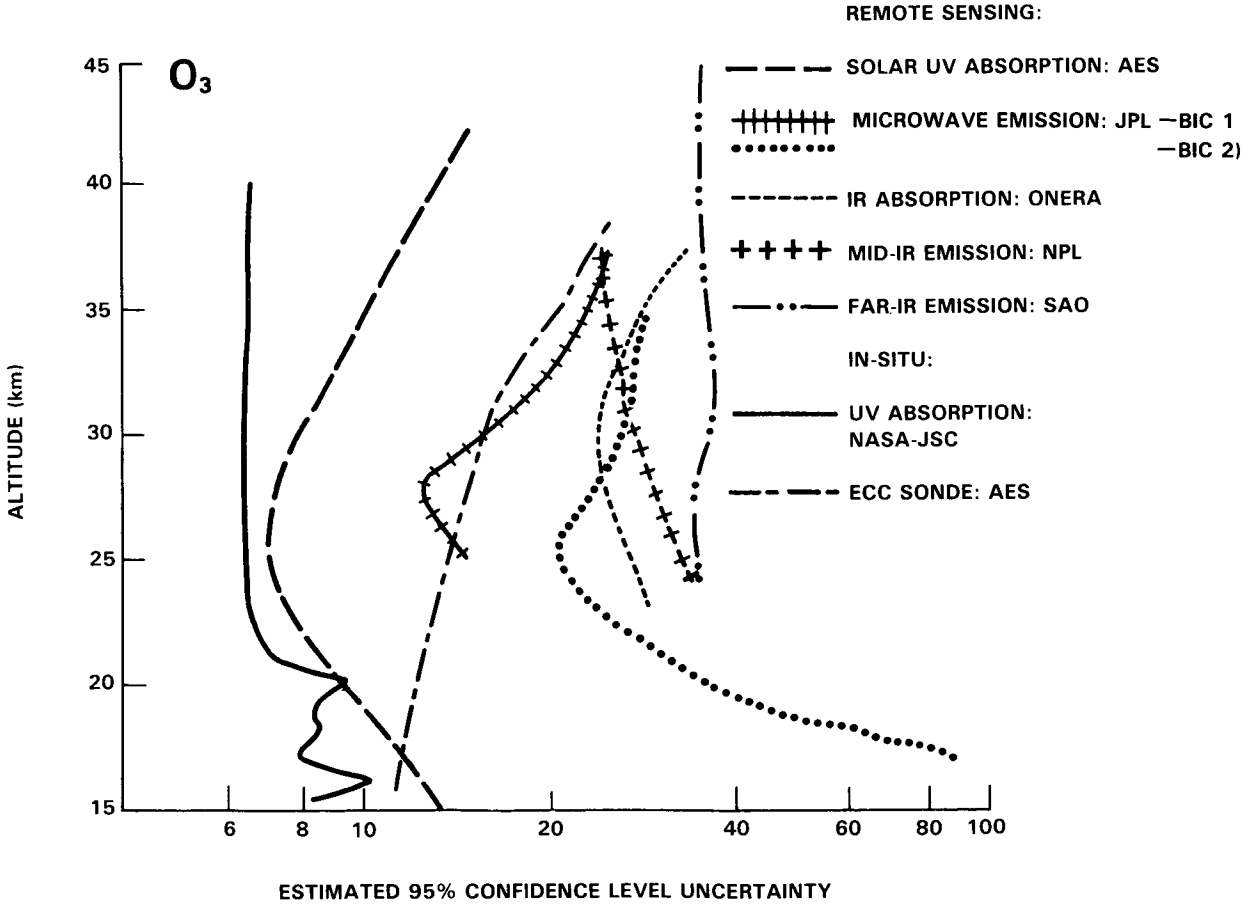

Figure C-5. The altitude-dependent, 95%-confidence-level uncertainties estimated for the ozone instruments in the Balloon Intercomparison Campaign. (Adapted from Robbins *et al.,* [1986]).

(b) *Particulars:* The solar UV absorption technique was the exception noted above. Its data at 31 km were higher than the others, a direction that the results of this technique have tended in the past. Furthermore, the ECC data were lower than the others at the highest altitudes, a tendency that is also consistent with earlier observations.

C-2 WATER VAPOR (H_2O)

The measurement of stratospheric water vapor by *in situ* techniques is difficult due to the potential problems of local contamination arising from outgassing in and around the instrument. Remote instruments are relatively less sensitive to contamination from this particular source, but could be influenced by outgassing from the balloon or gondola. The measurements that had been made over the past decade at different times and places by the various methods had shown differences as large as an order of magnitude. Consequently, there has been a keen interest in assessing the reliability of balloon-borne stratospheric water vapor measurements. Two major research efforts have addressed this question:

- *INTERNATIONAL INTERCOMPARISON OF STRATOSPHERIC WATER VAPOR INSTRUMENTATION* - primarily *in situ* methods, and
- *BALLOON INTERCOMPARISON CAMPAIGN* - remote methods.

The results of each are described here.

C-2.1 International Intercomparison of Stratospheric Water Vapor Instrumentation

The goal of this campaign was to better characterize the difference between the results of the different balloon-borne *in situ* methods that address stratospheric water vapor (Watson *et al.*, 1986). Some remote methods were also included, however.

Characteristics

(a) *Organization:* The campaign was conducted in Palestine, Texas,in two parts. The first was in 1981 and the second was in 1983. Eight different types of instrumentation were involved:

	1981 gondola and date	**1983 gondola and date**
• *in situ:*		
— NCAR: cryogenic whole-air sampler	A, 7 May	A, 13 Oct.
— UM: mass spectrometer	B, 7 May	B, 11 Oct.
— NOAA-AL: photofragmentation hygrometer	C, 7 May	C, 11 Oct.
— NOAA-GMCC: frostpoint hygrometer (free flyer)	7 May	11 Oct.
• remote:		
— DU: emission spectrometer	D, 7 June	D, 11 Oct.
— AES: scanning radiometer	D, 7 June	D, 11 Oct.
— NPL: far-IR radiometer	C, 7 May	

INTERCOMPARISONS

The methods whereby the different instruments acquire their samples (e.g., at float, on ascent, or on descent) were sufficiently different that four separate gondolas and balloons, designated above as A, B, C, D, as well as a small payload on handlaunched balloons, were required. In addition, several water vapor instruments were onboard a U-2 research aircraft that was to rendezvous with the balloons. The goal was, of course, to have all of these in the air at nearly the same time, but this could not be done. Here, only the results that were taken very nearly at the same time are intercompared.

Results

After the May 1981 flight, the investigators separately reduced their data and then examined the results as a group. While the differences were not the factor-of-ten variation from the individual studies of the previous decade, there were striking discrepancies between the data sets, as large as a factor of four. This situation prompted an intense re-evaluation by each investigator of their method and instrument. Several minor and major problems were caught in this soul-searching. Figure C-6 shows the May 1981 results,

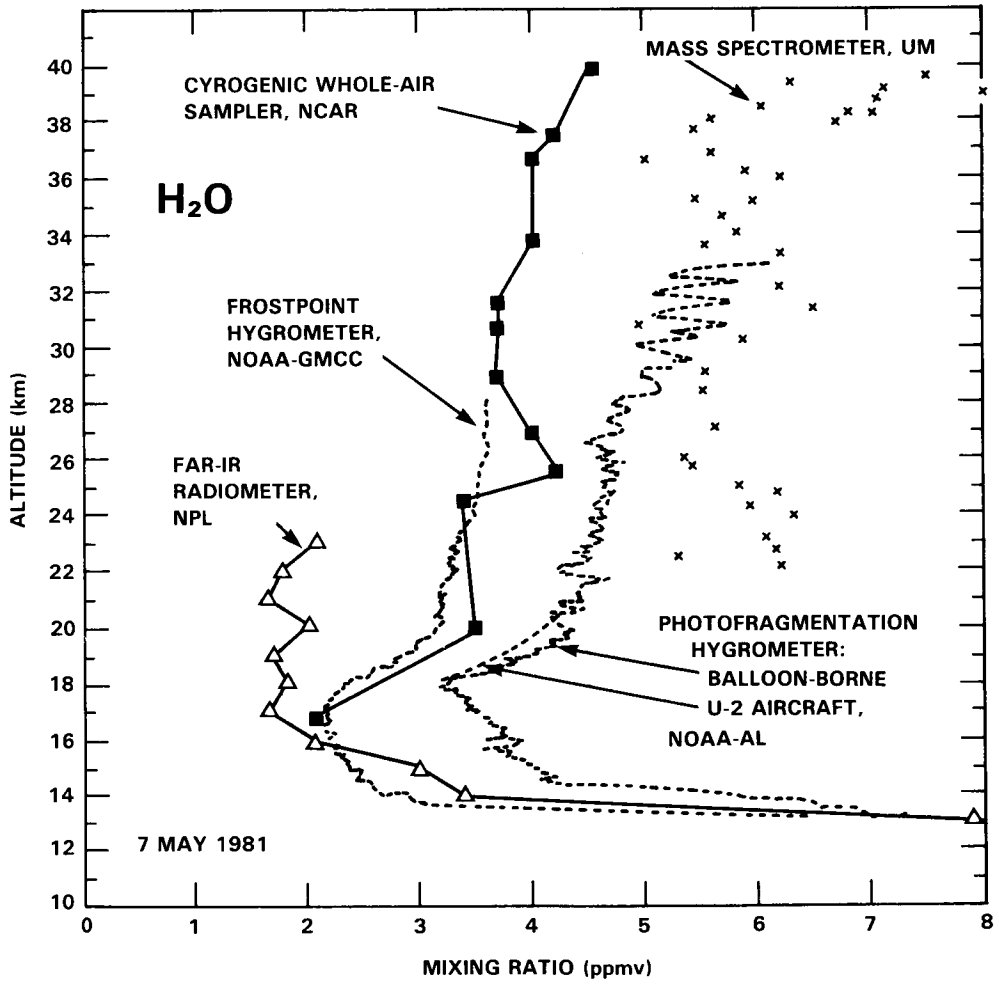

Figure C-6. Water vapor mixing ratios obtained in the first flight series of the international intercomparison of stratospheric water vapor instrumentation. (Adapted from Watson *et al.*, [1986]).

once these errors were corrected. While this re-examination resulted in a modest improvement in the overall agreement (factor-of-three worst case), there are still substantial differences. The stated error limits touch in most cases, but nevertheless there are intriguing regularities that suggest systematic problems with magnitudes of tens of percent.

Since the soul-searching presumably had improved the methods and instruments, a second flight series was carried out to see if the state of affairs portrayed by Figure C-6 was indeed the current state of the art of stratospheric water measurements. Figure C-7 shows the results of the October 1983 flights. Since the differences are comparable to those of the earlier study, both data sets are likely to be a fairly definitive statement regarding the reliabiity of *in situ* water vapor measurements in the stratosphere.

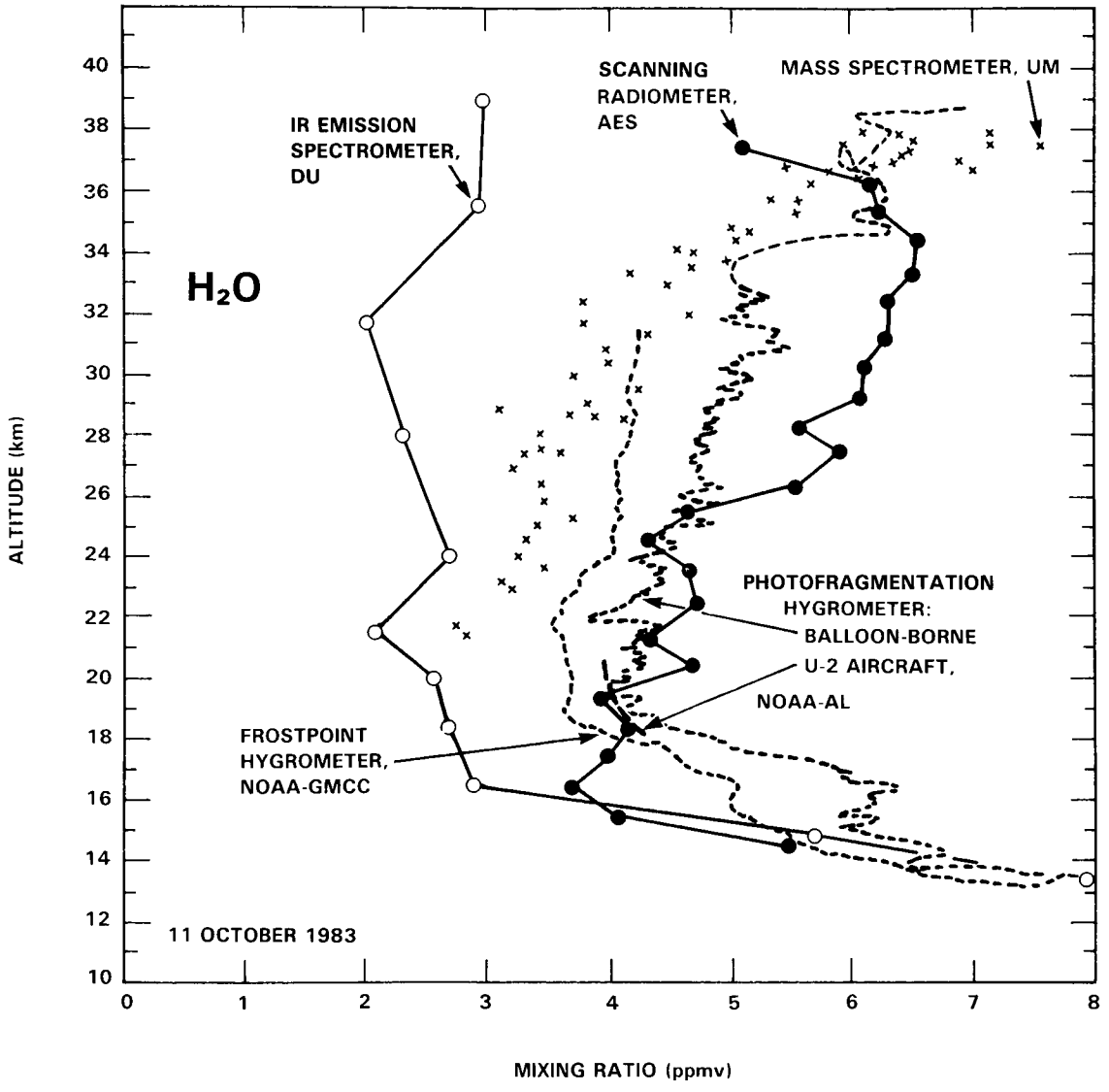

Figure C-7. Water vapor mixing ratios obtained in the second flight series of the international intercomparison of stratospheric water vapor instrumentation. (Adapted from Watson *et al.*, [1986]).

The patterns (or lack thereof) in Figure C-6 and C-7 are fairly clear. First, the photofragmentation and frostpoint hygrometers differ in a regular fashion, the latter being lower by 0.5 to 0.75 ppmv. The same magnitude and sign of this difference was also observed on simultaneous flights of these two instruments from Laramie, Wyoming in February 1983. This consistency has occurred even though different frostpoint instruments have been used in the studies, demonstrating that the problem does not lie in one particular frostpoint instrument. The mass spectrometer data are consistent with neither the photofragmentation nor the frostpoint data. The results of the three remote techniques, although not flown together on the same series, are both lower and higher than the *in situ* data.

C-2.2 Balloon Intercomparison Campaign

The Balloon Intercomparison Campaign (BIC) was carried out to assess the ability to measure remotely a number of compounds other than water vapor; however, this species has strong absorption features throughout the IR and mm-wave regions of the spectrum. Hence, many of the investigators had absorption or emission features due to water vapor in their data and have reported these results for intercomparison. While more data was, in fact, available for water vapor than any other species addressed in BIC, the spectral regions were generally chosen to optimize the measurement of species other than water vapor. Nevertheless, BIC does provide a useful first look at the level of agreement between remote techniques (Murcray *et al.*, 1986), hence complementing the earlier comparison of *in situ* methods.

Characteristics

As explained in Part 1.3 above, BIC was conducted in two parts, the first in 1982 and the second in 1983. Furthermore, in neither case were all of the gondolas launched on one day, but rather they were separated by 13 days in 1982 and 3 days in 1983. Since the latter is much more favorable for intercomparison, we focus here on it. The four emission and two absorption remote-measurement techniques were:

Group	Instrument	Method	Wavelength	Gondola and date
UL	Mid-IR grating spectrometer	absorption	4044 cm^{-1}	A, 17 June
DU	IR grating spectrometer	emission	25, 26 μm	B, 17 June
AES	IR scanning	emission	6.3 μm	C, 20 June
SAO	Far-IR Fourier spectrometer	emission	111, 188 cm^{-1}	D, 20 June
ONERA	IR grille spectrometer	absorption	1600–1608 cm^{-1}	D, 20 June
NPL	Mid-IR grating spectrometer	emission	1339–1350 cm^{-1}	E, 20 June

Results

Figure C-8 presents the results obtained. The data appear to split into two sets at the higher altitudes, a "high" set from ONERA and SAO and a "low" set from AES, DU, NPL, and UL. While the "high" pair were indeed on the same gondola, some of the data of the "low" set were taken, nevertheless, on the same day. Furthermore, the two sets do not reflect a division between emission and absorption methods.

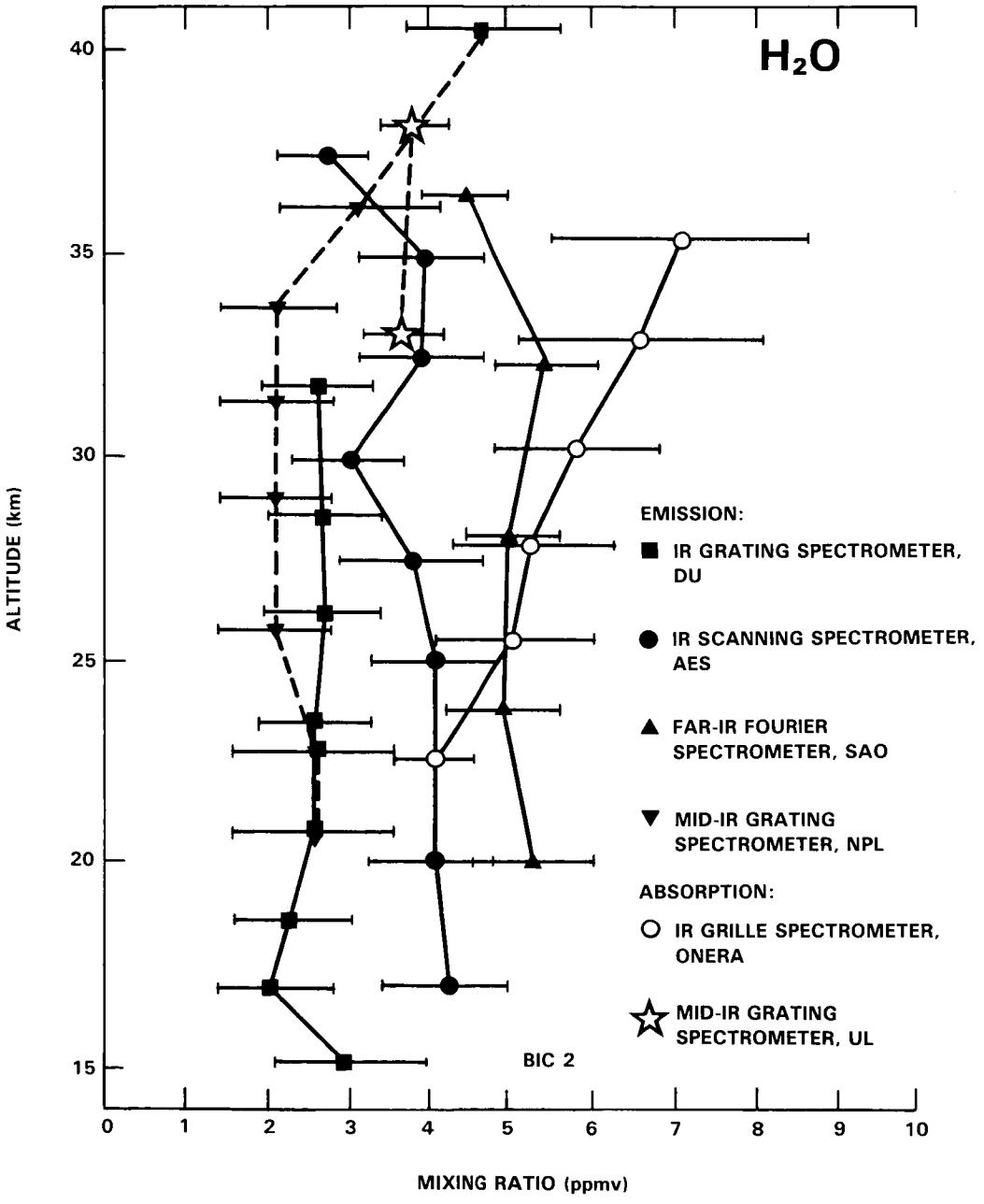

Figure C-8. Water vapor mixing ratios as observed in the Balloon Intercomparison Campaign 2. (Adapted from Murcray *et al.*, [1986]).

Thus, it is difficult to find a simple rationalization of the differences and, indeed, no satisfactory explanation is known currently. The discrepancy is a real one, since the uncertainty limits in Figure C-8 are deemed conservative estimates of the possible random and systematic errors. The differences were smaller on the BIC flights the year earlier, but the time spread over which those data were taken clouds the issue of whether the change reflects better instrumental performance. Thus, on the basis of one sample, the discrepancies among the results of non-optimized remote methods for measuring stratospheric water vapor are up to a factor of 3.5. One positive point can be made: the AES and DU results are in far better agreement in BIC 2 than they were in the October 1983 flights of the *in situ* water-vapor campaign (Figure C-7).

C-3. OTHER SPECIES

The direct assessment of the reliability with which other stratospheric species can be measured has been done only in the Balloon Intercomparison Campaign (BIC). As described in Sec. 1.3, BIC concentrated predominately on evaluating balloon-borne remote-sensing methods. The program was conducted in two parts; September-October 1982 (BIC 1) and June 1983 (BIC 2). Problems forced the BIC 1 flights to be separated by over two weeks, whereas all of the BIC 2 flights occurred within a 3-day period. Consequently, the data from BIC 2 are the emphasis in the intercomparisons described below.

C-3.1 Nitric Acid (HNO_3)

Characteristics

During BIC, remote-sensing methods using both emission and absorption spectroscopy were assessed for their reliability in determining height-profile and vertical-column abundances of HNO_3 (Pollitt *et al.*, 1986):

Height-profile, balloon-borne

Group	Instrument	Technique	Spectral Region (cm^{-1})	BIC
AES	cooled radiometer	emission, ascent	870–900	1&2
DU	cooled-grating spectrometer	emission, ascent	Q-branch 873.73	1&2
NPL	cooled-grating spectrometer	emission, limb-scanning	870–900	2
ONERA	grille spectrometer	absorption limb-scanning	1325.7	2

Total-column, balloon-borne

Group	Instrument	Technique	Spectral Region (cm^{-1})	BIC
DU	IR Fourier spectrometer	absorption, occulation	1720–1730	1&2

Total-column, aircraft

Group	Instrument	Technique	Spectral Region (cm^{-1})	BIC
NCAR	IR Fourier spectrometer	absorption, occultation	1720–1730	1&2

Special care was taken by the BIC investigators to intercompare only those data from the same air mass, wherever possible. For example, the AES radiometer and the DU spectrometer were on two gondolas that were launched on the same day in BIC 1 and hence were deemed comparable. Furthermore, the sunset solar absorption measurements of ONERA and the westward-looking emission measurements of NPL during BIC 2 were paired. While some possible effects of spatial variation could not be ruled out, the measurements of the HNO_3 column made in the region round the launch site showed little variation with latitude and time, thereby giving confidence that samples of dissimilar parts of an inhomogeneous distribution were not a significant source of differences between instruments.

Results

The initial comparisons of the results revealed substantial agreement for most of the data sets, but there were two notable exceptions. First, the emission data obtained by the cooled radiometer of AES at altitudes less than 22 km were significantly lower than the other data. The cause of this discrepancy was traced to spectral contamination by chlorofluorocarbons and hence corrections were made in the final data. The second anomaly was the absorption data set from the grille spectrometer of ONERA, which was significantly different in magnitude and shape from all of the other profile data. Despite preliminary re-examination of the laboratory calibration that was used to reduce the flight data, the cause of the discrepancy remains unknown.

The left-hand portion of Figure C-9 compares the percentage differences of the AES and DU data from their common mean for the averages over four altitude ranges in BIC 1. The $\pm 20\%$ differences are well within the possible uncertainties, except perhaps at the lowest elevations. However, both are emission measurements employing the 11.3 micron band of HNO_3 and reduced using the same band model; hence, systematic errors in the spectral parameters are common to both.

In BIC 2, a much more extensive intercomparison could be made: three emission techniques (AES, DU and NPL) and one absorption technique (ONERA). The right-hand portion of Figure C-9 shows the percentage deviations of these data sets from the mean of the emission data. The three emission experiments, which used similar wavelength regions, gave results that were in substantial harmony, generally $\pm 25\%$ and well within the possible uncertainties, except perhaps at the lowest altitudes. However, the absorption data of ONERA are quite different, being a factor of two larger at 27 km. It is not currently clear whether this is a problem associated with the ONERA instrument and/or techniques in particular or an unknown problem with emission and/or absorption methods in general.

An average of the three emission data sets on BIC 2 gave an integrated column abundance above 21 km that agrees satisfactorily with that that determined in one "best" scan by the absorption measurement of the balloon-borne IR Fourier transform spectrometer of DU. The aircraft absorption measurements of the HNO_3 above 13 km are 20% lower than those obtained from an integration of the height-profile data from the balloon-borne emission instruments, but this difference may not be outside of the combined uncertainties.

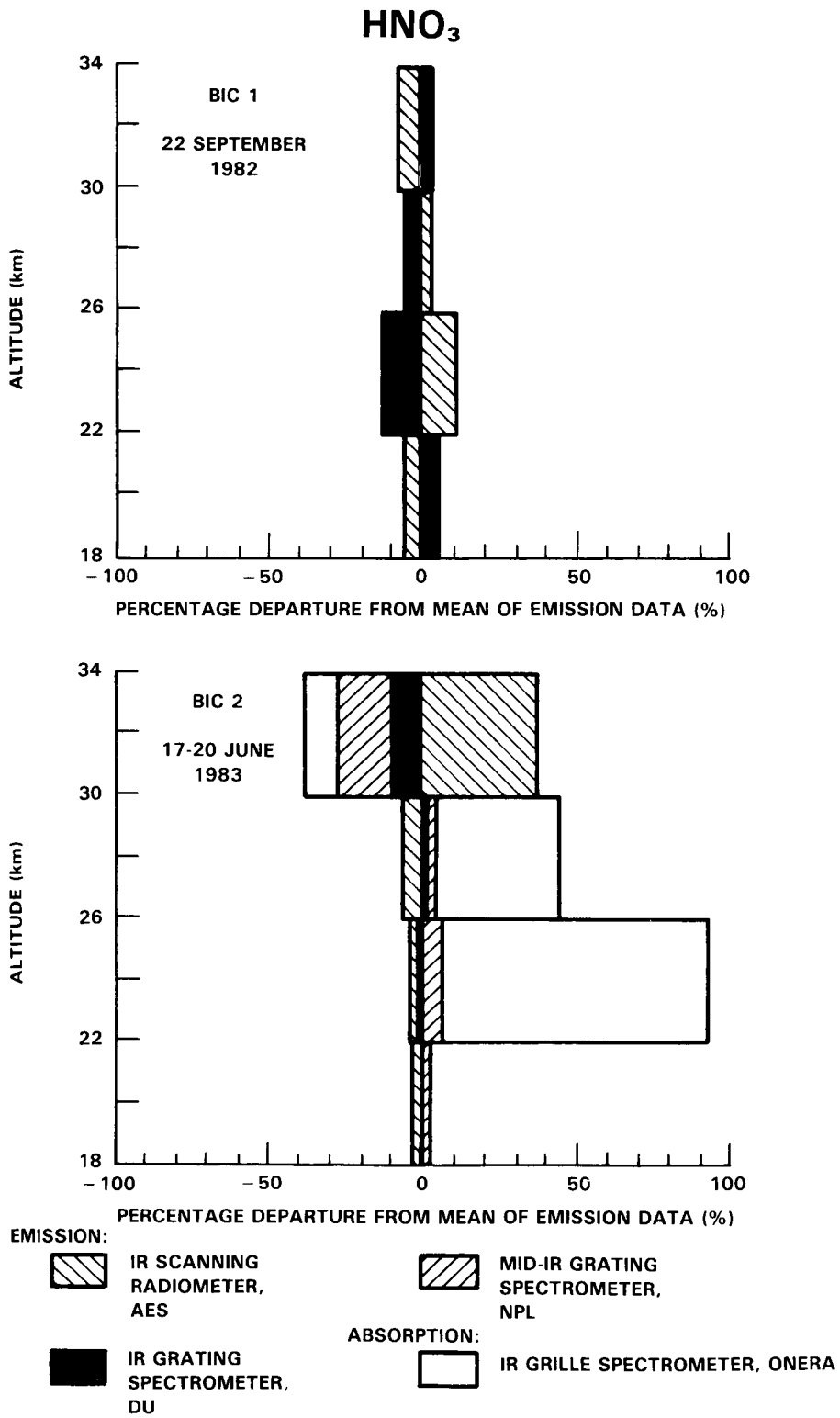

Figure C-9. Departures of the 4-km averages of the HNO_3 data from the mean in the Balloon Intercomparison Campaign. (Adapted from Pollitt *et al.*, [1986]).

C-3.2 Hydrogen Chloride (HCl) and Hydrogen Fluoride (HF)

Apart from its importance in the chemistry of the stratosphere, HCl provides an excellent test of the spectroscopic remote sensing methods that are currently used for measuring the composition of the upper atmosphere. HF also provides a useful test of such methods. Their lines are widely spaced, have well-known positions, are fairly clear from interferences, and have relatively well-understood spectral shapes and strengths. Hence, this spectroscopic "best case" was one of the primary focuses in BIC. There were a total of eight different instruments involved in the HCl and HF measurements (Farmer *et al.*, 1986; Mankin *et al.*, 1986). The most definitive test of the reliability with which HCl and HF can be quantified occurred in BIC 2.

Characteristics

HCl height-profiles were obtained by five balloon-borne instruments: three limb scanning in absorption and two in emission:

Group	Instrument	Technique	Spectral Region (cm^{-1})
AES	IR Fourier spectrometer	absorption	3000 (HCl)
ONERA	IR grille spectrometer	absorption	3000 (HCl)
UL	Mid-IR grating spectrometer	absorption	3000 (HCl), 4040 (HF)
IROE	Far-IR Fourier spectrometer	emission	41 and 62 (HCl), 164 (HF)
SAO	Far-IR Fourier spectrometer	emission	124, 145, and 165 164 (HF)

In addition to these ballon-borne instruments, there were vertical-column measurements of HCl made from balloons and aircraft, as well as ground sites. These data, however, are not yet fully available.

Results

Figure C-10 shows the height-profile data obtained for HCl by five instruments. It is clear that there is excellent agreement, generally within $\pm 20\%$ and well within the experimental uncertainties. The agreement for HF among three instruments was not quite as good, perhaps generally $\pm 35\%$.

C-3.3 Methane (CH_4)

Although CH_4 was not a main emphasis in BIC, some of the instruments, especially those making optical remote-sensing measurements in the mid-IR, could examine vibration-rotation bands of this molecule (Zander *et al.*, 1986). The more-coincident balloon flights of BIC 2 provided the best opportunity to intercompare the results of the instruments that could observe CH_4.

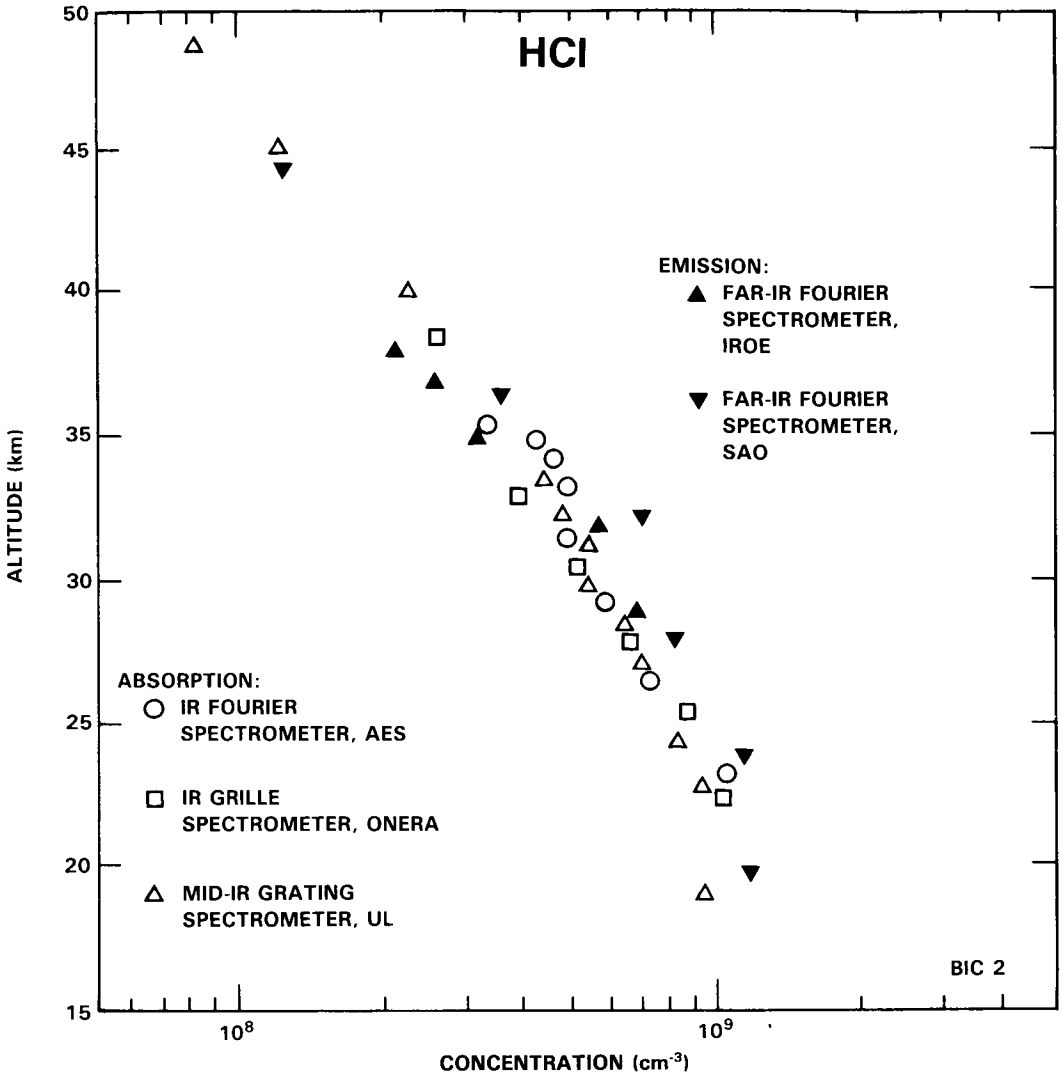

Figure C-10. The HCl concentrations measured in the Balloon Intercomparison Campaign. (Adapted from Farmer *et al.*, [1986]).

Characteristics

CH_4 height profiles were recorded by three instruments on BIC 2, two operating in absorption and one in emission:

Group	Instrument	Technique	Spectral Range (cm^{-1})
UL	Mid-IR grating spectrometer	solar absorption, occultation	2948
NPL	Mid-IR grating spectrometer	atmospheric emission, limb scan	1335–1350
ONERA	IR grille spectrometer	solar absorption, occultation	1322, 2927, 2948

Results

Figure C-11 shows the BIC results. A significant discrepancy is apparent. While both of the absorption studies, UL and ONERA, are in excellent agreement, the emission data of NPL are substantially lower. The emission technique was re-examined carefully, since it was the "outlier" and since its results for H_2O, which were from the same spectral region, also tend to be lower than others (Figures C-6 and C-8). However, the difference has not been rationalized satisfactorily at the present.

C-3.4 Nitrogen Oxides (NO and NO_2)

Nitric oxide and nitrogen dioxide were considered as prime targets in the BIC campaign. Not only are they the key reactive species in the stratospheric nitrogen chemistry that leads to ozone destruction,

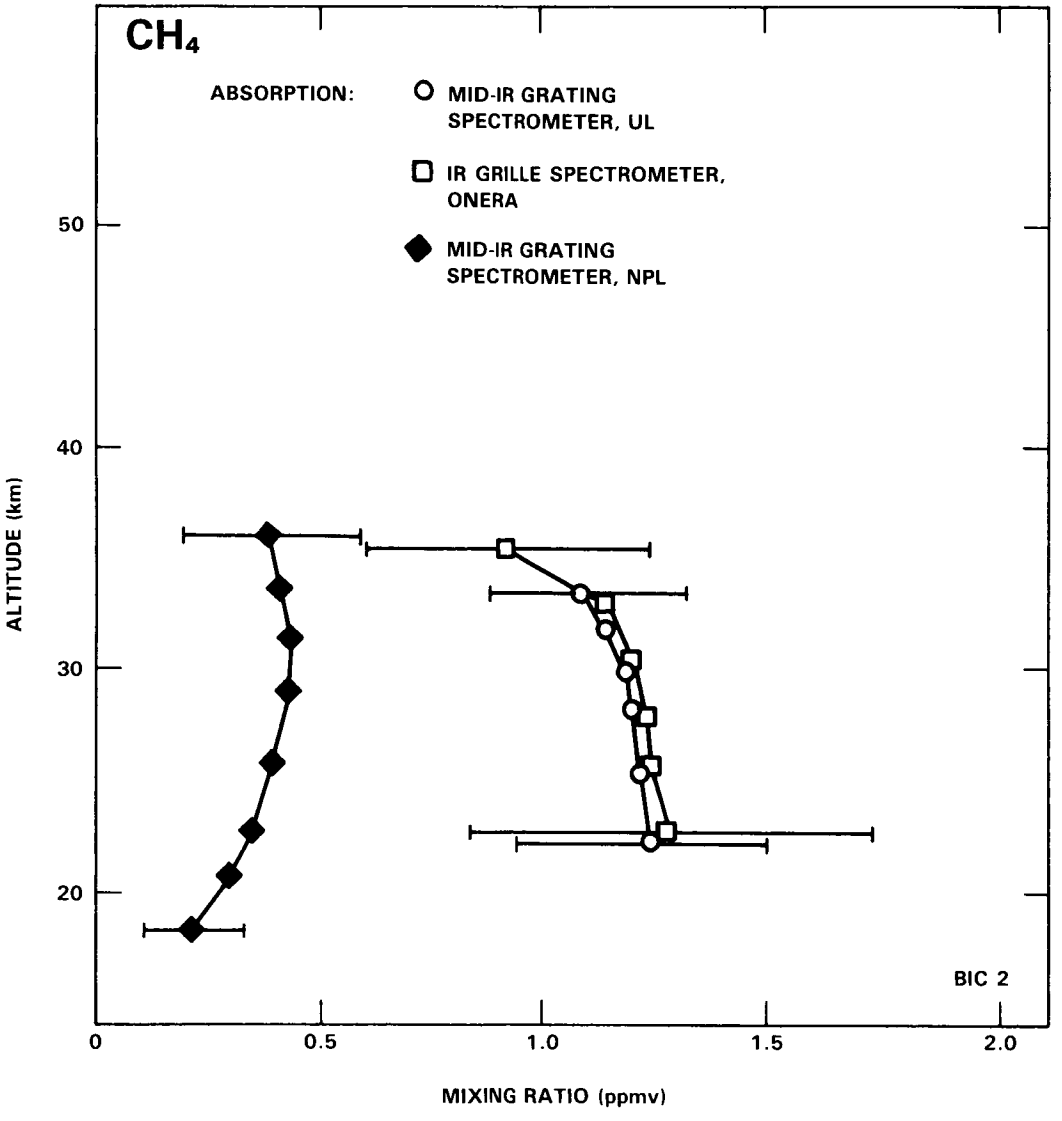

Figure C-11. The CH_4 mixing ratios measured in the Balloon Intercomparison Campaign 2. (Adapted from Zander *et al.*, [1986]).

but also a number of remote-sensing methods and instruments are capable and available to measure these species (Roscoe *et al.*, 1986).

Characteristics

BIC 1 and 2 involved not only balloon-borne instruments that obtained vertical-profile data, but also aircraft-borne and ground-based instruments that could obtain vertical-column data. Of particular concern for the species NO and NO_2 is the fact that the absorption measurements that use the sun as a source are generally made at sunrise and sunset, just at the time when the concentrations of these species are changing rapidly. Therefore, emission methods, which do not require the sun as a source and hence can be made at any time of the day, are an important complement to the more-common absorption instruments.

The suite of balloon-borne methods that were included in BIC for NO_2 were the following:

Group	Instrument	Technique	Spectral Range	BIC
UO	IR pressure modulated radiometer	emission	1570–1650 (cm^{-1})	1&2
NPL	Mid-IR grating spectrometer	emission	1600–1615	1&2
ONERA	IR grille spectrometer	absorption	1600–1608	2
AES	Visible spectrometer	absorption	437–450 (nm)	2
UT	Visible spectrometer	absorption	429–452	2
CNRS-SA	Visible spectrometer	absorption	432–450	2

The total-column data are only partially available at the present.

Results

There is still a considerable amount of analysis and scrutiny that must be done on the BIC data for the nitrogen oxides, and hence a complete picture is not yet available. However, it is clearly a very interesting and puzzling picture.

(a) *NO:* The nitric oxide observations were limited to two instruments on BIC 2: the UO emission radiometer and the ONERA absorption spectrometer. The results agree very well, $\pm 15\%$, over the 30–40 km altitude range, which is very significant since the two approaches are so different.

(b) *NO_2*: The puzzle arises for NO_2. The BIC 2 data from the four absorption instruments (ONERA in the infrared and AES, UT, and CNRS-SA in the visible) agree very well, typically within $\pm 25\%$, over the 20–40 km altitude range. Furthermore, the results of the NPL emission spectrometer are in accord with this absorption data set. However, the other emission instrument, UO's IR pressure modulated radiometer, gave results that are substantially less than the others at altitudes below about 30 km.

Although the discrepancy is only slightly larger than the (rather broad) limits of uncertainty, the pattern is similar to that seen in BIC 1 in the UO and NPL data and in the "historic" data sets that preceded BIC. Despite extensive searching for consistent reasons, none have been found. Thus far, the comparison to the vertical-column data has not shed any light.

C-4 CONCLUSIONS

Although not all of the analyses from the intercomparison campaigns have been completed, several conclusions presently stand out and are unlikely to change substantially when the picture is completed.

C-4.1 Ozone

(a) *UV absorption photometry appears to be able to measure the mixing ratios of ozone with a precision and relative accuracy of $\pm 4\%$ at stratospheric altitudes up to 40 km.*

The BOIC 3 data demonstrate that three very differently constructed and independently operated UV absorption photometers can agree to $\pm 3\%$, using a common measurement of ambient pressure and the same absorption cross section. Assuming that this one flight was not simply a fortuitous anomaly and indeed reflects approximately the current state of UV absorption photometry, then these results can be generalized as follows into an assessment of the state of the art of *in situ* stratospheric measurement capability. Pressure should be quantifiable to $\pm 1\%$. The uncertainty in the cross section is considered commonly to be about $\pm 2\%$. Therefore, UV absorption photometry should be capable of $\pm 4\%$ uncertainty relative to the cross section and $\pm 6\%$ uncertainty absolute. Since this technique has been woven deliberately as a common thread through all of the ozone intercomparisons (indeed, one of the NASA-JSC instruments has been on every campaign), it allows a common basis with which to assess the uncertainties of the other methods.

(b) *The electrochemical sondes, with state-of-the-art preflight preparation, are generally reliable to about $\pm 10\%$ overall uncertainty in the stratosphere at altitudes up to approximately 30 km, above which the readings are erroneously low.*

The extensive triplet intercomparisons of BOIC 1 and the sonde-to-UV intercomparison on BOIC 3 are the rationale for this $\pm 10\%$ figure of merit for the general monitoring-type sonde. All ozone intercomparison campaigns demonstrate the loss of sensitivity at the higher altitudes. While this figure of merit applies to the average performance, individual sondes are occasionally much better or much worse. The electrochemical sondes are "operator sensitive", as demonstrated in BOIC 1 and 3, and those of a single group can have a one-standard-deviation precision of $\pm 5\%$ in the stratosphere.

(c) *The remote solar UV absorption technique gives results that appear to be erroneously high by 5–20%.*

Every one of the recent intercomparisons campaigns have verified this pattern. Different types of solar absorption instruments operated by different groups were involved in these campaigns. Hence, the prob-

lem is very likely to be a property of the method. Since this remote solar UV absorption method could, in principle, have the same high accuracy as its *in situ* cousin, it remains an enigma why it does not.

(d) *The total vertical column of ozone can be measured to an absolute uncertainty of* $\pm 5\%$.

Several intercomparisons of ground-based methods for measuring the vertical column of ozone have shown the high precision of the Dobson and Brewer techniques and instruments. However, the balloon-borne studies summarized in this Appendix have afforded height-profile data of unparalleled accuracy. Hence, since ground-based total-column measurements were also a part of these studies, comparisons of these data to the integrations of the independent vertical-profile data provides a more sensitive test of the absolute accuracy of both approaches than was heretofore available. The analyses completed thus far provide the $\pm 5\%$ figure of merit.

C-4.2 Water Vapor

(a) *Concurrent stratospheric water vapor measurements by various balloon-borne methods differ by a factor 3 to 4, reflecting differences of 2–5 ppmv.*

While this is an improvement over the factor-of-ten differences reported over the earlier decade, the discrepancies among the results of nine different methods, if all are taken at face value, demonstrate that water vapor still remains a very difficult stratospheric constituent to measure with high absolute accuracy.

(b) *The frostpoint and photofragmentation in situ results differ consistently by 0.5 to 0.75 ppmv, with the latter being the larger values.*

This consistency is worth noting for two reasons. First, it is the only consistency among the water vapor intercomparison results. Secondly, these are the methods whereby the bulk of stratospheric water vapor data have been acquired. The consistency of the difference strongly indictates a bias in one or both of the methods, which has defied discovery thus far.

C-4.3 Other Species

(a) *Current balloon-borne measurements of* HNO_3 *by three instruments using emission spectroscopy in the same wavelength region agree within* $\pm 10\%$ *at altitudes between 22 and 30 km and* $\pm 25\%$ *between 30 and 37 km.*

In addition, these data yield column abundances above 21 km that agree to within 30% with a separate absorption measurement. It is tempting to conclude that this harmony represents the current ability to measure HNO_3 with remote sensing methods, but an unexplained serious discrepancy (factor of two) between these data and the height-profile measurements in absorption by another instrument currently prevent this.

(b) *Remote sensing techniques can determine the height profile of* HCl *over the altitude ranges 20–45 km to within* $\pm 20\%$ *and can determine* HCl *mixing ratios at 30 km to within* $\pm 35\%$.

HCl and HF pose a "best case" for remote sensing methods and BIC 2 states strongly that the best is indeed quite good. No systematic differences were observed between emission and absorption and between the two spectral regions that were employed.

(c) *Unresolved discrepancies among members of a small data set prevent an unequivocal assessment of remote methods for measuring stratospheric CH_4.*

Taking the 21 data points and their uncertainty estimates from the three instruments at face value, the methane mixing ratio at altitudes of 20–35 km lies between 0.2 and 1.5 ppmv, which is not a useful constraint.

(d) *The IR pressure modulated radiometer appear to rather consistenty give results for NO_2 that are significantly less than the results from other remote balloon-borne measurements at altitudes below about 30 km.*

This pattern was seen in both BIC 1 and 2 and in much of the "historic" data as well. Yet this emission method yields NO results that are consistent with those of other methods. The cause, if indeed it lies solely in IR pressure modulated radiometry, has resisted discovery thus far.

C-4.4 General

(a) *The intercomparison campaigns have improved the quality of the measurements of stratospheric trace gases.*

This is undoubtedly true. Specific examples of deficiencies that were discovered and corrected are the following: an error in a primary standard, an incorrectly measured length, a spectroscopic interference from chlorofluorocarbons, large and variable losses to the walls of inlet tubes at high elevations at night, a misapplied algorithm, an incorrect preception of the number of path lengths in a multipass cell, and a small persistent leak in a vacuum line. In the complex and challenging task of balloon-borne measurements of stratospheric trace gases, it is by no means surprising that some problems of this sort have occurred. It is very unlikely that they would have been discovered in the near future had the rigorous intercomparisons not been done. Many of the problems caused errors in the awkward 20–40% range, which is small enough to not be immediately obvious in the results of separate flights, but large enough to be of consequence.

C-5 FUTURE RESEARCH NEEDS

Although it is clear that the past intercomparison campaigns have been instructive and useful in assessing and improving stratospheric measurement capabilities, it is also clear that much still needs to be done in this regard. This includes, first of all, simply finishing the analyses and assessments of the large body of intercomparison data already in hand and, secondly, initiating new studies based on what has then been learned. The major short-term needs are as follows, expressed here as a series of questions:

C-5.1 Ozone

(a) *Does $\pm 3\%$ precision and relative accuracy indeed reflect the standard performance of in situ UV absorption photometry at stratospheric altitudes up to 40 km?*

While very encouraging, BOIC 3 is only one sampling of this technique's performance. Opportunities should not be missed to intercompare these instruments a few more times and with other techniques like lidar. If this performance is indeed standard, then the demonstration of that will be highly significant in future monitoring or ground-truth strategies.

(b) *What is the origin and cure for the operator sensitivity of the electrochemical monitoring sondes?*

Realistically, BOIC only represents a "best-case" assessment of the sondes, since they were lovingly prepared in the field by the leading authorities. The differences between the data of the institutions involved that occurred even under these ideal circumstances suggest that the sonde-to-sonde variation will likely be larger in a network of far-flung sites operated by a variety of people. Laboratory tests seem to be in order to seek the cause of these differences, so that network operation could have a smaller potential variance.

(c) *What are the details of the agreement between the integrals of the best height-profile data and the simultaneous total-column measurements?*

Although a preliminary examination has been done, the BOIC, and to a lesser extent the BIC, data have only just begun to be mined for this important information on these two separately measured quantities.

C-5.2 Water Vapor

(a) *What is the origin of the systematic 0.5–0.75 ppmv difference between the photofragment and frost-point hygrometers?*

Further flight investigations are not needed. Laboratory comparisons of the two methods under conditions were potential artifacts could be systematically tested would seem to be more fruitful. If these two methods were to agree eventually, they would serve as a benchmark against which the other methods, both *in situ* and remote, could be assessed in future balloon-borne intercomparisons, particularly ones in which the remote methods are optimized for water vapor.

C-5.3 Other Species

(a) *Is the discrepancy among the remote methods for measuring HNO_3 a problem with one instrument, the IR absorption grille spectrometer, or a more subtle difference between absorption and emission techniques in general?*

The laboratory calibration spectra used with the grille spectrometer are currently being examined in this regard, including effects of pressure dependence. This is an example of a need that is more broad and fundamental than this current discrepancy; namely, the remote methods, and HNO_3 in particular, could use better-quality spectroscopic data.

(b) *Since the vertical-profile data for HCl and HF appear to be very accurate, what are the details of the agreement with the total column data?*

This spectroscopic "best case" should be mined for all the information that it contains. Clearly, the stage is nearly set for an in situ vis-a-vis remote balloon-borne intercomparison.

(c) *The weight of evidence suggests that the IR pressure modulated spectrometer produces results that are too small at the stratospheric altitudes below about 30 km. Why?*

Laboratory tests are addressing this question, e.g., the possible temperature dependence of the NO_2 line shape. Emission methods for NO_2 are not plentiful and the daytime capability is important. This discrepancy is a key one.

C-5.4 General

Clearly there remains much more to be done and learned about instrument assessment via intercomparison. In addition to completing what has been started, there are the more general comparisons of *in situ* and remote methods for most of the BIC species. Furthermore, some of the key radical species, like ClO, are ripe for balloon-borne and ground-based intercomparisons. The pacing element is the existence of different techniques that address the same species with instruments that have completed the separate field-trial stage. Even with that necessary condition, the road to harmony can be long and twisting. For example, there is no one recipe for what to do when two or more methods significantly disagree.

Since both individual instrument development and tracking down the origin of will-o-the-wisp discrepancies are both arduous, time-consuming, and costly tasks, it should continue to be recognized that (a) multiple techniques are essential (and are not "wasteful" duplication) and that rigorous and blind intercomparisons under field conditions are vital (and are indeed as much a part of doing atmospheric science as is gathering data to test a geophysical hypothesis). The need is as simple as being able to unequivocally demonstrate that what we measure is correct.

APPENDIX D

MONTHLY MEAN DISTRIBUTION OF OZONE AND TEMPERATURE

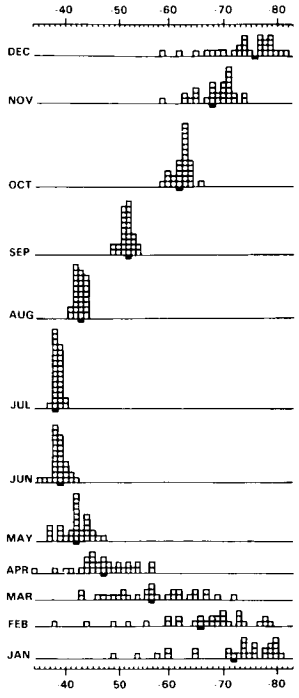

Panel Members

K. Labitzke, Chairperson

J. K. Angell
J. J. Barnett
P. Bowman
M. Corney
G. M. Keating
A. J. Krueger
A. J. Miller
R. M. Nagatani

APPENDIX D

MONTHLY MEAN DISTRIBUTION OF OZONE AND TEMPERATURE

TABLE OF CONTENTS

D-0 INTRODUCTION

This Appendix is provided because global monthly mean charts of ozone and temperature have become available, covering for the first time the height range 30 to 0.1-mbar, (approximately 24 to 64 km).

For both hemispheres these charts are given for the four mid-season months, and for the pressure levels 30, 10, 1, and 0.1 mbar for temperature, and 0.4 mbar for ozone. Charts of total ozone are provided separately. This set of charts shows clearly the very close coupling between the temperature and ozone distributions and demonstrates the influence of the large-scale planetary waves which give rise to very large longitudinal variations.

A discussion of the regular and interannual variability of temperature and ozone precedes the description of the mean state.

D-1 DATA

D-1.1 Temperature

The temperatures presented here are data which were prepared for a new REFERENCE ATMOSPHERE, published as *MAP-Handbook, Vol. 16*, by a COSPAR-SCOSTEP Task Group. These temperatures are based largely on satellite observations made by the Selective Chopper Radiometer (SCR) and the Pressure Modulator Radiometer (PMR) which both are nadir-viewing instruments which measure the infra-red emission from the carbon dioxide υ_2 band at about 15μm. These data are an average of the 5 year period 1973, 1974, July 1975 to June 1978, (Barnett and Corney, 1984). The 30-mbar temperatures are based on radiosonde observations, and are a 20-years average for the Northern Hemisphere (July 1964 to June 1984), *Meteorologische Abhandlungen, F.U.Berlin*, and a 5-years average for the Southern Hemisphere (1968 to 1972), Knittel, 1976.

D-1.2 Ozone

The ozone data presented here are based on measurements from the Solar Backscatter Ultraviolet (SBUV) Ozone Measurement System and on the Total Ozone Mapping Spectrometer (TOMS), covering the period October 1978 to September 1982, (R.M. Nagatani and A.J. Miller, personal communication).

SBUV, a nadir-viewing double monochromator, measures the radiances backscattered from the atmosphere at 12 discrete wavelengths from the 255 nm to 340 nm with a 1-nm bandpass (Heath *et al.*, 1975; McPeters *et al.*, 1984; Fleig *et al.*, 1982). Radiances between 255 nm and 306 nm are used in the ozone profile inversion, while radiances between 312 nm and 340 nm are used to calculate total ozone. In order to calculate backscattered albedo, the ratio of backscattered radiance to extraterrestrial solar irradiance must be measured daily by deploying a diffuser plate. The scan-to-scan precision of the albedo measurement is very high, a few tenths of a percent. A detailed discussion on the accuracy of these data is given in Chapter 8.

A comparison of results of different experiments measuring ozone during the period November 1978 - May 1979 is under preparation and will be published as a MAP-Handbook; (J.R. Russel *et al;* Middle Atmosphere Composition Revealed by Satellite Observations). Only one example is given here, pointing out the differences between LIMS and SBUV during January and February 1979, Figure D-1. It should be recalled that February 1979 was a month with a major stratospheric warming.

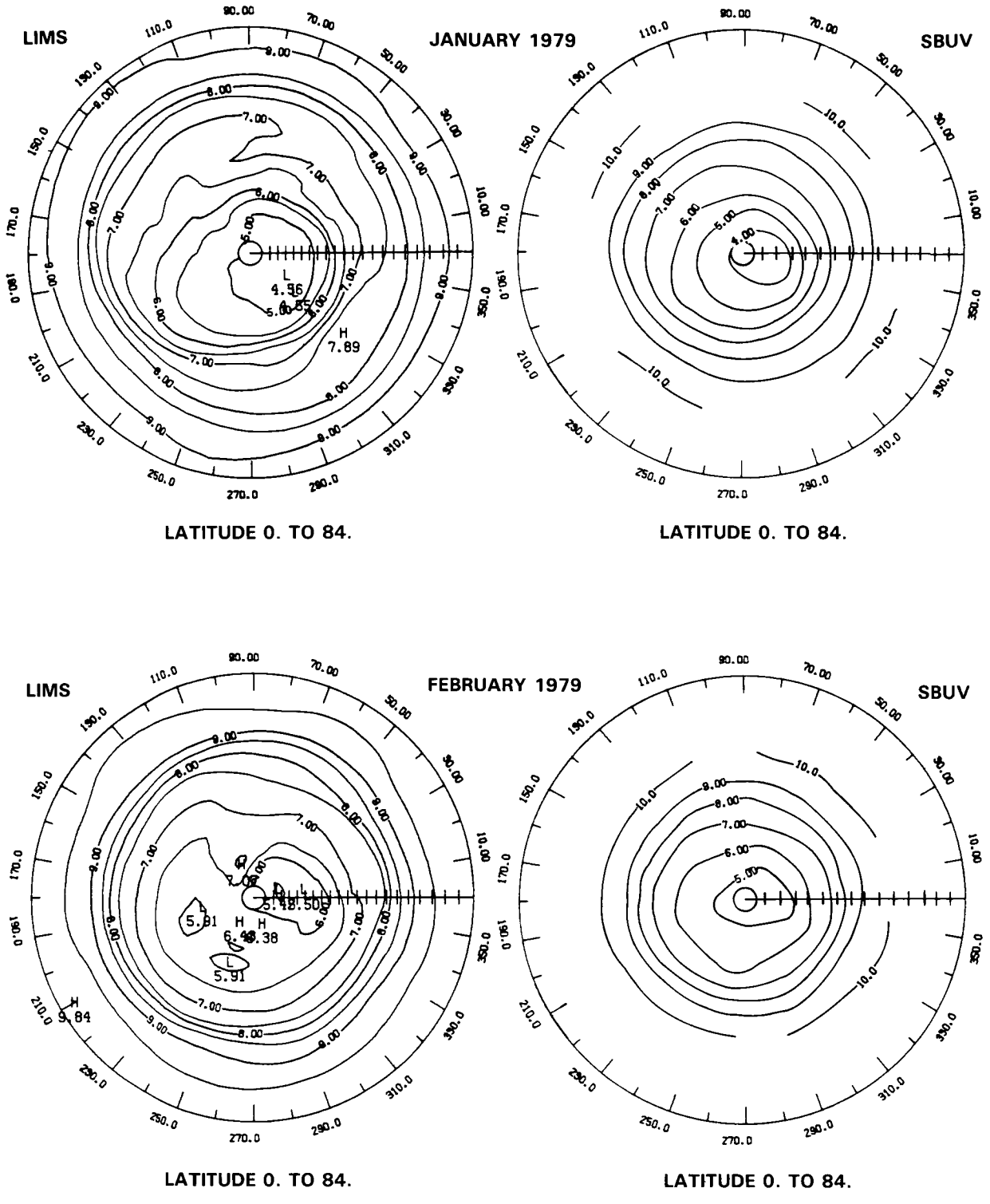

Figure D-1. Comparison of monthly mean values of ozone mixing ratio(ppmV) as measured at the 10-mbar level by LIMS and SBUV: upper part = January 1979; lower part = February 1979. (Russell *et al.*, 1986.)

Looking at the maps for January, we see that the overall placement of the major trough-ridge systems agree quite favorably, but LIMS shows a bit more detail than does SBUV. For example, the secondary high values at about 70 °E and 330 °E are not evident in SBUV. This is, most likely, due to the increased vertical resolution of LIMS as discussed in Chapter 8. A similar situation exists for the February maps with the LIMS indicating more detail in the high latitudes at about 100 °E, but with general agreement of the patterns. In general, the SBUV data as presented in Section D-4 tend to show a more detailed structure in the ozone distribution for the regions above and below the maximum of the ozone mixing ratio.

TOMS is similar in concept to the SBUV with two important distinctions, (Fleig *et al.*, 1982). The first is that it is limited to total ozone only. The second is that it incorporates a side scan feature with approximately 50×50 km field of view. This coupled with the several hundred thousand data points obtained in a single day provides considerable detail not generally observed by the nadir only SBUV.

Error sources of TOMS are very similar to those for SBUV and comparison with total ozone measurements from Dobson stations indicates that TOMS is lower, on average, by about 6%.

D-2 REGULAR COMPONENTS: ANNUAL, SEMI-ANNUAL AND QUASI-BIENNIAL WAVES

D-2.1 Temperature

D-2.1.a Annual and Semi-Annual Waves

The SCR/PMR monthly mean temperature values have been Fourier analysed at each latitude and pressure level to obtain the annual mean and the amplitude and phase of the annual and semi-annual cycles, Figure D-2. The phase is the month of the maximum, such that 1=January 1, 1.5=January 16, 2=February 1, etc. There are some very marked hemispheric differences, notably:

a) At 80 °N there is a maximum amplitude of the annual cycle of 26K at 2.5 mbar, the corresponding maximum at 80 °S is much stronger (35K) and at a lower altitude (11 mbar), Figure D-2.b. This is because in the middle stratosphere summers are warmer and winters colder over the Antarctic than over the Arctic, as shown in Section D-4.

(b) A semi-annual wave in temperature is found over both polar regions, Figure D-2.c. The one in the Arctic is 2-3 times larger than the one in the Antarctic. The latter is as large as the one over the equator.

(c) The annual mean, Figure D-2.a, shows a minimum at 50 °S, 1 mbar, and a corresponding weaker minimum at 60 °N. This is a general feature of the Southern Hemisphere winter, occurring to a smaller extent in the Northern Hemisphere, and clearly strong enough to affect the annual mean.

The annual wave reaches its maximum mostly during the summer solstices. The phase of the equatorial semi-annual wave in temperature is equinoctial and propagates downward, Figure D-2.c, while the first maximum of this wave in the polar regions falls in winter. This confirms earlier analyses (van Loon *et al.*, 1972).

In general the hemispheres are remarkably similar and six months out of phase above about 0.3 mbar (56 km). It will be shown in Section D-4 that the two hemispheres are significantly different especially in winter. However, changes from summer to winter are so large by comparison that the annual cycles appear to be very similar.

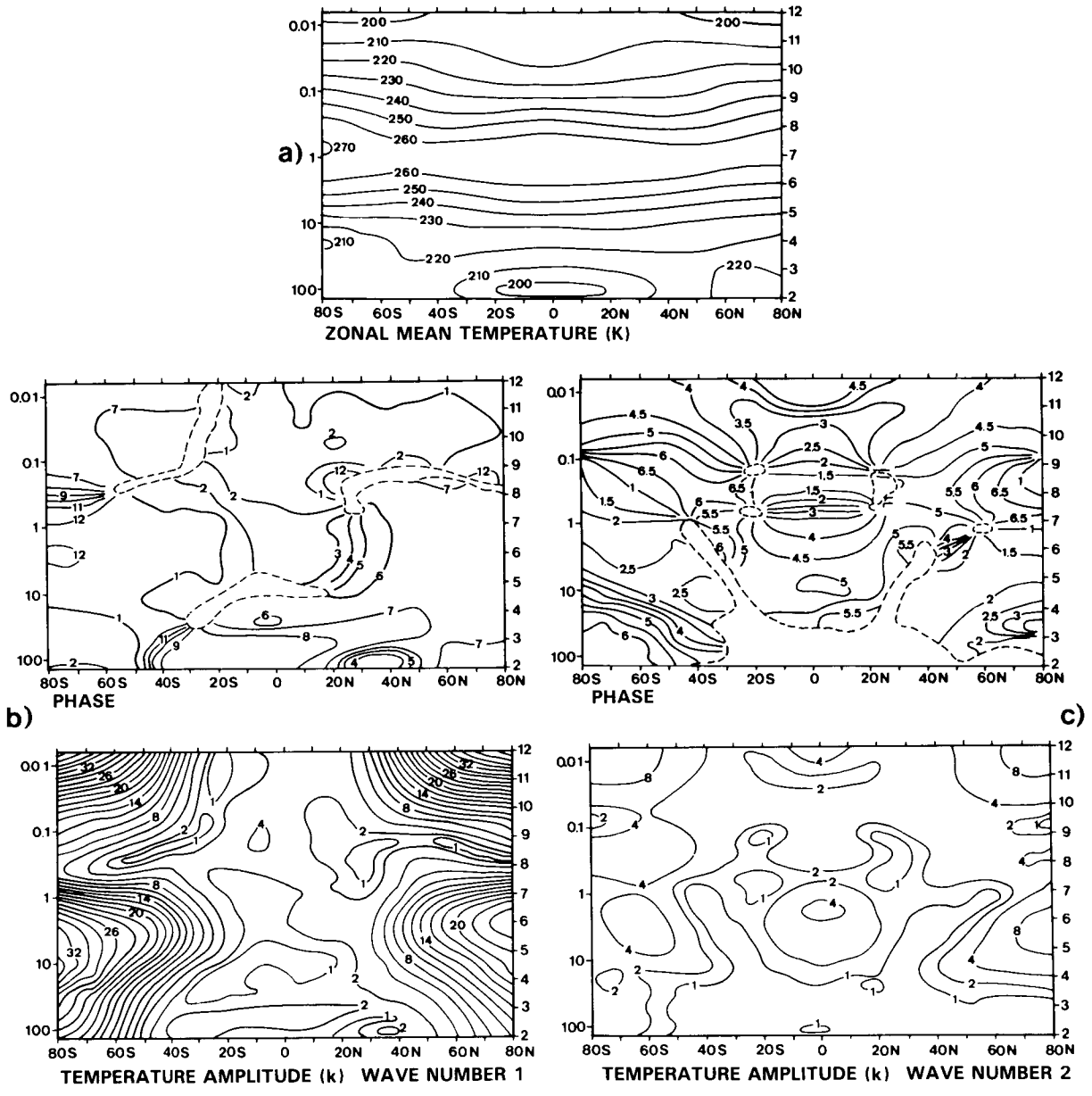

Figure D-2. Components of the annual variation of temperature (K) derived from the SCR/PMR combined means.

a) annual mean;
b) phase and amplitude of annual cycle;
c) phase and amplitude of semi-annual cycle; (Phase is given as the month of maximum temperature, e.g. 12 means December 1. (Barnett and Corney, 1984.)

Because of the existence in winter of large longitudinal temperature variations which are repeatedly in the same phase for several months, a given longitude might be consistently warm at some levels and cold at others, leading to annual and semi-annual cycles which differ markedly from those of the zonal mean. This is shown for the annual wave by means of horizontal maps of the 30-mbar level, Figure D-3, (Labitzke, 1977).

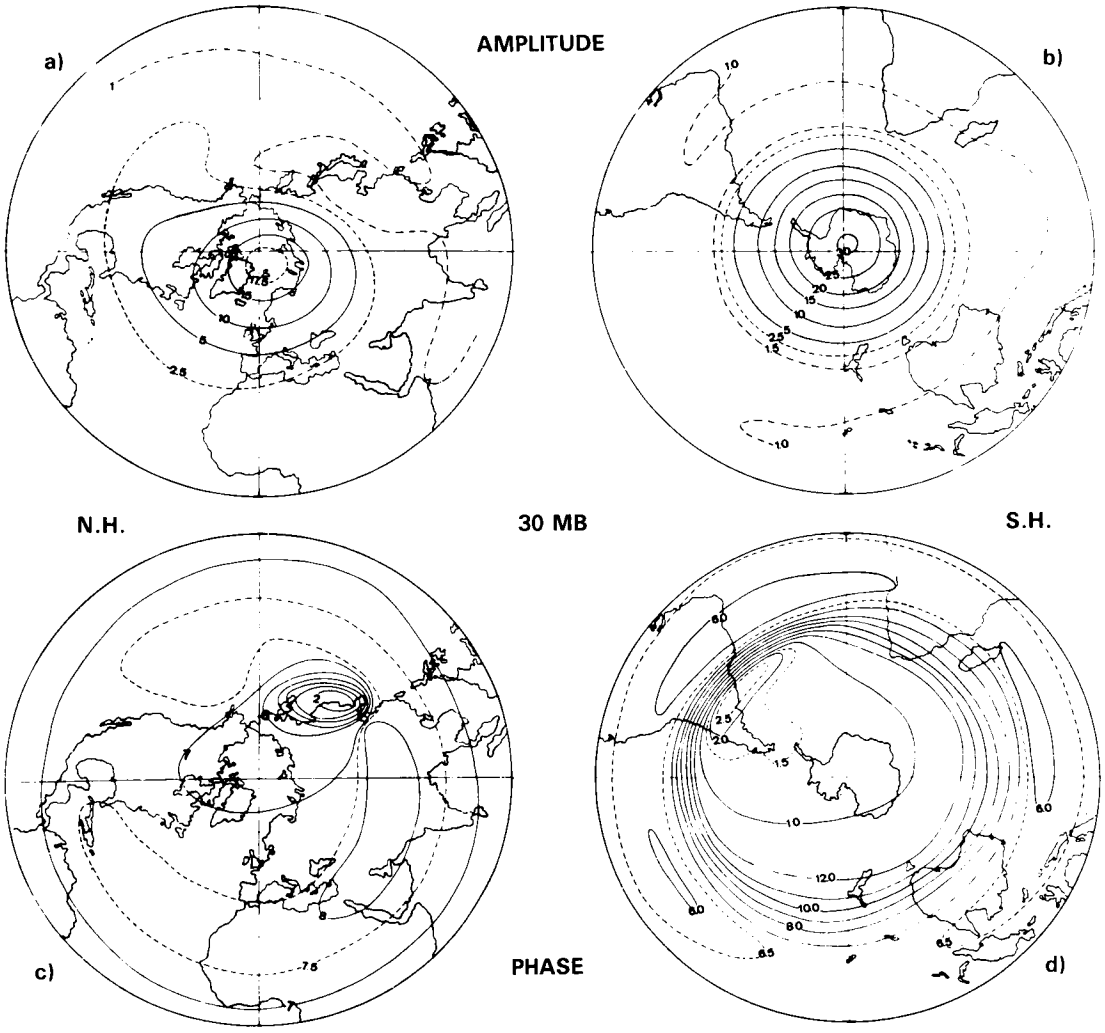

Figure D-3. a) and b): amplitude (K); c) and d) phases (month of maximum) of the annual temperature wave at the 30-mbar level. (Labitzke, 1977.)

Over the Northern Hemisphere large changes in phase occur within the regime of the Aleutian anticyclone. Here, the amplitude of the annual wave is small because it is warm in winter as well as in summer.

Over the Southern Hemisphere large phase changes occur over the southern part of South America. Here the maximum of the annual wave is reached late because the "Final Warmings" are starting over the Australian sector of the Antarctic and the transition into summer is finished last over South America, (Knittel, 1976). A similar pattern can be seen in the total ozone data, (cf. Section D-2.2 and Figure D-8).

The variations around the globe of annual and semi-annual cycles should be largest at 60–70 °S or N where planetary wave amplitudes are largest (cf. Section D-3), and Figure D-4 shows the temperature amplitudes and phases (time of maxima) for 64 °N as a function of longitude and pressure. Phase variations are relatively minor (except where the amplitudes are very small). However there are large amplitude variations, e.g. from 16 to 26 K at 3 mbar for the annual cycle, 5 to 8.3 K at 5 mbar for the semi-annual cycle.

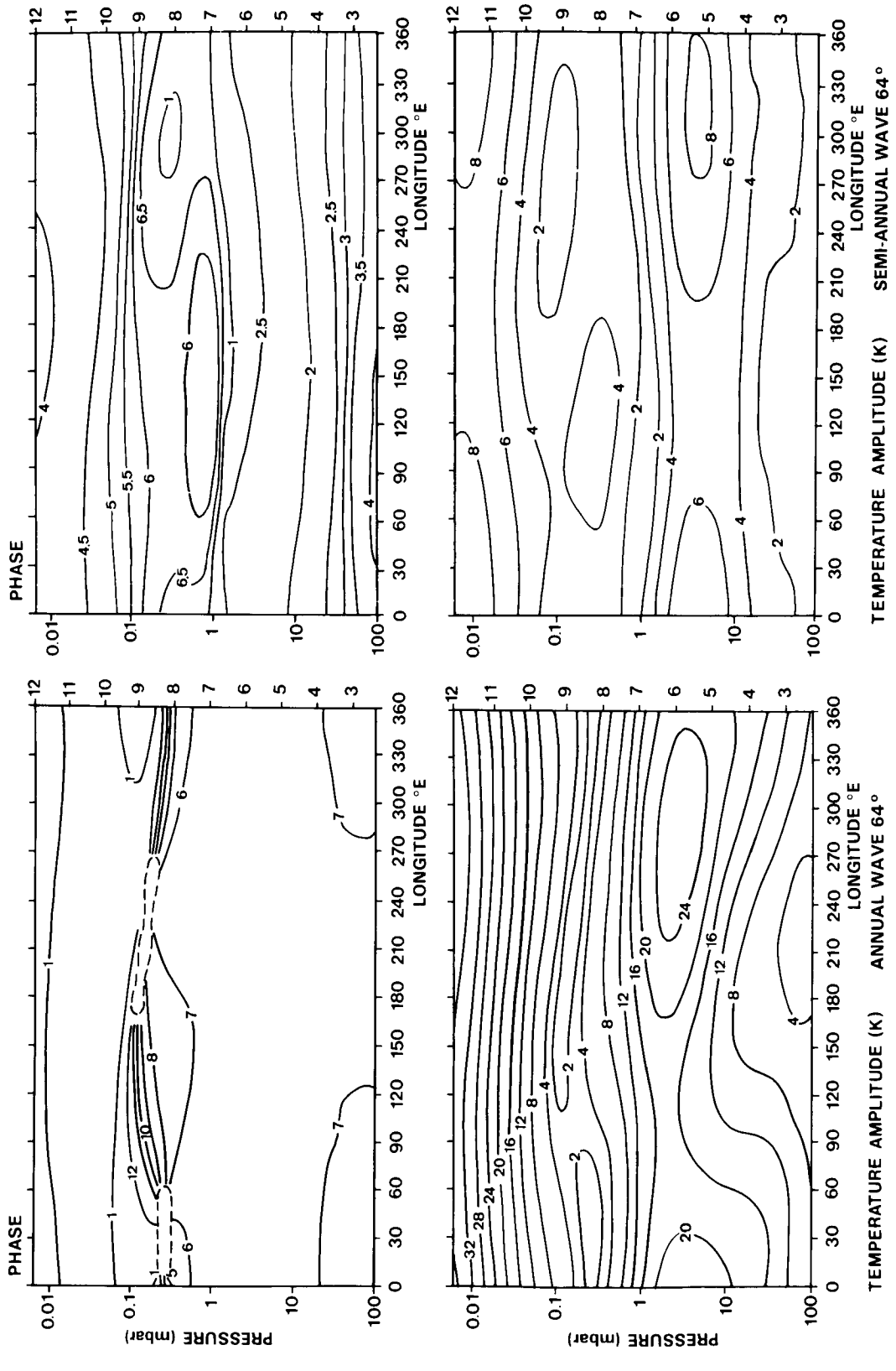

Figure D-4. Amplitude (K) and phase (month of maximum) of the annual and semi-annual cycles of temperature at 64°N as functions of longitude and pressure. (Barnett and Corney, 1984.)

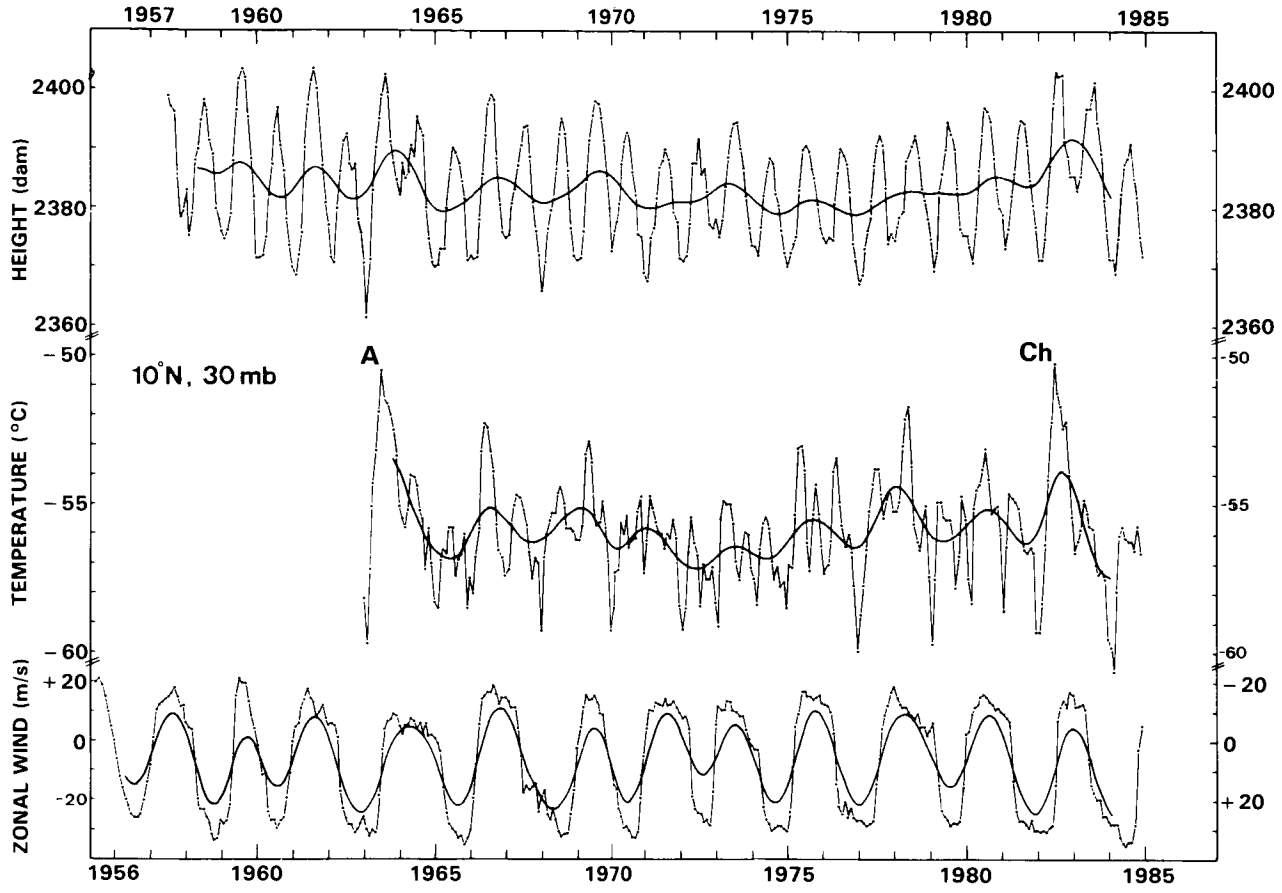

Figure D-5. Zonal means of monthly mean 30-mbar heights (a) and temperatures (b) for 10°N, (thin lines), together with a curve giving the filtered data (13-point filter to remove the annual and semi-annual wave, after Naujokat, 1981) (c) Monthly mean zonal winds over the equator based on different radiosonde stations, thin lines, (Naujokat, 1986) and filtered as above, heavy lines. (Labitzke and Naujokat, 1986.)

D-2.1.b Quasi-Biennial Wave (QBO)

The well known Quasi-Biennial Wave in the winds over the tropics has been discussed already in Chapter 6.

But this wave is also clearly pronounced in the temperatures of the stratosphere. This has been shown before, e.g., by Newell *et al.*, 1974. Here we show an update for the 30-mbar level at 10°N, Figure D-5. The zonal mean heights (curve a) and zonal mean temperatures (curve b) are plotted for each month and also after being filtered in such a way that the annual and semi-annual components are removed. These data are based on daily hemispheric analyses, using largely radiosondes, (F.U. Berlin). These series of data can be compared with a series of monthly mean winds over the equator (curve c) which is based on an analysis of Naujokat (1986), using different radiosonde stations close to the equator. Obviously, higher temperatures lead to westerlies and lower temperatures to easterlies, in accordance with the thermal wind relationship, (Reed, 1962).

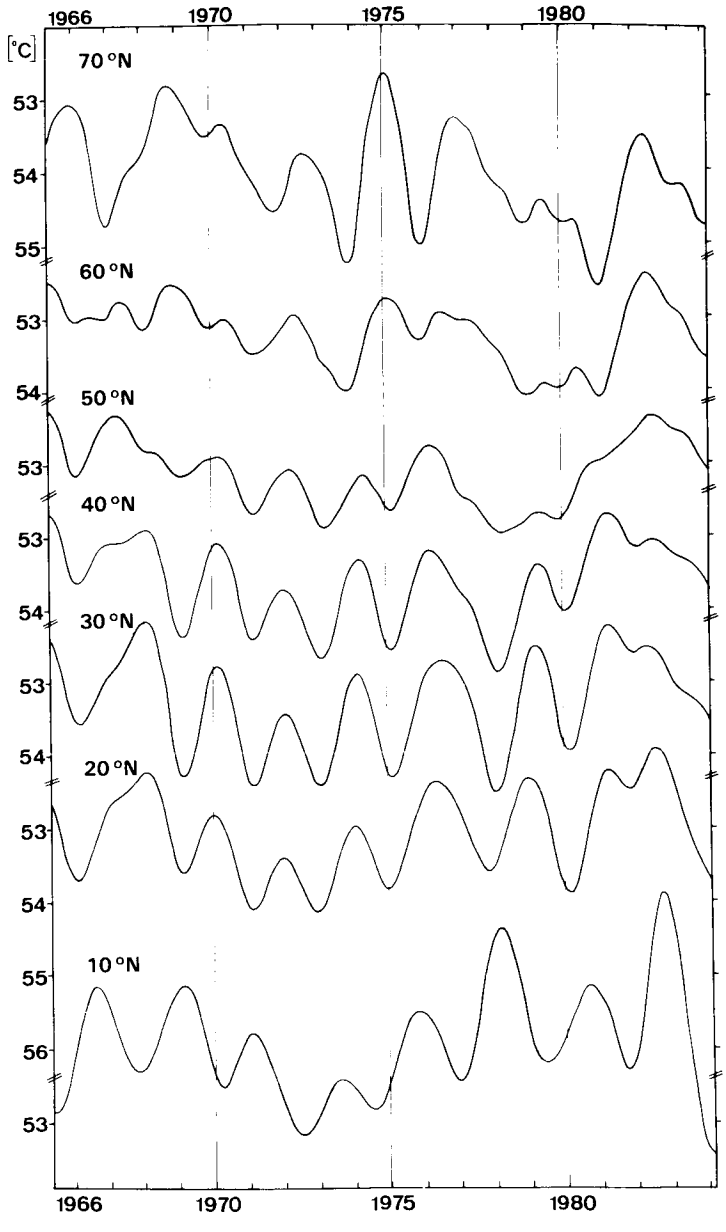

Figure D-6. Zonal mean 30-mbar temperatures (filtered to remove the annual and semi-annual wave) from 10 to 70°N. (Labitzke and Naujokat, 1986.)

The horizontal structure of the QBO in the temperature is shown for the 30-mbar level in Figure D-6. Here only the filtered temperatures are given, for every ten degrees latitude between 10 and 70 °N, (Labitzke and Naujokat, 1986).

The QBO in the 30-mbar temperatures is very well developed, with largest amplitudes at 30 °N. The amplitudes are leading at 10 °N, while they appear to be well in phase from 20 to 50 °N. Further north the signal is less clear, although evident, and the phase appears to be out of phase here, compared with the region 20 to 50 °N.

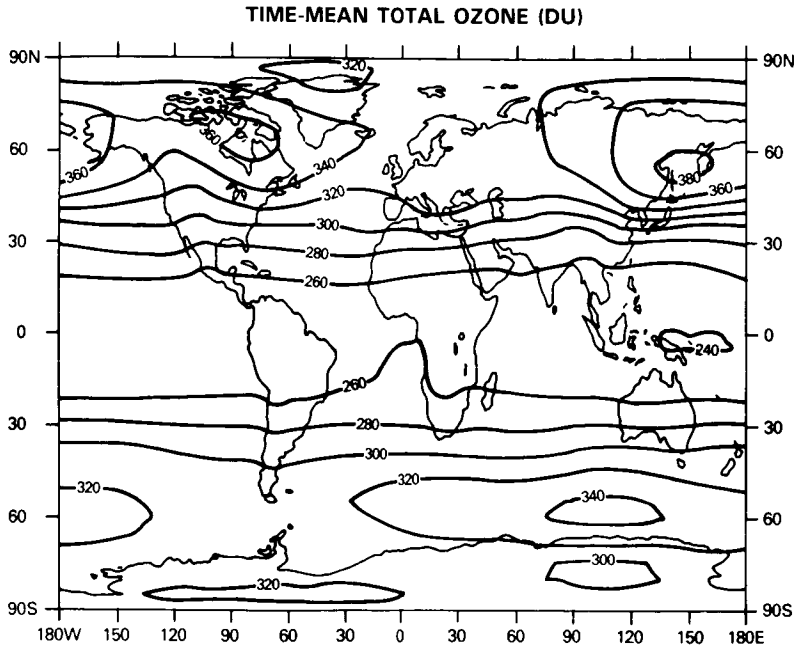

Figure D-7. TOMS time-mean total ozone, computed for the 4 year period 1978–1982, (Dobson units). (Bowman and Krueger, 1985.)

D-2.2 Total Ozone

D-2.2.a Annual and Semi-Annual Wave

Based on a global climatology of total ozone data as measured by the TOMS (Bowman and Krueger, 1985) global maps of the time-mean total ozone and of the amplitudes and phases of the annual and semi-annual waves are presented in Figures D-7–D-9. (For a detailed discussion of the quality of the data see Bowman and Krueger, 1985.)

In the Northern Hemisphere the amplitude of the annual wave in ozone increases nearly uniformly away from the equator, Figure D-8. There are two regions with large annual variations (fraction of variance) over the Sea of Okhotsk and the Canadian Arctic. Both are located coincident with maxima in the time mean ozone, Figure D-7. The minimum of the annual wave is located at about 10°S. The maximum of the annual wave in the Southern Hemisphere is also co-located with the maximum in the time mean. There is a very low minimum in the annual wave straddling the Antarctic penninsula. This coincides with the region of large phase changes of the annual wave of the 30-mbar temperature, as discussed above, Figure D-3.d. Obviously, the spring build up of ozone is weak here due to the delayed Final Warmings.

The annual harmonic in the Northern Hemisphere reaches a maximum in late winter to early spring. The earliest maximum occurs where the amplitude is largest, over the Sea of Okhotsk. The phase of the annual harmonic increases southward across the equator so that maxima in the Southern Hemisphere also occur in winter to early spring. Phase is difficult to determine near the poles, but there appear to be large differences between the annual harmonics in the Arctic and Antarctic regions. The annual harmonic explains a large fraction of the variance over much of the earth, especially in middle and high latitudes of the Northern Hemisphere and in the Northern Hemisphere tropics.

The amplitude, phase, and fraction of the variance explained by the semi-annual harmonic are shown in Figure D-9. The amplitude is flat throughout the tropics and generally increases towards the poles. At high latitudes the semi-annual wave becomes very unreliable due to the large amount of missing data and is probably largely an artifact of the analysis method. Hopkins (1975) has suggested that the semi-annual wave in the tropics results from the absorption of equartorward propagating planetary waves at the zero wind line. The total ozone shows no evidence for a maximum in the amplitude of the semi-annual harmonic in the tropics, although such a feature could occur locally in the vertical.

The maximum in the fraction of the variance explained over Asia appears to be associated with a real maximum in the amplitude of the semi-anual wave, but the maxima over the Indian Ocean stretching toward the west and over the Weddel Sea appear to be caused by the absence of a strong annual harmonic, Figure D-8.

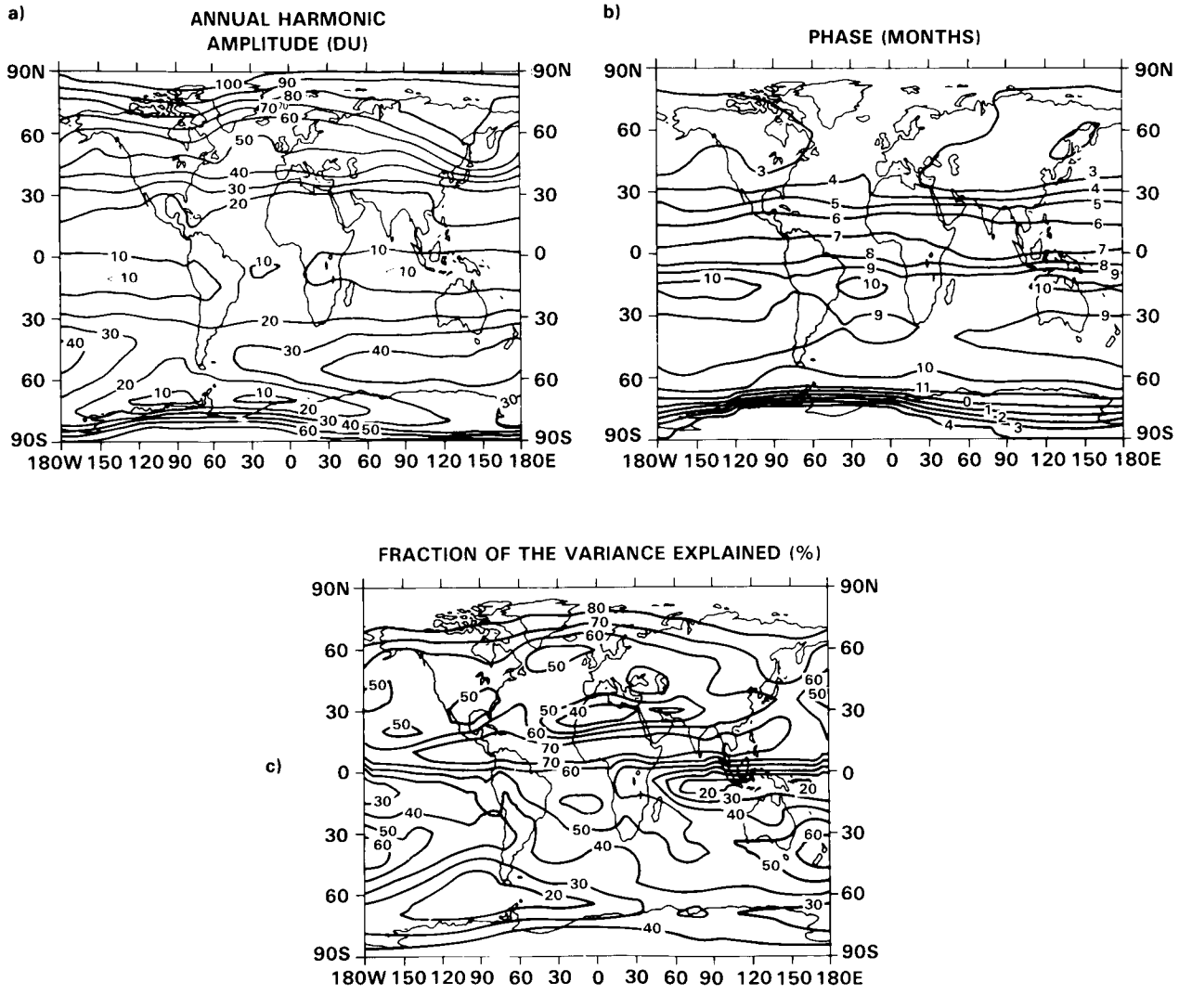

Figure D-8. (a) Amplitude (Dobson units),(b) Phase (months of maximum, after 1 January), and (c) fraction of the total variance explained by the annual harmonic (%). (Bowman and Krueger, 1985.)

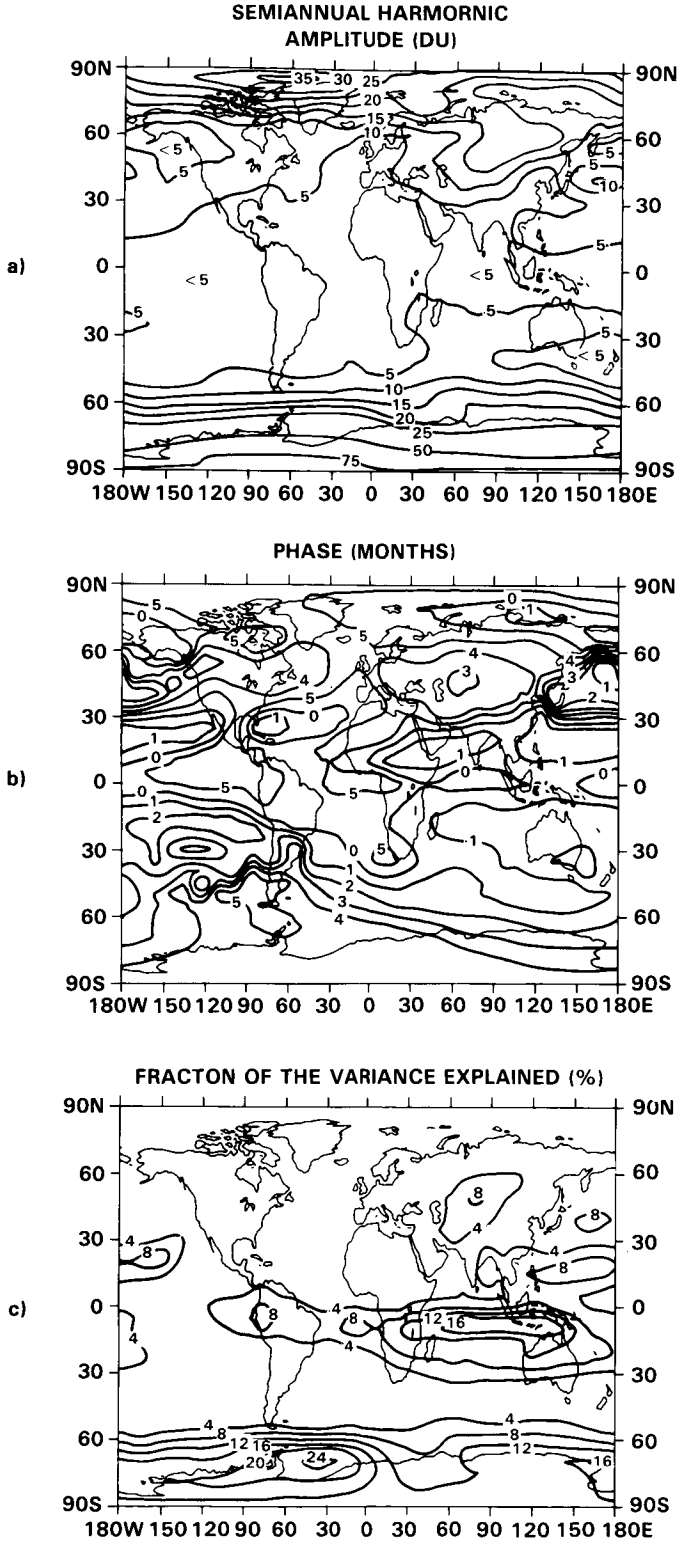

Figure D-9. (a) Amplitude (Dobson units), (b) Phase (month of first maximum after 1 January), and (c) fraction of the total variance explained by the semi-annual harmonic (%). (Bowman and Krueger, 1985.)

D-2.2.b Quasi-Biennial Wave

The quasi-biennial variation in ozone is thought to be related to the quasi-biennial variation in equatorial zonal winds (Oltmans and London, 1982). Shown in Figure D-10 (Tolson, 1981) is the biennial component of the zonal mean total ozone variation based on 7 years of Nimbus 4 BUV data. The contour interval is 2 Dobson units with the solid lines positive and the shaded area with dashed lines negative. However, since the variation is only quasi-biennial, the phase indicated in Figure D-10 will change with time. There is also evidence that the period of the quasi-biennial variation may vary somewhat with latitude (Hilsenrath and Schlesinger, 1981) and that the latitude of maximum quasi-biennial variation may vary somewhat with time (Hasebe, 1983).

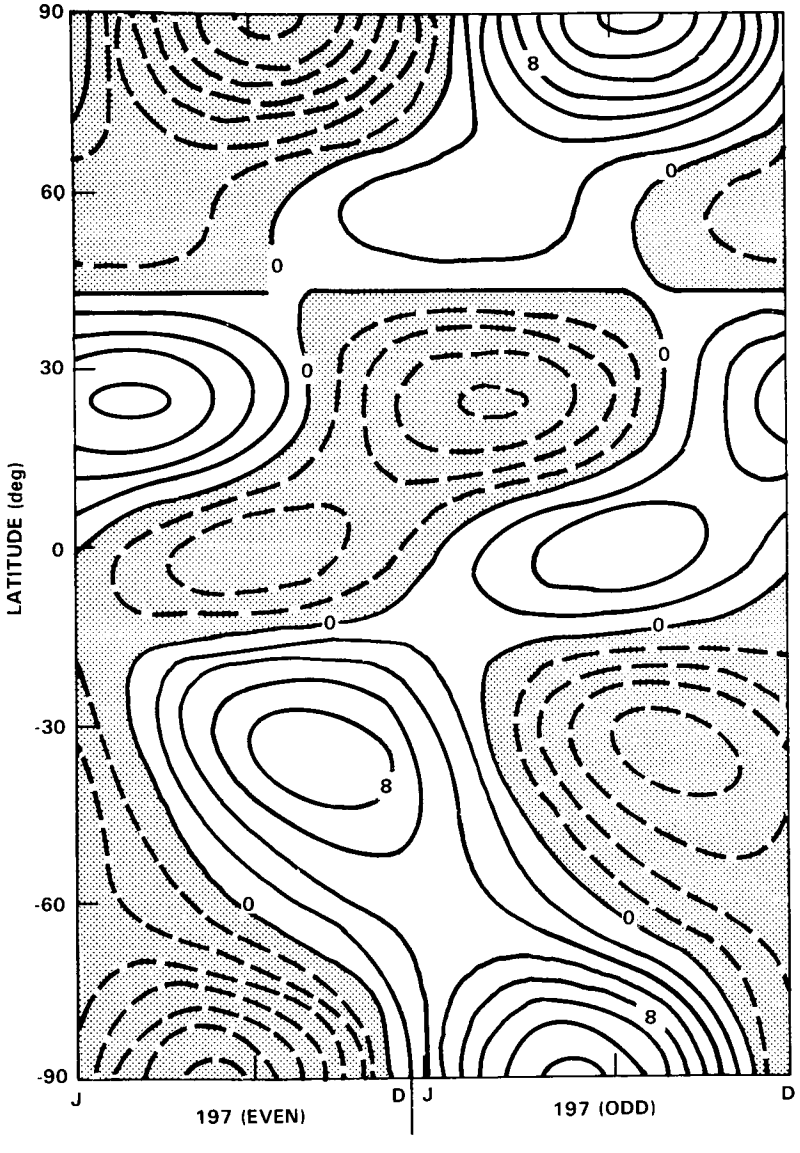

Figure D-10. Biennial component of zonal mean total ozone variation based on 7 years of Nimbus 4 BUV measurements. Contour interval is 2 Dobson units; solid lines are positive and shaded area negative. (Tolson, 1981.)

D-2.3 Vertical Ozone Profiles

D-2.3.a Annual and Semi-Annual Waves

Using data from the ozonesonde and Umkehr stations listed in Table D-1, standard harmonic analyses have been computed for the mandatory pressure surfaces of 700, 500, 300, 200, 150, 100, 70, 50, 30, 20 and 10 mbar from ozonesonde data, and for layer 6 (centered at 12 mbar), layer 7 (centered at 6 mbar), layer 8 (centered at 3 mbar) and layer 9 (centered at 1.5 mbar) from Umkehr data. Insofar as possible, stations were chosen about 15 degrees of latitude apart.

Table D-1. List of stations used in analysis of annual, semi-annual and biennial ozone components. Umkehr records have been terminated at the end of 1981 because of the biasing of the measurements by El Chichon volcanic eruption in the spring of 1982. (J.K. Angell, personal communication.)

Station	Latitude	Record Length
Ozonesonde		
Resolute	75°N	1967-1983
Churchill	59°N	1974-1983
Hohenpeissenberg	47°N	1967-1983
Kagoshima	31°N	1969-1983
Natal	6°S	1980-1981
Aspendale	38°S	1966-1981
Syowa	69°S	1966-1982*
Umkehr		
Edmonton	54°N	1970-1981
Arosa	47°N	1965-1981
New Delhi	28°N	1965-1981
Singapore	1°N	1981
Brisbane	27°N	1965-1981
Aspendale	38°S	1965-1981
Invercargill	46°S	1973-1981

* No data between 1974 and 1978.

OZONE AND TEMPERATURE DISTRIBUTIONS

Figure D-11 shows the annual amplitude of ozone in units of partial pressure (left) and percent of the average value at the given surface (middle). The latter is presented because at upper levels the values become very small and patterns are hard to discern otherwise. These results from ground-based data (Table D-1) are supplemented on the right by an analysis of the 4-year SBUV data set available from Nimbus 7, expressed in percent. The latter, while based on a limited time interval, has better spatial coverage than the ground-based data.

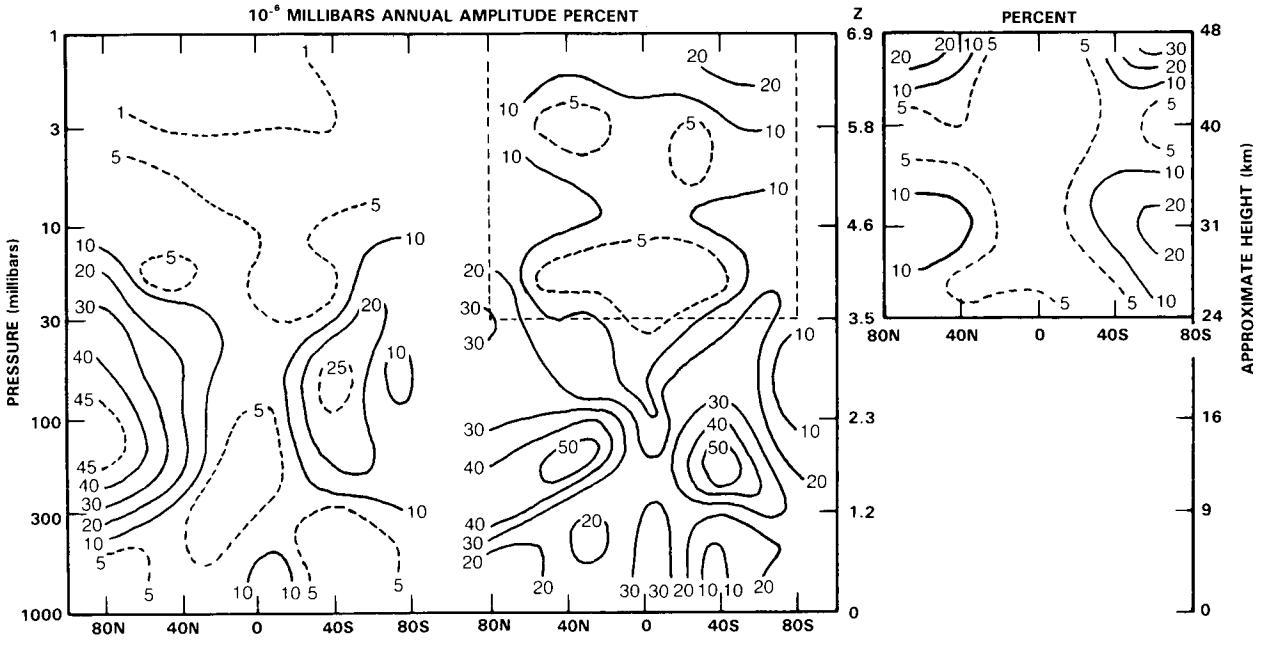

Figure D-11. Annual amplitude of ozone as a function of pressure and latitude from ground-based data and from SBUV data (right). The amplitude in units of mixing ratio (ppmv) is obtained by dividing the partial pressure in units of 10^{-6} mbar by the ordinate pressure in mbar; (J.K. Angell, private communication.)

In terms of partial pressure, the annual amplitude of ozone is a maximum between 100 and 200 mbar in north polar latitudes. In middle latitudes of the Southern Hemisphere the amplitude is indicated to be only half as large between 50 and 100 mbar. In these units the annual amplitude is not the same in the two hemispheres, either in magnitude or distribution. In the case of percent, however, the annual amplitude is a maximum near the tropopause, with a value of 50% at about 40 degrees latitude in both hemispheres. Here, the amplitude in the two hemispheres appears more nearly the same. At upper levels both ground-based and satellite data indicate a consistent analysis with a relative minimum in the tropics and the minimum at about 3 mbar in the vertical. At 1 mbar the SBUV shows a larger amplitude in the polar areas by about 10%.

The phase of the annual cycle determined from ground-based data is shown in Figure D-12. At the specified latitudes the phase is given as the time of maximum ozone. In middle and polar latitudes of the Northern Hemisphere the time of maximum ozone varies from June near the surface to March in the 30–100 mbar layer. At 30°N, however, there is little change in time of ozone maximum between the surface and low stratosphere. At 1–3 mbar the ozone is a maximum near the winter solstice, in agreement with SBUV results. The sparse Southern Hemisphere data suggest a similar variation with height, but 6 months out of phase.

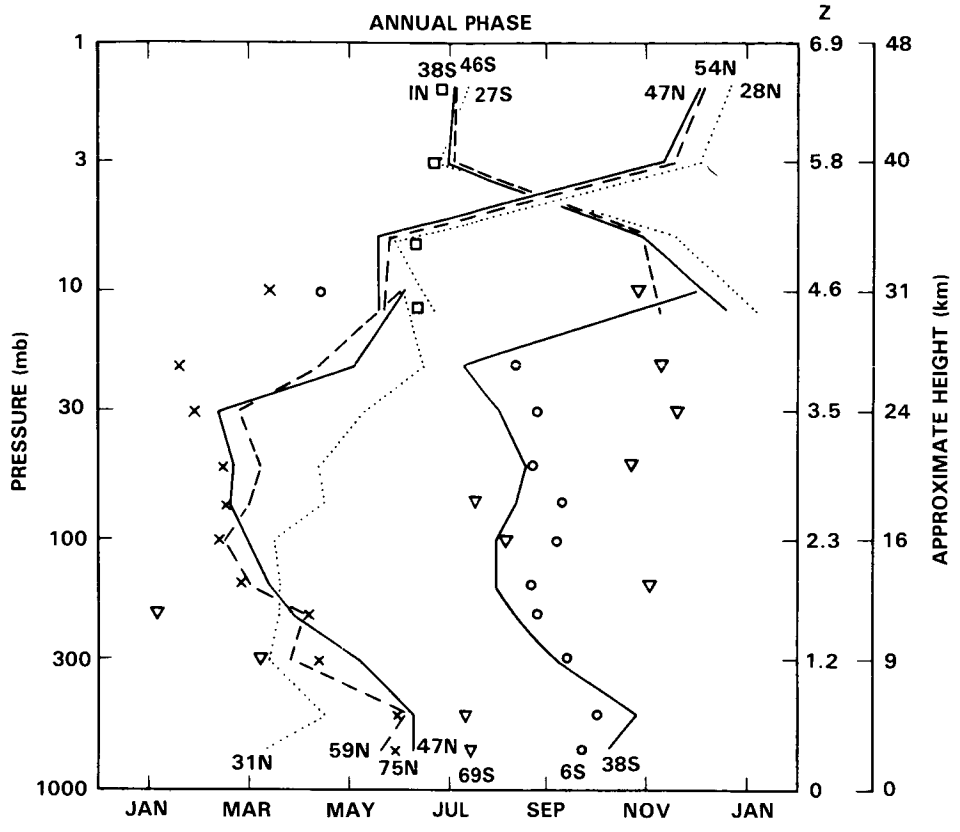

Figure D-12. Times of maximum ozone values for annual component. Latitude of ozonesonde and Umkehr stations indicated at bottom and top; (J.K. Angell, private communication.)

In Figure D-13 results for the semi-annual component are presented. The values tend to be much smaller than for the annual component. In terms of partial pressure, a polar maximum is observed in both hemispheres in the 30–100 mbar layer, with evidence for another maximum in the equatorial zone above 30 mbar. In the case of percent, the ground-based data indicate a maximum in the tropics of at least 12% between 100 and 300 mbar. At higher altitudes the semi-annual amplitudes are small and different from those calculated from the SBUV data. In the latter, a tropical maximum of about 5% is observed between 1 and 3 mbar, together with polar maxima of about 10% in the same layer, whereas polar maxima are not apparent from the ground-based data.

The phase of the semi-annual cycle determined from ground-based data is shown in Figure D-14. In the Northern Hemisphere the time of the earlier ozone maximum varies from about May near the surface to March at the tropopause. From the tropopause to the stratopause there is no compelling evidence of a change in phase. Southern Hemisphere phases are so scattered it is difficult to say whether semi-annual variations are in phase or out of phase in the two hemispheres. With such small amplitudes, the confidence of the phase depiction is rather low.

D-2.3.b Biennial Wave

In Figure D-15 are presented the results for the biennial (not quasi-biennial) component. In the Southern Hemisphere only the ozonesonde station at Aspendale has a record of sufficient length for consideration

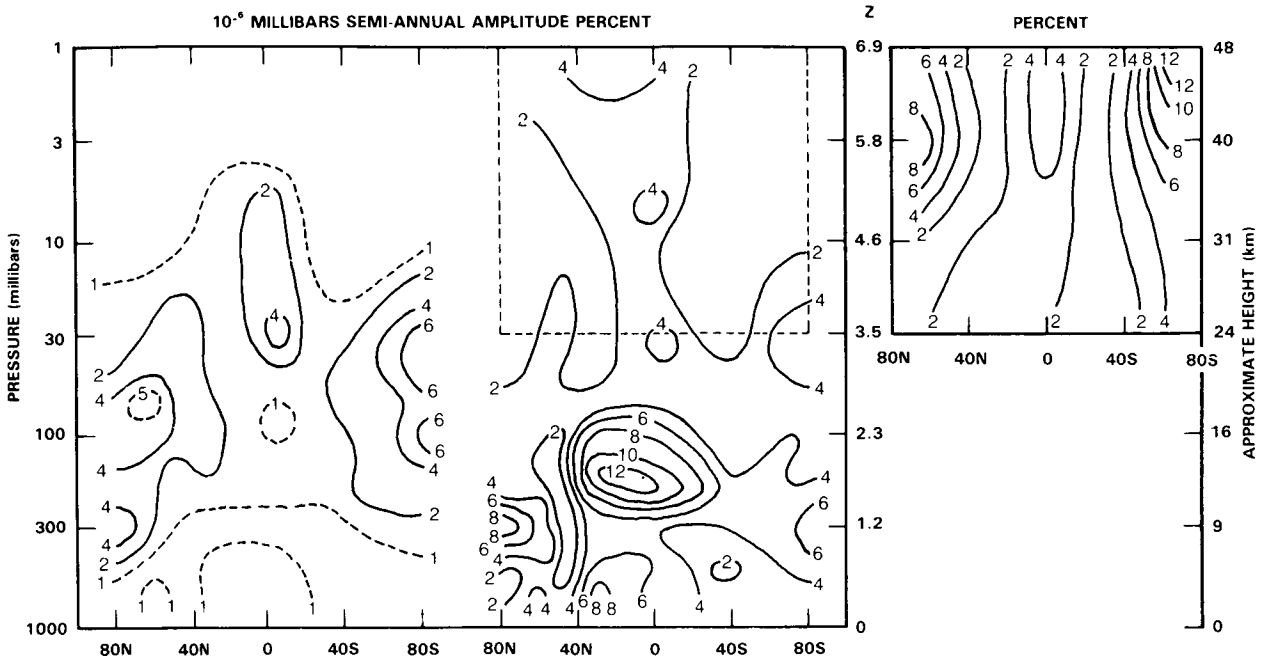

Figure D-13. Same as Figure D-11 for semi-annual component.

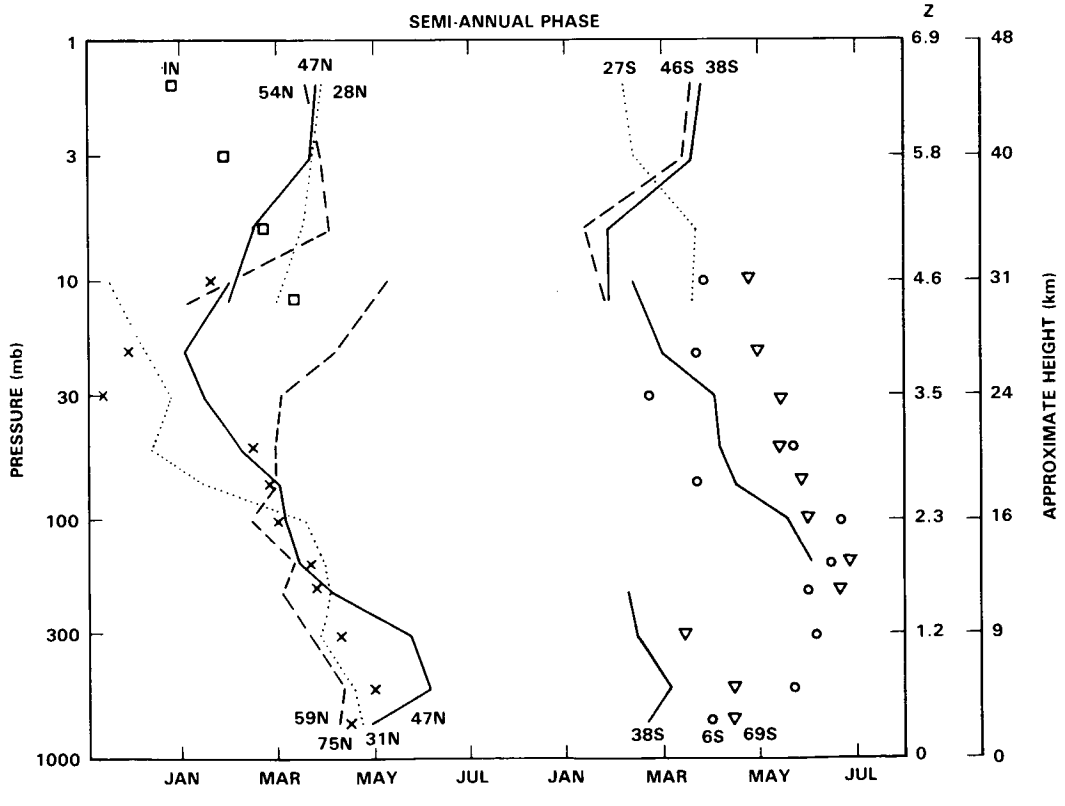

Figure D-14. Same as Figure D-12 for semi-annual component.

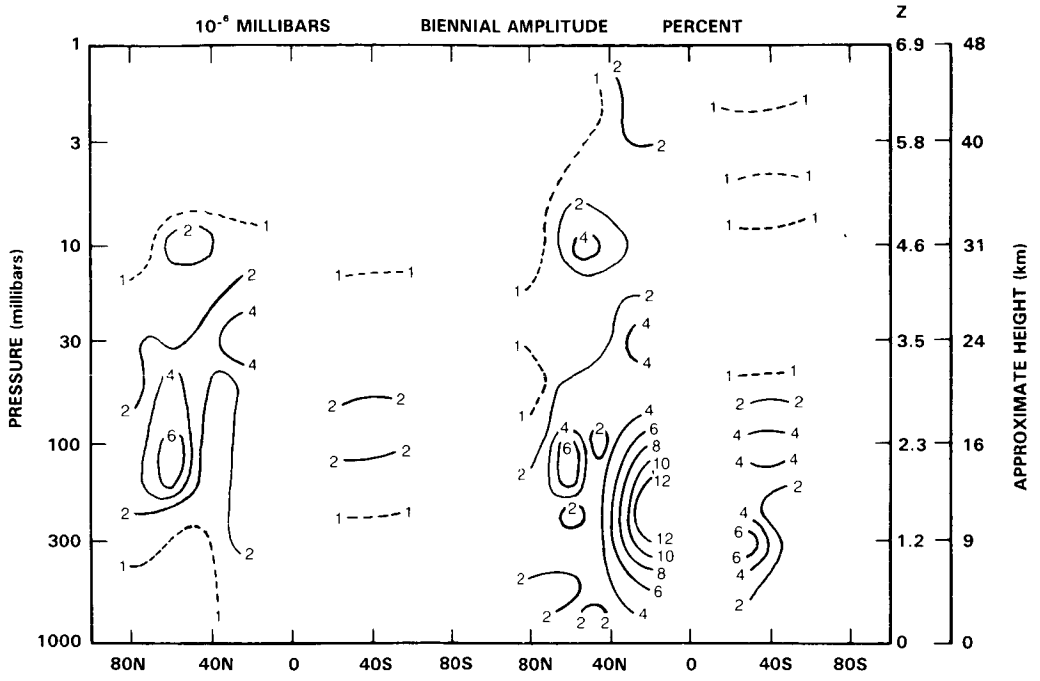

Figure D-15. Same as Figure D-11 for biennial component.

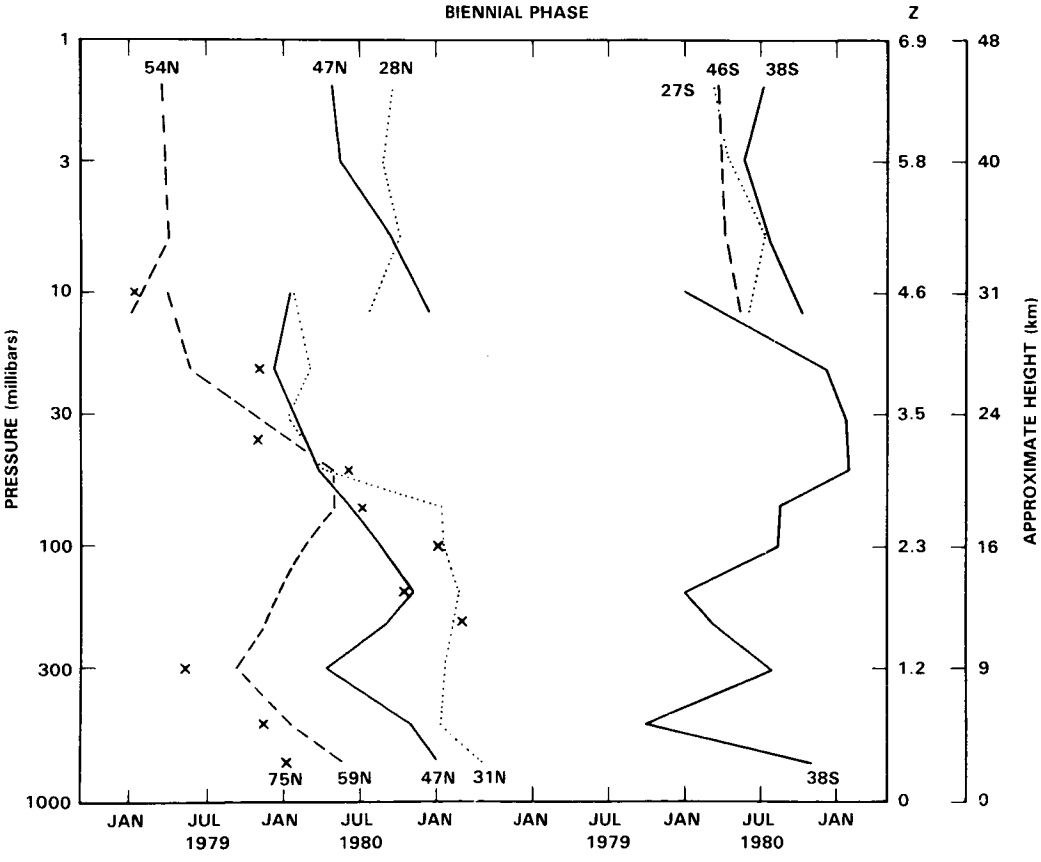

Figure D-16. Same as Figure D-12 for biennial component.

here. The absence of long-term records in the tropics makes the analysis particularly difficult. In terms of partial pressure, a maximum is observed around 100 mbar in northern mid-latitudes, but in the case of percent the maximum is indicated to be in the tropics between 100 and 300 mbar. With such small amplitudes the confidence of the biennial phase depiction in Figure D-16 is also low. In general, the ozone amount has been greater in even years (1980) than in odd years (1979) in both hemispheres.

D-3 INTERANNUAL VARIABILITY

The climatology which will be presented in Section D-4 is based on global satellite data and forms a very useful basis for climatological studies. When using such climatologies it is important to be aware of the interannual variability which in the middle atmosphere is particularly large during the northern winters and southern springs.Then the standard deviations of the monthly mean temperatures are particularly large.

D-3.1 Temperature

D-3.1.a Lower Stratosphere

For the discussion of the interannual variability of the lower stratosphere a long-term series of temperature data is available for the Northern Hemisphere. This series is based on daily maps derived largely from radiosonde data,(Free University Berlin). For the Southern Hemisphere only data of single radiosonde stations are available.

Variability of the Polar Region

For a comparison of the two polar regions, the monthly mean temperature data for 90 °N and 90 °S are shown in Figures D-17 (update of Figure 1 of Naujokat , 1981) and D-18 (Figure 1b, Labitzke and Naujokat, 1983) in the form of frequency distributions. The time-scale is shifted by 6 months so that both polar regions can be compared easily.The monthly mean values for the North Pole are based on daily 30-mbar charts derived from radiosonde data, while for the South Pole a radiosonde station is available directly.

The main features to be noted and which have been pointed out previously (e.g., Barnett, 1974; Labitzke, 1974; Knittel, 1976) are:

(1) In the *lower stratosphere* the interannual variability during the northern midwinters, Figure D-17, is much larger than during the southern midwinters, Figure D-18, due to the major midwinter warmings which take place only during the northern winters; the largest interannual variations over Antarctica are observed during late spring,i.e., October and November when very intense "Final Warmings" bring about the transition into summer.
(2) The variability in the middle stratosphere is very small in summer when the planetary waves of the troposphere cannot propagate upwards into the stratosphere due to the prevailing easterly winds. This is true for both polar regions.

Standard Deviations of Monthly Means

Figure D-19 gives the latitudinal distribution of the standard deviations of the 30-mbar temperatures for the Northern Hemisphere. This drawing indicates clearly where the interannual variability is smallest: at 60–70 °N, *in summer*; as well where it is largest: at 80–90 °N in *winter* and *spring*.

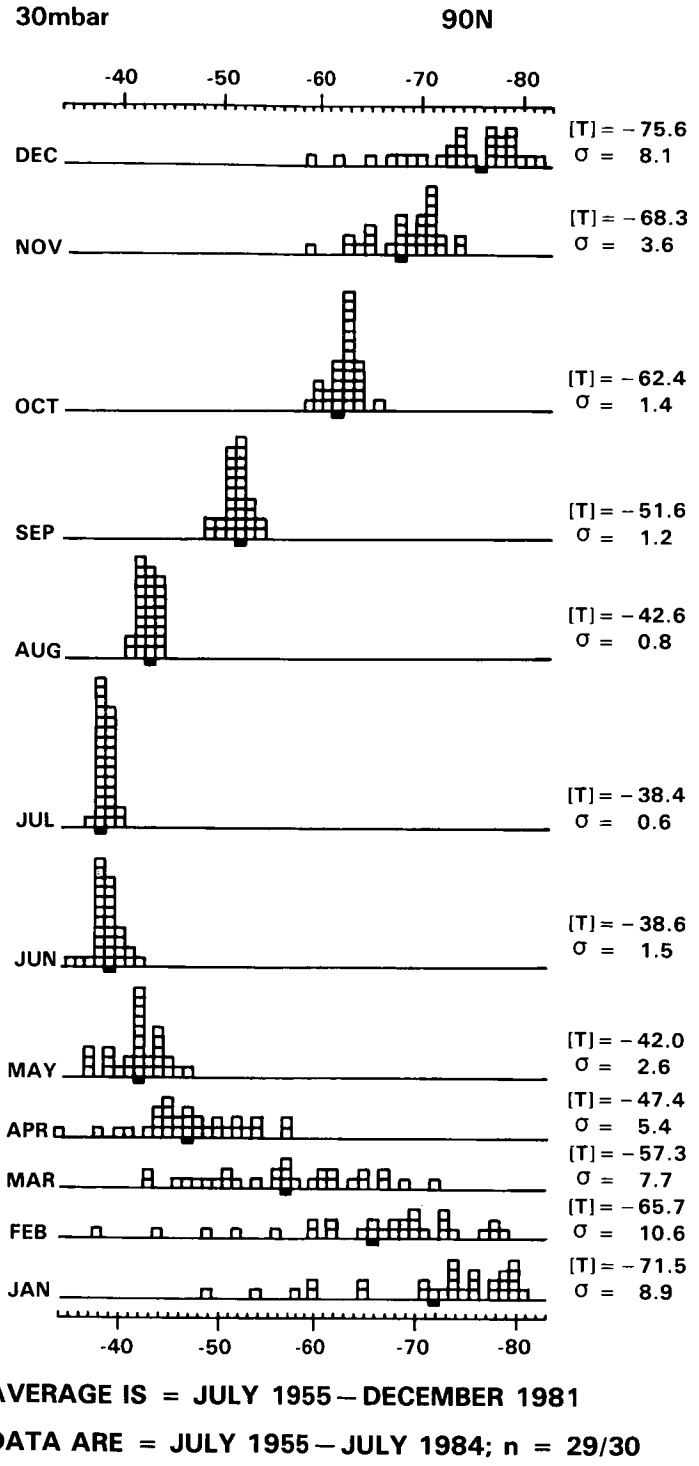

Figure D-17. Frequency distribution of the monthly mean 30-mbar temperatures (°C) over the North Pole, for the period July 1955 through July 1984. Interval is 1 K. The long-term average T is given at the right hand side of the picture, together with the standard derivation, and T is also marked as a black box in the frequency distribution. (Update of Figure 1, Naujokat, 1981.)

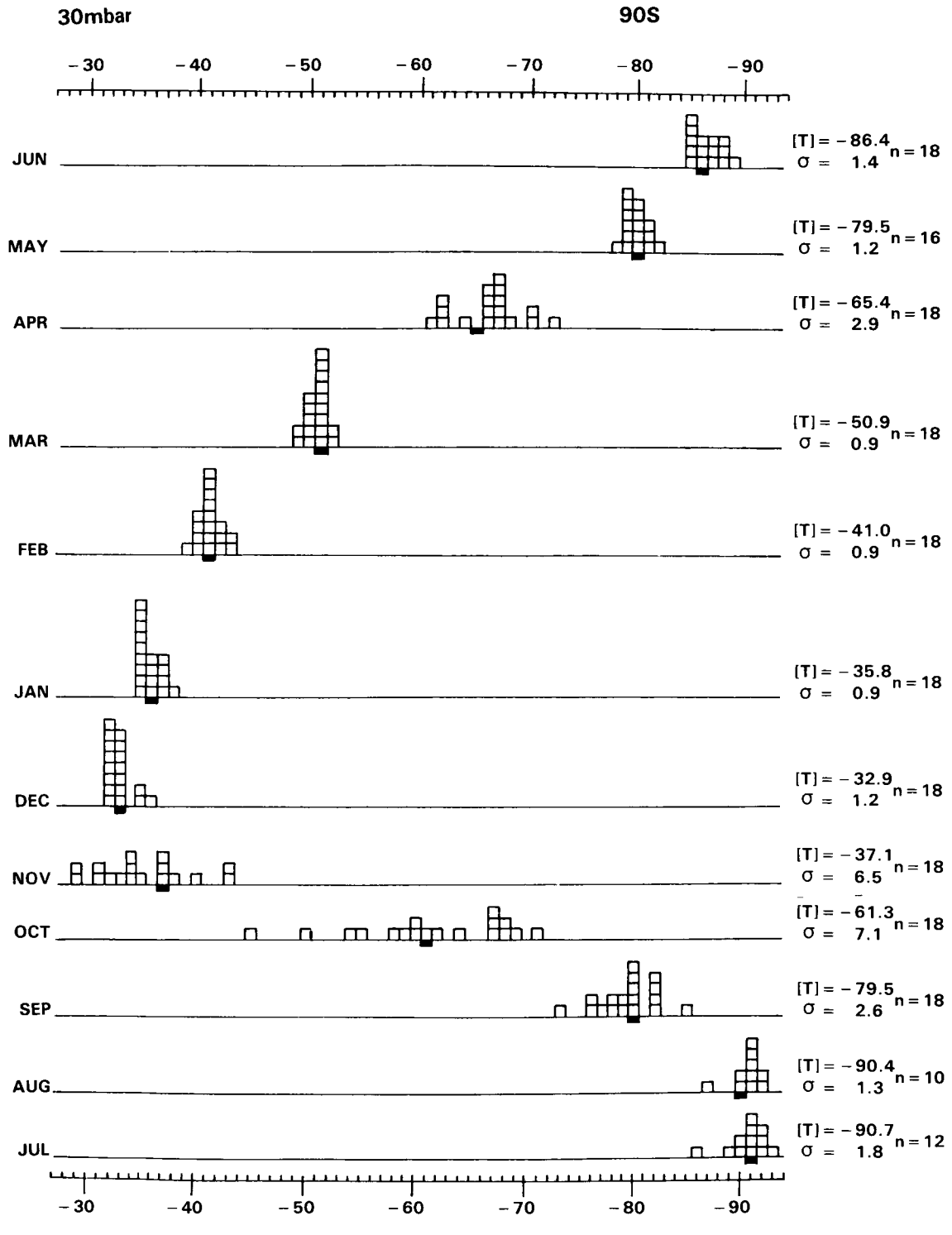

Figure D-18. Frequency distribution of the monthly mean 30-mbar temperatures (°C) over the South Pole, for the period 1961–1978. (Based on radiosonde data, not all months are complete, because of the very low temperatures in winter.) Otherwise same notation as in Figure D-17 (Figure 1b, Labitzke and Naujokat, 1983.)

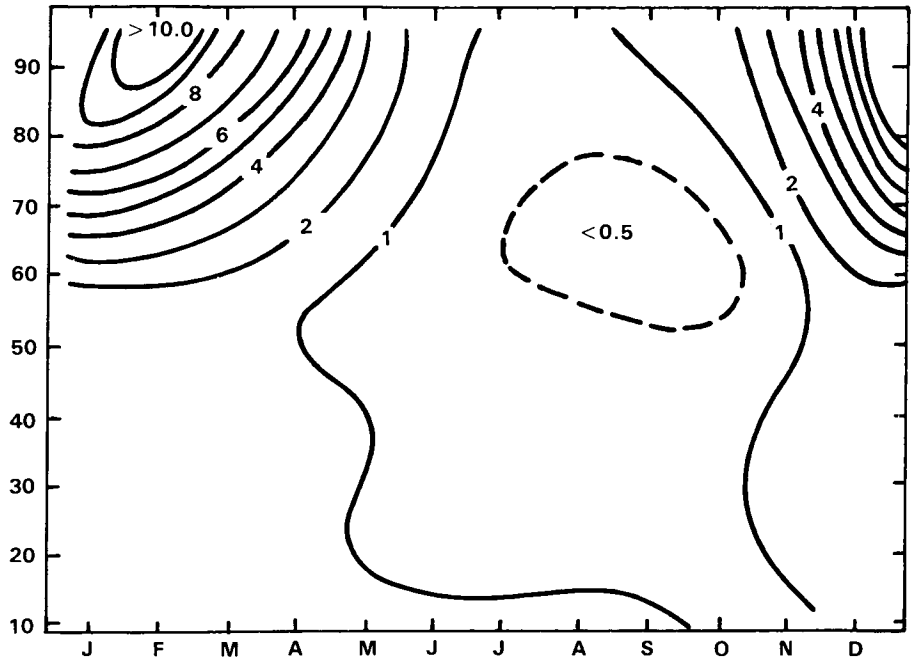

Figure D-19. Latitudinal distribution of the standard deviations (K) of the monthly mean 30-mbar temperatures throughout the year. (90°N: July 1955–December 1981, n = 26 or 27 years; 80–10°N: July 1964–December 1981, n = 17 or 18 years.) (Figure 3, Labitzke and Naujokat, 1983.)

D-3.1.b Upper Stratosphere

The discussion of the interannual variability of the upper stratosphere will concentrate on satellite data which are available for this region since the winter of 1970/71.

Variability of the Polar Regions

The same features as discussed for the lower stratosphere can be found in the upper stratosphere, namely highly disturbed northern winters. This is shown with daily zonal means of radiances at 80 deg.N from different upper stratospheric channels of the SCR (Selective Chopper Radiometer) and PMR (Pressure Modulated Radiometer) (Nimbus 4, 5, 6), Figure D-20. They are compared with the 10- and 30-mbar temperatures over the North Pole, (Labitzke, 1983). The data-set used for the preparation of the climatology, (as presented in Section D-4), includes most of these winters.

This survey over 8 northern winters illustrates distinctly the high variability of the stratospheric winters with the different timing and intensity of the stratospheric warmings. The "major warmings(*)" are connected with a break-down of the stratospheric polar vortex, followed by a "late winter cooling", thus influencing the whole winter season. (Definition of major warmings see, e.g., Labitzke, 1981).

In contrast, the southern winters show very little variation from year to year over the polar region. The temperature minimum is reached in early winter and therefore in the *upper stratosphere* the transition into summer starts much earlier over the Antarctic than over the Arctic. This is shown in Figure D-21, where the march of radiances at 80°N and 80°S is compared, (Labitzke, 1977).

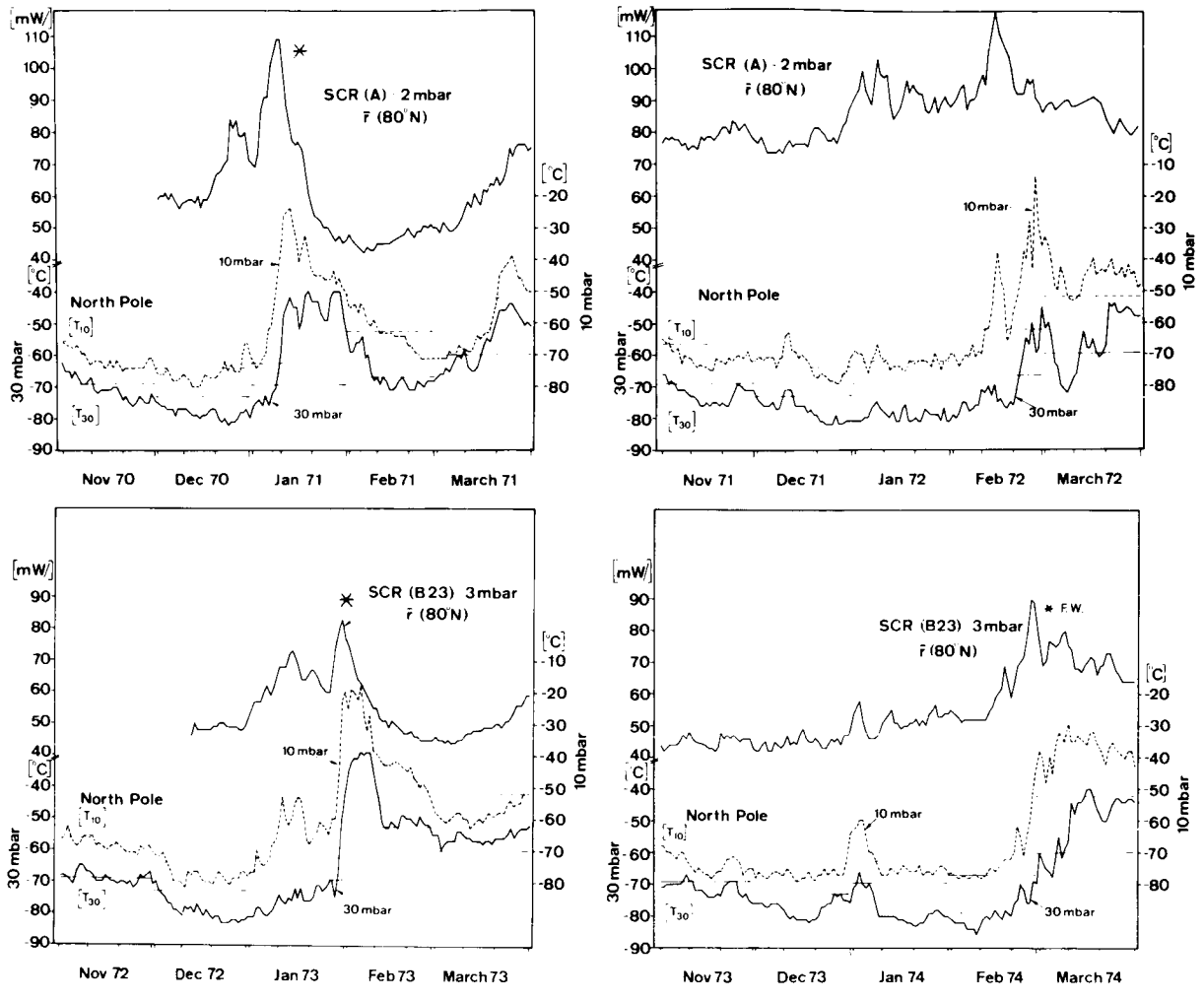

Figure D-20. Course of radiances or temperatures over the polar region: zonal mean radiances at 80°N in ($mW(m^2sr(cm^{-1})^{-1}$) or (K), i.e., equivalent blackbody temperature, from different experiments representing the upper stratosphere as indicated. Temperatures (°C) of the 10- and 30-mbar level over the North Pole. (Radiance data: Oxford University, U.K.; temperature data: Free University Berlin.) (Labitzke, 1983.)

These differences are most obvious in spring. Therefore, the 30- and 1-mbar temperature charts of March/N.H. and September/S.H. are compared in Figure D-22.

For the N.H. the temperature distributions show that the transition into spring is *well advanced in the lower stratosphere* while the cold wintertime polar vortex is still dominant in the upper stratosphere, Figure D-22, upper part.

This is very different from the developments in the S.H., Figure D-22, lower part. Here, the cold polar vortex of the lower stratosphere is still very strong in September while the transition into spring is *well advanced in the upper stratosphere* with the warm polar region, a reversed temperature gradient and the remnants of the cold polar vortex over middle latitudes.

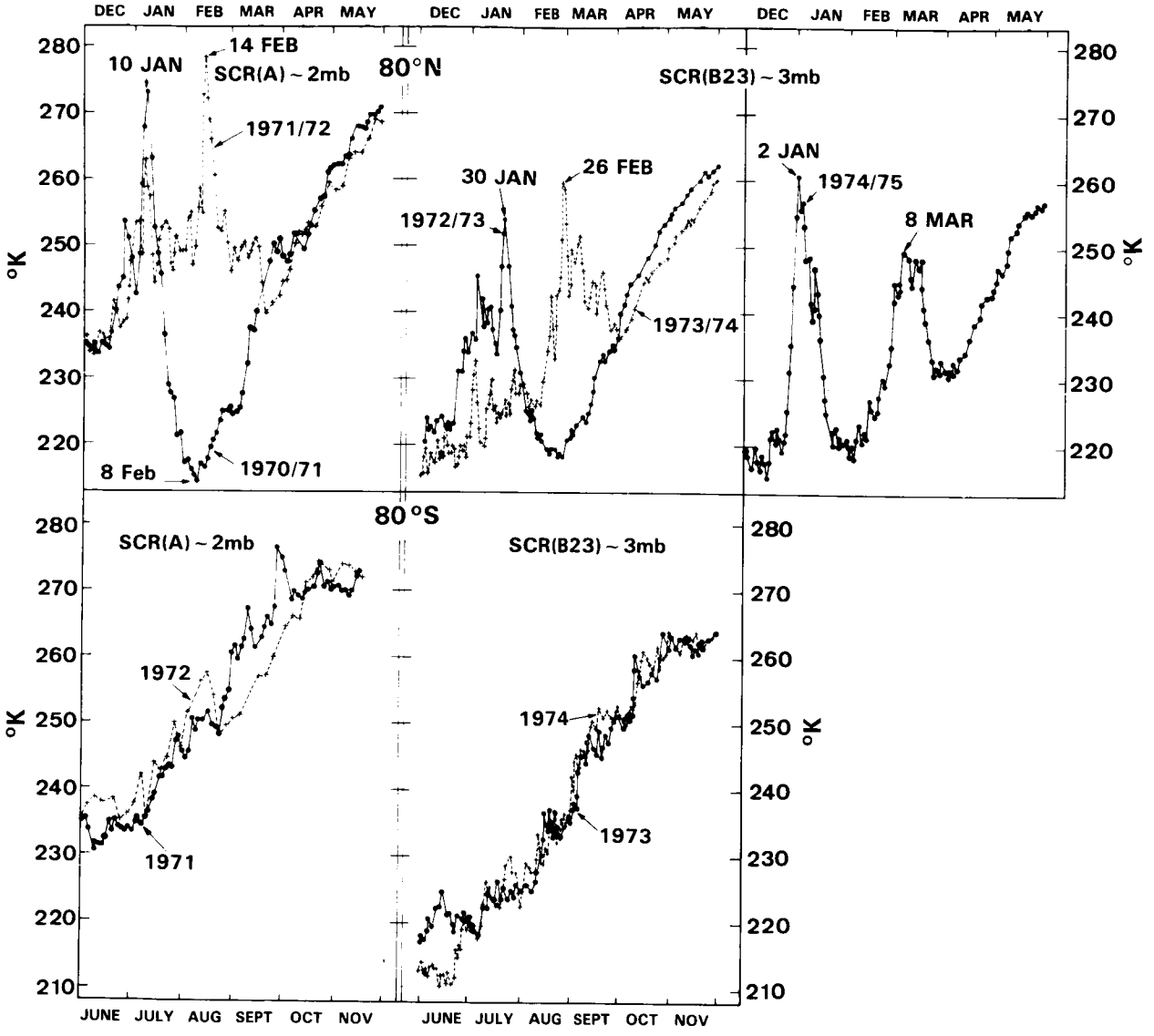

Daily zonal means at 80 deg. latitude of radiances of upper stratospheric channels of the SCR, flown on Nimbus 4 and 5.

(The radiances are converted into equiv. black body temperatures (°K)).

Figure D-21. Daily zonal means at 80° latitude of radiances of upper stratospheric channels of the SCR flown on Nimbus 4 and 5. The radiances are converted into equivalent blackbody temperatures. (Labitzke, 1977.)

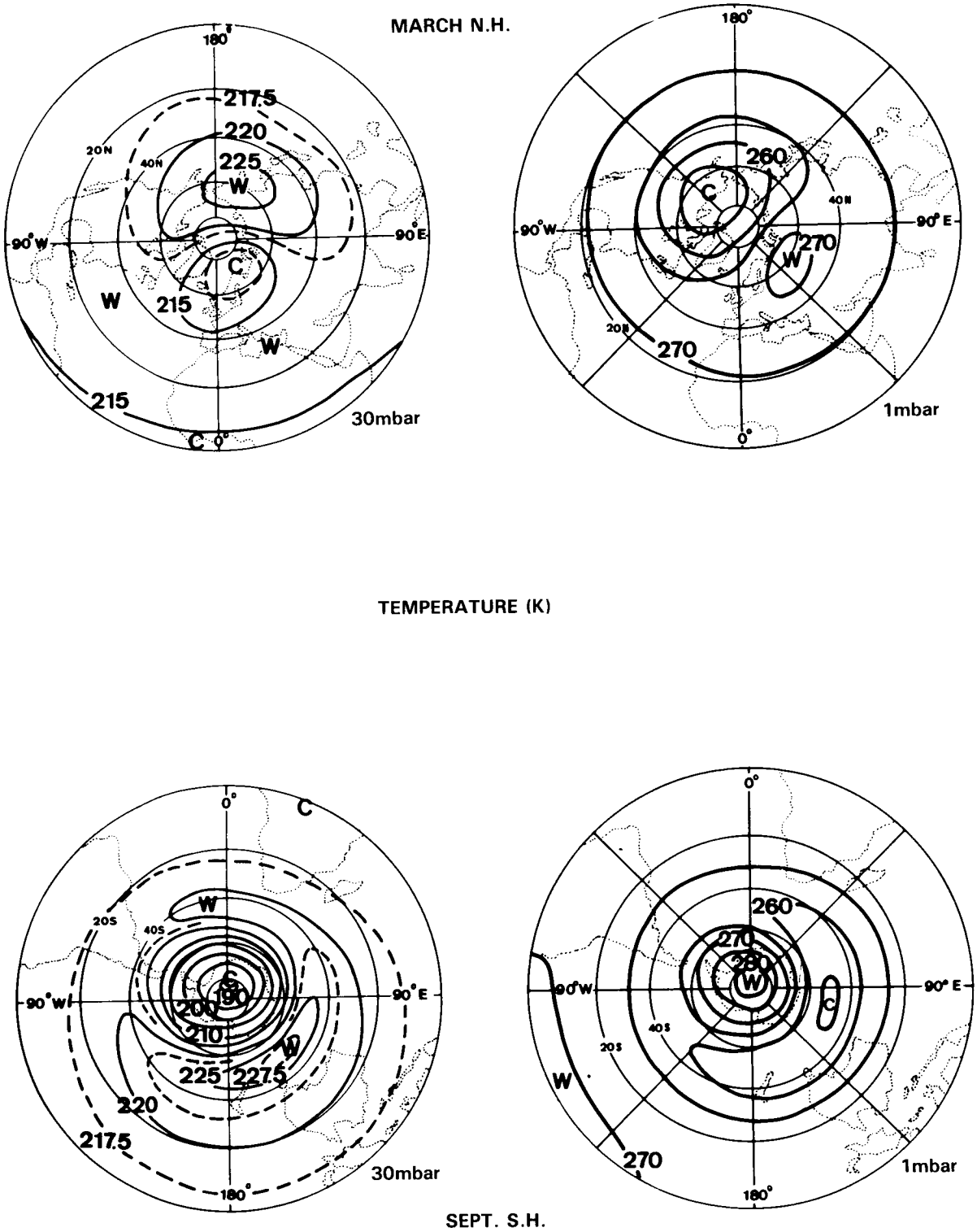

Figure D-22. Monthly mean 30- and 1-mbar temperatures for March, N.H. and September, S.H. (Data: F.U. Berlin and New Reference Atmosphere, MAP-Handbook, 16.)

D-3.2 Total Ozone

For a discussion of the interannual variability of ozone, data for many years are required but are not easily available.

But one excellent example is given here with Figure D-23, which shows the series of total ozone measurements in Arosa, Switzerland. This series of annual mean values starts by 1926, (Duetsch, 1985) and shows clearly very large interannual variations which are closely connected with the variability of the winter polar vortex, but also with volcanic eruptions like Mt. Agung in March 1963 and El Chichon in April 1982, which are responsible for the large minima in total ozone occurring after the eruptions.

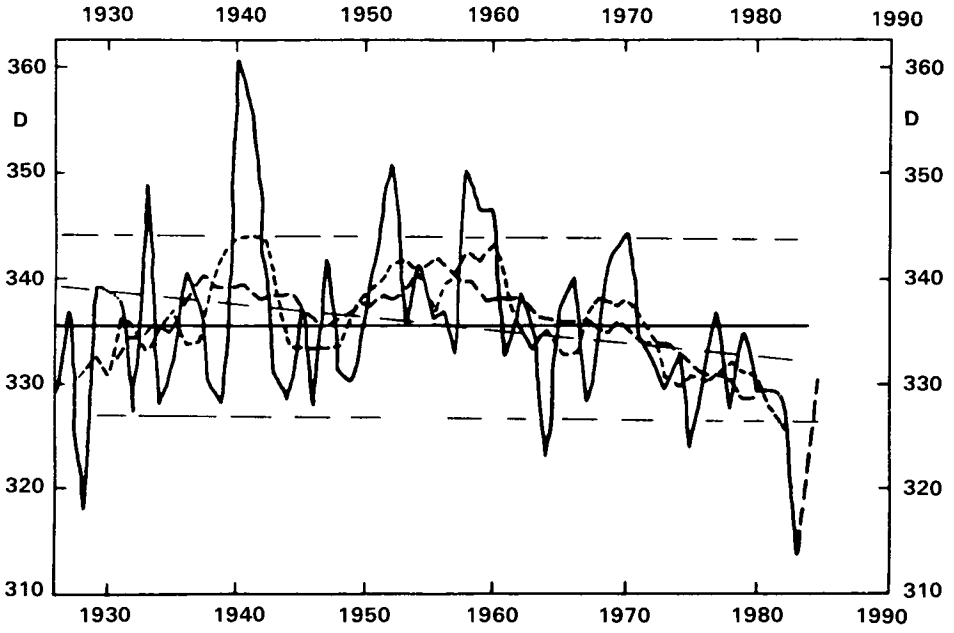

Figure D-23. Arosa total ozone series; annual mean values (C-wavelength pair): Full line; 5 year overlapping means: short dashed line; ten year overlapping means: dashed line; regression line: fine dashed. (Duetsch, 1984.)

D-3.3 Vertical Distribution of Ozone

Although there is interannual variability, comparison of the SBUV data over the 4-year period of measurements shows a remarkable similarity of structure from year to year. For example, shown in Figure D-24 is the vertical structure at 0°, 20°N, 40°N and 60°N for November of 1978, 1979, 1980 and 1981. Note how the 0° and 20°N profiles come together near 4 mbar. The 60°N profile changes in each case from the lowest profile at 4 mbar to the highest at 1.5 mbar.

Shown in Figure D-25 is the interannual variability of zonal mean ozone expressed as standard deviation (in percent) relative to the mean 4 years of SBUV data as a function of pressure and latitude for the months of November and July. As indicated in the previous Figure, the interannual variability of zonal means in November is very low, generally less than 4%. In contrast, the month of July gave the largest variability over this 4-year period with the maximum variability occurring at high southern winter latitudes. The interannual variability over the tropics appears to be strongly related to the quasi-biennial oscillation.

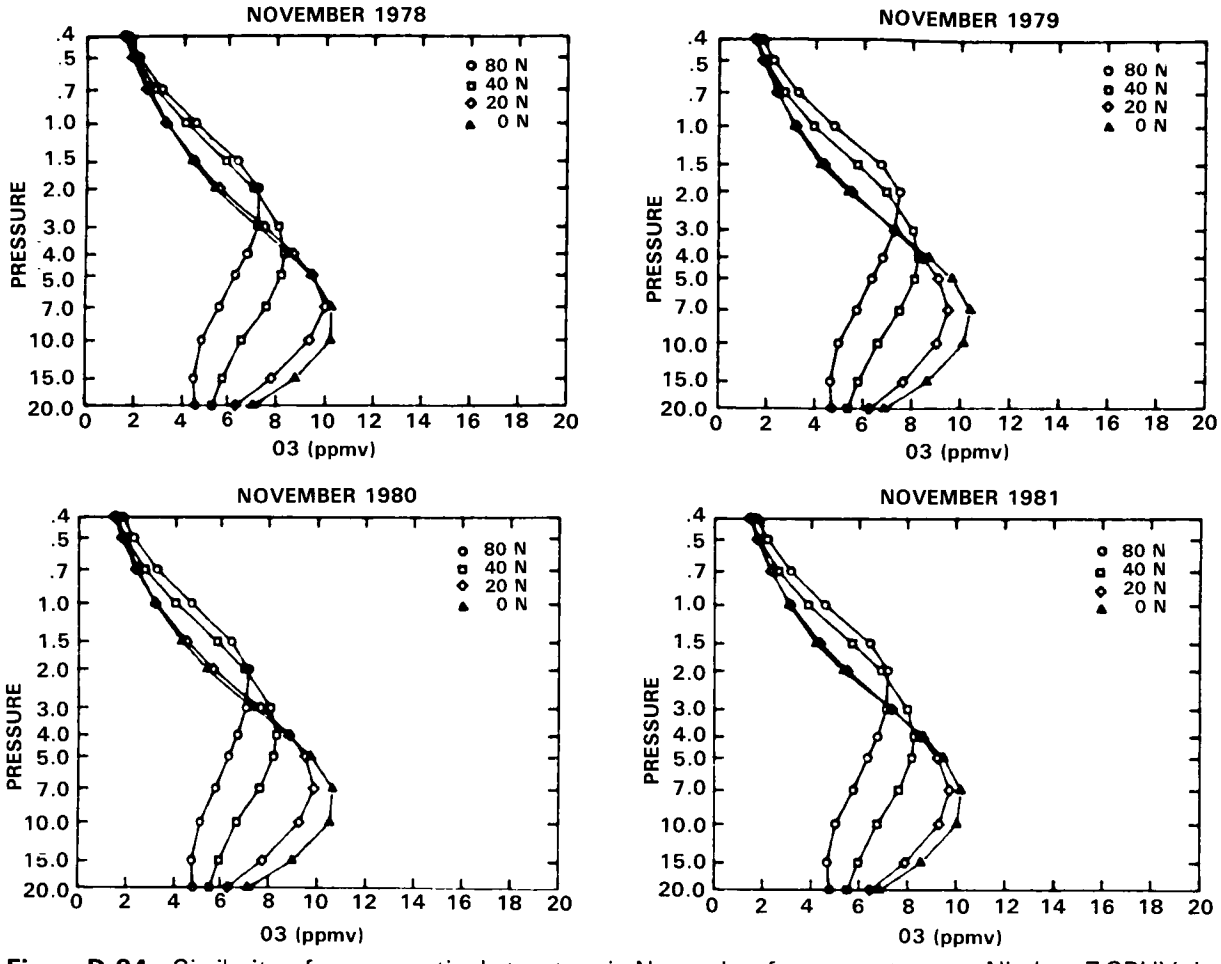

Figure D-24. Similarity of ozone vertical structure in November from year to year; Nimbus 7 SBUV data. (Keating and Young, 1985.)

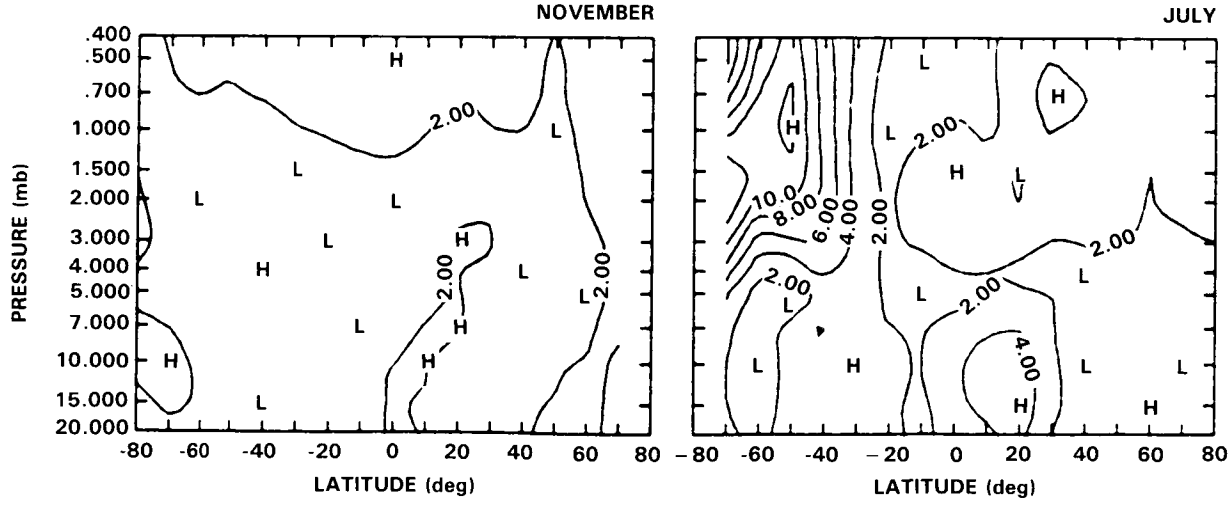

Figure D-25. Interannual variability of ozone vertical structure expressed as yearly standard deviation (percent) from 4-year zonal means for the months of November and July; Nimbus 7 SBUV data. (Keating and Young, 1985.)

D-4 MONTHLY MEAN CHARTS OF TOTAL OZONE, AND OF OZONE MIXING RATIOS AND TEMPERATURES AT SELECTED PRESSURE LEVELS

Based on the data described above, monthly mean charts of total ozone, Figure D-26 and of ozone mixing ratio and temperatures at selected pressure levels, Figures D-27–D-30, are presented for the mid-season months, together with meridional sections of the amplitudes and phases of the quasi-stationary planetary temperature waves 1 and 2, Figure D-31.

When comparing these temperature fields with the respective ozone fields, the following features are evident:

During summer the influence of the dynamics in connection with the planetary waves is negligable and we find a strong temperature dependance of ozone, i.e., minima of ozone mixing ratio are connected with the temperature maxima over the polar regions.

During all other seasons, however, when planetary waves are developed, the ozone distribution is coupled strongly to the horizontal and vertical motions in connection with the planetary waves. In the lower stratosphere (30 mbar) *maxima of ozone mixing ratio are connected with high temperatures*, (which are a result of sinking motions), and vice versa. The same is valid for the pattern of the total ozone.

In the upper stratosphere, 1-mbar, and lower mesosphere, 0.4-and 0.1-mbar, respectively, photochemical processes dominante and we find a negative correlation between ozone and temperature, and *high temperatures are connected with ozone minima*, and vice versa.

D-4.1 Total Ozone: Mid-Season Months, Northern and Southern Hemisphere

The charts of total ozone, Figure D-26, support the discussion in the previous Sections, particularly with respect to the differences between the hemispheres during the spring transition time. The distribution of total ozone is highly correlated with the temperature of the lower stratosphere and with the large-scale planetary waves. This will be discussed in more detail in Section D-4.2, where the ozone distribution is presented at selected pressure levels.

D-4.2 Ozone Mixing Ratios and Temperatures at Selected Pressure Levels

D-4.2.a January:

Northern Hemisphere

During the northern winters the large-scale planetary waves 1 and 2 can penetrate from the troposphere into the stratosphere as long as the mean zonal winds are from the west, (Charney and Drazin, 1961). The most prominent features of the stratosphere in winter are the well developed cold polar vortex and the strong quasi-stationary planetary wave 1. This wave which causes large longitudinal variability over middle and high latitudes, is most pronounced in the lower and middle stratosphere at the 30-and 10-mbar levels (23 and 30km), respectively, Figure D-27.2. The warm region over approx. 150 °E is connected with the well known Aleutian anticyclone which is responsible for the displacement of the polar vortex away from the North Pole.

Following are the charts for Section D-4.1 and D-4.2, Figures 26.1–31.4.

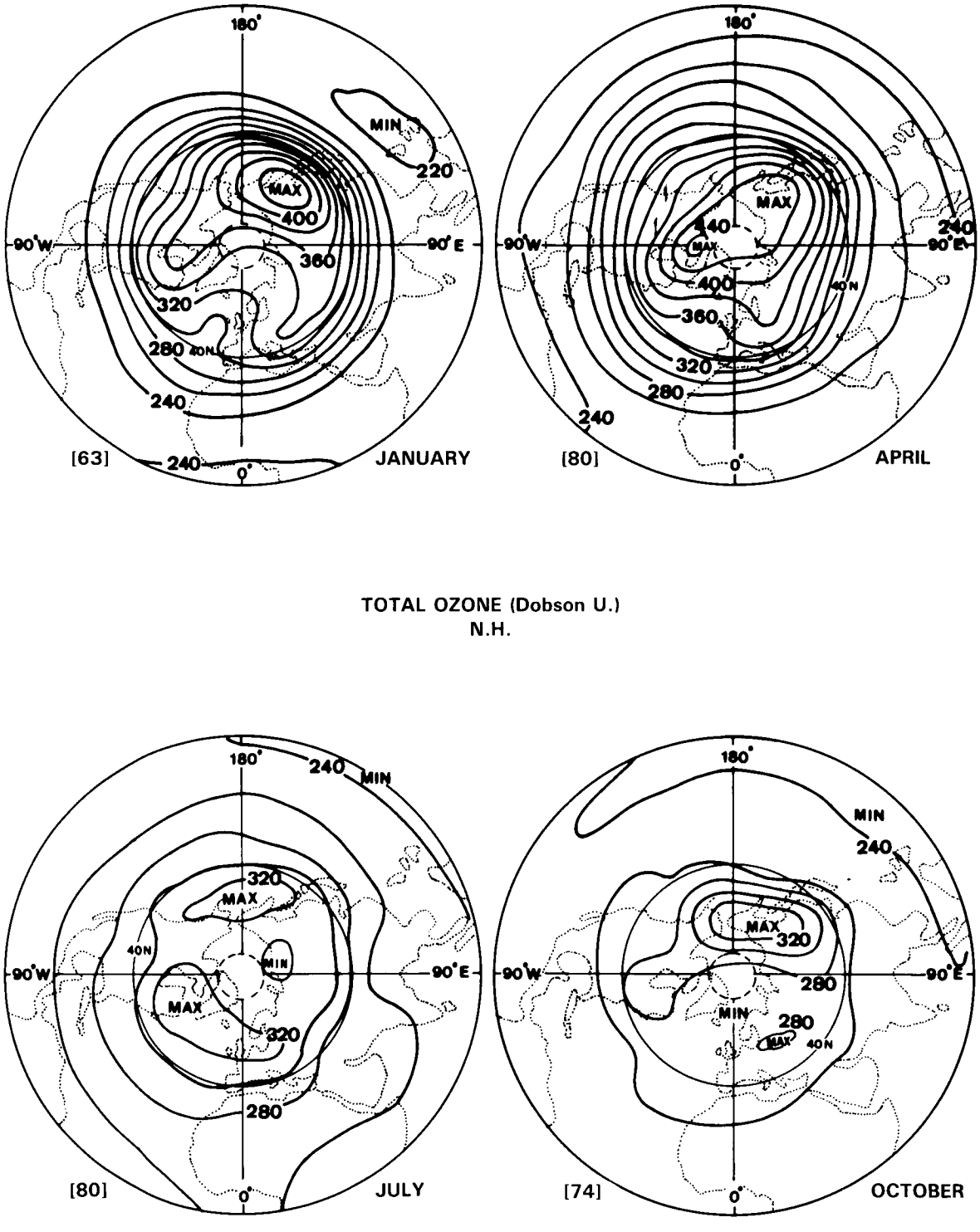

Figure D-26.1. Monthly average total ozone charts for the Northern Hemisphere from 1978–1982, for the mid-season months. Values in brackets outside of the charts indicate the latitude from which the analyses were extrapolated polewards. (R.M. Nagatani and A.J. Miller, personal communication.)

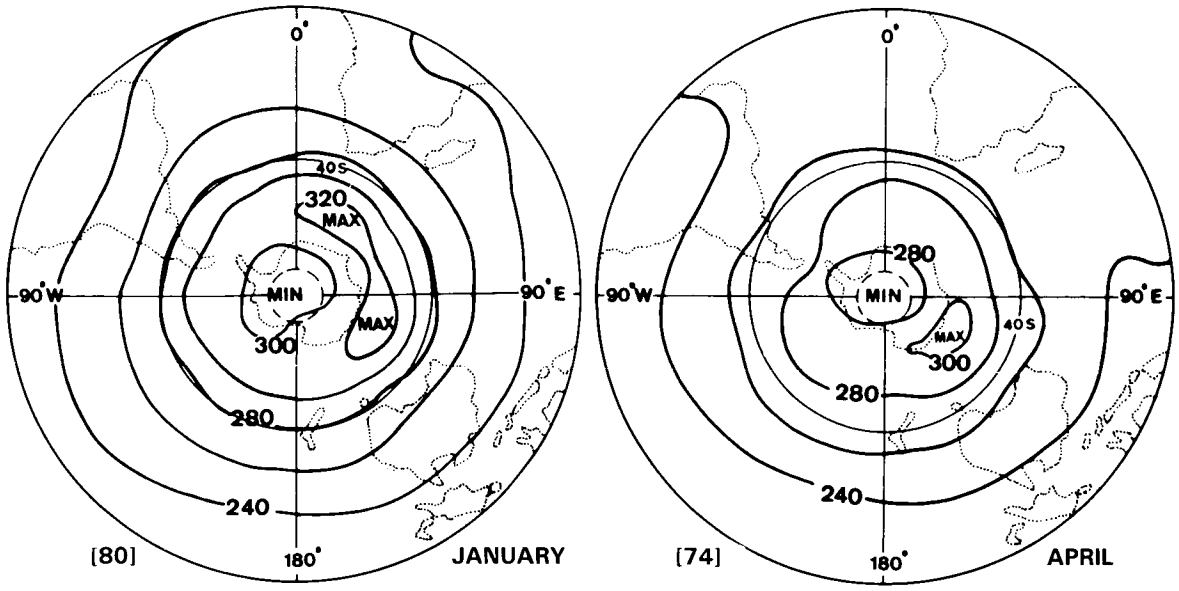

TOTAL OZONE (Dobson U.)
S.H.

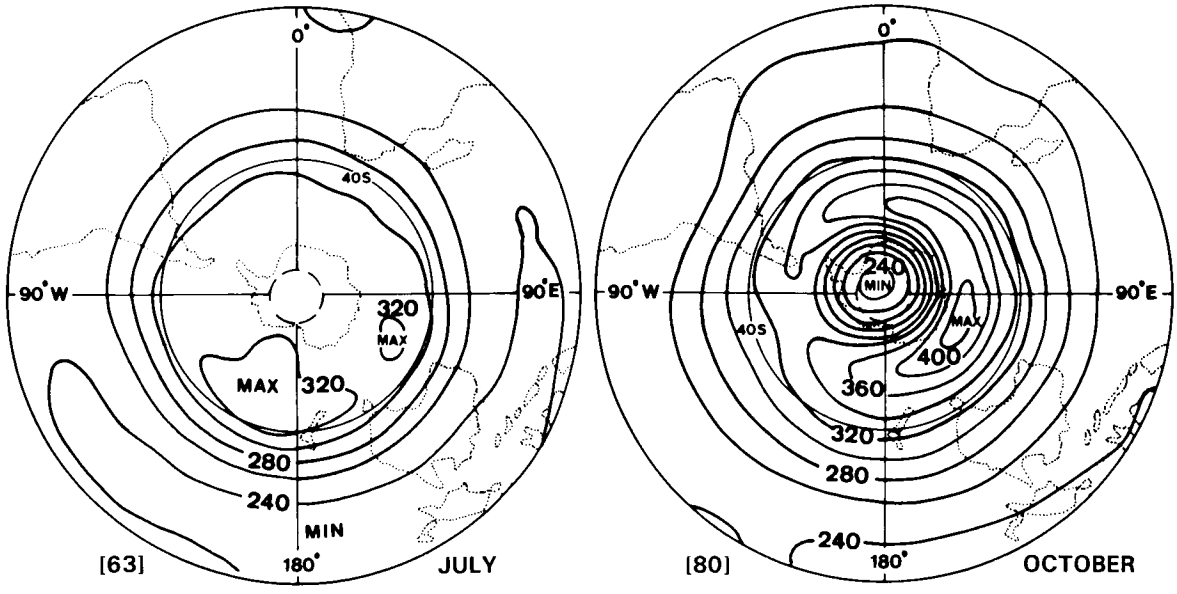

Figure D-26.2. Monthly average total ozone charts for the Southern Hemisphere from 1978–1982, for the mid-season months. For values in brackets see Figure D-26.1. (R.M. Nagatani and A.J. Miller, personal communication.)

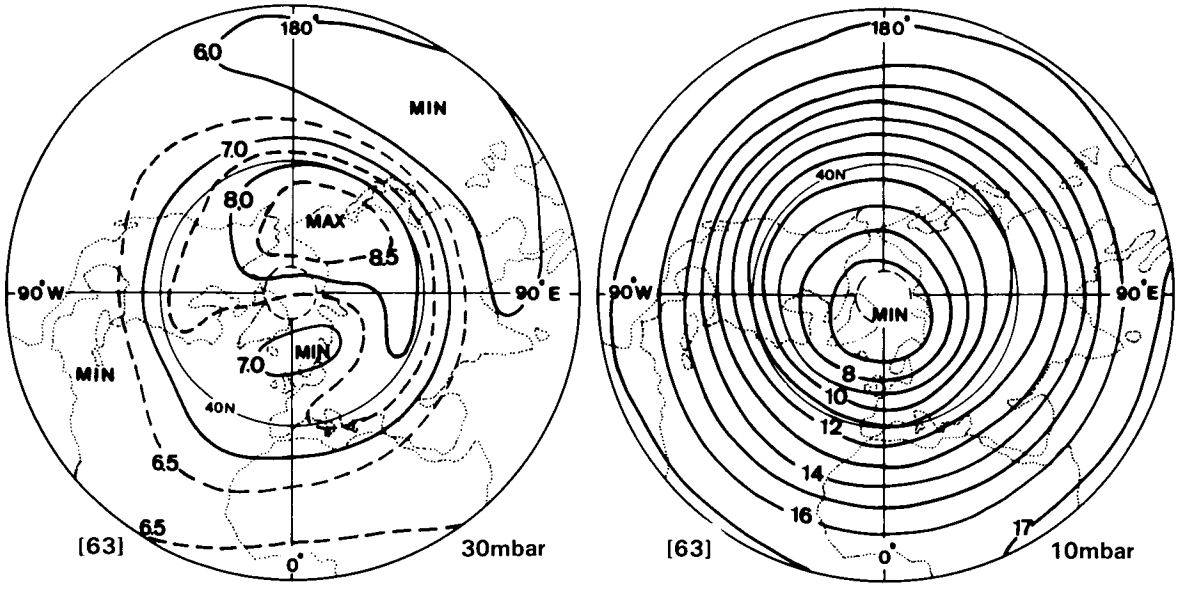

OZONE MASS MIXING RATIO (ppm)
JANUARY N.H.

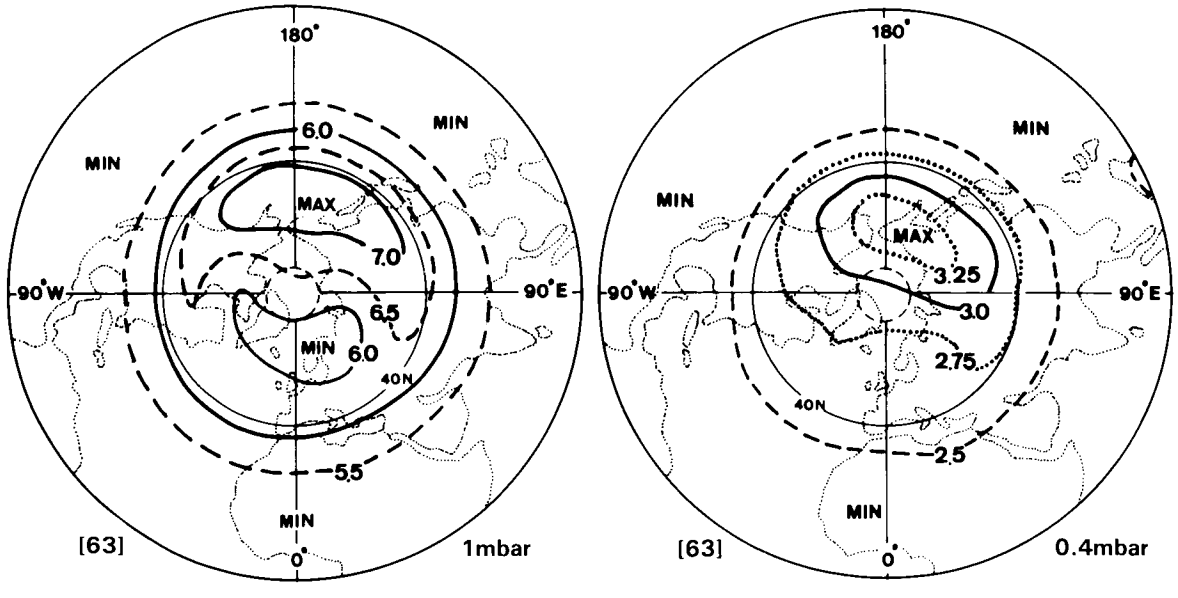

Figure D-27.1. Monthly average ozone mass mixing ratio (ppm) for the Northern Hemisphere from 1978–1982, for January. For values in brackets see Figure D-26.1. (R.M. Nagatani and A.J. Miller, personal communication.)

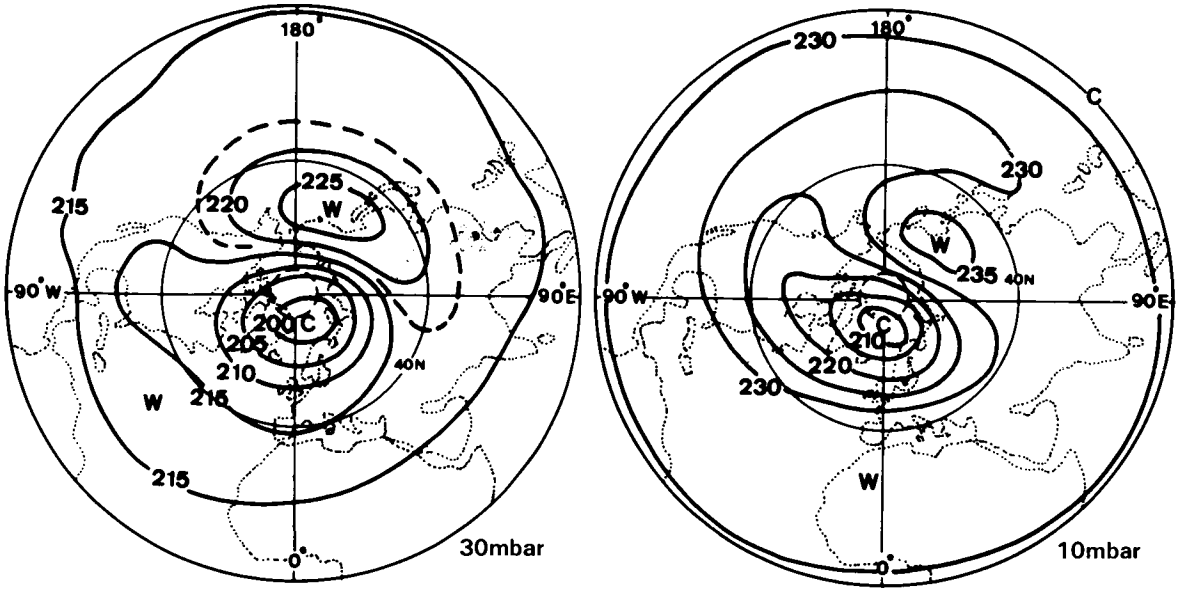

TEMPERATURE (K)
JANUARY N.H.

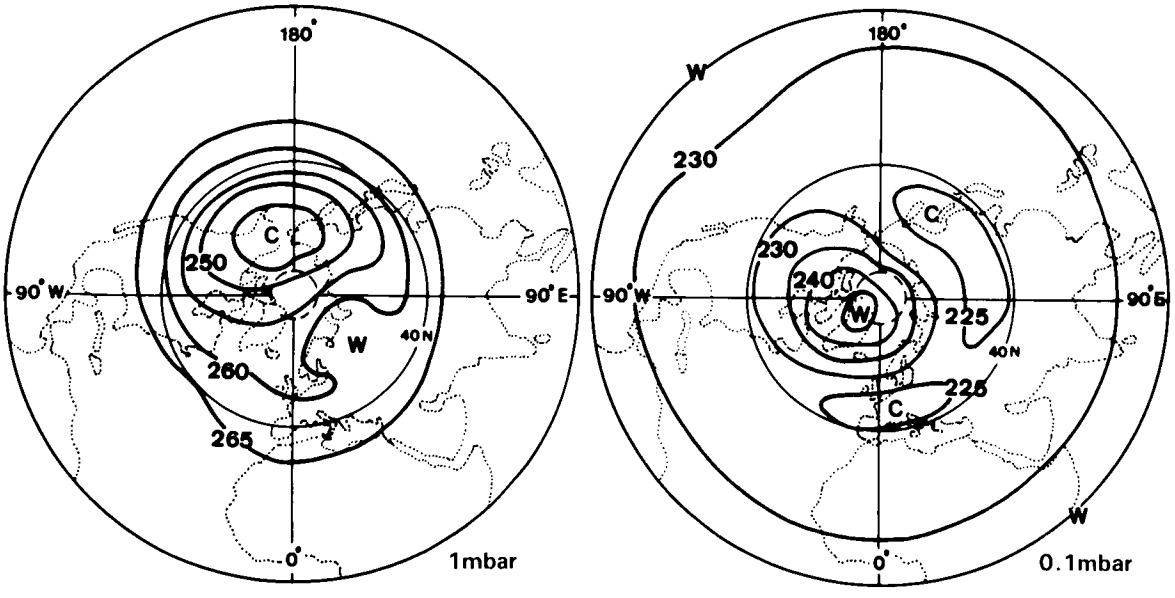

Figure D-27.2. Monthly mean temperature charts for January, Northern Hemisphere. (Data: 30-mbar: F.U. Berlin; otherwise: New Reference Atmosphere, MAP-Handbook, 16.)

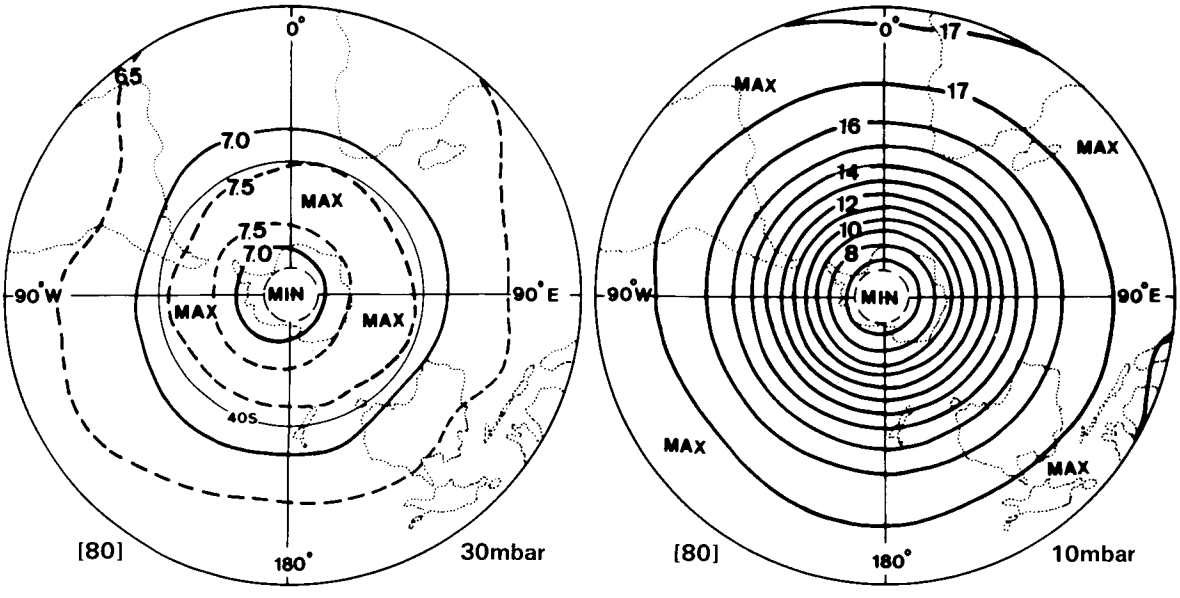

OZONE MASS MIXING RATIO (ppm)
JANUARY S.H.

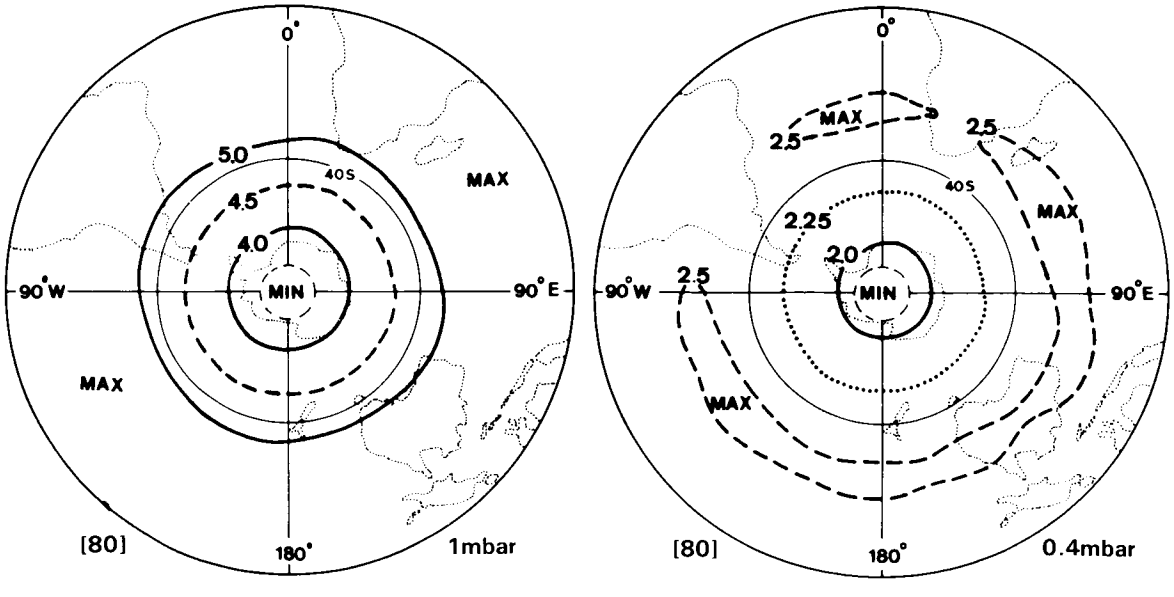

Figure D-27.3. Monthly average ozone mass mixing ratio (ppm) for the Southern Hemisphere from 1978–1982, for January. (R.M. Nagatani and A.J. Miller, personal communication.)

C·5

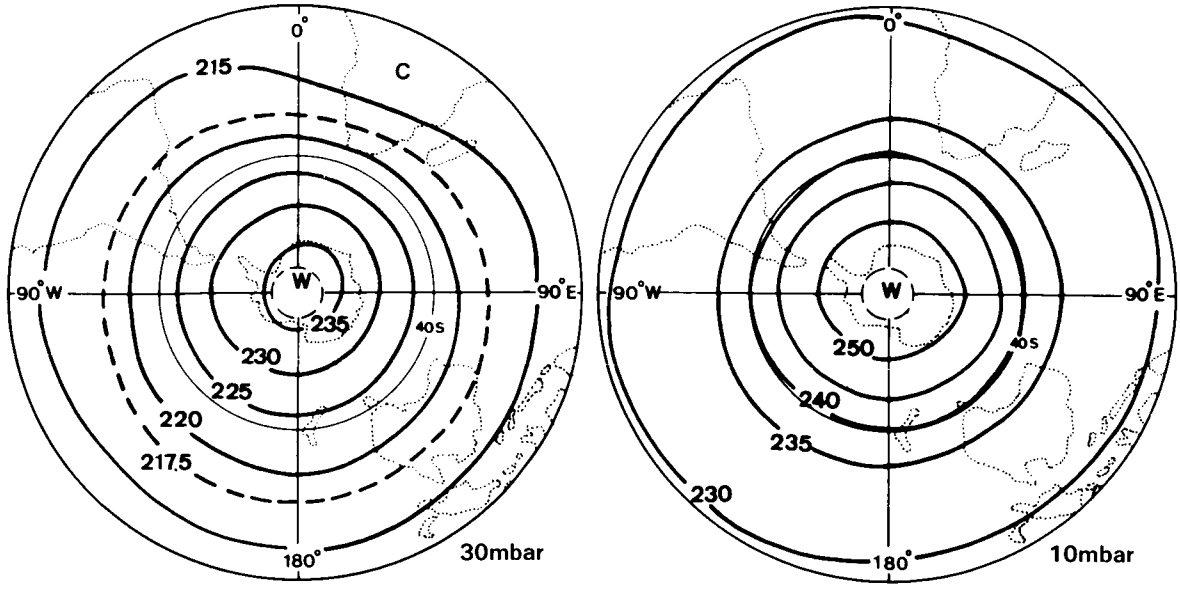

TEMPERATURE (K)
JANUARY S.H.

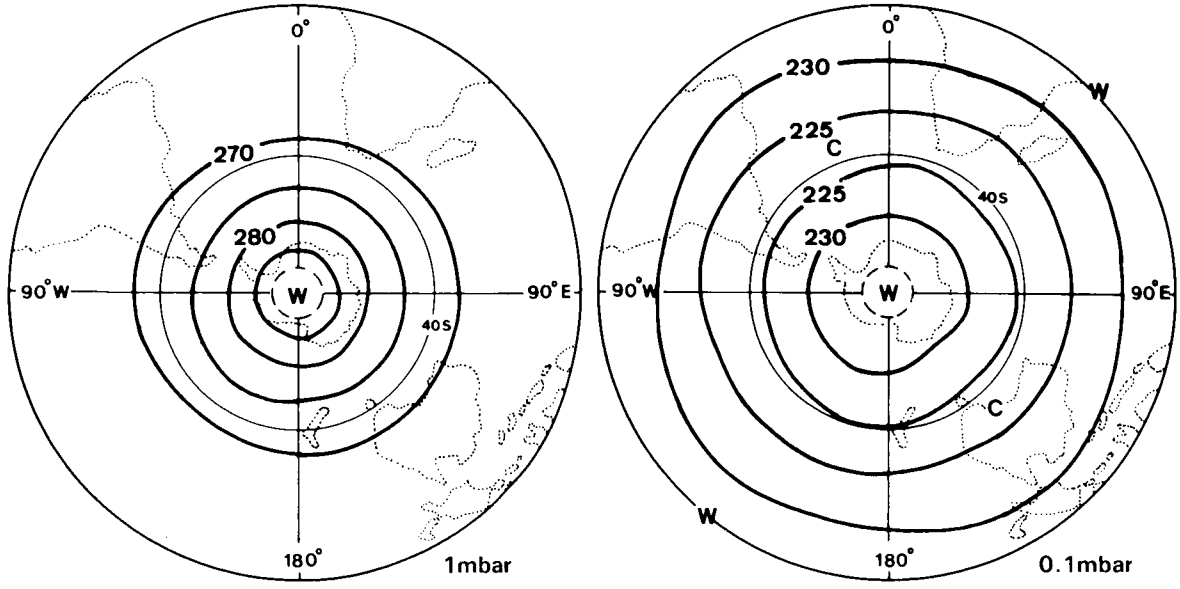

Figure D-27.4. Monthly mean temperature charts for January, Southern Hemisphere. (Data: 30-mbar: Knittel, 1976; otherwise: New Reference Atmosphere, MAP-Handbook, 16.)

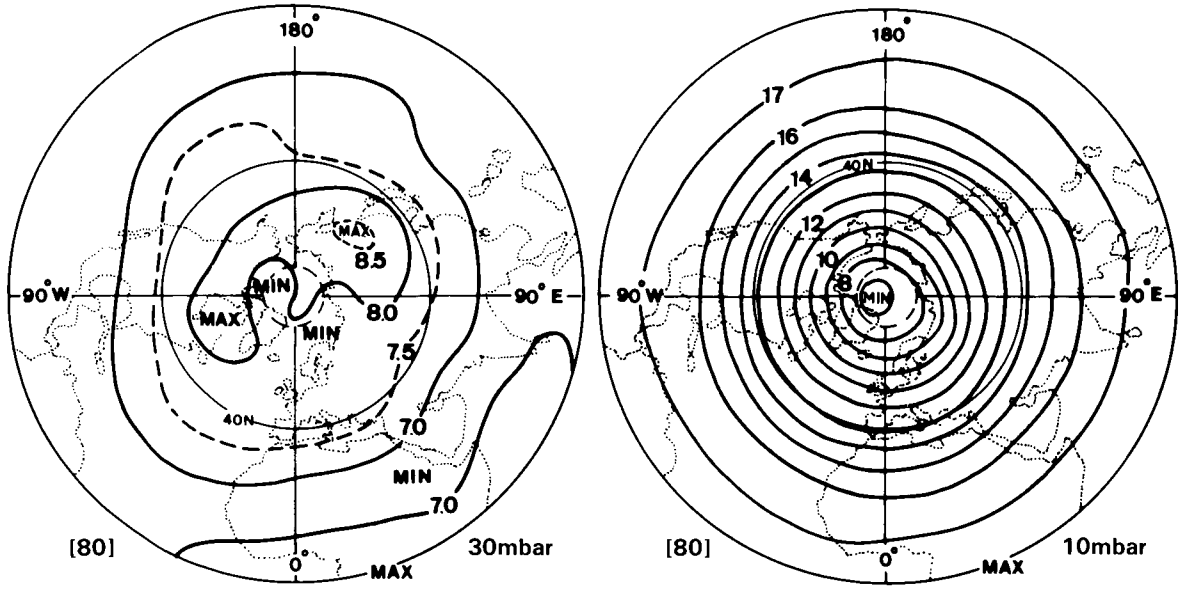

OZONE MASS MIXING RATIO (ppm)
APRIL N.H.

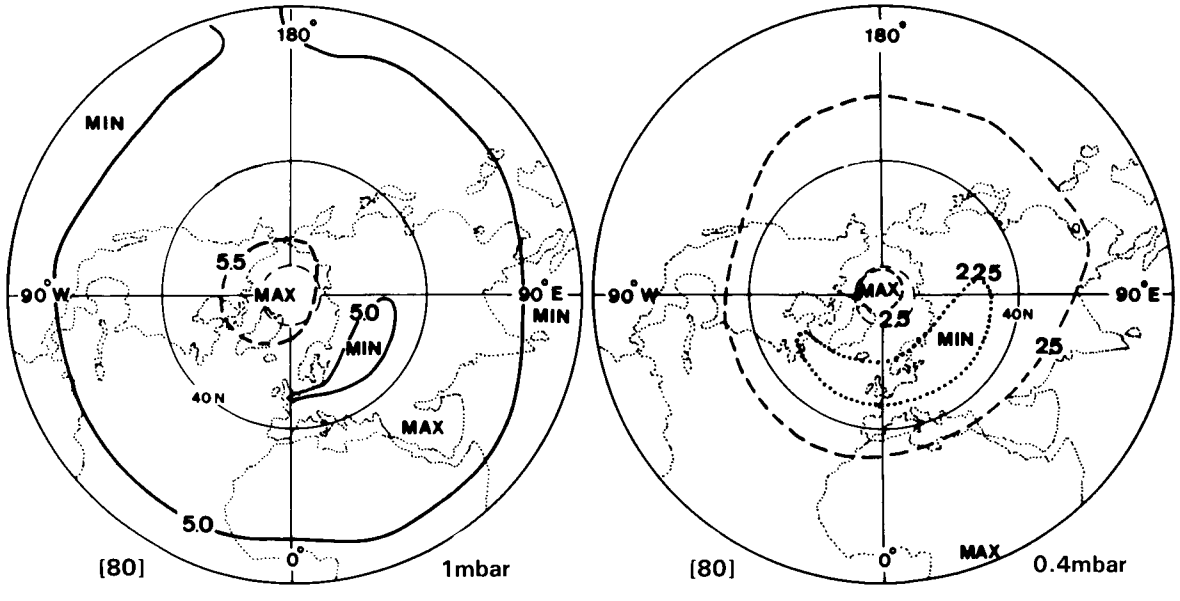

Figure D-28.1. Monthly average ozone mass mixing ratio (ppm) for the Northern Hemisphere from 1978–1982, for April. (R.M. Nagatani and A.J. Miller, personal communication.)

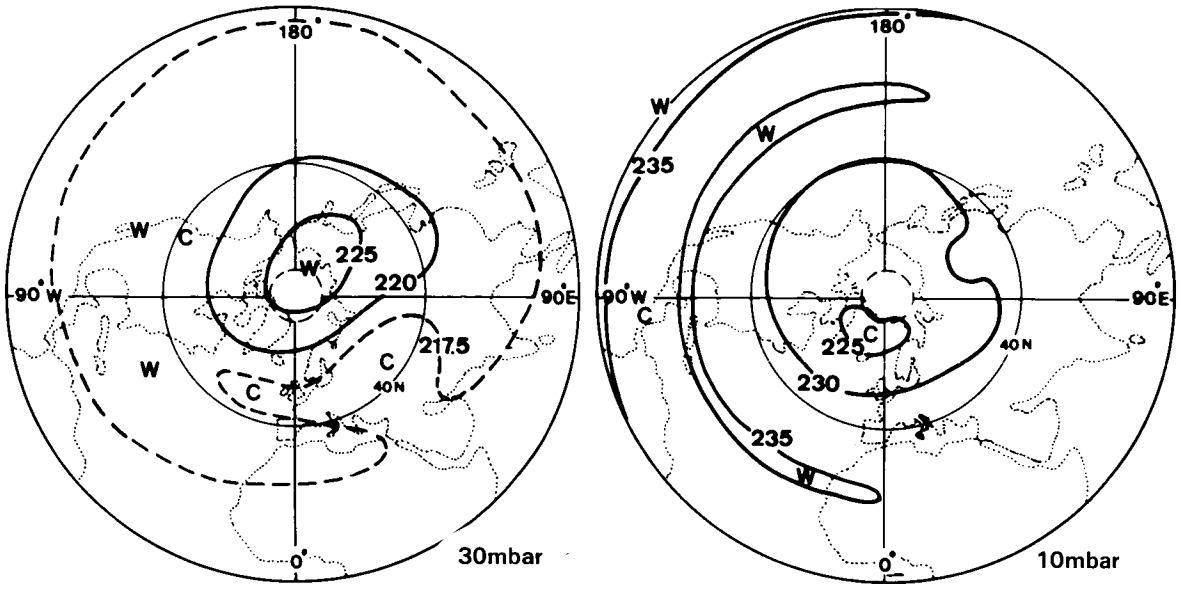

TEMPERATURE (K)
APRIL N.H.

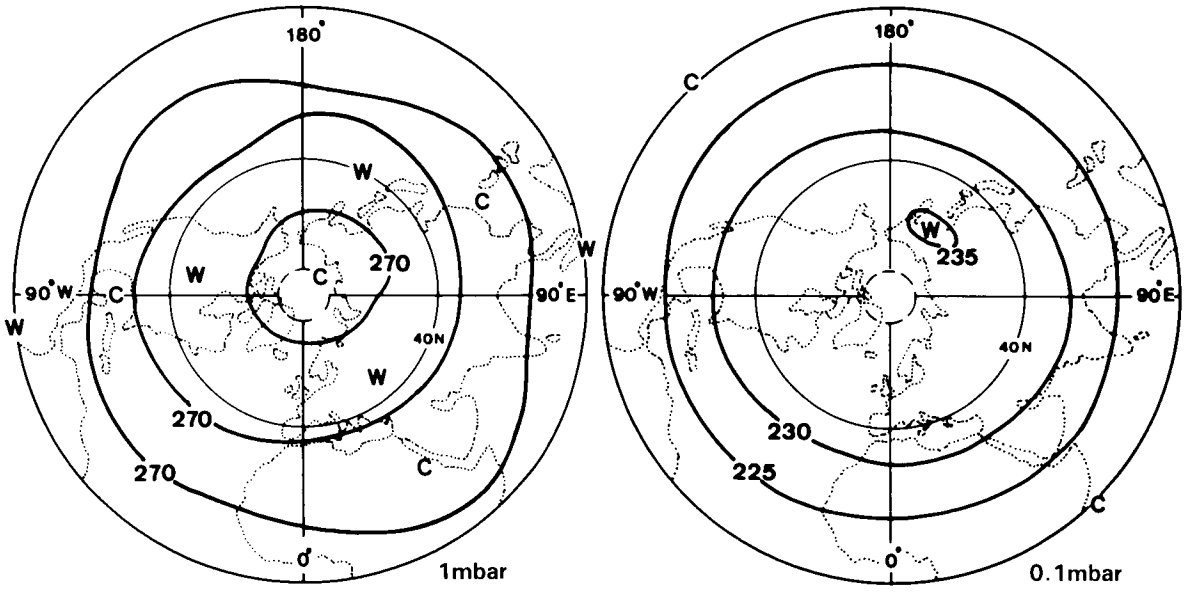

Figure D-28.2. Monthly mean temperature charts for April, Northern Hemisphere. (Data: 30-mbar: F.U. Berlin; otherwise: New Reference Atmosphere, MAP-Handbook, 16.)

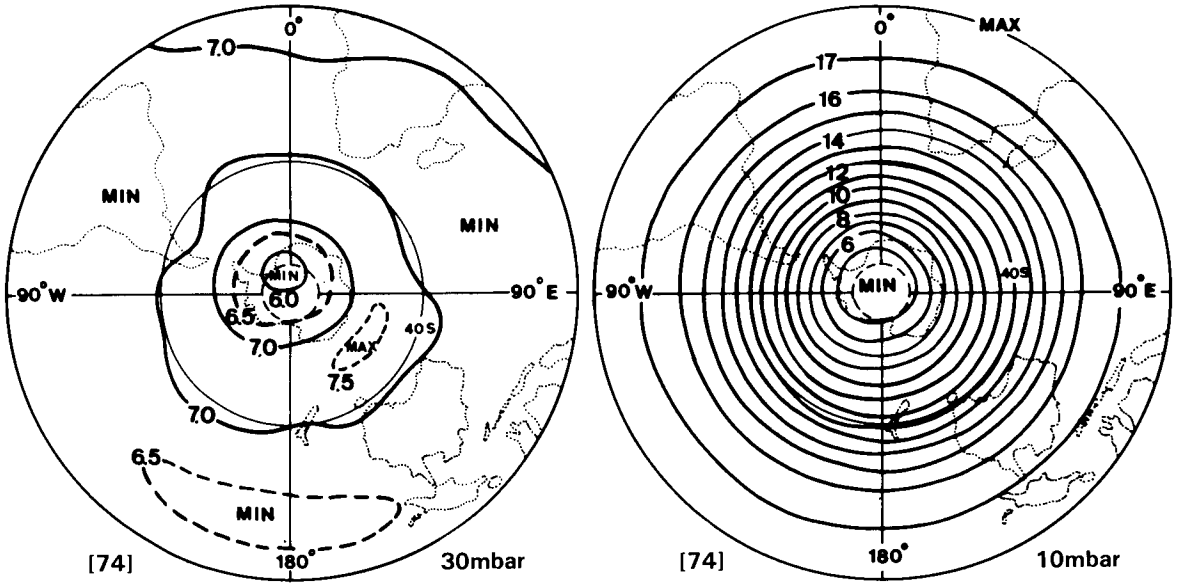

OZONE MASS MIXING RATIO (ppm)
APRIL S.H.

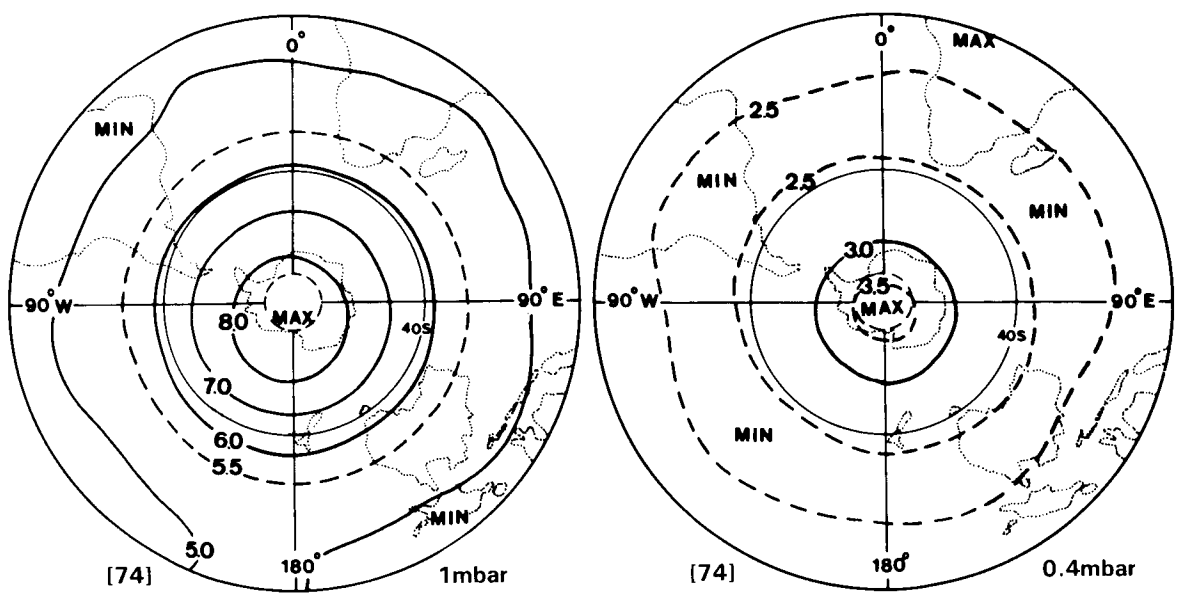

Figure D-28.3. Monthly average ozone mass mixing ratio (ppm) for the Southern Hemisphere from 1978–1982, for April. (R.M. Nagatani and A.J. Miller, personal communication.)

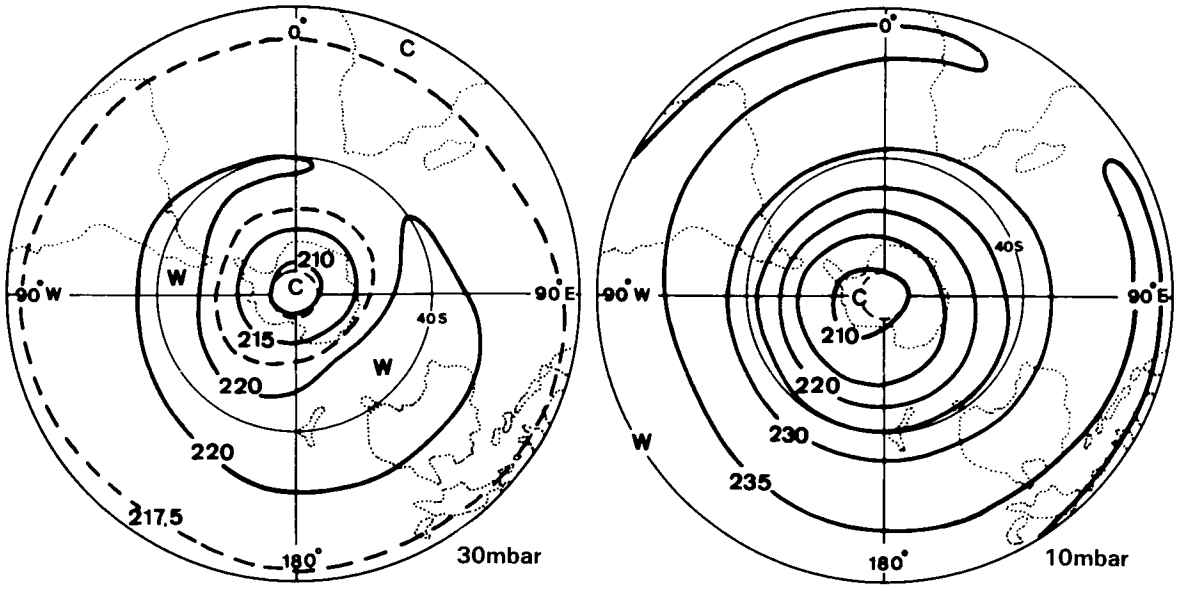

TEMPERATURE (K)
APRIL S.H.

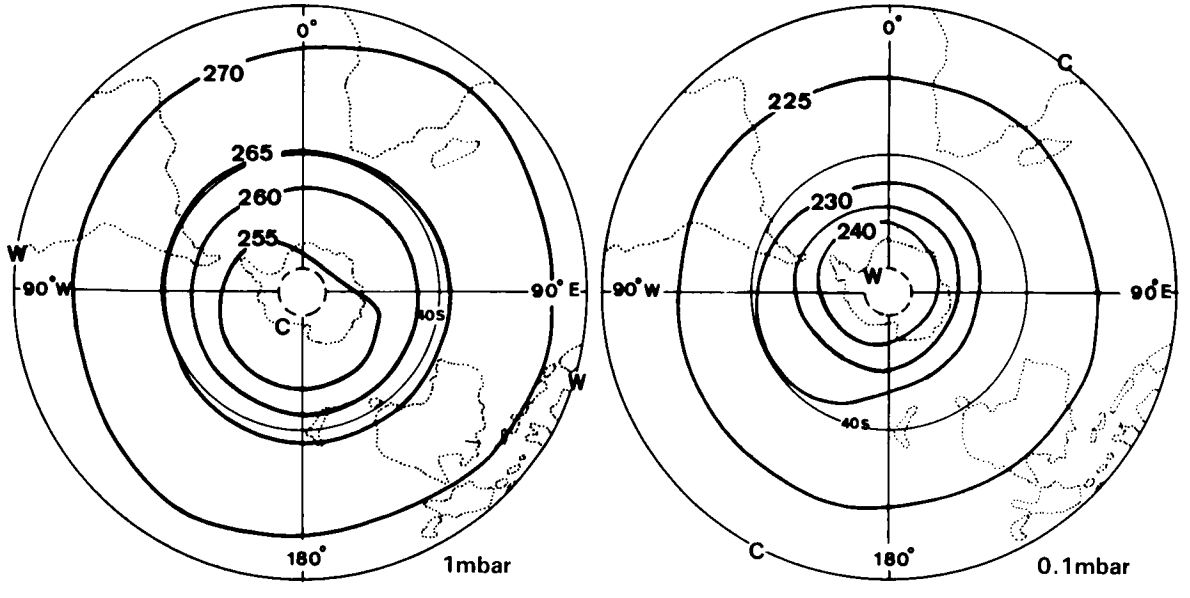

Figure D-28.4. Monthly mean temperature charts for April, Southern Hemisphere. (Data: 30-mbar: Knittel, 1976; otherwise: New Reference Atmosphere, MAP-Handbook, 16.)

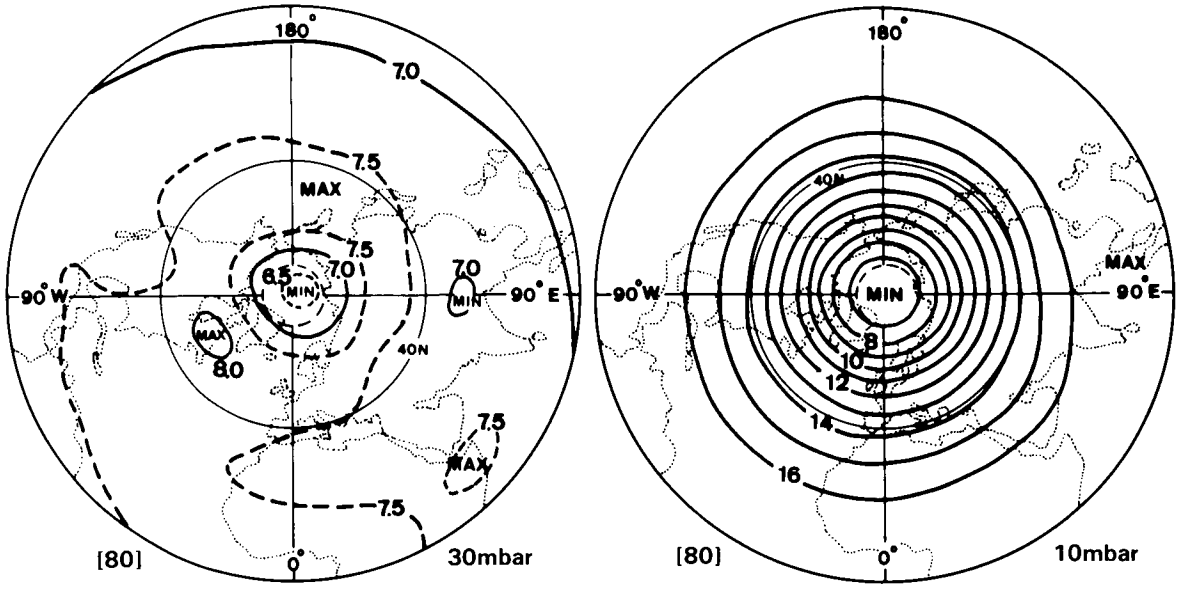

OZONE MASS MIXING RATIO (ppm)
JULY N.H.

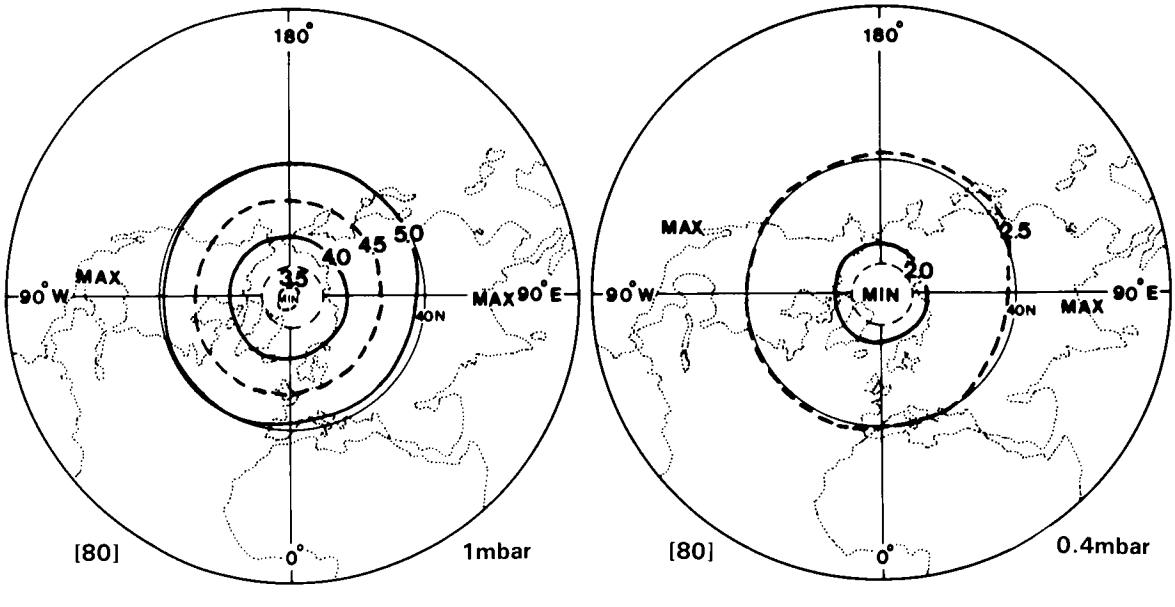

Figure D-29.1. Monthly average ozone mass mixing ratio (ppm) for the Northern Hemisphere from 1978–1982, for July. (R.M. Nagatani and A.J. Miller, personal communication.)

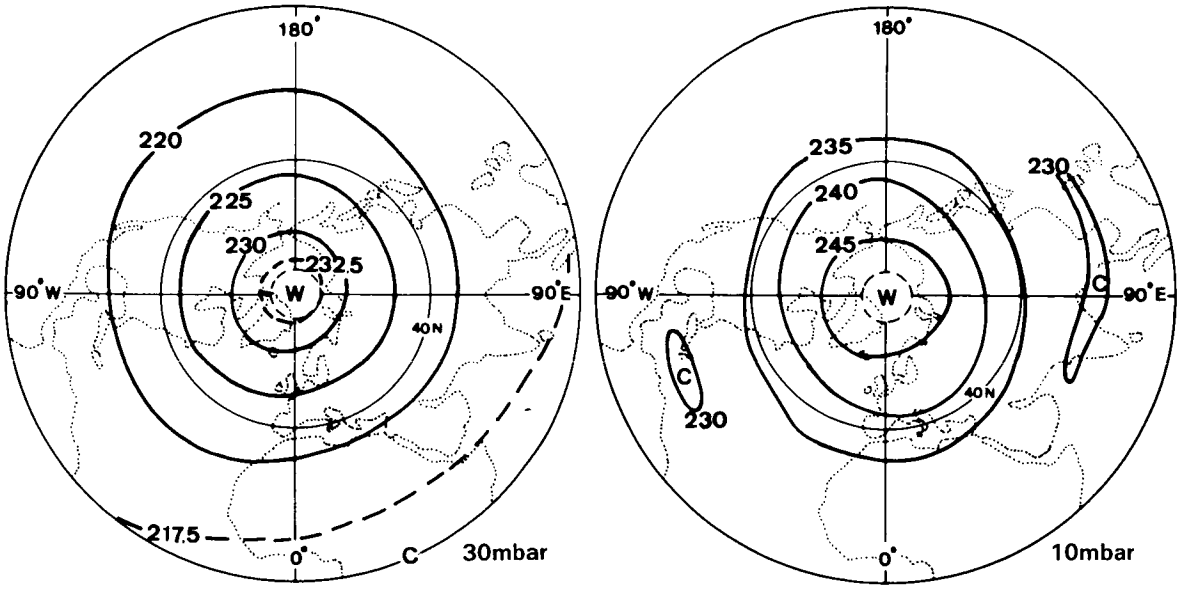

TEMPERATURE (K)
JULY N.H.

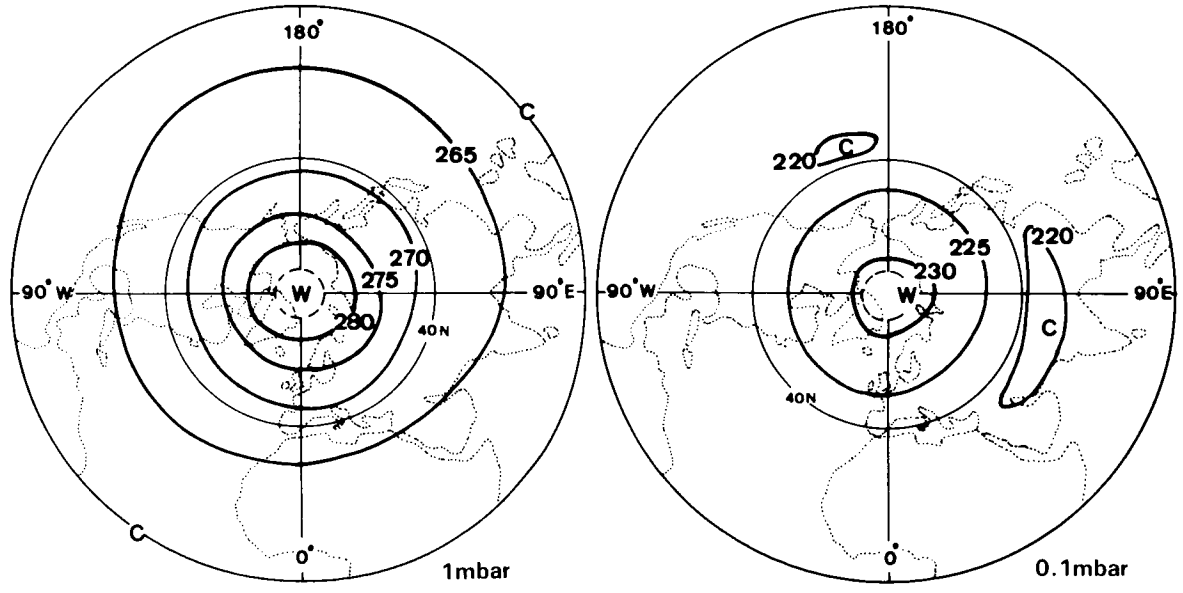

Figure D-29.2. Monthly mean temperature charts for July, Northern Hemisphere. (Data: 30-mbar: F.U. Berlin; otherwise: New Reference Atmosphere, MAP-Handbook, 16.)

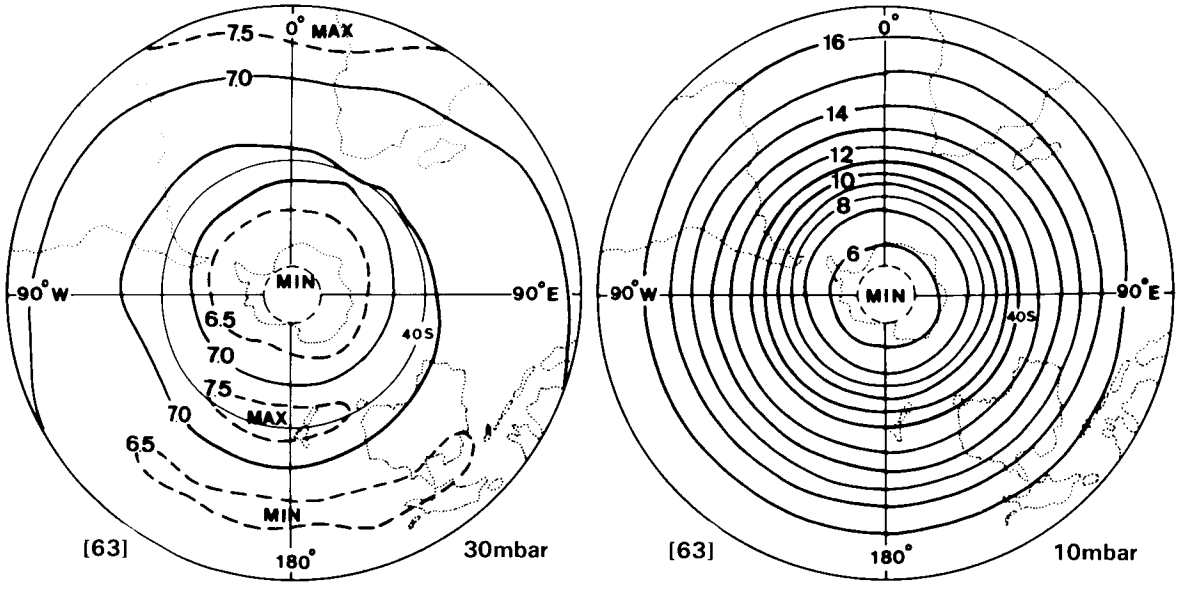

OZONE MASS MIXING RATIO (ppm)
JULY S.H.

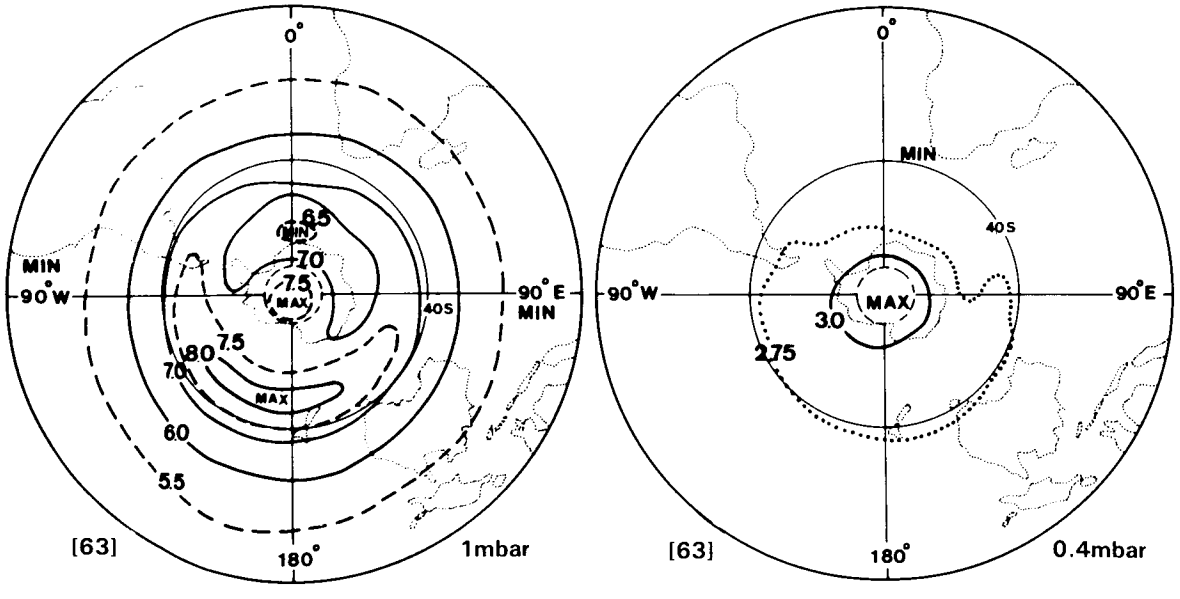

Figure D-29.3. Monthly average ozone mass mixing ration (ppm) for the Southern Hemisphere from 1978–1982, for July. (R.M. Nagatani and A.J. Miller, personal communication.)

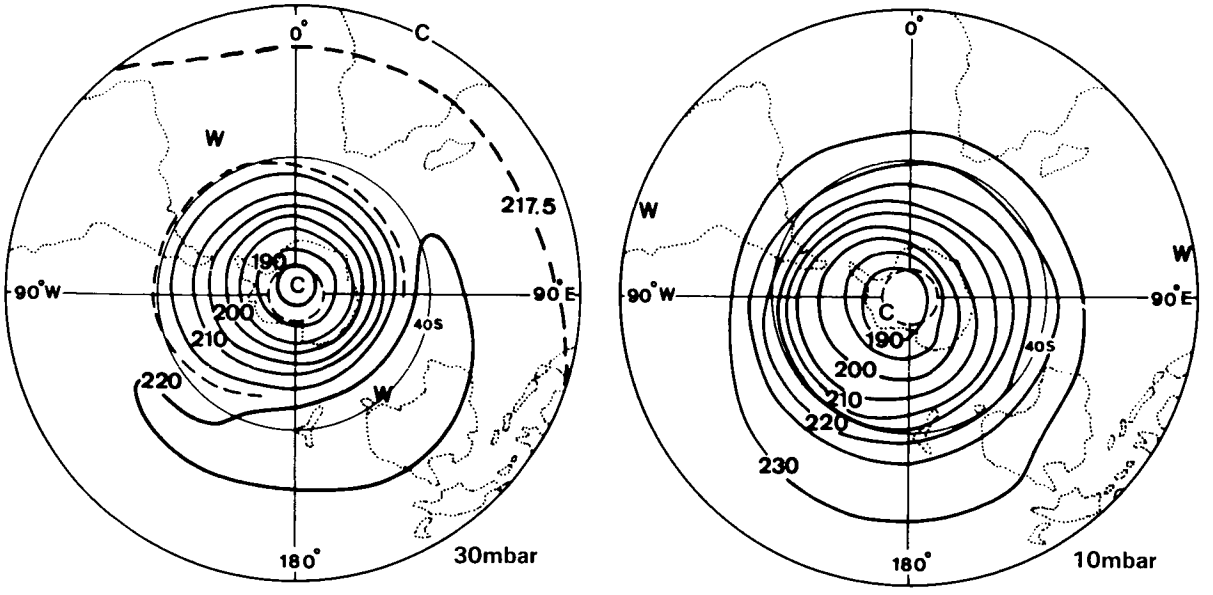

TEMPERATURE (K)
JULY S.H.

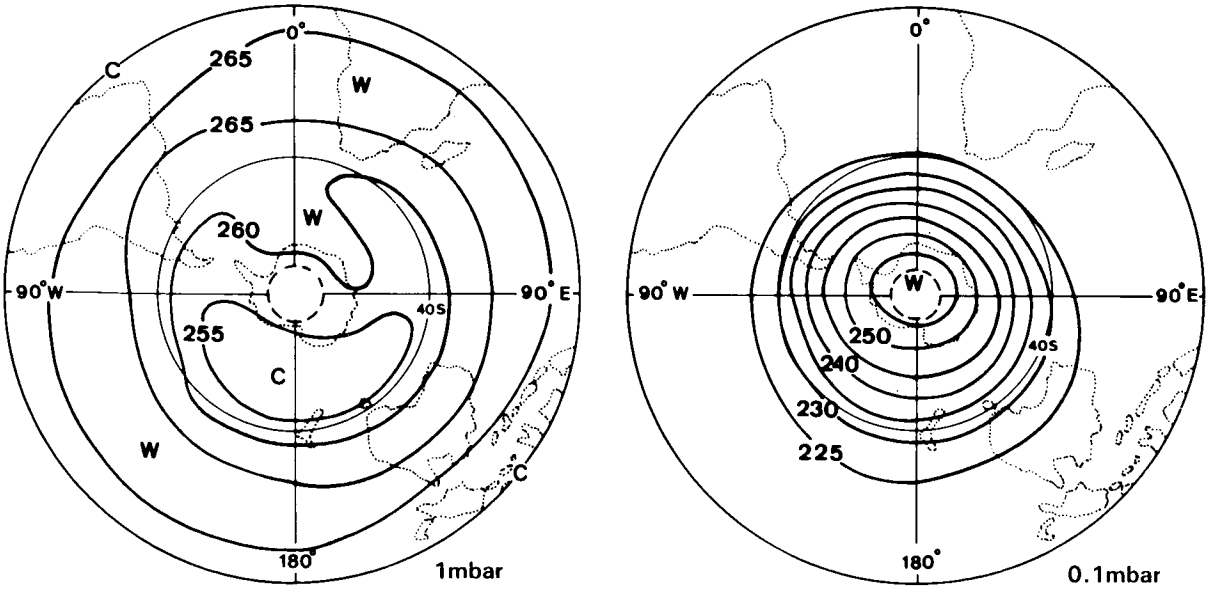

Figure D-29.4. Monthly mean temperature charts for July, Southern Hemisphere. (Data: 30-mbar: Knittel, 1976; otherwise: New Reference Atmosphere, MAP-Handbook, 16.)

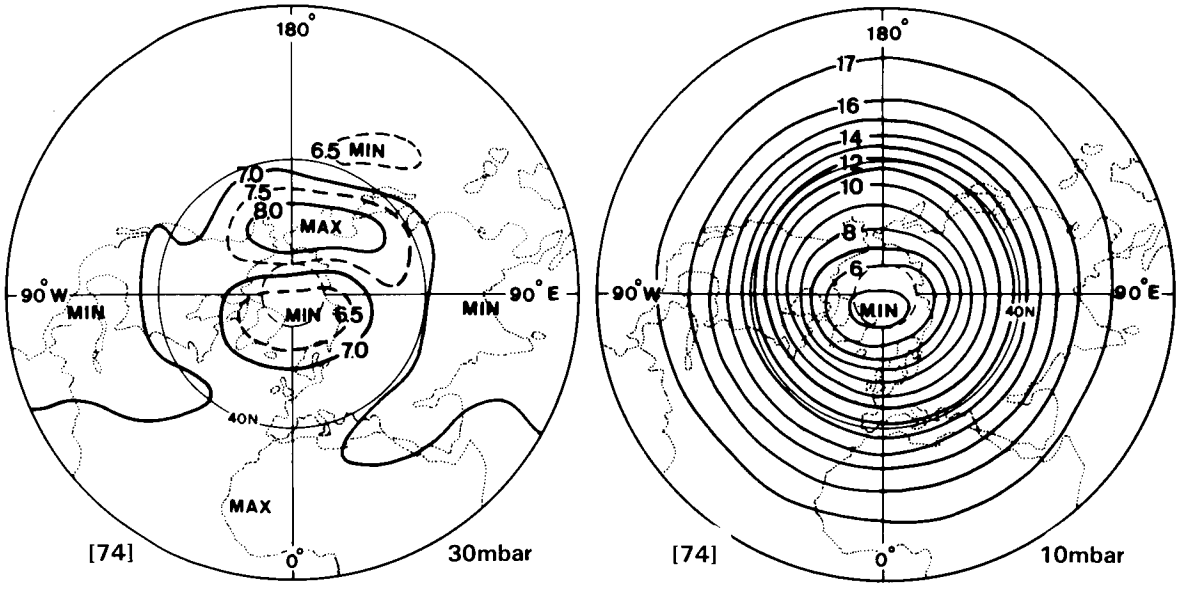

OZONE MASS MIXING RATIO (ppm)
OCTOBER N.H.

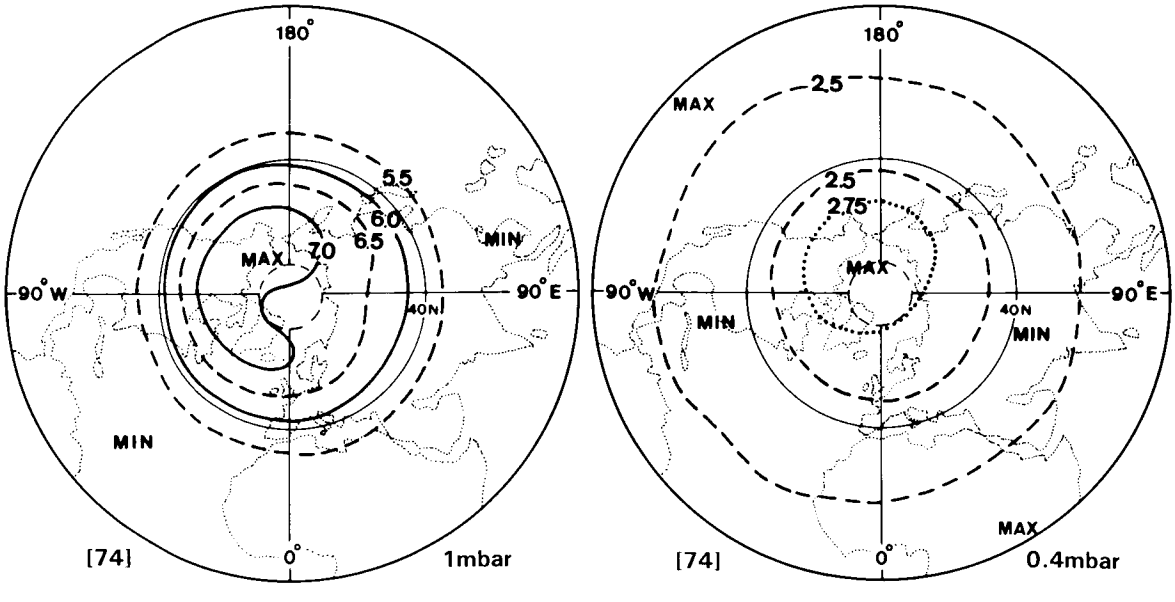

Figure D-30.1. Monthly average ozone mass mixing ratio (ppm) for the Northern Hemisphere from 1978–1982, for October. (R.M. Nagatani and A.J. Miller, personal communication.)

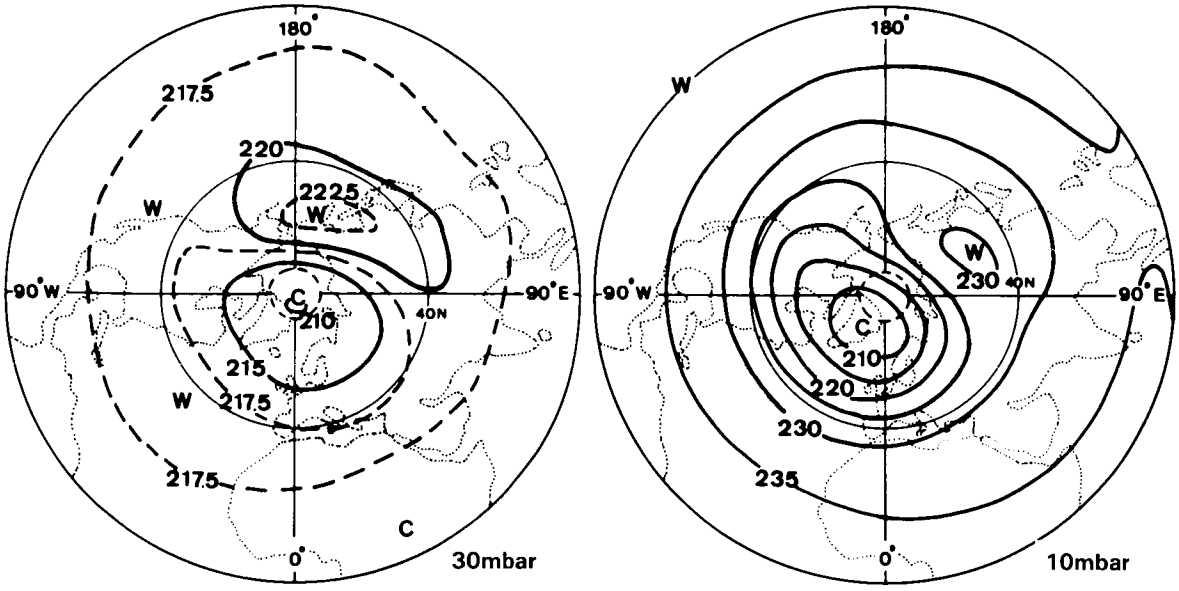

TEMPERATURE (K)
OCTOBER N.H.

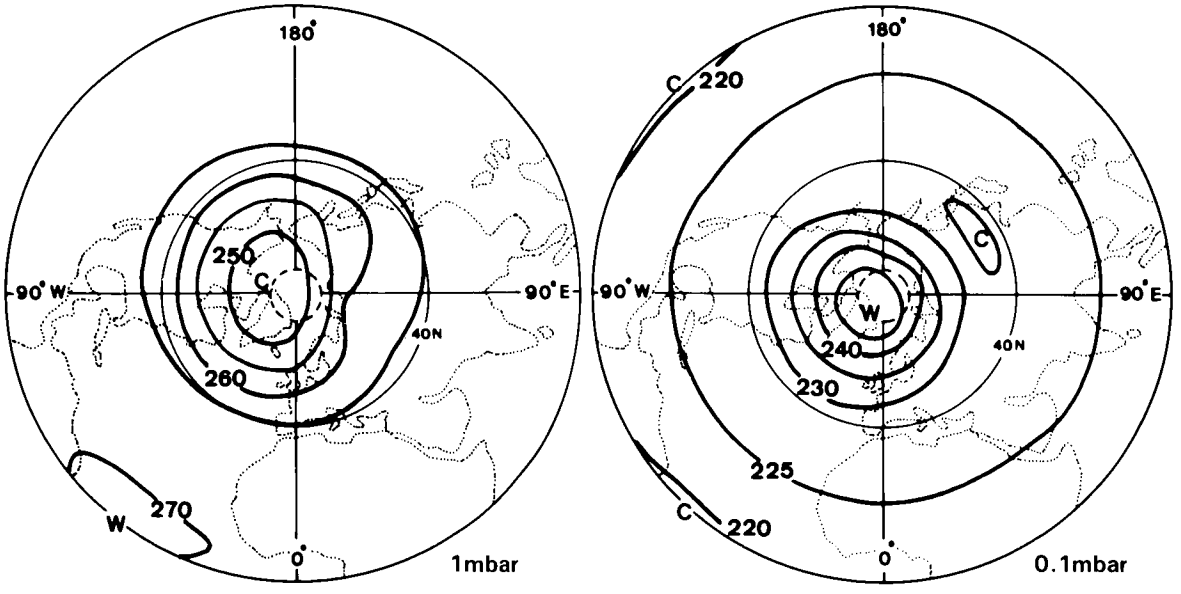

Figure D-30.2. Monthly mean temperature charts for October, Northern Hemisphere. (Data: 30-mbar: F.U. Berlin; otherwise: New Reference Atmosphere, MAP-Handbook, 16.)

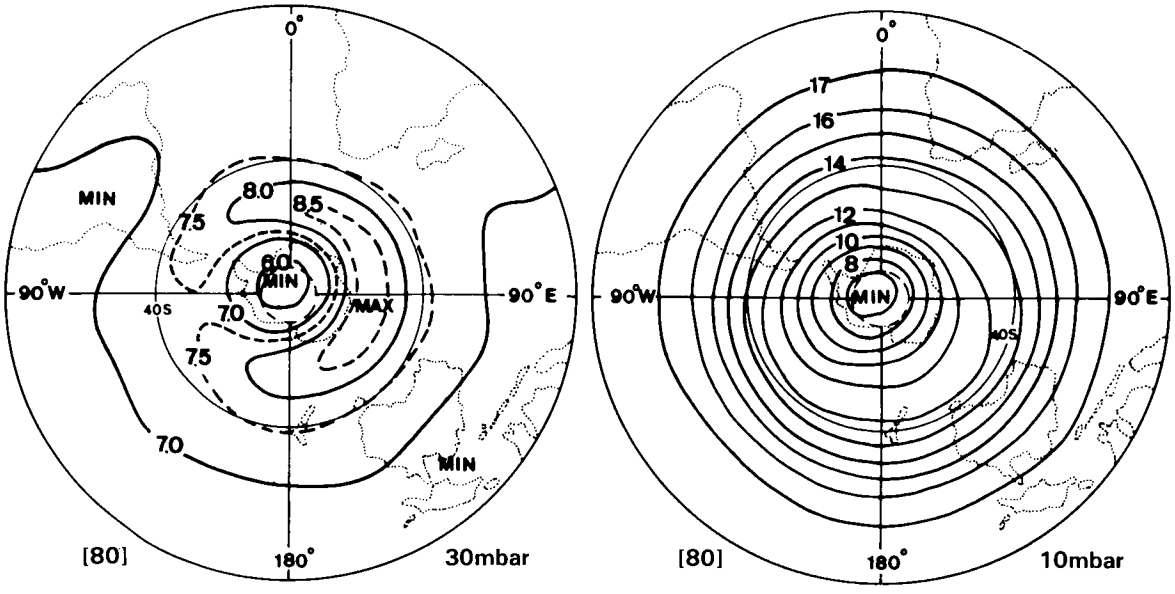

OZONE MASS MIXING RATIO (ppm)
OCTOBER S.H.

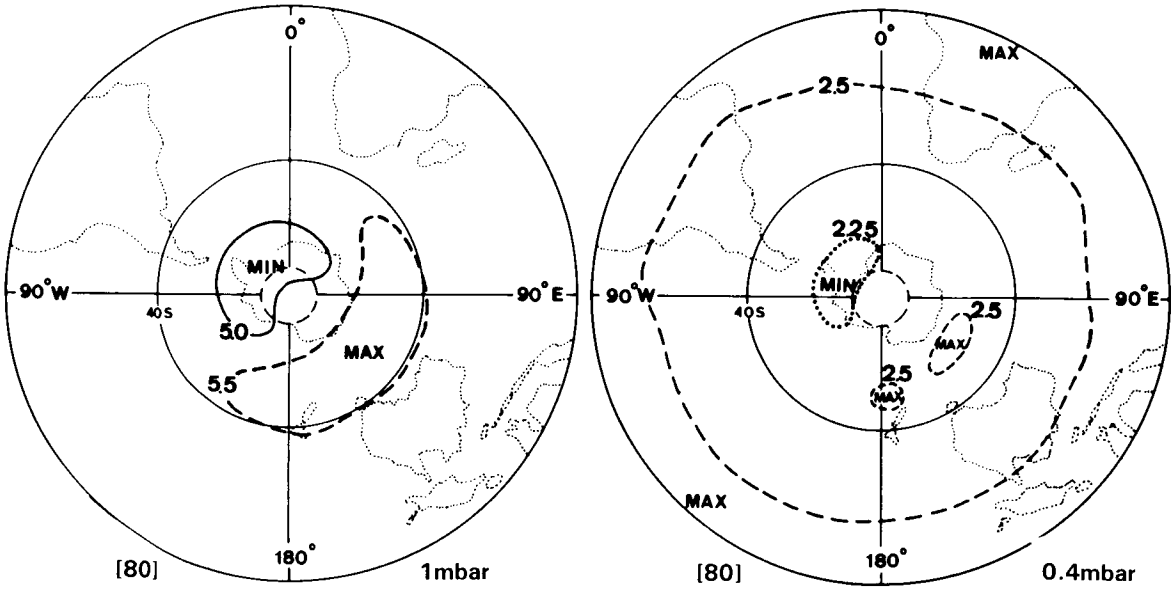

Figure D-30.3. Monthly average ozone mass mixing ratio (ppm) for the Southern Hemisphere from 1978–1982, for October. (R.M.Nagatani and A.J.Miller, personal communication.)

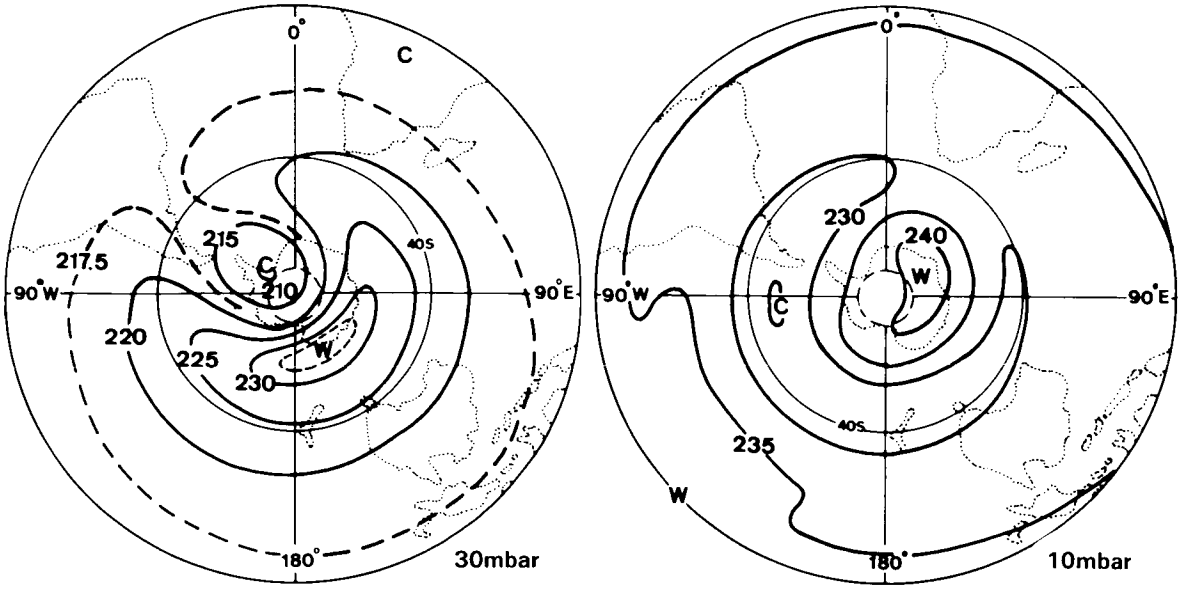

TEMPERATURE (K)
OCTOBER S.H.

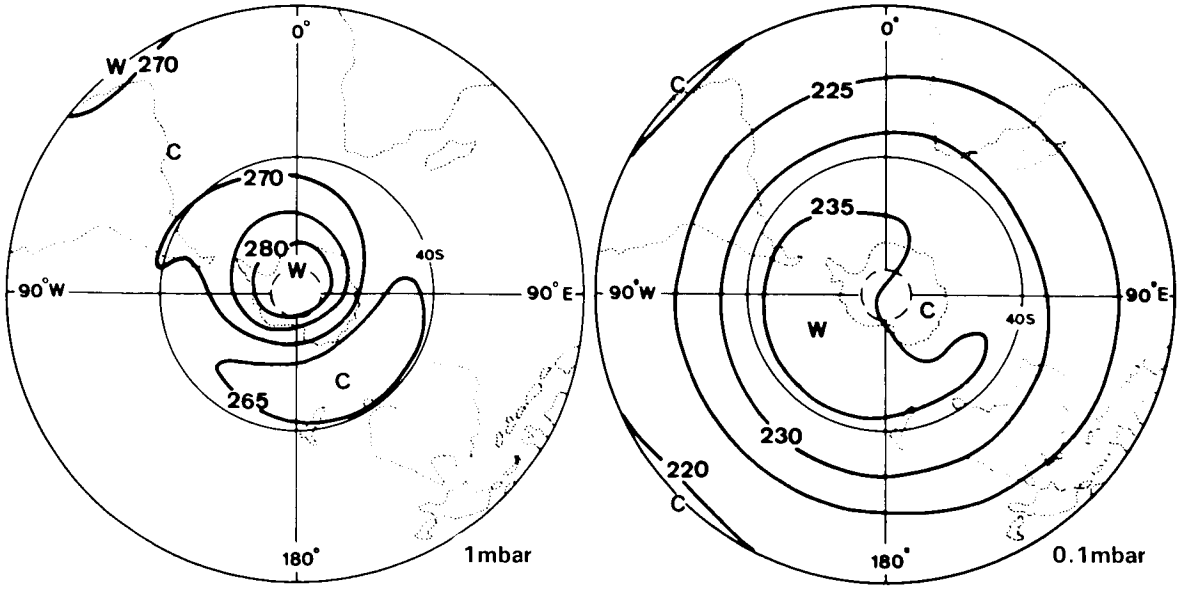

Figure D-30.4. Monthly mean temperature charts for October, Southern Hemisphere. (Data: 30-mbar: Knittel, 1976; otherwise: New Reference Atmosphere, MAP-Handbook, 16.)

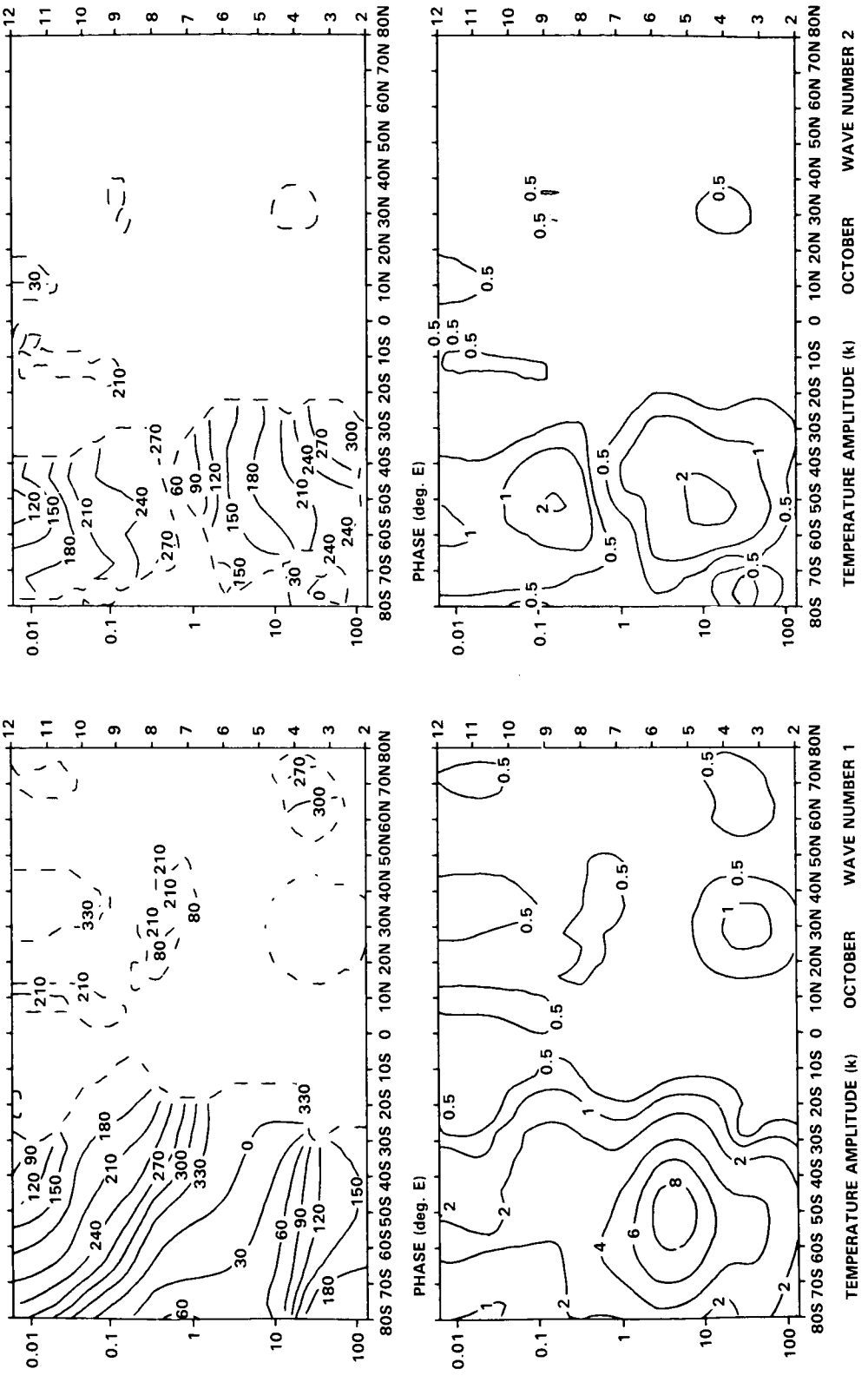

Figure D-31.1. Meridional height sections of temperature waves 1 and 2, January. (Data: New Reference Atmosphere, MAP-Handbook, 16.)

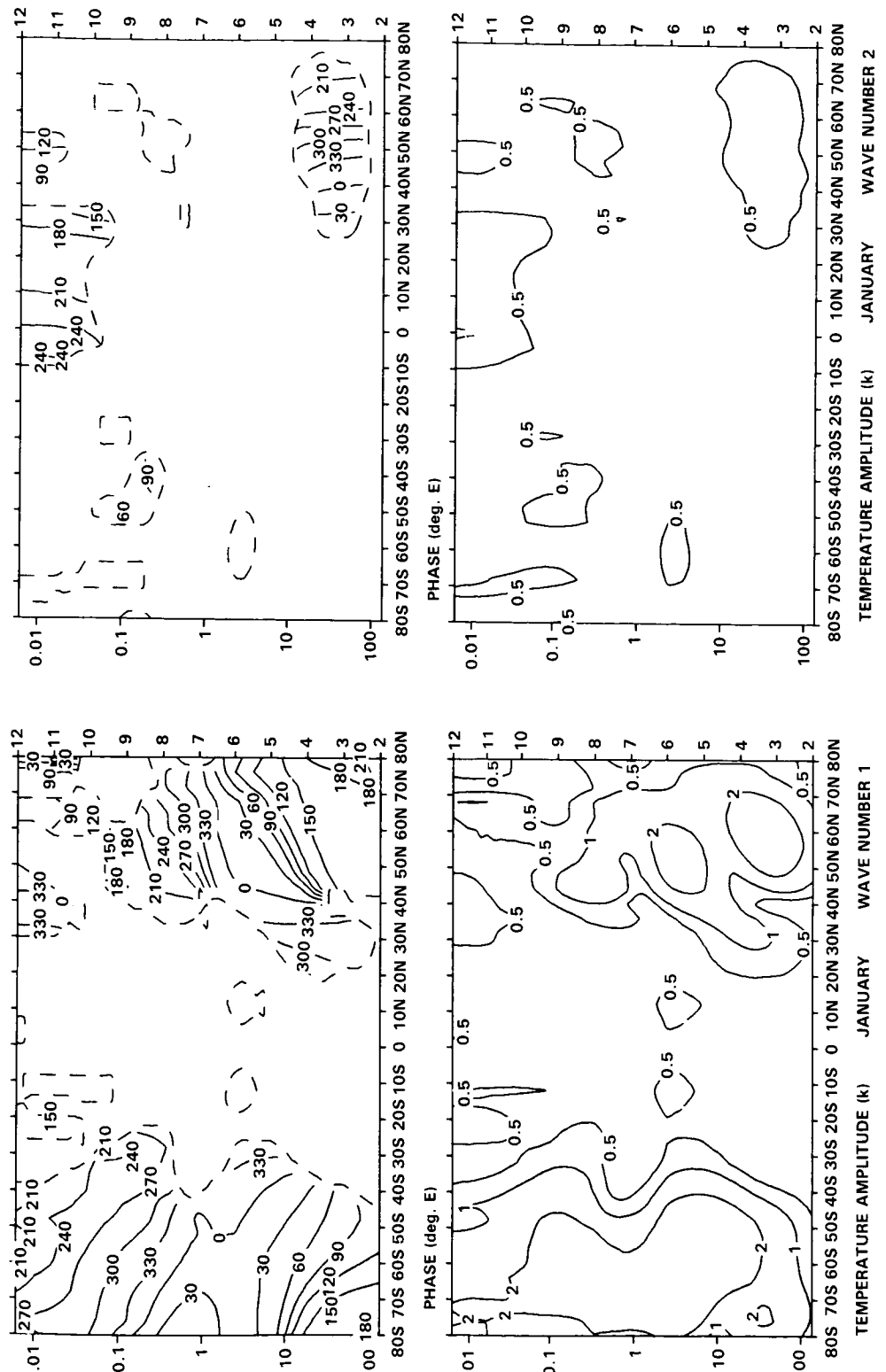

Figure D-31.2. Meridional height sections of temperature waves 1 and 2, April. (Data: New Reference Atmosphere, MAP-Handbook, 16.)

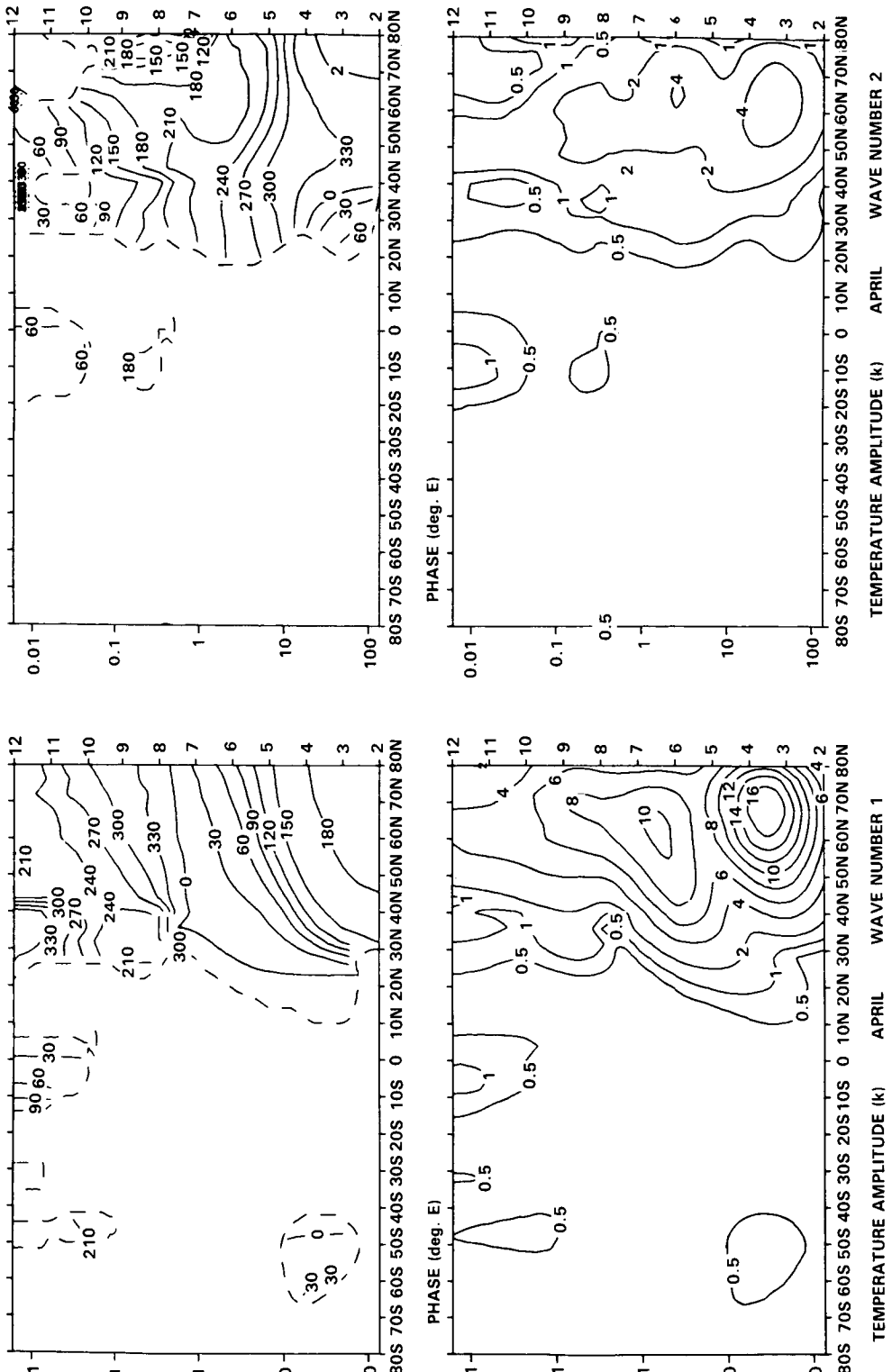

Figure D-31.3. Meridional height sections of temperature waves 1 and 2, July. (Data: New Reference Atmosphere, MAP-Handbook, 16.)

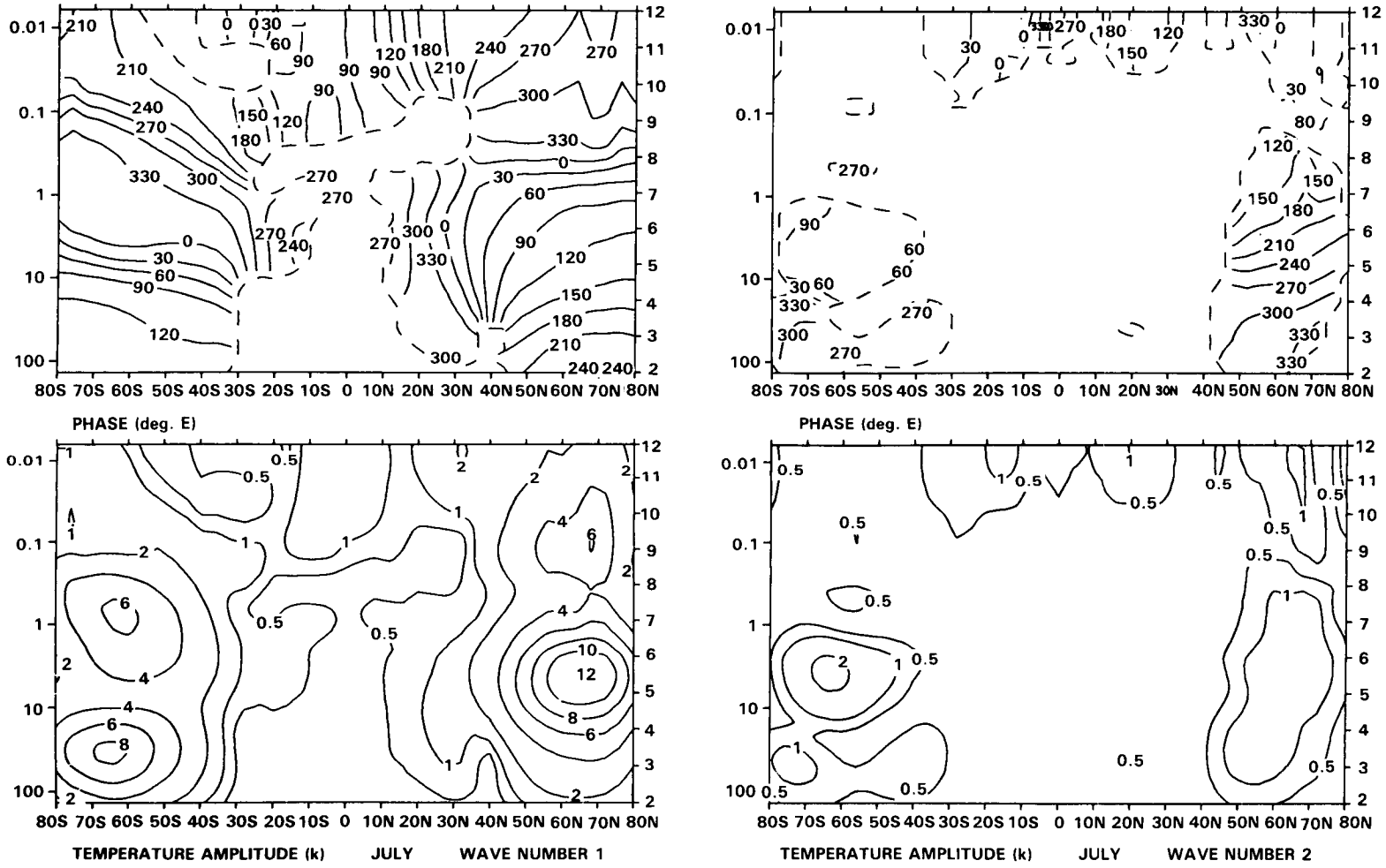

Figure D-31.4. Meridional height sections of temperature waves 1 and 2, October. (Data: New Reference Atmosphere, MAP-Handbook, 16.)

As pointed out before, wave 1 is approximately four times stronger than wave 2, both waves have their maximum in the lower and middle stratosphere over high northern latitudes, but extend into the upper mesosphere, and both waves are sloping westwards with height.

D-4.2.b April

Northern Hemisphere

Over the polar region the warming of the stratosphere and the cooling of the mesosphere is very large from midwinter to spring. But in April, during the spring transition time of the Northern Hemisphere, the remnants of the cold stratospheric polar vortex still dominate the temperature pattern, Figure D-28.2, longitudinal asymmetries still exist and the transition into summer is not completed. This is true also for the lower mesosphere and in strong contrast to the conditions during the spring reversal in the Southern Hemisphere, cf. Section D-3.1.b.

The charts of ozone mixing ratio show the same feature: the transition into summer is not yet completed, and the respective positive and negative correlations between ozone and temperature are remarkably large, considering the different types and times of the observations.

Southern Hemisphere

The radiational cooling of the stratosphere is extremely strong during the southern fall, resulting in an early establishment of the cold polar vortex and a concurrent warming of the mesosphere, Figure D-28.4. Typically, longitudinal variations are small over the Southern Hemisphere. But it is of interest to note the development of a weak warm area south of Australia at the 30-mbar level, Figure D-28.4, together with an ozone maximum at this level, Figure D-28.3.

Vertical Structure of Temperature Waves 1 and 2

During this time of the year both waves are approximately of the same size over both hemispheres, Figure D-31.2. This means that the waves during the northern spring are as weak as during the southern fall. And it is of interest to compare this with the respective Figure for October, cf. Figure D-31.4.

D-4.2.c July

Northern Hemisphere

During the northern summer the stratosphere is warmest over the polar region, Figure D-29.2, but not as warm as over the southern Arctic, cf. Figure D-27.4. This has been noted before (e.g., Barnett, 1974) and is due to the difference in solar heating of ozone, because of the ellipticity of the Earth's orbit, which produces a 6% modulation of the solar input. This temperature difference appears to exist throughout the mesosphere.

The ozone distribution is very regular during this time of the year.

Southern Hemisphere

During the southern winter the stratospheric polar vortex is extremely cold in the middle stratosphere, Figure D-29.4, and much colder than during the northern winter. In contrast, due to a more intense meri-

dional circulation the upper stratosphere and the lower mesosphere are less cold than during the northern winter, cf. Figure D-27.2. This explains why the height of the maximum of the annual temperature waves is lower over the Antarctic than over the Arctic, cf. Section D-2.1.a.

Note the very similar asymmetry of the temperature and ozone patterns at the 1-mbar level.

Vertical Structure of Temperature Waves 1 and 2

The vertical structure of the waves is given in Figure D-31.3. Compared with the respective Figure for January, Figure D-31.1, it is obvious that the amplitudes of the temperature waves 1 and 2 are only half of the values observed during the northern winters.

D-4.2.d October

Northern Hemisphere

During the northern fall the radiational cooling leads to the establishment of the cold stratospheric polar vortex together with the development of the "Aleutian High", i.e., the development of the planetary wave 1, Figures D-30.2 and D-31.4. This is one of the most important differences between the two hemispheres.

The build up of the ozone maximum in the lower stratosphere in conjunction with the build up of the Aleutian High is well in progress, Figure D-30.1.

Southern Hemisphere

In contrast to the Northern Hemisphere the transition into summer is already well advanced in the *upper* stratosphere, Figure D-30.4, (cf. Figure D-22). This characteristic difference has been described before, (Labitzke, 1974). One has to keep in mind, however, that this is not true for the *lower* stratosphere where the transition into summer is finished much later, cf. Section D-2.1.a.

Vertical Structure of Temperature Waves 1 and 2

The vertical structure of the temperature waves 1 and 2 is given in Figure D-31.4. As mentioned before the comparison with the respective Figure for April (Figure D-31.2) shows clearly the very different intensity of the planetary waves 1 and 2 over both hemispheres during spring and fall, respectively. In the lower stratosphere most of the wave activity of the Southern Hemisphere takes place during spring when the very intense "Final Warmings" bring the transition into summer. In contrast the largest wave activity in the Northern Hemisphere is observed during winter.

During the northern fall the planetary waves develop to much larger amplitudes than during the southern fall, Figs. D-31.4 and D-31.2.

A Fourier analysis along high latitudes results in large values of the amplitudes of wave 1, but also in relatively large values of wave 2, Figure D-31.1. For the quasi-stationary pattern which the monthly mean charts are presenting, these two waves account for 98% of the total variance, van Loon *et al.*, 1972.

Wave 1 is sloping westwards with height, Figure D-31.1, and is still well pronounced at the 1-mbar level (48km) which represents the upper stratosphere, Figure D-27.2.

The temperature gradient is reversed in the mesosphere, but wave 1 is still noticeable at the 0.1-mbar level (65km) which represents the lower mesosphere.

The charts showing the ozone mixing ratios, Figure D-27.1, reflect the strong positive correlation of ozone with temperature in the lower stratosphere as well as the strong negative correlation in the upper stratosphere and lower mesosphere. As regards the relatively regular pattern of ozone mixing ratio at the 10-mbar level, the reader is referred to Section D-1.2, Figure D-1. The weakest influence of dynamics must be expected in this region around the maximum of the ozone mixing ratio where the vertical advection term will be the smallest.

It should be noted that these maps represent an averaged state of the middle atmosphere and that the short-term variability during the northern winters is very large in connection with high-latitude stratospheric warmings-mesospheric coolings. This has been subject of many studies of which only a few are given here for reference: Labitzke, 1981 and 1982; McInturff,1978; Schoeberl, 1978.

Southern Hemisphere

During summer when the mean zonal winds in the stratosphere are from the east, the tropospheric waves cannot propagate into the stratosphere. Therefore the temperature distribution is very symmetric around the pole, Figure D-27.4.

The summer stratosphere is warmest over the polar region due to the heating of the ozone layer and the highest temperatures of the middle atmosphere are found over the South Pole at the stratopause, i.e., the 1-mbar level, and the lower mesosphere is still warmest over the polar region, although colder than at the stratopause, with a generally very flat temperature gradient.

The ozone distribution is similarly regular, Figure D-27.3. The negative correlation at the 0.1/0.4-mbar level is particularly worth noting, indicating rising motion within the belt of low temperatures/ large values of ozone mixing ratio.

Vertical Structure of Temperature Waves 1 and 2

The vertical structure of the temperature waves 1 and 2 is summarized in meridional height-sections, Figure D-31.1, which show the amplitudes and phases of these waves. For wave 1 the phase is the longitude (deg.E) of the maximum, while for wave 2 the phase is twice that longitude. Wave components are available for both hemispheres but are not given here for the Southern Hemisphere because they are small (about 0.5K) in summer. It should be noted that phases are not given where the amplitude is less than the lowest contour value and that this contour is indicated by a dashed line on the phase diagrams.

APPENDIX

LIST OF CONTRIBUTORS

CONTRIBUTORS

OVERALL CHAIRMAN

R.T. Watson
National Aeronautics and Space Administration—Headquarters
Washington, D.C. 20546

CHAPTER CHAIRMEN

D.L. Albritton—*Appendix C*
NOAA
Aeronomy Lab
R/E/AL6, Room 24-2107
325 Broadway
Boulder, Colorado 80303

G. Brasseur—*Chapter 8*
Institut d'Aeronomie Spatiale de Belgique
3 Avenue Circulaire
Brussels, B-1180 Belgium

R.A. Cox—*Chapter 2*
AERE Harwell
Environmental and Medical Science Div. B364
Oxfordshire OX11 ORA, England

W.B. DeMore—*Appendix A*
Jet Propulsion Laboratory
4800 Oak Grove Drive
Pasadena, California 91103

J.E. Frederick—*Chapter 7*
University of Chicago
Dept. of Geophysical Sciences
5734 South Ellis Avenue
Chicago, Illinois 60637

R. Gammon—*Chapter 3*
NOAA
PMEL/RE/PM
Bin #C25700
Building 3
7600 Sand Point Way, NE
Seattle, Washington 98115-0070

J.E. Harries—*Chapter 10*
Rutherford and Appleton Laboratories
Science Research Council
Chilton Didcot Oxon OQX, England

N. Husson—*Appendix B*
C.N.R.S.
Laboratoire de Meteorologie Dynamique
Ecole Polytechnique Route
Departmental 36
91198 Palaiseau Cedex, France

H.S. Johnston—*Chapter 13*
University of California
Department of Chemistry
Berkeley, California 94720

F. Kaufman, (deceased)—*Chapter 13*
University of Pittsburgh
Department of Chemistry
205 SRCC Building
Pittsburgh, Pennsylvania 15206

K. Labitzke—*Chapter 14* and *Appendix D*
Free University of Berlin
Dietrich-Schafer Weg 6-10
D-1000 Berlin 41, FRG

C.B. Leovy—*Chapter 7*
University of Washington
Department of Atmospheric Sciences
Seattle, Washington 98150

CONTRIBUTORS

A.J. Miller—*Chapters 8 and 14*
NOAA
National Meteorological Center
W333, Room 210
5200 Auth Road
Washington, D.C. 20233

V.A. Mohnen—*Chapter 4*
State University of New York
Atmospheric Science Research Center
400 Washington Avenue
Albany, New York 12222

M.J. Molina—*Chapter 11*
Jet Propulsion Laboratory
Mail Code: 183-601
4800 Oak Grove Drive
Pasadena, California 91109

R.A. Plumb—*Chapter 6*
CSIRO
Division of Atmospheric Research
Aspendale 3195 Victoria, Australia

J. Pyle—*Chapter 12*
University of Cambridge
Department of Physical Chemistry
Lensfield Rd.
Cambridge CB2 1EP England

V. Ramanathan—*Chapter 15*
National Center for Atmospheric Research
Climate Section
P.O. Box 3000
Boulder, Colorado 80307

H.I. Schiff—*Chapter 9*
York University
Department of Chemistry
4700 Keele Street
Downsview, Ontario M3J 1P3, Canada

A.F. Tuck—*Chapter 5*
Met.015
Meteorological Office
London Road
Bracknell Berkshire RG12 2SZ, England

S.C. Wofsy—*Chapter 3*
Harvard University
Pierce Hall
29 Oxford Street
Cambridge, Massachusetts 02138

R.J. Zander—*Appendix C*
University of Liege
Institute of Astrophysics
5 Avenue de Cointe
B-4200 Liege-Ougree, Belgium

OVERVIEW EDITORIAL COMMITTEE

Chapter Chairmen were responsible for editing their own chapters. The role of the editorial committee was to work with the chairmen to coordinate a wide range of activities associated with producing the chapters and to present a consistent style for the report.

F.M. Ormond
ORI, Inc.
Rockville, Maryland

R.S. Stolarski
NASA Goddard Space Flight Center
Greenbelt, Maryland

R.T. Watson
NASA Headquarters

PEER REVIEW PANEL AND AGENCY LIAISONS

Co-Chairmen

M. Geller
NASA Goddard

R.T. Watson
NASA Headquarters

D.L. Albritton—*Appendix C**
NOAA Aeronomy Laboratory

H. Bauer
Gesellschaft fur Strahlen und
Umweltforschung MBH Munchen
Bereich Projekttragerschaften
Josephspitalstr. 15
8000 Munchen 2, FRG

G. Brasseur—*Chapter 8*
Institut d'Aeronomie Spatiale de Belgique

R.A. Cox—*Chapter 2*
AERE Harwell

P. Crutzen
Max-Planck Institute for Atmospheric
Chemistry
SAARSTR 23, Postbox 3060
D-6500 Mainz, FRG

W.B. DeMore—*Appendix A*
Jet Propulsion Laboratory

D.H. Ehhalt
Institut fur Chemie
3 Atmosphaerische Chemie der
Kernforschung Sanlage
Julich GMBH Postfach 1913, FRG

J.E. Frederick—*Chapter 7*
University of Chicago

R. Gammon—*Chapter 3*
NOAA/PMEL

M.A. Geller
NASA
Goddard Space Flight Center
Code: 610
Greenbelt, Maryland 20771

A. Ghazi
Commission of the European Communities
Directorate-General for Science
Research and Development
Rue de la Loi 200
1049 Brussels, Belgium

R.F. Hampson
NASA Headquarters
Code: EE
Washington, D.C. 20546

J.E. Harries—*Chapter 10*
Rutherford and Appleton Laboratories

N. Husson—*Appendix B*
C.N.R.S.

H.S. Johnston—*Chapter 13*
University of California

N.P. Krull
Federal Aviation Administration
Office of Environment and Energy, AEE-30
800 Independence Avenue, S.W.
Washington, D.C. 20591

K. Labitzke—*Chapter 14 and Appendix D*
Free University of Berlin

*Full addresses for Chapter Chairmen are in first listing.

J. Mahlman
NOAA
Princeton University
Geophysical Fluid Dynamics Laboratory
P.O. Box 308
Princeton, New Jersey 08542

M.B. McElroy
Harvard University
Division of Applied Sciences
1350 Massachusetts Avenue
Cambridge, Massachusetts 02138

A.J. Miller—*Chapters 8 and 14*
NOAA

V. Mohnen—*Chapter 4*
State University of New York

M. Molina—*Chapter 11*
Jet Propulsion Laboratory

R.A. Plumb—*Chapter 6*
CSIRO

J. Pyle—*Chapter 12*
University of Cambridge

V. Ramanathan—*Chapter 15*
National Center for Atmospheric Research

F.S. Rowland
University of California
Department of Chemistry
Irvine, California 92717

H. I. Schiff—*Chapter 9*
York University

R.S. Stolarski
NASA
Goddard Space Flight Center
Code: 616
Greenbelt, Maryland 20771

N. Sundararaman
World Meteorological Organization
Case Postal 5
CH 1211 Geneva 20, Switzerland

N.D. Sze
Atmospheric and Environmental Research Inc.
840 Memorial Drive
Cambridge, Massachusetts 02139

A.F. Tuck—*Chapter 5*
Met. Office

P. Usher
United Nations Environment Program
P.O. Box 30552
Nairobi, Kenya

R.T. Watson
NASA Headquarters
Code: EE
Washington, D.C. 20546

PANEL MEMBERS

Alphabetical listing of all panel members. Some served on more than one panel. See the chapter title pages to identify membership of each panel.

D.E. Anderson, Jr.
Naval Research Laboratory

G.P. Anderson
Air Force Geophysical Laboratory

D.G. Andrews
Oxford University, England

J.K. Angell
National Oceanic and Atmospheric Administration

A. Barbe
Laboratoire de Physique Moleculaire
Faculte des Sciences, France

J.J. Barnett
Oxford University, England

P.K. Bhartia
Systems and Applied Sciences Corp.

P. Bowman
National Aeronautics and Space
Administration - Goddard

G. Brasseur
Institut d'Aeronomie Spatiale
de Belgique, Brussels, Belgium

E.V. Browell
National Aeronautics and Space
Administration - Langley

L.R. Brown
Jet Propulsion Laboratory

C. Burnett
National Oceanic and Atmospheric
Administration

D.M. Butler
National Aeronautics and Space
Administration - Headquarters

L.B. Callis, Jr.
National Aeronautics and Space
Administration - Langley

D. Cariolle
EERM/CNRM, France

B. Carli
Instituto de Ricerca
Onde Elettromagnetiche - CNR, Italy

R.D. Cess
State University of New York

W. Chameides
Georgia Institute of Technology

R.J. Cicerone
National Center for Atmospheric Research

M.T. Coffey
National Center for Atmospheric Research

M. Corney
Oxford University, England

E.F. Danielsen
National Aeronautics and Space
Administration - Ames

A.C. Delany
National Center for Atmospheric Research

J. DeLuisi
National Oceanic and Atmospheric
Administration

K.L. Demerjian
Environmental Protection Agency

W.B. DeMore
Jet Propulsion Laboratory

R. deZafra
State University of New York

R.E. Dickinson
National Center for Atmospheric Research

S.R. Drayson
University of Michigan

W.F.J. Evans
Atmospheric Environment Service, Canada

P. Fabian
Max-Planck Institute for
Aeronomie, FRG

C.B. Farmer
Jet Propulsion Laboratory

S. Fels
National Oceanic and Atmospheric Administration

E.E. Ferguson
National Oceanic and Atmospheric Administration

H. Fischer
University of Münich, FRG

A.J. Fleig
National Aeronautics and Space Administration - Goddard

J.E. Frederick
University of Chicago

L. Froidevaux
Jet Propulsion Laboratory

R.R. Garcia
National Center for Atmospheric Research

M.A. Geller
National Aeronautics and Space Administration - Goddard

J. Gille
National Center for Atmospheric Research

D.M. Golden
Stanford Research Institute

A. Goldman
University of Denver

W.L. Grose
National Aeronautics and Space Administration - Langley

P.D. Guthrie
National Aeronautics and Space Administration - Goddard

L.A. Hall
Air Force Geophysical Laboratory

R.F. Hampson
National Aeronautics and Space Administration - Headquarters

J.E. Hansen
Goddard Institute for Space Studies

R.T. Harriss
National Aeronautics and Space Administration - Langley

W. Heaps
National Aeronautics and Space Administration - Goddard

D. Heath
National Aeronautics and Space Administration - Goddard

E. Hilsenrath
National Aeronautics and Space Administration - Goddard

J. Holton
University of Washington

B. Hoskins
University of Reading, England

C.J. Howard
National Oceanic and Atmospheric Administration

I.S.A. Isaksen
National Center for Atmospheric Research

D.R. Johnson
University of Wisconsin

R. Jones
Meteorological Office, England

G.M. Keating
National Aeronautics and Space Administration - Langley

M.A.K. Khalil
Oregon Graduate Center

J. Kiehl
National Center for Atmospheric Research

D. Kley
Institut für Chemie, Julich, FRG

M. Ko
Atmospheric and Environmental
Research, Inc.

C.E. Kolb
Aerodyne Research, Inc.

A.J. Krueger
National Aeronautics and Space
Administration - Goddard

W.R. Kuhn
University of Michigan

M.J. Kurylo
National Bureau of Standards

A. Lacis
Goddard Institute of Space Studies

D. Lenschow
National Center for Atmospheric Research

R. Lesclaux
Universite de Bordeaux I, France

J.A. Logan
Harvard University

N. Louisnard
ONERA, France

F.M. Luther
Lawrence Livermore National Laboratory

J.D. Mahlman
NOAA Geophysical Fluid
Dynamics Laboratory

W.G. Mankin
National Center for Atmospheric Research

J.J. Margitan
Jet Propulsion Laboratory

C. Mateer
Atmospheric and Environment
Service, Canada

M.P. McCormick
National Aeronautics and Space
Administration - Langley

R.J. McNeal
National Aeronautics and Space
Administration - Headquarters

G. Megie
Service d'Aeronomie, CNRS, France

J.E. Mentall
National Aeronautics and Space
Administration - Goddard

P. Midgley
ICI Americas, Inc.

A.J. Miller
National Oceanic and Atmospheric
Administration

M.J. Molina
Jet Propulsion Laboratory

G.H. Mount
National Research Laboratory, England

D.G. Murcray
University of Denver

R.M. Nagatani
National Oceanic and Atmospheric
Administration

T.B. Narijokat
Free University of Berlin, FRG

R. Newell
Massachusetts Institute of Technology

CONTRIBUTORS

M. Nicolet
Aeronomy Laboratory, Brussels, Belgium

J. Noxon
National Oceanic and Atmospheric Administration

A. O'Neill
Meteorological Office, England

A.J. Owens
DuPont Company

S.A. Penkett
AERE Harwell, England

H.M. Pickett
Jet Propulsion Laboratory

U. Platt
Institut für Chemie - KFA, FRG

R.A. Plumb
CSIRO, Australia

S. Pollitt
National Physical Laboratory, England

M. Prather
Goddard Institute for Space Studies

J. Pyle
University of Cambridge, England

A.R. Ravishankara
National Oceanic and Atmospheric Administration

R.A. Reck
General Motors Research Laboratories

G. Reinsel
University of Wisconsin

B.A. Ridley
National Center for Atmospheric Research

D.E. Robbins
National Aeronautics and Space Administration - Johnson

A.E. Roche
Lockheed Palo Alto Research Laboratories

C.D. Rodgers
Oxford University, England

H. Roscoe
Oxford University, England

L.S. Rothman
Air Force Geophysical Laboratory

G. Rottman
University of Colorado

J.M. Russell, III
National Aeronautics and Space Administration - Langley

M.L. Salby
University of Colorado

S.P. Sander
Jet Propulsion Laboratory

M.E. Schlesinger
Oregon State University

U. Schmailzl
Max-Planck Institut für Chemie, FRG

A.L. Schmeltekopf
National Oceanic and Atmospheric Administration

U. Schmidt
Institut für Chemie, FRG

M.R. Schoeberl
National Aeronautics and Space Administration - Goddard

U. Schurath
University of Bonn, FRG

P. da Silva Dias
University of Sao Paulo, Brazil

P.C. Simon
Institut d'Aeronomie Spatiale
de Belgique, Brussels, Belgium

M.A.H. Smith
National Aeronautics and Space
Administration - Langley

S. Solomon
National Oceanic and Atmospheric
Administration

F. Stordal
National Center for Atmospheric Research

N.D. Sze
Atmospheric and Environmental
Research, Inc.

G. Tiao
University of Chicago

R.J. Thomas
University of Colorado

W.A. Traub
Smithsonian Astrophysical Observatory

K.K. Tung
Massachusetts Institute of Technology

G. Vaughan
University College of Wales, UK

R.A. Vincent
University of Adelaide, Australia

G. Visconti
University of Aquila, Italy

J.W. Waters
Jet Propulsion Laboratory

R.T. Watson
National Aeronautics and Space
Administration - Headquarters

D.J. Wuebbles
Lawrence Livermore National
Laboratory

R.J. Zander
University of Liege, Belgium

R. Zellner
Universitat Goettingen, FRG

ACKNOWLEDGEMENTS

(exclusive of those already listed above)

Reviewers

A. Aikin
NASA/Goddard

J.G. Anderson
Harvard University

A.M. Bass
National Bureau of Standards

C. Bruehl
Max Planck Institut für Chem.

A. Chedin
C.N.R.S.

P. Connell
Lawrence Livermore National Laboratory

A. Douglass
Applied Research Corporation

D.E. Freeman
Harvard University

CONTRIBUTORS

R. Greenstone
ORI, Inc.

J. Herman
NASA/Goddard

C. Jackman
NASA/Goddard

J. Kaye
NASA/Goddard

S. Liu
NOAA Aeronomy Lab.

S. Manabe
Geophysical Fluid Dynamics Lab.

D.S. McKenna
U.K. Met. Office

R. McPeters
NASA/Goddard

R.G. Prinn
MIT

R. Rood
Applied Research Corporation

R. Selkirk
MIT Met. Dept.

R. Stewart
NASA/Goddard

Editorial

M.A. Baldauf
RMS, Inc.

R. Duffy
NASA/Goddard

G. Escobar
NCAR

B. Kibling
ORI, Inc.

C.A. Meetre
SAR, Inc.

K. Taylor
ORI, Inc.

Design, Art, Typesetting and Production
Jands, Inc.
Silver Spring, Maryland

Jerry Mendelson, President

David Callahan, Studio Director

Dorothy Jenkins, Publications Manager

Jodine Bloom, Production Supervisor

Chris Miller, Senior Proofreader

and a dedicated group of 27 art,
typesetting and production personnel

APPENDIX F

LIST OF FIGURES

APPENDIX F
INDEX OF FIGURES

FIGURES

FIGURES

FIGURES

Page

FIGURES

FIGURES

FIGURES

FIGURES

FIGURES

FIGURES

FIGURES

FIGURES

Page

Page

FIGURES

FIGURES

FIGURES

FIGURES

FIGURES

APPENDIX

LIST OF TABLES

APPENDIX G
INDEX OF TABLES

TABLES

TABLES

TABLES

APPENDIX H

MAJOR ACRONYMS

APPENDIX H
ACRONYMS

Units, Instruments, Satellites, and Programs

AE	Atmospheric Explorer
AEM	Applications Explorer Mission
ATMOS	Atmospheric Trace Molecule Spectroscopy Experiment
AVHRR	Advanced Very High Resolution Radiometer
BMLS	Balloon-borne Microwave Limb Sounder
BSU	Basic Sounding Unit
BUV	Backscattered Ultraviolet Spectrometer
BIC	Balloon Intercomparison Campaign
BOIC	Balloon Ozone Intercomparison Campaign
CIAP	Climatic Impact Assessment Program
DMSP	Defense Meteorological Satellite Program
DU	Dobson Unit = milliatm-cm = 2.687×10^{16} molecules cm^{-2}
ECC	Electrochemical cell (ozonesonde)
ECD	Electron Capture Detection
ERBS	Earth Radiation Budget Satellite
FTS	Fourier Transform Spectrometer
GARP	Global Atmospheric Research Program
GATE	GARP Atlantic Tropical Experiment
GC	Gas Chromatography
GCM	General Circulation Model
GMCC	Geophysical Monitoring for Climatic Change
GOES	Geosynchronous Operational Environment Satellite
GLOBUS	Global Budget of Stratospheric Trace Constituents
HALOE	Halogen Occultation Experiment
HAPP	High Altitude Pollution Program
HIRS	High Resolution Infrared Radiation Sounder
IORI	International Ozone Rocketsonde Intercomparison
IRIS	Infrared Interferometer Spectrometer
ITCZ	Intertropical Convergence Zone
ITOS	Improved TIROS Operational Satellite
ITPR	Infrared Temperature Profile Radiometer

ACRONYMS

LHR	Laser Heterodyne Radiometer
LIMS	Limb Infrared Monitor of the Stratosphere
LRIR	Limb Radiance Inversion Radiometer
MAP	Middle Atmosphere Program
MFR	Multichannel Filter Radiometer
MM	Mechanistic Model
MS	Mass Spectrometry
MST	Mesosphere, Stratosphere, Troposphere (radar)
MSU	Microwave Sounding Unit
MUSE	Monitor of Ultraviolet Solar Energy
NOPS	Nimbus Operational Processing System
OAO	Orbiting Astronomical Observatory
OGO	Orbiting Geophysical Observatory
OSO	Orbiting Solar Observatory
PEPSIOS	Poly-Etalon Pressure Scanned Interferometer
PMR	Pressure Modulated Radiometer
SAGE	Stratospheric Aerosol and Gas Experiment
SAMS	Stratospheric and Mesospheric Sounder
SAM II	Stratospheric Aerosol Measurement II
SBUV	Solar and Backscatter Ultraviolet Spectrometer
SCR	Selective Chopper Radiometer
SIRS	Satellite Infrared Spectrometer
SME	Solar Mesosphere Explorer
SPE	Solar Proton Event
SSH	Special Sensor H (also called MFR)
SST	Supersonic Transport
SSU	Stratospheric Sounding Unit
TIROS	Television and Infrared Observation Satellite
TOMS	Total Ozone Mapping System/Spectrometer
TOVS	TIROS Operational Vertical Sounder
UARS	Upper Atmosphere Research Satellite
VTPR	Vertical Temperature Profile Radiometer

Institutions

AER, Inc.	Atmospheric and Environmental Research, Incorporated 872 Massachusetts Avenue Cambridge, Massachusetts 02139 USA
AERE Harwell	Atomic Energy Research Establishment Harwell Oxfordshire OX11 ORA, United Kingdom
AES	Atmospheric Environment Service 4905 Dufferin Street Downsview, Ontario M3H 5T4, Canada
AFGL	Air Force Geophysics Laboratory Bedford, Massachusetts USA
AIAA	American Institute of Aeronautics and Astronautics, Inc. Technical Information Center 555 West 57th Street New York, New York 10019 USA
ARC	Ames Research Center Moffett Field, California 94035 USA
ASL	Atmospheric Sciences Laboratory White Sands Missile Range New Mexico 88002 USA
BMFT	Bundesministerium für Forschung und Technologie Federal Republic of Germany
BMO	British Meteorological Office London Road Bracknell, Berkshire RG12 2SZ, United Kingdom
CEC	Commission of the European Communities Rue de la Loi 200 Brussels, Belgium
CMA	Chemical Manufacturers Association 2501 M Street, N.W. Washington, DC 20037 USA
CNRS	Center National de la Recherche Scientifique 91370 Verrieres le Buisson, France

ACRONYMS

CNRS-FRS	CNRS - Faculte des Sciences de Reims
CNRS-SA	CNRS - Service d'Aeronomie CNRS - Laboratoire de Meteorologie Dynamique
CODATA	Committee on Data for Science and Technology 51 Boulevard de Montmorency Paris, France
COMESA	Committee on Meteorological Effects of Stratospheric Aircraft Meteorological Office Bracknell, United Kingdom
CSIRO	Commonwealth Scientific and Industrial Research Organization Australia
DOD	Department of Defense (USA)
DOT	Department of Transportation (USA)
DU	Denver University
Du Pont	E.I. du Pont de Nemours & Co. Experimental Station Wilmington, Delaware 19898 USA
EERM	Meteorologie Nationale EERM Boulogne-Billancourt France
EPA	Environmental Protection Agency Washington, D.C. 20460 USA
FAA	Federal Aviation Administration Washington, D.C. 20591 USA
FPP	Fluorocarbon Program Panel (of the CMA)
GFDL	Geophysical Fluid Dynamics Laboratory P.O. Box 308, Princeton University Princeton, New Jersey 08540 USA
GISS	Goddard Institute of Space Studies New York, New York 10025 USA

GIT	Georgia Institute of Technology Atlanta, Georgia 30332 USA
GSFC	Goddard Space Flight Center Greenbelt, Maryland 20771 USA
HU	Harvard University Cambridge, Massachusetts USA
IASB	Institut d'Aeronomie Spatiale de Belgique Brussels, Belgium
IROE	Instituto diRicherca sulle Onde Electromagnetiche (Italy)
JPL	Jet Propulsion Laboratory 4800 Oak Grove Drive Pasadena, California 91103 USA
JSC	Johnson Space Center Houston, Texas USA
KFA	Institut für Chemie der Kernforschungsanlage Julich Postfach 1913, D-5170 Julich Federal Republic of Germany
KPNO	Kitt Peak National Observatory Tucson, Arizona USA
LaRC	Langley Research Center Hampton, Virginia 23665 USA
LLNL	Lawrence Livermore National Laboratory P.O. Box 808 Livermore, California 94550 USA
MET. O.	Meteorological Office London Road Bracknell, Berkshire RG12 2S2 United Kingdom
MIM	Met. Institut Munich, Federal Republic of Germany
MIT	Massachusetts Institute of Technology Cambridge, Massachusetts 02139 USA

ACRONYMS

MOH	Meteorologisches Observatorium Hohenpeissenberg, Federal Republic of Germany
MPAE	Max Planck Institut für Aeronomie Postfach 20, D-3411 Katlenburg, Lindau 3 Federal Republic of Germany
MPN	Meteorologie Nationale (France)
MPIC, MPI-Mainz	Max Planck Institut für Chemie Saarstrasse 23, D-65 Mainz Federal Republic of Germany
NAS	National Academy of Sciences 2101 Constitution Avenue, N.W. Washington, D.C. 20418 USA
NASA	National Aeronautics and Space Administration Headquarters Washington, D.C. 20546 USA
NBS	National Bureau of Standards Gaithersburg, Maryland 20899 USA
NCAR	National Center for Atmospheric Research P.O. Box 3000 Boulder, Colorado 80307 USA
NCC	National Climatic Center Asheville, North Carolina 28801 USA
NESS	National Earth Satellite Service Suitland, Maryland 20233 USA
NOAA	National Oceanic and Atmospheric Administration Headquarters Rockville, Maryland 20852 USA
NOAA-AL	NOAA Aeronomy Laboratory, Boulder, Colorado 80303 USA
NOAA-ERL	NOAA Environmental Research Lab., Boulder, Colorado 80303 USA
NOAA-GMCC	NOAA Geophysical Monitoring for Climate Change USA
NPL	National Physics Laboratory Teddington, Middlesex, United Kingdom
NRC	National Research Council (of the NAS) Washington, D.C. USA

NSF	National Science Foundation Washington, D.C. USA
NSSDC	National Space Science Data Center Goddard Space Flight Center Greenbelt, Maryland 20771 USA
NTIS	National Technical Information Service Springfield, Virginia 22151 USA
OECD	Organization for Economic Cooperation and Development Paris, France
OHP	Observatoire de Haute Provence Chiran, France
ONERA	Office National d'Etudes et de Recherches Aerospatiales Chatillion, Bagneux, France
ONR	Office of Naval Research, Washington, D.C. USA
NWS	National Weather Service Silver Spring, Maryland 20910 USA
RAL	Rutherford and Appleton Laboratories Chilton, Didcot OXON OQX, United Kingdom
SAO	Smithsonian Astrophysical Observatory Cambridge, Massachusetts USA
SUNY	State University of New York
UK DOE	United Kingdom Department of the Environment
UL	Universite de Liege Liege-Ougree, Belgium
UM	University of Minnesota
UNEP	United Nations Environment Program Nairobi, Kenya
UO	University of Oxford Oxford, United Kingdom

ACRONYMS

UT	University of Tokyo, Japan
WMO	World Meteorological Organization Case Postal No. 5 Geneva 20, Switzerland

APPENDIX

CHEMICAL FORMULAE AND NOMENCLATURE

APPENDIX I

Chemical Formulae and Nomenclature

Symbol	Name
O	atomic oxygen
O_2	molecular oxygen
O_3	ozone
O_x	odd oxygen (O,$O(^1D)$,O_3)
N_2	molecular nitrogen
N_2O	nitrous oxide
NO	nitric oxide
NO_2	nitrogen dioxide
NO_3	nitrogen trioxide, nitrate radical
NO_y	odd nitrogen (NO, NO_2, NO_3, N_2O_5, $ClONO_2$, HNO_4, HNO_3)
NO_x	oxides of nitrogen (NO, NO_2, NO_3)
N_2O_5	dinitrogen pentoxide
HNO_2, HONO	nitrous acid
HNO_3, $HONO_2$	nitric acid
HNO_4, HO_2NO_2	peroxynitric acid
NH_3	ammonia
H_2O	water vapor
H_2O_2	hydrogen peroxide
OH, HO	hydroxyl radical
HO_2	hydroperoxyl radical
HO_x	odd hydrogen (OH, HO_2, H_2O_2)

Symbol	Name
CO	carbon monoxide
CO_2	carbon dioxide
CS_2	carbon disulfide
COS, OCS	carbonyl sulfide
SO_2	sulfur dioxide
SF_6	sulfur hexafluoride
H_2SO_4	sulfuric acid
HF	hydrogen fluoride
HCl	hydrogen chloride
HCN	hydrogen cyanide
HOCl	hypochlorous acid
Cl	chlorine atom
ClO	chlorine monoxide
$ClONO_2$, $ClNO_3$	chlorine nitrate
Cl_x	odd chlorine, inorganic chlorine
CH_4	methane
C_2H_6	ethane
C_3H_8	propane
C_2H_4	ethylene
C_2H_2	acetylene
CH_2O	formaldehyde
CH_3CHO	acetaldehyde
$(CH_3)_2CO$	acetone

Symbol	Name
CH_3O_2H	methyl hydroperoxide
CH_2CHCHO	acrolein
C_2Cl_4	tetrachloroethylene
CH_3Cl	methyl chloride
CH_2Cl_2	methylene chloride, dichloromethane
$CHCl_3$	chloroform, trichloromethane
CFC	chlorofluorocarbon
HC	hydrocarbon
NMHC	non-methane hydrocarbons
PAN	peroxyacetylnitrate
CH_3CCl_3	methyl chloroform
C_2F_6	hexafluoroethane
CCl_4	carbon tetrachloride (FC-10)
CCl_3F	trichlorofluoromethane (FC-11)
CCl_2F_2	dichlorodifluoromethane (FC-12)
$CClF_3$	chlorotrifluoromethane (FC-13)
CF_4	tetrafluoromethane (FC-14)
$CHCl_2F$	dichlorofluoromethane (FC-21)
$CHClF_2$	chlorodifluoromethane (FC-22)
CCl_2FCClF_2	trichlorotrifluoroethane (FC-113)
$CClF_2CClF_2$	dichlorotetrafluoroethane (FC-114)
$CClF_2CF_3$	chloropentafluoroethane (FC-115)
CF_3CF_3	hexafluoroethane (FC-116)

FORMULAE

Symbol	Name
CH_3CN	methyl cyanide
CH_3I	methyl iodide
Br	bromine atom
BrO	bromine monoxide
BrO_x	odd bromine, inorganic bromine
$CBrF_3$	trifluorobromomethane
$CHBr_3$	bromoform, tribromomethane
CH_3Br	methyl bromide
CH_2Br_2	dibromomethane
$CHBr_2Cl$	dibromochloromethane
CH_2BrCl	bromochloromethane
$C_2H_4Br_2$	dibromoethane
$CBrClF_2$	Halon 1211 (BCF) FC-12B1
CF_3Br	Halon 1301 FC-13B1

APPENDIX J

PRESSURE—ALTITUDE CONVERSION CHART

APPENDIX J

PRESSURE-ALTITUDE CONVERSION CHART

PRESSURE-ALTITUDE

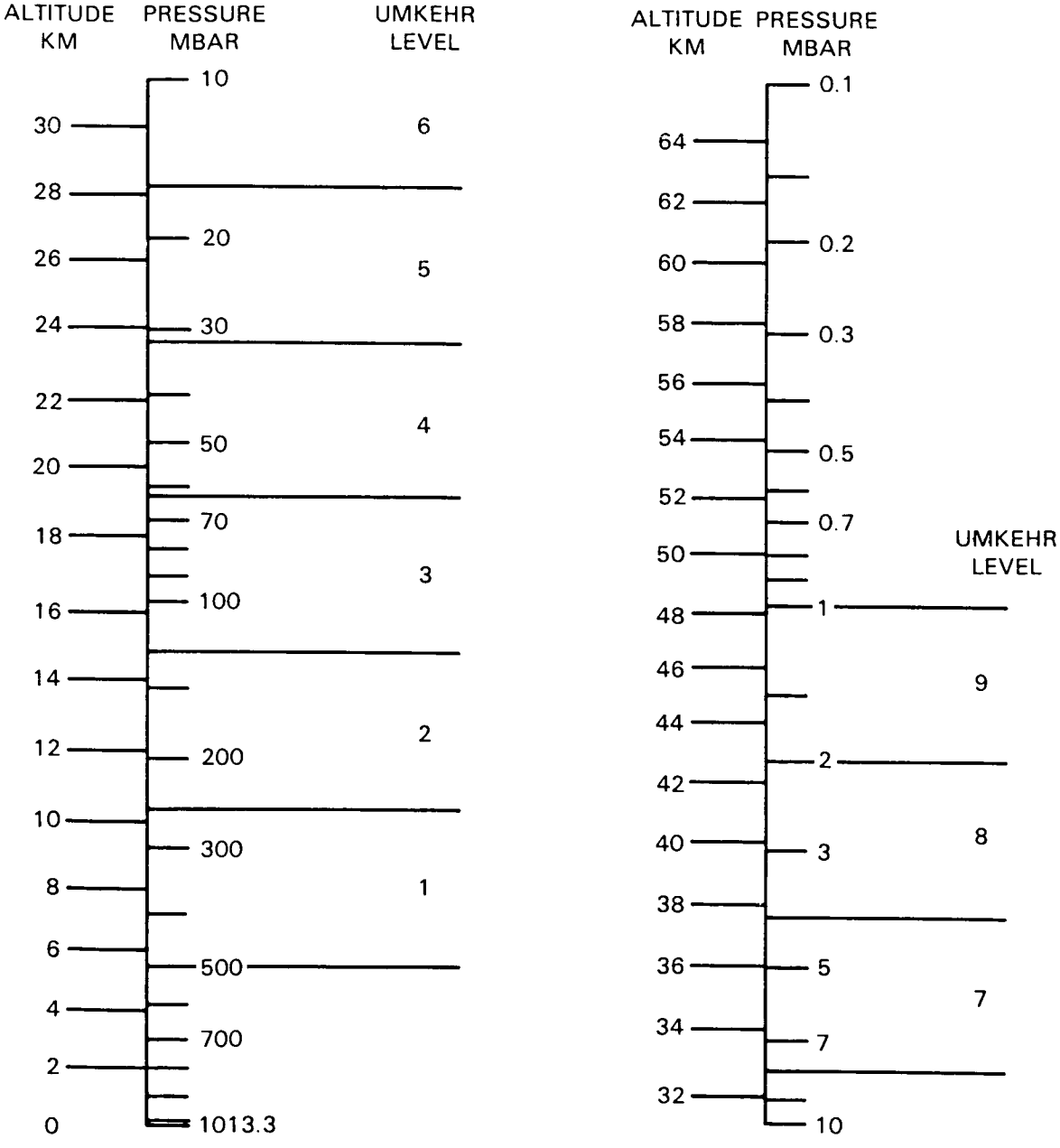

ALTITUDES ARE BASED ON U.S. STANDARD ATMOSPHERE, 1976. THE ACTUAL ALTITUDE FOR A GIVEN PRESSURE MAY DIFFER BY AS MUCH AS 2 KM, DEPENDING ON SEASON, LATITUDE, AND SHORT TERM VARIATIONS.

REFERENCES

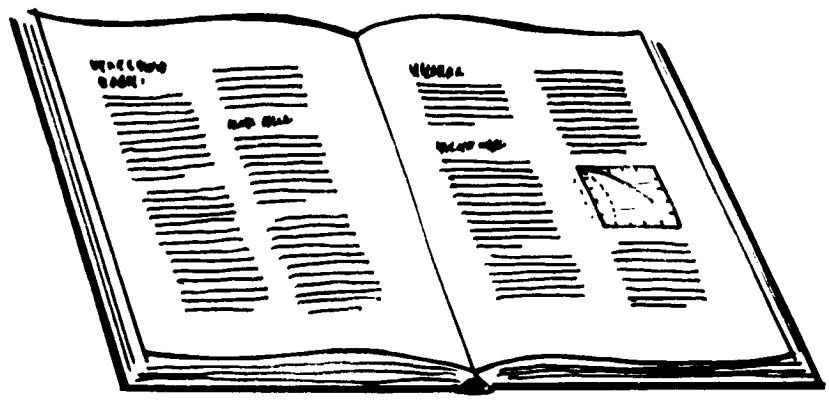

Research Panel

C. Meetre — Database Designer

M.A. Baldauf
K. Taylor

APPENDIX: REFERENCES

Abbas, M. M., T. Kostiuk, M. J. Mumma, D. Buhl, V. G. Kunde, and L. W. Brown, Stratospheric ozone measurement with an infrared heterodyne spectrometer, *Geophys. Res. Lett.*, *5*, 317-320, 1978.

Ackerman, M., Ultraviolet solar radiation related to mesospheric processes, in *Mesospheric Models and Related Experiments*, edited by G. Fiocco, pp. 149-159, D. Reidel, Dordrecht, 1971.

Ackerman, M., and C. Muller, Stratospheric methane and nitrogen dioxide from infrared spectra, *Pure Appl. Geophys.*, *106-108*, 1325-1335, 1973.

Ackerman, M., J. C. Fontanella, D. Frimout, A. Girard, N. Louisnard, and C. Muller, Simultaneous measurements of NO and NO_2 in the stratosphere, *Planet. Space Sci.*, *23*, 651-660, 1975.

Ackerman, M., D. Frimout, A. Girard, A. Gottignies, and C. Muller, Stratospheric HCl from infrared spectra, *Geophys. Res. Lett.*, *3*, 81-83, 1976.

Ackerman, M., D. Frimout, C. Muller, and D. J. Wuebbles, Stratospheric methane measurements and predictions, *Pure Appl. Geophys.*, *117*, 367-380, 1978/79.

Ackerman, M., C. Lippens, C. Muller, J. Vercheval, J. Besson, A. Girard, J. Laurent, and M. P. Lemaitre, Observations of middle atmosphere CH_4 and N_2O vertical distributions by the Spacelab one grille spectrometer, *Geophys. Res. Lett.*, submitted, 1985.

Ahlquist, J., Normal-mode global Rossby waves, theory and observations, *J. Atmos. Sci.*, *39*, 193-202, 1982.

Aikin, A. C., B. Woodgate, and H. J. P. Smith, Equatorial ozone profiles from the solar maximum mission - A comparison with theory, *Planet. Space Sci.*, *32*, 503-513, 1984.

Aimedieu, P., P. Rigaud, and J. Barat, The sunrise ozone depletion problem of the upper stratosphere, *Geophys. Res. Lett.*, *8*, 787-789, 1981.

Aimedieu, P., A. J. Krueger, D. E. Robbins, and P. C. Simon, Ozone profile intercomparison based on simultaneous observations between 20 and 40 km, *Planet. Space Sci.*, *31*, 801-807, 1983.

Al-Ajmi, D. N., R. S. Harwood, and T. Miles, A sudden warming in the middle atmosphere of the Southern Hemisphere, *Quart. J. Roy. Meteorol. Soc.*, *111*, 359-389, 1985.

Allam, R. J., and A. F. Tuck, Transport of water vapour in a stratosphere-troposphere general circulation model I. Fluxes, *Quart. J. Roy. Meteorol. Soc.*, *110*, 321-356, 1984a.

Allam, R. J., and A. F. Tuck, Transport of water vapour in a stratosphere-troposphere general circulation model II. Trajectories, *Quart. J. Roy. Meteorol. Soc.*, *110*, 357-392, 1984b.

Allam, R. J., K. S. Groves, and A. F. Tuck, Global OH distribution derived from general circulation model fields of ozone and water vapor, *J. Geophys. Res.*, *86*, 5303-5320, 1981.

Allen, D. C., J. D. Haigh, J. T. Houghton, and C. J. S. M. Simpson, Radiative cooling near the mesopause, *Nature*, *281*, 660-661, 1979.

Allen, D. C., T. Scragg, and C. J. S. M. Simpson, Low temperature fluorescence studies of the deactivation of the bend-stretch manifold of CO_2, *Chem. Phys.*, *51*, 279-298, 1980.

Allen, M., and J. E. Frederick, Effective photodissociation cross sections for molecular oxygen and nitric oxide in the Schumann-Runge bands, *J. Atmos. Sci.*, *39*, 2066-2075, 1982.

Allen, M., J. I. Lunine, and Y. L. Yung, The vertical distribution of ozone in the mesosphere and lower thermosphere, *J. Geophys. Res.*, *89*, 4841-4872, 1984.

Alpert, J. C., M. A. Geller, and S. K. Avery, The response of stationary planetary waves to tropospheric forcing, *J. Atmos. Sci.*, *40*, 2467-2483, 1983.

Altshuller, A. P., and J. J. Bufalini, Photochemical aspects of air pollution: A review, *Environ. Sci. Technol.*, *5*, 39-64, 1971.

Anderson, G. P., and L. A. Hall, Attenuation of solar irradiance in the stratosphere: Spectrometer measurements between 191 and 207 nm, *J. Geophys. Res.*, *88*, 6801-6806, 1983.

Anderson, J. G., The absolute concentration of OH ($X^2\pi$) in the Earth's stratosphere, *Geophys. Res. Lett.*, *3*, 165-168, 1976.

REFERENCES

Anderson, J. G., Free radicals in the earth's stratosphere: A review of recent results, in *Proceedings of the NATO Advanced Study Institute on Atmospheric Ozone: Its Variation and Human Influences, Rep. FAA-EE-80-20*, edited by A. C. Aikin, pp. 233-251, DOT, FAA, Washington, DC, 1980.

Anderson, J. G., The past five years-the next five years, paper presented at the International Workshop on Current Issues in our Understanding of the Stratosphere and the Future of the Ozone Layer, BMFT, NASA, FAA, WMO, Feldafing, FRG, June 11-16, 1984.

Anderson, J. G., J. J. Margitan, and D. H. Stedman, Atomic chlorine and the chlorine monoxide radical in the stratosphere: Three in-situ observations, *Science, 198*, 501-503, 1977.

Anderson, J. G., H. J. Grassl, R. E. Shetter, and J. J. Margitan, Stratospheric free chlorine measured by balloon-borne in situ resonance fluorescence, *J. Geophys. Res., 85*, 2869-2887, 1980.

Anderson, J. G., H. J. Grassl, R. E. Shetter, and J. J. Margitan, HO_2 in the stratosphere: Three in situ observations, *Geophys. Res. Lett., 8*, 289-292, 1981.

Anderson, J. R., and R. D. Rosen, The latitude-height structure of 40-50 day variations in atmospheric angular momentum., *J. Atmos. Sci., 40*, 1584-1591, 1983.

Anderson, P. W., Pressure broadening in the microwave and infrared regions, *Phys. Rev., 76*, 647-661, 1949.

Andrews, D. G., and M. E. McIntyre, Planetary waves in horizontal and vertical shear: The generalized Eliassen-Palm relation and the mean zonal acceleration, *J. Atmos. Sci., 33*, 2031-2048, 1976.

Andrews, D. G., and M. E. McIntyre, Generalized Eliassen-Palm and Charney-Drazin theorems for waves on axisymmetric mean flows in compressible atmospheres, *J. Atmos. Sci., 35*, 175-185, 1978a.

Andrews, D. G., and M. E. McIntyre, An exact theory of nonlinear waves on a Lagrangian mean flow, *J. Fluid. Mech., 89*, 609-646, 1978b.

Andrews, D. G., J. D. Mahlman, and R. W. Sinclair, Eliassen-Palm diagnostics of wave-mean flow interaction in the GFDL "SKYHI" general circulation model, *J. Atmos. Sci., 40*, 2768-2784, 1983.

Angell, J. K., and J. Korshover, Recent rocketsonde-derived temperature variations in the Western Hemisphere, *J. Atmos. Sci., 35*, 1758-1764, 1978a.

Angell, J. K., and J. Korshover, Estimate of global temperature variations in the 100-30 mb layer between 1958 and 1977, *Mon. Weather Rev., 106*, 1422-1432, 1978b.

Angell, J. K., and J. Korshover, Global temperature variations in the troposphere and stratosphere, *Mon. Weather Rev., 111*, 901-921, 1983a.

Angell, J. K., and J. Korshover, Global variations in total ozone and layer-mean ozone: An update through 1981, *J. Clim. Appl. Meteor., 22*, 1611-1627, 1983b.

Angell, J. K., J. Korshover, and W. G. Planet, Ground-based and satellite evidence for a pronounced total-ozone minimum in early 1983 and responsible atmospheric layers, *Mon. Weather Rev., 113*, 641-646, 1985.

Apruzese, J., and D. F. Strobel, Radiative relaxation rates for individual 15-micron CO_2 lines in the upper stratosphere and lower mesosphere, *J. Geophys. Res., 89*, 7187-7194, 1984.

Apruzese, J. P., M. R. Schoeberl, and D. F. Strobel, Parameterization of IR cooling in a middle atmosphere dynamics model. 1. Effect on the zonally averaged circulation, *J. Geophys. Res., 87*, 8951-8966, 1982.

Arakawa, A., and W. H. Schubert, Introduction of cloud ensemble with the large scale environment, *J. Atmos. Sci., 31*, 674-701, 1974.

Arijs, E., D. Neverjans, and J. Ingles, Unambiguous mass determination of major stratospheric positive ions, *Nature, 288*, 684-686, 1980.

Arijs, E., D. Neverjans, and J. Ingels, Stratospheric positive ion composition measurements, ion abundances and related trace gas detection, *J. Atmos. Terr. Phys., 44*, 43-53, 1982.

Arnold, F., Multi-ion complexes in the stratosphere-Implications for trace gases and aerosol, *Nature, 284*, 610-611, 1980.

Arnold, F., Stratospheric trace gas detection by rocket-, balloon-, and aircraft-borne chemical ionization mass spectrometry, paper presented at the International Workshop on Current Issues in our Understanding of the Stratosphere and the Future of the Ozone Layer, BMFT, NASA, FAA, WMO, Feldafing, FRG, June 11-16, 1984.

Arnold, F., and G. Henschen, First mass analysis of stratospheric negative ions, *Nature*, *275*, 521-522, 1978.

Arnold, F., and S. Qiu, Upper stratosphere negative ion composition measurements and inferred trace gas abundances., *Planet. Space Sci.*, *32*, 169-177, 1984.

Arnold, F., H. Bohringer, and G. Henschen, Composition measurements of stratospheric positive ions, *Geophys. Res. Lett.*, *5*, 653-656, 1978.

Arnold, P. W., Losses of nitrous oxide from soil, *J. Soil*, *5*, 116-128, 1955.

Arrhenius, S., On the influence of carbonic acid in the air upon the temperature of the ground, *Philos. Mag.*, *41*, 237, 1896.

Arvesen, J. C., R. N. Griffin, and B. D. Pearson, Jr., Determination of extraterrestrial solar spectral irradiance from a research aircraft, *Appl. Optics*, *8*, 2215-2232, 1969.

Asai, K., T. Itabe, and T. Igarashi, Range-resolved measurements of atmospheric ozone using a differential-absorption CO_2 laser radar, *Appl. Phys. Lett.*, *35*, 60-62, 1979.

Atkinson, R., and A. C. Lloyd, Evaluation of kinetic and mechanistic data for modeling of photochemical smog, *J. Phys. Chem. Ref. Data*, *13*, 315-444, 1984.

Atkinson, R., S. M. Aschmann, A. M. Winer, and W. P. L. Carter, Rate constants for the gas-phase reactions of NO_3 with furan, thiophene and pyrole at 295 1 K and atmospheric pressure, *Environ. Sci. Technol.*, *19*, 87-90, 1985.

Atticks, M. G., and G. D. Robinson, Some features of the structure of the tropical tropopause, *Quart. J. Roy. Meteorol. Soc.*, *109*, 295-308, 1983.

Attmannspacher, W., and H. U. Duetsch, International ozone sonde intercomparison at the Observatory Hohenpeissenberg 5-20 April 1978, *Ber. Deutschen Wetterdienstes*, *Nr. 20*, 1970.

Attmannspacher, W., and H. U. Duetsch, Second international ozone sonde intercomparison at the Observatory Hohenpeissenberg 5-20 April 1978, *Ber. Deutschen Wetterdienstes*, *Nr. 157*, 1981.

Augustsson, T., and V. Ramanathan, A radiative-convective model study of the CO_2 climate problem, *J. Atmos. Sci.*, *34*, 448-451, 1977.

Ausloos, P., R. E. Rebbert, and L. Glasgow, Photodecomposition of chloromethane absorbed on silica surfaces, *J. of Res. of Nat. Bureau of Standards*, *82*, 1-8, 1977.

Austin, J., Comparison of stratospheric air parcel trajectories calculated from SSU and LIMS satellite data, *J. Geophys. Res.*, in press, 1985.

Austin, J., and A. F. Tuck, The calculation of stratospheric air parcel trajectories using satellite data, *Quart. J. Roy. Meteorol. Soc.*, *111*, 279-307, 1985.

Austin, J., R. R. Garcia, J. M. Russell III, S. Solomon, and A. F. Tuck, On the atmospheric photochemistry of nitric acid, *J. Geophys. Res.*, in press, 1985a.

Austin, J., R. C. Pallister, J. A. Pyle, A. F. Tuck, and A. M. Zarody, Photochemical model comparisons with LIMS observations in a stratospheric trajectory coordinate system, *Quart. J. Roy. Meteorol. Soc.*, in press, 1985b.

Azouit, M., and J. Vernin, Remote investigation of tropospheric turbulence by two dimensional analysis of stellar scintillation, *J. Atmos. Sci.*, *37*, 1550-1557, 1980.

Bacastow, R. B., C. D. Keeling, and T. P. Whorf, Seasonal amplitude increase in atmospheric CO_2 concentration at Mauna Loa, Hawaii, 1959-1982, *J. Geophys. Res.*, *90*, 10529-10540, 1985.

Baker, C. B., W. R. Kuhn, and E. Ryzner, Effects of the El Chichon volcanic cloud on direct and diffuse irradiances, *J. Clim. Appl. Meteor*, *23*, 449-452, 1984.

Baker-Blocker, A., T. M. Donahue, and K. H. Mancy, Methane flux from wetlands areas, *Tellus*, *29*, 245-250, 1977.

REFERENCES

Baldecchi, M. G., B. Carli, F. Mencaraglia, A. Bonetti, and M. Carlotti, Atlas of stratospheric submillimeter lines: 1. The 7-20 cm^{-1} interval, *J. Geophys. Res.*, *89*, 11689-11704, 1984.

Baldwin, A. C., and D. M. Golden, Heterogeneous atmospheric reactions-Sulphuric acid aerosols as tropospheric sinks, *Science*, *206*, 562-563, 1979.

Baldwin, A. C., J. R. Barker, D. M. Golden, and D. G. Hendry, Photochemical smog. Rate parameter estimates and computer simulation, *J. Phys. Chem.*, *81*, 2483-2492, 1977.

Ballard, H. N., A review of seven papers concerning the measurement of temperature in the stratosphere and mesosphere, *Tech. Rep. ECOM-5125*, 67 pp., U.S. Atmos. Sci. Lab., White Sands Missile Range, NM, 1967.

Balsley, B. B., and D. A. Carter, The spectrum of atmospheric velocity fluctuations at 8 km and 86 km, *Geophys. Res. Lett.*, *9*, 465-468, 1982.

Balsley, B. B., and A. C. Riddle, Monthly mean values of the mesospheric wind field over Poker Flat, Alaska, *J. Atmos. Sci.*, *41*, 2368-2375, 1984.

Baluteau, J. P., A. Marten, E. Bussoletti, M. Anderegg, J. E. Beckman, A. F. M. Moorwood, and N. Coron, High resolution infrared spectra of the Earth's atmosphere-II. Ground-based observations in the 500-570 cm^{-1} range, *Infrared Phys.*, *17*, 211-224, 1977.

Bamber, D. J., P. G. W. Healey, B. M. R. Jones, S. A. Penkett, A. F. Tuck, and G. Vaughan, Vertical profiles of tropospheric gases: Chemical consequences of stratospheric intrusions, *Atmos. Environ.*, *18*, 1759-1766, 1984.

Barat, J., Some characteristics of clear-air turbulence in the middle atmosphere, *J. Atmos. Sci.*, *39*, 2553-2564, 1982.

Barbe, A., P. Marche, C. Secroun, and P. Jouve, Measurements of tropospheric and stratospheric H_2CO by an infrared high resolution technique, *Geophys. Res. Lett.*, *6*, 463-465, 1979.

Barnes, I., K. H. Becker, E. H. Fink, A. Reimer, F. Zabel, and H. Niki, Rate constant and products of the reaction CS_2 + OH in the presence of O_2, *Int. J. Chem. Kinet.*, *15*, 631-645, 1983.

Barnes, R. A., A. R. Bandy, and A. T. Torres, ECC ozonesonde accuracy and precision, *J. Geophys. Res.*, *90*, 7881-7887, 1985.

Barnett, J. J., The mean meridional temperature behaviour of the stratosphere from November 1970 to November 1971 derived from measurements by the selective chopper radiometer on Nimbus 4, *Quart. J. Roy. Meteorol. Soc.*, *100*, 505-530, 1974.

Barnett, J. J., and M. Corney, Temperature comparisons between the NIMBUS 7 SAMS, rocket/radiosondes and the NOAA-6 SSU, *J. Geophys. Res.*, *89*, 5294-5302, 1984.

Barnett, J. J., and M. Corney, A middle atmosphere temperature reference model from satellite measurements, *Adv. Space Res.*, *5*, 125-134, 1984.

Barnett, J. J., J. T. Houghton, and J. A. Pyle, The temperature dependence of the ozone concentration near the stratopause, *Quart. J. Roy. Meteorol. Soc.*, *101*, 245-257, 1975a.

Barnett, J. J., R. S. Harwood, J. T. Houghton, C. G. Morgan, C. D. Rodgers, and E. J. Williamson, Comparison between radiosonde, rocketsonde and satellite observations of atmospheric temperatures, *Quart. J. Roy. Meteorol. Soc.*, *101*, 423-436, 1975b.

Barrett, E. W., P. M. Kuhn, and A. Shlanta, Recent measurements of the injection of water vapor and ozone into the stratosphere by thunderstorms, in *Proceedings of the 2nd Conference on the Climatic Impact Assessment Program*, *DOT-TSC-OST-73-4*, edited by A. J. Broderick, pp. 34-46, Transportation Systems Center, Cambridge, MA, 1973.

Barth, C. A., D. W. Rusch, R. J. Thomas, G. H. Mount, G. J. Rottman, G. E. Thomas, R. W. Sanders, and G. M. Lawrence, Solar Mesosphere Explorer: Scientific objectives and results, *Geophys. Res. Lett.*, *10*, 237-240, 1983.

Barton, I. J., Upper level cloud climatology from an orbiting satellite, *J. Atmos. Sci.*, *40*, 435-447, 1983.

Basco, N., and J. E. Hunt, Mutual combination of ClO radicals, *Int. J. Chem. Kin.*, *11*, 649-664, 1979.

Bass, A. M., and R. J. Paur, The ultraviolet cross sections of ozone: I. The measurements, in *Atmospheric Ozone*, edited by C. S. Zerefos and A. Ghazi, pp. 606-610, D. Reidel, Dordrecht, 1984.

Bates, D. R., Rayleigh scattering by air, *Planet. Space Sci.*, *32*, 785-790, 1984.

Bauer, E., A catalog of perturbing influences on stratospheric ozone, 1955-1975, *J. Geophys. Res.*, *84*, 6929-6940, 1979.

Baulch, D. L., R. A. Cox, R. F. Hampson, Jr., J. A. Kerr, J. Troe, and R. T. Watson, Evaluated kinetic and photochemical data for atmospheric chemistry, *J. Phys. Chem. Ref. Data*, *9*, 295-471, 1980.

Baulch, D. L., R. A. Cox, P. J. Crutzen, R. F. Hampson, J. A. Kerr, J. Troe, and R. T. Watson, Evaluated kinetic and photochemical data for atmospheric chemistry: Supplement I. CODATA Task Group on Chemical Kinetics, *J. Phys. Chem. Ref. Data*, *11*, 327-496, 1982.

Baulch, D. L., R. A. Cox, R. F. Hampson, Jr., J. A. Kerr, J. Troe, and R. T. Watson, Evaluated kinetic and photochemical data for atmospheric chemistry supplement II. CODATA Task Group on Gas Phase Chemical Kinetics, *J. Phys. Chem. Ref. Data*, *13*, 1259-1380, 1984.

Belmont, A. D., and D. G. Dartt, Semiannual variation in zonal wind from 20 to 65 kilometers, at 80°N-10°S, *J. Geophys. Res.*, *78*, 6373-6376, 1973.

Belmont, A. D., D. G. Dartt, and G. D. Nastrom, Periodic variations in stratospheric zonal winds from 20 to 65 km, at 80°N to 70°S, *Quart. J. Roy. Meteorol. Soc.*, *100*, 203-211, 1974.

Berg, W. W., and P. D. Sperry, Atmospheric bromine in the Arctic, *J. Geophys. Res.*, *88*, 6719-6736, 1983.

Berg, W. W., P. J. Crutzen, F. E. Grahek, S. N. Gitlen, and W. A. Sedlacek, First measurements of total chlorine and bromine in the lower stratosphere, *Geophys. Res. Lett.*, *7*, 937-940, 1980.

Berg, W. W., L. E. Heidt, W. Pollock, P. D. Sperry, R. J. Cicerone, and E. S. Gladney, Brominated organic species in the Arctic atmosphere, *Geophys. Res. Lett.*, *11*, 429-432, 1984.

Berner, W., H. Oeschger, and B. Stauffer, Information on the CO_2 cycle from ice-core studies, *Radiocarbon*, *22*, 227-235, 1980.

Betts, A. K., Parametric interpretation of trade wind cumulus budget studies, *J. Atmos. Sci.*, *32*, 1934-1945, 1975.

Bevilacqua, R. M., J. J. Olivero, P. R. Schwartz, C. J. Gibbins, J. M. Bologna, and D. L. Thacker, An observational study of water vapor in the mid-latitude mesosphere using ground-based microwave techniques, *J. Geophys. Res.*, *88*, 8523-8534, 1983.

Bevilacqua, R. M., W. J. Wilson, W. B. Ricketts, P. R. Schwartz, and R. J. Howard, Possible seasonal variability of mesospheric water vapor, *Geophys. Res. Lett.*, 12, 397-400, 1985.

Bhartia, P. K., K. F. Klenk, A. J. Fleig, C. G. Wellemyer, and D. Gordon, Intercomparison of Nimbus 7 Solar Backscattered Ultraviolet ozone profiles with rocket, balloon and Umkehr profiles, *J. Geophys. Res.*, *89*, 5227-5238, 1984a.

Bhartia, P. K., K. F. Klenk, C. K. Wong, D. Gordon, and A. J. Fleig, Intercomparison of the Nimbus 7 SBUV/TOMS total ozone data sets with Dobson and M83 results, *J. Geophys. Res.*, *89*, 5239-5248, 1984b.

Bhartia, P. K., D. F. Heath, and A. J. Fleig, Observation of anomalously small ozone densities in South Polar Stratosphere during October 1983 and 1984, paper presented at 5th General Assembly, IAGA Symposium, Prague, Czechoslovakia, July, 1985.

Blackmer, A. M., and J. M. Bremner, Potential of soil as a sink for atmospheric nitrous oxide, *Geophys. Res. Lett.*, *3*, 739-742, 1976.

Blackshear, W. T. W. L. Grose, and R. E. Turner, Simulated sudden stratospheric warmings: Synoptic evaluations, *Quart. J. Roy. Meteorol. Soc.*, in press, 1986.

Blake, A. J., An atmospheric absorption model for the Schumann-Runge bands of oxygen, *J. Geophys. Res.*, *84*, 3272-3282, 1979.

REFERENCES

Blake, A. J., S. T. Gibson, and D. G. McCoy, Photodissociation of $^{16}O^{18}O$ in the atmosphere, *J. Geophys. Res.*, *89*, 7277-7284, 1984.

Blake, D. R., Increasing concentrations of atmospheric methane, 1979-1983, Ph.D. thesis, 213 pp., U. of California, Irvine, CA, 1984.

Blake, D. R., and F. S. Rowland, World-wide increase in tropospheric methane, *J. Atmos. Chem.*, in press, 1985.

Blake, D. R., W. E. Mayer, S. C. Tyler, Y. Makide, D. C. Montaque, and F. S. Rowland, Global increase in atmospheric methane concentrations between 1978 and 1980, *Geophys. Res. Lett.*, *9*, 477-480, 1982.

Blake, D. R., V. H. Woo, S. C. Tyler and F. S. Rowland, Methane concentrations and source strengths in urban locations, *Geophys. Res. Lett.*, *11*, 1211-1214, 1984.

Blanchet, J. P., and R. List, On the optical properties of Arctic haze, in *Aerosols and Their Climate Effects*, edited by H. E. Gerber and A. Deepak, pp. 179-196, A. Deepak Publ., Hampton, VA, 1984.

Blatherwick, R. D., A. Goldman, D. G. Murcray, F. J. Murcray, G. R. Cook, and J. W. Van Allen, Simultaneous mixing ratio profiles of stratospheric NO and NO_2 as derived from balloon-borne infrared solar spectra, *Geophys. Res. Lett.*, *7*, 471-473, 1980.

Blatherwick, R. D., F. J. Murcray, F. H. Murcray, A. Goldman, and D. G. Murcray, Atlas of South Pole IR solar spectra, *Appl. Opt.*, *21*, 2658-2659, 1982.

Bloomfield, P., M. L. Thompson, and S. Zeger, A statistical analysis of Umkehr measurements of 32-46 km ozone, *J. Appl. Meteorol.*, *21*, 1828-1837, 1982.

Bloomfield, P., G. Oehlert, M. L. Thompson, and S. Zeger, A frequency domain analysis of trends in Dobson total ozone records, *J. Geophys. Res.*, *88*, 8512-8522, 1983.

Blumenthal, D. L., W. S. Keifer, and J. A. McDonald, Aircraft measurements of pollutants and meteorological parameters during the Sulphate Regional Experiment (SURE), *Rep. EPRI-EA-1909*, 230 pp., Meteorology Research, Santa Rosa, CA, 1981.

Bohringer, H., D. W. Fahey, F. C. Fehsenfeld, and E. E. Ferguson, The role of ion molecule reactions in conversion of N_2O_5 to HNO_3 in the stratosphere, *Planet. Space Sci.*, *31*, 185-191, 1983.

Bojkov, R. D., Some characteristics of the total ozone deduced from Dobson-spectrophotometer and filter-ozonometer data and their application to determination of the effectiveness of the ozone station network, *Ann. Geoph.*, *25*, 293-299, 1969.

Bojkov, R. D., Tropospheric ozone, its changes and possible radiative effect, *WMO Special Environment Report 16*, 1983.

Bojkov, R. D., and G. C. Reinsel, Trends in tropospheric ozone concentration, in *Atmospheric Ozone*, edited by C. S. Zerefos and A. Ghazi, pp. 775-781, D. Reidel, Dordrecht, 1984.

Bollinger, M. J., C. J. Hahn, D. D. Parrish, P. C. Murphy, D. L. Albritton, and F. C. Fehsenfeld, NOx measurements in clean continental air and analysis of the contributing meteorology, *J. Geophys. Res.*, *89*, 9623-9631, 1984.

Bonsang, B., and G. Lambert, Nonmethane HC in an oceanic atmosphere, *J. Atmos. Chem.*, *2*, 257-271, 1985.

Borchers, R., P. Fabian, and S. A. Penkett, First measurements of the vertical distribution of CCl_4 and CH_3CCl_3 in the stratosphere, *Naturwiss.*, *70*, 514-516, 1983.

Borchers, R., P. Fabian, B. C. Krueger, S. Lal, U. Schmidt, D. Knapska, and S. A. Penkett, The vertical distribution of CCl_2F-$CClF_2$ (CFC-113) and $CClF_2$-$CClF_2$ (CFC-114) in the stratosphere, paper presented at 5th General Assembly, International Association of Geomagnetism and Aeronomy, Prague, 5-17 August 1985.

Borden, T. R., and W. S. Hering, Ozonesonde observations over North America, Vol I, 525 pp., II, 286 pp., III, 266 pp., IV, 376 pp., *Report AFCRL-65-913*, Air Force Cambridge Res. Labs., Hanscom AFB, MA, 1964.

Borden, T. R., and W. S. Hering, Mean distributions of ozone density over North America 1963-1964, *Environmental Research Paper No. 162, Report AFCRL-65-913*, 28 pp., Air Force Cambridge Research Labs., Hanscom AFB, MA, 1965.

Borghi, R., D. Cariolle, A. Girard, J. Laurent, and N. Louisnard, Comparison entre les resultats d'un modele une dimensionnel et des resultats de mesures stratospheriques de CH_4, H_2O et des oxydes d'azote, *Rev. Phys. Appl., 18*, 229-237, 1983.

Borisenkov, Ye. P., and Yu. Ye. Kazakov, Effect of freons and halocarbons on the ozone layer of the atmosphere and climate, typed manuscript, USSR, 1977.

Borucki, W. J., and W. L. Chameides, Lightning: Estimates of the rates of energy dissipation of nitrogen fixation, *Res. Geophys. and Space Phys., 22*, 363-372, 1984.

Bossy, L., and M. Nicolet, On the variability of Lyman alpha with solar activity, *Planet. Space Sci., 29*, 907-914, 1981.

Bottenheim, J. W., K. A. Brice, and K. G. Anlauf, Discussion of a Lagrangian trajectory model describing long-range transport of oxides of nitrogen, the incorporation of PAN in the chemical mechanism, and supporting measurements of PAN and nitrate species at rural sites in Ontario, Canada, *Atmos. Environ., 18*, 2609-2619, 1984.

Boughner, R. E., The effect of increased carbon dioxide concentrations on stratospheric ozone, *J. Geophys. Res., 83*, 1326-1332, 1978.

Boughner, R. E., and V. Ramanathan, Climatic consequence of increasing CO_2: A study of the feedback mechanism between increasing CO_2 concentrations and the atmospheric ozone, water vapor, and thermal structure balance, paper presented at Second Conf. Atmospheric Radiation, Amer. Meteor. Soc., Arlington, VA, 29-31 October, 1975.

Boughner, R., J. C. Larsen, and M. Natarajan, The influence of NO and ClO variations at twilight on the interpretation of solar occultation measurements, *Geophys. Res. Lett., 7*, 231-234, 1980.

Bowman, K. P., and A. J. Krueger, A global climatology of total ozone from the Nimbus 7 Total Ozone Mapping Spectrometer (TOMS), *J. Geophys. Res., 90*, 7967-7976, 1985.

Boyd, J. P., The noninteraction of waves with the zonally averaged flow on a spherical Earth and the interrelationships of eddy fluxes of energy, heat and momentum, *J. Atmos. Sci., 33*, 2285-2291, 1976.

Bradford, C. M., F. H. Murcray, J. W. Van Allen, J. N. Brooks, D. G. Murcray, and A. Goldman, Ground level detection and feasibility for monitoring of several trace atmospheric constituents by high resolution infrared spectroscopy, *Geophys. Res. Lett., 3*, 387-390, 1976.

Bradshaw, J. D., and D. D. Davis, Sequential two-photon laser-induced fluorescence—A new method for detecting atmospheric trace levels of NO, *Optics Letters, 7*, 224-226, 1982.

Bradshaw, J. D., S. KeSheng, M. O. Rodgers, S. T. Sandholm, and D. D. Davis, Measurements of tropospheric NO concentrations as part of the NASA GTE/CITE program, *Eos Trans. AGU, 65*, 835, 1984.

Brasseur, G., *Physique et chimie de l'atmosphere moyenne*, Masson, Paris, 1982.

Brasseur, G., and M. Bertin, The action of chlorine on the ozone layer as given by a zonally averaged two-dimensional model, *Pure Appl. Geophys., 117*, 436-450, 1978/79.

Brasseur, G., and M. Nicolet, Chemospheric process of nitric oxide in the mesophere and stratosphere, *Planet. Space Sci., 21*, 939-961, 1973.

Brasseur, G., and P. C. Simon, Stratospheric chemical and thermal response to long-term variability in solar UV irradiance, *J. Geophys. Res., 86*, 7343-7362, 1981.

Brasseur, G., and S. Solomon, *Aeronomy of the Middle Atmosphere: Chemistry and Physics in the Stratosphere and Mesosphere*, 441 pp., D. Reidel, Dordrecht, 1984.

Brasseur, G., P. De Baets, and A. De Rudder, Solar variability and minor constituents in the lower thermosphere and in the mesosphere, *Space Sci. Rev., 34*, 377-385, 1983a.

REFERENCES

Brasseur, G., A. De Rudder, and P. C. Simon, Implication for stratospheric composition of a reduced absorption cross section in the Herzberg continuum of molecular oxygen, *Geophys. Res. Lett.*, *10*, 20-23, 1983b.

Brasseur, G., A. De Rudder, and C. Tricot, Stratospheric response to chemical perturbations, *J. Atmos. Chem.*, *3*, 261-288, 1985.

Bremner, J. M., and A. M. Blackmer, Nitrous oxide: Emission from soils during nitrification of fertilizer nitrogen, *Science*, *199*, 295-298, 1978.

Bremner, J. M., S. G. Robbins, and A. M. Blackmer, Seasonal variability in emission of nitrous oxide in soil, *Geophys. Res. Lett.*, *7*, 611-643, 1980.

Bretherton, F. P., Momentum transport by gravity waves, *Quart. J. Roy. Meteorol. Soc.*, *95*, 213-243, 1969.

Brewer, A. W., Evidence for a world circulation provided by the measurements of helium and water vapour distribution in the stratosphere, *Quart. J. Roy. Meteorol. Soc.*, *75*, 351-363, 1949.

Brewer, A. W., and J. R. Milford, The Oxford-Kew ozonesonde, *Proc. Roy. Soc. London A*, *256*, 470-495, 1960.

Brewer, A. W., and A. W. Wilson, The regions of formation of atmospheric ozone, *Quart. J. Roy. Meteorol. Soc.*, *94*, 249-265, 1968.

Brice, K. A., R. G. Derwent, A. E. J. Eggleton, and S. A. Penkett, Measurements of CCl_3F and CCl_4 at Harwell 1/75-6/81, *Atmos. Environ.*, *16*, 2543-2554, 1982.

Brice, K. A., S. A. Penkett, D. H. F. Atkins, F. J. Sandalls, D. J. Bamber, A. F. Tuck, and G. Vaughan, Atmospheric measurements of peroxyacetylnitrate (PAN) in rural, South-East England: Seasonal variations, Winter photochemistry, and long-range transport, *Atmos. Environ.*, *18*, 2691-2702, 1984.

Brietenbeck, G. A., A. M. Blackmer, and J. M. Bremner, Effects of different nitrogen fertilizers on emissions of nitrous oxide from soil, *Geophys. Res. Lett.*, *7*, 85-88, 1980.

Briggs, J., and W. T. Roach, Aircraft observations near jet streams, *Quart. J. Roy. Meteorol. Soc.*, *89*, 225-247, 1963.

Broadfoot, A. L., The solar spectrum 2100-3200 /, *Astrophys. J.*, *173*, 681-689, 1972.

Broecker, W. S., T. H. Peng, and R. Engh, Modeling the carbon system, *Radiocarbon*, *22*, 565-598, 1980.

Browell, E. V., A. F. Carter, and S. T. Shipley, An airborne lidar system for ozone and aerosol profiling in the troposphere and lower stratosphere, in *Proceedings of the Quadrennial International Ozone Symposium, Vol. I*, edited by J. London, pp. 99-107, IAMAP, NCAR, Boulder, CO, 1981.

Browell, E. V., A. F. Carter, S. T. Shipley, R. J. Allen, C. F. Butler, M. N. Mayo, J. H. Siviter, Jr, and W. M. Hall, NASA multi purpose airborne DIAL system and measurements of ozone and aerosol profiles, *Appl. Opt.*, *22*, 522-534, 1983.

Browell, E. V., S. Ismail, E. F. Danielsen, G. L. Gregory, and S. M. Beck, Airborne lidar and in situ measurements of a tropopause fold event, in press, 1985.

Bruehl, C. H., and P. J. Crutzen, A radiative-convective model to study the sensitivity of climate and chemical composition to a variety of human activities, *Stratosphere*, Proceedings of a working party meeting, Brussels, May 18, 1984, *Commission of European Communities*, edited by A. Ghazi, pp. 85-94, 1984.

Brune, W. H., E. M. Weinstock, J. J. Schwab, R. M. Stimpfle, and J. G. Anderson, Stratospheric ClO: Insitu detection with a new approach, *Geophys. Res. Lett.*, *12*, 441-444, 1985.

Bryan, K., F. G. Komro, S. Manabe, and M. J. Spelman, Transient climate response to increasing atmospheric carbon dioxide, *Science*, *215*, 56-58, 1982.

Bryan, K., F. G. Komro, and C. Rooth, The ocean's transient response to global surface temperature anomalies, in *Climate Processes and Climate Sensitivity*, *Geophysical Monograph 29*, Maurice Ewing Series Vol. 5, edited by J. E. Hanson and T. Takahashi, pp. 29-38, American Geophysical Union, Washington, DC, 1984.

C-6

Bufton, J. L., R. W. Stewart, and Chi Weng, Remote measurement of tropospheric ozone, *Appl. Opt.*, *18*, 3363-3364, 1979.

Buijs, H. L., G. L. Vail, G. Tremblay, and D. J. W. Kendall, Simultaneous measurements of the volume mixing ratio of HCl and HF in the stratosphere, *Geophys. Res. Lett.*, *7*, 205-208, 1980.

Burkhardt, E. G., C. A. Lambert, and C. K. N. Patel, Stratospheric nitric oxide: Measurements during daytime and sunset, *Science*, *188*, 1111-1113, 1975.

Burnett, C. R., and E. B. Burnett, Spectroscopic measurements of the vertical column abundance of hydroxyl (OH) in the Earth's atmosphere, *J. Geophys. Res.*, *86*, 5185-5202, 1981.

Burnett, C. R., and E. B. Burnett, Vertical column abundance of atmospheric OH at solar maximum from Fritz Peak, Colorado, *Geophys. Res. Lett.*, *9*, 708-711, 1982.

Burnett, C. R., and E. B. Burnett, OH PEPSIOS, *Appl. Opt.*, *22*, 2887-2892, 1983a.

Burnett, C. R., and E. B. Burnett, OH column abundance measurements from Boca Raton, FL, Fritz Peak, CO, and Poker Flat, AK, *Eos Trans. AGU*, *64*, 781, 1983b.

Burnett, C. R., and E. B. Burnett, Observational results on the vertical column abundance of atmospheric hydroxyl: Description of its seasonal behavior 1977-1982 and of the 1982 El Chichon perturbation, *J. Geophys. Res.*, *89*, 9603-9611, 1984.

Burnett, C. R., and E. B. Burnett, Atmospheric hydroxyl response to the partial solar eclipse of May 30, 1984, *Geophys. Res. Lett.*, *12*, 263-266, 1985.

Burnham, J., Atmospheric gusts-A review of the results of some recent research at the Royal Aircraft Establishment, *Mon. Weather Rev.*, *98*, 723-734, 1970.

Burrows, J. P., T. J. Wallington, and R. P. Wayne, Kinetics of the reaction of OH with ClO, *J. Chem. Soc. Faraday Trans. 2*, *80*, 957-971, 1984.

Burrows, J. P., D. W. T. Griffith, G. K. Moortgat, and G. S. Tyndall, Matrix isolation Fourier transform infrared study of the products of the reaction between ClO and NO_2, *J. Phys. Chem.*, 266-271, 1985.

Butchart, N., and E. E. Remsberg, The area of the stratospheric polar vortex as a diagnostic for tracer transport on an isentropic surface, *J. Atmos. Sci.*, in press, 1985.

Butchart, N., S. A. Clough, T. N. Palmer, and P. J. Trevelyan, Simulations of an observed stratospheric warming with quasi-geostrophic refractive index as a model diagnostic, *Quart. J. Roy. Meteorol. Soc.*, *108*, 475-502, 1982.

Butler, D. M., Earth observing system. Science and mission requirements. Working group report, Volume I, Part 2, *NASA Technical Memorandum 86129*, NASA Goddard Space Flight Center, Greenbelt, MD, 1984.

Cadle, R. D., and G. W. Grams, Stratospheric aerosol particles and their optical properties, *Reviews of Geophysics and Space Physics*, *13(4)*, 475-501, 1975.

Cadle, R. D., P. J. Crutzen, and D. H. Ehhalt, Heterogeneous chemical reactions in the stratosphere, *J. Geophys. Res.*, *80*, 3381-3385, 1975.

Cahen, C., J. Pelon, P. Flamant, and G. Megie, Mesure de la vapeur d'eau tropospherique par absorption differentielle laser, *C. R. Acad. Sci.*, Paris, *292*, 29, 1981.

Callis, L. B., and M. Natarajan, Stratospheric ozone and temperature perturbations: An examination of synergistic effects, in *Proceedings of the Quadrennial International Ozone Symposium, Vol. II*, edited by J. London, pp. 910-917, IAMAP, NCAR, Boulder, CO, 1981.

Callis, L. B., and M. Natarajan, Atmospheric carbon dioxide and chlorofluoromethanes: Combined effects on stratospheric ozone, temperature, and surface temperature, *Geophys. Res. Lett.*, *8*, 587-590, 1981.

Callis, L. B., M. Natarajan, and R. E. Boughner, On the relationship between the greenhouse effect, atmospheric photochemistry and species distribution, *J. Geophys. Res.*, *88*, 1401-1426, 1983a.

REFERENCES

Callis, L. B., J. M. Russell III, K. V. Haggard, and M. Natarajan, Examination of winter-time latitudinal gradients in stratospheric NO_2 using theory and LIMS observations, *Geophys. Res. Lett.*, *10*, 945-948, 1983b.

Callis, L. B., M. Natarajan, and J. M. Russell III, Estimates of the stratospheric distributions of odd nitrogen from the LIMS data, *Geophys. Res. Lett.*, *12*, 259-262, 1985a.

Callis, L. B., M. Natarajan, R. E. Boughner, J. M. Russell III, and J. D. Lambeth, Stratospheric photochemical studies using Nimbus 7 data, Part II: Development of infrared trace species distributions, *J. Geophys. Res.*, in press, 1985b.

Calvert, J. G., Test of the theory of ozone generation in Los Angeles atmosphere, *Environ. Sci. Technol.*, *10*, 248-256, 1976.

Camy-Peyret, C., J.-M. Flaud, L. Delbouille, G. Roland, J. W. Brault, and L. Testerman, Quadrupole transitions of the 1-0 band of N_2 observed in high resolution atmospheric spectrum, *J. Physique Lett.*, *42*, 279-283, 1981.

Camy-Peyret, C., J.-M. Flaud, J. Laurent, and G. M. Stokes, First infrared measurement of atmospheric NO_2 from the ground, *Geophys. Res. Lett.*, *10*, 35-38, 1983.

Cariolle, D., and D. Brard, The distribution of ozone and active stratospheric species: Results of a two-dimensional atmospheric model, in *Atmospheric Ozone*, edited by C. S. Zerefos and A. Ghazi, pp. 77-81, D. Reidel, Dordrecht, 1984.

Cariolle, D., and M. Deque, A GCM study of the transport of heat, momentum and ozone in the stratosphere, in *Atmospheric Ozone*, edited by C. S. Zerefos and A. Ghazi, pp. 24-27, D. Reidel, Dordrecht, 1984.

Carli, B., F. Mencaraglia, and A. Bonetti, Fourier spectroscopy of the stratospheric emission, *Int. J. Infrared mm Waves*, *1*, 253-276, 1980.

Carli, B., F. Mencaraglia, and A. Bonetti, New assignments in the submillimeter emission of the stratosphere, *Int. J. Infrared mm Waves*, *3*, 385-394, 1982.

Carli, B., F. Mencaraglia, A. Bonetti, B. M. Dinelli, and F. Forni, Submillimeter detection of stratospheric OH and further line assignments in the stratospheric emission spectrum, *Int. J. Infrared mm Waves*, *4*, 475-488, 1983.

Carli, B., F. Mencaraglia, and A. Bonetti, Submillimeter high resolution FT spectrometer for atmospheric studies, *Appl. Opt.*, *23*, 2534-2603, 1984.

Carli, B., F. Mencaraglia, A. Bonetti, M. Carlotti, and I. Nolt, Detection of atomic oxygen and further line assignments in the far infrared stratospheric spectrum, *Int. J. Infrared mm Waves*, *6*, 149-176, 1985a.

Carli, B. M. Carlotti, D. M. Dinelli, F. Mencaraglia, and I. Nolt, Further evidence of stratospheric chlorine monoxide, in press, 1985b.

Carney, T. A., and J. Fishman, An investigation of the vertical distribution of trace constituents in the troposphere with a one-dimensional photochemical model and a model of the trade-wind boundary layer, *Eos Trans. AGU*, *65*, 836, 1984.

Carroll, M. A., and B. A. Ridley, Tropospheric NOx measurements, *Eos Trans. AGU*, *65*, 834, 1984.

Carter, W. P. L., A. C. Lloyd, J. L. Sprung, and J. N. Pitts, Jr., Progress in the validation of a detailed mechanism for the photooxidation of propene and nebutane in photochemical smog, *Int. J. Chem. Kinet.*, *11*, 45-111, 1979.

Carver, J. H., B. H. Horton, and F. G. Burger, Nocturnal ozone distribution in the upper atmosphere, *J. Geophys. Res.*, *71*, 4189-4191, 1966.

Carver, J. H., H. P. Giess, T. H. Hobbs, B. R. Lewis, and J. H. McCoy, Temperature dependence of the molecular oxygen photoabsorption cross section near the H Lyman alpha line, *J. Geophys. Res.*, *82*, 1955-1960, 1977.

CDAC: See National Research Council, *Changing Climate*, Carbon Dioxide Assessment Committee.

Cess, R. D., Climatic change: An appraisal of atmospheric feedback mechanisms employing zonal climatology, *J. Atmos. Sci.*, *33*, 1831-1843, 1976.

Cess, R. D., and S. C. Chen, The influence of ethane and acetylene upon the thermal structure of the Jovian atmosphere, *Icarus*, *26*, 444-450, 1975.

Cess, R. D., and S. D. Goldenberg, The effect of ocean heat capacity upon global warming due to increasing atmospheric carbon dioxide, *J. Geophys. Res.*, *86*, 498-502, 1981.

Cess, R. D., and G. L. Potter, A commentary on the recent CO_2-climate controversy, *Climatic Change*, *6*, 365-376, 1984.

Cess, R. D., and L. S. Wang, A band absorptance formulation for nonisothermal gaseous radiation, *Int. J. Heat Mass Transfer*, *13*, 547-555, 1970.

Cess, R. D., B. P. Briegleb and M. S. Lian, Low-latitude cloudiness and climate feedback: Comparative estimates from satellite data, *J. Atmos. Sci.*, *39*, 53-59, 1982.

Cess, R. D., D. P. Kratz, S. J. Kim and J. Caldwell, Infrared band models for atmospheric methane, *J. Geophys. Res.*, in press, 1985.

Chamberlin, T. C., An attempt to frame a working hypothesis of the cause of glacial periods on an atmospheric basis, *J. Geol.*, *7*, 545, 1899.

Chameides, W. L., The photochemistry of a remote marine stratiform cloud, *J. Geophys. Res.*, *89*, 4739-4755, 1984.

Chameides, W. L., and D. D. Davis, The free radical chemistry of cloud droplets and its impact upon the composition of rain, *J. Geophys. Res.*, *87*, 4863-4877, 1982.

Chameides, W. L., and A. Tan, The two dimensional diagnostic model for tropospheric OH: An uncertainty analysis, *J. Geophys. Res.*, *86*, 5209-5223, 1981.

Chameides, W. L., and J. C. G. Walker, A photochemical theory of tropospheric ozone, *J. Geophys. Res.*, *78*, 8751-8760, 1973.

Chameides, W. L., D. H. Stedman, R. R. Dickerson, D. W. Rusch, and R. J. Cicerone, NOx production in lightning, *J. Atmos. Sci.*, *34*, 143-149, 1977a.

Chameides, W. L., S. C. Liu, and R. J. Cicerone, Possible variations in atmospheric methane, *J. Geophys. Res.*, *82*, 1795-1798, 1977b.

Chan, S. H., and C. L. Tien, Total band absorptance of nonisothermal infrared-radiating gases, *J. Quant. Spectrosc. Radiat. Transfer*, *9*, 1261-1271, 1969.

Chance, K. V., and W. A. Traub, An upper limit for stratospheric hydrogen peroxide, *J. Geophys. Res.*, *89*, 11655-11660, 1984.

Chance, K. V., and W. A. Traub, to be published under BIC I, BIC II, 1986.

Chance, K. V., J. C. Brasunas, and W. A. Traub, Far infrared measurement of stratospheric HCl, *Geophys. Res. Lett.*, *9*, 704-706, 1980.

Chandra, S., Solar-induced oscillations in the stratosphere: A myth or reality?, *J. Geophys. Res.*, *90*, 2331-2339, 1985.

Chang, C. P., Forcing of stratospheric Kelvin waves by tropospheric heat sources, *J. Atmos. Sci.*, *35*, 740-744, 1976.

Chang, J. S., A. C. Baldwin, and D. M. Golden, An explanation of the preferential formation of less stable isomers in threebody reactions: Cl + NO_2 + M, ClO + NO_2 + M, *J. Chem. Phys.*, *71*, 2021-2024, 1979.

Chanin, M. L., The Intercomparison Ozone Campaign held in France in June 1981: Description of the campaign, *Planet. Space Sci.*, *31*, 707-715, 1983a.

Chanin, M. L., The Ozone Intercomparison Campaign, 1981: Concluding remarks, *Planet. Space Sci.*, *31*, 811-812, 1983b.

Chanin, M. L., and A. Hauchecorne, Lidar observations of gravity and tidal waves in the middle atmosphere, *J. Geophys. Res.*, *86*, 9715-9721, 1981.

Chao, W. C., and M. R. Schoeberl, On the linear approximation of gravity wave saturation in the mesosphere, *J. Atmos. Sci.*, *41*, 1893-1898, 1984.

Chapman, S., A theory of upper atmospheric ozone, *Mem. Roy. Met. Soc.*, *3*, 103-125, 1930.

Chapman, W., and G. Peckham, Spectral analysis of wave motions in the middle atmosphere, *Phil. Trans. Roy. Soc. London*, *A296*, 59-63, 1980.

Charlock, T. P., Cloud optical feedback and climate stability in a radiative-convective model, *Tellus*, *34*, 245-254, 1982.

Charney, J. G., The dynamics of long waves in a baroclinic westerly current, *J. Meteorol.*, *4*, 135-162, 1947.

Charney, J. G. (Chairman), *Carbon Dioxide and Climate: A Scientific Assessment*, 33 pp., National Academy Press, Washington, DC, 1979.

Charney, J. G., and P. G. Drazin, Propagation of planetary-scale disturbances from the lower into the upper atmosphere, *J. Geophys. Res.*, *66*, 83-109, 1961.

Charney, J. G., and M. E. Stern, On the stability of internal baroclinic jets in a rotating atmosphere, *J. Atmos. Sci.*, *19*, 159-172, 1962.

Chatfield, R. B., and P. J. Crutzen, Sulfur dioxide in remote oceanic air: Cloud transports of reactive precursors, *J. Geophys. Res.*, *89*, 7111-7132, 1984.

Chedin, A., and N. A. Scott, The impact of spectroscopic parameters on the comparison of the Jovian atmosphere discussed in connection with the recent laboratory, earth and planetary observation programs, *J. Quant. Spectrosc. Radiat. Transfer*, *32*, 453-461, 1984.

Chedin, A., N. Husson, N. A. Scott, I. Jobard, I. Cohen-Hallaleh, and A. Berroir, La Banque de donees GEISA, Description et logiciel d'utilisation, Laboratoire de Meteorologie Dynamique du C.N.R.S., *Internal Note 108*, Ecole Polytechnique, 91128 Palaiseau Cedex, France, October, 1980.

Chedin, A., N. Husson, N. A. Scott, I. Cohen-Hallaleh, and A. Berroir, The GEISA data bank: 1984 version, Laboratoire de Meteorologie Dynamique du C.N.R.S., *Internal Note 127*, Ecole Polytechnique, 91128 Palaiseau Cedex, France, February, 1985.

Chemical Manufacturers Association, CMA, *Effect of chlorofluorocarbons on the atmosphere, revision 17*, edited by B. P. Block, H. Magid, and R. B. Ward, 98 pp., Washington, DC, 1982.

Chemical Manufacturers Association, CMA, *Production, sales and calculated release of CFC 11 and CFC 12 through 1983*, October, 1984.

Chemical Manufacturers Association, CMA, *Production, sales and calculated release of CFC 11 and CFC 12 through 1984*, October, 1985.

Chemical Manufacturers Association-National Bureau of Standards, CMA-NBS, *Proceedings of CMA-NBS workshop on atmospheric spectra*, November 3-4, 1983, Gaithersburg, MD, edited by A. Weber, June, 1985.

Cheung, A.S.C., K. Yoshino, W. H. Parkinson, and D. E. Freeman, Herzberg continuum cross section of oxygen in the wavelength region 193.5-204.0 nm and band oscillator strengths of the (0,0) and (1,0) Schumann-Runge bands, *Can. J. Phys.*, *62*, 1752-1762, 1984a.

Cheung, A. S. C., K. Yoshino, W. H. Parkinson, and D. E. Freeman, Herzberg continuum cross-section of oxygen in the wavelength region 193.5-204 nm: New laboratory measurements and stratospheric implications, *Geophys. Res. Lett.*, *11*, 580-582, 1984b.

Chou, C. C., R. J. Milstein, W. S. Smith, H. Veraruiz, M. J. Molina, and F. S. Rowland, Stratospheric photodissociation of several saturated perhalo- chlorofluorocarbon compounds in current technological use (Fluorocarbons -13, -113, -114, and -115), *J. Phys. Chem.*, *82*, 1-7, 1978.

Chou, M.-D., L. Peng, and A. Arking, Climate studies with a multilayer energy balance model. Part III: Climatic impact of stratospheric volcanic aerosols, *J. Atmos. Sci.*, *41*, 759-767, 1984.

Chu, W. P., and M. P. McCormick, Inversion of stratospheric aerosol and gaseous constituents from spacecraft solar extinction data in the 0.38 - 1.0 μm wavelength region, *Appl. Opt.*, *18*, 1404-1413, 1979.

CIAP: See Climatic Impact Assessment Program.

Cicerone, R. J., Atmospheric carbon tetrafluoride: A nearly inert gas, *Science*, *206*, 59-61, 1979.

Cicerone, R. J., Methane in the atmosphere, in *Global Environment Problems*, edited by S. F. Singer, Paragon House, New York, in press, 1985.

Cicerone, R. J., and J. L. McCrumb, Photodissociation of isotopically heavy O_2 as a source of atmospheric O_3, *Geophys. Res. Lett.*, *7*, 251-254, 1980.

Cicerone, R. J., and J. D. Shetter, Sources of atmospheric methane: Measurements in rice paddies and a discussion, *J. Geophys. Res.*, *86*, 7203-7209, 1981.

Cicerone, R. J., and R. Zellner, The atmospheric chemistry of hydrogen cyanide, *J. Geophys. Res.*, *88*, 10689-10696, 1983.

Cicerone, R. J., S. Walters, and S. C. Liu, Non-linear response of stratospheric ozone column to chlorine injections, *J. Geophys. Res.*, *88*, 3647-3661, 1983a.

Cicerone, R. J., J. D. Shetter, and C. C. Delwiche, Seasonal variation of methane flux from a California rice paddy, *J. Geophys. Res.*, *88*, 11022-11024, 1983b.

Cieslik, S., and M. Nicolet, The aeronomic dissociation of nitric oxide, *Planet. Space Sci.*, *21*, 925-930, 1973.

Clancy, R. T., D. O. Muhleman, and G. L. Berge, Microwave spectra of terrestrial mesospheric CO, *J. Geophys. Res.*, *87*, 5009-5014, 1982.

Clark, J.H.E., and L. T. Morone, Mesospheric heating due to convectively excited gravity waves. A case study, *Mon. Weather Rev.*, *109*, 990-1001, 1981.

Clark, J.H.E., and T. G. Rogers, The transport of conservative trace gases by planetary waves, *J. Atmos. Sci.*, *35*, 2232-2235, 1978.

Clark, T. A., and D. J. W. Kendall, Far infrared emission spectrum of the stratosphere from balloon altitudes, *Nature*, *260*, 31-32, 1976.

Clark, T. A., and D. J. W. Kendall, Line positions and strengths of magnetic dipole transitions of molecular oxygen from stratospheric emission spectra, *J. Quant. Spectrosc. Radiat. Transfer*, *24*, 65-73, 1980.

Clark, T. A., D. A. Naylor, R. T. Boreiko, J. M. Hoogerdijk, B. Fitton, M. F. Kessler, and R. J. Emery, Downward flux of atmospheric 63)m emission from atomic oxygen at balloon altitudes, *Nature*, *313*, 206-207, 1985.

Climate Analysis Center, *Climate Diagnostics Bulletin*, Published monthly by the Climate Analysis Center, NOAA/NMC/NWS, Washington, DC, 1983.

Climate Analysis Center, *Climate Diagnostics Bulletin*, Published monthly by the Climate Analysis Center, NOAA/NMC/NWS, Washington, DC, 1984.

Climatic Impact Assessment Program, Report of findings: The effects of stratospheric pollution by aircraft, *DOT-TST-75-50*, edited by A. J. Grobecker, S. C. Coroniti, and R. H. Cannon, Jr., 551 pp., Department of Transportation, Washington, DC, 1974.

Clough, S. A., N. S. Grahame, and A. O'Neill, Potential vorticity in the stratosphere derived using data from satellites, *Quart. J. Roy. Meteorol. Soc.*, *111*, 335-358, 1985.

CMA: See Chemical Manufacturer's Association.

Coakley, J. A. Jr., and R. D. Cess, The effect of tropospheric aerosols on the earth's radiation budget: A parameterization for climate models, *J. Atmos. Sci.*, *40*, 116-138, 1983.

Coffey, M. T., W. G. Mankin, and A. Goldman, Simultaneous spectroscopic determination of the latitudinal, seasonal, and diurnal variability of stratospheric N_2O, NO, NO_2, and HNO_3, *J. Geophys. Res.*, *86*, 7331-7341, 1981a.

Coffey, M. T., W. G. Mankin, and R. J. Cicerone, Spectroscopic detection of stratospheric hydrogen cyanide, *Science*, *214*, 333-335, 1981b.

Coffey, M. T., W. G. Mankin, A. Goldman, C. P. Rinsland, G. A. Harvey, V. Malathy Devi, and G. M. Stokes, Infrared measurements of atmospheric ethane (C_2H_6) from aircraft and ground based solar absorption spectra in the 3000 cm^{-1} region, *Geophys. Res. Lett.*, *12*, 199-202, 1985.

REFERENCES

Coffey *et al.*, 1985: See Roscoe *et al.*, 1985.

Cohen, Y., and L. I. Gordon, Nitrous oxide in the oxygen minimum of the eastern tropical North Pacific: Evidence for its consumption during denitrification and possible mechanisms for its production, *Deep Sea Res.*, *6*, 509-524, 1978.

Cohen, Y., and L. I. Gordon, Nitrous oxide production in the ocean, *J. Geophys. Res.*, *84*, 347-353, 1979.

Cole, A. E., and A. J. Kantor, Air Force Reference Atmospheres, *Rep. AFGL-TR-78-0051*, 78 pp., Air Force Geophys. Lab., Hanscom AFB, MA, 1978.

Connell, P. S., D. J. Wuebbles, and J. S. Chang, Stratospheric hydrogen peroxide-The relationship of theory and observation, *J. Geophys. Res.*, 90, 10726-10732, 1985.

Cook, J. W., G. E. Brueckner, and M. E. Van Hoosier, Variability of the solar flux in the far ultraviolet 1175-2100Å, *J. Geophys. Res.*, *85*, 2257-2268, 1980.

Cornford, S. G., and C. S. Spavins, Some measurements of cumulonimbus tops in the pre-monsoon season in the north-east of India, *Met. Mag.*, *102*, 314-332, 1973.

COSPAR International Reference Atmosphere, CIRA, edited by A. C. Strickland, Akademie-Verlag, Berlin, 1972.

Cowley, J. R., and G. M. Lawrence, Earth Limb altitude determination for the Solar Mesosphere Explorer, paper presented at AIAA Aerospace Sciences Meeting, *AIAA Paper 83-0429*, 9 pp., Reno, Nevada, January 10-13, 1983.

Cox, R. A., and M. J. Coffey, Thermal decomposition of peroxyacetyl nitrate in the presence of NO, *Environ. Sci. Tech.*, *11*, 900-906, 1977.

Cox, R. A., and R. G. Derwent, Kinetics of chlorine oxide radical reactions using modulated photolysis, Part I, Disproportionation of ClO, *J. Chem. Soc. Far. I*, *75*, 1635-1647, 1979.

Cox, R. A., A.E.J. Eggleton, R. G. Derwent, J. E. Lovelock, and D. H. Pack, Long-range transport of photochemical ozone in north-western Europe, *Nature*, *255*, 118-121, 1975.

Cox, R. A., R. G. Derwent, A. E. J. Eggleton, and H. J. Reid, Kinetics of chlorine oxide radical reactions using modulated photolysis, Part 2, ClO and ClOO radical kinetics, *J. Chem. Soc. Far. I*, *75*, 1648-1666, 1979.

Cox, R. A., J. P. Burrows, and G. B. Coker, Product formation in the association reaction of ClO with NO_2 investigated by diode laser spectroscopy, *Int. J. Chem. Kinet.*, *16*, 445-467, 1984.

Coy, L., An unusually large westerly amplitude of the quasi-biennial oscillation, *J. Atmos. Sci.*, *36*, 174-176, 1979.

Coy, L., An unusually large westerly amplitude of the quasi-biennial oscillation, corrigendum, *J. Atmos. Sci.*, *37*, 913, 1980.

Coy, L., and M. Hitchman, Kelvin wave packets and flow acceleration: A comparison of modeling and observation, *J. Atmos. Sci.*, *41*, 1875-1880, 1984.

Craig, H., and C. C. Chou, Methane: The record in polar ice cores, *Geophys. Res. Lett.*, *9*, 1221-1224, 1982.

Craig, R. A., *The Upper Atmosphere: Meteorology and Physics*, 209 pp., Academic Press, New York, 1965.

Craig, R. L., R. A. Vincent, G. J. Fraser, and M. J. Smith, The quasi 2-day wave in the Southern Hemisphere mesosphere, *Nature*, *287*, 319-320, 1980.

Craig, R. L., R. A. Vincent, and R. A. Plumb, On the interaction between the quasi 2-day wave and the mean flow, in *Handbook for MAP*, *Vol. 18*, edited by S. Kato, pp. 76-79, SCOSTEP Secretariat, Univ. of Illinois, Urbana, 1985.

Crane, A. J., Uses of satellite data in studies of stratospheric dynamics, Ph.D. thesis, Oxford University, Oxford, 1977.

Crane, A. J., Aspects of the energetics of the upper stratosphere during the January-February 1973 major sudden warming, *Quart. J. Roy. Meteorol. Soc.*, *105*, 185-206, 1979.

Crane, A. J., J. D. Haigh, J. A. Pyle, and C. F. Rogers, Mean meridional circulations of the stratosphere and mesosphere, *Pure Appl. Geophys.*, *118*, 307-328, 1980.

Crutzen, P. J., discussion of "Absorption and emission by carbon dioxide in the mesosphere", *Quart. J. Roy. Meteorol. Soc.*, *96*, 767-769, 1970.

Crutzen, P. J., Ozone production rates in an oxygen, hydrogen, nitrogen-oxide atmosphere, *J. Geophys. Res.*, *76*, 7311-7327, 1971.

Crutzen, P. J., Gas phase nitrogen and methane chemistry in the atmosphere, in *Physics and Chemistry of Upper Atmospheres*, edited by B. M. McCormac, D. Reidel, Boston, MA, 1973a.

Crutzen, P. J., A discussion of the chemistry of some minor constituents in the stratosphere and troposphere, *Pure Appl. Geophys.*, *106-108*, 1385-1399, 1973b.

Crutzen, P. J., Photochemical reactions initiated by and influencing ozone in unpolluted tropospheric air, *Tellus*, *26*, 47-57, 1974.

Crutzen, P. J., The possible importance of CSO for the sulfate layer of the stratosphere, *Geophys. Res. Lett.*, *3*, 73-76, 1976.

Crutzen, P. J., The role of NO and NO_2 in the chemistry of the stratosphere and troposphere, *Ann. Rev. Earth Pl. Sci.*, *7*, 443-472, 1979.

Crutzen, P. J., Atmospheric interactions--Homogeneous gas reactions of C, N and S containing compounds, in *The Major Biogeochemical Cycles and Their Interactions*, edited by B. Bolin and R. Cook, pp. 67-112, Wiley, New York, 1983.

Crutzen, P. J., The role of the tropics in atmospheric chemistry, in *Geophysiology of Amazonia*, edited by R. Dickinson, Wiley, New York, in press, 1985.

Crutzen, P. J., and D. H. Ehhalt, Effects of nitrogen fertilizers and combustion on the stratospheric ozone layer, *Ambio*, *6*, 112-117, 1977.

Crutzen, P. J., and J. Fishman, Average concentrations of OH in the troposphere and the budgets of CH_4, CO, H_2, and CH_3CCl_3, *Geophys. Res. Lett.*, *4*, 321-324, 1977.

Crutzen, P. J., and L. T. Gidel, A two dimensional photochemical model of the atmosphere. 2. The tropospheric budgets of the anthropogenic chlorocarbons, CO, CH_4, CH_3Cl and the effect of various NO_x sources on tropospheric ozone, *J. Geophys. Res.*, *88*, 6641-6661, 1983.

Crutzen, P. J., and U. Schmailzl, Chemical budgets of the stratosphere, *Planet. Space Sci.*, *31*, 1009-1032, 1983.

Crutzen, P. J., and S. Solomon, Response of mesospheric ozone to particle precipitation, *Planet. Space Sci.*, *28*, 1147-1153, 1980.

Crutzen, P. J., I. S. A. Isaksen, and G. C. Reid, Solar proton events: Stratospheric sources of nitric oxide, *Science*, *189*, 457-459, 1975.

Crutzen, P. J., L. E. Heidt, J. P. Krasnec, W. H. Pollock, and W. Seiler, Biomass burning as a source of atmospheric gases CO, H_2, N_2O, NO, CH_3Cl and COS, *Nature*, *282*, 253-256, 1979.

Crutzen, P. J., W. Seiler, A. C. Delany, J. Greenburg, P. Haagensen, L. Heidt, R. Lueb, W. Pollock, A. Wartburg, and P. Zimmerman, Tropospheric chemical composition measurements in Brazil during the dry seasons, *J. Atmos. Chem.*, *2*, 233-256, 1983.

Cunnold, D., Fluorocarbon lifetime and releases from 5 years of ALE data, paper presented at CSIRO symposium, The Scientific Application of Baseline Observations of Atmospheric Composition, Aspendale, Australia, 7-9 November, 1984.

Cunnold, D., F. N. Alyea, N. Phillips, and R. G. Prinn, A three-dimensional dynamical chemical model of atmospheric ozone, *J. Atmos. Sci.*, *32*, 170-194, 1975.

Cunnold, D. M., F. N. Alyea, and R. G. Prinn, Relative effects on atmospheric ozone of latitude and altitude of supersonic flight, *AIAA Journal*, *15*, 337-345, 1977.

REFERENCES

Cunnold, D. M., F. N. Alyea, and R. G. Prinn, Preliminary calculations concerning the maintenance of the zonal mean ozone distribution in the Northern Hemisphere, *Pure Appl. Geophys.*, *118*, 329-354, 1980.

Cunnold, D. M., R. G. Prinn, R. A. Rasmussen, P. G. Simmonds, F. N. Alyea, C. A. Cardelino, A. J. Crawford, P. J. Fraser, and R. D. Rosen, The atmospheric lifetime experiment, 3, Lifetime methodology and application to 3 years of $CFCl_3$ data, *J. Geophys. Res.*, *88*, 8379-8400, 1983a.

Cunnold, D. M., R. G. Prinn, R. A. Rasmussen, P. G. Simmonds, F. N. Alyea, C. A. Cardelino, and A. J. Crawford, The atmospheric lifetime experiment, 4, Results for CF_2Cl_2 based on 3 years of data, *J. Geophys. Res.*, *88*, 8401-8414, 1983b.

Curtis, P. D., J. T. Houghton, G. D. Peskett, and C. D. Rodgers, The pressure modulator radiometer for Nimbus F, *Proc. Roy. Soc. London A*, *337*, 135-150, 1974.

Dacey, J., and M. J. Klug, Methane efflux from lake sediments through water lilies, *Science*, *203*, 1253-1255, 1979.

Danielsen, E. F., Trajectories: Isobaric, Isentropic and Actual, *J. Meteorol.*, *18*, 479-493, 1961.

Danielsen, E. F., *Project Springfield Report*, Defense Atomic Support Agency, DASA 1517, Washington, DC, 1964.

Danielsen, E. F., Transport and diffusion of stratospheric radioactivity based on synoptic hemispheric analyses of potential vorticity, Final report, *Report NYO-3317-3*, 97 pp., Pennsylvania State University, University Park, PA, 1967.

Danielsen, E. F., Stratospheric-tropospheric exchange based on radioactivity, ozone and potential vorticity, *J. Atmos. Sci.*, *25*, 502-518, 1968.

Danielsen, E. F., The relationship between severe weather, major dust storms and rapid large-scale cyclogenesis (II), in *Subsynoptic Extratropical Weather Systems: Observations, Analysis, Modeling, and Prediction, Notes from a colloquium, Summer, 1974, Volume II: Seminars and workshops,, Report PB-247286/8*, pp. 226-241, NCAR, Boulder, CO, 1974.

Danielsen, E. F., An objective method for determining the generalized transport tensor for two-dimensional Eulerian models, *J. Atmos. Sci.*, *38*, 1319-1339, 1981.

Danielsen, E. F., Statistics of cold cumulonimbus anvils based on enhanced infrared photographs, *Geophys. Res. Lett.*, *9*, 601-604, 1982.

Danielsen, E. F., Meteorological context for Global Tropospheric Experiments' instruments tests, paper presented to American Geophysical Union, San Francisco, California, December 3-7, 1984, *Eos Trans. AGU*, *65*, 834, 1984.

Danielsen, E. F., and R. S. Hipskind, Stratospheric-tropospheric exchange at polar latitudes in summer, *J. Geophys. Res.*, *85*, 393-400, 1980.

Danielsen, E. F., and D. Kley, A tropical cumulonimbus source for correlated water vapor and ozone minima in extratropical stratosphere, *J. Geophys. Res.*, in press, 1985.

Danielsen, E. F., and V. A. Mohnen, Project Dustorm Report: Ozone transport, in situ measurements and meteorological analyses of tropopause folding, *J. Geophys. Res.*, *82*, 5867-5877, 1977.

Danielson, E. F., R. Bleck, J. Shedlovsky, A. Wartburg, P. Haagensen and W. Pollock, Observed distribution of radioactivity, ozone and potential vorticity associated with tropopause folding, *J. Geophys. Res.*, *75*, 2353-2361, 1970.

Dave, J. V., J. J. DeLuisi, and C. L. Mateer, Results of a comprehensive theoretical examination of the optical effects of aerosols on the Umkehr measurements, *Spec. Environ. Rep. 14*, pp. 15-22, WMO, Geneva, 1979.

Davies, R. W., Many body treatment of pressure shifts associated with collisional broadening, *Phys. Rev.*, *A12*, 927-946, 1975.

Dawson, G. A., Nitrogen fixation by lightning, *J. Atmos. Sci.*, *37*, 174-178, 1980.

De La Noe, J., A. Baudry, M. Perault, P. Dierich, N. Monnanteuil, and J. M. Colmont, Measurements of the vertical distribution of ozone by ground-based microwave techniques at the Bordeaux Observatory during the June 1981 intercomparison campaign, *Planet. Space Sci.*, *31*, 737-741, 1983.

De More: See DeMore.

De Muer, D., Vertical ozone distributions over Uccle, Belgium from six years of soundings, *Beit. Phys. Atmos.*, *49*, 1-16, 1976.

De Rudder, A., and G. Brasseur, Ozone in the 21st century: Increase or decrease?, in *Atmospheric Ozone*, edited by C. S. Zerefos and A. Ghazi, pp. 92-96, D. Reidel, Dordrecht, 1984.

De Rudder, A., and G. Brasseur, A model calculation of the ozone response to the increase in the atmospheric emission of several gases, *Internal Report*, Inst. Aeronomie Spatiale de Belgique, Brussels, 1985.

de Zafra, R. L., A. Parrish, P. M. Solomon, and J. W. Barrett, A measurement of stratospheric HO_2 by ground-based millimeter-wave spectroscopy, *J. Geophys. Res.*, *89*, 1321-1326, 1984.

de Zafra, R. L., A. Parrish, P. M. Solomon, and J. W. Barrett, Quantitative observations of stratospheric chlorine monoxide as a function of latitude and season during the period 1980-1983, in *Atmospheric Ozone*, edited by C. S. Zerefos and A. Ghazi, pp. 206-209, D. Reidel, Dordrecht, 1985a.

de Zafra, R. L., A. Parrish, J. Barrett, and P. Solomon, An observed upper limit on stratospheric hydrogen peroxide, *J. Geophys. Res.*, *90*, 13087-13090, 1985b.

Deguchi, S., and D. O. Muhleman, Mesospheric water vapor, *J. Geophys. Res.*, *87*, 1343-1346, 1982.

Delany, A. C., P. J. Crutzen, P. Haagensen, S. Walters, and A. F. Wartburg, Photochemically produced ozone in the emission from large-scale tropical vegetation fires, *J. Geophys. Res.*, *90*, 2425-2429, 1985.

Delany, A. C., D. R. Fitzjarrald, D. Pearson, D. H. Lenschow, G. J. Wendel, and B. Woodruff, Direct measurements of fluxes of oxides of nitrogen and of ozone over grasslands, *J. Atmos. Chem.*, in press, 1986.

Delbouille, L., G. Roland, J. W. Brault, and L. Testerman, Photometric atlas of the solar spectrum from 1850 to 10,000 cm^{-1}, preliminary data, Kitt Peak National Observatory, 1981.

Delmas, R. J., J. M. Ascencia, and M. Legrand, Polar ice evidence that atmospheric CO_2 20,000 B.P. was 50% of present, *Nature*, *284*, 155-157, 1980.

DeLuisi, J. J., Umkehr vertical ozone profile errors caused by the presence of stratospheric aerosols, *J. Geophys. Res.*, *84*, 1766-1770, 1979.

Demerjian, K. L., J. A. Kerr, and J. G. Calvert, Mechanism of photochemical smog formation, *Adv. Environ. Sci. Technol.*, *10*, 1-262, 1974.

Demerjian, K. L., K. L. Schere, and J. T. Peterson, Theoretical estimates of active (spherically integrated) flux and photolytic rate constants of atmospheric species in the lower troposphere, *Adv. Environ. Sci. Technol.*, *10*, 369-459, 1980.

DeMore, W. B., Rate constants for the reactions of hydroxyl and hydroperoxyl radicals with ozone, *Science*, *180*, 735-737, 1973.

DeMore, W. B., Rate constant and possible pressure dependence of the reaction OH + HO_2, *J. Phys. Chem.*, *86*, 121-126, 1982.

DeMore, W. B., and O. Raper, Hartley band extinction coefficients of ozone in the gas phase and in liquid nitrogen, carbon monoxide and argon, *J. Phys. Chem.*, *68*, 412-414, 1964.

DeMore, W. B., M. J. Molina, R. T. Watson, D. M. Golden, R. F. Hampson, M. J. Kurylo, C. J. Howard, and A. R. Ravishankara, Chemical kinetics and photochemical data for use in stratospheric modeling, Evaluation number 6, *JPL Publication 83-62*, 219 pp., Jet Propulsion Lab., Pasadena, CA, 1983.

DeMore, W. B., J. J. Margitan, M. J. Molina, R. T. Watson, D. M. Golden, R. F. Hampson, M. J. Kurylo, C. J. Howard, and A. R. Ravishankara, Chemical kinetics and photochemical data for use in stratospheric modeling, Evaluation Number 7, *JPL Publication 85-37*, 226 pp., Jet Propulsion Lab., Pasadena, CA, 1985.

REFERENCES

Derwent, D. G., Two-dimensional model studies of the impact of aircraft emission on tropospheric ozone, *Atmos. Environ.*, *16*, 1997-2007, 1982.

Derwent, R. G., and A. E. J. Eggleton, Two dimensional model studies of methyl chloroform in the troposphere, *Quart. J. Roy. Meteorol. Soc.*, *107*, 231-242, 1981.

Derwent, R. G., and H. N. M. Steward, Elevated ozone levels in the air of central London, *Nature*, *241*, 342-343, 1973.

Dickerson, R. R., Measurements of reactive nitrogen compounds in the free troposphere, *Atmos. Chem.*, *18*, 2585-2593, 1984.

Dickenson, R. E., Planetary Rossby waves propagating vertically through weak westerly wind wave guides, *J. Atmos. Sci.*, *25*, 984-1002, 1968.

Dickinson, R. E., Theory of planetary wave-zonal flow interaction, *J. Atmos. Sci.*, *26*, 73-81, 1969.

Dickinson, R. E., Infrared radiative heating and cooling in the Venusian mesosphere, 1, Global mean radiative equilibrium, *J. Atmos. Sci.*, *29*, 1551-1556, 1972.

Dickinson, R. E., Method of parameterization for infrared cooling between altitudes of 30 and 70 kilometers, *J. Geophys. Res.*, *78*, 4451-4457, 1973.

Dickinson, R. E., Energetics of the stratosphere, *J. Atmos. Terr. Phys.*, *37*, 855-864, 1975.

Dickinson, R. E., Modeling climate changes due to carbon dioxide increases, in *Carbon Dioxide Review*, edited by W. C. Clark, pp. 101-133, Clarendon Press, New York, 1982.

Dickinson, R. E., Infrared radiative cooling in the mesosphere and lower thermosphere, *J. Atmos. Terr. Phys.*, *46*, 995-1008, 1984.

Dickinson, R. E., Modeling of future climate. WMO/ICSU/UNEP international assessment of the impact of an increased atmospheric concentration of carbon dioxide on the environment, in press, 1985.

Dickinson, R. E., S. C. Liu, and T. M. Donahue, Effect of chlorofluoromethane infrared radiation on zonal atmospheric temperature, *J. Atmos. Sci.*, *35*, 2142-2152, 1978.

Ditchburn, R. W., and P. A. Young, The absorption of molecular oxygen between 1850 and 2500Å, *J. Atmos. Terr. Phys.*, *24*, 127-139, 1962.

Dobson, G. M. B., Origin and distribution of polyatomic molecules in the atmosphere, *Proc. Roy. Soc. London*, *A236*, 187-193, 1956.

Dobson, G. M. B., The laminated structure of the ozone in the atmosphere, *Quart. J. Roy. Meteorol. Soc.*, *99*, 599-607, 1973.

Dobson, G. M. B., D. N. Harrison, and J. Lawrence, Measurements of the amount of ozone in the Earth's atmosphere and its relation to other geophysical conditions: Part III, *Proc. Roy. Soc. London*, *A122*, 456-486, 1929.

Dobson, G. M. B., A. W. Brewer, and B. M. Cwilong, Meteorology of the lower stratosphere, *Proc. Roy. Soc. London*, *A185*, 144-175, 1946.

Dodge, M. C., Combined effects of organic reactivity and NMHC/NOx ratio on photochemical oxidant formation--a modeling study, *Atmos. Environ.*, *18*, 1657-1665, 1984.

Dognon, A. M., F. Caralp, and R. Lesclaux, Reactions of chlorofluoromethyl peroxy radicals with NO: A kinetic study in the temperature range 230-430K, *J. Chem. Phys. Phys. Biol.*, in press, 1985.

Doherty, G. M., R. E. Newell, and E. F. Danielsen, Radiative heating rates near the stratospheric fountain, *J. Geophys. Res.*, *89*, 1380-1384, 1984.

Donner, L. J., and H.-L. Kuo, Radiative forcing of stationary planetary waves, *J. Atmos. Sci.*, *41*, 2849-2868, 1984.

Donner, L. J., and V. Ramanathan, Methane and nitrous oxide: Their effects on the terrestrial climate, *J. Atmos. Sci.*, *37*, 119-124, 1980.

Dopplick, T. G., Radiative heating of the global atmosphere: Corrigendum, *J. Atmos. Sci.*, *36*, 1812-1817, 1979.

Douglass, A. R., R. B. Rood, and R. S. Stolarski, Interpretation of ozone temperature correlations, 2. Analysis of SBUV ozone data, *J. Geophys. Res.*, 90, 10693-10708, 1985.

Drayson, S. R., Calculation of long-wave radiative transfer in planetary atmospheres, Ph.D. thesis, *Rep. 07584-1-T*, 110 pp., College of Engineering, University of Michigan, Ann Arbor, MI, 1967.

Drayson, S. R., P. L. Bailey, H. Fischer, J. C. Gille, A. Girard, L. L. Gordley, J. E. Harries, W. G. Planet, E. E. Remsberg, and J. M. Russell, III, Spectroscopy and transmittances for the LIMS experiment, *J. Geophys. Res.*, *89*, 5141-5146, 1984.

Drummond, J. R., and R. F. Jarnot, Infrared measurements of stratospheric composition II. Simultaneous NO and NO_2 measurements, *Proc. Roy. Soc. London A*, *364*, 237-254, 1978.

Drummond, J. R., J. T. Houghton, G. D. Peskett, C. D. Rodgers, M. J. Wale, J. Whitney, and E. J. Williamson, The stratospheric and mesospheric sounder on Nimbus 7, *Phil. Trans. Roy. Soc. London*, *A296*, 219-241, 1980.

Drummond, J. W., J. M. Rosen, and D. J. Hofmann, Balloon borne chemiluminescent measurement of NO to 45 km, *Nature*, *265*, 319-320, 1977.

Drummond, J. W., A. Volz, and D. H. Ehhalt, An optimized chemiluminescence detector for tropospheric NO measurements, *J. Atmos. Chem.*, *2*, 287-306, 1985.

Duce, R. A., V. A. Mohnen, P. R. Zimmerman, D. Grosjean, W. Cautreels, R. Chatfield, R. Jaenicke, J. A. Ogren, E. D. Pellizzari, and G. T. Wallace, Organic material in the global troposphere, *Revs. Geophys. Space Phys.*, *21*, 921-952, 1983.

Duetsch, H. U., Two years of regular ozone soundings over Boulder, Colorado, *NCAR Tech. Note No. 10*, 449 pp., NCAR, Boulder, CO, 1966.

Duetsch, H. U., Vertical ozone distribution on a global scale, *Pure Appl. Geophys.*, *116*, 511-529, 1978.

Duetsch, H. U., Total ozone trend in the light of ozone soundings, The impact of El Chichon, in *Atmospheric Ozone*, edited by C. S. Zerefos and A. Ghazi, pp. 263-268, D. Riedel, Dordrecht, 1985.

Duetsch, H. U., C. Ling, and W. Zuellig, Regular ozone observation at Thalwill, Switzerland and at Boulder, Colorado, *Rept. LAPETH-1*, 279 pp., Eidgenoessische Technische Hochschule, Zurich, 1970.

Dunkerton, T. J., On the mean meridional mass motions of the stratosphere and mesosphere, *J. Atmos. Sci.*, *35*, 2325-2333, 1978.

Dunkerton, T. J., On the role of Kelvin waves in the westerly phase of the semi-annual zonal wind oscillation, *J. Atmos. Sci.*, *36*, 32-41, 1979.

Dunkerton, T. J., Stochastic parameterization of gravity wave stresses, *J. Atmos. Sci.*, *39*, 1711-1725, 1982a.

Dunkerton, T. J., Theory of the mesopause semi-annual oscillation, *J. Atmos. Sci.*, *39*, 2681-2690, 1982b.

Dunkerton, T. J., Laterally-propagating planetary waves in the easterly phase of the quasi-biennial oscillation, *Atmosphere-Ocean*, *21*, 55-68, 1983a.

Dunkerton, T. J., Modification of stratospheric circulation by trace constituent changes?, *J. Geophys. Res.*, *88*, 10831-10836, 1983b.

Dunkerton, T. J., and N. Butchart, Propagation and selective transmission of internal gravity waves in a sudden warming, *J. Atmos. Sci.*, *41*, 1443-1460, 1984.

Dunkerton, T. J., and D. P. Delisi, Climatology of the equatorial lower stratosphere, *J. Atmos. Sci.*, *42*, 376-396, 1984.

Dunkerton, T. J., C. P. F. Hsu, and M. E. McIntyre, Some Eulerian and Lagrangian diagnostics for a model stratospheric warming, *J. Atmos. Sci.*, *38*, 819-843, 1981.

Dutton, J. A., *The Ceaseless Wind*, 579 pp., McGraw-Hill, New York, 1976.

Duxbury, J. M., D. R. Bouldin, R. E. Terry, and R. L. Tate, Emissions of nitrous oxide from soils, *Nature*, *298*, 462-464, 1982.

Dvoryashina, Y. V., V. I. Dianov-Klokov, and L. N. Yurganov, On the variations of atmospheric total column carbon monoxide abundance for 1970-1982, *Phys. Atmos. Oceans*, *20*, 40-47, 1984.

Eady, E. T., Long waves and cyclone waves, *Tellus*, *1*, 35-42, 1949.

Eastman, J. A., and D. H. Stedman, A fast response sensor for eddy-correlation flux measurement, *Atmos. Environ.*, *11*, 1209-1211, 1977.

Eaton, F., and G. Wendler, Some environmental effects of forest fires in interior Alaska, *Atmos. Environ.*, *17*, 1331-1337, 1983.

Edmon, Jr., H. J., B. J. Hoskins, and M. E. McIntyre, Eliassen-Palm cross sections for the troposphere, *J. Atmos. Sci.*, *37*, 2600-2616, 1980.

Edmonds, J. A., J. Reilly, J. R. Trabalka, and D. E. Reichle, An analysis of possible future atmospheric retention of fossil fuel CO_2, *DOE/OR-21400/1*, 169 pp., Institute for Energy Analysis, Washington, DC, 1984.

Edwards, D. K., and S. J. Morizumi, Scaling of vibration-rotation band parameters for nonhomogeneous gas radiation, *J. Quant. Spectrosc. Radiat. Transfer*, *10*, 175-188, 1970.

Ehhalt, D. H., The atmospheric cycle of methane, *Tellus*, *26*, 58-70, 1974.

Ehhalt, D. H., and J. W. Drummond, The tropospheric cycle of NOx, in *Chemistry of the Unpolluted and Polluted Troposphere*, edited by H. W. Georgii and W. Jaeschke, D. Reidel, Hingham, MA, 1982.

Ehhalt, D. H., and J. Rudolph, On the importance of light hydrocarbons in multiple atmospheric systems, in *Berichte der Kernforschungsanlage*, Julich GMbH, Juli, 1984.

Ehhalt, D. H., and U. Schmidt, Sources and sinks of atmospheric methane, *Pure Appl. Geophys.*, *116*, 452-464, 1978.

Ehhalt, D. H., and A. Toennissen, Hydrogen and carbon compounds in the stratosphere, in *Proceedings of the NATO Advanced Study Institute on Atmospheric Ozone: Its Variation and Human Influences*, *Rep. No. FAA-EE-80-20*, edited by A. C. Aikin, pp. 129-151, DOT, FAA, Washington, DC, 1980.

Ehhalt, D. H., L. E. Heidt, R. H. Lueb, and E. A. Martell, Concentrations of CH_4, CO, CO_2, H_2, H_2O, and N_2O in the upper stratosphere, *J. Atmos. Sci.*, *32*, 163-169, 1975.

Ehhalt, D. H., E. P. Roeth, and U. Schmidt, On the temporal variance of stratospheric trace gas concentrations, *J. Atmos. Chem.*, *1*, 27-51, 1983a.

Ehhalt, D. H., R. J. Zander, and R. A. Lamontagne, On the temporal increase of tropospheric CH_4, *J. Geophys. Res.*, *88*, 8442-8446, 1983b.

Ehhalt, D. H., J. Rudolph, F. Meixner, and U. Schmidt, Measurements of selected C_2-C_5 hydrocarbons in the background troposphere: Vertical and latitudinal variations, *J. Atmos. Chem.*, *3*, 29-52, 1985.

Elansky, N. F., A. Ya. Arabov, A. S. Elskhov, and I. A. Senik, Spatial and temporal variability of the NO_2 total content based on annual observation data in *Atmospheric Ozone*, edited by C. S. Zerefos and A. Ghazi, pp., 157-162, D. Reidel, Dordrecht, 1984.

Eliasen, E., and B. Machenhauer, A study of the fluctuations of atmospheric planetary flow patterns represented by spherical harmonics, *Tellus*, *17*, 220-238, 1965.

Eliasen, E., and B. Machenhauer, On the observed large-scale atmospheric wave motions, *Tellus*, *21*, 149-165, 1969.

Eliassen, A., On the vertical circulation in frontal zones, *Geofys. Pub.*, *24 (4)*, 147-160, 1962.

Eliassen, A., and E. Palm, On the transfer of energy in stationary mountain waves, *Geofys. Publ.*, *22*, *No. 3*, 1-23, 1961.

Elkins, J. W., S. C. Wofsy, M. B. McElroy, C. E. Kolb, and W. A. Kaplan, Aquatic sources and sinks for nitrous oxide, *Nature*, *275*, 602-606, 1978.

Ellingson, R. G., and G. N. Serafino, Observations and calculations of aerosol heating over the Arabian Sea during MONEX, *J. Atmos. Sci.*, *41*, 575-589, 1984.

Elliott, W. P., L. Machta and C. D. Keeling, An estimate of the biotic contribution to the atmospheric CO_2 increase based on direct measurements at Mauna Loa Observatory, *J. Geophys. Res.*, *90*, 3741-3746, 1985.

Ellis, P., G. Holah, J. T. Houghton, T. S. Jones, G. Peckham, G. D. Peskett, D. R. Pick, C. D. Rodgers, H. K. Roscoe, R. Sandwell, The selective chopper radiometer for Nimbus 5, *Proc. Roy. Soc. London A, 334*, 149-170, 1973.

Ellsaesser, H. W., Sources and sinks of stratospheric water vapor, in *Proceedings of the NATO Advanced Study Institute on Atmospheric Ozone: Its Variation and Human Influences, Rep. FAA-EE-80-20*, edited by A. C. Aikin, pp. 283-300, DOT, FAA, Washington,DC, 1980.

Ellsaesser, H. W., J. E. Harries, D. Kley and R. Penndorf, Stratospheric H_2O, *Planet Space Sci., 28*, 827-835, 1980.

Enting, I. G., Preliminary studies with a two-dimensional model using transport fields derived from a GCM, *J. Atmos. Chem.*, in press, 1985.

National air pollutant emission estimates, 1940-1983, *EPA-450/4-84-028*, Environmental Protection Agency, Research Triangle Park, NC, 1984.

EPA: See National Air Pollutant Estimates.

Ertel, H., Ein neuer hydrodynamischer wirbelsatz, *Meteor. Z., 59*, 277-281, 1942.

Evans, W. F. J., C. I. Lin, and C. L. Midwinter, The altitude distribution of nitric acid at Churchill, *Atmosphere, 14*, 172-179, 1976.

Evans, W. F. J., J. B. Kerr, C. T. McElroy, R. S. O'Brien, and J. C. McConnell, Measurements of NO_2 and HNO_3 during a stratospheric warming at 54 degrees N. in February, 1979, *Geophys. Res. Lett., 9*, 493-496, 1982a.

Evans, W. F. J., C. T. McElroy, J. B. Kerr, and J. C. McConnell, Simulations of the October 23, 1980 stratoprobe flight, *Geophys. Res. Lett., 9*, 223-226, 1982b.

Fabian, P., Halogenated hydrocarbons in the atmosphere, in *The Handbook of Environmental Chemistry, Vol. 4*, Springer-Verlag, Heidelberg, in press, 1985.

Fabian, P., and C. E. Junge, Global rate of ozone destruction at the earth's surface, *Arch. Met. Geophys. Bioklim., A19*, 161-172, 1970.

Fabian, P., J. A. Pyle, and R. J. Wells, The August 1972 solar proton event and the atmospheric ozone layer, *Nature, 277*, 458-460, 1979.

Fabian, P., R. Borchers, S. A. Penkett, and N. J. D. Prosser, Halocarbons in the stratosphere, *Nature, 294*, 733-735, 1981a.

Fabian, P., R. Borchers, G. Flentje, W. A. Matthews, W. Seiler, H. Giehl, K. Bunse, F. Muller, U. Schmidt, A. Volz, A. Khedim, and F. J. Johnen, The vertical distribution of stable trace gases at mid-latitudes, *J. Geophys. Res., 86*, 5179-5184, 1981b.

Fabian, P., J. A. Pyle, and R. J. Wells, Diurnal variation of minor constituents in the stratosphere modeled as a function of latitude and season., *J. Geophys. Res., 87*, 4981-5000, 1982.

Fabian, P., R. Borchers, B. C. Krueger, S. Lal, and S. A. Penkett, The vertical distribution of $CHClF_2$ (CFC-22) in the stratosphere, *Geophys. Res. Lett., 12*, 1-3, 1985a.

Fabian, P., G. Flentje, and W. A. Mathews, Stratospheric NO profiles from simultaneous measurements of two chemiluminescent balloon-borne sondes, *Planet. Space Sci.*, in press, 1985b.

Fabian, P., R. Borchers, B. C. Krueger, and S. Lal, The vertical distribution of CFC-114 ($CClF_2$-$CClF_2$) in the atmosphere, *J. Geophys. Res., 90*, 13091-13093, 1985c.

Falls, A. H., and J. H. Seinfeld, Continued development of a kinetic mechanism for photochemical smog, *Environ. Sci. Technol., 12*, 1398-1400, 1978.

Farman, J. C., B. G. Gardiner, and J. D. Shanklin, Large losses of total ozone in Antarctica reveal seasonal ClO_x/NO_x interaction, *Nature, 315*, 207-210, 1985.

Farmer, C. B., and O. F. Raper, The HF:HCl ratio in the 14-38 km region of the stratosphere, *Geophys. Res. Lett., 4*, 527-529, 1977.

REFERENCES

Farmer, C. B., O. F. Raper, and R. H. Norton, Spectroscopic detection and vertical distribution of HCl in the troposphere and stratosphere, *Geophys. Res. Lett.*, *3*, 13-16, 1976.

Farmer, C. B., O. F. Raper, B. D. Robbins, R. A. Toth, and C. Mueller, Simultaneous spectroscopic measurements of stratospheric species: O_3, CH_4, CO, CO_2, N_2O, HCl, and HF at northern and southern mid-latitudes, *J. Geophys. Res.*, *85*, 1621-1632, 1980.

Farmer, C. B., B. Carli, A. Bonetti, M. Carlotti, B. M. Dinelli, H. Fast, N. Louisnard, C. Alamichel, W. Mankin, M. Coffey, I. G. Nolt, D. G. Murcray, A. Goldman, G. Stokes, D. Johnson, W. Traub, K. Chance, R. Zander, L. Delbounille, and G. Roland, Balloon Intercomparison Campaigns: Results of remote sensing measurements of HCl, to be published, 1986.

Fast, H., W.F.J. Evans, G. L. Vail, and H. L. Buijs, A measurement of the stratospheric HCl profile at 82°N on November 8, 1978, *J. Geophys. Res.*, in press, 1985.

FCM: See *The National plan for stratospheric ozone monitoring*.

Feely, H. W., and J. Spar, Tungsten-185 from nuclear bomb tests as a tracer for stratospheric meteorology, *Nature*, *188*, 1062-1064, 1960.

Fehsenfeld, F. C., E. E. Ferguson, G. E. Streit, and D. L. Albritton, Stratospheric ion chemistry and the 11-year variation in polar ozone, *Science*, *194*, 544-545, 1976.

Fels, S. B., Simple strategies for inclusion of Voigt effects in infrared cooling rate calculations, *Appl. Opt.*, *18*, 2634-2637, 1979.

Fels, S. B., A parameterization of scale dependent radiative damping rates in the middle atmosphere, *J. Atmos. Sci.*, *39*, 1141-1152, 1982.

Fels, S. B., The radiative damping of short vertical scale waves in the mesosphere, *J. Atmos. Sci.*, *41*, 1755-1764, 1984.

Fels, S. B., Radiative-dynamical interactions in the middle atmosphere, in *Issues in Atmospheric and Oceanic Modeling*, edited by B. Saltzman, Advances in Geophysics 28, Part A, in press, 1985.

Fels, S. B., and L. D. Kaplan, A test of the role of longwave radiative transfer in a general circulation model, *J. Atmos. Sci.*, *33*, 779-789, 1975.

Fels, S. B., and M. D. Schwartzkopf, An efficient, accurate algorithm for calculating CO_2 15 μm band cooling rates, *J. Geophys. Res.*, *86*, 1205-1232, 1981.

Fels, S. B., J. D. Mahlman, M. D. Schwarzkopf, and R. W. Sinclair, Stratospheric sensitivity to perturbations in ozone and carbon dioxide: Radiative and dynamical response, *J. Atmos. Sci.*, *37*, 2265-2297, 1980.

Fiedler, B. H., An integral closure model for the vertical turbulent flux of a scalar in a mixed layer, *J. Atmos. Sci.*, *41*, 674-680, 1984.

Finger, F. G., M. E. Gelman, F. J. Schmidlin, R. Leviton, and B. Kennedy, Compatibility of meteorological rocketsonde data as indicated by International Comparison Tests, *J. Atmos. Sci.*, *32*, 1705-1714, 1975.

Firestone, M. K., and J. M. Tiedje, Temporal change in nitrous oxide and dinitrogen following the onset of an aerobiosis, *Appl. Environ. Microbiol.*, *38*, 673-679, 1979.

Firestone, M. K., M. S. Smith, R. B. Firestone, and J. M. Tiedje, The influence of nitrate, nitrite and oxygen on the gaseous products of denitrification in soil, *Soil Sci. Soc. Am. J.*, *43*, 1140-1144, 1979.

Fischer, H., F. Fergg, D. Rabus, and P. Burkert, Stratospheric H_2O and HNO_3 profiles derived from solar occultation measurements, *J. Geophys. Res.*, *90*, 3831-3835, 1985a.

Fischer, H., E. Redemann, F. Fergg, and D. Rabus, Measurements of stratospheric NO_2 profiles using a gas correlation radiometer in the solar occultation mode, *J. Atmos. Chem.*, in press, 1985b.

Fishman, J., Ozone in the troposphere, in *Ozone in the Free Atmosphere*, edited by R. C. Whitten and S. S. Prasad, pp. 161-194, Van Nostrand Reinhold, New York, 1985.

Fishman, J., and T. A. Carney, A one-dimensional photochemical model of the troposphere with planetary boundary-layer parameterization, *J. Atmos. Chem.*, 351-376, 1984.

Fishman, J., and P. J. Crutzen, The origin of ozone in the troposphere, *Nature*, *274*, 855-858, 1978.

Fishman, J., and W. Seiler, Correlative nature of ozone and carbon monoxide in the troposphere: Implications for the tropospheric ozone budget, *J. Geophys. Res.*, *88*, 3662-3670, 1983.

Fishman, J., V. Ramanathan, P. J. Crutzen, and S. C. Liu, Tropospheric ozone and climate, *Nature*, *282*, 818-820, 1979a.

Fishman, J., S. Solomon, and P. J. Crutzen, Observational and theoretical evidence in support of a significant in-situ photochemical source of tropospheric ozone, *Tellus*, *31*, 432-446, 1979b.

Fishman, J., W. Seiler, and P. Haagensen, Simultaneous presence of O_3 and CO bands in the troposphere, *Tellus*, *32*, 456-463, 1980.

Fitzjarrald, D. R., and M. Garstang, Boundary-layer growth over the tropical ocean, *Mon. Weather Rev.*, *109*, 1762-1772, 1981.

Fitzjarrald, D. R., and D. H. Lenschow, Mean concentration and flux profiles for chemically reactive species in the atmospheric surface layer, *Atmos. Environ.*, *17*, 2505-2512, 1983.

Flaud, J.-M., C. Camy-Peyret, and L. S. Rothman, Improved ozone line parameters in the 10- and 4.8 μm regions, *Appl. Opt.*, *19*, 655, 1980.

Flaud, J.-M., C. Camy-Peyret, D. Cariolle, J. Laurent, and G. M. Stokes, Daytime variations of atmospheric NO_2 from ground-based infrared measurements, *Geophys. Res. Lett.*, *10*, 1104-1107, 1983.

Fleig, A. J., K. F. Klenk, P. K. Bhartia, K. D. Lee, C. G. Wellemeyer, and V. G. Kaveeshwar, Vertical ozone profile results from Nimbus 4 data, in *Proc. 4th Conf. Atmos. Radiation*, pp. 20-26, AMS, Toronto, Canada, 1981.

Fleig, A. J., K. F. Klenk, P. K. Bhartia, D. Gordon, and W. H. Schneider, Users guide for the Solar Backscattered Ultraviolet (SBUV) instrument first-year ozone-S data set, *NASA Ref. Publ. 1095*, 72 pp., NASA Goddard Space Flight Center, Greenbelt, MD, 1982.

Fontanella, J., A. Girard, L. Gramont, and N. Louisnard, Vertical distribution of NO, NO_2, and HNO_3 as derived from stratospheric absorption infrared spectra, *Appl. Opt.*, *14*, 825-839, 1975.

Foot, J. S., Aircraft measurements of the humidity in the lower stratosphere from 1977 to 1980 between 45°N and 60°N, *Quart. J. Roy. Meteorol. Soc.*, *110*, 303-320, 1984.

Forbes, J. M., Middle atmosphere tides, *J. Atmos. Terr. Phys.*, *46*, 1049-1067, 1984.

Fouquart, Y., B. Bonnel, G. Brogniez, A. Cerf, M. Chaovi, L. Smith, and J. C. Vanhootte, Size distribution and optical properties of Saharan aerosols during Eclats, in *Aerosols and their Climate Effects*, edited by H. E. Gerber and A. Deepak, pp. 35-62, A. Deepak Publ., Hampton, VA, 1984.

Frank, W. M., The cumulus parameterization problem, *Mon. Weather Rev.*, *111*, 1859-1871, 1983.

Fraser, P. J., M. A. K. Khalil, R. A. Rasmussen, and A. J. Crawford, Trends of atmospheric methane in the Southern Hemisphere, *Geophys. Res. Lett.*, *8*, 1063-1066, 1981.

Fraser, P. J., G. I. Pearman, and P. Hyson, The global distribution of atmospheric CO_2: II. A review of provisional background observations 1978-1980, *J. Geophys. Res.*, *88*, 3591-3598, 1982.

Fraser, P. J., P. Hyson, I. G. Enting, and G. I. Pearman, Global distribution and Southern Hemisphere trend of atmospheric CCl_3F, *Nature*, *302*, 692-695, 1983a.

Fraser, P. J., M. A. K. Khalil, R. A. Rasmussen, and L. P. Steele, Tropospheric methane in the mid-latitudes of the Southern Hemisphere, *J. Atmos. Chem.*, *1*, 125-135, 1983b.

Fraser, P. J., P. Hyson, M. A. K. Khalil, and R. A. Rasmussen, Conference on Scientific Application of Baseline Observations on Atmospheric Composition, Aspendale, Australia, 7-9 November, 1984.

Frederick, J. E., Solar corpuscular emission and neutral chemistry in the Earth's middle atmosphere, *J. Geophys. Res.*, *81*, 3179-1976, 1976.

Frederick, J. E., Radiative-photochemical response of the mesosphere to dynamical forcing, *J. Geophys. Res.*, *86*, 5224-5230, 1981.

Frederick, J. E., and R. J. Cicerone, Dissociation of metastable O_2 as a potential source of atmospheric odd oxygen, *J. Geophys. Res.*, 90, 10733-10738, 1985.

REFERENCES

Frederick, J. E., and A. R. Douglass, Atmospheric temperatures near the tropical tropopause: Temporal variations, zonal asymmetry and implications for stratospheric water vapor, *Mon. Weather Rev.*, *111*, 397-1403, 1983.

Frederick, J. E., and R. D. Hudson, Predissociation linewidths and oscillator strengths for the 2-0 to 13-0 Schumann-Runge bands of O_2, *J. Molec. Spectrosc.*, *74*, 247-258, 1979a.

Frederick, J. E., and R. D. Hudson, Predissociation of nitric oxide in the mesosphere and stratosphere, *J. Atmos. Sci.*, *36*, 737-745, 1979b.

Frederick, J. E., and R. D. Hudson, Dissociation of molecular oxygen in the Schumann-Runge bands, *J. Atmos. Sci.*, *37*, 1099-1106, 1980a.

Frederick, J. E., and R. D. Hudson, Atmospheric opacity in the Schumann-Runge bands and the aeronomic dissociation of water vapor, *J. Atmos. Sci.*, *37*, 1088-1098, 1980b.

Frederick, J. E., and J. E. Mentall, Solar irradiance in the stratosphere: Implications for the Herzberg continuum absorption of O_2, *Geophys. Res. Lett.*, *9*, 461-464, 1982.

Frederick, J. E., and N. Orsini, The distribution and variability of mesospheric odd nitrogen: A theoretical investigation, *J. Atmos. Terr. Phys.*, *44*, 479-1982, 1982.

Frederick, J. E., and G. N. Serafino, Satellite observations of the nitric oxide dayglow: Implications for the behavior of mesospheric and lower thermospheric odd nitrogen, *J. Geophys. Res.*, *90*, 3821-3830, 1985.

Frederick, J. E., R. D. Hudson, and J. E. Mentall, Stratospheric observations of the attenuated solar irradiance in the Schumann-Runge band absorption region of molecular oxygen, *J. Geophys. Res.*, *86*, 9885-9890, 1981.

Frederick, J. E., A. J. Blake, D. E. Freeman, R. W. Nicholls, T. Ogawa, and P. C. Simon, MSG-7: Molecular absorption processes related to the penetration of ultraviolet solar radiation into the middle atmosphere, in *Handbook for MAP, Vol. 8*, edited by C. F. Sechrist, Jr., pp. 53-74, SCOSTEP Secretariat, Univ. of Illinois, Urbana, 1983a.

Frederick, J. E., F. T. Huang, A. R. Douglass, and C. A. Reber, The distribution and annual cycle of ozone in the upper stratosphere, *J. Geophys. Res.*, *88*, 3819-3828, 1983b.

Frederick, J. E., G. N. Serafino, and A. R. Douglass, An analysis of the annual cycle in upper stratospheric ozone, *J. Geophys. Res.*, *89*, 9547-9555, 1984.

Fredriksson, K., B. Galle, K. Nystrom, and S. Svanberg, Lidar system applied in atmospheric pollution monitoring, *Appl. Optics*, *18*, 2998-2998, 1979.

Freeman, D. E., K. Yoshino, J. R. Esmond, and W. H. Parkinson, High resolution absorption cross section measurements of ozone at 195 K in the wavelength region 240-350 nm, *Planet. Space Sci.*, *32*, 239-248, 1984.

Freney, J. R., O. T. Denmead, and J. R. Simpson, Nitrous oxide emissions from soils at low moisture contents, *Soil Biol. Biochem.*, *11*, 167-173, 1979.

Frerking, M. A., and D. J. Muehlner, Infrared heterodyne spectroscopy of atmospheric ozone, *Appl. Opt.*, *16*, 526-528, 1977.

Friedl, R. R., W. H. Brune, and J. G. Anderson, Kinetics of SH with NO_2, O_3, O_2, and H_2O_2, *J. Phys. Chem.*, *89*, 5505-5510, 1985.

Friedli, H., E. Moore, H. Oeschger, U. Siegenghaler, and B. Stauffer, $^{13}C/^{12}C$ ratios in CO_2 extracted from antarctic ice, *Geophys. Res. Lett.*, *11*, 1145-1148, 1984.

Fritts, D. C., Gravity wave saturation in the middle atmosphere: A review of theory and observations, *Rev. Geophys. and Space Phys.*, *22*, 275-308, 1984.

Fritts, D. C., and T. J. Dunkerton, Fluxes of heat and constituents due to convectively unstable gravity waves, *J. Atmos. Sci.*, *42*, 549-556, 1985.

Fritz, B., and R. Zellner, Reaction rate and equilibrium constant for $ClO + O_2 \rightarrow OClOO$, presented at CMA Chemistry Workshop, Goettingen, 1984.

Froidevaux, L., Photochemical modeling of the earth's stratosphere, Ph.D. thesis, 275 pp., California Institute of Technology, Pasadena, CA, 1983.

Froidevaux, L., and Y. L. Yung, Radiation and chemistry in the stratosphere: Sensitivity to O_2 absorption cross-sections in the Herzberg continuum, *Geophys. Res. Lett.*, *9*, 854-857, 1982.

Froidevaux, L., M. Allen, and Y. L. Yung, A critical analysis of ClO and O_3 in the mid-latitude stratosphere, *J. Geophys. Res.*, *90*, 12999-13030, 1985a.

Froidevaux, L., M. Allen, S. Berman, and A. Daughton, Analysis of LIMS observations in the upper stratosphere and lower mesosphere, I. The mean O_3 profile and its temperature sensitivity at mid-latitudes in May, 1979, in press, 1985b.

Funk, J. P., and G. J. Garnham, Australian ozone observations and a suggested 24-month cycle, *Tellus*, *14*, 378-382, 1962.

Gage, K. S., and B. B. Balsley, MST radar studies of wind and turbulence in the middle atmosphere, *J. Atmos. Terr. Phys.*, *46*, 739-753, 1984.

Galbally, I. E., Emission of fixed nitrogen compounds to the atmosphere in remote areas, in *Biogeochemical Cycling of Sulfur and Nitrogen in Remote Areas*, edited by J. N. Galloway, D. Reidel, Dordrecht, in press, 1985.

Galbally, I. E., and C. R. Roy, Loss of fixed nitrogen from soils by nitric oxide exhalation, *Nature*, *275*, 734-735, 1978.

Galbally, I. E., and C. R. Roy, Destruction of ozone at the earth's surface, *Quart. J. Roy. Meteorol. Soc.*, *106*, 599-620, 1980.

Galbally, I. E., and C. R. Roy, Ozone and nitrogen oxides in the Southern Hemisphere troposphere, in *Proceedings of the Quadrennial International Ozone Symposium, Vol. I*, edited by J. London, pp. 431-438, IAMAP, NCAR, Boulder, CO, 1981.

Galbally, I. E., C. R. Roy, R. S. O'Brien, B. A. Ridley, D. R. Hastie, W. F. J. Evans, C. T. McElroy, J. B. Kerr, P. Hyson, W. Knight, and J. E. Laby, Measurements of the trace composition of the Austral stratosphere: Chemical and meteorological data, *Technical Paper No. 1*, CSIRO, Div. of Atmos. Res., Australia, 1983.

Galindo, I., Anthropogenic aerosols and their regional scale climatic effects, in *Aerosols and their Climatic Effects*, edited by H. E. Gerber and A. Deepak, pp. 245-260, A. Deepak Publ., Hampton, VA, 1984.

Gallagher, C. C., C. A. Forsberg, A. S. Mason, B. W. Gandrud, and M. Janghorbani, Total chlorine content in the lower stratosphere, *J. Geophys. Res.*, *90*, 10747-10752, 1985.

Gamache, R. R., and R. W. Davies, Theoretical N_2-, O_2-, and air broadened halfwidths of O_3 calculated by quantum Fourier transform theory with realistic collision dynamics, *J. Molec. Spec.*, *109*, 283-299, 1985.

Gamlen, P. H., B. C. Lane, P. M. Midgley, and J. J. Steed, The production and release to atmosphere of $CHCl_3$ and CCl_2F_2, *Atmos. Environ.*, in press, 1985.

Gammon, R. H., and W. D. Komhyr, Response of the global atmospheric CO_2 distribution to the atmospheric/oceanic circulation perturbation in 1982, in *IUGG Symposium 19 (Oceans and CO_2 Climate Response), Vol. 2*, 828 pp., Hamburg, FRG, 1983.

Gammon, R. H., W. D. Komhyr, L. Waterman, T. Conway, K. Thoning, and D. Gillette, The 1982/83 ENSO event: Response of the global atmospheric CO_2 distribution, paper presented at Conference on Scientific Application of Baseline Observations of Atmospheric Composition, CSIRO, Aspendale, Australia, 7-9 November, 1984.

Gammon, R. H., E. T. Sandquist, and P. J. Fraser, History of carbon dioxide in the atmosphere, *U.S. Department of Energy State-of-the-Art Report on the Global Carbon Cycle (DOE)*, Chapter 3, in press, 1985a.

REFERENCES

Gammon, R. H., W. D. Komhyr, and J. T. Peterson, The global atmospheric CO_2 distribution 1968-83: Interpretation of the results of the NOAA/GMCC measurement program, in *The Global Carbon Cycle: Analysis of the Natural Cycle and Implications of Anthropogenic and Alterations for the Next Century*, edited by J. R. Trabalka and D. E. Reichle, Springer-Verlag, New York, in press, 1985b.

Garcia, R. R., and J. Geisler, Stochastic forcing of small amplitude oscillations in the stratosphere, *J. Atmos. Sci.*, *38*, 2187-2197, 1981.

Garcia, R. R., and S. Solomon, A numerical model of the zonally averaged dynamical and chemical structure of the middle atmosphere, *J. Geophys. Res.*, *88*, 1379-1400, 1983.

Garcia, R. R., and S. Solomon, The effect of breaking gravity waves on the dynamics and chemical composition of the mesosphere and lower thermosphere, *J. Geophys. Res.*, *90*, 3850-3868, 1985.

Garcia, R. R., S. Solomon, R. G. Roble, and D. W. Rusch, A numerical response of the middle atmosphere to the 11-year solar cycle., *Planet. Space Sci.*, *32*, 411-423, 1984.

Garland, J. A., and S. A. Penkett, Absorption of peroxyacetyl nitrate and ozone by natural surfaces, *Atmos. Environ.*, *10*, 1127-1131, 1976.

Garland, J. A., A. W. Elzerman, and F. A. Penkett, The mechanism for dry deposition of ozone to sea water surfaces, *J. Geophys. Res.*, *85*, 7488-7492, 1980.

Gates, W. L., Modeling the ice-age climate, *Science*, *191*, 1138-1144, 1976.

Gates, W. L., K. H. Cook, and M. E. Schlesinger, Preliminary analysis of experiments on the climatic effects of increased CO_2 with an atmospheric general circulation model and a climatological ocean, *J. Geophys. Res.*, *86*, 6385-6393, 1981.

Geisler, J. E., and R. E. Dickinson, The five-day wave on the sphere with realistic zonal winds, *J. Atmos. Sci.*, *33*, 632-641, 1976.

Geller, M. A., Dynamics of the middle atmosphere, *Space Sci. Rev.*, *34*, 359-375, 1983.

Geller, M. A., Modelling the middle atmosphere circulation, in *Dynamics of the Middle Atmosphere*, edited by J. R. Holton and T. Matsuno, pp. 467-500, Terrapub, Tokyo, 1984.

Geller, M. A., and J. C. Alpert, Planetary wave coupling between the troposphere and the middle atmosphere as a possible sun-weather mechanism, *J. Atmos. Sci.*, *37*, 1197-1215, 1980.

Geller, M. A., M. F. Wu, and M. E. Gelman, Troposphere-stratosphere (Surface-55 km) monthly winter general circulation statistics for the Northern Hemisphere-four year averages, *J. Atmos. Sci.*, *40*, 1334-1352, 1983.

Geller, M. A., M. F. Wu, and M. E. Gelman, Troposphere-stratosphere (Surface-55 km) monthly winter general circulation statistics for the Northern Hemisphere-interannual variations, *J. Atmos. Sci.*, *41*, 1726-1744, 1984.

Gelman, M. E., A. J. Miller, R. M. Nagatani, and H. D. Bowman II, Mean zonal wind and temperature structure during the PMP-1 winter periods, *Adv. Space Res.*, *10*, 159-162, 1983.

Geophysical Monitoring for Climatic Change: See Harris, J. M.

Georgii, H.-W., and F. X. Meixner, Measurement of the tropospheric and stratospheric SO_2 distribution, *J. Geophys. Res.*, *85*, 7433-7438, 1980.

Ghazi, A., *Atlas der Globalverteilung des Gesamtozonbetrages nach Satellitenmessungen (April 1970-Mai 1972).*, Mitteilungen aus dem Institut fuer Geophysik and Meteorologie der Universitat zu Koln, 1980.

Ghazi, A., and J. J. Barnett, Ozone behavior and stratospheric thermal structure during Southern Hemispheric spring, *Contr. to Atmos. Phys.*, *53*, 1-13, 1980.

Ghazi, A., A. Ebel, and D. F. Heath, A study of satellite observations of ozone and stratospheric temperatures during 1970-1971, *J. Geophys. Res.*, *81*, 5365-5373, 1976.

Ghazi, A., V. Ramanathan, and R. E. Dickinson, Acceleration of upper stratospheric radiative damping: Observational evidence, *Geophys. Res. Lett.*, *6*, 437-440, 1979.

Ghazi, A., R. H. Wang, and M. P. McCormick, A study on radiative damping of planetary waves utilizing stratospheric observations, *J. Atmos. Sci.*, *42*, 2032-2042, 1985.

Gibbins, C. J., P. R. Schwartz, D. L. Thacker, and R. M. Bevilacqua, The variability of mesospheric water vapor, *Geophys. Res. Lett.*, *9*, 131-134, 1982.

Gidel, L. T., Cumulus cloud transport of transient tracers, *J. Geophys. Res.*, *88*, 6587-6599, 1983.

Gidel, L. T., and M. A. Shapiro, The role of clear air turbulence in the production of potential vorticity in the vicinity of upper tropospheric jetstream-frontal systems., *J. Atmos. Sci.*, *36*, 2125-2138, 1979.

Gidel, L. T., and M. A. Shapiro, General circulation model estimates of the net vertical flux of ozone in the lower stratosphere and the implications for the troposheric ozone budget, *J. Geophys. Res.*, *85*, 4049-4058, 1980.

Gidel, L. T., P. J. Crutzen, and J. Fishman, A two-dimensional photochemical model of the atmosphere. 1: Chlorocarbon emissions and their effect on stratospheric ozone, *J. Geophys. Res.*, *88*, 6622-6640, 1983.

Gill, A. E., *Atmosphere-Ocean Dynamics*, 662 pp., Academic Press, New York, 1982.

Gill, P. S., T. E. Graedel, and C. J. Weschler, Organic films on atmospheric aerosol particles, fog droplets, cloud droplets, raindrops and snowflakes, *Rev. Geophys. Space Phys.*, *21*, 903-920, 1983.

Gille, J. C., and F. B. House, On the inversion of Limb radiance measurements, I, Temperature and thickness., *J. Atmos. Sci.*, *28*, 1427-1442, 1971.

Gille, J. C., and L. V. Lyjak, An overview of wave-mean flow interactions during the winter of 1978-1979 derived from LIMS observations, in *Dynamics of the Middle Atmospere*, edited by J. R. Holton and T. Matsuno, pp. 289-306, Terrapub, Tokyo, 1984.

Gille, J. C., and J. M. Russell III, The Limb Infrared Monitor of the Stratosphere: Experiment description, performance, and results, *J. Geophys. Res.*, *89*, 5125-5140, 1984.

Gille, J. C., P. L. Bailey, R. A. Craig, F. B. House, and G. P. Anderson, Sounding the stratosphere and mesosphere by infrared Limb scanning from space, *Science*, *208*, 397-399, 1980a.

Gille, J. C., P. L. Bailey, and J. M. Russell III., Temperature and composition measurements from the LRIR and LIMS experiments on Nimbus 6 and 7, *Phil. Trans. Roy. Soc. London*, *A296*, 205-218, 1980b.

Gille, J. C., P. L. Bailey, L. V. Lyjak, and J. M. Russell III, Results from the LIMS experiment for the PMP-1 winter 1978/79, *Adv. in Space Res.*, *2*, 163-167, 1983.

Gille, J. C., J. M. Russell III, P. L. Bailey, L. L. Gordley, E. E. Remsberg, J. H. Lienesch, W. G. Planet, F. B. House, L. V. Lyjak, and S. A. Beck, Validation of the temperature retrievals obtained by the Limb Infrared Monitor of the Stratosphere (LIMS) experiment on NIMBUS 7, *J. Geophys. Res.*, *89*, 5147-5160, 1984a.

Gille, J. C., J. M. Russell III, P. L. Bailey, E. E. Remsberg, L. L. Gordley, W. F. J. Evans, H. Fischer, B. W. Gandrud, A. Girard, J. E. Harries, and S. A. Beck, Accuracy and precision of the nitric acid concentrations determined by the Limb Infrared Monitor of the Stratosphere experiment on NIMBUS 7, *J. Geophys. Res.*, *89*, 5179-5190, 1984b.

Gille, J. C., C. M. Smythe, and D. F. Heath, Observed ozone response to variations in solar ultraviolet radiation, *Science*, *225*, 315-317, 1984c.

Giorgi, F., and W. L. Chameides, The rainout parameterization in a photochemical model, *J. Geophys. Res.*, *90*, 7872-7880, 1985.

Girard, A., and N. Louisnard, Stratospheric water vapor, nitrogen dioxide, nitric acid and ozone measurements deduced from spectroscopic observations, *J. Geophys. Res.*, *89*, 5109-5114, 1984.

Girard, A., J. Besson, R. Giraudet, and L. Gramont, Correlated seasonal and climatic variations of trace constituents in the stratosphere, *Pure Appl. Geophys.*, *117*, 381-393, 1978/79.

Girard, A., L. Gramont, N. Louisnard, S. Le Boiteux, and G. Fergant, Latitudinal variation of HNO_3, HCl, and HF vertical column density above 11.5 km, *Geophys. Res. Lett.*, *9*, 135-138, 1982.

Girard, A., G. Ferganti, L. Gramont, O. Lado-Bordowsky, J. Laurent, S. LeBoiteux, M. P. Lemaitre, and N. Louisnard, Latitudinal distribution of ten stratospheric species deduced from simultaneous spectroscopic measurements, *J. Geophys. Res.*, *88*, 5377-5392, 1983.

GMCC: See Harris, J. M.

Godson, W. L., Total ozone in the middle stratosphere over Arctic and sub-Arctic areas in winter and spring, *Quart. J. Roy. Meteorol. Soc.*, *86*, 301-317, 1960.

Goldan, P. D., W. C. Kuster, D. L. Albritton, and A. L. Schmeltekopf, Stratospheric $CFCl_3$, CF_2Cl_2, and N_2O height profile measurements at several latitudes, *J. Geophys. Res.*, *85*, 413-423, 1980.

Goldman, A., D. G. Murcray, F. H. Murcray, W. J. Williams, and F. S. Bonomo, Identification of the ν_3 NO_2 band in the solar spectrum observed from a balloon-borne spectrometer, *Nature*, *225*, 443-444, 1970.

Goldman, A., R. N. Stocker, D. Rolens, W. J. Williams, and D. G. Murcray, Stratospheric HNO_3 distributions from balloon-borne infrared atmospheric emission measurements from 1970-75, *Scientific Report*, University of Denver, Denver, CO, 1976.

Goldman, A., F. G. Fernald, W. J. Williams, and D. G. Murcray, Vertical distribution of NO_2 in the stratosphere as determined from balloon measurements of solar spectra in the 4500 Å region, *Geophys. Res. Lett.*, *5*, 257-260, 1978.

Goldman, A., D. G. Murcray, F. J. Murcray, G. R. Cook, J. W. Van Allen, F. S. Bonomo, and R. D. Blatherwick, Identification of the ν_3 vibration rotation band of CF_4 in balloon-borne infrared solar spectra, *Geophys. Res. Lett.*, *6*, 609-612, 1979.

Goldman, A., D. G. Murcray, F. J. Murcray, and E. Niple, High resolution IR balloon-borne solar spectra and laboratory spectra in the HNO_3 1720 cm^{-1} region: An analysis, *Appl. Opt.*, *19*, 3721-3724, 1980.

Goldman, A., F. J. Murcray, R. D. Blatherwick, J. R. Gillis, F. S. Bonomo, F. H. Murcray, D. G. Murcray, and R. J. Cicerone, Identification of acetylene (C_2H_2) in infrared atmospheric absorption spectra, *J. Geophys. Res.*, *86*, 12143-12146, 1981a.

Goldman, A., J. Reid, and L. S. Rothman, Identification of electric quadrupole O_2 and N_2 lines in the infrared atmospheric absorption spectrum due to the vibration-rotation fundamentals, *Geophys. Res. Lett.*, *8*, 77-78, 1981b.

Goldman, A., F. J. Murcray, J. R. Gillis, and D. G. Murcray, Identification of new solar OH lines in the 10-12 micron region, *Astrophys. J.*, *248*, L133-L135, 1981c.

Goldman, A., F. J. Murcray, R. D. Blatherwick, F. S. Bonomo, F. H. Murcray, and D. G. Murcray, Spectroscopic identification of $CHClF_2$ (F-22) in the lower stratosphere, *Geophys. Res. Lett.*, *8*, 1012-1014, 1981d.

Goldman, A., R. D. Blatherwick, F. J. Murcray, J. W. Van Allen, F. H. Murcray, and D. G. Murcray, *New Atlas of Stratospheric Infrared Absorption Spectra*, Univ. of Denver, Denver, CO, 1982.

Goldman, A., F. G. Fernald, F. J. Murcray, F. H. Murcray, and D. G. Murcray, Spectral least squares quantification of several atmospheric gases from high resolution infrared solar spectra obtained at the South Pole, *J. Quant. Spectrosc. Radiat. Transfer*, *29*, 189-204, 1983a.

Goldman, A., D. G. Murcray, D. L. Lambert, and J. F. Dominy, The pure rotation spectrum of the hydroxyl radical and the solar oxygen abundance, *Mon. Not. R. Astr.*, *203*, 767-776, 1983b.

Goldman, A., F. H. Murcray, D. G. Murcray, and C. P. Rinsland, A search for formic acid in the upper troposphere: A tentative identification of the 1105 cm^{-1} $\nu 6$ band Q branch in high-resolution balloon-borne solar absorption spectra, *Geophys. Res. Lett.*, *11*, 307-310, 1984a.

Goldman, A., C. P. Rinsland, F. J. Murcray, D. G. Murcray, M. T. Coffey, and W. G. Mankin, Balloon-borne and aircraft infrared measurements of ethane (C_2H_6) in the upper troposphere and lower stratosphere, *J. Atmos. Chem.*, *2*, 211-221, 1984b.

Goldman, A., J. R. Gillis, C. P. Rinsland, F. J. Murcray, and D. G. Murcray, Stratospheric HNO_3 quantification from line-by-line nonlinear least-squares analysis of high-resolution balloon-borne solar absorption spectra in the 870 cm^{-1} region, *Appl. Opt.*, *23*, 3252-3255, 1984c.

Golombek, A., A global three-dimensional model of the circulation and chemistry of long-lived atmospheric species, Ph.D. thesis, 201 pp., Dept. of Meteor. and Phys. Oceanography, MIT, Cambridge, MA, 1982.

Goody, R. M., A statistical model for water vapor absorption, *J. Meteorol.*, *78*, 165-169, 1952.

Goody, R. M., *Atmospheric Radiation*, 436 pp., Oxford University Press, London, 1964.

Goreau, T. J., The biogeochemistry of nitrous oxide, Ph.D. thesis, Harvard Univ., Boston, MA, 1981.

Goreau, T. J., and W. Z. DeMello, Effects of deforestation on sources and sinks of atmospheric carbon dioxide, nitrous oxide and methane from some Amazonian biota and soils, in press, 1985.

Goreau, T. J., W. A. Kaplan, S. C. Wofsy, M. B. McElroy, F. W. Valois, and S. W. Watson, Production of NO_2 and N_2O by nitrifying bacteria at reduced concentrations of oxygen, *Appl. Environ. Microbiology*, *40*, 526-532, 1985.

Gotz, F. W. P., A. R. Meetham, and G. M. B. Dobson, The vertical distribution of ozone in the atmosphere, *Proc. Roy. Soc. London*, *A145*, 416-446, 1934.

Graedel, T. E., and J. R. McRae, On the possible increase of the atmospheric methane and carbon monoxide concentrations during the last decade, *Geophys. Res. Lett.*, *7*, 977-979, 1980.

Grant, K. E., P. S. Connell, and D. J. Wuebbles, Monte Carlo uncertainty analysis of atmosphere ozone concentrations from large trace gas perturbations, in press, 1985.

Gray, L. J., and J. A. Pyle, Semi-annual oscillation and equatorial tracer distributions, *Quart. J. Roy. Meteorol. Soc.*, in press, 1986.

Gray, W. M., Global view of the origin of tropical disturbances and storms, *Mon. Weather Rev.*, *26*, 653-700, 1968.

Gray, W. M., Cumulus convection and large-scale circulations, Part I: Broadscale and mesoscale considerations, *Mon. Weather Rev.*, *101*, 839-855, 1973.

Greenberg, J. P., and P. R. Zimmerman, Nonmethane HC in remote tropical, continental, and marine atmospheres, *J. Geophys. Res.*, *89*, 4767-4778, 1984.

Greenberg, J. P., P. R. Zimmerman, L. Heidt, and W. Pollock, Hydrocarbons and carbon monoxide emissions from biomass burning in Brazil, *J. Geophys. Res.*, *89*, 1350-1354, 1984.

Grevesse, N., A. J. Sauval, and E. F. Van Dishoeck, An analysis of vibration-rotation lines of OH in the solar infrared spectrum, *Astron. Astrophys.*, *141*, 10-16, 1984.

Griffing, G. W., Ozone and nitrogen oxides production during thunderstorms, *J. Geophys. Res.*, *82*, 943-950, 1977.

Griggs, M., Absorption coefficients of ozone in the ultraviolet and visible regions, *J. Chem. Phys.*, *49*, 857-859, 1968.

Grose, W. L., Recent advances in understanding stratospheric dynamics and transport processes: Application of satellite data to their interpretation, *Adv. in Space Res.*, *4*, 19-28, 1984.

Grose, W. L., and J. M. Russell III, The use of isentropic potential vorticity in conjunction with quasi-conserved species in the study of stratospheric dynamics and transport, in press, 1985.

Grose, W. L., R. E. Turner, and J. E. Nealy, Transport processes in the stratosphere: Model simulations and comparisons with satellite observations, in *Proceedings of the International Middle Atmosphere Symposium*, Kyoto, Japan, in press, 1984.

Grose, W. L., R. E. Turner, and J. E. Nealy, Coupling between photochemistry and transport: Simulations with a 3-D model, *J. Atmos. Terr. Phys.*, in press, 1985.

Grosjean, D., Atmospheric reactions of ortho cresol: Gas phase and aerosol products, *Atmos. Environ.*, *18*, 1641-1652, 1984.

Groves, G. V., Seasonal and latitudinal models of atmospheric temperature, pressure and density, 25 to 100 km, *AFCRL-70-0261*, 78 pp., Air Force Cambridge Research Labs., Hanscom AFB, MA, 1970.

Groves, G. V., and J. M. Forbes, Equinox tidal heating of the upper atmosphere, *Planet. Space Sci.*, *32*, 447-436, 1984.

REFERENCES

Guedalia, D., C. Estournel, and R. Vehil, Effects of Sahel dust layers upon nocturnal cooling of the atmosphere, *ECLATS Experiment*, 644-650, 1984.

Guicherit, R., and H. Van Dop, Photochemical production of ozone in Western Europe (1971-1978) and its relation to meteorology, *Atmos. Environ.*, *11*, 145-155, 1977.

Guthrie, P. D., C. H. Jackman, J. R. Herman, and C. J. McQuillan, A diabatic circulation experiment in a two-dimensional photochemical model, *J. Geophys. Res.*, *89*, 9589-9602, 1984.

Hack, W., and H. Kurzke, The production of H-atoms in the energy transfer reaction of O_2 ($^1\Delta g$) with HO_2 (X^2A''), *Chem. Phys. Lett.*, *104*, 93-96, 1984.

Hack, W., and H. Kurzke, Kinetic study of the elementary chemical reaction $H(^2S) + O_2(^1\Delta g) \rightarrow OH$ ($^2\pi$) + $O(^3P)$ in the gas phase, *J. Phys. Chem.*, in press, 1985.

Haggard, K. V., and W. L. Grose, Numerical simulation of a sudden stratospheric warming with a three-dimensional spectral, quasi-geostrophic model, *J. Atmos. Sci.*, *38*, 1480-1497, 1981.

Hahn, J., and P. J. Crutzen, The role of fixed nitrogen in atmospheric photochemistry, *Phil. Trans. Roy. Soc. London*, *B296*, 521-541, 1982.

Haigh, J. D., and J. A. Pyle, Ozone perturbation experiments in a two-dimensional circulation model, *Quart. J. Roy. Meteorol. Soc.*, *108*, 551-574, 1982.

Haigh, J. D., Radiative heating in the lower stratosphere and the distribution of ozone in a two-dimensional model, *Quart. J. Roy. Meteorol. Soc.*, *110*, 167-185, 1984.

Hall, C. A. S., C. A. Ekdahl, and D. E. Wartenberg, A fifteen-year record of biotic metabolism in the Northern Hemisphere, *Nature*, *255*, 136-138, 1975.

Hameed, S., and R. D. Cess, The impact of a global warming on biospheric sources of methane and its climatic consequences, *Tellus*, *35*, 1-7, 1983.

Hameed, S., J. P. Pinto, and R. W. Stewart, Sensitivity of the predicted CO-OH-CH_4 perturbation to tropospheric NO_X concentrations, *J. Geophys. Res.*, *84*, 763-768, 1979.

Hameed, S., R. D. Cess, and J. S. Hogan, Response of the global climate to changes in atmospheric chemical composition due to fossil fuel burning, *J. Geophys. Res.*, *85*, 7537-7545, 1980.

Hamilton, K., Studies of wave-mean flow interaction in the stratosphere, mesophere and lower thermosphere, Ph.D. thesis, Princeton University, Princeton, NJ, 1981a.

Hamilton, K., The vertical structure of the quasi-biennial oscillation and its theory, *Atmos.-Ocean*, *19*, 236-250, 1981b.

Hamilton, K., Rocketsonde observation of the mesospheric semiannual oscillation at Kwajalein, *Atmos.-Ocean*, *20*, 281-286, 1982a.

Hamilton, K., Some features of the climatology of the Northern Hemisphere stratosphere revealed by NMC upper atmosphere analyses, *J. Atmos. Sci.*, *39*, 2737-2749, 1982b.

Hamilton, K., Diagnostic study of the momentum balance in the Northern Hemisphere winter stratosphere, *Mon. Weather Rev.*, *111*, 1434-1441, 1983a.

Hamilton, K., Aspects of wave behavior in the mid and upper troposphere of the Southern Hemisphere, *Atmos.-Ocean*, *21*, 40-54, 1983b.

Hamilton, K., Mean wind evolution through the quasi-biennial cycle in the tropical lower stratosphere, *J. Atmos. Sci.*, *41*, 2113-2125, 1984.

Hampson, J., Chemiluminescent emissions observed in the stratosphere and mesosphere, in *Les Problemes Meteorologiques de la Stratosphere et de la Mesosphere*, edited by CNES, Presses Universitaires de France, Paris, 1965.

Handwerk, V., and R. Zellner, Laboratory study of the reaction ClO + $O_2(^1\Delta) \rightarrow$ products, Final report to CMA, 1984.

Hanel, R. A., B. J. Conrath, V. G. Kunde, C. Prabhakara, I. Revah, V. V. Salomonson, and G. Wolford, The Nimbus 4 infrared spectroscopy experiment 1. Calibrated thermal emission spectra, *J. Geophys. Res.*, *77*, 2629-2641, 1972.

Hansen, J., D. Johnson, A. Lacis, S. Lebedeff, P. Lee, D. Rind, and G. Russell, Climate impact of increasing atmospheric carbon dioxide, *Science*, *213*, 957-966, 1981.

Hansen, J., A. Lacis, D. Rind, G. Russell, P. Stone, I. Fung, R. Ruedy, and J. Lerner, Climate sensitivity: Analysis of feedback mechanisms, in *Climate Processes and Climate Sensitivity*, Maurice Ewing Series 5, edited by J. E. Hansen and T. Takasashi, 368 pp., American Geophysical Union, Washington, DC, 1984.

Hao, W. M., Sources of N_2O from combustion, Ph.D. thesis, Harvard University, Boston, MA, 1985.

Harries, J. E., Ratio of HNO_3 to NO_2 concentrations in daytime stratosphere, *Nature*, *274*, 235, 1978.

Harries, J. E., Stratospheric composition measurements as tests of photochemical theory, *J. Atmos. Terr. Phys.*, *44*, 591-597, 1982.

Harries, J. E., D. G. Moss, N. R. W. Swann, G. F. Neill, and P. Gildwarg, Simultaneous measurements of H_2O, NO_2, and HNO_3 in the daytime stratosphere from 15 to 35 km, *Nature*, *259*, 300-302, 1976.

Harries, R. C., D. I. Sebacher, and F. P. Day, Methane flux in the Great Dismal Swamp, *Nature*, *297*, 673-674, 1982.

Harris, J. M. and B. A. Bodhaine (Eds.), *Geophysical Monitoring for Climatic Change, Summary Report 1982*, 160 pp., NOAA Air Resources Laboratory, Boulder, CO, 1983.

Harris, J. M., and E. C. Nickerson (Eds.), *Geophysical Monitoring for Climatic Change, No. 12, Summary Report, 1983*, 199 pp., NOAA Air Resources Laboratory, Boulder, CO, 1984.

Harshvardhan, A. Arking, M. D. King and M.-D. Chou, Impact of the El Chichon stratospheric aerosol layer on N. H. temperatures, paper presented at WMO(CAS)/IAMAP Workshop on Aerosols and Their Climatic Effects, Williamsburg, VA, 28-30 March 1983.

Hartmann, D. L., The structure of the stratosphere in the Southern Hemisphere during late winter 1973 as observed by satellite, *J. Atmos. Sci.*, *33*, 1141-1154, 1976a.

Hartmann, D. L., The dynamical climatology of the stratosphere in the Southern Hemisphere during late winter 1973, *J. Atmos. Sci.*, *33*, 1789-1802, 1976b.

Hartmann, D. L., A note concerning the effect of variable extinction on radiative-photochemical relaxation, *J. Atmos. Sci.*, *35*, 1125-1130, 1978.

Hartmann, D. L., Barotropic instability of the polar night jet stream, *J. Atmos. Sci.*, *40*, 817-835, 1983.

Hartmann, D. L., and R. R. Garcia, A mechanistic model of ozone transport by planetary waves in the stratosphere, *J. Atmos. Sci.*, *36*, 350-364, 1979.

Hartmann, D. L., C. R. Mechoso, and K. Yamazaki, Observations of wave mean-flow interaction in the Southern Hemisphere, *J. Atmos. Sci.*, *41*, 351-362, 1984.

Harwood, R. S., The temperature structure of the Southern Hemisphere stratosphere: August-October, 1971, *Quart. J. Roy. Meteorol. Soc.*, *102*, 757-770, 1975.

Harwood, R. S., and J. A. Pyle, A two-dimensional mean circulation model for the atmosphere below 80 km, *Quart. J. Roy. Meteorol. Soc.*, *101*, 723-747, 1975.

Harwood, R. S., and J. A. Pyle, Studies of the ozone budget using a zonal mean circulation model and linearized photochemistry, *Quart. J. Roy. Meteorol. Soc.*, *103*, 319-343, 1977.

Harwood, R. S., and J. A. Pyle, The dynamical behaviour of a two-dimensional model of the stratosphere, *Quart. J. Roy. Meteorol. Soc.*, *106*, 395-420, 1980.

Hasebe, F., Interannual variations of global total ozone revealed from Nimbus 4 BUV and ground-based observations, *J. Geophys. Res.*, *88*, 6819-6834, 1983.

Hasebe, F., The global structure of the total ozone fluctuations observed on the time scales of two to several years, in *Dynamics of the Middle Atmosphere*, edited by J. R. Holton and T. Matsuno, pp. 445-464, Terrapub, Tokyo, 1984.

Hashimoto, L. K., W. A. Kaplan, S. C. Wofsy, and W. B. McElroy, Transformations of fixed nitrogen in the Cariaco Trench, *Deep Sea Res.*, *30*, 575-590, 1983.

Hasson, V., and R. W. Nicholls, Absolute spectral absorption measurements in molecular oxygen from 2640-1920 Å: II. Continuum measurements 2430-1920 Å, *J. Phys. B.: Atom. Mol. Phys.*, *4*, 1789-1797, 1971.

Hastie, D. R., and M. D. Miller, A balloon-borne tunable diode laser absorption spectrometer for multi-species trace gas measurements in the stratosphere, *Appl. Opt.*, in press, 1985.

Hayashi, Y., A theory of large-scale equatorial waves generated by condensation heat and accelerating the zonal wind, *J. Meteorol. Soc. Japan*, *48*, 140-160, 1970.

Hayashi, Y., Spectral analysis of tropical disturbances appearing in a GFDL general circulation model, *J. Atmos. Sci.*, *31*, 180-218, 1974.

Hayashi, Y., Non-singular resonance of equatorial waves under the radiation condition, *J. Atmos. Sci.*, *33*, 183-201, 1976.

Hayashi, Y., D. Golder, and J. Mahlman, Stratospheric and mesospheric Kelvin waves simulated by the GFDL "SKYHI" general circulation model, *J. Atmos. Sci.*, *41*, 1971-1984, 1984.

Hayashi, Y., and D. Golder, Transient planetary waves simulated by GFDL spectral general circulation models. Part I: Effects of mountains, *J. Atmos. Sci.*, *40*, 941-950, 1983.

Hayashi, Y., D. Golder, and J. Mahlman, Stratospheric and mesospheric Kelvin waves simulated by the GFDL "SKYHI" general circulation model, *J. Atmos. Sci.*, *41*, 1971-1984, 1984.

Heaps, W. S., and T. J. McGee, Balloon borne lidar measurements of the stratospheric hydroxyl radical, *J. Geophys. Res.*, *88*, 5281-5285, 1983.

Heaps, W. S., and T. J. McGee, Progress in stratospheric hydroxyl measurement by balloon-borne lidar, *J. Geophys. Res.*, *90*, 7913-7922, 1985.

Heaps, W. S., T. J. McGee, R. D. Hudson, and L. O. Caudill, Stratospheric ozone and hydroxyl radical measurements by balloon-borne lidar, *Applied Opt.*, *21*, 2265-2274, 1982.

Hearn, A. G., The absorption of ozone in the ultraviolet and visible regions of the spectrum, *Proc. Phys. Soc. (London)*, *78*, 932-940, 1961.

Heaseman, C. H., Satellite observations of mesospheric wind structure, Ph.D. thesis, Oxford University, Oxford, 1981.

Heastie, H., and P. M. Stephenson, Upper winds over the world, *Geophys. Mem.*, No. 103, London: HMSO, *13*, 1-217, 1960.

Heath, D. F., A review of observational evidence for short and long term ultraviolet flux variability of the sun, in *Proceedings of the International Conference on Sun and Climate*, Centre National d'E-tudes Spatiales, Toulouse, Sept. 30-Oct. 3, 445-450, 1980.

Heath, D. F., and B. M. Schlesinger, Temporal variability of the UV solar spectral irradiance from 160-400 nm over periods of the evolution and rotation of active regions from maximum to minimum phases of the sunspot cycle, in press, 1985.

Heath, D. F., A. J. Krueger, H. A. Roeder, and B. D. Henderson, The solar backscatter ultraviolet and total ozone mapping spectrometer (SBUV/TOMS) for Nimbus G, *Opt. Eng.*, *14*, 323-331, 1975.

Heath, D. F., A. J. Krueger, and P. J. Crutzen, Solar proton event: Influence on stratospheric ozone, *Science*, *197*, 886-889, 1977.

Heath, D. F., T. P. Repoff, and R. F. Donnelly, Nimbus-7 SBUV observations of solar UV spectral irradiance variations caused by solar rotation and active-region evolution for the period November 7, 1978-November 1, 1980, *NOAA-TM-ERL-ARL-129*, 78 pp., NOAA Air Resources Laboratory, Rockville, MD, September, 1984.

Heicklen, J., *Atmospheric Chemistry*, 406 pp., Academic Press, New York, 1976.

Heidt, L. E., J. P. Krasnec, R. A. Lueb, W. H. Pollack, B. E. Henry, and P. J. Crutzen, Latitudinal distributions of CO and CH_4 over the Pacific, *J. Geophys. Res.*, *85*, 7329-7336, 1980.

Heikes, B., and A. M. Thompson, Effects of heterogeneous processes on NO_3, HONO, and HNO_3 chemistry in the troposphere, *J. Geophys. Res.*, *10*, 10883-10895, 1983.

Helas, G., and P. J. Warneck, Background NO_x mixing ratios in air masses over the North Atlantic Ocean, *J. Geophys. Res.*, *86*, 7283-7290, 1981.

Held, I. M., Stationary and quasi-stationary eddies in the extratropical troposphere: Theory, in *Large-scale Dynamical Processes in the Atmosphere*, edited by B. J. Hoskins and R. Pearce, pp. 127-168, Academic Press, New York, 1983.

Helten, M., W. Patz, M. Trainer, H. Fark, E. Klein, and D. H. Ehhalt, Measurements of stratospheric HO_2 and NO_2 by matrix isolation and ESR spectroscopy, *J. Atmos. Chem.*, *2*, 191-202, 1984a.

Helten, M., W. Patz, D. H. Ehhalt, and E. P. Roeth, Measurements of nighttime NO_3 and NO_2 in the stratosphere by matrix isolation and ESR spectroscopy, in *Atmospheric Ozone*, edited by C. S. Zerefos and A. Ghazi, pp. 196-200, D. Reidel, Dordrecht, 1984b.

Hendry, D. G., and R. A. Kenley, Chapter 7, in *Atmospheric chemistry of perioxynitrates, nitrogen air pollutants: Chemical and biological implications*, edited by D. Grosjean, Ann Arbor Science, Ann Arbor, MI, 1979.

Hering, W. S. and T. R. Borden: See Borden, T. R. and W. S. Hering.

Herman, J. R., and C. J. McQuillan, Atmospheric chlorine and stratospheric ozone nonlinearities and trend detection, *J. Geophys. Res.*, *90*, 5721-5732, 1985.

Herman, J. R., and J. E. Mentall, O_2 absorption cross sections (187-225 nm) from stratospheric solar flux measurements, *J. Geophys. Res.*, *87*, 8967-8975, 1982a.

Herman, J. R., and J. E. Mentall, The direct and scattered solar flux within the stratosphere, *J. Geophys. Res.*, *87*, 1319-1330, 1982b.

Hess, P. H., and J. R. Holton, The origin of temporal variance in long-lived trace constituents in the summer stratosphere, *J. Atmos. Sci.*, *42*, 1455-1463, 1985.

Hicks, B. B., M. L. Wesely, and J. L. Durham, *Critique of Methods to Measure Dry Deposition*, 83 pp., Environmental Sciences Research Laboratory, Office of Research and Development, U. S. Environmental Protection Agency, Research Triangle Park, NC, 1980.

Hidalgo, H., and P. J. Crutzen, The tropospheric and stratospheric composition perturbed by NO_x emissions of high-altitude aircraft, *J. Geophys. Res.*, *82*, 5833-5866, 1977.

Hide, R., and P. J. Mason, Sloping convection in a rotating fluid, *Advances in Physics*, *24*, 47-100, 1975.

Hill, W. J., P. N. Sheldon, and J. J. Tiede, Analyzing worldwide total ozone for trends, *Geophys. Res. Lett.*, *4*, 21-24, 1977.

Hills, A. J., and C. J. Howard, Rate coefficient temperature dependence and branching ratio for the OH + ClO reaction, *J. Chem. Phys.*, *81*, 4458-4465, 1984.

Hilsenrath, E., and B. M. Schlesinger, Total ozone seasonal and interannual variations derived from the 7 year Nimbus 4 data, *J. Geophys. Res.*, *86*, 12087-12096, 1981.

Hilsenrath, E., T. Seiden, and P. Goodman, An ozone measurement in the mesosphere and stratosphere by means of a rocketsonde, *J. Geophys. Res.*, *71*, 1385-1397, 1969.

Hilsenrath, E., J. Ainsworth, A. Holland, J. Mentall, A. Torres, W. Attmannspacher, A. Bass, W. Evans, W. Komhyr, K. Mauersberger, A. J. Miller, M. Proffitt, D. Robbins, S. Taylor, and E. Weinstock, Results from the balloon ozone intercomparison campaign (BOIC), in *Atmospheric Ozone*, edited by C. S. Zerefos and A. Ghazi, pp. 454-459, D. Reidel, Dordrecht, 1985.

Hilsenrath, E., J. Ainsworth, W. Attmannspacher, A. Bass, W. F. J. Evans, A. Holland, W. Komhyr, K. Mauersberger, J. Mentall, M. Proffitt, D. Robbins, S. Taylor, A. Torres, and E. Weinstock, Results from the Balloon Ozone Intercomparison Campaign (BOIC), to be published, 1986.

Hines, C. O., Dynamical heating of the upper atmosphere, *J. Geophys. Res.*, *70*, 177-183, 1965.

Hinteregger, H. E., Representations of solar EUV fluxes for aeronomical applications, in *The Mesosphere and Thermosphere*, edited by G. Schmidtke and K. S. W. Champion, pp. 39-52, Pergamon Press, Oxford, 1981.

Hirooka, T., and I. Hirota, Normal mode Rossby waves observed in the upper stratosphere. Part II. Second antisymmetric and symmetric modes of zonal wavenumbers 1 and 2, *J. Atmos. Sci.*, *42*, 536-548, 1985.

Hirota, I., Seasonal variation of planetary waves in the stratosphere observed by the Nimbus 5 SCR, *Quart. J. Roy. Meteorol. Soc.*, *102*, 757-770, 1976.

Hirota, I., Equatorial waves in the upper stratosphere and mesosphere in relation to the semi-annual oscillation of the zonal wind, *J. Atmos. Sci.*, *35*, 714-722, 1978.

Hirota, I., Kelvin waves in the equatorial middle atmosphere observed by the Nimbus-5 SCR, *J. Atmos. Sci.*, *36*, 217-222, 1979.

Hirota, I., Observational evidence of the semiannual oscillation in the tropical middle atmosphere-A review, *Pure Appl. Geophys.*, *118*, 217-238, 1980.

Hirota, I., Climatology of gravity waves in the middle atmosphere, *J. Atmos. Terr. Phys.*, *46*, 767-773, 1984.

Hirota, I., and T. Hirooka, Normal mode Rossby waves observed in the upper stratosphere. Part I: First symmetric modes of wavenumbers 1 and 2, *J. Atmos. Sci.*, *41*, 1253-1267, 1984.

Hirota, I., and Y. Sato, Periodic variation of the winter circulation and intermittent vertical propagation of planetary waves, *J. Meteorol. Soc. Japan*, *47*, 390-402, 1969.

Hirota, I., T. Hirooka, and M. Shiotani, Upper stratospheric circulation in the two hemispheres observed by satellites, *Quart. J. Roy. Meteorol. Soc.*, *109*, 443-454, 1983a.

Hirota, I., Y. Maekawa, S. Fukao, K. Fukuyama, M. P. Sulzer, J. L. Fellous, T. Tsudo, and S. Kato, Fifteen-day observation of mesospheric and lower thermospheric motions with the aid of the Arecibo UHF radar, *J. Geophys. Res.*, *88*, 6835-6842, 1983b.

Hitchman, M. H., An observational study of wave-mean flow interaction in the equatorial middle atmosphere, Ph.D. thesis, 360 pp., Dept. of Atmospheric Sciences, University of Washington, Seattle, WA, 1985.

Hitchman, M. H., and C. B. Leovy, Evolution of the zonal mean state in the equatorial middle atmosphere during October, 1978-May, 1979, *J. Atmos. Sci.*, *43*, in press, 1986.

Hocking, W. K., Mesospheric turbulence intensities measured with a HF radar at 35° S - II, *J. Atmos. Terr. Phys.*, *45*, 103-114, 1983.

Hocking, W. K., Turbulence in the region 80-120 km, in *Handbook for MAP*, *Vol. 16*, edited by K. Labitzke, J. J. Barnett, and B. Edwards, pp. 290-304, SCOSTEP Secretariat, Univ. of Illinois, Urbana, 1985.

Hodges, Jr., R. R., Generation of turbulence in the upper atmosphere by internal gravity waves, *J. Atmos. Sci.*, *72*, 3455-3458, 1967.

Hoell, J. M., C. N. Harward, and B. S. Williams, Remote infrared heterodyne radiometer measurements of atmospheric ammonia profiles, *Geophys. Res. Lett.*, *7*, 313-316, 1980.

Hoell, J. M., G. L. Gregory, M. A. Carroll, M. McFarland, B. A. Ridley, D. D. Davis, J. Bradshaw, M. O. Rodgers, A. L. Torres, G. W. Sachse, G. F. Hill, E. P. Condon, R. A. Rasmussen, M. C. Campbell, J. C. Farmer, J. C. Sheppard, C. C. Wang, and L. I. Davis, An intercomparison of carbon monoxide, nitric oxide, and hydroxyl measurement techniques: Overview of results, *J. Geophys. Res.*, *89*, 11819-11825, 1984.

Hoffert, M. I., A. J. Callegari, and C. T. Hsieh, The role of deep sea storage in the secular response to climate forcing, *J. Geophys. Res.*, *85*, 6667-6679, 1980.

Hoffman-Sievert, R., and A. W. Castleman, The reaction of SO_3 with water clusters and the formation of H_2SO_4, *J. Phys. Chem.*, *88*, 3329-3333, 1984.

Hofmann, D. J., and J. M. Rosen, Balloon-borne observations of stratospheric aerosol and condensation nuclei during the year following the Mt. St. Helens eruption, *Geophys. Res. Lett.*, *87*, 11039-11061, 1982.

Hofmann, D. J., and J. M. Rosen, Sulfuric acid droplet formation and growth in the stratosphere after the 1982 eruption of El Chichon, *Science*, *222*, 325-327, 1983.

Holland, A. J., T. D. Keenan, and G. D. Crane, Observations of a phenomenal temperature perturbation in tropical cyclone Kerry (1979), *Mon. Weather Rev.*, *112*, 1074-1082, 1984.

Holstein, K. J., E. H. Fink, J. Wildt, R. Winter, and F. Zabel, Mechanisms of $HO_2(A2A')$ excitation in various chemical systems, *J. Phys. Chem.*, *87*, 3943-3948, 1983.

Holton, J. R., Waves in the equatorial stratosphere generated by tropospheric heat sources, *J. Atmos. Sci.*, *29*, 368-375, 1972.

Holton, J. R., A note on the frequency distribution of atmospheric Kelvin waves, *J. Atmos. Sci.*, *30*, 499-501, 1973.

Holton, J. R., *The Dynamical Meteorology of the Stratosphere and Mesosphere*, 216 pp., American Meteorological Society, Boston, MA, 1975.

Holton, J. R., Wave propagation and transport in the middle atmosphere, *Phil. Tran. Roy. Soc. London*, *A296*, 73-85, 1980.

Holton, J. R., An advective model for two-dimensional transport of stratospheric trace species, *J. Geophys. Res.*, *86*, 11989-11994, 1981.

Holton, J. R., The role of gravity wave induced drag and diffusion in the momentum budget of the mesosphere, *J. Atmos. Sci.*, *39*, 791-799, 1982.

Holton, J. R., The influence of gravity wave breaking in the circulation of the middle atmosphere, *J. Atmos. Sci.*, *40*, 2497-2507, 1983.

Holton, J. R., The generation of mesospheric planetary waves by zonally asymmetric gravity wave breaking, *J. Atmos. Sci.*, *41*, 3427-3430, 1984a.

Holton, J. R., Troposphere-stratosphere exchange of trace constituents: The water vapor puzzle, in *Dynamics of the Middle Atmosphere*, edited by J. R. Holton and T. Matsuno, pp. 369-385, Terrapub, Tokyo, 1984b.

Holton, J. R., A dynamically based transport parameterization for one-dimensional photochemical models, in *Handbook for MAP, Vol. 18*, edited by S. Kato, Chap. 4, SCOSTEP Secretariat, Univ. of Illinois, Urbana, 1985.

Holton, J. R., A dynamically based transport parameterization for one-dimensional photochemical models of the stratosphere, *J. Geophys. Res.*, in press, 1986.

Holton, J. R., and R. S. Lindzen, An updated theory of the quasi-biennial oscillation of the tropical stratosphere, *J. Atmos. Sci.*, *29*, 1076-1080, 1972.

Holton, J. R., and H. C. Tan, The influence of the equatorial quasi-biennial oscillation on the global circulation at 50 mb, *J. Atmos. Sci.*, *37*, 2200-2208, 1980.

Holton, J. R., and H. C. Tan, The quasi-biennial oscillation in the Northern Hemisphere lower stratosphere, *J. Meteorol. Soc. Japan*, *60*, 140-148, 1982.

Holton, J. R., and W. M. Wehrbein, The role of forced planetary waves in the annual cycle of zonal mean circulation of the middle atmosphere, *J. Atmos. Sci.*, *37*, 1968-1983, 1980a.

Holton, J. R., and W. M. Wehrbein, A numerical model of the zonal mean circulation of the middle atmosphere, *Pure Appl. Geophys.*, *118*, 284-306, 1980b.

Holton, J. R., and X. Zhu, A further study of gravity wave induced drag and diffusion in the mesosphere, *J. Atmos. Sci.*, *41*, 2653-2662, 1984.

Hood, L. L., The temporal behavior of upper stratospheric ozone at low latitudes: Evidence from Nimbus 4 BUV data for short-term responses to solar ultraviolet variability, *J. Geophys. Res.*, *89*, 9557-9568, 1984.

Hopkins, R. H., Evidence of polar-tropical coupling in upper stratospheric zonal wind anomalies, *J. Atmos. Sci.*, *32*, 712-719, 1975.

REFERENCES

Horvath, J. J., J. E. Frederick, N. Orsini, and A. R. Douglass, Nitric oxide in the upper stratosphere: Measurements and geophysical interpretation, *J. Geophys. Res.*, *88*, 10809-10817, 1983.

Hoskins, B. J., Non-Boussinesq effects and further development in a model of upper troposheric frontogenesis, *Quart. J. Roy. Meteorol. Soc.*, *98*, 532-541, 1972.

Hoskins, B. J., The role of potential vorticity in symmetric stability and instability, *Quart. J. Roy. Meteorol. Soc.*, *100*, 480-482, 1974.

Hoskins, B. J., The geostrophic momentum approximation and the semi-geostrophic equations, *J. Atmos. Sci.*, *32*, 233-242, 1975.

Hoskins, B. J., Modelling of the transient eddies and their feedback on the mean flow, in *Large-scale Dynamical Processes in the Atmosphere*, edited by B. J. Hoskins and R. Pearce, pp. 169-199, Academic Press, New York, 1983.

Hoskins, B. J., and I. Draghici, The forcing of ageostrophic motion according to the semi-geostrophic equations and in an isentropic coordinate model, *J. Atmos. Sci.*, *34*, 1859-1867, 1977.

Hoskins, B. J., and W. A. Heckley, Baroclinic waves and frontogenesis in a non-uniform potential vorticity semi-geostrophic model, *J. Atmos. Sci.*, *39*, 1999-2016, 1982.

Hoskins, B. J., I. Draghici, and H. C. Davies, A new look at the omega equation, *Quart. J. Roy. Meteorol. Soc.*, *104*, 31-38, 1978.

Hoskins, B. J., M. E. McIntyre, and A. W. Robertson, On the use and significance of isentropic potential vorticity maps, *Quart. J. Roy. Meteorol. Soc.*, *111*, 877-946, 1985.

Houghton, J. T., *The Physics of Atmospheres*, 203 pp., Cambridge University Press, Cambridge, 1977.

Houghton, J. T., The stratosphere and mesosphere, *Quart. J. Roy. Meteorol. Soc.*, *104*, 1-30, 1978.

Houghton, J. T., F. W. Taylor, and C. D. Rodgers, Remote sounding of atmospheres, *Cambridge Planetary Science Series No. 5*, 343 pp., Cambridge University Press, Cambridge, 1984.

Houze, Jr., R. A., Cloud clusters and long-scale vertical motions in the tropics, *J. Meteorol. Soc. Japan*, *60*, 396-409, 1982.

Houze, R. A., and A. K. Betts, Convection in GATE, *Rev. Geophys. Space Phys.*, *19*, 541-576, 1981.

Houze, R. A., S. G. Geotis, F. D. Marks, and A. K. West, Winter monsoon convection in the vicinity of North Borneo. Part I: Structure and time evolution of the clouds and precipitation, *Mon. Weather Rev.*, *109*, 1595-1614, 1981.

Hov, O., S. A. Penkett, I. S. A. Isaksen, and A. Semb, Organic gases in the Norwegian Arctic, *Geophys. Res. Lett.*, *11*, 425-428, 1984.

Hoyt, S. D., The air-sea exchange of carbonyl sulfide (OCS) and halocarbons, Ph.D. thesis, Oregon Graduate Center, Beaverton, Oregon, 1982.

Hsu, C. P. F., Air parcel motions during a numerically simulated sudden stratospheric warming, *J. Atmos. Sci.*, *37*, 2768-2792, 1980.

Hubler, G., D. Perner, U. Platt, A. Tonnissen, and D. H. Ehhalt, Ground-level OH radical concentrations: New measurements by optical absorption, *J. Geophys. Res.*, *89*, 1309-1319, 1984.

Huddleston, R. K., and E. Weitz, A laser-induced fluorescence study of energy transfer between the symmetric stretching and bending modes of CO_2, *Chem. Phys. Lett.*, *83*, 174-179, 1981.

Hudson, R. D., Critical review of ultraviolet photoabsorption cross sections for molecules of astrophysical and aeronomic interest, *Rev. Geophys. Space Phys.*, *9*, 305-406, 1971.

Hudson, R. D. (Ed.), *The Stratosphere 1981. Theory and Measurements, WMO Global Ozone Research and Monitoring Project Report No. 11*, 516 pp., WMO, Geneva, 1982.

Hudson, R. D., and S. H. Mahle, Photodissociation rates of molecular oxygen in the mesosphere and lower thermosphere, *J. Geophys. Res.*, *77*, 2902-2914, 1972.

Hudson, R. D., and E. I. Reed (Eds.), *The Stratosphere: Present and Future, NASA Reference Publication 1049*, 432 pp., NASA Goddard Space Flight Center, Greenbelt, MD, 1979.

Huebert, B. J., The dry deposition of nitric acid to grass, *J. Geophys. Res.*, *90*, 2085-2090, 1985.

Huebert, B. J., and A. L. Lazrus, Tropospheric gas-phase and particulate nitrate measurements, *J. Geophys. Res.*, *85*, 7322-7328, 1980.

Hungate, R. E., *The Rumen and Its Microbes*, 533 pp., Academic Press, New York, 1960.

Hunt, B. G., Experiments with a stratospheric general circulation model. III. Large-scale diffusion of ozone including photochemistry. *Mon. Weather Rev.*, *97*, 287-306, 1969.

Hunt, B. G., The maintenance of the zonal mean state of the upper atmosphere as represented in a three-dimensional general circulation model extending to 100 km, *J. Atmos. Sci.*, *38*, 2172-2186, 1981.

Hunt, B. G., The impact of gravity wave drag and diurnal variability on the general circulation of the middle atmosphere, *J. Atmos. Sci.*, in press, 1985.

Hunt, B. G., and S. Manabe, Experiments with stratospheric general circulation model, II. Large-scale diffusion of tracers in the stratosphere, *Mon. Weather Rev.*, *96*, 503-539, 1968.

Hunten, D., The philosophy of one-dimensional modeling, in *Proceedings Fourth Conference Climatic Impact Assessment Program, DOT-TSC-OST-75-38*, edited by T. M. Hard and A. J. Broderick, pp. 147-155, Transportation Systems Center, Cambridge, MA, 1975.

Huntress, W. T. Jr., Upper Atmosphere Research Satellite Program—to study the chemistry, energetics, and dynamics, Final Report, *JPL Publ. 78-54*, 62 pp., Jet Propulsion Lab., Pasadena, CA, 1978.

Husson, N., A. Chedin, N. A. Scott, I. Cohen-Hallaleh, and A. Berroir, La Banque de donnees GEISA. Mise a jour no. 3, Laboratoire de Meteorologie Dynamique du C.N.R.S., *Internal Note 116*, Ecole Polytechnique, 91128 Palaiseau Cedex, France, July 1982.

Husson, N., A. Chedin, N. A. Scott, D. Bailly, G. Graner, N. Lacome, A. Levy, C. Rossetti, G. Tarrago, C. Camy-Peyret, J. M. Flaud, A. Bauer, J. M. Colmont, N. Monnanteuil, J. C. Hilico, G. Pierre, M. Loete, J. P. Champion, L. S. Rothman, L. R. Brown, G. Orton, P. Varanasi, C. P. Rinsland, M. A. H. Smith, and A. Goldman, The GEISA spectroscopic line parameters data bank in 1984, *Annales Geophysicae*, Fasc. 2, Series A, 1986.

Hutchinson, G. E., and A. R. Mosier, Nitrous oxide emissions from an irrigated cornfield, *Science*, *205*, 1125-1127, 1976.

Hyson, P., Stratospheric water vapor over Australia, *Quart. J. Roy. Meteorol. Soc.*, *109*, 285-294, 1983.

Idso, S. B., The climatological significance of a doubling of earth's atmospheric carbon dioxide concentration, *Science*, *207*, 1462-1463, 1980.

Iman, R. L., and M. J. Shortencarier, A Fortran 77 program and user's guide for the generation of Latin hypercube and random samples for use with computer models, *SAND 83-2365*, Sandia National Laboratories, Albuquerque, NM, 1984.

Iman, R. L., J. C. Helton, and J. E. Campbell, An approach to sensitivity analysis of computer models: Part I-Introduction, Input variable selection and preliminary variable assessment, *J. Quality Tech.*, *13*, 174-183, 1981.

Imbrie, J., and K. P. Imbrie, *Ice Ages, Solving the Mystery*, 224 pp., Enslow Pub., Short Hills, NJ, 1979.

Inn, E. C. Y., and Y. Tanaka, Absorption coefficient of ozone in the ultraviolet and visible regions, *J. Opt. Soc. Am.*, *43*, 870-873, 1953.

Inst. fur Met. des Frei Universiteit Berlin, Meteorologische Abhandlungen, Tagliche Hohenkarten der 30-Mbar-flache sowie monatliche mittelkarten fur das jahr 1980, Verlag Von Dietuch Reiner, Berlin, 1980.

Isaksen, I. S. A., Tropospheric ozone budget and possible man made effects, in *Quadrennial International Ozone Symposium, Vol. II*, edited by J. London, pp. 845-852, IAMAP, NCAR, Boulder, CO, 1981.

Isaksen, I. S. A., and O. Hov, Calculations of trends in the tropospheric concentration of O_3, OH, CO, CH_4 and NO_x, in press, 1985.

REFERENCES

Isaksen, I. S. A., and F. Stordal, Ozone perturbations by enhanced levels of CFCs, N_2O and CH_4: A two-dimensional diabatic circulation study including uncertainty estimates, *J. Geophys. Res.*, in press, 1985.

Ishiwata, T., I. Fujiwara, Y. Naruge, K. Obi, and I. Tanaka, Study of NO_3 by laser induced fluorescence, *J. Phys. Chem.*, *87*, 1349-1352, 1983.

Itoh, H., The response of equatorial waves to thermal forcing, *J. Meteorol. Soc. Japan*, *55*, 222-239, 1977.

Jackman, C. H., and P. D. Guthrie, Sensitivity of N_2O, $CFCl_3$ and CF_2Cl_2 two-dimensional distributions to O_2 absorption cross sections, *J. Geophys. Res.*, *90*, 3919-3923, 1985.

Jackman, C. H., and R. D. McPeters, The response of ozone to solar proton events during solar cycle 21: A theoretical interpretation, *J. Geophys. Res.*, *42*, 90, 7955-7966, 1985.

Jackman, C. H., J. E. Frederick, and R. S. Stolarski, Production of odd nitrogen in the stratosphere and mesosphere: An intercomparison of source strengths, *J. Geophys. Res.*, *85*, 7495-7505, 1980.

Jackman, C. H., J. A. Kaye, and P. D. Guthrie, LIMS HNO_3 data above 5 mbar: Corrections based on simultaneous observations of other species, *J. Geophys. Res.*, 90, 7923-7930, 1985.

Jackman, C. H., R. S. Stolarski, and J. A. Kaye, Two-dimensional monthly average ozone balance from Limb Infrared Monitor of the stratosphere and stratospheric and mesospheric sounder data, *J. Geophys. Res.*, *91*, 1103-1116, 1986.

Jesson, J. P., Release of industrial halocarbons and tropospheric budget, in *Proceedings of the NATO Advanced Study Institute on Atmospheric Ozone: Its Variation and Human Influences*, *Rep. FAA-EE-80-20*, edited by A. C. Aikin, pp. 373-396, DOT, FAA, Washington, DC, 1980.

Johansson, C., Field measurements of emission of nitric oxide from fertilized and unfertilized forest soils in Sweden, *J. Atmos. Chem.*, *1*, 429-442, 1984.

Johansson, C., and L. Granat, Emission of nitric oxide from arable land, *Tellus*, *36B*, 25-37, 1984.

Johnson, D. R., Systematic stratospheric-tropospheric exchange through quasi-horizontal transport within active baroclinic waves, in *The Long-Range Transport of Pollutants and its Relation to General Circulation including Stratospheric/Tropospheric Exchange Processes—Conference Proceedings*, *WMO No. 538*, pp. 401-408, WMO, Geneva, 1979.

Johnson, D. R., A generalized transport equation for use with meteorological coordinate systems, *Mon. Weather Rev.*, *108*, 733-745, 1980.

Johnson, D. R., On the forcing and maintenance of the isentropic zonally averaged circumpolar vortex, paper presented at *IAMAP-WMO Symposium on Maintenance of the Quasi-Stationary Components of the Flow in the Atmosphere and in Atmospheric Models*, pp 19-22, WMO, Geneva, Paris, August 30-September 2, 1983.

Johnson, D. R., On the global distribution of heat sources and sinks and their relation to mass and energy transport, paper presented at WMO Proceedings of the FGGE Tropics Seminar, Tallahassee, Florida, October 8-12, 1984a.

Johnson, D. R., The global circulation during the FGGE year: On the balance of mass, energy, and angular momentum within isentropic and isobaric coordinates as revealed by different FGGE data sets, paper presented at *WMO Proceedings of the Global Weather Experiment Scientific Seminar*, Helsinki, Finland, August 29-31, 1984b.

Johnson, D. R., and W. K. Downey, Azimuthally averaged transport and budget equations for storms: Quasi-Lagrangian diagnostics 1, *Mon. Weather Rev.*, *103*, 967-979, 1975.

Johnson, D. R., and R. D. Townsend, Diagnostics of the heat sources and sinks of the Asiatic monsoon and the thermally-forced planetary scale response, M. S. thesis, *AD-A119755*, 72 pp., Wisconsin Univ., Madison, WI, 1981.

Johnson, D. R., R. D. Townsend, and M-Y Wei, The thermally forced responses of the planetary scale circulation to the global distribution of heat sources and sinks, *Tellus*, *37A*, 106-125, 1985.

Johnson, F. S., J. D. Purcell, R. Tourey, and K. Watanabe, Direct measurements of the vertical distribution of atmospheric ozone to 70 kilometers altitude, *J. Geophys. Res.*, *57*, 157-176, 1952.

Johnson, J. E., The role of the oceans in the atmospheric cycle of carbonyl sulfide, Ph.D. thesis, University of Washington, Seattle, WA, 1985.

Johnson, K. W., and M. E. Gelman, Trends in the upper stratospheric temperatures as observed by rocketsondes (1965-1983), in *Handbook for MAP*, *Vol. 18*, edited by S. Kato, pp. 24-27, SCOSTEP Secretariat, Univ. of Illinois, Urbana, 1985.

Johnson, R. H., and D. C. Kriete, Thermodynamic circulation characteristics of winter monsoon tropical mesoscale convection, *Mon. Weather Rev.*, *110*, 1898-1911, 1982.

Johnston, D. A., Volcanic contribution of chlorine to the stratosphere: More significant to ozone than previously estimated?, *Science*, *209*, 491-493, 1980.

Johnston, H. S., Reduction of stratospheric ozone by nitrogen oxide catalysts from supersonic transport exhaust, *Science*, *173*, 517-522, 1971.

Johnston, H. S., Human effects on the global atmosphere, *Ann. Rev. Phys. Chem.*, *35*, 481-505, 1984.

Johnston, H. S., and J. Podolske, Interpretations of stratospheric photochemistry, *Rev. Geophys. Space Phys.*, *16*, 491-519, 1978.

Johnston, H. S., D. Kattenhorn, and G. Whitten, Use of excess carbon 14 data to calibrate models of stratospheric ozone depletion by supersonic transports, *J. Geophys. Res.*, *78*, 368-380, 1976.

Johnston, H. S., M. Paige, and F. Yao, Oxygen absorption cross sections in the Herzberg continuum and between 206 and 326 K, *J. Geophys. Res.*, *89*, 11661-11665, 1984.

Johnston, H. S., C. A. Cantrell, and J. G. Calvert, Unimolecular decomposition of NO_3 to NO and O_2, *J. Geophys. Res.*, in press, 1985.

Jones, B. M. R., J. P. Burrows, R. A. Cox, and S. A. Penkett, OCS formation in the reaction of OH with CS_2, *Chem. Phys. Lett.*, *88*, 372-376, 1982.

Jones, B. M. R., R. A. Cox, and S. A. Penkett, Atmospheric chemistry of carbon disulfide, *J. Atmos. Chem.*, *1*, 65-86, 1983.

Jones, R. L., Satellite measurements of atmospheric composition: Three years' observations of CH_4 and N_2O, *Adv. Space Res.*, *4*, 121-130, 1984.

Jones, R. L., and J. A. Pyle, Observations of CH_4 and N_2O by the Nimbus 7 SAMS: A comparison with in-situ data and two-dimensional numerical model calculations, *J. Geophys. Res.*, *89*, 5263-5279, 1984.

Jones, R. L., J. A. Pyle, J. E. Harries, A. M. Zavody, J. M. Russell III, and J. C. Gille, The water vapour budget of the stratosphere studied using LIMS and SAMS satellite data, *Quart. J. Roy. Meteorol. Soc.*, in press, 1985.

Joseph, J. H., The sensitivity of a numerical model of the global atmosphere to the presence of desert aerosols, Dept. of Geophysics and Planetary Sciences, Tel-Aviv Univ., Ramat Aviv, Israel, 6997, 1983.

JPL: See DeMore, et al. and NASA-JPL listings.

Junge, C., W. Seiler, and P. Warneck, The atmospheric ^{12}CO and ^{14}CO budget, *J. Geophys. Res.*, *76*, 2866-2879, 1971.

Junge, C. E., Global ozone budget and exchange between stratosphere and troposphere, *Tellus*, *14*, 363-377, 1962.

Junge, C. E., *Air chemistry and radioactivity*, 380 pp.,Academic Press, New York, 1963.

Just, T., and J. Troe, Theory of two-channel unimolecular reactions. 1. General formulation, *J. Phys. Chem.*, *84*, 3068-3072, 1980.

Kagann, R. H., J. W. Elkins, and R. L. Sams, Absolute band strengths of halocarbons F-11 and F-12 in the 8 to 16μm region, *J. Geophys. Res.*, *88*, 1427-1432, 1983.

Kanzawa, H., The behavior of mean zonal wind and planetary-scale disturbances in the troposphere and stratosphere during the 1973 sudden warming, *J. Meteorol. Soc. Japan*, *58*, 329-356, 1980.

Kanzawa, H., Eliassen-Palm flux diagnostics and the effect of the mean zonal wind on planetary wave propagation for an observed sudden stratospheric warming, *J. Meteorol. Soc. Japan*, *60*, 1063-1073, 1982.

Kanzawa, H., Four observed sudden warmings diagnosed by the Eliassen-Palm flux and refractive index, in *Dynamics of the Middle Atmosphere*, edited by J. R. Holton and T. Matsuno, pp. 307-331, Terrapub, Tokyo, 1984.

Karoly, D. J., and B. J. Hoskins, Three dimensional propagation of planetary waves, *J. Meteorol. Soc. Japan*, *60*, 109-123, 1982.

Katz, M., *Methods of Air Sampling and Analysis*, edited by M. Katz, pp. 549-555, American Public Health Assoc., Washington, DC, 1977.

Kawahira, K., A quasi-one-dimensional model of the ozone transport by planetary waves in the winter stratosphere, *J. Meteorol. Soc. Japan*, *60*, 831-849, 1982.

Keating, G. M., The response of ozone to solar activity variations. A review, *Solar Physics*, *74*, 321-347, 1981.

Keating, G. M., and D. F. Young, Interim reference ozone models for the middle atmosphere, in *Handbook for MAP, Vol. 16*, edited by K. Labitzke, J. J. Barnett, and B. Edwards, pp. 205-229, SCOSTEP Secretariat, Univ. of Illinois, Urbana, 1985.

Keating, G. M., G. P. Brasseur, J. Y. Nicholson III, and A. De Rudder, Detection of the response of ozone in the middle atmosphere to short-term solar ultraviolet variations, *Geophys. Res. Lett.*, *12*, 449-452, 1985.

Keeling, C. D., The Global Carbon Cycle: What we know and could know from atmospheric, biospheric, and oceanic observations, in *Proceedings of the CO_2 Research Conference: Carbon Dioxide, Science and Consensus, DOE CONF-820970*, pp. II.3-II.62, U.S. Dept. of Energy, Washington, DC, 1983.

Keeling, C. D., A. F. Carter, and W. G. Mook, Seasonal, latitudinal and secular variations in the abundance and isotopic ratios of atmospheric CO_2, *J. Geophys. Res.*, *89*, 4615-4628, 1984.

Keenan, T. D., and J. I. Templeton, A comparison of tropical cyclone, hurricane and typhoon mass and moisture structure, *Mon. Weather Rev.*, *111*, 320-327, 1983.

Keller, M., T. J. Goreau, S. C. Wofsy, W. A. Kaplan, and M. B. McElroy, Production of nitrous oxide and consumption of methane by forest soils, *Geophys. Res. Lett.*, *10*, 1156-1159, 1983.

Keller, M., W. A. Kaplan, and S. C. Wofsy, Emissions of N_2O, CH_4 and CO from tropical forest soils, in press, 1985.

Kelly, P. M., P. D. Jones, T. M. L. Wigley, R. S. Bradley, H. F. Diaz, and C. M. Goodess, The extended Northern Hemisphere surface air temperature record: 1851-1984, *Proceedings, AMS Conference on Climate Variations*, Boston, MA, 190 pp., 1984.

Kendall, D. J. W., and H. L. Buijs, Stratospheric NO_2 and upper limits of CH_3Cl and C_2H_6 from measurements at 3.4 μm, *Nature*, *303*, 221-222, 1983.

Kendall, D. J. W., and T. A. Clark, Balloon-borne far infrared atmospheric emission studies, *Infrared Phys.*, *18*, 803-813, 1978.

Kendall, D. J. W., and T. A. Clark, The pure rotational atmospheric lines of hydroxyl, *J. Quant. Spectrosc. Radiat. Transfer*, *21*, 511-526, 1979.

Kendall, D. J. W., and T. A. Clark, Detection of minor constituents of the stratosphere by far infrared emission spectroscopy, *Int. J. Infrared mm Waves*, *3*, 783-808, 1981.

Kennedy, P. J., and M. A. Shapiro, The energy budget in a clear air turbulence zone as observed by aircraft, *Mon. Weather Rev.*, *111*, 650-993, 1975.

Kennedy, P. J., and M. A. Shapiro, Further encounters with clear air turbulence in research aircraft, *J. Atmos. Sci.*, *37*, 986-993, 1980.

Kerr, J. B., and C. T. McElroy, Measurement of stratospheric nitrogen dioxide from the AES stratospheric balloon program, *Atmosphere*, *14*, 166-171, 1976.

Kerr, J. B., C. L. Mateer, C. T. McElroy, and D. I. Wardle, Intercomparison of the Dobson and grating ozone spectrophotometers, in *Proc. Joint Symp. on Atm. Ozone, Vol. 1*, pp. 109-120, Dresden, GDR, 1976.

Kerr, J. B., C. T. McElroy, and W. F. J. Evans, Mid-latitude summertime measurements of stratospheric NO_2, *Can. J. Phys., 60*, 196-200, 1982.

Keyser, L. F., High pressure flow kinetics. A study of the OH + HCl reaction from 2 to 100 torr, *J. Phys. Chem., 88*, 4759-4759, 1984.

Khalil, M. A. K., and R. A. Rasmussen, Increase of $CHClF_2$ in the earth's atmosphere, *Nature, 292*, 823-824, 1981.

Khalil, M. A. K., and R. A. Rasmussen, Secular trends of methane, *Chemosphere, 12*, 877-883, 1982.

Khalil, M. A. K., and R. A. Rasmussen, Gaseous tracers of Arctic haze, *Environ. Sci. and Tech., 17*, 157-164, 1983a.

Khalil, M. A. K., and R. A. Rasmussen, Increase and seasonal cycles of nitrous oxide in the Earth's atmosphere, *Tellus, 35B*, 161-169, 1983b.

Khalil, M. A. K., and R. A. Rasmussen, Sources, sinks and seasonal cycles of atmospheric methane, *J. Geophys. Res., 88*, 5131-5144, 1983c.

Khalil, M. A. K., and R. A. Rasmussen, Termites and methane, *Nature, 302*, 355, 1983d.

Khalil, M. A. K., and R. A. Rasmussen, The atmospheric lifetime of methylchloroform (CH_3CCl_3), *Tellus, 36B*, 317-332, 1984a.

Khalil, M. A. K., and R. A. Rasmussen, Global increase of carbon monoxide, in *Transactions of the APCA Specialty Conference on Environmental Impacts of Natural Emissions*, edited by V. P. Aneja, 1984b.

Khalil, M. A. K., and R. A. Rasmussen, Carbon monoxide in the Earth's atmosphere: Increasing trend, *Science, 224*, 54-56, 1984c.

Khalil, M. A. K., and R. A. Rasmussen, Causes of increasing atmospheric methane: Depletion of hydroxyl radicals and the rise of emissions, *Atmos. Environ., 19*, 397-407, 1985a.

Khalil, M. A. K., and R. A. Rasmussen, Global sources, lifetimes and mass balances of carbonyl sulfide (OCS) and carbon disulfide (CS_2) in the earth's atmosphere, *Atmos. Environ., 18*, 1805-1813, 1985b.

Khalil, M. A. K., and R. A. Rasmussen, The trend of bromodifluoromethane ($CBrClF_2$) and the concentration of other bromine containing gases at the South Pole, *Antarctic Journal of the U.S.*, in press, 1985c.

Khalil, M. A. K., and R. A. Rasmussen, Trichlorotrifluoroethane (F-113) trends at Pt. Barrow, Alaska, in *Geophysical Monitoring for Climate Change, No. 13, Summary Report 1984*, U.S. Department of Commerce, ERL/NOAA, Boulder, CO, in press, 1985d.

Khalil, M. A. K., and R. A. Rasmussen, Atmospheric carbon tetrafluoride (CF_4): Sources and trends, *Geophys. Res. Lett., 12*, 671-672, 1985e.

Khalil, M. A. K., and R. A. Rasmussen, Interannual variability of atmospheric methane, *Science*, in press, 1985f.

Khalil, M. A. K., R. A. Rasmussen, and S. D. Hoyt, Atmospheric chloroform ($CHCl_3$): Ocean-air exchange and global mass balance, *Tellus, 35B*, 266-274, 1983.

Kiang, C. S., D. Stauffer, V. J. Mohnen, J. Bricard, and D. Vigla, Heteromolecular nucleation theory applied to gas-to-particle conversion, *Atmos. Environ., 7*, 1279-1283, 1973.

Kida, H., A numerical investigation of the atmospheric general circulation and stratospheric-tropospheric mass exchange. I. Long-term integration of a simplified general circulation model. II. Lagrangian motion of the atmosphere, *J. Meteorol. Soc. Japan, 55*, 52-88, 1977.

Kida, H., General circulation of air parcels and transport characteristics from a hemispheric GCM, Part 1. A determination of advective mass flow in the lower stratosphere, *J. Meteorol. Soc. Japan, 61*, 171-188, 1983a.

Kida, H., General circulation of air parcels and transport characteristics derived from a hemispheric GCM. Part 2. Very long-term motions of air parcels in the troposphere and stratosphere, *J. Meteorol. Soc. Japan*, *61*, 510-523, 1983b.

Kida, H., A numerical experiment on the general circulation of the middle atmosphere with a three-dimensional model explicitly representing internal gravity waves and their breaking, *Pure Appl. Geophys.*, *122*, 731-746, 1985.

Kiehl, J. T., The effect of aerosols on radiative damping rates in the stratosphere, paper presented at *Proceedings of the International Radiation Symposium*, Perugia, Italy, Aug. 21-26, 1984.

Kiehl, J. T., The results cited under this citation refer to calculations performed by J. T. Kiehl employing the narrow band model described in Ramaswamy, V. and J. T. Kiehl, Sensitivities of the radiative forcing due to large loadings of smoke and dust aerosols, *J. Geophys. Res.*, *90*, 5597-5613, 1985.

Kiehl, J. T., and V. Ramanathan, CO_2 radiative parameterization used in climate models: Comparison with narrow band models and with laboratory data, *J. Geophys. Res.*, *88*, 5191-5202, 1983.

Kiehl, J. T., and S. Solomon, On the radiative balance of the stratosphere, *J. Atmos. Sci.*, *43*, in press, 1986.

Kircher, C., and S. P. Sander, Kinetics and mechanism of HO_2 and DO_2 disproportionations, *J. Phys. Chem.*, *88*, 2082-2091, 1984.

Kleinschmidt, E., Dynamic meteorology, in *Handbuch der Physik*, edited by A. Eliassen and E. Kleinschmidt, pp. 1-154, 1957.

Kley, D., Ly(α) absorption cross section of H_2O and O_2, *J. Atmos. Chem.*, *2*, 203-210, 1984.

Kley, D., and E. J. Stone, A measurement of water vapor in the stratosphere by photodissociation with Ly (α) (1216Å) light, *Rev. Sci. Instrum.*, *49*, 691-697, 1978.

Kley, D., E. J. Stone, W. R. Henderson, J. W. Drummond, W. Harrop, A. L. Schmeltekopf, and T. L. Thompson, *In situ* measurements of the mixing ratio of water vapor in the stratosphere, *J. Atmos. Sci.*, *36*, 2513-2534, 1979.

Kley, D., J. W. Drummond, and A. L. Schmeltekopf, On the structure and microstructure of stratospheric water vapor, in *Atmospheric Water Vapor* edited by A. Deepak, T. D. Wilkinson, and L. H. Ruhke. pp. 315-327, Academic Press, New York, 1980.

Kley, D., J. W. Drummond, M. McFarland, and S. C. Liu, Tropospheric profiles of NO_x, *J. Geophys. Res.*, *86*, 3153-3161, 1981.

Kley, D., A. L. Schmeltekopf, K. Kelley, R. H. Winkler, T. L. Thompson, and M. McFarland, Transport of water vapor through the tropical tropopause, *Geophys. Res. Lett.*, *9*, 617-620, 1982.

Kley, D., A. L. Schmeltekopf, K. Kelly, R. H. Winkler, T. L. Thompson, and M. McFarland, The U2 Lyman-alpha hygrometer results from the 1980 Panama experiment, in *The 1980 Stratospheric-Tropospheric Exchange Experiment*, *NASA Tech Memo 84297*, edited by A. Margozzi, NASA Ames Research Center, Moffett Field, CA, 425 pp., 1983.

Knapska, D., U. Schmidt, C. Jebsen, G. Kulessa, J. Rudolph and S. A. Penkett, Vertical profiles of chlorinated source gases in the mid-latitude stratosphere, in *Atmospheric Ozone*, edited by C. S. Zerefos and A. Ghazi, pp. 117-121, D. Reidel, Dordrecht, 1985a.

Knapska, D., U. Schmidt, C. Jebsen, F. J. Johnen, A. Khedim, and G. Kulessa, A laboratory test of cryogenic sampling of long lived trace gases under simulated stratospheric conditions, in *Atmospheric Ozone*, edited by C. S. Zerefos and A. Ghazi, pp. 122-128, D. Reidel, Dordrecht, 1985b.

Knight, W., D. R. Hastie, and B. A. Ridley, Measurements of nitric oxide during a stratospheric warming, *Geophys. Res. Lett.*, *9*, 489-492, 1982.

Knittel, J., Ein Beitrag zur Klimatologi der Stratosphaere der Suedhalbkugel, *Meteor. Abh. der F.U., Berlin*, A2, Nr.1, 1976.

Knollenberg, R. G., A. J. Dasher, and D. Huffman, Measurements of the aerosol and ice crystal population in tropical stratospheric cumulonimbus anvils, *Geophys. Res. Lett.*, *9*, 613-616, 1982.

Knop, G., and F. Arnold, Nitric acid vapor measurements in the troposphere and lower stratosphere by chemical ionization mass spectrometry, *Geophys. Res. Lett.*, in press, 1985.

Ko, M. K. W., and N. D. Sze, A 2-D model calculation of atmospheric lifetimes for N_2O, CFC-11 and CFC-12, *Nature*, *297*, 317-319, 1982.

Ko, M. K. W., and N. D. Sze, Effect of recent data revisions on stratospheric modeling, *Geophys. Res. Lett.*, *10*, 341-344, 1983.

Ko, M. K. W., and N. D. Sze, Diurnal variation of ClO: Implications for the stratospheric chemistries of $ClONO_2$, HOCl, and HCl, *J. Geophys. Res.*, *89*, 11619-11632, 1984.

Ko, M. K. W., N. D. Sze, M. Livshits, M. B. McElroy, and J. A. Pyle, The seasonal and latitudinal behavior of trace gases and O_3 as simulated by a two-dimensional model of the atmosphere, *J. Atmos. Sci.*, *41*, 2381-2408, 1984.

Ko, M. K. W., K. K. Tung, D. K. Weinstein, and N. D. Sze, A zonal-mean model of stratospheric tracer transport in isentropic coordinates: Numerical simulations for nitrous oxide and nitric acid, *J. Geophys. Res.*, *90*, 2313-2329, 1985.

Kobayashi, J., and Y. Toyama, On various methods of measuring the vertical distribution of atmospheric ozone 2, *Papers in Meteor. and Geoph.*, *17*, 97-112, 1966.

Kobayashi, J., M. Kyozuka, and H. Muamatsu, On various methods of measuring the vertical distribution of atmospheric ozone 1, *Papers in Meteor. and Geoph.*, *17*, 76-96, 1966.

Kohno, J., Stratospheric ozone transport due to transient large-amplitude planetary waves, *J. Meteorol. Soc. Japan*, *62*, 413-439, 1984.

Kohri, W. J., LRIR observations of the structure and propagation of the stationary planetary waves in the Northern Hemisphere during December 1975, Ph.D. thesis, *Cooperative Thesis No. 63*, Drexel Univ. and National Center for Atmospheric Research, Boulder, CO, 1981.

Komhyr, W. D., A carbon-iodine sensor for atmospheric soundings, paper presented at *Proc. Ozone Symp.*, Albuquerque, NM, pp. 26-30, 1965.

Komhyr, W. D., Electrochemical concentration cells for gas analysis, *Ann. Geoph.*, *25*, 203-210, 1969.

Komhyr, W. D., R. H. Gammon, J. Harriss, L. W. Waterman, T. J. Conway, W. R. Taylor, and K. W. Thoning, Global atmospheric CO_2 distribution and variation from 1968-1982 NOAA/GMCC flask sample data, *J. Geophys. Res.*, *90*, 5567-5596, 1985.

Kondo, Y., W. A. Matthews, A. Iwata, and M. Takagi, Measurements of nitric oxide from 7 to 32 km and its diurnal variation in the stratosphere, *J. Geophys. Res.*, *90*, 3813-3820, 1985.

Koyama, T., Gaseous metabolism in lake sediments and paddy soils and the production of atmospheric methane and hydrogen, *J. Geophys. Res.*, *68*, 3971-3973, 1963.

Koyama, T., Biogeochemical studies on lake sediments and paddy soils and the production of atmospheric methane and hydrogen, in *Recent Researches in the Fields of Hydrosphere, Atmosphere and Nuclear Geochemistry*, edited by Y. Miyake and T. Koyama, Water Research Laboratory, Nagoya University, Nagoya, Japan, 1964.

Krey, P. W., R. J. Lagomarsino, and L. E. Toonkel, Gaseous halogens in the atmosphere in 1975, *J. Geophys. Res.*, *82*, 1753-1766, 1977.

Krishnamurti, T. N., The subtropical jet stream of winter, *J. Meteorol.*, *18*, 172-191, 1961.

Krueger, A. J., Rocket measurements of ozone over Hawaii, *Ann. Geoph.*, *25*, 307-311, 1969.

Krueger, A. J., and R. A. Minzner, A mid-latitude ozone model for the 1976 U.S. standard atmosphere, *J. Geophys. Res.*, *81*, 4477-4481, 1976.

Krueger, A. J., B. Guenther, A. J. Fleig, D. F. Heath, E. Hilsenrath, R. McPeters, and C. Prabakhara, Satellite ozone measurements, *Phil. Trans. Roy. Soc. London*, *A296*, 191-204, 1980a.

Krueger, A. J., A. J. Fleig, J. A. Gatlin, D. F. Heath, P. K. Bhartia, V. G. Kaveeshwar, K. F. Klenk, and P. M. Smith, First results from the Nimbus 7 total ozone mapping spectrometer, in *Proceedings*

Quadrennial International Ozone Symposium, Vol. I, edited by J. London, pp. 322-327, IAMAP, NCAR, Boulder, CO, 1981.

Krumins, M. V., and W. C. Lyons, Corrections for the upper atmosphere temperatures using a thin-film loop mount, *Tech. Rep. NOLTR 72-152*, 46 pp., U.S. Nav. Ordnance Lab., White Oak, MD, 1972.

Kuhn, W. R., and J. London, Infrared radiative cooling in the middle atmosphere (30-110 km), *J. Atmos. Sci., 26*, 189-204, 1969.

Kulcke, W., and H. K. Paetzold, Uber eine radiosonde zur bestimmung der vertikalen ozonverteilung, *Ann. Meteorol., 8*, 47-53, 1957.

Kunde, V., B. Conrath, R. Hanel, J. Herman, D. Jennings, W. Maguire, J. Brasunas, H. Buijs, J. Berike, and J. McKinnon, Measurement of lower stratosphere gaseous constituents with a balloon-borne cryogenic spectrometer, *J. Geophys. Res.*, in press, 1985.

Kurzeja, R. J., The transport of trace chemicals by planetary waves in the stratosphere. Part 1: Steady waves, *J. Atmos. Sci., 38*, 2779-2788, 1981.

Kurzeja, R. J., K. V. Haggard, and W. L. Grose, Numerical experiments with a general circulation model concerning the distribution of ozone in the stratosphere, *J. Atmos. Sci., 41*, 2029-2051, 1984.

Kutepov, A. A., and G. M. Shved, Radiative transfer in the 15 μm CO_2 band with non-LTE in the Earth's atmosphere, *Izves. Atmos. and Ocean. Phys., 14*, 28-43, 1978.

Labitzke, K., The interaction between stratosphere and mesosphere in winter, *J. Atmos. Sci., 29*, 1395-1399, 1972.

Labitzke, K., The temperature in the upper stratosphere: Differences between hemispheres, *J. Geophys. Res., 79*, 2171-2175, 1974.

Labitzke, K., Comparison of the stratospheric temperature distribution over Northern and Southern Hemispheres, *COSPAR Space Research, XVII*, 159-165, 1977.

Labitzke, K., The major stratospheric warming during January/February 1979, *Beilage zur Berliner Wetterkarte, 8.5*, 1979.

Labitzke, K., Stratospheric-mesospheric midwinter disturbances: A summary of observed characteristics, *J. Geophys. Res., 86*, 9665-9678, 1981.

Labitzke, K., On the interannual variability of the middle stratosphere during the northern winters, *J. Meteorol. Soc. Japan, 60*, 124-139, 1982.

Labitzke, K., A survey over the PMP-1 winters 1978/79-1981/82 in comparison with earlier winters, *Adv. Space Res., 2*, 149-157, 1983.

Labitzke, K., On the interannual variability of the middle atmosphere during winter, in *Handbook for MAP, Vol. 18*, edited by S. Kato, pp. 1-9, SCOSTEP Secretariat, Univ. of Illinois, Urbana, 1985.

Labitzke, K., and J. J. Barnett, Review of climatological information obtained from remote sensing of the stratosphere and mesosphere, *Space Res., 19*, 97-106, 1979.

Labitzke, K., and B. Naujokat, On the variability and on trends of temperature in the middle stratosphere, *Beitr. Phys. Atmosph., 56*, 495-507, 1983.

Labitzke, K., and B. Naujokat, An update of the observed QBO of the stratospheric temperatures over the Northern Hemisphere, *Geophys. Res. Lett.*, in press, 1986.

Labitzke, K., R. Lenschow, B. Naujokat, and K. Petzoldt, The second winter of PMP-1: 1979/80, *Beilage zur Berliner Wetterkarte, 2.4*, 1980.

Labitzke, K., R. Lenschow, and B. Naujokat, The third winter of PMP-1: 1980/81, *Beilage zur Berliner Wetterkarte, 16.7*, 1981.

Labitzke, K., B. Naujokat, and M. P. McCormick, Temperature effects on the stratosphere of the April 4, 1982 eruption of El Chichon, Mexico, *Geophys. Res. Lett., 10*, 24-26, 1983.

Labitzke, K., J. J. Barnett and B. Edwards (Eds.), *Draft of a New Reference Middle Atmosphere, Handbook for MAP, Vol. 16*, 318 pp., SCOSTEP Secretariat, Univ. of Illinois, Urbana, 1985.

Labitzke, K., G. Brasseur, B. Naujokat, and A. de Rudder, Long-term temperature trends in the stratosphere: Possible influence of antropogenic gases, *Geophys. Res. Lett.*, *13*, 1152-1155, 1986.

Lacis, A., Chlorofluorocarbons and stratospheric ozone, in *Global Environmental Problems*, edited by S. F. Singer, Paragon House, New York, in press, 1985.

Lacis, A. A., and J. E. Hansen, A parameterization for the absorption of solar radiation in the Earth's atmosphere, *J. Atmos. Sci.*, *31*, 118-133, 1974.

Lacis, A., J. Hansen, P. Lee, T. Mitchell, and S. Lebedeth, Greenhouse effect of trace gases, *Geophys. Res. Lett.*, *8*, 1035-1038, 1981.

Lacome, N., A. Levy, and C. Boulet, Air broadened line width of nitrous oxide: An improved calculation, *J. Mol. Spectrosc.*, *97*, 139-153, 1983.

Lal, S., R. Borchers, P. Fabian, and B. C. Krueger, Increasing abundance of $CBrClF_2$ in the atmosphere, *Nature*, *316*, 135-136, 1985.

Lau, K-M, and P. H. Chan, Short term climate variability and atmospheric teleconnections from satellite-observed outgoing longwave radiation. Part I: Simultaneous relationships, *J. Atmos. Sci.*, *40*, 2735-2750, 1983.

Laurent, J., M. P. Lemaitre, C. Lippens, and C. Muller, *L'Aeronautique et l'Astronautique*, *98*, 60-61, 1983.

Laurent, J., M. P. Lemaitre, J. Besson, A. Girard, C. Lippens, C. Muller, J. Vercheval, and M. Ackerman, Middle atmosphere NO and NO_2 observed by means of the Spacelab 1 grille spectrometer, *Nature*, in press, 1985.

Lazrus, A. L., and B. W. Gandrud, Distribution of stratospheric nitric acid vapor, *J. Atmos. Sci.*, *31*, 1102-1108, 1974.

Lazrus, A. L., B. W. Gandrud, R. N. Woodard, and W. A. Sedlacek, Direct measurements of stratospheric chlorine and bromine, *J. Geophys. Res.*, *81*, 1067-1090, 1976.

Lean, J. L., Estimating the variability of the solar flux between 200 and 300 nm, *J. Geophys. Res.*, *89*, 1-9, 1984.

Lean, J. L., and A. Skumanich, Variability of the Lyman alpha flux with solar activity, *J. Geophys. Res.*, *88*, 5751-5759, 1983.

Lean, J. L., O. R. White, W. C. Livingston, D. F. Heath, R. F. Donnelly, and A. Skumanich, A three component model of the variability of the solar ultraviolet flux: 145-200 nm, *J. Geophys. Res.*, *87*, 10307-10317, 1982.

Leifer, R., R. Larsen, and L. Toonkel, Stratospheric distributions and inventories of trace gases in the Northern Hemisphere for 1976, *Report EML-349, I-211*, Environmental Measurements Lab., New York, 1979a.

Leifer, R., L. Toonkel, and R. Larsen, Project airstream, trace gases in the stratosphere, *Report EML-349, II-107*, Environmental Measurements Lab., New York, 1979b.

Leifer, R., K. C. Sommers, and S. F. Guggenheim, Atmospheric trace gas measurements with a new clean air sampling system, *Geophys. Res. Lett.*, *8*, 1079-1081, 1981.

Leighton, H., Influence of Arctic haze on the solar radiation budget, *Atmos. Environ.*, *17*, 2065-2068, 1983.

Leighton, P. A., *Photochemistry of Air Pollution*, Academic Press, New York, 1961.

Lemaitre, M. P., J. Laurent, J. Besson, A. Girard, C. Lippens, C. Muller, J. Vercheval, and M. Ackerman, Sample performance of the grille spectrometer, *Science*, *225*, 171-172, 1984.

Lenoble, J., A general survey of the problem of aerosol climatic impact, in *Aerosols and Their Climatic Effects*, edited by H. E. Gerber and A. Deepak, pp. 279-294, A. Deepak Publ., Hampton, VA, 1984.

Lenoble, J., D. Tanre, P. Y. Deschamps, and M. Hessman, A simple method to compute the change in earth-atmosphere radiative balance due to a stratospheric aerosol layer, *J. Atmos. Sci.*, *39*, 2565-2576, 1982.

Lenschow, D. H., R. Pearson, Jr., and B. B. Stankov, Measurements of ozone vertical flux to ocean and forest, *J. Geophys. Res.*, *87*, 8833-8837, 1982.

Leone, J. A., and J. H. Seinfeld, Analysis of the characteristics of complex chemical reaction mechanisms: Application to photochemical smog chemistry, *Environ. Sci. Technol.*, *18*, 280-287, 1984a.

Leone, J. A., and J. H. Seinfeld, Updated chemical mechanism for atmospheric photooxidation of toluene, *Int. J. Chem. Kinet.*, *16*, 159-193, 1984b.

Leovy, C. B., Simple models of thermally driven mesospheric circulations, *J. Atmos. Sci.*, *21*, 327-341, 1964a.

Leovy, C. B., Radiative equilibrium of the mesosphere, *J. Atmos. Sci.*, *21*, 238-248, 1964b.

Leovy, C. B., and P. J. Webster, Stratospheric long waves: Comparison of thermal structure in the northern and southern hemispheres, *J. Atmos. Sci.*, *33*, 1624-1638, 1976.

Leovy, C. B., C. R. Sun, M. H. Hitchman, E. E. Remsberg, J. M. Russell III, L. L. Gordley, J. C. Gille, and L. V. Lyjak, Transport of ozone in the middle stratosphere: Evidence for planetary wave breaking, *J. Atmos. Sci.*, *42*, 230-244, 1985.

Lesclaux, R., and F. Caralp, Determination of the rate constants for the reactions of $CFCl_2O_2$ radical with NO and NO_2 by laser photolysis and time resolved mass spectrometry, *Int. J. Chem. Kinet.*, *16*, 1117-1128, 1984.

Leu, M. T., Kinetics of the reaction O + ClO → Cl + O_2, *J. Phys. Chem.*, *88*, 1394-1398, 1984.

Levine, J. S., C. P. Rinsland, and G. M. Tennille, The photochemistry of methane and carbon monoxide in the troposphere in 1950 and 1985, *Nature*, *318*, 254-257, 1985.

Levine, S. Z., and S. E. Schwartz, In-cloud and below-cloud scavenging of nitric acid vapor, *Atmos. Environ.*, *16*, 1725-1734, 1982.

Levy II, H., Normal atmosphere: Large radical and formaldehyde concentrations predicted, *Science*, *173*, 141-143, 1971.

Levy II, H., Photochemistry of the lower troposphere, *Planet. Space Sci.*, *20*, 919-935, 1972.

Levy II, H., J. D. Mahlman, and W. J. Moxim, A preliminary report on the numerical simulation of the three-dimensional structure and variability of atmospheric N_2O, *Geophys. Res. Lett.*, *6*, 155-158, 1979.

Levy II, H., J. D. Mahlman, and W. J. Moxim, A stratospheric source of reactive nitrogen in the unpolluted troposphere, *Geophys. Res. Lett.*, *7*, 441-444, 1980.

Levy II, H. B., J. D. Mahlman, W. J. Moxim, and S. C. Liu, Tropospheric ozone: The role of transport, *J. Geophys. Res.*, *90*, 3753-3771, 1985.

Lewis, B. R., I. M. Vardavas, and J. H. Carver, The aeronomic dissociation of water vapor by H Lyman alpha radiation, *J. Geophys. Res.*, *88*, 4935-4940, 1983.

Lilly, D. K., D. E. Waco, and S. I. Adelfang, Stratospheric mixing estimated from high-altitude turbulence measurements, *J. Appl. Meteorol.*, *13*, 488-493, 1974.

Lin, B. D., The behavior of winter stationary planetary waves forced by topography and diabatic heating, *J. Atmos. Sci.*, *39*, 1206-1226, 1982.

Lindzen, R. S., Some speculations on the roles of critical level interactions between internal gravity waves and mean flows, in *Acoustic-Gravity Waves in the Atmosphere-Symposium Proceedings*, edited by T. M. Georges, Environmental Science Services Administration, Boulder, CO, 427 pp., 1968.

Lindzen, R. S., Turbulence and stress owing to gravity and tidal breakdown, *J. Geophys. Res.*, *86*, 9707-9714, 1981.

Lindzen, R. S., and J. R. Holton, A theory of the quasi-biennial oscillation, *J. Atmos. Sci.*, *25*, 1095-1107, 1968.

Lindzen, R. S., and C. Y. Tsay, Wave structure of the tropical stratosphere over the Marshall Islands area during 1 April-1 July 1958, *J. Atmos. Sci.*, *22*, 2008-2021, 1975.

Lindzen, R. S., D. M. Straus, and B. Katz, An observational study of large-scale atmospheric Rossby waves during FGGE, *J. Atmos. Sci.*, *41*, 1320-1335, 1984.

Ling, X., and J. London, A theoretical study of the quasi-biennial oscillation in the tropical stratosphere, in *Atmospheric Ozone*, edited by C. S. Zerefos and A. Ghazi, pp. 53-58, D. Reidel, Dordrecht, 1985.

Lippens, C., and C. Muller, Atmospheric nitric acid and chlorofluoromethane 11 from interferometric spectra obtained at the Observatoires du Pic du Midi, *J. Optics (Paris)*, *12*, 331-336, 1981.

Lippens, C., C. Muller, J. Vercheval, M. Ackerman, J. Laurent, M. P. Lemaitre, J. Besson, and A. Girard, Trace constituents measurements deduced from spectrometric observations onboard Spacelab, *Adv. Space Res.*, *4*, 75-79, 1984.

Lipschultz, F., O. C. Zafiriou, S. C. Wofsy, M. B. McElroy, F. W. Valois, and S. W. Watson, Production of NO and N_2O by soil nitrifying bacteria: A source of atmospheric nitrogen oxides, *Nature*, *294*, 641-643, 1981.

Liu, S. C., and G. C. Reid, Sodium and other minor constituents of meteoric origin in the atmosphere, *Geophys. Res. Lett.*, *6*, 283-286, 1979.

Liu, S. C., T. M. Donahue, R. J. Cicerone, and W. L. Chameides, Effect of water vapor on the destruction of ozone in the stratosphere perturbed by Cl_x or NO_x pollutants, *J. Geophys. Res.*, *81*, 3111-3118, 1976.

Liu, S. C., D. Kley, M. McFarland, J. D. Mahlman, and H. Levy II, On the origin of tropospheric ozone, *J. Geophys. Res.*, *85*, 7546-7552, 1980.

Liu, S. C., M. McFarland, D. Kley, O. Zafiriou, and B. J. Huebert, Tropospheric NO_x and O_3 budgets in the equatorial Pacific, *J. Geophys. Res.*, *88*, 1360-1368, 1983.

Loewenstein, M., W. J. Starr, and D. G. Murcray, Stratospheric NO and HNO_3 observations in the Northern Hemisphere for three seasons, *Geophys. Res. Lett.*, *5*, 531-534, 1978a.

Loewenstein, M., W. J. Borucki, H. F. Savage, J. G. Borucki, and R. C. Whitten, Geographical variations of NO and O_3 in the lower stratosphere, *J. Geophys. Res.*, *83*, 1874-1882, 1978b.

Logan, J. A., Nitrogen oxides in the troposphere: Global and regional budgets, *J. Geophys. Res.*, *88*, 10785-10807, 1983.

Logan, J. A., Tropospheric ozone: Seasonal behavior, trends and anthropogenic influence, *J. Geophys. Res.*, 90, 10463-10482, 1985.

Logan, J. A., M. J. Prather, S. C. Wofsy, and M. B. McElroy, Atmospheric chemistry: Response to human influence, *Phil. Trans. Roy. Soc. London*, *A290*, 187-234, 1978.

Logan, J. A., M. J. Prather, S. C. Wofsy, and M. B. McElroy, Tropospheric chemistry: A global perspective, *J. Geophys. Res.*, *86*, 7210-7254, 1981.

London, J., Radiative energy sources and sinks in the stratosphere and mesosphere, in *Proceedings of the NATO Advanced Study Institute on Atmospheric Ozone: Its Variation and Human Influences*, *Rep. FAA-EE-80-20*, edited by A. C. Aikin, pp. 703-721, DOT, FAA, Washington, DC, 1980a.

London, J., The observed distribution and variations of total ozone, in *Proceedings of the NATO Advanced Study Institute on Atmospheric Ozone: Its Variation and Human Influences*, *Report FAA-EE-80-20*, edited by A. C. Aikin, pp. 31-44, DOT, FAA, Washington,DC, 1980b.

London, J., and J. Park, Application of general circulation models to the study of stratospheric ozone, *Pure Appl. Geophys.*, *106-108*, 1611-1617, 1973.

London, J., and J. Park, The interaction of ozone photochemistry and dynamics in the stratosphere: A three-dimensional stratospheric model, *Can. J. Chem.*, *62*, 1599-1609, 1974.

London, J., B. D. Bojkov, S. Oltmans, and J. F. Kelly, Atlas of the global distribution of total ozone, July 1957-July 1967, *Tech. Note NCAR/TN/113* + STR, Nat. Center for Atmos. Res., Boulder, CO, Jan., 1976.

London, J., J. E. Frederick, and G. P. Anderson, Satellite observations of the global distribution of stratospheric ozone, *J. Geophys. Res.*, *82*, 2543-2556, 1977.

London, J., G. G. Bjarnason, and G. J. Rottman, 18 months of UV irradiance observations from the Solar Mesosphere Explorer, *Geophys. Res. Lett.*, *11*, 54-56, 1984.

Lorenc, A. C., The evolution of the planetary scale 200 mb divergent flow during the FGGE year, *Quart. J. Roy. Meteorol. Soc.*, *110*, 427-441, 1984.

Lorenz, E. N., The nature and theory of the general circulation of the atmosphere, *WMO No 218, WMO*, 1967.

Louis, J. F., A two-dimensional transport model of the atmosphere, Ph.D. thesis, Univ. of Colorado, Boulder, CO, 1974.

Louisnard, N., and O. Lado-Bordowsky, Spectroscopic measurements of carbon monoxide in the stratosphere, *J. Geophys. Res.*, *88*, 3781-3797, 1983.

Louisnard, N., and S. Pollitt, Measurements of neutral constituents using infrared and visible remote sensing, in *Handbook for MAP*, *Vol. 15*, edited by D. G. Murcray, pp. 37-70, SCOSTEP Secretariat, Univ. of Illinois, Urbana, 1985.

Louisnard, N., A. Girard, and G. Eichen, Mesures du profil vertical de concentration de la vapeur d'eau stratospherique, *C. R. Acad. Sc. Paris*, *290*, 385-388, 1980.

Louisnard, N., G. Fergant, A. Girard, L. Gramont, O. Lado-Bordowsky, J. Laurent, S. Le Boiteau, and M. P. Lemaitre, Infrared absorption spectroscopy applied to stratospheric profiles of minor constituents, *J. Geophys. Res.*, *88*, 5365-5376, 1983.

Lovelock, J. E., Atmospheric halocarbons and stratospheric ozone, *Nature*, *252*, 292-294, 1974.

Lovelock, J. E., Methyl chloroform in the troposphere as an indicator of OH radical abundance, *Nature*, *267*, 32, 1977.

Ludlam, F. H., *Clouds and Storms*, *Chapter 8*, Pennsylvania State University Press, University Park, PA, 1980.

Luther, F., Commentary on climatic effects of minor atmospheric constituents, in *Carbon Dioxide Review*, edited by W. C. Clark, pp. 290-294, Clarendon Press, New York, 1982.

Luther, F. M., and Y. Fouquart, *WMO Report WCP-93*, 37 pp., Geneva, 1984.

Luther, F., D. J. Wuebbles, and J. S. Chang, Temperature feedback in a stratospheric model, *J. Geophys. Res.*, *82*, 4935-4942, 1977.

Madden, R. A., Oscillations in the winter stratosphere. 2: The role of horizontal heat transport and the interaction of transient and stationary planetary-scale waves, *Mon. Weather Rev.*, *103*, 717-719, 1975.

Madden, R. A., Evidence for large-scale regularly propagating waves in a 73-year data set, in *Extended Summaries of Contributions*, IAGA/IAMAP, Seattle, Washington, International Assoc. for Atmos. Phys., NCAR, Boulder, CO, 1977.

Madden, R. A., Further evidence of traveling planetary waves, *J. Atmos. Sci.*, *35*, 1605-1618, 1978.

Madden, R. A., The effect of the interference of traveling and stationary waves on time variations of the large-scale circulation, *J. Atmos. Sci.*, *40*, 1110-1125, 1983.

Madden, R. A., and P. R. Julian, Detection of a 40-50 day oscillation in the zonal wind in the tropical Pacific, *J. Atmos. Sci.*, *28*, 702-708, 1971.

Madden, R. A., and P. R. Julian, Descriptions of global scale circulation cells in the tropics with a 40-50 period, *J. Atmos. Sci.*, *29*, 1109-1123, 1972a.

Madden, R. A., and P. Julian, Further evidence of global-scale 5-day pressure waves, *J. Atmos. Sci.*, *29*, 1464-1469, 1972b.

Madden, R. A., and P. Julian, Reply to comments by R. Deland, *J. Atmos. Sci.*, *30*, 935-940, 1973.

Madden, R. A., and K. Labitzke, A free Rossby wave in the troposphere and stratosphere during January 1979, *J. Geophys. Res.*, *86*, 1247-1254, 1981.

Madronich, S., D. R. Hastie, B. A. Ridley, and H. I. Schiff, Measurement of the photodissociation coefficient of NO_2 in the atmosphere, I. Method and surface measurements, *J. Atmos. Chem.*, *1*, 3-25, 1983.

Mahlman, J. D., Relation of stratospheric-tropospheric mass exchange mechanisms to surface radioactivity peaks, *Arch. Met. Geoph. Biokl. A.*, *15*, 1-25, 1965.

Mahlman, J. D., Long-term dependence of surface fallout fluctuations upon tropopause-level cyclogenesis, *Arch. Met. Geoph. Biokl. A.*, *18*, 299-311, 1969a.

Mahlman, J. D., Heat balance and mean meridional circulations in the polar stratosphere during the sudden warming of January 1958, *Mon. Weather Rev.*, *97*, 534-540, 1969b.

Mahlman, J. D., On the maintenance of the polar front jet stream, *J. Atmos. Sci.*, *30*, 544-557, 1973.

Mahlman, J. D., Some fundamental limitations of simplified transport models as implied by results from a three-dimensional general circulation/tracer model, in *Proceedings Fourth Conference Climatic Impact Assessment Program, DOT-TSC-OST-75-38*, edited by T. M. Hard and A. J. Broderick, pp. 132-146, Transportation Systems Command, Cambridge, MA, 1975.

Mahlman, J. D., Coupling in atmospheric observations with comprehensive numerical models, *Proc. of ICMUA Sessions and IUGG Symposium 18*, XVII IUGG General Assembly, Canberra, Australia, *18*, pp. 253-259, 1980.

Mahlman, J. D., "Strategies for equatorial lower stratospheric measurements" and "The status of stratospheric general circulation models", papers presented at International Workshop on Current Issues in our Understanding of the Stratosphere and the Future of the Ozone Layer, BMFT, NASA, FAA, WMO, Feldafing, FRG, June 11-16, 1984.

Mahlman, J. D., Mechanistic interpretation of stratospheric tracer transport, *Issues in Atmos. and Oceanic Modelling*, J. Smagorinsky Comm. Vol., 1985.

Mahlman, J. D., and W. J. Moxim, Tracer simulation using global circulation model: results from a midlatitude instantaneous source experiment, *J. Atmos. Sci.*, *35*, 1340-1374, 1978.

Mahlman, J. D., and R. W. Sinclair, Recent results from the GFDL troposphere-stratosphere-mesosphere general circulation model, *Proc. of ICMUA Sessions and IUGG Symposium 18*, XVII IUGG General Assembly, Canberra, Australia, 11-18, 1980.

Mahlman, J. D., and L. J. Umscheid, Dynamics of the middle atmosphere: Successes and problems of the GFDL "SKYHI" general circulation model, in *Dynamics of the Middle Atmosphere*, edited by J. R. Holton and T. Matsuno, pp. 501-525, Terrapub, Tokyo, 1984.

Mahlman, J. D., H. B. Levy II, and W. J. Moxim, Three-dimensional tracer structure and behavior as simulated in two ozone precursor experiments, *J. Atmos. Sci.*, *37*, 655-685, 1980.

Mahlman, J. D., D. G. Andrews, H. U. Duetsch, D. L. Hartmann, T. Matsuno, R. J. Murgatroyd, and J. F. Noxon, Transport of trace constituents in the stratosphere, in *Handbook for MAP, Vol. 3*, edited by C. F. Sechrist, Jr., pp. 14-43, SCOSTEP Secretariat, Univ. of Illinois, Urbana, 1981.

Mahlman, J. D., D. G. Andrews, D. L. Hartmann, T. Matsuno, and R. G. Murgatroyd, Transport of trace constituents in the stratosphere, in *Dynamics of the Middle Atmosphere*, edited by J. R. Holton and T. Matsuno, pp. 387-416, Terrapub, Tokyo, 1984.

Mahlman, J. D., H. B. Levy II, and W. J. Moxim, Three dimensional simulations of stratospheric N_2O: Predictions for other trace constituents, *J. Geophys. Res.*, in press, 1985.

Maier, E. J., A. C. Aikin, and J. E. Ainsworth, Stratospheric nitric oxide and ozone measurements using photoionization mass spectrometry and UV absorption, *Geophys. Res. Lett.*, *5*, 37-40, 1978.

Maki, A. G., F. J. Lovas, and W. B. Olson, Infrared frequency measurements on the ClO fundamental band, *J. Mol. Spectros.*, *92*, 410-418, 1982.

Makide, Y., and F. S. Rowland, Tropospheric concentrations of methyl chloroform, CH_3CCl_3, in January 1978 and estimates of atmospheric residence times for hydrocarbons, *Proceedings Natl. Acad. Sci., USA*, 5933-5937, 1981.

REFERENCES

Malcolm, K. W., K. O. Nien, and D. A. K. Sze, A 2-D model calculation of atmospheric lifetimes for N_2O, CFC-11 and CFC-12, *Nature*, *297*, 317-319, 1982.

Malko, M. W., and J. Troe, Analysis of the unimolecular reaction $N_2O_5 + M \rightarrow NO_2 + NO_3 + M$, *Int. J. Chem. Kinet.*, *14*, 399-416, 1982.

Malkmus, W., Random Lorentz band model with exponential tailed S^{-1} line-intensity distribution, *J. Opt. Soc. Amer.*, *57*, 323-329, 1967.

Malkus, J. S., Large-scale interactions, in *The Sea, Vol. 1*, edited by M. N. Hill, Interscience Publishers, New York, 1962.

Manabe, S., and B. G. Hunt, Experiments with a stratospheric general circulation model: I. radiative and dynamic effects, *Mon. Weather Rev.*, *96*, 477-539, 1968.

Manabe, S., and J. D. Mahlman, Simulation of seasonal and interhemispheric variations in the stratospheric circulation, *J. Atmos. Sci.*, *33*, 2185-2217, 1976.

Manabe, S., and R. J. Stouffer, Sensitivity of a global climate model to an increase of CO_2 concentration in the atmosphere, *J. Geophys. Res.*, *85*, 5529-5554, 1980.

Manabe, S., and R. T. Wetherald, Thermal equilibrium of the atmosphere with a given distribution of relative humidity, *J. Atmos. Sci.*, *24*, 241-259, 1967.

Manabe, S., and R. T. Wetherald, The effects of doubling the CO_2 concentration on the climate of a general circulation model, *J. Atmos. Sci.*, *32*, 3-15, 1975.

Manabe, S., and R. T. Wetherald, On the distribution of climate change resulting from an increase in CO_2-content of the atmosphere, *J. Atmos. Sci.*, *37*, 99-118, 1980.

Mankin, W. G., and M. T. Coffey, Latitudinal distributions and temporal changes of stratospheric HCl and HF, *J. Geophys. Res.*, *88*, 10776-10784, 1983.

Mankin, W. G., and M. T. Coffey, Increased stratospheric hydrogen chloride in the El Chichon cloud, *Science*, *226*, 170-172, 1984.

Mankin, W. G., M. T. Coffey, D. W. T. Griffith, and S. R. Drayson, Spectroscopic measurement of carbonyl sulfide (OCS) in the stratosphere, *Geophys. Res. Lett.*, *6*, 853-856, 1979.

Mankin, W. G., M. T. Coffey, K. V. Chance, W. A. Traub, B. Carli, A. Bonetti, I. G. Nolt, R. Zander, D. W. Johnson, G. Stokes, and C. B. Farmer, Intercomparison of measurements of stratospheric hydrogen fluoride, to be published, 1986.

Manson, A. H., C. E. Meek, and J. G. Gregory, Winds and waves (10 min - 30 days) in the mesosphere and lower thermosphere at Saskatoon (32 °N, 107 °W, L=4.3) during the year October 1979 to July 1980, *J. Geophys. Res.*, *86*, 9615-9625, 1981.

Marche, P., and C. Meunier, Atmospheric trace species measured above Haute-Provence Observatory, *Planet. Space Sci.*, *31*, 731-733, 1983.

Marche, P., A. Barbe, C. Secroun, J. Corr, and P. Jouve, Ground based spectroscopic measurements of HCl, *Geophys. Res. Lett.*, *7*, 869-872, 1980a.

Marche, P., A. Barbe, C. Secroun, J. Corr, and P. Jouve, Mesures des acides fluorhydrique et chlorhydrique dans l'atmosphere par spectroscopie infrarouge a partir du sol, *C. R. Acad. Sc. Paris*, *290B*, 369-371, 1980b.

Marche, P., C. Meunier, A. Barbe, and P. Jouve, Total atmospheric ozone measured by ground based high resolution infrared spectra-comparison with Dobson measurements, *Planet. Space Sci.*, *31*, 723-727, 1983.

Margitan, J. J., Chlorine nitrate: The sole product of the $ClO + NO_2 + M$ recombination, *J. Geophys. Res.*, *88*, 5416-5420, 1983.

Margitan, J. J., Kinetics of the reaction $O + ClO \rightarrow Cl + O_2$, *J. Phys. Chem.*, *88*, 3638-3643, 1984a.

Margitan, J. J., Mechanisms of the atmospheric oxidation of sulfur dioxide catalysis by hydroxyl radicals, *J. Phys. Chem.*, *88*, 3314-3318, 1984b.

Maroulis, P. J., A. I. Torres, and A. R. Bandy, Atmospheric concentrations of carbonyl sulfide in the southwestern and eastern United States, *Geophys. Res. Lett.*, *4*, 510-512, 1977.

Martin, L. R., H. S. Judeikis, and M. Wu, Heterogeneous reactions of Cl and ClO in the stratosphere, *J. Geophys. Res.*, *85*, 5511-5518, 1980.

Maruyama, T., Long-term behavior of Kelvin waves and mixed Rossby-gravity waves, *J. Meteorol. Soc. Japan*, *47*, 245-254, 1969.

Mason, C. J., and J. J. Horvath, The direct measurement of nitric oxide concentration in the upper atmosphere by a rocket-borne chemiluminescent detector, *Geophys. Res. Lett.*, *3*, 391-394, 1976.

Massman, W. J., An investigation of gravity waves on a global scale using TWERLE data, *J. Geophys. Res.*, *86*, 4072-4082, 1981.

Mastenbrook, H. J., Water vapor distribution in the stratosphere and high troposphere, *J. Atmos. Sci.*, *25*, 299-311, 1968.

Mastenbrook, H. J., and S. J. Oltmans, Stratospheric water vapor variability for Washington, DC/Boulder, CO: 1964-82, *J. Atmos. Sci.*, *40*, 2157-2165, 1983.

Mateer, C. L., and I. A. Asbridge, On the appropriate haze correction for direct sun total ozone measurements with the Dobson spectrophotometer, in *Proceedings of the Quadrennial International Ozone Symposium, Vol. I*, edited by J. London, pp. 236-242, IAMAP, NCAR, Boulder, CO, 1981.

Mateer, C. L., and J. J. DeLuisi, The estimation of the vertical distribution of ozone by the short Umkehr method, in *Proceedings of the Quadrennial International Ozone Symposium, Vol. I*, edited by J. London, pp. 64-73, IAMAP, NCAR, Boulder, CO, 1981.

Mateer, C. L., and H. U. Duetsch, Uniform evaluation of Umkehr observations from the World Ozone Network: Part 1, Proposed standard Umkehr evaluation technique, Nat'l Center for Atmos. Res., Boulder, Colorado, 1964.

Mathews, E. I. Fung, and S. Ross, Atmospheric methane: Global distributions of biogenic source locations, in press, 1986.

Matson, M., Eruptions of El Chichon volcano, in *Radiative Effects of the El Chichon Volcanic Eruption: Preliminary Results Concerning Remote Sensing, NASA Tech. Memo. 84959*, edited by W. R. Bandeen and R. S. Fraser, 103 pp., NASA Goddard Space Flight Center, Greenbelt, MD, 1982.

Matsuno, T., Vertical propagation of stationary planetary waves in the winter Northern Hemisphere, *J. Atmos. Sci.*, *27*, 871-883, 1970.

Matsuno, T., A dynamical model of the stratospheric sudden warming, *J. Atmos. Sci.*, *28*, 1479-1494, 1971.

Matsuno, T., Lagrangian motion of air parcels in the stratosphere in the presence of planetary waves, *Pure Appl. Geophys.*, *118*, 189-216, 1980.

Matsuno, T., A quasi one-dimensional model of the middle atmosphere circulation interacting with internal gravity waves, *J. Meteorol. Soc. Japan*, *60*, 215-226, 1982.

Mattingly, S. R., The contribution of extratropical severe storms to the stratospheric water vapour budget, *Met. Mag.*, *106*, 256-262, 1977.

Mayer, E. W., D. R. Blake, S. C. Tyler, Y. Makide, D. C. Montague, and F. S. Rowland, Methane: Interhemispheric concentration gradient and atmospheric residence time, *Proc. Nat. Acad. Sci., USA*, *79*, 1366-1370, 1982.

McClatchey, R. S., R. W. Fenn, J. E. A. Selby, F. E. Volz, and J. S. Garing, Optical properties of the atmosphere, *AFCRC-71-0279*, 85 pp., Air Force Cambridge Res. Lab., Bedford, MA, 1971.

McClatchey, R. A., W. S. Benedict, S. A. Clough, D. E. Burch, R. F. Calfee, K. Fox, L. S. Rothman, and J. S. Garing, AFCRL atmospheric absorption line parameters compilation, *AFCRL-TR-73-0096*, 83 pp., Air Force Cambridge Research Laboratory Report, Hanscom AFB, MA, 1973.

McCormick, M. P., and T. J. Swissler, Stratospheric aerosol mass and latitudinal distribution of the El Chichon eruption cloud for October 1982, *Geophys. Res. Lett.*, *10*, 877-880, 1983.

McCormick, M. P., P. Hamill, T. J. Pepin, W. P Chu, T. J. Swissler, and L. R. McMaster, Satellite studies of the stratospheric aerosol, *Bull. Amer. Meteor. Soc.*, *60*, 1038-1046, 1979.

McCormick, M. P., H. M. Steele, P. Hamill, W. P. Chu, and T. J. Swissler, Polar stratospheric cloud sightings by SAM II, *J. Atmos. Sci.*, *39*, 1387-1397, 1982.

McCormick, M. P., T. J. Swissler, E. Hilsenrath, A. J. Krueger, and M. T. Osborn, Satellite and correlative measurements of stratospheric ozone; Comparison of measurements made by SAGE, ECC balloons, chemiluminescent and optical rocketsondes, *J. Geophys. Res.*, *89*, 5315-5320, 1984.

McCormick, M. P., T. J. Swissler, W. H. Fuller, W. H. Hunt, M. T. Osborn, Airborne and ground-based lidar measurements of the El Chichon stratospheric aerosol from 90N to 56S, *Geof. Int.*, *23-2*, 187-221, 1984.

McElroy, M. B., Chemical processes in the solar system, in *Chemical Kinetics*, edited by D. R. Hersehbach, pp. 127-211, Int. Review of Science, Butterworths, London, 1976.

McElroy, M. B., and S. C. Wofsy, Tropical forests: Interactions with the atmosphere, in *Symposium volume on 'Tropical Forests and World Atmospheres'*, edited by G. T. Prance, in press, 1985.

McElroy, M., S. C. Wofsy, J. Penner and J. McConnell, Atmospheric ozone: Possible impact of stratospheric aviation, *J. Atmos. Sci.*, *31*, 287-303, 1974.

McElroy, M. B., S. C. Wofsy, and Y. L. Yung, The nitrogen cycle: Perturbations due to man and their impact on atmospheric N_2O and O_3, *Phil. Trans. Roy. Soc. London*, *A277*, 159-181, 1977.

McFarland, J., D. Kley, J. W. Drummond, A. L. Schmeltekopf, and R. H. Winkler, Nitric oxide measurements in the Equatorial Pacific region, *Geophys. Res. Lett.*, *6*, 605-608, 1979.

McFarland, M., B. A. Ridley, M. Profitt, and D. L. Albritton, Simultaneous in-situ measurements of stratospheric O_3, NO_2, and NO, in press, 1985.

McGregor, J., and W. A. Chapman, Stratospheric temperatures and geostrophic winds during 1973-1974, *Quart. J. Roy. Meteorol. Soc.*, *105*, 241-261, 1979.

McInturff, R. M. (Ed.), Stratospheric warmings: Synoptic, dynamic and general-circulation aspects, *NASA Ref. Publ. 1017*, 166 pp., NASA, Washington, DC, 1978.

McIntyre, M. E., Towards a Lagrangian-mean description of stratospheric circulations and chemical transports, *Phil. Trans. Roy. Soc. London*, *A296*, 129-148, 1980a.

McIntyre, M. E., An introduction to the generalized Lagrangian-mean description of wave, mean-flow interaction, *Pure Appl. Geophys.*, *118*, 152-176, 1980b.

McIntyre, M. E., How well do we understand the dynamics of stratospheric warmings?, *J. Meteorol. Soc. Japan*, *60*, 37-65, 1982.

McIntyre, M. E., and T. N. Palmer, Breaking planetary waves in the stratosphere, *Nature*, *305*, 593-600, 1983.

McIntyre, M. E., and T. N. Palmer, The 'surf zone' in the stratosphere, *J. Atmos. Terr. Phys.*, *46*, 825-850, 1984.

McKay, M. D., R. J. Beckman, and W. J. Conover, A comparison of three methods for selecting values of input variables in the analysis of output from a computer code, *Technometrics*, *21*, 239-245, 1979.

McKenney, D. J., D. L. Wade, and W. I. Findlay, Rates of N_2O evolution from N fertilized soil, *Geophys. Res. Lett.*, *5*, 777-780, 1978.

McKenney, D. J., K. F. Shuttleworth, J. R. Vriesacker, and W. T. Findlay, Production and loss of nitric oxide from denitrification in anaerobic Brookstone clay, *Appl. Env. Microbiol.*, *43*, 534-541, 1982.

McKenzie, R. L., and P. V. Johnston, Seasonal variation in stratospheric NO_2 at 45 degrees S, *Geophys. Res. Lett.*, *9*, 1255-1258, 1982.

McMahon, T. A., and P. J. Denison, Empirical atmospheric deposition parameters—A survey, *Atmos. Environ.*, *13*, 571-585, 1979.

McMillin, L. M., and C. Dean, Evaluation of a new operational technique for producing clear radiances, *J. Appl. Meteorol.*, *21*, 1005-1014, 1982.

McPeters, R. D., and C. H. Jackman, The response of ozone to solar proton events during solar cycle 21: The observations, *J. Geophys. Res.*, 90, 7945-7954, 1985.

McPeters, R. D., C. H. Jackman, and E. G. Stassinopoulos, Observations of ozone depletion associated with solar proton events, *J. Geophys. Res.*, *86*, 12071-12081, 1981.

McPeters, R. D., D. F. Heath, and P. K. Bhartia, Average ozone profiles for 1979 from the NIMBUS 7 SBUV instrument, *J. Geophys. Res.*, *89*, 5199-5214, 1984.

McPherson, R. D., K. H. Bergman, R. E. Kistler, G. E. Rasch, and D. S. Gordon, The NMC operational global data assimilation system, *Mon. Weather Rev.*, *107*, 1445-1461, 1979.

Mechoso, C. R., M. J. Suarez, K. Yamazaki, J. Spahr, and A. Arakawa, A study of the sensitivity of numerical forecasts to an upper boundary condition in the lower stratosphere, *Mon. Weather Rev.*, *110*, 1984-1993, 1982.

Mechoso, C. R., K. Yamazaki, A. Kitch, and A. Arakawa, Numerical forecasts of stratospheric warming events during the winter of 1979, *J. Atmos. Sci.*, in press, 1985.

Meek, C. E., I. M. Reid, and A. H. Manson, Observations of mesospheric wind velocities. I. Gravity wave horizontal scale and phase velocities determined from spaced wind observations, *Rad. Sci.*, in press, 1985a.

Meek, C. E., I. M. Reid, and A. H. Manson, Observations of mesospheric wind velocities. II. Cross sections of power spectral density for 48-8h, 8-1h, 1h-10 min over 60-110 km for 1981, *Rad. Sci.*, in press, 1985b.

Megie, G., and J. E. Blamont, Laser sounding of atmospheric sodium, Interpretation in terms of global atmospheric parameters, *Planet. Space Sci.*, *25*, 1093-1109, 1977.

Megie, G., and R. T. Menzies, Complementarity of UV and IR differential absorption lidar for global measurements of atmospheric species, *Appl. Optics*, *19*, 1173-1183, 1980.

Megie, G., J. Y. Allain, M. L. Chanin, and J. E. Blamont, Vertical profile of stratospheric ozone by lidar sounding from the ground, *Nature*, *270*, 329-331, 1977.

Meier, R. R., D. E. Anderson, Jr., and M. Nicolet, Radiation field in the troposphere and stratosphere from 240-1000 nm - I. General analysis, *Planet. Space Sci.*, *30*, 923-933, 1982.

Mentall, J. E., J. E. Frederick, and J. R. Herman, The solar irradiance from 200-330 nm, *J. Geophys. Res.*, *86*, 9881-9884, 1981.

Mentall, J. E., B. Guenther, and D. Williams, The solar spectral irradiance between 150 and 200 nm, *J. Geophys. Res.*, *90*, 2265-2272, 1985.

Menzies, T., Remote measurement of ClO in the stratosphere, *Geophys. Res. Lett.*, *6*, 151-154, 1979.

Menzies, T., A re-evaluation of laser heterodyne radiometer ClO measurements, *Geophys. Res. Lett.*, *10*, 729-732, 1983.

Michalsky, J. J., B. M. Herman and N. R. Larson, Mid-latitude stratospheric aerosol layer enhancement by El Chichon: The first year, *Geophys. Res. Lett.*, *11*, 76-79, 1984.

Mihelic, D., D. H. Ehhalt, G. F. Kulessa, J. Klomfass, M. Trainer, U. Schmidt, and H. Rohrs, Measurements of free radicals in the atmosphere by matrix isolation and electron paramagnetic resonance, *Pure Appl. Geophys.*, *116*, 530-536, 1978.

Miles, T., and W. A. Chapman, Intercomparison of planetary-scale diagnostics derived from seperate satellite and radiosonde time-mean temperature fields, *Quart. J. Roy. Meteorol. Soc.*, *110*, 1003-1021, 1984.

Miller, A. J., Periodic variation of atmospheric circulation at 14-16 days, *J. Atmos. Sci.*, *31*, 720-726, 1974.

Miller, A. J., T. G. Rogers, R. M. Nagatani, D. F. Heath, A. J. Krueger, W. Planet, and D. Crosby, Preliminary comparisons of daily total ozone fields derived from SBUV, TOMS and HIRS-2 satellite

instruments, in *Proc. XVII General Assembly of the International Union of Geodesy and Geophysics*, pp. 153-164, 1979.

Miller, A. J., R. M. Nagatani, T. G. Rogers, A. J. Fleig, and D. F. Heath, Total ozone variations 1970-1974 using Backscattered Ultraviolet (BUV) and ground-based observations, *J. Appl. Meteorol.*, *21*, 621-630, 1982.

Miller, A. J., R. M. Nagatani and J. E. Frederick, Ozone-temperature relationships in the stratosphere, in *Proceedings of the International Ozone Symposium*, pp. 321-324, Thessaloniki, Greece, D. Reidel, Dordrecht, 1985.

Miller, C., D. L. Filken, A. J. Owens, J. M. Steed, and J. P. Jesson, A two-dimensional model of stratospheric chemistry and transport, *J. Geophys. Res.*, *86*, 12039-12065, 1981.

Mitchell, J. F. B., The seasonal response of a general circulation model to changes in CO_2 and sea temperatures, *Quart. J. Roy. Meteorol. Soc.*, *109*, 113-152, 1983.

Mitchell, J. M., El Chichon: Weather-maker of the century?, *Weatherwise*, *35*, 252-261, 1982.

Miyahara, S., A numerical simulation of the zonal mean circulation of the middle atmosphere including effects of solar diurnal tidal waves and internal gravity waves; solstice condition, in *Dynamics of the Middle Atmosphere*, edited by J. R. Holton and T. Matsuno, pp. 271-287, Terrapub, Tokyo, 1984.

Miyahara, S., Suppression of stationary planetary waves by internal gravity waves in the mesosphere, *J. Atmos. Sci.*, *42*, 100-107, 1985.

Miyahara, S., Y. Hayashi, and J. D. Mahlman, Interactions between gravity waves and planetary scale flow simulated by GFDL "SKYHI" general circulation model, *J. Atmos. Sci.*, in press, 1985.

Miyakoda, K., R. F. Strickler, and G. D. Hembree, Numerical simulation of the breakdown of a polar-night vortex in the stratosphere, *J. Atmos. Sci.*, *27*, 139-154, 1970.

Moeng, C.-H., and J. C. Wyngaard, Statistics of conservative scalars in the convective boundary layer, *J. Atmos. Sci.*, *41*, 3161-3169, 1984.

Molina, L. T., M. J. Molina, and F. S. Rowland, Ultraviolet absorption cross sections of several brominated methanes and ethanes of atmospheric interest, *J. Phys. Chem.*, *86*, 2672-2676, 1982.

Molina, L. T., M. J. Molina, R. A. Stachnik and R. D. Tom, An upper limit to the rate of HCl + $ClONO_2$ reaction, *J. Phys. Chem.*, *89*, 3779-3781, 1985.

Molina, M. J., and F. S. Rowland, Stratospheric sink for chlorofluoromethanes: chorine atom catalyzed destruction of ozone, *Nature*, *249*, 810-814, 1974.

Molina, M. J., L. T. Molina, and T. Ishiwata, Kinetics of the ClO + NO_2 + M reaction, *J. Phys. Chem.*, *84*, 3100-3104, 1980.

Molina, M. J., L. T. Molina, and C. A. Smith, The rate of the reaction of OH with HCl, *Int. J. Chem. Kinet.*, *16*, 1151-1160, 1984.

Mook, W. M., M. Koopermans, A. F. Carter, and C. D. Keeling, Seasonal, latitudinal, and secular variations in the abundance and isotopic ratios of atmospheric carbon dioxide (1): Results from land stations, *J. Geophys. Res.*, *88*, 915-933, 1983.

Morel, O., R. Simonaitis, and J. Heicklen, Ultraviolet absorption spectra of HO_2NO_2, $CCl_3O_2NO_2$, $CCl_2FO_2NO_2$ and $CH_3O_2NO_2$, *Chem. Phys. Lett.*, *73*, 38-42, 1980.

Mount, G. H., and G. J. Rottman, The solar spectral irradiance 1200-3184 Å near solar maximum: 15 July 1980, *J. Geophys. Res.*, *86*, 9193-9198, 1981.

Mount, G. H., and G. J. Rottman, Solar absolute spectral irradiance 1150-3173 Å: May 17, 1982, *J. Geophys. Res.*, *88*, 5403-5410, 1983a.

Mount, G. H., and G. J. Rottman, The solar absolute spectral irradiance at 1216 Å and 1800-3173 Å: January 12, 1983, *J. Geophys. Res.*, *88*, 6807-6811, 1983b.

Mount, G. H., and G. J. Rottman, The solar absolute spectral irradiance 118-300 nm: July 25, 1983, *J. Geophys. Res.*, *90*, 13031-13036, 1985.

Mount, G. H., G. J. Rottman, and J. G. Timothy, The solar spectral irradiance 1200-2550 Å at solar maximum, *J. Geophys. Res.*, *85*, 4271-4274, 1980.

Mount, G. H., D. W. Rusch, J. M. Zawodny, J. F. Noxon, C. A. Barth, G. J. Rottman, R. J. Thomas, G. E. Thomas, R. W. Sanders, and G. M. Lawrence, Measurements of NO_2 in the Earth's stratosphere using a Limb scanning visible light spectrometer, *Geophys. Res. Lett.*, *10*, 265-268, 1983.

Mount, G. H., D. W. Rusch, J. F. Noxon, J. M. Zawodny, and C. A. Barth, Measurements of stratospheric NO_2 from the solar mesosphere explorer satellite, 1. An overview of the results, *J. Geophys. Res.*, *89*, 1327-1340, 1984.

Moxim, W. J., and J. D. Mahlman, Evaluation of the various total ozone sampling networks using the GFDL 3-D tracer model, *J. Geophys. Res.*, *85*, 4527-4539, 1980.

Mozurkewich, M., and S. Benson, Negative activation energies and curved Arrhenius plots. I. Theory of reaction over potential wells, *J. Phys. Chem.*, *88*, 6429-6435, 1984.

Mueller, P. K., and G. M. Hidy, The sulfate regional experiment: Report of findings, *EPRI-EA-1901*, Electric Power Research Institute, Palo Alto, CA, March, 1983.

Muller, C., J. Vercheval, M. Ackerman, C. Lippens, J. Laurent, M. P. Lamaitre, J. Besson, and A. Girard, Observations of middle atmospheric CH_4 and N_2O vertical distributions by the Spacelab 1 grille spectrometer, *Geophys. Res. Lett.*, *12*, 667-670, 1985.

Muller, H. G., Long period meteor wind oscillations, *Phil. Trans. Roy. Soc. London*, *A271*, 585-598, 1972.

Muller, H. G., G. A. Whitehurst, and A. O'Neill, Stratospheric warmings and their effects on the winds in the upper atmosphere during the winter of MAP/WINE 1983-1984, *J. Atmos. Terr. Phys.*, in press, 1985.

Mumma, M. J., J. D. Rogers, T. Kostiuk, D. Deming, J. J. Hillman, and D. Zipoy, Is there any chlorine monoxide in the stratosphere?, *Science*, *221*, 268-271, 1983.

Murad, E., W. Swider, and S. W. Benson, Possible role for metals in stratospheric chlorine chemistry, *Nature*, *289*, 273-275, 1981.

Murakami, T., Equatorial stratospheric waves induced by diabatic heat sources, *J. Atmos. Sci.*, *29*, 1129-1137, 1972.

Murcray, D. G., T. G. Kyle, F. H. Murcray, and W. J. Williams, Nitric acid and nitric oxide in the lower stratosphere, *Nature*, *218*, 78-79, 1968.

Murcray, D. G., A. Goldman, A. Csoeke-Poeckh, F. H. Murcray, W. J. Williams, and R. N. Stocker, Nitric acid distribution in the stratosphere, *J. Geophys. Res.*, *78*, 7033-7038, 1973.

Murcray, D. G., D. B. Barker, J. N. Brooks, A. Goldman, and W. J. Williams, Seasonal and latitudinal variations of the stratospheric concentration of HNO_3, *Geophys. Res. Lett.*, *6*, 223-225, 1975.

Murcray, D. G., A. Goldman, C. M. Bradford, G. R. Cook, J. W. Van Allen, F. S. Bonomo, and F. H. Murcray, Identification of the ν_2 vibration-rotation band of ammonia in ground level solar spectra, *Geophys. Res. Lett.*, *5*, 527-530, 1978.

Murcray, D. G., A. Goldman, F. H. Murcray, F. J. Murcray, and W. J. Williams, Stratospheric distribution of $ClONO_2$, *Geophys. Res. Lett.*, *6*, 857-859, 1979.

Murcray, D. G., F. J. Murcray, A. Goldman, F. H. Murcray, and J. J. Kosters, Balloon-borne remote sensing of stratospheric constituents, *22*, 2629-2640, 1983.

Murcray, D. G., A. Goldman, J. Kosters, R. Zander, W. Evans, N. Louisnard, C. Alamichel, M. Bangham, S. Pollitt, B. Carli, B. Dinelli, S. Piccioli, A. Volboni, W. Traub, and K. Chance, Intercomparison of stratospheric water vapor profiles obtained during the balloon intercomparison campaign, in *Atmospheric Ozone*, edited by C. S. Zerefos and A. Ghazi, pp. 144-148, D. Riedel, Dordrecht, 1985a.

Murcray, D. G., L. S. Rottman, G. A. Vanasse, F. H. Murcray, F. J. Murcray, and A. Goldman, Atmospheric emission spectra from the stratospheric cryogenic interferometer balloon experiment, paper presented at the Ninth colloquium on High Resolution Molecular Spectroscopy, Riccione, Italy, 1985b.

Murcray, D. G., A. Goldman, J. Kosters, R. Zander, W. F. J. Evans, N. Louisnard, D. Alamichel, M. Bangham, S. Pollitt, B. Carli, B. Dinelli, S. Piccioli, A. Volboni, W. Traub, and K. Chance, Intercomparison of stratospheric water vapor profiles obtained during the balloon intercomparison campaign, to be published, 1986.

Murcray, F. J., A. Goldman, D. G. Murcray, G. R. Cook, J. W. Van Allen, and R. D. Blatherwick, Identification of isolated NO lines in balloon-borne infrared solar spectra, *Geophys. Res. Lett.*, *7*, 673-676, 1980.

Murgatroyd, R. J., Recent progress in studies of the stratosphere, *Quart. J. Roy. Meteorol. Soc.*, *108*, 271-312, 1982.

Murgatroyd, R. J., and R. M. Goody, Sources and sinks of radiative energy from 30 to 90 km, *Quart. J. Roy. Meteorol. Soc.*, *84*, 225-234, 1958.

Murgatroyd, R. J., and F. Singleton, Possible meridional circulations in the stratosphere and mesosphere, *Quart. J. Roy. Meteorol. Soc.*, *87*, 125-135, 1961.

Murray, E. R., Remote measurement of gases using discretely tunable infrared lasers, *Opt. Eng.*, *16*, 284-290, 1977.

Myers, R. J. K., J. R. Simpson, R. Wetselaar, and G. T. McKinney, Problems in modelling the environmental aspects of the nitrogen cycle in agro-ecosystems, SCOPE workshop on "Dynamic Aspects of Nitrogen Cycling in the Australian Ecosystems," Aspendale, Vic., Australia, 1979.

Nagata, T., T. Tohmatsu, and T. Ogawa, Sounding rocket measurement of atmospheric ozone density, 1965-1970, *Space Res.*, *11*, 849-855, 1971.

NAS: See National Academy of Sciences.

NASA, Man's impact on the troposphere: Lectures in tropospheric chemistry, *NASA Reference Publication 1022*, edited by J. S. Levine and D. R. Schryer, Hampton, VA, Sept. 1978.

NASA, *The Stratosphere: Present and Future*, *NASA Reference Publication 1049*, edited by R. D. Hudson and E. I. Reed, 432 pp., NASA Goddard, Greenbelt, MD, 1979.

NASA-JPL, Chemical kinetics and photochemical data for use in stratospheric modeling, Evaluation No. 7, NASA Panel for Data Evaluation, *JPL Publication 85-37*, Jet Propulsion Laboratory, Pasadena, CA, 1982.

Nastrom, G. D., B. B. Balsley, and D. A. Carter, Mean meridional winds in the mid- and high-latitude summer mesosphere, *Geophys. Res. Lett.*, *9*, 139-142, 1982.

Nastrom, G. D., W. L. Ecklund, and K. S. Gage, Direct measurements of synoptic scale vertical velocities using clear air radars, *Mon. Weather Rev.*, *113*, 708-718, 1985.

Natarajan, M., L. B. Callis, and J. E. Nealy, Solar UV variability: Effects on stratospheric ozone, trace constituents and thermal structure, *Pure Appl. Geophys.*, *119*, 750-779, 1980/81.

National Academy of Sciences, NAS, *Halocarbons: Effect on Stratospheric Ozone*, National Academy Press, Washington, DC, 1976.

The National plan for stratospheric ozone monitoring and early detection of change, 1981-1986, *FCM-P17-1982*, 79 pp., Federal Coordinator for Meteorological Services and Supporting Research, NOAA, Rockville, MD, 1982.

National Research Council, *Environmental Impact of Stratospheric Flight*, National Academy of Sciences, Washington, DC, 1975.

National Research Council, *Effects on Stratospheric Ozone*, National Academy of Sciences, Washington, DC, 1976.

National Research Council, *Stratospheric Ozone Depletion by Halocarbons: Chemistry and Transport*, National Academy of Sciences, Washington, DC, 1979.

National Research Council, *Protection Against Depletion of Stratospheric Ozone by Chlorofluorocarbons*, Committee on Impacts of Stratospheric Change, 392 pp., National Academy of Sciences, Washington, DC, 1979.

National Research Council, *Changing Climate: Report of the Carbon Dioxide Assessment Committee*, CDAC, 496 pp., National Academy Press, Washington, DC, 1983.

National Research Council, *Causes and Effects of Changes in Stratospheric Ozone: Update 1983*, National Academy Press, Washington, DC, 1984.

National Research Council, *Global Tropospheric Chemistry, A Plan for Action*, National Academy Press, Washington, DC, 1984.

Naudet, J. P., P. Rigaud, and D. Huguenin, Stratospheric NO_2 at night from balloons, *J. Geophys. Res.*, *89*, 2583-2587, 1984.

Naudet, J. P., P. Rigaud, and D. Huguenin, Variabilite temporelle du NO_3 stratospherique, in *Atmospheric Ozone*, edited by C. S. Zerefos and A. Ghazi, pp. 201-205, D. Reidel, Dordrecht, 1985.

Naujokat, B., Long-term variations in the stratosphere of the Northern Hemisphere during the last two sunspot cycles, *J. Geophys. Res.*, *86*, 9811-9816, 1981.

Naujokat, B., An update of the observed QBO of the stratospheric winds over the tropics, *J. Atmos. Sci.*, in press, 1986.

Nava, D. F., J. V. Michael, and L. J. Stief, Rate constant for the reaction of atomic bromine with formaldehyde from 223 to 480K, *J. Phys. Chem.*, *85*, 1896-1899, 1981.

Naylor, D. A., T. A. Clark, and R. T. Boreiko, Determination of stratospheric H_2O and O_3 column densities from balloon altitude far infrared absorption spectra by a curve of growth method, *Infrared Phys.*, *21*, 271-281, 1981.

Naylor, D. A., R. T. Boreiko, T. A Clark, R. J. Emery, B. Fitton, and M. F. Kessler, Atmospheric emission in the 20 μm window from Mauna Kea, *Pub. Astron. Soc. Pacific*, *96*, 167-173, 1984.

Naylor, D. A., J. M. Hoogerdijk, R. T. Boreiko, T. A. Clark, B. Fitton, M. F. Kessler, and R. J. Emery, Observations of 63 micron atomic oxygen emission in the earth's atmosphere from balloon altitudes: Astronomical implications, in press, 1985.

Neckel, H., and D. Labs, Improved data of solar spectral irradiance from 0.33 to 1.25 μm, *Solar Physics*, *74*, 231-249, 1981.

Neckel, H., and D. Labs, The solar radiation between 3300 and 12500 Å, *Solar Physics*, *90*, 205-258, 1984.

Neftel, A., H. Oeschger, J. Schwander, B. Stauffer, and R. Zumbrunn, Ice core measurements give atmospheric CO_2 content during the past 40,000 years, *Nature*, *295*, 220-223, 1982.

Neftel, A., E. Moor, H. Oeschger, and B. Stauffer, Evidence from polar ice cores for the increase in atmospheric CO_2 in the past two centuries, *Nature*, *315*, 45-47, 1985.

Nelson, H. H., L. Pasternack, and J. R. McDonald, Laser-induced excitation and emissions spectra of NO_3, *J. Phys. Chem.*, *87*, 1286-1266, 1983.

Newell, R. E., The general circulation of the atmosphere and its effects on the movement of trace substances, *J. Geophys. Res.*, *68*, 3949-3962, 1963a.

Newell, R. E., The general circulation of the stratosphere above 60 km, *Meteor. Monogr.*, Amer. Meteor. Soc., Boston, *31*, 98-113, 1963b.

Newell, R. E., Further ozone transport calculations and the spring maximum in ozone amount, *Pure Appl. Geophys.*, *59*, 191-206, 1964.

Newell, R. E., and T. G. Dopplick, Questions concerning the possible influence of anthropogenic CO_2 on atmospheric temperature, *J. Appl. Meteor.*, *18*, 822-825, 1979.

Newell, R. E., and S. Gould-Stewart, A stratospheric fountain?, *J. Atmos. Sci.*, *38*, 2789-2796, 1981.

Newell, R. E., J. W. Kidson, D. G. Vincent, and G. J. Boer, *The General Circulation of the Tropical Atmosphere, Vol. I*, MIT Press, Cambridge, MA, 1969.

Newell, R. E., J. W. Kidson, D. G. Vincent, and G. J. Boer, *The General Circulation of the Tropical Atmosphere, Vol. 2*, MIT Press, Cambridge, MA, 1974.

REFERENCES

Newell, R. E., E. P. Condon, and H. G. Reichle, Measurements of CO and CH_4 in the troposphere over Saudi Arabia, India and the Arabian Sea during the 1979 International Summer Monsoon Experiment (MONEX), *J. Geophys. Res.*, *86*, 9833-9838, 1981.

Newman, P. A., M. R. Schoeberl, and R. A. Plumb, A computation of the horizontal mixing coefficients calculated from NMC data, *Geophys. Res. Lett.*, in press, 1986.

Newson, R. L., An experiment with a tropospheric and stratospheric three-dimensional general circulation model, in *Proceedings Third Conference on the Climatic Impact Assessment Program, DOT-TSC-OST-74-15*, edited by A. J. Broderick and T. M. Hard, pp. 461-474, Dept. of Transp., Washington, DC, 1974.

Newton, C. W., and E. Palmen, Kinematic and thermal properties of a large amplitude wave in the westerlies, *Tellus*, *15*, 99-119, 1963.

Newton, C. W., and A. Trevisan, Clinogenesis and frontogenesis in jet stream waves. Part I: Analytical relation, *J. Atmos. Sci.*, *41*, 2717-2734, 1984.

Nicolet, M., On the production of nitric oxide by cosmic rays in the mesosphere and stratosphere, *Planet. Space Sci.*, *23*, 637-649, 1975.

Nicolet, M., The solar spectral irradiance and its action in the atmospheric photodissociation processes, *Planet. Space Sci.*, *29*, 951-974, 1981.

Nicolet, M., The influence of solar radiation on atmospheric chemistry, *Annales Geophysicae*, *1*, 493-502, 1983.

Nicolet, M., On the molecular scattering in the terrestrial atmosphere: An empirical formula for its calculation in the homosphere, *Planet. Space Sci.*, *32*, 1467-1468, 1984a.

Nicolet, M., On the photodissociation of water vapor in the mesophere, *Planet. Space Sci.*, *32*, 871-880, 1984b.

Nicolet, M., Aeronomical aspects of mesospheric photodissociation: Processes resulting from the H Lyman-alpha line, *Planet. Space Sci.*, *33*, 69-80, 1985.

Nicolet, M., and S. Cieslik, The photodissociation of nitric oxide in the mesosphere and stratosphere, *Planet. Space Sci.*, *28*, 105-115, 1980.

Nicolet, M., and W. Peetermans, Atmospheric absorption in the O_2 Schumann-Runge band spectral region and photodissociation rates in the stratosphere and mesosphere, *Planet. Space Sci.*, *28*, 85-103, 1980.

Nicolet, M., R. R. Meier, and D. E. Anderson, Jr., Radiation field in the troposphere and stratosphere. II. Numerical analysis, *Planet. Space Sci.*, *30*, 935-983, 1982.

Niki, H., P. D. Maker, C. M. Savage, and L. P. Breitenbach, Fourier transform IR spectroscopic observation of pernitric acid formed via $HOO + NO_2 \rightarrow HOONO_2$, *Chem. Phys. Lett.*, *45*, 564-566, 1977.

Niki, H., P. D. Maker, C. M. Savage, and L. P. Breitenbach, A fourier transform infrared study of the kinetics and mechanisms for the reaction $HO + CH_3OOH$, *J. Phys. Chem.*, *87*, 2190-2193, 1983.

Niple, E., W. G. Mankin, A. Goldman, D. G. Murcray, and F. J. Murcray, Stratospheric NO_2 and H_2O mixing ratio profiles from high resolution infrared solar spectra using nonlinear least squares, *Geophys. Res. Lett.*, *7*, 489-492, 1980.

Nitta, T., Response of cumulus updraft and downdraft to GATE A/B-scale motion systems, *J. Atmos. Sci.*, *34*, 1163-1186, 1977.

Nordhaus, W. D., and G. W. Yohe, Future paths of energy and carbon dioxide emissions, in *Changing Climate*, pp. 87-153, National Academy of Sciences, Washington, DC, 1983.

North, G. R., R. F. Cahalan and J. A. Coakley, Energy-balance climate models, *Rev. Geophys. Space Phys.*, *19*, 91-122, 1981.

Norton, R. B., and J. F. Noxon, The dependence of stratospheric NO_3 upon latitude and season, *J. Geophys. Res.*, in press, 1985.

Noxon, J. F., Atmospheric nitrogen fixation by lightning, *Geophys. Res. Lett.*, *3*, 463-465, 1976.

Noxon, J. F., Stratospheric NO_2 in the Antarctic winter, *Geophys. Res. Lett.*, *5*, 1021-1022, 1978a.
Noxon, J. F., Tropospheric NO_2, *J. Geophys. Res.*, *83*, 3051-3057, 1978b.
Noxon, J. F., Stratospheric NO_2, 2, Global behavior, *J. Geophys. Res.*, *84*, 5067, 1979.
Noxon, J. F., Tropospheric NO_2 (Correction), *J. Geophys. Res.*, *85*, 4560-4561, 1981a.
Noxon, J. F., NO_x in the mid-Pacific troposphere, *Geophys. Res. Lett.*, *8*, 1223-1226, 1981b.
Noxon, J. F., NO_3 and NO_2 in the mid-Pacific troposphere, *J. Geophys. Res.*, *88*, 11017-11021, 1983.
Noxon, J. F., R. B. Norton, and W. R. Henderson, Observation of atmospheric NO_3, *Geophys. Res. Lett.*, *5*, 675-678, 1978.
Noxon, J. F., E. C. Whipple Jr., and R. S. Hyde, Stratospheric NO_2 1. Observational method and behavior at mid-latitude, *J. Geophys. Res.*, *84*, 5047-5065, 1979a.
Noxon, J. F., E. Marovich, and R. B. Norton, Effect of a major warming upon stratospheric NO_2, *J. Geophys. Res.*, *84*, 7883, 1979b.
Noxon, J. F., R. B. Norton, and E. Marovich, NO_3 in the troposphere, *Geophys. Res. Lett.*, *7*, 125-128, 1980.
Noxon, J. F., W. R. Henderson, and R. B. Norton, Stratospheric NO_2, 3. The effects of large scale horizontal transport, *J. Geophys. Res.*, 88, 5240-5248, 1983.
NRC: See National Research Council.
Oeschger, H., The contribution of ice core studies to the understanding of environmental processes, in *Green Ice Core: Geophysics, Geochemistry, and the Environment, American Geophysical Union Monograph No. 33*, edited by C. C. Langway, H. Oeschger, and W. Dansgaard, pp. 9-17, *33*, 1985.
Oeschger, H., U. Siegenthaler, U. Schotterer and A. Gugelmann, A box diffusion model to study the carbon dioxide exchange in nature, *Tellus*, *27*, 168-192, 1975.
Ogawa, M., Absorption cross sections of O_2 and CO_2 continua in the Schumann and far-UV regions, *J. Chem. Phys.*, *54*, 2550-2556, 1971.
Ogawa, T., K. Shibasaki, and K. Suzuki, Balloon observation of the stratospheric NO_2 profile by visible absorption spectroscopy, *J. Meteorol. Soc. Japan*, *59*, 410-416, 1981.
Oltmans, S. J., and J. London, The quasi-biennial oscillation in atmospheric ozone, *J. Geophys. Res.*, *87*, 8981-8989, 1982.
O'Neill, A., and C. Youngblut, Stratospheric warmings diagnosed using the transformed Eulerian-mean equations and the effect of the mean state on wave propagation, *J. Atmos. Sci.*, *39*, 1370-1386, 1982.
O'Neill, A., R. L. Newson, and R. J. Murgatroyd, An analysis of the large-scale features of the upper troposphere and the stratosphere in a global, three-dimensional, general circulation model, *Quart. J. Roy. Meteorol. Soc.*, *108*, 25-53, 1982.
Ongstad, A. P., and J. W. Birks, Studies of reactions of importance in the stratosphere. V. Rate constants for the reactions $O + NO_2 \rightarrow NO + O_2$ and $O + ClO \rightarrow Cl + O_2$ at 298K, *J. Chem. Phys.*, *81*, 3922-3930, 1984.
Oort, A. H., Global Atmospheric Statistics, 1958-1973, *NOAA Professional Paper*, *14*, 1983.
Ooyama, K., On the stability of the baroclinic circular vortex: A sufficient criterion for instability, *J. Atmos. Sci.*, *23*, 43-53, 1966.
Oran, E. S., P. S. Julienne, and D. F. Strobel, The aeronomy of odd nitrogen in the thermosphere, *J. Geophys. Res.*, *80*, 3068-3076, 1975.
Orton, G. S., and A. G. Robiette, A line parameter list for the ν_2 and ν_4 bands of $^{12}CH_4$ and $^{13}CH_4$, extended to $J^1=25$ and its application to planetary atmospheres, *J. Quant. Spectrosc. Radiat. Transfer*, *24*, 81-95, 1980.
Ostlund, H. G., H. G. Dorsey and R. Brescher, GEOSECS Atlantic radiocarbon and tritium results, *Report No. 5*, Univ. Miami Tritium Laboratory Data, 1976.

REFERENCES

Owens, A. J., J. M. Steed, D. L. Filkin, C. Miller, and J. P. Jesson, The potential effects of increased methane on atmosphere ozone, *Geophys. Res. Lett.*, *9*, 1105-1108, 1982a.

Owens, A. J., J. M. Steed, C. Miller, D. L. Fillim, and J. P. Jesson, The atmospheric lifetime of CFC-11 and CFC-12, *Geophys. Res. Lett.*, *9*, 700-703, 1982b.

Owens, A. J., C. H. Hales, D. L. Filkin, C. Miller, and M. McFarland, Multiple scenario ozone change calculations: The subtractive perturbation approach, in *Atmospheric Ozone*, edited by C. S. Zerefos and A. Ghazi, pp. 82-86, D. Reidel, Dordrecht, 1985a.

Owens, A. J., C. H. Hales, D. L. Filken, C. Miller, J. M. Steed, and J. P. Jesson, A coupled one-dimensional radiative-convective, chemistry-transport model of the atmosphere 1. Model structure and steady-state perturbation calculations, *J. Geophys. Res.*, *90*, 2283-2311, 1985b.

Paetzold, H. K., New experimental and theoretical investigation on the atmospheric ozone layer, *J. Atmos. Terr. Phys.*, *7*, 128-140, 1955.

Pallister, R. C., and A. F. Tuck, The diurnal variation of ozone in the upper stratosphere as a test of photochemical theory, *Quart. J. Roy. Meteorol. Soc.*, *109*, 271-284, 1983.

Palmen, E., and C. W. Newton, *Atmospheric Circulation Systems*, 603 pp., Academic Press, New York, 1969.

Palmer, T. N., Diagnostic study of wavenumber-2 stratospheric sudden warming in a transformed Eulerian mean formalism, *J. Atmos. Sci.*, *38*, 844-855, 1981a.

Palmer, T. N., Aspects of stratospheric sudden warmings studied from a transformed Eulerian-mean viewpoint, *J. Geophys. Res.*, *86*, 9679-9687, 1981b.

Palmer, T., and C. Hsu, Stratospheric sudden coolings and the role of nonlinear wave interactions in preconditioning the circumpolar flow, *J. Atmos. Sci.*, *40*, 909-928, 1983.

Park, J. H., D. J. W. Kendall, and H. L. Buijs, Stratospheric HF mixing ratio profiles in the Northern and Southern Hemispheres, *J. Geophys. Res.*, *89*, 11645-11653, 1984.

Parker, D. E., and J. L. Brownscombe, Stratospheric warming following the El Chichon volcanic eruption, *Nature*, *301*, 406-408, 1983.

Parrish, A., R. L. De Zafra, P. M. Solomon, J. W. Barrett, and E. R. Carlson, Chlorine oxide in the stratospheric ozone layer: Ground-based detection and measurement, *Science*, *211*, 1158-1161, 1981.

Patel, C. K. N., E. G. Burkhardt, and C. A. Lambert, Spectroscopic measurements of stratospheric nitric oxide and water vapor, *Science*, *184*, 1173-1176, 1974.

Patrick, R., J. R. Barker, and D. M. Golden, Computational study of the HO_2 + HO_2 and DO_2 + DO_2 reactions, *J. Phys. Chem.*, *88*, 128-136, 1984.

Patterson, E. M., B. T. Marshall and K. A. Rahn, Radiative properties of the Arctic aerosol, *Atmos. Environ.*, *16*, 2967-2977, 1982.

Paur, R. J., and A. M. Bass, The ultraviolet cross sections of ozone II. Results and temperature dependence, in *Atmospheric Ozone*, edited by C. S. Zerefos and A. Ghazi, pp. 611-616, D. Reidel, Dordrecht, 1985.

Payne, W. J., *Denitrification*, 214 pp., Wiley, New York, 1983.

Pearman, G. I., P. Hyson, and P. J. Fraser, The global distribution of atmospheric carbon dioxide: I. Aspects of observation and modelling, *J. Geophys. Res.*, *88*, 3581-3590, 1983.

Pearman, G. I., D. Etheridge, F. deSilva, and P. J. Fraser, Evidence of changing concentrations of atmospheric CO_2, N_2O and CH_4 from air bubbles in antarctica, *Nature*, 1985.

Pearman, G. I., and P. Hyson, Activities of the global biosphere as reflected in atmospheric CO_2 records, *J. Geophys. Res.*, *85*, 4457-4467, 1980.

Pearson, Jr., R., and D. H. Stedman, Instrumentation for fast response ozone measurements from aircraft, *Atmos. Techn.*, National Center for Atmospheric Research, Boulder, CO, *12*, 51-55, 1980.

Pelon, J., and G. Megie, Ozone monitoring in the troposphere and lower stratosphere: Evaluation and operation of a ground based lidar station, *Geoph. Res.*, *87*, 4947-4955, 1982a.

Pelon, J., and G. Megie, Ozone vertical distribution and total content using a ground-based active remote sensing technique, *Nature*, *299*, 137-139, 1982b.

Pelon, J., and G. Megie, Ozone monitoring in the troposphere and lower stratosphere: Evaluation and operation of a ground-based lidar station, *J. Geophys. Res.*, *87*, 4947-4955, 1982c.

Pelon, J., and G. Megie, Lidar measurements of the vertical ozone distribution during the June 1981 intercomparison campaign GAP/OHP, *Planet. Space Sci.*, *31*, 717-721, 1983.

Penkett, S. A., The application of analytical techniques to the understanding of chemical processes occurring in the atmosphere, *Toxicol. Environ. Chem.*, *3*, 291-321, 1981.

Penkett, S. A., R. G. Derwent, P. Fabian, R. Borchers, and U. Schmidt, Methyl chloride in the stratosphere, *Nature*, *283*, 58-60, 1980.

Penkett, S. A., N. J. D. Prosser, R. A. Rasmussen, and M. A. K. Khalil, Atmospheric measurements of CF_4 and other fluorocarbons containing the CF_3 grouping, *J. Geophys. Res.*, *86*, 5172-5178, 1981.

Penn, S., A case study using ozone to determine structure and air motions at the tropopause, *J. Appl. Meteorol.*, *3*, 581-586, 1964.

Perner, D., D. H. Ehhalt, H. W. Paetz, U. Platt, E. P. Roeth, and A. Volz, OH radicals in the lower troposphere, *Geophys. Res. Lett.*, *3*, 466-468, 1976.

Perry, R., Kinetics of the reactions of NCO radicals with H_2, NO and O_2 using laser photolysis-laser induced fluorescence, paper presented at 16th Informal Conference on Photochemistry, *Abstract T-12*, Cambridge, MA, August, 1984.

Perry, R. A., R. Atkinson, and J. N. Pitts, Jr., Kinetics and mechanism of the gas phase reactions of OH radicals with aromatic hydrocarbons over the temperature range 296 - 435K, *J. Phys. Chem.*, *82*, 296-304, 1977.

Philbrick, C. R., Measurements of structural features in profiles of mesospheric density, in *Handbook for MAP*, *Vol. 2*. edited by S. K. Avery, pp. 333-340, SCOSTEP Secretariat, Univ. of Illinois, Urbana, 1981.

Pick, D. R., and J. L. Brownscombe, Early results based on the stratospheric channels of TOVS on the TIROS-N series of operational satellites, *Adv. in Space Res.*, *1*, 247-260, 1981.

Pickett, H. M., D. E. Brinza, and E. A. Cohen, Pressure broadening of ClO by nitrogen, *J. Geophys. Res.*, *86*, 7279-7282, 1981.

Pierotti, D., and R. A. Rasmussen, Combustion as a source of nitrous oxide in the atmosphere, *Geophys. Res. Lett.*, *3*, 265-267, 1976.

Pierotti, D., and R. A. Rasmussen, The atmosphere distribution of nitrous oxide, *J. Geophys. Res.*, *82*, 5823-5832, 1977.

Pirre, M., P. Rigaud, and D. Huguenin, New in-situ measurements of the absorption cross section of O_2 in the Herzberg continuum, *Geophys. Res. Lett.*, *11*, 1199-1202, 1984.

Pirre, M., P. Rigaud, and D. Huguenin, Mesure de l'absorption par la haute atmosphere dans le domame de hugeus donde de la fenetre atmosphenigue an voisinage de 200 nm, in *Atmospheric Ozone*, edited by C. S. Zerefos and A. Ghazi, pp. 630-634, G. Reidel, Dordrecht, 1985.

Pitari, G., and G. Visconti, Two-dimensional tracer transport: Derivation of residual mean circulation and eddy transport tensor from a 3-D model data set, *J. Geophys. Res.*, *90*, 8019-8032, 1985.

Pittock, A. B., Climatology of the vertical distribution of ozone over Aspendale, *Quart. J. Roy. Meteorol. Soc.*, *103*, 575-584, 1977.

Planet, W. G., D. S. Crosby, J. H. Lienesch, and M. L. Hill, Determination of total ozone amounts from TIROS radiance measurements, *J. Clim. and Appl. Meteor.*, *23*, 308-316, 1984.

Platt, C. M. R., Cirrus clouds in tropical Australia, *Weatherwise*, *36*, 132-133, 1983.

Platt, U., and D. Perner, Direct measurements of atmospheric CH_2O, HNO_2, O_3, NO_2, and SO_2 by differential optical absorption in the near UV, *J. Geophys. Res.*, *85*, 7453-7458, 1980.

Platt, U., D. Perner, G. W. Harris, A. M. Winer, and J. N. Pitts, Jr., Observations of nitrous acid in an urban atmosphere by differential optical absorption, *Nature*, *285*, 312-314, 1980a.

Platt, U., D. Perner, A. M. Winer, G. W. Harris, and J. N. Pitts, Jr., Detection of NO_3 in the polluted troposphere by differential optical absorption, *Geophys. Res. Lett.*, *7*, 89-92, 1980b.

Platt, U., D. Perner, J. Schroder, C. Kessler, and A. Toennissen, The diurnal variation of NO_3, *J. Geophys. Res.*, *86*, 11965-11970, 1981.

Platt, U. F., A. M. Winer, H. W. Biermann, R. Atkinson, and J. H. Pitts, Jr., Measurement of nitrate radical concentrations in continental air, *Environ. Sci. Technol.*, *18*, 365-369, 1984.

Plumb, R. A., The interaction of two internal waves with the mean flow: Implications for the theory of the quasi-biennial oscillation, *J. Atmos. Sci.*, *34*, 1847-1858, 1977.

Plumb, R. A., Eddy fluxes of conserved quantities by small-amplitude waves, *J. Atmos. Sci.*, *36*, 1699-1704, 1979.

Plumb, R. A., Instability of the distorted polar night vortex: A theory of stratospheric warmings, *J. Atmos. Sci.*, *38*, 2514-2531, 1981.

Plumb, R. A., The circulation of the middle atmosphere, *Aus. Meteorol. Mag.*, *30*, 107-121, 1982.

Plumb, R. A., Baroclinic instability of the summer mesosphere: A mechanism for the quasi-two-day-wave?, *J. Atmos. Sci.*, *40*, 262-270, 1983a.

Plumb, R. A., A new look at the energy cycle, *J. Atmos. Sci.*, *40*, 1669-1688, 1983b.

Plumb, R. A., The quasi-biennial oscillation, in *Dynamics of the Middle Atmosphere*, edited by J. R. Holton and T. Matsuno, pp. 217-251, Terrapub, Tokyo, 1984.

Plumb, R. A., and R. C. Bell, A model of the quasi-bienniel oscillation on an equatorial beta-plane, *Quart. J. Roy. Meteorol. Soc.*, *108*, 335-352, 1982.

Plumb, R. A., and J. D. Mahlman, The zonally-averaged transport characteristics of the GFDL general circulation/tracer model, *J. Atmos. Sci.*, in press, 1986.

Plumb, R. A., and A. D. McEwan, The instability of a forced standing wave in a viscous stratified fluid: A laboratory analogue of the quasi-biennial oscillation, *J. Atmos. Sci.*, *35*, 1827-1839, 1978.

Pollack, J. B., and T. P. Ackerman, Possible effects of the El Chichon volcanic cloud on the radiation budget of the northern tropics, *Geophys. Res. Lett.*, *10*, 1057-1060, 1983.

Pollack, J. B., and C. P. McKay, The impact of polar stratospheric clouds on the heating rates of the winter polar stratosphere, *J. Atmos. Sci.*, *42*, 245-262, 1985.

Pollitt, S., M. Coffey, W. Evans, A. Goldman, J. J. Kosters, N. Louisnard, W. G. Mankin, D. G. Murcray, and W. J. Williams, Intercomparative measurements of stratospheric nitric acid, in *Atmospheric Ozone*, edited by C. S. Zerefos and A. Ghazi, pp. 151-156, D. Reidel, Dordrecht, 1985.

Pollitt, S., D. G. Murcray, A. Goldman, J. J. Kosters, W. J. Williams, N. Louisnard, W. F. J. Evans, M. Coffey, W. G. Mankin, R. Zander, D. W. Johnson, G. Stokes, and R. K. Seals, BIC nitric acid intercomparison, to be published, 1986.

Pollock, W., L. E. Heidt, R. Lueb, and D. H. Ehhalt, Measurement of stratospheric water vapor by cryogenic collection, *J. Geophys. Res.*, *85*, 5555-5568, 1980.

Pommereau, J. P., Observation of NO_2 diurnal variation in the stratosphere, *Geophys. Res. Lett.*, *9*, 850-853, 1982.

Porch, W. M., and M. C. MacCracken, Parametric study to the effects of Arctic soot on solar radiation, *Atmos. Environ.*, *16*, 1365-1371, 1982.

Posey, J., J. Sherwell, and M. Kaufman, Kinetics of the reactions of atomic bromine with HO_2 and H_2O_2, *Chem. Phys. Lett.*, *77*, 476-479, 1981.

Poulet, G., G. Laverdet, and G. Le Bras, Discharge flow-mass spectrometric determination of the rate coefficient for the reactions of formaldehyde with bromine atoms and chlorine atoms, *J. Phys. Chem.*, *85*, 1891-1895, 1981.

Poulet, G., G. Laverdet, and G. Le Bras, Kinetics of the reactions of atomic bromine with HO_2 and HCO at 298K, *J. Chem. Phys.*, *80*, 1922-1928, 1984.

Poulet, G., G. Laverdet, and G. LeBras, Rate constant and branching ratio for the reaction of OH with ClO, *J. Phys. Chem.*, in press, 1985.

Poynter, R. L., and H. M. Pickett, Submillimeter, millimeter, and microwave spectral line catalogue, *JPL Publication 80-23, Revision 1*, 151 pp., Jet Propulsion Laboratory, California Institute of Technology, Pasadena, CA, 1981.

Poynter, R. L., and H. M. Pickett, Submillimeter, millimeter, and microwave spectral line catalogue, *JPL Publication 80-23, Revision 2*, 171 pp., Jet Propulsion Laboratory, California Institute of Technology, Pasadena, CA, 1984.

Prabhakara, C., Effects of non-photochemical processes on the meridional distribution and total amount of ozone in the atmosphere, *Mon. Weather Rev.*, *91*, 411-431, 1963.

Prasad, S. S., Possible existence and chemistry of $ClO.O_2$ in the stratosphere, *Nature*, *285*, 152-154, 1980.

Prata, A., The 4-day wave, *J. Atmos. Sci.*, *41*, 150-155, 1984.

Prather, M. J., Ozone in the upper stratosphere and mesosphere, *J. Geophys. Res.*, *86*, 5325-5338, 1981.

Prather, M. J., Continental sources of halocarbons and nitrous oxide, *Nature*, *317*, 221-225, 1985.

Prather, M. J., M. B. McElroy, and S. C. Wofsy, Reductions in ozone at high concentrations of stratospheric halogens, *Nature*, *312*, 227-231, 1984.

Prinn, R. G., P. G. Simmonds, R. A. Rasmussen, R. D. Rosen, F. N. Alyea, C. A. Cardelino, A. J. Crawford, D. M. Cunnold, P. J. Fraser, and J. E. Lovelock, The atmospheric lifetime experiment, 1, Introduction, instrumentation and overview, *J. Geophys. Res.*, *88*, 8353-8367, 1983a.

Prinn, R. G., R. A. Rasmussen, P. G. Simmonds, F. N. Alyea, D. M. Cunnold, B. C. Lane, C. A. Cardelino, and A. J. Crawford, The atmospheric lifetime experiments, 5, Results for CH_3CCl_3 based on three years of data, *J. Geophys. Res.*, *88*, 8415-8426, 1983b.

Pugh, L. A., and K. N. Rao, Intensities from infrared spectra, *Mol. Spectros., Mod. Res.*, *2*, 165-225, 1976.

Pyle, J. A., A calculation of the possible depletion of ozone by chlorofluorocarbons using a two-dimensional model, *Pure Appl. Geophys.*, *118*, 355-377, 1980.

Pyle, J. A., and C. F. Rogers, A modified diabatic circulation model for stratospheric tracer transport, *Nature*, *287*, 711-714, 1980a.

Pyle, J. A., and C. F. Rogers, Stratospheric transport by stationary planetary waves: The importance of chemical processes, *Quart. J. Roy. Meteorol. Soc.*, *106*, 421-446, 1980b.

Pyle, J. A., and C. F. Rogers, Modelling tracer budgets in the stratosphere, *Quart. J. Roy. Meteorol. Soc.*, *110*, 1097-1106, 1984.

Pyle, J. A., and A. M. Zavody, The derivation of near-global fields of hydrogen containing radical concentrations from satellite data sets, *Quart. J. Roy. Meteorol. Soc.*, in press, 1985a.

Pyle, J. A., and A. M. Zavody, The variability of stratospheric radicals, paper presented at the 5th General Assembly, International Association of Geomagnetism and Aeronomy, Prague, 5-17 August 1985b.

Pyle, J. A., A. M. Zavody, J. E. Harries, and P. H. Moffat, Derivation of OH concentration from satellite infrared measurements of NO_2 and HNO_3, *Nature*, *305*, 690-692, 1983.

Quinn, T. H., K. A. Wolf, W. E. Mooz, J. K. Hammitt, T. W. Chesnutt and S. Sarma, Projected use, emissions, and banks of potential ozone depleting substances, *N-2282-EPA*, Rand Corp., Santa Monica, CA, 1985.

Quiroz, R. S., Stratospheric temperatures during solar cycle 20, *J. Geophys. Res.*, *84*, 2415-2420, 1979a.

Quiroz, R. S., Tropospheric-stratospheric interaction in the major warming event of January-February 1979, *Geophys. Res. Lett.*, *6*, 645-648, 1979b.

REFERENCES

Quiroz, R. S., The isolation of stratospheric temperature change due to the El Chichon volcanic signals, *J. Geophys. Res.*, *88*, 6773-6780, 1983a.

Quiroz, R. S., The climate of the "El Nino" winter of 1982-83. A season of extraordinary climatic anomalies, *Mon. Weather Rev.*, *111*, 1685-1706, 1983b.

Quiroz, R. S., and M. E. Gelman, An evaluation of temperature profiles from falling sphere soundings, *J. Geophys. Res.*, *81*, 406-412, 1976.

Quiroz, R. S., A. J. Miller, and R. M. Nagatani, A comparison of observed and simulated properties of sudden stratospheric warmings, *J. Atmos. Sci.*, *32*, 1723-1736, 1975.

Ramanathan, V., Greenhouse effect due to chlorofluorocarbons: Climatic implications, *Science*, *190*, 50-52, 1975.

Ramanathan, V., Radiative transfer within the Earth's troposphere and stratosphere: A simplified radiative-convective model, *J. Atmos. Sci.*, *33*, 1330-1346, 1976.

Ramanathan, V., Climatic effects of anthropogenic trace gases, in *Energy/Climate Interactions*, pp. 269-280, D. Reidel, Dordrecht, 1980.

Ramanathan, V., The role of ocean-atmosphere interactions in the CO_2 climate problem, *J. Atmos. Sci.*, *38*, 918-930, 1981.

Ramanathan, V., and J. A. Coakley, Jr., Climate modeling through radiative-convective models, *Rev. Geophys. Space Phys.*, *16*, 465-490, 1978.

Ramanathan, V., and R. E. Dickinson, The role of stratospheric ozone in the zonal and seasonal radiative energy balance of the earth-troposphere system, *J. Atmos. Sci.*, *36*, 1084-1104, 1979.

Ramanathan, V., and P. Downey, A non-isothermal emissivity and absorptivity formulation for water vapor, *J. Geophys. Res.*, *91*, in press, 1986.

Ramanathan, V., L. B. Callis and R. E. Boughner, Sensitivity of atmospheric and surface temperature to perturbations in the stratospheric concentration of ozone and nitrogen dioxide, *J. Atmos. Sci.*, *33*, 1092-1112, 1976.

Ramanathan, V., M. S. Lian and R. D. Cess, Increased atmospheric CO_2: Zonal and seasonal estimates of the effect on the radiation energy balance and surface temperature, *J. Geophys. Res.*, *84*, 4949-4958, 1979.

Ramanathan, V., E. J. Pitcher, R. C. Malone and M. L. Blackmon, The response of a spectral general circulation model to refinements in radiative processes, *J. Atmos. Sci.*, *40*, 605-630, 1983.

Ramanathan, V., R. J. Cicerone, H. B. Singh and J. T. Kiehl, Trace gas trends and their potential role in climate change, *J. Geophys. Res.*, *90*, 5547-5566, 1985.

Ramaswamy, V., and A. Detwiler, Interdependence of radiation and microphysics in cirrus clouds, *J. Atmos. Sci.*, *43*, in press, 1985.

Ramaswamy, V., and J. T. Kiehl, Sensitivities of the radiative forcing due to large loadings of smoke and dust aerosols, *J. Geophys. Res.*, *90*, 5597-5613, 1985.

Randal, W. J., and J. L. Stanford, Structure of medium-scale atmospheric waves in the Southern Hemisphere summer, *J. Atmos. Sci.*, *40*, 2312-2318, 1983.

Randhawa, J. S., Ozonesonde for rocket flight, *Nature*, *213*, 53-54, 1967.

Rao, M. S. V., Retrieval of worldwide precipitation and allied parameters from satellite microwave observations, in *Advances in Geophysics*, *Vol. 26*, edited by B. Saltzman, pp. 1238-1336, Academic Press, New York, 1984.

Rao (Vupputuri), R. K., Numerical experiment on the steady state meridional structure and ozone distribution in the stratosphere, *Mon. Weather Rev.*, *101*, 510-527, 1973.

Raper, O. F., C. B. Farmer, R. A. Toth, and B. D. Robbins, The vertical distribution of HCl in the stratosphere, *Geophys. Res. Lett.*, *4*, 531-534, 1977.

Rasmussen, R. A., and M. A. K. Khalil, Atmospheric halocarbons: Measurements and analyses of selected trace gases, in *Proceedings of the NATO Advanced Study Institute on Atmospheric Ozone: Its Variation and Human Influences, Rep. FAA-EE-80-20*, edited by A. C. Aikin, pp. 209-231, DOT, FAA, Washington, DC, 1980.

Rasmussen, R. A., and M. A. K. Khalil, Global atmospheric distribution and trend of methylchloroform (CH_3CCl_3), *Geophys. Res. Lett.*, *8*, 1005-1007, 1981a.

Rasmussen, R. A., and M. A. K. Khalil, Atmospheric methane (CH_4); Trends and seasonal cycles, *J. Geophys. Res.*, *86*, 9826-9832, 1981b.

Rasmussen, R. A., and M. A. K. Khalil, Differences in the concentrations of atmospheric trace gases in and above tropical boundary layer, *Pure Appl. Geophys.*, *119*, 990-997, 1981c.

Rasmussen, R. A., and M. A. K. Khalil, Increase in the concentration of atmospheric methane, *Atmos. Environ.*, *15*, 883-886, 1981d.

Rasmussen, R. A., and M. A. K. Khalil, Latitudinal distributions of trace gases in and above the boundary layer, *Chemosphere*, *11*, 227-235, 1982.

Rasmussen, R. A., and M. A. K. Khalil, Natural and anthropogenic trace gases in the lower troposphere of the Arctic, Dept. of Environ. Sci., Beaverton, OR, 1983a.

Rasmussen, R. A., and M. A. K. Khalil, Atmospheric fluorocarbons and methyl chloroform at the South Pole, *1982 Annual Issue of the Antarctic Journal of the United States*, *17*, 203-205, 1983b.

Rasmussen, R. A., and M. A. K. Khalil, Global production of methane by termites, *Nature*, *301*, 700-702, 1983c.

Rasmussen, R. A., and M. A. K. Khalil, Natural and anthropogenic trace gases in the lower troposphere in the arctic, *Chemosphere*, *12*, 371-375, 1983d.

Rasmussen, R. A., and M. A. K. Khalil, Trace gases at Point Barrow and Arctic haze, in *Geophysical Monitoring for Climatic Change Annual Report 10*, edited by B. A. Bodhaine and J. M. Harris, NOAA/ERL, U.S. Dept. of Commerce, Boulder, CO, 1983e.

Rasmussen, R. A., and M. A. K. Khalil, Rare trace gases at the South Pole: $CHClF_2$, CH_3I, $CHCl_3$ and SF_6, 1984a.

Rasmussen, R. A., and M. A. K. Khalil, Atmospheric methane in recent and ancient atmospheres: Concentrations, trends and interhemispheric gradients, *J. Geophys. Res.*, *89*, 11599-11605, 1984b.

Rasmussen, R. A., and M. A. K. Khalil, Gaseous bromine in the Arctic and Arctic haze, *Geophys. Res. Lett.*, *11*, 433-436, 1984c.

Rasmussen, R. A., S. A. Penkett, and N. Prosser, Measurements of carbontetrafluoride in the atmosphere, *Nature*, *277*, 549-550, 1979.

Rasmussen, R. A., L. E. Rasmussen, M. A. K. Khalil, and R. W. Dalluge, Concentration distribution of methyl chloride in the atmosphere, *J. Geophys. Res.*, *85*, 7350-7356, 1980.

Rasmussen, R. A., M. A. K. Khalil, and R. W. Dalluge, Atmospheric trace gases in Antarctica, *Science*, *211*, 285-287, 1981.

Rasmussen, R. A., M. A. K. Khalil, A. J. Crawford, and P. J. Fraser, Natural and anthropogenic trace gases in the Southern Hemisphere, *Geophys. Res. Lett.*, *9*, 704-707, 1982a.

Rasmussen, R. A., M. A. K. Khalil, R. Gunawardena, and S. D. Hoyt, Atmospheric methyl iodide (CH_3I), *J. Geophys. Res.*, *87*, 3086-3090, 1982b.

Rasmussen, R. A., M. A. K. Khalil, and R. J. Fox, Altitudinal and temporal variations of hydrocarbons and other gaseous tracers of Arctic haze, *Geophys. Res. Lett.*, *10*, 144-147, 1983.

Ravishankara, A. R., and P. H. Wine, Absorption cross sections for HNO_3 between 565 and 673 nm, *Chemical Physics Letters*, *101*, 73-78, 1983.

Ravishankara, A. R., P. H. Wine, A. Torabi, C. A. Smith, and R. Wells, Photodissociation of N_2O_5, *J. Phys. Chem.*, in press, 1985.

REFERENCES

Rayez, J. C., B. Veyret, and R. Lesclaux, Thermodynamical and structural data of free radicals of atmospheric interest calculated by MNDO-CI, paper presented at XVth Int. Symp. on Free Radicals, Lauzelle-Ottignies, Belgium, 1983.

Raynaud, D., and J. M. Barnola, An Antarctica ice core reveals atmospheric CO_2 variations over the past few centuries, *Nature*, *315*, 309-311, 1985.

Reagan, J. B., R. E. Meyerott, R. W. Nightingale, R. C. Gunton, R. G. Johnson, J. E. Evans, W. L. Imhof, D. F. Heath, and A. J. Krueger, Effects of the August 1972 solar particle events on stratospheric ozone, *J. Geophys. Res.*, *86*, 1473-1494, 1981.

Reber, C. A., Upper Atmosphere Research Satellite (UARS) Mission, *NASA Goddard Space Flight Center Publication 430-1003-001*, NASA Goddard Space Flight Center, Greenbelt, MD, 1985.

Reck, R. A., Stratospheric ozone effects on temperature, *Science*, *192*, 557-559, 1976.

Reck, R. A., Atmospheric temperature calculated for ozone depletion, *Nature*, *263*, 116-117, 1976.

Reck, R. A., Thermal effect of stratospheric ozone depletion at 85° latitude as influenced by airborne particles, *Geophys. Res. Lett.*, *5*, 361-364, 1978.

Reck, R. A., and D. L. Fry, The direct effect of chlorofluoromethanes on the atmospheric surface temperature, *Atmos. Environ.*, *12*, 2501-2503, 1978.

Reck, R. A., and J. R. Hummel, Influence of aerosol optical properties on surface temperatures computed with a radiative-convective model, *Atmos. Environ.*, *15*, 1727-1731, 1981.

Reed, R. J., The role of vertical motions in ozone-weather relationships, *J. Meteorol.*, *7*, 263-267, 1950.

Reed, R. J., A study of a characteristic type of upper level frontogenesis, *J. Meteorol.*, *12*, 226-237, 1955.

Reed, R. J., The structure and dynamics of the 26-month oscillation, paper presented at 40th anniv. meeting of the Amer. Met. Soc., Boston, 1960.

Reed, R. J., Evidence of geostrophic motion in the equatorial stratosphere, *Quart. J. Roy. Meteorol. Soc.*, *88*, 324-327, 1962.

Reed, R. J. A tentative model of the 26-month oscillation in tropical latitudes, *Quart. J. Roy. Meteorol. Soc.*, *90*, 441-466, 1964.

Reed, R. J., The quasi-biennial oscillation of the atmosphere between 30 and 50 km over Ascension Island, *J. Atmos. Sci.*, *22*, 331-333, 1965.

Reed, R. J., Zonal wind behaviour in the equatorial stratosphere and lower mesosphere, *J. Geophys. Res.*, *71*, 4223-4233, 1966.

Reed, R. J., and E. F. Danielson, Fronts in the vicinity of the tropopause, *Arch. Met. Geophys. Bioklim.*, *11*, 1-17, 1959.

Reed, R. J., and K. E. German, A contribution to the problem of stratospheric diffusion by large-scale mixing, *Mon. Weather Rev.*, *93*, 313-321, 1965.

Reed, R. J., and C. L. Vlcek, The annual temperature variation in the lower tropical stratosphere, *J. Atmos. Sci.*, *26*, 163-167, 1969.

Reed, R. J., D. C. Norquist, and E. F. Recker, The structure and properties of African wave disturbances as observed during Phase III of GATE, *Mon. Weather Rev.*, *105*, 317-333, 1977.

Regener, V. H., Vertical flux of atmospheric ozone, *J. Geophys. Res.*, *62*, 221-228, 1957.

Regener, V. H., Measurement of ozone with the chemiluminescent method, *J. Geophys. Res.*, *69*, 3795-3800, 1964.

Reid, G. C., and K. S. Gage, A relation between the height of the tropical tropopause and the global angular momentum of the atmosphere, *Geophys. Res. Lett.*, *11*, 840-842, 1984.

Reinsel, G., G. C. Tiao, M. N. Wang, R. Lewis, and D. Nychka, Statistical analysis of stratospheric ozone data for the detection of trend, *Atmos. Environ.*, *15*, 1569-1577, 1981.

Reinsel, G., G. C. Tiao, R. Lewis, and M. Bobkoski, Analysis of upper stratospheric ozone profile data from the ground-based Umkehr method and the Nimbus-4 BUV satellite experiment, *J. Geophys. Res.*, *88*, 5393-5403, 1983.

Reinsel, G. C., G. C. Tiao, J. L. De Luisi, C. L. Mateer, A. J. Miller, and J. E. Frederick, Analysis of upper stratospheric Umkehr ozone profile data for trends and the effects of stratospheric aerosols, *J. Geophys. Res.*, *89*, 4833-4840, 1984.

Reiter, E. R., Atmospheric transport processes. Part 1: Energy transfers and transformation, *USAEC Report TID-24868*, 253 pp., Colorado State Univ., Fort Collins, CO, 1968.

Reiter, E. R., Atmospheric transport processes. Part 2: Chemical tracers, *USAEC Report TID-25314*, 382 pp., Colorado State Univ., Fort Collins, CO, 1971.

Reiter, E. R., Atmospheric transport processes. Part 3: Hydrodynamic tracers, *USAEC Report TID-25731*, 212 pp., Colorado State Univ., Fort Collins, CO, 1972.

Reiter, E. R., Stratospheric-tropospheric exchange processes, *Rev. Geophys. Space Phys.*, *13*, 459-474, 1975.

Reiter, E. R., Tropospheric-stratospheric transport processes: Indications of their interannual variability, paper presented at WMO Symp. on Long Range Transport of Pollutants and its Relation to General Circulation including Stratosphere/Troposphere Exchange Processes, *WMO No. 538*, pp. 393-400, 1979.

Reiter, E. R., and H. J. Kanter, Time behavior of CO_2 and O_3 in the lower troposphere based on recordings from neighbouring mountain stations between 0.7 and 3.0 km ASL including the effects of meteorological parameters, *Arch. Met. Geoph. Biokl. Ser. B*, *30*, 191-225, 1982.

Reiter, E. R., and J. D. Mahlman, A case study of mass transport from stratosphere to troposphere not associated with surface fallout, in *Atmospheric Science Paper No. 70*, pp. 54-83, Colorado State University, Ft. Collins, CO, 1971.

Reiter, E. R., and M. P. McCormick, SAGE-European ozonesonde comparison, *Nature*, *300*, 337-339, 1982.

Reiter, E. R., and A. Nania, Jet stream structure and clear air turbulence (CAT), *J. Appl. Meteorol.*, *3*, 247-260, 1963.

Reiter, E. R., M. E. Glasser, and J. D. Mahlman, The role of the tropopause in stratospheric-tropospheric processes, *Pure Appl. Geophys.*, *75*, 185-218, 1969.

Remsberg, E. E., and L. L. Gordley, Analysis of differential absorption lidar from the Space Shuttle, *Appl. Optics*, *17*, 624-630, 1978.

Remsberg, E. E., J. M. Russell III, J. C. Gille, L. L. Gordley, P. L. Bailey, W. G. Planet, and J. E. Harries, The validation of Nimbus 7 LIMS measurements of ozone, *J. Geophys. Res.*, *89*, 5161-5178, 1984a.

Remsberg, E. E., J. M. Russell III, L. L. Gordley, J. C. Gille, and P. L. Bailey, Implications of stratospheric water vapor distribution as determined from the Nimbus 7 LIMS experiment, *J. Atmos. Sci.*, 2934-2945, 1984b.

Ridley, B. A., and D. R. Hastie, Stratospheric odd nitrogen: NO measurements at 51 °N in summer, *J. Geophys. Res.*, *86*, 3162-3166, 1981.

Ridley, B. A., and H. I. Schiff, Stratospheric odd nitrogen: Nitric oxide measurements at 32 °N in autumn, *J. Geophys. Res.*, *86*, 3167-3172, 1981.

Ridley, B. A., J. T. Bruin, H. I. Schiff, and J. C. McConnell, Altitude profile and sunset decay measurements of stratospheric nitric oxide, *Atmosphere*, *14*, 180-188, 1976.

Ridley, B. A., M. McFarland, J. T. Bruin, H. I. Schiff, and J. C. McConnell, Sunrise measurements of stratospheric nitric oxide, *Can. J. Phys.*, *55*, 212-221, 1977.

Ridley, B. A., S. H. Luu, D. R. Hastie, H. I. Schiff, J. C. McConnell, W. F. J. Evans, C. T. McElroy, J. B. Kerr, H. Fast, and R. S. O'Brien, Stratospheric odd nitrogen: Measurements of HNO_3, NO, NO_2 and O_3 near 54° N. in winter, *J. Geophys. Res.*, *89*, 4797-4820, 1984.

Riehl, H., *Climate and Weather in the Tropics*, Academic Press, New York, 611 pp., 1979.

Rigaud, P., J. P. Naudet, and D. Huguenin, Simultaneous measurements of vertical distribution of stratospheric NO_3 and O_3 at different periods of the night, *J. Geophys. Res.*, *88*, 1463-1467, 1983.

REFERENCES

Rind, D., and S. Lebedeff, Potential climatic impacts of increasing atmospheric CO_2 with emphasis on water availability and hydrology in the United States, *NASA-TM-87479*, 106 pp., NASA Goddard Space Flight Center, Greenbelt, MD, 1984.

Rind, D., R. Suozzo, A. Lacis, G. Russell, and J. Hansen, 21 layer troposphere-stratosphere climate model, *Mon. Weather Rev.*, in press, 1985.

Rinsland, C. P., and J. S. Levine, Free tropospheric carbon monoxide concentrations in 1950 and 1951 deduced from infrared total column amount measurements, *Nature*, *318*, 250-254, 1985.

Rinsland, C. P., M. A. H. Smith, J. M. Russell, J. H. Park, and C. B. Farmer, Stratospheric measurements of continuous absorption near 2400 cm^{-1}, *Appl. Opt.*, *20*, 4167-4171, 1981.

Rinsland, C. P., M. A. H. Smith, P. L. Rinsland, A. Goldman, J. W. Brault, and G. M. Stokes, Ground-based infrared spectroscopic measurements of atmospheric hydrogen cyanide, *J. Geophys. Res.*, *87*, 1119-1124, 1982a.

Rinsland, C. P., M. A. H. Smith, R. K. Seals, Jr., A. Goldman, F. J. Murcray, D. G. Murcray, J. C. Larsen, and P. L. Rarig, Stratospheric measurements of collision-induced absorption by molecular oxygen, *J. Geophys. Res.*, *87*, 3119-3122, 1982b.

Rinsland, C. P., A. Goldman, F. J. Murcray, D. G. Murcray, M. A. H. Smith, R. K. Seals, Jr., J. C. Larsen, and P. L. Rinsland, Stratospheric N_2O mixing ratio profile from high-resolution balloon-borne solar absorption spectra and laboratory spectra near 1880 cm^{-1}, *Appl. Opt.*, *21*, 4351-4355, 1982c.

Rinsland, C. P., R. E. Boughner, J. C. Larsen, G. M. Stokes, and J. W. Brault, Diurnal variations of atmospheric nitric oxide: Ground-based infrared spectroscopic measurements and their interpretation with time-dependent photochemical model calculations, *J. Geophys. Res.*, *89*, 9613-9622, 1984a.

Rinsland, C. P., A. Goldman, V. M. Devi, B. Fridovich, D. G. S. Snyder, G. D. Jones, F. J. Murcray, D. G. Murcray, M. A. H. Smith, R. K. Seals, Jr., M. T. Coffey, and W. G. Mankin, Simultaneous stratospheric measurements of H_2O, HDO, and CH_4 from balloon-borne and aircraft infrared solar absorption spectra and tunable diode laser laboratory spectra of HDO, *J. Geophys. Res.*, *89*, 7259-7266, 1984b.

Rinsland, C. P., R. E. Boughner, J. C. Larsen, A. Goldman, F. J. Murcray, and D. G. Murcray, Stratospheric NO and NO_2 profiles at sunset from analysis of high resolution balloon-borne infrared solar absorption spectra obtained at 33 °N. and calculations with a time-dependent photochemical model, *NASA Tech. Memo 86285*, 46 pp., NASA Langley Research Center, Hampton, VA, 1984c.

Rinsland, C. P., J. S. Levine, and T. Miles, Concentration of methane in the troposphere deduced from 1951 solar spectra, *Nature*, *318*, 245-249, 1985a.

Rinsland, C. P., A. Goldman, D. G. Murcray, F. J. Murcray, F. S. Bonomo, R. D. Blatherwick, V. M. Devi, M. A. H. Smith, and P. L. Rinsland, Tentative identification of the 780 cm^{-1} ν_4 band Q branch of chlorine nitrate in high-resolution solar absorption spectra of the stratosphere, *J. Geophys. Res.*, *90*, 7931-7943, 1985b.

Rinsland, C. P., V. M. Devi, J.-M. Flaud, C. Camy-Peyret, M. A. H. Smith, and G. M. Stokes, Identification of ^{18}O-isotopic lines of ozone in infrared ground-based solar absorption spectra, *J. Geophys. Res.*, *90*, 10719-10725, 1985c.

Rinsland, C. P., A. Goldman, and G. M. Stokes, Identification of atmospheric C_2H_2 lines in the 3230-3340 cm^{-1} region of high resolution solar absorption spectra recorded at the National Solar Observatory, *Appl. Opt.*, *24*, 2044-2046, 1985d.

Rippel, H., A helium cooled balloon experiment for measuring infrared emission from stratospheric gases, Ph.D. Thesis, Univ. Wuppertal, Dept. of Atmospheric Physics, W. Germany, 1984a.

Rippel, H., Ein Heliumgekuhltes Ballonexperiment zur Messung der Infrarotemissionen stratospharischer Spurengase., Ph.D. Thesis, University of Wuppertal, F.R.G., 1984b.

Roach, W. T., Aircraft observations in the lower sub-arctic stratosphere in winter, *Meteorological Research Committee Paper 121*, (available at National Meteorological Library, UK Meteorological Office), 1962.

Roach, W. T., and B. F. James, A climatology of the potential vertical extent of giant cumulonimbus clouds in some selected areas, *Met. Mag.*, *101*, 161-181, 1973.

Robbins, D., W. Evans, N. Louisnard, S. Pollitt, W. Traub, and J. Waters, Ozone intercomparisons from the balloon intercomparison campaign, in *Atmospheric Ozone*, edited by C. S. Zerefos and A. Ghazi, pp. 465-469, D. Reidel, Dordrecht, 1985.

Robbins, D., J. Waters, P. Zimmermann, R. Jarnot, J. Hardy, H. Pickett, S. Pollitt, W. Traub, K. Chance, N. Louisnard, W. F. J. Evans, and J. Kerr, Ozone measurements during the balloon intercomparison campaign, to be published, 1986.

Robbins, R. C., L. A. Cavanagh, and L. J. Salas, Analysis of ancient atmospheres, *J. Geophys. Res.*, *78*, 5341-5344, 1973.

Robert, D., and J. Bonamy, Short range force effects in semiclassical molecular line broadening calculations, *Jl. de Physique*, *40*, 923-943, 1979.

Robertson, J. P., and J. M. Tiedje, Denitrification and nitrous oxide production in successful and old growth Michigan forests, *Soil Sci. Soc. Am. J.*, *48*, 383-389, 1984.

Robinson, E., and R. C. Robbins, Sources, abundance and fate of gaseous atmospheric pollutants, *Res. Proj. PR-6755*, Suppl. rep., Stanford Res. Inst., Menlo, CA, 1969.

Robinson, E., R. A. Rasmussen, J. Krasnec, D. Pierotti, and M. Jakubovic, Halocarbon measurements in the Alaskan troposphere and lower stratosphere, *Atmos. Environ.*, *11*, 215-218, 1977.

Roche, A. E., *UARS Spectroscopy Requirements: Report of the UARS Spectroscopy Working Group*, in press, 1985.

Rodgers, C. D., The radiative heat budget of the troposphere and lower stratosphere, Planet. Circ. Project, MIT Dept. Meteorol., *Rep.* #A2, 1967.

Rodgers, C. D., Evidence for the five-day wave in the upper stratosphere, *J. Atmos. Sci.*, *33*, 710-711, 1976a.

Rodgers, C. D., Retrieval of atmospheric temperature and composition from remote measurements of thermal radiation, *Rev. Geophys. Space Phys.*, *14*, 609-624, 1976b.

Rodgers, C. D., Statistical principles of inversion theory., in *Inversion Methods in Atmospheric Remote Sounding*, edited by A. Deepak, pp. 117-138, Academic Press, New York, 1977.

Rodgers, C. D. (Ed.), Coordinated Study of the Behavior of the Middle Atmosphere in Winter (PMP-1), *Handbook for MAP, Vol. 12*, 154 pp., SCOSTEP Secretariat, Univ. of Illinois, Urbana, 1984.

Rodgers, C. D., and W. L. Grose, PMP-1 Data Comparison Workshop, Part II, in *Handbook for MAP*, SCOSTEP Secretariat, Univ. of Illinois, Urbana, in press, 1985.

Rodgers, C. D., and A. J. Prata, Evidence for a travelling 2-day wave in the middle atmosphere, *J. Geophys. Res.*, *86*, 9661-9664, 1981.

Rodgers, C. D., and C. D. Walshaw, The computation of infra-red cooling rate in planetary atmospheres, *Quart. J. Roy. Meteorol. Soc.*, *92*, 67-92, 1966.

Rodgers, C. D., R. L. Jones, and J. J. Barnett, Retrieval of temperature and composition from Nimbus 7 SAMS measurements, *J. Geophys. Res.*, *89*, 5280-5286, 1984.

Rogers, C. F., and J. A. Pyle, Stratospheric tracer transport: A modified diabatic circulation model, *Quart. J. Roy. Meteorol. Soc.*, *110*, 219-237, 1984.

Rood, R. B., and A. R. Douglass, Interpretation of ozone temperature correlations 1. Theory, *J. Geophys. Res.*, *90*, 5733-5743, 1985.

Roscoe, H., Tentative observation of stratospheric N_2O_5, *Geophys. Res. Lett.*, *9*, 901-902, 1982.

Roscoe, H. K., J. R. Drummond, and R. F. Jarnot, Infrared measurements of stratospheric composition III. The daytime changes of NO and NO_2., *Proc. Roy. Soc. London A*, *375*, 507-528, 1981.

Roscoe, H. K., B. J. Kerridge, S. Pollitt, M. Bangham, N. Louisnard, C. Alamichel, J. P. Pommereau, T. Ogawa, N. Iwagami, M. T. Coffey, W. Mankin, J. M. Fland, C. Camay-Peret, F. J. Murcray,

A. Goldman, W. F. J. Evans, and T. McElroy, Intercomparison of stratospheric measurements of NO and NO_2, in *Atmospheric Ozone*, edited by C. S. Zerefos and A. Ghazi, pp. 149-156, D. Reidel, Dordrecht, 1985a.

Roscoe, H. K., B. J. Kerridge, J. A. Pyle, L. J. Gray, and R. J. Wells, Simultaneous measurements of stratospheric NO and NO_2 and their comparison with model predictions, *J. Geophys. Res.*, in press, 1985b.

Roscoe, H. K., B. J. Kerridge, S. Pollitt, M. Bangham, N. Louisnard, C. Alamichel, J. M. Flaud, C. Camy-Peyret, J. R. Pommereau, T. Ogawa, N. Iwagami, M. T. Coffey, W. Mankin, F. J. Murcray, A. Goldman, W. F. J. Evans, T. McElroy, and J. Kerr, Intercomparison of remote measurements of stratospheric NO and NO_2, to be published, 1986.

Rose, K., and G. Brasseur, Ozone during sudden stratospheric warmings: A three-dimensional simulation, in *Atmospheric Ozone*, edited by C. S. Zerefos and A. Ghazi, pp. 28-32, D. Reidel, Dordrecht, 1985.

Rothman, L. S., *AFGL atmospheric absorption line parameters compilation: 1985 Edition*, in press, 1985.

Rothman, L. S., A. Goldman, J. R. Gillis, R. R. Gamache, H. M. Pickett, R. L. Poynter, N. Husson, and A. Chedin, AFGL trace gas compilation: 1982 version, *Appl. Opt.*, *22*, 1616-1627, 1983a.

Rothman, L. S., R. R. Gamache, A. Barbe, A. Goldman, J. R. Gillis, L. R. Brown, R. A. Toth, J. M. Flaud, and C. Camy-Peyret, AFGL atmospheric absorption line parameters compilation: 1982 Edition, *Appl. Opt.*, *22*, 2247-2256, 1983b.

Rothman, L. S., G. A. Vanasse, Murcray, D. G., F. H. Murcray, F. J. Murcray, and A. Goldman, Atmospheric emission spectra from the stratospheric cryogenic interferometer balloon experiment, in *Ninth Colloquium on High Resolution Molecular Spectroscopy*, pp. 19, University Press, Bologna, Italy, 1985.

Rottger, J., Structure and dynamics of the stratosphere and mesosphere revealed by VHF radar investigations, *Pure Appl. Geophys.*, *118*, 494-527, 1980.

Rottman, G. J., 27-day variations observed in solar ultraviolet (120-300 nm) irradiance, *Planet. Space Sci.*, *31*, 1001-1007, 1983.

Rowe, B. R., A. A. Viggiano, F. C. Fehsenfeld, D. W. Fahey, and E. E. Ferguson, Reactions between neutrals clustered on ions, *J. Chem. Phys.*, *76*, 742-743, 1982.

Rowland, F. S., and M. J. Molina, Chlorofluoromethanes in the environment, *Rev. of Geophys. Space Phys.*, *13*, 1-36, 1975.

Rowland, F. S., and P. J. Rogers, Upper stratospheric photolysis of NaCl and KCl, *Proc. Natl. Acad. Sci. USA*, *79*, 2737-2739, 1982.

Rowland, F. S., E. W. Mayer, D. R. Blake and Y. Makide, Trends in atmospheric methane concentrations since 1978, paper presented at Proc. Symp. Composition of the Non-urban Troposphere, Williamsburg, VA, 25-28 May 1982.

Rowland, F. S., D. R. Blake, and E. W. Mayer, World-wide increase in concentration of atmospheric methane since 1978, in *Symposium Proceedings* of WMO Technical Conference on Observation and Measurement of Atmospheric Contaminants, in press, 1984.

Roy, C. R., I. E. Galbally, and B. A. Ridley, Measurements of nitric oxide in the stratosphere of the Southern Hemisphere, *Quart. J. Roy. Meteorol. Soc.*, *106*, 887-894, 1980.

Ruderman, M. A., H. M. Folet, and J. W. Chamberlain, Eleven-year variation in polar ozone and stratospheric-ion chemistry, *Science*, *192*, 555-557, 1976.

Rudolph, J., and D. H. Ehhalt, Measurements of C_2-C_5 hydrocarbons over the North Atlantic, *J. Geophys. Res.*, *86*, 11959-11964, 1981.

Rudolph, J., D. H. Ehhalt, and A. Toennissen, Vertical profiles of ethane and propane in the stratosphere, *J. Geophys. Res.*, *86*, 7267-7272, 1981.

Rundel, R. D., D. M. Butler, and R. S. Stolarski, Uncertainty propagation in a stratospheric model 1. Development of a concise stratospheric model, *J. Geophys. Res.*, *83*, 3063-3072, 1978.

Rusch, D. W., and R. S. Eckman, Implications of the comparison of ozone abundances measured by the Solar Mesosphere Explorer to model calculations, *J. Geophys. Res.*, *90*, 12991-12998, 1985.

Rusch, D. W., J. C. Gerard, S. Solomon, P. J. Crutzen, and G. C. Reid, The effect of particle precipitation on the neutral and ion chemistry of the middle atmosphere—I. Odd nitrogen, *Planet. Space Sci.*, *29*, 767-774, 1981.

Rusch, D. W., G. H. Mount, C. A. Barth, G. J. Rottman, R. J. Thomas, G. E. Thomas, R. W. Sanders, G. M. Lawrence, and R. S. Eckman, Ozone densities in the lower mesosphere measured by a Limb Scanning Ultraviolet Spectrometer, *Geophys. Res. Lett.*, *10*, 241-244, 1983.

Rusch, D. W., G. H. Mount, C. A. Barth, and M. Callan, Global measurements of ozone in the 1.0 to 0.1 mb region by an ultraviolet spectrometer on the Solar Mesosphere Explorer, *J. Geophys. Res.*, *89*, 11677-11687, 1984.

Rusch, D. W., R. J. Thomas, and E. Hilsenrath, Satellite-rocket ozone profile comparisons over Natal, *J. Geophys. Res.*, in press, 1985.

Russell III, J. M., Global distribution and variability of stratospheric constituents measured by LIMS, *Adv. Space Res.*, *4*, 107-116, 1984.

Russell III, J. M, and J. C. Gille, The Limb Infared Monitor of the Stratosphere (LIMS) experiment, in *The Nimbus 7 Users' Guide*, edited by C. R. Madrid, pp. 71-103, NASA Goddard Space Flight Center, Greenbelt, MD, 1978.

Russell III, J. M., J. C. Gille, E. E. Remsberg, L. L. Gordley, P. L. Bailey, S. R. Drayson, J. Fischer, A. Girard, J. E. Harries, and W. F. J. Evans, Validation of nitrogen dioxide results measured by the Limb Infrared Monitor of the Stratosphere (LIMS) experiment on Nimbus 7, *J. Geophys. Res.*, *89*, 5099-5107, 1984a.

Russell III, J. M., S. Solomon, L. L. Gordley, E. E. Remsberg, and L. B. Callis, The variability of stratospheric and mesospheric NO_2 in the polar winter night observed by LIMS, *J. Geophys. Res.*, *89*, 7267-7275, 1984b.

Russell III, J. M., J. C. Gille, E. M. Remsberg, L. L. Gordley, P. L. Bailey, H. Fischer, A. Girard, S. R. Drayson, W. F. J. Evans, and J. E. Harries, Validation of water vapor results measured by the Limb Infrared Monitor of the Stratosphere experiment on NIMBUS 7, *J. Geophys. Res.*, *89*, 5115-5124, 1984c.

Russell III, J. M., S. Solomon, M. P. McCormick, A. J. Miller, D. W. Rusch, and J. J. Barnett, Middle atmosphere composition revealed by satellite observations, in *Handbook for MAP*, in press, 1986.

Ryden, J. C., N_2O exchange between grassland and the atmosphere, *Nature*, *292*, 235-237, 1981.

SRI International, *Chemical Economics Handbook Product Review: Fluorocarbons*, August, 1982.

Salby, M. L., Rossby normal modes in nonuniform background configurations. I: Simple fields, *J. Atmos. Sci.*, *38*, 1803-1826, 1981a.

Salby, M. L., Rossby normal modes in nonuniform background configurations. II: Equinox and solstice conditions, *J. Atmos. Sci.*, *38*, 1827-1840, 1981b.

Salby, M. L., The 2-day wave in the middle atmosphere—Observations and theory, *J. Geophys. Res.*, *86*, 9654-9660, 1981c.

Salby, M. L., A ubiquitous wavenumber-5 anomaly in the Southern Hemisphere during FGGE, *Mon. Weather Rev.*, *110*, 1712-1720, 1982a.

Salby, M. L., Sampling theory for asynoptic satellite observations. Part I. Space-time spectra, resolution and aliasing. Part II. Fast Fourier synoptic mapping, *J. Atmos. Sci.*, *39*, 2577-2614, 1982b.

Salby, M. L., Survey of planetary-scale traveling waves: The state of theory and observations, *Rev. Geophys. Space. Phys.*, *22*, 209-236, 1984a.

Salby, M. L., Transient disturbances in the stratosphere: Implications for theory and observing systems, *J. Atmos. Terr. Phys.*, 46, 1009-1047, 1984b.

Salby, M. L., and R. Garcia, Vacillations induced by interference of stationary and traveling waves, in *Handbook for MAP, Vol. 18*, edited by S. Kato, pp. 170-174, SCOSTEP Secretariat, Univ. of Illinois, Urbana, 1985.

Salby, M. L., and R. G. Roper, Long-period oscillations in the meteor region, *J. Atmos. Sci.*, *37*, 237-244, 1980.

Salby, M. L., D. L. Hartmann, P. L. Bailey, and J. C. Gille, Evidence for equatorial Kelvin modes in Nimbus-7 LIMS, *J. Atmos. Sci.*, *41*, 220-235, 1984.

Samain, D., and P. C. Simon, Solar flux determination in the spectral range 150-210 nm, *Solar Physics*, *49*, 33-41, 1976.

Sandalls, F. J., and S. A. Penkett, Measurements of carbonyl sulfide and carbon disulfide in the atmosphere, *Atmos. Environ.*, *11*, 197-199, 1977.

Sander, S. P., and M. Peterson, Kinetics of the reaction $HO_2 + NO_2 + M \rightarrow HO_2NO_2 + M$, *J. Phys. Chem.*, *88*, 1566-1571, 1984.

Sanheuza, E., and J. Heicklen, Chlorine atom sensitized oxidation of dichloromethane and chloromethane, *J. Phys. Chem.*, *79*, 7-11, 1975.

Sato, T., and R. F. Woodman, Fine altitude resolution observations of stratospheric turbulent layers by the Arecibo 430 MHz radar, *J. Atmos. Sci.*, *39*, 2546-2552, 1982.

Savoie, D. L., and J. M. Prospero, Particle size distribution of nitrate and sulfate in the marine atmosphere, *Geophys. Res. Lett.*, *9*, 1207-1210, 1982.

Sawyer, J. S., The vertical circulation at meteorological fronts and its relation to frontogenesis, *Proc. Roy. Soc. London*, *A234*, 346-362, 1956.

Schenkel, A., and B. Broder, Interference of some trace gases with ozone measurements by the KI method, *Atmos. Environ.*, *16*, 2187-2190, 1982.

Schlesinger, M. E., A review of climate model simulations of CO_2-induced climatic change, *Rep. No. 41*, 135 pp., Climatic Research Institute, Oregon State University, Corvalalis, OR, 1983.

Schlesinger, M. E., Climate model simulation of CO_2-induced climatic change, in *Advances in Geophysics*, *26*, edited by B. Saltzman, pp. 141-235, Academic Press, New York, 1984.

Schlesinger, M. E., and Y. Mintz, Numerical simulation of ozone production, transport and distribution with a global general circulation model, *J. Atmos. Sci.*, *36*, 1325-1361, 1979.

Schlesinger, M. E., and J. F. B. Mitchell, Model projections of equilibrium climate response to increased CO_2, edited M. C. MacCracken and F. M. Luther, U.S. Department of Energy, in press, 1985.

Schlesinger, M. E., W. L. Gates, and Y. J. Han, The role of the ocean in CO_2-induced climate change: Preliminary results from the OSU coupled atmosphere-ocean general circulation model, in *Coupled Ocean Atmosphere Models*, edited by J. C. Nichol, pp. 447-478, Elsevier Science, New York, 1985.

Schmailzl, U., and P. J. Crutzen, Budgets of stratospheric trace gases from 2-D-model calculations and satellite observations, in *Atmospheric Ozone*, edited by C. S. Zerefos and A. Ghazi, pp. 43-47, D. Reidel, Dordrecht, 1985.

Schmeisser, M., and K. Brandle, Halogennitrate und ihre Reaktionen, *Angew. Chem.*, *73*, 388-393, 1961.

Schmidt, U., G. Kulessa, A. Khedim, D. Knapska, and J. Rudolph, Sampling of long lived trace gases in the middle and upper stratosphere, in *Sixth ESA Symposium on European Rocket and Balloon Programmes and Related Research—-Conferences, ESA SP-183*, edited by W. R. Burke, pp. 141-145, European Space Agency, Paris, 1983.

Schmidt, U., A. Khedim, D. Knapska, G. Kulessa, and F. J. Johnen, Stratospheric trace gas distributions observed in different seasons, *Adv. Space Res.*, *4*, 131-134, 1984.

Schmidt, U., D. Knapska, and S. A. Penkett, A study of the vertical distribution of methyl chloride (CH_3Cl) in the midlatitude stratosphere, *J. Atmos. Chem.*, in press, 1985a.

Schmidt, U., P. Fabian, and R. Borchers, Intercomparison of balloon-borne cryogenic whole air samplers during the MAP/Globus campaign, *Planet. Space Sci.*, in press, 1985b.

Schneider, S. H., On the carbon dioxide-climate confusion, *J. Atmos. Sci.*, *32*, 2060-2066, 1975.

Schneider, S. H., and S. L. Thompson, Atmospheric CO_2 and climate: Importance of the transient response, *J. Geophys. Res.*, *86*, 3135-3147, 1981.

Schneider, W. H., P. K. Bhartia, K. F. Klenk, and C. L. Mateer, An optimum statistical technique for ozone profile retrieval from backscattered UV radiances, paper presented at Fourth Conference on Atmospheric Radiation, Am. Meteorol. Soc., Toronto, Ontario, Canada, June 16-18, 1981.

Schoeberl, M. R., Stratospheric warmings: Observations and theory, *Rev. Geophys. Space Phys.*, *16*, 521-538, 1978.

Schoeberl, M. R., Medium-scale disturbances in total ozone during Southern Hemisphere summer, *Bull. Amer. Meteorol. Soc.*, *64*, 1358-1365, 1983.

Schoeberl, M. R., On the penetration of mountain waves into the middle atmosphere, *J. Atmos. Sci.*, *42*, 2856-2864, 1985.

Schoeberl, M. R., and M. A. Geller, A calculation of the structure of stationary planetary waves in winter, *J. Atmos. Sci.*, *34*, 1235-1255, 1977.

Schoeberl, M. R., and D. F. Strobel, The response of the zonally averaged circulation to stratospheric ozone reductions, *J. Atmos. Sci.*, *35*, 1751-1757, 1978a.

Schoeberl, M. R., and D. F. Strobel, The zonally averaged circulation of the middle atmosphere, *J. Atmos. Sci.*, *35*, 577-591, 1978b.

Schoeberl, M. R., and D. F. Strobel, Nonzonal gravity wave breaking in the winter mesosphere, in *Dynamics of the Middle Atmosphere*, edited by J. R. Holton and T. Matsuno, pp. 45-64, D. Reidel, Dordrecht, 1984.

Schoeberl, M. R., D. F. Strobel, and J. Apruzese, A numerical model of gravity wave breaking and stress in the mesosphere, *J. Geophys. Res.*, *88*, 5249-5259, 1983.

Schryer, D. R., *Heterogeneous Atmospheric Chemistry, Geophysical Monograph 26*, American Geophysical Union, Washington, DC, 1982.

Schwab, J. J., D. W. Toohey, W. H. Brune, and J. G. Anderson, Reaction kinetics of $O + ClO \rightarrow Cl + O_2$ between 252-347K, *J. Geophys. Res.*, *89*, 9581-9587, 1984.

Schwartz, P. R., C. L. Croskey, R. M. Bevilacqua, and J. J. Olivero, Microwave spectroscopy of H_2O in the stratosphere and mesosphere, *Nature*, *305*, 294-295, 1983.

Schwartz, S. E., Gas- and aqueous-phase chemistry of HO_2 in liquid-water clouds, paper presented at the meeting of the American Chemical Society, Division of Environmental Chemistry, Washington, DC, September, 1983.

Secroun, C., A. Barbe, P. Jouve, P. Arcas, and E. Arie, Intensity of the $\nu 3$ band of ozone from a study of its anomalous dispersion at 10 μm, *J. Molec. Spectrosc.*, *85*, 8-15, 1981.

Sehmel, G. A., Particle and gas dry deposition: A review, *Atmos. Environ.*, *14*, 983-1011, 1980.

Seiler, W., The cycle of carbon monoxide in the atmosphere, in *Proceedings of the ICESA Conference, Vol. 2*, I.E.E.E., New York, 1976.

Seiler, W., Contributions of biological processes to the global budget of CH_4 in the atmosphere, in *Current Perspectives in Microbial Ecology*, American Soc. for Microbiology, Washington, DC, edited by M. J. Klug and C. A. Reddy, 710 pp., 1984.

Seiler, W., and R. Conrad, Field measurements of natural and fertilizer-induced N_2O release rates from soils, *APCA Journal*, *31*, 767-772, 1981.

Seiler, W., and R. Conrad, Contributions of tropical ecosystems to the global budgets of trace gases, especially CH_4, H_2, CO and N_2O, in *Geophysiology of Amazonia*, edited by R. Dickinson, Wiley, New York, in press, 1985.

Seiler, W., and P. Crutzen, Estimates of the gross and net flux of carbon between the biosphere and the atmosphere from biomass burning, *Climate Change*, *2*, 207-247, 1980.

Seiler, W., and J. Fishman, The distribution of carbon monoxide and ozone in the free troposphere, *J. Geophys. Res.*, *86*, 7255-7265, 1981.

Seiler, W., and U. Schmidt, New aspects of CO and H_2 cycles in the atmosphere, in *Proceedings of the Int'l Conf. on the Structure, Composition, and Gen'l Circulation of the Upper and Lower Atmospheres and Possible Anthropogenic Perturbations*, pp. 192-222, IAMAP, Melbourne, 1974.

Seiler, W., F. Muller, and H. Oeser, Vertical distribution of chlorofluoromethanes in the upper troposphere and lower stratosphere, *Pure Appl. Geophys.*, *116*, 554-566, 1978.

Seiler, W., A. Holzafel-Pschorn, R. Conrad, and D. Scharffe, Methane emissions from rice paddies, *J. Atmos. Chem.*, *1*, 241-268, 1984a.

Seiler, W., H. Giehl, E. Brunke, and E. Halliday, The seasonality of CO abundance in the Southern Hemisphere, *Tellus*, *36B*, 219-231, 1984b.

Seiler, W., R. Conrad, and D. Scharffe, Field studies of CH_4 emissions from termite nests into the atmosphere and measurements of CH_4 uptake by tropical soils, *J. Atmos. Chem.*, *1*, 171-187, 1984c.

Seinfeld, J. H., *Air Pollution: Physical and Chemical Fundamentals*, 523 pp., McGraw-Hill Book Co., New York, 1975.

Senum, G. I., Y. N. Lee, and Gaffrey, Ultraviolet absorption spectrum of peroxyacetyl nitrate and peroxypropionyl nitrate, *J. Phys. Chem.*, *88*, 1269-1270, 1984.

Sexstone, A. J., N. P. Reusbeck, T. B. Parkin, and J. M. Tiedje, Direct measurement of oxygen profiles and denitrification rates in soil aggregates, *Soil Sci. Am. J.*, *49*, 645-651, 1985.

Sexton, K. and H. Westberg, Nonmethane HC composition of urban and rural atmospheres, *Atmos. Environ.*, *18*, 1125-1132, 1984.

Shapiro, M. A., A multiple-structured frontal zone-jet stream system as revealed by meteorologically instrumented aircraft, *Mon. Weather Rev.*, *102*, 244-253, 1974.

Shapiro, M. A., Simulation of upper level frontogenesis with a 20-level isentropic coordinate primitive equation model, *Mon. Weather Rev.*, *103*, 591-604, 1975.

Shapiro, M. A., The role of turbulent heat flux in the generation of potential vorticity in the vicinity of upper level jetstream systems, *Mon. Weather Rev.*, *102*, 892-896, 1976.

Shapiro, M. A., Further evidence of the mesoscale and turbulent structure of upper jet stream-frontal zone systems, *Mon. Weather Rev.*, *106*, 1101-1111, 1978.

Shapiro, M. A., Turbulent mixing within tropopause folds as a mechanism for exchange of chemical constituents between the stratosphere and troposphere, *J. Atmos. Sci.*, *37*, 994-1004, 1980.

Shapiro, M. A., Frontogenesis and geostrophically forced secondary circulations in the vicinity of jetstream-frontal zone systems, *J. Atmos. Sci.*, *38*, 954-973, 1981.

Shapiro, M. A., E. R. Reiter, R. D. Cadle, and W. A. Sedlacek, Vertical mass and trace constituent transports in the vicinity of jet streams, *Arch. Met. Geoph. Biokl.*, *B28*, 193-206, 1980.

Shapiro, M. A., A. J. Krueger, and P. J. Kennedy, Nowcasting the position and intensity of jet streams using a satellite-borne total ozone mapping spectrometer, in *Nowcasting*, edited by K. A. Browning, pp. 137-145, Academic Press, New York, 1982.

Shapiro, M. A., R. C. Schnell, F. P. Parungo, S. J. Oltmans, and B. A. Bodhaine, El Chichon volcanic debris in an Arctic tropopause fold, *Geophys. Res. Lett.*, *11*, 421-424, 1984.

Shardanand, and A. D. Prasad Rao, Collision induced absorption of O_2 in the Herzberg continuum, *J. Quant. Spectrosc. Radiat. Transfer*, *17*, 433-439, 1977.

Sharma, R. D., and R. M. Nadile, Carbon dioxide (v2) radiative results using a new non-equilibrium model, *AIAA 81-0426*, paper presented at AIAA 19th Aerospace Sciences meeting, St. Louis, MO, 1981.

Shaw, Napier Sir, *Manual of Meteorology, The Physical Processes of Weather, Vol. III*, 445 pp., Cambridge University Press, Cambridge, 1942.

Shiotani, M., and I. Hirota, Planetary wave-mean flow interaction in the stratosphere: A comparison between the Northern and Southern Hemisphere, *Quart. J. Roy. Meteorol. Soc.*, *111*, 309-334, 1985.

Siegenthaler, U., and H. Oeschger, Transient temperature changes due to increasing CO_2 using simple models, *Ann. of Glaciology*, *5*, 153-159, 1984.

Silver, J. A., and C. E. Kolb, Measurement of molecular sodium species in the upper atmosphere, *Report No. ARI-RP-199*, Aerodyne Research, Inc., Billerica, MA, May, 1985.

Silver, J. A., A. C. Stanton, M. S. Zahniser, and C. E. Kolb, Gas phase reaction rate of sodium hydroxide with hydrochloric acid, *J. Phys. Chem.*, *88*, 3123-3129, 1984a.

Silver, J. A., M. S. Zahniser, A. C. Stanton, and C. E. Kolb, Temperature dependent thermolecular reaction rate constants for potassium and sodium superoxides formation, paper presented at 20th Symposium (International) on Combustion, Ann Arbor, MI, August, 1984b.

Simmonds, P. G., F. N. Alyea, C. A. Cardelino, A. J. Crawford, D. M. Cunnold, B. C. Lane, J. E. Lovelock, R. G. Prinn, and R. A. Rasmussen, The atmospheric lifetime experiment, 6, Results for carbon tetrachloride based on 3 years data, *J. Geophys. Res.*, *88*, 8427-8441, 1983.

Simmons, A. J., and R. Struefing, Numerical forecasts of stratospheric warming events using a model with a hybrid vertical coordinate, *Quart. J. Roy. Meteorol. Soc.*, *109*, 81-111, 1983.

Simon, P. C., Balloon measurements of solar fluxes between 1960 and 2300 A, in *Proceedings of the Third Conference on the Climatic Impact Assessment Program, DOT-TSC-OST-74-15*, edited by A. J. Broderick and T. M. Hard, pp. 137-140, Dept. of Transp., Washington, DC, 1975.

Simon, P. C., Solar irradiance between 120 and 400 nm and its variations, *Solar Physics*, *74*, 273-291, 1981.

Simon, P. C., and G. Brasseur, Photodissociation effects of solar UV radiation, *Planet. Space Sci.*, *31*, 987-999, 1983.

Simon, P. C., R. Pastiels, and D. Nevejans, Balloon observations of solar ultraviolet irradiance at solar minimum, *Planet. Space Sci.*, *30*, 68-71, 1982.

Simonaitis, R., Oxidation of the CH_3 radical and some halomethyl and haloethyl radicals of atmospheric interest, in *Proceedings of the NATO Advanced Study Institute on Atmospheric Ozone, Rep. FAA-EE-80-20*, edited by A. C. Aikin, pp. 501-515, DOT, FAA, Washington, DC, 1980.

Simonaitis, R., and J. Heicklen, Temperature dependence of the reactions of HO_2 with NO and NO_2, *Int. J. Chem. Kinet.*, *10*, 67-87, 1978.

Simons, J. W., R. J. Paur, H. A. Webster III, and E. J. Bair, Ozone ultraviolet photolysis. VI. The ultraviolet spectrum, *J. Chem. Phys.*, *59*, 1203-1208, 1973.

Singh, H. B., Atmospheric halocarbons: Evidence in favour of reduced average hydroxyl radical concentration in the troposphere, *Geophys. Res. Lett.*, *4*, 101-104, 1977a.

Singh, H. B., Preliminary estimates of average tropospheric OH concentrations in the Northern and Southern Hemispheres, *Geophys. Res. Lett.*, *4*, 453-456, 1977b.

Singh, H. B., and L. J. Salas, Measurement of selected light hydrocarbons over the Pacific Ocean: Latitudinal and seasonal variations, *Geophys. Res. Lett.*, *9*, 842-845, 1982.

Singh, H. B., and L. J. Salas, Methodology for the analysis of peroxyacetyl nitrate (PAN) in the unpolluted troposphere, *Atmos. Environ.*, *17*, 1507-1516, 1983a.

Singh, H. B., and L. J. Salas, Peroxyacetylnitrate in the free troposphere, *Nature*, *302*, 326-328, 1983b.

Singh, H. B., L. J. Salas, H. Shigeishi, and A. Crawford, Urban-nonurban relationships of halocarbons, SF_6, N_2O and other atmospheric trace constituents, *Atmos. Environ.*, *11*, 819-823, 1977.

Singh, H. B., L. J. Salas, H. Shigeishi, and E. Scibner, Atmospheric halocarbons, hydrocarbons, and sulfur hexafluride: Global distributions, sources, and sinks, *Science*, *203*, 899-903, 1979.

Singh, H. B., L. J. Salas, and R. E. Stiles, Methyl halides in and over the eastern Pacific (40°N-32°S), *J. Geophys. Res.*, *88*, 3684-3690, 1983a.

Singh, H. B., L. J. Salas, and R. E. Stiles, Selected man-made halogenated chemicals in the air and oceanic environment, *J. Geophys. Res.*, *88*, 3675-3683, 1983b.

Singh, H. B., L. J. Salas, B. A. Ridley, J. Shetter, N. M. Donahue, F. C. Fehsenfeld, D. W. Fahey, D. D. Parrish, E. J. Williams, S. C. Liu, G. Hubler, P. C. Murphy, Relationship between peroxyacetyl nitrate (PAN) and nitrogen oxides in the clean troposphere, in press, 1985.

Slemr, F., and W. Seiler, Field measurements of NO and NO_2 emissions from fertilized and unfertilized soils, *J. Atmos. Chem.*, *2*, 1-24, 1984.

Smagorinsky, J. (Chairman), *Carbon Dioxide and Climate: A Second Assessment*, 92 pp., National Academy Press, Washington, DC, 1982.

Smagorinsky, J., S. Manabe, and J. L. Holloway Jr., Numerical results from a nine-level general circulation model of the atmosphere, *Mon. Weather Rev.*, *93*, 727-788, 1965.

Smith, A. K., An observational study of planetary wave propagation in the winter stratosphere, Ph.D. thesis, 71 pp., Washington Univ., Seattle, WA, 1982.

Smith, A. K., Observations of wave-wave interactions in the stratosphere, *J. Atmos. Sci.*, *40*, 2484-2496, 1983.

Smith, A. K., and L. V. Lyjak, An observational estimate of gravity wave drag from the momentum balance in the middle atmosphere, *J. Geophys. Res.*, *90*, 2233-2241, 1985.

Smith, A. K., J. C. Gille, and L. V. Lyjak, Wave-wave interactions in the stratosphere: Observations during quiet and active wintertime periods, *J. Atmos. Sci.*, *41*, 363-373, 1984.

Smith, C. J., R. D. DeLaure, and W. H. Patrick, Jr., Nitrous oxide emission from Gulf Coast wetlands, *Geochim. Cosmochim. Acta*, *47*, 1805-1814, 1983.

Smith, M. A. H. (Ed.), Review of spectroscopic parameters for upper atmospheric measurements, *NASA Conference Publication 2396*, 28 pp., NASA, Langley Research Center, Hampton, VA, 1985.

Smith, M. A. H., and C. P. Rinsland, Spectroscopic measurements of atmospheric HCN at northern and southern latitudes, *Geophys. Res. Lett.*, *12*, 5-8, 1985.

Smith, M. A. H., C. P. Rinsland, D. Frieourch and K. Narahari Rao, Intensities and collision broadening parameters from infrared spectra, in *Molecular Spectroscopy in Modern Research*, *Vol. 3*, pp. 111-248, Academic Press, New York, 1985.

Smith, P. L., H. E. Griesinger, J. H. Black, K. Yoshino, and D. E. Freeman, Interstellar O_2. II. VUV oscillator strengths of Schumann-Runge lines and prospects for space telescope observations, *Astrophys. J.*, *277*, 569-575, 1984.

Smith, R. M., A preview of the detection of mass return flow of air and water into the stratosphere using tritium as a tracer, *Tellus*, *20*, 76-81, 1968.

Smith, W. L., H. M. Woolf, C. M. Hayden, D. Q. Wark, and L. M. McMillin, The TIROS-N operational vertical sounder, *Bull. Amer. Meteor. Soc.*, *60*, 1177-1187, 1979.

Solomon, P. M., R. L. de Zafra, A. Parrish, and J. W. Barrett, Diurnal variation of stratospheric chlorine monoxide: A critical test of chlorine chemistry in the ozone layer, *Science*, *224*, 1210-1214, 1984.

Solomon, S., and P. J. Crutzen, Analysis of the August 1972 solar proton event including chlorine chemistry, *J. Geophys. Res.*, *86*, 1140-1146, 1981.

Solomon, S., and R. R. Garcia, On the distribution of nitrogen dioxide in the high-latitude stratosphere, *J. Geophys. Res.*, *88*, 5229-5239, 1983a.

Solomon, S., and R. R. Garcia, Simulation of NO_x partitioning along isobaric parcel trajectories, *J. Geophys. Res.*, *89*, 5497-5501, 1983b.

Solomon, S., and R. R. Garcia, Transport of thermospheric NO to the upper stratosphere, *Planet. Space Sci.*, *32*, 399-409, 1984a.

Solomon, S., and R. R. Garcia, On the distribution of long-lived tracers and chlorine species in the middle atmosphere, *J. Geophys. Res.*, *89*, 11633-11644, 1984b.

Solomon, S., D. W. Rusch, J.-C. Gerard, G. C. Reid, and P. J. Crutzen, The effect of particle precipitation events on the neutral and ion chemistry of the middle atmosphere: II. Odd hydrogen, *Planet. Space Sci.*, *29*, 885-892, 1981.

Solomon, S., P. J. Crutzen, and R. G. Roble, Photochemical coupling between the thermosphere and the lower atmosphere 1. Odd nitrogen from 50 to 120 km, *J. Geophys. Res.*, *87*, 7206-7220, 1982.

Solomon, S., D. W. Rusch, R. J. Thomas, and R. S. Eckman, Comparison of mesospheric ozone abundances measured by the Solar Mesosphere Explorer and model calculations, *Geophys. Res. Lett.*, *10*, 249-252, 1983a.

Solomon, S., G. C. Reid, D. W. Rusch, and R. J. Thomas, Mesospheric ozone depletion during the solar proton event of July 13, 1983, Part II. Comparison between theory and measurements, *Geophys. Res. Lett.*, *10*, 257-260, 1983b.

Solomon, P. M., R. de Zafra, A. Parrish and J. W. Barrett, Diurnal variation of stratospheric chlorine oxide: A critical test of chlorine chemistry in the ozone layer, *Science*, *224*, 1210-1214, 1984.

Solomon, S., J. M. Russell III, M. P. McCormick, D. W. Rusch, and J. M. Zawodny, Intercomparison of satellite datasets for NO_2 and odd nitrogen photo-chemistry, in press, 1985a.

Solomon, S., R. R. Garcia, and F. Stordal, Transport processes and ozone perturbations, *J. Geophys. Res.*, *90*, 12981-12990, 1985b.

Solomon, S., J. T. Kiehl, R. R. Garcia, and W. Grose, Tracer transport by the diabatic circulation deduced from satellite observations, *J. Atmos. Sci.*, in press, 1986.

Somerville, R. C. J., and L. A. Remer, Cloud optical thickness feedbacks in the CO_2 climate problem, *J. Geophys. Res.*, *89*, 9668-9672, 1984.

Spelman, M. J., and S. Manabe, Influence of oceanic heat transport upon the sensitivity of a model climate, *J. Geophys. Res.*, *89*, 571-586, 1984.

Speth, P., and R. Madden, Space-time spectral analyses of Northern Hemisphere geopotential heights, *J. Atmos. Sci.*, *40*, 1086-1100, 1983.

Spicer, C. W., M. W. Holdren, and C. W. Keigley, The ubiquity of peroxyacetyl nitrate in the continental boundary layer, *Atmos. Environ.*, *17*, 1055-1058, 1983.

Sridharan, U. C., L. X. Qui, and F. Kaufman, Kinetics and product channels of the reactions of HO_2 with O and H atoms at 296K, *J. Phys. Chem.*, *86*, 4569-4574, 1982.

Sridharan, U. C., L. X. Qui, and F. Kaufman, Rate constant of the OH + HO_2 reaction from 252 to 420K, *J. Phys. Chem.*, *88*, 1281-1282, 1984.

St. John, D., W. H. Bailey, W. H. Fellner, J. M. Minor, and R. D. Sull, Time series analysis of stratospheric ozone, *Commun. Statist. Theory Methods*, *11*, 1293-1333, 1982.

Staff, Upper Air Branch National Weather Service, Synoptic analyses, 5-, 2-, and 0.4-millibar surfaces for July 1974 through June 1976, *NASA Ref. Publ. 1023*, 330 pp., National Weather Service, Camp Springs, MD, 1978.

Staffensen, F. L., S. Kikkawa, and R. G. Phibbs, Meteorological rocket data processor and results from the solar eclipse of 7 March 1970, *J. Appl. Meteorol.*, *11*, 722-730, 1972.

Staley, D. O., Evaluation of potential vorticity changes near the tropopause and the related vertical motions, vertical advection of vorticity, and transfer of radioactive debris from stratosphere to troposphere, *J. Meteorol.*, *17*, 591-620, 1960.

Staley, D. O., On the mechanism of mass and radioactivity transport from stratosphere to troposphere, *J. Atmos. Sci.*, *19*, 450-467, 1962.

Starr, W. L., R. A. Craig, M. Loewenstein, and M. E. McGhan, Measurements of NO, O_3, and temperature at 19.8 km during the total solar eclipse of 26 February 1979, *Geophys. Res. Lett.*, *7*, 553-555, 1980.

REFERENCES

Stauffer, B., A. Neftel, H. Oeschger, and J. Schwander, CO_2 concentrations in air extracted from Greenland ice samples, in *Greenland Ice Core: Geophysical Geochemistry, and the Environment, American Geophysical Union Monograph No. 33*, edited by C. C. Langway, H. Oeschger, and W. Dansgaard, pp. 83-89, Washington, DC, 1985.

Stedman, D. H., and J. O. Jackson, The photostationary state in photochemical smog, *Int. J. Chem. Kinetics Symposium, 1*, 493-501, 1975.

Steed, J. M., A. J. Owens, C. D. Miller, D. L. Filkin, and J. P. Jesson, Two-dimensional model calculations of potential ozone perturbation by chlorofluorocarbons, *Nature, 295*, 308-311, 1982.

Steele, L. P., P. J. Fraser, R. A. Rasmussen, M. A. K. Khalil, T. J. Conway, A. J. Crawford, R. H. Gammon, K. A. Masarie, and K. W. Thoning, The global distribution of methane in the troposphere, *J. Atmos. Chem.*, in press, 1985.

Stelson, A. W., and J. H. Seinfeld, Relative humidity and temperature dependence of the ammonium nitrate dissociation constant, *Atmos. Environ., 16*, 983-993, 1982.

Stephens, G. L., and P. J. Webster, Sensitivity of radiative forcing to variable cloud and moisture, *J. Atmos. Sci., 36*, 1450-1466, 1979.

Stephens, G. L., S. Ackerman and E. A. Smith, A shortwave parameterization revised to improve cloud absorption, *J. Atmos. Sci., 41*, 687-690, 1984.

Stern, A. C., *Air Pollution, Vol. III*, Academic Press, New York, 1977.

Stevens, C. M., and A. Engelkemeir, *J. Geophys. Res.*, in press, 1986.

Stockwell, W. R., and J. G. Calvert, The mechanism of the HO-SO_2 reaction, *Atmos. Environ., 17*, 2231-2235, 1983.

Stolarski, R. S., Impact of large amounts of chlorine on stratospheric ozone, paper presented at the International Workshop on Current Issues in our Understanding of the Stratosphere and the Future of the Ozone Layer, BMFT, NASA, FAA, WMO, Feldafing, FRG, June 11-16, 1984.

Stolarski, R. S., and R. J. Cicerone, Stratospheric chlorine: A possible sink for ozone, *Can. J. Chem., 52*, 1610-1615, 1974.

Stolarski, R. S., and A. R. Douglass, Parameterization of the photochemistry of stratospheric ozone including catalytic loss processes, *J. Geophys. Res.*, 90, 10709-10718, 1985.

Stolarski, R. S., D. M. Butler, and R. D. Rundel, Uncertainty propagation in a stratospheric model. 2. Monte Carlo analysis of imprecisions due to reaction rates, *J. Geophys. Res., 83*, 3074-3078, 1978.

Stordal, F., I. S. A. Isaksen, and K. Horntveth, A diabatic circulation two-dimensional model with photochemistry: Simulations of ozone and ground released tracers, *J. Geophys. Res., 90*, 5757-5776, 1985.

Stout, J., E. B. Rogers, and E. Nunez, abst, 16th Conf. Hurricanes and Tropical Meteorol 14-17 May 1985, Houston, Texas., 1985.

STRAC, Chlorofluorocarbons and their effects on stratospheric ozone, *Pollution Paper No 15, HMSO*, 1979.

Stratospheric Analysis Group, *Meteor. Abh. Met. Inst. Berlin*, 1980.

Strickland, A. C. (Ed.), *COSPAR International Reference Atmosphere*, Akademie-Verlag, Berlin, 1972.

Strobel, D. F., Parameterization of the atmospheric heating from 15-120 km due to O_2 and O_3 absorption of solar radiation, *J. Geophys. Res., 83*, 6225-6230, 1978a.

Strobel, D. F., Photochemical radiative damping and instability in the stratosphere, II. Numerical results, *Geophys. Res. Lett., 5*, 523-525, 1978b.

Strobel, D. F., D. M. Hunten, and M. B. McElroy, Production and diffusion of nitric oxide, *J. Geophys. Res., 75*, 4307-4321, 1970.

Susskind, J., and J. E. Searl, Atmospheric absorption near 2400 cm^{-1}, *J. Quant. Spectrosc. Radiat. Transfer, 18*, 581-589, 1977.

Swanson, D., K. Brian, and H. S. Johnston, NO_3 quantum yield from N_2O_5 photolysis, *J. Phys. Chem., 88*, 3115-3115, 1984.

Swider, W., and T. J. Keneshea, Decrease of ozone and atomic oxygen in the lower mesosphere during a PCA event, *Planet. Space Sci.*, *21*, 1969-1973, 1973.

Swider, W., T. J. Keneshea, and C. I. Foley, An SPE-distributed D-region model, *Planet. Space Sci.*, *26*, 883-892, 1978.

Syed, M. Q., and A. W. Harrison, Ground based observations of stratospheric nitrogen dioxide, *J. Canad. Phys.*, *58*, 788-802, 1980.

Syed, M. Q., and A. W. Harrison, Seasonal trend of stratospheric NO_2 over Calgary, *Can. J. Phys.*, *59*, 1278-1279, 1981.

Sze, N. D., Anthropogenic CO emissions: Implications for the atmospheric CO-OH-CH_4 cycle, *Science*, *195*, 673-675, 1977.

Sze, N. D., paper presented at CMA Workshop on Stratospheric Chemistry, Gottingen, FRG, October, 1984.

Sze, N. D., and M. K. Ko, CS_2 and COS in the stratospheric sulfur budget, *Nature*, *280*, 308-310, 1979.

Sze, N. D., M. K. W. Ko, W. Swider, and E. Murad, Atmospheric sodium chemistry. 1. The altitude region 70-100 km, *Geophys. Res. Lett.*, *9*, 1187-1190, 1982.

Sze, N. D., M. K. W. Ko, M. Livshits, W. C. Wang, P. B. Ryan, R. E. Specht, M. B. McElroy, and S. C. Wofsy, *Annual Report on the Atmospheric Chemistry, Radiation and Dynamics Program*, Atmospheric and Environmental Research, Inc., Cambridge, MA, 1983.

Taine, J., and F. LePoutre, A photoacoustic study of the collisional deactivation of the first vibrational levels of CO_2 by N_2 and CO, *Chem. Phys. Lett.*, *65*, 554-558, 1979.

Takahashi, M., A two-dimensional numerical model of the semi-annual zonal wind oscillation, in *Dynamics of the Middle Atmosphere*, edited by J. R. Holton and T. Matsuno, pp. 253-269, Terrapub, Tokyo, 1984.

Tang, I. N., On the equilibrium partial pressures of nitric acid and ammonia in the atmosphere, *Atmos. Environ.*, *14*, 819-828, 1980.

Telegades, K., The seasonal stratospheric distribution and inventory of excess carbon-14 from March 1955 to July 1969, *Rep. 243*, Health and Safety Lab., U.S. Atomic Energy Comm., Washington, DC, 1971.

Tenenbaum, J., Integrated and spectral energetics studies of the GLAS general circulation model, *Mon. Weather Rev.*, *110*, 962-980, 1982.

Terry, R. E., R. L. Tate, and J. M. Duxbury, Nitrous oxide emissions from drained, cultivated organic soils of S. Florida, *J. Air Poll. Control Assoc.*, *31*, 1173-1176, 1981.

Thacker, D. L., C. J. Gibbins, P. R. Schwartz, and R. M. Bevilacqua, Ground-based microwave observations of mesospheric H_2O in January, April, July, and September, 1980, *Geophys. Res. Lett.*, *8*, 1059-1062, 1981.

Theon, J. S., W. Nordberg, C. B. Katchen, and J. J. Horvath, Some observations on the thermal behavior of the mesosphere, *J. Atmos. Sci.*, *24*, 428-438, 1967.

Thomas, M. E., and R. J. Nordstrum, The N_2-broadened water vapor absorption line shape and infrared continuum absorption, I. Theoretical development, *J. Quant. Spectrosc. Radiat. Transfer*, *28*, 81-101, 1982.

Thomas, R. J., C. A. Barth, G. J. Rottman, D. W. Rusch, G. H. Mount, G. M. Lawrence, R. W. Sanders, G. E. Thomas, and L. E. Clemens, Ozone density distribution in the mesosphere (50-90 km) measured by the SME Limb Scanning Near Infared Spectrometer, *Geophys. Res. Lett.*, *10*, 245-248, 1983a.

Thomas, R. J., C. A. Barth, G. J. Rottman, D. W. Rusch, G. H. Mount, G. M. Lawrence, R. W. Sanders, G. E. Thomas, and L. E. Clemens, Mesospheric ozone depletion during the solar proton event of July 13, 1982, Part I-Measurement, *Geophys. Res. Lett.*, *10*, 253-255, 1983b.

Thomas, R. J., C. A. Barth, D. W. Rusch, and R. W. Sanders, Solar Mesosphere Explorer Near Infrared Spectrometer: Measurements of 1.27 μm radiances and the inference of mesospheric ozone, *J. Geophys. Res.*, *89*, 9569-9580, 1984a.

Thomas, R. J., C. A. Barth, and S. Solomon, Seasonal variations of ozone in the upper mesosphere and gravity waves, *Geophys. Res. Lett.*, *11*, 673-676, 1984b.

Thompson, A. M., and D. H. Lenschow, Mean profiles of trace reactive species in the unpolluted marine surface layer, *J. Geophys. Res.*, *89*, 4788-4796, 1984.

Thompson, A. M., and O. C. Zafiriou, Air-sea fluxes of transient atmospheric species, *J. Geophys. Res.*, *88*, 6696-6708, 1983.

Tolson, R. H., Spatial and temporal variations of monthly mean total columnar ozone derived from 7 years of BUV data, *J. Geophys. Res.*, *86*, 7312-7330, 1981.

Tomatsu, K., Spectral energetics of the troposphere and lower stratosphere, *Advances in Geophysics*, *21*, 189-205, 1979.

Torabi, A., An investigation of the kinetics and excited state dynamics of the nitrate free radical, Ph.D. thesis, Georgia Institute of Technology, Atlanta, Georgia, 1985.

Torres, A. L., Tropospheric nitric oxide measurements during GTE/CITE, *Eos Trans. AGU*, *65*, 835, 1984.

Torres, A. L., and A. R. Bandy, Performance characteristics of the electrochemical concentration cell ozonesondes, *J. Geophys. Res.*, *83*, 5501-5504, 1978.

Torres, A. L., P. J. Maroulis, A. B. Goldberg, and A. R. Bandy, Atmospheric OCS measurements on Project Gametag, *J. Geophys. Res.*, *85*, 7357-7360, 1980.

Townsend, R. D., A diagnostic study of the zonally-averaged global circulation in isentropic coordinates. Ph.D. thesis, 221 pp., University of Wisconsin, Madison, 1980.

Townsend, R. D., and D. R. Johnson, The mass and angular momentum balance of the zonally averaged general circulation, paper presented at Int. Conf. Prelim. FGGE Data Anal. Res., pp. 542-552, Bergen, 23-27 June 1980.

Townsend, R. D., and D. R. Johnson, A diagnostic study of the isentropic zonally-averaged mass circulation during the first GARP global experiment, *J. Atmos. Sci.*, *42*, 1565-1579, 1985.

Traub, W. A., "An upper limit for stratospheric hydrogen peroxide" and "Measurements of OH from 18 to 48 km", papers presented at the International Workshop on Current Issues in our Understanding of the Stratosphere and the Future of the Ozone Layer, BMFT, NASA, FAA, WMO, Feldafing, FRGl, June 11-16, 1984.

Traub, W. A., and K. V. Chance, Stratospheric HF and HCl observations, *Geophys. Res. Lett.*, *8*, 1075-1077, 1981.

Traub, W. A., K. V. Chance, J. C. Brasunas, J. M. Vrtilek, and N. P. Carleton, Use of a Fourier Transform spectrometer on a balloon borne telescope and at the MMT, in *Proc. Soc. Photo-Opt. Instrum. Eng. Instrumentation in Astronomy IV*, *331*, 209-218, 1982.

Tsao, C. J., and B. Curnutte, Line widths of pressure broadened spectral lines, *J. Quant. Spectrosc. Radiat. Transfer*, *2*, 41-91, 1962.

Tsay, C. Y., Analysis of large scale wave disturbances simulated by an NCAR global circulation model, *J. Atmos. Sci.*, *31*, 330-339, 1974.

Tuazon, E. C., R. Atkinson, C. N. Plum, A. M. Winer, and J. N. Pitts, The reaction of gas phase N_2O_5 with water vapor, *Geophys. Res. Lett.*, *10*, 953-956, 1983.

Tuazon, E. C., A. M. Winer, and J. N. Pitts, Jr., Trace pollutant concentrations in a multiday smog episode in the California South Coast air basin by long path length fourier transform infrared spectroscopy, *Environ. Sci. Technol.*, *15*, 1232-1237, 1981.

Tuazon, E. C., R. Atkinson, H. MacLeod, H. W. Biermann, A. M. Winer, W. P. L. Carter, and J. N. Pitts, Jr., Yields of glyoxal and methylglyoxal from the NOx-air photooxidations of toluene and m- and p- xylene, *Environ. Sci. Technol.*, *18*, 981-984, 1984.

Tuck, A. F., Production of nitrogen oxides by lightning discharges, *Quart. J. Roy. Meteorol. Soc.*, *102*, 749-755, 1976.

Tuck, A. K., A comparison of one- two- and three-dimensional model representations of stratospheric gases, *Phil. Trans. Roy. Soc. London*, *A290*, 477-494, 1979.

Tucker, B. J., P. J. Maroulis, and A. R. Bandy, Free tropospheric measurements of CS_2 over a 45 °N to 45 °S latitude range, *Geophys. Res. Lett.*, *12*, 9-11, 1983.

Tucker, C. J., I. Y. Fung, C. D. Keeling, and R. H. Gammon, The relationship of global spectral vegetation indices to atmospheric CO_2 concentrations, *Nature*, in press, 1985.

Tung, Ka Kit, On the two-dimensional transport of stratospheric trace gases in isentropic coordinates, *J. Atmos. Sci.*, *39*, 2330-2355, 1982.

Tung, Ka Kit, Modeling of tracer transport in the middle atmosphere, in *Dynamics of the Middle Atmosphere*, edited by J. R. Holton and T. Matsuno, pp. 417-444, Terrapub, Tokyo, 1984.

Tung, Ka Kit, and R. S. Lindzen, A theory of stationary long waves. Part II: Resonant Rossby waves in the presence of realistic vertical shears, *Mon. Weather Rev.*, *107*, 735-750, 1979.

Turco, R. P., R. C. Whitten, O. B. Toon, J. B. Pollack, and P. Hamill, OCS stratospheric aerosols and climate, *Nature*, *283*, 283-286, 1980.

Turco, R. P., O. B. Toon, R. C. Whitten, R. G. Keesee, and P. Hamill, Importance of heterogeneous processes to tropospheric chemistry: Studies with a one-dimensional model, in *Heterogeneous Atmospheric Chemistry*, *Geophysical Monograph 26*, edited by David R. Schryer, pp. 231-240, American Geophysical Union, Washington, DC, 1982.

Turner, N. C., S. Rich, and P. E. Waggoner, Removal of ozone by soil, *J. Environ. Qual.*, *2*, 259-264, 1973.

Turner, N. C., P. E. Waggoner, and S. Rich, Removal of ozone from the atmosphere by soil and vegetation, *Nature*, *250*, 486-489, 1974.

Twomey, S. A., M. Piepgrass and T. L. Wolfe, An assessment of the impact of pollution on global albedo, *Tellus*, *36B*, 356-366, 1984.

Tyndall, J., On radiation through the Earth's atmosphere, *Philos. Mag.*, *4*, 200, 1863.

Tyson, B. J., J. C. Arvesen, and D. O'Hara, Interhemispheric gradients of CF_2Cl_2, $CFCl_3$, CCl_4, and N_2O, *Geophys. Res. Lett.*, *5*, 535-538, 1978b.

Uccellini, L. W., and D. R. Johnson, The coupling of upper and lower tropospheric jet streaks and implications for the development of severe convective storms, *Mon. Weather Rev.*, *107*, 682-702, 1979.

Uchino, O., M. Maeda, and M. Hirono, Applications of excimer lasers to laser-radar observations of the upper atmosphere, *IEEE J. Quant. Elec.*, *QE-15*, 1094-1107, 1979.

U.S. Dept. of HEW, Public Health Service, *Air Quality Criteria for Photochemical Oxidants*, *NAPCA-PUB-AP-63*, 202 pp., National Air Pollution Control Administration, Arlington, VA, 1970.

U.S. Standard Atmosphere Supplements, Superintendent of Documents, 289 pp., U.S. Government Printing Office, Washington, DC, 1966.

U.S. Standard Atmosphere, 1976, U.S. Government Printing Office, Washington, DC, 1976.

van Loon, H. K., K. Labitzke, and R. L. Jeene, Half-yearly wave in the stratosphere, *J. Geophys. Res.*, *77*, 3846-3855, 1972.

van Loon, H., C. S. Zerefos, and C. C. Repapis, Evidence of the southern oscillation in the stratosphere, *Publication No.3*, Academy of Athens, Research Center for Atmospheric Physics and Climatology, Athens, 1981.

Varanasi, P., and F. K. Ko, Intensity and transmission measurements in the nu-3 fundamental of N_2O at low temperatures, *J. Quant. Spectros. Radiat. Transfer*, *18*, 465-470, 1977.

Varanasi, P., L. P. Giver, and F. P. J. Valero, Intensity measurements in the V_4-fundamental of $^{13}CH_4$ at planetary atmospheric temperatures, *J. Quant. Spectros. Radiat. Transfer*, *30*, 491-495, 1983.

Vassy, A., Radiosonde speciale pour la mesure de la repartition verticale de l'ozone atmospherique, *J. Sci. Meteorol.*, *10*, 63-75, 1958.

Vaughan, G., and A. F. Tuck, Aircraft measurements near jet streams, in *Atmospheric Ozone*, edited by C. S. Zerefos and A. Ghazi, pp. 572-579, D. Reidel, Dordrecht, 1985.

REFERENCES

Vedder, J. F., B. J. Tyson, R. B. Brewer, C. A. Boitnott, and E. C. Y. Inn, Lower stratospheric measurements of variation with latitude of CF_2Cl_2, $CFCl_3$, CCl_4, and N_2O profiles in the Northern Hemisphere, *Geophys. Res. Lett.*, *5*, 33-36, 1978.

Venne, D., The horizontal structure of traveling planetary-scale waves in the upper stratosphere, *J. Geophys. Res.*, 1984.

Venne, D., and J. Stanford, An observational study of high-latitude stratospheric planetary waves in winter, *J. Atmos. Sci.*, *39*, 1026-1084, 1982.

Veryard, R. G., and R. A. Ebdon, Fluctuations in tropical stratospheric winds, *Meteor. Mag.*, *90*, 125-143, 1961.

Vienkorn-Rudolph, B., K. Bachmann, and B. Schwartz, Vertical profiles of hydrogen chloride in the troposphere, *J. Atmos. Chem.*, *2*, 47-63, 1984.

Vigroux, E., Contribution a l'etude experimentale de l'absorption de l'ozone, *Ann. Phys.*, *8*, 709-762, 1953.

Vincent, D. G., Mean meridional circulation in the Northern Hemisphere lower stratosphere during 1964 and 1965, *Quart. J. Roy. Meteorol. Soc.*, *94*, 333-349, 1968.

Vincent, R. A., Gravity wave motions in the mesosphere, *J. Atmos. Terr. Phys.*, *46*, 119-128, 1984a.

Vincent, R. A., MF/HF radar measurements of the dynamics of the mesopause region-A review, *J. Atmos. Terr. Phys.*, *46*, 961-974, 1984b.

Vincent, R. A., Planetary and gravity waves in the mesosphere and lower thermosphere, in *Handbook for MAP, Vol. 16*, edited by K. Labitzke, J. J. Barnett, and B. Edwards, pp. 269-277, SCOSTEP Secretariat, Univ. of Illinois, Urbana, 1985.

Vincent, R. A., and I. M. Reid, HF Doppler measurements of mesospheric gravity wave momentum fluxes, *J. Atmos. Sci.*, *40*, 1321-1333, 1983.

Volz, A., U. Schmidt, J. Rudolph, D. H. Ehhalt, F. J. Johnen, and A. Khedim, Vertical profiles of trace gases at mid latitudes, *Jul-Report 1742*, Kernforschungsanlage Julich GmbH, D-5170 Julich, FRG, 1981.

Vukovich, F. M., J. Fishman and E. V. Browell, The reservoir of ozone in the boundary layer of the eastern United States and its potential impact on the global tropospheric ozone budget, *J. Geophys. Res.*, *90*, 5687-5690, 1985.

Vupputuri, R. K. R., The structure of the natural stratosphere and the impact of chlorofluoromethanes on the ozone layer investigated in a 2-D time dependent model, *Pure Appl. Geophys.*, *117*, 448-485, 1978/79.

Vupputuri, R. K. R., Study the effect of El Chichon volcanic cloud on the stratospheric temperature structure and ozone distribution in a 2-D model, in *Atmospheric Ozone*, edited by C. S. Zerefos and A. Ghazi, pp. 59-60, D. Reidel, Dordrecht, 1985.

Vyas, N., Numerical modelling of atmospheric processes, Ph.D. thesis, Oxford University, Oxford, 1984.

Wale, M. J., and G. D. Peskett, Some aspects of the design and behavior of the Stratospheric and Mesospheric Sounder, *J. Geophys. Res.*, *89*, 5287-5293, 1984.

Wallace, J. M., General circulation of the tropical lower stratosphere, *Rev. Geophys. Spa. Phys.*, *11*, 191-222, 1973.

Wallace, J. M., The climatological mean stationary waves: Observational evidence, in *Large-scale Dynamical Processes in the Atmosphere*, edited by B. J. Hoskins and R. Pearce, pp. 27-53, Academic Press, New York, 1983.

Wallace, J. M., and V. Kousky, Observational evidence of Kelvin waves in the tropical stratosphere, *J. Atmos. Sci.*, *25*, 900-907, 1968.

Wallington, T. J., R. Atkinson, and A. M. Winer, Rate constants for the gas phase reaction of OH radicals with peroxyacetyl nitrate (PAN) at 273 and 297K, *Geophys. Res. Lett.*, *11*, 861-864, 1984.

Wang, P.-H., M. P. McCormick, and W. P. Chu, A study on the planetary wave transport of ozone during the late February 1979 stratospheric warming using the SAGE ozone observation and meteorological information, *J. Atmos. Sci.*, *40*, 2419-2431, 1983.

Wang, W.-C., and P. H. Stone, Effect of ice-albedo on global sensitivity in a one-dimensional radiative-convective climate model, *J. Atmos. Sci.*, *37*, 545-552, 1980

Wang, W.-C., and N. D. Sze, Coupled effects of atmospheric N_2O and O_3 on the Earth's climate, *Nature*, *268*, 589-590, 1980.

Wang, W.-C., J. P. Pinto and Y. L. Yung, Climatic effects due to halogenated compounds in the Earth's atmosphere, *J. Atmos. Sci.*, *37*, 333-338, 1980.

Wang, W.-C., Y. L. Yung, A. A. Lacis, T. Mo and J. E. Hansen, Greenhouse effects due to man-made perturbations of trace gases, *Science*, *194*, 685-690, 1976.

Wang, W.-C., W. B. Rossow, M.-S. Yao and M. Wolfson, Climate sensitivity of a one-dimensional radiative-convective model with cloud feedback, *J. Atmos. Sci.*, *38*, 1167-1178, 1981.

Wang, W.-C., D. J. Wuebbles, W. M. Washington, R. G. Isaacs and G. Molnar, Potential climatic effects of perturbations other than CO_2, Chapter 6, in *State-of-the-art report*, edited by M. C. MacCracken and F. M. Luther, Dept. of Energy, Washington, DC, 1985

Warmbt, W., Results of long term measurements of near surface ozone in the GDR, *Zeit. fuer Met.*, *29*, 24-31, 1979.

Warneck, P., On the role of OH and HO_2 radicals in the troposphere, *Tellus*, *26*, 39-46, 1974.

Washington, W. M., and G. A. Meehl, General circulation model experiments on the climatic effects due to a doubling and quadrupling of carbon dioxide concentration, *J. Geophys. Res.*, *88*, 6600-6610, 1983.

Washington, W. M., and G. A. Meehl, Seasonal cycle experiment on the climate sensitivity due to a doubling of CO_2 with an atmospheric general circulation model coupled to a simple mixed-layer ocean model, *J. Geophys. Res.*, *89*, 9475-9503, 1984.

Watanabe, K., M. Zelikoff, and E. C. Y. Inn, Absorption coefficients of several atmospheric gases, *Geophysical Research Paper No. 21*, Air Force Cambridge Research Lab., Bedford, MA, 1953.

Waters, J. W., J. J. Gustincic, R. K. Kakar, H. K. Roscoe, P. N. Swanson, T. G. Phillips, T. de Graauw, A. R. Kerr, and R. J. Mattauch, Aircraft search for millimeter wavelength emission by stratospheric ClO, *J. Geophys. Res.*, *84*, 7034-7040, 1979.

Waters, J. W., J. C. Hardy, R. F. Jarnot, and H. M. Pickett, Chlorine monoxide radical, ozone, and hydrogen peroxide: Stratospheric measurements by microwave limb sounding, *Science*, *214*, 61-64, 1981.

Waters, J. W., J. C. Hardy, R. F. Jarnot, H. M. Pickett, and P. Zimmermann, A balloon-borne microwave limb sounder for stratospheric measurements, *J. Quant. Spectrosc. Radiat. Transfer*, *32*, 407-433, 1984.

Watson, R. T., Rate constants of reactions of ClO_x of atmospheric interest, *J. Phys. Chem. Ref. Data*, *6*, 871-918, 1977.

Watson, R. T., Balloon intercomparison measurements of minor species, to be published, 1986.

Watson, R. T., J. Rogers, L. Heidt, W. Pollock, K. Mauersberger, D. Kley, A. L. Schmeltekopf, D. L. Albritton, S. Oltmans, J. Mastenbrook, D. Murcray, W. F. J. Evans, C. Midwinter, N. Swann, and E. F. Danielsen, An intercomparison of stratospheric water vapor instruments, to be published, 1986.

Wayne, R. P., *Chemistry of Atmospheres*, 361 pp., Clarendon Press, Oxford, 1985.

WCP, Aerosols and their climatic effects, paper presented at World Climate Research Programme Report, *WCP-55*, Report of the experts meeting, Williamsburg, VA, 28-30 March 1983.

Weaver, C., and R. Pearson, Ozone conservation and transport in cumulus clouds, *Eos Trans. AGU*, *65*, 836, 1984.

Weaver, H., M. J. Mumma, J. L. Faris, T. Kostiuk, and J. J. Hillman, Infrared heterodyne spectroscopy of seven gases in the vicinity of chlorine monoxide lines, *Appl. Opt.*, *22*, 1562-1567, 1983.

REFERENCES

Webster, C. R., and R. T. Menzies, In situ measurements of stratospheric nitric oxide using a balloon-borne tunable diode laser spectrometer, *Appl. Opt.*, *23*, 1140-1142, 1984.

Webster, P. J., and G. L. Stephens, Tropical upper-tropospheric extended clouds: Inferences from Winter MONEX, *J. Atmos. Sci.*, *37*, 1521-1541, 1980.

Weeks, L. H., and L. G. Smith, A rocket measurement of ozone near sunrise, *Planet. Space Sci.*, *16*, 1189-1195, 1968.

Weeks, L. H., R. S. CuiKay, and J. R. Corbin, Ozone measurements in the mesosphere during the solar proton event of 2 November 1969, *J. Atmos. Sci.*, *29*, 1138-1142, 1972.

Wehrbein, W. M., and C. B. Leovy, An accurate radiative heating and cooling algorithm for use in a dynamical model of the middle atmosphere, *J. Atmos. Sci.*, *39*, 1532-1544, 1982.

Weiler, K. H., P. Fabian, G. Flentje, and W. A. Mathews, Stratospheric NO measurements: A new balloon-borne chemiluminescence instrument, *J. Geophys. Res.*, *85*, 7445-7452, 1980.

Weinreb, M. P., W. A. Morgan, I-Lok Chang, L. D. Johnson, P. A. Bridges, and A. C. Neuendorffer, High-altitude balloon test of satellite solar occultation instrument for monitoring stratospheric O_3, H_2O and HNO_3., *J. Atmos. Oc. Tech.*, *1*, 87-100, 1984.

Weinstock, E. M., M. J. Phillips, and J. G. Anderson, In situ observations of ClO in the stratosphere: A review of recent results, *J. Geophys. Res.*, *86*, 7273-7278, 1981.

Weinstock, B., and H. Niki, Carbon monoxide balance in nature, *Science*, *176*, 290-292, 1972.

Weinstock, J., Nonlinear theory of gravity waves: Momentum deposition, generalized Rayleigh friction and diffusion, *J. Atmos. Sci.*, *39*, 1698-1710, 1982.

Weiss, R. F., The temporal and spatial distribution of tropospheric nitrous oxide, *J. Geophys. Res.*, *86*, 7185-7195, 1981.

Weiss, R. F., and H. Craig, Production of atmospheric nitrous oxide by combustion, *Geophys. Res. Lett.*, *3*, 751-753, 1976.

Wesely, M. L., Turbulent transport of ozone to surfaces common in the eastern half of the United States, in *Trace Atmospheric Constituents*, edited by S. E. Schwartz, pp. 345-370, Wiley, New York, 1983.

Wesley, M. L., and B. B. Hicks, Some factors that affect the deposition rates of sulfur dioxide and similar gases on vegetation, *J. Air Poll. Control Assoc.*, *27*, 1110-1116, 1977.

Wesely, M. L., J. A. Eastman, D. R. Cook, and B. B. Hicks, Daytime variations of ozone eddy fluxes to maize, *Boundary-Layer Meteorol.*, *15*, 361-363, 1978.

Wesely, M. L., D. R. Cook, and R. M. Williams, Field measurement of small ozone fluxes to snow, bare wet soil, and lake water, *Boundary-Layer Meteorol.*, *20*, 459-471, 1981.

Wesely, M. L., J. A. Eastman, D. H. Stedman, and E. D. Yalvac, An eddy correlation measurement of NO_2 flux to vegetation and comparison to O_3 flux, *Atmos. Environ.*, *16*, 815-820, 1982.

Wetherald, R. T., and S. Manabe, The effects of changing the solar constant on the climate of a general circulation model, *J. Atmos. Sci.*, *32*, 2044-2059, 1975.

Whitten, G. Z., H. Hogo, and J. P. Killus, The carbon bond mechanism: A condensed kinetic mechanism for photochemical smog, *Environ. Sci. Technol.*, *14*, 690-700, 1980.

Whitten, R. C., W. J. Borucki, H. T. Woodward, L. A. Capone, C. A. Riegel, R. P. Turner, I. G. Poppoff, and K. Santhanam, Implications of smaller concentrations of stratospheric OH: A two-dimensional model study of ozone perturbations, *Atmos. Environ.*, *15*, 1583-1589, 1981.

Wigley, T. M. L., and M. E. Schlesinger, Analytical solution for the effect of increasing CO_2 on global mean temperature, *Nature*, *315*, 649-652, 1985.

Wilkniss, P. E., and R. E. Larson, Atmospheric radon measurements in the Arctic fronts, seasonal observations and transport of continental air to polar regions, *J. Atmos. Sci.*, *41*, 2347-2358, 1984.

Wilkniss, P. E., R. A. Lamontagne, R. E. Larson, J. W. Swinnerton, C. R. Dickson, and T. Thompson, Atmospheric trace gases in the Southern Hemisphere, *Nature*, *245*, 45-47, 1973.

Williams, A. P., Relaxation of the 2.7γ and 4.3γ bands of carbon dioxide, in *Mesospheric Models and Related Experiments*, edited by G. Fiocco, pp. 177-187, D. Reidel, Dordrecht, 1971.

Williams, R. M., Uncertainties in the use of box models for estimating dry deposition velocity, *Atmos. Envir.*, *16*, 2707-2708, 1982.

Williams, W. J., J. J. Kosters, A. Goldman, and D. G. Murcray, Measurements of stratospheric halocarbon distributions using infrared techniques, *Geophys. Res. Lett.*, *3*, 379-382, 1976.

Wine, P. H., and A. R. Ravishankara, Kinetics of OH reactions with tropospheric sulfur compounds, in *2nd Symposium Composition of the Nonurban Troposphere*, pp. 258-260, May 25-28, 1982, Williamsburg, VA, AMS, Boston, MA, 1982.

WMO, *The Stratosphere 1981. Theory and Measurements*, *WMO Global Ozone Research and Monitoring Project Report No. 11*, 516 pp., WMO, Geneva, 1982.

WMO, Report of the WMO meeting of experts on potential climatic effects of ozone and other minor trace gases, *WMO Global Ozone Research and Monitoring Project*, *Report No. 14*, WMO, Geneva, 1983a.

WMO, World Meteorological Organization project on research and monitoring of atmospheric CO_2, *Report No. 10*, edited by R. J. Bojkov, 42 pp., Geneva, 1983b.

WMO, Report of the WMO (CAS) Meeting of Experts on the CO_2 Concentrations from Pre-Industrial Times to I.G.Y. World Climate Programme, *WCP-53*, WMO/ICSU, 34 pp., Geneva, 1983c.

Wofsy, S. C., Interactions of CH_4 and CO in the earth's atmosphere, *Ann. Rev. Earth Planet. Sci.*, *4*, 441-469, 1976.

Wofsy, S. C., J. C. McConnell, and M. B. McElroy, Atmospheric CH_4, CO and CO_2, *J. Geophys. Res.*, *77*, 4477-4493, 1972.

Wofsy, S. C., M. B. McElroy, and Y. L. Yung, The chemistry of atmospheric bromine, *Geophys. Res. Lett.*, *2*, 215-218, 1975.

Wolff, G. T., and P. J. Lioy, Development of an ozone river associated with synoptic scale episodes in the eastern United States, *Environ. Sci. Tech.*, *14*, 1257-1261, 1980.

Woodman, R. F., and A. Giullen, Radar observaqtions of winds and turbulence in the stratosphere and mesosphere, *J. Atmos. Sci.*, *31*, 493-505, 1974.

Wu, M. F., M. A. Geller, J. G. Olson, and M. E. Gelman, Troposphere-Stratosphere (surface-55 km) monthly general circulation statistics for the Northern Hemisphere; 4 year averages, *NASA Techn. Memo. 86182*, NASA Goddard Space Flight Center, Greenbelt, MD, 1984.

Wuebbles, D. J., Chlorocarbon emission scenarios: Potential impact on stratospheric ozone, *J. Geophys. Res.*, *88*, 1433-1443, 1983a.

Wuebbles, D. J., A theoretical analysis of the past variations in global atmospheric composition and temperature structure, *UCRL-53423*, Lawrence Livermore National Laboratory, Livermore, CA, 1983b.

Wuebbles, D. J., and P. S. Connell, Interpreting the 1-D model-calculated nonlinearities from chlorocarbon perturbations, paper presented at International Workshop on Current Issues in our Understanding of the Stratosphere and the Future of the Ozone Layer, BMFT, NASA, FAA, WMO, Feldafing, FRG, June 11-16, 1984.

Wuebbles, D. J., F. M. Luther, and J. E. Penner, Effect of coupled anthropogenic perturbations on stratospheric ozone, *J. Geophys. Res.*, *88*, 1444-1456, 1983.

Wuebbles, D. J., M. C. MacCracken, and F. M. Luther, A proposed reference set of scenarios for radiatively active atmospheric constituents, *Carbon Dioxide Research Division Report DOE/NBB-0066*, U.S. Department of Energy, Lawrence Livermore National Laboratory, Livermore, CA, 1984.

Wyngaard, J. C., Toward convective boundary layer parameterization: A scalar transport module, *J. Atmos. Sci.*, *41*, 1959-1969, 1984.

Yamazaki, K. and C. R. Mechoso, Observations of the final warming in the stratosphere of the Southern Hemisphere during 1979, *J. Atmos. Sci.*, *42*, 1198-1205, 1985.

Yanai, M., J.-H. Chu, T. E. Stark, and T. Nitta, Response of deep and shallow tropical maritime cumuli to large-scale processes, *J. Atmos. Sci.*, *33*, 976-991, 1976.

Yao, F., I. Wilson, and H. Johnston, Temperature dependent ultraviolet absorption spectrum for dinitrogen pentoxide, *J. Phys. Chem.*, *86*, 3611-3615, 1982.

Yoshida, T., and M. Alexander, Nitrous oxide formations by nitrosomoses europsea and heterotrophic organisms, *Soil Sci. Soc. Am. Proc.*, *34*, 880-882, 1970.

Yoshida, T., and M. Alexander, Hydroxylamine oxidation by nitrosomoses europea, *Soil Sci.*, *3*, 307-312, 1971.

Yoshino, K., D. E. Freeman, J. R. Esmond, and W. H. Parkinson, High resolution absorption cross section measurements and band oscillator strengths of the (1,0) - (12-0) Schumann-Runge bands of O_2, *Planet. Space Sci.*, *31*, 339-353, 1983.

Yung, Y. L., M. B. McElroy, and S. C. Wofsy, Atmospheric halocarbons: A discussion with emphasis on chloroform, *Geophys. Res. Lett.*, *2*, 397-399, 1975.

Yung, Y. L., J. P. Pinto, R. T. Watson, and S. P. Sander, Atmospheric bromine and ozone perturbations in the lower stratosphere, *J. Atmos. Sci.*, *37*, 339-353, 1980.

Zafiriou, O. C., and M. McFarland, Nitric oxide from nitrite photolysis in the central equatorial Pacific, *J. Geophys. Res.*, *86*, 3173-3182, 1981.

Zander, R., Presence de HF dans la stratosphere superieure, *C. R. Acad. Sc. Paris*, *281B*, 213-214, 1975.

Zander, R., Recent observations of HF and HCl in the upper stratosphere, *Geophys. Res. Lett.*, *8*, 413-416, 1981a, Corrections, *Geophys. Res. Lett.*, *8*, 850, 1981.

Zander, R., Evidence for variability in the total column of HCl over the Jungfraujoch Station, to be published, 1986.

Zander, R., Trend in HF above the Jungfraujoch Station, to be published, 1986.

Zander, R., H. Leclerq, and L. D. Kaplan, Concentration of carbon monoxide in the upper stratosphere, *Geophys. Res. Lett.*, *8*, 365-368, 1981.

Zander, R., G. M. Stokes, and J. W. Brault, Simultaneous detection of FC-11, FC-12, and FC-22 through 8 to 13 micrometers IR solar observations from the ground, *Geophys. Res. Lett.*, *10*, 521-524, 1983.

Zander, R., G. M. Stokes, and J. W. Brault, Spectroscopic detection of acetylene and ethane in the earth's atmosphere, through ground-based solar observations, *C. R. Acad. Sc. Paris*, *295*, 583-586, 1982.

Zander, R., N. Louisnard, and M. Bangham, Stratospheric methane concentration profiles measured during the Balloon Intercomparison Campaigns, to be published, 1986.

Zangvil, A. and M. Yanai, Upper tropospheric waves in the tropics. Part I: Dynamical analysis in the wavenumber frequency domain, *J. Atmos. Sci.*, *37*, 283-298, 1980.

Zawodny, J. M., Short-term variability of nitrogen dioxide in the winter stratosphere., *J. Geophys. Res.*, in press, 1985a.

Zawodny, J. M., Short term variability of nitrogen dioxide in the winter stratosphere., Ph.D. thesis, University of Colorado, Boulder, CO, 1985b.

Zipf, E. C., and S. S. Prasad, A mesosphere source of nitrous oxide, *Nature*, *295*, 133-135, 1982.

Zumbrunn, R., A. Neftel, and H. Oeschger, CO_2 measurements on l-cm^3 ice samples with an IR laser spectrometer (IRLS) combined with a new dry extraction device, *Earth and Planetary Space Letters*, *60*, 318-324, 1982.